Proceedings of the V Ibero-American

Congress of Smart Cities

ICSC-CITIES 2022

Cuenca, Ecuador, November 28th to 30th
Hosted and sponsored by Universidad de Cuenca

Editors:

Pedro Moreno-Bernal
Luis Hernández-Callejo
Sergio Nesmachnow
Diego Rossit
Danny Ochoa-Correa

UCUENCA

CITIES

CIUDADES INTELIGENTES TOTALMENTE INTEGRALES, EFICIENTES Y SOSTENIBLES

UVa

UNIVERSIDAD
DE LA REPÚBLICA
URUGUAY

UNIVERSIDAD AUTÓNOMA DEL
ESTADO DE MORELOS

UNIVERSIDAD NACIONAL DEL SUR
BAHIA BLANCA

Proceedings of the V Ibero-American

Congress of Smart Cities

ICSC-CITIES 2022

Cuenca, Ecuador, November 28th to 30th

CITIES

CIUDADES INTELIGENTES TOTALMENTE INTEGRALES, EFICIENTES Y SOSTENIBLES

Editors

Pedro Moreno-Bernal (iD)
Universidad Autónoma del Estado de Morelos (UAEM), México

Luis Hernández-Callejo (iD)
Universidad de Valladolid (UVa), España

Sergio Nesmachnow (iD)
Universidad de la República (UDELAR), Uruguay

Diego Rossit (iD)
DI, INMABB, Universidad Nacional del Sur (UNS)-CONICET, Argentina

Danny Ochoa-Correa (iD)
Universidad de Cuenca (UCUENCA), Ecuador

About the event

A Smart City is a framework composed mainly of Internet of Things systems and Information and Communication Technologies (ICT), integrated to develop, implement and promote sustainable development practices and face the challenges of urbanization. The Ibero-American Congress of Smart Cities (ICSC-CITIES) is a discussion forum that aims to create synergies among different research groups to promote the development of Smart Cities, and contribute to their knowledge and integration in different scenarios. The conference is held yearly since 2018 and is sponsored by the Ibero-American Program of Science and Technology for Development (CYTED). The first and the second editions, i.e., 2018 and 2019, were celebrated in Soria, Spain. The third edition was celebrated virtually, but hosted by the Costa Rica Institute of Technology. The fourth edition was hosted by Instituto Politécnico Nacional de México (IPN), celebrate in presencial and virtual mode in Cancún, México.

The fifth Ibero-American Congress of Smart Cities (ICSC-CITIES 2022) was held in a hybrid way (face-to-face and virtual) from November 28th to 30th, 2022, in Cuenca, Ecuador, hosted and sponsored by Universidad de Cuenca, Ecuador. Eighty five technical presentations were given by researchers from 24 different countries during the ICSC-CITIES 2022. Ten papers were included as posters. Papers were divided into four topics, i.e., Governance and Citizenship, Mobility and IoT, Infrastructures, Energy and the Environment and Energy Efficiency. After a rigorous peer-review process, those contributions were selected from a pool of 116 submitted papers, yielding an acceptance rate of 92%.

ICSC-CITIES 2022 program also included the participation of government representatives from several American countries. More specifically, two panel discussion sessions were held. The first one was related to Urban Sustainability. In this panel participated María Augusta Hermida, Rector of the University of Cuenca (Ecuador), Representatives of local governments and governmental entities of Ecuador: Minister of Telecommunications. Vice-Minister of Electricity, Vice-Mayor of Cuenca. A second discussion panel was held which was related to the "Challenges and opportunities of the new urban agenda for intermediary cities", moderated by Prof. Dr. Pedro Martín Cervantes. In this panel participated Dr. Roberto Ramírez Basterrechea, PhD in Political Administration and Economics, Founder of the Startups SmartCitGreen, EcoCitFarmS and CivesSolutions, Dr. Ruben Raedo Santos, PhD in Economics, Consultant to Local Public Administration and Prof. Dr. Pablo de Frutos Madrazo of the Department of Applied Economics Faculty of Business and Labour Sciences, Promoter and first Director of the Chair Urban Agenda 2030 for Local Development University of Valladolid (Spain).

Organization

General Chairs

Luis Hernández Callejo, Universidad de Valladolid, Spain
Sergio Nesmachnow, Universidad de la República, Uruguay

Organizing Committee

Luis Hernández Callejo, Universidad de Valladolid, Spain
Sergio Nesmachnow, Universidad de la República, Uruguay
Pedro Moreno Bernal, Universidad Autónoma del Estado de Morelos, México
Juan Leonardo Espinoza, Universidad de Cuenca, Ecuador
Danny Ochoa Correa, Universidad de Cuenca, Ecuador
Luis Manuel Navas, Universidad de Valladolid, Spain

Publication Chairs

Luis Hernández Callejo, Universidad de Valladolid, Spain, Spain
Sergio Nesmachnow, Universidad de la República, Uruguay
Pedro Moreno Bernal, Universidad Autónoma del Estado de Morelos, México
Diego Rossit, Universidad Nacional del Sur, Argentina
Danny Ochoa Correa, Universidad de Cuenca, Ecuador

Submission and Conference Management Chair

Santiago Iturriaga, Universidad de la República, Uruguay

Track Chairs

Fabián Castillo Peña, Universidad Libre Seccional Cali, Colombia
Ponciano Jorge Escamilla Ambrosio, Instituto Politécnico Nacional, México
Paulo Gondim, Universidade de Brasília, Brasil
Luis Eduardo Tobón, Pontificia Universidad Javeriana, Cali, Colombia
Bernabé Dorronsoro, Universidad de Cádiz, Spain
Ana Ruiz, Universidad San Jorge, Cátedra Mobility Experience, Spain
Humberto Sossa, Instituto Politécnico Nacional, México
Jesús Armando Aguilar Jiménez, Universidad Autónoma de Baja California, México
Victor Alonso Gómez, Universidad de Valladolid, Spain
Sara Gallardo Saavedra, Universidad de Valladolid, Spain
Luis Hernández Callejo, Universidad de Valladolid, Spain
Roberto Villafáfila Robles, Universidad Politécnica de Cataluña, Spain
Irene Lebrusan, Instituto Complutense de Sociología para el Estudio de las Transformaciones Sociales Contemporáneas, Spain
Andrés Navarro, Pontificia Universidad Javeriana, Cali, Colombia
Adriana Correa Guimaraes, Universidad de Valladolid, Spain
Óscar Duque Pérez, Universidad de Valladolid, Spain
Luis Manuel Navas, Universidad de Valladolid, Spain
Jorge Luis Mírez Tarrillo, Universidad Nacional de Ingeniería, Perú

Lorena Parra, Universitat Politécnica de Valencia, Spain
Carlos E. Torres Aguilar, Centro Nacional de Investigación y Desarrollo Tecnológico, México
Daniel Rossit, Universidad Nacional del Sur, Argentina
Pedro Moreno Bernal, Universidad Autónoma del Estado de Morelos, México
Jesús del Carmen Peralta Abarca, Universidad Autónoma del Estado de Morelos, México
Ana Carolina Olivera, CONICET, Argentina
Sergio Nesmachnow, Universidad de la República, Uruguay
Diego Rossit, Universidad Nacional del Sur, Argentina
Mariano Frutos, Universidad Nacional del Sur, Argentina
Teodoro Calonge Cano, Universidad de Valladolid, Spain
Ponciano Jorge Escamilla Ambrosio, Instituto Politécnico Nacional, México
Renzo Massobrio, Universidad de la República, Uruguay and Universidad de Cádiz, Spain
Luis Angelo Steffenel, Université de Reims Champagne-Ardenne, France
Jamal Toutouh, Universidad de Málaga, Spain

Program Committee

Adolfo Ruelas Puente, Universidad Autónoma de Baja California, México
Adrian Toncovich, Universidad Nacional del Sur, Argentina
Adriana Correa-Guimaraes, Universidad de Valladolid, España
Agustín Laguarda, Universidad de la República, Uruguay
Alejandro Otero, Universidad de Buenos Aires-CONICET, Argentina
Alejandro Paz Parra, Pontificia Universidad Javeriana, Colombia
Alessandra Bussador, Universidade Federal da Integração Latino-Americana, Brasil
Alexander Vallejo Díaz, Santo Domingo Institute of Technology, República Dominicana
Alexis Acuna, Universidad Autónoma de Baja California, México
Ana Carolina Olivera, Universidad Nacional de Cuyo, Argentina
Ana Ruiz, San Jorge University, España
Andrei Tchernykh, CICESE Research Center, México
Andrés Adolfo Navarro Newball, Pontificia Universidad Javeriana, Colombia
Ángel Zorita Lamadrid, Universidad de Valladolid, España
Ângela Ferreira, Polytechnic Institute of Bragança, Portugal
Antonella Cavallin, Universidad Nacional del Sur, Argentina
Antonio Mauttone, Universidad de la República, Uruguay
Antonio Muñoz, University of Málaga, España
Armando Huicochea, Research Center for Engineering and Applied Science, México
Bernabe Dorronsoro, Universidad de Cádiz, España
Bernardo Pulido-Gaytan, CICESE Research Center, México
Bouras Abdelkarim, Badji Mokhtar University, Algeria
Carlos Grande, Universidad Centroamericana José Simeón Cañas, El Salvador
Carlos Meza Benavides, Anhalt University of Applied Sciences, Alemania
Carlos E. Torres, Tecnológico Nacional de México/CENIDET, México
Christian Cintrano, Universidad de Málaga, España
Claudio Paz, Universidad Tecnológica Nacional - FRC, Argentina
Claudio Risso, Universidad de la República, Uruguay
Cleonilson Protasio, Federal University of Paraíba, Portugal

Cristina Sáez Blázquez, Department of Cartographic and Land Engineering - University of Salamanca, España

Daniel Rossit, Universidad Nacional del Sur, Argentina

Daniel H. Stolfi, University of Luxembourg, Luxemburgo

David Peña Morales, Universidad de Cádiz, España

Deyslen Mariano, Instituto Tecnológico de Santo Domingo, República Dominicana

Diego Arcos-Aviles, Universidad de las Fuerzas Armadas ESPE, Ecuador

Diego Alberto Godoy, Universidad Gastón Dachary, Argentina

Diego Gabriel Rossit, Universidad Nacional del Sur-CONICET, Argentina

Edgardo Aníbal Belloni, Universidad Gastón Dachary, Argentina

Edgar V. Macias Melo, Universidad Juárez Autónoma de Tabasco, México

Edith Gabriela Manchego Huaquipaco, Universidad Nacional de San Agustín de Arequipa, Perú

Eduardo Fernández, Universidad de la República, Uruguay

Emmanuel Millan, UNcuyo, Argentina

Enrique González, Universidad de Salamanca, España

Esteban Mocskos, Universidad de Buenos Aires, Argentina

Fabian Castillo Peña, Universidad Libre - Cali, Colombia

Fabio Miguel, Universidad Nacional de Río Negro-CONICET, Argentina

Francisco David Moya Chaves, Universidad Distrital Francisco José de Caldas, Colombia

Francisco Valbuena, Universidad de Valladolid, España

Franco Robledo, Universidad de la República, Uruguay

Gilberto Martinez, CIC-IPN, México

Gina Paola Maestre Gongora, Universidad Cooperativa de Colombia, Colombia

Gustavo Richmond-Navarro, Instituto Tecnológico de Costa Rica, Costa Rica

Ignacio de Godos, Universidad de Valladolid, España

Ignacio Martín Nieto, Universidad de Salamanca, España

Irene Lebrusán, Harvard University, Estados Unidos de América

Ivania Aguirre, University of Cuenca, Ecuador

Jamal Toutouh, Massachusetts Institute of Technology, Estados Unidos de América

Javier Rocher, Universitat Politècnica de València, España

Jesús Vegas, Universidad de Valladolid, España

Jesús Armando Aguilar, Autonomous University of Baja California, México

Jesús Del Carmen Peralta Abarca, Universidad Autónoma del Estado de Morelos, México

Joao Coelho, Instituto Politécnico de Bragança, Portugal

Jonathan Muraña, UDELAR, Uruguay

Jorge Arturo Del Ángel Ramos, Universidad Veracruzana, México

Jorge Mario Cortés-Mendoza, University of Luxembourg, Luxembourg

Jorge Mírez, Universidad Nacional de Ingeniería, Perú

Jorge Nájera, Centro de Investigaciones Energéticas, Medioambientales y Tecnológicas, España

José Alberto Hernández, Universidad Autónoma del Estado de Morelos, México

José Ángel Morell Martínez, Universidad de Málaga, España

José Antonio Ferrer, CIEMAT, España

José-Ramón Aira, Universidad de Valladolid, España

Juan Chavat, Universidad de la República, Uruguay

Juan Espinoza, Universidad de Cuenca, Ecuador

Juan Francisco Cabrera Sánchez, Universidad de Cádiz, España

Juan Humberto Sossa Azuela, CIC-IPN, México
Juan José Tarrio, Comisión Nacional de Energía Atómica, Argentina
Juan Manuel Ramírez Alcaraz, Universidad de Colima, México
Juan Mauricio, Universidade Federal da Paraíba, Brasil
Juan Pavón, Universidad Complutense de Madrid, España
Juan R. Coca, Universidad de Valladolid, España
Karla M. Aguilar Castro, Universidad Juárez Autónoma de Tabasco, México
Leonardo Cardinale, Instituto Tecnológico de Costa Rica, Costa Rica
Lilian Obregon, Universidad de Valladolid, España
Lorena Parra, Universitat Politècnica de València, España
Luis G. Montané Jiménez, Universidad Veracruzana, México
Luis Garcia, Universidad de Concepción, Chile
Luis Hernandez-Callejo, Universidad de Valladolid, España
Luis Manuel Navas García, Universidad de Valladolid, España
Luis Marrone, UNLP, Argentina
Luis Tobon, Pontificia Universidad Javeriana Cali, Colombia
Luisana Fernandez, Universidad del Zulia, Venezuela
Manuel Gonzalez, Universidad de Valladolid, España
Marcin Seredynski, E-Bus Competence Center, Francia
Maria Teresa Cepero, Universidad Veracruzana, México
Mariano Frutos, Department of Engineering, Argentina
Mario Andrés Paredes Valverde, TecNM/ITS de Teziutlán, México
Melva Inés Gómez Caicedo, Fundación Universitaria Los Libertadores, Colombia
Miguel Davila, Universidad Politécnica Salesiana, Ecuador
Miguel Angel Che Pan, Tecnológico Nacional de México/CENIDET, México
Monica Alonso, University Carlos III de Madrid, España
Mónica Montoya Giraldo, CIDET, Colombia
Neiel Israel Leyva Santes, Barcelona Supercomputing Center, España
Noelia Uribe-Perez, Tecnalia Research & Innovation, España
Noelia Soledad Pinto, Universidad Tecnológica Nacional, Argentina
Oscar Duque-Perez, University of Valladolid, España
Oscar Izquierdo, CEDER-CIEMAT, España
Pablo Daniel Godoy, Universidad Nacional de Cuyo, Argentina
Pablo Monzon, Universidad de la República, Uruguay
Paul Ayala, Universidad de las Fuerzas Armadas, Ecuador
Paula de Andrés Anaya, Escuela Politécnica Superior de Ávila, España
Paula Peña Carro, CIEMAT, España
Paulo Gondim, Universidade de Brasilia, Brasil
Pedro Curto, Universidad de la República, Uruguay
Pedro Moreno Bernal, Universidad Autónoma del Estado de Morelos, México
Pedro Piñeyro, Universidad de la República, Uruguay
Ponciano Jorge Escamilla-Ambrosio, CIC-IPN, México
Ramiro Martins, Polytechnic Institute of Bragança, Portugal
Raúl Alberto López Meraz, Universidad Veracruzana, México
Renato Andara, Universidad Nacional Experimental Politécnica Antonio José de Sucre, Venezuela

Renzo Massobrio, Universidad de la República, Uruguay

Ricardo Beltrán, Centro de Investigación en Materiales Avanzados, México

Roberto Villafafila, Universitat Politècnica de Catalunya, España

Rodrigo Porteiro, UTE, Uruguay

Rogelio Vargas Lopez, Universidad Autónoma de Guadalajara, México

Santiago Iturriaga, Universidad de la República, Uruguay

Sara Gallardo-Saavedra, Universidad de Valladolid, España

Sergio Nesmachnow, Universidad de la República, Uruguay

Sesil Koutra, University of Mons, Bélgica

Silvia Soutullo, CIEMAT, España

Teodoro Calonge, Universidad de Valladolid, España

Teresa Batista, Universidade de Évora, Portugal

Tiago Carneiro Pessoa, INRIA, Francia

Vanessa Guimarães, CEFET/RJ, Brasil

Vicente Leite, Instituto Politécnico de Bragança, Portugal

Vicente Canals, Universidad de las Islas Baleares, España

Víctor Alonso Gómez, Universidad de Valladolid, España

Víctor Manuel Padrón Nápoles, Universidad Europea de Madrid, España

Program

ICSC-CITIES 2022 took place simultaneously in more than 24 countries throughout Latin America, Spain, and Portugal. To facilitate the attendance of students, researchers and professionals from these countries, the event was schedule in such a way that it was in a suitable period of the day for everyone. The conference program is shown below at the local time of the hosting institution (UTC-5).

Monday, November 28th

Hour (UTC-5)	Activity	Speaker	
8:30 a 9:00	Acto de Inauguración	Dr. Juan Leonardo Espinoza Abad	Vicerrector Académico de la Universidad de Cuenca
		Prof. Dra. Viridiana Aydee León Hernández	Decana de la Facultad de Ciencias Químicas e Ingeniería, Universidad Autónoma del Estado de Morelos, México
		Prof. Dr. Luis Hernández Callejo	Profesor e Investigador de la Universidad de Valladolid (España) y Organizador Académico ICSC-CITIES
		Arq. Pablo Burbano	Vicealcalde de Cuenca
		Dra. Monserrtah Jerves	Vicerrectora de Investigación de la Universidad de Cuenca
		Ing. Enith Carrión	Viceministra de Electricidad
		Ing. Vianna Maino	Ministra de Telecomunicaciones
		Dra. María Augusta Hermida Palacios	Rectora de la Universidad de Cuenca
9:00 a 10:00	**Panel de discusión:** Sostenibilidad Urbana Moderadores: Prof. Dr. Luis Hernández Callejo, Universidad de Valladolid (España)	Autoridades de la Universidad de Cuenca: Rectora María Augusta Hermida Representantes de gobiernos locales y entidades gubernamentales del Ecuador: Ministra de Telecomunicaciones. Viceministra de Electricidad, Vicealcalde de Cuenca	
10:00 a 10:30	Receso para café		

	1658 - Operational strategies to maximize the use of renewable energies in an isolated microgrid: A case study for Puertecitos, B.C., Mexico	Edgar González-San Pedro, Nicolás Velázquez, Adolfo Ruelas, Jesús Armando Aguilar-Jiménez and Ricardo López-Zavala
	2706 - Wind energy forecasting and power ramp: a review	Brian Loza and Ismael Minchala
	4426 - Sistema de control auto-optimizado para maximizar la extracción de potencia y minimizar las cargas en las aspas de un aerogenerador	Gilson Daniel Malo Méndez, Carlor Eduardo Rivas Vásquez and Luis Ismael Minchala
	9575 - Modelamiento numérico de la capacidad de transporte de un gasoducto mediante el uso de ecuaciones convencionales de flujo	Abelardo Contreras Panibra and Jorge Mírez
	7720 - Development of Electric Vehicles Charging Corridors for Steep Elevation Highways. Case study: Cuenca-Ecuador	Miguel Davila, Marco Toledo, Luis Hernández Callejo, Luis Gonzalez and Carlos Alvarez
	2936 - Technical, economic and environmental feasibility study for the implementation of ecotechnologies in a non-residential building	Mariana Romero-Aguilar, Jesús Martínez-Domínguez, Esteban Montiel-Palacios, Roberto Alvarado-Juárez and Moisés Montiel-González
10:30 a 12:30	**9253** - PV and Storage System to reduce distribution network losses: a case study	Gustavo Adolfo Gomez Ramirez, Gonzalo Mora-Jiménez, Isaac A. Luévano-Reyes, Luis García-Santander, Markel Zubiaga Laskano and Carlos Meza
	9300 - Technical-Economic Study of the replacement of internal combustion motorcycle taxis by electric motor motorcycle taxis using RETScreen Software in the city of Lima, Peru	Estefani Gabriela Mendoza Guerra and Guillermo Perez
	2380 - MPC for Active and Reactive Power Dispatch in Islanded Microgrids	Juan Gabriel Ordoñez Ordoñez, John Barco Jiménez, Andres Pantoja, Javier Revelo Fuelagán and José Aguado
	3793 - General economic comparison in heating demand supply: geothermal energy Vs natural gas	Natalia Nuño-Villanueva, Ignacio Martín Nieto, Cristina Sáez Blázquez and Arturo Farfán Martín
	710 - Hybrid AC/DC Microgrids. A state of Art	Oscar Izquierdo, Gonzalo Manuel Martín Rodríguez, Paula Peña-Carro, Inés Fraile Martín, Luis Hernández Callejo and Angel Zorita Lamadrid
	3845 - Development of a gas-absorption packed column simulator for power plants with CO2 capture	Miriam Navarrete, Gustavo Urquiza and Laura Castro

S1. Energy & Energy efficiency and sustainability & Smart Grid

Track Chair: Prof. Dr. Víctor Alonso Gómez

12:30 a 14:30	**1968** - Solar-driven drinking water supply in rural areas under different climate scenarios	Alfonso Garcia Alvaro, María Nafría Martín, Víctor Alonso Gómez, Raúl Muñoz Torre, Daphne Hermosilla Redondo and Ignacio de Godos Crespo	**S2**. Governance & Smart Economy, Development and Education & Smart Environment & Smart Public Services & Sustainability **Track Chair:** Prof. Dr. Luis Manuel Navas
	717 - Deep Neural Networks for Global Horizontal Irradiation Forecasting: A comparative study	Cristian Arbeláez-Duque, Alejandro Duque-Ciro, Walter Villa-Acevedo and Álvaro Jaramillo-Duque	
	6216 - Sustainable Production Planning Optimization Using Integer Programming	Fernando Zanella and Clara Bento Vaz	
	6394 - Repensando un Sistema Integral de RSU para el Centro Histórico de Cuernavaca, Morelos, México	Ivonne Yazmín Arce García, María del Carmen Torres Salazar, José Gerardo Vera Dimas, Hugo Albeiro Saldarriaga Noreña, Viridiana Aydeé León Hernández, Jesús del Carmen Peralta Abarca and Pedro Moreno Bernal	
	1217 - Study of the greenhouse gas emissions and fuel consumption effect, caused by passive and aggressive behavior in driving public service buses in Pasto city	Fredy Dulce, Jackeline Murillo and Eduardo Caicedo	
	876 - SMART CITY INDEX PROPOSAL FOR LATIN AMERICA AND THE CARIBBEAN COUNTRIES	Jorge Najera, Richard Posso, Heiner Camacho, Gustavo Rivas and Junseok Hwang	
	1743 - LA IDEA DE CIUDAD INTELIGENTE EN AMÉRICA LATINA: CONCEPTO, EXPERIENCIAS Y RASGOS COMUNES DE IMPLEMENTACIÓN	Ryszard Edward Rozga Luter and Raúl Hernández Mar	
	4341 - Methodology for watermills localization: A case study of Soria province (Spain)	Jesus Bachiller Martinez, Alberto Redondo, Ana María Barrena Medina, Lilian Johanna Obregón, Héctor Felipe Mateo Romero, Lidia Sanz Molina, Susana Gómez Redondo, Víctor Alonso Gómez and Luis Hernández Callejo	
	7052 - Clustering Analysis of Solar Photovoltaic Electricity Generation at CIC-IPN in North of Mexico City	Ponciano Jorge Escamilla-Ambrosio, Ricardo Alcaraz-Fraga, Gilberto Lorenzo Martínez-Luna, Maria Guadalupe Pulido-Navarro and Juan Humberto Sossa-Azuela	
	9519 - LEVELS OF SULFUR EMITTED IN THE PORT OF GUAYAQUIL AND ITS ATMOSPHERIC CONCENTRATION	Olga Quevedo, Franklin Lopez and Sandra Ronquillo	
	9461 - Global energy balances for energy analysis in buildings	Carlos Enrique Torres-Aguilar, Pedro Moreno-Bernal, Sergio Nesmachnow and Luis Cisneros-Villalobos	
	4420 - Smart mobility for public transportation systems: Improved bus timetabling for synchronizing transfers	Claudio Risso, Sergio Nesmachnow and Diego Rossit	

Tuesday, November 29th

Hour (UTC-5)	Activity	Speaker	Sesion
08:30 a 10:30	**4471** - Impact analysis of the implementation of V2G technology on electric distribution networks	Erick Delgado, Luis Medina, Miguel Davila, Luis Gonzalez, Luis Hernández Callejo and Juan Espinoza	**S3**. Energy & Energy efficiency and sustainability & Smart Grid

Track Chair: Prof. Dr. Carlos Meza Benavides |
	6282 - PVT systems in high summer temperature cities: technical feasibility	Jesús Armando Aguilar-Jiménez, Luis Hernández-Callejo, José Alejandro Suástegui-Macías and Raúl Alberto López-Meraz	
	6794 - Estimación de la presión de falla en defectos por corrosión según ASME B31G para ductos de Transporte de Hidrocarburos utilizando Matlab	José Alberto Navarro Campos and Jorge Mírez	
	7226 - Minimización del requerimiento de almacenamiento de energía en parques eólicos a través del control del estado de carga del banco de baterías	Miguel Mendieta, Wilson Pavón and Luis Ismael Minchala	
	407 - Pump as Turbine in Small-Scale Hydro Generation	Vicente Leite	
	472 - Seguimiento simplificado de consumos para reducción de gasto eléctrico	Jorge Gomez-Sanz	
	2155 - The Impact of COVID-19 on Solar PV Electricity Generation and Consumption Patterns at CIC-IPN	Ponciano Escamilla-Ambrosio and Maria Guadalupe Pulido-Navarro	
	3876 - Variable light intensity system for greenhouse applications	Halleluyah Kupolati, Víctor Alonso Gómez and Luis Hernández Callejo	
	5185 - Biomethane production in isolated farms powered by solar energy: Anaerobic digestion/Solar hybridization technology	Alfonso García Alvaro, César Ruiz Palomar, Luis Hernández-Callejo, Víctor Alonso Gómez, Raúl Muñoz Torre, Daphne Hermosilla Redondo and Ignacio de Godos Crespo	
	1943 - Control Strategies in Microgrid Management: A state of Art	Oscar Izquierdo, Paula Peña Carro, Inés Fraile Martín, Gonzalo Manuel Martín Rojo, Ángel Zorita Lamadrid and Luis Hernandez Callejo	
	893 - IoT platform for monitoring nutritional and weather conditions of avocado production	Pedro Moreno-Bernal, Paris Arizmendi-Peralta, J. Alberto Hernández-Aguilar, Sergio Nesmachnow, J. del Carmen Peralta-Abarca and J. Guadalupe Velásquez-Aguilar	
10:30 a 11:00	Receso para café		

11:00 a 12:00	Título de la mesa redonda: **RETOS Y OPORTUNIDADES DE LA NUEVA AGENDA URBANA PARA LAS CIUDADES INTERMEDIAS** Moderador: **Prof. Dr. PEDRO MARTÍN CERVANTES** Departamento de Economía Financiera y Contabilidad Facultad de Ciencias Empresariales y del Trabajo, Socio de la Cátedra Agenda Urbana 2030 para el Desarrollo Local, Universidad de Valladolid (España)	**Dr. ROBERTO RAMÍREZ BASTERRECHEA** Doctor en Administración Política y Economía, Fundador de las Startup SmartCitGreen, EcoCitFarmS y CivesSolutions	SMART CITY GREEN
		Dr. RUBEN RAEDO SANTOS Doctor en Economía, Consultor de la Administración Pública Local	LA NECESIDAD DE CUANTIFICAR LOS PROCESOS DE IMPLANTACIÓN DE LA AGENDA URBANA El caso de la ciudad de Medellín
		Prof. Dr. PABLO DE FRUTOS MADRAZO Departamento de Economía Aplicada Facultad de Ciencias Empresariales y del Trabajo Promotor y primer Director de la Cátedra Agenda Urbana 2030 para el Desarrollo Local Universidad de Valladolid (España)	EL PAPEL DE LA ACADEMIA EN LA METODOLOGÍA DE IMPLANTACIÓN DE LA NUEVA AGENDA URBANA Una visión transversal y multidisciplinar del proceso
12:00 a 14:00	9749 - Sustainable House Manufacturing for Smart Matching Cities	Paolo Piantanida, Claudia Pilar, Valentina Villa and Antonio Vottari	**S4**. Governance & Smart Economy, Development and Education & Smart Environment & Smart Public Services & Sustainability **Track Chair:** Prof. Dr. Jorge Mírez Tarrillo
	7676 - Lean Office approach for muda identification in the admission process of university students	Jesús Del Carmen Peralta-Abarca, Pedro Moreno-Bernal, Sergio Nesmachnow and Viridiana Aydeé León Hernández	
	2581 - Analyzing the feasibility of the use of computational analysis in lighting improvement projects: The case of the Aerospace Engineering School of UPM (Spain)	Álvaro Pérez-Rees, Daniel Alfonso-Corcuera and Santiago Pindado	
	8969 - Energy efficiency in buildings: Experimental test about the thermal behavior of mortars with different additives	Jorge López-Rebollo, Natalia Nuño Villanueva, Ignacio Martín-Nieto, Cristina Sáez Blázquez and Susana Del Pozo	
	7337 - The role of small cities in achieving carbon neutrality Co-creating carbon neutral cities: a case study of transition management in small European cities	Lola Cadarso, Pablo de Frutos and Marcia Eugenio	
	6448 - Effect of sustainable Local Energy Communities on low	Samuel Borroy, Daniel Marquina, Andrés Llombart and Luis Hernández-Callejo	
	4276 - Energy and economic analysis of renewable energy-based isolated microgrids: Case study Bigene, Guinea-Bissau	Jesús Armando Aguilar Jiménez, Luis Hernández Callejo, Víctor Alonso Gómez, Alfonso García Álvaro, Lilian Johanna Obregón and Raúl Maján Navalón	

2576 - Analysis of the Use of Active Technologies to Convert Traditional Buildings into Net Zero Energy Buildings Using Building Energy Modeling	David Zabala-Pedraza, Ricardo Peña-Guzman, Diego Morales-Polanco, Genesis Sanchez-Sosa, Arismendy Del Orbe, Jose Duran, Nabil Sbriz, Miguel Aybar-Mejía and Deyslen Mariano-Hernández	
6215 - Expanded Realities for Smart Inclusive Education	Andres Adolfo Navarro-Newball, Martín V. A. Sierra G., Juan Carlos Martinez, Juan Jose Betancourt, Katherine Ramirez, Andres Velasquez, Valeria Quinto, Juan Miguel Cardona, Andres Enrique Calderon, Gerardo Restrepo, Andres Dario Castillo, Elizabeth Asprilla, Anita Portilla, Laura L. Serrano, Frank A. Rodriguez and Eliana Peñaloza	
2560 - El desarrollo de Ciudades Inteligentes desde la mirada de los criterios ASG y el enfoque de Sustentabilidad Corporativa en el sector industrial	Angeles Dennis Figueroa-Negrete, Karen Gallegos-Hernandez, Viridiana Aydee Leon-Hernandez and Maria Del Carmen Torres-Salazar	
9028 - Key factors influencing urban wind energy: A case study from the Dominican Republic	Alexander Vallejo Díaz, Idalberto Herrera, Carlos Pereyra and Candida Casilla	
2672 - Classification of Polyethylene Terephthalate bottles in a recycling plant	Diego Alberto Godoy, Nicolas Ibarra, Ricardo Selva, Cesar Gallardo and Enrique Marcelo Albornoz	
4874 - Study of the inactivation of Escherichia coli strain vs. native bacteria during UV disinfection treatment with a flow-trough reactor	Paola Duque-Sarango, Leonardo Romero Martinez, Verónica Pinos, Esteban Sanchez and Esteban Samaniego	

Wednesday, November 30th

Hour (UTC-5)	Activity	Speaker	Sesion
08:00 a 10:00	**7767** - Impact of Power Ramps of Photovoltaic Systems on the Electricity Grid. Case Study: Girasol Solar Park	Miguel Aybar, Darwin Santos, Adellin-Anderson Contreras-Álvarez, Dinelson Rosario-Weeks, Mischael Smith, Elvin Jiménez Matos, Deyslen Mariano-Hernández and Rene Báez-Santana	**S5.** Energy & Energy efficiency and sustainability & Smart Grid **Track Chair:** Prof. Dr. Américo Vicente Teixeira Leite
	2794 - Solar energy integration to achieve the Net-Zero Standard in Educational Buildings.	Esteban Zalamea, Alfredo Ordoñez, Boris Orellana and Juan Hidalgo	
	7323 - Partial photoluminescence imaging of silicon solar cells	Alberto Redondo Plaza, Víctor Alonso Gómez and Luis Hernández Callejo	
	2356 - Analyzing the influence of the building energy demand in the final design of shallow geothermal systems	Cristina Sáez Blázquez, Ignacio Martín Nieto, Natalia Nuño Villanueva, Miguel Ángel Maté González, Arturo Farfán Martín and Diego González Aguilera	
	3837 - Operation Analysis of the Electrical System in Areas with Growth of Tourist Complexes. Case Study: Enriquillo Region, Dominican Republic	Miguel Aybar-Mejía, Randy Andrés, Alam Cabral-Soto, Carlos Montás, Wilmer-Johann Núñez-García, Elvin Arnaldo Jiménez Matos and Deyslen Mariano-Hernández	
	8981 - Harmonic impact of Electric vehicles in Electrical Distribution Systems with high photovoltaic penetration	Miguel Davila, Luis Gonzalez, Luis Hernández Callejo, Oscar Duque-Perez, Ángel L Zorita Lamadrid and Juan Espinoza	
	4169 - Super resolution generative adversarial network for velocity fields in Large Eddy Simulations	Maximiliano Bove, Sergio Nesmachnow and Martín Draper	
	7316 - BB-PLC over LV networks - a step forward towards Smart Grid implementation	Jon González-Ramos, Itziar Angulo, Amaia Arrinda, Igor Fernández, David de la Vega and Alexander Gallarreta	
	7852 - Energy management of the CEDER's smart microgrid with different battery technologies	Oscar Izquierdo-Monge, Paula Peña-Carro and Marcos Martínez Gurría	
	6233 - Power quality improvement techniques in SmartGrids	Daniel Alcalá González, M. Isabel Más-López, Eva Maria García del Toro, Sara Garcia-Salgado and Santiago Pindado	
	1067 - Operation and maintenance of smart microgrids: A case study of the CEDER Microgrid	Oscar Izquierdo-Monge, Paula Peña-Carro, Alberto Redondo, Luis Hernandez Callejo, Gonzalo Martin Jimenez and Angel Zorita Lamadrid	
	8308 - Flexibility Management System for Executing Energy Program with Distributed Resources	Jose-Fernando Forero-Quintero, Roberto Villafafila Robles, Daniel Montesinos-Miracle and Sara Barja-Martinez	
10:00 a 10:30	Receso para café		

10:30 a 12:30	**2640** - Synthetic Dataset of Electroluminescence images of Photovoltaic cells by Deep Convolutional Generative Adversarial Networks	Héctor Felipe Mateo Romero, Miguel Angel González Rebollo, Valentín Cardeñoso Payo, Victor Alonso Gomez, Hugo Jose Bello, Alberto Redondo Plaza and Luis Hernández Callejo	**S6.** Artificial Intelligence & Urban Informatics **Track Chair:** Prof. Dr. Pedro Moreno Bernal
	502 - Distribution of Police Patrols as a Covering Problem in Smart Cities: Fuengirola Use Case	Jamal Toutouh, Francisco Chicano and Rodrigo Gil-Merino	
	9704 - Artificial intelligence for automatic building extraction from urban aerial images	Lucas Gonzalez Petti, Sergio Nesmachnow and Jamal Toutouh	
	7484 - Detecting air conditioning usage in households using unsupervised machine learning on smart meter data	Rodrigo Porteiro and Sergio Nesmachnow	
	6732 - IDE Y MOVILIDAD SOSTENIBLE: ESTADO DEL ARTE EN IBEROAMÉRICA	Maria Teresa Folgôa Batista, Carlos Grande, Carmen Luisa Vásquez Stanescu, Leonardo Suárez Matarrita, Luis Manuel Navas, Rodrigo Ramírez-Pisco, Renato Andara, Carla Fajardo and Rhonmer Pérez	
	596 - Synthesized data generation for public transportation systems	Federico Gómez and Sergio Nesmachnow	
	1815 - Big data analysis for delay estimation of public transportation systems	Santiago Olmedo, Santiago Guridi and Sergio Nesmachnow	
	434 - Big Data trends in the analysis of city resources	Regina Gubareva and Rui Pedro Lopes	
	427 - Walking Accessibility to the Public Transport Network in Montevideo, Uruguay	Sara Perera, Renzo Massobrio and Sergio Nesmachnow	
	7325 - Analysis of public transportation in Montevideo, Uruguay during the COVID-19 pandemic	Andrés Collares, Diego Helal, Andrei Tchernykh and Sergio Nesmachnow	
	6753 - Sistema de Análisis de la Movilidad Regular (Morebike): El Caso del Sistema ECOBICI de la Ciudad de México	Samuel Benitez, Gilberto Martinez and Adolfo Guzman	

12:30 a 14:30	**2947** - Dispositivo IoT para monitorizar aerogeneradores Vortex	Enrique González, Susana Lagüela, María Sánchez Aparicio, Paula de Andrés Anaya, Jose Antonio Martín-Jimenez and Susana del Pozo	**S7.** IoT & Smart Industry & Other Developments
	6034 - Cyber-Physical System through Internet of the Things for the Monitoring of Meteorological Conditions	José-Isidro Hernandez-Vega, Jonam-Leonel Sanchez-Cuevas, Luis-Alejandro Reynoso-Guajardo, Elda Reyes-Varela, Rene Sanjuan-Galindo and Lesly-Yamilett Treviño-Reyna	**Track Chair:** Prof. Dr. Ponciano Jorge Escamilla
	7739 - A new approach to automate the connectivity of electronic devices with an IoT Platform	Juan Flores-Sedano, Hugo Estrada-Esquivel, Alicia Martínez-Rebollar and Jassón Flores-Prieto	
	4773 - An AC/DC hybrid microgrid: a case study at CE.D.E.R.-CIEMAT	Oscar Izquierdo-Monge and Paula Peña-Carro	
	8283 - SNS-Based Secret Sharing Scheme for Security of Smart City Communication Systems	Andrei Gladkov, Egor Shiriaev, Andrei Tchernykh, Maxim Deryabin, Ekaterina Bezuglova, Georgii Valuev, Mikhail Babenko and Sergio Nesmachnow	
	5204 - IoT system for thermography analysis of photovoltaic installations	Leonardo Cardinale-Villalobos, Luis Antonio Solís-García and Luis Alonso Araya-Solano	
	3314 - Método para la transformación digital para espacios de salud (CLÍNICAS). Caso de estudio áreas de telemedicina	Fabian Peñaloza and Villie Morocho	
	1239 - Aplicación de tecnologías LPWAN basadas en LoRa en el monitoreo de fuentes hídricas de los páramos andinos	Luis Eduardo González Armijos, Andrés Amauta Gonzales Zapata, Santiago Renán González Martínez and Alonso Cartuche Paqui	
	4192 - Assessment of a vertical Agrivoltaics installation in the area of Chanco, Maule Region in Chile	Roxane Bruhwyler, Hugo Sanchez, Carlos Meza, Sebastian Dittmann and Frederic Lebau	
	6498 - Preparation of Zinc Oxide from Used Batteries as a Catalyst in the Transesterification of Recycled Oil for the Production of Biodiesel	Domenica Seminario, Melissa Ortega, Andrés Montero, Paola Duque, Paúl Álvarez and Veronica Pinos	
	2874 - Identificación automática de fases en redes de distribución en baja tensión mediante aprendizaje automático	Lluc Crespí-Castañer, Miquel Roca, Josep Lluís Rosselló, Lluís Juncosa and Vicente Canals	
	8120 - Análisis sobre la pérdida de las Lomas de Lima Este y su Impacto en la Reducción de los Servicios Eco-sistémicos	Flor Karin Sueldo Nieto and Jorge Mírez	

Posters

Smart cities and their relationship with ontological engineering	Cindy Espinoza-Aguirre
Planificación óptima de rutas de ambulancias eléctricas en situación de pandemia	Luis Santiago Martin Sevilla, Monica Alonso Martinez and Hortensia Amaris Duarte
Reciclado de Álabes de los Parques Eólicos implementados en Perú. Análisis y propuestas	Alejandro León-Benavides and Jorge Mírez
Progressive regression model to project the behavior of photovoltaic generation in municipalities of Mexico City	Raúl Alberto López Meraz, Yanitzia Reyes Cárcamo and Luis Omar Jamed Boza
A Review of Computational and Mathematical Techniques for Urban Mobility Data Analysis	Hugo Alatrista-Salas, Erick Cuenca, Rigoberto Fonseca-Delgado, Aracelis Hernandez, Saba Infante, Raúl Manzanilla, Diego Morales-Navarrete, Miguel Nunez-Del-Prado, Israel Pineda, Pascal Poncelet and Arnaud Sallaberry
Quantification of Resilience in the electric grid of CENTROSUR. A study case	Pablo Arias-Reyes, Antonio Barragán-Escandón, Javier González-Redrovan and Sergio Zambrano-Asanza
Energy Efficiency: characteristic that achieves the collaborative and sustainable perspective to incorporate IoT in a Smart City	Roberto Ferro-Escobar, Harold Vacca-González and Harvey Gómez-Castillo
Influencia del Desarrollo de Infraestructura Sostenible en el Sector Industria sobre la Vulnerabilidad Socioambiental	Ramsés David Villalobos Núñez and Jorge Mírez
EL PATRIMONIO DE LA HUMANIDAD COMO ELEMENTO COMPETITIVO Y DIFERENCIADOR PARA CIUDADES EN EL DESARROLLO ECONÓMICO DEL TURISMO DE NEGOCIOS	Víctor Hernández Andrés, Pablo de Frutos Madrazo, Pedro Antonio Martín Cervantes and Juan Carlos Frechoso Remiro
Herramienta de simulación de plantas de autoconsumo y su aplicación a un conjunto turístico	Jacinto Vidal-Noguera, Victor Martínez-Moll, Ivan Alonso de Miguel, Andreu Moià- Pol y Vicente Canals

Contents

Posters

Operational strategies to maximize the use of renewable energies in an isolated microgrid: A case study for Puertecitos, B.C., Mexico.

E. González [1,2], N. Velázquez [1], A. Ruelas [2], J.A. Aguilar-Jimenez [2], R. López [1].

[1] Centro de Estudios de las Energías Renovables (CEENER), Instituto de Ingeniería, Universidad Autónoma de Baja California, Mexicali, Baja California, México
[2] Facultad de Ingeniería, Universidad Autónoma de Baja California, Mexicali, Baja California, México
nicolas.velazquez@uabc.edu.mx(N.V.)

Abstract. This paper presents a study of the operation of an isolated microgrid in Puertecitos, B.C., Mexico to determine the operational strategies that would maximize the renewable energies use, in which it establishes the adequate use of fossil fuel and increases the battery bank lifespan. These strategies were obtained from the microgrid operational study through a dynamic simulation using TRNSYS software, where the operation in winter, equinox, and summer was evaluated. The results of the implementation of the generated strategies demonstrate that the energy dumped in winter was reduced by 1.6% and 1.3% in the equinox. Also, the battery lifetime was increased by decreasing the depth of discharge from 80 to 30% when the load is very high during the summer. On the other hand, it was possible to satisfy 12% more load in June and 96% in August, through the adequate use of the diesel electric generator. Therefore, new strategies represent a better use of the generation infrastructure with renewable energies, the minimum cost of operation due to the use of fossil fuel and a method of continuous operation by controlling the reduction of load during the summer months.

Keywords: Microgrid; Operational strategies; TRNSYS.

1 Introduction

Around the world, more than 1.3 billion people do not have access to electricity; more than 84% of this population lives in rural areas[1]. The United Nations proposes a sustainable electrification through electricity generation with renewable energies [2]. In Mexico, there are 45,000 communities in rural areas without access to energy [3] in which the plans of the Secretary of Energy, with support from the World Bank, are to bring rural electrification by installing systems activated with renewable energy, mainly with solar photovoltaic (PV)[4]. The electrical generation systems for isolated communities go from small photovoltaic installations with backup energy in batteries in every house up to a microgrid that includes a single generation system that is interconnected with the electrical loads of the whole community. The microgrids can work in different ways, its operation dynamics depends on its capacity and relationship between generation and storage, it is also required to establish a limit of energy supply [5–8] because the system cannot provide more energy from other generation systems as the case of

grid-connected. Furthermore, community load can vary between seasons due to extreme climates, which makes it difficult to establish criteria that adequately optimal microgrid sizing for winter and summer. However, the electrical load of a community can have great variations in the different seasons of the year, which makes it difficult to establish a sizing criterion that adequately balances the energy supply in winter and summer, which can be translated into a waste of renewable energies, when the design of the microgrid is under or over-dimensioned [9,10]. The last one being the reason for an increase in the initial investment and the time of return of the investment [11]. On the other hand, climate forecasts through numerical models allow generation estimates to be made by inferring the probabilities of cloud formation and variations in solar radiation, directly affecting PV generation through intermittent intervals of minutes to hours or days [12,13]. The evolution in the ways of renewable energies utilization has caused new challenges in designs of equipment, being the main ones the coupling between the generators (PV, Wind Turbine, Diesel generator) and energy storage in batteries, in such a way that the ranges of work of the different parameters from operation make difficult the coupling of technologies [14–17]. Currently, there is work in standardization to have general and defined rules for interoperability between generators, storage, power converters, and load (energy-consuming equipment) [18,19]. However, one of the main challenges is to establish the background for the implementation of an energy management system (EMS) [19–23]; microgrids have evolved rapidly, unlike low-capacity stand-alone systems (< 100 kW) [24–26] in which it is still required that the power converters fluidly communicate with a master system and allow decision making in its local control (tertiary control), which helps to mitigate operating problems in the local equipment caused by lack of visibility (communication) of the control actions to other parts of the microgrid, this has had the consequence of reducing the battery lifetime, inverters and controllers, reaching strong damage in storage systems with over-charged and over-discharged battery [27–30], which, in the meantime, causes the interruption of the operation. On the other hand, the importance of operating strategies that maximize the use of renewable energy is observed, [31] co optimizes the use of water-energy by distributing water in the hours of lowest energy cost, it develops a dispatch model to minimize the cost of energy while maximizing the generation with renewable energy, in [32,33] maximize the use of renewable energy by establishing operational strategies that maximize the use of a fuel cell in combination with PV and batteries. [34] Optimizes load dispatch by using an operational strategy that promotes charging of electric vehicles by shifting the peak load, allowing maximum use of renewable energy and reducing 8.97% of daily costs. [35] Using Homer software, a technical-economic study of a microgrid is carried out, the results show that load follow strategy is the best operation option when taking maximum advantage of renewable energies, ensuring that 85.6% of energy supply to the population and only 14.4% by fossil fuels. Finally, to reduce operating costs and maximize the use of renewable energies, it is necessary to define operating strategies for diesel-electric generators that minimize maintenance and the use of fossil fuels [36-39] , in the particular case of rural areas it is much more expensive to supply fuel [40-41].

Therefore, this article presents an operational study of an isolated microgrid and establishes the operational strategies that allow the maximum use of renewable energies, as well as establishing the optimal use of fossil fuel and increasing the battery bank life. The definition of the strategies is carried out through a quantitative analysis derived from the annual hourly operational study of the microgrid. This is obtained from a dynamic simulation using the TRNSYS simulator. It also takes into consideration a balance point between the battery lifetime and the cost of fossil fuel use. This document is organized as follows: Section 2 describes the system; its location, the components of the microgrid, and its operation. Section 3 presents in five steps, the methodology to improve the microgrid operation strategies, in addition to the weathering profile of Puertecitos, the electric load profile, and the mathematical models representing the components for the simulation. Section 4 presents a validation of the electricity generation with experimental data and simulation results. Section 5 presents the discussion of simulation results where current microgrid operation dynamics (base case scenario) and new operation strategies are shown. Section 6 presents the conclusions.

2 System description

The operational strategies are generated and implemented in the Sustainable Electrical Generation System (microgrid) of the isolated community of Puertecitos, which has been in operation since November 2015. The community is located in Baja California, Mexico, east of the Sea of Cortez (30°21′2.37″ N, 114°38′29.7′ ′ W). Diagram in figure 1 shows that the microgrid is composed of 54.6 kW of photovoltaic (PV) field, comprising 182 panels of 300 W which are connected in 13 arrays of 14 panels connected in series (see figure2 (a)). These are connected at two solar charge controllers of 26 kW each with a single output on a direct current bus of 348 V nominal, in which a battery bank is interconnected (522 kWh storage system, composed of 174 batteries connected in series, of 2V @1500 Ah) and a 100 kVA inverter, the installation of these components can be seen in Figure 2 (b), after this last one, there is a 480V AC bus, in which a 5 kW wind turbine(WT) is interconnected in Figure 2 (a) and a 75 kVA three-phase 480V diesel generator in Figure 2 (d). The inverter in Figure 2 (b) contains a 40 A DC rectifier that allows charge battery from AC power produced by the diesel generator and distributed through the distribution network shown in Figure 2 (c).
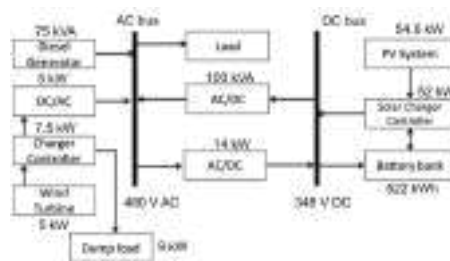
Fig. 1. Puertecitos microgrid diagram.

Fig. 2. Puertecitos, Baja California Power Generation System a), Inverter and battery bank b) Medium voltage power distribution system 13.3 kV c) and diesel electric generator d).

3 Methodology

This section presents the methodology to determine the operating strategies that will allow for the maximum use of renewable energies, an increase lifespan of equipment, and the optimal operation of a diesel-electric generator. To this achievement, the procedure shown in Figure 3 was established. The first step establishes weather conditions and the load profile of the Puertecitos to specify the equipment characteristics previously shown in section 2. In the second step, the simulation model for the operational study of the microgrid is carried out using the TRNSYS environment. In the third step, the microgrid operating procedure was established to define the conditions of the base case and formulated the cases for the new operational strategies to maximize microgrid performance. In the fourth and fifth steps, simulation results were analyzed and discussed.
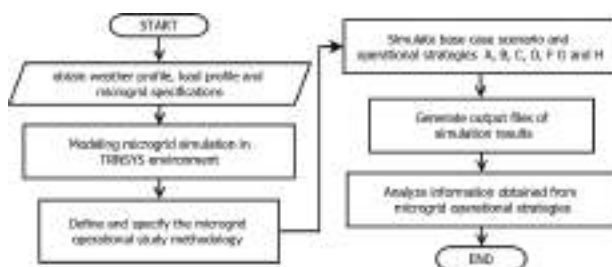
Fig. 3. Process of Puertecitos microgrid operational strategies study.

3.1 Weather data and load profile

To estimate PV/WT power generation, it is necessary Puertecitos Weather data. Measurements data are from a Delta Ohm weather station model HD52.3D147. Variables extracted from measurements are ambient temperature, barometric pressure, relative humidity, wind speed and direction, and global radiation (LPPYRA02 pyranometer). One second measurement interval and average, maximum, and minimum values were

collected at two-second intervals for one year. Data were processed to generate a Puertecitos typical meteorological file in TMY2 format.

Table 1 shows a summary of representative average weather data for winter, summer, and equinox. An increase in the availability of solar radiation during the summer months is observed, as well as an increase in the ambient temperature. Maximum wind speeds increase during winter and equinox.

Table 1. Average weather data.

Month	Average solar energy per day [kWh/m²]	Average wind speed [m/s]	Minimum and maximum wind speed [m/s]	Minimum and maximum temperature [°C]
March	6.75	3.17	0-13	15-30
June	8.49	2.94	0-9	22-41
August	7.4	3.2	0-10	24-43
December	3.59	3	0-14	7-26

The annual hourly load profile for 20 homes obtained from consumption data measured in a social interest home in Mexicali, B.C. Mexico (maximum expected load), in addition to the load from the community's public lighting system. The data were averaged in 10-minute intervals for the main household appliances: refrigerator, air conditioning, electronic equipment, and total consumption. Figure 4 shows that Mexicali and Puertecitos have very similar temperatures because they are in a very close geographic area and extreme climates, so the same energy consumption requirements are expected. As the ambient temperature increases between 30 and 40 °C, the load also increases due to the use of air conditioning for the air conditioning of spaces.
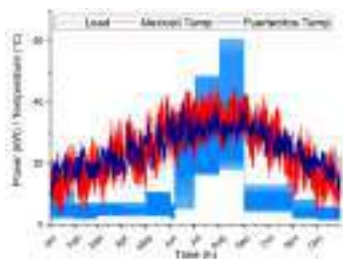
Fig. 4. Load profile and temperature expected in Mexicali and Puertecitos.
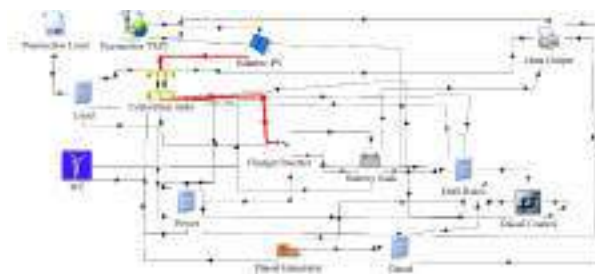
Fig. 5. TRNSYS simulation of Puertecitos Microgrid.

3.2   Modeling Puertecitos microgrid in TRNSYS environment

To evaluate the operational microgrid performance, a simulation was developed in a quasi-dynamic state, with an interval of 15 minutes, and is composed of interconnected types where each one contains a validated mathematical model. [42]. Figure 5 shows the microgrid configuration in simulation with Type 109, is a TMY file reader that extracts data on horizontal and tilt solar radiation, wind speed and direction, ambient temperature and atmospheric pressure. Type 9, CSV file reader where the load profile information is located, it moves forward according to each iteration in the simulation process within the time interval programmed. Type 94, calculates PV generation and takes the output data of type 109, it contains a mathematical model based on finding 4 parameters (*IL,ref*, *Io,ref,* γ, y R_s) that are complemented with the technical information of the PV panel model to be used, where the IV curve shown in the equation (1) depends directly on the incident radiation and cell temperature.

$$I = I_L - I_o \left[exp\left(\frac{q}{\gamma k T_c} (V + I R_s) \right) - 1 \right]$$ **(1)**

Where R_s y γ are constants and the I_L current shown in equation (2), depends linearly on the radiation of incidence on the panel.

$$I_L = I_{Lref} \frac{G_t}{G_{T,ref}}$$ (2)

Type 90, it represents the wind turbine which power output (p) is expressed in equation (3) and comes from the blades area (A_R) that receive the kinetic Energy and convert into mechanical Energy, in addition, air density (ρ), wind speed (U) and power coefficient (C_p) of the wind turbine. These conditions are only met under the wind power curve which is obtained from the manufacturer and is input to obtain real results. Type 47a, represents the battery bank. The input variable to this type is given in Power and the outputs are Power, voltage, current, and SoC. Battery voltage model represented in equation (4), accuracy increases by adjusting the parameters e_q, r_q and m depending on if it is being charged or discharged.

$$P = \frac{1}{2} \rho A_R U^3 C_p$$ (3)

$$V = e_q - gH + I r_q \left(1 + \frac{mH}{\frac{Q}{Q_m - H}} \right)$$ (4)

3.3   Microgrid operational study methodology

The base case scenario was analyzed through a quantitative study according to the simulation established in 3.1 in two steps (4 and 5). In step 4, a microgrid operation study was carried out, where it is analyzed how generation is complemented with renewable energies and the energy storage system for the load supply. In this way, operation problems presented in the different seasons of the year are quantified and identified. For this purpose, operation study is considered by representative weeks of winter, equinox, and-summer, where it is divided into the average load of the season in the month of June and the point of maximum ambient temperature and load in August. Therefore, the annual operating performance is obtained. The operating strategy of the base case scenario is illustrated in Figure 6, where it can be seen that the continuous operation of the microgrid depends on the load about generation capacity and available energy storage. When the generation power is greater than the load, the remaining energy is stored in

battery, as long as they are not fully State of Charge (SoCmax = 100%). Otherwise, the PV panels decrease their generation to meet the load by utilizing a solar charger controller. On the other hand, when the load is higher than the generation, energy comes from battery, only if there is a SoCmin is higher than 20%, otherwise, as there is not enough energy, loads are disconnected from the microgrid and battery are charged with the PV until the generation is greater than the load and the consumers can be connected again.
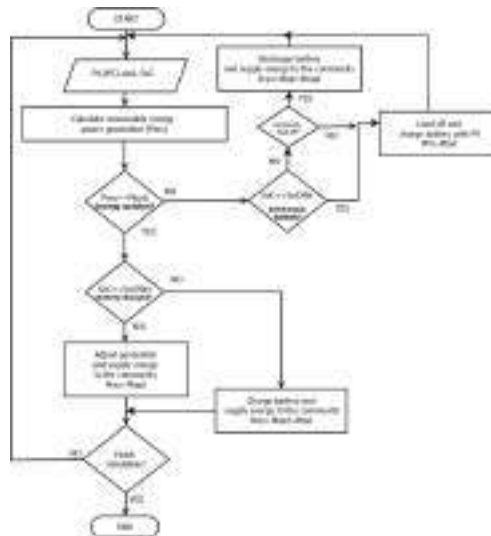
Fig. 6. Microgrid base case scenario algorithm.

Step 5 defines and evaluates operating strategies based on variations in solar PV generation, WT, diesel generator, battery, and load:

1. Winter operation. December 19-25 was selected as a representative winter data to analyze the surplus energy because of a low load profile compared to generation. Also, the maximum autonomy was studied for low generation days that occur more frequently in this season of the year. New load profiles were determined to take maximum use of the available renewable energy without compromising the battery life. Also, the community has a deficit of potable water, it is proposed to integrate a reverse osmosis desalination system, where the surplus energy can produce potable water considering an average specific energy consumption (SEC) of 3.8 kWh/m^3 ([43]), as part of the strategies to maximize the use of renewable energies.
2. Operation in Equinox. The week of March 14-20 was chosen to analyze the transition dynamics of the increase of the load in the community according to increases in the local temperature. Like in winter, new load profiles are being explored to maximize the use of renewable energies.

3. Summer operation. The week of June 21-27 was considered representative of the summer dynamics. The energy consumption was increased to mitigate the requirements of air-conditioned spaces due to the temperature and humidity of Puertecitos climate. The Load adjustment to the maximum generation/storage capacity was analyzed. On the other hand, continuous operation of the microgrid was analyzed using the diesel generator, to establish an operational strategy that minimizes its use and operation cost.

4 Analysis and discussion of results.

This section presents the validation of PV power output and the results of the microgrid simulations, in which the base case scenario operation (normal operation) was analyzed, in addition to the performance with the implementation of the proposed operation strategies, which allow the management of energy sources to increase their use, longer battery life, and the reduction of the operation cost by the diesel generator. Then, the algorithms for the new operation strategies are presented and finally, a comparison of the microgrid performance between the base case operation and the new proposal.

4.1 Validation of PV power output.

The results of PV generation were compared between the experimentally measured data of PV generation in the microgrid and the simulations carried out in TRNSYS, with climatological measured data (see Figure 7) where an average error of 5% was obtained when comparing the representative days of the equinox, summer, and winter.

4.2 A Base case scenario, microgrid normal operation

The base case scenario involves the microgrid operation analyzing in the different climates expected in Puertecitos, according to section 3.1, in which three types of climates during the year are explained. Therefore, the microgrid is evaluated in a week representative of the winter, equinox, and summer months.

Winter operation, figure 8(a) shows the generation of renewable energy, the load profile, the State of Charge (SoC) of the battery bank, and the amount of energy dumped. It can be seen that during all the days of the week that the generation is greater than the load, so there is waste energy that goes from 106 to 140 kWh per day, about the battery SoC is maintained between 90 and 100%. This means that the battery are under-utilized
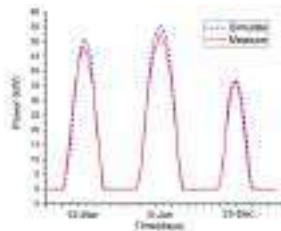
Fig. 7. PV generation comparison between experimental and simulation data.

by 70% since they can be used with an SoC greater than 20% so as not to damage their useful life. Also, the renewable energy generation infrastructure is under-utilized and battery capacity is not optimally used. This is because of the very low load profile in winter and local weather conditions. However, in summer the load increases due to the need for air conditioning.

Equinox operation, in March, the load increases by 26% and generation by 43% to winter (see Figure 8 b). Energy dumped that goes from 170 to 240 kWh per day. This is why at the equinox the battery have a low discharge profile that varies between 10 and 15% of Depth of Discharge (DoD) for a day of operation. Therefore, in these months of the year, there is also a waste of generation and storage infrastructure.

Summer operation in June, Figure 9(a) shows the generation with renewable energies, the expected load profile, the load supplied, the battery SoC and the energy dumped. The community does not want to use the diesel generator, so it is disconnected at night for 2 hours a day. The simulation considers the disconnection of the microgrid as can be seen when the load on the dotted lines falls, so it results in a daily supply of 406 kWh. Moreover, the battery bank is used at 40% of its capacity, with its SoC fluctuating from 60 to 100%. It is also observed that when the battery are fully charged, there is a minimum energy waste of 14 kWh per day in the first two days of the week. For all the above reasons, it can be seen that the use of the generation and storage capacity is optimal. In addition, the increase in ambient temperature in summer directly influences the increase in the load of the community.

Summer operation maximum load in August, Figure 9 (b) shows an increase in the load profile to 786 kWh per day, also the daily generation is 380 kWh, which is not enough to meet the load profile. This is why the energy supply is interrupted for 10 hours a day, without considering the diesel generator use. Therefore the load supplied is 369 kWh per day, which allows the battery bank to be used in an optimal range of charge and discharge cycles in a range of 50 to 98% SoC.

a)   b)
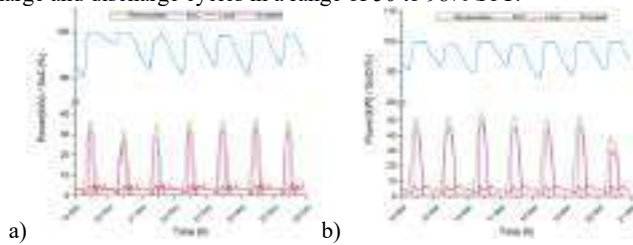
Fig. 8. One week Winter operation a) and one week Equinox operation b).

a)   b)
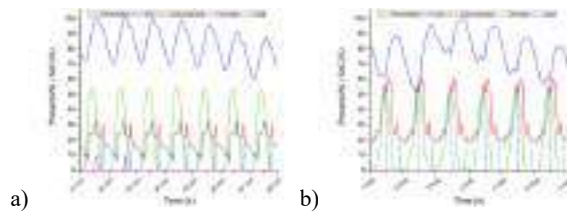
Fig. 9. Summer operation at June a) and Summer operation at load peak on August b).

4.2   Operational strategies to maximize the microgrid performance.
 Winter operation strategies

The operation of the base case scenario allowed the establishment of new operating strategies that aim to achieve maximum energy efficiency in winter. For this purpose,

a schedule was established where load is increased with non-priority equipment without compromising the battery lifetime. Also, the operation was determined under the worst winter generation conditions due to the low or non-availability of renewable resources. ***Case A***, maximizing renewable Energy performance in winter. From an exploratory analysis of the data obtained from the simulation in TRNSYS, a new load profile was determined which allows for maximizing the use of generation with renewable energies during winter. Figure 10 (a) shows a 20 kW load increase from 10:00 to 16:00 hours to coincide with the hours of the generation with PV panels and thus avoid greater use of the storage subsystem. The surplus energy can be used by non-priority or secondary systems for commercial or community purposes, such as producing 32 m^3/d of desalinated water, considering 121.6 kWh daily surplus. For its implementation, it is proposed to identify the users of the commercial sector who wish to consume a part of this energy and in which schedules to define a scheme of programmed loads that allows satisfying the non-priority commercial loads, water production, and domestic load. In this way, the microgrid delivers energy to the community and at 10 AM, the programmed non-priority loads are enabled, and at 4 PM all non-priority loads must be deactivated, keeping only the homes and public lighting connected. Therefore, an operation strategy is obtained which takes maximum advantage of renewable energies without reducing the battery lifespan. **Case B**, operation strategy for maximum autonomy in winter. Figure 10 (b) shows after one day of normal operation, renewable energy generation is interrupted for 3 days and battery SoC reaches 50% before restarting to store energy on the 4th day of operation. This operation strategy supports autonomy in the case of cloudy days or when maintenance or disconnection is required in the generation systems. Therefore, is determined that when having cloudy days, the system can operate without any problem under the normal profile established for winter, up to three days, then three days of operation are required with normal generation for the battery bank to reach 100% SoC, this is very important because the battery have a longer life when they are in charge and discharge cycles close to 100% SoC.

a)   b)
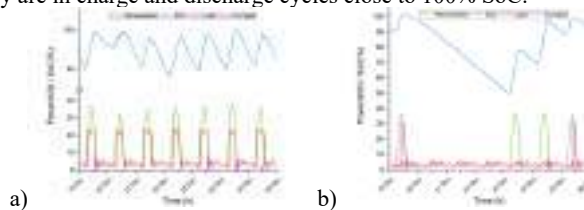
Fig. 10. Maximum use of renewable energies strategy a) and One week Winter simulation with 3 days of non-generation with renewable energy.

Operational strategies on equinox

Case C, maximum utilization of renewable energies, figure 11 (a) shows the generation with renewable energies, battery SoC, load, and dumped energy. An increase of 200 kWh in the load profile is observed compared to the operation of the base case at equinox. This corresponds to an extra load of 40 kW from 9:00 to 14:00 hours that can be used by non-priority or secondary electricity consumer systems, without compromising the use of stored energy, because it is only used when renewable energies are available. On the other hand, at this time of the year, 64 m^3/d of desalinated water can be produced daily, which can be used for daily community consumption or stored for later use. As

in the operation in winter, it is required to implement a scheme of connection and disconnection of electrical loads from the commercial sector and the water desalination system. Case D, maximum autonomy of operation without generation, figure 11 (b) shows that after the first day of operation, the storage system has 100% SoC and the next three days there is no generation, reaching 28% SoC in battery. In the fifth operation, there is a generation with renewable energy, so the load is satisfied and there is enough energy to charge battery at 100% SoC in 2 days, considering the load profile of the base case scenario operation. Therefore, a scenario was established to determine the maximum capacities of the microgrid when a maintenance disconnection is required or there is no renewable resource available, considering the battery bank lifespan will not be damaged.

a)   b)
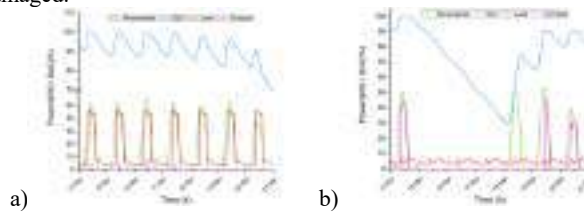
Fig. 11. Maximum utilization in equinox a) and b) Maximum autonomy for 3 days without generation.

Operational strategies in summer

In summer it is required a continuous operation (24/7) that allows having thermal comfort in air-conditioned spaces due to the high temperatures of the environment, so we propose operation strategies that enable the diesel-electric generator use to the minimum required and a load control strategy. *Case E, Load control on June.* Figure 12 (a) shows that the microgrid can satisfy the load if the daily profile is reduced by 14%. This improves the life of the battery bank since the SoC oscillates at higher levels (60-94%). Moreover, the objective of the uninterrupted operation is achieved. On the other hand, to carry out this strategy, the load shifting technique was used [44], by readjusting the "strategic conservation" type of load profile that allows for a readjustment of the electrical loads around the day. A more detailed analysis is shown in Figure 12 (b), where the total daily load profile within the houses where higher energy consumption is observed due to the use of air conditioning equipment to obtain thermal comfort. On the other hand, the participation of the residents is extremely important for the implementation of this type of strategy [45], where the first step is the manually connections and disconnections, so the results depend on the users and an information campaign must be carried out for the community to explain the limits of their consumption according to the electrical appliances they use and the schedule they can use. In a second step, it is required to implement automation through a direct load control that allows a load disconnection/connection based on each user's priorities, under the consideration that all houses have the same priority of use, so they have the same energy assigned. **Case F, Continuous operation with use of diesel electric generator.** Figure 13 shows the generation

with renewable energies, diesel generator, supplied load, expected load, battery bank state of charge, and Energy dumped. It can be seen that on the morning of June 26, the storage system was at 31% SoC and during the night, when there is no generation with PV panels, the diesel generator was turned on until sunrise. Therefore, on June 27, the battery bank was 100% charged and was able to satisfy the load of the community along with the generation until the early morning of June 28, when the SoC was close to the minimum (20%). Therefore, the generator is turned on again all night, this achieves to complement the charge of the battery to reach 100% with renewable energy in the afternoon. Hence, the diesel generator operation is optimal because no energy is wasted. On the other hand, the switching on and off of the diesel generator is carried out manually with the support of the microgrid operator. In a second step, an automatic generator starter (AGS) system will be used to program the generator's start and stop. Therefore, it is determined that the diesel generator should be used as long as the battery have reached an SoC close to 30% before having generation with solar energy. The diesel generator must be turned on when there is no more solar resource available.

a) b)
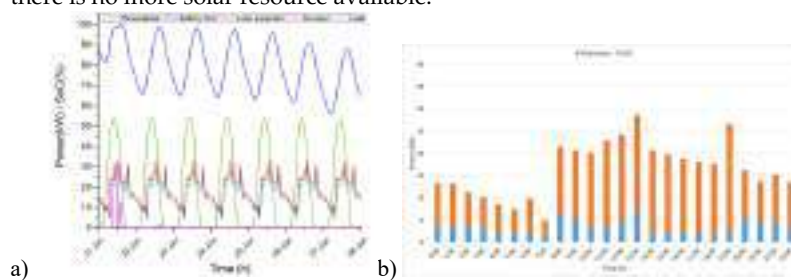
Fig. 12. Load adjust on summer week and Load profile adjust on summer (b).
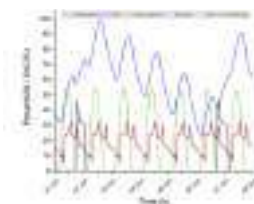
Figure 13. 24/7 operation with electric diesel generator.

5   Conclusions

In this work, which is a study of the operation, implementation, simulation through TRNSYS, it was obtained the behavior of the microgrid in different modes of operation in extreme climates, this determined operational strategies to maximize the use of renewable energies, establish the optimal use of the diesel-electric generator and extend

the life of the battery bank for the Puertecitos microgrid. Therefore, they reached the following conclusions: The strategies of operation in winter (case A) and equinox (case C), where the load is increased in hours that match the generation with renewable energies, demonstrated that it is possible to reduce the waste of energy that reached 63% to a maximum waste of 1.6%. Therefore, it is concluded that these strategies maximize the use of renewable energies without compromising the battery lifetime and it is valid to use them in isolated microgrids. The simulation model used to calculate the energy and operation dynamics during winter (case B) and equinox (case D), reduces the uncertainty of shutdowns in the microgrid when operating without generation, and also protects the life of the storage system as it determines an operation time without over-discharging. Therefore, it is a good option to schedule maintenance actions and avoid blackouts. Having a load profile that varies in the different seasons of the year, it was observed that there was a 63% waste of generation with renewable energies in the winter months. So with the proposed strategies, it is possible to satisfy the load, with optimal use of the generation and storage infrastructure throughout the year. The operational strategy of load control and the use of the diesel generator, increased the SoC levels to 95% and decreased the DoD 30%, so it is concluded that any strategy that reduces the work cycles during the high demands of use of the battery bank will help prevent damage from over-discharge and increase its life. In the region where Puertecitos microgrid has been installed, there are other locations with the same energy supply needs for people without access to energy, so the results of this work can be used for the implementation of other isolated microgrids on the same region.

References

1. Viteri, J.P.; Henao, F.; Cherni, J.; Dyner, I. Optimizing the insertion of renewable energy in the off-grid regions of Colombia. J. Clean. Prod., pp 235, 535–548, (2019).

2. Dioha, M.O.; Emodi, N.V. Investigating the Impacts of Energy Access Scenarios in the Nigerian Household Sector by 2030. Resources, pp. 8, 127 (2019).

3. Secretaria de energía Fondo del Servicio Universal Eléctrico, el rostro social de la Reforma Energética (2017).

4. Comunidades rurales alejadas de la red eléctrica logran acceso a electricidad en México, https://projects.bancomundial.org/es/results/2017/11/01/switching-on-remote-communities-through-electricity-access-in-mexico, last accessed 2019/11/21.

5. Khodayar, M.E., Rural electrification and expansion planning of off-grid microgrids. Electr. J., pp 30, 68–74 (2017).

6. Z., X.; M., N.; S., C. Rural electrification implementation strategies through microgrid approach in South African context. Int. J. Electr. Power Energy Syst., pp. 82, 452–465, (2016).

7. Zomers, A., Remote Access: Context, Challenges, and Obstacles in Rural Electrification. IEEE Power Energy Mag., pp. 12, 26–34 (2014).

8. Singh, S.; Singh, M.; Kaushik, S.C. Feasibility study of an islanded microgrid in rural area consisting of PV, wind, biomass and battery energy storage system. Energy Convers. Manag., pp. 128, 178–190 (2016).

9. The impact of climate change on the European energy system. Energy Policy, pp. 60, 406–417, (2013).

10. Perera, A.T.D.; Nik, V.M.; Scartezzini, J.-L. Impacts of extreme climate conditions due to climate change on the energy system design and operation. Energy Procedia, pp. 159, 358–363, (2019).

11. Siddaiah, R.; Saini, R.P. A review on planning, configurations, modeling and optimization techniques of hybrid renewable energy systems for off grid applications. Renew. Sustain. Energy Rev., pp. 58, 376–396, (2016).

12. Monaaf D.A. Al-falahi; S.D.G. Jayasinghe; H. Enshaei A review on recent size optimization methodologies for standalone solar and wind hybrid renewable energy system. Energy Convers. Manag., pp. 143, 252–274, (2017).

13. Agüera A.; Palomares, J.C.; González J.J., Weather forecasts for microgrid energy management: Review, discussion and recommendations. Appl. Energy, pp. 228, 265–278, (2018).

14. Planas, E.; Andreu, J.; Gárate, J.I.; Martínez , I.; Ibarra, E. AC and DC technology in microgrids: A review. Renew. Sustain. Energy Rev., pp. 43, 726–749, (2015).

15. Hirsch, A.; Parag, Y.; Guerrero, J. Microgrids: A review of technologies, key drivers, and outstanding issues. Renew. Sustain. Energy Rev., pp. 90, 402–411, (2018).

16. García, Y.E.; Dufo, R.; Bernal J.L., Optimization of Isolated Hybrid Microgrids with Renewable Energy Based on Different Battery Models and Technologies. Energies, 13, 581, (2020).

17. Marín, L.G., Sumner, M.; Muñoz, D.; Köbrich, D.; Pholboon, S.; Sáez, D.; Núñez, A., Hierarchical Energy Management System for Microgrid Operation Based on Robust Model Predictive Control. Energies, 12, 4453, (2019).

18. IEEE Standard for the Specification of Microgrid Controllers - IEEE Standard, https://ieeexplore.ieee.org/document/8295083, last accessed 2019/09/10.

19. Hannan, M.A.; Lipu, M.S.H.; Ker, P.J.; Begum, R.A.; Agelidis, V.G.; Blaabjerg, F. Power electronics contribution to renewable energy conversion addressing emission reduction: Applications, issues, and recommendations. Appl. Energy, pag. 251, (2019).

20. Anoune, K.; Bouya, M.; Astito, A.; Abdellah, A.B. Sizing methods and optimization techniques for PV-wind based hybrid renewable energy system: A review. Renew. Sustain. Energy Rev., pp. 93, 652–673, (2018).

21. Anoune, K.; Laknizi, A.; Bouya, M.; Astito, A.; Ben Abdellah, A. Sizing a PV-Wind based hybrid system using deterministic approach. Energy Convers. Manag., pp. 169, 137–148, (2018).

22. El-Bidairi, K.S.; Duc Nguyen, H.; Jayasinghe, S.D.G.; Mahmoud, T.S.; Penesis, I., A hybrid energy management and battery size optimization for standalone microgrids: A case study for Flinders Island, Australia. Energy Convers. Manag., pp. 175, 192–212, (2018).

23. Bonkile, M.P.; Ramadesigan, V., Power management control strategy using physics-based battery models in standalone PV-battery hybrid systems. J. Energy Storage, pp. 23, 258–268, (2019).

24. Henao, A.; Saavedra, A.; Ramos, C., Optimal Power Dispatch of Small-Scale Standalone Microgrid Located in Colombian Territory. Energies, pp. 11, 1877, (2018).

25. S., M.; S., G.K.; M., R., Microgrid energy management and control: Technical review. 2016 IEEE Int. Conf. Autom. ICA-ACCA, pp. 1–7.

26. Lanre, O.; Saad, M.; M.S., I.; M., M. Energy management strategies in hybrid renewable energy systems: A review, (2016).

27.   Meng, L.; Sanseverino, E.R.; Luna, A.; Dragicevic, T.; Vasquez, J.C.; Guerrero, J.M. Microgrid supervisory controllers and energy management systems: A literature review. Renew. Sustain. Energy Rev., pp. 60, 1263–1273, (2016).

28. Azuatalam, D.; Paridari, K.; Ma, Y.; Förstl, M.; Chapman, A.C.; Verbič, G. Energy management of small-scale PV-battery systems: A systematic review considering practical implementation, computational requirements, quality of input data and battery degradation. Renew. Sustain. Energy Rev., pp. 112, 555–570, (2019).

29. Yang, Y.; Bremner, S.; Menictas, C.; Kay, M. Battery energy storage system size determination in renewable energy systems: A review. Renew. Sustain. Energy Rev., pp. 91, 109–125, (2018).

30. Das, C.K.; Bass, O.; Kothapalli, G.; Mahmoud, T.S.; Habibi, D. Overview of energy storage systems in distribution networks: Placement, sizing, operation, and power quality. Renew. Sustain. Energy Rev., pp. 91, 1205–1230, (2018).

31. Moazeni, F.; Khazaei, J. Optimal operation of water-energy microgrids; a mixed integer linear programming formulation. J. Clean. Prod., 275, 122776, (2020).

32. Dursun, E.; Kilic, O. Comparative evaluation of different power management strategies of a stand-alone PV/Wind/PEMFC hybrid power system. Int. J. Electr. Power Energy Syst., pp. 34, 81–89, (2012).

33. Mohammad Sadigh Behzadi Comparative performance analysis of a hybrid PV/FC/battery stand-alone system using different power management strategies and sizing approaches | Elsevier Enhanced Reader., doi:10.1016/j.ijhydene.2014.10.097.

34. Wen, L.; Zhou, K.; Yang, S.; Lu, X. Optimal load dispatch of community microgrid with deep learning based solar power and load forecasting. Energy, 171, pp. 1053–1065, (2019).

35. Costa, T.S.; Villalva, M.G. Technical Evaluation of a PV-Diesel Hybrid System with Energy Storage: Case Study in the Tapajós-Arapiuns Extractive Reserve, Amazon, Brazil. Energies, 13, 2969, (2020).

36. Fodhil, F., Potential, optimization and sensitivity analysis of photovoltaic-diesel-battery hybrid energy system for rural electrification in Algeria. Energy, pp., 169, 613–624, (2019).

37. Olivares, D.E.; Mehrizi, A.; Etemadi, A.H.; Cañizares, C.A.; Iravani, R.; Kazerani, M.; Hajimiragha, A.H.; Gomis, O.; Saeedifard, M.; Palma-Behnke, R.; et al. Trends in Microgrid Control. IEEE Trans. Smart Grid, 5, pp.1905–1919, (2014).

38. Mohammed, Y.S.; Mustafa, M.W.; Bashir, N. Hybrid renewable energy systems for off-grid electric power: Review of substantial issues. Renew. Sustain. Energy Rev., 35, 527–539, (2014).

39. Shi, R.; Zhang, X. VSG-Based Dynamic Frequency Support Control for Autonomous PV–Diesel Microgrids. Energies, 11, 1814, (2018).

40. Tazvinga, H.; Xia, X.; Zhang, J., Minimum cost solution of photovoltaic–diesel–battery hybrid power systems for remote consumers. Solar Energy, 96, pp. 292–299, (2013).

41. Zia, M.F.; Elbouchikhi, E.; Benbouzid, M. Microgrids energy management systems: A critical review on methods, solutions, and prospects. Appl. Energy, pp. 222, 1033–1055, (2018).

42. Klein, S.A.; Beckman, W.A.; Mitchell, J.W.; Duffie, J.A.; Duffy, M.J. TRNSYS 17. Volume 4. Mathematical Reference. a TRaNsient SYstem Simulation program.

43. Meer A.M.Khan; S.Rehman; Fahad A. Al-Sulaiman A hybrid renewable energy system as a potential energy source for water desalination using reverse osmosis: A review. Renew. Sustain. Energy Rev., 97, 456–477, (2018).

44. Mohandes, B.; Acharya, S.; El Moursi, M.S.; Al-Sumaiti, A.; Doukas, H.; Sgouridis, S. Optimal Design of an Islanded Microgrid with Load Shifting Mechanism Between Electrical and Thermal Energy Storage Systems. IEEE Trans. Power Syst. 2020.

45. Wang, Y.; Su, P.; Zhao, J.; Deng, S.; Li, H.; Jin, Y. Intelligent Control Methods of Demand Side Management in Integrated Energy System: Literature Review and Case Study, Advanced Computational Methods in Energy, Power, Electric Vehicles, and Their Integration, 2017; Vol. 763, pp. 556–565 (2017).

Wind energy forecasting and power ramp: a review

B Loza[1] and I Minchala[1]

Universidad de Cuenca, Av. 12 de Abril y Agustín Cuenva, 0101168, Cuenca AZ, Ecuador

bandres.lozao@ucuenca.edu.ec - ismael.minchala@ucuenca.edu.ec

Abstract. Wind energy is one of the renewable energy sources with the largest installed capacity worldwide due to the advancement of technology that has allowed the implementation of large-scale wind farms. High levels of wind energy penetration affect the stability and security of the electrical grid due to the stochastic nature of the wind. Wind energy forecasting or ramp event forecasting methods have been developed to reduce the variability of this energy source. Ramp events are sudden changes in wind power over time. The combination of hybrid methods has achieved promising simulation results. In addition, the variety of energy storage systems (ESS) is a viable solution to reduce the variability of wind energy. This review article analyzes the latest scientific contributions related to wind power forecasting, ramp events, and hybrid wind and ESS power plants. Finally, a new research topic is proposed to be developed for future work.

Keywords: Wind energy, power ramp, forecasting, machine learning.

1 Introduction

In recent years, renewable energy sources have increased to reduce greenhouse gas emissions [1]. The innovation of new technologies facilitates the installation of large-scale wind and photovoltaic power plants, which are the most technologically developed [2]. These energy sources depend on a natural resource, wind or solar radiation, which have a stochastic behavior, making them a variable energy source. This variability causes stability and security problems for the electrical grid to which they are connected, especially when the level of penetration of renewable sources is high. Variability and intermittency are terms that can be defined based on wind power density (WPD). In [3], authors determine that wind power cannot be produced in situations of WPD less than $200 \text{ W}/\text{m}^2$. Therefore, variability describes the variations of the WPD measurements, while intermittency describes the alternation when $\text{WPD} > 200 \text{ W}/\text{m}^2$ and when $\text{WPD} < 200 \text{ W}/\text{m}^2$ [4]. The wind resource variability can be minimized with early detection of ramp events, which are sudden changes in wind power over a given period. In this case, different methods for forecasting ramp events have been developed, taking advantage of varying machine learning techniques. In this literature review, several investigations have been found that combine signal pre-processing

techniques for training regression models and neural networks. In [5], the authors analyze the investigations that have been developed considering physical approaches, statistical approaches, and combined approaches for the forecast of wind and power ramps. The approaches for forecasting ramp events with better results are deterministic and statistical. Fig. 1 shows the wind power forecasting methods discussed in this paper.
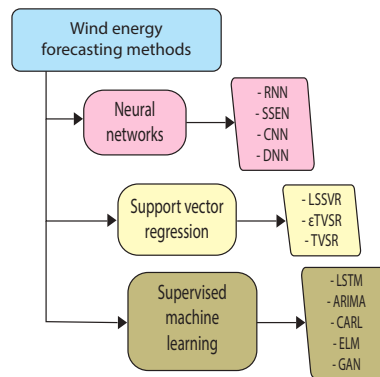
Fig. 1. Wind energy forecasting methods analyzed.

Another alternative to minimize the variability of wind resources are hybrid power plants. The combination of a wind farm and an energy storage system (ESS) helps the integration of wind farms into the electrical network. Different energy storage technologies such as flywheels, pumped hydro storage, compressed air energy storage, different types of batteries, magnetic superconductor energy storage, supercapacitors, hydrogen energy storage, and grid-connected vehicles have been implemented. All these energy storage technologies applied as a support system for the integration of wind energy are explained in [6, 7]. In [4] the authors carry out a review of the metrics used for the quantification of the variability of wind energy. Also, there are reviews about the technology available for the mitigation of wind energy variability and support systems for the integration of large-scale wind energy [6] and [7], respectively. Our paper provides a summary of new forecasting techniques for wind power and ramp events, focusing in statistical and hybrid models based on machine learning techniques. In this sense, the disadvantage of this review is that it does not analyze research focused on physical models. This article is structured as follows: Section 2 presents a categorization of wind energy forecasting methods according to horizon time. Section 3 presents a definition of wind power ramp events and its performance metrics. Section 4 presents forecasting methods applied to wind energy. Section 5 presents a review of forecasting techniques applied to wind energy. Section 6 draws a discussion. Section 7 presents the conclusion of this work.

2   Categorization of wind energy forecasting methods according to horizon time

The forecast for wind speed, wind power, and ramp events are divided into three categories according to their forecast lead time or horizon: short-term, medium-term, and long-term, as Fig.2 shows. These predetermined times are defined in [8] for wind speed forecasts. The same horizon times can be considered for wind energy forecasts. In the case of ramp events, short and medium-term forecasts with horizons ranging from 10 minutes to 6 hours have been found in the literature, as shown in Table 1. This categorization of wind power or wind
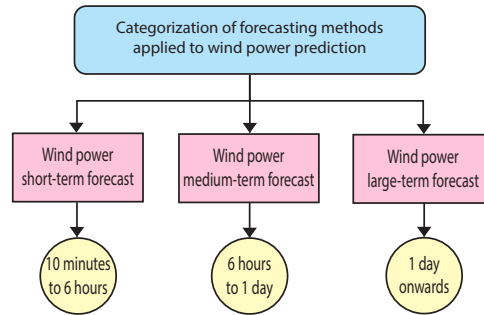
Fig. 2. Categorization of wind power forecast methods according to the horizon.

Table 1. Ramp event forecast times.

Study	Horizon time	
[11, 18]	Short-term	1 − 6 hours
[12, 17, 19]	Short-term	1 hour
[10, 13]	Short-term	10 and 60 minutes
[14, 15]	Short-term	15 minutes, incresed to 4 hours
[16]	Short-term	30 minutes − 3 hours

speed forecasts allow for proper choice of a forecast method according of the time frame and on the use of the prediction technique. In this sense, for the energy dispatch schedule of a wind farm, the short-term forecast, between 30 minutes to 3 hours, is the preferred option, according to [9]. In addition, short and medium-term forecasts are the methods that present results with greater accuracy and robustness [8]. Instead, the effectiveness of long-term forecasting methods is affected by changes in different climatological factors.

3 Definition of wind power ram events and performance metrics

An exact definition of wind energy power ramp is not determined in the literature [10–12, 20]. But in general terms, a ramp event is a sudden variation in the magnitude of wind energy in a given time.

$$\frac{|P_w\,(t + \Delta t) - P_w(t)|}{\Delta t} > P_{val} \tag{1}$$

where $P_w(t)$ is the wind power produced in time t, Δt is the duration of the ramp, and P_{val} is a limit value of wind energy variation. In [11], P_{val} is 25% of the installed wind capacity for time intervals of less than 4 hours. On the other hand, in [9], P_{val} is 50% of the installed wind capacity, which is the most common specification. Ramp events can be classified into two types: positive ramps and negative ramps. For every kind of ramp, it is required to carry out specific actions to solve the variations of wind energy. The performance of different methods of forecasting wind energy and ramp events is evaluated by means of metrics or performance indices. Table 2 summarizes the performance metrics of the investigations analyzed in this document.

Table 2: Performance metrics used in research analyzed.

Performance metrics	Study	Mathematical expression
MAE	[9, 10, 12, 13, 17, 22, 23, 25]	$MAE = \frac{1}{N} \sum_i^N |\hat{x}_i - x_i|$
MAPE	[10, 12, 25]	$MAPE(\%) = \frac{100}{N} \sum_i^N \frac{|\hat{x}_i - x_i|}{x_i}$
RMSE	[9–13, 17, 22, 25]	$RMSE = \sqrt{\frac{1}{N} \sum_i^N |\hat{x}_i - x_i|^2}$
Theil's U1 and U2 statistics	[9, 10]	$U_1 = \frac{\sqrt{\frac{1}{N} \sum_i^N (\hat{x}_i - x_i)^2}}{(\sqrt{\frac{1}{N} \sum_i^N x_i^2} + \sqrt{\frac{1}{N} \sum_i^N \hat{x}_i^2})}, U_2 = \frac{\sqrt{\frac{1}{N} \sum_i^N (\frac{x_{i+1} - \hat{x}_{i+1}}{x_i})^2}}{\sqrt{\frac{1}{N} \sum_i^N (\frac{x_{i+1} - \hat{x}_i}{x_i})^2}}$
Correlation coefficient	[22]	$I_{cc} = \frac{cov(x_i, \hat{x_i})}{\sqrt{Dx_i}\sqrt{D\hat{x_i}}}$
Ramp Capture Rate (RC)	[12]	$RC = \frac{TF}{TF + MR} 100\%$
SSR/SST and SSE/SST	[9]	$\frac{SSR}{SST} = \frac{\sum_i^N (\hat{x}_i - \bar{x})^2}{\sum_i^N (x_i - \bar{x})^2}, \quad \frac{SSE}{SST} = \frac{\sum_i^N (\hat{x}_i - x_i)^2}{\sum_i^N (x_i - \bar{x})^2}$
Agreement index (IOA)	[9]	$IOA = 1 - \frac{\sum_i^n (\hat{x}_i - x_i)^2}{\sum_i^N (|\hat{x}_i - \bar{x}| + |x_i + \bar{x}|)^2}$

Geometric mean	[18, 21, 23]	$GMS = \sqrt[3]{S_{NR}S_{NoR}S_{PR}}, S_{NR} = \frac{CC_{NR}}{N_{NR}}, S_{NoR} = \frac{CC_{NoR}}{N_{NoR}}, S_{PR} = \frac{CC_{PR}}{N_{PR}}$
Correct classification ratio (CCR)	[23]	$CCR = \frac{1}{N}\sum_i^N I(y_i^* = y_i)$
Percentage of wind energy reduced in 24 h (CR)	[27]	$CR = \frac{\sum(P_c^t \Delta t)}{\sum(P_w^t \Delta t)}100\%$
Thermo-ecological compensation cost indicator (TEC_{comp}) in 24h	[28]	$TEC_{comp} = \frac{TEC_{coal}*\sum \Delta n*\Delta E_{ch}}{E_{elwind}}$
Annual thermal efficiency $\bar{\eta}_{el}$	[28]	$\bar{\eta}_{el} = \frac{E_{elcoal}}{\sum \frac{\sum N_{tpp}(\tau)\Delta\tau}{\eta_{elav}(\tau)} + \sum \Delta n*\Delta E_{chloss}}$

The most commonly used performance metrics to verify the result of a model prediction are MAE, MAPE, and RMSE. MAE is more robust than RMSE because it does not consider outliers in its results. Instead, RMSE and MAPE are influenced to a greater extent by outliers. On the other hand, the geometric mean is less sensitive to outliers. Theil's statistics are widely used in economics to indicate the quality of forecasting performed by a method. The SSR/SST and SSE/SST ratios give an estimate of the goodness of fit of the model. The value of of SSR/SST ratio greater than 1 implies an overfitting during the training process. The CCR parameter represents the global performance in classification tasks. It is not recommended for unbalanced data sets [23].

4   Forecasting methods applied to wind energy

Wind power forecasting methods can be classified into physical, statistical, and hybrid approaches. Physical methods are based on meteorological data to determine the wind power output of a particular area. The most significant disadvantage of these methods is that they require large amounts of meteorological data and computational resources. For this reason, physical method is not used in short-term forecasting [35]. Statistical methods have significantly developed in the last decades due to the innovation of new time series analysis techniques and machine learning. Autoregressive model (AR), and the autoregressive moving average model (ARIMA) are the most used [4]. These methods determine a relationship between a system's input and output data that represents the random behavior of wind speed [34]. Their most significant disadvantage is a low performance with non-linear events [12]. On the other hand, hybrid methods are characterized by combining machine learning techniques with signal pre-processing techniques or optimization methods. The most widely used machine learning methods are neural networks and support vector machines (SVM) that improve the performance of forecast [8]. Hybrid methods combined with signal pre-processing techniques such as wavelet, empirical mode decomposition (EDM), and oversampling techniques are used to analyze the time series.

5　Review on forecasting method applied to wind power and wind power ramps

This article analyzes the research related to the forecast of wind energy and ramp events developed in the last decade. In addition, researchers that develop hybrid systems that combine ESS for the integration of wind farms and reduce the variability of wind energy are analyzed.

As mentioned in the previous section, the combination of forecasting methods based on machine learning and signal pre-processing techniques improves the performance of the proposed method. Authors of [10], develop a hybrid approach, which combines the discrete wavelet transform (DWT) to perform a pre-processing of the training data sets of a twin support vector regression (TVSR) algorithm. In addition, the authors compare the hybrid method with a convolutional network (CNN) and a random forest regression network (RFR). The hybrid method is 74.04% more efficient than CNN with 3-month training data and 53.07% with 12-month training data. Instead, with 3-month training data, CNN performs better than TVSR and RFR concerning RMSE.

In reference [9], authors presented a comparative study between a persistent model and variants of SVR combined with wavelet transform. The hybrid methods analyzed are wavelet combined with: SVR, LSSVR, TSVR, εTSVR and εSVR. The training time series is decomposed into low and high-frequency components using a *Daubechies* filter "db4" level 5. The results show that εTSVR and TVSR outperform LSSVR and εSVR in terms of RMSE and MAE. LSSVR minimizes the processing time due to the optimization problem posed by this model. TVSR obtained optimal values of SSR/SST and SSE/SST indexes. The authors concludes that εTVSR and TVSR present better performances in the short-term wind speed forecast. In the case of forecasting power ramp events, εTVSR gives a better performance concerning the absolute error indicator. One point to consider from this research is that the time series used came from different countries, with other sampling times at different heights.

Wavelet packet decomposition (WPD) combined with a recurrent neural network (RNN) is implemented in [11] for short-term ramp event forecasting. This study compare 4 mother functions for the discrete wavelet transform, determining that the *dmey* function presents the best results. Additionally, the authors used actual data from wind turbines installed in tropical and subtropical regions of Brazil and Uruguay. After the simulations were carried out, the authors concluded that the proposed method can be implemented in a wind farm. A hybrid model based on a regenerative adversarial network (C-AN) and a semi-supervised regression is applied in [12] to obtain the wind energy time series' characteristics. Semi-supervised regression minimizes the C-AN network function to optimize wind power forecast accuracy. Ramp event classification is based on ramp rate and predefined thresholds. The performance of the proposed method is compared with: ANN, SVM, CNN, RNN, and others. The C-AN method presents the best values of MAE, RMSE and MAPE, 0.7044, 0.8349 and 4.80%, respectively. RNN is the second best method, with MAE, RMSE and MAPE values of 1.5400, 2.345 and 14.04%.

The method proposed in [13] is based on a self-evolving seasonal neural network (SSEN) that classifies historical data into positive, negative, and no ramps. The training process was carried out with NEAT. NEAT combines genetic algorithms that determine the best topology and weight parameters. The proposed method is compared with different neural networks: BP model, BP Markov chain-based model, BP-enhanced SVM, and LSTM. The 10-minute ramp event forecast results show that SSEN outperforms all other neural networks by reducing MAE by 23% with test data. For 60-minute predictions, the results show that SSEN reduces MAE by 9.9% with the same data used above.

The OpSDA algorithm (optimized swinging door algorithm) is used to detect ramp events in historical wind energy data [14]. The proposed method accepts a relationship between wind power and ramp characteristics. Finally, the wind power and ramp characteristics are used as input data for a long short-term memory (LSTM) system that improves ramp event detection. The ramp characteristics are rate, amplitude, start time, and duration. The proposed method is compared with an LSTM system without the OpSDA algorithm and a neural network with a backpropagation algorithm (BP). For a forecast of 4 hours and with samples every 10 minutes, the method proposed gets 85% success for the estimates of wind power ramp events.

The ramp events are discriminated through the SDAM algorithm, and with an LSTM system. In reference [15] proposed a LSTM combined with an ESS and a synchronized dispatch strategy between the ESS and thermal generation units. This strategy decreases the stress of the ESS. This strategy limits the wind power for a particular time after the positive ramp event and minimizes the generation units' dispatch time and ESS. In the case of a negative ramp, wind generation is reduced a particular time before the start of the ramp event, and the ESS dispatches the required energy during the time of the ramp event. This ramp event forecasting method is compared with BP, Elman, and C-P neural networks. The authors performed robustness tests by changing the forecast time from 15 minutes to 4 hours. The normalized MAE of LSTM - SDAM changed 0.99%. The neural network with BP has a rate of change of 16.77%. For Elman, normalized MAE changed by 16.49%, and for the C-P network, it changed by 14.25%. These results indicate that the LSTM-SDAM method is the most robust method against changes in the forecast time.

A new index that identifies wind power intermittency is studied in [16]. This index, called wind power ramp work ratio (DBWPR), and it is defined as the time duration of the event (positive or negative ramp) over the total observation time of the historical data of a time series. The implementation of this index is done through a SVR. The disadvantage of this method is that its efficiency is drastically affected by climatic processes.

The training data for an extreme learning machine (ELM) method applied to ramp event forecasting shows an imbalance in relation to ramp events. So, in reference [17], is applied a technique of synthetic minority oversampling (SMOTE) to create synthetic samples of class with a lower likelihood of occurrence. This method uses wind speed and temperature data as input data. The SMOTE out-

put data is input to the ELM for ramp event forecasting. Authors of this research carry out simulations in 3 different wind farms, obtaining the best result of 80% correct answers and the worst of 67%. Authors of [18], employ a forecast method with a strong statistical component of ramp events through conditional logit autoregressive models (CLAR) with different thresholds from -0.3 to 0.3 with steps of 0.1. The objective of the method is to forecast the probability that the wind power exceeds the predefined threshold. The CLAR model can be adapted for ramp events with large amplitude changes at non-successive times. Reference [19], presents an ARIMA to predict ramp events based on time series and analyze ACF and PACF plots. Two case studies are carried out: a wind turbine and a 61 MW wind farm. In both cases, there is a false prediction when the nominal plant capacity threshold (PNC) is in the 50% range. The surplus of wind energy is controlled using pitch control or mechanical control.

In reference [21], a modified ADAM learning algorithm solve the imbalance in the training data of a multi-task learning deep neural network (MTL-DNN). This method obtains more robust results than a single-task learning (STL) model. The method proposed in [22] uses power curves to build a primary model based on historical data. The forecast residuals of the primary model are corrected by applying an MSAR, a combination of autoregressive models and Markov chains. Employing a swinging door algorithm, the ramp segments are extracted, and together with the definition of the ramp event, the prediction of these events is carried out. The proposed method presents lower power prediction errors and a higher correlation. The research results show that MSAR has the best performance for predicting wind power ramp events, followed by ARMA and, finally, the primary model. The SMOTE method is combined with a kernel mapping classifier to improve oversampling processing of the training data.

Authors of [23], used a kernel mapping to train an echo state network (ESN) and compare it with four methods: ordinary logistic regression (OLR), Kernel mapping OLR (KOLR), nominal logistic regression (NLR), and NLR with Kernel mapping (KNLR). The tests concluded that oversampling classes with a low probability of occurrence is necessary for more efficient classification of ramp events. In addition, the Kernel mapping methods presented better results. In reference [24], the authors proposed a pre-processing of training data through dimensionality reduction. The authors used principal component analysis (PCA) combined with an SVR. This research uses metrics developed by the authors, accounting for the number of predicted true ramps and false ramps, the number of missed ramps, and forecast accuracy.

In reference [25], is used the wavelet transform to eliminate the volatility of the wind speed series, decomposing the series into two components: an approximate signal, and a detailed signal. An SVM models an approximation signal of the wind speed whose input signal is analyzed through an ARIMA, and a genetic algorithm refines its parameters for a generalization of the SVM. With the granger causality test, they perform a comprehensive analysis and adequately select the input data of the SVM. Authors compare the proposed method with a persistent model and an SVM model combined with a genetic algorithm. The

result of the analysis is that with wavelet transform, the wind speed forecast improves despite 4 m/s peaks in the residuals of the SVM output. In reference [26], is presented a forecast of generated energy, demand, and the state of the generators of a wind farm. The generated power must not exceed its maximum and minimum limits. Ramp detection is made up of 2 stages: ramp detection and ramp quantification. The authors conclude that not all ramp events can be considered of high risk, which depends on the security region determined by the maximum and minimum limits of power generated.

Another alternative to mitigate the variability of wind energy is the combination of energy storage systems to manage the variability of wind power. Authors of [27], perform the ramp control through an ESS and redefine the ramp events. The ESS is controlled by a first-order low-filter (FLF) with and optimized, flexible time constant. The method consists of two parts: characterization of 4 types of ramps, considering the state of the ESS and the second part consider ESS energy loading/unloading strategy according to the wind power conditions. The proposed method is compared with: fixed time FLF, flexible time FLF and a combined output power limiter. The proposed method presents a better SRT (100% for events of 1 and 30 minutes) than the other three models. In addition, this control strategy keeps the SOC of the ESS between $10 - 90\%$. The second best method is the power limiter, which operates within the limits of the SOC, an undesired situation. Reference [28], presents simulations of 4 scenarios to reduce conventional thermal units' on/off cycles to integrate wind farms. The four scenarios are analyzed with the following indicators: thermo-ecological cost, the average efficiency of thermal plants, storage requirement, and energy capacity. The research concludes that higher penetration of wind energy, a greater storage capacity required. Parallel control of the fast and slow responses of an ESS to mitigate the power variability of a wind farm is developed in [29]. The authors use the desired power profile or load demand approach. The slow response ESS implements a SOC band control that uses hysteresis limits for SOC control and fuzzy control. To measure the performance of the parallel control system, authors use condition range (CRM) and depth discharge (DOD) metrics. CRM quantifies the power variations of short thermals using a probabilistic data model based on the wind power series. DOD is used to analyze the status of the ESS batteries.

Using the conventional categorization of ramp events: positive ramp, negative ramp, and no ramp, reference [30] optimizes the ESS-wind farm hybrid model to reduce ESS and wind power demand using a change-of-scenario adjustment (SSA) based on a fuzzy controller. This method is compared with a primary FLF controller, a flexible time FLF controller, and a power limiter. The proposed method presents significant improvements in the administration of the ESS compared to the rest of the ways. Determining the optimal dimension of an ESS is the research topic developed in [31] to reduce the variability of wind energy. To select the size of the ESS, authors use the conditional range metric (CRM). They use two parameters of the gamma distribution (α and β) to model the deviation of the time series, which are estimated through a maximum likelihood estimator (MLE). With CRM, it is quantified the variability of

wind energy. The developed analysis minimizes the variability of a 30 MW wind farm. Due to the high rates of variation of wind power, two possible cases are obtained:an excess wind power is more significant than the ESS capacity and a surplus wind power is less than ESS capacity. For the case study, which is a 30 MW wind farm, the best result is obtained with a 15 MW ESS.

The authors of [32] develop a range-based dispatch algorithm applied to a BESS unit to maximize the lifetime of each of the BESS elements during the charge/discharge periods and thus mitigate the wind power fluctuation. The maximization problem is posed with stochastic programming, where the decision variable is a monetary income, which considers the lifetime of BESS units and the combined power output of wind turbines and BESS. The BESS system is modeled as the parallel battery bank combination. The main objective of the algorithm is to maintain the charge/discharge cycles of each BESS unit equally and to support the variability of the wind energy produced. In reference [33], a wind energy dispatch model with economic factors is developed. This method considers the generated and forecasted power, the size of the storage system, and the price of energy, determining the energy export rate and maximizing profits. The method forecasted energy one day in advance to create a smooth dispatch schedule considering energy generated, energy exported, overflow, and storage losses. The generation, export, and waste models are of the cumulative type. A linear problem and an overflow restriction with mixed integer programming are considered to solve the programming problem, preventing the system from wasting energy in cases where the battery is incomplete. The authors do not mention the method or technique used for wind energy forecasting. Table 3. summarizes the analyzed research, method used, comparison, and results.

Table 3: Summary of analyzed investigations.

Study	Proposed method	Comparison	Result
[10]	WT–TVSR	CNN and RFR	DWT most efficient TVSR with 12-month training data, improves CNN and RFR by 53.94% at RMSE.
[9]	Wavelet and SVR variants	Persistent model	ε-TVSR and TVSR improve in terms of RMSE and MAE to LSSVR and εSVR.
[11]	WPD–RNN	The authors did not perform a comparative study	The mother function $dmey$ presented the best result RMSE = 0.5 m/s and R^2 = 0.97. The second-best performing family was $Symelt$ follow by $daubechies$.

[25]	Wavelet SVM ARIMA	Persistent model and SVM with genetic algorithm	The wavelet transform improves the wind speed forecast and the proposed method has a maximum error variation of 4 m/s.
[12]	C-ANN–semi-supervised regression	ANN, ARIMA, SVM, DBN, DBN + WT, CNN, RNN, ELM and RVFLN	C-AN presented MAE, RMSE and MAPE values of 0.5044, 0.8349 and 4.80%, respectively. The second-best method was RNN.
[13]	SSEN-NEAT	AR model, MC Markov chain-based model, MC-enhanced SVM, NEAT model without ramp classification, and LSTM	For 10-minute forecasts, SSEN reduces MAE by 28%. For 60-minute forecasts, SSEN reduces MAE by 10%. In both tests, SSEN outperformed all the neural networks used in the comparative study.
[14]	CpSDAE–CNN-LSTM	LSTM and NN with BP	CpSDAE–CNN–LSTM has an average absolute error of 10%, LSTM has an average absolute error of 15% and a neural network with BP of 32%.
[17]	SMOTE-ELM	The authors did not perform a comparative study	They apply the method in 3 different wind farms. The best result is 90% correct and the worst is 67%.
[21]	MLT–DNN-ADAM modified	STL	MTL–DNN-ADAM more robust results compared to an STL.
[22]	MSAR	Basic models and ARMA model	MSAR presented better results followed by the ARMA model and finally the primary model.
[23]	SMOTE–ESN	ORL, KORL, NRL and KNRL	Kernel mapping methods presented better results and the process of oversampling classes with low probability of occurrence is necessary for a better classification of ramp events.
[20]	Forecast of energy and status of wind farm	The authors did not perform a comparative study	They conclude that not all ramp events should be considered high risk.

[27]	Forecast of ramp events and ESS control optimized FLF	FLF control with fixed time, flexible time FLF and a power limiter	This new method keeps the SOC of the ESS between 10% and 90%. The second-best method is the power limiter.
[28]	ESS combined with ramp event forecasting	Conventional plant system, wind farm with ESS, ESS combined with conventional plants	The method that reduces on/off cycles is the proposed method.
[29]	ESS slow and fast response control	The authors did not perform a comparative study	The proposed method is analyzed by means of CRM, DoD metrics and counts the on/off cycles with a rainflow counter.
[30]	ESS control with SSA	FLF control with fixed time, flexible time FLF and a power limiter	Significant improvements found in the proposed method.

6 Discussion

The performance of forecasting wind energy or ramp events improves with a previous stage of pre-processing the time series with which the training is carried out. This pre-processing stage aims to break down the time series used or perform an oversampling process to solve the existing imbalance problem in the time series because power ramps are events with a low probability of occurrence. This review article determines that the wavelet transform is the most used method, followed by the SMOTE method. There are also combinations of neural networks and SVM with statistical methods such as ARIMA which are used to forecast wind power and ramp events. The disadvantage of ARIMA is a lower performance than that obtained with wavelet or SMOTE. Another solution is using ESS to supply power during negative ramp events. A possible problem with using ESS is the sizing of the entire storage system since, in some practical cases, there are not enough resources available to install the ESS. In addition, there may be a hypothetical case that the surplus energy of a ramp event is greater than the ESS's installed capacity, causing the wind energy reduction.

A wind energy forecasting method combined with a pre-processing stage is proposed using other approaches such as Fourier transform, short-time Fourier transform, Fourier synchronized transform, and cosine transform. A comparison study to determine which transform may be helpful for wind power forecasting. Fig 3 shows the flowchart of the wind energy forecasting method with pre-processing stage. If the training process doesn't present a good response all training process repeat until the response of the method is the required.
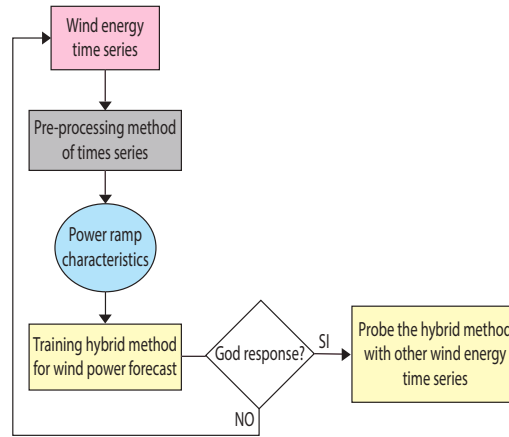
Fig. 3. Flowchart of wind energy forecasting method with pre-processing stage.

7   Conclusion

Short-term wind energy forecasting methods have been developed using various statistical models, machine learning-based methods, and hybrid methods combining pre-processing techniques to the time series used for forecast method training. The latter method has better performance. The most used pre-processing techniques are wavelet and SMOTE. An alternative solution to minimize wind energy variability is using ESS as an auxiliary support system during ramp events. The proper dimensioning and design of the energy dispatch strategy are essential for the hybrid system to have high performance. The use of other pre-processing techniques such as the Fourier transform and its variants, cosine transform, and Laplace transform is established to develop a new wind energy forecasting method. These possible techniques could improve the performance of a new a new forecasting method for wind energy or ramp events. An analytical study of these signal-processing techniques is proposed as future work.

References

1. Xavier Labandeira, Pedro Linares, and Klaas Würzburg. Energías renovables y cambio climático. *Cuadernos económicos de ICE*, 83:37–60, 2012.
2. Chun Sing Lai and Malcolm D McCulloch. Levelized cost of electricity for solar photovoltaic and electrical energy storage. *Applied energy*, 190:191–203, 2017.
3. Udaya Bhaskar Gunturu and Adam Schlosser. Characterization of wind power resource in the united states and its intermittency. Technical report, Mit joint Program on the science and policy of global change, 2011.
4. Guorui Ren, Jinfu Liu, Jie Wan, Yufeng Guo, and Daren Yu. Overview of wind power intermittency: Impacts, measurements, and mitigation solutions. *Applied Energy*, 204:47–65, 2017.

5. Bo Yang, Linen Zhong, Jingbo Wang, Hongchun Shu, Xiaoshun Zhang, Tao Yu, and Liming Sun. State-of-the-art one-stop handbook on wind forecasting technologies: an overview of classifications, methodologies, and analysis. *Journal of Cleaner Production*, 283:124628, 2021.

6. TR Ayodele and ASO Ogunjuyigbe. Mitigation of wind power intermittency: Storage technology approach. *Renewable and Sustainable Energy Reviews*, 44:447–456, 2015.

7. Haoran Zhao, Qiuwei Wu, Shuju Hu, Honghua Xu, and Claus Nygaard Rasmussen. Review of energy storage system for wind power integration support. *Applied energy*, 137:545–553, 2015.

8. Harsh S Dhiman, Dipankar Deb, and Valentina E Balas. *Supervised machine learning in wind forecasting and ramp event prediction*. Academic Press, 2020.

9. Harsh S Dhiman and Dipankar Deb. Machine intelligent and deep learning techniques for large training data in short-term wind speed and ramp event forecasting. *International Transactions on Electrical Energy Systems*, 31(9):e12818, 2021.

10. PJ Zucatelli, EGS Nascimento, AÁB Santos, AMG Arce, and DM Moreira. An investigation on deep learning and wavelet transform to nowcast wind power and wind power ramp: A case study in brazil and uruguay. *Energy*, 230:120842, 2021.

11. Bin Zhou, Haoran Duan, Qiuwei Wu, Huaizhi Wang, Siu Wing Or, Ka Wing Chan, and Yunfan Meng. Short-term prediction of wind power and its ramp events based on semi-supervised generative adversarial network. *International Journal of Electrical Power & Energy Systems*, 125:106411, 2021.

12. Yunchuan Liu, Amir Ghasemkhani, Lei Yang, Jun Zhao, Junshan Zhang, and Vijay Vittal. Seasonal self-evolving neural networks based short-term wind farm generation forecast. In *2020 IEEE International Conference on Communications, Control, and Computing Technologies for Smart Grids (SmartGridComm)*, pages 1–6. IEEE, 2020.

13. Li Han, Yan Qiao, Mengjie Li, and Liping Shi. Wind power ramp event forecasting based on feature extraction and deep learning. *Energies*, 13(23):6449, 2020.

14. Li Han, Rongchang Zhang, and Kai Chen. A coordinated dispatch method for energy storage power system considering wind power ramp event. *Applied Soft Computing*, 84:105732, 2019.

15. Guorui Ren, Jie Wan, Jinfu Liu, Daren Yu, and Lennart Söder. Analysis of wind power intermittency based on historical wind power data. *Energy*, 150:482–492, 2018.

16. Laura Cornejo-Bueno, Carlos Camacho-Gómez, Adrián Aybar-Ruíz, Luis Prieto, Alberto Barea-Ropero, and Sancho Salcedo-Sanz. Wind power ramp event detection with a hybrid neuro-evolutionary approach. *Neural Computing and Applications*, 32(2):391–402, 2020.

17. James W Taylor. Probabilistic forecasting of wind power ramp events using autoregressive logit models. *European Journal of Operational Research*, 259(2):703–712, 2017.

18. Arun Kumar Nayak, Kailash Chand Sharma, Rohit Bhakar, and Jyotirmay Mathur. Arima based statistical approach to predict wind power ramps. In *2015 IEEE Power & Energy Society General Meeting*, pages 1–5. IEEE, 2015.

19. Harsh S Dhiman, Dipankar Deb, and Josep M Guerrero. Hybrid machine intelligent svr variants for wind forecasting and ramp events. *Renewable and Sustainable Energy Reviews*, 108:369–379, 2019.

20. Jie Zhang, Anthony Florita, Bri-Mathias Hodge, and Jeffrey Freedman. Ramp forecasting performance from improved short-term wind power forecasting. In *In-*

ternational Design Engineering Technical Conferences and Computers and Information in Engineering Conference, volume 46315, page V02AT03A022. American Society of Mechanical Engineers, 2014.

21. Manuel Dorado-Moreno, Nicolò Navarin, Pedro Antonio Gutiérrez, Luis Prieto, Alessandro Sperduti, Sancho Salcedo-Sanz, and César Hervás-Martínez. Multi-task learning for the prediction of wind power ramp events with deep neural networks. *Neural Networks*, 123:401–411, 2020.

22. Tinghui Ouyang, Xiaoming Zha, Liang Qin, Yusen He, and Zhenhao Tang. Prediction of wind power ramp events based on residual correction. *Renewable Energy*, 136:781–792, 2019.

23. Manuel Dorado-Moreno, Laura Cornejo-Bueno, Pedro Antonio Gutiérrez, Luis Prieto, Sancho Salcedo-Sanz, and César Hervás-Martínez. Combining reservoir computing and over-sampling for ordinal wind power ramp prediction. In *International Work-Conference on Artificial Neural Networks*, pages 708–719. Springer, 2017.

24. Oliver Kramer, Nils André Treiber, and Michael Sonnenschein. Wind power ramp event prediction with support vector machines. In *International Conference on Hybrid Artificial Intelligence Systems*, pages 37–48. Springer, 2014.

25. Da Liu, Dongxiao Niu, Hui Wang, and Leilei Fan. Short-term wind speed forecasting using wavelet transform and support vector machines optimized by genetic algorithm. *Renewable energy*, 62:592–597, 2014.

26. Hao Wang, Hongtao Wang, and Hao Dong. A region-based method for high-risk wind power ramp events detection. In *International Conference on Renewable Power Generation (RPG 2015)*, pages 1–5. IET, 2015.

27. Wenlong Liu, Yuzhong Dong, Guangchao Deng, and Quanyuan Jiang. Refined ramp event characterisation for wind power ramp control using energy storage system. *IET Renewable Power Generation*, 13(10):1731–1740, 2019.

28. Tomasz Simla and Wojciech Stanek. Reducing the impact of wind farms on the electric power system by the use of energy storage. *Renewable Energy*, 145:772–782, 2020.

29. Yichuan Niu and Surya Santoso. Sizing and coordinating fast-and slow-response energy storage systems to mitigate hourly wind power variations. *IEEE Transactions on Smart Grid*, 9(2):1107–1117, 2016.

30. Yichuan Niu and Surya Santoso. Sizing and coordinating fast-and slow-response energy storage systems to mitigate hourly wind power variations. *IEEE Transactions on Smart Grid*, 9(2):1107–1117, 2016.

31. Yichuan Niu and Surya Santoso. Determining optimal energy storage size to mitigate intra-hour wind power variability. In *2015 IEEE Industry Applications Society Annual Meeting*, pages 1–6. IEEE, 2015.

32. Md Abu Abdullah, Kashem M Muttaqi, Danny Sutanto, and Ashish P Agalgaonkar. An effective power dispatch control strategy to improve generation schedulability and supply reliability of a wind farm using a battery energy storage system. *IEEE Transactions on Sustainable Energy*, 6(3):1093–1102, 2014.

33. Kalyanaraman Arya, Dutta. On mitigating wind energy variability with storage. In *International Conference on Communication Systems and Networks (COMSNETS)*, pages 1–9. IEEE, 2013.

34. Li C. Q. Wang G. B. Peng J. C. Jiang H. Liu Y. T. Wang, H. Z. Deep learning based ensemble approach for probabilistic wind power forecasting. *Applied energy*, 13(188):56–70, 2017.

35. Focken U. Lange, M. *Physical approach to short-term wind power prediction*. Berlin: Springer, 2006.

Sistema de control auto-optimizado para maximizar la extracción de potencia y minimizar las cargas en las aspas de un aerogenerador

Gilson D. Malo Méndez[1][0000−0003−1840−3345], Carlos E. Rivas Vásquez[1][0000−0001−6987−568X], y Luis I. Minchala[1][0000−0003−0822−0705]

Departamento de Ingeniería Eléctrica, Electrónica y Telecomunicaciones
Universidad de Cuenca
Ave. 12 de Abril y Agustín Cueva, Cuenca, Ecuador.
{daniel.malo,eduardo.rivas,ismael.minchala}@ucuenca.edu.ec

Resumen. Esta investigación presenta un método de diseño y prueba del esquema de control auto-optimizado (Self-Optimizing Control) para maximizar la potencia de salida de un sistema de conversión de energía eólica (Wind Energy Conversion System) mientras se reduce la tensión mecánica o estrés en las aspas del aerogenerador (Wind Turbine). El esquema abordado implica el planteamiento y optimización de una función de costo multiobjetivo que relaciona la potencia de salida y el factor de estrés, en presencia de incertidumbre o perturbación, que se asume como la variación de la velocidad del viento. Para el cálculo de la función de costo y la simulación del algoritmo de control auto-optimizado se utilizó MATLAB/Simulink, partiendo de un modelo de mecánica computacional combinado de la teoría del momento elemental del aspa (Blade Element Momentum) y la teoría de vigas de pared delgada (Thin-Walled Beams). Los resultados de la simulación indican la viabilidad del controlador propuesto para la operación eficiente del aerogenerador, ya que presenta un bajo coste computacional debido a la reducción del espacio de optimización mediante una proyección matricial. Finalmente, en términos de maximización de la potencia extraída y reducción de estrés, existe una mejora en el rendimiento del sistema de conversión de energía eólica cuando opera con el esquema de control auto-optimizado en comparación con el esquema de control clásico de línea base (Base-line Control System).

Keywords: Aerogenerador, Auto-Optimización, Aerodinámico, Máxima Extracción de Potencia, Reducción de Estrés Mecánico, Sistema de Conversión de Energía Eólica.

1 Introducción

Las políticas públicas para mitigar el cambio climático han favorecido el incremento de los sistemas de energía renovable, entre ellos, la producción energética eólica. A través de innovaciones tecnológicas y economías de escala, el mercado

mundial de energía eólica ha tenido un incremento durante la última década y se ha establecido como una de las fuentes de energía renovable más eficientes y rentables del mundo. La capacidad global instalada de energía eólica alcanzó 837 GW al final del 2021 y esto ha ocasionado el aumento en la oferta comercial de aerogeneradores de todo tamaño [1].

Los sistemas de conversión de energía eólica (Wind Energy Conversion Systems (WECS)) transforman la energía cinética del viento en energía eléctrica mediante una combinación de aerogeneradores (Wind Turbines (WT)) y generadores eléctricos [2–4]. Si bien es cierto de que existen diferencias y variaciones en el tamaño, todos los aerogeneradores, desde el más pequeño (Small Wind Turbine (SWT)) hasta el más grande (Large Wind Turbine (LWT)) trabajan de la misma manera [5–7]. Existen varias configuraciones posibles de aerogeneradores y generadores eléctricos, las cuales permiten diferentes enfoques basados en el control clásico y en el control moderno [8, 9] con el único objetivo de mejorar la captación de energía y mejorar el rendimiento de los WECS. Las técnicas de control [2, 8, 9], clásicamente aplicadas en aerogeneradores son: $stall^1$ activo y pasivo, y control por $pitch^2$. En cualquiera de estos casos pueden aplicarse técnicas de control moderno como [10–13]: el esquema de modelo predictivo no lineal (Nonlinear Model Predictive Control (NMPC)), adaptativo predictivo (Adaptive Predictive Control), el esquema proporcional-integral-derivativo basado en una red neuronal (Neural Network Proportional–Integral–Derivative (NN-PID)), etc.

Sin embargo, la mayoría de esquemas de control, se enfocan principalmente en el seguimiento del punto de máxima potencia (Maximum Power Point Tracking (MPPT)) [14, 15], dejando, en la mayoría de los casos, desatendidas otras variables de funcionamiento importantes, como el estrés o esfuerzo mecánico producido en los componentes estructurales del aerogenerador, principalmente en las aspas. Así, el diseño y evaluación de sistemas de control enfocados a la operación confiable y que atiendan variables típicamente no abordadas en los sistemas de control tradicionales para aerogeneradores, es importante, pues permite generar valor agregado a todo el sistema de conversión de energía eólica sin incurrir en costos adicionales [3, 16, 17].

1.1   Trabajos relacionados

En [10] se presenta dos esquemas de control: el APC y el control PID. Los resultados obtenidos muestran que el esquema de control APC logra una reducción de la tensión promedio que se genera por el estrés en las aspas para un nivel de potencia de salida dado, de esta manera, se obtiene un aumento en la potencia de salida en función del nivel de estrés. Por otro lado, en [11] se aplica el modelo NMPC al control supervisado de un aerogenerador, que integra en su base de procesamiento un modelo combinado de la teoría del momento elemental del aspa (Blade Element Momentum (BEM)) [18–20] y la teoría de vigas de pared delgada (Thin-Walled Beams (TWB)) [21]. El esquema NMPC gestiona

---

[1] Control por régimen o pérdida de sustentación de las aspas del aerogenerador.

[2] Control del ángulo de paso, ataque, de inclinación, cabeceo o elevación de las aspas.

simultáneamente el ángulo *pitch* de las aspas y el par eléctrico (torque) para la región II y III de funcionamiento del aerogenerador. Así también, NMPC realiza la maximización de la producción de energía y el alivio de estrés, los autores muestran que para el esquema propuesto se consigue una reducción instantánea del factor de estrés de hasta un 19% con una reducción de potencia variable de 0.5% al 12%.

El estudio realizado en [22] investiga el efecto del sistema de control de línea base (Base-line Control System (BCS)) en las características aerodinámicas y de fatiga en los aerogeneradores modernos. El modelo BCS, permite controlar la potencia de salida regulando el ángulo *pitch* y el torque del generador. Se utiliza el software FAST/NREL para simular un aerogenerador de 5 MW sometido a un conjunto de cargas de viento con velocidades entre 3 a 25 m/s. En el análisis de resultados se simulan dos casos diferentes, con BCS y sin BCS. En el primer caso, el ángulo *pitch* y la velocidad del rotor se regulan en función de las variables del controlador. En el segundo caso, el ángulo *pitch* y la velocidad del rotor son 0° y 12.1 rpm, respectivamente. Los valores medios y máximos de las respuestas dinámicas estructurales en el primer caso tienen una gran reducción con la velocidad del viento que excede la velocidad nominal en comparación con el segundo escenario. Así, el BCS tiene un gran efecto sobre los valores medios de las respuestas dinámicas estructurales en los aerogeneradores modernos.

En [23] se presenta al esquema de control auto-optimizado (SOC) como una estrategia de control generalizado (generalized Self-Optimizing Control (gSOC)) aplicado a un aerogenerador marino (Offshore Wind Turbine (OWT)) de 5 MW, con la finalidad de maximizar la extracción de potencia. El esquema propuesto se basa completamente en las mediciones de los datos operativos de la planta, siendo estos, la potencia de salida (P), el ángulo *pitch* (β), la velocidad angular y torque del rotor (ω_G y Γ, respectivamente), y la eficiencia del generador (η). El objetivo es determinar la ley de control óptima aplicando el esquema gSOC, considerando: β y ω_G, como las variables manipuladas, la velocidad del viento (v) como la perturbación, y la función objetivo J, a ser maximizada, como la potencia de salida ($P = \Gamma \cdot \omega_G \cdot \eta$). Así, mediante regresión y combinación lineal se encuentran los valores de las variables controladas que se aproximan a las condiciones de optimización. Los resultados muestran que el esquema gSOC maximiza con éxito J en la región II de operación del aerogenerador, sin ningún conocimiento de la dinámica de este sistema relativamente complejo, sino únicamente con base en los datos operativos proporcionados. Además, los autores mencionan que el esquema gSOC para entregar la máxima potencia intenta alcanzar siempre el máximo coeficiente de potencia (C_p), y esto puede hacerse manteniendo β constante y variando Γ de tal manera que la relación de velocidad-punta (Tip-Speed Ratio (TSR)) se mantenga constante en su valor óptimo. De esta manera, se logra obtener mayor extracción de potencia promedio para diferentes velocidades de viento.

1.2 Alcance y contribución

En esta investigación se implementará el esquema de control auto-optimizado (SOC) [24–27], con la finalidad de conciliar los objetivos de minimizar el estrés mecánico (fatiga) en las aspas del aerogenerador y maximizar la extracción de potencia. El modelo de sistema de conversión de energía eólica (WECS) utilizado corresponde al de un modelo de tipo fasorial [28, 29] desarrollado en MATLAB/Simulink, y está conformado por un aerogenerador de eje horizontal (Horizontal-Axis Wind Turbine (HAWT)) de 3 aspas y cuya potencia nominal es de 1.5 MW, un generador síncrono de imanes permanentes (Permanent Magnet Synchronous Generator (PMSG)), el control del ángulo *pitch* y el sistema de conversión de potencia en configuración *back-to-back*[3]. Además, considerando los resultados obtenidos en [11, 13], se integra un modelo aeroelástico que emplea las teorías BEM y TWB, a manera de visualizar el comportamiento aerodinámico de las aspas del aerogenerador frente al factor de estrés producido por fuertes cargas de viento. La implementación del esquema SOC no requiere el conocimiento de un modelo analítico de la planta, pues como su teoría lo indica, las variables controladas (**c**) requeridas en el esquema se obtienen a partir de las señales de interés obtenidas en las mediciones (**y**) a la salida de la planta simulada. Los valores para los datos correspondientes a la velocidad del viento fueron generados a partir de la herramienta *TurbSim* de NREL. Finalmente, se propone comparar los resultados obtenidos al aplicar el esquema SOC con el esquema de control clásico de línea base (BCS).

2 Metodología

El esquema de control SOC se implementa en un modelo simulado de tipo fasorial de un aerogenerador. A partir de los parámetros de la función de costo y la combinación lineal de mediciones se calcula el valor de la variable controlada, ω_{ref}, que cuando se mantiene constante el sistema se mantiene cerca del punto óptimo de operación. El valor óptimo consiste en minimizar la función de costo con el objetivo de extraer la máxima potencia y reducir el estrés mecánico en las aspas del aerogenerador. El valor del estrés normalizado se calcula a partir del modelo integrado de las teorías BEM/TWB.

2.1 Modelo integrado BEM/TWM

En [11, 30] se presenta la formulación del modelo BEM/TWB que genera un perfil aerodinámico del aspa de un aerogenerador mediante mecánica computacional. La ventaja de utilizar un modelo TWB es que se puede reducir la información geométrica del material, así como la anisotropía, la deformación y tensión en cada punto de la superficie del aspa. Los detalles de la geometría externa del

---

[3] Convertidores de potencia *espalda con espalda*. Hace referencia al control por *stall* electrónico

aspa, la distribución de la disposición y las propiedades de los materiales se pueden encontrar en [31].

Las deformaciones axiales y cortantes se pueden escribir de la siguiente manera:

$$\epsilon_{zz} = \epsilon_{zz}^0 + [y(s) - n\cos\alpha(s)]\kappa_x + [x(s) + n\sin\alpha(s)]\kappa_y + [\omega(s) - nq(s)]\kappa_w \quad (1)$$

$$\gamma_{sz} = \overline{\gamma}_{sz} + 2n\kappa_{xy} \quad (2)$$

donde, ϵ_{zz} es la deformación axial en la superficie a lo largo del eje (z), γ_{sz} es la deformación cortante en el plano del material del aspa (s, z); las coordenadas cartesianas (x, y, z) se encuentran alineadas con los movimientos *flapwise*, *edgewise* y *axial*, respectivamente; n, s corresponde a un sistema de coordenadas normales y tangenciales de un punto arbitrario ubicado en la superficie y con el origen ubicado en la mitad de la sección transversal del aspa; κ_x, κ_y, κ_{xy}, κ_ω son las curvaturas de la superficie en las direcciones xz, yz, tasa de torsión y curvatura de torsión, respectivamente; ϵ_{zz}^0 es la tensión axial de primer orden en la línea axial. $\overline{\gamma}_{sz}$ contiene términos de acoplamiento entre la deformación axial y la deformación cortante.

Las aspas de un aerogenerador se fabrican con capas de material que tienen características como: grosor específico, propiedades elásticas y diferentes orientaciones (direccional y bidireccional). Con (1) y (2) se puede determinar el esfuerzo axial (σ_{zz}) y cortante (σ_{sz}) en la capa k en cualquier posición del aspa utilizando una ley constitutiva ortogonal de tensión plana, así:

$$\begin{bmatrix} \sigma_{zz} \\ \sigma_{sz} \end{bmatrix}_k = \begin{bmatrix} \overline{\mathbf{Q}}_{11} & \overline{\mathbf{Q}}_{12} \\ \overline{\mathbf{Q}}_{12} & \overline{\mathbf{Q}}_{66} \end{bmatrix}_k \begin{bmatrix} \epsilon_{zz} \\ \gamma_{zz} \end{bmatrix} \quad (3)$$

donde $\overline{\mathbf{Q}}_{ij}$ son los coeficientes de rigidez del material en el sistema de coordenadas globales, que se reducen a través de una ley ortotrópica a condiciones de tensión planas.

Los esfuerzos de (3) son transformados al sistema de coordenadas del material utilizando la matriz de rotación $[\mathbf{R}]$ como sigue:

$$\begin{bmatrix} \sigma_{11} \\ \sigma_{22} \\ \sigma_{12} \end{bmatrix}_k = [\mathbf{R}]_k \begin{bmatrix} \epsilon_{zz} \\ \gamma_{sz} \end{bmatrix}_k \quad (4)$$

El modelo TWB calcula el valor de estrés en cada punto de la superficie de la capa del material, el factor de estrés en el aspa corresponde al valor máximo de estrés en cada punto de la superficie. El factor de estrés normalizado (ξ) se define como la razón entre el esfuerzo en la capa del material debido a las cargas aerodinámicas, y la resistencia del material $(S_{i,j})$ en la dirección especificada por (i, j).

$$\xi_{i,j} = \frac{\sigma_{i,j}}{S_{i,j}} \quad (5)$$

en este sentido, $(1, 1)$ a lo largo de la fibra del material, $(2, 2)$ perpendicular a la fibra del material y $(1, 2)$ en sentido de corte.

(a) Nivel de estrés medio con ángulo *pitch* fijo.

(b) Nivel de estrés bajo debido a la variación del ángulo *pitch*.
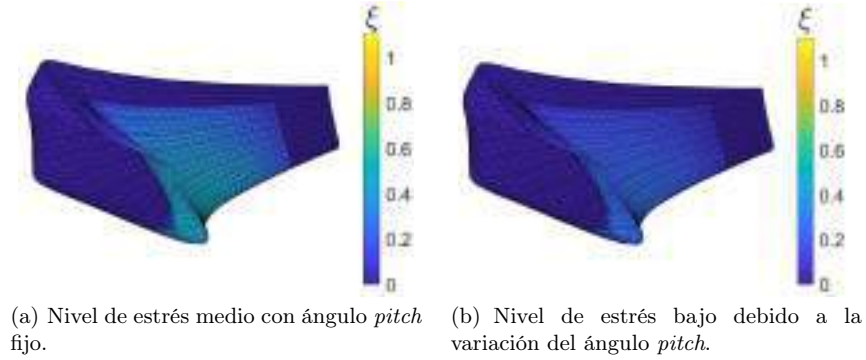
Fig. 1. Cálculo del estrés (ξ) utilizando el modelo BEM/TWB.

La Figura 1 presenta el perfil aerodinámico del aspa con un nivel bajo y medio de estrés que se calcula a través del modelo integrado BEM/TWB implementado en MATLAB [11]. La Figura 1(a) muestra que las zonas de color amarillo (con niveles altos de estrés) se ubican cerca de la raíz y el borde de salida del aspa. Las fallas en el borde de salida son causadas principalmente por los momentos de torsión y aleteo (flapwise). Uno de los factores que aumenta el estrés en la raíz del aspa es su tamaño, cuando este aumenta existen mayores fuerzas gravitatorias, lo que provoca que la frecuencia de torsión sea más baja, permitiendo que se acople a modos de flexión más bajos, lo que puede provocar inestabilidad y posteriormente la ruptura general del aspa [32]. La Figura 1(b) corresponde al resultado de variar la velocidad angular de la turbina a partir de manipular el ángulo *pitch*, β, con lo cual, se obtiene un nivel bajo de estrés.

2.2   Diseño del esquema de control auto-optimizado

El objetivo es maximizar la extracción de potencia, mientras se minimiza el estrés sobre las aspas del aerogenerador. Por lo que, la función de costo considera estas dos variables, tal como:

$$J = \alpha \left(P_{nom} - P_{cal} \right)^2 + \theta \xi^2 \tag{6}$$

donde, P_{nom} es la potencia nominal, P_{cal} es la potencia calculada, ξ es el estrés máximo de (5) calculado a lo largo del aspa, α y θ son parámetros de optimización cuyo valor se calcula según las restricciones operativas del sistema.

La variable manipulada ($\mathbf{u}$), mediciones ($\mathbf{y}$) y la perturbación ($\mathbf{d}$) del control auto-optimizado se definen como:

$$\mathbf{u} = [\omega_r]^T, \quad \mathbf{y} = [\omega_r, \beta, I_{sq}, I_{gq}, P_g, \xi]^T, \quad \mathbf{d} = [v_w]^T \tag{7}$$

donde, ω_r es la velocidad angular del generador, β es el ángulo *pitch* cuyo valor máximo es de 25 grados, I_{sq} es la corriente en cuadratura de generador, I_{gq} es

la corriente en cuadratura en la red, P_g es la potencia activa en la red y ξ es el estrés normalizado calculado por el modelo BEM/TWB. Las perturbaciones están relacionadas directamente con la función de costo definida por (6), por lo que, la optimización se realiza para cada valor de la serie de viento utilizadas en este estudio.

Para encontrar las variables controladas ($\mathbf{c}$) utilizando (8), además de conocer las mediciones ($\mathbf{y}$) a la salida del sistema, se requiere determinar la matriz de combinaciones, $\mathbf{H}$ [25], utilizando (9).

$$\mathbf{c} = \mathbf{Hy} \tag{8}$$

$$\mathbf{H} = \left(\tilde{\mathbf{F}}\tilde{\mathbf{F}}^T\right)^{-1} \mathbf{G}^y \left(\mathbf{G}^{y^T}\left(\tilde{\mathbf{F}}\tilde{\mathbf{F}}^T\right)^{-1}\mathbf{G}^y\right)^{-1} \mathbf{J}_{uu}^{1/2} \tag{9}$$

donde, $\mathbf{F}$ es la matriz de sensibilidad óptima definida por (10), $\mathbf{G}_y^d$ es la matriz de ganancias correspondientes a $\mathbf{y}$ frente a $\mathbf{d}$, y $\mathbf{G}^y$ es la matriz de ganancias correspondiente a $\mathbf{y}$ frente a $\mathbf{u}$.

$$\mathbf{F} = \mathbf{G}_y^d - \mathbf{G}^y\mathbf{J}_{uu}^{-1}\mathbf{J}_{ud} \tag{10}$$

$$\tilde{\mathbf{F}} \cong [\mathbf{FW}_d \quad \mathbf{W}_e] \tag{11}$$

La matriz diagonal del valor esperado de la perturbación, $\mathbf{W_d}$, y la matriz diagonal de los errores de implementación, $\mathbf{W_e}$; se eligen después de realizar varios experimentos en los cuales se verifica que se cumpla los objetivos individuales y restricciones de la función de costo (6). Los mejores resultados se consigue con:

$$\mathbf{W_d} = diag(1.2) \tag{12}$$

y el error de implementación para ω_r es de 4.5%; β, 14%; I_{sq}, I_{gq} y P_g, 9.5% y ξ, 3.7%. Así,

$$\mathbf{W_e} = diag(0.045, 3.5, 0.095, 0.095, 0.095, 0.037) \tag{13}$$

La matriz de ganancias, $\mathbf{G^y}$, se obtiene al evaluar la variable manipulada (ω) alrededor del punto de operación nominalmente óptimo. Con el uso de diferencias finitas se obtiene el valor de la ganancia para cada medición individual y perturbaciones. Los resultados obtenidos en [11] cuyo estudio se basa en un optimizador, son de utilidad para calcular la matriz de ganancias evaluando la variable manipulada cerca del valor nominal que corresponde a la región donde el generador se mantiene en velocidad constante. La matriz de ganancia frente a las mediciones es:

$$\mathbf{G^y} = \frac{\partial y}{\partial u}$$

$$\mathbf{G^y} = [1, 27.556, 0.219, 0.033, -0.876, 0.753]^T \tag{14}$$

mientras que la matriz de ganancia frente a la perturbación es:

$$\mathbf{G_y^d} = \frac{\partial y}{\partial d}$$

$$\mathbf{G_y^d} = [0.097, 34.701, 0.151, 0.014, 0.253, 0.868]^T \tag{15}$$

Al igual que las matrices de ganancia ($\mathbf{G_y^d}$ y $\mathbf{G^y}$), la matriz Hessiana representada en (16) se obtiene al rededor del punto nominalmente óptimo.

$$\mathbf{H}_J(\mathbf{u}, \mathbf{d}) = \begin{bmatrix} \mathbf{J}_{uu} & \mathbf{J}_{ud} \\ \mathbf{J}_{du} & \mathbf{J}_{dd} \end{bmatrix} \tag{16}$$

Utilizando las herramientas simbólicas de MATLAB se calcula (16) como: (`hessian(J, [w, v])`), donde: `J` es la función de costo en función de las variables simbólicas, `w`, y `v`, que representan la variable controlada ($u = \omega_r$) y la perturbación ($d = v_w$), respectivamente.

Los parámetros α y θ de la función de costo (6) se calculan utilizando la teoría de Pareto, con la precaución de no violar las restricciones en la dinámica del sistema.

La Figura 2 muestra la estructura del esquema de control auto-optimizado (SOC). Este esquema de control opera como supervisor sobre el modelo simulado de tipo fasorial del aerogenerador. En este estudio se elige el grado de
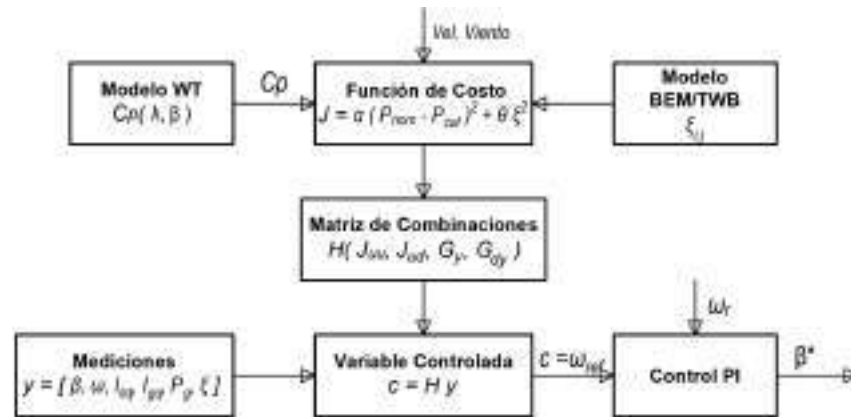
Fig. 2. Arquitectura del esquema de control SOC.

libertad, β^*, ya que es posible manipular la velocidad de rotación del aerogenerador variando correctamente esta variable. La Figura 3 muestra el sistema de control para manipular el ángulo *pitch*, la referencia es la velocidad normalizada en *pu* (por unidad) del generador. Este controlador se activa con velocidades de viento mayores a la nominal ($v_w > 10m/s$). Por el contrario, para velocidades por debajo de la nominal, $\beta^* = 0$.

El coeficiente de potencia (C_p) está en función de la relación de velocidad-punta λ (TSR) y el ángulo pitch. En [33, 34] se define una relación del coeficiente
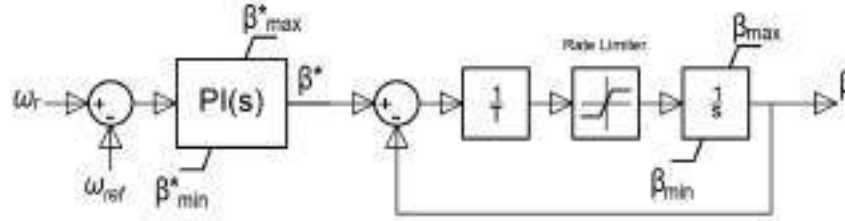
Fig. 3. Control del ángulo *pitch*.

de potencia como:

$$C_p\left(\lambda, \beta\right) = c_1\left(c_2/\lambda_i - c_3\beta - c_4\right)e^{-c_5/\lambda_i} + c_6\lambda \tag{17}$$

$$\frac{1}{\lambda_i} = \frac{1}{\lambda + 0.08\beta} - \frac{0.035}{\beta^3 + 1} \tag{18}$$

las constantes de (17) se toman de [35], esto es: $c_1 = 0.5176$, $c_2 = 116$, $c_3 = 0.4$, $c_4 = 5$, $c_5 = 21$, $c_6 = 0.0068$.

3 Resultados

El esquema de control auto-optimizado lleva a cabo el control de potencia en la tercera zona de operación del aerogenerador. Los controladores del convertidor del lado del estator (Stator Side Converter (SSC)) y del convertidor del lado de la red (Grid Side Converter (GSC)) regulan la velocidad de la turbina a través del torque del generador para maximizar la extracción de energía en velocidades de viento menores al valor nominal; ω_{ref} se calcula para maximizar la relación inversa entre la potencia extraída y el factor de estrés. El rendimiento del aerogenerador que se consigue aplicando el esquema de control auto-optimizado (SOC) para diferentes condiciones de funcionamiento, es comparado con el esquema de control referente de línea base (BCS).

La serie de viento empleada en la simulación se presenta en la Figura 4, la línea de color rojo indica el valor nominal de la velocidad de viento (10 m/s). Los datos de la serie de viento han sido generados utilizando la herramienta *TurbSim* de NREL. Al variar el valor del ángulo *pitch* (β^*) se consigue regular la velocidad angular del rotor. Además se observa que cuando la velocidad de viento supera el valor nominal, el valor de β^* presenta variaciones a lo largo del tiempo, por otro lado, cuando se mantiene velocidades de viento por debajo del valor nominal el ángulo de paso se mantiene en cero. Esto cumple con el objetivo de llevar y mantener la velocidad angular del rotor cerca del valor nominalmente óptimo.
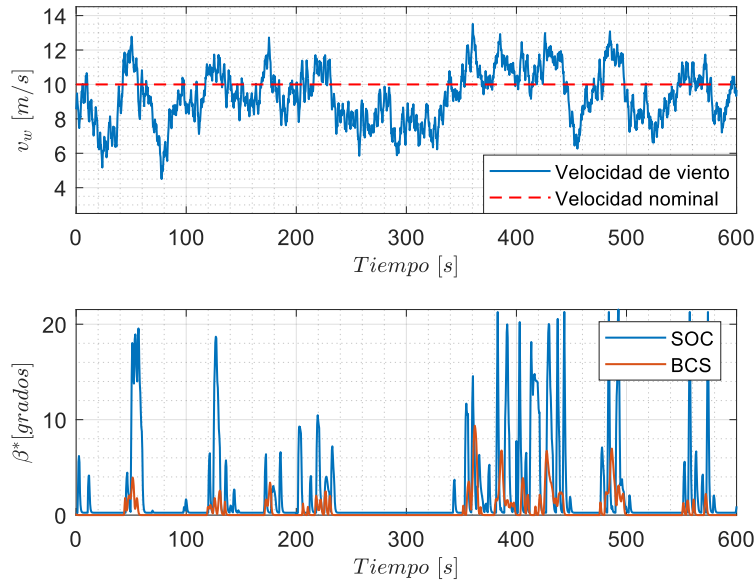
Fig. 4. Velocidad de viento (arriba) y comportamiento del ángulo *pitch* (abajo) para los esquemas de control SOC y BCS.

La Figura 5 muestra la gráfica de la velocidad del viento y la velocidad angular para el esquema de control diseñado en este estudio y el esquema de referencia. El valor promedio (μ_{SOC} y μ_{BCS}) y varianza (σ_{SOC} y σ_{BCS}) del control auto-optimizable y de línea base se incluye en esta figura. Para la serie de viento, el control auto-optimizable disminuye la velocidad angular de la turbina, cuando la velocidad del viento supera el valor nominal, en comparación con el control de línea base.

La aplicación de densidad espectral de potencia (Power Spectral Density (PSD)) normalizada a cada uno de los esquemas de control se muestra en la Figura 6. Los resultados obtenidos tanto de la potencia extraída como del factor de estrés en el aspa del aerogenerador muestran que la implementación del control auto-optimizado logra una leve ampliación en las fluctuaciones de la potencia, así como una reducción considerable de la mayoría de los componentes espectrales del factor de estrés.

La Tabla 1 muestra el resumen de los resultados del rendimiento para diferentes velocidades de viento e intensidades de turbulencia. Las series de viento empleadas en este estudio tienen una duración de 605 segundos. Las simulaciones se llevan a cabo en computador personal con procesador Intel(R) Core(TM) i7-7700HQ CPU @2.80GHz y 16 GB de memoria RAM. Con el esquema de control
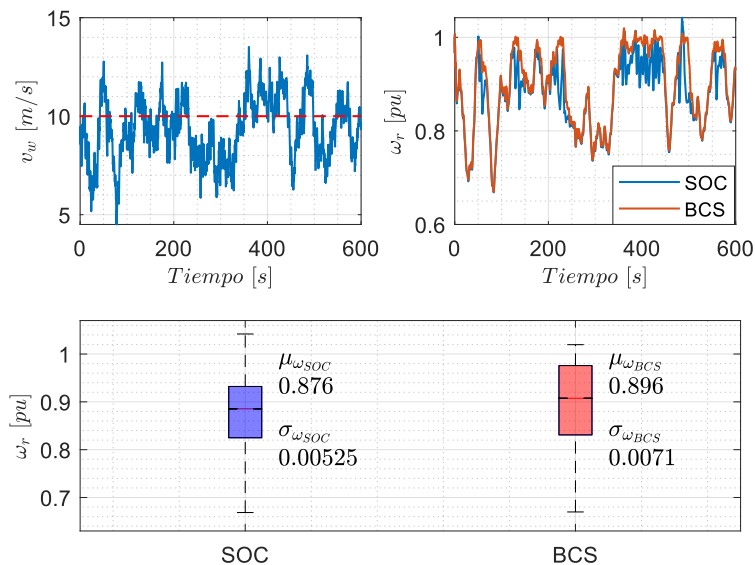
Fig. 5. Velocidad de viento (arriba izquierda), Velocidad angular en el tiempo (arriba derecha) y diagrama estadístico para la velocidad angular (abajo); para esquemas de control SOC y BCS.

SOC, la mayor reducción (cerca del 18%) del factor de estrés se tiene para la serie de viento de 10.434 m/s. Este resultado corresponde con la reducción de potencia alrededor del 11.5%.

Tabla 1. Resumen de resultados de operación para los diferentes esquemas de control.

Velocidad del viento	% de turbulencia	% de reducción del factor de estrés (ξ)	% de reducción de potencia
8.59 m/s	27.56 %	9.1601 %	6.274 %
9.21 m/s	15.00 %	9.863 %	5.938 %
10.434 m/s	21.51 %	17.982 %	11.523 %

4   Conclusiones

El funcionamiento y desempeño adecuado del aerogenerador en la producción de energía eólica se puede asegurar mediante el análisis dinámico de los componentes
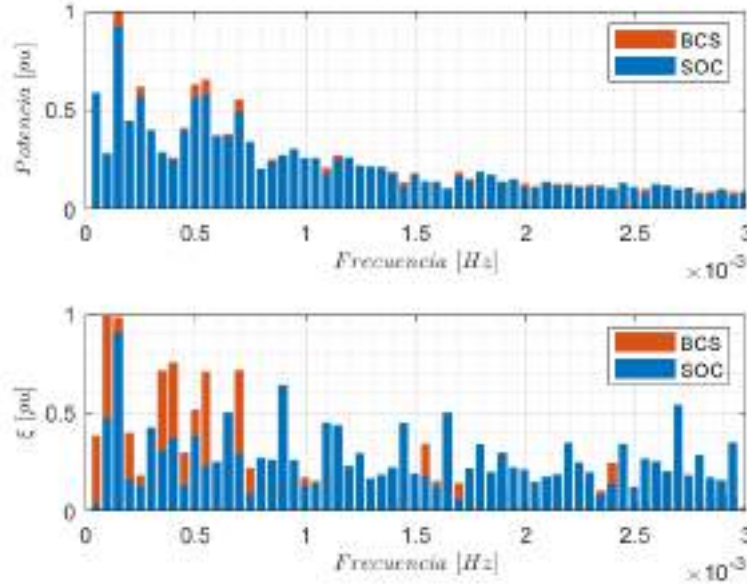
Fig. 6. Comparación de la respuesta en frecuencia de potencia (arriba) y el factor de estrés (abajo) para los controladores utilizando la PSD.

estructurales, especialmente de las aspas frente a esfuerzos mecánicos y esfuerzos adicionales que producen valores de fatiga o estrés elevados, ocasionando el deterioro y la posible destrucción del aerogenerador. La finalidad de todo análisis dinámico en un sistema de conversión de energía eólica, principalmente, en el aerogenerador, es aprovechar el máximo rendimiento del mismo, considerando extraer la máxima potencia disponible frente a variables típicas y de tratamiento crítico, como es el caso del estrés mecánico. Adicionalmente, los enfoques de control clásico y control moderno, aplicados a un aerogenerador, tienen el propósito de garantizar el desempeño eficiente, seguro y confiable de todo el sistema. Así, en este trabajo se investigó e implementó el esquema de control auto-optimizado (SOC), y se analizó su respuesta frente a los objetivos de maximización de la extracción de potencia y minimización de la fatiga en las aspas de un aerogenerador. De esta manera, es concluyente mencionar que el esquema de control abordado en esta investigación, no es invasivo y concilia los objetivos planteados mediante la optimización de variables de forma automática. Los resultados obtenidos mostraron que al variar el ángulo de paso y la velocidad angular del rotor, permite maximizar la extracción de potencia y reducir el factor de estrés en las aspas, contribuyendo así en la seguridad de la estructura del aerogenerador, frente a las respuestas dinámicas inducidas por las condiciones del viento.

La ventaja que presenta el esquema de control SOC frente a otros esquemas, es que, se reduce el tiempo de cálculo de los puntos de ajuste óptimos para la variable controlada, ya que el esquema propuesto se basa en la proyección de la matriz $\mathbf{H}$ óptima aplicada a un vector de mediciones, reduciendo así el tiempo de procesamiento computacional. Finalmente, la aplicación del esquema SOC puede ser extendida, desempeñando el rol de un control supervisor y optimizar el rendimiento de todo un sistema de conversión de energía eólica, implementado restricciones de operación específicas sobre las variables de interés.

References

1. GWEC: Global Wind Report 2022 (2021), https://gwec.net/global-wind-report-2022/, [Accessed: 20-Aug.-2022]
2. Wu, B., Lang, Y., Zargari, N., Kouro, S.: Power Conversion and Control of Wind Energy Systems. IEEE Press Series on Power Engineering, Wiley-IEEE Press, 1 edn. (2011), isbn: 9780470593653
3. Heier, S.: Grid Integration of Wind Energy, Onshore and Offshore Conversion Systems. John Wiley & Sons, Ltd, 3 edn. (2014). https://doi.org/10.1002/9781118703274, isbn: 9781118703274
4. Söder, L., Ackermann, T.: Wind Power in Power Systems: An Introduction. In: Thomas Ackermann (ed.) Wind Power in Power Systems, chap. 3, pp. 25–51. Electric Power Systems, John Wiley & Sons, Ltd, 1 edn. (2005). https://doi.org/10.1002/0470012684.ch3
5. Rojas Maita, C.P.: Evaluación de los Recursos Eólicos para la Generación de Energía Eléctrica a Pequeña Escala en el Distrito de Huachac. Tesis, Universidad Nacional del Centro del Perú (UNCP) (2020), https://repositorio.uncp.edu.pe/handle/20.500.12894/6337
6. Ackermann, T.: Historical Development and Current Status of Wind Power. In: Thomas Ackermann (ed.) Wind Power in Power Systems, chap. 2, pp. 7–24. Electric Power Systems, John Wiley & Sons, Ltd, 1 edn. (2005). https://doi.org/10.1002/0470012684.ch2
7. Rayyan Fazal, M.: Wind energy. In: Kamran, M., Rayyan Fazal, M. (eds.) Renewable Energy Conversion Systems, chap. 5, pp. 153–192. Academic Press (2021). https://doi.org/10.1016/B978-0-12-823538-6.00003-8, https://www.sciencedirect.com/science/article/pii/B9780128235386000038
8. Pao, L.Y., Johnson, K.E.: Control of Wind Turbines: Approaches, Challenges, and Recent Developments. IEEE Control Systems Magazine **31**(2), 44–62 (2011). https://doi.org/10.1109/MCS.2010.939962
9. Johnson, K., Pao, L., Balas, M., Fingersh, L.: Control of Variable-Speed Wind Turbines: Standard and Adaptive Techniques for Maximizing Energy Capture. IEEE Control Systems Magazine **26**(3), 70–81 (2006). https://doi.org/10.1109/MCS.2006.1636311
10. Garcia, M., San-Martin, J., Favela-Contreras, A., Minchala, I., Cárdenas, D., Probst, O.: A Simple Approach to Predictive Control for Small Wind Turbines with an Application to Stress Alleviation. Control Engineering and Applied Informatics **20**, 69–77 (12 2018), https://www.researchgate.net/publication/329813823
11. Minchala, I., Probst, O., Cárdenas, D.: Wind turbine predictive control focused on the alleviation of mechanical stress over the blades. IFAC-PapersOnLine **51**, 149–154 (01 2018). https://doi.org/10.1016/j.ifacol.2018.07.270, https://www.researchgate.net/publication/327353810

12. Loza, B., Pacheco-Chérrez, J., Cárdenas, D., Minchala, L.I., Probst, O.: Comparative Fatigue Life Assessment of Wind Turbine Blades Operating with Different Regulation Schemes. Applied Sciences **9**(21), 1–22 (2019). https://doi.org/10.3390/app9214632, https://www.mdpi.com/2076-3417/9/21/4632

13. Mínchala, L.I., Cárdenas-Fuentes, D., Probst, O.: Control of mechanical loads in wind turbines using an integrated aeroelastic model. In: 2017 IEEE PES Innovative Smart Grid Technologies Conference - Latin America (ISGT Latin America). pp. 1–6 (09 2017). https://doi.org/10.1109/ISGT-LA.2017.8126732, https://ieeexplore.ieee.org/document/8126732

14. Bianchi, F.D., Battista, H.D., Mantz, R.J.: Wind Turbine Control Systems Principles, Model and Gain Scheduling Design. Advances in Industrial Control, Springer, 1 edn. (2007), https://es.b-ok.lat/book/542739/245201, isbn: 9781849966115

15. Kot, R., Rolak, M., Malinowski, M.: Comparison of maximum peak power tracking algorithms for a small wind turbine. Mathematics and Computers in Simulation **91**, 29–40 (2013). https://doi.org/10.1016/j.matcom.2013.03.010, https://www.sciencedirect.com/science/article/pii/S0378475413000657, ELECTRIMACS 2011 - PART II

16. Abdullah, M., Yatim, A., Tan, C., Saidur, R.: A review of maximum power point tracking algorithms for wind energy systems. Renewable and Sustainable Energy Reviews **16**(5), 3220–3227 (2012). https://doi.org/10.1016/j.rser.2012.02.016, https://www.sciencedirect.com/science/article/pii/S1364032112001098

17. Lio, W.H.A.: Blade-Pitch Control for Wind Turbine Load Reductions. Springer Theses, Springer, Cham, 1 edn. (2018). https://doi.org/10.1007/978-3-319-75532-8, https://link.springer.com/book/10.1007/978-3-319-75532-8

18. Manwell, J.F., McGowan, J.G., Rogers, A.L.: Wind Energy Explained: Theory, Design and Application. John Wiley & Sons, Ltd, 2 edn. (2010), isbn: 9780470015001

19. Burton, T., Jenkins, N., Sharpe, D., Bossanyi, E.: Wind Energy Handbook. John Wiley & Sons, Ltd, 2 edn. (2011). https://doi.org/10.1002/9781119992714, isbn: 9781119992714

20. Knudsen, H., Nielsen, J.N.: Introduction to the Modelling of Wind Turbines. In: Thomas Ackermann (ed.) Wind Power in Power Systems, chap. 24, pp. 525–553. Electric Power Systems, John Wiley & Sons, Ltd, 1 edn. (2005). https://doi.org/10.1002/0470012684.ch24

21. Librescu, L., Song, O.: Kinematics of Thin Walled Beams. In: G.M.L. GLADWELL (ed.) Thin-Walled Composite Beams: Theory and Application, chap. 2, pp. 7–52. Springer Netherlands (2006). https://doi.org/10.1007/1-4020-4203-5_2, isbn: 9781402042034

22. Yuan, C., Li, J., Xie, Y., Bai, W., Wang, J.: Investigation on the Effect of the Baseline Control System on Dynamic and Fatigue Characteristics of Modern Wind Turbines. Applied Sciences **12**, 2968 (03 2022). https://doi.org/10.3390/app12062968

23. Gueorguiev Iordanov, S., Collu, M., Cao, Y.: Can a Wind Turbine Learn to Operate Itself? Evaluation of the potential of a heuristic, data-driven self-optimizing control system for a 5 MW offshore wind turbine. Energy Procedia **137**, 26–37 (2017). https://doi.org/10.1016/j.egypro.2017.10.332, https://www.sciencedirect.com/science/article/pii/S187661021735292X, 14th Deep Sea Offshore Wind R&D Conference, EERA DeepWind 2017

24. Jäschke, J., Cao, Y., Kariwala, V.: Self-optimizing control – A survey. Annual Reviews in Control **43**, 199–223 (2017). https://doi.org/10.1016/j.arcontrol.2017.03.001, https://www.sciencedirect.com/science/article/pii/S1367578816301055

25. Alstad, V., Skogestad, S., Hori, E.S.: Optimal measurement combinations as controlled variables. Journal of Process Control **19**, 138–148 (01 2009). https://doi.org/10.1016/j.jprocont.2008.01.002

26. Halvorsen, I.J., Skogestad, S., Morud, J.C., Alstad, V.: Optimal Selection of Controlled Variables. Process design and Control **42**, 3273–3284 (2003). https://doi.org/10.1021/ie020833t

27. Kariwala, V., Cao, Y., Janardhanan, S.: Optimal measurement combinations as controlled variables. IFAC Proceedings Volumes **40**, 257–262 (2007). https://doi.org/10.3182/20070606-3-MX-2915.00161

28. Martyanov, A., Martyanov, N., Anikin, A.: Comparative Analysis of Wind Turbine Control Strategies. Procedia Engineering **129**, 607–614 (2015). https://doi.org/10.1016/j.proeng.2015.12.077, https://www.sciencedirect.com/science/article/pii/S1877705815039612, International Conference on Industrial Engineering (ICIE-2015)

29. Rosyadi, M., Umemura, A., Takahashi, R., Tamura, J., Kondo, S., Ide, K.: Development of phasor type model of PMSG based wind farm for dynamic simulation analysis. In: 2015 IEEE Eindhoven PowerTech. pp. 1–6 (06 2015). https://doi.org/10.1109/PTC.2015.7232485, https://ieeexplore.ieee.org/document/7232485

30. Cárdenas, D., Elizalde, H., Marzocca, P., Gallegos, S., Probst, O.: A coupled aeroelastic damage progression model for wind turbine blades. Composite Structures **94**(10), 3072–3081 (2012). https://doi.org/10.1016/j.compstruct.2012.03.034, https://www.sciencedirect.com/science/article/pii/S0263822312001493

31. Cárdenas, D., Escárpita, A.A., Elizalde, H., Aguirre, J.J., Ahuett, H., Marzocca, P., Probst, O.: Numerical validation of a finite element thin-walled beam model of a composite wind turbine blade. Wind Energy **15**(2), 203–223 (2012). https://doi.org/10.1002/we.462, https://onlinelibrary.wiley.com/doi/abs/10.1002/we.462

32. Mishnaevsky, L.: Root Causes and Mechanisms of Failure of Wind Turbine Blades: Overview. Materials **15**(9) (2022). https://doi.org/10.3390/ma15092959, https://www.mdpi.com/1996-1944/15/9/2959

33. Carpintero Renteria, M., Santos-Martin, D., Lent, A., Ramos, C.: Wind turbine power coefficient models based on neural networks and polynomial fitting. IET Renewable Power Generation **14**(11), 1841–1849 (2020). https://doi.org/10.1049/iet-rpg.2019.1162, https://ietresearch.onlinelibrary.wiley.com/doi/abs/10.1049/iet-rpg.2019.1162

34. González, J., Salas, R.: Representation and estimation of the power coefficient in wind energy conversion systems. Revista Facultad de Ingeniería Uptc **28(50)**, 77–90 (2019). https://doi.org/10.19053/01211129.v28.n50.2019.8816

35. Parikshit, G., Jamdade, Santosh, V.P., Vishal, B.P.: Assessment of Power Coefficient of an Offline Wind Turbine Generator System. International Journal of Engineering Research & Technology (IJERT) **02**(09) (09 2013), https://www.ijert.org/assessment-of-power-coefficient-of-an-offline-wind-turbine-generator-system

Modelamiento numérico de la capacidad de transporte de un gasoducto mediante el uso de ecuaciones convencionales de flujo

Contreras Panibra, Abelardo[1][0000-0002-0977-8236] Jorge Mírez[1][0000-0002-5614-5853] Javier El-
mar Franco[1][0000-0002-4712-0726] and Adrián Zapata Sernaque[1][0000-0002-5303-8286]

[1] Universidad Nacional de Ingeniería (UNI), Perú
acontreras@fip.uni.edu.pe
jmirez@uni.edu.pe
efrancog@uni.edu.pe
azapatas@uni.edu.pe

Abstract. Los gasoductos forman parte de uno de los activos más importantes de la industria Oil&Gas y por ello es importante conocer la información técnica que nos permita conocer el comportamiento de estos sistemas en base a la literatura técnica así como a las herramientas informáticas, siendo el transporte de gas natural en uno de los pilares energéticos de las ciudades inteligentes. Es por ello que el presente trabajo tiene por objetivo desarrollar el uso de las diferentes ecuaciones convencionales de flujo, las cuales podrían ser utilizadas para estimar la capacidad de un gasoducto, así como una comparativa entre las mismas de manera que se pueda evidenciar aquella o aquellas que generen una mayor predictibilidad en el sistema de transporte elegido. Para ello, se presenta los modelos matemáticos, los resultados de las simulaciones numéricas y su comparación entre modelos usando software de alto nivel, considerando como caso de estudio, el principal gaseoducto del Perú de 34" de diámetro y 408 km de extensión.

Keywords: Gaseoducto, Ecuaciones de flujo, Gas Natural, Simulación.

1   Introducción

Los sistemas de transporte por tuberías consisten en un gran número de instalaciones que se utilizan para el transporte de diversos fluidos, siendo uno de sus usos principales el transporte de hidrocarburos líquidos y gaseosos. Por lo general, son la forma más segura, eficiente y económica de transporte [1].

Desde los grandes descubrimientos de gas natural en Egipto en la década de 1990, el gas natural aumentó su importancia como fuente de energía, incrementando su preponderancia en la matriz energética de diversos países a nivel mundial, siendo Perú uno de los países que ha adquirido relevancia debido a los diversos proyectos relacionados al transporte como distribución de gas natural. En ese sentido, dentro del desarrollo de las diferentes disciplinas técnicas asociadas a los mencionados proyec-

tos se encuentra el modelamiento numérico de estos sistemas de gasoductos de manera que sea posible estimar parámetros operativos de relevancia como son, la capacidad de transporte del sistema y los perfiles hidráulico y térmicos.

Con la finalidad de cubrir esta necesidad técnica, el presente trabajo tiene por objetivo desarrollar el uso de las diferentes ecuaciones convencionales de flujo las cuales podrían ser utilizadas para estimar la capacidad de un gasoducto, así como una comparativa entre las mismas de manera que se pueda evidenciar aquella o aquellas que generen una mayor predictibilidad en el sistema de transporte elegido como ejemplificación. Para la consecución del objetivo mencionado se empleó como herramienta de modelamiento el software Matlab R2015a la cual permitió registrar las rutinas y general los resultados numéricos, así como las gráficas correspondientes al caso elegido.

2   Fundamentos teóricos para la estimación de capacidad de un gasoducto

Menon [2] establece que la resistencia de la tubería, también denominada capacidad máxima de flujo en una tubería depende en gran medida de las propiedades físicas de las tuberías y de la composición del gas. Se han propuesto varias ecuaciones durante el siglo pasado para simular flujos de gas comprimible en tuberías largas, incluida la ecuación de Weymouth (desarrollada en 1912), la ecuación Panhandle A (desarrollada en 1940) y la ecuación Panhandle B (desarrollada en 1956). Estas ecuaciones se desarrollan a partir de la ecuación general de flujos para fluidos compresibles, sin embargo, cada una tiene una representación especial del factor de fricción para permitir que las ecuaciones se resuelvan analíticamente. Además, se diferencian entre sí por el método utilizado para crearlos y la cantidad de parámetros utilizados para definirlos.

2.1   Ecuaciones asociadas al flujo de gas por tuberías

Ecuaciones de gobierno. Entre las ecuaciones que gobiernan el comportamiento del gas natural tenemos: la ecuación de continuidad, la ecuación de cantidad de movimiento, la ecuación de energía y la ecuación de Bernoulli.

Supuestos para calcular la presión y el caudal. La ecuación general se puede derivar del balance total de cantidad de movimiento alrededor de un elemento de fluidos a través de un diferencial de longitud de tubería bajo los siguientes supuestos:

   a)   Es un flujo isotérmico
   b)   Es un flujo en estado estacionario
   c)   Es un flujo monofásico
   d)   No se presenta transferencia de calor del gas hacia el entorno.
   e)   No se realiza ningún trabajo mecánico por o hacia el fluido.
   f)   Se considera un fluido newtoniano.

Ecuaciones de flujo. Existen varias ecuaciones disponibles que relacionan el transporte de gas natural con las propiedades del gas, diámetro de la tubería, longitud y presiones aguas arriba y aguas abajo. Estas ecuaciones son [2]:

   a)   Ecuación general de flujo

b) Ecuación de Colebrook-White
c) Ecuación de Colebrook-White modificado
d) Ecuación AGA
e) Ecuación de Weymouth
f) Ecuación de Panhandle A
g) Ecuación de Panhandle B
h) Ecuación IGT
i) Ecuación de Spitzglass
j) Ecuación de Mueller
k) Ecuación de Fritzsche

De acuerdo con el GPSA [3], las ecuaciones de Weymouth, Panhandle A y Panhandle B se desarrollaron para simular el flujo de gas compresible en tuberías de gran extensión. En tal sentido la presente publicación tomará como caso de estudio la ecuación general de flujo y las ecuaciones anteriormente mencionadas con el fin de evaluarlas numéricamente y así realizar un análisis comparativo para el caso específico de una tubería de 34" de diámetro y 408 km de extensión ubicado en la Sierra del Perú. A continuación, describiremos cada una de las propiedades de estas tres ecuaciones:

2.2   Ecuaciones convencionales de flujo de gas para tuberías de gran extensión.

Ecuación general. La ecuación general es la ecuación básica que relaciona el caudal con la caída de presión. También se le llama ecuación de flujo fundamental para el flujo isotérmico en estado estacionario en gasoductos. Esta ecuación se aplica en todos los rangos de presión y es la base de muchas de las ecuaciones de flujo utilizadas en el análisis de redes de transporte y distribución de gas, asimismo la forma estándar que incluye los cambios de elevación a lo largo de la traza se describe en la Ec. (1), donde: Q es flujo de gas, medido a condiciones estándar, $ft^3/día$ (SCFD); F es un factor de transmisión, equivalente a $2f^{1/2}$, adimensional; P_b es la presión a condiciones base, psia; T_b es la temperatura a condiciones base, °R (460+°F); P_1 es la presión aguas arriba, psia; P_2 es la presión aguas abajo, psia; G es la gravedad específica (air=1.00); T_f es la temperatura promedio de gas, °R (460+°F); L es la longitud del segmento de tubería, mi; Z es el factor de compresibilidad a la temperatura de flujo, adimensional, y; D es el diámetro interno de tubería, in.

$$Q = 38.77F\left(\frac{T_b}{P_b}\right)\left(\frac{P_1^2 - e^s P_2^2}{GT_f L_e Z}\right)^{0.5} D^{2.5} \text{ [UCSC units]} \qquad (1)$$

El factor de fricción se puede estimar por medio de la ecuación de Colebrook-White según Ec. (2) donde Re es el número de Reynolds y Rr es la rugosidad relativa definidos según Ec. (3) y (4).

$$\frac{1}{\sqrt{f}} = -2log_{10}\left(\frac{e}{3.7D} + \frac{2.51}{Re\sqrt{f}}\right); Re > 4000 \qquad (2)$$

$$Re = 0.0004778 \left(\frac{P_b}{T_b}\right)\left(\frac{GQ}{\mu D}\right) \tag{3}$$

$$Rr = \frac{e}{D} \tag{4}$$

Respecto a los parámetros operativos, P_{avg} es la presión promedio y Z es el factor de compresibilidad se calculan según las Ec. (5) y (6).

$$P_{avg} = \frac{2}{3}\left(P_1 + P_2 - \frac{P_1 P_2}{P_1 + P_2}\right) \tag{5}$$

$$Z = \frac{1}{\left[1 + \left(\frac{P_{avg}\, 344,400\, (10)^{1.785G}}{T_f^{3.825}}\right)\right]} \tag{6}$$

Asimismo, L_e es la longitud equivalente del sistema analizado, estimado según Ec. (7).

$$L_e = j_1 L_1 + j_2 L_2 e^{s1} + j_3 L_3 e^{s2} + \cdots \tag{7}$$

Para el cálculo de la longitud equivalente L_e, se considera L_1, L_2, L_3... L_n como las longitudes discretizadas del sistema las cuales se encuentran asociadas a los cambios de elevación. Asimismo "j" corresponde a un parámetro calculado para cada cambio de pendiente en el segmento según Ec. (8) donde "s" es el parámetro de ajuste por elevación, calculado como la relación entre las elevaciones del segmento discretizado de tubería, la gravedad específica, la temperatura promedio y el factor de compresibilidad calculado según Ec. (9).

$$j = \frac{e^s - 1}{s} \tag{8}$$

$$s = 0.0375 G \left(\frac{H_2 - H_1}{T_f Z}\right) \tag{9}$$

Ecuación de Weymouth. La ecuación de Weymouth es apropiada para diámetros menores a 15 pulgadas, segmentos de tubería menores a 20 millas y presiones de entre 100 a 1000 psia [4]. Esta fórmula calcula directamente el caudal a través de una tubería para valores dados de gravedad del gas, compresibilidad, presiones de entrada y salida, diámetro y longitud de la tubería. En unidades USCS, la ecuación de Weymouth se establece según la Ec. (10).

$$Q = 433.5E \left(\frac{T_b}{P_b}\right)\left(\frac{P_1^2 - e^s P_2^2}{G T_f L_e Z}\right)^{0.5} D^{2.5} \tag{10}$$

Ecuación de Panhandle A. La Ecuación Panhandle A es apropiada para diámetros entre 12 a 60 pulgadas, sistemas de gran extensión, flujos de gas moderado y presiones entre 800 a 1500 psia [4]. Se desarrolló para su uso en gasoductos de gas natural incorporando un factor de eficiencia para los números de Reynolds en el rango de 5 a 11 millones. En esta ecuación no se utiliza la rugosidad de la tubería. La forma general de la ecuación Panhandle A se expresa en unidades USCS según Ec. (11).

$$Q = 433.5E\left(\frac{T_b}{P_b}\right)^{1.0788}\left(\frac{P_1^2 - e^s P_2^2}{G^{0.8539}T_f L_e Z}\right)^{0.5394} D^{2.6182} \tag{11}$$

Ecuación de Panhandle B. La ecuación Panhandle B es apropiada para diámetros de 36 pulgadas en adelante, flujos de gas alto y presiones por encima de los 1000 psia [4]. También es conocida como la ecuación Panhandle revisada y en flujo completamente turbulento, se encuentra que es preciso para valores del número de Reynolds en el rango de 4 a 40 millones. Esta ecuación en unidades USCS es la Ec. (12).

$$Q = 737E\left(\frac{T_b}{P_b}\right)^{1.02}\left(\frac{P_1^2 - e^s P_2^2}{G^{0.961}T_f L_e Z}\right)^{0.51} D^{2.53} \tag{12}$$

La descripción de las variables, sistema de unidades, así como parámetros asociados a los cambios de elevación para las ecuaciones de Weymouth, Panhandle A y B son los mismos que los descritos en la ecuación general.

3   Metodología

Para someter la evaluación de las tres ecuaciones convencionales de flujo se consideró la configuración de un gasoducto de 34" de diámetro y 408 km de extensión ubicado en la Sierra del Perú [5]. Las características técnicas y operativas del mismo se describen en la Tabla 1.

Tabla 1. Características técnicas y operativas del gasoducto evaluado

Parámetro	Valor	Unidades
Gravedad específica	0.612	adimensional
Temperatura inicial	549.27	°R
Temperatura final	528.39	°R
Temperatura promedio	538.83	°R
Viscosidad	0.0000101	lb/ft.s
Rugosidad	0.0004	in
Diámetro externo	34.00	in
Espesor	0.75	in
Diámetro interno	32.50	in
Presión inicial	1751.48	psia
Presión final	1388.01	psia

Asimismo, se relevó la información relacionada al perfil de elevación en las cuales se identifica la progresiva, los segmentos discretizados, así como la altura identificada en cada cota del ducto. Estos parámetros se encuentran almacenados en el archivo *Pipeline Elevation Profile.xlsx*. A continuación, se elaboraron las rutinas de Matlab con la finalidad de vincular los parámetros indicados en la Tabla 1 con las diferentes ecua-

ciones convencionales de flujo: Ecuación general, ecuación de Weymouth, Panhandle A y B, obteniéndose los siguientes archivos indicados en la Tabla 2.

Tabla 2. Archivos generados en Matlab para el modelamiento del gasoducto

Nombre	Tipo	Descripción
Ecuacionbasicageneral.m	función	Cálculo de factor de fricción y caudal Eq.General
EcuacionPanhandleA.m	función	Cálculo de caudal por medio de Panhandle A
EcuacionPanhandleB.m	función	Cálculo de caudal por medio de Panhandle B
EcuacionWeymouth.m	función	Cálculo de caudal por medio de Weymouth
Suelo.m	función	Gráfica del perfil de elevación en $f(L,H)$
Caudal.m	script	Script que consolida las rutinas y graficas

En base a los archivos señalados se obtuvieron los resultados comparativos.

4   Resultados

Las rutinas elaboradas en Matlab nos dan como resultado la gráfica del perfil de elevación del gasoducto descrito en la sección anterior (ver Fig. 1) así como los resultados de capacidad estimada para cada una de las ecuaciones en consideración: General, Weymouth, Panhandle A y Panhandle B y adicionalmente la presión inicial y final en el gasoducto (ver Fig. 2).
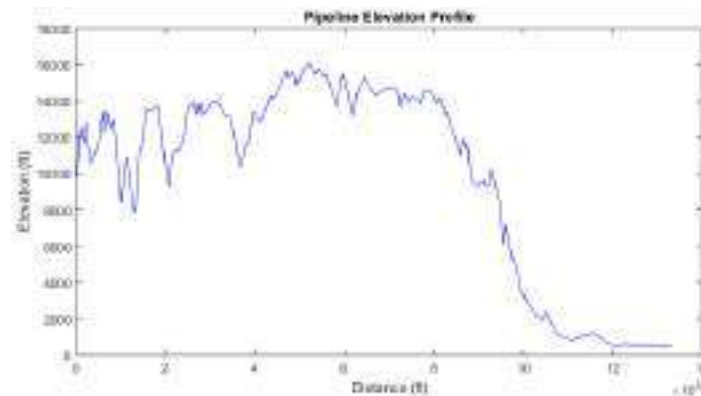
Fig. 1. Perfil de elevación generado en Matlab con la información de longitudes de tubería discretizada y altura de cotas. Ver archivo función *suelo.m*
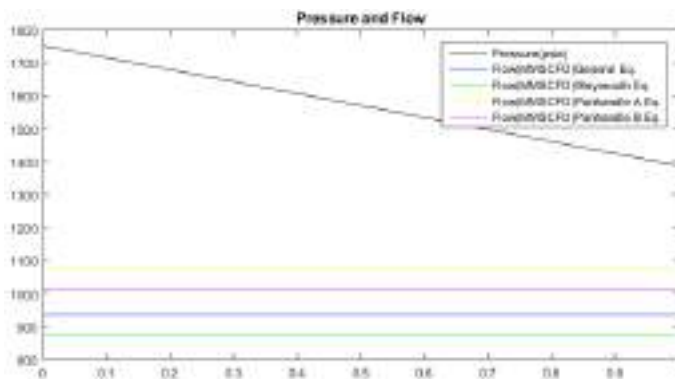
Fig. 2. Comparativa de estimaciones de flujo generado en Matlab para cada una de las ecuaciones convencionales. Ver script *caudal.m*

Por medio del software Matlab se obtuvieron las siguientes estimaciones de caudal, así como las respectivas desviaciones respecto de la ecuación general, que se muestran en la Tabla 2.

Tabla 2. Características técnicas y operativas del gasoducto evaluado

Ecuación	Caudal (MMSCFD)	Desviación respecto de la Ecuación General
General	934.75	-
Weymouth	873.49	- 61.26
Panhandle A	1076.66	141.91
Panhandle B	1013.46	78.71

Razón por la cual se determina que para el gasoducto modelo de 34" de diámetro y 408 km de extensión ubicado en la Sierra del Perú, la ecuación de Panhandle B presenta la menor desviación respecto de la Ecuación General, siendo en consecuencia la que contiene una mejor aproximación numérica.

5   Conclusiones

a. Para el caso de un gasoducto de 34" de diámetro, 408 km de extensión, flujos de gas alto y presiones por encima de los 1000 psia, la ecuación Panhandle B sostiene mayor aproximación respecto de la ecuación general, comprobando su utilidad de manera coincidente con la literatura referenciada.
b. Es posible reflejar las distintas ecuaciones relacionadas a la hidráulica por tuberías en la herramienta de modelamiento numérica Matlab, con resultados

de alta precisión y generación de gráficos que refuercen las prestaciones y utilidad de la herramienta.

c. Matlab permite conectar el suministro de data de entrada a través de la herramienta Excel, permitiendo, para el caso de gasoductos de gran extensión, vincular extensa información topográfica que nos permita resultados con una exactitud similar a los simuladores hidráulicos de la industria del Oil&Gas.

d. Es posible construir modelos de mayor complejidad y procesamiento de datos debido a las prestaciones de la herramienta.

6   Referencias

1. Gamal, A. (2015). Analysis of Pressure Drop Characteristics in Natural Gas Networks. International Journal of Engineering Research & Technology (IJERT). Vol. 4 Issue 10, October (2015). Disponible en: https://www.ijert.org/research/analysis-of-pressure-drop-characteristics-in-natural-gas-networks-IJERTV4IS100308.pdf
2. Shashi Menon, E., "Gas Pipeline Hydraulics", CRC Press, Taylor and Francis, (2005).
3. GPSA (Gas Processors Suppliers Association). Engineering Data Book. 11ed. 1998.
4. Bengtson, H. (2019). CE-080 Natural Gas Pipeline Flow Calculations. Disponible en: https://pdhstar.com/wp-content/uploads/2019/04/CE-080-Natural-Gas-Pipeline-Flow-Calculations.pdf
5. Organismo Supervisor de la Inversión en Energía y Minería – OSINERGMIN "La Industria del Gas Natural en el Perú". (2014). Disponible en: https://www.osinergmin.gob.pe/seccion/centro_documental/Institucional/Estudios_Economicos/Libros/Libro-Industria-Gas-Natural-Peru-10anios-Camisea.pdf

7   Anexos

Función: Ecuacionbasicageneral.m

```
function [qf1] = Ecuacionbasicageneral(G,D,e,P1,P2,Tf,L,H,Mu)
Pb = 14.7; % psia
Tb = 519.7; % °R
Qi = 10000000; %SCFD
Pavg = 2/3*(P1+P2-(P1*P2/(P1+P2)))-14.7; %psia
z1 = 1/(1+(Pavg*344400*(10^(1.785*G))/(Tf^3.825)));
n = length(L);
s = zeros(n,1);
j = zeros(n,1);
for I = 1:n
    s(i) = 0.0375*G.*(H(i+1)-H(i))/(Tf*z1);
    if s(i) == 0
        j(i) = 1;
    else
        j(i) = (exp(s(i))-1)./s(i);
    end
end
```

```
S = 0.0375*G*(H(n+1)-H(1))/(Tf*z1);
l = j(1).*L(1);
for I = 2:n
  Le = l+j(i).*L(i).*exp(s(i-1));
  l = Le;
end
f1 = 0.01;
Re = 0.0004778*(Pb/Tb)*(G*Qi/(Mu*D));
error = 1;
emin = 0.00000001;
while error > emin
  f = 1/(-2*log10(e/(3.7*D) + 2.51/(Re*sqrt(f1))))^2;
  F = 2/sqrt(f);
  qf1 = 38.77*F*(Tb/Pb)*((P1^2-P2^2*exp(S))/(G*Tf*Le*z1))^0.5*D^2.5; %SCFD
  Re1 = 0.0004778*(Pb/Tb)*(G*qf1/(Mu*D));
  error = abs(qf1-Qi);
  Re = Re1;
  Qi = qf1;
  f1 = f;
end
fprintf('Pipeline Capacity estimated with General equation(MMSCFD): Qf = %g\n',
qf1/1000000);


Función: EcuacionWeymouth.m
function [qf2] = EcuacionWeymouth(G,D,P1,P2,Tf,L,H)
Pb = 14.7; % psia
Tb = 519.7; % °R
Pavg = 2/3*(P1+P2-(P1*P2/(P1+P2)))-14.7; %psia
z1 = 1/(1+(Pavg*344400*(10^(1.785*G))/(Tf^3.825)));
n = length(L);
s = zeros(n,1);
j = zeros(n,1);
for i = 1:n
  s(i) = 0.0375*G.*(H(i+1)-H(i))/(Tf*z1);
  if s(i) == 0
  j(i) = 1;
  else
  j(i) = (exp(s(i))-1)./s(i);
  end
end
S = 0.0375*G*(H(n+1)-H(1))/(Tf*z1);
l = j(1).*L(1);
for i = 2:n
  Le = l+j(i).*L(i).*exp(s(i-1));
  l = Le;
end
```

```matlab
qf2 = 433.5*(Tb/Pb)*((((P1^2)-exp(S)*(P2^2))/(G*Tf*Le*z1))^0.5)*(D^2.667);
%SCFD
fprintf('Pipeline Capacity estimated with Weymouth equation(MMSCFD): Qf =
%g\n', qf2/1e+6);
end
```

Función: EcuacionPanhandleA.m
```matlab
function [qf3] = EcuacionPanhandleA(G,D,P1,P2,Tf,L,H)
Pb = 14.7; % psia
Tb = 519.7; % °R
Pavg = 2/3*(P1+P2-(P1*P2/(P1+P2)))-14.7; %psia
z1 = 1/(1+(Pavg*344400*(10^(1.785*G))/(Tf^3.825)));
n = length(L);
s = zeros(n,1);
j = zeros(n,1);
for i = 1:n
   s(i) = 0.0375*G.*(H(i+1)-H(i))/(Tf*z1);
   if s(i) == 0
   j(i) = 1;
   else
   j(i) = (exp(s(i))-1)./s(i);
   end
end
S = 0.0375*G*(H(n+1)-H(1))/(Tf*z1);
l = j(1).*L(1);
for I = 2:n
  Le = l+j(i).*L(i).*exp(s(i-1));
  l = Le;
end
qf3 = 435.87*((Tb/Pb)^1.0788)*((((P1^2)-
exp(S)*(P2^2))/((G^0.8539)*Tf*Le*z1))^0.5394)*(D^2.6182); %%SCFD
fprintf('Pipeline Capacity estimated with Panhandle A equation(MMSCFD): Qf =
%g\n', qf3/1e+6);
end
```

Función: EcuacionPanhandleB.m
```matlab
function [qf4] = EcuacionPanhandleB(G,D,P1,P2,Tf,L,H)
Pb = 14.7; % psia
Tb = 519.7; % °R
Pavg = 2/3*(P1+P2-(P1*P2/(P1+P2)))-14.7; %psia
z1 = 1/(1+(Pavg*344400*(10^(1.785*G))/(Tf^3.825)));
n = length(L);
s = zeros(n,1);
j = zeros(n,1);
for i = 1:n
   s(i) = 0.0375*G.*(H(i+1)-H(i))/(Tf*z1);
   if s(i) == 0
```

```
    j(i) = 1;
    else
    j(i) = (exp(s(i))-1)./s(i);
    end
end
S = 0.0375*G*(H(n+1)-H(1))/(Tf*z1);
l = j(1).*L(1);
for i = 2:n
  Le = l +j(i).*L(i).*exp(s(i-1));
  l = Le;
end
qf4 = 737*((Tb/Pb)^1.02)*((((P1^2)-
exp(S)*(P2^2))/((G^0.961)*Tf*Le*z1))^0.51)*(D^2.53); %SCFD
fprintf('Pipeline Capacity estimated with Panhandle B equation(MMSCFD): Qf =
%g\n', qf4/1e+6);
end
```

Función: suelo.m
```
function [M] = suelo(L,H)
n = length(L);
M = zeros(n+1,1);
M(1) = 0;
for i = 2:n+1
   M(i) = ((L(i-1)*5280)^2-((H(i)-H(i-1))^2))^(1/2)+M(i-1);
end
end
```

Script: Caudal.m
```
L = xlsread('Pipeline Elevation Profile.xlsx','USCS','G5:G1706');
H = xlsread('Pipeline Elevation Profile.xlsx','USCS','H5:H1707');
G = 0.612;
D = 32.5; %in
e = 0.0004; %in
P1 = 1751.48; %psia
P2 = 1388.01; %psia
Tf = 538.83; %°R
Mu = 0.0000101; %lb/ft-s
[qf1] = Ecuacionbasicageneral(G,D,e,P1,P2,Tf,L,H,Mu);
[qf2] = EcuacionWeymouth(G,D,P1,P2,Tf,L,H);
[qf3] = EcuacionPanhandleA(G,D,P1,P2,Tf,L,H);
[qf4] = EcuacionPanhandleB(G,D,P1,P2,Tf,L,H);
[M] = suelo(L,H);
P = [P1;P2]; %psia
N = [0;1];
Q1 = [qf1;qf1]/1e+6; %MMSCFD
Q2 = [qf2;qf2]/1e+6; %MMSCFD
Q3 = [qf3;qf3]/1e+6; %MMSCFD
```

```
Q4 = [qf4;qf4]/1e+6; %MMSCFD
fprintf('Estimated Flow (MMSCFD) \n');
fprintf('Q(G.Eq.)   Qf(W.Eq)   Qf(PA.Eq)   Qf(PB.Eq)\n');
fprintf('%9.6f  %9.6f  %9.6f  %9.6f\n',qf1/1e+6,qf2/1e+6,qf3/1e+6,qf4/1e+6);
figure;
plot(M,H,'b'); %recorrido del ducto Vs altura del ducto
xlabel('Distance (ft)');
ylabel('Elevation (ft)');
title('Pipeline Elevation Profile')
figure;
plot(N,P,'k',N,Q1,'b',N,Q2,'g',N,Q3,'y',N,Q4,'m'); % Presión y Caudales
legend('Pressure(psia)','Flow(MMSCFD)General Eq.','Flow(MMSCFD)Weymouth
Eq.','Flow(MMSCFD)Panhandle A Eq.','Flow(MMSCFD)Panhandle B Eq.');
title('Pressure and Flow')
```

Development of Electric Vehicles Charging Corridors for Steep Elevation Highways. Case study: Cuenca-Ecuador

Miguel Davila-Sacoto[1][0000-0001-6318-2137] , Marco A. Toledo[2][0000-0001-6570-850X] , Luis Hernández-Callejo[1][0000-0002-8822-2948] , L.G. González[3][0000-0001-9992-3494] , and Carlos Alvarez Bel[2][0000-0002-8238-1606]

[1] Department of Agricultural and Forestry Engineering, University of Valladolid, Duques de Soria University Campus, 42004 Soria, Spain
[2] Institute of Energy Engineering, Polytechnic University of Valencia, 46022 Valencia, Spain
[3] Department of Electrical Engineering, University of Cuenca, Central Campus, 010104 Cuenca, Ecuador

```
miguelalberto.davila@uva.es M.D-S.
   martoor@doctor.upv.es M.A.T.
luis.hernandez.callejo@uva.es L.H-C.
 luis.gonzalez@ucuenca.edu.ec L.G.G
     calvarez@die.upv.es C.A.B
```

Abstract. This research aims to study mobility behavior patterns, location of charging stations, autonomy, distances, and topology, to build the first electric corridor in topologically irregular intermediate cities. The city's mobility plan, battery discharge simulations, altitude monitoring through GPS, and surveys are used to estimate the use and levels of acceptance of this technology. The methodology for locating electric vehicle charging stations in mountainous terrain is studied.

Keywords: Electric Vehicle, Elevation effects, Electric Vehicle Autonomy, Electric Vehicle charging, Electric Vehicle charging corridor.

1   Introduction

Technological advances in the field of electric vehicles (EVs) have allowed developing countries to modify their mobility plans through projects in public and private transport. The transport sector consumes around 49.7 % of petroleum products and is responsible for 24 % of CO_2 emissions worldwide [1]. In Ecuador, population growth in the last decade was 1.4 % per year [2], and the city of Cuenca uses 62% of fossil fuels for transportation and is responsible for 58.4 % of total CO_2 emissions [3]. Conventional vehicles with internal combustion engines (ICE) emit between 400 and 450 gCO_2-eq/mile, therefore, a conventional vehicle in intermediate cities emits between 9 and 10 kg CO_2/day, on an average daily trip of 36 km/day [4].

In Latin America, the population growth rate was 1.05 % per year [5] between 2010 and 2015, while the rate of new vehicles in the same period was on average 10.6

vehicles per thousand inhabitants. Today, EVs are accepted as an alternative to replacing ICE vehicles, some manufacturers offer energy autonomy in the range of 120 km and 500 km, with exceptional cases, such as Tesla, which according to [6, 7, 8], its latest model can reach up to 900km, based on this premise the electricity demand will increase considerably.

One of the main barriers to the adoption of EVs on a large scale is the existence of a charging infrastructure that allows users to feel comfortable using an EV both for short trips within a city and for long trips in the city. Highway. For this reason, the optimal location of the charging stations in both cases is a requirement that must be developed based on the intrinsic characteristics of the implementation area of a vehicle charging network that meets the needs of the user.

In Ecuador, an additional consideration in the implementation of charging stations on highways is the variation in altitude, which affects the contribution of the regenerative brake [12]. Also, on the highways of mountainous areas in Ecuador, there are normally no tourist places where charging stations can be located to provide the user with entertainment during the recharging time of an EV.

Within the National Electromobility Strategy for Ecuador [9], it was established that Ecuador has a goal of 10,000 EVs by the year 2025, 100,000 EVs by the year 2030, and 750,000 EVs by the year 2040. To supply the charging needs of EVs, it is necessary to have a network of public charging stations that allow the development of this sector, considering the safety aspects for the user and technical aspects of the distribution network where these stations will be connected.

The installation of public charging stations in Ecuador are initiatives that arise from the government sector due to the cost of implementation and required studies, for which the electrical distribution company "Empresa Eléctrica Regional Centro Sur C.A". Executed the implementation of the first charging corridor that interconnects the city of Cuenca with the canton of La Troncal, two of the main urban areas within its concession area to promote the technological development required for the adoption of EVs.

Electromobility in the city of Cuenca is a process that is under development due to the short time that technology has evolved in the region and the country. This reality can be classified as a research opportunity for both academia and public companies to obtain information on mobilization issues in EVs and their impact on society, on the electrical and telecommunications infrastructure.

The present work constitutes the review of the methodology considered to implement the first highway charging corridor for EVs in Ecuador, which was carried out by the authors, and the joint work between the University of Cuenca and Empresa Eléctrica Regional Centro Sur C.A.

2   Problem definition

The location of stations in freight corridors has been the subject of analysis in some studies in recent years. The freight corridor concept is based on the activity of carrying out several loads in a route from a point of origin to a specific destination. In the existing literature, two methodologies have been determined in the selection of the location of

charging stations, the first based on nodes and the second based on flows [13]. The node model is based on the location of N charging stations minimizing the distance between nodes and applies to any type of vehicle energy storage technology [13], [14]. However, for the specific cases of alternative energies, due to the limitations of the range of travel that the batteries can give, these vehicles must have several recharging stations along a road [15] for which the authors use the flow model of charging based on capturing the nearby charging demand of users who use a particular road and considers the range of the vehicle; However, the model is limited to short trips.

Studies of the location of charging stations for long trips through corridors base the selection of charging points based on cost [16] or the division of the journey into N parts according to the average range of vehicles [17].

The recharging of vehicles on long trips along mountainous roads that present considerable elevation variations has been shallow studied, having only the general models for the location of stations, and in the case of Latin American countries crossed by the Andes Mountains, has specific studies.

Specifically for the city of Cuenca, one of the most used highways is the one that connects with the city of Guayaquil. The route crosses the Andes mountains to the equatorial coast in a 196 km route (see Fig. 1a) from an elevation of 2500 m to 61 m with a maximum of 4157 m (see Fig. 1b) in a trip of approximately 3 hours duration in a light vehicle, with road grades up to 38 degrees.

(a)
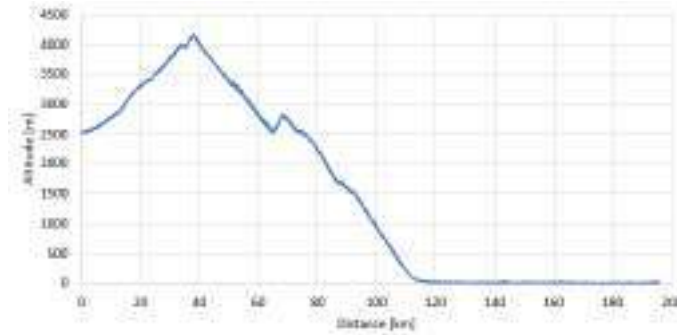
(b)

Fig. 1. Cuenca-Guayaquil Route (a) Route (b) Elevation.

We can see that the route from Cuenca to Guayaquil has the first section until reaching the highest point known as Tres Cruces de El Cajas, from which the route is downhill which would allow the EVs to recharge their battery due to the action of the regenerative braking, however, the return path has a section with a minimum elevation and then begins an approximately 80 km drive uphill which considerably decreases the range of the EV.

Another inconvenience that this route has, which is caused exclusively by an operational limitation, is that the Empresa Eléctrica Regional Centro Sur C.A. does not have facilities in the city of Guayaquil, having offices up to the La Troncal canton located 79 km away. from Guayaquil and 152 km from Cuenca. For this reason, only the Cuenca - La Troncal route was considered, which likewise crosses the Andes mountains in a common section with the Cuenca-Guayaquil road (see Fig. 2).

(a)

(b)
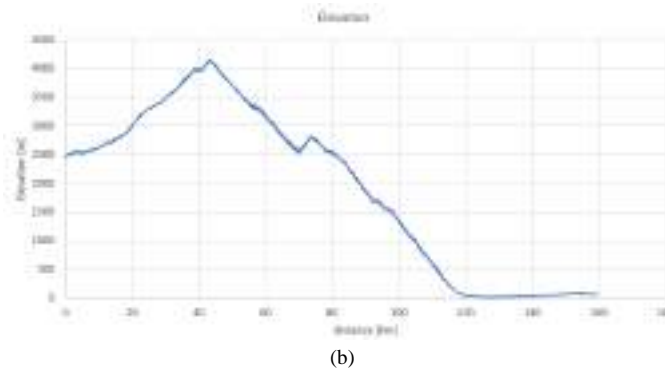
Fig. 2. Cuenca-La Troncal Route (a) Route (b) Elevation.

3 Charging stations location

The location of La Troncal was considered as the first alternative for the location of an EV charging station due to its proximity to the city of Guayaquil and because of Empresa Eléctrica Regional Centro Sur C.A it has its own infrastructure (office and electrical) in La Troncal to supply the electrical energy required by the station. The second charging station was located in the central offices located in the city of Cuenca in the urban part of the city and has the company's parking lot. The intermediate station location problem was carried out considering the following aspects:

- Perception analysis of EVs
- Average range of existing EVs
- Nearby tourist infrastructure
- Effect of elevation on EV range

3.1 Perception analysis of Electric Vehicles

In the first instance, an analysis of the perception of electromobility in the city was carried out to determine if the stations are going to have a real use. The technical analyzes used to estimate the degree of penetration that EVs will have in the selected route are carried out through a general survey carried out for electromobility in the city, therefore, based on 545 samples, distributed in three different areas of the city of Cuenca (the main source of traffic through the selected route). The questions asked have the objective of knowing the use of the vehicle in citizenship and the charging preferences in the case of having an EV. From the question What type of transport do you use daily?, it was obtained that 66 % use their car and 20% use public transport, these data show that the car continues to be the most used means of transport in Cuenca. Fig. 3 shows the distribution of the most used means of transport.
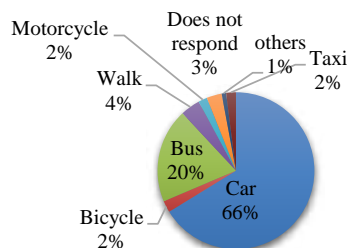
Fig. 3. Most used means of transport in Cuenca.

Regarding the question What is the average distance traveled in a day?, it was found that 10 % of citizens travel less than 3 km, 43 % travel between 3 km and 10 km, 42% travel more than 10km, and the people who did not respond are 5 %. In another question related to the frequency of car use per week (see Fig. 4), it was stated that 69 % use their car daily. Likewise, to the question Would you be willing to buy an electric vehicle?, 75 % answered YES, 21% said NO, and 4% did not answer. Finally, for the question What would be the preferred place to charge EVs?, 71.38% of the surveyed population preferred their home as a place to charge EVs and the rest preferred their place of work, the results are summarized in figure 5.
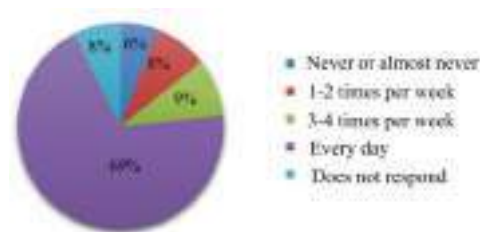
Fig. 4. Frequency of vehicle use in Cuenca

Fig. 5. The place chosen to recharge EVs

3.2　The average range of existing electric vehicles in the Ecuadorian market

In Ecuador the adoption of EVs is a process that is beginning, having until August 2022 a total of 1170 EVs registered of a total of 2,361,175 motorized vehicles in the country (4.95 %) [18] which have been registered by independent magazines since there are no official statistics that determine it, however, they coincide with the predictions of the country's electromobility plan. Table 1 shows the autonomy of the best-selling EVs in Ecuador, having an average autonomy of 225.33 km. The autonomy showed is what the manufacturer reports, however, there is no information on this value in mountainous areas or with considerable variations in altitude.

Table 1. Autonomy of the best-selling electric vehicles in Ecuador.

Brand	Model	Range [km]
Dayang	Chock G2	100
KIA	Soul	276
BYD	E5	300
Mean		225.33

3.3　Nearby tourist infrastructure

The Cuenca-La Troncal route crosses El Cajas National Park, an area known for its tourist attractions for mountain activities, walks, visits to lagoons, and observation of wild flora and fauna. Although the route has several restaurants and rest areas that are potential locations for the location of charging stations (see Fig. 6) as a government company, additional parameters had to be considered such as security of the facilities, ease of access both for the user and for maintenance personnel and above all the willingness of the owners of the premises to house an EV charging station.

Fig. 6. Existing restaurants and rest areas on the Cuenca-La Troncal route. Source: Google Maps.

3.4 Effect of Elevation Variation on EV Range

With the above parameters, a simulation of the effect of the variation of the elevation of the Cuenca-La Troncal route in the EV range was carried out to properly choose the location of the intermediate charging stations. Thus, a simulation was carried out in Matlab using the basic model of an EV (see Fig. 7a) with a battery controller, driving cycle, and environmental conditions [19] to which the elevation of the analyzed road was added and used a WLTP class 2 driving cycle (see Fig. 7b) because the maximum speed of the route is 90 km/h.

(a)

(b)
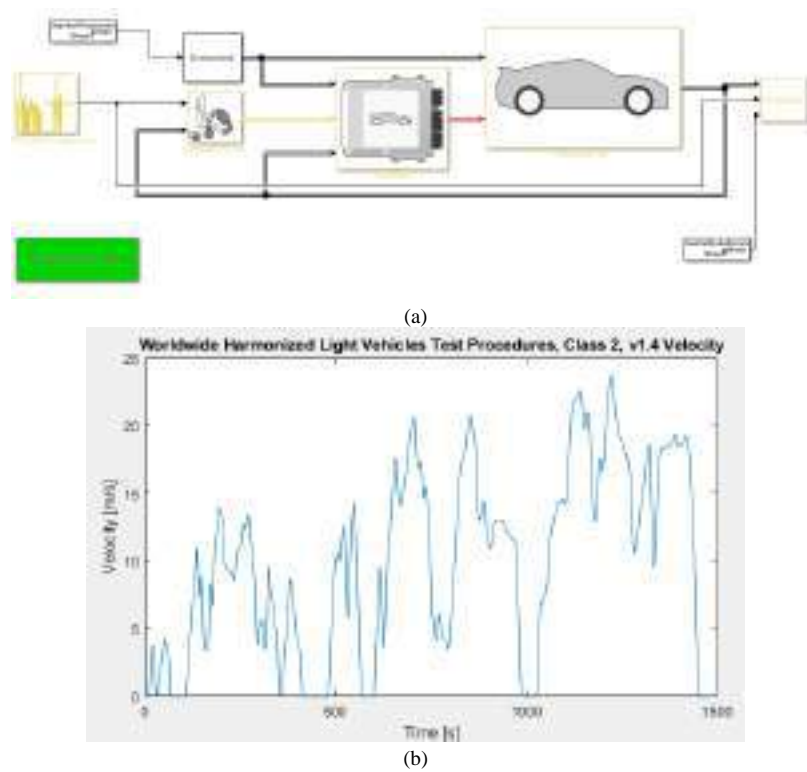
Fig. 7. Simulation in Matlab-Simulink (a) Electric vehicle model considering road elevation (b) Driving cycle.

4 Results

Simulations were carried out in Matlab in two cases, the first in the Cuenca-La Troncal path and the second in the La Troncal-Cuenca path, in both cases an initial state of

charge (SOC) of 80 % is assumed. Speed, engine revolutions, engine torque, battery state of charge (SOC), battery current, and elevation are analyzed (see Fig. 8).
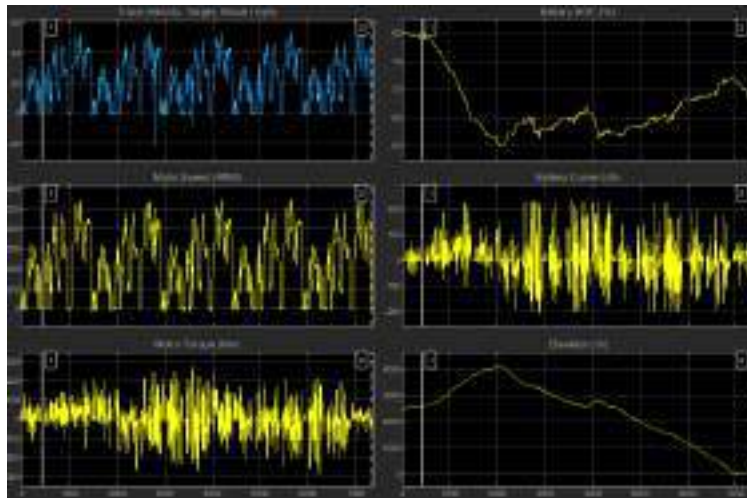
Fig. 8. Results obtained from the Simulation in Matlab-Simulink

In the first case, it is observed that on the first uphill path the EV reaches a SOC=60 %, while with the use of the regenerative brake it recovers up to 9 % at its destination (see Fig. 9).
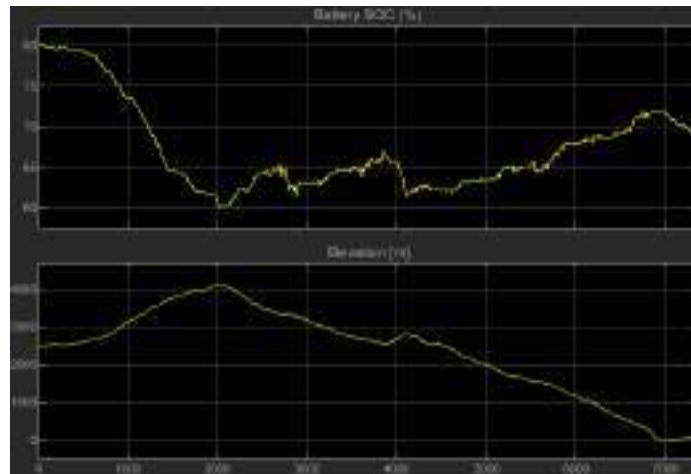
Fig. 9. SOC and elevation of the Cuenca-La Troncal route

In the second case, for the La Troncal-Cuenca route, it is observed that the SOC reaches a minimum value of 3.8 %, which can cause damage to the battery and increase the driver's charge anxiety (see Fig. 10).
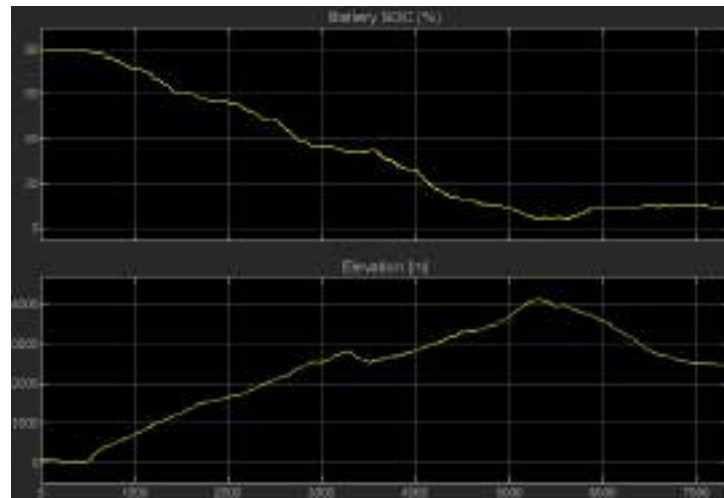
Fig. 10. SOC and elevation of the La Troncal-Cuenca route

Although the vehicle would arrive at its destination with a SOC=8.8 %, this scenario depends on the driving cycle and external parameters such as rain, traffic, etc. For this reason, the need for an intermediate charging station is determined, which must be selected based on the parameters described in the previous subsections.

Among the places of interest to locate charging stations on the highway, which are at an elevation at which there is a soc between 20 and 40 %, El Mestizo restaurant stands out, located at 3383m altitude and 68 km from Cuenca and 84km from La Troncal, where there would be a SOC=34 %. The location was also selected for having facilities for the construction of the infrastructure required for the charging station, for presenting rest activities for users, and for its proximity to the electrical distribution network (see Fig. 11). The installed station is a 50 kW direct current fast charge station. This type of direct current charging station offers advantages such as a reduction in charging time and results in a balance between installation costs and the impact on the electrical network.

Fig. 11. Charging station - Installation

5   Conclusions

This case study presents the basic methodology used to select the location of EV charging stations on the Cuenca-La Troncal highway, characterized by mostly mountainous routes. The charging stations installed on the Cuenca-La Troncal route constitute the first EV charging corridor in Ecuador and have been operating since August 2022. The location of this station allows even EVs with less autonomy such as the Chock G2 to charge. However, in the case of vehicles with low autonomy, a full charge is required, which can take between 1 to 2 hours in fast charge and up to 6 hours in slow charge according to the common profiles in this type of vehicle. For this, the user has nearby leisure activities such as observation of flora in the area and walks, however these activities are limited, which constitutes an opportunity for the public company and the authorities to improve the offer of these activities and promote tourism around the area of charging corridors.

When determining the perception of citizens regarding electromobility, it was observed that 66 % of citizens use their private vehicles with routes between 3 km and 10 km, the survey found that only 19 % of respondents are willing to purchase an EV, while the rest are reluctant due to lack of knowledge of the technology associated mainly with maintenance and customer service issues.

At an altitude of 2,250 and 4,100 meters above sea level, an average autonomy of 225 km was obtained based on market data since Ecuador does not have official electromobility statistics. According to the routes surveyed, the EVs in Cuenca, in the least favorable scenario, will receive 10 monthly recharges, using 257 kWh/month.

Future Work

The Cuenca-La Troncal corridor is the first cargo corridor in Ecuador, however, the interconnection of Cuenca with other cities such as Cañar and Loja are required. In addition, the study of short-distance urban charging corridors is required for the location of stations that cover the future demand for electromobility in the city.

Acknowledgments

The authors thank the University of Cuenca for providing the fast-charging station installed in this project and the Empresa Eléctrica Regional Centro Sur for the installation of the infrastructure resulting from this research.

References

1. CO2 Emissions from Fuel Combustion, International Energy Agency, https://www.iea.org/publications/freepublications/publication/KeyWorld2017.pdf, Abril 2017.
2. El Telégrafo, se vendieron 103.000 vehículos n.d., https://www.eltelegrafo.com.ec/noticias/economia/4/en-2017-sevendieron- 103-000-vehiculos, 2017.
3. EMOV EP. "Inventario de Emisiones Atmosféricas del Cantón Cuenca 2014", 2014. https://:www.researchgate.net/profile/ReneParra/publication.
4. Banco Interamericano de Desarrollo, La Incorporación de los Vehículos Eléctricos en América Latina.
5. CEPALSTAT Indicador 31n.d. http://estadisticas.cepal.org/sisgen/Consulta Integrada.asp?IdAplicacion=1&idTema=1&idIndicador=31&idioma=e.
6. Clairand J-M, Arriaga M, Canizares CA, Alvarez C. Power generation planning of Galapagos microgrid considering electric vehicles and induction stoves, IEEE Trans Sustain Energy2018:1., https://doi.org/10.1109/TSTE.2018.2876059.
7. Martínez-Lao J, Montoya FG, Montoya MG, Manzano-Agugliaro F. Electric vehicles in Spain: an overview of charging systems, Renew Sustain Energy, Rev 2017;77:970–83, https://doi.org/10.1016/J.RSER.2016.11.239.
8. Model 3—Tesla n.d. https://www.tesla.com/model3. https://publications.iadb.org/bitstream/handle/11319/7854/Laincorporacion-de-los-vehiculos-electricos-en-America.pdf
9. Ministerio de Transporte y Obras Públicas del Ecuador, "Estrategia Nacional de Electromovilidad para Ecuador," 2021. Accessed: Oct. 04, 2022. [Online]. Available: https://varusecuador.com/wp-content/uploads/2021/05/Estrategia_Nacional_de_Electromovilidad_Ecuador.pdf.
10. Norma J1772: SAE Electric Vehicle Conductive Charge Coupler SAE International n.d.,https://www.sae.org/standards/content/j1772199610/;2019.
11. Plan de Movilidad del IMC, caracterización de la movilidad, 20 páginas, año 2015.
12. D. Antanaitis, "In-Depth Considerations for Electric Vehicle Braking Systems Operation with Steep Elevation Changes and Trailering," Oct. 2021, DOI: 10.4271/2021-01-1263.
13. S. Erdoğan, İ. Çapar, İ. Çapar, and M. M. Nejad, "Establishing a statewide electric vehicle charging station network in Maryland: A corridor-based station location problem," Socioecon. Plan. Sci., vol. 79, no. June 2021, 2022, DOI: 10.1016/j.seps.2021.101127.

14. M. A. Nicholas and J. Ogden, "Detailed Analysis of Urban Station Siting for California Hydrogen Highway Network," Transp. Res. Rec. J. Transp. Res. Board, vol. 1983, no. 1, pp. 121–128, Jan. 2006, DOI: 10.1177/0361198106198300117.
15. M. Kuby and S. Lim, "The flow-refueling location problem for alternative-fuel vehicles," Socioecon. Plan. Sci., vol. 39, no. 2, pp. 125–145, Jun. 2005, DOI: 10.1016/j.seps.2004.03.001.
16. N. Marco and G. Mehrnaz, "A Corridor - Centric Approach to Planning Electric Vehicle Charging Infrastructure", 2022. https://supernet.isenberg.umass.edu/photos/RSAI-2013/NARC2013-EV.pdf/ (accessed Oct. 04, 2022).
17. M. Ghamami, A. Zockaie, and Y. M. Nie, "A general corridor model for designing plug-in electric vehicle charging infrastructure to support intercity travel," Transp. Res. Part C Emerg. Technol., vol. 68, pp. 389–402, 2016, DOI: 10.1016/j.trc.2016.04.016.
18. Varus, "Vehículos eléctricos vendidos en Ecuador," 2022. https://varusecuador.com/esta-disticas-vehiculos-electricos-vendidos/ (accessed Oct. 04, 2022).
19. MathWorks, "EV Reference Application - MATLAB & Simulink," 2022. https://www.mathworks.com/help/autoblks/ug/electric-vehicle-reference-application.html (accessed Oct. 04, 2022).

Technical, economic and environmental feasibility study for the implementation of ecotechnologies in a non-residential building

Mariana Romero-Aguilar [1][0000-0003-2460-4450], Jesús Martínez-Domínguez [1][0000-0002-7949-5581],

Esteban Montiel-Palacios [2][0000-0001-8949-4112], Roberto Alvarado-Juárez[3][0000-0002-4153-3626],

Moisés Montiel-González[1][0000-0001-6726-9344],

[1] Facultad de Ciencias Químicas e Ingeniería. Universidad Autónoma del Estado de Morelos. México

[2] Escuela de Estudios Superiores de Xalostoc. Universidad Autónoma del Estado de Morelos. México

[3] Instituto Tecnológico Superior de Perote. Veracruz. México

Abstract

Nowadays, the intensive consumption of fossil fuels has led to an increase in greenhouse gases, which has induced the acceleration of climate change. Therefore, this research focuses on a technical, economic, and environmental feasibility study for the implementation of ecotechnologies in a non-residential building, considering as a case study a supermarket in Jojutla Morelos, Mexico. An earth-air heat exchanger was designed for the air conditioning of the building and a solar photovoltaic system interconnected to the grid for electricity supply, which satisfies the needs of thermal comfort and electricity demand. The earth-air heat exchanger was technically and economically feasible due to the availability of affordable space and materials and a payback time of less than 2 years. The photovoltaic system with 400 W panels was technically and economically feasible because the proposed arrangement has a payback time of less than 3 years. Furthermore, if both systems are implemented, 108.18 tCO_{2eq} would be avoided annually and 15,037.02 hectares of lowland rainforest are required to absorb the concentration of CO_{2eq} emissions.

Keywords: Earth-air heat exchanger, Photovoltaic system, Avoided CO_2 emissions.

1　　Introduction

Human development is historically related to the production and consumption of energy. The availability of energy represents a key factor for the economic growth of any country and an improvement in the quality of life of its inhabitants [1]. Primary energy sources are classified as renewable and non-renewable. Renewable energy sources are defined as the energy available from permanent and natural processes and that are replenished faster than they can be consumed [2]. Among the main renewable sources are solar energy, wind energy, geothermal energy, hydroelectric energy, ocean energy and bioenergy [2, 3]. The national energy consumption represents the availability of energy in the territory of a country, which can be used for transformation processes, distribution, and final consumption. Final consumption is made up of energy and raw material that are destined for use by the different sectors of the economy. This item covers the use of primary and secondary fuels to meet the energy needs of the residential, commercial, and public, transportation, agricultural and industrial sectors, as well as the use of raw materials to produce non-energy goods [4].

Energy consumption is increasing rapidly around the world due to population growth. In 2019, world energy consumption by type of energy was oil products (40.43%), electricity (19.68%), natural gas (16.37%), renewables (14.01%) and coal and its derivatives (9.52%). The industrial sector reflected higher consumption worldwide (28.94%), followed by the transportation sector (28.94%). In Mexico, in the year 2020, the final energy consumption of the different sectors was: transportation (38.87%), industrial (32.35%), residential, commercial, and public (24.54%) and agricultural (4.24%) [4]. Moreover, the production of primary energy was obtained through oil (56.32%), natural gas and condensates (27.75%), renewable energies (11.25%), coal (2.83 %) and nuclear power (1.85%). Accordingly, 87 percent of the Mexican economy is based on the production of energy from fossil fuels, mainly oil and natural gas. The problem is that fossil fuels are expensive to extract and pollute the air, water, and soil [5, 6]. According to Mexico's national inventory, 33.7% of greenhouse gas emissions come from the energy sector [7]. It is therefore important to consider energy generation from renewable sources to reduce Mexico's dependence on fossil fuels and to introduce "clean" technology [8] that reduces environmental pollution and lead to sustainable development because of fossil fuel reserves are limited and will not be enough to cater to future global energy demands [9].

The building sector (residential and non-residential) is one of the major sectors that consume energy and heating, ventilation, and air conditioning (HVAC) systems are responsible for more than 40% of a building's total energy consumption [10, 11]. Besides, there are several problems associated with the use of conventional HVAC systems: its energy consumption is high, its use increases the peak load, it is harmful to the environment and reduces indoor air quality. Therefore, all these issues with conventional HVAC system led to the exploration of energy efficient and environment friendly systems for heating/cooling of buildings [9]. For this reason, in recent years models, methodologies and strategies have been developed to replace conventional technologies with innovative ecotechnologies that operate with clean energy. In this sense, this paper focuses on how to achieve energetically sustainable non-residential buildings, considering as a case study a supermarket.

Supermarkets during their operation consume electrical energy due to air conditioning systems and the refrigeration of food and other products that require it. Considering this, it is necessary to implement actions that allow supermarkets to reduce their energy consumption coming from fossil fuels. For this purpose, a technical, economic, and environmental feasibility study was conducted in a supermarket located in Jojutla, which is a municipality located in the south of the state of Morelos, Mexico, with a sub-humid climate and summer rainfall, registering average temperatures of 28°C [12]. This municipality has a solar radiation greater than 5 kWh/m^2 throughout the year, so supermarkets located in the southern part of the state of Morelos have a high demand for air conditioning, especially in summer.

The implementation of ecotechnologies, such as photovoltaic systems and Earth-air heat exchangers (EAHE), will reduce the demand and consumption of electrical energy in the supermarket under study. "Ecotechnologies are human interventions in social ecological systems in the form of biological, physical and chemical practices and/or processes designed to minimize damage to the environment and provide ser-vices of value to society" [13]. Photovoltaic technology makes it possible to convert solar radiation into electricity, without emitting greenhouse gases. This technology uses solar cells, which through the photovoltaic effect, allow the transformation of solar energy into electrical energy. The potential for electricity generation using photovoltaic solar energy depends on the availability of solar radiation at the required location [5]. Mexico has an average annual solar radiation of 5 kWh/m^2/day, enough energy to supply the energy demand of a house inhabited by five people.

Commonly, stand-alone photovoltaic (SAPV) systems have been employed in places where power supply may not be readily accessible. In modern cities, most of the buildings are high-rise and the roof area is very limited for the installation of a SAPV system. Building-integrated photovoltaic (BIPV) systems, in which part of the external vertical walls are replaced with photovoltaic modules, are an appropriate alternative for these structures [5]. Photovoltaic panels decrease their efficiency as their temperature increases and to prevent this inconvenience, they can be cooled using fluids such as air or water (the heated fluid can be used for different purposes). The system that incorporates a fluid to cool the photovoltaic panels is known as a photovoltaic-thermal (PVT) unit [6]. Hybrid photovoltaic-thermal solar systems have been used to increase solar utilization and re-duce the relative cost per installation area [14]. PVT systems have been integrated into buildings to produce heat and electricity. The use of this system would reduce energy consumption [15].

On the other hand, HVAC systems based on geothermal energy have received significant attention during the last decades. Geothermal energy stored under the earth's surface can be effectively used for cooling/heating buildings. More than a meter depth, below the ground surface, the ground temperature remains almost constant throughout the year and is equal to the mean annual ambient temperature at that location. The Earth-air heat exchanger (EAHE) system is a green and energy efficient technology for heating and cooling applications in buildings [6, 11, 16, 17].

Many studies have been carried out and the influence of different factors on the performance of EAHE has been analyzed. Installation depth, pipe length, pipe diameter, air velocity of the pipe [16], climatic conditions, physical properties of the soil around the pipe and the operation mode have a great influence on the performance of EAHE [11, 18]. The application of different BIPVT-EAHE hybrid systems has been reported to preheat and precool outdoor air in winter and summer, respectively, and to generate electricity [6]. Yildiz et al. implemented a solar photovoltaic system (PV) assisted earth-to-air heat exchanger (underground air tunnel) for greenhouse cooling [19]. Chel and Tiwari studied photovoltaic energy integrated EAHE system to analyze its potential to mitigate CO_2 emissions compared to a coal-fired power

plant. They determined that the total amount of CO_2 emissions mitigated due to the energy supply during the useful life of the SAPV system is considerably higher than those produced by this system [5]. Nayak and Tiwari combined a EAHE with a photovoltaic cell and used it for heating and cooling a greenhouse [17]. They concluded that the general temperature of the air inside the greenhouse increases between 7 and 8 °C than that of the ambient air, when operating with photovoltaic energy (PVT) during the day and with an EAHE during the night, which is considered suitable for plant growth during the winter period. Argiriou et al. designed and installed a combined system, consisting of an EAHE and a photovoltaic panel, for the purpose of cooling a building [16].

This research seeks to address the problem caused by excessive energy consumption, proposing alternatives to mitigate the energy and environmental impact generated by a non-residential building. The main objective of the study is to evaluate the technical, economic, and environmental feasibility by analyzing real data on the energy consumption of a supermarket in the southern part of the state of Morelos, Mexico, with the aim of proposing the implementation of EAHEs as an air conditioning system and a photovoltaic system interconnected to the electricity grid to generate and supply the electricity required by the establishment. Thus, contributing to energy savings in the supermarket and diminishing the emission of CO2 into the environment.

2   Materials and Methods

2.1. Study area

Jojutla is in Morelos, Mexico. Between latitudes 18° 31' - 18° 41' N, longitudes 99° 09' - 99° 18' E and altitude 882 meters above sea level, with a total area of 153.942 km^2. It has a warm sub-humid climate with summer rains that range between 800-1000 mm per year. The average temperature is 28°C, with maximum of 39°C (in May) and minimum of 4.5°C (in November).

2.2 General Description of the Building

Beside the factors to analyze for the installation of an energy saving system, there are characteristics of the building needed to be aware of, such as size, occupant load and passive ventilation.

As a case study, a supermarket located in Jojutla is proposed. The building structure is an irregular polygon, with a total construction area of 6,882 m^2, and height of 5 m. The occupant load is 2,500 people per day. The hours of operation are 10:00 am to 10:00 pm. The building has small sources of passive ventilation, which are in the entrances that are oriented east-west.

Identification and diagnosis of energy consumption

From route of the building facilities, the main areas of higher energy consumption in the building were identified, which are: lights, air conditioning system and food refrigeration. The installed unit power and the total energy consumed were estimates, from of the quantification of the hours of operation, unit power, installed power and energy per day. The monthly and annual expense was calculated from the electricity rate (expense/kWh) and the electricity consumption of each area.

2.3 Ecotechnology 1: Earth-air heat exchanger (EAHE)

The air conditioning volume of the building was calculated using Equation (1):

$$\dot{V}_{Conditioning} = \frac{Total\ Volume}{Hours\ of\ operation} \qquad (1)$$

With relative humidity and wind speed data in Jojutla (from NASA's data) [19] the fluid flow required for the thermal comfort of the building was determined. Then, the air flow rate through the EAHE is a function of duct area (A_d) and wind speed (v) and is calculated by equation 2:

$$\dot{V}_{Air} = A_d * v \qquad (2)$$

In this equation, $\dot{V}_{Air}$ air conditioning volume per hour (m^3/h)

With these flow rates, the number of ducts necessary to provide thermal comfort to the interior of the building is calculated by equation (3).

$$N_D = \frac{\dot{V}_{Climatización}}{\dot{V}_{Aire}} \tag{3}$$

To determine the average temperature of the internal air of the duct, equation 4 was used:

$$T_m = \frac{T_e + T_s}{2} \tag{4}$$

Where:

Tm: average temperature of the internal air of the duct (°C)

Te: Input temperature to the duct (°C) (room temperature)

Ts: outlet temperature (°C)

The exchange of heat between the soil and the air that circulates inside the duct must be evaluated, for this, the total thermal resistance of the duct is calculated, which is the sum of the convection resistance and conduction resistance.

To determine the conduction resistance, the thickness of the duct and its thermal conductivity are needed. Equation 6 is used with these values:

$$R_{cond} = \frac{\epsilon}{k} \tag{5}$$

Where:

R_{cond}: conduction resistance (m^2/W)

ϵ: duct wall thickness (m)

k: Duct thermal conductivity (W m^2/K)

The convection resistance is calculated with equation 7:

$$R_{conv} = \frac{1}{5.55*(v^{0.8})} \tag{6}$$

With equation 8, the average heat flow per unit area was determined

$$q_m = \frac{T_{suelo} - T_m}{R_t} \tag{7}$$

To determine the amount of energy to be removed from the internal air of the duct, data of relative humidity, input and outlet temperature of the piping system are needed. The enthalpy value of dry air and the volume of air are obtained by the psychometric chart (equation 8):

$$E_R = \frac{h_s}{(V_s)out} - \frac{h_e}{(V_s)in} \tag{8}$$

In equation 8:

E_R: Energy to be removed from the internal air of the duct (kJ/m^3)

h: enthalpy of dry air (kJ/kg)

V_s: Specific volume of air (m^3/kg)

The determination of the total exchange area (m^2), is calculated with the equation (9):

$$A_{IC} = \frac{E_C * \dot{V}_{climatización}}{q_m} \tag{9}$$

For the determination of the length of the ducts that will be three meters deep in the soil, the value of S and the diameter of the ducts (D) are used (eq. 10)

$$L = \frac{A_{IC}}{\pi\,D} \tag{10}$$

2.4 Feasibility of implementation of an EAHE

The main factors to consider are the following [20]:

- Type of soil determines if its conditions are optimal to function as a heat exchanger.

- Sufficient space for installation: the existence of space within the area, which serves as an environment for eco-technologies

- Thermal balance: it determines the number and diameter of the ducts, since the size of the fluid flow will depend on this to provide thermal comfort to the building.

3. Ecotechnology 2: Grid-connected photovoltaic system

To determine if the use of photovoltaic solar systems is viable for the supermarket, the following factors were investigated and considered:

- Number of cloudy days
- Average annual rainfall
- Daily consumption (W)
- Solar resource (kWh/m2)
- Maximum temperature
- Optimum inclination
- Total peak power of the photovoltaic design (Pp)
- Number of photovoltaic panels
- Selection of the right inverter
- Number of panels connected in series and parallel

3.1 Optimum inclination

An adequate inclination of the photovoltaic panels will guarantee a maximum efficiency in the conversion of sunlight into electrical energy, this inclination is based on the latitude of the selected region and is given by Equation (11).

$$\beta opt = 3.7 + 0.69|\emptyset| \tag{11}$$

Where:

βopt: Optimum inclination angle (sexagesimal degrees).

$|\emptyset|$: Latitude (sexagesimal degrees)

3.2 Eficiency

An efficiency of the selected inverter of 95% and 97% efficiency of the wiring for a voltage drop of 3% are considered. The total efficiency is then calculated.

Photovoltaic panels are designed to provide maximum efficiency at standard temperature. However, the temperature fluctuates depending on the study area. For this, the maximum temperature reached in Jojutla, Morelos, must be known, data that will be obtained from the NASA page. To determine the thermal performance [19], equation 12 will be used.

$$Tc = T\,amb + C1 * G \tag{12}$$

Where:

Tc: Panel temperature

T amb.: Maximum temperature of Jojutla, Morelos

C1: nominal temperature of the cell when subjected to radiation of 800 W/m^2 spectral distribution of AM 1.5, ambiental temperature of 20 °C and wind velocity of 1 m/s, $(TOCN = 45°C)$.

G: measured radiation, which depends on the period in which it is (G = 1000 W/m²).

For the calculation of C1, equation 13 is used.

$$C1 = \frac{45-20}{800} = 0.03125 \tag{13}$$

The determination of the temperature loss was calculated with equation 14.

$$\Delta P = (0.47 \% /°C) * (\Delta T) \tag{14}$$

Where:

ΔT: temperature difference (°C)

To obtain the temperature differential, Equation 16 must be applied

$$\Delta T = Tc - Tce \tag{15}$$

Donde:

Tce: Temperature at standard condition (°C)

Equation (16) allows the calculation of the maximum power supplied by the panels.

$$\text{Maximum power} = (Pot.\,panel) - (\Delta T) \tag{16}$$

To obtain the thermal performance, which will be given by the calculated maximum power divided by the nominal power of the panel (Equation 17).

$$RT = \frac{\text{Maximum power}}{\text{Nominal power}} \tag{17}$$

Finally, to determine the peak power in kWh to be supplied, the daily consumption, the thermal efficiency and the total efficiency need to be known:

$$P_P = \frac{E_R}{R_S * R_T * \eta_t} \tag{18}$$

Where:

Pp: Peak power

Ec: Daily consumed energy

Rs: Solar resource

3.3 Inverter selection

The inverter is based on the maximum power to be installed. The selection criteria are that the maximum input power is equal to or greater than the maximum power generated by the photovoltaic panels. Several small inverters will be chosen so that together they cover the required demand even if the maximum power is large [21].

3.4. Serial and parallel connections

In the parallel connection, all the positive poles are connected and all the negative poles separately, therefore, the voltages accumulate while the currents are maintained. While for series connections, a positive pole of a negative module is connected to the positive of the next one, so that the current is increased, the initial voltage is maintained [22].

4. Results and discussion

4.1 Balance of thermal and electrical loads

Based on observations and frequent visits made in 2021 to the supermarket it was identified that:

- This has 144 skylights located on the roof of the building, so it has sufficient natural lighting.

- The air-conditioning system is used even in winter.

To determine the energy consumed for lighting, air conditioning and food refrigeration, an inventory of the devices that demand electrical energy was made. Accordingly, Table 1 shows the energy consumption and operational functions of the devices installed in the supermarket.

Table 1. Energy consumption and operational functions of the devices

Consumer device	Quantity of devices	Operating hours (h)	Unit power (W)	Installed power per device (W)	Energy consumed per day (kWh)
Luminaries	261	6	40	10,440	62.640
Air conditioning system	30	10	1,500	45,000	450
	10 cooling walls	13	330	3,330	43.29
	36 coolers	24	70	2,520	60.48
Food refrigeration	3 ice preservers	24	220.375	661.125	15.867
	3 cold chambers	24	640	1,920	46.08
	6 refrigerated cabinets	13	164.12	984.72	12.801
	4 ice-cream freezers	24	100	400	9.6
Total energy consumption					**700.758 kWh/day**

Although the building has natural lighting, it is important to consider the hours of operation of the luminaires (6:30 am - 7:30 am and 7:00 pm - 00:00 am) during the summer, because in this season there are days with up to 12 hours of sunshine, so it is recommended that the luminaires be turned on at 7:30 pm, in which case the lighting consumption would be 57,420 kWh/day and a saving of 4,820 kWh/day, which translates into an annual saving of 1,759.3 kWh.

Based on the data shown in Table 1 and the consumption fee, the average monthly and annual energy consumption for each of the areas was estimated. The monthly consumption and cost are shown in Table 2.

Table 2. Energy consumption and estimated monthly cost

Month	Days	Total consumption (kWh)	Monthly cost ($)
January	31	21,723.49	106,010.14
February	28	19,621.22	95,751.55
March	31	21,723.49	106,010.14
April	30	21,022.74	102,590.97
May	31	21,723.49	106,010.14
June	30	21,022.74	102,590.97
July	31	21,723.49	106,010.14
August	31	21,723.49	106,010.14
September	30	21,022.74	102,590.97
October	31	21,723.49	106,010.14
November	30	21,022.74	102,590.97
December	31	21,723.49	106,010.14
		255,776.61	**1,248,186.41**

Table 3 shows the estimated monthly and annual expense for energy consumption of the building.

Table 3. Estimated monthly cost of each energy consumption sector

Month	Air conditioning	Lighting	Food refrigeration
January	$68,076.00	$9,476.18	$28,458.49
February	$61,488.00	$8,559.13	$25,704.44
March	$68,076.00	$9,476.18	$28,458.49
April	$65,880.00	$9170.50	$27,540.47
May	$68,076.00	$9,476.18	$28,458.49
June	$65,880.00	$9170.50	$27,540.47
July	$68,076.00	$9,476.18	$28,458.49
August	$68,076.00	$9,476.18	$28,458.49
September	$65,880.00	$9170.50	$27,540.47
October	$68,076.00	$9,476.18	$28,458.49
November	$65,880.00	$9170.50	$27,540.47
December	$68,076.00	$9,476.18	$28,458.49
	$801,540.00	**$111,572.39**	**$335,051.15**

Based on the results gathered tables 2 and 3, the energy consumption for air conditioning is higher than the sum of the consumption for lighting and food refrigeration, being 13,950 kWh/month and 7,773.49 kWh/month, respectively, this is the estimated consumption in a monthly period of 31 days.

The results obtained are like those obtained by Morillón et al. [23], who determined the percentages for final energy use in different types of buildings and climates in Mexico. Among their findings they found that, for commercial buildings in hot sub-humid climates, the highest consumption is allocated in the following order: air conditioning, lighting, and refrigeration, while for hot dry climates they obtained the same order in terms of consumption, but in different proportions.

4.2 Design and proposal of an EAHE

Due to the higher energy consumption for air-conditioning, it is possible to design and propose an earth-air heat exchanger (EAHE), which would meet the objective of reducing energy consumption. The parameters and factors considered for the design of the EAHE are:

- The building has a total construction of 6,882 m^2 by 5 m high.

- The supermarket operational hours are 10:00 a.m. to 10:00 p.m., so it is open 12 hours at day, 7 days at week.

- The air conditioning systems operate 10 hours at day.

- Three typical relative humidities for Jojutla, Morelos were considered: 59%, 49% and 63%.

- Three temperatures were analyzed, an average temperature of 28 °C, the maximum of 39 °C recorded in the month of May and the minimum of 4.51 °C reported for the month of November.

- Three wind speeds were evaluated: 5.8 m/s, 4.49 m/s and 4.28 m/s.

- Five duct diameters were analyzed.

All the climatological values were taken from the NASA database, 2021 [19]. This is done with the objective of proposing several different arrangements to select the most viable and feasible one. The results are shown in table 4.

Table 4. Results for wind speed, relative humidity and temperature analyzed in the present study

Geometric parameter	Wind speed 5.8 m/s, relative humidity 59 % and temperature 28 °C		Wind speed 4. 49 m/s, relative humidity 49% and temperature 32 °C		Wind speed 4.28 m/s, relative humidity 63% and temperature 4.51 °C	
Duct Diameter (inches)	N_D	Length (m)	N_D	Length (m)	N_D	Length (m)
6	10	92.5	8	80.18	11	90.14
8	6	131.16	5	114.46	6	127.65
10	4	183.18	3	161.7	4	177.9
12	3	219.96	2	194.16	3	213.62
14	2	256.74	2	226.63	2	249.34

The proposed space for the implementation of the EAHEs is located on the west side of the building, due to the prevailing winds in this direction, this space has the following dimensions: 42.8 m long and 31.5 m wide, so the total area is 1,348.20 m^2. Once the results were obtained, the best design for the EAHEs was chosen and proposed, which consists of a duct system with a total length of 183.18 m and a diameter of 10 inches, distributed in a serpentine arrangement as shown in Figure 1.
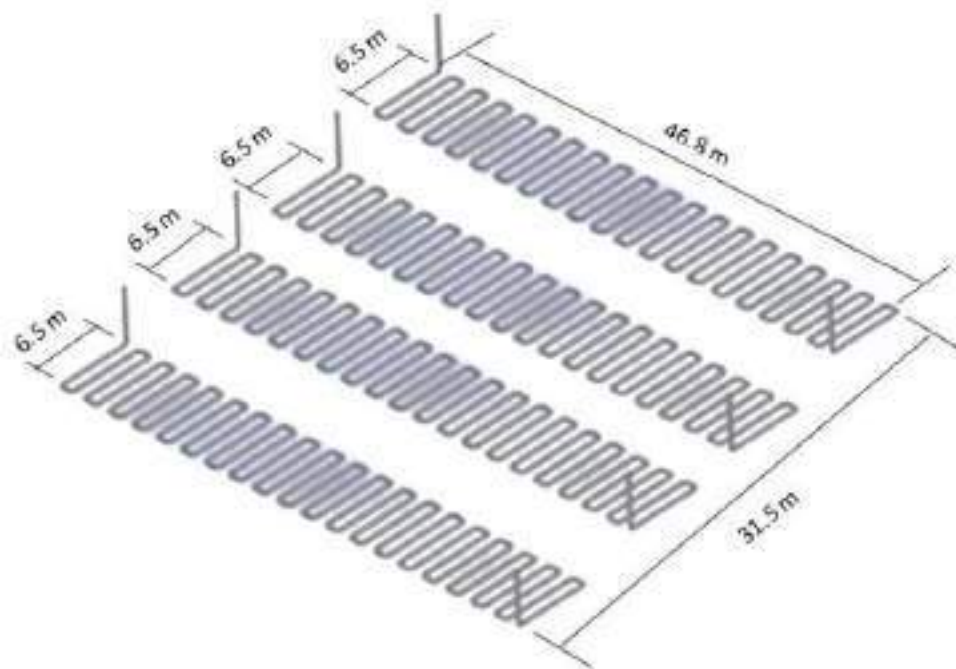
Fig. 1. Design of the EAHEs

Table 9 shows the components and costs for the implementation of EAHEs.

Table 5. Total investment for the implementation of an EAHE

Description	Amount	Unit price	Total price
Ducts	122 sections of 6.10 m	$2,699	$329,278
Elbows	120	$480	$57,600
Couplings	240 of 10 inches	$129	$30,960
Air filters	3	$1,100	$3,300
Thermal insulation	2 rolls of 10.7 m	$4,406	$8,812
Excavation	735 m^2	$240,000	$592,000
			$1,021,950.00

The total cost of the air conditioning system is $1,021,950.00, while the annual cost of the air conditioning system is $801,540.00, which gives a payback time of 1.27 years. Therefore, the payback time of the investment is approximately 15 months and 24 days, so the economic investment of the EAHE is viable and feasible for the supermarket.

4.3 Design and proposal of a grid-connected photovoltaic system

The study area has an average solar radiation of 6.69 kWh/m^2 with a maximum value of 8.15 kWh/m^2 in March, while the minimum value was in August with 5.01 kWh/m^2. Moreover, during the months of June, July, and September there was a similar value. Therefore, these months are considered as a critical season with respect to solar radiation. The solar resource in the municipality of Jojutla is viable for the implementation and use of solar photovoltaic energy.

Considering that the EAHE can replace the air-conditioning system of the supermarket, then the PV system is designed only to satisfy the energy demand for lighting and cooling of food and products, which was 250,758 kWh/day. Based on equation (18), it is obtained that the PV design should cover a total demand of 55 kWh per day, with this value the appropriate inverter was selected. Table 6 shows the number of panels required per array, total power, and associated costs with each proposed PV system. In all proposed arrays, 9 Epcom EPIG7K type inverters will be used.

Table 6. Total investment for the PV system

Panel (W)	Unit price	Amount	Total price	Unit price of inverter	Total price of inverter	Total Cost
330	$3,336	180	$600,480	$22,679.7	$204,117.7	$804,597.3
400	$4,044	144	$582,236	$22,679.7	$204,117.7	$786,353.7
500	$9,009.7	118	$1,063,146.9	$22,679.7	$204,117.7	$1,267,264.6

Table 6 shows that the lowest investment would be made with the 400 W PV panel array, followed by the 330 W panel type and the highest initial investment despite the minimum number of panels is obtained with the 500 W panels. Table 7 shows the total investment costs for each of the designs analyzed and proposed in this work.

Table 7. Total amount of investment.

Panel type	Cost of structures	Cost of PV panels	Inverters costs	Total cost
330 W	$210,130	$600,480	$204,117.7	$1,014,727.7
400 W	$193,743.9	$582,236	$204,117.7	$980,096.7
500 W	$146,298.6	$1,063,146.9	$204,117.7	$1,413,563.2

The 500 W design presents some technical difficulties, since, as it is a series-connected array, electrical failures can occur in all the modules if any of the panels have problems, which is why it is considered technically unfeasible, as well as being the one that requires the greatest initial investment. On the other hand, the 330 W design has the highest energy surplus. It is also observed that the design that requires the least investment is the 400 W photovoltaic system, which is also the most efficient. Therefore, this is the technically and economically feasible option.

Table 8 presents the time to return on investment for each proposed design, which was obtained with equation (19).

$$TRI = \frac{Total\ invesment}{Annual\ energy\ cost} \qquad (19)$$

Table 8. Time to return on investment

Panel type	Monthly consumption	Annual energy cost without PV panels	Total investment	Payback time (years)
330 W			$1,014,727.7	2.27
400 W	250.758 kWh	$446,327.53	$980,096.73	2.19
500 W			$1,413,563.29	3.16

As shown in Table 8, the shortest period to return on investment was obtained with the 400 W panels, while the design with 500 W panels represents the highest payback time, even though the total number of panels was lower than the other two proposed designs.

According to the results obtained in this research, when compared to those obtained by Molina and Muñoz [24] for 20 PYMES, the payback time was similar.

4.4 Environmental feasibility study

For the environmental feasibility study, we first calculate the emissions avoided using conventional air conditioning systems, which represent a daily consumption of 450 kWh.

The annual carbon equivalent (CO2e) emissions for lighting and food refrigeration were then calculated, this energy consumption resulted in 250,758 kWh/day. Equation (20) is used for this purpose:

$$HC = (C_E)(FC)(FE) \tag{20}$$

Where:

C_E=Electricity consumption (kWh)

FE=Emission factor

FC=Conversion factor

HC=Carbon footprint

The emission factor of the National Electricity System is the one indicated by the Energy Regulatory Commission (CRE) for the calculation of indirect greenhouse gas emissions from electricity consumption for the year 2021 [25]: $FE = 0.423 \, tCO_2eq/MWh$

On the other hand, the figure 2 shows the generation of CO_{2eq} by the consumption of electrical energy (kWh for diary and MWh per year). It be clearly appreciated, that the largest energy consumption is from the air conditioning, therefore, it presents the highest carbon footprint production. According to the INECC, 139,139 hectares of lowland forest (vegetation in Jojutla) are required to absorb one ton of CO_{2eq}, therefore, 15,037.02 ha are required to absorb the concentration of CO_{2eq} generated.
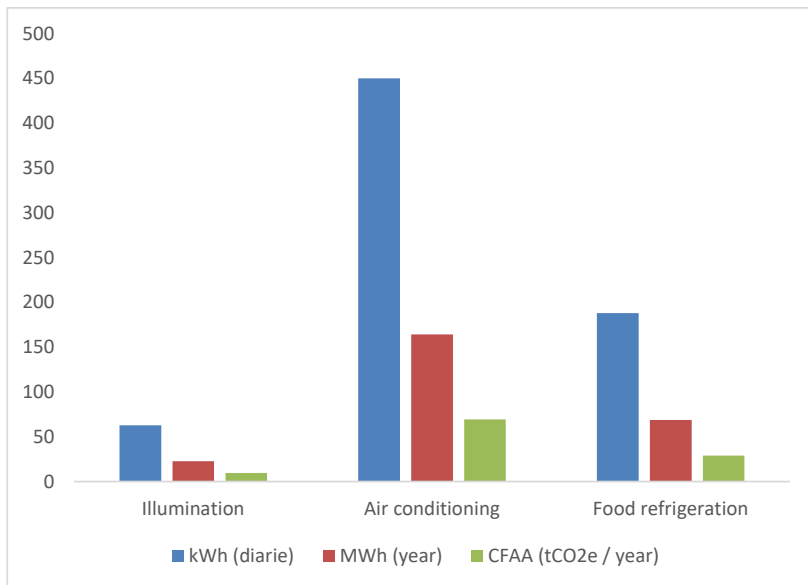
Fig. 1. Carbon footprint for electricity consumption

5. Conclusions and future work

From the technical, economic, and environmental feasibility study of the EAHE and the grid-connected photovoltaic system proposed in this work, the following conclusions can be drawn:

1. The EAHE was technically and economically feasible due to the availability of space for the proposed design, as well as materials, components, and the payback time.

2. The photovoltaic system with 400 W panels was technically and economically feasible with respect to the other proposed arrays.

3. The EAHE and the photovoltaic system were environmentally feasible because 108.18 tCO_{2eq} would be avoided annually.

4. The air conditioning presents the highest energy and economic consumption of the building, therefore, the implementation of ecotechnologies such as EAHE and photovoltaic systems would meet the needs of reducing the cost/ payment of the commercial establishment, as well as reducing its carbon footprint and reducing its economic expenditure in the short and medium term.

The main lines of future work are related to the following perspectives:

Elaborate a strategy for the private sector to have a broader perspective and thus actively collaborate in the design and implementation of eco-technologies.

Develop further technical, economic, and environmental feasibility studies for other buildings, considering different climatic conditions.

References

1. Ouedraogo, N.S.: Energy consumption and human development: Evidence from a panel cointegration and error correction model. Energy 63, 28-41 (2013).
2. UN. What is renewable energy? https://www.un.org/es/climatechange/what-is-renewable-energy, last accessed: 2022/09/30.
3. IRENA. Renewable Energy Sources, https://www.irena.org/, last accessed: 2022/09/30.
4. SENER. Balance Nacional de Energía 2020, https://www.gob.mx/cms/uploads/attachment/file/707654/BALANCE_NACIONAL_ENERGIA_0403.pdf, last accessed: 2022/09/30.
5. Chel, A., Tiwari, G. N.: Stand-alone photovoltaic (PV) integrated with earth to air heat exchanger (EAHE) for space heating/cooling of adobe house in New Delhi (India). Energy Conversion and Management 51, 393–409 (2010).
6. Shahsavar, A., Talebizadehsardari, P., Arıcı, M.: Comparative energy, exergy, environmental, exergoeconomic, and enviroeconomic analysis of building integrated photovoltaic/thermal, earth-air heat exchanger, and hybrid systems. Journal of Cleaner Production 362, 1-11 (2022).
7. INECC. Inventario Nacional de Emisiones de Gases y Compuestos de Efecto Invernadero, https://www.gob.mx/inecc/acciones-y-programas/inventario-nacional-de-emisiones-de-gases-y-compuestos-de-efecto-invernadero, last accessed: 2021/11/30.
8. Mundo-Hernández, J., de Celis Alonso, B., Hernández-Álvarez, J., de Celis-Carrillo, B.: An overview of solar photovoltaic energy in Mexico and Germany. Renewable and Sustainable Energy Reviews 31, 639-649 (2014).
9. Agrawal, K.K., Misra, R., Agrawal, G.D.: To study the effect of different parameters on the thermal performance of ground-air heat exchanger system: In situ measurement. Renewable Energy 146, 2070-2083 (2020).
10. Sedaghat, A., Habibi, M., Hakkaki-Fard, A.: A novel ground thermal recovery system for horizontal ground heat exchangers in a hot climate. Energy Conversion and Management 224, 1-15 (2020).
11. Cao, S., Li, F., Li, X., Yang, B.: Feasibility analysis of Earth-Air Heat Exchanger (EAHE) in a sports and culture center in Tianjin, China. Case Studies in Thermal Engineering 26, 1-9 (2021).

12. Síntesis   estadística   municipal   2019, https://coespo.morelos.gob.mx/images/Datos_municipales/2020/JOJUTLA2019.pdf,   last   accessed 2022/09/23.

13. Haddaway, N.R., McConville, J., Piniewski, M.: How is the term 'ecotechnology' used in the research literature? A systematic review with thematic synthesis. Eco-hydrology and Hydrobiology 18, 247-261 (2018).

14. Barone, G., Buonomano, A., Forzano, C., Giuzio, G. F., Palombo, A.: Passive and active performance assessment of building integrated hybrid solar photovolta-ic/thermal collector prototypes: Energy, comfort, and economic analyses. Energy 209, 1-13 (2020).

15. Abdelrazik, A.S., Shboul, B., Elwardany, M., Zohny, R.N., Osama, A.: The recent advancements in the building integrated photovoltaic/thermal (BIPV/T) systems: An updated review. Renewable and Sustainable Energy Reviews 170, 112988, (2022).

16. Argiriou, A.A., Lykoudis, S.P., Balaras, C.A., Asimakopoulos, D.N.: Experimental Study of a Earth-to-Air Heat Exchanger Coupled to a Photovoltaic System. Journal of Solar Energy Engineering 126, 620-625 (2004).

17. Nayak, S., Tiwari, G.N.: Theoretical performance assessment of an integrated photovoltaic and earth air heat exchanger greenhouse using energy and exergy analysis methods. Energy and Buildings 41, 888–896 (2009).

18. Yildiz, A., Ozgener, O., Ozgener, L.: Exergetic performance assessment of solar photovoltaic cell (PV) assisted earth to air heat exchanger (EAHE) system for solar greenhouse cooling. Energy and Buildings 43, 3154–3160 (2011).

19. NASA POWER | Data Access Viewer. NASA. https://power.larc.nasa.goV/data-access-Viewer/, last accessed: 2022/09/30.

20. Arcos, V.M. Estudio experimental del desempeño térmico de un intercambiador de calor tierra-aire en la ciudad de Chetumal, Quintana Roo. Universidad de Quintana Roo (2016).

21. Moro, M. Instalaciones solares fotovoltaicas. Paraninfo. Madrid, España (2010).

22. Pareja, M. Energía Solar Fotovoltaica. Marcombo. Barcelona, España (2010).

23. Morillón, D., Escobedo, A., García, I. Retos y Oportunidades Para la Sustentabi-lidad Energética en Edificios de México: Consumo y Uso Final de Energía en Edificios Residenciales, Comerciales y de Servicio. Serie Investigación y Desarrollo, Instituto de Ingeniería-UNAM. México City, México. (2015).

24. Molina, R, G., Muñoz, A. C. Propuesta de Inversión de paneles solares para Py-mes en el Sureste de México. Revista Universitaria Ruta 22(1), 2-31 (2020).

25. SEMARNAT. FACTOR DE EMISIÓN DEL SISTEMA ELÉCTRICO NACIONAL 2021. https://www.gob.mx/cms/uploads/attachment/file/706809/aviso_fesen_2021.pdf   last   accessed: 2022/09/30.

PV and Storage System to reduce distribution network losses: a case study. [*]

Gustavo A. Gómez-Ramírez[1][0000−0001−9195−072X], Gonzalo Mora-Jiménez[2][0000−0001−9059−3388], Isaac A. Luévano-Reyes[3], Luis García-Santander[4][0000−0002−6474−6528], Markel Zubiaga Laskano[5], and Carlos Meza[6][0000−0002−7374−505X]

[1] Electromechanics Engineering School. Instituto Tecnológico de Costa Rica
[2] CENCE-Instituto Costarricense de Electricidad
[3] ETAP Latin America Support Manager and Instructor
[4] Electrical Engineering Department. Universidad de Concepción. Concepción, Chile
[5] Ingeteam R&D Europe S. L., 48170 Zamudio, Spain
[6] Anhalt University of Applied Sciences, Germany

Abstract. Low- and middle-income countries struggled to develop a reliable power system while investing in non-traditional renewable energy sources. Also, developing remote regions requires energy, especially in high-energy activities such as mining. Robust and high-quality power transmission and distribution infrastructure will, in many cases, help the reliability of a power system. Nevertheless, investing in power infrastructure might be too costly for some nations. In this paper, we analysed the case of a high-energy intensive power load located in an unreliable power distribution section of the Honduran power system. The power transmission losses and the voltage instability have produced several outages in this section. Using an electrical power system analysis software (ETAP), we simulated this section of the distribution system. The simulation results demonstrate that a PV plant and storage unit can reduce power transmission losses by up to 63 %. Moreover, with the addition of a capacitor compensationbank, the voltage levels achieve values above 0.98 pu.

Keywords: Load Management · Solar Energy · Storage · Power Generation · Power System Planning.

1   Introduction

Power grids are inherently heterogeneous and, if not developed in a planned manner, can lead to significant power imbalances that can affect their performance. This is even more severe in power grids with high impedance and low inertia generation power plants. Photovoltaic (PV) based distributed power generation can make imbalance problems more severe due to its intrinsic variability.

Use of technologies such as PV and wind in combination with storage (especially electro-chemical) have displaced non-renewable resource options in Transmission and Distribution grids (T&D). Variability of PV and wind resources must be compensated with the use of storage to guarantee the reliability and continuous operation.

Storage can provide ancillary services, congestion relief of the T&D, voltage regulation, and allow grid investment deferral [1-3]. Ancillary services, congestion relief of the T&D, and voltage regulation are problems that storage can solve in times of economic crisis. Also, instability problems can be resolved using storage if used strategically. Therefore, considering it as a power reserve is a reasonable option. Due to this, strategic planning can take into account distributed or concentrated options.

Storage use with distributed generation is an option to mitigate the effects previously mentioned and thus improve stability, reliability, and loadability, among others. In addition, works such as [4-8] have shown that distributed generation and storage can also help stability in power grids by improving system demand, increasing available power capacity, reserve, frequency regulation, energy availability in black starts, and load management.

However, it should be taken into account the costs and benefits towards the grid power. Furthermore, integrating distributed storage can bring environmental benefits, mainly because it can remove non-renewable generation (of transmission) and replace it with PV and wind generation if it is managed with storage.

Storage distributed penetration could increase the distribution generation if used with PV generation [7], [8]. In future, there will be a transition from a concentrated generation to a distributed generation supported by storage. This option may benefit the distribution system by improving power demand, increasing available power capacity, reserve, frequency regulation, energy availability in black starts, and load management. Benefits in power transmission comprise load management, line congestion and investment deferral (planning), voltage stability and regulation, and power quality.

The size of the storage system [7], [9], [10], so the costs and benefits will be a problem to be solved. Therefore, economic evaluation analysis methods should consider the benefits of storage, energy flows, battery degradation, and ancillary services, such as frequency regulation, seasonal storage, and power reserves [11-13] for sizing.

Strategies formulation to minimise the costs of acquiring electricity from storage have been proposed by researchers [14]. Nowadays, interconnection contracts are established for the power system taking into account storage and daily

energy management. Furthermore, second-life use (from electric vehicle batteries) can be greatly beneficial if used [15] as a complementary subsystem to PV generation, reducing the cost of storage.

Therefore, distributed storage combined with PV generation is a potential solution to take advantage of the benefits of distributed generation by improving and relieving the T&D system [16][17]. Furthermore, PV generation can increase its penetration if strategic storage is integrated to mitigate generation intermittency. Storage and PV generation can substitute traditional non-renewable generation, as reported in [18], for the microgrid in Sein Island (French Brittany).

Regarding Central American, Gomez et. al in [19] have identified the potential in the Central American region to use PV and wind generation with storage. In the same way, Honduras and El Salvador have been studied in [20] and [21], where storage is used to manage the power system's demand and improve voltage regulation. Such analysis requires considering power flows, battery degradation and the ancillary services, such as frequency regulation, seasonal storage, and power reserves [18-21].

The present article evaluates and identifies the benefits of using storage and distributed generation to reduce losses in weak power networks. The case analysed is taken from a current situation occurring in the Honduran network. The rest of the paper is structured as follows: Section 2 describes the study case, Section 3 presents the methodology. The results and discussions are presented in section 4 and the conclusions are shown in section 5.
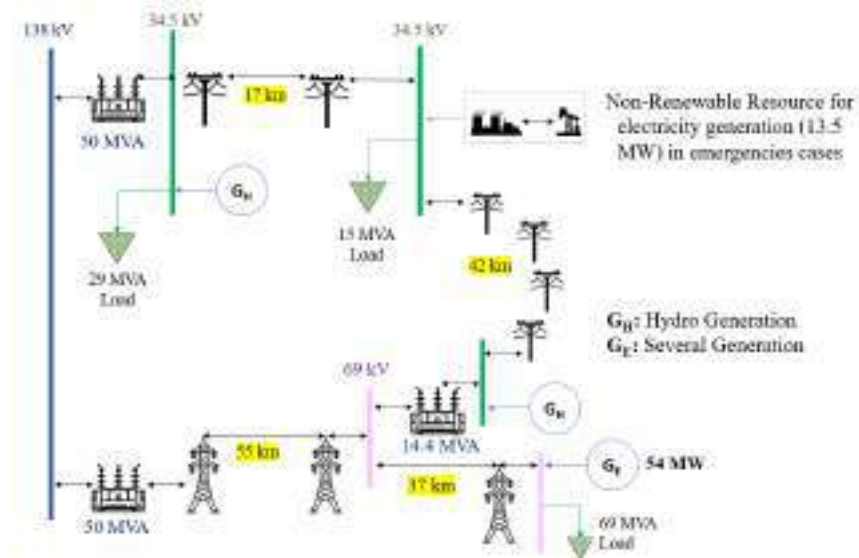
Fig. 1: Actual Power System

2   Study case

This article analyses the case of a constant power consumption point located in a section of a distribution network with high losses. The case is taken from an actual situation in the Honduras distribution network, as illustrated in Fig. 1. The power load is a mining facility that requires 15 MVA of power virtually 24/7 due to water pumping, illumination and the power of the other equipment needed to extract minerals.

Due to the nature of the mining facility, it is located relatively far from power generation sources. The two power distribution lines, labelled **Line254** and **Line256**, that power the load are 34.5 kV and at 17 km and are located at 42 km distance from the power sources, as shown in Fig. 1 and 2.

Due to the relative distribution lines length and the losses of the Honduran power system, several inconveniences have been reported, such as power outages and high distribution losses. Additionally, there is a fossil-fuel-based power generator to maintain the operation during a power outage.

Fig. 2: Electrical diagram of Power System using ETAP

3 Methodology

We develop a model of the section of the distribution line for the system under study. The model was constructed based on the information provided by one of the regional power companies, which also provided the values of the parameters of the transmission lines, transformers, power generators and other power grid elements. To evaluate a critical scenario, we use the maximum power demand curve for the Honduran power system for 2021. Fig. 2 shows the single-line diagram of the system under study.

Table 1: Power System Characteristics

Element	Description	Requirements
Power System		
	30-Bus	No
	25 T&D lines	No
	5 Generator	No
	10 Loads	No
	2 Capacitor of 3 MVAR	No
PV Generation		
	Irradiance: 811 W/m^2	Power Transformer
	Inverter: 480V/15.1 MW	12/15 MVA
	Capacity: 10.4 MW	0.48/34.5 kV
Storage System		
	Inverter: 7.5 MW/480V	Power Transformer
	Rated Voc: 947.2V	12/15 MVA
	Capacity: 4MW/36.4 MW h	0.48/34.5 kV

The distribution power system was modelled and analysed using the Electrical Transient Analyser Program (ETAP). ETAP is an engineering design and analysis program for power systems that have been used extensively for power generators [22], microgrids [23] and renewable energy [24]. A second model of the system was developed. In this case, a hypothetical 10 MW of PV plant with a 4 MW/36.4 MW h storage unit is added, as indicated in Fig. 3.

Table 1 shows the characteristics of the modelled power system and the requirements as indicated in Fig. 3. It is proposed to use two banks of 3 MVAR capacitors to have more reactive power from the storage system. The detected problem is low voltage due to the lack of MVAR support from power grid.

Hourly irradiation and simulation data was used to estimate the power generation profile of the PV system. The irradiance and temperature data from a typical meteorological day in Honduras were used using meteorological data from the National Solar Radiation Database (NSRDB) of the National Renewable Energy Laboratory.

The storage unit was programmed to supply reactive power and maintain voltage profiles at current operation values. Also, this unit constantly delivers
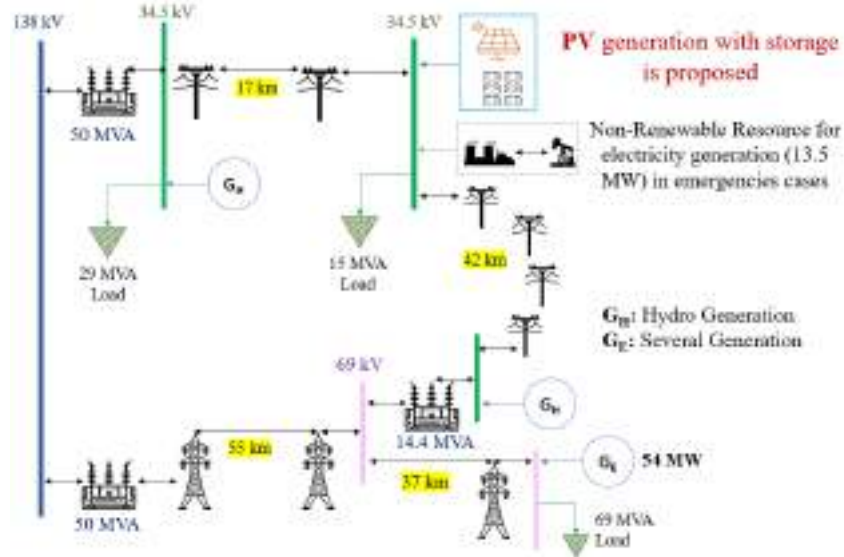
Fig. 3: Power System Proposed

power to the system (self-managed) when there is no solar generation to reduce the power transferred in the distribution lines. The PV plant delivers power to the grid and the storage unit. The storage unit and PV plant have been sized to reduce losses in the distribution lines.

4   Results

Fig. 4, 5, 6, and 7 present the comparison of the simulation results between the actual situation and the hypothetical case with PV generation and storage. The PV generation profile is shown in the yellow curve in Fig. 4, where the power flow to the storage unit is shown in green. When the power is negative it means that the storage unit is delivering power. Notice that in high irradiance conditions the PV plant delivers power both to the grid and the storage unit.

The green area in Fig. 5 represents the power loss reduction in distribution lines **254-sC** and **256-sC** that is achieved when the storage and PV plant are included due to the no-Compensation **sC** with proposed of storage. Notice that in this specific case, a maximal loss reduction of 66.4% is obtained (11 am) and the reduction are always greater than 30%. This figure also shows the current reduction obtained in both distribution lines (Line 254 and Line 256). On the other hand, the improvement of the performance in the curves **254-cC** and **256-cC** are observed. In this case, the system is compensated (**cC**) with proposed of section 3.
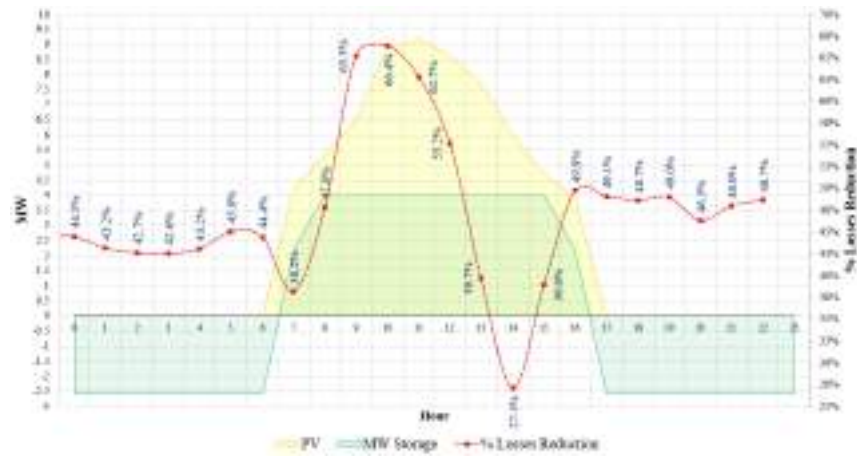
Fig. 4: Storage and PV Generation Management
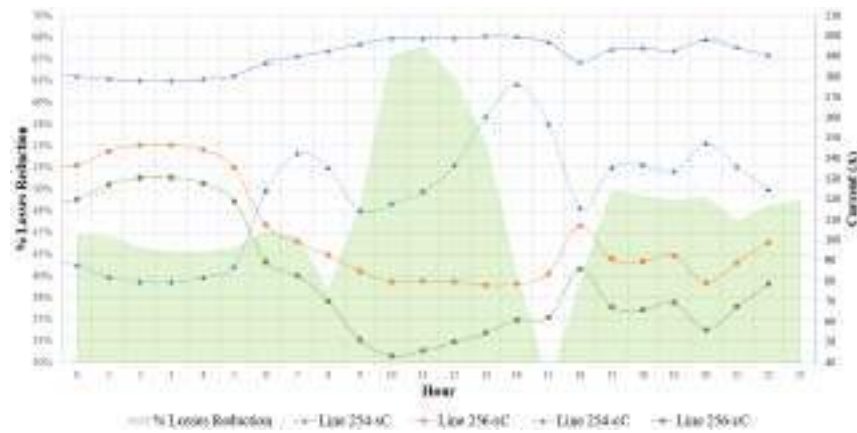
Fig. 5: Power loss reduction in the distribution lines. Current in the distribution lines in the actual situation (Line 254-sC, Line 256-sC) and including PV generation and storage (Line 254-cC, Line 256-cC)
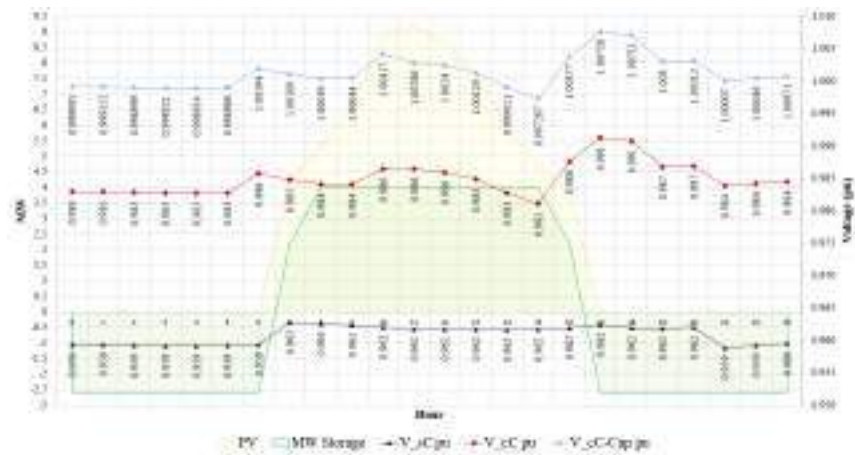
Fig. 6: Dynamic behaviour of the voltage on the bus that power the load. V_{sC} represents the voltage in the actual situation, V_{cC} the voltage with the storage unit and the PV plant and $V_{cC_{Cap}}$ the voltage with a storage unit, a PV plant and a capacitor bank).
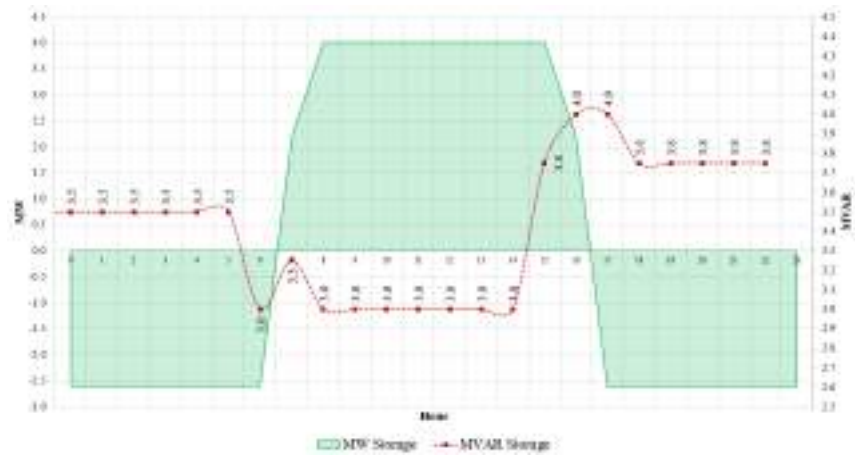
Fig. 7: Power Storage Management + Capacitor in 34.5 kV circuit

Fig. 6 depicts the voltage dynamics in the bus that power the load under study. For the actual case, a low voltage is observed (< 0.97 pu) in 24 hours (black line). When a storage unit and a PV plant is added the voltage dynamics improves. In this case, the voltage is always greater than 0.97. It is important to mention that the inverter was adjusted to deliverer reactive power to improve the voltage profiles.

To obtain more stable voltage values a static compensation was added. The voltage was compensated with a 3 MVAR and the inverter was allowed to supply the reactive power difference to maintain the voltage profiles near to 1 pu.

The results are shown in Fig. 6 with a light blue curve (**V_cC-Cap pu**). In this case the voltage was always greater than 0.99 pu. The power flow dynamics, both active and reactive, of this case is shown in Fig. 7. This figure shows the active and reactive power behaviour during *24 hour* profiles of the storage system. The system supply the demand and maintain the voltage over 0.99 pu.

As can be seen in Fig. 1, the current mining industry owns a fossil fuel-based power plant to provide electricity during power outages. In this regard, we have calculated the savings this industry may incur if they implement the proposed PV plant and storage unit.

Table 2: Non Renewable Generation Equivalent Cost

Substitution	Per Day (MW h)	Per Year (MW h)	Cost/Year (USD)
Power from PV	65.06	23421.60	2.34M
Power from storage	51.30	18460.00	1.84M
Avoid technical losses	0.18	1555.2	0.15M
Total	101.72	43436.8	4.34M

Table 2 shows the costs of generating energy with a fossil fuel-based power plant, *i.e.*, 4.34M USD per year. This cost was calculated taking into account the energy generated by the storage and PV system, *i.e.*, 101.72 MWh, losses was also considered. The price of electricity was taken from the projected value of the Network Operator (100 USD/MWh), [25].

5   Conclusion and future work

A section of the Honduran distribution system that presented voltage instabilities and high losses due to a relative electrical load was analysed by employing numerical simulations. This work demonstrated that including a photovoltaic system together with storage can significantly reduce the losses in the distribution line. For the case investigated the losses were reduced by more than 30% which represented 4.34M USD of cost-savings compared to the case in which this energy will have to be produced using fossil-fuel based generation.

Likewise, high-quality voltage levels can be obtained if a capacitor compensation bank is included. In future work, a procedure for the location and sizing of

storage in weak distribution grid will be determined. Also its economical benefits will be further analysed. Furthermore, a comparative techno-economic analysis of other options for solving the problem will also be carried out.

A distribution power grid presents excellent opportunities to use storage to improve system performance, reduce losses, and increase voltage profiles. The proposal in this article can contribute to relief T&D, giving planners time to prepare the grid for medium and long-term investments. PV Generation + storage offers opportunities in power systems to decarbonise power generation, especially when there is a significant dependence on non-renewable generation. PV generation and storage technologies can provide more advantages than fossil-fuel-based power generation.

It may consider the costs and benefits of penetration into the power grid. The self-sufficient power generation can be an opportunity to reduce the centralised generation so that, focusing on the load, the possibilities for improving performance are highest and unlimited.

References

1. IEEE-PES, Energy Storage Opportunities and Research Needs' (The Industry Technical Support Leadership Committee-IEEE, 2020)
2. Batarseh, Issa and Alluhaybi, Khalil: 'Emerging opportunities in distributed power electronics and battery integration: setting the stage for an energy storage revolution', IEEE Power Electronics Magazine, 2020, 7, (2), pp 22–32
3. Bistline, John et al.: 'Energy storage in long-term system models: a review of considerations, best practices, and research needs', Progress in Energy-IOP Publishing, 2020, 2, (3).
4. Burger, Scott P. et al.: 'Why Distributed?: A critical review of the tradeoffs between centralized and decentralized resources', IEEE Power and Energy Magazine, 2019, 17, (2), pp 16–24
5. Guney, Mukrimin Sevket and Tepe, Yalcin: 'Classification and assessment of energy storage systems', Renewable and Sustainable Energy Reviews-ELSEVIER, 2017, 175, pp 1187–1197
6. Iweh, Chu et al.: 'Distributed Generation and Renewable Energy Integration into the Grid: Prerequisites, Push Factors, Practical Options, Issues and Merits', Energies, 2021, 14, (17), pp 1996–1073
7. Gunter, Niklas and Marinopoulos, Antonios: 'Energy storage for grid services and applications: Classification, market review, metrics, and methodology for evaluation of deployment cases', Journal of Energy Storage-ELSEVIER, 2016, 8, pp 226–234
8. Lai, Chun Sing, et al.: 'A review on long-term electrical power system modeling with energy storage', Journal of Cleaner Production-ELSEVIER, 2021, 180, pp 1–9

9. Yang, Yuqing et al.: 'Battery energy storage system size determination in renewable energy systems: A review', Renewable and Sustainable Energy Reviews-ELSEVIER, 2018, 91, pp 109–125

10. Hesse, Holger C. et al.: 'Lithium-ion battery storage for the grid—A review of stationary battery storage system design tailored for applications in modern power grids', Multidisciplinary Digital Publishing Institute-ENERGIES, 2017, 10, (12).

11. Sperstad, Iver Bakken, et al.: 'Cost-Benefit Analysis of Battery Energy Storage in Electric Power Grids: Research and Practices'. 2020 IEEE PES Innovative Smart Grid Technologies Europe (ISGT-Europe), 2020, pp. 314–318

12. Nikolaidis, Pavlos and Poullikkas, Andreas: 'Cost metrics of electrical energy storage technologies in potential power system operations', Sustainable Energy Technologies and Assessments-ELSEVIER, 2018, 25, pp 43–59

13. Argyrou, Maria C. et al.: 'Energy storage for electricity generation and related processes: Technologies appraisal and grid scale applications', Renewable and Sustainable Energy Reviews-ELSEVIER, 2018, 94, pp 804–821

14. Kim, Jun-Mo, et al.: 'Power Conversion System Operation to Reduce the Electricity Purchasing Cost of Energy Storage Systems', Multidisciplinary Digital Publishing Institute-ENERGIES, 2021, 14, (16)

15. Deng, Youjun, et al.: 'Operational Planning of Centralized Charging Stations Utilizing Second-Life Battery Energy Storage Systems', IEEE Transactions on Sustainable Energy, 2020, 12, (1), pp 387–399

16. Cheng, Feng et al.: 'Applying battery energy storage to enhance the benefits of photovoltaics'. 2012 IEEE Energytech, 2012, pp. 1–5

17. Hill, Cody A., et al.: 'Battery Energy Storage for Enabling Integration of Distributed Solar Power Generation', IEEE Transactions on Smart Grid, 2012, 3, (2), pp 850–857

18. Lancel, Gilles et al.: 'Energy storage systems (ESS) and microgrids in Brittany islands', CIRED-Open Access Proceedings Journal, 2017, 1, pp 1741–1744

19. Gómez-Ramírez, Gustavo Adolfo et al.: 'Oportunidades y desafíos para la integración de almacenamiento electroquímico en las redes eléctricas centroamericanas', Revista Tecnología en Marcha, 2021

20. Gómez-Ramírez, Gustavo A. et al.: 'Demand Response Improvement using Storage Power Systems: Case study of Honduras'. 2021 IEEE CHILEAN Conference on Electrical, Electronics Engineering, Information and Communication Technologies (CHILECON), Santiago, Chile, Dec 2021, pp. 1–6

21. Gómez-Ramírez, Gustavo A and Meza, Carlos: 'Challenges of Storage in Large Power Systems', Revista Tecnología en Marcha, 2021, pp 95–105.

22. Waqfi, Rashed R. and Nour, Mutasim: 'Impact of PV and wind penetration into a distribution network using Etap', 7th International Conference on Modeling, 2017.

23. A. Sharma and B. K. Panigrahi: 'Phase Fault Protection Scheme for Reliable Operation of Microgrids,' IEEE Transactions on Industry Applications, vol. 54, no. 3, pp. 2646-2655, May-June 2018

24. E. G. Luna, R. F. Manrique and E. L. Palacios Bocanegra: 'Monitoring and Control System Using ETAP Real-Time on Generation Plant Emulation Using OPAL-RT,' 2018 IEEE ANDESCON, 2018, pp. 1-6

25. Operador del Sistema Honduras, 'Plan Indicativo de Expansión de la Generación 2022 – 2031' (GERENCIA DE PLANIFICACIÓN DEL SISTEMA)

Technical-Economic Study of the replacement of internal combustion motorcycle taxis by electric motor motorcycle taxis using RETScreen Software in the city of Lima, Peru

Estefani Gabriela Mendoza Guerra [1][0000-0001-5028-9816] and Guillermo Pérez [2][1001-14-1289533]

[1]Universidad Nacional de Ingeniería, Lima Perú

[2]Escuela Politécnica Nacional, Quito, Ecuador

[1]estefani.mendoza.g@uni.pe

[2]guillermo.perez.ee@gmail.com

Abstract: This work reports a proposal for the implementation of motorcycle taxis with electric motor in the city of Lima, Peru with the purpose of replacing motorcycle taxis with internal combustion engine. To this end, a compilation of information has been made from cities of interest that have committed themselves and have taken steps to improve the quality of life and preserve the environment by reducing CO_2 emissions. It is necessary to determine the amount of motor vehicles (mototaxis in Lima), characteristics and/or differences between mototaxis with electric motors and internal combustion mototaxis, calculation of greenhouse gas emissions. The implementation is carried out through simulation with the RetScreen Expert software, the number of mototaxis units in the city of Lima is entered, and the technical parameters of mototaxis with internal combustion (base case) and mototaxis with motor electrical (proposal case) with the purpose of doing a feasibility study, both technical and economic.

Keywords: Mototaxi, electric motor, internal combustion engine, emissions, RetScreen Expert, simulation.

1. Introduction

Our country has not been oblivious to the phenomenon of electromobility. In recent years, some incipient advances have been developed that include, among others, the approval of tax reductions to the selective consumption tax (ISC), the presentation of commercial and mining bus drivers, and the pilot electrification of motorcycle taxis in Pucallpa [1] .

However, due to the increase in population and the concentration of inhabitants in the capital (Lima) according to the National Institute of Statistics and Informatics (INEI), according to

population estimates and projections as of June 30 of this year, the population of the province of Lima, that is, the 43 districts that comprise it, reaches 10 million 4 thousand 141 inhabitants, which represent 29.9% of the projected population of Peru (33 million 396 thousand 698 habitants)[2], therefore, Lima is more vulnerable to the consequences of poor management of public transport (traffic), environmental pollution, lack of parking and high passages.

In the year 2022 the most congested country in the world was Peru, with the capital Lima being particularly known for its traffic problems. The country scored low across the board, but particularly when it came to the average congestion level of 42%, meaning a trip here would take 42% longer than it would without traffic [3].

Table 1: Ranking of the slowest countries in the word [3]

N	Country	Averege congestion level	Average days with low traffic	Highest speed limit (km/h)	Road quality score/7	Numbeo traffic Index score	Overall traffic score /10
1	Perú	42.0%	144.0	100	3.2	216.4	2.28
2	Colombia	53.0%	116.0	100	3.4	198.2	2.40
3	Filipinas	53.0%	128.0	100	3.7	192.9	2.48
4	Indonesia	36.0%	141.0	100	4.2	195.5	3.35
5	India	48.3%	124.5	120	4.5	205.2	3.46
6	Brasil	27.7%	102.1	110	3.0	175.6	3.99
7	México	36.0%	139.0	120	4.5	176.1	4.20
8	Argentina	24.0%	153.0	130	3.6	169.8	4.43
9	Rumania	42.0%	66.0	130	3.0	125.8	4.76
10	Tailandia	44.0%	44.0	120	4.4	178.8	4.79

In Table 1 the Numbeo traffic index score is a score that takes into account time spent in traffic, dissatisfaction with time spent, CO_2 consumed in traffic, and general inefficiencies in the traffic system. , according to Numbeo , with a lower score being better [3].

At least 600 thousand motorcycle taxis circulate without control in the capital, of this total 40% do so informally; this was determined by a study by the NGO Luz Ambar with data from the National Federation of Motorcycle Taxi Drivers [4]. So much informality in this type of public transport is due to the fact that the municipalities do not control this service [4]. A fleet of motorcycle taxis with an electric motor, in addition to reducing the emission of greenhouse gases (GHG), can also be considered a start of order and registration of the units, in order to offer a clean and formal transport service.

Considering that motorcycle taxis are used in other countries such as: Cuba with the name of cocotaxis [5]; El Salvador, Honduras and Guatemala known as Tuc tuc [6].

On the other hand, in Peru, three-wheel tricycles contributed 36.7% of sales of minor vehicles in January, although they fell 10.4% compared to January 2018. The top 10 of this segment used mainly for the transport of passengers and merchandise (mototaxis) was made up of Bajaj, Motokar/Honda, Zongshen, TVS, Wanxing, GM23/TTGM23, ZEUZ2211, Katsumoto, Raudo and Lifan [7] .

Carbon dioxide (CO_2) is the main greenhouse gas emitted as a result of human activities. The main human activity that emits CO_2 is the combustion of fossil fuels (coal, natural gas and oil) to generate energy and for transportation purposes, although certain industrial processes and changes in land use also emit CO_2 [8].
In Figure 1 it can be seen that the GHG emission by the transport sector is 14% [9].
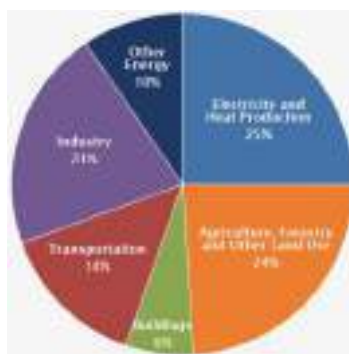
Figure 1: Global GHG emissions by economic sector, year 2014[9]

Figure *2* provides information on annual energy-related CO_2 emissions by sector and region for the reference case and the REmap case per year.[10], the transport sector for the year 2050 it is appreciated that for the energy scenario there will be an emission of 9633 Mt/yr compared to the energy transformation scenario of the same year with 2410 Mt/yr and the 1.5 C scenario that indicates 372 Mt/yr of CO_2 emission.
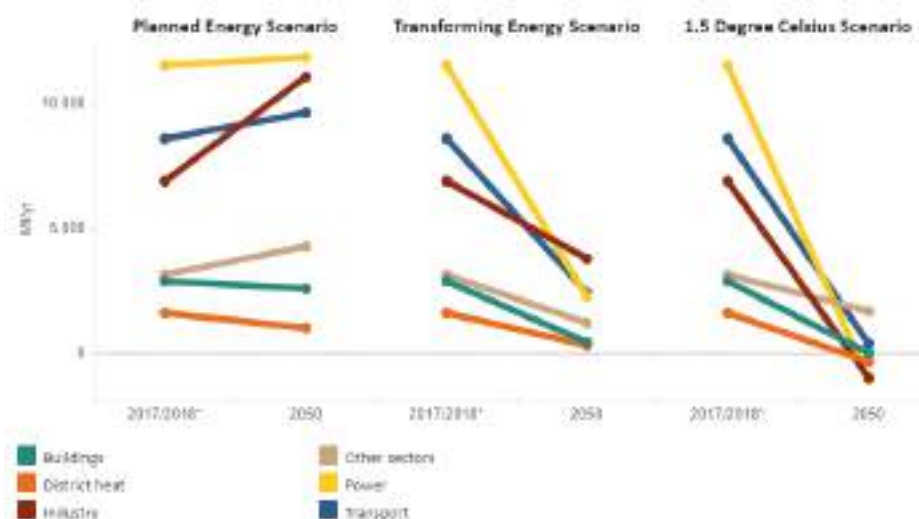
Figure 2 : REmap Emisiones relacionadas con la energía [10].

By promoting electromobility, by replacing units with internal combustion engines, we are directly participating in the reduction of CO_2 emissions, which is why it is important to involve everyone through talks, training, conferences, etc. This paper wants to simulate through the RETScreen Expert software the implementation of electric motorcycles by combustion engine motorcycles, in order to determine if it is technically and economically viable.

2. Theoretical Framework

2.1. Classification of electric vehicles [11]:
- BEV are battery electric vehicles
- PHEV are plug-in hybrid electric vehicles.

- FCEV are fuel cell electric vehicles.

2.2. Internal combustion engine:

Internal combustion engines are thermal fluid-mechanical machines in which, through the combustion of a mixture of fuel and air, mechanical energy is generated. All work processes take place in one work area, in the work cylinder. **Table 2** compares the engines: 2-stroke gasoline, 4-stroke gasoline and 4-stroke diesel [12].

Table 2: Engine comparison: 2-stroke gasoline, 4-stroke gasoline and 4-stroke diesel [12].

	2-stroke gasoline engine	4-stroke gasoline engine	4-stroke diesel engine
Charge	air fuel mixture	air fuel mixture	fresh air
Fuel supply	carburetor	carburetor	injection nozzle
Switched on	spark	spark	compression
Compression ratio	5...8	5...12	14...21
Air-fuel ratio	0.8...1.2	0,.8...1.2	1.5...10
Fuel	gasoline	gasoline	diesel

2.3. Technical characteristics of mototaxi models:

Technical characteristics in [13] , according to mototaxis model:

According to the Ministry of Transportation and Communications of Peru, the physical characteristics of the units are as follows: they measure an average of 2 meters long by 1.8 meters wide and 1.70 meters high, with a net weight of 250 kg and a load capacity of 350 Kg. The maximum speed it can reach is approximately 50 Km/h [14].

Table 3: Characteristics of mototaxi models [13]

	TORITO CROM UG GLP	TORITO 2T UG GSL	TORITO 2T UG-GLP
Power	9.32 Hp a 5000 RPM	8.44 Hp a 4000 RPM	8.58 Hp a 5000 RPM
Torque	16 NM a 3500 RPM	17 NM a 3000 RPM	15 NM a 3300 RPM
Engine	198.88 cc/DTS-i	145.45 cc	145.55 cc

For comparative purposes, a Mijie brand mototaxi of Chinese origin is considered, more detail in the **Table 4**.

Table 4: Detail of Tuk Tuk with 72V 3kW three wheel electric mototaxi [15]

Tuk Tuk with 72V 3kW three wheel electric mototaxi [15]		
Factory	Measures	Battery
Use for: Passenger Driving type: Electric Body Type: Closed Power:> 800W Voltage: 72V Brand:Mijie Place of Origin: Fujian, China Model: MJ168	Dimensions:3060*1500*1710mm Net weight: 600KGS Loading weight: 400KGS Speed: 55-60KM Maximum capacity: 30% Driver and passengers: 3-4 Power Type: Brushless Differential DC Motor Brake: Hydraulic Disc Parking Brake: Rear Mechanical Parking Brake Cable Gearbox: Automatic Transmission: Automatic Tires: 145-70R-12/155-65R-13	Operating voltage 72 V Capacity (80AH/100AH/120AH)

2.4. RETScreen Expert

The RETScreen Clean Energy Management Software platform enables low-carbon planning, implementation, monitoring and reporting [16].

Fuel Calorific Value: The calorific value is the energy contained in the fuel per unit mass or volume. It is necessary to know 100% of the energy contained in the fuel, how much is transformed into mechanical energy or torque and revolutions per minute.

For the modeling, the heating value of gasoline equivalent to 43.3 MJ/kg is considered, which a value that the software delivers directly is. The reference values of the calorific value for gasoline in Peru are 42.8 MJ/kg[21]

Internal combustion vehicle performance indicator: This value depends on environmental conditions, type of road, acceleration, number of passengers and distance travelled. For this reason, it is necessary to know how many liters of gasoline it consumes per 100 km of travel (L/100 km).

Electric vehicle performance indicator: The performance of an electric vehicle will depend on the electrical power of the motor and the time it will take to travel 100 km. In this way, the electrical kWh consumed to travel the 100 km (kWh/100 km) is considered [21] .

2.5. Fuel price and electricity rate

To run the simulation in the RETScreen Expert software, the data of the Torito CROM UG GLP motorcycle taxi with combustion engine and the MIJIE model MJ168 motorcycle taxi with electric motor were entered, since they have speed, size, number of passengers; except that the mototaxi with electric motor bears more net weight and cargo weight. The simulation will allow to determine if there is a saving in energy consumption and if the project is technically, environmentally and economically viable.

The prices are shown from 13-Jun-2022 to 19-Sep-2022The mean value during this period was 6.05 (Peruvian New Sol) with a minimum of 5.26 (Peruvian New Sol) to 12-Sep-2022 and a maximum of 6.63 (Peruvian New Sol) to 27-jun-2022. For comparison, the average price of gasoline in the world for this period is 7.66 (Peruvian New Sol) and the values in USD as of 19-Sep-2022 per liter is 1.356 USD and per gallon is 5.133 USD [17] .

The tariff schedule considered for residential North Lima corresponds to 0.6481 Soles per kWh, which is equivalent to 0.16 USD [18].

Under certain operating conditions, a motorcycle can have an approximate performance of up to 35 km per liter of gasoline (if it is for passengers), while a car can travel approximately 10 to 24 km per liter [19]. It is necessary to note that if we compare with the electric motorcycle taxi [20] "Elfi Motors TA-3" with a 2.5 Kw AC motor, a range of 120 to 150 km is obtained with a battery charging time between 6-8 hours, however, due to price issues, the model in Table 4 is selected.

3. Simulations

The modeling of the technical, economic and environmental feasibility is carried out with the help of the RETScreen Expert version 8.1.2 software considering the following parameters:

3.1. Technical analysis

The comparison of two vehicles with the same characteristics and capacity with different energy source and to supply the same travel distance is made. For the base case, a vehicle with an internal

combustion engine is considered, and in the proposed case, a vehicle with an electric motor, its energy demand is calculated in each case [22].

The calculation of the energy demand in the vehicle consider the following variables:
- ✓ Type of vehicle
- ✓ Average anual travel distance (X_p)
- ✓ Number of vehicles($N°$)
- ✓ Type of fuel
- ✓ Lower heating value (PCI)
- ✓ Vehicle performance with internal combustion engine (R_{CI})
  - • Per vehicle (L/100 km)
  - • Per passenger (L/ N°*100 km)
  - • Per weight or freight (L/kg*100 km)
- ✓ Vehicle performance with electric motor (R_{ME})
  - • Per vehicle (kWh/100 km)
  - • Per passenger (kWh/ N°*100 km)
  - • Per weight or freight (kWh/kg*100 km)
- ✓ Average annual fuel consumption (D_c)
- ✓ Annual energy demand ($DE_{vehículo}$)
- ✓ Energy saving (kWh)

$$DE_{vehicle\,CI}\left(\frac{kWh}{year*vehicle}\right) = X_p\left(\frac{km}{year}\right) * R_{CI}\left(\frac{L}{100km}\right) * PCI\left(\frac{kWh}{L}\right)$$

$$D_c\left(\frac{L}{year}\right) = X_p\left(\frac{km}{year}\right) * R_{CI}\left(\frac{L}{100km}\right) * N^{\underline{o}}$$

$$DE_{total\,CI}\left(\frac{kWh}{year}\right) = DE_{vehicle\,CI}\left(\frac{kWh}{year*vehicle}\right) * N^{\underline{o}}$$

$$DE_{vehicle\,ME}\left(\frac{kWh}{year*vehicle}\right) = X_p\left(\frac{km}{year}\right) * R_{ME}\left(\frac{kWh}{100km}\right)$$

$$DE_{total\,ME}\left(\frac{kWh}{year}\right) = DE_{vehicle\,ME}\left(\frac{kWh}{year*vehicle}\right) * N^{\underline{o}}$$

$$AE_{total}\left(\frac{kWh}{year}\right) = DE_{total\,CI}\left(\frac{kWh}{year}\right) - DE_{total\,ME}\left(\frac{kWh}{year}\right)$$

$$\%AE_{total}\left(\frac{kWh}{year}\right) = \frac{AE_{total}\left(\frac{kWh}{year}\right)}{DE_{total\,CI}\left(\frac{kWh}{year}\right)} * 100$$

3.2. Environmental analysis

The model proposes the calculation of the reduction of greenhouse gases (GHG) by replacing gasoline consumption with electricity from power generation plants. For the estimation of greenhouse gases, the following elements are considered:

- ✓ Combustion produces not only carbon dioxide, but also methane and nitrous oxide, however, a total equivalent value is presented in only carbon dioxide according to its "global warming potential" (GWP).

- ✓ The model considers the values of the Intergovernmental Panel on Climate Change (IPCC) differentiated by country and type of fuel: gasoline and electric.
- ✓ Losses due to transmission and distribution (T&D) of electrical energy are considered, from the generation plant to the point of supply to the electric vehicle.

GHG emission reduction: Gasoline to electricity

The model calculates the greenhouse gases of each case and the difference is considered as the GHG avoided to the atmosphere.

The amount of GHG will depend on the total energy demand and its emission factor based on the type of fuel consumed.

In the case of electrical energy consumption, transmission and distribution losses are considered up to the final point of consumption of the electric vehicle [22].

$$GEI_{gasoline} = (e_{base})DE_{gasoline}$$

$$GEI_{electric} = (e_{prop})DE_{electric}(1 - \lambda_{prop})$$

$$\Delta_{GEI} = (GEI_{gasoline} - GEI_{electric})(1 - e_{cr})$$

Where:

e_{base}, gasoline emission factor (ton CO_2/kWh thermal)

e_{prop}, electric energy emission factor (ton CO_2/kWh electric)

$DE_{gasoline}$, energy demand through gasoline consumption (kWh thermal)

$DE_{electric}$, demand for electrical energy (kWh electric)

λ_{prop}, losses due to transmission and distribution of electrical energy (%)

e_{cr}, rate or benefit for GHG emission reduction (%)

Δ_{GHG}, reduction to the environment (ton CO_2)

3.3. Economic and financial analysis

To carry out the economic-financial analysis, the unit cost of each energy source and the total energy demand of the internal combustion vehicle and the vehicle with an electric motor are considered. The model obtains the economic-financial profitability of the proposal by replacing the gasoline vehicle with a vehicle with an electric motor.

To calculate profitability, the following premises are considered:

- ✓ The initial investment year is year 0
- ✓ Costs and credits are given in terms of year 0, so the inflation rate applies from year 1 onwards
- ✓ Synchronization of cash flows occurs at the end of the year

The following **Table 5** summarizes the calculation of the necessary components to evaluate the profitability of a project:

Table 5: Equations for economic analysis *[22]*

Name	Equation	Nomenclature
Debt payment	$D = Cf_d \dfrac{i_d}{1 - \dfrac{1}{(1 + i_d)^N}}$	C, total initial cost of the project f_d, debt ratio i_d, bank interest rate N, duration of debt D, debt payment
Asset depreciation	$CCA_0 = C(1 - \partial)$ $CCA_n = \dfrac{C\partial}{N_d}$	∂, depreciation tax base used to specify how much of the initial costs are capitalized and can be depreciated for tax purposes. The portion that is not depreciated is considered fully spent during the year of construction (year 0). N_d, depreciation period C, total inversion CCA_0, zero year depreciation CCA_n, depreciation in subsequent years
Internal rate of return (IRR)	$0 = \displaystyle\sum_{n=0}^{N} \dfrac{C_n}{(1 + IRR)^n}$	C_n, cash flow for year n N, project life in years IRR, internal rate of return
Simple recovery period – PayBack (PB)	$PB = \dfrac{C - IG}{C_n}$	IG, incentives and subsidies C, total inversion C_n, cash flow for year n PB, Simple PayBack
Net Present Value (NPV)	$NPV = \displaystyle\sum_{n=0}^{N} \dfrac{C_n}{(1 + r)^n}$	r, discount rate N, project life in years C_n, cash flow for year n NPV, Net present value
Annual Life Cycle Savings (ACV)	$ACV = \dfrac{NPV}{\dfrac{1}{r}\left(1 - \dfrac{1}{(1 + r)^N}\right)}$	r, discount rate N, project life in years NPV, Net present value ACV, annual life cycle savings
Cost benefit relation	$B/C = \dfrac{NPV + (1 - f_d)C}{(1 - f_d)C}$	f_d, debt ratio C, total inversion NPV, Net present value B/C, cost benefit relation
GHG emission reduction cost	$GE_{GHG} = -\dfrac{ACV}{\Delta_{GHG}}$	ACV, annual life cycle savings Δ_{GEI}, reduction of GHG to the environment (ton CO_2) GE_{GHG}, GHG reduction cost

4. Results

4.1. Location:

For this simulation, 100 000 internal combustion mototaxis units located in Lima Peru are considered.

4.2. The yields considered for modeling are the following:
✓ Motorcycle with internal combustion engine: 2.86 l/100 km
✓ Motorcycle with electric motor: 4.1 kWh/100 km

The modeling considers an annual average route for each case equal to 12 000 km per year, in addition, the proposal to replace 100 000 internal combustion motorcycles with electric motors is considered.

4.3. Technical analysis

Once the corresponding values have been entered, a current energy demand of 304 755 MWh/year is obtained, or what is equivalent to the consumption of 9 066 385 gal/year. For the proposed case, when making the change for equipment that has higher energy efficiency, a new energy demand equal to 49 200 MWh/year is proposed. This proposal allows us a significant energy saving that represents 83.9% see Figure 3 and Table 6
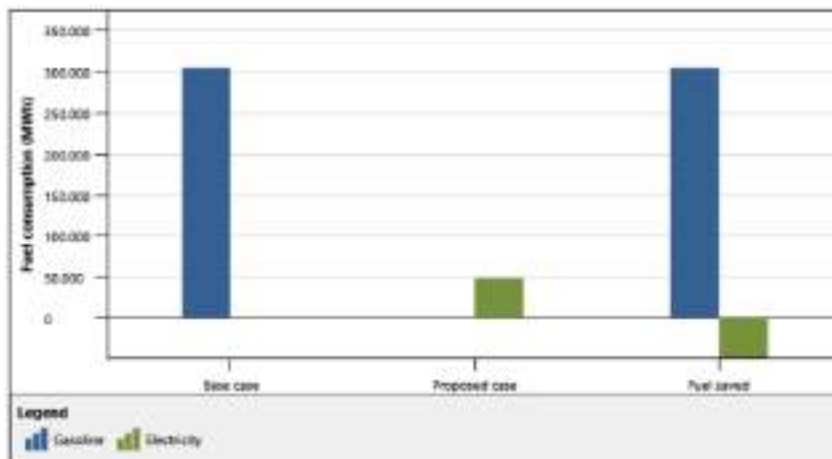
Figure 3: Summary of fuels *[22]*

Table 5 shows the summary of energy savings in kWh when comparing the base case (internal combustion mototaxis) and the proposed case (electric motor mototaxis).

Table 6: Energy savings in kWh *[22]*

Fuel consumption	Total kWh
Base case	304.755.207
Proposed case	49.200.000
Fuel saved	255.555.207
Fuel saved - percent	83.9%

4.4. Environmental analysis

Figure 4 shows the emission of greenhouse gases, obtaining a gross annual reduction of 85.5%, considering that the base case emits 72 621.4 tCO_2 and with the proposed case 10 544.9 tCO_2, the emission is avoided. of 62 076.5 tCO_2, which represents 5 709 Ha of forest absorbing carbon. Therefore, the software allows us to affirm that it is an environmentally attractive project and very viable if the importance of reducing greenhouse gases is considered.
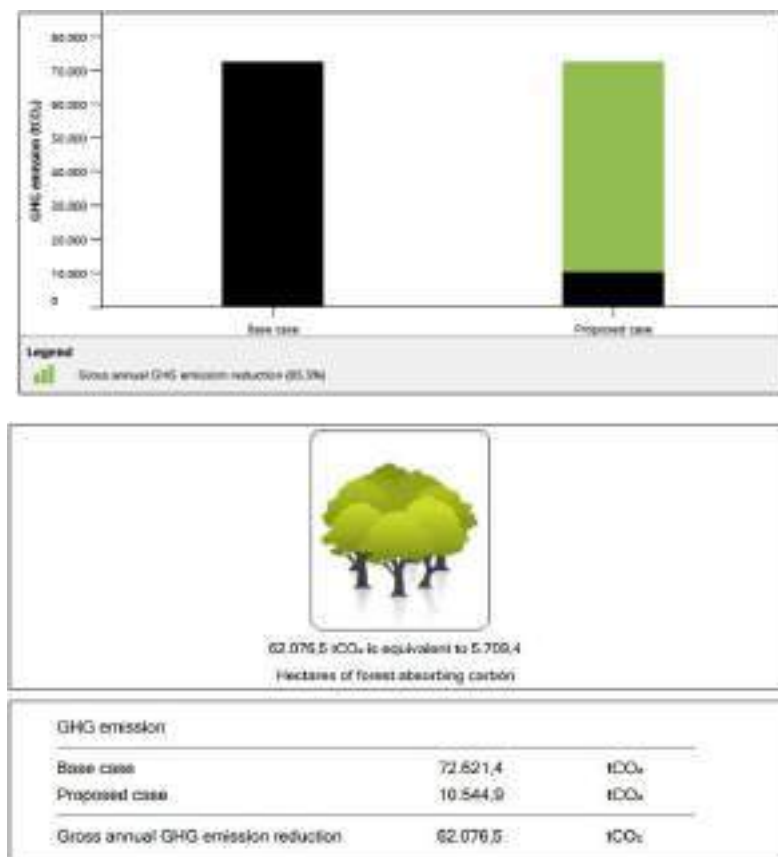
Figure 4: GHG emissions *[22]*

4.5. The economic and financial analysis

Considers an initial investment required of USD 250 000 000 for the acquisition of 100 000 electric motorcycle taxis, which represents a unit cost per electric motorcycle taxi equal to USD 2 500.

This modeling considers an economic saving due to the difference in maintenance costs between the internal combustion motorcycle and an electric motorcycle equivalent to 18 000 000 USD per year for 100 000 motorcycles. In addition, the economic savings due to the decrease in energy demand are considered, considering the following unit costs in the city of Lima-Peru:

Gasoline cost: 5.13 USD/gal = 0.15 USD/kWh

Electricity cost: 0.16 USD/kWh

As can be seen, the unit cost of electricity is greater than the unit cost of gasoline, however, as there is significant energy savings, it generates economic savings.

This analysis considers the financing option of 60% of the total investment through the acquisition of a bank loan with an interest rate of 12% for 10 years.

In addition, a fuel escalation rate of 0.5% per year is considered, with a local inflation rate of 7%, with a referential discount rate of 20%, during the 10-year life of the project.

An important variable to consider is the depreciation of the motorcycles, for this reason, a linear depreciation of 100% of the capital during the 10 years is considered, see Table 7.

Table 7: Financial parameters *[22]*

General		
Fuel cost escalation rate	%	0.5%
Inflation rate	%	7%
Discount rate	%	20%
Reinvestment rate	%	20%
Project life	yr	10
Finance		
Debt ratio	%	60%
Debt	USD	150.000.000
Equity	USD	100.000.000
Debt interest rate	%	12%
Debt term	yr	10
Debt payments	USD/yr	26.547.625
Income tax analysis		
Effective income tax rate	%	0%
Loss carryforward?		No
Depreciation method		Straight-line
Depreciation tax basis	%	100%
Depreciation period	yr	10

Figure 5 shows a return on investment from year 3, for which the support of the government is essential and thus provide an attractive offer to motorcycle taxi drivers in order to commit to caring for the environment using motorcycle taxis with electric motors.
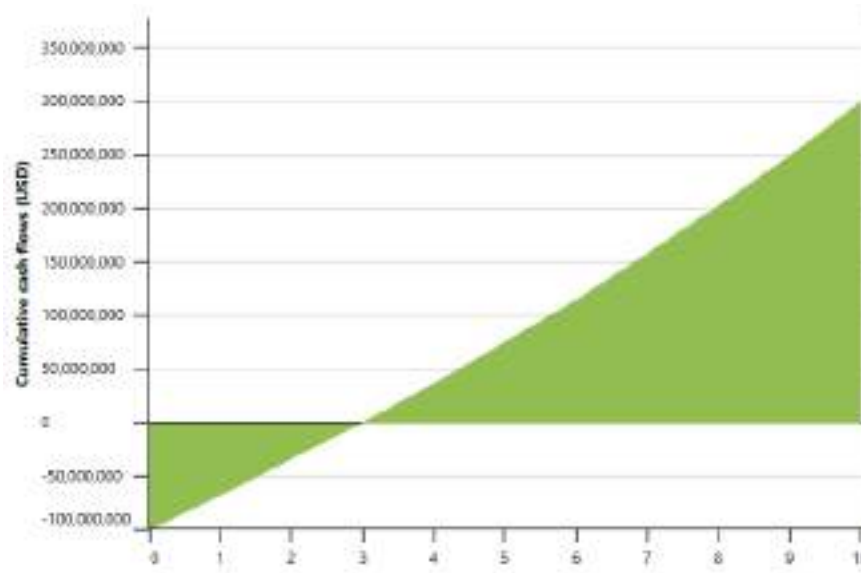
Figure 5: Cumulative Cash Flow *[22]*

5. Discussion

Obtaining a gross annual reduction of 85.5%, through simulation in the RetScreen Expert software, considering that the base case (internal combustion motorcycle taxi) emits 72 621.4 tCO_2 and with the proposed case (electric motorcycle taxi) the emission of 10 544.9 tCO_2. the emission of 62 076.5 tCO_2 is avoided, which represents 5 709 Ha of forest absorbing carbon, it is concluded that it is environmentally viable.

The return on investment is in the time of 4.4 years, likewise if a green bond is obtained, the time of return on investment can be reduced, it is very important that the government promote incentives and investment in motorcycle taxis with electric motors to reduce the emission of greenhouse gases.

The government could choose to reduce the price of the kWh required by electric motorcycle taxis, not charge taxes if an electric motorcycle taxi is purchased, or finance the purchase of electric motorcycle taxis at 70%, in order to promote the use of electric motorcycle taxis.

Acknowledgment

References

[1] Organismo Supervisor de la Inversión en Energía y Minería, *ELECTROMOVILIDAD Conceptos, políticas y lecciones aprendidas para EL PERÚ*, Primera. Lima, Perú, 2019. [En línea]. Disponible en: https://www.osinergmin.gob.pe/seccion/centro_documental/Institucional/Estudios_Economicos/Libros/Osinerg min-Electromovilidad-conceptos-politicas-lecciones-aprendidas-para-el-Peru.pdf

[2] Instituto Nacional de Estadística e Informática, «Lima supera los 10 millones de habitantes al año 2022», *Instituto Nacional de Estadística e Informática*, 17 de enero de 2022. https://www.inei.gob.pe/prensa/noticias/lima-supera-los-10-millones-de-habitantes-al-ano-2022-13297/ (accedido 5 de septiembre de 2022).

[3] Moneybarn, «The Slowest Cities in the World | Moneybarn», *Slowest Cities*, 2022. https://www.moneybarn.com/slowest-cities/ (accedido 5 de septiembre de 2022).

[4] TVPerú, «El 40% de mototaxis en Lima son informales», *TVPerú*, Lima, Perú, p. 1, 19 de abril de 2019.

[5] *El imperio del MOTOTAXI en Perú ¿Dónde se originó y cómo llegó al país?*, (26 de julio de 2020). Accedido: 6 de septiembre de 2022. [En línea Video]. Disponible en: https://www.youtube.com/watch?v=CP0WY--ape8

[6] E. Quiñónez, «Qué son los tuc tuc y en qué países se usan», *República.gt*. https://republica.gt/vive-guatemala/que-son-los-tuc-tuc-y-en-que-paises-se-usan-20227216180 (accedido 6 de septiembre de 2022).

[7] Asociación Automotriz del Perú, «Las 10 principales marcas de motos y trimotos de enero», *Asociación Automotriz del Perú*, 16 de febrero de 2019. https://aap.org.pe/las-10-principales-marcas-de-motos-y-trimotos-de-enero/ (accedido 6 de septiembre de 2022).

[8] O. US EPA, «Emisiones de dióxido de carbono», 26 de marzo de 2021. https://espanol.epa.gov/la-energia-y-el-medioambiente/emisiones-de-dioxido-de-carbono (accedido 23 de septiembre de 2022).

[9] O. US EPA, «Global Greenhouse Gas Emissions Data», 12 de enero de 2016. https://www.epa.gov/ghgemissions/global-greenhouse-gas-emissions-data (accedido 23 de septiembre de 2022).

[10] International Renewable Energy Agency, «REmap Energy-related Emissions», */Statistics/View-Data-by-Topic/Energy-Transition/REmap-Annual-Energy-related-Emissions*. https://www.irena.org/Statistics/View-Data-by-Topic/Energy-Transition/REmap-Annual-Energy-related-Emissions (accedido 6 de septiembre de 2022).

[11] International Energy Agency, «Global EV Data Explorer – Data Tools», *IEA*. https://www.iea.org/data-and-statistics/data-tools/global-ev-data-explorer (accedido 6 de septiembre de 2022).

[12] Gunt Hamburg, «Motores de combustión interna». [En línea]. Disponible en: https://www.gunt.de/images/download/int_comb_engines_spanish.pdf

[13] A. / CASO, «Torito Bajaj». https://torito.com.pe// (accedido 6 de septiembre de 2022).

[14] Congreso de la República del Perú, *PROYECTO DE LEY N 4389 /2018-CR LEY QUE COMPRENDE A LOS CONDUCTORES DE VEHICULOS MOTOTAXIS Y SUS DERECHOHABIENTES AL SEGURO INTEGRAL DE SALUD (SIS)*. 2019. [En línea]. Disponible en: https://www.leyes.congreso.gob.pe/Documentos/2016_2021/Proyectos_de_Ley_y_de_Resoluciones_Legislativas/PL0438920190524.pdf

[15] «PASSENGER TAX». https://www.dongbenmotors.com/page/passenger-tax?gclid=Cj0KCQjwsrWZBhC4ARIsAGGUJuqNNKNEi9gl9i_AevJWUahzKyy7p3E5wZn7uFhBKmoiryt4dCmMnWMaAlh1EALw_wcB (accedido 23 de septiembre de 2022).

[16] N. R. Canada, «retscreen», 10 de marzo de 2010. https://www.nrcan.gc.ca/maps-tools-and-publications/tools/modelling-tools/retscreen/7465 (accedido 24 de noviembre de 2022).

[17] «Perú precios de la gasolina, 19-sept-2022», *GlobalPetrolPrices.com*. https://es.globalpetrolprices.com/Peru/gasoline_prices/ (accedido 27 de septiembre de 2022).

[18] «Pliego Tarifario Máximo del Servicio Público de Electricidad». https://www.osinergmin.gob.pe/Tarifas/Electricidad/PliegoTarifario?Id=150000 (accedido 27 de septiembre de 2022).

[19] «Rendimiento de un motocarro: ¿Qué tanto combustible gasta? - ATUL», *ATUL México*, 16 de enero de 2019. https://www.atul.com.mx/rendimiento-de-un-motocarro/ (accedido 27 de septiembre de 2022).

[20] Elfi Motors, «ELFi Motors Movilidad Ecológica a tu alcance.» [En línea]. Disponible en: https://elfimotors.com/wp-content/uploads/2019/08/TA3-elfimotors.pdf

[21] G. J. Tipián Tipián, «Análisis experimental del uso de mezclas etanol-gasolina en motores de encendido por chispa», Tesis para obtención de título en Ingeniería Mecánica, Pontificia Universidad Católica del Perú, Lima, Perú, 2015. Accedido: 6 de octubre de 2022. [En línea]. Disponible en: https://tesis.pucp.edu.pe/repositorio/handle/20.500.12404/6163

[22] RETScreen Expert, «RETScreen Expert engineering book». Natural Resources Canada, Canadá. [En línea]. Disponible en: www.retscreen.net

MPC for Active and Reactive Power Dispatch in Islanded Microgrids[*]

Juan G. Ordoñez[1][0000−0001−7418−3717], John
Barco-Jiménez[2,3,4][0000−0002−9152−2132], Andrés Pantoja[1][0000−0002−0196−3269],
Javier Revelo[1][0000−0002−2652−8351], and José A. Aguado[3][0000−0003−3954−3646]

[1] Departamento de Electrónica, Universidad de Nariño, Pasto, Colombia
`jgabriel@udenar.edu.co`, `ad_pantoja@udenar.edu.co`,
`javierrevelof@udenar.edu.co`
[2] PPIEE, Universidad del Valle, Santiago de Cali, Colombia
`john.barco@correounivalle.edu.co`
[3] Departamento de Ingeniería Eléctrica, Universidad de Málaga, Málaga, España
`jbarco@uma.es`, `jaguado@uma.es`
[4] Departamento de Ingeniería Electrónica, Universidad CESMAG, Pasto, Colombia
`jebarco@unicesmag.edu.co`

Abstract. The optimal power dispatch of a microgrid is a challenging problem that must be addressed to achieve technical and economic objectives. Besides, the power balance generation-demand must be satisfied considering that the renewable generators and loads have an intrinsic stochastic behavior. In this sense, this paper proposes an approach based on model predictive control (MPC) for the optimal dispatch of active and reactive power in isolated microgrids. Two optimization problems are formulated (for active and reactive power dispatches), where power flows are considered within the constraints of the controller, so that the solutions guarantee the convergence. The proposed algorithm solves the problems in sequence, optimizing operating costs, improving voltage profiles, reducing losses, and diminishing unsupplied demand. The validation is performed in a co-simulation scheme on a modified version of the IEEE 13-bus test Feeder.

Keywords: Active power dispatch · Microgrid · Model predictive control · Reactive power dispatch.

1 Introduction

Microgrids are small-scale distribution systems, mainly composed of distributed generators (DGs), energy storage units (SUs), and interconnected loads, which can operate connected or isolated from the main grid [10]. Therefore, microgrids are an efficient option to integrate renewable generation sources with conventional ones, reduce greenhouse gas emissions, and provide power to remote

populations far from the main grid [12]. However, for a microgrid to provide optimal and reliable power, it is necessary to perform power management that faces several technical and economic complexities [11].

Optimal power dispatch is among the critical and challenging problems that must be addressed to ensure efficient and low-cost operation [2]. As a solution to this problem, different optimization problems have been formulated and several solution methods have been proposed. Heuristic methods have been widely used due to the nonlinearity of dispatch problems. In [18] and [14], economic dispatch is performed using genetic algorithms and in [1,21,22] the problem is solved using particle swarm optimization (PSO). These methods do not require simplifications in the optimization problems, but they do not guarantee convergence to global optima and convergence times are high for real-time applications [6].

Other studies have proposed novel methods for the solution of dispatch problems. In [7], a distributed strategy based on the replicator dynamics method is proposed, and in [17], a recently developed linearization based on the Wirtinger calculus is used to guarantee the convergence of the interior point method. These methods present shorter convergence times and are applicable to large power systems, however, they do not consider a forecast horizon in the management and [7] do not include energy storage in the model.

MPC controllers allow energy management in microgrids considering the future behavior of the system and maintaining short convergence times. In [3,4,15] a prediction horizon is considered and MPC is used for the economic dispatch of active power. In [6] and [2], mixed integer nonlinear problems (MINLP) are formulated and MPC is used for the economic dispatch of active and reactive power. Other studies such as [23] and [13], employ MPC for power dispatch and voltage and frequency control, respectively.

In this work, an MPC is proposed for joint dispatch of active and reactive power in isolated microgrids, which is capable of performing economic dispatch, voltage control, and decreasing losses in the whole system. The main contributions are: first, the formulation of two linked optimization problems, one defined in a time horizon for the economic dispatch of active power and the other one for the dispatch of reactive power. Second, an MPC algorithm capable of finding optimal operating points by anticipating phenomena such as consumption peaks and generation reductions. Finally, the validation of the algorithm is performed in a real-time co-simulation scheme, between a software that solves the optimization problems and a power-analysis software.

The rest of the document is organized as follows. Section 2 formulates the optimization problem for active power dispatch. Then, Section 3 presents the optimization problem for reactive power dispatch. Next, Section 4 describes the MPC algorithm. To introduce the simulation scenario and analysis of results in Section 5. Finally, Section 6 concludes and proposes future work.

2 Economic Active Power Dispatch

The economic dispatch of active power allows the system to minimize costs, taking the power available in the cheap generators and compensating the deficit with the most expensive ones. For this purpose, constrained optimization problem is formulated, which looks for finding the operating points of the DGs and the SUs to minimize a cost function respecting the operating conditions of the microgrid.

2.1 Objective Function

According to [24], the cost of a generator can be approximated by quadratic functions dependent on the active power generated, such as

$$C_i^G(P_i) = a_i P^2 + b_i P + c_i, \tag{1}$$

where a_i, b_i, and c_i are specific parameters of each GD. Likewise, the SUs also have a cost related. Hawever, in this work, only the discharge cost is considered, since the power that charges the batteries already has an associated cost when it is generated. A simplified model to include the discharging cost of the ith SU, depending on its discharging power P_j^{dis} is adapted from [8] as

$$C_j^B(P_j^{dis}) = b_j P_j^{dis}, \tag{2}$$

$$b_j = \frac{C_j^{inv}}{4(C_j^f)(n_j^{dis})}, \tag{3}$$

where, n_j^{dis}, C_j^{inv}, and C_j^f correspond to the efficiency, the investment cost, and the life cycles of the storage unit j, respectively. Then, if the system has N_G generators and N_B storage units, the objective function for active power dispatch is

$$J = \sum_{i=1}^{N_G} C_i^G(P_i) + \sum_{j=1}^{N_B} C_j^B(P_j^{dis}). \tag{4}$$

2.2 Constraints

The first constraint is the energy balance, which ensures that at each instant, the total power dispatched power seeks to satisfy the power demanded by the loads P^L and the losses P^{loss}. Then, the constraint is given by

$$\sum_{i=1}^{N_G} P_i + \sum_{j=1}^{N_B} P_j = P^L + P^{loss}, \tag{5}$$

where, the variable P_j is equal to the discharge power P_j^{dis} when the SU delivers power, or is equal to the charge power P_j^{ch} when the SU demands power to store.

In the GDs and SUs, it is necessary to constraint the operating limits to ensure they work in the intervals $[P^{min}, P^{max}]$. Consequently, the second and third constraints are defined as

$$P_i^{min} \leq P_i \leq P_i^{max}; \ \forall i \in (1, \cdots, N_G), \tag{6}$$

$$P_j^{min} \leq P_j \leq P_j^{max}; \ \forall j \in (1, \cdots, N_B). \tag{7}$$

It is worth clarifying that the limits in renewable generators vary according to the energy resources available at each instant of time.

Finally, in the storage units, the limits in the load states are dynamic and for K instants of management they are given by

$$S_j^{min} \leq S_j(k+1) \leq S_j^{max}; \ \forall j \in (1, \cdots, N_B); \ \forall k \in (1, \cdots, K), \tag{8}$$

where, S_j^{min} is the minimum capacity, S_j^{max} is the maximum capacity, and $S(k+1)$ represents the next state of charge, which is obtained by

$$S_j(k+1) = S_j(k) - P_j^B; \ \forall j \in (1, \cdots, N_B); \ \forall k \in (1, \cdots, K). \tag{9}$$

Here, $S_j(k)$ represents the current state of charge and P_j^B is defined as [2]

$$P_j^B = sw_j n_j^{ch} P_j^{ch} + (1 - sw_j) \frac{P_j^{dis}}{n_j^{dis}}; \ \forall j \in (1, \cdots, N_B), \tag{10}$$

where n_j^{ch} is the charging efficiency and sw_j is a binary control variable used to identify whether the battery bank is in charging or discharged state. If $sw_j = 1$ the storage unit j is charging and, if $sw_j = 0$ it is in the discharge state. If we rewrite (8) from (9) and (10), the constraints for the state of charge of the SUs are

$$P_j^B \leq -S_j^{min} + S_j(k); \ \forall j \in (1, \cdots, N_B); \ \forall k \in (1, \cdots, K), \tag{11}$$

$$-P_j^B \leq S_j^{max} - S_j(k); \ \forall j \in (1, \cdots, N_B); \ \forall k \in (1, \cdots, K). \tag{12}$$

2.3 Predictive Model

The dynamics of the storage units allow the control to implement an of MPC strategy for the energy management in microgrids. Then, it is necessary to extend the optimization problem in a time horizon H_p to incorporate the future behavior of the system to determine the operating points of the DGs and the SUs. The MPC, allows the system to anticipate disturbances such as consumption peaks and variations in the generation capacity of the microgrids, consolidating more reliable systems. In this work, the predictive model is derived from the active power dispatch problem as

$$J_{MPC} = \sum_{l=1}^{H_P} \sum_{i=1}^{N_G} C_i^G(P_{l,i}) + \sum_{l=1}^{H_P} \sum_{j=1}^{N_B} C_j^B(P_{l,j}^{dis}) \tag{13}$$

Subject to:

$$\sum_{i=1}^{N_G} P_{l,i} + \sum_{j=1}^{N_B} P_{l,j} = P_l^L + P_l^{loss} \tag{14}$$

$$P_i^{min} \leq P_{l,i} \leq P_i^{max}; \ \forall i \in (1, \cdots, N_G) \tag{15}$$

$$P_j^{min} \leq P_{l,j} \leq P_j^{max}; \ \forall j \in (1, \cdots, N_B) \tag{16}$$

$$P_{l,j}^B \leq -S_j^{min} + S_{l,j}(k); \ \forall j \in (1, \cdots, N_B) \tag{17}$$

$$-P_{l,j}^B \leq S_j^{max} - S_{l,j}(k); \ \forall j \in (1, \cdots, N_B), \tag{18}$$

where, $P_{l,i}$, $P_{l,j}$, and $S_{l,j}$ are the power of generator i, the power of battery j and the state of charge of battery j at instant of prediction l, respectively.

3 Reactive Power Dispatch

For reactive power dispatch, a constrained optimization problem is also formulated, which seeks to correct voltage profiles and minimize the losses in the system.

3.1 Objective Function

In an isolated microgrid with N_n nodes and with N_i nodes coupled to node i, an objective function that approximates the active power losses can be defined according to [5] as

$$P^{loss}(V, \theta) = \sum_{i=1}^{N_n} \sum_{j=1}^{N_i} G_{i,j}(V_i^2 + V_j^2 - 2V_i V_j cos(\theta_i - \theta_j)), \tag{19}$$

where, V_i, V_j, θ_i, and θ_j are the voltages and the phase angles of the nodes i and j respectively, connected by the line (i, j) with conductance $G_{i,j}$.

3.2 Constraints

The equality constraints are determined by the load flow equations, set in [5] as

$$P_i(V, \theta) = V_i \sum_{j=1}^{N_i} V_j(G_{i,j}cos(\theta_i - \theta_j) + B_{i,j}sin(\theta_i - \theta_j))$$

$$= P_i^G - P_i^L, \tag{20}$$

$$Q_i(V, \theta, Q_i^G) = V_i \sum_{j=1}^{N_i} V_j(G_{i,j}sin(\theta_i - \theta_j) - B_{i,j}cos(\theta_i - \theta_j))$$

$$= Q_i^G - Q_i^L, \tag{21}$$

where, P_i^G and Q_i^G are the active and reactive power generated in node i, P_i^L and Q_i^L are the active and reactive load demanded at node i, and $G_{i,j}$ and $B_{i,j}$ are the conductance and susceptance of the element connecting nodes $i - j$. As $i \in N_n$, each equation represents N_n restrictions. On the other hand, the inequality constraints set the operating limits of the variables as

   − Voltage limits

$$V_i^{min} \leq V_i \leq V_i^{max}; \ \forall i \in (1, \cdots, N_n). \tag{22}$$

   − Phase limits

$$\theta_i^{min} \leq \theta_i \leq \theta_i^{max}; \ \forall i \in (1, \cdots, N_n). \tag{23}$$

   − Reactive power generation limits

$$Q_i^{min} \leq Q_i \leq Q_i^{max}; \ \forall i \in (1, \cdots, N_G), \tag{24}$$

$$Q_j^{min} \leq Q_j \leq Q_j^{max}; \ \forall j \in (1, \cdots, N_B). \tag{25}$$

The storage units dispatch reactive power in both, charge and discharge states [9], and their generation limits vary depending on the active power and the power factor PF as

$$Q_j^{max} = -Q_j^{min} = |P_j| tan(cos^{-1}(FP_j)); \ \forall j \in (1, \cdots, N_B). \tag{26}$$

4 MPC Algorithm.

The main features of the MPC family have been adapted to the current application as follows: first, an optimization problem for active power dispatch over a time horizon (proposed in Section 2) is formulated. Second, the optimization problem is solved to find the optimal powers of each instant into the horizon. Subsequently, only the first control action is taken in the DGs and SUs to establish the current setpoints in active power. Then, the limits in reactive power of the SUs and the active power generated in each node are calculated, according to the active power operating points. Finally, the optimization problem proposed in Section 3 is solved for the reactive power dispatch.

The validation of the controller is performed in a co-simulation scheme between Matlab® and DigSilent®, in such a way that DigSilent® estimates the electrical variables through power flows and Matlab® solves the optimization problems and save the data of interest. The exchange of information between the two programs is done by means of .txt files, as it is detailed in the block diagram in Fig. 1, where the process performed for K instants management is summarized.

5 Simulation Results and Discussion

The study case corresponds to the IEEE 13-bus test feeder [19] with some changes to evaluate the proposed MPC: First, the external grid is replaced by
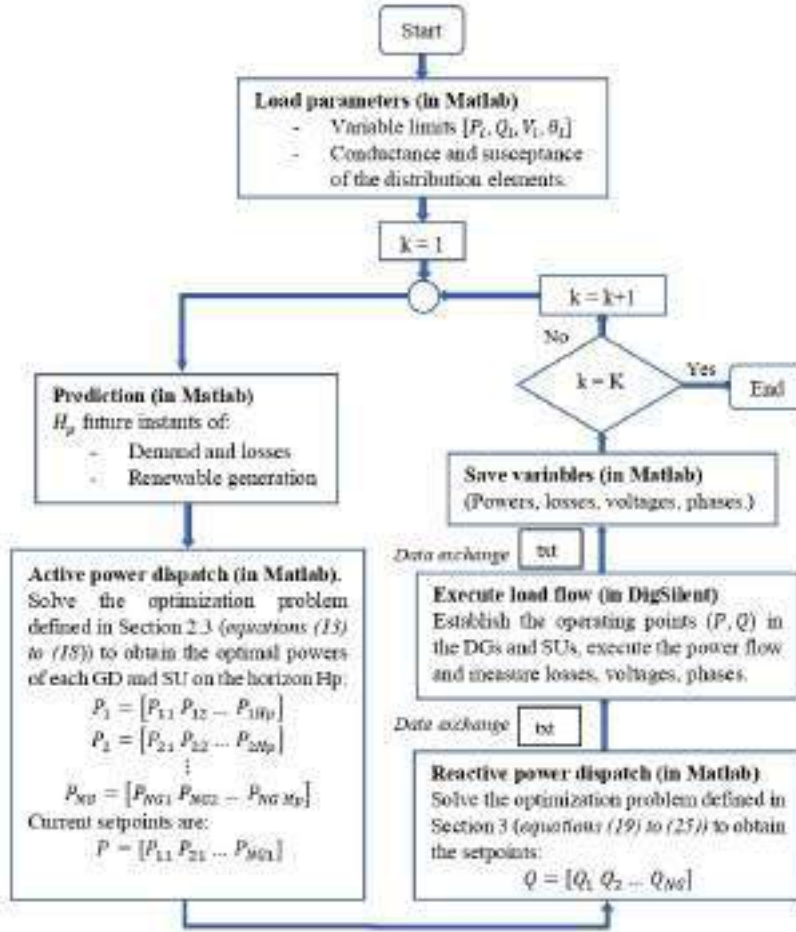
Fig. 1. Co-simulation block diagram and MPC algorithm.

a diesel generator. Second, based on the study realized in [20], four distributed generators (one solar, one wind and two storage units) are added. Finally, the system is balanced. The microgrid obtained is shown in Fig. 2.

The cost coefficients related to (1) are adapted from [7] and are shown in Table 1. The storage units are of two technologies: lead acid (BTl) and lithium-ion (BT2). In the former, the cost parameter $b_1 = 900$ and in the latter, $b_2 = 800$, since, although ion lithium batteries require a higher investment cost, they have 30% better efficiency and a higher number of life cycles [16]. These costs will
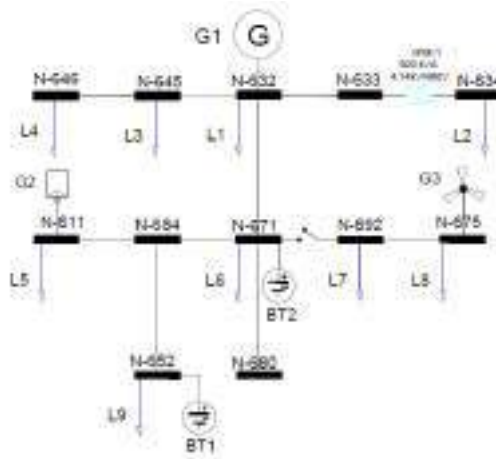
Fig. 2. Schematic diagram of the study case corresponding to a modified IEEE-13-node Feeder.

Table 1. Cost coefficients for each generator type.

Generator type	a_i	b_i	c_i
Diesel	104.44	1150.5	1.53
Photovoltaic	28.77	903.00	0.00
Wind	35.90	999.90	0.00

vary according to the scenarios or requirements of the users, so the difference in costs between the SUs may be properly adjusted.

Table 2 details the active power limits and the power factor configured in each device. The limits on the node voltages are set according to Colombian standards at 0.95 p.u and 1.05 p.u and the limits on reactive power can be estimated by

$$Q_{max} = -Q_{min} = |P_{max}|tan(cos^{-1}(FP)). \quad (27)$$

Table 2. Capacity limits of active power and power factor for the GDs and SUs in the microgrid.

GD/SU	Type	Pmax [kW]	Pmin [kW]	FP
G1	Diesel	2000	200	0.8
G2	Photovoltaic	1200	0	0.8
G3	Wind	1000	0	0.8
BT1	Battery Bank	800	-800	0.8
BT2	Battery Bank	1200	-1200	0.8

5.1 Energy Demand and Resources

Based on the consumption dynamics measured at the University of Nariño located in the southwest of Colombia and the nominal values of the loads presented in [19], the demand curves for the nine loads of the system are estimated for ten consecutive days, with sampling times of one hour. Fig. 3, shows the aggregate demand, where the weekend is clearly identification by the low energy consumption.

The renewable generation curves (solar and wind) are also estimated according to the energy resources available on the university campus and shown in Fig. 4.
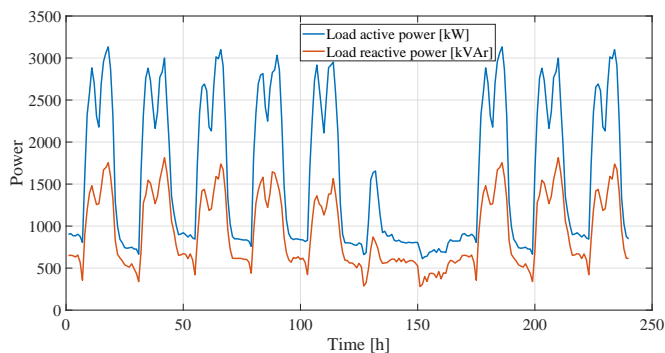
Fig. 3. Aggregate demand profile for active and reactive power.
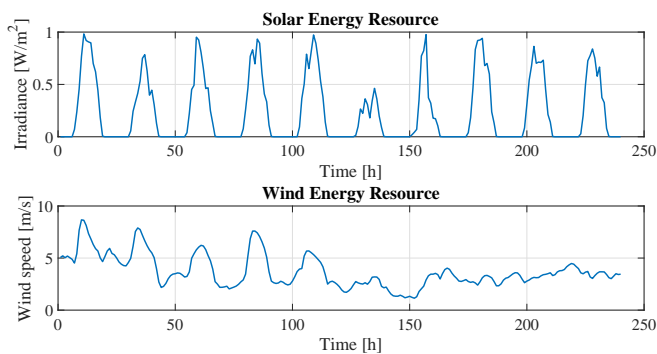
Fig. 4. Solar and wind profile resources for the university campus.

5.2   Results and Discussion

Figs. 5 and 6 present the results of the dispatch problems for 240 hours of management. The first one shows the active power profiles for the three generators and the two storage units, while the second one shows the reactive power profiles. Each figure shows the results obtained when no predictive control is applied and when MPC is applied with a prediction horizon of 24 hours. In both cases, sequential quadratic programming (SQP) is used to solve the optimization problems and convergence times of less than $10s$ are achieved, with an average increase of $2s$ when MPC is used.
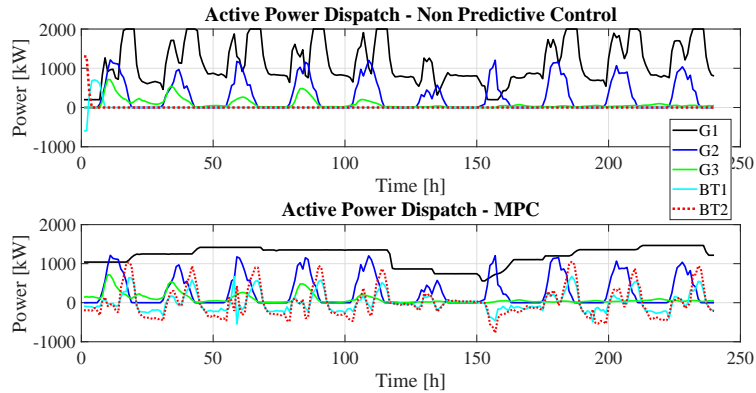
Fig. 5. Active power dispatch: non predictive control and MPC.

In the active power-dispatch curves, it is evident that when applying MPC, the dynamics of the diesel generator (G1) change, while the solar generator (G2) and the wind generator (G3) are always dispatched at their maximum capacity, following the availability of resources according to Fig. 4. The difference is produced since, when considering a prediction horizon, the diesel generator charges the batteries in the moments of low consumption to supply future demand peaks, while, when not considering a prediction horizon, the dispatch only complies the objective of supplying the current demand and the batteries are not charged. The details are shown in Fig. 7, which compares the charging states of the SUs in the two management methods.

Fig. 6 details the influence of the MPC in the reactive power dispatch. The profiles show that when MPC is applied, a large part of the demand is supplied by the batteries and the participation of diesel (G1) and photovoltaic (G2) generators decreases considerably.

Fig. 8 compares the unsupplied active and reactive power demand when no predictive control is applied and when MPC is working. The curves show how the
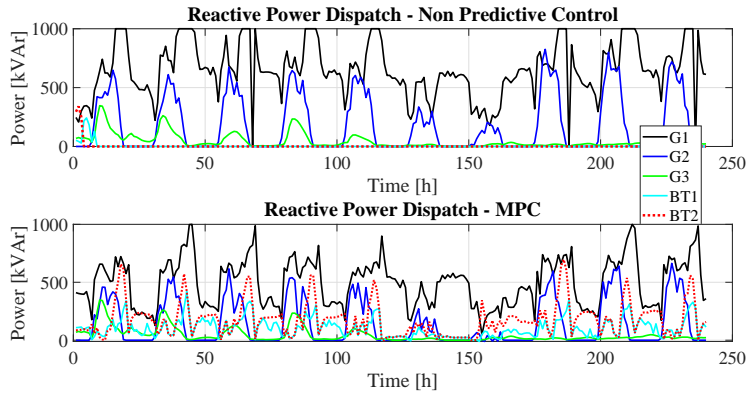
Fig. 6. Reactive power dispatch: non predictive control and MPC.
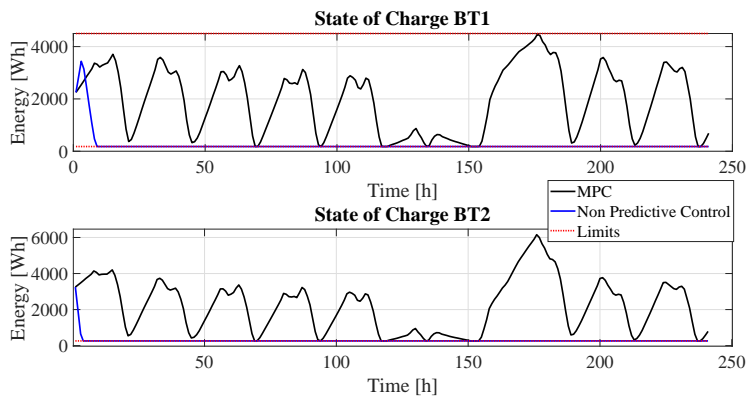
Fig. 7. Comparison of state of charge of storage systems: non predictive control and MPC.

non-predictive method does not supply the total demand in consumption peaks, presenting a total error of 4.8% in active power and 8.2% in reactive power, while MPC reduces the errors in demand to practically zero. This is due to the fact that the predictive control allows programming the charging and discharging of the storage units, in such a way that reserve energy is guaranteed for the demand all the time. However, supplying all demand increases the operating cost by 4.3% due to the greater participation of the SUs and the diesel generator to charge them.

Fig. 9 compares the voltage profiles of 4 nodes of the microgrid in 3 scenarios: when no predictive control is applied, when MPC is applied with active power
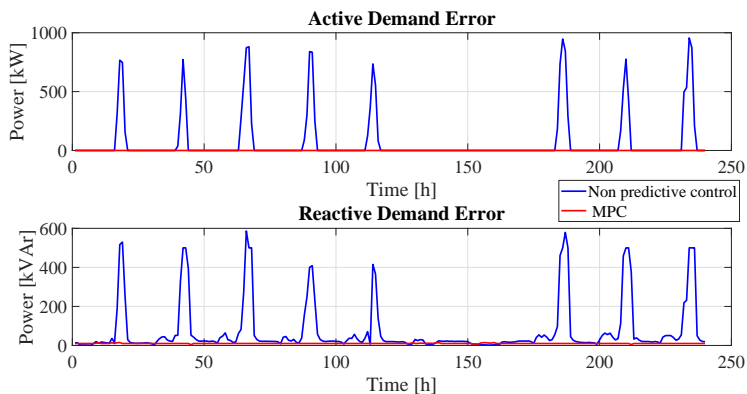
Fig. 8. Comparison of active and reactive power demand error: non predictive control and MPC

dispatch and when MPC is applied with active and reactive power dispatch. The results show that when predictive control is applied, the voltage deviation is corrected to the desired range of 5% and when reactive power dispatch is included, a better correction is achieved.
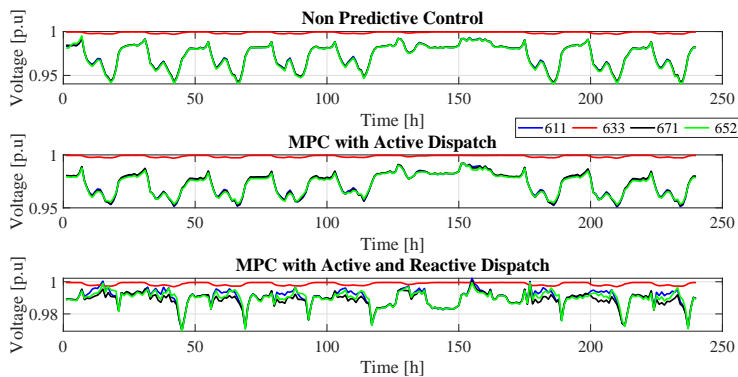
Fig. 9. Voltage deviation comparison: non predictive control, MPC with active dispatch and MPC with active and reactive dispatch.

Finally, Fig. 10 shows the active power losses. The curves prove how applying MPC and performing joint dispatch of active and reactive power reduces losses in the system. Predictive control decreases losses by 9.5% when management is

performed only with active power (blue curves) and by 26.4% when active and reactive power is dispatched (red curves).
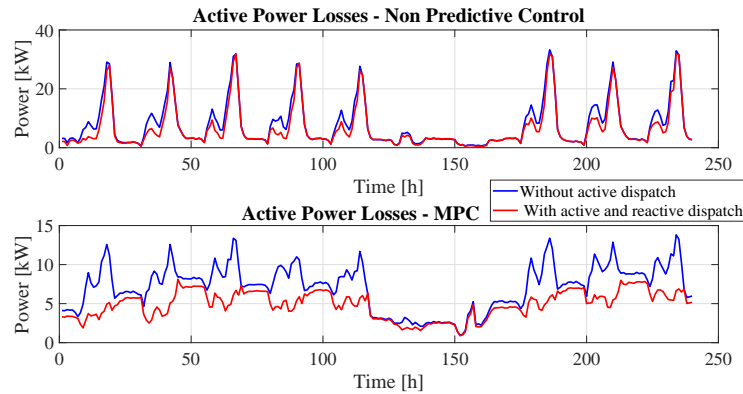
Fig. 10. Active power losses: non predictive control and MPC with active dispacth and active and reactive dispacth.

6　Conclusions

This paper presents an approach based on MPC for the optimal dispatch of active and reactive power in isolated microgrids. The management is performed in order to minimize operating costs and active power losses in the system. For this purpose, two optimization problems are formulated: one for the economic dispatch of active power and another one for the reactive power dispatch. The proposed algorithm is validated in a co-simulation scheme, where DigSilent estimates the electrical variables and Matlab solves the optimization problems. Summarizing results, the algorithm is able to find an optimal solution in less than 10 seconds, a low convergence time and ideal for real-time applications. Second, the error in both active and reactive power demand is removed, consolidating a more reliable and constant-service microgrid. Finally, a significant reduction in active power losses is achieved, improving the efficiency of the entire system. Future works could study the algorithm distribution, including the application in large power systems.

References

1. Ahmed, S., Tarek, B., Djemai, N.: Economic dispatch resolution using adaptive acceleration coefficients based PSO considering generator constraints. In: 2013 International Conference on Control, Decision and Information Technologies (CoDIT). pp. 212–217. IEEE (2013)

2. Alramlawi, M., Mohagheghi, E., Li, P.: Predictive active-reactive optimal power dispatch in PV-battery-diesel microgrid considering reactive power and battery lifetime costs. Solar Energy **193**, 529–544 (2019)

3. Clarke, W.C., Manzie, C., Brear, M.J.: An economic MPC approach to microgrid control. In: 2016 Australian Control Conference (AuCC). pp. 276–281. IEEE (2016)

4. Du, Y., Pei, W., Chen, N., Ge, X., Xiao, H.: Real-time microgrid economic dispatch based on model predictive control strategy. Journal of modern power systems and clean energy **5**(5), 787–796 (2017)

5. Duman, S., Sönmez, Y., Güvenç, U., Yörükeren, N.: Optimal reactive power dispatch using a gravitational search algorithm. IET generation, transmission & distribution **6**(6), 563–576 (2012)

6. Erazo-Caicedo, D., Mojica-Nava, E., Revelo-Fuelagán, J.: Model predictive control for optimal power flow in grid-connected unbalanced microgrids. Electric Power Systems Research **209**, 108000 (2022)

7. España, N., Barco-Jiménez, J., Pantoja, A., Quijano, N.: Distributed population dynamics for active and reactive power dispatch in islanded microgrids. International Journal of Electrical Power & Energy Systems **125**, 106407 (2021)

8. Garcia-Torres, F., Bordons, C.: Optimal economical schedule of hydrogen-based microgrids with hybrid storage using model predictive control. IEEE Transactions on Industrial Electronics **62**(8), 5195–5207 (2015)

9. Gevorgian, V., Wallen, R., Koralewicz, P., Mendiola, E., Shah, S., Morjaria, M.: Provision of grid services by PV plants with integrated battery energy storage system. Tech. rep., National Renewable Energy Lab.(NREL), Golden, CO (United States) (2020)

10. Hatziargyriou, N.: Microgrids: architectures and control. John Wiley & Sons (2014)

11. Hosseini, S.S.S., Gandomi, A.H.: Discussion of "economic load dispatch—a comparative study on heuristic optimization techniques with an improved coordinated aggregation-based PSO". IEEE Transactions on Power Systems **25**(1), 590–590 (2009)

12. Jiménez-Estévez, G.A., Palma-Behnke, R., Ortiz-Villalba, D., Mata, O.N., Montes, C.S.: It takes a village: Social SCADA and approaches to community engagement in isolated microgrids. IEEE Power and Energy Magazine **12**(4), 60–69 (2014)

13. Liu, K., Liu, T., Tang, Z., Hill, D.J.: Distributed MPC-based frequency control in networked microgrids with voltage constraints. IEEE Transactions on Smart Grid **10**(6), 6343–6354 (2019)

14. Ma, Z.l., Liu, S., Lan, H., et al.: A new solution to economic emission load dispatch using immune genetic algorithm. In: 2006 IEEE Conference on Cybernetics and Intelligent Systems. pp. 1–6. IEEE (2006)

15. Nassourou, M., Puig, V., Blesa, J., Ocampo-Martínez, C.: Economic model predictive control for energy dispatch of a smart micro-grid system. In: 2017 4th International Conference on Control, Decision and Information Technologies (CoDIT). pp. 0944–0949. IEEE (2017)

16. Power-Sonic: The complete guide to lithium vs lead acid batteries. https://www.power-sonic.com/blog/lithium-vs-lead-acid-batteries/, last accessed 25 Sep 2022

17. Ramirez, D.A., Garces, A., Mora-Florez, J.J.: A convex approximation for the tertiary control of unbalanced microgrids. Electric Power Systems Research **199**, 107423 (2021)

18. Sahay, K.B., Sonkar, A., Kumar, A.: Economic load dispatch using genetic algorithm optimization technique. In: 2018 International Conference and Utility Ex-

hibition on Green Energy for Sustainable Development (ICUE). pp. 1–5. IEEE (2018)

19. Schneider, K.P., Mather, B., Pal, B., Ten, C.W., Shirek, G.J., Zhu, H., Fuller, J.C., Pereira, J.L.R., Ochoa, L.F., de Araujo, L.R., et al.: Analytic considerations and design basis for the IEEE distribution test feeders. IEEE Transactions on power systems **33**(3), 3181–3188 (2017)

20. Tautiva, C., Cadena, A., Rodriguez, F.: Optimal placement of distributed generation on distribution networks. In: 2009 44th International Universities Power Engineering Conference (UPEC). pp. 1–5. IEEE (2009)

21. Yalcinoz, T., Rudion, K.: Economic load dispatch using an improved particle swarm optimization based on functional constriction factor and functional inertia weight. In: 2019 IEEE International Conference on Environment and Electrical Engineering and 2019 IEEE Industrial and Commercial Power Systems Europe (EEEIC/I&CPS Europe). pp. 1–5. IEEE (2019)

22. Yousif, M., Ai, Q., Gao, Y., Wattoo, W.A., Jiang, Z., Hao, R.: An optimal dispatch strategy for distributed microgrids using PSO. CSEE Journal of Power and Energy Systems **6**(3), 724–734 (2019)

23. Zeng, P., Li, H., He, H., Li, S.: Dynamic energy management of a microgrid using approximate dynamic programming and deep recurrent neural network learning. IEEE Transactions on Smart Grid **10**(4), 4435–4445 (2018)

24. Zhu, J.: Optimization of power system operation. John Wiley & Sons (2015)

General economic comparison in heating demand supply: geothermal energy Vs natural gas

Natalia Nuño-Villanueva[1][0000-0001-7022-119X], Ignacio Martín Nieto[1][0000-0003-3984-7228], Cristina Sáez Blázquez[2][0000-0002-5333-0076], Arturo Farfán Martín[1][0000-0002-1506-1207]

[1] Department of Cartographic and Land Engineering, University of Salamanca, Higher Polytechnic School of Avila, Hornos Caleros 50, 05003 Avila, Spain.
[2] Department of Electric, System and Automatic Engineering, University of Leon, 24071 León, Spain.
id00816629@usal.es

Abstract. Renewable energies such as geothermal presents in the current scenario a solution to the fragility of the market, in this case it is a solution to conventional heating systems powered by natural gas, which are the most used in Spain. In addition to the advantages of using renewable energy, a comparative economic study of a general nature would shed light when choosing a heating supply. For this reason, the present study exposes an economic comparison for the same set of buildings (single-family homes) on its heating system if it were powered by geothermal energy or natural gas, based on the initial investment, initial installation of the natural gas system and the wellfield of the geothermal system, and the annual expense due to that installation in order to supply the heating demand needed. This will lead to the approximate calculation of the payback period for the geothermal installation based in the market prices of 2022, 2020 and 2019, which in the worst scenario presented, the payback period is achieved at only 32% of the useful life expected of the installation (8 years).

Keywords: Geothermal, natural gas, investment, renewable energy, payback period, heating demand.

1   Introduction

Geothermal energy has proven to be a valuable source of renewable energy for supplying not only domestic hot water (DHW) [1] but also heating [2], which, taking into account the current state of the fossil fuel market and its fragility due to recent events, such as the Russia-Ukraine war of 2022 with its consequent influence on the supply of liquefied natural gas, further emphasizes this type of energy as an alternative of commonly used supplies based on natural gas.

Over the years, research has been carried out on the efficiency of geothermal-based supply installations [3] [4], including studies on the advantages of collective installations compared to individual ones [5]. This has led to the development of a heating system known as district heating (DH) whose objective is to supply an entire group of

buildings, a system used in Europe since the 14th century [6] with more weight in northern European countries where installations of this type currently exist and new models are being investigated [5] [7] [8].

In addition to being a mature technology with its fourth generation (4GDH) [9] [10] [11] and the development of its fifth (5GDHC) [12] [13] [14] [15], this type of heating offers various advantages compared to the conventional model, including the reduction in fossil fuel consumption with its consequent reduction in CO_2 and greenhouse gas emissions[16].

However, despite these benefits, the initial investment in geothermal DH represents a point against natural gas, which is why this study intends to consider the annual expenditure during the same period of years in order to verify the payback period and observer in general terms which solution is the most economical.

2   Methodology

The methodology present in this research is a simplified calculation of the demand of an entire urbanization for its subsequent comparison between two different types of heating supply sources: geothermal energy and natural gas.

The workflow diagram described in Fig 1 shows the steps followed, with the consequent software's used specified by stage, until reaching the economic comparison between both sources of supply, conclusion of this article.
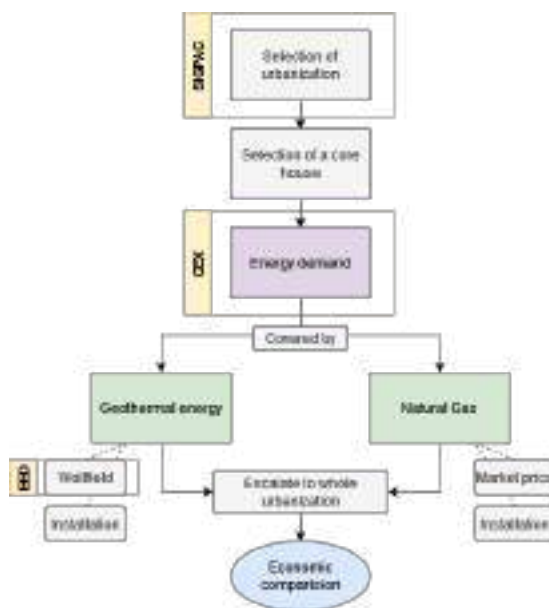
Fig. 1. Workflow diagram of the methodology used.

The starting point of this methodology consists in the selection of a residential area that can be classified in such a way that the houses can be individualized (explained in more detail in the third point of this article). The Geographic Information System of Agricultural Parcels (SIGPAC)[17], from Spain, is a tool that allows the visualization and measurement of desired zones on a map, however any Geographic Information System (GIS) can be used to define a zone of interest since it uses geographically referenced information, making the replicability of the methodology feasible.

Once the residential state is selected, the next step would be defining a single plot with its individual house to consider it the base of the calculation. The more similar the houses are within the residential development, the smaller the error in the calculation of the demand since it will later be scaled to all the houses.

There are numerous programs for calculating the energy demand based on the construction itself that also perform the calculations based on the current regulations of the normative building code, they are usually based in the energetic certification of the building studied, some examples of this tools are: LIDER/CALENER (HULC), CERMA, CEX, CE3 and CYPETHERM HE Plus. In this case the software used for the calculation is CEX.

As it was stated before, the comparison proposed in this study is an economic comparison between two means of supplying heating demand, the traditional and commonly used natural gas and a renewable energy supply alternative such as geothermal energy. Both means of supply will be calculated based on the same time of use and the price of the installation will be considered to obtain a general conclusion on the economical difference in the initial investment and maintenance.

3   Applicable study sites and location

The study can be replicated and carried out in housing states whose houses are either identical or similar since the base of this research is based in the individual study of a single house of the urbanization that later will be scaled.

In this regard, any urbanization already made, or planned, whose houses are design as clones could benefit from this calculation. This does not mean that a calculation cannot be estimated in other types of residential developments, but the error is bound to increase.

It should be noted that geothermal energy is highly dependent of the terrain in which it is located since it affects the performance of the geothermal heat pump installations. As the intention of this research is to create the wellfield within the residential area, the calculations will be more favorable the greater the thermal conductivity of the land on which said urbanization is built.

The study site selected in this research is based in Ávila in the autonomous community of Castilla y León, Spain. The exact location is presented in Fig 2 using SIGPAC.

Fig. 2. Study site selected as example (Ávila, Castilla y León, Spain)

As can be seen in Fig 2, this urbanization has the same type of house built despite the change in the distribution of its individual plot which doesn't interfere with the calculations and consists of 83 houses as shown in Fig 3.

Fig. 3. Selection of the totality of the houses in the housing development.

Furthermore, using the geothermal map of the Ávila region[18], the thermal conductivity of the terrain in which the urbanization was built can be obtained as shown in Fig 4.
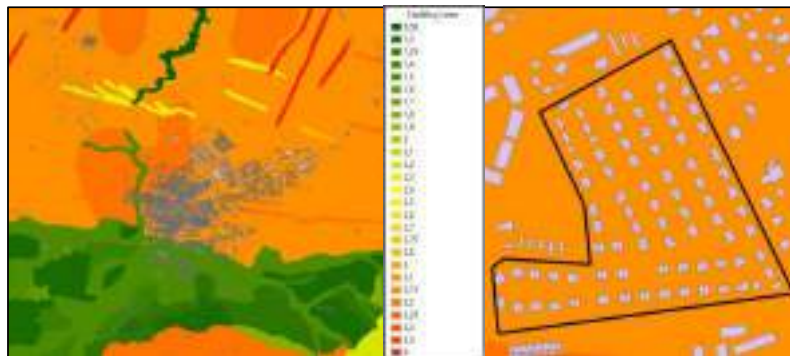
Fig. 4. Selected study site with its thermal conductivity presented.

The selected example of site results in a terrain with high thermal conductivity, approximately 2,8-3W/m·K.

4   Calculation, results and discussion

4.1   Calculation of energy demand

As specified in Fig 1 the selection of a core house has to be made in order to ease the calculation of the demand. Therefore, the example house plot consists of an area of $783m^2$ (27x29m), this area is maintained approximately for the rest of the houses even if the length and width of the plots change. The house itself is $210m^2$ seen from above (15x14m) and consist of 3 floors where one of them is half the surface due to the indoor parking, this results in $525m^2$ in total.

In order to calculate the demand with the CEX software it is necessary to make some estimates and previous calculations:

— The corresponding factors included in the Technical Building Code will be applied, that is, among others, the reference demand of DHW for buildings of private residential use will be obtained considering needs of 28l/day·person[19].
— The average distribution of the house will be two bedrooms that are equivalent to 3 people.[19]

Considering the advantages of CEX when it comes to autocomplete according to regulations and climatic zone, only the general data of the house and its structure in terms of facades needs to be provided. In this case Table 1 presents the data used for the calculation.

Table 1. Building data entered in CEX software.

Building characteristics	Value
Construction year	1999
Usable living area	525 m^2
Number of habitable floors	2
Daily DHW demand	84 l/day

A heating demand of 99.1 kWh/m^2 has been calculated for a single house, resulting in 52MWh. It must be considered that other factors influences this heating demand, as per example the orientation or the residents habits, so it will be adjusted to a rounding of **55MWh of heating demand per house per plot annually**.

4.2   Natural gas installation

The calculation of the installation and maintenance of natural gas for heating is simpler than the calculation of geothermal supply, since natural gas is the most widely used in Spain, therefore there are more estimated prices of the calculation of the facilities. An example of the cost of an average natural gas installation in single-family homes is presented in Table 2.

Table 2. Price of natural gas installation in single-family homes[20].

Description	Total (€)
Individual receiver facility	1420
Technical calculation report and individual gas installation certificate	
Management and processing of licenses, permits and commissioning	
Regulation cabinet	
Connection steam to service	
Condensing boiler	1000
TOTAL	**2420**

Scaling the cost to the 83 total homes that make up the urban complex a **total of 200.860€.**

4.3   Geothermal installation

So as to meet the heating demand with geothermal energy, it is necessary to calculate two factors: the design and sizing of the wellfield and the installation per se.

The EED[21] (Earth Energy Designer) software has been used as a tool for designing ground source heat pump systems and borehole thermal storage. With an estimated annual heating demand of 55MWh, the monthly distribution with the corresponding consumption factors and a peak demand of 8kWh (Fig 5.) a design can be optimized.
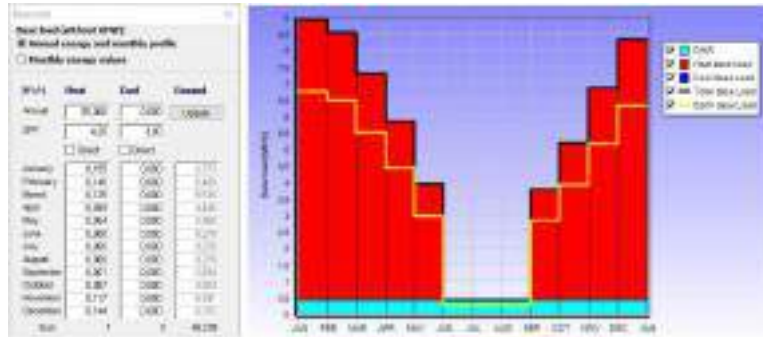
Fig. 5. Base load of heating demand and its graphic representation.

In Fig 6 different optimized configurations created by EED can be seen. The first part has as priority the least number of boreholes whereas the second prioritizes the depth of the boreholes.

Fig. 6. Design solutions provided by EED software.

For this comparison, the first configuration of 2 boreholes of 115m depth will be used. This configuration presents in Fig 7 its fluid temperature curve for 25 years. It can be verified that the final temperature (approximately -6ºC) is far from the freezing point of the selected fluid: Monopropylenglycole and water at 33%, this fluid has a freezing point of -17ºC and is commonly used for this type of installations since it reduces the freezing point, its environmentally friendly (unlike its predecessor the monoetylene glycol) and it also maintains the water flow at the selected operating temperature, key point of the installation.
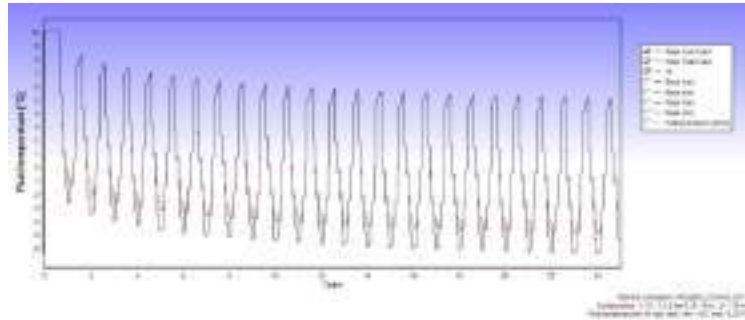
Fig. 7. Temperature evolution in 25 years provided by EED software.

With the wellfield calculated, it is necessary to calculate the heat pump needed. An estimated calculation with a COP of 4 and 2400h of work a **0,01MW of pump power** is obtained. Table 3 shows the summary of the design selected.

Table 3. Summary of design and installation per house.

Wellfield	Nº of boreholes	Depth (m)	Spacing (m)
	2	115	15
Heat pump	Power (MW)	COP	Operating hours
	0,01	4	2400

CYPE engineers [22] has an extensive library of Spanish work prices which will be used for estimated calculation of the installation work. Table 4 breaks down the required budget for the wellfield installation using CYPEs registered data.

Table 4. Estimated price of the wellfield installation per house.

Unit	Description	Efficiency	Unitary price (€)	Total (€)
h	Hydraulic equipment on crawler carriage […].	0,130	105,84	13,76
h	Injection equipment for geothermal drilling.	0,130	34,16	4,44
			Equipment subtotal	**18,20**
h	Official construction of civil works.	0,459	19,93	9,15
h	Civil works construction assistant.	0,459	18,92	8,68
			Workforce subtotal	**17,83**
%	additional direct costs	2	36,03	0,72
			TOTAL	**36,75***

*Rounded up for further calculations to 40€/m

Doing the calculations with the design selected of 2 boreholes of 115m each, total of 230m, escalated to the totality of the 83 houses, results in **763.600€ the cost of the total wellfield**.

Regarding the necessary heat pump, it must be considered that larger heat pumps work with higher COP, therefore the COP used will be changed from 4 to 4,5 as estimation, maintaining the same operating hours.

In order to calculate the heating power needed, the demand obtained per house will be multiplied for the total number of houses in the housing development (83) divided by the COP of the heat pump. This results in **a total demand of 1015MWh or 0,43MW, which for this study purposes will be rounded up to 0,5MW**.

As an example of geothermal heat pump the geotherm variant of Vaillant[22] will be used as estimated price as shown in Table 5.

Table 5. Price of heating pump for the housing development.

Description	Heating power (kW)	Quantity	Unitary price (€)	Total (€)
Vaillant geoTHERM VWS 460/3 400 V	49,9	10	18.235,91	182.359,1

As a result, the geothermal installation costs are shown in Table 6.

Table 6. Summary of total cost of geothermal installation

Description	Total (€)
Wellfield installation	763.600
Heat pump installation	182.359,1
TOTAL	**945.959**

4.4　Comparison result

The difference obtained in the initial installation of each of the supplies shown in Table 7 was expected due to the wellfield design and excavation.

Table 7. Summary of initial cost of installation

Description	Total (€)
Natural gas initial installation	**200.860**
Geothermal initial installation	**945.959**

However, the comparison presented in this article is not only with the initial investment but also with its prolonged use. This calculation is complex since it depends on the market price of electricity and natural gas. As the objective of this research is the

comparison in general terms of the cost, the values presented in Table 8 are estimations of the mean market value.

Table 8. Market value of electric kWh and natural gas in different significant years.

Year	Market value	
	Electricity (€/kWh)	**Natural gas (€/kWh)**
2022	0,2773	0,2166
2020	0,1214	0,0480
2019	0,1115	0,0736

The price of electricity has been taken as the average of the electricity market for the month of October, while for natural gas the average price of three companies has been used: Endesa, Iberdrola and Repsol, all three of them operate in Spain.

Fig 8 and Fig 9 are the graphical representation of the cost of both systems, starting with the initial investment detailed in Table 7 plus the annual cost of covering the heating demand and maintaining this coverage for 10 years.
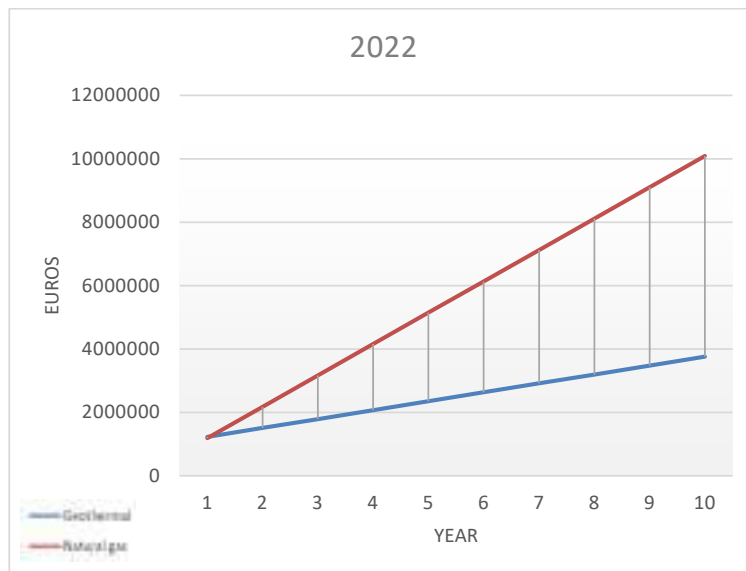
Fig. 8. Graphic representation of the cost of both systems in 10 years (2022).
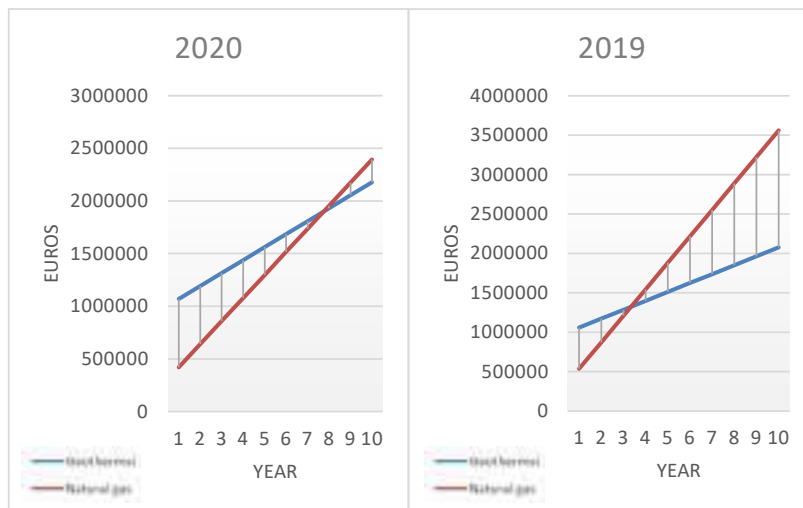
Fig. 9. Graphic representation of the cost of both systems in 10 years (2020 and 2019).

The cut-off points of the graphs presented (year 1 in 2022, year 8 in 2020 and year 4 in 2019) represents the year in which the geothermal system starts equals the natural gas system and begins the payback period. As it can be seen in the graphs, the savings once this point is passed is of great magnitude.

5   Conclusions

An undeniable point of geothermal energy is its great initial cost (Table 7), being approximately one fifth of the initial cost of the natural gas installation, however this initial outlay is compensated by the annual cost of its use, highly dependant on the market and its stability. Due to the influence in this market of political disputes, it can be seen in the period of 4 years how prices have varied to the current point where compared to 2019 there has been an increase of 149% in the case of electricity and a rise of 195% in the case of natural gas, but within the most stable period between 2019 and 2020 prices hardly vary. Even so, the return period is reached early, considering that the temperature of the fluid and the installations are guaranteed for 25 years, since none of them reach 10 years.

A more conservative approach considering other factors ignored in this study, such as the fluctuation of the market or selecting the electric kWh during off-peak hours since the heat pump can be programmed to work on determined hours, can be taken and expect a payback return around half the years needed to maintain the heat pump or the boiler (25 years approximately depending on the model, not counting the annual revisions for both systems).

This study is interesting not only as a concept of investment in this type of technology, but also as a renewable resource available to any country. If the correct study of the construction zone is done and it results in an acceptable thermal conductivity, geothermal system is to consider for any country that is not a main producer of natural gas, thus making it less dependent on the conditions of the supply.

References

1. T. Kitzberger, D. Kilian, J. Kotik, and T. Pröll, «Comprehensive analysis of the performance and intrinsic energy losses of centralized Domestic Hot Water (DHW) systems in commercial (educational) buildings», *Energy Build.*, vol. 195, pp. 126-138, jul. 2019, doi: 10.1016/j.enbuild.2019.05.016.
2. K. Duus and G. Schmitz, «Experimental investigation of sustainable and energy efficient management of a geothermal field as a heat source and heat sink for a large office building», *Energy Build.*, vol. 235, pp. 110726, mar. 2021, doi: 10.1016/j.enbuild.2021.110726.
3. M. H. Kristensen and S. Petersen, «District heating energy efficiency of Danish building typologies», *Energy Build.*, vol. 231, pp. 110602, ene. 2021, doi: 10.1016/j.enbuild.2020.110602.
4. «06/02326 Effect of reference state on the performance of energy and exergy evaluation of geothermal district heating systems: Balcova example: Ozgener, L. et al. Building and Environment, 2006, 41, (6), 699–709.», *Fuel Energy Abstr.*, vol. 47, n.º 5, pp. 354, sep. 2006, doi: 10.1016/S0140-6701(06)82334-9.
5. U. Persson and S. Werner, «Heat distribution and the future competitiveness of district heating», *Appl. Energy*, vol. 88, n.º 3, pp. 568-576, mar. 2011, doi: 10.1016/j.apenergy.2010.09.020.
6. B. Rezaie and M. A. Rosen, «District heating and cooling: Review of technology and potential enhancements», *Appl. Energy*, vol. 93, pp. 2-10, may 2012, doi: 10.1016/j.apenergy.2011.04.020.
7. M. Gong and S. Werner, «Exergy analysis of network temperature levels in Swedish and Danish district heating systems», *Renew. Energy*, vol. 84, pp. 106-113, dic. 2015, doi: 10.1016/j.renene.2015.06.001.
8. S. Paiho and F. Reda, «Towards next generation district heating in Finland», *Renew. Sustain. Energy Rev.*, vol. 65, pp. 915-924, nov. 2016, doi: 10.1016/j.rser.2016.07.049.
9. H. Averfalk and S. Werner, «Economic benefits of fourth generation district heating», *Energy*, vol. 193, pp. 116727, feb. 2020, doi: 10.1016/j.energy.2019.116727.
10. B. van der Heijde, A. Vandermeulen, R. Salenbien, and L. Helsen, «Integrated Optimal Design and Control of Fourth Generation District Heating Networks with Thermal Energy Storage», *Energies*, vol. 12, n.º 14, Art. n.º 14, ene. 2019, doi: 10.3390/en12142766.
11. H. Lund *et al.*, «4th Generation District Heating (4GDH): Integrating smart thermal grids into future sustainable energy systems», *Energy*, vol. 68, pp. 1-11, abr. 2014, doi: 10.1016/j.energy.2014.02.089.

12. H. Lund *et al.*, «Perspectives on fourth and fifth generation district heating», *Energy*, vol. 227, pp. 120520, jul. 2021, doi: 10.1016/j.energy.2021.120520.

13. S. Buffa, M. Cozzini, M. D'Antoni, M. Baratieri, and R. Fedrizzi, «5th generation district heating and cooling systems: A review of existing cases in Europe», *Renew. Sustain. Energy Rev.*, vol. 104, pp. 504-522, abr. 2019, doi: 10.1016/j.rser.2018.12.059.

14. S. S. Meibodi and F. Loveridge, «The future role of energy geostructures in fifth generation district heating and cooling networks», *Energy*, vol. 240, pp. 122481, feb. 2022, doi: 10.1016/j.energy.2021.122481.

15. A. Volkova, I. Pakere, L. Murauskaite, P. Huang, K. Lepiksaar, and X. Zhang, «5th generation district heating and cooling (5GDHC) implementation potential in urban areas with existing district heating systems», *Energy Rep.*, vol. 8, pp. 10037-10047, nov. 2022, doi: 10.1016/j.egyr.2022.07.162.

16. J. W. Lund and P. J. Lienau, «GEOTHERMAL DISTRICT HEATING», pp. 18.

17. «Visor SigPac V 4.8». https://sigpac.mapama.gob.es/fega/visor/ , last accessed 2022/09/29.

18. C. Sáez Blázquez, A. Farfán Martín, I. Martín Nieto, P. Carrasco García, L. S. Sánchez Pérez, and D. González Aguilera, «Thermal conductivity map of the Avila region (Spain) based on thermal conductivity measurements of different rock and soil samples», *Geothermics*, vol. 65, pp. 60-71, ene. 2017, doi: 10.1016/j.geothermics.2016.09.001.

19. «DccHE.pdf». Last accessed 2022/10/03. [On-line]. Available in: https://www.codigotecnico.org/pdf/Documentos/HE/DccHE.pdf

20. «¿Cuánto cuesta instalar el gas natural?», *preciogas.com*. https://preciogas.com/instalaciones/gas-natural/precio, last accessed 2022/10/03.

21. «EED – Earth Energy Designer – Buildingphysics.com». https://buildingphysics.com/eed-2/ , last accessed 2022/10/03.

22. «Bombas de calor geotérmica Vaillant geoTHERM alta potencia VWS 460/3 400 V», *Gasfriocalor.com*. https://www.gasfriocalor.com/bombas-de-calor-geotermica-vaillant-geotherm-alta-potencia-vws-460-3-400-v , last accessed 2022/10/04.

Hybrid AC/DC Microgrids. A state of Art

Óscar Izquierdo-Monge[1], Gonzalo Manuel Martín Rodríguez[2], Paula Peña-Carro[1],
Inés Fraile Martín[2], Angel Zorita-Lamadrid[3] and Luis Hernández-Callejo[4]

[1] CEDER-CIEMAT, Autovía de Navarra A15 salida 56, 422290 Lubia (Soria), Spain.
[2] University of Salamanca, Plaza de la Merced 18, 37008 Salamanca, Spain.
[3] ADIRE-ITAP. University of Valladolid, Campus Duques de Soria, 42004 Soria, Spain.
[4] ADIRE-ITAP. University of Valladolid, Paseo del Cauce 59, 47011 Valladolid, Spain.

oscar.izquierdo@ciemat.es; gonmarro@usal.es; paula.pena@ciemat.es; inesfraile@usal.es;
zorita@eii.uva.es and luis.hernandez.callejo@uva.es.

Abstract: Microgrids (MG) are a compilation of loads, distributed generation (DG) elements and storage systems (SSs), they are a green and reliability solution to generate and supply electricity. Alternating current (AC) MGs are the most researched at the moment. Direct current (DC) MGs have gained a lot of interest in recent years as researchers have determined a number of advantages of DC MGs over AC ones. Furthermore, hybrid microgrids (HMGs) compile the advantages of both types turning them into a very interesting field of study. Nevertheless, the development of DC and HMGs is more recent, topic that is being investigated in an extensive way in recent years. This paper presents the state-of-the-art on DC and HMGs compiling the most actual and fundamental information and compares it with the basic knowledge on AC MGs. The most important advantages and disadvantages of AC, DC and HMGs are presented. Different aspects of the proper operation of these MGs are exposed, such as several methods of interconnection in HMGs. Also, a review of the current situation of DC and HMGs, as well as certain aspects to be improved in the coming years and future trends are described. Some examples have been presented in different sections with the aim of creating a broader view of the subject under discussion.

Keywords: Hybrid AC/DC microgrid, control methods, microgrid, interconnection, future trends.

1　　Introduction

Due to the climate emergency and the current energy crisis, the development and implementation of MGs is becoming necessary. MGs are capable of producing energy using renewable energy sources (RES) such as wind energy and photovoltaic (PV), so their use is optimal for reducing greenhouse gas emissions, decreasing the consumption

of fossil fuels, saving energy, improving supply reliability, producing clean energy and reducing costs [1]. MGs are the future of electric distribution networks.

A microgrid is a small power system that can supply power self-sufficiently. The U.S. Department of Energy defines it as: "A group of inter-connected loads and distributed energy resources (DERs), with clearly defined electrical boundaries, that acts as a single controllable entity with respect to the grid and can connect and disconnect from the grid to enable it to operate in both grid-connected or island modes" [2]. MGs can collect and analyse information in real time, thus optimizing its consumption. They mainly include these elements: loads, DG and SSs [3] .

There are several types of DGs, so a classification can be made [4]. On the one hand, there is energy generation from RES such as ocean waves, tides, geothermal, biomass, wind turbines or PV systems. On the other hand, there are clean alternative energy (AE) such as microturbines or fuel cells (FCs). Finally, there are traditional rotational machine-based technologies such as diesel generators.

There are also two categories of ESSs, presented in Table 1.

Table 1. Categories of energy SSs [4].

Categories	Description/function	Examples
Capacity-oriented	Slow response time Balance long-term energy Dampen low-frequency power oscillation Respond to the intermittence of the RES	Batteries, pumped hydroelectric systems, compressed air energy storage or hydrogen storage.
Access-oriented	Fast response time Generate the short duration disturbances in the MGs, providing the high frequency energy component Supply or absorb the high-power transients with high-power density	Supercapacitors, flywheels or superconducting magnetic energy storage

Loads, distributed generation elements and SSs can be classified depending on the type of current (AC or DC) from which they are fed [3], [5], [6]. Several examples of these types of elements are exposed below. Some examples of AC loads can be: washing machines, coffee pots or microwaves; some DC examples of loads are: electric vehicles, TVs, PCs or air conditioners. Examples of DC DGs elements are: wind turbines, gas turbines or diesel generators; AC DGs elements can be: PV or fuel cells. Finally, some DC SSs elements are flywheels or battery energy storage system (BESS).

Three types of MGs have been developed so far, so they can be differentiated between: 1) AC MGs, 2) DC MGs, and 3) HMGs. AC MGs have already been extensively investigated, they mainly include AC loads and sources. DC MGs are rising and have not been as developed as AC ones, they are made of DC loads and sources.

In recent years, HMGs have gained great relevance as they combine the advantages of AC and DC MGs.

The HMGs can be classified depending on the configuration of AC and DC buses and on the connection of sources and loads to the system [4], [5], [7]:

- HMGs with AC coupling: they have a considerable number of DC loads connected to a common AC coupling bus via interface DC/AC power converters (IPCs).
- HMGs with DC coupling: they are made up of a remarkable number of AC loads that are connected to a common DC coupling bus via AC/DC IPCs.
- HMGs with AC and DC coupling: these types of MGs are formed by the two previously mentioned MGs, commonly interconnected by Bidirectional Interlink Power Converters (BILPCs).

We can see an example of a hybrid AC/DC microgrid with AC and DC coupling in Figure 1:
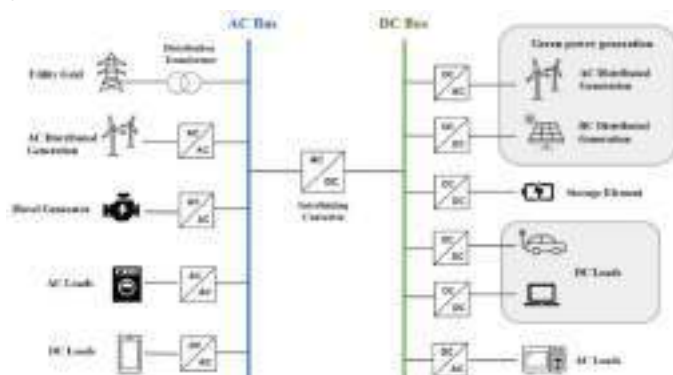
Figure 1. Hybrid AC/DC microgrid with AC and DC coupling example.

Figure 1 is an example of a hybrid microgrid, it is made up of storage elements, AC and DC loads and DGs connected to the AC and DC buses by means of power converters. These power converters are called interface power converters (IPCs) [5], depending on the type of current IPCs transform, there are different structures: AC/AC, DC/DC, AC/DC and DC/AC. This hybrid microgrid can be understood as the connection of an AC microgrid with a DC microgrid through the interlinking converter (IC). The IC allows power exchange between the AC and DC sub-grid. Different types and forms of interconnection of these MGs will be studied in Section 0.

The development of the article continues in Section 2, which presents some advantages and drawbacks of the MGs. In Section 0, some interconnection methods for HMGs are presented. Different control methods are shown in Section 4. Section 5 talks about some future trends. Finally, Section 6 shows the conclusions.

2   Advantages and drawbacks of AC, DC and HMGs

2.1   AC Microgrids

Although AC MGs were the first to be developed, they present a series of benefits [8]:
- High efficiency: The voltage of AC MGs can be stepped up and down with high-efficiency transformers for distribution purposes or for local loads use.
- Stable voltage: It can be obtained when reactive power is controlled independently.
- Security: If any fault occurs in grid-tied mode, the AC microgrid disconnects itself. The load will not be influenced from the disturbances that occur in the main grid.
- Protection: There is natural zero crossing of the current in AC grids, so protection schemes are advantageous because current can be interrupted in a safer way than in a DC grid.

The use of AC microgrid also presents certain drawbacks [8]:
- Harmonics: The use of power electronic converters introduces harmonics in the main grid.
- Complexity: It is complicated to interconnect DC RESs because inverters must be used to convert DC output to AC.
- Conversions: There is a loss of efficiency when AC power needs to be converted for DC loads such as computers, TVs, battery charging, DC fluorescent lamps, electric vehicles, etc.

2.2   DC Microgrids

Research and development of AC MGs is greater than for DC MGs. Despite this, starting to implement DC MGs brings a series of advantages:
- Reduction of CO_2 emissions: DC MGs use a fewer number of energy converters, minimizing CO_2 emissions [9].
- Effective integration of DC loads: There is no need to convert AC power to DC for DC loads. Because of this, the quality of the energy is higher, reducing costs and losses [9].
- Easier integration of RESs and Energy Storage Systems (ESSs): Most of RES and ESS produce DC power, so they are easily integrated into a DC microgrid than into an AC one.
- No need for synchronization: The operational complexity of the system can be reduced because, in DC systems, there is no need to synchronize the grid-connected renewable energy systems with the main AC grid [10].
- No skin effect: In DC systems, skin effect is not produced. The current can flow through the entire cable and not just through the outer edges. Because of this, power losses are reduced and smaller cables can be used in DC distributions [9].

- Increased energy efficiency and reliability: DC MGs are more energy efficient than AC ones. This is because a DC/AC converter, which has lower efficiency than a DC/DC one, is required in order to convert the DC power coming from the sources into AC power for the loads.

As seen, the implementation of DC MGs increases power quality, efficiency, reliability, stability and controllability of the system. However, the use of DC MGs has some drawbacks, mainly due to the lack of research on DC technologies. Some obstacles in the implementation of DC networks are [9], [10]:

- Protection: The protection in a DC microgrid is more complicated than in an AC one because, in the first one, there is no natural zero crossing of the current.
- Lack of expertise: Due to the existing MGs being mostly AC, their technology is well developed and expanded. Nevertheless, DC technology is in the process of improvement.
- Higher cost: Because of the recent development of DC technology, the overall cost of AC technology is lower than the DC one.
- Lack of specific standards: It is necessary to specify some parameters such as the voltage levels to implement DC technology.

2.3   Hybrid AC/DC Microgrids

HMGs combine the advantages of both AC MGs and DC MGs. Therefore, the implementation of HMGs presents a series of advantages [1], [11]:

- Reduction of energy losses: AC and DC devices are connected to the main grid with the minimum number of interface elements and, because of that, the number of conversion stages is reduced and there are less energy losses.
- Simplification of the voltage transformation: In the AC grid, the voltage modification is performed by transformers, and in the DC grid the modification is performed by DC-DC converters.
- Economic advantages: A hybrid microgrid is developed by adding a power converter to the current distribution grid and the communication network for the connected devices. If the number of connected devices is high, investment in converters results profitable as the number of total interface converters is reduced.
- Control strategies simplification: Because of the DGs and SSs are directly connected to the AC or DC grid.

Apart from the drawbacks that the DC microgrid presents, there are a series of inconveniences that the implementation of a hybrid microgrid entails:

- Increased complexity: Managing a HMG is more complex than an AC MG or a DC MG, as in HMGs, it is necessary to perform the control of the devices attached to the AC and DC networks and the interface power converter

between them. Both types of MGs (AC and DC ones) must be able to access a stable and reliable power supply.

- ▪ Reliability reduction: It is reduced because an interface power converter must be introduced in the distribution network to generate the DC-link, but if the number of converter stages is reduced, the reliability of the connected devices of the HMG improves.

In general terms, both AC and DC MGs have good efficiency, although the efficiency of DC MGs is higher because in DC MGs no inverter is required to convert the DC power coming from the sources into AC for the loads.

As has been seen, despite DC MGs are more efficient, their implementation is complicated mainly due to the lack of standardization, which is closely related to a lack of development and research in this type of MGs.

These issues also affect hybrid AC/DC MGs, making these systems complex. Investment in DC microgrid research is needed to make both DC and HMGs the best options.

3 Interconnection of AC and DC microgrids in HMGs

A very important issue to deal with is the connection between the AC and DC MGs that form the hybrid microgrid. Hybrid AC/DC MGs consists of three main parts, which are: AC microgrid, DC microgrid, and power electronics interlinking converters (ICs). One of the most relevant elements of HMGs is the IC because it oversees connecting AC-DC MGs.

Some of the features and operability that are obtained thanks to ICs are presented by authors of [12] in Table 2:

Table 2. ICs features [12].

Features	Description
Easier connectivity	ICs allow to asynchronously interconnect AC MGs with different frequency or DC MGs with different voltage.
Power flow control	The ICs allow to control the flow of active and reactive power between the MGs. This allows faster and more precise regulation than direct connection. In addition, greater stability is achieved due to the minimization of impedance effects.
Simplified network	The power grid is easier to control as ICs handle the interactions between the interconnected systems. The complexity of the system

	does not increase when new networks are added. ICs manage to simplify the synchronization and connection of MGs.
Ancillary services	Apart from regulating the power flow, ICs can provide ancillary services to the grid. Ancillary services provided by the ICs have been studied, especially for solid-state transformer (SST), as seen in **[13], [14]**.
Grid decoupling	ICs allow voltage decoupling between connected networks to prevent the propagation of voltage surges and sags from one network to another. ICs also allow current decoupling to isolate current harmonics, which cause efficiency losses.

As seen in Section 1, there are several types of HMGs depending on how the elements are connected to the microgrid and how AC and DC MGs are connected between them. These types of MGs are: AC Coupled Hybrid MG, DC Coupled Hybrid MG and AC-DC Coupled Hybrid MG [4], [7].

ICs provide some relevant ancillary services which are presented by authors of [12]. Therefore, ICs provide the regulation of active and reactive power, harmonic and unbalance compensation, black-start and back-up operation, smart protection or harmonic and resonance damping.

Due to the growing interest in hybrid AC/DC MGs, the implementation and development of ICs has been extensively researched last years. The growing interest in ICs is due to the fact that they generate a simplification of the grid, as well as making it more controllable, modular and reconfigurable.

There are many ways of using ICs. The different types of IC and their uses, which were found in various literature, are exposed here. Authors of [15] propose a new structure of interlinking converter called hybrid coupled interlinking converter (HCIC), which is composed of a converter in series with a static VAR compensator (SVC). This structure is proposed for hybrid AC and low voltage DC MGs.

The point of common coupling (PCC) is the gateway between the MGs and the main grid, this connection is done through a switchgear (three main types of switchgears are used: circuit breakers (CBs), contactors and switches) [3]. Authors of [16] develop a control scheme for the IC in order to maintain a sinusoidal PCC voltage under nonlinear load conditions in islanded HMGs.

In the following scheme (Figure 2), raised by authors of [5], different methods of interconnection of AC and DC MGs are presented.
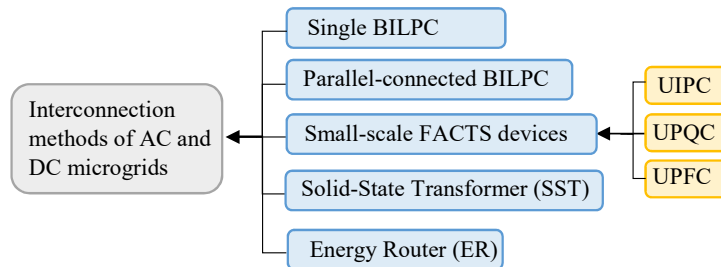
Figure 2. Classification of interconnection methods of AC and DC MGs [5].

These different forms of interconnection methods of AC and DC MGs are described by authors of [5]:

- Single BILPC: Bidirectional interlink power converter is one of the most developed methods in recent years, the amount of transferred power is limited. There is no high reliability.
- Parallel-connected BILPC: Reliability and the amount of exchanged power increase if they are connected in parallel. However, several control challenges appear in control design and operation levels.
- Small-scale FACTS: HMGs can be connected through several methods that add flexibility in power flow, such as unified interphase power controller (UIPC), unified power quality conditioner (UPQC), and unified power flow controller (UPFC).
- Solid state transformer: This element provides a low voltage DC link that makes the integration of DGs and SSs easier. Also, it provides more degree of freedom in power transfer performance [17].
- Energy Router: Consists in various DC/DC and DC/AC power conversion units [18].

It has been seen that the most common interconnection method between AC and DC MGs is through the BILPC. In addition, the most used control methods of the BILPC is the droop-control-based method [5].

4 Control methods

In order to guarantee a correct operation of the system, AC, DC and HMGs require different control tasks [3]. MGs differ from conventional networks mainly because of the control strategies that manage the devices connected to the network. These control strategies are necessary for an adequate management of the microgrid and, in fact, MGs control is a field in which it is necessary to investigate to find the most appropriate method for each case. Therefore, the main characteristics that must fulfil a MG are: protection, transition, synchronization, stability, power balance, power transmission and optimization [19].

The distributed generation units can be controlled by various algorithms that can be classified as centralized or decentralized [20]:

- Centralized control: In this type of control, the microgrid centralized controller (MGCC) controls the DG units. Each individual primary controller of the DGs is commanded by the MGCC. A disadvantage of this control method is that it does not

allow plug-and-play technology [20]. However, this control method allows an easy management of energy between multiple converters connected to the distribution network [21].

▪ Decentralized control: In this control method all the DG units work independently without a secondary master controller. Each controller operates with local measurements themselves effectively and it also allows plug-and-play-technology. Authors of [20] propose a decentralized control for the integration and coordination of various DG units of the system. An important advantage of this type of control method is that the system capacity can be easily extended [21].

Most MGs use centralized control which, due to its simplicity, is suitable for small-scale MGs. In recent years, decentralized control is on the rise, as it allows plug-and-play technology and is more suitable for large MGs and multiple users, as it is more adaptable to changes.
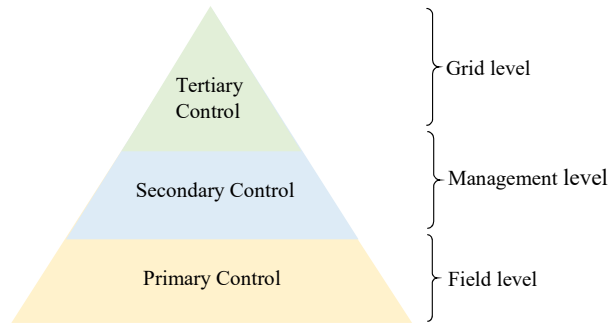
Figure 3. Hierarchical control.

MGs control strategies principally depend on the characteristics of the microgrid, even so, the most adopted control strategies are based on a hierarchical structure [19]. Then, for both AC and DC MGs, three control levels can be differentiated: grid-level/global/tertiary control, management-level/microgrid/secondary control and field-level/local/primary control. Each level controls a different scale of the microgrid. This hierarchical control can be seen schematically in Figure 5. In some articles, such as in the work presented by [22], these levels are called primary, secondary and central.

The three main levels of hierarchical control are [3], [23], [19]:

▪ Primary Control: Each element of the microgrid (DGs, SSs and loads) is connected to a local controller (LC) [3]. Depending on the element connected to the LC, it performs various tasks [3]:

▪ DGs connected to LC: Controllable DGs (gas turbines, small diesel generators, etc.) are controlled by droop control, which offers a good reliability and does not require communication between DERs. Non-controllable DGs (PV, wind turbines, etc.) are managed by nonlinear droop control and hybrid droop control with maximum power point tracking.

- SSs connected to LC: SSs are controlled by state of charge (SoC)-based adaptative droops
  - Loads connected to LC: MGCC controls loads shedding if a centralised hierarchical control is used.
- Secondary Control: The management of the MG is performed by a MGCC [3]. The MGCC restores the frequency and synchronizes the microgrid and the grid only in AC MGs. For both AC and DC, the MGCC restores the voltage, manages load shedding and the optimisation of the production of the MG.
- Tertiary Control: This control sets the power flow between the DC MG and the upper grid [23]. At this level, the distribution network operator (DNO) and the market operator (MO) stand out. On the one hand, MO ensures that the microgrid participates in energy markets following different market policies ranging from supplying the microgrid with its own energy to buying and selling power to the grid [3]. On the other hand, the DNO decides the schedule of power exchange with the MG [23].

Some demands of the MG are expected to be fulfilled in a stable manner: active and reactive power support to loads, voltage and frequency regulation at their nominal values, power flow control with the grid, and optimal and economic operation of the microgrid [24]. All these demands are managed by the microgrid through the hierarchical control.

Another efficient way to control power in a hybrid AC/DC microgrid is proposed by authors of [21], where an energy management method based on ANN theory is proposed to efficiently operate small-scale hybrid AC/DC MGs. Also, a control scheme for coordinating DGs in MGs is reviewed by authors of [25]. Moreover, a control scheme for regulating power flows in a hybrid AC/DC MG interlinked by power converters is explained. The article [26] proposes and designs the control of a system that can operate in connected and isolated mode and shows that the system can maintain stable operation under the proposed coordination control schemes when the network is switched from one operating condition to another.

A useful way of working with hierarchical control can be seen in article [27], where it is concluded that the tertiary control can be made to act as the primary control, thus being able to interconnect more MGs. This could scale the hierarchy of control as needed. This is the reason why the system becomes more flexible and expandable and, consequently, more MGs can be integrated without changing the local hierarchical control system associated to each MG.

5   Future trends

As exposed throughout the article, MGs are useful and increasing in use. Climate change and the reduction in the consumption of fossil fuels or the current energy crisis are precursors to the necessary development and implementation of HMGs. In this section, the most important topics to be discussed in the coming years are presented in order to favourably develop DC MGs and AC/DC HMGs.

As reviewed throughout the article, unlike DC MGs, AC MGs have been extensively studied. Further research on DC MGs is required in order to develop better AC/DC HMGs.

DC devices need to be connected to DC-AC converters to connect to AC MGs. Due to the increasing number of DC devices, the implementation of DC MGs reduces the losses caused by this conversion [9]. In addition, DC MGs and AC/DC HMGs reduce the number of power conversion processes, thus increasing the efficiency of the system [4]. By the way, it is important to promote the development of DC-compatible equipment [9].

There are a number of research areas that should be taken into account in the next years:

- Control: Droop-based control strategies are useful to achieve plug-and-play-technology [19], but it needs to be researched more in the future because it presents some disadvantages [28]. Also, power flow between AC and DC sub-grids can be more suitable if the control strategy for the interface converter is improved. Therefore, the control and management of interface converters is an important topic to investigate further in the coming years [19]. Furthermore, the efficiency of the microgrid can be improved if a high-level control technique is included. This will achieve an improvement in the control of the power flow on the utility grid [29].

- Real-time operation: Due to the increasing incorporation of new RES in MG, there is a need for safer, more reliable, faster and cheaper testing methods.

- Standardization: The standardisation of AC MGs has greatly advanced in the last years, unlike DC MGs [3]. A very important issue that needs to be addressed is the regulatory framework and standardization for DC MGs. There is an important lack of adequate standards since there is no one specific DC voltage level or clear limits between low, medium and high voltage. For this reason, without voltage standardization it is difficult to customize appliances, safety equipment and devices which are connected to the DC buses of the MGs [9].

- Operation mode and protection: The transition between grid-tied and islanded modes of operation needs to be more researched, but no matter the case, this transition should be seamless and smooth [4], [19]. Related to this, the protection technique must be developed to operate in any framework of the microgrid. In addition, future research can be done on artificial intelligence-based microgrid protection that can work in both grid-connected and islanded modes [8]. In any case, the design of protection scheme must guarantee a safe operation [3]. Protection research should also be developed to control cyber-attacks that disrupt the operation of the microgrid [8].

- Cybersecurity: Cyber-physical systems are those that integrate computing, communication, physical processes and security issues [30]; these systems require more research. MGs are cyber-physical systems that can be affected by cyber-attacks. In hybrid AC/DC MGs, cybersecurity has an important effect on the control structure. This is the reason why real-time control and

monitoring systems must be developed in future research for detecting attack scenarios [31].

- Power quality issues: Related to power quality issues, the development of ancillary services such as harmonic compensation, power factor correction, flicker mitigation, etc., is a good research direction for future MG systems [4].
- Economic issues: Regarding economic issues, as MGs are developed and researched, their costs will be reduced and MGs will become cheaper and more accessible [4].
- Interface converters: It is necessary to improve the performance of power interface converters since they control the power flow between networks while ensuring an efficient, reliable and adequate distribution of the power. Also, the modularization of power converters is a topic that needs further research [32], [11]. Depending on the input and output voltage levels of the MGs, different approaches need to be developed [11].
- AC-DC Coupled Hybrid Microgrid: This type of structure, which is presented in Sections 1 and 0, has many benefits compared to the other structures. That is why this will be the most promising microgrid structures in the next years [4], [7].

6   Conclusions

This work presents a review and state-of-the-art of DC and HMGs. As it has been seen throughout the paper, the use and implementation of MGs is growing due to the need for greater consumption and supply of energy from renewable energies such as PV and wind power. In recent years, more research has been done on DC and HMGs, which combine both AC and DC grids, due to the advantages that these MGs offer over AC MGs.

Despite DC MGs having a number of disadvantages due to the lack of research such as the need for specific standards, higher costs than AC MGs and the absence of a highly developed technology that allows a better implementation; DC MGs have advantages that cannot be disregarded and that make them a viable option. These advantages are the increasing number of DC loads, improving the effectiveness and power quality of MGs by reducing power losses due to power conversions; and an easier integration of RES in DC MG, thus reducing CO_2 emissions. This is why the use of hybrid AC/DC MGs is a good option, as they encompass the advantages of both DC and AC MGs.

HMGs consist of an AC microgrid, a DC microgrid and an interlinking converter that enables the interconnection between both MGs. The growing interest in ICs is due to the fact that they simplify the grid, make it more controllable, modular, reconfigurable and offers easier connectivity. The BILPC is one of the most developed interconnection methods in recent years.

The importance of hierarchical control has been described and highlighted, and several examples of control methods investigated in various works such as making the tertiary control to act as the primary one to achieve a more expandable MG or the use

of ANN to control the MGs have been presented. Centralized control, due to its simplicity, is suitable for small-scale MGs. In recent years, decentralized control is on the rise, as it allows plug-and-play technology and is more suitable for large MGs and multiple users, as it is more adaptable to changes.

Finally, several topics have been discussed about what further research should be carried out in the future in order to improve the implementation of hybrid and DC MGs. Some of the most important future trends are the need for standardization for DC MGs, cost reduction or cybersecurity.

References

1. S. Mishra and R. K. Viral, "Introduction to hybrid AC/DC microgrids," in *Microgrids*, Elsevier, 2022, pp. 159–189. doi: 10.1016/b978-0-323-85463-4.00005-8.
2. J. T. Seo, "Towards the advanced security architecture for Microgrid systems and applications," *J Supercomput*, vol. 72, pp. 3535–3548, 2016, doi: 10.1007/s11227-016-1786-8.
3. E. Planas, J. Andreu, J. I. Gárate, I. Martínez De Alegría, and E. Ibarra, "AC and DC technology in microgrids: A review," *Renewable and Sustainable Energy Reviews*, vol. 43, pp. 726–749, Mar. 2015, doi: 10.1016/J.RSER.2014.11.067.
4. F. Nejabatkhah and Y. L. Wei, "Overview of Power Management Strategies of Hybrid AC/DC Microgrid," *IEEE Trans Power Electron*, vol. 30, no. 12, 2015, doi: 10.1109/TPEL.2014.2384999.
5. M. Zolfaghari, G. B. Gharehpetian, M. Shafie-khah, and J. P. S. Catalão, "Comprehensive review on the strategies for controlling the interconnection of AC and DC microgrids," *International Journal of Electrical Power & Energy Systems*, vol. 136, p. 107742, Mar. 2022, doi: 10.1016/J.IJEPES.2021.107742.
6. J. J. Justo, F. Mwasilu, J. Lee, and J. W. Jung, "AC-microgrids versus DC-microgrids with distributed energy resources: A review," *Renewable and Sustainable Energy Reviews*, vol. 24, pp. 387–405, Aug. 2013, doi: 10.1016/J.RSER.2013.03.067.
7. O. Azeem *et al.*, "A comprehensive review on integration challenges, optimization techniques and control strategies of hybrid ac/dc microgrid," *Applied Sciences (Switzerland)*, vol. 11, no. 14, Jul. 2021, doi: 10.3390/app11146242.
8. A. Dagar, P. Gupta, and V. Niranjan, "Microgrid protection: A comprehensive review," *Renewable and Sustainable Energy Reviews*, vol. 149. Elsevier Ltd, Oct. 01, 2021. doi: 10.1016/j.rser.2021.111401.
9. M. Fotopoulou, D. Rakopoulos, D. Trigkas, F. Stergiopoulos, O. Blanas, and S. Voutetakis, "State of the Art of Low and Medium Voltage Direct Current (DC) Microgrids," vol. 14, 2021, doi: 10.3390/en14185595.
10. D. Kumar, F. Zare, and A. Ghosh, "DC Microgrid Technology: System Architectures, AC Grid Interfaces, Grounding Schemes, PowerQuality, Communication Networks, Applications, and Standardizations Aspects", doi: 10.1109/ACCESS.2017.2705914.
11. E. Unamuno and J. A. Barrena, "Hybrid ac/dc microgrids—Part I: Review and classification of topologies," *Renewable and Sustainable Energy Reviews*, vol. 52, pp. 1251–1259, 2015, doi: https://doi.org/10.1016/j.rser.2015.07.194.

12. A. Ordono, E. Unamuno, J. A. Barrena, and J. Paniagua, "Interlinking converters and their contribution to primary regulation: a review," *International Journal of Electrical Power and Energy Systems*, vol. 111, pp. 44–57, Oct. 2019, doi: 10.1016/j.ijepes.2019.03.057.

13. L. F. Costa, G. de Carne, G. Buticchi, and M. Liserre, "The Smart Transformer: A solid-state transformer tailored to provide ancillary services to the distribution grid," *IEEE Power Electronics Magazine*, vol. 4, no. 2, pp. 56–67, 2017, doi: 10.1109/MPEL.2017.2692381.

14. Z.-X. Zou, G. Buticchi, and M. Liserre, "Control and communication in the Smart Transformer-fed grid," in *2016 IEEE 21st International Conference on Emerging Technologies and Factory Automation (ETFA)*, 2016, pp. 1–9. doi: 10.1109/ETFA.2016.7733495.

15. L. Wang, X. Fu, and M.-C. Wong, "Operation and Control of a Hybrid Coupled Interlinking Converter for Hybrid AC/Low Voltage DC Microgrids," *IEEE TRANSACTIONS ON INDUSTRIAL ELECTRONICS*, vol. 68, no. 8, 2021, doi: 10.1109/TIE.2020.3001802.

16. D. M. Phan and H. H. Lee, "Interlinking Converter to Improve Power Quality in Hybrid AC-DC Microgrids with Nonlinear Loads," *IEEE J Emerg Sel Top Power Electron*, vol. 7, no. 3, pp. 1959–1968, Sep. 2019, doi: 10.1109/JESTPE.2018.2870741.

17. J. E. Huber and J. W. Kolar, "Applicability of Solid-State Transformers in Today's and Future Distribution Grids," *IEEE Trans Smart Grid*, vol. 10, no. 1, pp. 317–326, Jan. 2019, doi: 10.1109/TSG.2017.2738610.

18. Y. Liu, Y. Fang, and J. Li, "Interconnecting microgrids via the energy router with smart energy management," *Energies (Basel)*, vol. 10, no. 9, Aug. 2017, doi: 10.3390/en10091297.

19. E. Unamuno and J. A. Barrena, "Hybrid ac/dc microgrids—Part II: Review and classification of control strategies," *Renewable and Sustainable Energy Reviews*, vol. 52, pp. 1123–1134, Dec. 2015, doi: 10.1016/J.RSER.2015.07.186.

20. L. Domínguez-García, G. Kyriakarakos, J. Jayaram, M. Srinivasan, N. Prabaharan, and T. Senjyu, "Design of Decentralized Hybrid Microgrid Integrating Multiple Renewable Energy Sources with Power Quality Improvement," 2022, doi: 10.3390/su14137777.

21. K.-M. Kang *et al.*, "Energy Management Method of Hybrid AC/DC Microgrid Using Artificial Neural Network," 2021, doi: 10.3390/electronics10161939.

22. P. S. Prasad, A. M. Parimi, and L. Renuka, "Control of hybrid AC/DC microgrids," in *Microgrids*, Elsevier, 2022, pp. 191–225. doi: 10.1016/b978-0-323-85463-4.00003-4.

23. C. N. Papadimitriou, E. I. Zountouridou, and N. D. Hatziargyriou, "Review of hierarchical control in DC microgrids," *Electric Power Systems Research*, vol. 122, pp. 159–167, May 2015, doi: 10.1016/J.EPSR.2015.01.006.

24. K. Dubey, Sanat, and P. Jena, "Protection schemes in microgrid," in *Microgrid Cyberphysical Systems*, Elsevier, 2022, pp. 255–276. doi: 10.1016/b978-0-323-99910-6.00003-7.

25. J. M. Guerrero, P. Chiang Loh, T.-L. Lee, and M. Chandorkar, "Advanced Control Architectures for Intelligent Microgrids 2014;Part II: Power Quality, Energy Storage, and AC/DC Microgrids," *IEEE Transactions on Industrial Electronics*, vol. 60, no. 4, p. 1263, 2013, doi: 10.1109/TIE.2012.2196889.

26. X. Liu, P. Wang, and P. C. Loh, "A Hybrid AC/DC Microgrid and Its Coordination Control," *IEEE Trans Smart Grid*, vol. 2, no. 2, 2011, doi: 10.1109/TSG.2011.2116162.

27. J. M. Guerrero, J. C. Vasquez, J. Matas, L. Garci de Vicuna, and M. Castilla, "Hierarchical Control of Droop-Controlled AC and DC Microgrids-A General Approach Toward

Standardization," *IEEE TRANSACTIONS ON INDUSTRIAL ELECTRONICS*, vol. 58, no. 1, pp. 158–172, 2011, doi: 10.1109/TIE.2010.2066534.

28. A. Bidram and A. Davoudi, "Hierarchical Structure of Microgrids Control System," *IEEE Trans Smart Grid*, vol. 3, no. 4, 2012, doi: 10.1109/TSG.2012.2197425.

29. Q. Shafiee, T. Dragičević, J. C. Vasquez, and J. M. Guerrero, "Hierarchical control for multiple DC-microgrids clusters," *IEEE Transactions on Energy Conversion*, vol. 29, no. 4, pp. 922–933, 2014, doi: 10.1109/TEC.2014.2362191.

30. T. v. Vu, B. L. H. Nguyen, Z. Cheng, M. Y. Chow, and B. Zhang, "Cyber-Physical Microgrids: Toward Future Resilient Communities," *IEEE Industrial Electronics Magazine*, vol. 14, no. 3. Institute of Electrical and Electronics Engineers Inc., pp. 4–17, Sep. 01, 2020. doi: 10.1109/MIE.2019.2958039.

31. M. Najafzadeh, R. Ahmadiahangar, O. Husev, I. Roasto, T. Jalakas, and A. Blinov, "Recent Contributions, Future Prospects and Limitations of Interlinking Converter Control in Hybrid AC/DC Microgrids," *IEEE Access*, vol. 9, pp. 7960–7984, 2021, doi: 10.1109/ACCESS.2020.3049023.

32. J. W. Kolar, G. Ortiz, J. W. Kolar, and G. Ortiz, "Solid-State-Transformers: Key Components of Future Traction and Smart Grid Systems."

Development of a gas-absorption packed column simulator for power plants with CO_2 capture

Miriam Navarrete Procopio[1][0000−0002−0247−9647], Gustavo
Urquiza[1][0000−0001−5075−3631], and Laura Castro[1][0000−0003−2507−0067]

Centro de Investigación en Ingeniería y Ciencias Aplicadas (CIICAP), Universidad
Autónoma del Estado de Morelos, Cuernavaca, Morelos, México
miriam.navarrete@uaem.mx

Abstract. The electricity generation process from fossil fuels is one of
the main sources of CO_2 emissions, post-combustion CO_2 capture is an
alternative to minimize emissions. The packed absorption column is the
first unit of the CO_2 capture process. In this work, a simulator of gas
absorption columns was developed using Matlab as a programming lan-
guage with RefProp to calculate the thermodynamic and thermophysical
properties of the substances used in the processes. The model was vali-
dated by measurements in a laboratory-scale absorption unit, simulations
were carried out with the same operating conditions as measurements
and two different fuels were treated, coal and natural gas. Once having a
reliable model the combined cycle power plant in Mexico was simulated,
with the objective of evaluating the main parameters in the absorption
process and have the dimensions of the packed absorption column re-
quired to carry out the capture of CO_2 in the power plant. From the
result of the simulations it is established 5 columns treatment with 4
m of diameter and 11 m of height to removed of 95% of the CO_2 con-
tained in the flue gases with a solution of 30% monoethanolamine using
Mellapak 250Y structured packaging.

Keywords: Post-combustion capture, Absorption column, Power Plant,
Process system modelling

1 Introduction

The electricity generation process from fossil fuels is the second main source of
CO_2 emissions in Mexico, [1], which is the greenhouse gas with largest contrib-
utor to global warming. The "Special climate change program" issued by the
Mexican Federal Government, study the postcombustion CO_2 capture process
for application in power plants was carried out as a possible alternative to reduce
CO_2 emissions in Mexico, it ranked the first fifteen emitting countries in 2010
with 1.4% of global emissions, with this trend in 2020 national CO_2 emissions
would reach one billion tons. [2].

Carbon capture and storage (CCS) consists of the separation of CO_2 from in-
dustrial source, transportation of CO_2 to a storage location, and long-term isola-
tion of CO_2 from the atmosphere, CCS represents an option for the mitigation of

anthropogenic greenhouse gas emissions caused by fossil fuel use [3,4]. There are three technological pathways that can be used for CO_2 capture from coal-derived power generation: oxy-combustion, pre-combustion, and post-combustion capture.

From the available methods of CO_2 capture, post-combustion is the only method that can be retrofitted to existing plants. In power plant with Post-combustion capture, the separation of CO_2 from flue gas derived from combustion fossil fuels is carried out using amine solvents, and then absorbed CO_2 is liberated from the solvent and is compressed for transportation and storage. [1–8]. In the literature discuss the two main paths; trying different solvents and optimization of the process configuration [9–12]. Some parameters are important to determine the amine type to be used as an absorbent solution, these parameters could be concentration of the amine solutions, solution temperature, CO_2 loading and corrosion behavior. Solvents have been proposed for the chemical CO_2 absorption process, but these may not fulfill the expectations of capture of CO_2 in a global scenario due to energetic and environmental penalty that takes place during its use, monoethanolamine (MEA) is the most used industrially. [13–15].

Simulators are of great importance in industrial processes since they provide valuable information, these are a friendly tool that performs all the relevant calculations with indispensable input data. The simulator can prevent results that could be unfavorable before including a new unit to the process or modify the operating conditions. A higher number of chemical companies have decided to use them for operational training, with the aim of improving and increasing the efficiency of industries by modifying the conditions of the process [16–18].

The Post-combustion capture consists of the next components: absorber, heat exchanger and stripper as well as auxiliary equipment such as pumps, valves and reservoirs. The aim of this study is to have a gas-absorption packed column simulator, which is the first component that begin with capture process. The model was validated with experimental data, varying the following parameters: the CO_2 content of the entering gas, the gas flow, the MEA weight percentage and the solvent flow. In additions, a Thermoelectric Plant in Mexico was simulated to obtained the needed dimensions and operating conditions of absorption column to capture its CO_2 emissions.

This work contains the development of the mathematical model (section 2), the validation of the mathematical model (section 3) and the simulation of a power plant (section 4).

2 Mathematical model

2.1 Process unit description

For this work, an absorption packed column is the processing unit. It is an equipment with a gas inlet at the bottom (G_1) and liquid inlet on the top (L_2), liquid flows downward by gravity and outlet is at bottom (L_1), while gas flows upward through the wetted packing, contacting the liquid and coming out at the top (G_2) (countercurrent flow). Figure 1 show the absorber unit for the model.
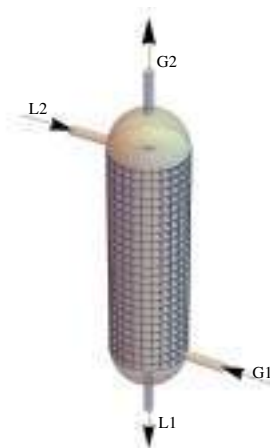
Fig. 1. Packed column process unit.

The reaction between the amines and CO_2 are quite complex. However the overall reactions can be represented as follows [19, 20]:

$$MEA + CO_2 \leftrightarrow MEACOO^- + H^+$$
$$MEA + H^+ \leftrightarrow MEAH^+$$

$$\overline{2MEA + CO_2 \leftrightarrow MEACOO^- + MEAH^+}$$
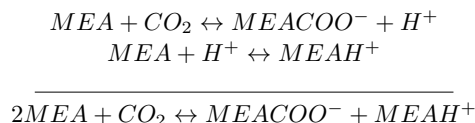
The gas absorption is a mass-transfer operation through diffusion, the driving force for transfer is a concentration difference, where a solute contained in a gas mixture is absorbed by a solvent in the packing. The packing increase contact between the liquid and gas, random and structured are principal types of packings. Table 1 shows the specifications of the types of packaging used in this work, random plastic packs were used for model validation (Pall Ring) and structured metal packs were used for power plant simulations (Mellapak).

Table 1. Specifications of packings.

Type	Material	Size (in)	a_t (m^2/m^3)	ε
Pall rings	Polypropylene	5/8	274	0.90
Mellapak	Metal	250Y	250	0.97

2.2 Equations of balance and design

The evaluation of an absorption column involves the determination of its dimensions. The diameter of an absorption column is in function of the flows of the gas to be treated and absorbent solvent, the total volume of packing, which determines the size of the column, depends on the finally concentration of solute and the overall mass transfer coefficient. Calculations of material balances and design parameters, the equilibrium data for the systems as well as their properties are necessary.

The main assumptions used to simplify the analysis are:

— The processes are in steady-state conditions
— The absorption process is adiabatic
— The species in the gas mixture are ideal gases
— Thermodynamic and transport properties were modelled using RefProp for CO_2, O_2, N_2 and H_2O.
— The insert MEA property was included of the base version of Aspen Plus

The overall material balance for the column in the figure 1 can be write as follow:

$$G_1 y_1 + L_2 x_2 = G_2 y_2 + L_1 x_1 \tag{1}$$

The relationship between x and y at any point in the column, obtained by rearranging Eq1, is called operating-line equation

$$\left(\frac{y_2}{1-y_2}\right) = \frac{L_s}{G_s}\left(\frac{x_2}{1-x_2} - \frac{x_1}{1-x_1}\right) + \left(\frac{y_1}{1-y_1}\right) \tag{2}$$

Where $\left(\frac{y_2}{1-y_2}\right)$ represent the molar ratio for gas and $\left(\frac{x_2}{1-x_2}\right)$ for the liquid.

Figure 2 shows the equilibrium curve for $MEA - CO_2$ 30% wt system [21], in the same can be plotted the minimum and real operating line, these have to be drawn above the equilibrium for the absorption process to take place, since this gives a positive driving force $y - y^*$ for absorption.

The height of the column (Z_T) required for the relevant separation process can be obtained from this equation:

$$Z_T = \frac{G_G}{K_G} \int \frac{dy}{y - y^*} \tag{3}$$

The integral in Eq. 3 is called number of transfer units (NTU) based on the global driving force for the gas phase, the simulator solves NTU for diluted and concentrated conditions, the other hand side of Eq. 3 has the units of length and
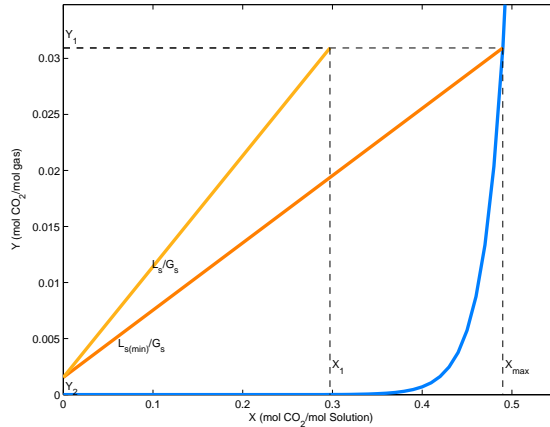
Fig. 2. Construction of the operation line for the $MEA - CO_2$ 30% wt system.

is called height of a transfer unit (HTU) is calculated from the mass transfer correlations.

$$Z_T = HTU \ NTU \tag{4}$$

In the field of process engineering, the overall mass transfer coefficient of liquid and gas, have been predicted with different correlations. The correlation that allows determination of mass transfer coefficients (k_G), is the Onda model [22] to random packaging and the Bravo model to structured packaging are written as follows [23]:

$$\frac{k_G RT}{a_t D_G} = 5.23 \left(\frac{G}{a_t \mu_G} \right)^{0.7} \left(\frac{\mu_G}{\rho_G \mu_G} \right)^{1/3} (a_t D_G)^{-2} \tag{5}$$

$$k_G = 0.054 \left(\frac{\rho_G (U_G + U_L)s}{\mu_G} \right)^{0.8} \left(\frac{\mu_G}{D_G \rho_G} \right)^{0.333} \left(\frac{D_G}{s} \right) \tag{6}$$

Where R is the gas constant ($m^3/atm \ mol \ K$), T is temperature (K), ρ_G is density (kg/m^3), μ_G is viscosity ($kg/m \ h$), D_G is diffusivity (m^2/h) of gas phase and U is the speed (m/s) of gas (G) and liquid (L) phase.

Diffusivity is best estimated by experimental measurements and where such information is available for the system of interest, it should be used directly. Often the desired values are not available, however, it must be estimated from published correlations. The value of the binary diffusion is obtained using the potential of Lennard-Jones with parameters ϵ and σ for CO_2 and air to the following equation:

$$D_G = \frac{0.00185 T^{3/2} \left[(MW_a + MW_b) / MW_a MW_b \right]^{1/2}}{P \sigma_{ab}^2 \Omega_D} \tag{7}$$

Where MW is the molecular weights $(kg/kmol)$, P is pressure (atm) and the subscripts a, b are CO_2 and air.

The programming algorithm presented in Figure 3 was used in this study. The algorithm consists of two main input cases: case (1) the percent CO_2 removed ($\cdot\cdot$) to returd the column packed size and case (2) the column height to returd CO_2 concentration in the out flue gas. The algorithm was programming at ┌-UIDE MATLAB version P201Na. Example of simulator main window is shown in Figure 4.
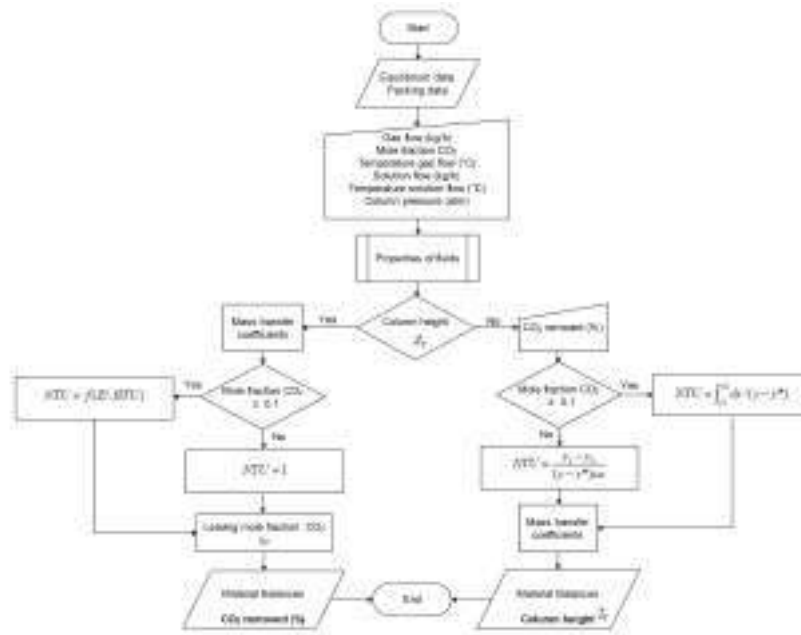
Fig. 3. Programming algorithm.
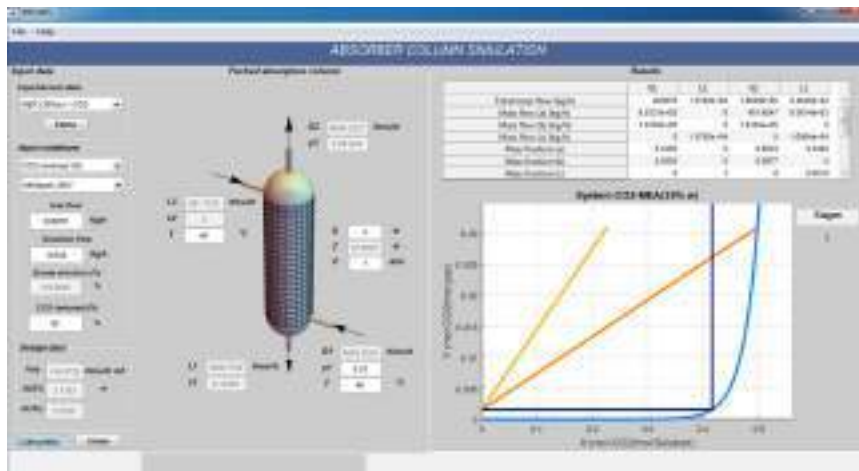
Fig. 4. Simulator main window.

3   Model validation

The validation of the model was performed with experiments in a laboratory-scale absorption unit at INEEL (Instituto Nacional de Electricidad y Energías Limpias).

3.1   Experimental section

The experimental column absorption is shown in Figure 5. The lab unit includes a column ($T-101$) made of borosilicate glass Duran 3.3, with a height of 1.70 m and internal diameter of 4", the type of packaging used was 5/8" polypropylene pall ring, the total height of the packing is 1.20 m. Additionally, there are two atmospheric tanks: one for holding a CO_2-free MEA solution ($TK-101$) and another for the reception of CO_2 rich solution ($TK-104$); a pump for feeding of the MEA to the column ($P-101$); for the gas conditioning there are: a pressurized tank contained CO_2 ($TK-102$), an air compressor ($TK-103$) and volumetric flow measurement instruments (gas mixer, "M", and rotameters).There is a reacts chemically between the absorbent solution and the carbon dioxide when the gases flow (Stream 3) through the packed bed absorber ($T-101$) countercurrent to the solution. CO_2 gas is absorbed into an amine solution (Stream 1) and it becomes a "rich" CO_2 concentration (Stream 2) solution. The purified gas is vented to the atmosphere from the top of the absorber (Stream 4) using a certified analyzer gas (Testo 350 Portable Emission Analyzer) and humidity-temperature meter (Vaisala M170), respectively.

(a) Schematic flow diagram.   (b) CO_2 capture lab unit.
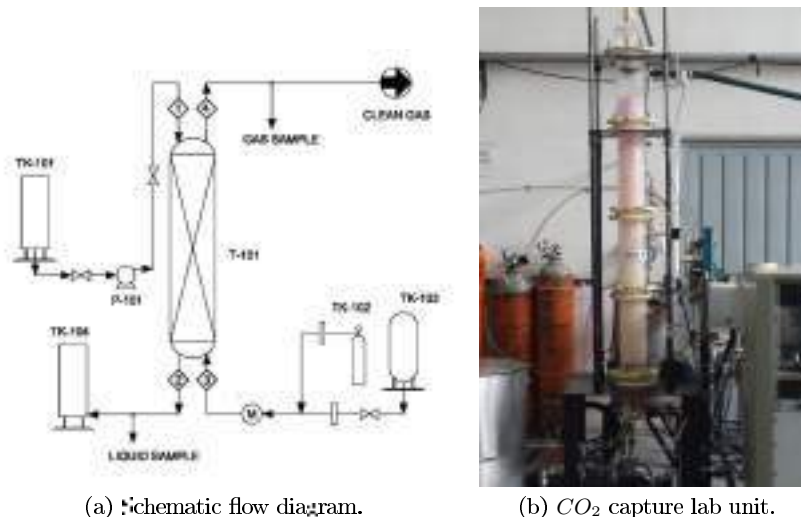
Fig. 5. Experimental process.

Table 2 shows the parameters used during in experiments and later in simulations. They were conducted using two different gas flow rate, 104 NL/min (Normal Liters per minute) with 12 % CO_2 concentration and 76 NL/min with 5.1 % CO_2 concentration, tests for CO_2 composition of a Coal Electric and a Combined Cycle Power Plant respectively, besides two different MEA concentration 25 and 30 % wt, the flow rates of MEA solution were varied to have different ratios of $CO_2 : MEA$.

Table 2. Experiment configurations.

Case	Flue gas flow (NL/min)	CO_2 composition $(vol\%)$	MEA composition $(wt\%)$	Flow MEA solution (mL/min)
1	104	12	25	410
2	104	12	25	675
3	104	12	30	344
4	104	12	30	559
5	76	5.1	25	128
6	76	5.1	25	299

The results based on the developed model and the laboratory-scale absorption unit were compared. Table 3 includes them.

There are coincidence between simulation and experimentation values in all cases. Several studies that propose models for the capture of CO_2 by absorption columns have reported results with higher relative errors than this work [24,25].

The higher relative errors is to calculated Z_T, this is due to use a correlation mass transfer coefficient.

Table 3. Experimental results with the developed model.

Case	CO_2 removed (%) Exp	CO_2 removed (%) Sim	Rel.Error (%)	Column height (m) Exp	Column height (m) Sim	Rel.Error (%)
1	77.30	83.50	8.02	1.20	1.01	15.93
2	83.50	83.50	0.00	1.20	1.23	2.31
3	81.20	83.66	3.03	1.20	1.13	5.47
4	85.00	83.80	1.41	1.20	1.29	7.54
5	53.70	53.88	0.33	1.20	1.19	0.27
6	62.70	59.70	4.78	1.20	1.23	2.52

4 Power Plant Simulation

The reference plant is a natural-gas-fired combined-cycle with 244 MW power located in the center region of Mexico. Table 4 shows power plant key data.

Table 4. Base case power plant summary.

Process variable	Value
Power (MW)	244
Natural gas consumption (t/h)	16.63
Flow of gases to be treated (t/h)	1004.35
Exhaust gas pressure (atm)	1.18
Exhaust gas temperature (^{o}C)	146

In order to know the composition of the exhaust gases to be treated in the combined cycle plant, stoichiometric calculations of the methane combustion reaction were made, taking as input data the flow of fuel and exhaust gases.

The Eq. 8 establishes the combustion reaction of methane, the major component of natural gas:

$$CH_4 + a\left[O_2 + 3.76N_2\right] \rightarrow iCO_2 + jH_2O + eN_2 + gO_2 \tag{8}$$
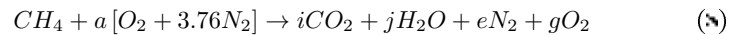
The molar composition of the exhaust gases are: 3% CO_2, 13% O_2, 7% H_2O, 77% N_2 with CO_2 emission rate of the plant is 124 kg/MWh.

3　Results and discussion

In the absorption process, the flow of the inlet gas G_1, its composition y_1 and a given separation task are usually fixed values. Accordingly, the amount of inlet liquid flow L_2 and the main dimensions of the column is left to the designer's choice. The aim of this work is to supplement the theoretical considerations by the results of relevant studies that were performed in the simulations.

Using the simulator developed in this work, the following discussion how to estimate the dimensions of the absorption column and the solution flow required for CO_2 capture process:

1. One fifth of the total gas flow presented in Table 4 was treated with a MEA solution 30% wt, the corresponding flue gas flow rate is 200.87 t/h, with low CO_2 concentration (3% mol). The structure packing type used was shown in Table 1.

2. Both the removed amount of CO_2 and required absorbent solution influence the size. The first analysis was carried out to determined the diameter of the column, Fig. 6(a) shows the effect of percentage of excess solution and column height on absorber diameter. It is clear that increasing the amount of solution decreases the column height required, this happens because the most important factor affecting column height is residence time in the fluid, it is the time in which CO_2 and MEA are in contact through the packed column. The column diameters were varying of 2, 3, 4, 5 and 6 m, there is a height difference of almost 4 meters between 2 and 3 m of diameter and almost 2.5 meters between 3 and 4 m. Nevertheless, the smallest height difference occurs between diameters 4 and 5, with this comparison a column diameter of 4 m was selected.

3. Another significant contribution to the dimensions of the column is the removal efficiency which is also strongly influenced by amount solution, the process parameter was varied (90, 92, 95 and 98% removal). The results are shown in Fig. 6(b), the column size is reduced almost 7 m, if you choose to remove 95% instead of the maximum simulated. Within 92 - 95% the size of the column is reduced almost 3 m, from the results the best CO_2 removal efficiency by MEA (30%) was 95% with a column height of 13 m.

4. The last parameter to analyze is the amount of solution, in both graphics 20-200 % of excess MEA solution was varied, it was managed to reduce 2 m more to the column height by feeding a percentage of excess amine solution of 120% with a greater amount of solution the decrease in height is negligible.The calculation of the Z_T is based on the NTU, which is the result of the area under the curve between the line of operation and the equilibrium curve as shown in the Fig. 2, the greater L the less area under the curve and therefore less Z_T.

(a)   (b)
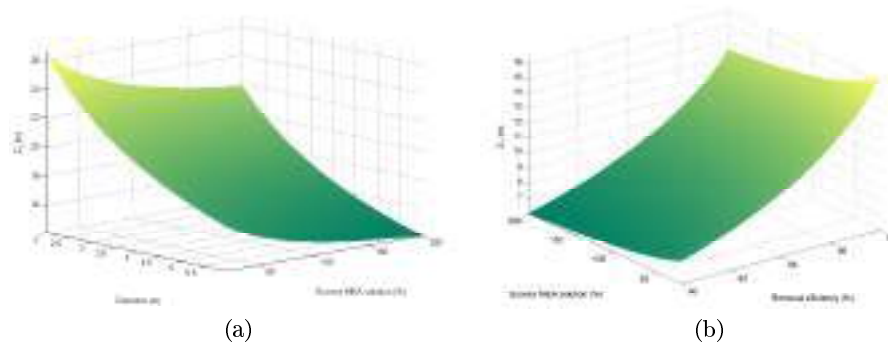
Fig. 6. Excess MEA solution profiles for height of the column with diameters from 2 to 6 (a) and 4 different removal efficiencies (b).

In this study, absorption columns were used to remove CO_2, 5 columns are required to treat 200.87 t/h of exhaust of the combined cycle power plant, it is possible to absorb 0.37 $MtCO_2/year$ having a favourable environmental impact. Table 5 shows the overall results for a column absorption.

Table 5. Results of the baseline case.

Parameter	Value
Flue gas components	CO_2, O_2, N_2, H_2O
Pressure (atm)	1.0
Temperature (^oC)	40
Inlet flue gas flow-rate (t/h)	200.87
CO_2 (vol %)	3
Packing type	Mellapak 250 Y
MEA composition (w %)	30
CO_2 capture (%)	95
Column diameter (m)	4
Column height (m)	11
Excess solution (%)	120
flue liquid flow-rate (t/h)	19.70

6 Conclusions

The developed model solves the dimensions of the absorption column for concentrated and diluted gas flows to be treated, making the analogy to a natural

gas combined cycle power plant or a coal-electric power plant respectively and on the other hand determines the conditions of the output flows, establishing as input data the dimensions of the equipment. Unlike commercial software for simulating processes, the simulator developed in this work is user friendly, the flowsheet is easy for balance results checking.

The mathematical model was validated with data from a laboratory-scale absorption unit obtaining favourable results. The CO_2 removed is predicted by the developed simulator with a deviation from 0-8% , while the height of the column about 0.27-17.13%. The higher relative errors were to calculate Z_T, this is due to use a correlation mass transfer coefficient.

A test case was made to determine if the model was built according to the requirements of the user. A combined cycle electric power station was simulated to determine the dimensions of the absorption column necessary to remove the CO_2 contained in its exhaust gases, making several parametrizations it was obtained that 5 columns treatment with 4 m of diameter and 11 m of height to removed of 85% of the CO_2 contained in the flue gases with a solution of 30% monoethanolamine using Mellapak 250Y structured packaging.

References

1. INECC-SEMARNAT, Primer Informe Bienal de Actualización ante la Convención Marco de las Naciones Unidas sobre el Cambio Climático, México, (2015).
2. PROGRAMA Especial de Cambio Climático, Diario Oficial de la Federación. 28 de abril de 2019
3. Cau, Giorgio, et al. CO2-free coal-fired power generation by partial oxy-fuel and post-combustion CO_2 capture: Techno-economic analysis. Fuel 214 423-435 (2018)https: doi.org 10.1016 j.fuel.2017.10.023
4. Wang, Yuan, et al. A review of post-combustion CO_2 capture technologies from coal-fired power plants. Energy Procedia 114 650-665 (2017) https: doi.org 10.1016 j.egypro.2017.03.1209
5. Arroyave, Juan D., et al. Evaluation of CO_2 production for enhanced oil recovery from four power plants. Energy 206 118161 (2020) https: doi.org 10.1016 j.energy.2020.118161
6. Koytsoumpa, Efthymia Ioanna, Christian Bergins, and Emmanouil Kakaras. The CO_2 economy: Review of CO_2 capture and reuse technologies. The Journal of Supercritical Fluids 132 3-16 (2018) https: doi.org 10.1016 j.supflu.2017.07.029
7. Olaleye, Akeem K., Meihong Wang, and Greg Kelsall. Steady state simulation and exergy analysis of supercritical coal-fired power plant with CO_2 capture. Fuel 151 57-72 (2015) https: doi.org 10.1016 j.fuel.2015.01.013
8. Cao, Yang, et al. Energy and exergy investigation on two improved IGCC power plants with different CO_2 capture schemes. Energy 140 47-57 (2017): https: doi.org 10.1016 j.energy.2017.08.044

9. Sang-Jun Han. Jung-Ho Wee. Estimation of CO_2 Absorption Capacity via Correlating Measured Electrical Conductivity in a Diethanolamine Solvent System Compared to Monoethanolamine Solvent Systems, Journal of Chemical & Engineering data , 62, 1570-1580 (2017) https: doi.org 10.1021 acs.jced.6b00862

10. Sang-Jun Han. Jung-Ho Wee. Estimation of CO_2 Absorption Capacity via Correlating Measured Electrical Conductivity in a Diethanolamine Solvent System Compared to Monoethanolamine Solvent Systems, Journal of Chemical & Engineering data , 62, 1570-1580 (2017) https: doi.org 10.1021 acs.jced.6b00862

11. Kaiyun Fu. Guangying Chen. Zhiwu Liang. Teerawat Sema. Raphael Idem, Analysis of Mass Transfer Performance of Monoethanolamine-Based CO_2 Absorption in a Packed Column Using Artificial Neural Networks, Industrial & Engineering Chemistry Research , 53, 4413-4423 (2014)https: doi.org 10.1021 ie403259g

12. Xiaofei Li. Shujuan Wang. Changhe Chen, Experimental Study of the Dynamic Behavior of the Stripping Column for Post-combustion CO_2 Capture with Monoethanolamine, Energy & fuels , 28, 1230-1241 (2014) https: doi.org 10.1021 ef40213sm

13. Amornvadee Veawab, Paitoon Tontiwachwuthikul, Amit Chakma, Corrosion Behavior of Carbon Steel in the CO_2 Absorption Process Using Aqueous Amine Solutions, Industrial & Engineering Chemistry Research, 38, 3917-3924 (1999)https: doi.org 10.1021 ie9901630

14. Huertas, José I. Gomez, Martin D. Giraldo, Nicolas and Garzón, Jessica, CO_2 absorbing capacity of MEA, Journal of Chemistry, 2015, 925-931 (2015)https: doi.org 10.1155 2015 965015

15. Patricia Luis, Use of monoethanolamine (MEA) for CO_2 capture in a global scenario: Consequences and alternatives, Desalination, 380, 93-99 (2016)https: doi.org 10.1016 j.desal.2015.08.004

16. Olaleye, Akeem K., and Meihong Wang. Conventional and Advanced Exergy Analysis of Post-combustion CO_2 Capture in the Context of Supercritical Coal-Fired Power Plant. Exergy for A Better Environment and Improved Sustainability 1. Springer 1235-1248 (2018) https: doi.org 10.1007 978-3-319-62572-0_79

17. Jokar, Seyyed Mohammad and Rahimpour, Hamid Reza and Momeni, Hossein and Rahimpour, Mohammad Reza and Abbasfard, Hamed, Simulation and feasibility analysis of structured packing replacement in absorption column of natural gas dehydration process: A case study for Farashband gas processing plant, Iran, Journal of Natural Gas Science and Engineering, 18, 336-350 (2014)https: doi.org 10.1016 j.jngse.2014.03.005

18. Fan, Zhen and Liu, Kun and Ji, Guojie and Frimpong, Reynolds and Nikolic, Heather and Liu, Kunlei, Aspen modeling for $MEA-CO_2$ loop: Dynamic gridding for accurate column profile, International Journal of Greenhouse Gas Control, 37, 318-324 (2015)https: doi.org 10.1016 j.ijggc.2015.03.035

19. Celia, Michael A. Geological storage of captured carbon dioxide as a large-scale carbon mitigation option. Water Resources Research 53 5 3527-3533 (2017) https: doi.org 10.1002 2017WR020841

20. Desideri, U., and Paolucci, A. Performance modelling of a carbon dioxide removal system for power plants. Energy conversion and management, 40(18), 1899-1915 (1999). https: doi.org 10.1016 S0196-8904(99)00074-6

21. Ugochukwu E. Aronu, Shahla Gondal, Erik T. Hessen, Tore Haug-Warberg, Ardi Hartono, Karl A. Hoff, Hallvard F. Svendsen, Solubility of CO_2 in 15, 30, 45 and 60 mass% MEA from 40 to 120 $°C$ and model representation using the extended UNIQUAC framework, Chemical Engineering Science, 66, 6393–6406 (2011) https: doi.org 10.1016 j.ces.2011.08.042

22. Kim, Seongyup and Deshusses, Marc A., Determination of mass transfer coefficients for packing materials used in biofilters and biotrickling filters for air pollution control-2: Development of mass transfer coefficients correlations, Chemical Engineering Science, 63, 856-861 (2008) https://doi.org/10.1016/j.ces.2007.10.021

23. Wang, G. Q. and Yuan, X. G. and Yu, K. T., Review of mass-transfer correlations for packed columns, Industrial and Engineering Chemistry Research, 44, 8715-8729 (2005) https://doi.org/10.1021/ie050017w

24. Kvamsdal, H. M., Jakobsen, J. P., and Hoff, K. A. Dynamic modeling and simulation of a CO2 absorber column for post-combustion CO2 capture. Chemical Engineering and Processing: Process Intensification, 48, 135-144 (2009).https://doi.org/10.1016/j.cep.2008.03.002

25. Nicolas von Solms, A new pilot absorber for CO_2 capture from flue gases: Measuring and modelling capture with MEA solution, International Journal of Greenhouse Gas Control, 12, 181-192 (2013) https://doi.org/10.1016/j.ijggc.2012.10.010

Conflict of interest statement: On behalf of all authors, the corresponding author states that there is no conflict of interest.

Solar-driven drinking water supply in rural areas under different climate scenarios

A. García Álvaro [1, 2]*, M. Nafría Martín [3], V. Alonso Gómez [4], R. Muñoz Torre [1], D. Hermosilla Redondo [5], I. de Godos Crespo [1, 2]*

[1]University of Valladolid, Institute of Sustainable Process, Valladolid, Spain,

[2] Department of Chemical Engineering and Environmental Technology, University of Valladolid (UVA), Campus Universitario Duques de Soria, 42004 Soria, Spain.

[3]Solarig Global Services, Calle Naranjos 4, 42190 Soria, Spain

[4]Department of Applied Physics, University of Valladolid (UVA), Campus Universitario Duques de Soria, 42004 Soria, Spain.

[5]Department of Forest and Environmental Engineering and Management, Universidad Politécnica de Madrid, José Antonio Novais 10, 28040 Madrid, Spain.

*Corresponding author

Abstract.

Implementation of drinking water systems is limited in rural areas with reduced electrical connectivity. Water extraction from groundwater wells powered by solar light offers a sustainable and low-cost solution easy to replicate. A complete unit of drinking water supply has been designed for providing high quality water for a population of 500 inhabitants.

Selection of equipment and sizing was based on the simulation of available solar energy and equipment consumption performed by specific software. This approach indicates that power storage should be slightly oversized to minimize de energy losses and ensure water supply. In the light of the results battery accumulation is not recommended since water storage tanks can match energy availability and water requirements with less money inversion and maintenance.

The system design will serve as prototype for similar communities on the world taking account the need of a proper ad hoc field study.

Keywords: Distributed generation, Drinking water, Renewable Energies, Rural areas

1　Introduction

1.1　Drinking water supply challenge

771 million people worldwide still lack elementary water services, that means safe drinking water and sanitation systems. Among these, 80 percent live in rural areas and nearly half live in the least developed countries [1]. Which means a large population at health risk due to consumption of untreated water containing pathogens, chemicals or

undesired materials. This issue has been addressed in the Sustainable Development Goals (SDG) set up by United Nations in 2015 under SDG number 6: Clean Water and Sanitation [2]. The solutions provided by the organizations and the different stakeholders involved in the water sector include improvements in the information about water resources, optimized financing of local communities and innovation in the technologies applied. In case of drinking water systems placed in rural areas of emergent nations the implementation of water facilities is limited not only by the economic resources of municipalities but by general development of the areas.

1.2 Solution based on endogenous energy resources. Solar energy

Isolated rural areas of extended areas of Africa and Latin America are barely connected to the electrical grids [3]. Therefore, conventional drinking water facilities, which requires electricity for pumps, mixers and filtration units are rarely implemented. In this sense, distributed generation technologies based on renewable energy coupled to small scale water treatment units can provide a new model for drinking water supply [4]. In case of rural communities (100 to 500 inhabitants) with access to groundwater reservoirs, photovoltaic panels coupled to pumping and filtering devices are a doable alternative with very low capital and operational costs.

1.3 The case study

Taking into account the data on access to drinking water free from an improved water source which is located on premises, available when needed and free from faecal and priority chemical contamination from the UN-Water SDG6 platform [5], the regions of sub-Saharan Africa, Latin America, Central, Western and Southern Asia and Northern Africa have been identified as the most vulnerable (see figure 1). Also, at the global level there is a notable difference in the greater difficulty in rural areas (see figure 2).
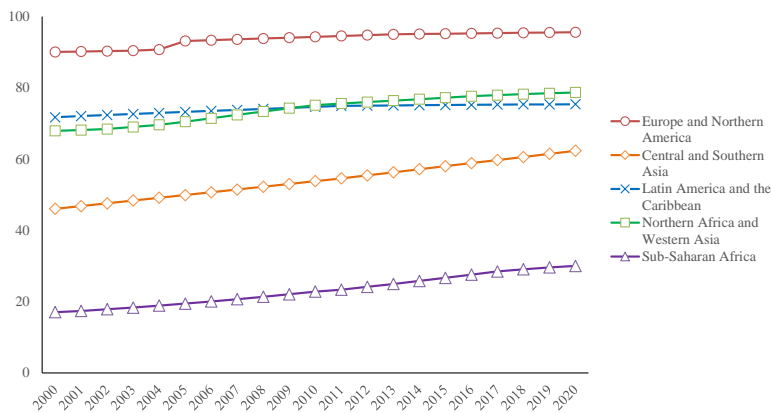
Figure 1. Proportion of population using safely managed drinking water services in the SDG regions between 2000 and 2020
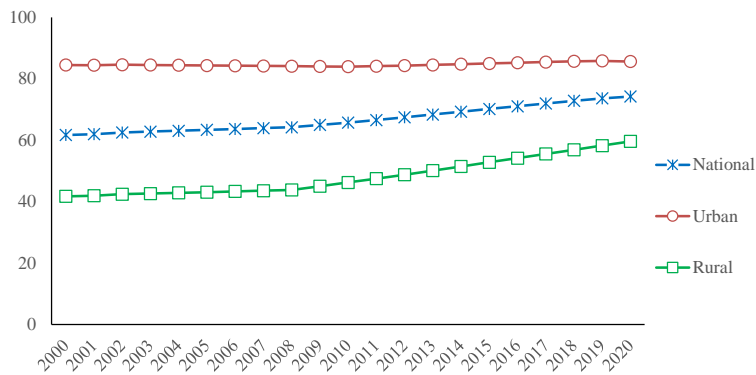
Figure 2. Proportion of population using safely managed drinking water services on the world (Urban and rural areas) between 2000 and 2020

In the present work a study has been carried out in four different locations of the efficiency of a solar supported water pumping system in three different working scenarios for the storage of the available solar energy: with energy storage in batteries, with energy storage in the water tank or without energy storage. An economic evaluation has also been made for the three cases in each region (see figure 3)
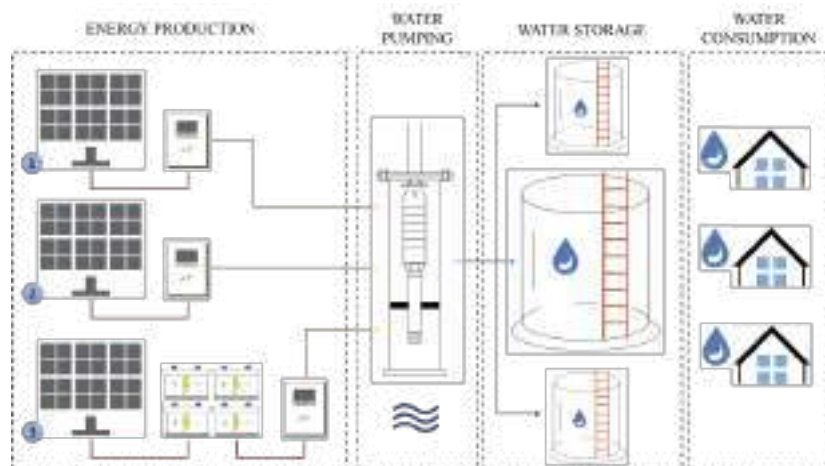
Figure 3. Three scenarios proposed for the drinking water supply in rural areas.

2   Materials and Methods

2.1   Water demand

Calculation of water requirement were done according to the standards value reported by UN of 50 liters per person and day. The population was estimated in 500 inhabitants with a variation considered for a period of 25 years taking into account the average annual increase of the region (0.5 %). Water demand was only calculated considering domestic consumption.

The groundwater reservoir is available through a 100 m depth well placed at 300 meters from distribution tank. A water treatment is included to accomplish the elimination of microorganisms in the water

2.2   Installation for drinking water supply

The design of the water treatment unit driven by solar light was based in conventional groundwater extraction from wells (see figure 4). A submergible 6kW pump introduced into the well extracts water, according to the possible water consumption of the community. A sand filter is connected to the pipe in order to remove suspended solids and microorganisms. Hypochlorite is dosed by a specific pump before the distribution tank, this treatment will remove heterotrophic bacteria present in water. A net of pipes delivers water to family houses from the tank.
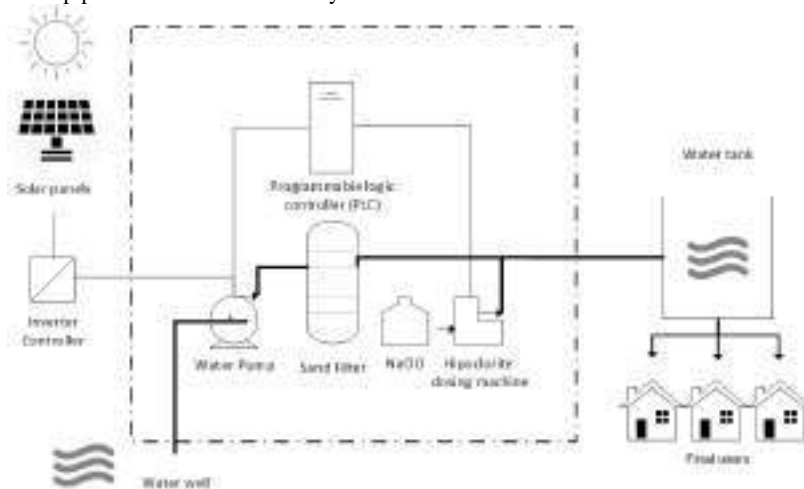
Figure 4. Equipment diagram of the water treatment unit.

16 solar panels connected to an MPPT-AC inverter supply the energy to all the equipment. The photovoltaic (PV) solar module chosen is a generic model 400 W peak power and the inverter chosen is a generic model MPPT-AC (Maximum Power Point Tracker – Alternating Current). A System operating control device adjusts the operation parameters according to the water level at the tank

The energy storage was differenced in three scenarios (see table 1) changing the water tank size from 20 to 100 m^3 and the use of Lead-acid batteries (12 V/160 AH) [6].

Table 1. Three scenarios proposed for the energy storage

	Scenario 1	Scenario 2	Scenario 3
Water tank (m^3)	20	100	20
Battery 12V / 160 Ah (units)	0	0	10

2.3   Simulations of conditions

PVSyst V7.2.2 software was used to estimate the power requirements. Solar irradiation availability in the selected area was estimated with Meteonorm software.

2.4   Study localizations

In order to analyze the effect of the proposed system under different climatic scenarios, where the solar resource allow a comparison, four different regions has been chosen considering rural areas and countries with a low proportion of drinking water access. In figure 5 irradiation conditions can be seen identifying the winter and summer differences that will be critical for the final water supply.

Table 2. Regions selected for the study and main characteristics

	Bigene (Guinea-Bissau)	Makonis (Zimbabue)	Teel (Mongolia)	Los Achiotes (Guatemala)
Latitude and longitude	12.44 -15.58	-18.72, 31.98	48.04, 100.5	13.99, -90.08
Proportion of population using safely managed drinking water services (%)	24.33	29.54	30.06	55.83
Annual irradiation (MWh/m^2)	1936.5	2343.4	1413.6	2113.1
Optimum inclination angle (º)	15	23	46	20
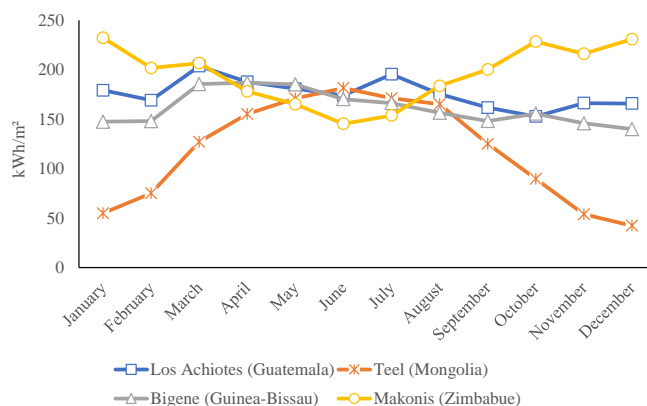
Figure 5. Monthly irradiation in the four regions selected

2.5   Economic evaluation

An economic evaluation of the three scenarios has been studied taking into account the overall cost of the installation and the operation and maintenance costs for 25 years (see Table 3).

Table 3. Unit prices for the installation. * The water tank price will depend on the volume; ** Batteries will be installed just on the scenario 3

Description	Quantity	Unit Price ($)	Description	Quantity	Unit Price ($)
Solar panel 400 Wp	16	250	Water treatment	1	1500
Structure	16	40	Engineering study	1	100
Pump 6.3 kW	1	750	licences	1	250
Engine 6.3 kW	1	750	Transport	1	600
Controller	1	900	Accesories	1	350
Water tank	1	3,000*	Wiring	1	200
Hydraulic circuit	1	1,100	Well (drilling, building)	1	2,500
Batery	10**	700			

3   Results and Discussion

The simulation results presented in Table 4 show the large difference in drinking water availability for each region. While in Makonis (Zimbabwe) the missing water arrives to 0% in scenarios 2 and 3, in the cases of Bigene (Guinea-Bissau) and Teel (Mongolia) it does not go below 20%. In Los Achiotes (Guatemala) the missing water is between 3.8 and 13.5% (see figure 6). This difference is due to the higher irradiation in Makonis with 2343.4 kWh/m² which is also evenly distributed all year round. In the case of Teel, with 1413.6 kWh/m², it is the winter months between December and February where more water would be missing to be pumped to final consumers.

Table 4. Simulation results in each region. Scenarios 1-3

	Bigene (Guinea-Bissau)	Makonis (Zimbabue)	Teel (Mongolia)	Los Achiotes (Guatemala)
	Scenario 1			
Water needs (m³)	9125	9125	9125	9125
Water pumped (m³)	6894	8731	6371	7893
Missing water (%)	24,5	4,3	30,2	13,5
Energy at pump (kWh)	6622	7172	5297	6931
Specific energy (kWh/m³)	0,96	0,82	0,83	0,88
Unused PV energy (kWh)	30	2222	568	729
System efficiency (%)	67,5	57,8	52,2	63,8

	Scenario 2			
Water needs (m^3)	9125	9125	9125	9125
Water pumped (m^3)	6927	9125	6996	8518
Missing water (%)	24,1	0	23,3	6,7
Energy at pump (kWh)	6653	7508	5766	7448
Specific energy (kWh/m^3)	0,96	0,82	0,82	0,87
Unused PV energy (kWh)	0	1886	99	212
System efficiency (%)	67,8	60,5	56,8	68,5
	Scenario 3			
Water needs (m^3)	9125	9125	9125	9125
Water pumped (m^3)	6927	9125	7126	8779
Missing water (%)	24,1	0	21,9	3,8
Energy at pump (kWh)	6653	7508	5865	7659
Specific energy (kWh/m^3)	0,96	0,82	0,82	0,87
Unused PV energy (kWh)	0	1886	0	0
System efficiency (%)	67,8	63,3	57,8	70,5
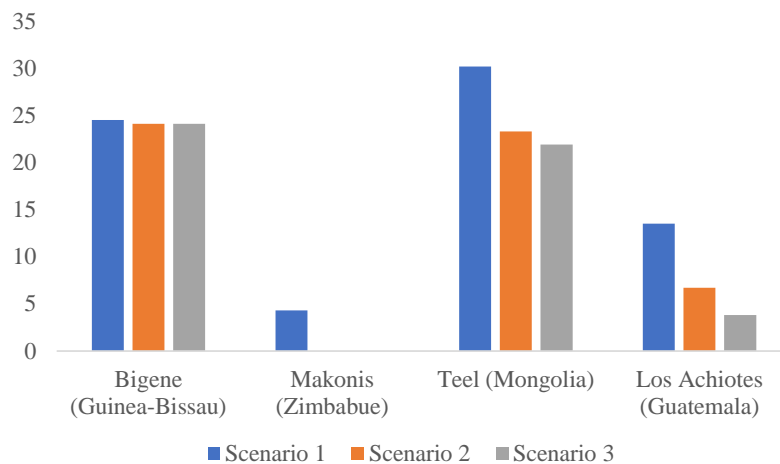
Figure 6. Missing water (%) in the three scenarios

On the other hand, efficiency of the system, measured in terms of energy lost, shows that scenario 3 is around 5% more efficient than scenario 1 and 2% than scenario 2 (see figure 7). This difference is due to with a water full tank in scenarios 1 and 2, the pump is forced to stop and the PV energy is unused.
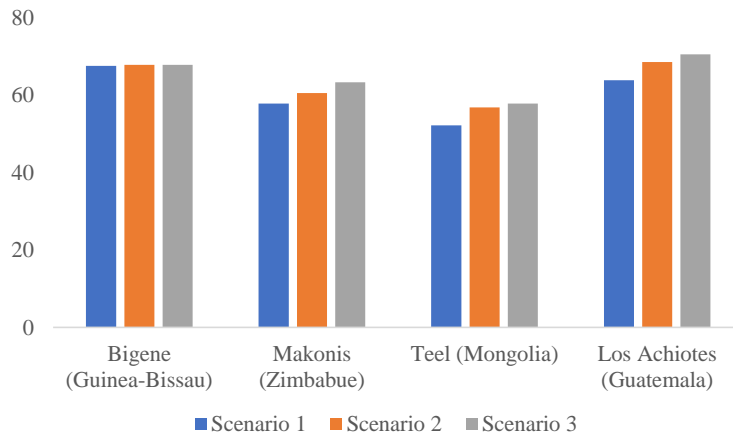
Figure 7. System efficiency (%) in the three studied scenarios

The economic study, taking into account that the system described has been considered similar in the four regions, shows that the price of the storage system in scenario 3 is more expensive, followed by scenarios 2 and 1 (see Figure 8).

Finally, Table 5 shows the price of pumped water for each region taking into account the cost of the total installation and its operation and maintenance cost during the 25 years considered. It can be seen how scenarios 1 and 2 are the most profitable in an evaluation from an economic point of view with a water price between 0.241 and 0.330 $/m^3). Scenario 3 is a 18% more expensive than the cheapest scenario. Batteries are not recommended since large storage tanks will match solar energy availability and water requirements without excess of installation and operational cost.
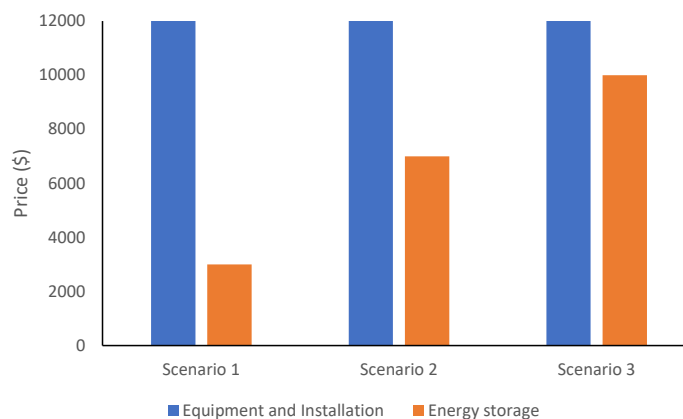
Figure 8. Effective energy in each process step per scenario. Loss diagram.

	Bigene (Guinea-Bissau)			Makonis (Zimbabue)		
	Scenario 1	Scenario 2	Scenario 3	Scenario 1	Scenario 2	Scenario 3
Water pumped (m3)	6894	6927	6927	8731	9125	9125
Installation price ($)	15140	19140	22140	15140	19140	22140
Operation&maintenance ($/year)	1500	1500	1750	1500	1500	1750
Water price ($/m3)	0.305	0.327	0.380	0.241	0.248	0.289
Price differenced (%)	0%	7%	25%	0%	3%	20%

	Teel (Mongolia)			Los Achiotes (Guatemala)		
	Scenario 1	Scenario 2	Scenario 3	Scenario 1	Scenario 2	Scenario 3
Water pumped (m3)	6371	6996	7126	7893	8518	8779
Installation price ($)	15140	19140	22140	15140	19140	22140
Operation&maintenance ($/year)	1500	1500	1750	1500	1500	1750
water price ($/m3)	0.330	0.324	0.370	0.267	0.266	0.300
Price differenced (%)	2%	0%	14%	0%	0%	13%

Similar works in the field of photovoltaic water pumping have reported comparable systems in isolated conditions in other regions of Asia and Africa [7], [8]. Naval et al. (2021) also proposes a pumping system based on photovoltaic energy since the increase in the cost of energy of the water pumping facilities puts at risk the economic sustainability of the recent investments in the modernization of the systems.

To address this problem, the application of renewable technologies for the production of electricity is essential, and photovoltaic energy is especially attractive due to its reduced cost and recent technological advances [9]. Viability of photovoltaic-based water systems has been reported for irrigation and domestic supply in urban and rural regions of countries with high solar irradiation levels where a considerable part of the rural population lives in remote areas [10].

The use of software simulations allows to design the equipment and shows impact of the different parameters affecting performance results of the system [11].

4　　Acknowledgments

Declaration of competing interest
The authors declare that they have no known competing financial interests or personal relationships that could have appeared to influence the work reported in this paper.

References

[1]   UN-Water, "Summary Progress Update 2021 : SDG 6 — water and sanitation for all,"
        UN-Water Integr. Monit. Initiat., pp. 1–58, 2021, [Online]. Available:
        https://www.unwater.org/new-data-on-global-progress-towards-ensuring-water-and-
        sanitation-for-all-by-2030/.

[2]   N. Ferri, "United nations general assembly," *Int. J. Mar. Coast. Law*, vol. 25, no. 2, pp.
        271–287, 2010, doi: 10.1163/157180910X12665776638740.

[3]   EIA,   "No   Title,"   *IEA   (2020),   SDG7   Data   Proj.   IEA,   Paris
        https//www.iea.org/reports/sdg7-data-and-projections*.

[4]   J. Marsden, "Distributed generation systems: A new paradigm for sustainable energy,"
        2011 IEEE Green Technol. Conf. Green 2011, no. May 2011, 2011, doi:
        10.1109/GREEN.2011.5754858.

[5]   UN-Water, "SDG 6 – Data portal", (2022) [Online]. Available: https://sdg6data.org/

[6]   Eugene A. Esparcia, Michael T. Castro, Carl Michael F. Odulio, Joey D. Ocon, A
        stochastic   techno-economic   comparison   of   generation-integrated   long   duration
        flywheel, lithium-ion battery, and lead-acid battery energy storage technologies for
        isolated microgrid applications, Journal of Energy Storage, Volume 52, Part A, 2022,
        104681, ISSN 2352-152X, https://doi.org/10.1016/j.est.2022.104681.

[7]   I.Togola. "Solar energy use water supply of rural areas in East Africa", [PhD. Thesis],
        2003

[8]   Kazem, H.A., Al-Waeli, A.H.A., Chaichan, M.T. et al. Design, measurement and
        evaluation of photovoltaic pumping system for rural areas in Oman. Environ Dev
        Sustain 19, 1041–1053 (2017). https://doi.org/10.1007/s10668-016-9773-z

[9]   Natalia Naval, Jose M. Yusta, Optimal short-term water-energy dispatch for pumping
        stations   with   grid-connected   photovoltaic   self-generation,   Journal   of   Cleaner
        Production,   Volume   316,   2021,   128386,   ISSN   0959-6526,
        https://doi.org/10.1016/j.jclepro.2021.128386

[10]   Olga V. Shepovalova, Alexander T. Belenov, Sergei V. Chirkov, Review of
        photovoltaic wa-ter pumping system research, Energy Reports, Volume 6, Supplement
        6, 2020, Pages 306-324, ISSN 2352-4847, https://doi.org/10.1016/j.egyr.2020.08.053.

[11]   Rakhi Sharma, Shivanshu Sharma, Sumit Tiwari, Design optimization of solar PV water
        pumping system, Materials Today: Proceedings, Volume 21, Part 3, 2020, Pages 1673-
        1679, ISSN 2214-7853, https://doi.org/10.1016/j.matpr.2019.11.322.

Deep Neural Networks for Global Horizontal Irradiation Forecasting: A comparative study

Cristian Arbeláez-Duque [0000-0003-0932-2746], Alejandro Duque-Ciro [0000-0002-0128-6878],
Walter Villa-Acevedo [0000-0002-1466-7266] and Álvaro Jaramillo-Duque [0000-0002-0128-6878]

Universidad de Antioquia, Cl. 67 #53-108, Medellín, Colombia
grupo.gimel@udea.edu.co

Abstract. In order to contribute to the integration of photovoltaic renewable energy into power system, this paper addresses the problem of forecasting solar irradiance or Global Horizontal Irradiation (GHI). The collection, adjustment and processing of meteorological data used as input is carried out, in addition various Deep Neural Networks (DNN) models are implemented and analyzed, among which are the Artificial Neural Networks (ANN) of type as Transformer, LSTM, GRU, and mixed between Convolutional ANN (CNN)-LSTM, and CNN-GRU. These ANN variants are implemented, and a comparative study are made. Finally, the results obtained show that the ANN transformer has less error in the GHI forecasting.

Keywords: Deep Neural Networks, Artificial Neural Network, Global Horizontal Irradiation Forecasting, Transformer, LSTM, GRU, Convolution.

1   Introduction

Electrical energy has become a fundamental support for modern society that uses technology powered by it, constituting itself as the essential hub in the development of daily activities worldwide. Electricity is used in sectors such as industrial, agricultural, domestic and many others, making it a primary and fundamental service for the global economy. Due to aforementioned, electricity consumption worldwide maintains a constant growth; therefore, technologies focused on energy efficiency and the management of the renewable resources for electricity generation have been developed in the last decades [1].

1.1   Background

As the consumption of electricity increases globally, it is a challenge to supply this demand without generating additional environmental impacts. In addition, the infrastructure of electricity systems and conventional technologies of electricity generation must be adapted to achieve an energy transition towards sustainable and more environmentally friendly technologies. Due to the above, the energy sector has been driven to develop and to integrate alternatives of non-conventional technologies for elec-

tricity generation such as renewable energies, which allow diversifying the energy matrix and energy transition. This without neglecting environmental responsibility and guaranteeing competitive and accessible prices in the electricity market [2].

In the many countries, there has been an increase in the use of non-conventional technology for electrical energy generation, whose availability of natural resources is intermittent, for example, photovoltaic solar energy or wind energy. Also the implementing costs of these technologies have been greatly reduced in the last decades, making those options cost-effective electricity sources. In addition, these reduce greenhouse gas emissions and have lower environmental impacts [2]. Unlike of the conventional technologies, one of the biggest challenges presented by intermittent technologies are to determine exactly how much energy will be generated at each moment of the day [3].

One of the tasks in the power system operation, is to dispatch of power plants, in order to meet the electricity demand. For conventional power plants, it can be quantified very precisely how much energy can be generated in the future, considering the amount of fuel available in a thermal power plant, or from the water stored in the case of a hydroelectric power plant [3]. On the other hand, the electricity production from photovoltaic and wind power plants may be affected by weather conditions, such as solar radiation, wind speed, geographical location, temperature, humidity, atmospheric pressure, among other weather factors. These factors cannot be controlled and do not allow to forecast with precise accuracy how much energy will be available in the future. Therefore, a challenge arises when it make planning of energy dispatch in power systems that includes intermittent energy sources electricity generation [4].

For photovoltaic (PV) power plants, the challenge is to determine the availability of the solar irradiance or Global Horizontal Irradiation resource (GHI) to estimate the energy production. There exist several forecasting models for solar irradiance are classified into physical models, statistical and Machine Learning (ML) models.

1.2   Literature review

Physical models, such as numerical weather prediction (NWP), are computationally expensive because they consider several environmental aspects to calculate the future irradiance. Statistical models, such as the autoregressive integrated and moving average model (ARIMA) perform temporal mappings over past data and produce forecasts and have been used in several irradiance forecasting applications [5].

Machine Learning (ML) models are one of the most promising computational methods for forecasting GHI and energy production, because they are more suitable for mapping nonlinear patterns [5]. ML models are not only capable of performing nonlinear mappings in the data but also present some flexibility regarding noisy data [5].

A ML model can be described as a group of mathematical expression to find patterns or make predictions. Once a ML model is built to forecast the GHI, a training process is carried out from a set of historical data, called a training set. After the training process is completed, the performance of the model is evaluated with another set of data, called test set. If the performance metrics have adequate values, it moves on

to the stage of forecasting the future values of the variable of interest with new data. Otherwise, to improve performance models a hyperparameters tuning process or a architecture modification of the ML model is carried out. This process is made until reaching adequate performance metrics according to the nature of the problem.

Predictions problems can be divided into two types of tasks: classification and regression tasks. The intermittent renewable resource forecasting or the power generated from intermittent renewable technologies is classified as a regression task, in which the time series of future values is forecasted from data from the past. For example, to calculate the forecast of GHI for the next day, with an hourly resolution, radiation data from previous days are used [6].

For the time series forecasting problem there is a type of ANN, which has characteristics suitable for the management of temporal sequences and the temporal dependence of the data that make up the time series. This advantage makes it suitable for GHI time series forecasting. This ANN is known as Recurrent Neural Network (RNN), it has the particularity of having connections between neurons, which propagate information forward and backward (recurrent connection), so RNN present a good response processing data sequences as is the case of time series, without this affecting the size or number of layers that make up the RNN [7].

According to [7]–[12], a type of RNN is Long Short Term Memory (LSTM) that has the ability to process long time series sequences, allowing to handle short and long term dependencies on the data stream. Due to the recurrence in LSTM structure, those models can remember previous states and from them forecast which will be the next state [6]. The LSTM models are capable by predicting variables that have trend and seasonal behaviors, and in general long term dependencies into data [6].

In [13], a simple RNN and an LSTM are proposed to make the next day of solar irradiance forecasting. To reduce the error into forecasting and given the high dependence that the climate state has on solar irradiance, four different states are proposed to make the forecast, which are sunny, cloudy, rainy and intense rainy states. The proposed model is composed of three main parts which are: 1) Preprocessing of the solar irradiance data using Discrete Wavelet Transformation (DWT), 2) Extraction of the local features based on a Convolutional layer, and 3) the processing of the sequence using an LSTM layer. The results presented according to the performance metrics obtained less error for sunny days. On the other hand, in [9], an LSTM is also used, to make the forecasting of the GHI in Atlanta, New York and Hawaii. To do the prediction, three classifications of the weather are proposed, which are: sunny, cloudy and mixed. The presented model has a hidden single layer structure with a Relu activation function. The dropout is added to the hidden layer allowing some connections to be discarded randomly during training process; which allows to reduce the overfitting problem in the LSTM response. The proposed LSTM has less forecasting error on cloudy and mixed days.

In [14] is present a LSTM network used to predict the power produced from a photovoltaic power plan, and compares it to a simple RNN, a Generalized Regression Neural Network (GRNN), and an Extreme Learning Machine (ELM). The LSTM network consists of an input layer, hidden layers, and an output layer in sequential manner. The results show that the performance of the LSTM for the four seasons of

the year is superior with respect to the others ANN since it presents a lower forecasting error due to the LSTM cells, which allows to maintain the long-term temporal dependencies.

In [15] the authors perform a forecasting task for which, in training different ANN models, then combine their results to solve the same problem. The same data is entered simultaneously to the ANN, and then averaging the forecasts given by each one. In this case, two types of ANN were used: MultiLayer Perceptron (MLP) and LSTM. After training the ANN with four different databases, the results of the combined forecasting have less error compared to the results of MLP and LSTM individually.

In [16] a forecast combiner is proposed in which the outputs generated individually by LSTM and GRU models are used to finally deliver a combined forecast. These two RNNs are used because they allow long term information to be retained and thus maintain correlations between the values of the time series. The results show that LSTM and GRU individually delivered values of performance metrics with higher errors compared to the proposed forecast combination process showing a significant improvement in the forecasting of the variables.

A forecast model based on Deep Neural Networks (DNN) combined with self-attention mechanisms, known as Transformers, which are characterized by parallelizing computational processes, have shown great potential in natural language and image processing; so they are shown as promising candidates to make forecasts in time series [15].

In this work, different ANN are implemented to the task of short-term forecasting of GHI, with a horizon of 24 hours and a temporal resolution of 15 minutes. This forecast will serve as an input to establish the future generation of photovoltaic power plants. Among the ANN to be considered are LSTM, GRU, CNN-LSTM, CNN-GRU and Transformer, architectures and hyperparameters based on those found in the technical literature such as those obtained by hyperparameter tuning tools will be considered. A database of meteorological variables of two years that are used for the experiments. The performance evaluation of each ANN model is done with metrics for both training and validation data [7].

The contribution of this work focuses on determining from an evaluation and comparison of different ANN models, what is the best model configuration for the GHI forecast of a full day using historical data. Different architectures, scaling types, and data inputs were used for ANN types, including the Transformer model. A one-day time window with a resolution of fifteen minutes between each measurement was used for all experiments [18].

2   Background

This section presents the basic concepts for the implementation of ANN models for the GHI forecast.

2.1　　Factors influencing GHI forecast

In [6], [8], [9], [15], [19] were found that, in order to forecast GHI and electrical energy from a solar power plant, it is vitally important to consider these important aspects: 1) Forecast time horizons, 2) Data preparation and model inputs, 3) Artificial intelligence (AI) tools, and 4) Model performance evaluation metrics.

Forecast time horizons.
For the development of a prediction model, aspects such as: prediction horizon and temporal resolution must be considered in the model design. The prediction horizon of the data corresponds to the period towards the future in which the forecast is made, starting from a given moment in which the prediction is made. Depending on the forecast horizon of the GHI, the following classification is available: very short term (ranging from one hour to three hours); short term (comprises up to 24 hours); medium term (includes up to a week) and long term (includes up to weeks). For the temporal resolution of the data, each horizon must be considered. They must be fractions of the prediction horizon, which adjust to the nature of the problem and the user needs. For example, for very short term it must be 1, 5, 10, 15 or 30 minutes are handled. The horizon and resolution must be considered in the forecast task so that the data is prepared according to the available information and the type of forecast will be implemented.

Data preparation and model inputs.
Input data is critical in any ML model, as these are what feed the models. Based on [8], [9] and [17], a cleaning and preparation of the data is performed, replacing the missing data with the closest previous value in the time series, not zero. A resampling of the data is also carried out, to avoid missing values, if the missing values do not exceed the new resolution of the resampling time. Subsequently, the normalization and standardization of the set of data obtained is used. It is worth highlighting the importance of the selection of the input variables of the model, in [7] and [9] the most important variables are selected and with more correlation with the generated power of the PV power plant, making use of a correlation map. It is found that the most important variables for the data set are irradiance, global irradiance and direct irradiance. Likewise, other variables that can be useful are air temperature and hour.

2.2　　Artificial intelligence models

In [14], [16] the methods that were used for the forecasting of the solar resource are based on AI techniques, especially machine learning models. The term AI adheres to systems that have the ability to imitate human intelligence to perform tasks and improve according to the information that they collect.

　ANN are a broad family of algorithms that form the basis of the so-called AI, which has been called Deep Learning (DL). These types of AI techniques have been very well accepted, getting satisfactory results forecasting natural resources, such as

solar irradiance and wind speed. ANN has become a very popular AI technique, due to their high degree of application in multiple tasks. ANN creates an interconnection system between layers and artificial neurons that processes a set of data and generates an output. Likewise, other types of neural networks have been developed that have had great acceptance in forecasting applications, which are mainly used in others works [6].

MultiLayer Perceptron - MLP.
It is a feedforward approach since the information present in the inputs flows in just one direction, from the input layer to the output layer. The general principle of MLP consists of a set of artificial neurons that are connected to each other with the aim of transmitting the signals forward. Each output value of the previous neuron is multiplied by a weight, then to the output of the neuron is applied a limiting function or activation function which is responsible for modifying or limiting the output value that will be propagated to the other neurons.
In addition, the values assigned to the weights are updated in the training process, through the minimization of a loss function; known as back propagation algorithm [6]. The MLP is a universal function approximator because it can map any continuous, nonlinear, limited, and differentiable function with a predetermined error threshold [5].

Recurrent Neural Networks - RNN.
It is an ANN that has a greater capacity to handle and learn different computational structures. Which in practical terms means that it can learn the trend and seasonal behaviors into the time series as the solar irradiance. RNN not only includes feedforward connections like an MLP, but also backward connections; thus, having a kind of feedback with the other neurons that are in the layers [6]. RNN has different variants to handle the recurrence connections into architecture such as the LSTM and Gated Recurrent Unit (GRU).

Long Short-Term Memory - LSTM.
RNN has a problem due to the form of time sequence information propagation within its architecture, since it propagates not only forward, but also backward. Sometimes an accumulated error into the neural network response is produced, commonly this problem appears when RNN handles time series with long-term dependencies; called long-term memory problems. LSTM solves the problem of long-term memory in simply RNNs, since these have as their main characteristic that information can persist by introducing loops in the flow of information from the network. So, basically, LSTM can remember previous states and use this information to decide what the next state will be. This feature makes them very suitable for handling long time series. Therefore, it can be stated that LSTM can learn long dependencies and thanks to this they have a long-term memory [7].

Gated Recurrent Unit - GRU.

GRU is a new generation of RNN and is like the LSTM network but has less complex architecture and allows you to control the flow of information to capture time series dependencies without using an internal memory cell. This characteristic solves the problems that arise from local minimums and gradient descent. In addition, as it is a less complex network, it uses less computational resources, therefore it spends less time to carry out its training [7].

Convolutional Neural Networks - CNN.

This is a type of network that integrates the convolution mathematical operator, which transforms the input data, reducing its dimensions and computational complexity when processing it. These networks instead of neurons have filters, kernels and the amount of them is determined according to the needs of the problem [7]. For the forecast of time series, a CNN with a layer of one dimension is used, which allows it to process temporal sequences instead of images that have information structures in two dimensions, for which the CNNs were created.
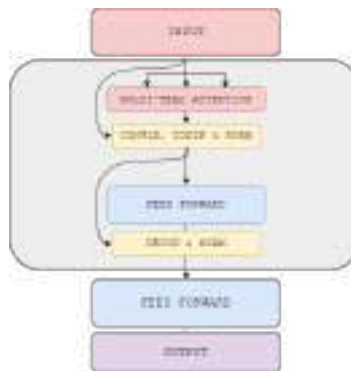
Fig. 1. Transformer ANN Architecture shows the structuring of the Attention function, normalization, the final layer of with convolution, in addition to simple ANNs, also called Feed Forward.

Transformer Model.

As presented in [20] and Figure 1, Transformer deep learning model is based on the combination of two stages (Encoder and Decoder). The Encoder stage starts with a positional coding block, a Multi-Head Attention block, a block of simple neurons, and finally Decoder stage that is the output of the model.

As presented in [21], an Attention function can be described as assigning a query (encoding) and a set of key-value pairs as output. Where the query, keys, values, and output are all vectors. The output is calculated as a weighted sum of the values, where

the weight assigned to each value is calculated using a query compatibility function with the corresponding key.

Next with the development of the study of the Attention functions, in [21] it was found that better performances were produced in the models by linearly projecting the queries, keys and values a certain number of times with different linear projections in three-dimensional space. For each projection, an Attention function is applied in parallel to the others, then a concatenation is performed that is projected and results in the output of the model. The Multi-Head Attention function allows the model to process information as a set. This function is included in the structure of the Transformer model [17]. The Transformer network used in this work is presented in Figure 1. Its main features are that in the encoder block it uses a one-dimensional convolutional layer after the Multi-head Attention block and in the decoding stage it uses a layer of an MLP feed forward network.

2.3   Evaluation of model performance

Usually, the most used metrics to measure the error of DL forecasting models are: 1) MSE (Mean Square Error), 2) RMSE (Root Mean Square Error), 3) MAE (Mean Absolute Error), 4) MAPE (Mean Absolute Percentage Error). These metrics are used for the evaluation of the models in regression problems, these metrics are appropriate to evaluate performance in time series forecasting contexts such as the one addressed in this work. As is showed below, in the equations (1) and (2), two values are required for the calculations, the real value y_i and forecasted value $\check{y}_i$.

RMSE.
This index measures the root of the average square error of the forecasts made, using the expression shown in equation (1). For each sample what it does is calculate the square difference between the forecasts and the target outputs, and then average these values [7].

$$RMSE = \sqrt{\frac{1}{n}\sum_{i=1}^{n}(y_i - \check{y}_i)^2} \qquad (1)$$

MAE.
In this metric the error is calculated as the average of absolute differences between the target values and the forecasts, as presented in equation (2). The MAE is a linear score, which means that all individual differences are weighted equally in the average. An advantage of this metric is that it penalizes huge errors, therefore, it is not as sensitive to outliers [6].

$$MAE = \frac{1}{n}\sum_{i=1}^{n}|y_i - \check{y}_i| \qquad (2)$$

In [14], [16], the most used metrics to evaluate the performance of the implemented models are RMSE and MAE. In [8], [11], [14] and [22], it is observed that the chosen metric is RMSE. Unlike [6], [10], [12], [15], [16], [23], [24], where the metric used is MAE.

3   Implementation of ANN

This section will explain the general structure carried out for the assembly and realization of the experiments. It is important to note that the same programming and organization structure was maintained for each of the models that were implemented. The structure and development of the models is available at [18].

3.1   Problem definition

It seeks to make a forecast of GHI or solar irradiance using various ML models. Where at the model inputs are historical data of a full day taken from zero hour to twenty-fourth hour are entered, with a resolution of fifteen minutes between each data. Each model will deliver the forecast of a forecasting horizon or time window with the same amount of data and the same input resolution, which corresponds to the forecasts of the solar irradiance of the day immediately following the one entered.

3.2   Dataset

To carry out the experiment, freely accessible historical data, never used before for this propose, recorded by a weather station located in Kenya, were used. With the following measurements: GHI, wind speed, humidity and air temperature, Zenith, and Azimuth angles. The data has a measurement resolution of one minute for a full year. The database was separated into two sets, one with 80% of the data to train the models and a second set with the other 20% of data to validate models performance [25].

3.3   Data preparation

A preparation of the data was carried out that would allow an objective and global analysis of the data. The first adjustment was to change the headings and indexes with the appropriate names and order that in the case of the index was converted to date format. Then the resolution of the measures was changed from one minute to fifteen minutes. Finally, the missing data were filled in using arithmetic means to avoid altering the statistical measures of the data.

Data preprocessing.
   This step is performed to adjust the data with the sequence and dimensions required by the ML models. The first step is to scale the data using normalization or standardization. For the different models, the two types were used to analyze the differences in the results. The second step is to segment the data into time windows, with

96 data, equivalents to a full last day with a resolution of 15 minutes, that will be the input of the model as illustrated in (3).

$$Datos = \begin{bmatrix} [x_{1,1} & x_{1,2} & x_{1,3} & \dots & x_{1,96}] \\ [x_{2,1} & x_{2,2} & x_{2,3} & \dots & x_{2,96}] \\ \vdots & \vdots & \vdots & \ddots & \vdots \\ [x_{n,1} & x_{n.2} & x_{n,3} & \dots & x_{n,96}] \end{bmatrix} \tag{3}$$

Where the first subscript refers to the day on which the data was taken, and the second subscript refers to the data number of the day the measurement was taken. It is also important to note that x can be in addition a number or a data vector. For example, it can contain GHI, humidity, temperature, as data of an instant of time for the case of multivariate models.

3.4   Definition of models

In this step, the ML models with an architecture and hyperparameters that correspond to a particular model under study were defined. The Python programming language, Keras and TensorFlow libraries were used to implement the ML models. The models implemented are those presented in Table 1, which also includes the main characteristics of these.

3.5   Model performance measures

The RMSE and MAE, shown in equations (1) and (2), were taken as global performance measures for the models. The training process of the models with a learning curve was also monitored. Finally, random forecasting was taken from the dataset to graphically analyze the behavior of the forecasts compared to the actual results.

4   Results and analysis

Table 1 presents the results obtained for the different models implemented in this work. It considers performance metrics, architecture and the scaling type used in the input data. It is important to note that these work results can be replicated using the scripts hosted in the public repository in [18]. All scripts are available with the implemented models, their parameters, hyperparameters, the structuring of the data, and all the specific information needed.

4.1   Forecast errors

As shown in Table 1, architectures are shown, and number of neurons in each layer for the LSTM, CNN-LSTM, GRU, CNN-GRU models. For the Transformer model are shown number of heads, blocks, and units in each block. The best performing models, based on MAE metric, were marked in bold. For the LSTM, CNN-LSTM, GRU and CNN-GRU models, a fixed structure was used, varying the way of scaling the data in addition to entering one or more variables (univariate or multivariable) as

the case may be. In the case of multivariate models, the variables used were GHI, rainfall, relative air humidity, time of day and wind speed.

Table 1. Implemented ANN Models

ANN type	Architecture	Input	Scaling	MAE	RMSE
LSTM	100/150	Univariable	Standard	40,54	77,41
LSTM	100/150	Univariable	MinMax	38,91	74,92
LSTM	100/150	Multivariable	Standard	39,46	74,88
LSTM	**100/150**	**Multivariable**	**MinMax**	**39,94**	**76,53**
CNN-LSTM	32/100/150	Univariable	Standard	41,05	77,06
CNN-LSTM	32/100/150	Univariable	MinMax	39,14	75,46
CNN-LSTM	32/100/150	Multivariable	Standard	40,17	76,94
CNN-LSTM	**32/100/150**	**Multivariable**	**MinMax**	**39,24**	**75,12**
GRU	100/150	Univariable	Standard	43,79	77,04
GRU	100/150	Univariable	MinMax	52,97	83,78
GRU	100/150	Multivariable	Standard	41,12	76,46
GRU	**100/150**	**Multivariable**	**MinMax**	**38,63**	**74,34**
CNN-GRU	32/100/150	Univariable	Standard	46,47	80,87
CNN-GRU	32/100/150	Univariable	MinMax	75,57	104,0
CNN-GRU	32/100/150	Multivariable	Standard	44,06	78,38
CNN-GRU	**32/100/150**	**Multivariable**	**MinMax**	**39,07**	**74,50**
Transformer	**24 h/ 4 b/ 200 u**	**Univariable**	**MinMax**	**37,85**	**72,24**

The performance metrics presented in Table 1 were calculated by forecasting the complete validation dataset and then the MAE and RMSE, described in equitation (2) and (1), were computed for each model. After executing each script multiple times, no significant change was found in the errors shown, so the last result obtained was presented. It should be noted that in other studies MAPE is commonly used, which is like MAE, but is presented in a relative percentage way. However, its use was ruled out because when the values to be estimated are close to zero, the error tends to very high values, although the forecast is correct.

Considering the 24 hours forecast horizon with a resolution of 15 minutes, resulting in a total of 96 total data for one day. The results obtained, compared to those presented in [20], are similar. However, the maximum forecast horizon proposed in this study was 12 hours with a resolution of 1 hour, being a smaller and less complex problem.

In [20], the model that yields the best performance is the Transformer as found in this work and observed in Table 1. It is also relevant to mention the results of [10], which makes forecasts with a maximum horizon of 9 hours and a resolution of one hour; where their lowest error was 2.82 W/m^2 with an LSTM model, in addition to that, authors use the clear sky index as input data for their implemented models.

In [16] as in this work, they predicted 24 hours of solar irradiance, however, values with a resolution of 1 hour between each data were used, obtaining as a minimum error of 5.78 W/m^2 unlike this work, where the time resolution used it is 15 minutes, four times longer. Another aspect that influences in [16], is the maximum irradiance values recorded in its database, is in the order of 600 W/m^2, while the database used in this study records values that are around 1200 W/m^2. This is reasoning the performances of both models are not directly comparable, but in proportion to this analysis, the Transformer model yields similar results in the error, even minor.

4.2   Forecasts

Figure 2 shows the forecast on the same day with clear weather conditions (sunny day). These cases were randomly taken from the validation dataset, for the Transformer, LSTM, CNN-LSTM, GRU and CNN-GRU models, respectively. In the face of clear sky conditions, all models make good forecasts with low errors. The forecast in the hours of sunrise and sunset have low error, as well as in the peak value of irradiance. In general, the models are adjusted almost superimposing the real data, as it also happens in [16], [9] and [19].
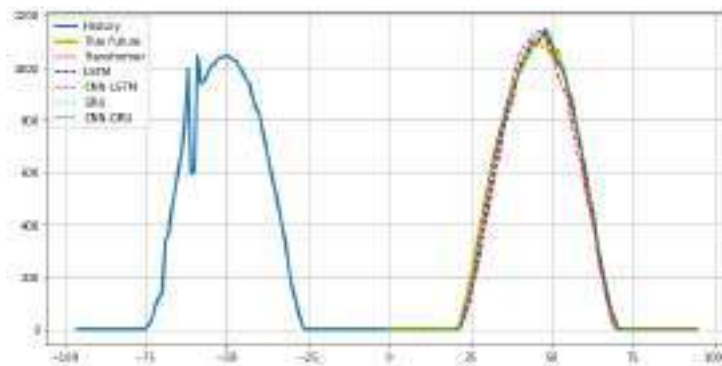
Fig. 2. Forecast of a full day of irradiance given in W/m^2, made by the Transformer, LSTM, GRU and CNN models, compared to the actual values for a sunny day.
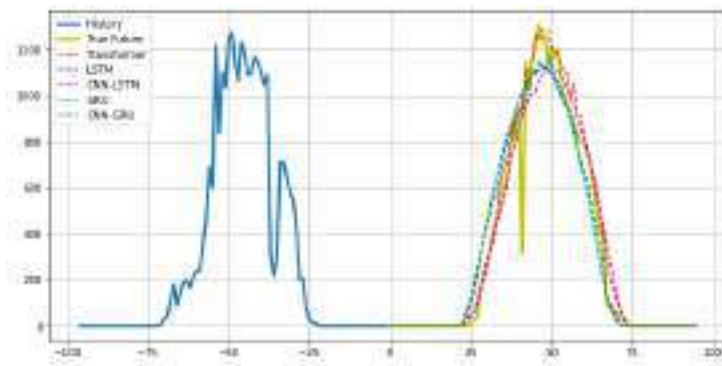
Fig. 3. Forecast of a full day of irradiance given in units performed W/m^2 by the Transformer, LSTM, GRU and CNN models, compared to the actual values for a cloudy day.

Figure 3 shows the forecast for the same day, with cloudy conditions for a few hours during it. These cases were randomly taken from the validation dataset, for the Transformer, LSTM, CNN-LSTM, GRU and CNN-GRU models respectively. The best

forecast is made by the Transformer model, and it is also worth highlighting the behavior of the CNN-LSTM, since they correctly forecast the time of sunrise and sunset. The Transformer model, in this case, is the only one capable of correctly forecasting the peak irradiance value of the day. However, like the other models, it cannot adequately predict sudden changes in the behavior of the variable. Finally, it is important to note that the overall performance of the models is quite accurate, since they all manage to adjust tendentially to the real behavior they intend to forecast. When deviations in the results occur, the responses are not distant. All the above considering that no variables were entered that could provide information for the forecasting regarding cloudiness and therefore solar irradiance.

5   Conclusions

In the proposed work, different ML models were proposed, implemented, and evaluated, currently used for the solution of similar problems, obtaining forecasts with lower errors compared to those analyzed from other previously published works.

Transformer model gives outstanding results for the problem of GHI forecasting. For this reason, and due to the few findings in the literature, it is highly recommended to further investigate the behavior of this type of neural network.

The clear sky index is an input variable that provides valuable information, which enriches the models to generate good estimates of GHI. Therefore, it becomes convenient for subsequent work, to obtain a historical dataset with this index or information to calculate it.

Finally, all models performed in a good way, but considering the results obtained, the model with the best performance in the development of this work was the Transformer model and the lowest performance was the Univariable CNN-GRU model with MinMax scaling.

6   Funding

References

[1]   D. Morales Ramírez y J. R. Luyando Cuevas, «Analisis del Consumo de Energia Electrica Residencial en el Area Metropolitana de Monterrey», vol. 31, n.º 62, Art. n.º 62.

[2]   REN21, «Renewables Global Status Report», Paris, France, 22 de marzo de 2022. Accedido: 22 de marzo de 2022. [En línea]. Disponible en: https://www.ren21.net/reports/global-status-report/

[3]   «Demanda de energía eléctrica en tiempo real, estructura de generación y emisiones de CO2», *REE*, 22 de marzo de 2022. https://demanda.ree.es/visiona/seleccionar-sistema (accedido 22 de marzo de 2022).

[4]　Á. Robledo Quintero, «Predicción de la radiación global utilizando redes de neuronas artificiales», jul. 2018, Accedido: 22 de marzo de 2022. [En línea]. Disponible en: https://e-archivo.uc3m.es/handle/10016/29002

[5]　D. S. de O. Santos Jr *et al.*, «Solar Irradiance Forecasting Using Dynamic Ensemble Selection», *Appl. Sci.*, vol. 12, n.º 7, p. 3510, 2022.

[6]　A. Aliberti, D. Fucini, L. Bottaccioli, E. Macii, A. Acquaviva, y E. Patti, «Comparative Analysis of Neural Networks Techniques to Forecast Global Horizontal Irradiance», *IEEE Access*, vol. 9, pp. 122829-122846, 2021, doi: 10.1109/ACCESS.2021.3110167.

[7]　A. Géron, *Hands-On Machine Learning with Scikit-Learn, Keras, and TensorFlow: Concepts, Tools, and Techniques to Build Intelligent Systems*. O'Reilly Media, Inc., 2019.

[8]　C.-H. Liu, J.-C. Gu, y M.-T. Yang, «A Simplified LSTM Neural Networks for One Day-Ahead Solar Power Forecasting», *IEEE Access*, vol. 9, pp. 17174-17195, 2021, doi: 10.1109/ACCESS.2021.3053638.

[9]　M. Aslam, S.-J. Lee, S.-H. Khang, y S. Hong, «Two-Stage Attention Over LSTM With Bayesian Optimization for Day-Ahead Solar Power Forecasting», *IEEE Access*, vol. 9, pp. 107387-107398, 2021, doi: 10.1109/ACCESS.2021.3100105.

[10]　Y. Yu, J. Cao, y J. Zhu, «An LSTM Short-Term Solar Irradiance Forecasting Under Complicated Weather Conditions», *IEEE Access*, vol. 7, pp. 145651-145666, 2019, doi: 10.1109/ACCESS.2019.2946057.

[11]　M. Konstantinou, S. Peratikou, y A. G. Charalambides, «Solar Photovoltaic Forecasting of Power Output Using LSTM Networks», *Atmosphere*, vol. 12, n.º 1, Art. n.º 1, 2021, doi: 10.3390/atmos12010124.

[12]　S. M. J. Jalali, S. Ahmadian, A. Kavousi-Fard, A. Khosravi, y S. Nahavandi, «Automated Deep CNN-LSTM Architecture Design for Solar Irradiance Forecasting», *IEEE Trans. Syst. Man Cybern. Syst.*, vol. 52, n.º 1, Art. n.º 1, 2022, doi: 10.1109/TSMC.2021.3093519.

[13]　F. Wang, Y. Yu, Z. Zhang, J. Li, Z. Zhen, y K. Li, «Wavelet Decomposition and Convolutional LSTM Networks Based Improved Deep Learning Model for Solar Irradiance Forecasting», *Appl. Sci.*, vol. 8, n.º 8, Art. n.º 8, ago. 2018, doi: 10.3390/app8081286.

[14]　I.-I. Prado-Rujas, A. García-Dopico, E. Serrano, y M. S. Pérez, «A Flexible and Robust Deep Learning-Based System for Solar Irradiance Forecasting», *IEEE Access*, vol. 9, pp. 12348-12361, 2021, doi: 10.1109/ACCESS.2021.3051839.

[15]　W. Khan, S. Walker, y W. Zeiler, «Improved solar photovoltaic energy generation forecast using deep learning-based ensemble stacking approach», *Energy*, vol. 240, p. 122812, 2022, doi: https://doi.org/10.1016/j.energy.2021.122812.

[16]　M. Abdel-Nasser, K. Mahmoud, y M. Lehtonen, «HIFA: Promising Heterogeneous Solar Irradiance Forecasting Approach Based on Kernel Mapping», *IEEE Access*, vol. 9, pp. 144906-144915, 2021, doi: 10.1109/ACCESS.2021.3122826.

[17]　A. Katrompas, T. Ntakouris, y V. Metsis, «Recurrence and Self-attention vs the Transformer for Time-Series Classification: A Comparative Study», en *International Conference on Artificial Intelligence in Medicine*, 2022, pp. 99-109.

[18]　A. D. Cristian Arbelaez-Duque, «SolarForecastingElecEngUdeA». Medellin, 25 de julio de 2022. Accedido: 23 de septiembre de 2022. [En línea]. Disponible en: https://github.com/cdarbelaez/SolarForecastingElecEngUdeA

[19]   J. M. Romero Rodríguez, «Modelo para predicción de potencia de paneles fotovoltaicos utilizando técnicas de clasificación no supervisada y redes neuronales artificiales», 2020, Accedido: 22 de marzo de 2022. [En línea]. Disponible en: https://manglar.uninorte.edu.co/handle/10584/9049

[20]   S. Sharda, M. Singh, y K. Sharma, «RSAM: Robust Self-Attention Based Multi-Horizon Model for Solar Irradiance Forecasting», *IEEE Trans. Sustain. Energy*, vol. 12, n.º 2, pp. 1394-1405, abr. 2021, doi: 10.1109/TSTE.2020.3046098.

[21]   A. Vaswani *et al.*, «Attention is All you Need», en *Advances in Neural Information Processing Systems*, 2017, vol. 30. [En línea]. Disponible en: https://proceedings.neurips.cc/paper/2017/file/3f5ee243547dee91fbd053c1c4a845aa-Paper.pdf

[22]   X. Huang, C. Zhang, Q. Li, Y. Tai, B. Gao, y J. Shi, «A Comparison of Hour-Ahead Solar Irradiance Forecasting Models Based on LSTM Network», *Math. Probl. Eng.*, vol. 2020, p. e4251517, ago. 2020, doi: 10.1155/2020/4251517.

[23]   Q. Ashfaq, A. Ulasyar, H. S. Zad, S. Nisar, A. Khattak, y K. Imran, «Multi-Step Forecasting of Global Horizontal Irradiance Using Long Short-Term Memory Network for Solving Economic Dispatch Problem», en *2021 International Conference on Innovative Computing (ICIC)*, 2021, pp. 1-9. doi: 10.1109/ICIC53490.2021.9693031.

[24]   N. Vakitbilir, A. Hilal, y C. Direkoğlu, «Hybrid deep learning models for multivariate forecasting of global horizontal irradiation», *Neural Comput. Appl.*, ene. 2022, doi: 10.1007/s00521-022-06907-0.

[25]   GeoSUN Africa, «Kenya - Solar Radiation Measurement Data», *EnergyData.info*, 2020. https://energydata.info/dataset/kenya-solar-radiation-measurement-data (accedido 23 de septiembre de 2022).

Sustainable Production Planning Optimization Using Integer Programming

Fernando Zanella[1][0000000314686771] and Clara Bento Vaz[1,2,3][0000000198626068]

[1] Research Centre in Digitalization and Intelligent Robotics (CeDRI), Instituto Politécnico de Bragança (IPB), Campus Santa Apolónia, 5300-253 Bragança, Portugal
[2] Laboratório para a Sustentabilidade e Tecnologia em Regiões de Montanha (SusTEC), Instituto Politécnico de Bragança, Campus de Santa Apolónia, 5300-253 Bragança, Portugal

[3] Centre for Management and Industrial Engineering (CEGI/INESC TEC)
`a52494@alunos.ipb.pt,clvaz@ipb.pt`

Abstract. This paper presents how integer linear programming can be used to optimize and develop a sustainable production plan for a medium-sized cold stamping company. The objective is to develop a model to minimize the total production cost, which includes the manufacturing process cost, inventory holding cost, and unproductive machine cost. The model takes into account weekly demands, inventory levels, and idle machine time during a planning horizon of one month. The output is a plan containing all products that have to be manufactured, their weekly optimal quantities, and a prediction of the final inventory level. By minimizing the total production cost, the model ensures that the company is consuming only the necessary amount of resources. The mathematical model is related to the real-world constraints that are part of the company's production scenario, reflecting both direct and indirect impacts of resource usage. This model enables to simulate three scenarios, and their results indicate that the total production cost is minimum when a company produces in volumes slightly greater than the demand. By better allocating resources, the company can contribute to sustainability in the context of responsible production.

Keywords: Integer Programming · Production planning · Sustainability

1 Introduction

The United Nations (UN) has set 17 Sustainable Development Goals (SDGs), which are a group of guidelines that intend to build a better world by 2030. The topic of these goals involves all aspects of society, such as social (hunger, poverty, equality), economic (industry, innovation, partnership), and environmental (natural resources, fauna, flora) [1]. This paper intends to contribute to the 12th SDG, entitled "Responsible Consumption and Production", which states that the global economy's dependence on the natural environment and its

resources increased over 65% from 2000 to 2019 [2]. All targets set by the 12th SDG are related to sustainable management and efficient use of resources while reducing all kinds of waste through prevention, reduction, recycling, and reuse. In this context, the optimization technique, Linear Programming (LP), can be used as an efficient approach to promote sustainable production, since it allows companies to save resources and operate in an optimal way, independent of their economic sector [3]. The most common application of LP involves determining the optimal scenario for a set of activities toward an objective. Most of the time, these activities compete for resources between each other, such as energy and raw material.

Production planning is an essential and complex activity inside a company that requires simultaneous cooperation between everyone responsible for the decision-making process. A good plan will always lead to a good workflow, promoting efficient resource usage and responsible production. Usually, production planning can be separated into three different time horizons: (i) long-range plans, (ii) medium-range plans, and (iii) short-range plans [4]. Long-range plans are related to new infrastructure, research and development, new products, and facility location and/or capacity. Medium-range plans are elaborated to always match supply and demand in terms of rough volume and product mix, which mean maintaining enough raw material, work in process, and inventory level to meet the demand while also absorbing possible demand fluctuations. The ultimate output of a medium-range plan is the master production schedule (MPS), which outlines all products that need to be manufactured, when, and in what quantities, usually referring to finished goods. Finally, short-range plans are concerned with determining job assignments, ordering, job scheduling, and dispatching [5].

Omara et al. [6] developed a model to optimize the MPS using Fuzzy Mixed Integer Linear Programming (FMILP). Herrmann [7] proposed a linear model to optimize the MPS using a commercially available software ILOG. Sawik [8] addressed production scheduling optimization based on Mixed Integer Linear Programming (MILP), seeking to minimize tardiness. Al-Ashhab and Fadag [9] developed a model to optimize the MPS based on maximizing profit using MILP and Genetic Algorithms (GA). Within this context, no studies that integrate directly the sustainability in the MPS planning were found. To fill this gap, this study intends to propose an Integer Linear Programming model - or simply Integer Programming (IP) - that allows a real medium-sized cold stamping company to create a sustainable MPS. Hence, this model seeks to minimize costs, proposing an efficient and responsible production plan.

This paper is organized as follows: the next section describes the MPS planning, and how IP can be used to optimize it. Section 3 proposes an IP model for a medium-sized cold stamping company and describes all data that are required; section 4 discusses three different scenarios of the proposed model; Finally, section 5 presents the conclusions and further work.

2   Literature Review

This section aims to present some important topics regarding manufacturing planning and control optimization. First, it is intended to state a brief introduction to MPS and its basic concepts and definitions; next, it is discussed some general methods that are used by many industries to plan their production activities; afterwards, IP is introduced under a production planning context.

2.1   Master Production Planning

Creating the MPS is the task of disaggregating the company's sales and operations plan (S&OP) into a tangible manufacturing schedule, determining all products that must be manufactured with their quantities and production timing. For the MPS to be developed, two other plans must have already been done: long-term capacity planning and Aggregate Production Planning (APP) [4, 5].

Every MPS aims to develop a production schedule over a medium-term period, usually in terms of weeks. For each product manufactured within the planning period, the MPS indicates production quantities, machine capacity, required levels of raw materials and unfinished goods, and any other pertinent detail. Lastly, it is possible to estimate both intermediate and final inventory levels, based on what is planned to be consumed [10]. In most scenarios, some of the leading MPS guidelines and constraints are the time available for production, whether or not including overtime, the demand, the availability of resources, and the maximum inventory capacity for each product.

Since every MPS belongs to the medium-range plans, when unexpected adversities occur, such as machine breakdowns or quality problems, planned tasks may not be executed accordingly to the schedule, leading to delays. In other words, planning does not guarantee due dates compliance, precisely because of these unpredictable factors that are intrinsic to the production process. Still, having a well-defined plan helps to react to these adversities in the best possible way [4, 5].

Concerning loading capacity, which is the process of assigning jobs to specific machines, workstations, or processes, it is important to consider that, in reality, all machines and equipment have limited capacity, usually defined in terms of available time to operate. When production schedules consider this assumption, the planning is said to have finite loading. Production planning techniques that ignore the maximum capacity of machines and equipment are called infinite loading models. In this case, there is a greater probability of not meeting delivery deadlines, and in cases of overload, it is required overtime or outsourcing [4].

Omara et al. [6] proposed a model to minimize the costs of the MPS using FMILP, taking into account production cost, setup cost, inventory, and backorder costs. However, none direct analysis was done regarding sustainability.

Herrmann [7] developed a model to minimize tardiness for companies that produce in small batches while having to meet high demand. This approach involves detailed scheduling based on production completion times, leading to

reduced capacity problems, out-of-stock situations, and most importantly, tardiness. The commercially available tool ILOG was used to run the linear model.

Sawik [8] also addressed production planning optimization based on tardiness, elaborating a model based on IP that divides and allocates customer orders into planning periods to meet due dates while minimizing the total number of delays. Despite referring to reducing operational costs, the model is not directly attached to sustainability.

Al-Ashhab and Fadag [9] proposed a model to maximize the profit of a company considering transportation logistics and production costs, selling prices, inventory, batch size and capacity. MILP and GA were used to solve the model, and both methods gave the same optimal values for most variables, seeming to be equally efficient.

As can be noticed, sustainability is not a prominent topic when it comes to optimizing the MPS of a company. Hence, the model proposed in this paper intends to contribute to sustainable production by minimizing costs.

2.2   Integer Programming (IP)

Integer programming is a method that uses a set of mathematical linear functions to describe a certain problem and then solve it to obtain a set of optimal decision variables expressed in integer numbers [11, 3]. When defining an IP mathematical model, four groups of elements should be defined: the decision variables, the objective function, the functional constraints, and the nonnegativity constraints [3].

The decision variables represent the model's solution. When an IP problem is modeled, the goal is to find a set of optimal integer values - the decision variables - that satisfy all constraints while maximizing or minimizing the objective function[3]. Most of the time, within the context of the MPS, the decision variables represent the quantities to be produced for each different product.

The objective function is a mathematical expression that relates directly every decision variable to the objective of the model, which can be a maximization or minimization function, depending on the approach to solve the problem. In the literature review carried out concerning MPS optimization problems, three objectives were identified: (i) to minimize costs [6], (ii) to minimize tardiness [7], and (iii) to maximize profit [9].

The functional constraints are a set of inequalities that give realism to the model by restricting the solution span based on certain criteria, imposing upper and bottom limits to the decision variables. In the MPS model, these constraints often represent the machine capacity, the minimum demand, the maximum quantities able to be stocked, and so forth [11, 3].

3   Methodology

This section aims to describe the methodology used to develop the proposed IP model, by introducing the context of the problem and its elements, correlating them with sustainable production planning.

3.1 Context setting

The company under study is a medium-sized firm that produces cold stamping parts of exhaust systems for the automobile industry. These parts are sold to customers who assemble the full exhaust system. Specifically, the company is in the middle of the automobile industry supply chain, and therefore, there is huge pressure on accomplishing due dates.

In the company's stamping sector, there are four hydraulic presses: (i) Zani 600 tons, (ii) Rovetta I 600 tons, (iii) Rovetta II 600 tons, and (iv) Cattaneo 1000 tons. Each machine is capable of producing a limited range of products, although some products can be manufactured on more than one machine. Despite this, the proposed model involves the MPS of one machine at a time, because based on production costs and productivity rates, the company already knows in which machine (first option) a particular product is more viable to be manufactured. The alternative machine is only used when the first option machine is unavailable due to unscheduled maintenance or breakdown.

The company's production process is briefly explained through Figure 1.
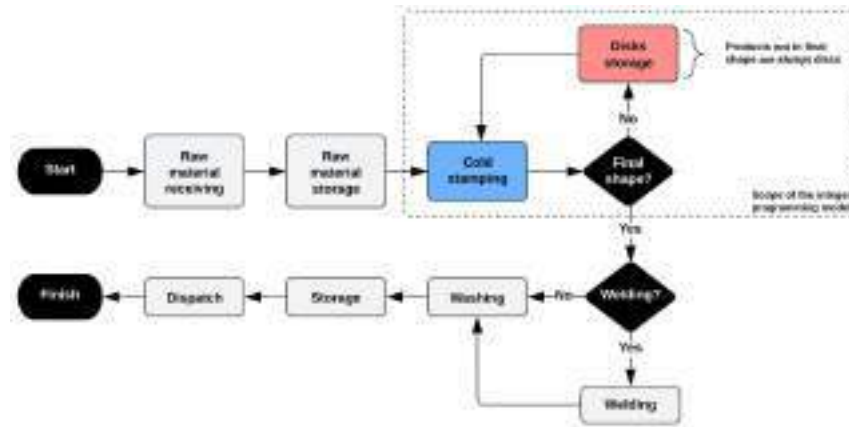
Fig. 1. Company's production chain

The production process begins with raw material receiving, most of the time in the form of metal coils. When the raw materials arrive from the suppliers, they are stocked in the warehouse and stay there until demand occurs, when then one of the hydraulic presses is fed with these metal coils. From this point, there are two possibilities: (i) the metal sheet is stamped by the press and the output is a part in its final shape; (ii) the metal sheet is cut into disks by the hydraulic press, and these disks are stocked to later be stamped again and finally be shaped to their final form. After going through the stamping sector, a part may be welded by a semi-automatic machine. Later, the part is washed and dried by another

machine, obtaining the product in its finished state. Finally, the product has to be stocked in the warehouse until its dispatched.

Throughout this entire production process, only the cold stamping sector presents bottlenecks, and therefore this is the main scope of the proposed model.

3.2 Integer Programming Model

The following notation concerning indices, sets, parameters, and variables are used in the model formulation.

i	Product code to be manufactured (i=1, 2, 3, ..., 10)
j	Week designation (j= 1, 2, 3, 4)
TPC	Total production cost [€]
MPC_i	Manufacturing process cost for the product i [€/unit]
IHC_i	Inventory holding cost per week for the product i [€/unit]
II_{ij}	Initial inventory for the product i at the beginning of week j [unit]
SS_i	Safety stock level for the product i [unit]
FS_i	Final inventory for the product i at the end of the four weeks [unit]
D_{ij}	Demand for the product i and week j [unit]
UMC	Unproductive machine cost [€/hour]
S_j	Number of shifts available to work during week j [unit]
P_i	Time required to produce one unit of product i [hour/unit]
PT	Total productive time [hour]
UT	Total unproductive time [hour]

The formulation of the proposed integer programming model is presented in 3.2(1).

Minimize

$$\sum_{i=1}^{10}\sum_{j=1}^{4} MPC_i \cdot X_{ij} +$$
$$\sum_{i=1}^{10}\sum_{j=1}^{4} IHC_i \cdot (X_{ij} + II_{ij} - D_{ij}) + \qquad (1)$$
$$\sum_{i=1}^{10}\sum_{j=1}^{4} UMC.(7.25 \cdot S_j - P_{ij} \cdot X_{ij})$$

s.t.

$$SS_i + D_{ij} - II_{ij} \leq X_{ij} \qquad (C1)$$

$$\sum_{j=1}^{4} X_{ij} \leq M_i \qquad (C2)$$

$$\sum_{i=1}^{10} X_{ij} \cdot P_{ij} \leq 7.25 \cdot S_j \qquad (C3)$$

$$X_{ij} \geq 0 \qquad (C4)$$

$$X_{ij} \in \mathbb{Z}$$

$$i = \{1, 2, 3, \ldots, 10\}$$
$$j = \{1, 2, 3, 4\}$$

The integer programming model (1) allows determining the optimum quantity to be produced of each product i in week j (X_{ij}). These are the decision variables required to develop the MPS of the company. The sub-index i can vary from 1 to 10, because historically this is the maximum amount of product types that a single machine produces per month, while the sub-index j ranges from 1 to 4 weeks, corresponding to a planning horizon of one month. Since X_{ij} represents a set of quantities, all values must be positive integer numbers.

To ensure sustainability within a productive and competitive context, a company always aims to increase its profit margin by using fewer resources. These imply minimizing the production costs which means that only the necessary amount of all associated resources are being used. In practice, the model should determine the optimal quantities to produce for each product at the right moment, leading to reduced costs and waste. This is captured by the definition of the objective function which minimizes the total production cost that includes three main production cost factors within the company: (i) manufacturing pro-

cess costs (MPC_i), (ii) inventory holding cost (IHC_i), and (iii) unproductive machine cost (UMC).

The MPC_i represents the cost for a certain machine to operate and produce one unit of product i. For a product i that can be manufactured on more than one machine, its MPC_i will probably be different for each one of them. The MPC_i tends to increase proportionally to the power of the hydraulic press in which the product i is produced. The second term of the objective function is the inventory holding cost (IHC_i) which includes all the fees and expenses required to maintain the product i in the company's warehouse. These costs involve security, fixed costs, product depreciation, and salaries which are proportional to the stored quantity of the product i. The third and last term UMC is linked to the unproductive machine cost (UMC), which is different for each of the four machines and is mainly determined by the hourly cost of depreciation, fees, and insurance.

To reflect the reality of the production process, three functional constraints were considered: (i) the minimum quantity to be produced to satisfy the demand (C1), (ii) the maximum quantity allowed to be produced (C2), and (iii) the machine availability (C3).

Concerning the minimum quantity to be produced (C1), it is determined based on the week's initial inventory (II_{ij}), safety stock level (SS_i), and demand (D_{ij}). Regarding demand, the company works with production forecasts that support medium-term planning. These forecasts provide aggregated volumes of demand that must be met during the next four months, however, they are subject to change. In other words, the company always has an aggregate production planning (APP) for four months from the present. Production volumes are only disaggregated for the current month, that is, for the next 28 days from the present. This process originates weekly demands for each product for the next four weeks. To absorb possible market fluctuations or unexpected setbacks, the company works with a predetermined safety stock level (SS_i), which is equivalent to the two-week average demand for the planning period.

The maximum quantity allowed to be produced (C2) for each product i in week j takes into account the manager's expertise, as it may depend on the combined effect of numerous factors, such as raw material shortage, forecasted demand, warehouse capacity, and so forth. In other words, the manager's knowledge is essential to set an upper limit (M_i) to all products that must be manufactured over the planning horizon.

The planning model adopted by the company is based on limited loading, and therefore, the total available time to produce (C3) must be sufficient to cover all product units that are going to be manufactured. In practice, knowing the number of available working shifts (S_j) in each week j and the productive hours per shift (7.25), it is possible to calculate how many working hours each machine will be able to operate over the planning horizon. Based on the average time to produce one unit of each product (P_i), these available working hours end up as an upper limit on the total number of parts that can be manufactured.

3.3　Data

The data used to test, validate, and implement the model were collected in the company. It is possible to classify the required data into three large groups: (i) product structure, (ii) machines, and (iii) storage information.

All product structure information was obtained directly through a formal document, containing all levels of each product, from raw material to the finished good. In terms of cold stamping, among the entire company's portfolio, the vast majority of parts is only submitted to a single stamping step, but on the other hand, there is a range of products that must go through two subsequent stamping steps, as described before. Despite being dependent on each other in terms of manufacturing, these two subsequent processes can be considered independent in the proposed model, simply because they occur at two very different moments. In practice, the first stamping process generates disks that are stocked to be used later, meaning a complete planning cycle. When there is demand, the second stamping process is planned and executed, consuming some of those disks and leading to the product in its final shape, meaning another complete planning cycle. The same disk type can be used for more than one product, which is why the company adopts the strategy of stocking disks, seeking to absorb any fluctuations or unforeseen events.

All machine data were easily accessible, as it was only necessary to regroup and rearrange them. The main set of information was obtained from an electronic spreadsheet frequently used by the company. For all hydraulic presses, it was possible to extract what products each of them can produce, their respective average production rates (P_i), the costs of each stamping process (MPC_i), and their unproductive costs (UMC_i).

The information about inventory costs (IHC_i) for both finished and unfinished products required processing before they could be used. With the company's support, for each product, finished or not, storage costs were determined based on the volume that each product container occupies inside the warehouse and the logistic costs involved to manipulate it.

To select the most suitable software for solving the model, the main concern was the dimension of the problem in terms of the number of decision variables and constraints, as well as the ability of the company to use it. Since the company uses Excel extensively, it was necessary to improve and adjust the mathematical formulation for it to be solved by the add-on Solver from Excel.

4　Results and Discussion

In order to relate the total production cost (TPC) with sustainability, model (1) was used to simulate and compare three different situations: no initial inventory and no safety stock (NINS); no initial inventory but with safety stock (NIWS); with initial inventory and safety stock (WIWS). In all scenarios, the same products were considered as well their respective weekly demand (D_{ij}) and maximum production levels (M_i), according to Table 1.

Table 1. Weekly demand and maximum production level per product

Product code i	D_{i1}	D_{i2}	D_{i3}	D_{i4}	M_i
Product 1	9000	9000	0	0	36000
Product 2	0	0	4500	4500	18000
Product 3	0	4500	4500	0	18000
Product 4	0	0	15000	15000	60000
Product 5	3000	3000	3000	0	18000
Product 6	0	9000	9000	0	36000
Product 7	0	0	0	20000	40000
Product 8	0	8000	8000	0	32000
Product 9	15000	15000	0	0	60000
Product 10	4500	4500	4500	4500	36000

The first scenario (NINS) refers to a situation in which initial inventory (IS_i) and safety stock level (SS_i) are null. In practice, this means that the company does not have inventory and will only produce surplus if the model identifies that this approach is more beneficial than leaving the machine unproductive. The optimum solution for the first scenario is shown in Table 2.

Table 2. Quantities to be produced of each product in scenario NINS.

Product code i	SS_i	IS_i	X_{i1}	X_{i2}	X_{i3}	X_{i4}	FS_i	$FS_i - SS_i$
Product 1	0	0	9000	9000	0	18000	18000	18000
Product 2	0	0	0	0	4500	4500	0	0
Product 3	0	0	0	4500	4500	0	0	0
Product 4	0	0	0	0	15000	15000	0	0
Product 5	0	0	3000	3000	3000	0	0	0
Product 6	0	0	0	9000	14840	12160	18000	18000
Product 7	0	0	0	0	0	20000	0	0
Product 8	0	0	0	8000	8000	0	0	0
Product 9	0	0	15000	15000	0	30000	30000	30000
Product 10	0	0	4500	4500	4500	22500	18000	18000

Analyzing Table 2, it is clear that the model (1) identified that most of the time, it is better to leave the machine not operating rather than producing surplus units. The only exceptions identified that would compensate the unproductive costs are products 1, 6, 9, and 10, which are suggested to be produced to

stock. In other words, producing surplus units of these products and generating inventory is better than keeping the machine in an unproductive state.

The second scenario (NIWS) represents a situation where initial stocks (IS_i) are null, but now it considers a safety stock (SS_i) equivalent to 50% of the sum of the total demand. This 50% margin is the current value that the company uses to determine its safety stock level. The optimum solution for the second scenario is shown in Table 3.

Table 3. Quantities to be produced of each product in scenario NIWS.

Product code i	SS_i	IS_i	X_{i1}	X_{i2}	X_{i3}	X_{i4}	FS_i	$FS_i - SS_i$
Product 1	9000	0	18000	9000	0	27000	36000	27000
Product 2	4500	0	4500	0	4500	4500	4500	0
Product 3	4500	0	4500	4500	4500	0	4500	0
Product 4	15000	0	15000	0	15000	15000	15000	0
Product 5	4500	0	7500	3000	3000	0	4500	0
Product 6	9000	0	9000	9000	36000	0	36000	27000
Product 7	10000	0	10000	0	0	20000	10000	0
Product 8	8000	0	8000	8000	8000	0	8000	0
Product 9	15000	0	30000	15000	0	45000	60000	45000
Product 10	9000	0	13500	4500	11145	24855	36000	27000

As shown in Table 3, during the first week of the NIWS scenario, all products have to be produced in order to achieve their respective safety stock level, but during the following weeks, most production is only to meet demand. Similarly to the NINS scenario, the products 1, 6, 9, and 10 are suggested to be overproduced, but now differing from the first scenario by their quantities.

The third scenario (WIWS) considers both initial (IS_i) and safety stock (SS_i), with an initial inventory level higher than the safety level. In this simulation, the safety stock corresponds to 50% of the sum of the total demand (such as in the NIWS scenario), while the initial inventory is 60% of that sum. The 60% margin enables to represent how the model would react to a situation when it can consume stocked units to partially satisfy the demand. The optimum solution for the third scenario is shown in Table 4.

Based on Table 4, the scenario WIWS is very different from the others. This time, only products 1, 5, 9, and 10 are to be produced in the first week, whereas by the end of the planning horizon, only products 6, 9, and 10 are recommended to be overproduced.

Table 5 summarizes all results for each scenario at the optimum solution, presenting their values regarding the total production cost (TPC) and its components, the manufacturing production cost (MPC), the inventory holding cost (IHC), and the unproductive machine cost (UMC). Moreover, the total unpro-

Table 4. Quantities to be produced of each product in scenario WIWS.

Product code i	SS_i	IS_i	X_{i1}	X_{i2}	X_{i3}	X_{i4}	FS_i	$FS_i - SS_i$
Product 1	9000	10800	7200	9000	0	0	9000	0
Product 2	4500	5400	0	0	3600	4500	4500	0
Product 3	4500	5400	0	3600	4500	0	4500	0
Product 4	15000	18000	0	0	12000	15000	15000	0
Product 5	4500	5400	2100	3000	3000	0	4500	0
Product 6	9000	10800	0	7200	46800	0	46800	37800
Product 7	10000	12000	0	0	0	18000	10000	0
Product 8	8000	9600	0	6400	8000	0	8000	0
Product 9	15000	18000	12000	15000	0	49532	64532	49532
Product 10	9000	10800	2700	4500	7224	39576	46800	37800

ductive time (UT) and the total productive time (PT) are also shown for each scenario.

Table 5. Production costs and working time results

Scenario	MPC [€]	IHC [€]	UMC [€]	TPC [€]	UT [h]	PT [h]
NINS	4.511,40	718,71	8.052,66	13.282,77	136	154
NIWS	6.767,08	4.109,15	3.483,42	14.359,65	59	231
WIWS	5.241,53	4.302,06	6.079,67	15.623,26	102	188

As stated in Table 5, the total production cost (TPC) for the first scenario (NINS) is €13.282,77, of which €4.511,40 (34%) are from the MPC, €718,71 (5%) from the IHC, and €8.052,66 (61%) from the UMC. Relating to these costs, it is estimated a total of 136 unproductive hours that lead to the UMC, whereas the 154 productive hours lead to both the MPC and the IHC. This means that the model found the balance between the costs to produce surplus units and leaving the machine in an unproductive state.

For the second scenario (NIWS), the total cost (TPC) is €14.359,65, composed by €6.767,08 (47%) from the MPC, €4.109,15 (29%) from the IHC, and €3.483,42 (24%) from the UMC. This plan results in a total of 59 unproductive hours face 231 productive hours. This time, because it is necessary to replenish all units required by the safety stock level, the UMC represents the lowest contribution to the total cost (TPC), whereas the MPC is the highest, exactly because there is a an incentive to produce more (demand plus safety stock).

In the third scenario (WIWS), there is a need to replace the safety stock. Thus, the total cost (TPC) is €15.623,26, in which the MPC is €5.241,53 (34%),

the IHC is €4.302,06 (28%), and the UMC is €6.079,67 (39%). The third plan leads to 188 productive hours and 102 unproductive hours.

Comparing all scenarios, it is clear that the most sustainable is the first one (NINS), where the approach is to produce only what is necessary, avoiding to keep inventory. This is aligned with lean manufacturing, which is known to promote efficiency and reduce waste. However, the second scenario (NIWS) is a better planning approach for the company under study, because it works with high demand levels, and if there is a machine breakdown, safety stock can reduce or even avoid delays, leading to less impact on customer expectation. The third scenario (WIWS) shows that excessive production above the safety level generates high costs and higher consumption of resources, just because all surplus units are costing to be maintained over time.

5   Conclusion

Bear in mind what has been presented, one can assure that IP consists of a powerful tool for developing a sustainable MPS model. This approach gives the possibility of predicting and analyzing a vast number of different scenarios which is fundamental for a firm that wants to prosper and grow, using a sustainable and a competitive strategy.

The main contribution of this paper is to develop a sustainable MPS model based on IP, which allows a medium-sized cold stamping company to find the optimal balance between letting unproductive machines or generating inventory by producing units in surplus, which means producing more with less waste in order to obtain a responsible and sustainable production.

Three different scenarios (NINS, NIWS, WIWS) were simulated using the proposed model, and the results indicate that the total production cost is lower when a company produces in volumes close to the demand. However, not every company is capable of doing it, because of possible unscheduled events intrinsic to the production process that can lead to delays and decrease customer satisfaction. The worst scenario is when a company generates an excessive inventory, since it turns into high costs required to maintain them in the warehouse.

The proposed model does not consider uncertainty for two main reasons: (i) it was designed to be continuously applied at the end of each week, meaning that only during the first week the proposed plan is going to be executed, whereas all plans concerning the following weeks (2, 3, and 4) are going to be weekly rescheduled until they take place; (ii) given that the company has a limited number of customers and produces based on orders, the demand fluctuation is predictable and absorbed by the weekly review of all plans.

Since the model is still in development, no comparisons were made with the real plan developed and applied by the company. Some of the further work intends to extend the model to determine the short-range plans based on an effective job sequencing rule, involving setup time. With the final model in hand, the validation encompasses the comparison of the MPS planning of the proposed

model with the real planning of the company. Additionally, the proposed model will be tested to support the real production planning of the decision makers.

Acknowledgement

References

1. United Nations: 17 Sustainable Development Goals. Available at: https://sdgs.un.org/goals (Accessed: October 1, 2022).
2. United Nations: Sustainable Development Goal Nº 12. Available at: https://sdgs.un.org/goals/goal12 (Accessed: October 1, 2022).
3. Hillier, F., Lieberman, G.: Introduction to operations research. 9th ed. Higher Education (2010)
4. Heizer, J., et al.: Operations management: sustainability and supply chain management. 12th ed. Pearson (2017)
5. Vollmann, T., et al.: Manufacturing planning and control systems for supply chain management: the definitive guide for professionals. 5th ed. McGraw-Hill Professional (2004)
6. Omara, M. K., Mohd-Jusohb, M.; Omarc, M.: Developing a Master Production Schedule Using Fuzzy Mixed Integer Linear Programming. International Journal of Computers (2021)
7. Herrmann, F.: Using optimization models for scheduling in enterprise resource planning systems. Systems (2016)
8. Sawik, T.: Integer programming approach to production scheduling for make-to-order manufacturing. Mathematical and Computer Modelling (2005)
9. Al-Ashhab, M. S., Fadag, H.: Multi-Product Master Production Scheduling Optimization Modelling Using Mixed Integer Linear Programming And Genetic Algorithms. International Journal of Research-Granthaalayah. (2018)
10. Stadtler, H., et al.: Supply chain management and advanced planning: concepts, models, software, and case studies. 3rd ed. Springer (2015)
11. Lachtermacher, G.: Pesquisa operacional na tomada de decisões. Editora Campos (2004)

Repensando un Sistema Integral de RSU para el Centro Histórico de Cuernavaca, Morelos, México

Arce-García Ivonne Yazmín[1][0000-0001-8486-3038], Torres-Salazar María del Carmen[2][0000-0002-2119-8998], Vera-Dimas José Gerardo[1][0000-0002-3880-3568], Saldarriaga-Noreña Hugo Albeiro[2][0000-0002-0676-0639], León-Hernández Viridiana Aydeé[1][0000-0002-5070-9320], Peralta-Abarca Jesús del Carmen[1][0000-0003-2995-9277] y Moreno-Bernal Pedro[1][0000-0002-2811-5331]

[1] Facultad de Ciencias Químicas e Ingeniería (FCQeI)
[2] Centro de Investigaciones Químicas (CIQ),
Universidad Autónoma del Estado de Morelos (UAEM),
Cuernavaca, Morelos, México
yazmin.arcegrc@uaem.edu.mx

Resumen. ¿Cómo se puede migrar un sistema de recolección municipal convencional hacia uno de carácter sostenible? La respuesta a esta interrogante para la mayoría de las ciudades de México aún se encuentra en construcción, como en el caso de Cuernavaca y su Centro Histórico. Sin embargo, hay sistemas de recolección urbanos que se están volviendo un modelo de referencia en el tema de recuperación y valorización de los Residuos Sólidos Urbanos (RSU) en nuestro país, los cuales pueden aportar aspectos significativos para poder repensar una forma distinta de sistema de recolección municipal. Por ello, el objetivo de este artículo es analizar el sistema actual del Centro Histórico de Cuernavaca, Morelos, considerando las estrategias que han sido abordadas, los retos que se han presentado al trascurrir de los años, y como podría migrar su sistema de recolección hacia un sistema más adecuado, visto a través de la mirada de los generadores y de la observación de aquellas ciudades que han obtenido la presea de la escoba de platino, oro, y plata, por ser las ciudades que destacan en su labor a favor del medioambiente y ser las más limpias en nuestro país, reconocimiento que es emitido por la Asociación Técnica para la Gestión de Residuos y Medio Ambiente (ATEGRUS) con sede en España.

Palabras clave: Gestión de RSU, Sistema Integral de RSU, Repensando sistemas.

1   Introducción

El manejo de los RSU y los sistemas de gestión integral forman parte del campo de estudio de los países emergentes o en desarrollo, precisamente porque la capacidad instalada no va acorde con su generación y su crecimiento poblacional. No obstante, también se integran países que buscan ayudar a mitigar los efectos del cambio climático. Esto debido a que al hablar de residuos se están involucrando diferentes vertientes, no solo es desechar un producto/embalaje o parte de un servicio, es desperdiciar recursos

útiles en la economía e incrementar los impactos ambientales, sociales y económicos que están relacionados de manera directa e indirecta a su inadecuado manejo. Bajo este contexto, el manejo de los RSU para la mayoría de las Ciudades de México, y de algunos países, integra un sistema básico de recolección de residuos de manera no diferenciada, en donde la recuperación de materiales valorizables es mínima y se está llevando a cabo a través del sector informal (recolectores/pepenadores). En el mejor de los casos, los residuos son dispuestos en rellenos sanitarios, los cuales, cabe señalar que tampoco cuentan con un control ambiental adecuado. La principal problemática que se presenta sobre este tema está dada en cómo se genera y se disponen los residuos desde la fuente, donde al menos se debería de requerir la clasificación primaria (orgánicos e inorgánicos). En segundo lugar, la infraestructura instalada, el presupuesto asignado, la topografía del lugar y la falta de capacitación y concientización de todos los actores involucrados también viene a repercutir en la cadena de manejo de los residuos [5].

El desechar elementos útiles ha fomentado el consumo de materias primas, y este consumo ha alcanzado un ritmo que comprometerá la capacidad del planeta, si se continúa esta tendencia lineal de consumo y desecho [9], [18]. Tan es así que el escenario previsto para la población estimada para el 2030 y 2050, requerirá la demanda de recursos naturales equivalente a tener tres planetas para poder satisfacer sus necesidades básicas [13]. Esta proyección pone en riesgo no solo el equilibrio de nuestro planeta, sino que también la subsistencia del ser humano. Por ello, se le ha dado vital importancia a este tema dentro de las convenciones macro, con la firma de acuerdos y compromisos internacionales, como el convenio de Basilea, el tratado de París los objetivos del milenio y los del desarrollo sostenible (ODS) de la Agenda 2030. Dentro de estos últimos, están especificadas 11 metas relacionadas con el manejo de los RSU, y cuyo rubros son: ciudades y comunidades sostenibles (11.6), producción y consumo responsable (12.5 y 12.a), acciones por el clima (13.2 y 13.3), alianzas para lograr los objetivos (17); y de manera indirecta, con agua limpia y saneamiento (6.6), trabajo decente y crecimiento económico (8.4), vida submarina (14.1), y vida de ecosistemas terrestres (15.1 y 15.2) [15], con los cuales se pretende mitigar/minimizar en medida de lo posible, los efectos adversos en el presente, los cuales se pueden agravar en el futuro. Como lo ha dicho la Fundación Ellen MacArthur, "¡el momento de actuar es ahora!"- y este cambio solo ocurrirá cuando se trabaje en conjunto: gobierno, sociedad, empresas y la academia, empezando desde el ámbito local.

Para que estas metas puedan cumplirse, se vuelve indispensable conocer de manera particular cuales son las situaciones que se viven y se practican en las localidades, observándolas como un sitio de estudio, para identificar cuáles son las oportunidades potencialmente que se pueden presentar. Una vez reunida la información se puede construir una hoja de ruta que coadyuve a la recuperación y valorización de los materiales. El Sistema por proponer tendrá que ajustarse a las necesidades del sitio, maximizando los recursos existentes. En este contexto, se mostrará parte del estudio que se está realizando en la localidad del Centro Histórico de Cuernavaca, Morelos, México, cuyo objetivo es analizar el sistema de manejo de RSU, considerando las estrategias que han sido abordadas, los retos que se han presentado al trascurrir de los años, y como podría

migrar hacia un sistema más adecuado, visto a través de la mirada de los generadores (UE) y de la observación de aquellas Ciudades modelo que han implementado buenas prácticas para la recuperación y valorización de RSU.

2　　Referentes teóricos

El Programa de las Naciones Unidas para el Desarrollo (PNUD) [16], Rosario [20] y Jacob [9] recomiendan que antes de generar una propuesta de intervención, es necesario saber cuáles son los conocimientos que presentan los generadores, porque a partir de ello, se pueden establecer estrategias que vayan direccionadas a suplir carencias o a reforzar conocimiento, y con ello se detone mayor conciencia sobre el manejo de los RSU, involucrándose en las actividades y generando el compromiso personal de ayudar a mejorar nuestro planeta. Por ello, este primer acercamiento de referentes teóricos está basado en conceptos que sirven como aspectos claves para entender el tema de los residuos desde la participación del aspecto social.

2.1　　Basura vs residuo

Un residuo es todo material o producto cuyo propietario o poseedor desecha y que se encuentra en estado sólido o semisólido, o es un líquido o gas contenido en recipientes o depósitos, y que puede ser susceptible de ser valorizado (material y económicamente) o que requieren sujetarse a tratamiento o disposición final conforme a lo dispuesto en la Ley General de Prevención y Gestión Integral de los Residuos (LGPGIR), mientras que el concepto de basura será dado a todos los residuos en conjunto, que van mezclados y que son susceptibles de contaminarse entre sí, perdiendo su valor material [22]; [3].

2.2　　Sistemas de Gestión Integral de RSU

Un Sistema Integral se muestra como parte de la solución para el manejo adecuado de los RSU, debido a que conlleva acciones normativas, de planeación y operación, administrativas, sociales, de educación, monitoreo, supervisión y evaluación, desde que se está generando un residuo, hasta su disposición final [14], direccionándolos hacia los sitios adecuados para poder reutilizar, transformar y/o confinar. Estos sistemas estarán basados en los principios de la economía circular y la sustentabilidad, que, al conjuntar el aspecto social, ambiental y económico en la circularidad de materiales, se podrán modificar los sistemas lineales de extracción, producción, consumo y desecho.

2.3 Responsabilidad compartida vs responsabilidad extendida del productor (REP) según la LGPGIR

La responsabilidad compartida ocurre cuando se reconoce que los RSU son generados a partir de la realización de actividades, que satisfacen necesidades de la sociedad, mediante cadenas de valor tipo producción, proceso, envasado, distribución, consumo de productos, y que, en consecuencia, su manejo integral es una corresponsabilidad social y requiere de la participación conjunta, coordinada y diferenciada de productores, distribuidores, consumidores, usuarios de subproductos, y de los tres órdenes de gobierno según corresponda, bajo un esquema de factibilidad de mercado y eficiencia ambiental, tecnológica, económica y social. Por su lado, la Responsabilidad Extendida del Productor (REP) se trata de un principio para promover mejoras ambientales, a través de ciclos de vida completos de los sistemas de los productos, ya que su objetivo es extender las responsabilidades de los fabricantes del producto a varias fases del ciclo total de su vida útil, y especialmente las acciones que van encaminadas hacia la recuperación, reciclaje y disposición final de los mismos [6].

3 Materiales y métodos

Se realizó una investigación documental referente al Centro Histórico de Cuernavaca, Morelos. En donde se abordaron reportajes de periódicos en línea sobre datos históricos de la crisis de basura que enfrenta y de las estrategias que se han implementado.

Posteriormente, se aplicaron de manera aleatoria 196 cuestionarios de recopilación de información sobre generación y manejo de RSU en el sitio de estudio, a UE pertenecientes a los sectores de: alimentos y bebidas, y/o alojamiento temporal; prestación de servicios; comercio; instituciones educativas; industria manufacturera; y otras. El levantamiento de información corresponde al periodo de junio-septiembre de 2022, y representan un avance del 60 % de una muestra poblacional de 326 UE. Cabe señalar que la muestra poblacional fue determinada con el software Decision Analyst STATS 2.0 considerando el 95% de confiabilidad y el 5% de margen de error, sobre un universo de 2,154 UE. Universo que está basado en el censo reportado del año 2020 en el Directorio Estadístico Nacional de Unidades Económicas (DENUE) del Instituto Nacional de Estadística, Geografía e Informática (INEGI). El instrumento de recolección de datos fue revisado por expertos en la materia, fue piloteado y validado estadísticamente, y presentó un alfa de Cronbach de .727, por lo tanto, está dentro del parámetro de fiabilidad para el levantamiento de información en el sitio de estudio. Para el análisis de los datos se utilizó el software estadístico SPSS y Microsoft Excel.

Finalmente, se hizo una revisión exploratoria sobre ciudades modelo que están siendo punta de lanza en México a través de sus buenas prácticas en la recuperación y

valorización de RSU. Los resultados obtenidos en conjunto se muestran de manera descriptiva y correlacional.

4   Resultados y discusión

4.1   Recopilación de retos y estrategias abordadas para el manejo de los RSU en el Centro Histórico de Cuernavaca, Morelos

Cuernavaca representa el 2.95% de la superficie total del Estado de Morelos [15]. Es reconocida como "la ciudad de la eterna primavera", y fue elegida durante muchos años como uno de los lugares turísticos y de descanso favoritos de la población del centro de México [13] y de algunos turistas extranjeros. Con el paso del tiempo la Ciudad creció a un ritmo sin precedentes, en donde las inadecuadas decisiones administrativas sobre los servicios públicos municipales han ocasionado que la imagen urbana decayera y con ello, su calidad turística, también se mermara. Una de las problemáticas que más se ha hecho evidente es el manejo inadecuado de los RSU, cuya demanda estimada es de 557.87 ton/día [5] en un área aproximada de 151.20 Km^2 [17]. Esta actividad desde el año 2005 trae aparejados periodos de crisis en los trienios municipales, con la presencia de bolsas de basura que quedan expuestas en la vía pública de la Ciudad, así como el problema del pago de salarios a los trabajadores de limpia y recolección, presentándose especialmente cuando termina y/o se renueva una administración municipal.

Dentro de las primeras estrategias abordadas en el año 2013, para mejorar la imagen urbana, consistió en la instalación de contenedores de basura en las plazas de la ciudad capital (Plaza Emiliano Zapata y Jardín Juárez) (ver Fig. 1), es decir, en el Centro Histórico [12], por ser un sitio de relevancia económica, social y ambiental (está integrado en mayor medida por comercios, sitios gubernamentales y sitios de interés turístico). Esta dinámica económica es la responsable de generar cerca de 49 ton/diarias de RSU [10] en un área aproximada de 1.3 Km^2. Si comparamos la generación estimada de todo el municipio de Cuernavaca con respecto a la del Centro Histórico, toma un efecto relevante el poder actuar en este sitio, debido a que representa el 9% de la generación total de residuos de la Ciudad, en un área geográfica relativamente pequeña.

La instalación de estos contenedores de basura tenía el objetivo de poder cubrir la demanda de generación de RSU que se suscitaban al consumir productos/servicios dentro del Centro Histórico. No obstante, los botes de basura terminaron ampliando su cobertura de confinamiento temporal de residuos hacia la comunidad, puesto que en ellos no solo se depositaba lo que se generaban de este espacio, sino que alojó también bolsas de basura domiciliaria de localidades vecinas, sobrepasando así la capacidad de carga y volumen de los contenedores, y promoviendo de esta forma una imagen de una Ciudad con basura. Motivo por el cual fueron retirados, con la idea de "si no hay donde depositar la basura, deberán de llevársela a su casa, y la Ciudad permanecerá limpia". Estrategia que tampoco dio resultados positivos, al contrario, comenzaron a acumularse montañas pequeñas de residuos en las esquinas de las calles y avenidas. El contar con

contenedores/botes de basura mixtos tampoco es una solución viable a largo plazo, porque los residuos se depositan de manera no diferenciada, es decir, que todos los materiales desechados, así como fueron depositados, estarían siendo trasladados hacia el Centro de Transferencia de la Ciudad y posteriormente, al relleno sanitario. No hay recuperación de materiales.

Poco tiempo después, la problemática sobre el manejo de los RSU se extendió hacia la acción de respuesta del H. Ayuntamiento de Cuernavaca, quien se vio rebasado en la capacidad operativa y técnica. Se habló de la construcción de un relleno sanitario para la ciudad, el cual no fue aprobado por el Congreso, y terminó concesionándose el servicio de recolección, manejo y traslado hacia empresas particulares (PASA, SIREC y actualmente con el corporativo ambiental DKDA, S.A. de C.V. (KS ambiental)) [4] y trasladando de esta forma los derechos del manejo de los residuos de Cuernavaca.

A partir del año 2015, se decretó que el Centro Histórico de Cuernavaca, Morelos se convertiría en la 1ª Ecozona del Estado, la primera de México y de Latinoamérica con carácter de zona metropolitana, por lo cual tendrían injerencia los tres niveles de gobierno (federal, estatal y municipal). En el proyecto se planteó su remodelación para convertirlo en una zona más saludable, regresarle su actividad turística, encaminar este espacio para reducir las emisiones contaminantes en aire y agua, recuperar el espacio público, detonando zonas de valor ambiental, así como la creación de un sistema integrado de movilidad sustentable para poder reorganizar el territorio [11]; [23]. Acciones que contribuirían directamente a la mitigación de los efectos negativos del cambio climático a través del Programa de Manejo de Residuos Sólidos y del adiós a los plásticos de un solo uso [7]. Con este concepto regresaron los contenedores de basura a la Ciudad, pero en esta ocasión de manera diferenciada, con tres separaciones para poder recuperar el residuo orgánico; el papel y cartón; y el vidrio y las latas (ver Fig. 1).

Fig. 1. Botes de basura año 2013 vs Contenedores de residuos clasificados 2015. Elaboración a partir de trabajo de campo y de imágenes de internet.

A su vez, se colocaron contenedores no diferenciados en puntos estratégicos y se dio pauta a una serie de acciones de jornadas de limpieza, campañas de concientización, sobre reusar/rechazar ciertos materiales como las bolsas de plástico, los popotes y el unicel [7], [19], por estar relacionados con la amenaza para la vida silvestre, previniendo de esta manera, la contaminación del suelo y los cuerpos de agua, así como las

posibles inundaciones por el taponamiento de alcantarillas [21]. Se implementó el uso de camiones compactadores, el establecimiento de rutas, horarios, campaneo, etc., con los cuales se intentaría regular la manera en cómo se disponen, recolectan y se transfieren los residuos. Incluso dentro de la cláusula del contrato de prestación de servicios concesionados para la recolección domiciliaria, descarga y operación en el Centro de Transferencia, se mostró la pauta de llevar a cabo acciones de recogida diferenciada sobre residuos orgánicos e inorgánicos, teniendo lugar los lunes, martes, viernes y sábados, para el primero, y los miércoles y viernes para recolectar los segundos [8]. Esta estrategia estaría ligada al reglamento de Aseo Urbano de Cuernavaca, donde se estipula que los generadores de RSU tendrían que realizar al menos la separación primaria, y entregar los residuos directamente al trabajador de limpia, o en su caso, depositarlos en los contenedores municipales [2].

A pesar de contar con reglamentos, iniciativas y contratos armonizados, la dinámica que se muestra en el Centro Histórico dista mucho de apegarse a las reglas, esto en parte por la ausencia de la difusión de los ordenamientos, de la continuidad de acciones y de las campañas de concientización, pero también por falta de capacitación de los operadores del servicio municipal. Por lo que la valorización de los RSU se ha y se sigue realizando a partir de la participación de los "recolectores/pepenadores". Si bien, el volumen de recuperación es ineficiente e insuficiente comparado con el potencial de revalorización existente de lo que se está desechando [5], también es cierto, que esta parte de recurso humano debería de poder ser integrado dentro de la cadena de valor del sistema de recolección de residuos, porque son los que están recuperando los recursos útiles para la economía (se estaría logrando cumplir la meta 8.7 de los ODS).

Actualmente, el camión recolector recorre las calles y avenidas del Centro Histórico de Cuernavaca, Morelos, en los tres turnos (mañana, tarde y noche), compactando los residuos que son entregados directamente, utilizan el campaneo para avisar de su llegada, sin embargo, su sistema de operación es de continuo movimiento (no se detiene, avanza lento), por lo que de esta manera incita a que las UE, en lugar de entregar directamente los RSU al trabajador de limpia, terminen colocándolo en la acera (banqueta) (ver Fig. 2). El camión puede pasar en el momento en que están expuestas las bolsas de basura en la vía pública, y recogerlas, pero también se da el caso, en que estas bolsas terminen siendo colocadas después de su partida. La idea del funcionamiento de los camiones compactadores es que los residuos que logre recuperar sean heterogéneos, es decir, recolección de orgánicos en ciertos días, e inorgánicos en otros, objetivo que no se está logrando.

Fig. 2. Presencia de basura en calles y avenidas del Centro Histórico de Cuernavaca. Elaboración propia a través de trabajo de campo y de imágenes de internet.

4.2 Perspectiva de las UE generadoras de RSU en el Centro Histórico de Cuernavaca, Morelos, México

A través del análisis de los resultados del cuestionario exploratorio sobre generación y manejo de RSU de las UE del Centro Histórico de Cuernavaca, Morelos, se lograron obtener datos que están relacionados con las prácticas de separación, periodicidad de entrega de residuos, y de quienes consideraban que son los responsables del manejo adecuado de los mismos (Fig. 3), datos que se muestran a continuación:
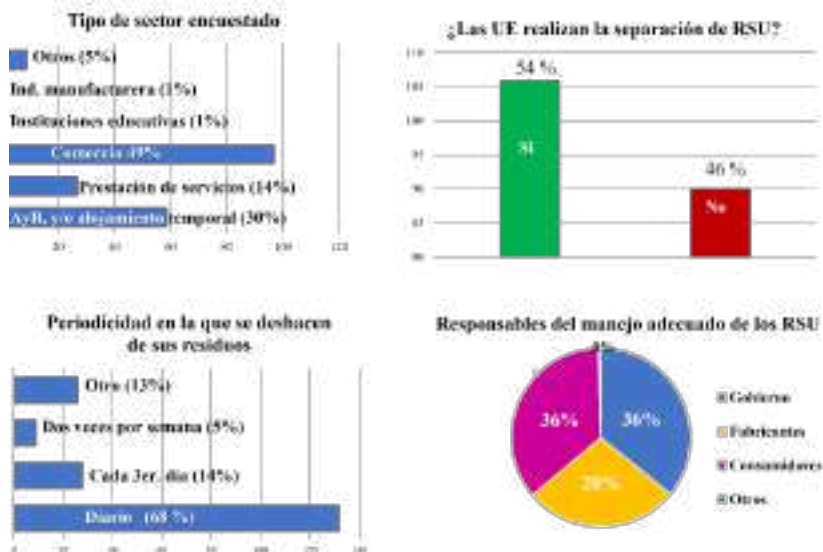
Fig. 3. Prácticas de generación de RSU y responsables de su manejo. Elaboración propia a través del análisis de datos del cuestionario exploratorio.

Con respecto al análisis de los datos, se observó que el 54 % de las UE tiene el hábito de realizar al menos algún tipo de separación de residuos, y estos están asociados a elementos inorgánicos, como el plástico, el papel y el cartón. Donde el 68% (132 UE) estará entregando o depositando sus residuos de manera diaria. El resto lo estarán realizando cada tercer día, dos veces por semana o incluso, cada 15 días, porque los residuos que generan son inorgánicos y el volumen de su generación es mínima. Cabe señalar que esta entrega de materiales tiene tres salidas: el primero con el servicio de recolección municipal; el segundo a través de la entrega a los recolectores/pepenadores; y el tercero, por la venta directa de estos materiales para el personal que labora en las UE.

Por su parte, el 46% de las UE (55% comercio, 30 % sector de alimentos y bebidas, 11% servicios; 2% industria manufacturera, 1% sistema educativo) que no separan sus residuos, refirieron como motivos:

- Que generan una cantidad mínima de residuos;
- Que no tiene caso separarla si el camión compactador revuelve los materiales, y de igual forma, ocurre con los pocos botes/contenedores que están instalados para depositar la basura;
- Por comodidad de poder disponerlo en un solo lugar, así como el ahorro en bolsas para basura (se entregan cuando estas están cubriendo su capacidad real de confinamiento);
- El no ver la separación como algo necesario;
- El que no haya infraestructura pública o se desconoce de sitios para ir a depositarlos de manera diferenciada;
- Qué el espacio físico dentro de los locales no permite el colocar diferentes botes, para clasificar los residuos;
- Por el tiempo relativo destinado a separar y atender al público, sobre todo en el sector de preparación de alimentos y bebidas y de hospedaje temporal;
- El no haber planteado o adquirido el hábito de separación;
- Que los RSU que se desechan no tienen un mercado valorizable;
- El que existen personas que ya se dedican a realizar la separación de RSU, visto como una actividad laboral (recolectores/pepenadores, sistema municipal, etc.);
- Que el tema de separación sale del control de las UE, debido a que reciben basura pública, originada por el consumo de los usuarios del Centro Histórico. Este causal fue comúnmente referenciado por UE cuyo giro es la prestación de servicios a partir de estacionamientos públicos.
- Que no han emitido una recomendación por parte de la autoridad correspondiente para entregarlos de manera diferenciada.
- Finalmente, que no están desechando RSU valorizables. En este caso en particular, se retomó el apartado de listado de materiales del cuestionario, en donde se abordan los residuos que desechan comúnmente, y se pudo observar que al menos el 80% de los que refirieron esta categoría, están generando RSU que si tienen un mercado de valor en Cuernavaca, Morelos. Estos materiales son: PET, cartón, papelería, tetrabrik, hojalata, latas de aluminio, envases de plástico duro (comúnmente conocido como "soplado"), por lo que se puede deducir que hay

desconocimiento sobre los materiales/elementos que se están desechando y que pueden ser valorizados económica y materialmente.

Con respecto a la asignación de responsabilidades, el 60 % de las UE mostró que el tema del manejo de los RSU conlleva un compromiso compartido entre gobierno, fabricantes y consumidores. Sin embargo, si se toma como referencia el porcentaje acumulado, se estaría observando que el 36% de la responsabilidad se la confieren al gobierno, por ser el actor principal en la recolección, manejo y disposición de RSU, mientras que el 28% sitúan a los fabricantes, en donde se estaría abordando el principio de responsabilidad extendida del productor (REP), a través de impulsar la logística inversa, en donde el producto o parte de este, que son desechados, incluyendo su embalaje, pase por ciclos completos durante la totalidad de su vida útil [6]. Este porcentaje, ha hecho énfasis en la necesidad de eliminar la obsolescencia programada de ciertos productos eléctricos/electrónicos, porque el material que podría reincorporarse en otros aparatos o venderse en los centros de acopio de RSU inorgánicos, no está siendo recibido, y el camión recolector tampoco permite el poder transferirlo hacia los sitios de disposición final, por ser residuos de manejo especial. Mientras que el 36% asumen como responsables a los consumidores, en donde contribuyen con un compromiso individual de practicar ciertas acciones de separación diferenciada o entrega directa al camión recolector.

4.3 Estrategias formuladas para repensar un Sistema integral de RSU

En la construcción de estrategias que fueron mencionadas por las UE encuestadas para poder repensar un sistema adecuado de RSU para el Centro Histórico de Cuernavaca se encuentran aspectos de infraestructura, del fomento de la educación ambiental, de la colaboración entre terceros y del seguimiento sobre la estructura normativa que debe de cumplirse por parte del H. Ayuntamiento (ver Fig. 4).
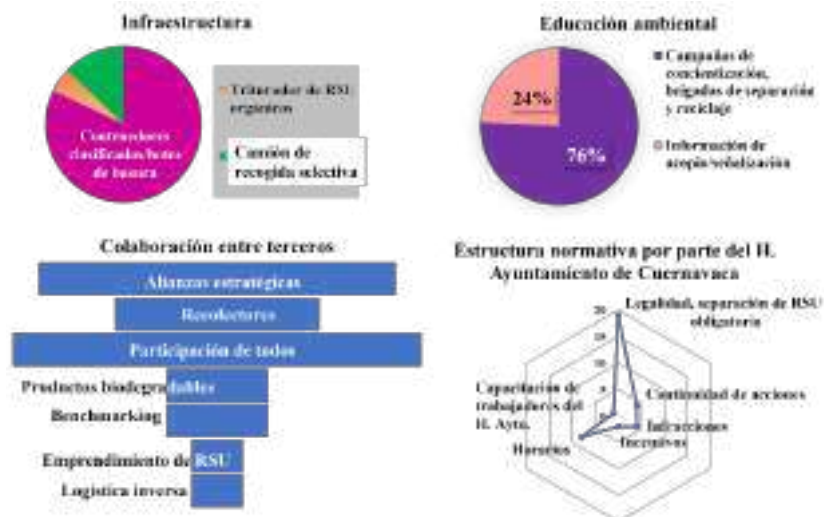
Fig. 4. Estrategias obtenidas a partir del análisis de datos del cuestionario exploratorio.

Las estrategias significativas de común acuerdo muestran la necesidad de instalar contenedores diferenciados de RSU, utilizar camiones de recogida selectiva, de realizar campañas de concientización, brigadas de separación y reciclaje, de fomentar la participación y alianzas estratégicas, así como realizar la separación obligatoria de los RSU, y el establecimiento y difusión de los horarios de recolección municipal, estos últimos, porque en el sitio de estudio se desconocen o las rutas de recolección no son constantes.

Dentro de las opciones con menor repetición, pero no por ello menos importante, se habla de poder tener acceso a la *información de centros de acopio y señalización*, del *benchmarking* (tomar como referencia los mejores aspectos o prácticas de otras empresas) y el *emprendimiento de empresas de residuos*, con los cuales se lograría migrar hacia sistemas sostenibles de residuos. Con estas tres acciones, se describen a continuación parte de las estrategias que se tendrían que analizar o tomar como referencia para poder repensar un Sistema sostenible de RSU adecuado hacia el sitio de estudio.

Requerimientos de información de centros de acopio-señalización. Existe un desconocimiento entre la mayoría de las UE con respecto hacia donde pueden canalizar los diversos tipos de RSU que están produciendo, tanto valorizables, como aquellos que representan un riesgo para la salud y el ambiente. De igual forma, se ha solicitado que dentro de las estrategias se dé difusión y señalización sobre que residuos pueden recuperarse y cuál es la forma más pertinente para realizarlo (cómo se deben de disponer).

Benchmarking. En esta primera parte exploratoria de benchmarking, se toma como referencia algunas estrategias que han sido implementadas por algunas Ciudades de

México y las cuales han sido galardonadas por ser las más limpias del país. Entre estas estrategias sobresalen:

- La implementación de desarrollo tecnológico;
- Adquisición de parques vehiculares;
- Compra de infraestructura;
- Incentivos;
- Generación de alianzas estratégicas;
- Realización y difusión de campañas de concientización.

En la Tabla 1 se muestran cinco Ciudades, en donde sus programas y acciones han tenido avances significativos en el manejo de los RSU. Todas tienen como objetivo, el disminuir el impacto ambiental ocasionado por los RSU, no obstante, esta acción trae consigo diversos beneficios.

Tabla 1. Estrategias de Ciudades Mexicanas que han innovado en el servicio de recolección y revalorización de RSU

Ciudad y generación de RSU	Programas y estrategias abordadas	Beneficios del programa
Orizaba, Veracruz *120 ton/día*	"Predial por basura", se realiza la separación de RSU desde la fuente (casa/UE), se entrega al servicio de recolección y a cambio se dan puntos como incentivo para posteriormente descontarlo del monto total del pago de predial. Se utiliza un calendario municipal para recoger RSU orgánicos, los cuales son utilizados en el proceso industrial del cemento. En el 2020, se llevó a cabo la instalación de la Planta Separadora y Trituradora de residuos orgánicos y sólidos (ECORI), y cuentan con asistencia técnica de GEOCYCLE. También se requirió de contar con personal de limpia las 24 horas del día, en turnos diferenciados.	Los RSU entregados entran en la cadena productiva, no llegan al relleno sanitario. Genera un recurso económico, para recolectores, empleados del ayuntamiento y gobierno. Además de que se ha logrado cerca del 90% de pago de contribuyentes, que se traduce en más obras y beneficios de servicios públicos para la ciudadanía.
Puebla, Puebla *1,700 ton/día*	Se ha realizado la instalación de "puntos verdes" de acopio de PET, cartón, Tetrapak, plástico duro, vidrio, latas y aluminio, en donde se realiza el cambio de hábitos de la ciudadanía, a través de la separación y clasificación de los RSU desde el hogar.	Tiene un impacto estimado de 20 % de recuperación de RSU valorizables, sujetos a reciclaje en comparación al 2% que se recolectaba comúnmente.

Guadalajara, Jalisco *7,000 ton/día*	"Base Cero", se realiza la instalación de módulos de separación de RSU, y el mejoramiento del Centro Integral de Economía Circular (CIEC).	Se ha logrado construir una red de puntos de acopio, que ha traído como beneficio el mejoramiento de la operación de los centros de transferencia, y con ello, se ha podido desarrollar el mercado de los RSU-valorizables. Consolidando a su vez, la red de rellenos sanitarios en el área metropolitana de Guadalajara (AMG).
Santa Catarina, Monterrey, Nuevo León *--*	"Súmate", a través de acciones de voluntarios (empresas, ONG's, organizaciones religiosas, empleados municipales, ciudadanos comprometidos con el ambiente, y el equipo de Red Ambiental), se ha logrado la recuperación y limpieza de espacios públicos.	Se ha creado un modelo de colaboración, encaminado hacia la cultura de una ciudad limpia, generando un cambio positivo en el medio ambiente y en la sociedad.
Veracruz, Veracruz *5,719 ton/día*	"Veracruz Puerto Limpio", con este programa se ha implementado una app para identificar en tiempo real las rutas de recolección. Esta permite realizar comentarios y reportar incidencias.	Se ha creado un canal de comunicación personalizado, asignando una ruta adecuada a la ubicación proporcionada por el ciudadano. Se tiene transparencia del servicio, rutas más eficientes, mejor control de unidades e imagen de la ciudad.

Elaboración propia a través de trabajo de campo y de ATEGRUS [1].

Emprendimiento de empresas de residuos. Este concepto está relacionado con la economía circular, en donde supone una invitación a redescubrir el valor del producto más allá de su primer ciclo de vida y arriesgarse a innovar para salvaguardarlo [14]. Desde el año 2013, este punto se ha impulsado a través de la incorporación de los mercados y tianguis verdes que se presentan los fines de semana en el Centro Histórico de Cuernavaca. Sin embargo, este mercado requiere de mayor difusión y de generar redes de coparticipación, que le permitan el desarrollar una cadena de valor, iniciando con la incorporación de materiales generados desde el sitio de estudio, para seguir con el reuso/transformación, venta y comercialización, y llegar a culminar con el fin de su vida útil, integrándose hasta ese momento, al relleno sanitario. El emprendimiento de empresas de residuos integra la mayor parte de los RSU que son valorizables, y tiene un potencial de destacar como acción social, debido a que estos materiales también pueden ser utilizados en grupo de artesanos, instituciones educativas de nivel prescolar y básico (manualidades), para talleres ambientales, e incluso servir como insumo en la decoración de calles para los días festivos. Con ello, además de preservar los materiales, traer mejoras ambientales, sociales y económicas, también se estarían generando

fuentes de empleo, solo hace falta despuntar la creatividad. Por ello es importante enfatizar que es necesaria una separación de RSU desde la fuente, para poder direccionarlos hacia procesos más sostenibles.

5　　Conclusiones preliminares y trabajo futuro

Para poder repensar el sistema de recolección de RSU siempre será indispensable estudiar el sitio, adentrarse en su historia, conocer cuáles han sido las estrategias abordadas, que ha funcionado o como se ha mostrado la dinámica social, operativa, técnica y financiera. A partir de ese panorama, se lograrán tomar las mejores decisiones. En este contexto, con los resultados presentados en este trabajo de campo, se pudo recrear el panorama que se vive en el Centro Histórico, mediante la recopilación de información de las UE y de las estrategias que se han llevado a cabo, los cuales, sumado al trabajo futuro, del estudio de generación y caracterización de RSU, se podrá comenzar a proponer la estructura de un Sistema Integral sostenible.

En la hoja de ruta, el punto primordial será la educación ambiental (enseñanza/instrucción), con un enfoque de participación y generación de redes de colaboradores de todas las partes interesadas. Todos desde el ámbito de su competencia pueden aportar para poder hablar de sustentabilidad en el sistema de recuperación y valorización de RSU, y con ello mitigar/reducir varios de los impactos ambientales, sociales y económicos que están relacionados con el inadecuado manejo de los RSU, generando a partir de esto riqueza en todos los aspectos. El segundo punto prioritario, estará basado en la optimización de procesos y materiales, a través de tener un mejor control sobre la infraestructura instalada o por instalar, así como las herramientas, maquinaria y equipo destinados para la recolección y manejo de los residuos.

Cabe resaltar, que el papel que juega el H. Ayuntamiento de Cuernavaca es de vital importancia y más aún, que sus ordenamientos cumplan la función para lo cual fueron escritos. En este caso, la estrategia que se vislumbra es retomar este espacio como un producto turístico, y que las acciones vayan encaminadas a un mejor aprovechamiento de los residuos, del espacio y de la imagen urbana. Sin lugar a duda, el camino trazado ha traído consigo experiencias, no hay estrategias inadecuadas, solo hace falta integrarla en conjunto para crear cadenas de valor. Estos esfuerzos deben de ir encaminados a una meta en común: lograr un espacio de consumo responsable, que migre hacia un entorno de Ciudad sostenible. Por último, es importante destacar que, gracias a los acuerdos internacionales, planes de desarrollo municipal, estatal y federal, leyes y reglamentos, se le está dando un seguimiento al tema de los residuos, y tenemos como ejemplo algunas Ciudades que están teniendo resultados muy favorables en este tema, por lo que parte de estas estrategias pueden ser replicadas con ciertas adecuaciones a la dinámica del sitio.

Referencias

1. ATEGRUS. https://www.ategrus.org/noticias/escobas-de-plata-oro-y-platino-2020-21/, fecha de acceso 2022/10/2022.
2. Ayuntamiento Constitucional de Cuernavaca: Reglamento de Aseo Urbano del Municipio de Cuernavaca. H. Ayuntamiento de Cuernavaca (2008).
3. Cámara de Diputados del H. Congreso de la Unión: Ley General para la Prevención y Gestión Integral de los Residuos (LGPGIR). Última Reforma DOF 19/01/2018. (2018).
4. Cinta, G.: https://www.guillermocinta.com/opinion/antecedentes-de-la-nueva-crisis-de-la-basura-en-cuernavaca/, fecha de acceso 2022/10/01.
5. Consejería Jurídica del Poder Ejecutivo del Estado de Morelos: Estrategia para la Gestión Integral de los Residuos del estado de Morelos, Gobierno del Estado de Morelos (2017).
6. Consejería Jurídica del Poder Ejecutivo del Estado de Morelos: Ley de Residuos Sólidos para el Estado de Morelos, Gobierno del Estado de Morelos (2020).
7. Gobierno del Estado de Morelos: https://morelos.gob.mx/?q=prensa/nota/adios-plasticos-de-un-solo-uso-en-la-ecozona-de-cuernavaca , fecha de acceso 2022/10/01.
8. H. Ayuntamiento de Cuernavaca: PM/SA/SDSySP/CJ/002/2021-CT (2021).
9. Jacob, S.: Gestión Integral de RSU para Mar del Plata, propuesta del marco legal a nivel local, Facultad de Ingeniería UNMDP Universidad Nacional de Mar del Plata, 01.05-01.07 (n.d.).
10. Martínez, G.: https://www.diariodemorelos.com/noticias/refuerzan-limpieza-en-el-centro-de-cuernavaca , fecha de acceso 2022/10/02.
11. Martínez, K.: https://iki-alliance.mx/cuernavaca-emprende-la-primera-ecozona-en-mexico-y-latinoamerica/ , fecha de acceso 2022/10/02.
12. Maximocerdio: https://conurbados.com/morelos/2013/instalan-botes-de-basura-tipo-arturito/, fecha de acceso 2022/10/03.
13. México desconocido: https://www.mexicodesconocido.com.mx/cuernavaca.html, fecha de acceso 2022/10/04.
14. Müller, P. y Fontrodona, J.: Economía circular, una revolución en marcha. 48, Cuadernos de la Cátedra CaixaBank de Responsabilidad Social Corporativa IESE, Navarra (2021).
15. Naciones Unidas-CEPAL: Agenda 2030 y los Objetivos de Desarrollo Sostenible, una oportunidad para América Latina y el Caribe. Naciones Unidas (2018).
16. PNUD, NBSAP Fórum, Secretaría del CDB y Rare: Comunicando el valor de la biodiversidad, Learning for Nature UNPD (2021)
17. Poder Ejecutivo del Estado de Morelos: Diagnóstico municipal, Cuernavaca. Gobierno del Estado de Morelos (2017).
18. Prieto V., Jaca, C. y Ormazabal, M.: Circular economy: Relationship with the evolution of the concept of sustainability and strategies for its implementation. Memoria Investigaciones en Ingeniería, (15), 85-95 (2017).
19. Redacción AND: https://www.informateymas.com/2018/05/30/promueve-ecozona-campana-evitar-uso-popotes-bolsas-unicel/, fecha de acceso 2022/10/01.
20. Rosario, R.: Manejo de residuos sólidos urbanos para la prevención de daños a la salud en el municipio de Cuernavaca, Morelos, [Tesis de maestría] Instituto Nacional de Salud Pública, Escuela de Salud Pública de México, Cuernavaca, Morelos (2016).
21. Secretaría de Medio Ambiente y Recursos Naturales (SEMARNAT): https://www.gob.mx/semarnat/acciones-y-programas/residuos-solidos-urbanos-rsu, fecha de acceso 2022/10/03.
22. Tecnozoes: https://www.tecnozono.com/basura/, fecha de acceso 2022/10/05.
23. Universidad Autónoma del Estado de Morelos (UAEM): Programa de manejo para la implementación de la Ecozona de Cuernavaca (Centro). UAEM, Morelos (2018).

Study of the greenhouse gas emissions and fuel consumption effect, caused by passive and aggressive behavior in driving public service buses in Pasto city⋆

Fredy Dulce$^{1,3[0000-0001-8937-2334]}$, Jackeline Murillo$^{2[0000-0003-0644-0923]}$, and
Eduardo Caicedo$^{1[0000-0003-0727-2917]}$

^{1} Programa de Posgrado en Ingeniería Eléctrica y Electrónica - PPIEE, Universidad del Valle, Cali, Colombia
^{2} Escuela de Ingeniería Civil y Geomática - EICG, Universidad del Valle, Cali, Colombia
^{3} Programa de Ingeniería Electrónica, Universidad CESMAG, Pasto, Colombia

Abstract. Public transport systems have great importance in planning any city; currently, the increase in population is not the only factor to consider, but also the pollution levels and the social impact. In general, the public transport system in Pasto has aggressive behavior from the bus drivers due to the goals that they should achieve. These goals are related to the route time and directly affect the salary of the bus drivers, which is why they tend to have aggressive driving behavior. This article focuses on the simulation of driving behaviors, aggressive and passive, considering the rush hour and peak-off-hour traffic to determine what effect it has on fuel consumption and greenhouse gas emissions. Four public transport routes were used in Pasto city as the study case. The simulations were carried out in Eclipse SUMO, a widely used tool for performing complex analyses that include many variables to make a realistic enough simulation.

Keywords: Driving behavior · Rush hour · Peak-off-hour · Public transport · Greenhouse Gas Emissions · SUMO

1 Introduction

It is very known that the transport sector is one of the most significant contributors to greenhouse gas emissions, making the research related to this sector relevant. Considering this, Colombia aims to reduce greenhouse emissions by 36 million tCO2eq, and one of the challenges is to migrate forward to sustainable transport due to 78% of these emissions coming from this sector [1]. Vehicle fuel

consumption and carbon emissions are influenced by driving behaviour, as well as traffic conditions and average driving distance for safety [2].

Traffic-related emissions, such as CO2, CO, NOx and HC, have negatively affected the environment and led to poor air quality [3]. Highlighting that CO2 has the most significant impact [4]. According to [5], improving the driving conditions in major Latin American cities could bring potential economic benefits on the order of billions of US dollars per year.

For example, in the case of Bogotá, implementing driving patterns similar to those represented by test driving cycles used in Europe or Japan could reduce CO, CO2, and HC emissions by at least 11% and by as much as 20% for NOx. Modifying driving conditions usually requires hefty, expensive, and difficult-to-build infrastructure. In this context, eco-driving becomes a cost-effective alternative to reduce vehicle emissions, especially if the practice is prioritized for large-engine vehicles and those lacking emission control technologies [5].

Considering the previous fact, we aim to assess the driving behavior (passive and aggressive) on public bus transport systems, adding the rush hour and peak-off-hour traffic to determine its effect on fuel consumption and greenhouse gas emissions. For this, we take the Strategic Public Transport System (SETP for its acronym in Spanish) of Pasto city as a study case. Moreover, using all input variables such as speed, routes, stops, acceleration, driving behavior, rush hour and peak-off-hour, Euro norm, and vehicle type allows us to simulate the reality of the city, which is a significant contribution. Eclipse SUMO is the software selected to achieve the objective proposed.

SUMO is an open-source, highly portable, microscopic, and continuous traffic simulation package designed to handle large networks. Several studies have used SUMO to simulate road systems with a high level of detail. Thus the simulations and their results can be as realistic as possible.

For this article, SUMO is used to analyze driving behavior, adding the rush hour and peak-off-hour traffic to determine what effect it has on fuel consumption and greenhouse gas emissions with the SETP of Pasto city as the study case.

2   Methodology

The simulation process was defined as follows. First, the Pasto city map with the road network was downloaded from Open Street Map (OSM). Secondly, four routes of the SETP were defined to make the simulations, and we created the road corridors in NetEdit. For this, the streets were extracted from the SETP website [11]. The next step involves defining the vehicle characteristics such as speed, acceleration, deceleration, emission standards, and weight, among others. Finally, the bus stop points for passenger boarding and alighting are defined.

On the other hand, two simulation scenarios were defined. These are periods of high demand (morning and afternoon rush hour) and periods that consider free-flow volume, i.e., without congestion. Because of that, the bus in the simulation will have more stops during rush hour and fewer stops during peak-off-hour. Likewise, the duration of stops is larger during rush hour than peak-off-hour.

Subsequently, the acceleration of the buses is changed. The work carried out in [13] was taken as a reference to calibrate the acceleration. It has been estimated that aggressive driving occurs when the acceleration is carried out with 4.0 m/s2, and passive driving is assumed when the driver accelerates at a rate of 2.0 m/s2.

2.1　Road Corridors

Pasto city had about 825 buses until 2017, with an average age of 12 years for the entire fleet; the fuel used for all vehicles is Diesel or ACPM. The SETP operation is under the organization "Unión Temporal Ciudad Sorpresa," which is made up of four companies. In addition, the fare for a bus ticket is 2000 COP for the year 2022 and has an approximate annual increase of 100 COP.

Routes E1 and E3 are part of the so-called strategic routes. They have been assigned this name because they make relatively short journeys to reduce transport times, connecting strategic points such as the city center and some outlying sectors. On the other hand, routes C1 and C16 are part of the so-called complementary routes. Unlike the strategic ones, these routes were not designed to have shorter routes but to connect the most significant number of sectors possible so that most of the population has access to public transport services and can be mobilized from anywhere in the city.

The Table 1 and Figure 1 present the set of selected collective public transport routes.

Table 1. Selected Routes - Collective Public Transportation. Source: http://181.49.177.91/

Road Corridor	Origin - Destination	Distance [Km]	Approximate Time [min]
E1	(North - South) Barrio Dolores – Universidad de Nariño	10.4	56
E2	(North - South) Altos de chapalito – Torobajo	9.4	51
C1	(South - North - West) Obonuco – Altos de Chapalito	12.1	59
C16	(East - West Outside of the municipal capital) Cabrera/La Laguna – Anganoy	14.6	66

2.2　Critical transport hours

Pasto city has three daily rush hours between 6 am and 7 am, 12 pm and 1 pm, and 6 pm and 7 pm. Likewise, the peak-off hours are between 9 am and 10 am

Fig. 1. SETP selected routes, a) E1 route, b) E2 route, c) C1 route and d) C16 route. Source: http://181.49.177.91/

and 3 pm and 4 pm. Table 2 shows the average daily travel people make using the SETP [12].

Table 2. Average of travel per day in the SETP. Source [12]

Hour	6am - 7am	9am - 10am	12pm - 1pm	3pm - 4pm	6pm - 7pm
Number of travels	13000	4000	14000	4000	10000

The people in Pasto start their activities around 7 am, take lunch at 1 pm, and return to work or study at 2 pm; finally, they finish the activities at 6 pm. Due to this schedule, there are three rush hours daily. Instead, while most people work or study, few people need to get away from home, and the number of travel is minor. Because of that, there are two peak-off hours daily. This behavior is taken into account too. Thus the simulations could be more realistic and the results more accurate.

2.3   Simulation Parameters

The simulation parameters are described in Table 3. The parameters acceleration and acceleration duration have two values because these are the parameters used to simulate driving behavior, a regular acceleration is obtained with 2.0 m/s^2, and an aggressive acceleration is obtained with 4.0 m/s^2.

The EURO III standard is used since most of the SETP buses in Pasto comply with this standard as Figure 2 shows [12].

Table 3. Simulation Parameters

Parameter	Value
MaxSpeed $[m/s]$	16.67
Acceleration $[m/s^2]$	[2.0, 4.0]
Deceleration $[m/s^2]$	3.0
Vehicle Mass $[kg]$	11000
Emission Class	HBEFA3/HDV_D_EU3
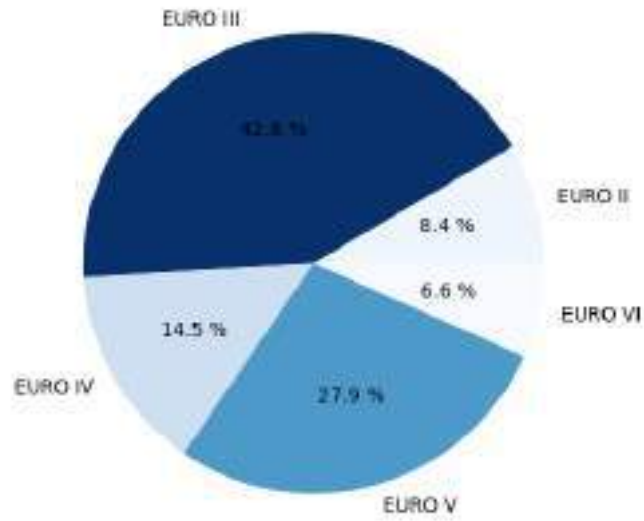
Fig. 2. Percentage of buses per European standard in Pasto

3　Simulations and results

SUMO is used in conjunction with Python to perform the simulations, which allows for speeding up the process. It is possible to perform a better analysis of the information through Python. Figure 3 shows an explanatory diagram of the communication between SUMO and Python.
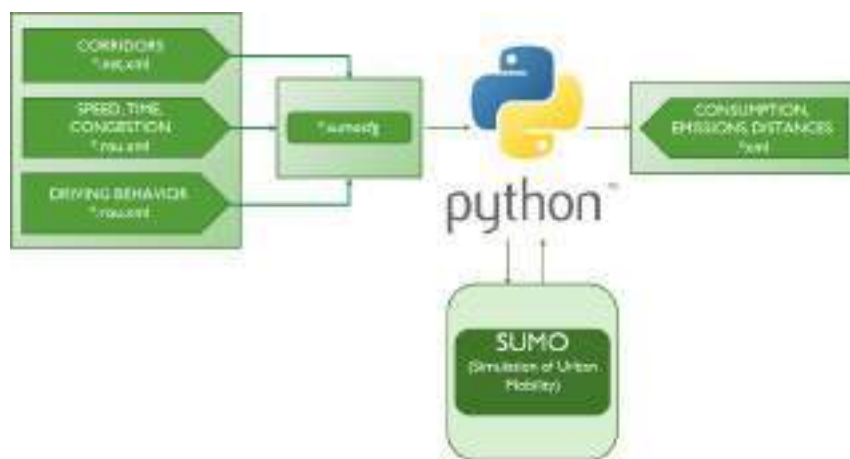
Fig. 3. Simulation SUMO-PYTHON

3.1　Validation

First, we compared the CO emissions at different speeds to validate that the Euro III standard is met, for which a trial test was carried out under track conditions. The result shows that the vehicle complies with the European standard. Once this was verified, the experiments were carried out with the four selected routes.

　　The figure 4 shows that all the values are below the maximum value of the Euro III norm; in this case, the maximum value allowed by the norm is 2.1 [g/kwh] [14]. With this outcome, we can validate the results given by SUMO.

3.2　Results

Figure 5 contains the simulated cases' outcomes. Each subplot shows the result for a single variable, for example, fuel consumption in Gl or CO2 emissions in Kg. Moreover, each subplot has a bar plot with results for aggressive behavior appointed with "A" and passive behavior with "P" on the axis below the figure. Likewise, there are results related to the traffic, either rush hour or peak-off-hour traffic. Finally, there are results for each selected route, C1, C16, E1, or
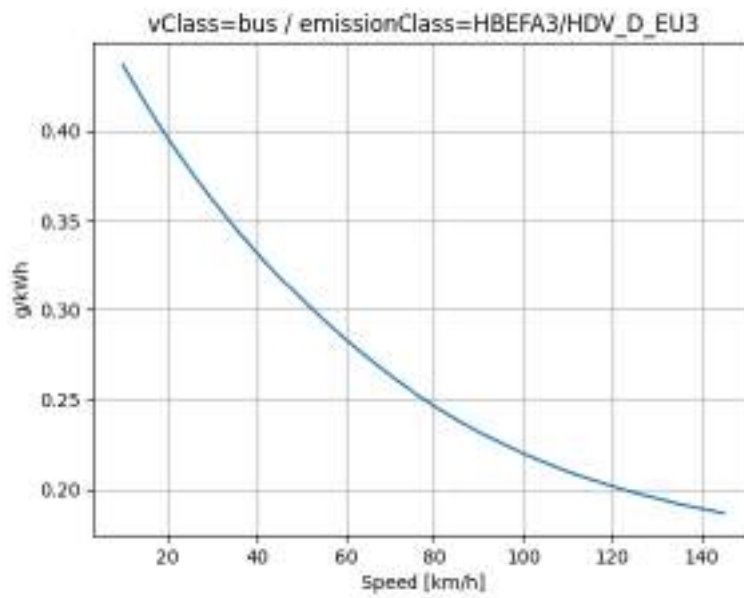
Fig. 4. For the Euro III norm, CO emissions in g/kWh vs. vehicle speed [km/h].

E2. Notably, the CO2 emissions are in kilograms scale while the other emissions are in grams scale, highlighting that CO2 is the most gas emission generated by fuel combustion in a diesel bus.

Visibly the emissions and fuel consumption are most considerable when the bus transit in rush hour than peak-off-hour. Because of that, we calculated the increasing percentage of rush hour fuel consumption and emissions concerning peak-off-hour. The results were plotted in the figure 6.

It is interesting to observe that the general emissions and fuel consumption increase around 50% or more, only in the C16 case, the increase is around 20%. Moreover, the increase is most considerable for passive behavior than aggressive behavior. The above indicates that rush hour traffic affects passive drivers more; one possible explanation is that aggressive drivers have high values in both hours of traffic cases; thus, the increase between each case is not that significant.

Finally, we expected the most significant increase in fuel consumption and emissions for aggressive behavior than passive behavior. To check it, we calculated the percentage increase of all aggressive outcomes concerning passive, and the results were plotted in the figure 7. However, the expected idea was only fulfilled for fuel consumption, CO2, and NOx emissions, but this idea was wrong for CO, HC, and PMx emissions.

As figure 7 shows, there are some negative bars. This fact indicates a decrease in emissions for aggressive behavior concerning passive behavior. Doing a literature review, we found two references that support this finding. The articles show that CO and HC decrease with higher engine loads. The load on the motor can be assumed to be directly proportional to the acceleration since if the load is increased, the acceleration must increase so that the force will be greater and thus maintain the speed approximately constant. In this order of ideas, if the acceleration increases, the CO and HC tend to decrease. A plausible reason for the decrease in CO, HC, and PMx emissions could be the increase in combustion temperature caused by a higher engine load, thereby enhancing the oxidation of unburnt hydrocarbons in the exhaust. Moreover, aggressive driving characterized by rapid acceleration might have required the engine to operate at a higher peak speed (rpm). A previous study showed that an internal combustion engine could emit lower concentrations of hydrocarbons with increasing engine speed [15], [16].

On the other hand, the case of route C1 is different from the others because this route has more direction changes, which requires a more frequent deceleration and acceleration, preventing the vehicle from reaching a high speed. If the speed is necessarily low, emissions will be higher in any case. On the other hand, the other routes do not have as many direction changes, which can allow them to reach higher speeds through higher accelerations, which is consistent with the results of HC, CO, and PMx.
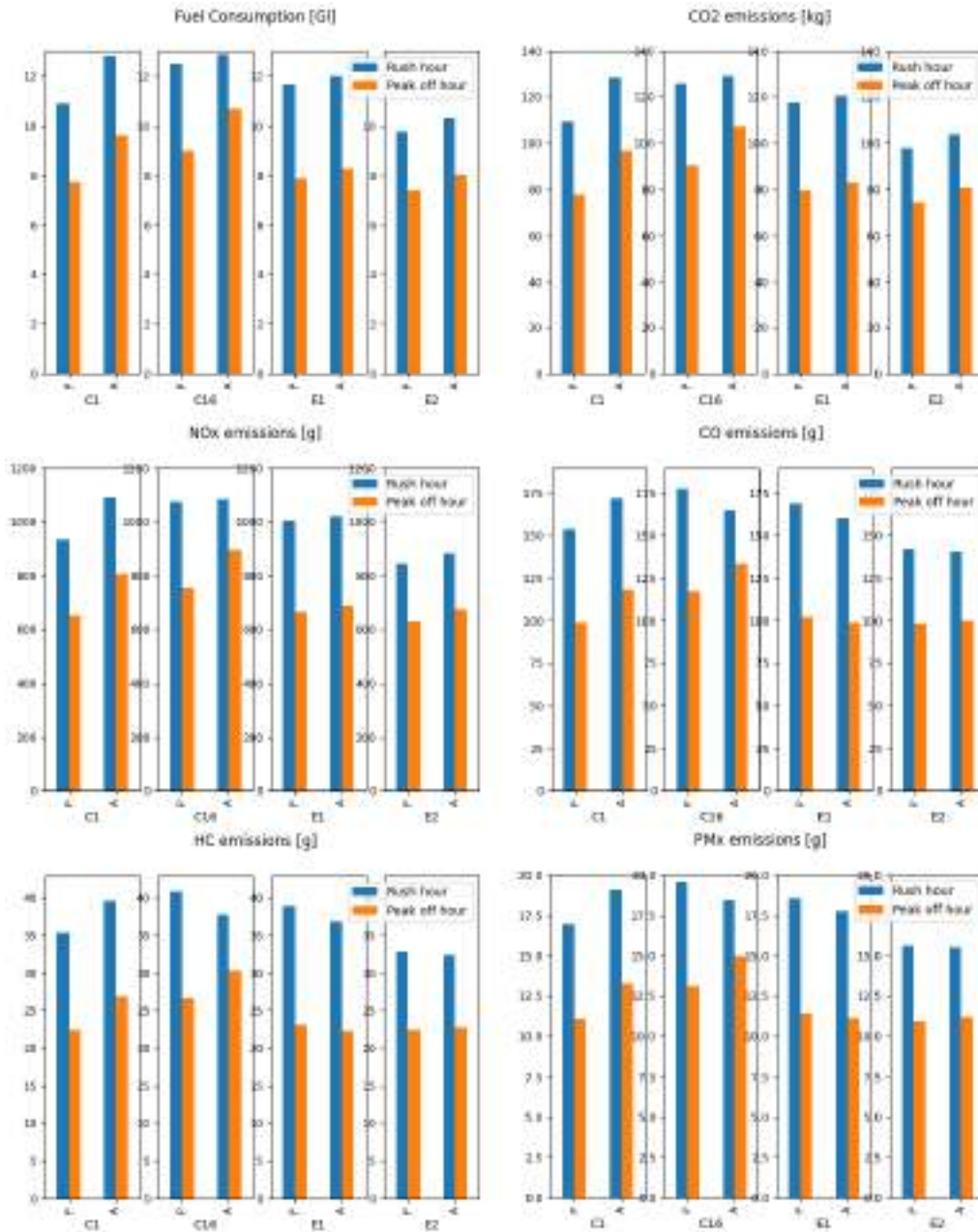
Fig. 5. Total emissions and fuel consumption for each simulated case
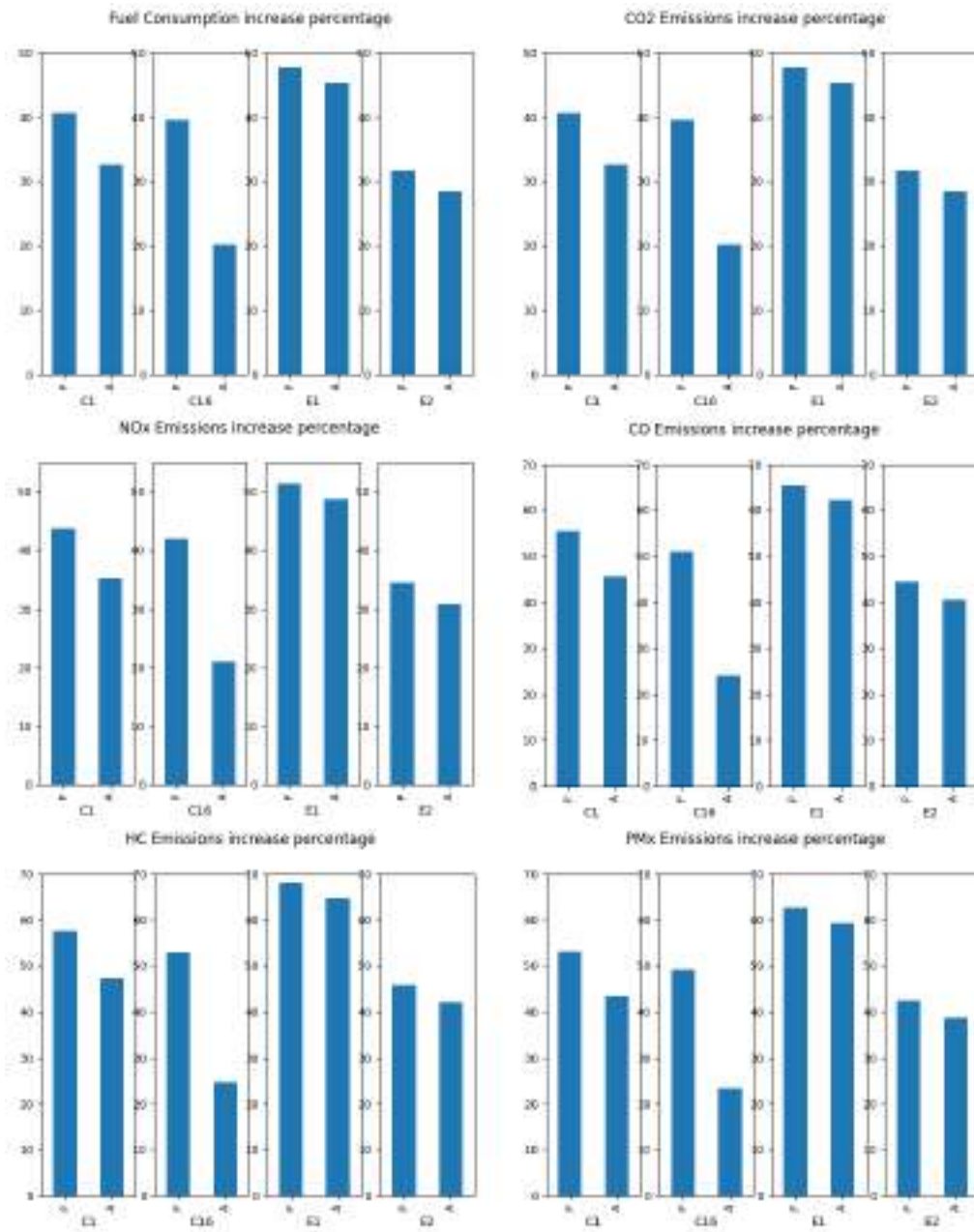
Fig. 6. Percentage increase of emissions and fuel consumption of rush hour traffic respect peak-off-hour traffic
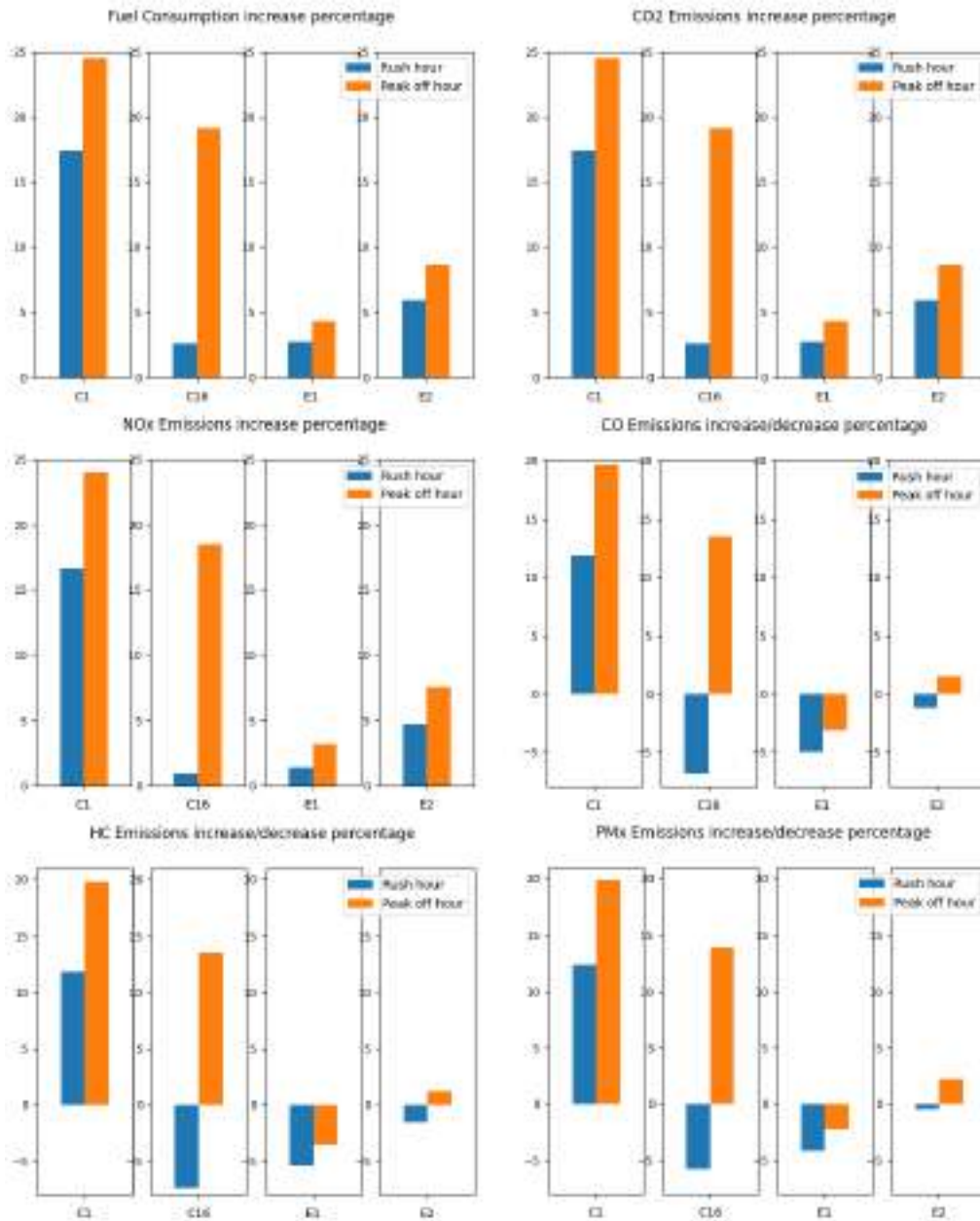
Fig. 7. Percentage increase/decrease of emissions and fuel consumption of aggressive behavior respect passive behavior

4 Conclusions

The results obtained in the four simulation cases show several generalized behaviors. First, fuel consumption and gas emissions are always higher during rush hours. Regarding fuel consumption costs, moving during rush hours is more expensive than during peak-off-hours. However, the behavior also influences since passive behavior has lower fuel consumption and, therefore, a lower fuel expense.

Regarding emissions, moving around a traffic jam harms the environment since emissions at peak hours are much higher than at off-peak hours, around 50% higher. Regarding behavior, it is impossible to state that passive driving will be better for avoiding significant emissions of polluting gases. This statement is only correct for CO_2 and NOx, but in the case of intermediate driving behavior between aggressive and passive could have fewer emissions in cases of mobilization within the cities. This fact could be different if mobilizations on highways or between cities, where it is possible to reach higher speeds and less aggressive behavior regarding acceleration.

References

1. Departamento DE Nacional Planeación. (2019). Plan Nacional de Desarrollo 2018-2022. pacto por colombia.
2. Keyvanfar, Ali & Shafaghat, Arezou & Muhammad, Nasiru & Ferwati, M Salim. (2018). Driving Behaviour and Sustainable Mobility—Policies and Approaches Revisited. Sustainability. 10. 1152. 10.3390/su10041152.
3. Shafaghat, Arezou, et al. "Environmental-conscious factors affecting street microclimate and individuals' respiratory health in tropical coastal cities." Sustainable Cities and Society 21 (2016): 35-50
4. Sun, Longsheng, Mark H. Karwan, and Changhyun Kwon. "Incorporating driver behaviors in network design problems: Challenges and opportunities." Transport Reviews 36.4 (2016): 454-478.
5. Keyvanfar, Ali, et al. "Driving behaviour and sustainable mobility—policies and approaches revisited." Sustainability 10.4 (2018): 1152.
6. sumo.dlr.de. (2022). Documentation - SUMO Documentation. SUMO. https://sumo.dlr.de/docs/index.html
7. Almatrudi, Sulaiman & Parvate, Kanaad & Rothchild, Daniel & Vijay, Upadhi. (2022. Using Automated Vehicle (AV) Technology to Smooth Traffic Flow and Reduce Greenhouse Gas Emissions. 10.7922/G2JS9NRB.
8. Aditya, F., Nasution, S. M., & Virgono, A. (2020). Traffic Flow Prediction using SUMO Application with K-Nearest Neighbor (KNN) Method. International Journal of Integrated Engineering, 12(7), 98–103. https://doi.org/10.30880/ijie.2020.12.07.011
9. Ruiz, S., Arroyo, N., Acosta, A., Portilla, C., & Espinosa, J. (2018). An optimal battery charging and schedule control strategy for electric bus rapid transit. IET Seminar Digest, 2018(1), 23–30. https://doi.org/10.1049/ic.2018.0004
10. Srivastava, R., & Kumar, V. (2020). Accident avoidance simulation using SUMO. Proceedings of the 2020 9th International Conference on System Modeling and Advancement in Research Trends, SMART 2020, 179–183. https://doi.org/10.1109/SMART50582.2020.9337079

11. RUTA C1 - SETPasto - Sistema Estratégico de Transporte Público de Pasto. (n.d.). Retrieved July 3, 2022, from http://181.49.177.91/index.php/rutas/rutas-complementarias/c1

12. Movilidad Sostenible LTDA. (2018). Elaboración del Plan Maestro de Movilidad y Espacio Público para el Municipio de Pasto, Nariño. 170.

13. Perrotta, Deborah & Macedo, José & Rossetti, Rosaldo & Afonso, J.L. & Kokkinogenis, Zafeiris & Ribeiro, Bernardo. (2014). Driver Attitude and Its Influence on the Energy Waste of Electric Buses. 99-108. 10.1007/978-3-662-45079-6_8.

14. Emission Standards: Europe: Cars and Light Trucks, url: https://dieselnet.com/standards/eu/ld.php

15. Dhital, Narayan Babu, et al. "Effects of driving behavior on real-world emissions of particulate matter, gaseous pollutants and particle-bound PAHs for diesel trucks." Environmental Pollution 286 (2021): 117292.

16. Shirneshan, Alireza. "HC, CO, CO2 and NOx emission evaluation of a diesel engine fueled with waste frying oil methyl ester." Procedia-Social and Behavioral Sciences 75 (2013): 292-297.

Smart Cities Index Proposal for Latin America and the Caribbean Region

Jorge Nájera Gómez, Richard Posso, Heiner Camacho, Gustavo Rivas, Junseok Hwang

Seoul National University, Integrated Major in Smart City Global Convergence, 1 Gwanak-ro, Gwanak-gu, Seoul, 08826, Republic of Korea

jnajera@snu.ac.kr,richardposso@gmail.com,2020925730@snu.ac.kr,
grivasb@gmail.com,junhwang@snu.ac.kr

Abstract. The increasing world population, world aggregated demand, and raw materials extraction (mainly from developing economies), have led society to face challenging scenarios characterized by increasing global warming, inequality, poverty, injustice, poor governance, and violence. Latin America and the Caribbean (LAC) region is not exempt from this global trend. Indeed, the Economic Commission for Latin America and the Caribbean (ECLAC) identifies that LAC cities, in addition to high levels of urbanization, are facing similar issues. The LAC cities are formulating smart city development initiatives to mitigate the effects of the problems described. However, how do city managers ensure that these initiatives are appropriate? Practitioners, politicians, and academics suggest using evaluation mechanisms that objectively and quantitatively measure the cities' evolution. Nevertheless, despite the substantial number of available indexes for evaluating smart cities, the literature reveals a gap in studies considering specific characteristics of the LAC region. According to ECLAC, LAC has a latent need for smart city indicators considering Sustainable Development Goals (SDGs) and Digital Transformation (DX). The most popular world smart city rankings were reviewed, analyzed, and paired with SDGs and the LAC needs characterization based on the ECLAC report. By re-evaluating those indicators, this research aims to create a set of new indicators for a real evaluation of the smartification level of LAC cities. Based on the proposed indicators, new ways for enhancing smartification in LAC will be identified. By applying the proposed methodology, it may be possible to improve the diagnosis for cities by region characterization in the future.

Keywords: Evaluation Model, Smart City, Latin America and the Caribbean, Sustainable Development Goals, KPI.

1   Introduction

As the world continues to urbanize, particularly in low-income and lower-middle-income countries, sustainable development is increasingly dependent on the successful management of urban expansion [1]. According to the United Nations (UN), the global

population was around 2.6 billion in 1950, and 7.7 billion in 2019, and it is projected to reach 9.7 billion by 2050 [2]. Urban administrators and planners will struggle to satisfy the needs of their rising urban populations in terms of housing, transportation, energy, infrastructure, jobs, and key services such as education and healthcare. Therefore, several initiatives have been proposed, including smart city conceptualization.

However, there has been no clear, distinctive, and accepted definition of a smart city. A pioneer definition suggests that a smart city "*makes optimal use of all the interconnected information available today to better understand and control its operations and optimize the use of limited resources*" [3]. This concept has evolved and currently, the ECLAC states that "*the smart city model is based on the generalized use of the Information and Communication Technologies (ICT) that among others allow promoting intensive and highly-productive economic activities*" [4]. In addition, the ECLAC identifies three primary clusters: i) city and mobility, ii) technology and energy, and iii) industrial policy for constructing smart LAC while contributing to the achievement of DX and SDGs [5]. During DX, public employees, cities, and residents must adapt, employ, and embrace these technologies as allied instruments, not as enemies [6],[7],[8]. A DX supported by the gradual introduction of smart city initiatives is crucial for developing sustainable solutions geared toward citizens and individuals. The IDB recently released a study on DX as a key driver for cities' smartification by identifying the technology needs of LAC as recipients. This study created a linkage with those sources to create a multilateral technology transfer process [8]. Using this approach, LAC countries developed Urban 2030 Agendas to lead their cities for achieving an ecosystem of solutions and standards supporting SDG action plans or roadmaps [15][16]. Effective action plan implementation requires to measure and to integrate information from city projects with the SDGs, supporting the creation of policies aimed to advance a better society and increase citizens' quality of life [11]. Therefore, strategic and operational goals must align with automated measurements and indicators [12]. The SDGs aim to promote economic growth and satisfy social needs like education, health, equality, and job opportunities while fighting climate change and preserving seas and forests [1].

Fig. 1. Sustainable Development Goals. (Own elaboration)

Some cases focused on SDG 11, "Sustainable Cities and Communities", as the major goal for their smart city projects by emphasizing the importance of the urban process over global social and environmental problems [9], [14]–[17]. This strategy lacks specificity for low- and middle-income nations, which are particularly vulnerable to climate change [18]. This papers aims to stablish the smart city projects pillars in LAC which must include SDG 11, as aforementioned cases, but also consider other suitable SDGs (see Fig. 1).

1.1 LAC Smart Cities Cases

LAC region is among the most urbanized regions internationally [19]; but it does not mean its cities have well-organized growth. Lack of accurate growth plans combined with varied features [20] create cities in the region facing difficulties and threats to infrastructure, services, sustainability, resilience, economic, social, and environmental.

ECLAC's paper "Multidimensional review of urban development in Latin America and the Caribbean" notes that LAC region cities face social, economic, environmental, infrastructure, and governance concerns that city planners should consider [21]. LAC region cities are devising smart city development projects to mitigate the concerns stated. Expanding internet connections or incorporating technology into daily life does not mean a city has finished the evolutionary process needed to be called "smart." How do city administrators know if these programs are successful? Practitioners, policymakers, and academics recommend objective, quantitative appraisal of city growth [22], [23].

Using evaluation models is one way to determine city growth and interaction with enabling technology [24]. The same assessment model can yield various outcomes depending on its use [25]. Since their invention, evaluation models have considered many elements and qualities that, while acceptable for the region they were designed, may not be for another. In this regard, it is vital to evaluate the location where they will be deployed and the technologies closely associated to economic, social, and environmental development areas that contribute most to local growth. Academics do not agree on a precise evaluation framework due to the variety of smart city aspects and attributes. Most evaluation frameworks are holistic [26]. The United for Smart Sustainable Cities (U4SSC) provides a collection technique for Key Performance Indicators (KPI) for Smart Sustainable Cities to evaluate cities' smartification projects in compliance with the SDGs [27]. Despite the many existing approaches for evaluating smart cities (government, non-government, business, and academy-based) [28], there are few studies that address the LAC region's SDGs. This study aims to provide a novel diagnostic model, based on a mixed approach considering SDGs, the ECLAC report and the U4SSC methodology, suitable to determine the LAC city's position on the road to smartification. It is important to highlight that both ECLAC and U4SSC embed the SDGs as a key element within their structure. It will serve as a basis for formulating strategies and action plans for developing smart cities in LAC. The next section describes the relevant academic works and publications. In section 3 the Systematic Indexes Crossed-Comparison methodology is described. The Results are listed in

section 4; some conclusions are listed in section 5; and some limitations and future research are presented in section 6.

2   Literature Review

A literature review was conducted to establish what academic publications in LAC support the research goal. Web of Science (WoS) and Scopus were chosen since they are primary sources for citation-based transdisciplinary scientific data [29],[30]. "Smart Cities Index in Latin America" and other synonyms were used to develop search terms. It resulted in the following keywords: 'Smart, Cit*, index*, metric*, indicator*, Latin America, LAC region, and LATAM region. In the literature review, following equation (1), 18 papers were identified as relevant to support this paper's research gap and purpose.

Smart* AND Cit* AND (index*OR metric*OR indicator* AND ("Latin America " OR
"LAC region" OR "LATAM region"))   (1)

The primary findings provide evidence for developing a comprehensive index for LAC smart cities and identifying the region's needs. First, several publications stressed the importance of evaluation for a city to be considered "smart" [28] [31] [32]. Due to the complexity of constituent aspects, "Smart City" evaluation is challenging [28].

Carrion et al (2021) compared 21 variables and suggested EU CITY keys indicators for LAC. The study suggested that indicators should include the following criteria: relevance, completeness, availability, measurability, reliability, familiarity, non-redundancy, and independence [28]. In the LAC region, the indicators were not applicable due to a lack of data sources [28]. It shows the complexity of measuring and the need to adapt international metrics to the LAC region.

A different technique to acquiring some indicators involved developing an electronic platform based on Boyd Cohen's Smart Cities Wheel (tool) to collect data, simplify tracking, measure indicators, and offer reliable information. This platform provides access to information with varied degrees of usefulness, helping users to improve their quality of life and engage in Smart Cities programs [31]. Nevertheless, LAC data is scant, and the platform's trustworthy information was incomplete.

Other authors admit that the LAC area is different from the rest of the globe and say it needs a tailored model to measure its sustainable efforts [32] or to identify local impediments to implementing smart cities [33].The reality of developed economies contrasts with the absence of essential services, weak governance, low value for citizen participation, and social and political constraints that the LAC region faces [32]. Consequently, smart cities in developed countries present higher rankings than the LAC smart cities region because of different conditions.

These regional differences support the statement to identify real needs and link them to useful metrics in LAC cities. The authors say LAC cities should design a proper plan [33]. This reasoning supports the current study objective of determining LAC concerns and linking solutions to smart city master plans.

Other scholarly publications for LAC focus on developing indicators only for specific areas. For instance, mobility [34], [35] [36], energy [37] [38], [39], e-participation [40] living conditions [41], productivity [42], services [43], and transportation [44]. Other studies took a more general approach to analyze patterns of mortality [45], diseases [46], or health [47] under same parameters of developed countries without differentiating variables for LAC countries. This tendency supports the objective of this research to establish a comprehensive approach to evaluate the present needs of LAC cities and to customize smart city index that help meet those demands and improve the quality of life for citizens as outlined in the SDGs.

2.1   LAC cities' needs in concordance with the Sustainable Development Goals

ECLAC is a UN regional commission. It was created to boost Latin America's economy, coordinate activities, and strengthen economic ties. Later, social development promotion was added [48]. 2017 ECLAC report on sustainable growth highlighted that inequality hinders healthy urban expansion. Despite a rise in GDP per capita and a decline in poverty rates, urban inequality has not decreased [49]. The document analyzes situations, difficulties, challenges, and advancements in the LAC region framed in the SDGs [49].

Considering that technology drives smart city development and the need to create synergy between urban space development and SDG challenges, different authors have proposed SDG-based measurement tools to capture and measure the smart city contribution to building sustainable and resilient societies. Teixeira et al (2022) measured the sustainability and smartness of cities using the SDGs, the Human Development Index (HDI), and the Urban Quality of Life (UQoL) indexes. Adam Przybyowski says quality of life can be quantified using ISO37120 indicators in the SDG context [50].

Giuseppe Grossi and Olga Trunova assess the UN's KPI for smart cities combined with the SDGs as a measurement instrument. The authors found that the complexity of the smart city concept and the unique characteristics of cities prevent universally applying a set of metrics to measure a smart city's core nature [51]. Following this approach, Clarissa Lima Loureiro understands the need for accurate measuring items that reflect the city's reality. Otherwise, the usability of models such as ISO 37120, 37122, or 37123 can be non-viable [52]. The U4SSC methodology is the result of the organizations described in Annex I, table 5 for giving a standard way to collect data and measure performance and progress in the cities' roadmap for becoming more innovative and sustainable entities embracing the SDGs [27].

In this regard, the U4SSC methodology satisfies the purpose of this work since it contextualizes ISO 37120, 37122, and 37123 KPI into the SDGs. Some authors have used this method to measure city smartness with inconsistent results. Mashhad, Iran, research shows that, according to the U4SSC approach, the city's evolution cannot be quantified because it lacks the necessary infrastructure and services. The author also discussed the U4SSC methodology's access limits to private organizations' information and data [53]. Nora Faroun used U4SSC metrics to measure the transition of Egypt's East Mansoura District into a smart and sustainable city. As part of the reported study

challenges, the author states that due to their extent, it is challenging to apply all U4SSC indicators (eleven KPI) [54].

Although U4SSC has proven to be a complete and normed instrument for the smartness, resilience, and sustainability measurement of cities framed in the SDGs [27], it is necessary to narrow down its scope and consider those specific indicators that reflect the current conditions where it will be applied. On the other hand, the ECLAC report analyses the conditions, problems, challenges, and advancements in several dimensions in the LAC region framed in the SDGs and the 2030 agenda [21]. Considering these premises and having the SDGs as a convergence point, this research has included the U4SSC methodology as part of the evaluation indexes proposed for the LAC region.

3 Methodology

3.1 Smart cities' Systematic Indexes Crossed-Comparison of evaluation for LAC region

The aim of this study is to consider the current limitations in the general implementation of smart city indexes over specific populations in LAC. Such kind of limitations may include data availability, the smart city complex definition, and the development orientation (e.g., agriculture vs. industry) [28] [32]. In addition, the case for the LAC region will analyze smart city indexes and methodologies containing the domains and indicators that represent the specific needs of the region and pursuing the data integrity (relevance, completeness, availability, measurability, reliability, familiarity, non-redundancy, and independence) as described in the literature review. To approach this goal, a Systematic Indexes Crossed-Comparison is proposed, divided into three stages.

Table 1. SCI-ECLAC Matching Coincidence Index

SCI-ECLAC	
Smart City Index	Coincidence Level
IMD-SUTD Smart City Index (SCI)	5
City Keys	5
IESE Cities in Motion Index (CIMI)	5
ISB Smart City index SHAKTI	4
DTM Smart City Index Report	3
ISO 37122 Sustainable Cities	3
ITU Smart Sustainable City Index	3
Sitkom Smart City Index	2
Kearney Global Cities Index	2
Mori Global Power Index	2
Smart Eco City Index	2
Economist Digital City Index	1
EasyPark Cities of Future	1
Solactive Smart City Index TR	1
Huawei Global connectivity Index	0

First stage: Identification of international Indexes based on multidimensional needs for LAC cities.

In this stage, Google was used to find smart cities-related indexes. Due to the large number of international rankings results for gauging smart cities, it was required to rank the results under the criteria proposed in the ECLAC report. This document uses five dimensions to examine LAC needs and issues.   Consequently, fifteen indexes were obtained. Table 1 shows that IMD-SUTD Smart City Index (SCI), City Keys, and IESE Cities in Motion Index (ICIM) have the highest coincidence level with the evaluated parameters and describes the coincidence level between Smart City Indexes.

  In other situations, the nomenclature differed, thus a subsequent analysis was undertaken by specifying the objectives of each subdimension and establishing the similitude degree. See Table 2. Notice that the U4SCC index is also included in this list, despite not being found in the search results. The reason for including this index is stated in the section 2.1.

Table 2. ECLAC Dimensions vs Smart Cities Indexes Dimensions

ECLAC vs SCI Coincidence				
ECLAC	U4SCC	IMD-SUTD Smart City Index 2021 (SCI)	IESE Cities in Motion Index 2020 (CIM)	City Keys Index 2021
Economy	Economy	Country	Economy	Green Economy
Environment	Environment	Health & Safety	Environment	Ecosystem / Climate / Pollution Waste
Social	Society & Culture	Opportunities (Work & School)	Social cohesion / Human capital	Community Involvement / Education / Employment / Health / Housing
Government	X	Governance	Governance	Multi-Level Gov
Infrastructure	X	Priority Areas	Urban planning	Services Acces
		Mobility	Mobility and transportation	Energy / Materials

Overcoming inequality is the biggest challenge for the city's development in LAC. This socioeconomic distortion goes beyond income and capital inequality. It affects social links with gender, ethnicity, age, or religious inequities, which builds up poverty in the region. Elders, women, and minorities are the most vulnerable in LAC, making them a carefully examined category [55]. The economic dimension assesses not only minority economic performance, but also planning and labor engagement.

   Environmentalists promote a comprehensive approach to societal problems. First, urban ecosystems and environmental sustainability are key to citizen well-being. Second, environmental services (water, green areas, energy, solid waste disposal) must be used in an ecological way. Third, climate-related severe events and environmental adversity. Fourth, the present urbanization model is needed as a major aspect of SDG-

aligned sustainable development. This dimension includes credible information regarding environmental services, quality, planning, policies, and waste management.

Government dimension measures government and urban citizenship. Urban administration, governance, citizenship, and human rights. Examining government and governance, particularly institutional capacity indicators, reveals how inequalities hinder public engagement. Public engagement is also acknowledged. This includes urban alliances.

Social dimension addresses regional inequalities. Inequality varies across LAC region, thus it's necessary to identify its causes. Despite progress in reducing inequality, spatial inequalities in urban poverty, informal settlements, and violence remain [49]. This dimension covers equity, social cohesiveness, service access, safety, and opportunities.

Inequality in society causes poverty clusters, unequal access to housing, public services, and urban infrastructure [49]. Therefore, infrastructural indicators are needed. Additionally, considering the fourth industrial revolution and its relevance in economic processes, governments must take into account the coverage of internet service in all urban spaces and how local places are influenced by global ones and vice versa. Thus, this dimension includes some metrics for service coverage overall.

Second stage: Nomenclature definition scheme for the indicators.

To guarantee a unique identity for the indicators, ease of understanding, and applicability, the following process was elaborated to create the nomenclature scheme. While the smart city indexes implement diverse structures and methodologies, the first step to standardize the nomenclature was based on the name of the source document. Then, the dimensions were defined, taking as reference the ECLAC report. Each dimension contains sub-dimensions that represent the sector of the city. In addition, each subdimension includes a category that represents the area in which the index could be applied. Lastly, a sequence number is assigned to avoid duplicity. The proposed scheme is shown in table 3.

Table 3. Smart Cities Index Dimensions Vs ECLAC Dimensions

XX: Document Source		XX : Dimension		X(XX) : Sub-Dimension		X(XX): Category		X(XX): Category (*cont.*)	
U4	U4SSC	EC	Economy	E	Energy	AQ	Air Quality	HO	Housing
CM	Cities in Motion	EN	Environment	EH	Education, Health and Culture	B	Buildings	IN	Innovation
CK	City Keys	SC	Society and Culture	EN	Environment	C	Culture	ICT	ICT Infrastructure
SC	IMD Smart City Index	GV	Government	I	Infrastructure	D	Drainage	PS	Public Sector
		IN	Infraestructure	ICT	ICT	E	Energy	PSN	Public Spaces and Nature
				P	Productivity	ED	Education	SA	Safety
				SH	Safety, Housing and Social Inclusion	EM	Employment	SI	Social Inclusion
						EQ	Environmental Quality	T	Transport
						ES	Electricity Supply	UP	Urban Planning
						FS	Food Security	WA	Waste
						H	Health	WS	Water and Sanitation

Third stage: Cross-comparison indexes with ECLAC dimensions.
The documents source teardown analysis identified more than six hundred indicators and fifty categories. It supports the challenges described by [53] and [54] regarding the vast number of indicators. Subsequently, indicators and categories were analyzed to identify duplicates, synonyms, or similarities in the definitions and targets. The result of this process identified five domains with a significant level of closeness with the ECLAC report. As stated in 1.1 section, exist different frameworks [28], but not all of them align with the SDGs. Therefore, the U4SSC document is suitable since it intrinsically incorporates the SDGS [27]. In summary, following the proposed scheme for nomenclature and comparing all the relevant indicators a suggested indicators list was elaborated and presented in the following section.

4   Results

Descriptive statistics is utilized to evaluate the relevance of the dimensions from the total results of the cross-comparison indexes. As a result, the present research proposes a set of five dimensions and one hundred thirteen indicators to measure the level of smartification in LAC cities (See table 4).

The results demonstrate that for the LAC region, a vast number of indicators belongs to the social category (31%), closely followed by the government (30%). These results are in concordance with the ECLAC report, that describes that most of the regional needs comes from those two categories [49].

Economy (13%) and infrastructure (13%) dimensions which contain similar number of indicators. This result demonstrates the relevance in these sectors for the LAC region smartification process.

Results also show the difference between LAC region and developed countries for smart cities' needs. According to the IMD index, the main concerns of high ranked cities are related to housing, and environment; whereas, lower ranked ones' priorities are aimed to health and safety issues [56]. Thus, several indicators are proposed to measure their smartness in this area [56]. However, in the case of LAC region, the applicable number of smart city indicators is lower. This outcome may suggest further research to evaluate and investigate the suitable environment (12%) indicators for the LAC region.

The number of indicators in this study is similar to the number used by other indexes to measure economic prosperity of cities. A detailed table with the description of dimension, sub-dimensions, indicators and the nomenclature are presented in Annex I.

Table 4. Results according to dimensions, indicators per dimension, and weighted percentage.

Dimension	Indicators per Dimension	Weigthed Percentage
ECONOMY	15	13%
ENVIRONMENT	14	12%
GOVERNMENT	34	30%
INFRAESTRUCTURE	15	13%
SOCIAL	35	31%
	113	100%

5   Conclusion

Despite the fact that many countries in LAC are still developing their economies and industries, designing new cities or improving existing ones can be approached, from a comprehensive perspective, from the smart city's methodology. This approach emphasizes the environmental and social assets to shift the current urbanization trend into a more holistic, systematic, organized, human oriented and aligned with the SDGs.

The international smart city indicators are not suitable for LAC region since there exist several differences between developed and developing countries in terms of income, infrastructure and technology penetration. This particularity decreases the effectiveness of international indexes when evaluating LAC region smart cities. Therefore, the current set of dimensions and indicators are proposed to help policy and decision makers to identify the milestones in the smartification process for LAC cities.

Based on the previous section, infrastructure dimension is a primordial element for the development of smart cities and it is gaining importance in the region. However, achieving optimal development levels will require more than a 70% increase in investment [57]. Although this dimension is important, the current economic conditions of the region do not allow reaching the necessary level of investment, slowing down its development. This is the main reason the number of indicators under this dimension is lower with the number of indicators embedded by the social or governance dimensions.

Economy dimension indicators describe factors that promote the development of a country, region, or city. Many studies consider GDP as the only indicator of growth; however, this study propose to consider other indicators that, individually, or as a whole, provide spaces for the economic development of cities framed within the Smart city concept.

The present work aims to identify the current societal needs and evaluate the most important smart city index in response to the SDG; this methodology could be used as a reference in other low- and middle-income countries in Africa, Asia, or Europe.

6   Limitations and future research

The aim of the present research is to propose an index evaluation for smartification in LAC cities. The literature review revealed flaws within international indexes to cope with evaluation in LAC region mainly due to specificity factors. Great efforts were done to determine the appropriate indicators and create a comprehensive index for LAC region; however, the present research is limited because the needs in the region were mainly identified from ECLAC report. Future research may tackle this limitation by spanning the documentation source related to the needs in the region.

The scope of this research includes economy, environment, government, infrastructure, and social dimensions; however, there exist others such as education and food. They were not included since the analyzed indexes contain scarce measurements items to match up with these dimensions described in the ECLAC report. Therefore, future research may identify appropriate indicators to fit with education, food, or more

dimensions deriving in results with more significance. To demonstrate the pertinence and effectiveness of the proposed set of indicators, it is necessary to define specific metrics for each indicator, then evaluate those indicators and compare the results between cities in LAC. Further research is needed to determine and stablish the metrics and methods for measuring and calculating each indicator.

7　Acknowledgement

References

[1]　Martin, "68% of the world population projected to live in urban areas by 2050, says UN," *United Nations Sustainable Development*, May 16, 2018. https://www.un.org/sustainabledevelopment/blog/2018/05/68-of-the-world-population-projected-to-live-in-urban-areas-by-2050-says-un/ (accessed Sep. 02, 2022).

[2]　UN, "Growing at a slower pace, world population is expected to reach 9.7 billion in 2050 and could peak at nearly 11 billion around 2100 | UN DESA | United Nations Department of Economic and Social Affairs," 2019. https://www.un.org/development/desa/en/news/population/world-population-prospects-2019.html (accessed Sep. 02, 2022).

[3]　V. Scuotto, A. Ferraris, and S. Bresciani, "Internet of Things: Applications and challenges in smart cities: a case study of IBM smart city projects," *Business Process Management Journal*, 2016.

[4]　ECLAC, "CEPAL: Las ciudades inteligentes pueden apoyar el urbanismo sostenible que propone la Agenda 2030," Oct. 16, 2016. https://www.cepal.org/es/noticias/cepal-ciudades-inteligentes-pueden-apoyar-urbanismo-sostenible-que-propone-la-agenda-2030 (accessed Sep. 05, 2022).

[5]　ECLAC, "2020-2022 Programme," Nov. 03, 2020. https://www.cepal.org/en/programa-cooperacion-cepal-bmzgiz/2020-2022-programme (accessed Sep. 05, 2022).

[6]　M. A. Ahad, S. Paiva, G. Tripathi, and N. Feroz, "Enabling technologies and sustainable smart cities," *Sustainable Cities and Society*, vol. 61, p. 102301, Oct. 2020, doi: 10.1016/j.scs.2020.102301.

[7]　I. Bouzguenda, C. Alalouch, and N. Fava, "Towards smart sustainable cities: A review of the role digital citizen participation could play in advancing social sustainability," *Sustainable Cities and Society*, vol. 50, p. 101627, Oct. 2019, doi: 10.1016/j.scs.2019.101627.

[8]   IDB, "Research on the Digital Transformation and Ecosystem of Korea applicable to Latin American and Caribbean companies," Dec. 13, 2021. https://idbinvest.org/en/publications/research-digital-transformation-and-ecosystem-korea-applicable-latin-american-and (accessed Nov. 14, 2022).

[9]   S. Blasi, A. Ganzaroli, and I. De Noni, "Smartening sustainable development in cities: Strengthening the theoretical linkage between smart cities and SDGs," *Sustainable Cities and Society*, vol. 80, p. 103793, May 2022, doi: 10.1016/j.scs.2022.103793.

[10]   UN, "Transforming our world: the 2030 Agenda for Sustainable Development | Department of Economic and Social Affairs," 2022. https://sdgs.un.org/2030agenda (accessed Sep. 12, 2022).

[11]   J. C. F. De Guimarães, E. A. Severo, L. A. Felix Júnior, W. P. L. B. Da Costa, and F. T. Salmoria, "Governance and quality of life in smart cities: Towards sustainable development goals," *Journal of Cleaner Production*, vol. 253, p. 119926, Apr. 2020, doi: 10.1016/j.jclepro.2019.119926.

[12]   A. Visvizi and R. P. del Hoyo, *Smart Cities and the UN SDGs*. Elsevier, 2021.

[13]   German Development Institute (DIE), "The Financing of Agenda 2030 Falls Short of Its Goals," *diplomatisches-magazin.de*, 2022. https://www.diplomatisches-magazin.de/en/article/deutsches-institut-fuer-entwicklungspolitik-die-finanzierung-der-agenda-2030-verfehlt-ihre-ziele/ (accessed Sep. 13, 2022).

[14]   A. Bhatnagar, T. P. Nanda, S. Singh, K. Upadhyay, A. Sawhney, and D. T. V. R. R. Swamy, "Analysing the Role of India's Smart Cities Mission in Achieving Sustainable Development Goal 11 and the New Urban Agenda," in *Sustainable Development Research in the Asia-Pacific Region: Education, Cities, Infrastructure and Buildings*, W. Leal Filho, J. Rogers, and U. Iyer-Raniga, Eds. Cham: Springer International Publishing, 2018, pp. 275–292. doi: 10.1007/978-3-319-73293-0_16.

[15]   R. C. Estoque *et al.*, "Heat health risk assessment in Philippine cities using remotely sensed data and social-ecological indicators," *Nat Commun*, vol. 11, no. 1, Art. no. 1, Mar. 2020, doi: 10.1038/s41467-020-15218-8.

[16]   R. K. Goel, C. S. Yadav, and S. Vishnoi, "Self-sustainable smart cities: Socio-spatial society using participative bottom-up and cognitive top-down approach," *Cities*, vol. 118, p. 103370, Nov. 2021, doi: 10.1016/j.cities.2021.103370.

[17]   M. A. Mycoo and K. Bharath, "Sustainable Development Goal 11 and a New Urban Agenda for Caribbean Small Island Developing States: Policy, Practice, and Action," *Frontiers in Sustainable Cities*, vol. 3, 2021, Accessed: Sep. 13, 2022. [Online]. Available: https://www.frontiersin.org/articles/10.3389/frsc.2021.554377

[18]   Z. Allam and Z. A. Dhunny, "On big data, artificial intelligence and smart cities," *Cities*, vol. 89, pp. 80–91, Jun. 2019, doi: 10.1016/j.cities.2019.01.032.

[19]   WorldBank, "Demographic Trends and Urbanization," *World Bank*, 2021. https://www.worldbank.org/en/topic/urbandevelopment/publication/demographic-trends-and-urbanization (accessed Sep. 02, 2022).

[20] A. Escudero, "Ciudad y arquitectura. Seis generaciones que construyeron la América Latina moderna, de Silvia Arango Cardinal," *Anales del Instituto de Investigaciones Estéticas*, vol. 1, p. 277, Oct. 2016, doi: 10.22201/iie.18703062e.2016.109.2582.

[21] L. Montero, J. García, and C. R. Francesa, "Panorama multidimensional del desarrollo urbano en América Latina y el Caribe," 2017.

[22] M. Cavada, D. Hunt, and C. Rogers, "Smart cities: Contradicting definitions and unclear measures," presented at the World sustainability forum, 2014, pp. 1–12.

[23] M. Zuccardi Merli and E. Bonollo, "Performance measurement in the smart cities," in *Smart city*, Springer, 2014, pp. 139–155.

[24] OECD, "Do Smart Cities Benefit Everyone," *Organisation for Economic Co-operation and Development: Paris, France*, 2020.

[25] E. B. Sheldon and W. E. Moore, *Indicators of social change: Concepts and measurements*. Russell Sage Foundation, 1968.

[26] R. G. Hollands, "Will the real smart city please stand up?: Intelligent, progressive or entrepreneurial?," in *The Routledge companion to smart cities*, Routledge, 2020, pp. 179–199.

[27] ITU, "U4SSC - Collection Methodology for Key Performance Indicators for Smart Sustainable Cities," *ITU*, 2017. https://www.itu.int:443/en/publications/ITU-T/Pages/publications.aspx?parent=T-TUT-SMARTCITY-2017-9&media=electronic (accessed Sep. 05, 2022).

[28] J. Carrión, P. Coba, and M. Pérez, "An Evaluation of the Relevance of Global Models of Indicators for Latin American Cities," in *Advances in Emerging Trends and Technologies*, vol. 1066, M. Botto-Tobar, J. León-Acurio, A. Díaz Cadena, and P. Montiel Díaz, Eds. Cham: Springer International Publishing, 2020, pp. 67–78. doi: 10.1007/978-3-030-32022-5_7.

[29] B. S. Ballew, "Elsevier's Scopus® Database," *Journal of Electronic Resources in Medical Libraries*, vol. 6, no. 3, pp. 245–252, Sep. 2009, doi: 10.1080/15424060903167252.

[30] W. M. Sweileh, "Research trends on human trafficking: a bibliometric analysis using Scopus database," *Globalization and Health*, vol. 14, no. 1, p. 106, Nov. 2018, doi: 10.1186/s12992-018-0427-9.

[31] M. Limon, V. M. Larios, R. Maciel, R. Beltran, J. A. Orizaga-Trejo, and G. R. Ceballos, "User-oriented representation of Smart Cities indicators to support citizens governments decision-making processes," in *2019 IEEE International Smart Cities Conference (ISC2)*, Casablanca, Morocco, Oct. 2019, pp. 396–401. doi: 10.1109/ISC246665.2019.9071742.

[32] D. Marchetti, R. Oliveira, and A. R. Figueira, "Are global north smart city models capable to assess Latin American cities? A model and indicators for a new context," *Cities*, vol. 92, pp. 197–207, Sep. 2019, doi: 10.1016/j.cities.2019.04.001.

[33] M. Calderon, G. Lopez, and G. Marin, "Smartness and Technical Readiness of Latin American Cities: A Critical Assessment," *IEEE Access*, vol. 6, pp. 56839–56850, 2018, doi: 10.1109/ACCESS.2018.2864218.

[34]　E. E. M. Toro, A. van der Krogt, and R. S. Flores, "Mobility and Integration of Public Transport Systems in Latin America," in *Proceedings of the 2019 2nd International Conference on Machine Learning and Machine Intelligence*, Jakarta Indonesia, Sep. 2019, pp. 58–62. doi: 10.1145/3366750.3366760.

[35]　J. I. Huertas *et al.*, "Methodology to Assess Sustainable Mobility in LATAM Cities," *Applied Sciences*, vol. 11, no. 20, p. 9592, Oct. 2021, doi: 10.3390/app11209592.

[36]　E. Pena-Ancavil, F. Tejada-Estay, C. Estevez, A. Zacepins, and V. Komasilovs, "Effect of street geometry on the vehicular traffic throughput and its impact on smart cities mapping design," in *2017 International Smart Cities Conference (ISC2)*, Wuxi, China, Sep. 2017, pp. 1–6. doi: 10.1109/ISC2.2017.8090801.

[37]　A. Mutule, I. Zikmanis, and A.-M. Dumitrescu, "Electric Consumption Assessment using Smart Meter Data and KPI Methodology," *Latvian Journal of Physics and Technical Sciences*, vol. 57, no. 3, pp. 3–19, Jun. 2020, doi: 10.2478/lpts-2020-0011.

[38]　D. P. Duarte *et al.*, "Intelligent system to management of reclosers and proposition of maneuvers in distribution network," in *2013 IEEE PES Conference on Innovative Smart Grid Technologies (ISGT Latin America)*, Sao Paulo, Brazil, Apr. 2013, pp. 1–8. doi: 10.1109/ISGT-LA.2013.6554407.

[39]　J. Helder, A. Molar-Cruz, and V. M. Larios-Rosillo, "Urban Energy Innovation Index for Latin American Cities," in *2019 IEEE International Smart Cities Conference (ISC2)*, Casablanca, Morocco, Oct. 2019, pp. 336–341. doi: 10.1109/ISC246665.2019.9071741.

[40]　F. Dias Cordeiro A and N. Cacho Alessandro, "A Platform for Measuring e-Participation in Smart Cities: A Case Study with Brazilian Capitals," *IEEE Latin Am. Trans.*, vol. 16, no. 2, pp. 542–548, Feb. 2018, doi: 10.1109/TLA.2018.8327411.

[41]　Ms. E. S. M. Nunez and Ms. J. R. M. Chirinos, "Impact of Business Intelligence on Coexistence and Citizen Security," in *2019 IEEE 39th Central America and Panama Convention (CONCAPAN XXXIX)*, Guatemala City, Guatemala, Nov. 2019, pp. 1–6. doi: 10.1109/CONCAPANXXXIX47272.2019.8977024.

[42]　R. A. S. Fernandes, A. O. Queiroz, J. T. A. V. L. Wilmers, and W. A. M. Hoffmann, "Urban governance in Latin America: Bibliometrics applied to the context of smart cities," *Transinformação*, vol. 31, p. e190014, 2019, doi: 10.1590/2318-0889201931e190014.

[43]　S. H. A. Koop and C. J. van Leeuwen, "The challenges of water, waste and climate change in cities," *Environ Dev Sustain*, vol. 19, no. 2, pp. 385–418, Apr. 2017, doi: 10.1007/s10668-016-9760-4.

[44]　J. A. Mahady, C. Octaviano, O. S. Araiza Bolaños, E. R. López, D. M. Kammen, and S. Castellanos, "Mapping Opportunities for Transportation Electrification to Address Social Marginalization and Air Pollution Challenges in Greater Mexico City," *Environ. Sci. Technol.*, vol. 54, no. 4, pp. 2103–2111, Feb. 2020, doi: 10.1021/acs.est.9b06148.

[45]　M. Naghavi *et al.*, "Global, regional, and national age-sex specific mortality for 264 causes of death, 1980–2016: a systematic analysis for the Global Burden of

Disease Study 2016," *The Lancet*, vol. 390, no. 10100, pp. 1151–1210, Sep. 2017, doi: 10.1016/S0140-6736(17)32152-9.

[46] T. Vos *et al.*, "Global, regional, and national incidence, prevalence, and years lived with disability for 310 diseases and injuries, 1990–2015: a systematic analysis for the Global Burden of Disease Study 2015," *The Lancet*, vol. 388, no. 10053, pp. 1545–1602, Oct. 2016, doi: 10.1016/S0140-6736(16)31678-6.

[47] J. D. Stanaway *et al.*, "Global, regional, and national comparative risk assessment of 84 behavioural, environmental and occupational, and metabolic risks or clusters of risks for 195 countries and territories, 1990–2017: a systematic analysis for the Global Burden of Disease Study 2017," *The Lancet*, vol. 392, no. 10159, pp. 1923–1994, Nov. 2018, doi: 10.1016/S0140-6736(18)32225-6.

[48] ECLAC, "About ECLAC," 2017a. https://www.cepal.org/en/about (accessed Sep. 11, 2022).

[49] ECLAC, *Panorama multidimensional del desarrollo urbano en América Latina y el Caribe*. CEPAL, 2017b. Accessed: Sep. 11, 2022. [Online]. Available: https://www.cepal.org/es/publicaciones/41974-panorama-multidimensional-desarrollo-urbano-america-latina-caribe

[50] A. Przybyłowski, A. Kałaska, and P. Przybyłowski, "Quest for a Tool Measuring Urban Quality of Life: ISO 37120 Standard Sustainable Development Indicators," *Energies*, vol. 15, no. 8, p. 2841, 2022.

[51] G. Grossi and O. Trunova, "Are UN SDGs useful for capturing multiple values of smart city?," *Cities*, vol. 114, p. 103193, 2021.

[52] L. C. Loureiro, C. Muniz, C. Pereira, L. Paseto, M. Martinez, and A. M. Alves, "A new methodology for smart cities in developing countries: a case study," presented at the 2021 IEEE International Smart Cities Conference (ISC2), 2021, pp. 1–6.

[53] S. M. Mirsarraf, A. Yari, N. Zohdi, and A. Motevalizadeh, "Smart City Standardized Evaluation: Use Case of Mashhad," presented at the 2021 12th International Conference on Information and Knowledge Technology (IKT), 2021, pp. 16–21.

[54] N. M. Faroun, A. N. El-Badrawy, and L. S. El-Gizawi, "Transforming Old Cities into Smart Cities Using Environmental Key Performance Indicators to Solve Environmental Problems," *cea*, vol. 10, no. 5, pp. 2075–2088, Sep. 2022, doi: 10.13189/cea.2022.100528.

[55] UN, "Estado de las Ciudades de América Latina y el Caribe (State of the Latin America and the Caribbean Cities report) - Espanol | UN-Habitat," 2012. https://unhabitat.org/estado-de-las-ciudades-de-america-latina-y-el-caribe-state-of-the-latin-america-and-the-caribbean (accessed Sep. 27, 2022).

[56] IMD, "Data shows effects of COVID-19 and climate change on citizens' perceptions of how smart their cities are," *IMD business school*, 2021. https://www.imd.org/news/updates/data-shows-effects-of-covid-and-climate-change-on-citizens-perceptions-of-how-smart-their-cities-are/ (accessed Sep/22)

[57] J. P. Brichetti, L. Mastronardi, M. E. Rivas, T. Serebrisky, and B. Solís, "The Infrastructure Gap in Latin America and the Caribbean: Investment Needed Through 2030 to Meet the Sustainable Development Goals," 2021.

Annex I

Table 5. International organizations participating in the U4SSC collection methodology

NAME	ACRONYM
Convention of Biological Diversity	BD
Economic Commission for Latin America and the Caribbean	ECLAC
Food and Agriculture Commission	FAO
International Telecommunication Union	ITU
United Nations Development Programme	UNDP
United Nations Economic Commission for Africa	UNECA
United Nations Economic Commission for Europe	UNECE
Regional Bureau of Sciences in Latin American and the Caribbean of the United Nations Educational, Scientific and Cultural Organization	UNESCO
United Nations Environment	UN environment
United Nations Environment Programme Finance Initiative	UNEP-FI
United Nations Framework Convention for Climate Change	UNFCCC
United Nations Human Settlements Programme	UN-Habitat
United Nations Industrial Development Organization	UNIDO
United Nations University-Operating Unit on Policy-Driven Electronic Governance	UNU-EGOV
United Nations Entity for Gender Equality and Empowerment of Women	UN-Women
World Meteorological Organization	WMO

Table 6. Indicators contained in the "Economy" dimension

SSSI4LAC - Economy Smart City Sustainable Indicators for Latinamerica and Caribean Region

#	Dimension	Sub-Dimension	Indicator	Nomeclature
1	ECONOMY	Economic performance	Productivity	U4:EC:P:IN:18
2	ECONOMY	Economic performance	Productivity	U4:EC:P:IN:20
3	ECONOMY	Economic performance	Productivity	U4:EC:P:EM23
4	ECONOMY	Economic performance	Productivity	U4:EC:P:EM24
5	ECONOMY	Economic performance	Productivity	U4:EC:P:IN:19
6	ECONOMY	Economic performance	Productivity	U4:EC:P:EM:21
7	ECONOMY	Economic performance	Productivity	U4:EC:P:EM:22
8	ECONOMY	Economic performance	Productivity	CM:EC:P:PS:04
9	ECONOMY	Opportunities	Young woman with limited labour participation	U4:EC:P:EM:22
10	ECONOMY	Opportunities	Young woman with limited labour participation	CM:SC:SH:SI:01
11	ECONOMY	Planning	Inefficient expansion of the urban sprawl	U4:EC:I:UP:45
12	ECONOMY	Planning	Saturated Urban Sapces	CK:EN:EN:PSN:16
13	ECONOMY	Opportunities	Urban Work	CK:EC:P:EM:05
14	ECONOMY	Planning	The surplus value of urban land	CK:EC:SH:HO:11
15	ECONOMY	Planning	The surplus value of urban land	CK:EC:P:PS:12

Table 7. Indicators contained in the "Environment" dimension

SSSI4LAC - Environment Smart City Sustainable Indicators for Latinamerica and Caribean Region				
#	**Dimension**	**Sub-Dimension**	**Indicator**	**Nomeclature**
1	ENVIRONMENT	Environmental Services Administration	Inefficient water management	U4:EC:I:WS:25
2	ENVIRONMENT	Environmental Services Administration	Inefficient water management	U4:EC:I:WS:26
3	ENVIRONMENT	Environmental Services Administration	Inefficient water management	U4:EC:I:WS:27
4	ENVIRONMENT	Environmental Services Administration	Inefficient water management	U4:EC:I:WS:28
5	ENVIRONMENT	Environmental Services Administration	Inefficient water management	U4:EN:EN:WS:51
6	ENVIRONMENT	Environmental Services Administration	Green areas Protection	U4:EN:EN:PSN:57
7	ENVIRONMENT	Environmental quality	Atmopheric Protection	U4: EN:EN:AQ:46
8	ENVIRONMENT	Environmental quality	Atmopheric Protection	U4:EN:EN:AQ:47
9	ENVIRONMENT	Waste	Improper management of solid waste	U4:EN:EN:WA:52
10	ENVIRONMENT	Waste	Improper management of solid waste	U4:EC:I:WS:29
11	ENVIRONMENT	Environmental quality	Contamination	U4:EN:EN:EQ:54
12	ENVIRONMENT	Environmental quality	Contaminación	U4:EN:EN:EQ:53
13	ENVIRONMENT	Planning	Waste Management	U4:EC:I:WS:30
14	ENVIRONMENT	Environmental Security	Risk Management	U4:SC:SH:SA:85

Table 8. Indicators contained in the "Government" dimension

SSSI4LAC - Government Smart City Sustainable Indicators for Latinamerica and Caribean Region				
#	**Dimension**	**Sub-Dimension**	**Indicator**	**Nomeclature**
1	GOVERNMENT	Citizenship	Citizen participation	U4:SC:SH:SI:80
2	GOVERNMENT	Citizenship	Citizen participation	CK:SC:SH:SI:09
3	GOVERNMENT	Citizenship	Citizen participation	CK:SC:SH:SI:10
4	GOVERNMENT	Citizenship	Citizen participation	CK:GV:P:PS:21
5	GOVERNMENT	Citizenship	Citizen participation	CK:GV:SH:SI:22
6	GOVERNMENT	Citizenship	Citizen participation	CK:GV:SH:SI:23
7	GOVERNMENT	Citizenship	Citizen participation	CK:GV:I:SI:06
8	GOVERNMENT	Citizenship	Citizen participation	CK:GV:SH:PS:07
9	GOVERNMENT	Citizenship	Citizen participation	CK:SC:SH:SI:10
10	GOVERNMENT	Citizenship	Citizen participation	CM:GV:SH:SI:03
11	GOVERNMENT	Citizenship	Citizen participation	CK:IN:SH:SI:03
12	GOVERNMENT	City	City Information	U4:EC:I:T12
13	GOVERNMENT	City	City Information	EC:ICT:PS:15
14	GOVERNMENT	City	City Information	CK:EC:I:IN:13
15	GOVERNMENT	City	City Information	CK:EC:I:ICT:17
16	GOVERNMENT	City	City Information	SC:GV:ICT:PS:02
17	GOVERNMENT	City	City Information	SC:GV:SH:PS:03
18	GOVERNMENT	City	City Information	SC:GV:SH:PS:04
19	GOVERNMENT	City	City Information	CM:GV:ICT:ICT:02
20	GOVERNMENT	City	City Information	CK:SC:SH:SA:01
21	GOVERNMENT	Governance	Institutional Capabilities	CK:GV:I:PS:18
22	GOVERNMENT	Governance	Institutional Capabilities	CK:GV:I:PS:19
23	GOVERNMENT	Governance	Institutional Capabilities	CK:GV:I:PS:20
24	GOVERNMENT	Governance	Urban Financement	CK:GV:ICT:PS:15
25	GOVERNMENT	Governance	Policies and Regulations	CK:GV:ICT:ICT:14
26	GOVERNMENT	Governance	Policies and Regulations	CK:GV:SH:SI:24
27	GOVERNMENT	Governance	Policies and Regulations	CK:I:ICT:ICT25
28	GOVERNMENT	Governance	Policies and Regulations	CK:IN:SH:ICT:02
29	GOVERNMENT	Governance	Policies and Regulations	SC:IN:I:T:01
30	GOVERNMENT	Governance	Strategic Aliance	CK:GV:SH:SI:24
31	GOVERNMENT	Governance	Strategic Aliance	SC:GV:ICT:PS:02
32	GOVERNMENT	Governance	Strategic Aliance	SC:GV:SH:PS:03
33	GOVERNMENT	Governance	Strategic Aliance	SC:GV:SH:PS:04
34	GOVERNMENT	Governance	Citizen participation	CK:IN:SH:SI:04

Table 9. Indicators contained in the "Infrastructure" dimension

#	Dimension	Sub-Dimension	Indicator	Nomeclature
	SSSI4LAC - Infraestructure Smart City Sustainable Indicators for Latinamerica and Caribean Region			
1	INFRAESTRUCTURE	Environment	Public Building Sustainability	U4:EC:I:B:42
2	INFRAESTRUCTURE	Governance	e-Government	U4:EC:ICT:PS:16
3	INFRAESTRUCTURE	Governance	Public Sector e-procurement	U4:EC:ICT:PS:17
4	INFRAESTRUCTURE	Internet	Fixed Broadband Subscriptions	U4:EC:ICT:ICT:2
5	INFRAESTRUCTURE	Internet	Wireless Broadband Subscriptions	U4:EC:ICT:ICT:3
6	INFRAESTRUCTURE	Internet	Wireless Broadband Coverage	U4:EC:ICT:ICT:4
7	INFRAESTRUCTURE	Services	Smart Water Meters	U4:EC:ICT:WS:6
8	INFRAESTRUCTURE	Services	Water Supply ICT Monitoring	U4:EC:ICT:WS:7
9	INFRAESTRUCTURE	Services	Drainage / Storm Water System ICT Monitoring	U4:EC:ICT:D:8
10	INFRAESTRUCTURE	Services	Smart Electricity Meters	U4:EC:ICT:ES:9
11	INFRAESTRUCTURE	Services	Electricity Supply ICT Monitoring	U4:EC:ICT:ES:10
12	INFRAESTRUCTURE	Services	Demand Response Penetration	U4:EC:ICT:ES:11
13	INFRAESTRUCTURE	Services	Integrated Building Management Systems in Public Buildings	U4:EC:I:B:43
14	INFRAESTRUCTURE	Transportation	Traffic Monitoring	U4:EC:ICT:T:13
15	INFRAESTRUCTURE	Transportation	Intersection Control	U4:EC:ICT:T:14

Table 10. Indicators contained in the "Social" dimension

#	Dimension	Sub-Dimension	Indicator	Nomeclature
	SSSI4LAC - Social Smart City Sustainable Indicators for Latinamerica and Caribean Region			
1	SOCIAL	Equity and Social Cohesion	Economic Inequality	U4:SC:SH:SI:78
2	SOCIAL	Equity and Social Cohesion	Gender Inequality	U4:SC:SH:SI:77
3	SOCIAL	Equity and Social Cohesion	Neigborhood Poverty	U4:U4:SC:SH:HO:75
4	SOCIAL	Equity and Social Cohesion	Neigborhood Poverty	U4:SC:SH:HO:76
5	SOCIAL	Equity and Social Cohesion	Neigborhood Poverty	U4:SO:SH:SA:85
6	SOCIAL	Equity and Social Cohesion	Poberty	U4:SC:SH:SI:79
7	SOCIAL	Service Access	Service Access	U4:EN:EN:PSN:55
8	SOCIAL	Service Access	Service Access	U4:EC:ICT:ICT:5
9	SOCIAL	Service Access	Service Access	U4:EC:I:ES:33
10	SOCIAL	Service Access	Service Access	U4:EC:I:ES:31
11	SOCIAL	Service Access	Service Access	U4:EC:I:ES:32
12	SOCIAL	Service Access	Service Access	U4:SO:SH:SA:86
13	SOCIAL	Service Access	Service Access	U4:EN:EN:PSN:56
14	SOCIAL	Service Access	Service Access	U4:EN:EN:PSN:58
15	SOCIAL	Service Access	Service Access	U4:EC:I:T:38
16	SOCIAL	Service Access	Service Access	U4:EC:I:T:35
17	SOCIAL	Service Access	Service Access	U4:EC:ICT:ICT:1
18	SOCIAL	Service Access	Service Access	U4:SO:SH:SA:87
19	SOCIAL	Service Access	Service Access	U4:SO:SH:SA:88
20	SOCIAL	Service Access	Urban mobility	U4:EC:I:UP:44
21	SOCIAL	Service Access	Urban mobility	U4:EC:I:T:37
22	SOCIAL	Service Access	Urban mobility	U4:EC:I:T:39
23	SOCIAL	Service Access	Urban mobility	U4:EC:I:T:40
24	SOCIAL	Service Access	Urban mobility	U4:EC:I:T:41
25	SOCIAL	Service Access	Urban mobility	U4:SO:SH:SA:90
26	SOCIAL	Service Access	Urban mobility	U4:EC:I:T:34
27	SOCIAL	Service Access	Urban mobility	U4:EC:I:T:36
28	SOCIAL	Safety	Violence	U4:SC:SH:SA:89
29	SOCIAL	Opportunities	Human capital low qualified	U4:SC:EH:ED:64
30	SOCIAL	Opportunities	Human capital low qualified	U4:SO:EH:ED:63
31	SOCIAL	Opportunities	Human capital low qualified	U4:SC:EH:ED:65
32	SOCIAL	Opportunities	Human capital low qualified	U4:SO:EH:ED:66
33	SOCIAL	Opportunities	Employment	U4:EC:P:EM:21
34	SOCIAL	Opportunities	Employment	U4:EC:P:EM:22
35	SOCIAL	Opportunities	Human capital without social protection	U4:SC:EH:H:72

LA IDEA DE CIUDAD INTELIGENTE EN AMÉRICA LATINA: CONCEPTO, EXPERIENCIAS Y RAZGOS COMUNES DE IMPLEMENTACIÓN

Ryszard Edward Rozga Luter[1]
Raúl Hernández Mar[2]

Resumen

El trabajo parte de la característica de la red de asentamientos humanos que describen las condiciones de implementación de la idea de Ciudad Inteligente en América Latina. El papel importante en esta implementación tiene la existencia de las estructuras organizativas en apoyo de implementación, que desempeñan tanto las diferentes instituciones supranacionales como algunas nacionales. El objetivo de este trabajo consiste en revisar las diferentes experiencias de los principales países de América Latina (Argentina, Brasil, Chile, Colombia y México) para tratar de responder a la pregunta cuales son los avances en la elaboración de idea de la Ciudad Inteligente, cuáles son los ejemplos de pruebas de la construcción de un modelo abstracto de ciudad inteligente en América Latina y por consecuencia ¿si se puede hablar de un modelo latinoamericano de implementación de la de Ciudad Inteligente? Con base en la presentación de algunos modelos abstractos se termina con algunas conclusiones referentes al estado actual de la idea del modelo latinoamericano de la Ciudad Inteligente y su implementación.

Palabras clave: Ciudad Inteligente, concepto, experiencias, América Latina

Introducción

Los procesos de urbanización que se realizan en América Latina son acelerados, caóticos y en la mayoría de los casos con planeación y políticas públicas de urbanización insuficientemente efectivas para orientar y organizar este proceso. En tal situación hay una búsqueda de nuevas ideas del futuro de la ciudad y una de ellas son las pruebas de implementación de la idea de la Ciudad Inteligente *(smart city)* que declara la mayoría de las autoridades de los países de América Latina y que se puede considerar como una búsqueda del nuevo paradigma del desarrollo urbano.

La idea de la Ciudad Inteligente nació en otros ambientes geográficos, económicos y culturales, en los países europeos y en América del Norte - altamente desarrollados, sin embargo, se ha difundido por todo el mundo tomando forma desde - las declaraciones comerciales a través de las cuales se realizan las iniciativas de grandes corporaciones de la producción electrónica avanzada, de vender sus productos a nuevos mercados, pasando por unas propuestas de promover el desarrollo tecnológico en los ambientes regionales a través de esta

forma de ciudades y regiones inteligentes, hasta llegar a las declaraciones políticas en búsqueda de legitimización de los gobiernos y autoridades muchas veces poco eficientes en la gestión urbana.

En los principales países más grandes de América Latina (Argentina, Brasil, Chile, Colombia y México) pero también en algunos otros (Ecuador, Uruguay) ya existen diferentes experiencias en la elaboración de idea de la Ciudad Inteligente, los ejemplos de pruebas de su implementación y por consecuencia nace la pregunta ¿si se puede hablar de un modelo latinoamericano de la Ciudad Inteligente? La hipótesis de este trabajo es que no existe tal modelo y los diferentes países siguen diferentes pautas en la implementación. Sin embargo, ya después de aproximadamente veinte años de tales políticas se puede hablar de algunas experiencias comunes que deben servir como indicaciones de las futuras políticas públicas urbanas.

El objetivo de este trabajo consiste en revisar las diferentes experiencias de los principales países de América Latina (Argentina, Brasil, Chile, Colombia y México) para tratar de responder a la pregunta cuales son los avances en la elaboración de idea de la Ciudad Inteligente, cuáles son los ejemplos de pruebas de la construcción de un modelo abstracto de ciudad inteligente en América Latina y por consecuencia ¿si se puede hablar de un modelo latinoamericano de implementación de la de Ciudad Inteligente?

La metodología que se emplea consiste en la revisión de la literatura y los documentos disponibles sobre el tema, la sistematización de los datos y de la información y, la exposición crítica del tema.

Los primeros resultados muestran qué implementación del modelo de la ciudad inteligente en países de América Latina se lleva a cabo de manera bastante heterogénea realizada tanto por los gobiernos centrales, autoridades de ciudades grandes, pero también por las empresas abastecedores del equipamiento electrónico informático. Evidencias de eso son las formas de organización de difusión de la idea de la Ciudad Inteligente, así como promoción e implementación de la idea de parte de los organismos gubernamentales.

1. La característica de la red de asentamientos humanos en América Latina.

Las condiciones geográficas de América Latina son bastante heterogéneas y por esa razón también el sistema de asentamientos humanos tiene características diferenciadas. En primer término, hay que mencionar relativa polarización de los elementos de la red de asentamientos humanos ya que en América Latina además de mega-metropolis[3] que en este momento ya son entre 6 y 8 (para 2018 estos fueron, Ciudad de México, Sao Paulo, Buenos Aires, Rio de Janeiro y Lima), zonas

---

[3] Por mega-metropolis se entiende las grandes zonas metropolitanas que cuentan con más de 10 millones de habitantes.

metropolitanas[4] y el resto de la estructura se caracteriza por relativamente pequeños ciudades que muchas veces no sobrepasan 100 mil habitantes. Esta característica probablemente produce que la mayoría de la población urbana que conforma aproximadamente 80% de la población, vive en mega-metropolis y zonas metropolitanas.

Sin embargo, por esa razón también las ciudades latinoamericanas presentan gran polarización dentro de sus áreas. Son tanto las concentraciones de la población, actividad económica y riqueza, así como presentan amplias áreas de zonas pobres y marginadas que en diferentes países obtienen diferentes nombres (favelas, zonas marginadas, asentamientos irregulares, etc.).

Todo esto crea la situación específica para la implementación de la idea de la Ciudad Inteligente, ya que prácticamente fuera de megaciudades y grandes ciudades es muy difícil hablar sobre desarrollos maduros de implementación. La mayoría de las pequeñas ciudades latinoamericanas sufre falta de recursos económicos, poca organización de la vida urbana y por consecuencia es muy difícil hablar de la implementación de la idea de ciudad avanzada. Sin embargo, todo esto no nos libera de considerar cuáles podrían ser las líneas futuras de implementación de la idea de Ciudad Inteligente, también en ambientes de ciudades pequeñas y medianas.

2. La existencia de las estructuras organizativas supranacionales en apoyo de Ciudades Inteligentes

En la búsqueda, para las necesidades de este trabajo, de las estructuras organizativas supranacionales en apoyo a la implementación de idea de la ciudad inteligente, en primer término, se encontró una plataforma de la CEPAL - La Plataforma Urbana y de Ciudades de América Latina y el Caribe. La División de Desarrollo Sostenible y Asentamientos Humanos de la Comisión Económica para América Latina y el Caribe (CEPAL), elabora estudios, proyectos y programas de investigación en el tema de Ciudades Inteligentes y Sostenibles.

Por otro lado, parece que la más conocida iniciativa de promover la idea de la Ciudad Inteligente es la de asociación privado-gubernamental (PPP) que produjo una serie de Congresos de Ciudades Inteligentes Expo-LATAM. Los congresos se realizan desde el año 2016, primero por cuatro años en Puebla y los últimos tres años en Mérida, Yucatán. Smart City Expo LATAM Congress es el evento que impulsa la colaboración e implementación de las acciones que, a través de tecnología e innovación, se requieren para la transformación y evolución de la región, todo bajo el eje rector "activar, actual, acelerar".

---

[4] Por zonas metropolitanas se entiende las áreas urbanas donde vive entre 1 y 10 millones de habitantes.

Según los organizadores, este congreso representa una oportunidad de generar networking, promover alianzas estratégicas y debatir tendencias, así como dialogar con los actores principales del ecosistema urbano y territorial. Se trata de los eventos en los cuales (en el último del año 2022) participaron los representantes de más de 300 ciudades de 45 países.[5]

Desde hace algunos años se realizan los Congresos Iberoamericanos de Ciudades Inteligente (ICSC-CITIES) patrocinados por el Programa Iberoamericano de Ciencia y Tecnología para el Desarrollo (CYTED)[6]. El siguiente Quinto Congreso tendrá lugar en la ciudad de Cuenca, Ecuador, en noviembre de este año.

Las noticias de las redes sociales informan también sobre la instalación el día 3 de abril de este año, de la Red Latinoamericana de Ciudades Inteligentes de FLACMA[7] en el marco del evento "EXPERIENCIA PUERTO RICO 2022" cuya temática de este año eran las ciudades inteligentes y sostenibles.

3. Las características generales de las ciudades inteligentes latinoamericanas

En esta parte del trabajo analizaremos diferentes casos de países latinoamericanos donde se implementa la idea de la ciudad inteligente, por lo menos de manera declarativa. Lo interesante es que, por lo menos en algunos países, funcionan o se declaran programas gubernamentales como son los casos de Argentina, Brasil o Colombia.

ARGENTINA

En Argentina en 2019 apareció un documento elaborado para las necesidades de SMART CITY EXPO CURITIBA 2019, titulado: Estrategia argentina de Ciudades Inteligentes, de la autoría de Catalina Palacio Cortés, de la Dirección de Investigación, Innovación y Control, Subsecretaría País Digital, Secretaría de Modernización de la Nación, Presidencia de la Nación. (Palacio Cortés, 2019)

---

[5] Los principales organizadores del Congreso son: LATAM, Fira Barcelona México y la Universidad Panamericana Campus México (UP).

[6] El Programa Iberoamericano de Ciencia y Tecnología para el Desarrollo (CYTED) es un programa que promueve la cooperación en temas de ciencia, tecnología e innovación para el desarrollo armónico de Iberoamérica. El Programa CYTED fue creado en 1984 mediante un Acuerdo Marco Interinstitucional, el cual fue firmado por el gobierno de los 21 países de lengua hispano--portuguesa (Argentina, Bolivia, Brasil, Chile, Colombia, Costa Rica, Cuba, Ecuador, El Salvador, España, Guatemala, Honduras, México, Nicaragua, Panamá, Paraguay, Perú, Portugal, República Dominicana, Uruguay y Venezuela). Este Programa se encuentra incluido a partir de 1995 entre los Programas de Cooperación de las Cumbres Iberoamericanas de Jefes de Estado y de Gobierno.

[7] Federación Latinoamericana de Ciudades, Municipios y Asociaciones Municipalistas (FLACMA) es una organización propositiva de libre adhesión que representa a los 16.132 municipios, intendencias y prefecturas, a las ciudades y a las asociaciones de gobiernos locales, redes y gremios, municipalistas de América Latina y El Caribe.

En este documento se presenta un diagnóstico que se hace por medio de la aplicación del "Modelo de Ciudades Inteligentes de País Digital". El modelo está compuesto por 5 dimensiones: Gobernanza, Ambiente, Desarrollo Humano, Planeamiento Urbano y Competitividad. Cada dimensión está estructurada por 3 Ejes (exceptuando Desarrollo Humano que tiene 4 ejes) y cada Eje está compuesto por Factores (un promedio de 3 Factores por cada Eje). La unidad mínima de medida es el indicador y el modelo cuenta con más de 300 de ellos entre cualitativos y cuantitativos internacionalmente usados y reconocidos. (Ibid.) Sin embargo, en este documento no se presentan ningunos casos específicos de las Ciudades Inteligentes.

Este tipo de evaluación de la situación en Argentina encontramos en otra fuente donde se presenta el siguiente diagnóstico: "Según el ranking Cities in Motion, la ciudad de Buenos Aires ocupa el puesto 85 de ciudades inteligentes en el mundo. Los especialistas coinciden en resaltar que la tecnología ayuda, pero no suma, ya que la capital ha mantenido este lugar en las últimas tres ediciones. El ámbito porteño posee buenas puntuaciones en materia de "gobernanza" pero falla en ítems como la "gestión pública" y la "economía". (Tridia, 2022)

También en publicaciones de este índice (Cities in Motion) aparecen otras ciudades en como Córdoba y Rosario, en los puestos 107 y 139 respectivamente. La capital de la provincia cordobesa se destaca por su nivel tecnológico y planificación urbana, superando a la propia ciudad de Buenos Aires. Además, estas dos ciudades hacen lo propio en el ámbito medioambiental dejando a los porteños muy por detrás. (Ídem).

¿Pero cuál es el panorama de las Smart Cities en Argentina? Sebastián García Marra, uno de los fundadores de Less, empresa argentina dedicada al desarrollo del monitoreo inteligente, explicó que la ciudad de Buenos Aires es una isla dentro del país ya que en la capital federal hace mucho tiempo que se vienen implementando soluciones inteligentes, como el *smart lighting*, pero el resto del país queda a la espera de estas acciones. El mismo entrevistado quien trabaja para diseñar dispositivos capaces de medir una gran cantidad de variables que pueden ayudar a diferentes industrias, explica que en Argentina hay grupos trabajando en aplicaciones específicas que están al nivel de cualquier otro país del mundo. "Nos falta ese gran paso que es que se tome una decisión de gran escala" (Ibid.). Se puede entender que el entrevistado se refiere a las decisiones que ampliarían la idea de Ciudad Inteligente a otras ciudades argentinas. Siguiendo "El panorama de las Smart Cities en Argentina es muy prometedor ya que el capital humano se encuentra disponible para avanzar en soluciones que mejoren la vida de la ciudadanía. Mediante la optimización de procesos y el aumento de eficiencia, las soluciones tecnológicas se presentan como una gran vía para aumentar la eficiencia energética de las ciudades." (Tridia, 2022). Sin embargo, podríamos concluir que por lo pronto la idea de Ciudad Inteligente se mantiene en ambiente de las tres ciudades mencionadas.

BRASIL

El programa Pró-Cidades de Brasil, que fue lanzado en 2019 con 4 mil millones de reales, disponibles para financiar proyectos de rehabilitación y modernización tecnológica en zonas urbanas, aparentemente debería permitir al país avanzar en el proyecto de ciudades inteligentes. Dicho proyecto fue preparado por el Ministerio de Desarrollo Regional (MDR) y el Ministerio de Ciencia, Tecnología, Innovaciones y Comunicaciones (MCTIC). (Careño, 2020)

En este contexto es interesante el "Ranking de Ciudades Inteligentes Conectadas" que es un estudio desarrollado por la empresa Urban Systems para el evento homónimo, concebido por la misma empresa y Necta y celebrado desde 2015, y donde también se creó una plataforma de discusión y negocios sobre las Smart Cities. Con siete ediciones ya realizadas, versiones de 2015 a 2021, el Ranking de Ciudades Inteligentes Conectadas es un esfuerzo en la comprensión de los sistemas urbanos y definición de los indicadores que señalan la etapa de las ciudades brasileñas para su desarrollo inteligente, sostenible y humano." (Connected Smart Cities Ranking, 2021)

El Ranking consta de 11 ejes temáticos, y 75 indicadores que se conectan entre sí y presentan la clasificación de 100 municipios de Brasil clasificados en 3 grupos (más de 500 mil habitantes, entre 100 y 500 mil y menos que 100 mil). La clasificación de los primeros municipios de cada grupo presenta la Tabla 4.

Tabla 4: Los primeros 20 municipios clasificados en 3 grupos del ranking de 100 municipios de Brasil, según el Ranking de Ciudades Inteligentes Conectadas, 2021.

más de 500 mil hab.	Sao Paulo (1), Florianópolis (2), Curitiba (3), Brasil (4), Rio de Janeiro (7), Campinas (8), Niterói (9), Salvador (10), Campo Grande (13), Belo Horizonte (15), Goiania (18),
entre 100 y 500 mil hab.	Vitória (5), Sao Caetano do Sul (6), Barueri (11), Balneario Camboriu (12), Santos (14), Blumenau (16), Jaragua do Sul (17), Jundaí (20).
entre 50 y 100 mil hab.	Jaguariúna (19)

Fuente: (Ranking Connected Smart Cities, 2021)

La Tabla 4 de la clasificación de los primeros 20 municipios del Ranking de Ciudades Inteligentes Conectadas, realizado para 2021 proporciona una buena orientación sobre el rumbo del desarrollo de este tipo de ciudades. En primer término, se puede notar que predominan las ciudades grandes por arriba de medio millón, mucho menos representados son las ciudades del tamaño mediano (entre 100 y 500 mil habitantes) y prácticamente no aparecen las ciudades pequeñas por abajo de 100 mil. En segundo término, notamos que entre los primeros 20 municipios sólo se

encuentra un municipio del noreste de Brasil, que es la ciudad de Salvador, capital de la provincia Bahía.

Sobre las características de las áreas en las cuales se desarrollan las ciudades inteligentes en Brasil nos informa el mismo Ranking de Ciudades Inteligentes Conectadas, ya que entre sus once ejes de evaluación predominan las relacionadas con el desarrollo urbano tales como: Movilidad, Urbanismo, Gobernanza y otros cinco parecidos, mientras que a las cuestiones tecnológicas y económicas están dedicadas sólo tres ejes, que son: Tecnología e Innovación, Economía y Emprendedurismo. Esto sugiere claramente que en caso de Brasil la idea de Ciudad Inteligente tiene principalmente como objetivo el desarrollo urbano y en menor grado la promoción de tecnología e innovación.

Chile

Según las fuentes consultadas, Chile desde hace por lo menos 10 años "está comenzando a incursionar en el tema de Ciudades Inteligentes y está impulsando varias iniciativas al respecto. Entre éstas, se encuentran: Agenda Digital 2020, creación de la Mesa Institucional de Smart Cities y Mesa Técnica de Smart Cities, ambas organizadas por Fundación País Digital y Cepal." (Cohen y Obediente, 2014: 3).

La situación es bastante específica en este país que tiene una red de asentamientos humanos dispersa con la mayoría de las ciudades menores y predominancia de la Zona Metropolitana de Santiago. Por esa razón en la clasificación de Ciudades Inteligentes de Chile no aparece ninguna ciudad que no es el área metropolitana.

Tabla 5: Los primeros 10 áreas metropolitanas
de Chile según tamaño de población

Gran Santiago	7 112 808
Gran Concepción	971 285
Gran Valparaíso	944 498
Gran La Serena	448 784
Antofagasta	361 873
Gran Temuco	358 541
Gran Iquique	299 843
Gran Rancagua	294 279
Gran Puerto Montt	290 480
Arica	221 364

La Fundación País Digital y la Universidad del Desarrollo, desarrollaron el estudio, donde se utilizaron 28 indicadores repartidos en seis ejes o componentes que son: medio ambiente, movilidad, gobierno, economía, sociedad y calidad de vida. Este esquema ha sido utilizado para medir el avance de la idea de Ciudad Inteligente.

Dentro del estudio realizado en 2014, hay una clasificación de las ciudades inteligentes donde se toma en cuenta las siguientes once ciudades (Ídem):

Tabla 6: Ranking de las 11 ciudades de Chile considerados más inteligentes, 2014

CIUDAD	PUNTAJE	CIUDAD	PUNTAJE
1.Santiago	86.15	7. Antofagasta	57.91
2. Puerto Montt	72.81	8. Talca	57.85
3. Temuco	62.85	9. Chillan	57.65
4. Coquimbo-La Serena	61.72	10. Rancagua	55.30
5. Concepción	60.37	11. Arica	53.0
6. Valparaíso	59.46		

Fuente: (Cohen y Obediente, 2014: 7)

Vale la pena subrayar que las únicas dos ciudades que no se repitan en las Tablas 5 y 6, son el área metropolitana de Gran Iquique y la ciudad de Arica, lo que muestra claramente que la política del desarrollo de las ciudades inteligentes está dirigida a las grandes áreas metropolitanas del país.

Por otro lado, en el 2019, el Corfo[8] anunció que "Antofagasta, Valparaíso, Chillán, Concepción y Temuco serán las ciudades en que se comenzará a aplicar desde 2019, el Plan Nacional de Ciudades Inteligentes. El Plan Nacional de Ciudades Inteligentes responde al interés de Corfo por promover y facilitar las condiciones para el desarrollo de ciudades más innovadoras, sostenibles y competitivas, como también más habitables para sus ciudadanos. En una segunda etapa de la propuesta se evaluará su extensión a otras ciudades del país." (Espinoza, 2018). Sin embargo, como vemos las 5 ciudades anunciadas para promover en dicho Plan, se encuentran entre 11 ciudades consideradas que mejor implementan la idea de Ciudad Inteligente.

Por último, vale la pena mencionar que también dentro del Ministerio de Transportes y Comunicaciones existe Unidad de Ciudades Inteligentes que supuestamente actúa de acuerdo con la idea de *Smart City* (Unidad de Ciudades Inteligentes, 2022). Sin embargo, si hubiéramos tratado de evaluar la política del desarrollo de las ciudades inteligentes en Chile tendríamos que llegar a la conclusión parecida a los dos casos anteriores (Argentina, Brasil) de que la idea se trata básicamente implementar en las ciudades grandes.

COLOMBIA

Tampoco en el caso de Colombia, en las comparaciones internacionales del desarrollo de las ciudades inteligentes, aparecen otras ciudades que la capitalina ciudad de Bogotá y Medellín. Sin embargo, "El Ministerio de Tecnologías de

---

[8] La Corporación de Fomento de la Producción (Corfo) es la agencia del Gobierno de Chile, organismo de ámbito multisectorial, encargado del fomento de la producción nacional y promotora del crecimiento económico regional.

Información y de Comunicaciones (TIC) dio a conocer el año pasado los municipios que probablemente se conviertan en "ciudades inteligentes"; son más de 60 ciudades que el Ministerio de TIC promete impulsar para que se conviertan en territorios inteligentes, entre ellas se encuentran varias capitales, así como otros de menor población, pero los cuales proyectan gran crecimiento en los próximos años. (…)

El Ministerio TIC planea la ejecución de un "modelo de medición de madurez de ciudades y territorios inteligentes" que permitirá identificar oportunidades y prioridades para definir una visión futura y una hoja de ruta concreta y viable para el proceso de transformación digital, e invita a los empresarios, la población civil, las instituciones educativas y las entidades gubernamentales a expresar sus puntos de vista para colaborar en la implementación de este proceso." (Haddad, 2022) Es así que:

> "Por segunda vez en el país, el Ministerio de Tecnologías de la Información y las Comunicaciones (MinTIC), aplica el Modelo de Madurez en Ciudades y Territorios Inteligentes para reconocer las capacidades y oportunidades de mejora de 115 territorios de Colombia, en relación con su ruta de transformación digital territorial para ser un territorio inteligente. Este despliegue ha permitido identificar e integrar al diseño del modelo de Ciudad Inteligente, la visión que sus habitantes tienen sobre el desarrollo de sus territorios, a fin de construir un modelo plural e incluyente que refleje las opiniones e intereses de quienes la conforman." (Ministerio de Tecnologías, 2021)

Los resultados de aplicación de este modelo, aquí presentadas sólo para las primeras 10 alcaldías presenta la Tabla 7.

Tabla 7: Las primeras 10 alcaldías de Colombia, según el Índice de Ciudades y Territorios Inteligentes, 2021

Departamento	Entidad Territorial	Índice de Madurez
1. Antioquia	Sabaneta	4,9
2. Antioquia	Itagüí	4,6
3. Cundinamarca	Sopó	4,4
4. Tolima	Ibagué	4,3
5. Antioquia	Marinilla	4,3
6. Antioquia	San Jerónimo	4,2
7. Santander	Onzaga	4,2
8. Antioquia	Medellín	4,2
9. Boyacá	Paipa	4,1
10. Antioquia	Caucasia	4,0

Fuente: (Ministerio de Tecnologías, 2021: 10)

Muy interesante es el documento emitido en el año 2020, en su versión de borrador, por el Gobierno de Colombia, titulado: "Documento de lineamientos de política de Ciudades Inteligentes, Versión Borrador" (Documento, 2020). En este documento

se precisa el apoyo a la introducción de la idea de Ciudad Inteligente de los dos instrumentos existentes que son: el Índice de Ciudades Modernas (Tabla 8) y el Modelo de Medición de Madurez de Ciudades y Territorios Inteligentes.

Tabla 8: Las primeras 10 ciudades de Colombia, según el Índice de Ciudades Modernas, 2019

Ciudad	Índice
Bogotá	68
Medellín	62
Manizales	61
Tunja	61
Barranquilla	60
Bucaramanga	60
Cali	58
Pereira	57
Armenia	55
Cartagena	55

Fuente: (Observatorio, 2020)

En este sentido podemos observar que la política de implementación de la idea de ciudad inteligente en Colombia parece bastante madura y avanzada. En diferentes dependencias del gobierno de Colombia se desarrollan diferentes iniciativas para promover esta idea además de tratar de desarrollar su propio concepto.

MEXICO

En México no existe ningún plan gubernamental para promoción de la idea de Ciudad Inteligente y tampoco muchas ciudades mexicanas aparecen en las comparaciones internacionales. La única ciudad que aparece constantemente en estas comparaciones es la Ciudad de México, aunque las iniciativas para promover la idea de las Ciudades Inteligentes se pueden encontrar por lo menos en otras tres grandes ciudades de México.

El día 16 de febrero 2016 se firmó acta de constitución de La Asociación Mexicana de Ciudades Inteligentes (AMECI) que se realizó en el marco de Smart City Expo Puebla (México) (Se constituye AMECI, 2016). La AMECI tiene entre sus objetivos impulsar en los municipios mexicanos el uso de infraestructura de innovación y tecnología para disminuir el consumo energético y reducir las emisiones de CO_2, mejorar la gobernanza, la movilidad y el capital humano. Esta asociación forma parte de la Conferencia Nacional de Municipios de México (CONAMM). Hoy día este mismo organismo aparece como Asociación Mexicana de Municipios y Ciudades Inteligentes – diluyendo so objetivo original.

De la revisión básicamente de fuentes hemerográficas, encontramos en este momento que hay por lo menos cinco casos de pruebas de implementación de la idea de Ciudad Inteligente, aunque débilmente documentados. Añadiendo los experimentos en la Ciudad de México, según Nieves (2018, p. 30) existen proyectos

de CI tales como: Ciudad Maderas, Querétaro; Ciudad Creativa Digital, Guadalajara; Tequila, Jalisco y, Smart Puebla, Puebla. Estos cuatro proyectos se pueden considerar como más consistentes y ya estables desde hace algunos años. Revisando estos casos, tres son ejemplos de ciudades grandes: Ciudad de México, Guadalajara y Puebla, una iniciativa dentro de una ciudad mediana que es la de Ciudad Madero de Querétaro y un ejemplo que parece más como experimento, en el municipio de Tequila, Jalisco.

La opinión general que podemos presentar después de revisar brevemente estos cinco casos es que en México los proyectos de Ciudad Inteligente, más se encuentran en la esfera de los deseos políticos y pruebas parciales de implementación de algunos elementos de la idea, especialmente referente a la creación de las islas de innovación (Ciudad Maderas o Ciudad Creativa Digital) o pruebas de mejoramiento de alguna infraestructura o servicios públicos (alumbrado en Puebla).

4. Hacia un modelo latinoamericano de la idea de Ciudad Inteligente

En la realidad latinoamericana se han realizado algunas pruebas de conceptualización abstracta del modelo de Ciudad Inteligente. En la revisión de la literatura se encontró realmente tres de este tipo de modelos que se presentan a continuación (Figuras 1, 2 y 3).

Figura 1: El modelo 1 - Elementos de una ciudad inteligente y sostenible
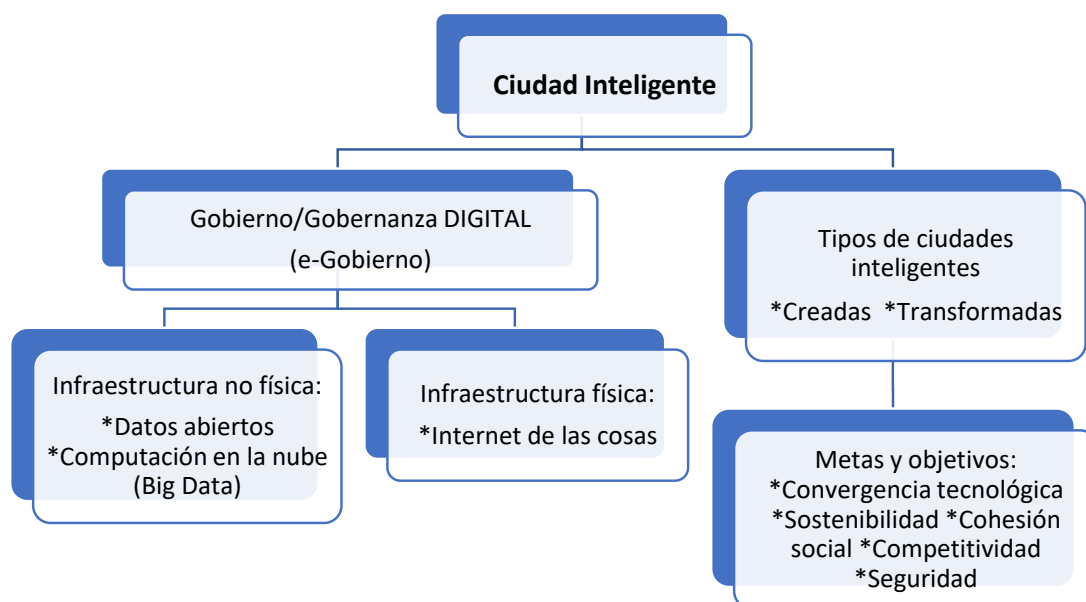
En el primero de los modelos presentados (Figura 1), es difícil encontrar alguna lógica fuera de probar de enumerar elementos de la ciudad inteligente, tipos de estas ciudades y sus metas y objetivos.

Figura 2: El modelo 2 - Arquitectura de una ciudad o territorio Inteligente
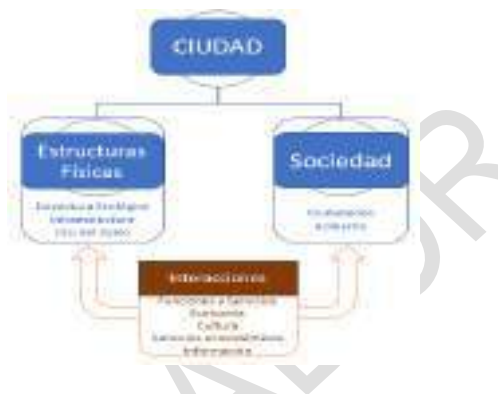
Fuente: Departamento Nacional de Planeación (2020: 18)

El segundo de los modelos (Figura 2) presenta los principales elementos conceptuales que son: las Estructuras físicas, la Sociedad y las interacciones entre ellos.

El tercero de los modelos (Figura 3) presenta la lógica bastante diferente ya que se trata de diseñar las etapas de implementación de la idea de Ciudad Inteligente en los países de América Latina.

Resumiendo, esta parte podemos decir que hay algunos avances en las pruebas de encontrar un modelo abstracto de Ciudad Inteligente en América Latina, sin embargo, como se puede observar en estos modelos el papel de tecnología es claramente secundario.

Figura 3: Modelo de la Ciudad Inteligente (CI) 3 –Escalable para los países emergentes

ETAPA 1: CI INCIPIENTE

Objetivos:

- Convergencia tecnológica

- Competitividad

- Seguridad

Actores básicos:

Lideres locales, ciudadanía y empresa

REDES SOCIALES

ETAPA 2: CI EN PROCESO

Objetivos:

- Convergencia social

- Convergencia tecnológica

- Competitividad

- Seguridad

Actores básicos:

Autoridades locales, lideres locales, ciudadanía y empresa

REDES SOCIALES

ETAPA 3: CI EN MADURACIÓN

Objetivos:

- Sustentabilidad

- Convergencia social

- Convergencia tecnológica

- Competitividad

- Seguridad

Actores básicos:

Autoridades centrales y locales, lideres locales, ciudadanía y empresa

----

REDES SOCIALES

Fuente: Rozga Luter y Hernández Mar (2020) con base en (Alvarado López, 2017), (Sikora-Fernández, 2017), (Stawasz y Sikora-Fernández, 2015) y (Colado García et. al., 2014).

Conclusiones

Si analizamos las urbes latinoamericanas que aparecen, primero, en los rankings de Ciudades Inteligentes (*Smart Cities*), debemos tener en cuenta que la mayoría de ellas (Buenos Aires, Santiago de Chile, Sao Paulo, Ciudad de México) son mega-metropolias de más de 10 millones de habitantes. Sin embargo, para muchos ideólogos de Smart Cities, las grandes «manchas» urbanas son la antítesis de la idea y valores de una Ciudad Inteligente.

En su camino hacia la a implementación de nuevas tecnologías las autoridades y los tomadores de decisiones de la política pública de las ciudades no siempre actúan de manera coordinada con la agenda nacional de innovación y los reguladores sectoriales. Esto puede responder, entre otras causas, a que poseen otra estructura de incentivos, alineamientos políticos divergentes, o simplemente, a que no comparten los objetivos.

Respondiendo a la pregunta de Introducción de este trabajo ¿si se puede hablar de un modelo latinoamericano de implementación de la de Ciudad Inteligente? Podemos decir que **no existe modelo latinoamericano de la ciudad inteligente y los diferentes países siguen diferentes pautas en la implementación de esta idea.**

En diferentes países latinoamericanos se usa el modelo general (de seis áreas) de la Ciudad Inteligente, así como se promueve diferentes propuestas de su implementación. En términos generales estos modelos podríamos caracterizar como modelos de implementación de las nuevas tecnologías para facilitar funcionamiento de las ciudades y mejorar la calidad de vida de sus ciudadanos. Por otro lado, en los modelos de implementación, lo que se busca es la gradualidad, que permite su mejor realización.

Resumiendo, se puede decir que Los primeros resultados muestran qué implementación del modelo de la ciudad inteligente en países de América Latina se lleva a cabo de manera bastante heterogénea realizada tanto por los gobiernos centrales, autoridades de ciudades grandes, pero también por las empresas abastecedores del equipamiento electrónico informático. Evidencias de eso son las formas de organización de difusión de la idea de la Ciudad Inteligente, así como promoción e implementación de la idea de parte de los organismos gubernamentales.

Bibliografía

Cabello, Sebastián (2022), El camino de desarrollo de las ciudades inteligentes Una evaluación de Bogotá, Buenos Aires, Ciudad de México y São Paulo, Documentos de Proyectos (LC/TS.2022/86), Santiago: Comisión Económica para América Latina y el Caribe (CEPAL).

Careño, Itzel (03.01.2020), "Brasil avanza con ciudades inteligentes a través del programa Pró-Cidades", DPL News, Consultado el día 07.06.2022 en: https://dplnews.com/brasil-avanza-con-ciudades-inteligentes-a-traves-del-programa-pro-cidades/#:~:text=Brasil%20avanza%20con%20ciudades%20 inteligentes%20a%20través%20del,de%20reconocimiento%20facial%20para%20el%20área%20de%20seguridad.

Cohen, Boyd y Elizabeth Obediente (2014), Estudio "Ranking de Ciudades Inteligentes En Chile", Fundación País Digital, Universidad del desarrollo, (s/l), Consultado el día 05.06.2022 en: https://dg6223fhel5c2.cloudfront.net/PD/wp-content/uploads/2014/06/Ranking-Ciudades-Inteligentes-en-Chile.pdf

Departamento Nacional de Planeación (2020), "Documento de lineamientos de política de Ciudades Inteligentes, Versión Borrador", (04.09.2020), Departamento Nacional de Planeación, Gobierno de Colombia, Consultado el día 06.06.2022 en:

https://dnp.gov.co/DNPN/Documents/Borrador-Lineamientos-Ciudades-Inteligentes.pdf.

Espinoza, Felipe, (19.12.2018), "Chile anuncia el Plan Nacional de Ciudades Inteligentes", LA NETWORK, Consultado el día 05.06.2022 en: https://la.network/chile-anuncia-plan-nacional-de-ciudades-inteligentes/

X-Global Smart City Index 2021 (2021), Consultado en: https://asyparkgroup.com/studies/cities-of-the-future/en/ (2022-06-03)

Haddad, Michele (28.01.2022), "Ciudades inteligentes en Colombia", Diseño Web & Marketing Digital, Consultado el día 06.06.2022 en: https://internetedadinero.com/ciudades-inteligentes-en-colombia/

X-IMD Smart City Index, 2020. City Performance Overview, (2021), Consultado en: https://www.imd.org/smart-city-observatory/home/#_book (2022-06-03).

X-Índice IESE Cities in Motion 2020, (2020), ISE Business School University of Navarra, Consultado en: https://media.iese.edu/research/pdfs/ST-0542.pdf, (2022-06-03).

Ministerio de Tecnologías de las Informaciones y las Comunicaciones, (2021) "Índice de Ciudades y Territorios Inteligentes, 2021", MinTIC, Gobierno de Colombia, Consultado el día 06.06.2022 en: https://gobiernodigital.mintic.gov.co/portal/Iniciativas/Ciudades-y-Territorios-Inteligentes/

Nieves Lahaba, Yadira Rosario (2018). "Ciudades inteligentes, una oportunidad para la ciencia de la información." CIENCIA UANL.21(92), pp. 30-35. doi.org/10.29105/cienciauanl21.92-2

Observatorio de Sistema de Ciudades, DNP, (septiembre 2020), "Indice de Ciudades Modernas, 2019", Observatorio de Sistema de Ciudades, Departamento Nacional de Planeación, Gobierno de Colombia, Consultado el día 06.06.2022 en: ttps://colaboracion.dnp.gov.co/CDT/Prensa/IIndice_Ciudades_Modernas_2019.pdf.

Palacio Cortés, Catalina, (2019), "Estrategia argentina de Ciudades Inteligentes", (s/l), Dirección de Investigación, Innovación y Control, Subsecretaría País Digital, Secretaría de Modernización de la Nación, Presidencia de la Nación, Consultado el día 03.06.2022 en: https://www.argentina.gob.ar/sites/default/files/estrategia_argentina_de_ciudades_inteligentes.pdf.

Ranking Connected Smart Cities, (2021), Urban Systemas, NECTA, Consultado el día 29. 05. 2022. en: https://ranking.connectedsmartcities.com.br/sobre-o-ranking.php.

Requena, Carlos, (2016), *CiudadMX 360. Modelo de ciudad inteligente*, LID Editorial Mexicana, México D.F.

Se constituye AMECI, la Asociación Mexicana de Ciudades Inteligentes, (22.02.2016), eSmart City. Es. Todo sobre Ciudades Inteligentes, Consultado el día 06.06.2022 en: https://www.esmartcity.es/2016/02/22/se-constituye-ameci-asociacion-mexicana-ciudades-inteligentes#:~:text=La%20Asociación% 20Mexicana%20de%20Ciudades%20Inteligentes%20%28AMECI%29%20es,la%2 0movilidad%20y%20el%20capital%20humano%2C%20entre%20otros.

Tridia. Ingeniería y Eficiencia. Revista Electrónica (2022) "¿Cuál es la situación de las Smart Cities en Argentina?", Consultado en: https://ingenieriayeficiencia.com/smart-cities-en-argentina/ (2022-06-03)

Unidad de Ciudades Inteligentes, Ministerio de Transportes y Comunicaciones, Gobierno de Chile (2022), Consultado el día 05.06.2022 en: https://www.mtt.gob.cl/pyd/unidad-de-ciudades-inteligentes

Methodology for watermills localization: A case study of Soria province (Spain)

Jesús Bachiller Martínez [1], Alberto Redondo Plaza [1 [0000-0002-2109-5614]], Ana María Barrena Medina [1], Lilian Johanna Obregón [1], Héctor Felipe Mateo Romero [1 [0000-0002-5569-3532]], Lidia Sanz Molina [1], Susana Gómez Redondo [1], Víctor Alonso Gómez [1 [0000-0001-5107-4892]] and Luis Hernández Callejo [1 [0000-0002-8822-2948]]

[1] University of Valladolid, Spain
J.B.M. jesusmaria.bachiller@uva.es
A.R.P. alberredon@gmail.com
A.M.B.M. anamaria.barrena@uva.es
L.J.O. liliancitaobregon@gmail.com
H.F.M.R. hectorfelipe.mateo@uva.es
L.S.M. lidia.sanz.molina@uva.es
S.G.R. susana.gomezr@uva.es
V.A.G. victor.alonso.gomez@uva.es
L.H.C. luis.hernandez.callejo@uva.es

Abstract: Watermills have played an important role in the ancient industrial development. The invention of the steam engine and later the electric motor together the electricity price reduction, gave rise to the abandonment of most watermills. It is estimated that more than 350,000 watermills existed in Europe at one time or another. These infrastructures have low water head and low power configuration. So, the watermills restoration may be an attractive solution for micro-mini hydropower application. This paper shows the methodology implement in a project whose aim is the localization of the different ancient watermills located in Soria, a province of Spain with 10,306 km^2. The choose of several sources has been one of the project keys since it has allowed a complete watermills localization. Ignoring duplicate information in the several sources used, the present methodology has allowed the identification of 1,265 potential watermills. This assumes a density of 123 watermills per 1.000 km^2. The current project status is at an early stage and future work will involve field work that allow to create datasheets about the watermill and identify duplicate information between the several analysed sources.

Keywords: Watermill, Micro hydropower.

1   Introduction: Watermill overview

Rivers and streams have been significant impact in the human history of technology and economics. The watermill has played a significant role in the European industrialism from the Late Middle Ages [1]. Not only has the watermill probably been the first mover in the human hand, but also the oldest turbomachine. Moreover, these devices

had a great territorial diffusion, being used by the Roman, Egyptian, and Greek civilizations among others [1].

A watermill is a device that converts the potential energy of the water into mechanical energy which can be used in order to mill grain into flour (gristmills), oil extraction (oil mills), cloth production (fulling, cotton mills and textile mills), paper production (paper mills) or cut timber into lumber (sawmills). The appearance and diffusion of watermills represented a great advance in the ancient industrial processes. For example, a mill moved by two persons could produce 5 kg of flour per hour while a typical low head gristmill exceeded 100 kg of flour per hour [2].

Watermill is not a uniform concept. There are several kinds of watermill because each one has been designed contingent on orography, water head and water flow. However, watermill can be classified in two main types, according to the relative position of the water wheel: horizontal axis water wheels and vertical axis water wheels [3]. The main feature of the horizontal axis wheel relies on the rotation mainly under the action of the gravity of the water. Three types of wheels can be found among horizontal axis water wheels (see Fig.1.). The choice of wheel depends on the conditions of the place: water head and water flow mainly. Overshot wheels fit with a low water flow and a high-water head while undershot wheels are ideal for low water head and a high-water flow. Breastshot wheels are variant of undershot wheels that can improve the device efficiency.
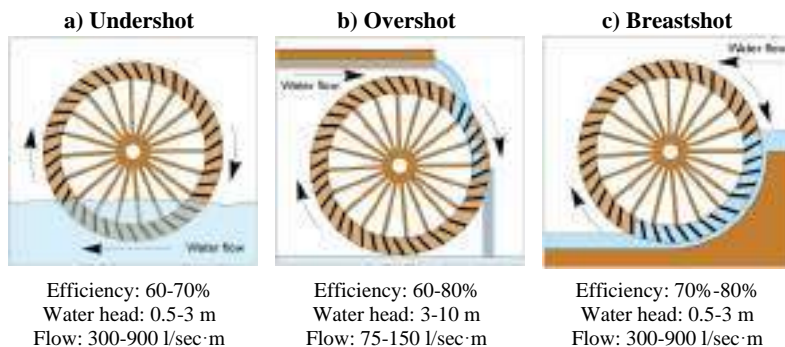
a) Undershot	b) Overshot	c) Breastshot

Efficiency: 60-70%	Efficiency: 60-80%	Efficiency: 70%-80%
Water head: 0.5-3 m	Water head: 3-10 m	Water head: 0.5-3 m
Flow: 300-900 l/sec·m	Flow: 75-150 l/sec·m	Flow: 300-900 l/sec·m

Fig. 1. Types of horizontal axis water wheels [1], [3].

Horizontal axis water wheel was the first wheels used in the ancient watermills. Later, technological development gave rise to vertical axis water wheels, devices that shows more similarities to modern water turbines. This water wheels have a higher efficiency and a great diffusion through the Mediterranean area [1]. Most Spanish watermills, that were mostly built during the first half of the 20th century, have a vertical axis water wheel configuration [4], [5].

To the pioneers of water-milling, the water supply was not a problem. The real challenge was how to control the water in order to achieve the highest possible efficiency.

Initially, the water wheels were fixed in river or brooks flow at specific level. Nevertheless, this is not the most optimal configuration because the water level tends to rise in winter and early spring and drop in summer and early autumn. Moreover, it is impossible to stop the water wheel for repairs. The derivation of a mill race from a natural watercourse allow to protect the water wheel from to high water levels. This also allow to control the water flow through the mill race using a sluice-gat. Secondly, weirs could be built in other to raise the water level and achieve the enough water head for an optimal water wheel performance. An example of a vertical waterwheel configuration is shown below (see. Fig. 2.).
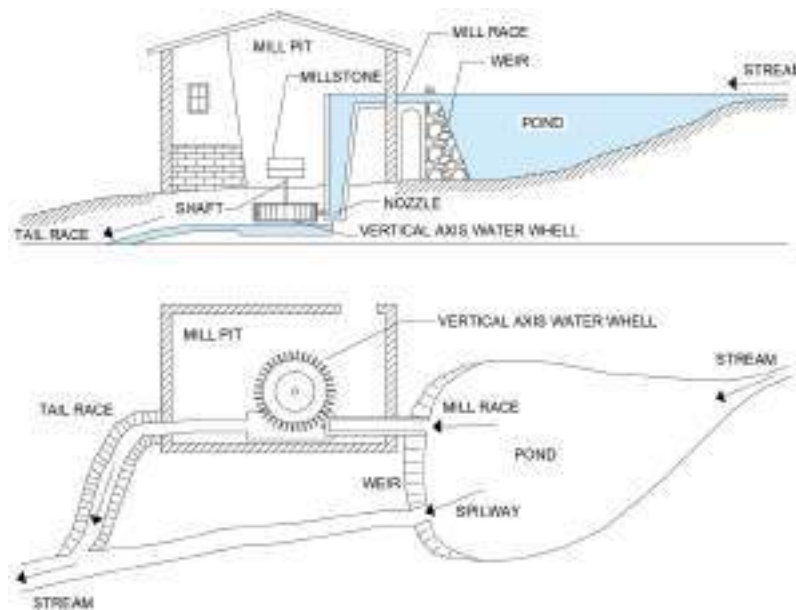

Fig. 2. Vertical axis waterwheel mill configuration.

It is estimated that more than 350,000 watermills may have exist in Europe at one time or another [3]. Most watermill were abandoned due to several reason like the changes in streams water flows. Furthermore, the invention of the steam engine and later the electric motor together low prices of electricity, explain the watermill abandonment. However, some spots were adapted to produce electrical energy.

These ancient watermills have a great potential for hydropower generation. Most watermill are low water head with potentials below 40 kW [6]. Gristmills for flour production, one of the most common artefacts within watermills, had an average 3 kW power [3]. These low water head and power configuration fits perfectly with micro-mini hydropower generation. Low head micro-hydropower stations present an attrac-

tive and efficient way for electricity generation in rural and remotes areas [7]. In addition, there are turbines designed specifically for low water head and water flow configurations such as Turgo, crossflow, Kaplan, Francis, or Archimedes screw turbine [7].

The ancient watermills restoration for micro-mini hydropower applications could be an attractive way for a clean and cheap electricity generation and recovering industrial heritage at once. Ancient watermills restoration for hydropower applications has other advantages such as the promotion of distributed generation or the electrical generation in isolated areas of the grid [8]. Micro-mini hydropower turbines installation in ancient watermills involves a cost reduction because watermills have already part of the civil works built. This is interesting because civil works are 40% of the levelized cost of energy (LCEO) in micro-mini hydraulic power stations [7]. Nevertheless, watermills restoration presents several challenges. First, heritage issues must be considered. Secondly, the rivers flow decrease in last years may make it unfeasible the hydropower exploitation in the smallest streams. Finally, each spots requires a different design of the generation and control system in function of the water head, water flow, terrain orography or heritage considerations.

Historical and non-powered weirs or dams could also be an attractive solution for micro-mini hydropower generation [9], [10]. Many of the monetary costs and environmental impacts of weirs have already been incurred at non-powered weirs, so adding power to the existing weir structure can often be achieved at lower cost, with less risk, and in a shorter timeframe than development requiring new weir construction.

RESTOR Hydro [11] is a project whose aim is to increase the renewable energy production from micro-mini hydropower, by identifying and restoring suitable historical watermills, weirs, or inoperative hydropower stations. RESTOR Hydro database contains 67,500 potential micro-mini hydropower sites in the European Union. Nonetheless, some countries such as Spain have a low density of potential hydro sites. It evidences the low-quality database of these countries and show the challenge of identifying historic watermills in large tracts of land.

This paper explains the methodology used in a project whose purpose is to locate watermills in the province of Soria. The second paper section show an overview of Soria province and its hydrological configuration. The third section present the implemented methodology while the fourth section show the first result of the research. Finally, the conclusion and futures work are presented in the fifth section.

2   Soria province

The province of Soria is located at the northeastern end of the Spanish plateau (see Fig. 3). Its physiognomy resembles a great natural amphitheatre between the Iberian Mountain Range, to the north and northeast, and a series of mountainous thresholds -appendages of the Central System- to the south. This arrangement configures the structure of its river network [12]. The province sits on the headwaters of two basins: one wider, the Duero, and another in a border arch that runs from northeast to southeast, which drains into the Ebro River (see Fig. 3.). This river system irrigates a territory of more than 10,000 km^2, with a large area traditionally dedicated to the cultivation of cereals.

The source of the Duero River is located in Urbión peaks, at 2,100 m altitude. It runs through the mountainous region of Pinares heading east and changes path around Soria city, heading west through the sedimentary basin in the interior of the province. Its head runs between mountains of high rainfall, which allow a contribution of de rains and snowy. In this first section it receives several tributaries that collect the waters of large sub-basins. On the left bank, the Revinuesa, Tera and Merdancho; on the right bank, the Ebrillos. In the central section, flatter and with less power source, it receives on the left bank the rivers that descend from some outer mountain ranges of the Ibérica and from the moorlands of the south. The rivers Rituerto, Escalote, Talegones, Caracena and Pedro stand out. On the right bank, also with its source in some outer mountains, the Izana, Fuentepinilla and, above all, the Ucero river stand out.

The rivers that descend to the Ebro basin along the eastern slopes of the Iberian peaks are short and steep. To the northeast, the headwater sections of the Cidacos, Mayor, Alhama and Queiles rivers stand out. To the southeast appears a somewhat larger sub-basin, that of the Jalón River, which has two important tributaries, the Henar and the Nágima.
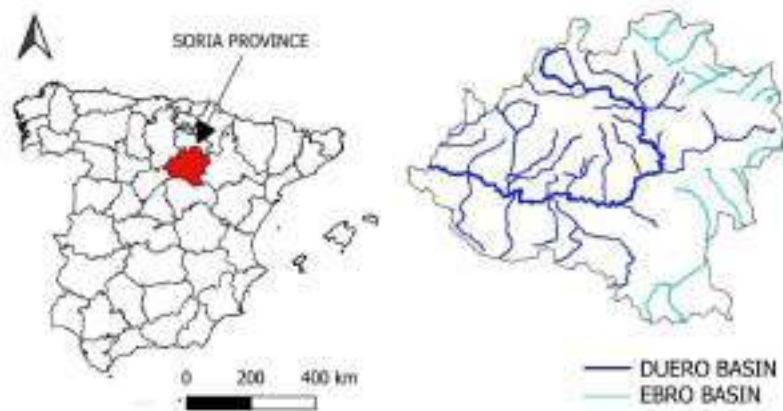
Fig. 3. Soria province location at Spain and Soria province hydrologic configuration. [13]

3   Methodology

The project is in an early stage. Although the sources searching is done, most of the performance that involves field labours have not been carried out yet. The project called "Infrastructure network for milling and other uses in Soria province rivers" (RIOS-SO) aim to search and localize all the ancient watermills in the Soria province ($10,306 \text{ km}^2$) for futures applications such as the watermill restoration for hydropower applications.

The methodology that has been used in the current project is schematized bellow (see Fig. 4.).

Fig. 4. Flow diagram of the watermill localization methodology used.

The methodology starts with the sources searching. Here, different sources have been identified.
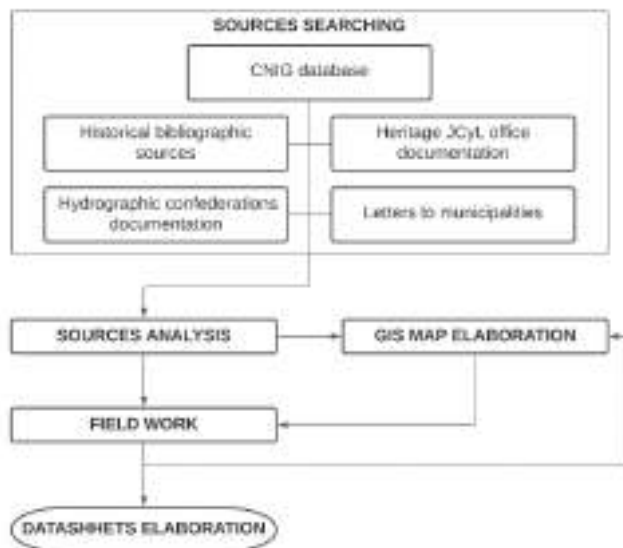
- "CNIG" database: "CNIG" is the geographic information national centre in Spain. This centre has a watermill database throughout the territory of Spain.
- Historical bibliographic sources: different historical sources have been used for the water mill localization. Among them we find the following ones.
  - Madoz: It is a statistical dictionary that was carried out between 1835 and 1850.
  - 1910 document: a document about the industrial infrastructures in Soria in 1910 has been found.
- Hydrographic confederation documentation: both hydrographic confederations have ancient itineraries that were carried out during the S. XIX. These itineraries were done in the main rivers of Soria province and show the kilometric point of different artifacts along the rivers.
- Heritage JCyL office documentation: a study about the industrial heritage in Soria have been found. The study has a database that show information about several industrial infrastructures like gristmills, sawmills, or fullings.

- Letters to municipalities: Soria is a province divided into 183 municipalities. Letters to each municipality have been send in order to identify persons that know about the existence of watermill in their respective municipalities.

After sources searching it is needed a proper sources analysis that allows to distinguish infrastructures of interest. Moreover, in some cases, sources analysis enables to identify data duplication in different sources.

Geographical coordinates of the watermills identified and located are added to a GIS map together the watermill main features such us stream or river in which it is situated, state of conservation, type of infrastructure and (gristmill, sawmill, fulling, power station and other). So, it is created a database that are able to collect all the information achieved.

On the one hand, some sources have geographic information that allows to create a GIS map where watermills are localized. This watermill localization allows to arrange the field work to visit watermills. On the other hand, other sources do not allow direct localization. So, it is needed a previous field work for the watermill localization on the GIS map. Before each field work it is important to identify all the potential watermills of the nearby area that is going to be visited. This makes easier the location of watermills that sources do not provide their coordinates. Tours of riverbeds, oral sources with local people and drone flights will play an important role in order to locale these watermills.

Finally, field work allows to collect information about the watermill for completing the GIS map database and creating datasheets. These datasheets collect deeper details about the watermills like machinery description, year of construction, history of the watermill and pictures of the watermill elements among others.

4   Results

After the sources analysis many potential watermills spots have been identified. Table 1 shows the several sources used and the number of watermills identified. Moreover, each source provides different data that help in the watermill localization. Some sources like CNIG database or JCyL Industrial Heritage study provide the exact coordinates where the watermills are place. Secondly, rivers itineraries just provide the name of the river and the kilometric point where the watermills are places. This allow a partial localization because it has been detected significant errors in the kilometric points. Finally, historical sources just show the river or the village where the watermills were place. In this case, direct watermills localization is impossible and even more field and researching work is required for the emplacement.

Table 1. Watermills identified by sources.

Source	Number of watermills	Geographic information about watermills
1910 document	358	River and village
Madoz document	279	Village
JCyL Industrial heritage study	134	Coordinates
Duero rivers itineraries	310	River and kilometric point
Ebro rivers itineraries	66	River and kilometric point
CNIG database	97	Coordinates
Letters to municipalities	21*	-

* A few municipalities been contacted so far. So, an increase in the number of watermills is expected.

A total 1,265 potential watermills have been identified among the several sources analysed. However, it is needed a further analysis and field works that allow to eliminate all the duplicate information and a proper localization. The status of the GIS map that place all the watermills located is shown in the Fig. 5. Field work will allow to improve the GIS map and locate new watermills.
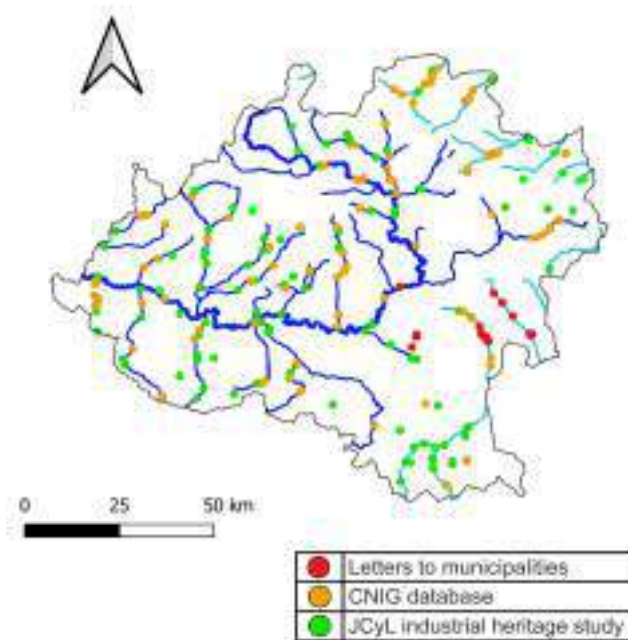

Fig. 5. GIS map of watermills located in Soria province. [13]

As mentioned in the introduction, there are several types of watermills. The Fig. 6. shows the different types of infrastructures identified. The most common by far are the gristmill, followed by fullings and sawmills. The study has also identified some ancient hydropower stations. In fact, some of these hydropower stations were ancient gristmills that were adapted for electricity production. Finally, other infrastructures such as textiles mills, flour factories or other kind of water wheels.
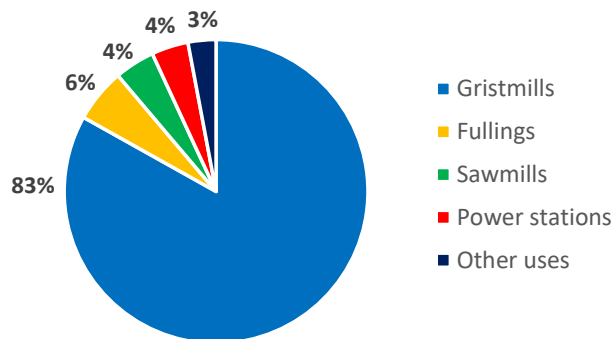

Fig. 6. Types of infrastructures identified.

5   Conclusions and future work

Watermill localization could be a great challenge in those studies whose aim is to analyse a large land extension. The methodology shown in this paper has allowed the identification of a large number of watermills in a total land of 10,306 km^2. The first project phase has identified a total of 1,265 potential watermills sites before duplicate information checking. It assumes a density of 123 watermills per 1,000 km^2. The most common infrastructure identified are the gristmills, followed by fullings, sawmills and power stations. Restoring these watermills and powers stations could be an attractive solution for micro-hydropower applications and heritage recovery.

Although there is duplicate or triplicate information in the several sources analysed, each one present information about some watermills that cannot be identified with the rest of the sources. Indeed, choosing a wide variety of sources allows a correct and complete watermills identification.

The sources analysis will allow arranging the field work. Future works will involve different visits in order to collect data about watermills already located. Moreover, field works will play an important role to localize watermills whose coordinates do not appear in the used sources. The result of the project will be a database that collet datasheets about all the watermills in Soria province. These study results will play a key role for different issues that could revive local and rural economies:

— Identify potential sites for micro-mini hydropower applications.
— Restore ancient watermills for other uses such as rural hotels, restaurants, or museums.
— Create tourist routes in those river and areas with a large number of well-preserved mills.

Acknowledgment

This study has been supported by "Cátedra de Agenda Urbana 2030 para Desarrollo Local" and "Ayuntamiento de Soria".

We would like to thank "Conferación Hidrografica del Duero", "Confederación hidrográfica del Ebro"and "Junta de Castilla y León" for the collaboration and help given.

References

[1] *Handbook of Ancient Water Technology*, Örjan Wikander., vol. 2. Brill, 2021. doi: 10.1163/9789004473829.

[2] G. Morís Menéndez -Valdés, "INGENIOS HIDRÁULICOS HISTÓRICOS MOLINOS, BATANES Y PERRERÍAS," 1995. [Online]. Available: http://iwaponline.com/IA/article-pdf/2/4/25/576316/ia19952685.pdf

[3] "Small and Micro Hydropower Restoration Handbook," 2014. Accessed: Sep. 19, 2022. [Online]. Available: http://www.restor-hydro.eu/

[4] J. I. Rojas-Sola and R. López-García, "Engineering graphics and watermills: Ancient technology in Spain," *Renew Energy*, vol. 32, no. 12, pp. 2019–2033, Oct. 2007, doi: 10.1016/j.renene.2006.10.013.

[5] T. Pujol, J. Solà, L. Montoro, and M. Pelegrí, "Hydraulic performance of an ancient Spanish watermill," *Renew Energy*, vol. 35, no. 2, pp. 387–396, Feb. 2010, doi: 10.1016/j.renene.2009.03.033.

[6] P. Punys, A. Kvaraciejus, A. Dumbrauskas, L. Šilinis, and B. Popa, "An assessment of micro-hydropower potential at historic watermill, weir, and non-powered dam sites in selected EU countries," *Renew Energy*, vol. 133, pp. 1108–1123, Apr. 2019, doi: 10.1016/j.renene.2018.10.086.

[7] A. H. Elbatran, O. B. Yaakob, Y. M. Ahmed, and H. M. Shabara, "Operation, performance and economic analysis of low head micro-hydropower turbines for rural and remote areas: A review," *Renewable and Sustainable Energy Reviews*, vol. 43. Elsevier Ltd, pp. 40–50, 2015. doi: 10.1016/j.rser.2014.11.045.

[8] R. C. Sharma, Y. Bisht, R. Sharma, and D. Singh, "Gharats (watermills): Indigenous device for sustainable development of renewable hydro-energy in Uttrakhand Himalayas," *Renew Energy*, vol. 33, no. 10, pp. 2199–2206, Oct. 2008, doi: 10.1016/j.renene.2007.12.023.

[9] A. Gagliano, G. M. Tina, F. Nocera, and F. Patania, "Technical and economic perspective for repowering of micro hydro power plants: A case study of an early XX century power plant," in *Energy Procedia*, 2014, vol. 62, pp. 512–521. doi: 10.1016/j.egypro.2014.12.413.

[10]   B. Hadjerioua, Y. Wei, and S.-C. Kao, "An Assessment of Energy Potential at Non-Powered Dams in the United States Report," 2012. [Online]. Available: http://www.osti.gov/contact.html

[11]   "Micro HydroPower in Europe." https://www.restor-hydro.eu/en/ (accessed Sep. 20, 2022).

[12]   J. Pala Bastaras, *Análisis del Medio Físico de Soria*. Junta de Castilla y León. Consejería de fomento, 1988.

[13]   "BTN 2021 CC-BY 4.0 INSTITUTO GEOGRÁFICO NACIONAL."

Clustering Analysis of Solar Photovoltaic Electricity Generation at CIC-IPN in North of Mexico City

P.J. Escamilla-Ambrosio [0000-0003-3772-3651], R. Alcaraz-Fraga[2], G.L. Martínez-Luna [0000-0002-0105-1112], M.G. Pulido-Navarro, J.H. Sossa-Azuela [0000-0002-0521-4898]

Centro de Investigación en Computación, Instituto Politécnico Nacional, Ciudad de México 07738, Mexico
pescamilla@cic.ipn.mx

Abstract. In this work, clustering of daily photovoltaic production profiles registered in a photovoltaic installation located at CIC-IPN in north of Mexico City was carried out. Data was collected for a period of 14 months, with a sampling frequency of 5 min. The electricity production profiles were grouped into four different categories using the k-means clustering algorithm, implemented in Python. Clustering was performed considering two options: the first one considers the daily production profile, while the second one considers summary statistics obtained from daily photovoltaic production, irradiance, module temperature, and ambient temperature. Clustering can help to better understand the state of the installation and classify the electricity production behavior at a specific site trough the months of a year. This in turns can be used to train more complex algorithms with the aim of making predictions of the energy production from solar photovoltaic plants.

Keywords: Photovoltaic production profile, Clustering algorithm, Energy generation, Solar photovoltaic.

1   Introduction

Solar photovoltaic (SPV) is a type of power generation that directly converts light into electrical energy using solar panels. Due to the cost reduction of solar panels and their increase of power generation efficiency, SPV electricity generation is attracting attention as one of the renewable energy sources that can replace existing fossil fuel-based power generation.

   Data clustering of power generation profiles of SPV plants is becoming increasingly popular because it allows to characterize SPV systems at a specific site without extensive analysis and simulation. Furthermore, clustering is considered as the first stage for reliable SPV power generation prediction. In this paper, clustering of SPV production profiles data, registered from a SPV installation located at Centro de Investigación en Computación, Instituto Politécnico Nacional (CIC-IPN) in north of Mexico City, is presented. Data was collected for a period of 14 months, with a sampling frequency of 5

min. The classification was performed considering two options; the first one considers the daily production profile, while the second one considers summary statistics obtained from photovoltaic production, irradiance, module temperature, and ambient temperature. SPV production data are classified into clusters by the k-means clustering algorithm. The remaining of the paper is organized as follows, Section 2 presents related research on SPV data clustering and production analysis; Section 3 presents the SPV plant from which data was collected; Section 4 presents the results of applying k-means clustering to the collected SPV data; finally, Section 5 presents the conclusion and future work.

2　　Related work

Nowadays green power generation, such as SPV is becoming of great interest. Nevertheless, there are some points to be considered when it comes to generate energy by this means and get connected to the grid. One problem is that solar photovoltaic generation is not constant; therefore, there is the need for a reliable photovoltaic power prediction, where clustering analysis is a first step. The authors in [1] propose a clustering analysis, which enhances the accuracy of the prediction model of RBF (Radial Basis Function) photovoltaic power. The method is divided into time series analysis method, artificial neural networks, support vector machine, etc. Then, meteorological information is fed to the RBF and the back propagation (BP) neural network in order to predict the photovoltaic power generation. Although the method is quite accurate there are still some issues that need to be considered, for example, improve data processing, strengthening clusters analysis and enhancing extraction modes.

In [2] the authors search and propose a new methodology to classify data of off grid solar energy. They analyzed the curves of the voltage and current obtained from a photovoltaic station formed of 24 solar panels for three years in order to understand the behavior of the energy obtained. They classified 5 types of situations which led to a better understanding of the solar station to develop robust prediction algorithms. For the study the authors divided the day into two, daytime taken as charge, and the discharge when there were no generation or sunlight. And instead of processing the whole curves that were produced during the day they took seven curves' characteristics to train the algorithm. For pattern recognition, cluster search and database visualization, SOM (Self Organized Maps) was used.

Prediction of solar radiation is quite important for photovoltaic power generation. In [3] the authors propose the use of neural networks to model such prediction. The robustness of the neural network depends on the type of data obtained from the photovoltaic network study. Then, the type of data used to train the neural network is important as well as the way this data is processed. Pre-processing and dividing the data gives a better approximation model. To pre-process the data usually clustering is used for training a neural network. In their work, the authors proposed a prediction model for soiled photovoltaic modules, as it was observed that dust on the panels may lead to power loss

of up to 30%. They considered soil characteristics such as physical, chemical, or spectral properties and used specialized data processing techniques to improve the accuracy of prediction.

Connecting photovoltaic power into the electrical grid requires an accurate analysis and simulation as the power output fluctuation may have negative effects to the grid. In the work presented in [4], the ideal number of clusters for photovoltaic power patterns data is determined that would achieve the best results. Here, a combination of conventional clustering algorithms and bio-inspired optimization clustering algorithms was presented. Clustering of photovoltaic power patterns is realized by utilizing a pattern recognition methodology on historical data such as irradiance and ambient temperature for a couple of years.

Trying to predict solar radiation for photovoltaic power generation brings about the big problem that even small changes in weather conditions really affect radiation. That is why modelling forecasting is so important and will help in the determination of the best possible number of clusters. First, time forecasting is divided into different conditions so modelling can be applied to specific environments, at this point two processes are required: clustering and classification. Clustering (unsupervised process) consists in characterize and label the types of each time period in the training data. Classification (supervised process) identifies the category of a time period in the forecasting stage. In [5] the authors propose an enhanced solar data clustering, pattern recognition and forecasting learning abilities simultaneously for an accurate weather forecasting. A clustering method is developed that only uses global horizontal radiance. After that, pattern recognition identifies the cluster to which a forecasting day belongs with first few hour's data. Finally, a two-layer machine learning based multimodel forecasting framework is developed to strengthen learning abilities for the machine learning models.

3   Solar Photovoltaic Electricity Generation Data Clustering

In this section, the solar photovoltaic electricity generation plant installed at CIC-IPN is described, along with the electricity generation data that have been obtained since the activation of the SPV plant. Afterwards, data clustering of the collected data is performed and the results obtained are presented.

3.1   Solar Photovoltaic Plant

The data used were obtained from the solar photovoltaic (SPV) electricity generation plant installed at CIC-IPN [6], located in north Mexico City, 19° 30' 11.1" North-latitude, 99° 08' 52.1" West-longitude at 2,243 m altitude, see Fig.1. The SPV plant has 186 solar panels (Canadian Solar CS3U), connected to three inverters (each Fronius Symo, 22.7 kW) with a maximum power capacity of 66.96 kW.

Fig. 1. SPV electricity generation plant installed at CIC-IPN.

3.2 SPV Data

Data collected from this SPV plant includes several parameters, but the ones used in this research include photovoltaic production (Wh), irradiance (W/m^2), ambient temperature (°C), and panel temperature (°C). There are data corresponding to 14 months, from April 2021 to May 2022, sampled every 5 minutes. Fig. 2 shows the plot of the values corresponding to the daily photovoltaic production (Wh), daily irradiance (W/m^2), daily average ambient temperature (°C), and daily average panel temperature (°C).
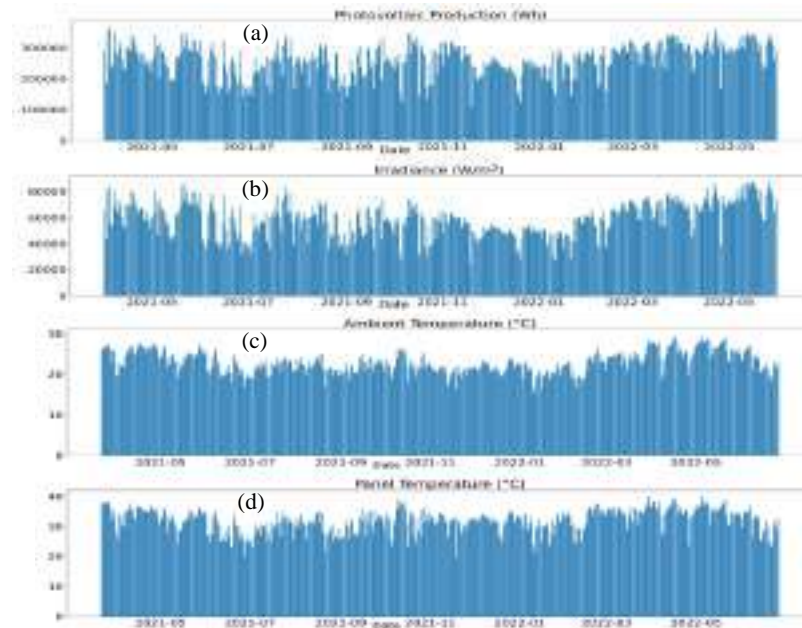
Fig. 2. Plots of (a) daily Photovoltaic Production (Wh), (b) daily Irradiance (W/m^2), (c) daily average Ambient Temperature (°C), and (d) daily average Panel Temperture (°C).

For a clear sky day, the photovoltaic production has a pattern as the shown in Fig. 3, this pattern changes depending if a given day is clear, cloudy or rainy. Hence, a first intuitive analysis is to average the photovoltaic production profile of every month, the resulting averaged production profiles are shown in Fig. 4.

Fig. 3. Hourly distribution of photovoltaic production for the day 27/05/2022.

Fig. 4. Daily photovoltaic production profile averaged by month for a year.

From Fig. 3, can be deduced that, depending on the month and the season of the year, the production profiles change. Hence, clustering algorithms can be applied to explore if effectively there are profiles that can be grouped together and if they correspond to a determined season of the year. This is performed in the next section.
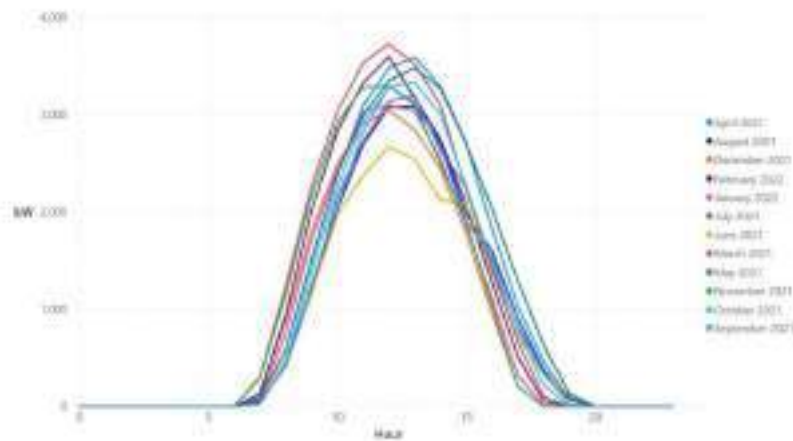
4   Clustering analysis

In this section the k-means clustering algorithm is applied to the collected SPV data. Clustering is performed considering two scenarios, the first one applies the k-means clustering algorithm to the data points of daily photovoltaic production (the daily production profiles, considered as vectors with 288 elements for every day, see Section 4.2). The second case applies k-means clustering to summary statistics of daily photovoltaic production, irradiance, ambient temperature, and panel temperature.

4.1   K-means Clustering Algorithm

One of the most popular unsupervised learning algorithms that solve the well-known clustering problem is the k-means clustering algorithm [7]. Let $\mathbf{X} = \{x_1,\ldots, x_n\}$ be a data set in a d-dimensional Euclidean space $\mathbb{R}^d$. Let $A = \{a_1,\ldots, a_n\}$ be the c cluster centers. Let $z = [z_{ik}]_{n \times c}$, where z_{ik} is a binary variable (i.e. $z_{ik} \in \{0, 1\}$) indicating if the data point x_i belongs to k-th cluster, $k = 1,\ldots, c$. The k-means objective function is $J(z, A) = \sum_{i=1}^n \sum_{k=1}^c z_{ik} \|x_i - a_k\|^2$. The k-means algorithm is iterated through necessary conditions for minimizing the k-means objective function $J(z, A)$ with updating equations for cluster centers and memberships, respectively, as:

$$a_k = \frac{\sum_{i=1}^n z_{ik} x_{ij}}{\sum_{i=1}^n z_{ik}} \qquad \text{and} \tag{1}$$

$$z_{ik} = \begin{cases} 1 & if \ \|x_i - a_i\|^2 = \min_{1 \leq k \leq c} \|x_i - a_i\|^2 \\ 0 & otherwise \end{cases} \tag{2}$$

where $\|x_i - a_k\|$ is the Euclidean distance between the data point x_i and the cluster centre a_k.

There exists a difficult problem in k-means, i.e., the number of clusters, the k, needs to be defined a priori. To solve this problem, the elbow method [8] is usually used to select the best k. The elbow method calculates the squared difference of different k values. The performance of the algorithm is calculated for different numbers of centroids and the percentage of variance is explained as a function of the number of clusters. Hence, a number of clusters is chosen so that adding another cluster does not give much better modelling of the data. The percentage of variance explained by the clusters is plotted against the number of clusters. The first clusters will add much information, but at some point, the marginal gain will drop dramatically and will produce an angle in the graph. The correct "k" i.e., the number of clusters, is chosen at this point, from here is the "elbow criterion".

Hence, in the next subsections the k-means clustering algorithm is applied considering the two cases explained before and using the elbow criterion to determine the optimum number of clusters.

4.2   Clustering Using Daily Production Profiles

To cluster daily production profiles, it was verified that the data points for every day have the same number of points. This was done by comparing the data length of all days, observing that the length is 288, which corresponds to the sample rate of 5 minutes. It is important to notice that at the start and at the end of the day all production values drop to 0, as can be verified in Fig. 3. Anyway, the 288 points of photovoltaic production for every day were considered for clustering purposes. Therefore, the k-means clustering algorithm was applied to the data. The optimum number of clusters was determined using the elbow method, from which the values obtained are shown in Fig. 5. As can be seen, according to this method, the optimum number of clusters is 4.
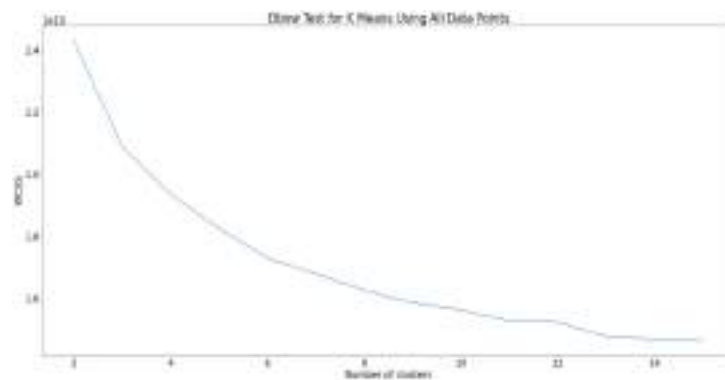
Fig. 5. Elbow method applied to choose the number of clusters for daily photovoltaic production profiles.

Once the k-means clustering algorithm has been applied, and considered the 4 clusters determined by the elbow method, the histogram of daily photovoltaic production profiles for each one of the four clusters is shown in Fig. 6. As can be seen in the figure, cluster 1 is the one with most daily production profiles, while cluster 0 is the one with less daily production profiles. To verify this, a plot with all the production profiles for every one of the clusters is presented in Fig. 7.

Fig. 6. Histogram of daily photovoltaic production profiles for each one of the four clusters.
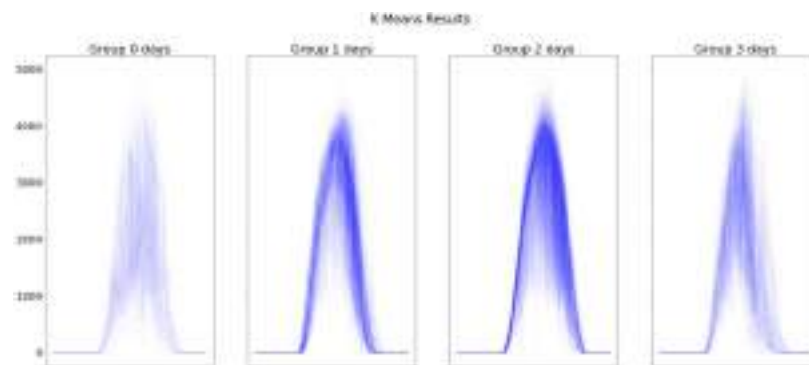
Fig. 7. Plot of all the daily production profiles among the four groups obtained.

From Figs. 6 and 7, it seems that the groups correspond to each one of the four seasons of the year. To investigate this, the cluster distribution by date of daily photovoltaic production was plot, as shown in Fig. 8. Furthermore, Fig. 9 shows the distribution of daily photovoltaic production profiles according with the cluster at which each daily production profile has been grouped and the season of the year.

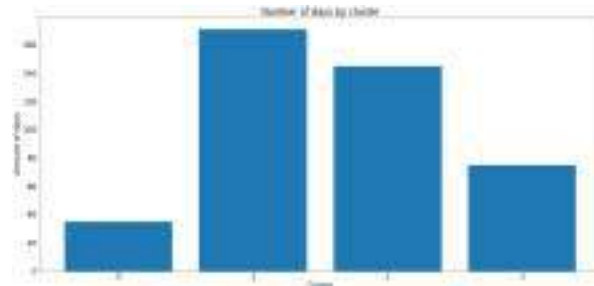From Figs. 8 and 9, it seems clear that at least two groups are clearly defined, the first one, marked in green color corresponding to cluster group 2, concentrate the daily production profiles corresponding to spring; while the second one, marked in purple color corresponding to cluster group 1, concentrate the daily production profiles corresponding to winter. For the other seasons, it seems that autumn tends to have similar production profiles than winter; however, summer contains profiles from all the groups. In what respects to daily production, it is clear that the days with higher production were grouped in clusters 1 and 2; while the days with lesser production were grouped in clusters 0 and 3. However, it seems that group 0 contains the profiles with the least production, which by the patter of the daily profile, see Fig. 7, seems to correspond to rainy or cloudy days.
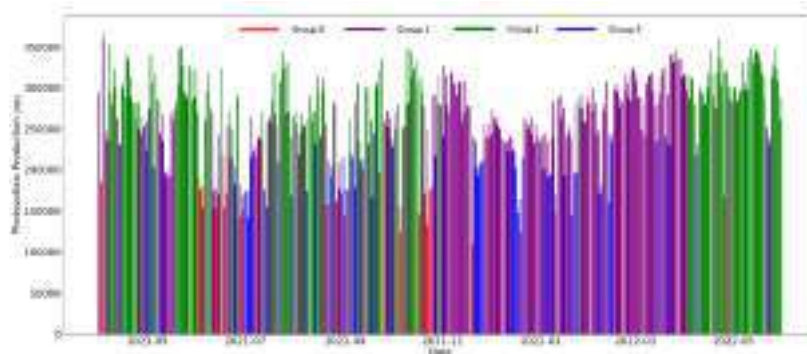
Fig. 8. Cluster distribution by date of daily photovoltaic production.
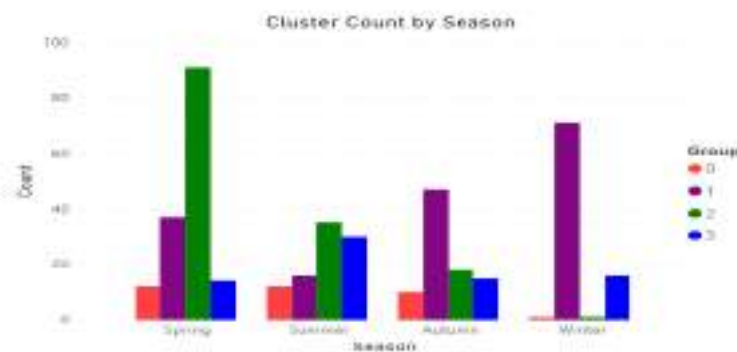
Fig. 9. Distribution of daily photovoltaic production profiles according to clusters and seasons.

4.3   Clustering Using Summary Statistics of Photovoltaic Production

The summary statistics used correspond to the variables photovoltaic production (Wh), irradiance (W/m^2), ambient temperature (°C), and panel temperature (°C); and the statistics used are the mean, median, standard deviation, and daily totals for each variable.

Conceptually, it makes sense to have three clusters to cluster the days into categories like High Production, Medium Production, and Low Production. However, using the elbow method to find the optimum number of clusters, four clusters were obtained, see Fig. 10, similar to the number of clusters for the previous case.

The clustering algorithm was performed on the summary statistics to group them into four clusters. Fig. 11 shows the histogram of daily photovoltaic production profiles for each one of the four clusters. Fig. 12 shows the plot of all the daily production profiles among the four groups obtained. Fig. 13 shows the cluster distribution by date of daily photovoltaic production profiles. Finally, Fig. 14 shows the distribution of daily

photovoltaic production profiles according with the cluster at which each daily production profile has been grouped and the season of the year.

From Figs. 12 and 13, as suspected, clustering based on the statistic of the data has produced four groups from higher production, cluster 2, followed by cluster 3, followed by cluster 0, to lower production, cluster 1. From Figs. 13 and 14, it seems that in this case there is not a clear relationship between the clusters and the seasons. However, again it is clear that the days with higher production are in the spring season. Also, in this case cluster 1, seems to contain the days rainy or cloudy, whit the lower production per day.
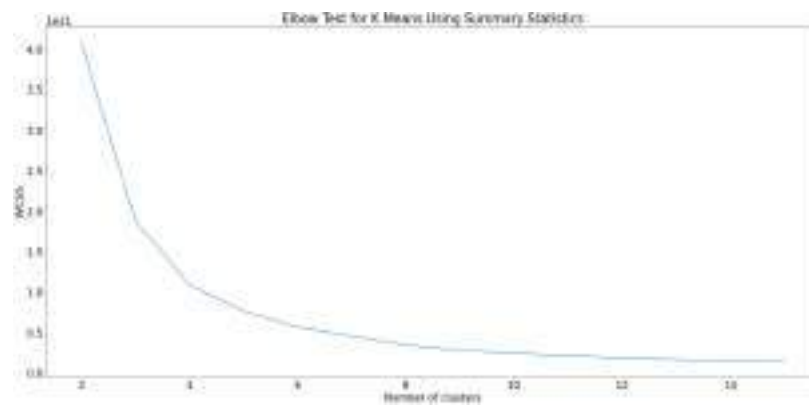
Fig. 10. Elbow method applied to choose the number of clusters for summary statistics.
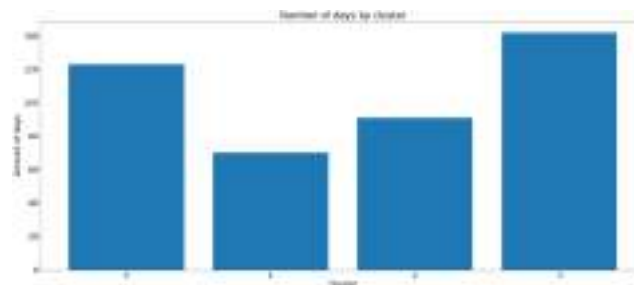
Fig. 11. Histogram of daily photovoltaic production profiles for each one of the four clusters using summary statistics.
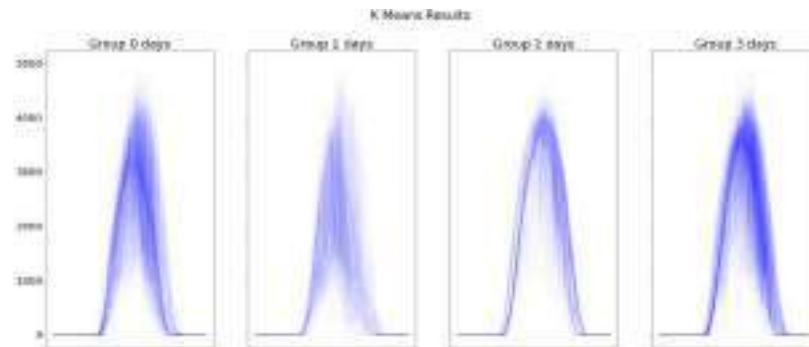
Fig. 12. Plot of all the daily production profiles among the four groups obtained from summary statistics.
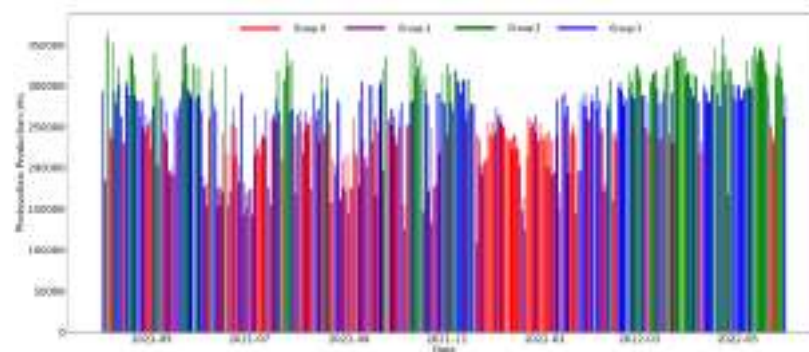
Fig. 13. Cluster distribution by date of daily photovoltaic production (clustering summary statistics).

To evaluate the separation between clusters in each of the two cases presented, the Davis-Bouldin index was used [7]. The lower the score the better the clusters are defined. For the first case, clustering of the daily production profiles, the score obtained was 1.6866. For the second case, clustering of the summary statistics, the score was 0.5374. Hence, although the clusters for the second case are better determined, these do not have a clear relationship with the season of the year.
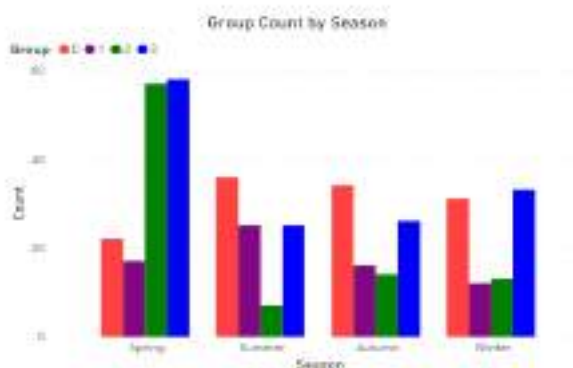
Fig. 14. Distribution of daily photovoltaic production profiles according to clusters and seasons (clustering summary statistics).

5   Conclusions and Future Work

In this work, a first approach to applying k-means clustering to data collected from the SPV plant installed at CIC-IPN in north Mexico City, is presented. The data used include photovoltaic production, irradiance, ambient temperature, and panel temperature. K-means clustering was performed considering two cases. In the first case, the daily photovoltaic production profiles were grouped. In the second case, summary statistics of daily photovoltaic production, irradiance, ambient temperature, and panel temperature were grouped.

For the first case, it was found that two of the clusters seem to correspond to the seasons of spring (cluster 2) and winter (cluster 1). For the other clusters, it seems that autumn tends to have similar production profiles than winter; however, summer contains profiles from all the clusters. Clusters 1 and 2 clearly contain the days with higher production, while cluster 0 contains the profiles with the least production, and seems to correspond to rainy (or cloudy) days.

For the second case, it was not found that the clusters correspond to the seasons of the year. However, the clusters are better defined, as the Davis-Bouldin idex showed. The clusters produced in this case clearly formed groups corresponding to higher to lower photovoltaic production, higher production corresponds to cluster 2, followed by cluster 3, followed by cluster 0, to lower production corresponding to cluster 1.

In the two cases considered here, two groups are clearly distinguished from the others, the one with correspond to profiles of higher photovoltaic production and the one which corresponds to the lower photovoltaic production.

Future work includes using the k-means clustering results into a scheme to perform predictions of photovoltaic production, for which neural and deep neural networks are going to be compared. Furthermore, other clustering methods will be applied to the data, for example, fuzzy C-means.

References

1. Si J., Cai Y., Wang Y., Liu H., Song W., Liu Q., Su X., and Ren J. "Piecewise Clustering Prediction Model of Distributed Photovoltaic Power Based on Principal Component Analysis", 2021 IEEE IAS Industrial and Commercial Power System Asia, pp. 437-443, July 2021.

2. Sanz-Gorrachategui P., Pastor-Flores A., Guillén-Asensio J.S., Artal-Sevil A., Bono-Nuez B., Martín-del-Brío C., and Bernal-Ruiz C. "Unsupervised clustering of battery waveforms in off grid PV installations", 2020 Fifteenth International Conference on Ecological Vehicles and Renewable Energies (EVER).

3. Pulipaka S. and Kumar R. "Power prediction of soiled PV module with neural networks using hybrid data clustering and division techniques", Solar Energy vol. 133 (2016), pp. 485–500.

4. Munshi A. and Mohamed Y. "Photovoltaic power pattern clustering based on conventional and swarm clustering methods", Solar Energy vol. 124 (2016), pp. 39–56.

5. Feng C., Cui M., Hodge B., Lu S., Hamann H. and Zhang J. "Unsupervised Clustering-Based Short-Term Solar Forecasting", IEEE Transactions on Sustainable Energy, vol. 10, no. 4, October 2019.

6. Escamilla-Ambrosio, P. J., Ramírez-Salinas, M. A., Espinosa-Sosa, O., Gallegos-García, G., Morales-Olea, M., & Hernández-Callejo, L. IPN sustainability program: solar photovoltaic electricity generation and consumption reduction. In Ibero-American Congress of Smart Cities, pp. 109-120., Springer, Cham (2019).

7. Sinaga, K. P., & Yang, M. S.: Unsupervised K-means clustering algorithm. IEEE Access 8, 80716-80727 (2020).

8. Bholowalia, P. and Kumar, A.: EBK-means: A clustering technique based on elbow method and k-means in WSN. International Journal of Computer Applications 105(9), 17-24 (2014).

9. Davies, David L., and Donald W. Bouldin.: A cluster separation measure. IEEE transactions on pattern analysis and machine intelligence 2, 224-227 (1979).

LEVELS OF SULFUR EMITTED IN THE PORT OF GUAYAQUIL AND ITS ATMOSPHERIC CONCENTRATION

Olga Quevedo[1] [0000-0002-0250-9228], Franklin López[2] [0000-0002-0645-1756], Sandra Ronquillo[3] [0000-0002-9048-8454], Freddy Espinoza[4] y Fernando Rodríguez[5].

University of Guayaquil, Faculty of Chemical Engineering Delta Av. and Kennedy Av. Guayaquil - Ecuador [1,2,3.]

olga.quevedop@ug.edu.ec

Armada del Ecuador, Dirección Nacional de Espacios Acuáticos Calle Malecón Simón Bolívar e Illingworth, Guayaquil - Ecuador [4 y5]

Abstract. Emissions from the smokestacks of the different types of shipping transport at the port level are closely linked to the ambient air quality in the areas of influence to the ports, and also to the aquatic ecosystems. The objective of this study is to demonstrate the potential concentrations of sulfur emitted by ships from burned diesel oil, and the presence of atmospheric sulfur in the ports of Guayaquil. Results are presented from the calculation of sulfur emissions and atmospheric sulfur using passive samplers during the period 2018 - 2019. The study consisted of analyzing databases from the Maritime and Port Information Management System (SIGMAP) and applying the Atmospheric Pollutant Emissions guide, in addition to the collection of 208 data from 16 sampled sites, categorized as urban, industrial and protected natural areas, in the area of influence of the Port of Guayaquil. The data were analyzed with a simple one-way Anova and the Kruskal-Wallis test for hypothesis testing with a p-value of 0.05. The sulfur concentrations emitted by the ships ranged from 297.14 to 976.77 kg, with the tugboats contributing the most pollution. The sulfur present in the atmosphere ranges from 52 - 172 mg/L, which is related to meteorological conditions such as winds and rain; during the dry season, the highest concentration is 211.6 mg/L as sulfate ion. Emissions of gases from shipping vessels are data obtained in real time from the port of Guayaquil by fuel consumed.

Keywords: plum ship, diesel oil, sulfur.

1   INTRODUCTION

Worldwide, commercial maritime transport is generally recognized as the most widely used mode of international trade and accounts for 90% [1], being one of the main causes of pollution both as a route of entry of harmful substances into the oceans and as a source of air pollution [2].

In maritime transport, two types of fuels are mainly used, diesel oil and fuel oil, with the use of gas oil being limited to fast, low-power engines for electric power generation and recreational vessels; the latter are vessels dedicated to pleasure trips. Additionally, it is considered that the type of fuel consumed is 80% fuel oil and 20% diesel oil [3].

Greenhouse gas (GHG) emissions, originating from the different transport systems on a global scale, are subdivided as follows: Land transport (11.9 %) derived from gasoline and diesel consumption: which includes cars, trucks, motorcycles and buses. Aviation (1.9 %) are emissions from passenger and freight air transport, and domestic and international aviation. Maritime transport (1.7 %), due to fuel consumption in ships [4].

With the objective of reducing air pollution generated by ships in mind, the International Maritime Organization (IMO), through the Marine Environment Protection Committee (MEPC), amends Annex VI of the MARPOL Convention and introduces a new maximum limit, expressed as a percentage by mass, for sulfur content in marine fuel oil. This new value reduces the sulfur content to 0.50% by mass for ships operating outside designated emission control areas [5].

Sulfur oxide is a colorless and non-flammable gas, with a strong and irritating odor, under normal conditions it is $6\text{-}112 \times 10^6$, its half-life in the atmosphere is about 2 to 4 days, but it remains in the atmosphere for up to 13 days, where it is converted into secondary pollutant gases such as SO_4H_2, and practically half of these emissions are re-deposited on the surface, while others are transformed into sulfate ions. With time in contact with air and humidity, it is converted into sulfur trioxide which is soluble in water forming an acidic solution [6].

Sulfur oxides are a group of gaseous compounds recognized by the problems of environmental pollution, the affectation to human health are linked to the quality of life of people and ecosystems, the latter in the case of the oceans, the acidification processes are caused by sulfuric acid that is present in the atmosphere as the main strong acid and is largely neutralized by the gaseous phase of ammonium that passes to the aqueous phase in the form of ammonium ions (NH4 +) [7]. One of the many reasons for its concentration is related to port emissions from the chimneys of ships, which do not comply with the use of filters or a cleaning system that is standardized by the countries where they operate [8].

Studies carried out by [9] analyzed the effects on the quality of the mangrove forest surrounding the port of Guayaquil, showing that there is a close relationship between sulfur concentrations in Kg/ha/year and photosynthetic pigments, including proteins. Greenhouse gases are related to the global warming of the earth and how water-soluble organic matter aerosols (WSOM) are key in the role of climate [10], i.e. they influenced the increase in temperature by approximately 0.6°C between 1850 and 2000 [11].

The increase in global maritime traffic, the opening of new shipping lines with emerging countries, such as China and India, and short sea shipping through the Nordic region have led to an increase in emissions of pollutants to Europe. This emission of toxic gases causes problems such as acid rain, increased causes of the greenhouse effect and more elements that deplete the ozone layer [12].

The majority of NOx, SOx, and particulate matter emissions in the coastal areas of the EU (European Union) are emitted by ships with a cargo capacity exceeding 500 GRT (Gross Registered Tonnage), of which about 45% of the emissions are from ships flying flags of EU countries and about 20% of the emissions are within 12 miles of territorial waters. It should be noted that the gas emitted by ships can travel hundreds of kilometers, so even in areas where the city and/or land on the coast is not accessible, it can cause air quality problems [12].

Greenhouse gases are elements generated from anthropogenic activities, one of them is SO2 in normal conditions is $6\text{-}112 \times 10^6$, and is maintained for 6 to 13 days in the atmosphere, where it is converted into secondary pollutant gases such as SO_4H_2, one of the many reasons for its concentration is linked to the emissions of port origin from the chimneys of ships, which do not comply with the use of filters or a cleaning system, which is regulated in the country where they dock [8].

The Port of Guayaquil is on the border of the city of the same name, in the estuary of the Guayas River and the distance to the exit to the Pacific Ocean is approximately 150 km. It began operations in 1958, and is considered the most important port of Ecuador for the approximate cargo volume of six hundred thousand tons. [13], 85% corresponds to containers with bulk products in general (solids and liquids), registering a total of 2583 shipments by 2019, and tourist cruises, Guayaquil Port Authority [14].

According to data from the Directorate of Maritime Traffic Control of the APG, public and private termini-nals in the port of Guayaquil received 231 ships of different types in November 2019 [14]. The concentrations of sulfur emissions generated by diesel oil-burning ships docking at the Port of Gua-yaquil have not been studied, nor how it influences the health of the surrounding populations. The diversification of port operations impacts the environment to different degrees, such as prolonged fumes with high concentrations of gases, particles, and soot, as well as the presence of particulate matter in the port areas, to which port personnel are exposed. These fumes can cause respiratory problems and skin problems that in many cases can be irreversible [15].

The main objective of this research is to analyze the contributions of sulfur to the atmosphere from the burning of fuel oil burned by ships and the existing contributions in urban areas around the Port of Guayaquil, in the period 2018-2019.

2   Methodology

2.1   Study area

The study area comprised 18282 ha of the city of Guayaquil, within six urban parishes in the south, northwest and northeast, influenced by anthropogenic activities such as industries, shipping transportation, and motor vehicles, which border the Estero Salado [16] and Santay Island [17] Protected Natural Areas, in the study are considered as the control or witness, since it is within the city. (Fig. 1).
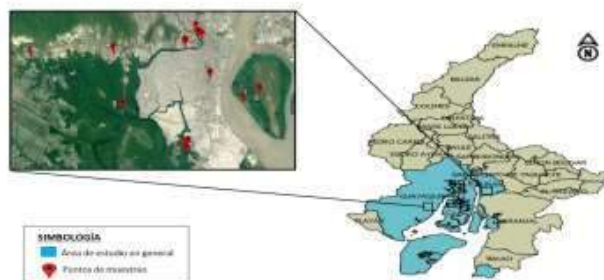
Fig. 1. Study area in the city of Guayaquil.

2.2   Research Design

The method is composed of two parts: the first consisted of placing passive samplers in areas with the highest vehicular, shipping, and industrial activity in the city of Guayaquil and in nearby places such as Cantón Durán. The passive samplers are used to determine the sulfate ions present in the atmosphere and are useful for both the dry and rainy seasons; they are placed in open places without interruption of adjacent buildings, roofs or vegetation, for 22 to 30 days, they are changed and replaced, in total 16 samplers were placed during 13 months from April 2018 to May 2019, a total of 208 samples were obtained (Table 1).

Table 1. Geographical location of study sites

Samples	Land use	Sites	Sulfur	East (X)**	North (Y)
1		3 Bocas	x	6157558	97535508
2	Shipping	Pto. Guayaquil	x	6219745	97478440
3	industry	Trinipuerto	x	6208584	97500126
4		COGUAR	x	6195417	97487390
5		Centro cívico	x	6230208	97555852
6		Chongón	x	6024519	97533016
7	Vehicular landyard	San Eduardo	x	6191502	97583086
8		Inst. Invest. UG	x	6220198	97592057
9		Cenest Harvard	x	6122010	97588200
10		El Recreo	x	6335901	97598993
11		Eva Adriana	x	6084713	97576688
12		Terra Nostra	x	6110796	97583124
13	City	Floresta	x	6231947	97499716
14		Acacias	x	6219133	97545263
15		Primavera 1	x	6291116	97611544
16	Control	Isla Santay y El Salado*	x	6270231	97542720

* Protected natural areas ** Southern hemisphere Zone 17

The second stage consisted of tabulating the information on fuel consumed contained in the Maritime and Port Information Management System (SIGMAP) provided by the National Directorate of Aquatic Spaces (DIRNEA) of the National Navy of Ecuador, information that contains data on the amount of fuel consumed, Gross Registered Tonnage (GRT) of the ships, distances traveled, port of departure and arrival, which was tabulated in an Excel spreadsheet.

2.3   Passive samplers

Los muestreadores pasivos o througfall (trampas de caída) [18] su ventaja es que pueden ser usados por largos periodos de tiempo, son de bajo costo porque utilizan materiales que pueden ser fácilmente remplazados en campo, su número por áreas hace factible caracterizar patrones espaciales [19], [20], [21].

2.4   Determination of sulfur concentration

The [22] presents to the NMX-AA-074-1981 standard, the samplers are suspended previously in a universal support, previously the glass wool is extracted from the upper part of the tube, to which a tube of 30 cm is coupled, and the valve is closed. It is poured 100 ml of distilled water, and it is left to rest for 20 minutes, then the valve is opened so that the washing water flows at a speed of two drops per second for 10 minutes, this water of the first washing is discarded. The second wash is added 100 ml of ClK2N (149.1 gauged to 1 liter) for 10 minutes, the valve is opened slightly so that the speed of dripping is of two drops per second until it comes out all, a volume of approximately 100 ml is collected in polyethylene bottles and they are refrigerated until their analysis. The stock solution is used to calculate the calibration curve whose R2 value was 0.9813.

2.5   Conditioning solution

For sulfur determination, 50 ml of glycerol is mixed with a solution containing 30 ml of concentrated hydrochloric acid, 300 ml of water, 100 ml of 95% ethyl or isopropyl alcohol and 75 g of sodium chloride, barium chloride (ClBa) in crystals and the sulfate standard solution (NMX-AA-074-1981).

In the THERMO spectrophotometer model Genesys 10 UV, in a quartz cuvette, 3 ml of the following solution are read: 40 ml of the washed solution and 2 ml of the conditioning solution, which is placed in a magnetic stirrer, once it begins to stir, a teaspoon with crystals of ClBa is poured in 1 minute.

reading should be made in the spectrophotometer at 30-second intervals for 4 minutes at 420 nm.

Quantification is done by mathematical methods where they are expressed using equations:

$$y\left(SO_4^{2-}\right) = [a(\lambda) - a]/b \quad \textbf{(1)}$$

b: corresponds to slope.
a: origin.
$\boldsymbol{\alpha(\lambda)}$**:** Absorbance reading of sulfate ion samples at wavelength λ.
y γ(SO4 2-): Concentration of sulfate ion expressed in mg/L of SO4 2-.

For the estimation of reservoir flows, it involves established variables and basic volumetric equations.

Aliquot value
Sulfate concentration
Funnel area
Exposure period
Equations:

$$\text{Mass concentration} = \text{Abs} * \text{alicuota} = \text{mg} * \left(1\text{E}^{-6}\frac{\text{kg}}{\text{mg}}\right) = [\text{kg}]$$

$$\text{Area} = (\pi * r^2) = \text{cm}^2 * \left(1\text{E}^{-8}\frac{\text{ha}}{\text{cm}^2}\right) = [ha]$$

$$\text{Exposure time} = \text{period} = [\text{years}]$$

$$\text{Flux} = \frac{\text{Concentration}}{\text{area} * \text{period}} = \left[\frac{\text{kg}}{\text{Ha year}}\right]$$

2.6   Sulfur determination in diesel oil fuel

The SIGMAP tabulation corresponding to the 2018 - 2019 study period, the fuel consumption by ships was determined which were classified by GRT (Gross Registered Ton) weight, and tabulated with the Air Pollutant Emission Inventory Guidelines (EMEP/EEA) [23] for its acronym in English. The respective equations were applied to determine the sulfur content in grams per liter of fuel consumed. The sulfur concentration to be used is 3.5 ppm %mass, a regulatory value obtained from the regulations [24] Annex VI of the IMO. The sulfur concentration in ppm % mass was converted to mg/L to perform the necessary calculations.

Equations:

$$m = V * [\,] \qquad (2)$$

m = mass of pollutant in milligrams

V = volume of fuel consumed in liters

$[\,]$ = concentration of the solute

Conversion factors were used to arrive at required units.

$$m = V * \rho$$

mm = mass of fuel in kilograms

V = volume of fuel consumed in liters

ρ = density of fuel in kilograms per liter

$$E_i = \sum_m(FC_m * EF_{i,m}) \qquad (3)$$

E_i = pollutant emission in kilograms

FC_m = fuel mass

EF_{im} = emission factor for the pollutant in kilograms / tonne

m = fuel type

Equation 3 was obtained from EMEP/EEA, this standard also contains the specific emission factor for sulfur $20\ \frac{\text{kg}}{\text{tonn}}$, indicating that this value can be taken as a reference

for those countries where the inventory of atmospheric emissions has not yet been carried out or updated.

2.7   Statistic

To demonstrate the robustness of the data, they were examined by one-way analysis of variance (ANOVA), and significant differences between sampling sites, seasonality and, by land use, validated with the Kruskal, & Wallis 1987 test, with a confidence level of 95% ($p < 0.05$) using Statgraphic CENTURION XVI software. The whisker box was used to observe the dispersion of sulfur in the study area and by land use.

Results

The concentrations of sulfur emitted into the atmosphere at the Port of Guayaquil are related to the volume of diesel oil fuel burned by the ships, the highest values fluctuate between 297.14 to 976.77 kg of sulfur emitted. The analysis of sulfur in the atmosphere determined by passive samplers is related to the atmospheric conditions at that time, and the contribution of gases from other anthropogenic activities, thus proximal differences are marked between July, September and October with respect to the concentrations of 211.6; 145, 6; and 179, 6 mg / L respectively are the highest during the dry season, the lowest values coincide with the rainy season from January to May. (Table 2).

Table 2. Sulfur concentrations in diesel oil in the port of Guayaquil and its area of influence during 2018-2019.

Month	Fuel consumed (L)	(g) S in the fuel consumed	Sulfur emissions (Kg)	[ ] S in the atmosphere * (mg/L)
May	28.149,05	83,88	478,53	71,6
Jun	23.569,20	70,24	400,67	39,6
Jul	17.479,13	52,09	297,14	211,6
Ago.	21.407,96	63,8	363,93	65,6
Sep.	21.149,07	63,02	359,53	145,6
Oct	57.457,81	171,22	976,77	179,6
Nov	38.102,08	113,54	647,73	127
Dic	33.537,37	99,94	570,13	127
Ene	52.481,30	156,39	892,18	97
Feb	31.570,69	94,08	536,7	172
Mar	20.896,99	62,27	355,25	109,5

Abr	63.345,02	188,77	926,85	109,5
May	30.581,29	91,13	519,88	52

The atmospheric conditions related to rainfall for the study period between January - March 2019, in the case of rainfall were between the minimum and maximum ranges of 168.7 to 432.8 mm. (National Institute of Meteorology and Hydrology. 2011) The accumulated values presented by INAMHI relating to the INOCAR weather station have been considered because it is the closest to the Port of Guayaquil, the values for 2018 were only considered to present April and May for comparisons. (**Table 3**).

Table 3. Atmospheric conditions accumulated during the study periods.

	2018			**2019**		
	Factors			**Factors**		
	Wind (m)	**Rain (acumulada) mm**	**Tempe-rature ºC mín/ max**	**Wind (m)**	**Rain (accu-mulated) mm**	**Temperature ºC mín / max**
Jan				2-3 SW	168,7	23,3 – 32,9
Febr				2-2 SW	100,4	22,7 - 30,4
Mar				1-4 SW	316,3	23,8 - 32,2
April	1-3 SW	10,9	21,3 - 34,0	1-3 SW	2,6	22,2 – 34,4
May	1-3SW	55,3	21,3 – 31,6	1-3 SE	2,6	23,7-34,6

Source: (National Institute of Meteorology and Hydrology. 2018b; 2019a).

Sulfur emissions ranged from 130 kg to 210.7 kg for domestic transit vessels, as opposed to international vessels whose values ranged from 19.48 to 190.4 kg. The out-liers were recorded for the tugboats (GRT 3281), which are the most polluting.

Ships with GRT 3830 - 3999 produced the most sulfur emissions during 2018-2019 with 210.7 kg of sulfur emissions followed by Tier 2 GRT 490 - 3500 which emitted 190.48 kg. The ports of departure with the highest sulfur emissions are Guayaquil and Galapagos.
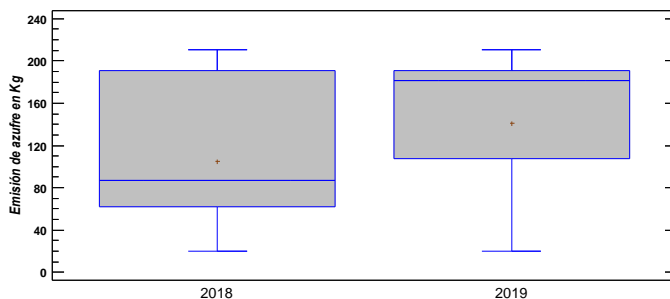
Fig 2. Sulfur emission in kg per diesel oil burned in the port of Guayaquil.

From the analysis of the medians with the Kruskal-Wallis test there is no statistically significant difference between the sulfur concentrations emitted in 2018 - 2019 by diesel oil burned by ships, their distribution is homo-generic in the study area since the P-value is greater than or equal to 0.05.
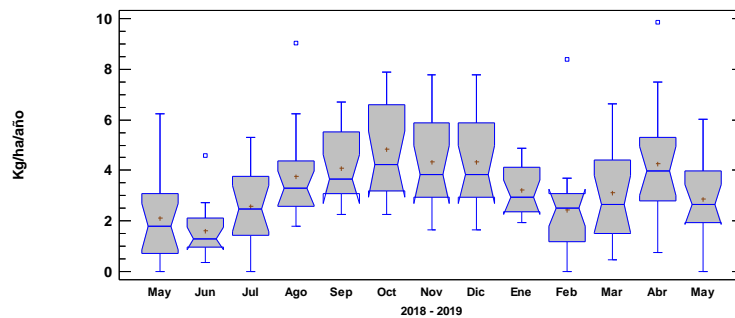
Fig. 3. Annual sulfur distribution in kg/ha/year period 2018 -2019.

From the analysis of the thirteen monthly data corresponding to the period 2018 - 2019 the means reflect statistically significant differences, since the P-value is less than 0.05; with a level of 95.0% confidence, with respect to the months of study, and the relationship with atmospheric conditions and land use, noting outlier data up to 10 kg/ha /year corresponding to the Port of Guayaquil (Figure 3).
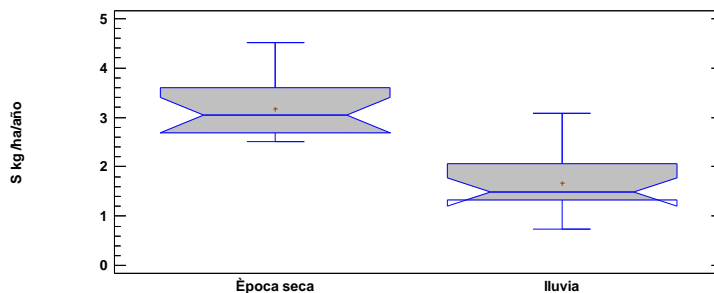
Fig. 4 Sulfur concentrations during dry and rainy seasons.

Sulfur concentrations during the dry season are higher than during the rainy season, showing differences between the medians with values of 3.0 to 1.5 kg/ha/year respectively in the city of Guayaquil during the study period (Figture 4).
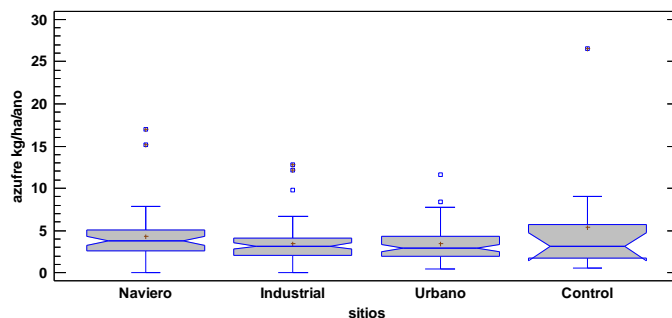
Fig. 5. Sulfur distribution categorized by land use.

With respect to land use, the sites that potentially contribute SO2 to the atmosphere were identified and categorized as shipping zone, industrial, urban and control (natural protected area), obtaining that the distribution of sulfur in these sites is homogeneous since there is no statistically significant difference between the medians, the p-value is 0.139 with a confidence level of 95.0% according to the Kruskal-Wallis test (Figture 5).

Discussion

The maritime activity during 2018-2019, presents moments in which there is higher fuel consumption with ranges of 63,345.02 - 52. 481.30 L, these as the most significant

and are not presented in any increasing or decreasing order, with respect to sulfur calculated in mg/L for the atmosphere, the highest concentrations are presented in the months when it does not rain, independent of the high com-fuel consumption that occurs in the rainy months; also the GRT, the distances traveled by the ships and the type of vessel.

The sulfur present in the exhaust gases derived from the burning of diesel oil depends entirely on its concentration in the fuel, the combustion of this compound is complete and much of the sulfur is released into the atmosphere as SO_2 and by continuing to react with the air continues to form sulfates causing much of the acid rain, the latter causes molecular reactions that affect mangrove forest ecosystems and infrastructure such as monuments or buildings [28].

Acid deposition in the port of Guayaquil responds to a regional distribution of SO_2, and is therefore related to sulfur concentrations in kg emitted by the burning of diesel oil from ships, as well as to the annual distribution in kg/ha/year of sulfur during the study period. [29] identified and prioritized interdisciplinary research at the air-ocean interface because of analyses of the impact of ships worldwide, data needed to improve understanding of the impact of stack gas emissions.

This study contributes to the port of Guayaquil for future studies and revisions of current regulations, as well as their enforcement, since concentrations affect the quality of life of people living near the port and the mangrove ecosystem on which the local economy depends.

The rules established by the IMO regarding the reduction of sulfur emissions in port centers and maritime traffic in general have not been fully implemented by the public authorities in the face of the global growth of maritime trade [30]. Even if the sulfur content of marine fuels is lowered without stricter oil control and release resolutions, emissions will more than double today's values by 2050, keeping pace with the growth in shipping traffic.

The International Plant Protection Convention (IPPC) indicates that the threshold for sulfur emissions is 150 tons in total per year, only for the Port of Gua-yaquil - Ecuador produced about seven tons of SO_x, one of the regulations imposed by the IMO to mitigate SO_x emissions is that from January 1, 2020 the concentration of sulfur must fall from 3.5 ppm to 0. 5 ppm, % mass/mass, a rule that does not yet apply in Ecuador because it has not complied with all the requirements necessary to become a signatory to MARPOL Annex VI.

Acknowledgments

References

[1] Ministerio de Defensa Nacional, "Marítimo." Dirección General Marítima, p. 20, 2019, [Online]. Available: https://www.dimar.mil.co/sites/default/files/informes/Brochuer de Transporte Maritimo 2019.pdf#:~:text=El Transporte Marítimoes una herramienta fundamental para la,a nivel mundial se transportan por vía marítima.

[2] B. Brito Mesa and Á. I. Hernández Alonso, "Implantación de la normativa IMO2020 y su consecuencia en los buques mercantes," 2020.

[3] P. Alarcón, "Movilidad urbana, consumo de energía y calidad del aire," *Let. Verdes, Rev. Latinoam. Estud. Socioambientales*, vol. 8, p. 3, 2011, doi: 10.17141/letrasverdes.8.2011.893.

[4] B. J. M. Recio, *calidad del aire y el cambio climático La movilidad urbana condicionada por la calidad del aire y el cambio climático*. Barcelona, 2021.

[5] Fundación de la Universidad de Oviedo. Grupo de Investigación del Transporte Marítimo., *Consumo de energía y emisiones asociadas al transporte por barco*, Grupo Gest., vol. 15. Grupo de Investigación del transporte marítimo de la Fundación Universidad de Oviedo., 2009.

[6] X. Querol, J. J. Ramasco, M. Viana, and T. Moreno, "Movilidad urbana y calidad del aire Urban mobility and air quality," *Bol. Grup. Españos Carbón*, vol. 58, no. 2, pp. 9–14, 2020, [Online]. Available: https://digital.csic.es/bitstream/10261/236203/1/BoletinGEC_058-art2.pdf.

[7] A. R. Baker *et al.*, "Changing atmospheric acidity as a modulator of nutrient deposition and ocean biogeochemistry," *Sci. Adv.*, vol. 7, no. 28, pp. 1–10, 2021, doi: 10.1126/sciadv.abd8800.

[8] F. Calderón and O. Quevedo, "Distribución espacial del azufre en la atmósfera del estuario interior del Golfo de Guayaquil, a partir de muestreadores pasivos (Fenn y Poth, 2004) Guayaquil, Ecuador," Mar. 2018. .

[9] O. Quevedo *et al.*, "Morphological responses of Rhizophora harrisonii by pollution in the main port zone of Guayaquil - Ecuador," *AIP Conf. Proc.*, vol. 1982, 2018, doi: 10.1063/1.5045429.

[10] R. M. B. O. Duarte, P. Duan, J. Mao, W. Chu, A. C. Duarte, and K. Schmidt-Rohr, "Exploring water-soluble organic aerosols structures in urban atmosphere using advanced solid-state 13C NMR spectroscopy," *Atmos. Environ.*, vol. 230, pp. 1–25, 2020, doi: 10.1016/j.atmosenv.2020.117503.

[11] Tillero Pintos María Laura, "Emisiones De Co 2 En el transporte marítimo," Universidad Pontificia ICADE Madrid, 2017.

[12] J. Egüen, "Estudio Técnico Del Cambio De Combustible Hsfo/Lsfo En Un Buque Petrolero Debido a Navegación En Zona Seca," Universidad de Cantabria, 2015.

[13]　J. Jiménez, "LA INDUSTRIA PORTUARIA Y EL IMPACTO AMBIENTAL," *AUTORIDAD PORTUARIA DE GUAYAQUIL*. Guayaquil.

[14]　APG, "El puerto de Guayaquil ha recibido 2.583 buques hasta noviembre de 2019 – Autoridad Portuaria de Guayaquil," *AUTORIDAD PORTUARIA DE GUAYAQUIL* . Guayaquil , 2019.

[15]　J. Zambrano, ""IDENTIFICACIÓN DE LA CONTAMINACIÓN ATMOSFERICA GENERADA POR BUQUES DE CARGA EN EL PUERTO DE GUAYAQUIL," Guayaquil, 2014.

[16]　Ministerio de Ambiente del Ecuador, *SUMARIO :* Ecuador, 2010, pp. 2–13.

[17]　Ministerio de Ambiente del Ecuador, *SUMARIO : Registro Oficial*. Ecuador, 2010, p. 2.

[18]　M. E. Fenn, M. A. Poth, S. L. Schilling, and D. B. Grainger, "Throughfall and fog deposition of nitrogen and sulfur at an N-limited and N-saturated site in the San Bernardino Mountains, southern California," *Can. J. For. Res.*, vol. 30, no. 9, pp. 1476–1488, 2000, doi: 10.1139/cjfr-30-9-1476.

[19]　M. E. Fenn, M. a. Poth, and M. J. Arbaugh, "A Throughfall Collection Method Using Mixed Bed Ion Exchange Resin Columns," *Sci. World J.*, vol. 2, pp. 122–130, 2002, doi: 10.1100/tsw.2002.84.

[20]　D. W. Clow, H. A. Roop, L. Nanus, M. E. Fenn, and G. A. Sexstone, "Spatial patterns of atmospheric deposition of nitrogen and sulfur using ion-exchange resin collectors in Rocky Mountain National Park, USA," *Atmos. Environ.*, vol. 101, pp. 149–157, 2015, doi: 10.1016/j.atmosenv.2014.11.027.

[21]　J. Cerón *et al.*, "Mapping temporal and spatial variation of sulphur and nitrogen deposition to a complex ecosystem in Campeche, Mexico," *WIT Trans. Ecol. Environ.*, vol. 203, no. Eid, pp. 113–123, 2016, doi: 10.2495/EID160111.

[22]　Secretaria de Comercio y Fomento Industrial, "NMX-AA-074-1981 'Análisis de agua-Determinación del ión sulfato'.," 1981.

[23]　N. Ole Kenneth, "EMEP/EEA air pollutant emission inventory guidebook 2019: Technical guidance to prepare national emission inventories," 2019. [Online]. Available: https://www.eea.europa.eu/publications/emep-eea-guidebook-2019.

[24]　O. M. I. Marpol, *Marpol 73/78 Edición refundida, 2002*, 3era ed. Londres: Organización Marítima Internacional, 2002.

[25]　W. & . A. W. Kruskal, "This Week ' s Citation Classic ® sE ~," *Am. Stat.*, vol. 5, pp. 583–621, 1987, [Online]. Available: http://garfield.library.upenn.edu/classics1987/A1987K083100001.pdf.

[26]　Instituto Nacional de Meteorología e Hidrologia., "Guía práctica para el cálculo de emisiones de gases de efecto invernadero (GEI)," 2011.

[27]　Instituto Nacional de Meteorología e Hidrologia., "ABRIL," 2018.

[28]　C. S. Ajiaco - Parra AC, Barrera - Barrera, "Origen, Acciòn y Daños causados por presencia de Sales en Materiales de Construcción," *In L`esprit Ingènieux.*, vol. 8, pp. 52–67, 2017.

[29]　S. Endres *et al.*, "A new perspective at the ship-air-sea-interface: The environmental impacts of exhaust gas scrubber discharge," *Front. Mar. Sci.*, vol. 5, no. APR, pp. 1–13, 2018, doi: 10.3389/fmars.2018.00139.

[30]   V. Eyring *et al.*, *Transport impacts on atmosphere and climate: Shipping*, vol. 44, no. 37. Elsevier Ltd, 2010.

Global energy balances for energy analysis in buildings

Carlos E. Torres-Aguilar[1][0000−0001−6187−4519],
Pedro Moreno-Bernal[2][0000−0002−2811−5331],
Jesús Xamán†[1], Sergio Nesmachnow[3][0000−0002−8146−4012], and
Luis Cisneros-Villalobos[2][0000−0002−9409−1374]

[1] Centro Nacional de Investigación y Desarrollo Tecnológico, México
carlos.torres17ma@cenidet.edu.mx
[2] Facultad de Ciencias Químicas e Ingeniería,
Universidad Autónoma del Estado de Morelos, México
{pmoreno,luis.cisneros}@uaem.mx
[3] Universidad de la República, Uruguay
sergion@fing.edu.uy

Abstract. This article presents a global energy balance solution for a one-dimension wall of multiple nodes in an unsteady state by diffusion in the context of energy efficiency and sustainability. The studied system considered Dirichlet boundary conditions. Experimental validation compares the proposed energy balance with an analytical solution reported in the literature. The main results indicate that the energy balance solution approximates the analytical solution in 6.81% when using a time step of 0.1s, and in 0.006% when using a time step of 0.0001s.

Keywords: Global energy balance, energy efficiency, thermal comfort in buildings

1 Introduction

Nowadays, human activities are related to energy production and consumption for economic and social interests. New advances in human welfare and societies have permitted the World population increases with considerable acceleration. According to the United Nations Department of Economic and Social Affairs, demographic growth expectations will increase from 7.7 billion in 2020 to 9.7 billion persons in 2050 [15]. The demographic growth implies an increase in electrical energy consumption for the following years. Exclusively, electrical energy consumption in the residential sector has been increasing over the years, mainly due to active refrigeration and air conditioning systems that provide thermal comfort to the interior. Recently, electrical energy consumption in the residential

---

This article is dedicated to the memory of our friend Jesús Perfecto Xamán Villaseñor (academically known as J. Xamán), who was the forerunner of this work.

sector was quantified at 27.1% of world energy consumption [7]. As an alternative to active systems, passive systems provide thermal comfort in buildings, in a sustainably and environmentally friendly manner [3,6,9,19].

The use of passive elements to provide thermal comfort in buildings positively has a positive impact on the reduction of the use of natural resources such as fossil fuels, which on the one hand are scarce resources and on the other hand are an important source of environmental pollution. Thermal comfort for buildings involves different physical processes, including solar radiation, thermophysical, optical, thermal, etc., which interact with the environment. For this reason, it is required to carry out energy analysis of the building through experimental or theoretical studies of its thermal behavior. Experimental analysis are recommended for tangibly studying the phenomena such as heat transfer and fluid mechanics that correspond to passive systems. Nevertheless, building scale models or mock-ups demands a considerable economic investment and time for development [13]. On the other hand, theoretical analysis implies mathematical modeling of the phenomena of interest. Theoretical analysis is performed through an analytical solution. The analytical or exact solution of the governing equations of the physical phenomenon under specific realistic boundary conditions is hard to determine, especially when complex mathematical models are needed to properly model realistic situations and problem instances. Therefore, an approximate solution permits addressing complex physical phenomenon models when the analytical solution is unknown or hard to determine.

Numerical methods allow addressing problems of fluid dynamics, heat transfer, and systems of partial differential equations when the analytical solution is complex to obtain due to real-life conditions or when it is not possible to fund ad-hoc experimental analysis [18]. Such physical phenomena are complex due to strong nonlinearity, complex geometry, sensitive fluid-property variations or complicated boundary conditions. However, numerical solution must be verified and validated to determine if the results represent the reality of the physical phenomenon. Occasionally, the mathematical model admits more than one numerical solution, and it is not easy to determine whether the numerical solution corresponds to reality. Hence, the verification can be performed through experimental analysis, the analytical solution of the mathematical model, or by comparing some theoretical solutions reported in the literature [14].

Advanced computational infrastructures and the development of custom numerical solutions employing Computational Fluid Dynamics (CFD) are necessary to address complex energy problems in buildings; however, accessible tools such as the Global Energy Balance (GEB) methodology are used as an alternative to studying building energy efficiency. GEB models based on thermal resistance theory have been used to address non-stationary state heat transfer problems in short computational times [1,5,8,17]. The GEB information consists of the temperature of every device component considered in the energy balance. Although GEB is unable to compute the vector field of the velocity of fluids, the model provides an overall estimation of the thermal system under steady

or unsteady conditions. Indeed, GEB is used as the primary tool in commercial software like DesignBuilder or open-source software like Energy Plus.

In this line of work, this article presents a GEB solution for a one-dimension wall of multiple nodes in an unsteady state by diffusion in the context of energy efficiency in buildings. The studied system considered Dirichlet boundary conditions and an iterative methodology to solve non-linear effects of the system, considering multiple nodes in the system to model. The experimental validation compares the proposed energy balance with an analytical solution reported in the literature. The main results indicate that the GEB solution approximates the analytical solution in 6.81% when using a time step of 0.1s, and in 0.006% when using a time step of 0.0001s. Results of the study system indicate that the GEB solution is capable of providing an acceptable solution at every time in the context of energy efficiency analysis.

The article is organized as follows. Section 2 describes the heat transfer by diffusion, and the energy balance methodology for a one-dimension wall of multiple nodes in an unsteady state. Section 3 presents the analytical solution and the solution methodology for diffusion heat transfer through energy balances of the evaluated system. The experimental evaluation and discussion of the numerical solution approach are described in section 4. Finally, section 5 presents the conclusions of the research and formulates the main lines for future work.

2   Global energy balance applied to heat diffusion

This section describes the heat transfer by diffusion. Also, the energy balance methodology for a one-dimension wall of multiple nodes in an unsteady state is described.

2.1   Diffusion and heat transfer

In nature, non-uniform physical properties in bodies that influence each other tend to balance through transport phenomena. The transport phenomenon depends on the nature of a physical property, e.g., the thermal diffusivity for heat conduction, a degree of imbalance, and the characteristics of the medium through which the transport is carried out [4]. The transport of energy or heat transfer plays an essential role in studying those processes that provide well-being to people, to satisfy their basic requirements such as health, food, and comfort in the home.

Energy is a property determined through its effects. The temperature that a system has in the heat transfer over time is a quantifiable magnitude.

The transfer of energy is carried out through three transport mechanisms: diffusion, convection, and radiation. The diffusion of properties occurs in dense matter or in bodies that contact each other through molecular interactions, such as heat conduction. The conduction or diffusion of heat relates the speed with which heat is transmitted with the temperature difference and with the

properties of the system through a series of equations of conservation of mass, momentum, energy, concentrations, chemicals, etc. [10,18]

In this context, the study of energy transfer in buildings is of interest to analyze the energy consumption that satisfies the need for thermal comfort.

2.2   Global energy balance

GEB method emerges as an alternative to model complex problems that demand higher performance from computing platforms, i.e., finite difference, finite element, and finite volume methods. The GEB method uses thermodynamic principles that do not depend on space, as with CFD. In the GEB method, the variable of interest in the energy analysis in buildings is the scalar variable of temperature. Temperature variable allows for estimating the heat fluxes through an element of a system [18,4]. Next, the equation of the energy conservation principle of the first law of thermodynamics on which the GEB method is based is presented.

The first law of thermodynamics states the principle of energy conservation: "energy is neither created nor destroyed; it only changes from one form to another". Energy ($\dot{E}$) can be transferred in a system in three modes: heat ($\dot{Q}$), work ($\dot{W}$), and mass flow (E_{mass}). The difference between the amounts transferred into (in) and out (out) of the system determines the amount of net energy transfer [2]. Eq. 1 and Eq. 2 determine an energy balance of a general system.

$$\dot{E}_{in} - \dot{E}_{out} = (\dot{Q}_{in} - \dot{Q}_{out}) + (\dot{W}_{in} - \dot{W}_{out}) + (E_{mass,in} - E_{mass,out}) \qquad (1)$$

$$\underbrace{\dot{E}_{in} - \dot{E}_{out}}_{\text{Net transfer of energy by heat, work, and mass}} = \underbrace{\Delta\dot{E}_{system}}_{\text{System energy rate of change}} \qquad (2)$$

When the heat transfer in an adiabatic system is zero, the work transfer in a system without any work interaction is zero, and the mass transfer in a system without mass flow in its boundaries is zero. This is defined as a closed system. A stationary system is a closed system that keeps the speed and elevation of the gravity center constant; the kinetic (KE) and potential (PE) energy do not experience changes, $\Delta KE = \Delta PE = 0$. Therefore, the total energy change of a closed system is equal to the change in its internal energy (U), $\Delta E = \Delta U$.

Eq. 3 expresses the energy balance of a system considering the three energy transfer mechanisms.

$$\dot{Q} - \dot{W} + \sum E_{mass,in} - \sum E_{mass,out} = \Delta\dot{E}_{system} \qquad (3)$$

Considering the change in internal energy without varying the state of matter, the change in internal energy by involving the enthalpy is expressed as $\dot{Q} - \dot{W} = mC_p\Delta T$. In the expression of internal energy change involving enthalpy, m is the mass of the object or substance, C_p is the specific heat ($Jkg^{-1}K^{-1}$), and

ΔT is the change in temperature (T). The situation that does not consider work $(W = 0)$ in the energy balance, and there is variation over time is expressed as $Q = mC_p \left(\frac{\delta T}{\delta t} \right)$. Q represents the transmission mechanisms of heat transfer and the transmission mechanisms are represented by Q_{cond} for diffusion, Q_{conv} for convection, and Q_{rad} for radiation.

Based on the principle of energy conservation, a GEB method applies only to the components of the physical model of a system. GEB method determines the amount of energy exchanged and stored in a system from a macroscopic perspective. The GEB method aims to determine the global effects of a system without analyzing the phenomenology details from the conditions between the system and its environment[16].

A GEB model is based on the analogy of thermal resistances from electrical circuit theory (Ohm's law) [2]. Thermal resistance (R_T) is analogous to electrical resistance (I). The heat transfer mechanisms through thermal resistance represent the heat flow (q) in the thermal system. Thermal resistances in the GEB model are represented as conductive thermal resistance (R_T^{cond}), convective thermal resistance (R_T^{conv}), and radiative thermal resistance (R_T^{rad}). Fig. 1 shows the representation of an energy flow in an element and an electrical resistance.

(a) Thermal resistance element (b) Electrical resistance element
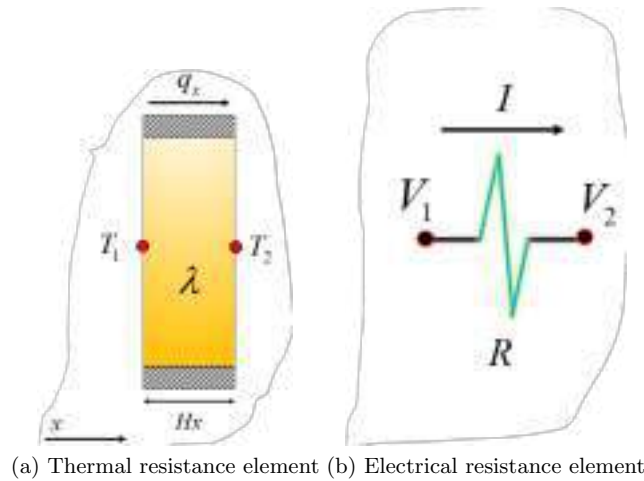
Fig. 1: Heat flow or energy flux through an system element

Fig. 1a shows the representation of thermal resistance. In Fig. 1a, x represents the coordinate in the x direction, Hx represents the dimension or length of the system, $T1$ and $T2$ represent the temperature at the edges of the system, q_x represents the heat flux in direction x, and λ represents the thermal conductivity. Fig. 1b shows the representation of electrical resistance. In Fig. 1b, I represents the electrical current, V_1 and V_2 the input and output voltage, respectively, and

R the resistance of the electrical circuit. From Fig. 1a and Ohm's Law resistivity equation the heat flux equation is expressed as $q = \lambda \frac{\Delta T}{Hx} = \frac{T_1 - T_2}{\frac{Hx}{\lambda}} = \frac{T_1 - T_2}{R_T}$.

The difference in electrical potential is analogous to the temperature difference between two points in the system. The resistance is equal to the density of the material factor of the inverse of material thermal conductivity (only for heat conduction). Applying Fourier's law, each heat flux equation element is substituted by its respective analog in an electrical circuit. In this context, conductance is expressed as $C = \frac{1}{R_T} = \frac{\lambda}{Hx}$.

The correct location of the nodes to evaluate the temperature difference is in the center of the element (node) of the system. The analysis of the heat flux in the system can be performed in a steady state or a transient (unsteady) state. The system element of interest is a thin plate represented by a node centered inside the element. A node at the center of an element is a generalization susceptible to an erroneous estimation of the temperature value in an energy balance. However, a GEB method allows analyzing heat flow in an element as an alternative to CFD.

2.3 Physical and mathematical model for a wall of multiple nodes in an unsteady state

Next, using GEB, physical and mathematical models of a one-dimension wall of multiple nodes in an unsteady state are presented.

Physical model. Fig. 2 shows the physical model of a one-dimension system in an unsteady state where the heat transfer will be analyzed in an established modeling time under homogeneous boundary conditions. In addition, the system will not have a source of heat generation inside, and the properties of the system are constant.

Fig. 2a shows the physical model of a solid element with multiple nodes. The solid element is subjected to first-class boundary conditions, where $T_b > T_a$. The behavior of the system is evaluated by the conduct of temperatures in a set time (Fig. 2b). Therefore, equation 4 expresses the energy balance adjustment for each node of the system element over time.

$$q_{in} - q_{out} = \rho C_p \frac{\partial T}{\partial t} \Delta x \qquad (4)$$

The input and output flux of energy difference is equal to the energy accumulated in the element; for this reason, the temperature variation term concerning time (t) is considered in the equation. The temperature-time analysis introduces a finite-difference approximation for the first derivative term in time by an implicit low-order approximation (Euler's method) in a backward scheme. The approximation used increases the stability of the solution through higher time intervals. The first derivative is replaced by the difference between the central node information at the current time (unknown) and the central node information at a previous time divided by the established time interval (Eq. 5).

(a) Physical model   (b) Approximation of temperature in time
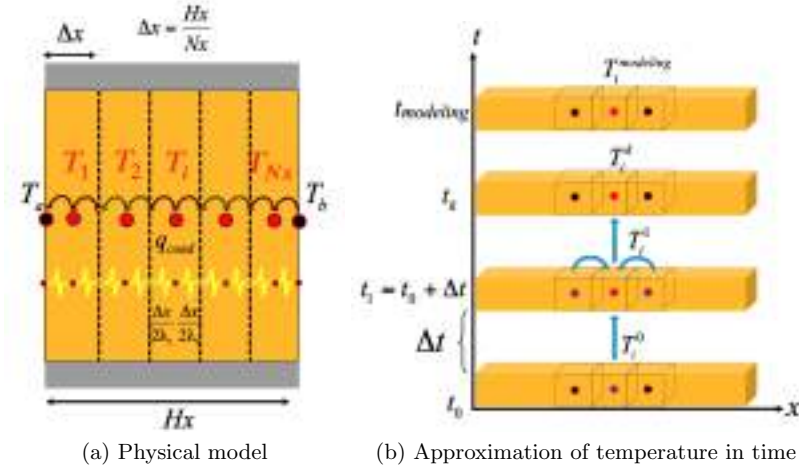
Fig. 2: Physical model of a system in an unsteady state

$$\frac{\partial T}{\partial t} = \frac{T_i^t - T_i^{t-\Delta t}}{\Delta t} \tag{5}$$

This way, Eq. 6 expresses the substitution of Eq. 5 in Eq. 4.

$$q_{in} - q_{out} = \rho C_p \left(\frac{T_i^t - T_i^{t-\Delta t}}{\Delta t} \right) \Delta x \tag{6}$$

Mathematical model. The heat transfer by diffusion for a one-dimension wall of multiple nodes in an unsteady state by energy balances is expressed mathematically next. Eq. 7 and Eq. 8 express the global energy balance for node 1:

$$q_{in(2-1)} - q_{out(1-a)} = \rho C_p \left(\frac{T_1^t - T_1^{t-\Delta t}}{\Delta t} \right) \Delta x \tag{7}$$

$$\left(\frac{1}{\frac{\Delta x}{2\lambda_2} + \frac{\Delta x}{2\lambda_1}} \right) (T_2^t - T_1^t) - \left(\frac{1}{\frac{\Delta x}{2\lambda_1}} \right) (T_1^t - T_a) = \left(\frac{\rho C_p}{\Delta t} \Delta x \right) (T_1^t - T_1^{t-\Delta t}) \tag{8}$$

Eq. 9 and Eq. 10 express the global energy balance for node i:

$$q_{in(N_{i+1}-N_i)} - q_{out(N_i-N_{i-1})} = \rho C_p \left(\frac{T_i^t - T_i^{t-\Delta t}}{\Delta t} \right) \Delta x \tag{9}$$

$$\left(\frac{1}{\frac{\Delta x}{2\lambda_{i+1}} + \frac{\Delta x}{2\lambda_i}}\right)\left(T_{i+1}^t - T_i^t\right) - \left(\frac{1}{\frac{\Delta x}{2\lambda_i} + \frac{\Delta x}{2\lambda_{i-1}}}\right)\left(T_i^t - T_{i-1}^t\right) =$$

$$\left(\frac{\rho C_p}{\Delta t}\Delta x\right)\left(T_i^t - T_i^{t-\Delta t}\right) \quad (10)$$

Eq. 11 and Eq. 12 express the global energy balance for node Nx:

$$q_{entra(b-(Nx))} - q_{sale(Nx-(Nx-1))} = \rho C_p \left(\frac{T_{Nx}^t - T_{Nx}^{t-\Delta t}}{\Delta t}\right)\Delta x \qquad (11)$$

$$\left(\frac{1}{\frac{\Delta x}{2\lambda_{Nx}}}\right)\left(T_b - T_{Nx}^t\right) - \left(\frac{1}{\frac{\Delta x}{2\lambda_{Nx}} + \frac{\Delta x}{2\lambda_{Nx-1}}}\right)\left(T_{Nx}^t - T_{Nx-1}^t\right) =$$

$$\left(\frac{\rho C_p}{\Delta t}\Delta x\right)\left(T_{Nx}^t - T_{Nx}^{t-\Delta t}\right) \quad (12)$$

Eqs. 8, 10 and 12 are grouped in a matrix which represents a linear equation system:

$$\begin{bmatrix} (a_1 + a_2 + a_{P0,1}a_1a_2) & (-a_2) & 0 & 0 & 0 \\ \ddots & \ddots & \ddots & 0 & 0 \\ 0 & (-b_1) & (b_1 + b_2 + a_{P0,i}b_1b_2) & (-b_2) & 0 \\ 0 & 0 & \ddots & \ddots & \ddots \\ 0 & 0 & 0 & (-c_1) & (c_1 + c_2 + a_{P0,Nx}c_1c_2) \end{bmatrix} \begin{bmatrix} T_1^t \\ \vdots \\ T_i^t \\ \vdots \\ T_{Nx}^t \end{bmatrix}$$

$$= \begin{bmatrix} a_1 T_a + a_{P0,1}a_1a_2 T_1^{t-\Delta t} \\ \vdots \\ a_{P0,i}b_1b_2 T_i^{t-\Delta t} \\ \vdots \\ c_2 T_b + a_{P0,Nx}c_1c_2 T_{Nx}^{t-\Delta t} \end{bmatrix}$$

$$(13)$$

In Eq. 13, coefficients are expressed as:

$$a_1 = \left(\frac{1}{\frac{\Delta x}{2\lambda_2} + \frac{\Delta x}{2\lambda_1}}\right); a_2 = \left(\frac{1}{\frac{\Delta x}{2\lambda_1}}\right); a_{P0,1} = \left(\frac{\rho_1 C_{p,1}}{\Delta t}\Delta x_1\right)$$

$$b_1 = \left(\frac{1}{\frac{\Delta x}{2\lambda_{i+1}} + \frac{\Delta x}{2\lambda_i}}\right); b_2 = \left(\frac{1}{\frac{\Delta x}{2\lambda_i} + \frac{\Delta x}{2\lambda_{i-1}}}\right); a_{P0,Nx} = \left(\frac{\rho_i C_{p,i}}{\Delta t}\Delta x_i\right) \qquad (14)$$

$$c_1 = \left(\frac{1}{\frac{\Delta x}{2\lambda_{Nx}}}\right); c_2 = \left(\frac{1}{\frac{\Delta x}{2\lambda_{Nx}} + \frac{\Delta x}{2\lambda_{Nx-1}}}\right); a_{P0,Nx} = \left(\frac{\rho_{Nx} C_{p,Nx}}{\Delta t}\Delta x_{Nx}\right)$$

Eq. 13 allows evaluating massive materials with multiple nodes to achieve grid and temporal independence. Eq. 8 and 12 describe the global energy balance considering first-class boundary conditions (Dirichlet condition), whereas Eq. 10 refers to the internal elements of material divided into a discrete number of elements. The arrangement of elements of Eq. 13 in the coefficients matrix refers to a tridiagonal shape of the elements that can be solved using a direct method like the Tridiagonal Matrix Algorithm.

Next section describes the experimental analysis using energy balances for a one-dimension wall of multiple nodes in an unsteady state and the comparison with the analytical solution.

3   Numerical solution and verification

This section describes the analytical solution for verification of the mathematical model of the evaluated system. Also, the solution methodology for diffusion heat transfer through energy balances for a wall of multiple nodes in an unsteady state is presented.

3.1   Analytical solution

The analytical solution for the proposed GEB application was reported in the literature. Eq. 15 expresses the analytical solution for verifying the evaluated multimodal system [12].

$$T(x,t) = T_0 e^{-\alpha\beta^2 t} \sin(\beta x) \qquad 0 \leq x \leq Hx; t > 0 \tag{15}$$

In Eq. 15, $\alpha = \frac{\lambda}{\rho C_P}$ and $\beta = \frac{\pi}{Hx}$. Eq. 16 expresses the initial condition for numerical solution.

$$T = T_0 \sin(\pi x) \qquad 0 \leq x \leq Hx; t = 0 \tag{16}$$

3.2   Energy balance method for a wall of multiple nodes in an unsteady state

Numerical solution based on GEB implements an iterative solver (Jacobi method) to analyze boundary conditions and properties, generating non-linear equations. Precisely, the characteristics of system and how easy the study case can be converted into a non-linear problem are the main reasons to consider a iterative solver like Jacobi´s method or Gauss-Seidel.

Jacobi's method starts to discretize the equation of grouping coefficients by $a_P \phi_P = a_W \phi_W + a_E \phi_E + b$. Eq. 17 expresses the Jacobi method to obtain the variable ϕ on each node at any element of the system, including boundary nodes.

$$\phi_P = \frac{a_W \phi_W + a_E \phi_E + b}{a_P} \qquad (17)$$

Summarizing, Jacobi's method consists of the following steps:

1. a distribution of the variable (ϕ_P^*) is guested in the computational domain
2. coefficients of computational nodes are calculated: a_W, a_E, a_P, b
3. ϕ_P is calculated by Eq. 17 using guest values of step one $\phi_P = \frac{a_W \phi_W^* + a_E \phi_E^* + b}{a_P}$; it applies to all discrete nodes, one by one
4. a convergence criterion is applied; if the criterion is satisfied, then ϕ_P is the problem solution; otherwise, the ϕ variable is renamed $\phi_P^* = \phi_P$, and step two is executed iteratively until the convergence criterion is satisfied

Algorithm 1 presents the iterative procedure to solve the system of multiple nodes in an unsteady state using a GEB method.

Algorithm 1: GEB method for solving a wall of multiple nodes in an unsteady state

---

Data: $Nx, Hx, \lambda, C_p, T_A, T_B, \varepsilon$
Result: Temperature Matrix ϕ
1 Set variables (T), properties and boundary conditions of system
2 Fill matrix $\phi = T_{guest}$
3 Generate mesh $\Delta x = \frac{Hx}{Nx-2}$
4 $k = 0$
5 **while** $t \leq t_{modeling}$ **do**
6   Rename matrix $\phi = \phi^t$
7      $t = k\Delta t$
8   **while** $R_\phi^k \geq \varepsilon$ **do**
9   Computing coefficients a_W, a_E, a_P, b
10   Jacobi solver $a_P = \frac{a_W \phi_W + a_E \phi_E + b}{a_P}$
11   Rename matrix $\phi^* = \phi$
12   Compute residual $R_\phi^k = \sum_{i=1}^{i=Nx} [a_P \phi_P - (a_E \phi_E + a_W \phi_W + b)]$
13   **end**
14     $k = k + 1$
15 **end**
16 Print temperature matrix ϕ

In Algorithm 1, a_E corresponds to the terms of the right side of the main diagonal of the coefficient matrix, a_W represents the terms of the left side of the main diagonal of the coefficient matrix, a_P corresponds to the terms on the main diagonal, and b is the resultant vector of Eq. 13. Steps 1-3 correspond to the declaration of system characteristics and other considerations, like the number of nodes that divides the system into small elements. Step 5 initializes the iterative process of time steps for the unsteady state of the system. Step 6

initializes the temperature variable by renaming the current variable with the new temperature value in time. Step 7 calculates the time step according to the specific time rate of interest. Step 8 initializes the iterative process of the Jacobi solver until the residual calculated at each iteration is greater or equal to an epsilon specified as a stop criterion. Step 9 calculates the matrix coefficients for been used in the Jacobi solver. Once the Jacobi solver finalizes, step 11 renames the new variable with the value of temperature calculated. Step 12 calculates the residual for the stop criterion. Finally, the temperature matrix results are printed with the heat transfer behavior for the system of multiple nodes in an unsteady state.

Next, the experimental analysis and results of the GEB solution for a wall of multiple nodes in an unsteady state are discussed.

4 Experimental analysis and discussion

This section reports the experimental analysis for a one-dimension wall of multiple nodes in an unsteady state by diffusion. Also, the development and execution platform are described. Finally, the computational efficiency results are reported and discussed.

4.1 Development and execution platform

The numerical codes were implemented in the ANSI-C programming language. The experimental evaluation was performed on the high performance computing infrastructure of National Supercomputing Center (Cluster-UY), Uruguay [11].

4.2 Problem features

Next, the problem features are presented. The one-dimension wall is divided into five nodes ($Nx = 5$). The wall length was established at 1m ($Hx = 1$m). Thermal conductivity was $\lambda = 2.0$ WmK^{-1}, density was $\rho = 1$ kgm^{-3}, and specific heat was $C_P = 1$WmK^{-2}°C^{-1}. The first class boudary values were $T_a = 0$°C and $T_b = 0$°C. The initial temperature was $T_0 = 20$°C, which is part of the initial condition (Eq. 16).

The modeling time for this study was 0.1s, while the time steps evaluated were $\Delta_t = 0.0001, 0.001, 0.01$ and 0.1 seconds. The problem conditions were selected to solve temperature variations in a short time in an ideal case since the purpose stated the effectiveness of the GEB methodology to analyze unsteady state conditions by heat conduction.

4.3 Results and discussion

Numerical results computed by the GEB method using different time steps were compared with the analytical solution (exact) of the mathematical model (Eq. 15).

Table 1 reports the numerical solutions obtained by GEB at different time steps for a wall of multiple nodes in an unsteady state.

Table 1: Energy balance and exact solution comparison four time steps for Δt=0.0001s

Position $x[m]$	$T[°C]$ Exact sol.	$T[°C]$ GEB sol.
t=0.0001s; Percentage difference [%]=0.006		
0.1	6.16	6.16
0.3	16.14	16.14
0.5	19.96	19.96
0.7	16.14	16.14
0.9	6.16	6.16
t=0.05s; Percentage difference [%]=3.35		
0.1	2.30	2.38
0.3	6.03	6.23
0.5	7.45	7.70
0.7	6.03	6.23
0.9	2.30	2.38
t=0.08s; Percentage difference [%]=5.41		
0.1	1.27	1.34
0.3	3.33	3.51
0.5	4.12	4.34
0.7	3.33	3.51
0.9	1.27	1.34
t=0.1s; Percentage difference [%]=6.81		
0.1	0.85	0.91
0.3	2.24	2.40
0.5	2.77	2.96
0.7	2.24	2.40
0.9	0.85	0.91

Results in Table 1 indicate that GEB is capable of obtaining a numerical solution for a wall of multiple nodes in an unsteady state, approximating the

analytical solution in 6.81% for time step t=0.1s. The percent difference was reduced in 0.006% when using a time step of t=0.0001s.

Fig. 3 graphically summarizes the profile temperatures for different times along the wall. Fig. 3 shows the behavior of heat transfer for a wall of multiple nodes in an unsteady state for times t=0.1s, t=0.01s, t=0.001s, t=0.0001s and the value obtained by the analytical solution of the mathematical model.
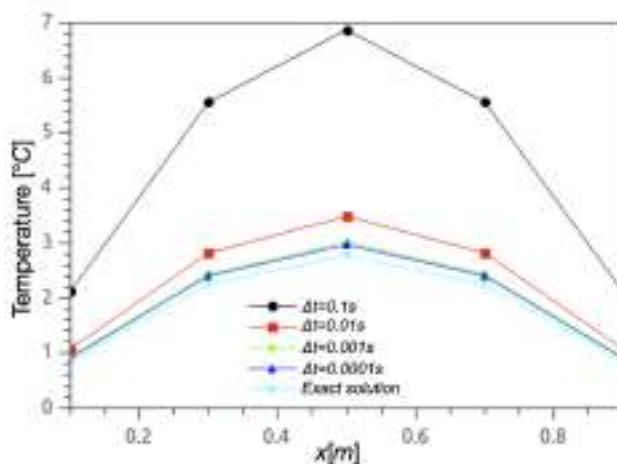
Fig. 3: Temperature condition for $t = 0.1s$

Different time steps were proposed, since the correct value which achieves the independence time of the system is unknown. However, Fig. 3 shows that the temperature profile is better adaptable to the analytical solution as the time step was reduced.

Summarizing, results of the experimental evaluation demonstrate that the percentage difference was reduced until achieving 6.81% respect for the analytical solution for a time step of t=0.1s, and it was reduced in 0.006% when using a time step of t=0.0001s, which is acceptable for an energy efficiency buildings analysis.

The results were also affected by the approximation of the temporal term in the energy balance (Eq. 12) and the non-uniform temperature distribution as the initial condition. Therefore, as an alternative solution, a future study must evaluate the effect of high-order approximations of the differential term, which is the temporal variation of temperature for each node or element, to improve the accuracy of the numerical results using GEB.

5   Conclusions and future work

This article presented a global energy balance solution for a one-dimension wall of multiple nodes in an unsteady state by diffusion in the context of energy efficiency analysis.

The proposed GEB methodology solved the heat conduction in an unsteady state for relevant energy efficiency analysis in buildings. The studied system considered Dirichlet boundary conditions with a generic structure for multiple nodes to permit heat conduction in materials with high thermal inertia.

The experimental validation compares the proposed GEB for a wall of multiple nodes in an unsteady state with an analytical solution reported in the literature.

The main results indicate that the percentage difference between the numerical solution (GEB) and the analytical solution was in 6.81% when using a time step of 0.1s, and in 0.006% when using a time step of 0.0001s. GEB behavior was expected to be similar to computational fluid dynamic solutions. The proposed study demonstrated the GEB capacity to obtain a suitable heat conduction solution through an iterative solution (linear equation system) at different time steps.

The main lines for future work are oriented to extend the proposed GEB methodology to include non-linear terms in the coefficients. Also, the GEB method can determine the temperature variation of a wall or building with thermal and thermodynamic properties in temperature function using phase change materials (PCM) or insulating layers. Likewise, the GEB method can address system boundary conditions in function of time, e.g., a building exposed to external environmental conditions. Finally, CFD and GEB comparison is of interest to analyze heat transfer with a suitable accuracy for energy efficiency applications.

References

1. Bahrehmand, D., Ameri, M.: Energy and exergy analysis of different solar air collector systems with natural convection. Renewable Energy **74**, 357–368 (2015)
2. Bergman, T.L., Lavine, A.S., Incropera, F.P., DeWitt, D.P.: Fundamentals of Heat and Mass Transfer. Wiley, 8 edn. (2018)
3. González-Julián, E., Xamán, J., Moraga, N.O., Chávez, Y., Zavala-Guillén, I., Simá, E.: Annual thermal evaluation of a double pane window using glazing available in the mexican market. Applied Thermal Engineering **143**, 100–111 (2018)
4. Cervantes de Gortari, J.: Fundamentos de Transferencia de Calor. Fondo de Cultura Economica, México (1999)
5. Hamed, M., Fellah, A., Ben Brahim, A.: Parametric sensitivity studies on the performance of a flat plate solar collector in transient behavior. Energy Conversion and Management **78**, 938–947 (2014)
6. Hernández-López, I., Xamán, J., Zavala-Guillén, I., Hernández-Pérez, I., Moreno-Bernal, P., Chávez, Y.: Thermal performance of a solar façade system for building ventilation in the southeast of mexico. Renewable Energy **145**, 294–307 (2020)
7. International Energy Agency: World energy outlook 2017 (2017)

8. Jiménez-Xamán, C., Xamán, J., Moraga, N.O., Hernández-Pérez, I., Zavala-Guillén, I., Arce, J., Jiménez, M.: Solar chimneys with a phase change material for buildings: An overview using cfd and global energy balance. Energy and Buildings **186**, 384–404 (2019)

9. Lima-Téllez, T., Chávez, Y., Hernández-López, I., Xamán, J., Hernández-Pérez, I.: Annual thermal evaluation of a ventilated roof under warm weather conditions of mexico. Energy **246**, 123412 (2022)

10. Mazumder, S.: Numerical Methods for Partial Differential Equations: Finite Difference and Finite Volume Methods. Academic Press (2016)

11. Nesmachnow, S., Iturriaga, S.: Cluster-UY: Collaborative Scientific High Performance Computing in Uruguay. In: Supercomputing, Communications in Computer and Information Science, vol. 1151, pp. 188–202. Springer (2019)

12. Ozisik, M.N.: Heat Transfer: a Basic Approach. McGraw-Hill (1985)

13. Patankar, S.: Numerical Heat Transfer and Fluid Flow. CRC Press (1980)

14. Roache, P.J.: Verification and validation in computational science and engineering. Hermosa Publishers, Albuquerque New Mexico (1998)

15. United Nations Department of Economic and Social Affairs, Population Division: World population prospects 2022: Summary of results (2022)

16. Uriarte, J.: Análisis Térmico de una Habitación con Techo de Geometría Irregular y Cubiertas Reflectivas. Ph.D. thesis, Centro Nacional de Investigación y Desarrollo Tecnológico, Tecnológico Nacional de México (2022)

17. Vargas-López, R., Xamán, J., Hernández-Pérez, I., Arce, J., Zavala-Guillén, I., Jiménez, M., Heras, M.: Mathematical models of solar chimneys with a phase change material for ventilation of buildings: A review using global energy balance. Energy **170**, 683–708 (2019)

18. Xamán, J., Guijon-Rivera, M.: Dinámica de Fluidos Computacionales para ingenieros. Palibrio, México (2018)

19. Zavala-Guillén, I., Xamán, J., Hernández-Pérez, I., Hernández-Lopéz, I., Jiménez-Xamán, C., Moreno-Bernal, P., Sauceda, D.: Ventilation potential of an absorber-partitioned air channel solar chimney for diurnal use under mexican climate conditions. Applied Thermal Engineering **149**, 807–821 (2019)

Smart mobility for public transportation systems: Improved bus timetabling for synchronizing transfers

Claudio Risso[0000−0003−0580−3083], Sergio Nesmachnow[0000−0002−8146−4012], and Diego Rossit[0000−0002−8531−445X]

Instituto de Computación, Universidad de la República, Uruguay
{crisso,sergion}@fing.edu.uy
INMABB, Department of Engineering, Universidad Nacional del Sur-CONICET,
Argentina
diego.rossit@uns.edu.ar

Abstract. Providing an efficient public transportation system is a key issue to increase the livability and sustainability of modern cities. This article addresses the bus timetabling problem for enhancing multi-leg trips or transfers. For this purpose, a mixed-integer programming model is proposed, aimed at maximizing the amount of transfers while considering budgetary and quality of service constraints. The proposed model is evaluated on real scenarios from the case study of the public transportation system in Montevideo, Uruguay. Results indicate that the solutions of the proposed model outperforms the current timetable used in the city in terms of number of transfers, cost, and number of required buses.

Keywords: public transportation, timetable synchronization, transfers, quality of service, MILP model

1 Introduction

Smart mobility is a key component of smart cities [9]. Smart mobility is based on the design and operation of intelligent transportation networks, by applying innovative technologies and planning/management methods.

A crucial problem for administrations is the increasing number of automobiles and other private non-sustainable transportation modes, which prevent a correct preservation of the environment [21,29]. For addressing this problem, the smart mobility paradigm heavily relies on public transportation systems, using efficient motor vehicles, electric vehicles, and other innovative transportation modes. The main goal is to promote a behavioral change of citizens, towards lowering private car ownership, reducing pollution, traffic congestion, and other related issues.

Public transportation is recognized as one of the key services for smart cities [11,20]. A proper design and operation of public transportation systems is crucial to guarantee efficient mobility. Important problems include route design,

timetabling and planning, drivers scheduling, etc., whose main goals are providing citizens a proper travel experience [5] and promoting sustainability [12].

The problem of designing timetables for public transportation systems is a crucial issue within the transit planning process. Timetable definition involves determining bus trip frequencies for a given operation period. An important subproblem is synchronizing multi-leg trips or *transfers*, which allows providing passengers adequate waiting times for transfers from one bus route to another.

Synchronizing timetables has been identified as a very difficult problem within public transportation planning and optimization [4]. Usually, experienced bus operators and planners define ad-hoc intuitive solutions that provide reasonable quality of service (QoS) to citizens. Our previous articles proposed exact and metaheuristic methods for an extended variant of the timetable synchronization problem, considering extended transfer zones [17,23,24]

In this line of work, this article presents a mathematical formulation of the timetable synchronization problem with the main goal of maximizing the number of transfers, while considering specific constraints for the minimal QoS and the available budget. The proposed model improves over our previous works [23,24] by including specific models for the cost of each bus trip, considering vehicle-time and vehicle-distance variables, and a model to assess the QoS provided by the public transportation system to users that perform direct trips (no transfers). A Mixed-Integer Linear Programming (MILP) model is proposed for solving realistic problems by taking advantage of modern high performance computing infrastructures.

The proposed formulation is evaluated on 25 scenarios defined with real data of the public transportation system in Montevideo, Uruguay. Results demonstrate that the proposed model is able to compute accurate solutions, significantly improving over the current timetable in Montevideo regarding synchronized transfers, while guaranteeing a proper cost and QoS for directs trips.

This article is organized as follows. Section 2 describes the Bus Synchronization Problem (BSP), its mathematical formulation, and reviews relevant related works. The case study is described in Section 3. Section 4 reports the experimental evaluation performed on a set of real-world instances. Finally, the conclusions and main lines for future work lines are outlined in Section 5.

2   The Bus Synchronization Problem

This section describes the BSP model and reviews related work. The problem data, the mathematical formulation, and the cost model are also described.

2.1   Conceptual problem model

The problem proposes finding the best configuration of headways (i.e., intervals between consecutive trips of the same line) for each line to optimize the number of transfers. Transfers are only effective when two trips are synchronized. A synchronization is achieved when not only the passenger has enough time to walk

from the bus stop in which he has got off the first trip to the stop in which he has to take the second trip, but also when the waiting time at the bus stop for the second trip is not larger than a certain threshold that guarantees a minimum QoS for passengers. The schedule is defined over a reference interval, within which, relevant data for the problem –such as buses traveling times between points and the number of passengers per unit of time – is steady and has a uniform distribution. Considering reference intervals within which certain parameters are constant is common in the related literature [10,13] and allows making the complex timetabling problem more tractable and, thus, to obtain (near) optimal plannings in a period of interest (e.g., peak hours of the system).

The problem does not assume a prefixed number of trips per line. It only considers that headways must be within minimum and maximum values that are pre-established for each bus line. Additionally, the estimated cost of the bus schedule is limited by a maximum budget that the decision makers are willing to spend. The cost of the bus schedules is affected by the working times of drivers and the distances traveled by buses, as explained in Section 2.5.

The reference QoS model combines random boarding with deterministic alighting. The Poisson process is the de-facto reference for independent and identically distributed random arrivals. Due to the regularity hypothesis along the planning period, the Poisson process is assumed of fixed rate. Thus, given the per-line average daily number of tickets ts_i sold by line i in $[0, T]$, $\Lambda_i = ts_i/T$ is the rate of boardings to the whole set of running buses of that line. The process actually alludes to the number of passengers arriving to some bus stop in order to be picked up, but the number of stops is large enough to refer to both processes as equivalent. Per-line descents are assumed fixed in this model. Let L_i be the traveling distance of passengers of line i. The average speed V_i of buses of line i is also known. Therefore, the time each passenger rides a bus before alighting is simply $td_i = L_i/V_i$. All the buses of each line i start their trips empty. Since the alighting time is fixed, buses only load new passengers along the interval $[0, td_i]$ (the ramp-up period). The end-to-end travel time $T2E_i$ for buses of line i is also known (i.e., it is computed from GPS records on each bus). For consistency, the model assumes that there is also a ramp-down period at the end $[T2E_i - td_i, T2E_i]$ where no passengers board. Finally, the QoS model assumes fixed headways F^i for every line i. If the passengers of that line arrived along the entire end-to-end travel time, the arrival rate of each bus is $\Lambda_i \cdot F^i/T2E_i$. However, to preserve the expected number of tickets sold, the rate must be adjusted to $\overline{\Lambda_i} = \Lambda_i \cdot F^i/(T2E_i - td_i)$, because of the ramp-down period.

The previous model was implemented by means of and ad-hoc discrete event simulator. A sample distribution of passengers over a bus is sketched in Fig. 1. Red crosses are samples identified as outliers. Regarding occupation, higher outliers (those placed above upper whiskers) were discarded. The considered QoS objective is that the whiskers are at most in the capacity of the buses, which is 65 passengers for the considered case study. So, for each line i, higher F^i values are explored until an upper whisker attains the limit of passengers. Let $\overline{F^i}$ be the maximum headway complying the target QoS for line i.
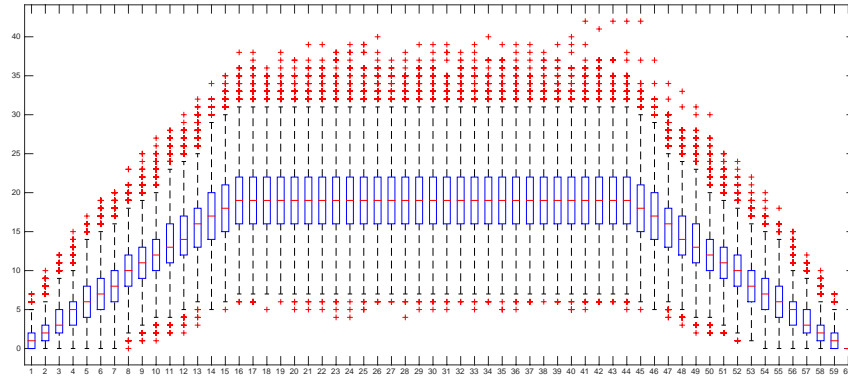
Fig. 1: Sample boxplot of a bus occupation along a 60min end-to-end travel with $td_i = 16$min and $\overline{\Lambda_i} = \frac{9}{8}$min^{-1}, after 10,000 simulations.

2.2   Related work

Bus timetabling has been addressed in the related literature under different criteria [13]. The most common optimization criteria are: minimizing the waiting time of users, minimizing the fleet size and travel time of buses, and maximizing the load factor of buses. However, few works considered setting frequencies to optimize the synchronization between buses or with other mobility means [13]. Moreover, being a problem which is recognized as computationally complex problem [31], works which use exact approaches to solve BSP are quite scarce.

Synchronizations improve as trips schedules promote buses with relaying passengers to arrive at times that allow convenient transfers to other buses. A convenient transfer simultaneously satisfies having waiting times short enough to provide good QoS for passengers but also long enough to allow passengers to move from one line to another [10]. Thus, the Synchronization Bus Problem consists in determining the departure time of every bus trip to maximize the synchronization of different bus lines of a network.

Ibarra and Rios [14] presented a MILP formulation for solving small instances. Due to the NP-hard of the problem, large instances are intractable with this model. Fouilhoux et al. [10] presented a plain MILP formulation with the addition of valid inequalities to solve a problem in which the number of trips per bus line is fixed. They proved that the valid inequalities are able to provide a stronger formulation of the problem allowing to address practical instances that cannot be solved with the plain MILP without these inequalities. Chu et al. [8] presented a more comprehensive model in which the primary objective is to reduce the travel time of the passengers from the origin to the destination and the bus synchronization is performed as a subordinated consequence in order to reduce the travel time. They proposed two mathematical formulations: a direct formulation like others in the literature and set-partitioning formulation. The set-partitioning formulation computed better results. Our previous article

[24] addressed two different variants of the BSP for peak hours. In the first variant, regularly spaced departures of buses of the same line are considered (thus only the offset –departure of the first bus– has to be determined). In the second variant, the headways of consecutive departures of buses of the same bus line can vary within certain limits. Both variants were solved with an exact MILP formulation for real instances of the city of Montevideo, proposing buses schedules that clearly overcome in terms of number of synchronizations and average waiting times for transfers the real schedules used in the city.

This article contributes with a mathematical formulation for the timetable synchronization problem to maximize the number of transfers for users that are willing to perform multi-leg trips, while considering specific constraints regarding the QoS and the available budget. Thus, the proposed model improves over previous works [23,24] through the inclusion of a specific cost model, which takes into account the distance and travel time of the buses, and a model to estimate the QoS that is provided to users that perform direct trips. Moreover, this problem is applied to realistic instances using an exact resolution approach.

2.3   Problem data

The formulation of the studied problem considers the following datasets:

– The planning period $[0, T]$, expressed in minutes. It corresponds to a reference interval within which relevant data for the problem (traveling times, number of passengers. etc.) are steady and has a uniform distribution.
– A set of bus lines $I = \{i_1, \ldots, i_n\}$, whose routes are fixed and known beforehand. Each trip of a line has an also known end-to-end cost, c_i.
– This problem does not assume a prefixed number of trips per line. Instead, headways and offset values are to be determined within a range of minimum (h_i) and maximum (H_i) values for each line i. The upper bound for the number of trips of any line within the planning period is $f_i = \lceil \frac{T}{h_i} \rceil$.
– A set of *synchronization nodes*, or *transfer zones*, $B = \{b_1, \ldots, b_m\}$. Each transfer zone $b \in B$ has three elements $<i, j, d_b^{ij}>$: i and j are the lines to synchronize, whereas d_b^{ij} is the distance that separates the bus stops for lines i and j in b. Each b considers two bus stops with registered transfer demand between lines i and j. The distance d_b^{ij} is expressed in time-units rather than distance, accounting for the time a passenger must walk to transfer from the bus stop of line i to the bus stop of line j in the considered transfer zone.
– A *traveling time function* $TT : I \times B \to \mathbf{Z}$. $TT_b^i = TT(i, b)$ defining the time that buses of line i need to travel to reach the transfer zone b. The time is measured from the departure of the line. The traveling time depends on the studied scenario and is affected by several factors such as the maximum allowed speed, the traffic in the city, the travel demands, etc., but it is considered fixed within the planning period.
– A *demand function* $P : I \times I \times B \to \mathbf{Z}$. $P_b^{ij} = P(i, j, b)$ defines how many passengers perform a transfer from line i to line j at transfer zone b along

the entire $[0, T]$ period. As described previously in this subsection, a hypothesis of uniformity is assumed. Hence, the potential number of transfers between any two trips of lines i and j are proportional to the time between two consecutive trips of buses in line i, i.e., to headways of the line from whom passengers alight. As we see next, not every potential transfer is considered successful, among other conditions, because of the quality-of-service expectations of passengers. The uniform demand hypothesis is realistic for short periods, such as in the problem instances studied.

– The maximum time that passengers are willing to wait to board to line j, after alighting from line i and walking to the corresponding stop of line j at the transfer zone b, W_b^{ij}. Two trips of line i and j are synchronized for transfers if, and only if: i) passengers alighting from i get to the second bus stop in time to board the trip from line j; ii) waiting time of those passengers standing there to transfer between lines is lower or equal to W_b^{ij}; and iii) all of these events happen within the planning period.

– The number of trips for line i to fulfill the QoS occupation goal, $N_i = \lceil T/\overline{F^i} \rceil$.

2.4 Problem formulation

Control variables in this problem are those in the set of departing times X_r^i of each trip r of every line i. Given any line i, the *headways* of the line are the times between consecutive trips. They can be easily derived from control variables using the expression $F_r^i = (X_r^i - X_{r-1}^i)$. Without losing generality, the model assumes $X_0^i = 0$, so the *offset* of a line i (departure time of the first trip of that line) is F_1^i, which matches X_1^i. Headway values must be within a range of minimum (h_i) and maximum (H_i) values for that line.

Since the number of trips of a line is a-priori unknown, control variables for trips are indexed from 1 to the upper bound $f_i = \lceil \frac{T}{h_i} \rceil$. Trips whose departing time are greater than T are not scheduled in the solution.

The mathematical model of the considered BSP variant as MILP problem is formulated in Eq. 1. The objective function is Eq. 1a. It aims upon maximizing the total number of successful transfers along the planning period, which is accounted by adding up effective transfers between any combination of lines at every transfer zone. Because of the uniformity hypothesis, $P_b^{ij} \cdot (X_r^i - X_{r-1}^i)/T$ is the number of potential transfers from the r-th trip of line i to some trip of line j at zone b. Passengers can only board into one of those trips, and not every passenger succeeds to board the next trip of a line j before awaiting its maximum tolerance W_b^{ij} at the relaying bus stop. These additional conditions are captured through Z_{rsb}^{ij} auxiliary binary variables that take the value 1 whenever the r-th trip of line i and the s-th trip of line j are synchronized at node b. Thus, $Z_{rsb}^{ij} \cdot P_b^{ij} \cdot (X_r^i - X_{r-1}^i)/T$ matches the number of successful transfers between trips r and s at b. Note that an active Z_{rsb}^{ij} increases the number of nonzero terms in the objective function, thus improving the overall result. In other words, the more variables where $Z_{rsb}^{ij} = 1$, the better. So, constraints are to be added in order to preserve consistency, i.e., to only account for successful transfers.

$$\max \quad \sum_{b \in B} (\sum_{r=1}^{f_i} \sum_{s=1}^{f_j} Z_{rsb}^{ij}) \cdot \frac{P_b^{ij} \times (X_r^i - X_{r-1}^i)}{T} \tag{1a}$$

$$\text{s.t.} \quad Z_{rsb}^{ij} \leq 1 + \frac{(A_{rb}^i + d_b^{ij} + W_b^{ij}) - A_{sb}^j}{M}, \quad \begin{array}{l} \forall b = < i, j, d_b^{ij} > \in B, \\ 1 \leq r \leq f_i, 1 \leq s \leq f_j, \end{array} \tag{1b}$$

$$Z_{rsb}^{ij} \leq 1 + \frac{A_{sb}^j - (A_{rb}^i + d_b^{ij})}{M}, \quad \begin{array}{l} \forall b = < i, j, d_b^{ij} > \in B, \\ 1 \leq r \leq f_i, 1 \leq s \leq f_j, \end{array} \tag{1c}$$

with $A_{rb}^i = X_r^i + TT_b^i, \; A_{sb}^j = X_s^j + TT_b^j$

$$\sum_{s=1}^{f_j} Z_{rsb}^{ij} \leq 1, \, \forall i, j \in I, 1 \leq r \leq f_i \tag{1d}$$

$$Q_r^i \leq 1 + \frac{T - X_r^i}{N}, \quad \forall 1 \leq r \leq f_i, \tag{1e}$$

$$\frac{T + 1 - X_r^i}{T + 1} \leq Q_r^i, \quad \forall 1 \leq r \leq f_i, \tag{1f}$$

$$Z_{rsb}^{ij} \leq Q_s^j, \quad \begin{array}{l} \forall b = < i, j, d_b^{ij} > \in B, \\ 1 \leq r \leq f_i, 1 \leq s \leq f_j, \end{array} \tag{1g}$$

$$h_i \leq X_r^i - X_{r-1}^i, \quad \forall r \in 2, .., f_i \tag{1h}$$

$$X_r^i - X_{r-1}^i \leq H_i, \quad \forall r \in 2, .., f_i \tag{1i}$$

$$\sum_{r=1}^{f_i} Q_r^i \geq N_i, \quad \forall i, 1 \leq i \leq n \tag{1j}$$

$$\sum_{i=1}^{n} c_i \cdot (\sum_{r=1}^{f_i} Q_r^i) \leq C \tag{1k}$$

$$0 \leq X_1^i \leq H_i \tag{1l}$$

$$Z_{rsb}^{ij}, Q_r^i \in \{0, 1\} \tag{1m}$$

Eq. 1b prevents Z_{rsb}^{ij} from taking the value 1 whenever passengers should wait longer than W_b^{ij} at zone b before the next trip of line j arrives. The expression A_{rb}^i corresponds to the alighting time to the zone b of passengers coming from line-i/trip-r, while A_{sb}^j is the time at which the s-th trip of line j arrives to this zone. So, $A_{rb}^i + d_b^{ij}$ is the time at which relaying passengers get to the next stop after walking, and that time should not exceed W_b^{ij} before the s-th trip reaches that point (i.e. A_{sb}^j). Whenever that does not hold, Z_{rsb}^{ij} must be lower than 1, ergo 0. The constant M is large enough to prevent the right-hand side to be lower than 0, what would make equations inconsistent. Complementarily, Eq. 1c inhibits Z_{rsb}^{ij} to be 1 if passengers of trip-r/line-i cannot reach the next bus stop at b in time to take the s-th line of j. In addition, Eq. 1d prevents from transfers to be accounted more than once.

It is not mandatory using all the available trips of each bus line. Unused trips are represented by a departing time beyond the planning horizon T. Considering that binary variable Q_r^i indicates whether trip r of line i is to be scheduled, Eq. 1e deactivates Q_r^i variables whose departure times X_r^i are greater than T, and Eq. 1f forces $Q_r^i = 1$ for those where $X_r^i \leq T$. Furthermore, transfers to unused trips are not accounted as synchronizations. This is guaranteed by Eq. 1g, which enforces variable Z_{rsb}^{ij} to be deactivated in line with the decision taken on variable Q_r^i.

Eq. 1h and Eq. 1i force headways F_r^i to be within limits h_i and H_i, while Eq. 1l does the proper for offsets X_1^i. Eq. 1m simply states the integrity of Z_{rsb}^{ij} and Q_r^i variables. Since the more trips scheduled, the higher the number of possible successful transfers, the number of trips is controlled through the operational cost. $\sum_{r=1}^{f_i} Q_r^i$ is the total number of trips scheduled for line i. Besides, the cost of each one of these trips is c_i. Therefore, the left-hand side of Eq. 1k matches the operational cost of the fleet, which must be limited to a parameter C. Consequently, the problem seeks for the maximum number of successful transfers within a reference period for a given operational budget. Conversely, lower bounds for the number of effective trips of each line are forced to prevent saturation of the capacity of buses, as it is described in Section 2.1. Eq. 1j guarantees that the necessary minimum number of trips N_i is achieved.

Products $Z_{rsb}^{ij}(X_r^i - X_{r-1}^i)$ in the objective function make the formulation as that of a Mixed-Integer Quadratic Programming, what is nomerically undesirable. This issue is tackled by a change of variables and additional constraints. Let $y_{rsb}^{ij} = Z_{rsb}^{ij}(X_r^i - X_{r-1}^i)$, so the objective is $\frac{1}{T} \sum_{b \in B} \sum_{r=1}^{f_i} \sum_{s=1}^{f_j} y_{rsb}^{ij} \cdot P_b^{ij}$, which is linear. To guarantee both objective functions match after this change, two equations are added per-each y_{rsb}^{ij} variable: i) $y_{rsb}^{ij} \leq (X_r^i - X_{r-1}^i)$ and ii) $y_{rsb}^{ij} \leq H_i \cdot Z_{rsb}^{ij}$. Within a maximization problem, variables y_{rsb}^{ij} will take a value as high as possible. H_i is an upper bound for $(X_r^i - X_{r-1}^i)$ because of Eq. 1i, so, whenever $Z_{rsb}^{ij} = 1$, the second equation results $y_{rsb}^{ij} \leq H_i$ and it is the first equation that guarantees y's value to be $(X_r^i - X_{r-1}^i)$ at most, which is then exactly the value variable y_{rsb}^{ij} will take. Conversely, when $Z_{rsb}^{ij} = 0$, the second equation forces y_{rsb}^{ij} to be 0. This behavior replicates that of $Z_{rsb}^{ij}(X_r^i - X_{r-1}^i)$ product, so the change of variables turns the problem into a linear one.

2.5   Cost model

The complexity of the cost models considered in public transportation systems varies significantly, depending on the specific purposes of the model [2]. This article focuses on the tactical problem of defining the headways of the bus schedule. Thus, the layout of the bus lines is not affected. For cases in which the layout of the bus lines is fixed, costs functions that are composed by the linear aggregation of different unitary costs per key parameters, such as the time the buses on road or the distance they travel have been extensively used in the related literature [1,18,19,28]. Moreover, these linear functions are usually used by practitioners [27]. Thus, a cost function related to vehicle-time and vehicle-distance variables is applied.

Vehicle-time. Some operating costs such as the salaries of the drivers, which usually represents a large proportion of the total operating cost, and hours of administrative supervision are directly linked to the amount of vehicle hours. Thus, these expenses are appropriately allocated to vehicle hours. Moreover, the use of vehicle hours is usually a surrogate for working hours of employees in cost allocation models since it is much easier to compute [7].

Vehicle-distance. Among the several operating costs which are related directly to the distance traveled by buses are the fuel, oil, tires and other vehicle maintenance expenses. These models are so-called allocation cost models, where key operating expense items are allocated to a specific operating statistic, such as vehicle-time or vehicle-distance [6]. Several linear costs models also consider the number of buses or the fleet size [19] or, more specifically, the number of buses required to cover the demand on peak hours (generally different to off-peak hours) [7]. The model considered in this article aims at analyzing short time windows in peak hours and, thus, the size of the fleet is considered as fixed. Furthermore, the case study solved is also an example of a public transportation system that operates with a rather fixed-size fleet, since the acquisition of new buses occurs each five years or more. The cost function used in this article is $Cost = U_{VH}VH + U_{VKM}VKM$ where VH and VM are the hours and distance that buses are used, respectively. U_{VH} and U_{VKM} are the unitary costs per hour and kilometer respectively.

Operating costs in the public transportation system of Montevideo. The different expenses of the bus system in Montevideo are regularly analyzed by the local authorities to estimate the tariff per kilometer, which is used as input information for defining the amount of the state subsidies that are received by the system. In Montevideo, there are different types of subsidies [3]. Two of the most important subsidies are the reduced price of fuel for the bus system and the reduced ticket for specific target users (students, pensioners, frequent commuters, etc.). Subsidies strongly influence the impact of each cost item in the cost structure of the system. For example, the reduced price of fuel provokes that the impact of this item in the cost structure is remarkably lower than it is in other bus systems just explaining 5% of the total estimated cost in Montevideo [15] against 13% in other similar systems [2]. However, the reduced price for fuel represents a large expense for the Uruguayan state. In the last years, the city of Montevideo has started to replace diesel buses with electric buses (e-buses) [12]. Shifting to electric buses is an environmentally friendly policy which involves the reduction of fossil fuels consumption [26] and greenhouse gases emission of the system [30].

Two of the main costs in the system are the salary of drivers and the fuel. and/or electricity (if the system uses e-buses). Thus, these two costs are considered associated with the vehicles-hours in the case of salary of drivers and vehicle-distance in the case of fuel and/or electricity (parameters U_{VH} and U_{VKM}) The salary of the drivers is approximately 9.2 USD per hour (8 USD of the basic wage and 1.2 USD of social charges). Regarding the fuel, the average consumption of fuel for a typical diesel bus in the system of Montevideo is 0.396 liters per km [15] and the cost per liter of fuel in the city is about 1.6 USD per liter.

3   Case study: the public transportation system in Montevideo, Uruguay

In Montevideo, Uruguay, the public transportation system is under the Metropolitan Transportation System (STM) [25]. The STM was proposed to integrate in a common system all the public transportation of Montevideo and its metropolitan area, including all urban agglomerations around Montevideo located in nearby departments of Canelones and San José.

STM introduced new technologies that allow a more efficient public transportation. One of the most significant technologies introduced by the STM was the use of a smart card to pay for trips [16]. The smart card allows gathering relevant data and also extracting useful knowledge about the mobility patterns of citizens of Montevideo [24].

STM provides two main alternatives for passengers to get to their destination. One the one hand, the traditional *direct* (i.e., end-to-end) trips. On the other hand, multi-leg trips (*transfers*) either under the 'one hour' or 'two hours' tickets, are enabled by the STM card. The system stores historical data about both direct and transfer trips, tickets sold, and also several other relevant data, including GPS records for each bus [16]. Using these data, official and third-party apps have been designed to provide accurate information and interact with users.

Overall, the STM comprises 145 main lines, more than one thousand line variants, and approximately five thousand bus stops in three departments. This numbers are remarkable large for a city like Montevideo, and highlights the importance of a proper planning for providing a good QoS for citizens that use public transportation.

4   Experimental evaluation

This section presents the computational experimentation performed over real-world instances of the city of Montevideo is presented, including the implementation details, a description of the set of instances, and the report and analysis of the results obtained.

4.1   Methodology

The main details of the methodology applied in the experimental evaluation are presented next.

Implementation details. The proposed MILP formulation for the BSP was implemented in IBM ILOG CPLEX Interactive Optimizer 12.6.3.0. A C program was developed to convert problem instances (in .csv format) to the LP-format used by CPLEX. Matlab version R2015a-8.5.0 was used for the pre-processing, analysis, and post-processing of the computed solutions. The ad-hoc discrete event simulator used for the reference QoS model was also developed in Matlab.

Problem Instances. The computational experimentation was performed over 25 instances built using real information of the city of Montevideo. For building the problem instances several sources of information were used. The bus lines description, routes, timetables, and bus stop locations in the city were retrieved from the National Open Catalog of Uruguay. The information regarding transfers was provided by Intendencia de Montevideo and processed applying a urban data analysis approach [16]. The considered period is the rush hour at midday (12:00 to 14:00) [21]. The demand function is computed from transfers information registered by smart cards used to sell tickets. The synchronization points are chosen according to their demand, i.e., the pairs of bus stops with the largest number of registered transfers for the period are selected; the bus lines correspond to the lines passing by the synchronization points.

The instances include 30 synchronization points, randomly selected from the most demanded transfer zones for the considered period in the city (a total number of 170 zones). The time traveling function TT for each line is computed empirically by using GPS data. The walking time function is the estimated walking speed of a person (6 km/h) multiplied by the distance between bus stops in each transfer zone computed using geospatial information about stops. The maximum waiting time is equal to λH, with $\lambda \in [0.5, 0.7, 0.9, 1]$, to configure instances with different levels of tolerance/QoS. The name of the problem instances is NL.λ.id. NL is the number of bus lines, λ is the coefficient applied to the waiting time of the line in percentage, i.e., different threshold of tolerance to the time that the users are willing to stay are considered, and *id* is a relative identifier for instances with the same NL and λ.

Execution platform. The computational experimentation was performed in an HP ProLiant DL380 G9 high end server with two Intel Xeon Gold 6138 processors (20 cores each) and 128 GB RAM, from the high performance computing infrastructure of National Supercomputing Center, Uruguay (Cluster-UY [22]).

Comparison with current real situation. A relevant baseline for comparison is the current timetable (CT) applied in the transportation system of Montevideo (the real timetable). The metrics for comparing the MILP solutions and the CT are: i) the number of transfers, as is proposed in the objective function ii) the cost of the bus schedule, and iii) the number of buses required for the solution.

4.2   Numerical results

Results of the MILP model and the comparison to the baseline CT in Montevideo are presented in Table 1. The Table reports three metrics: from left to right, the number of successful transfers, the cost of the bus schedule in monetary units and the number of buses required for operation of the computed schedule. For each metric, the value computed by the MILP model, the CT of the city and the percentage of improvement of MILP over CT (*impr.*) are reported.

Table 1: Results of the MILP model and comparison to CT in Montevideo.

instance	successful transfers			cost			number of buses		
	MILP	CT	impr.	MILP	CT	impr.	MILP	CT	impr.
37.30.1	298.99	110.40	170.82%	8,711.71	8,721.80	-0.12%	442	439	0.68%
37.100.1	311.37	263.41	18.21%	8,697.71	8,721.80	-0.28%	436	439	-0.68%
37.50.1	308.88	175.67	75.83%	8,713.82	8,721.80	-0.09%	435	439	-0.91%
37.70.1	310.22	236.18	31.35%	8,679.70	8,721.80	-0.48%	437	439	-0.46%
37.90.1	310.55	263.41	17.90%	8,687.76	8,721.80	-0.39%	433	439	-1.37%
40.100.0	243.83	209.02	16.65%	8,568.87	8,592.64	-0.28%	426	419	1.67%
40.100.4	270.57	226.72	19.34%	7,634.73	8,717.53	-12.42%	374	428	-12.62%
40.90.0	239.38	92.19	159.66%	8,566.40	8,592.64	-0.31%	423	419	0.95%
40.100.4	262.24	106.48	146.28%	7,943.69	8,717.53	-8.88%	388	428	-9.35%
40.50.0	243.73	136.12	79.06%	8,387.31	8,592.64	-2.39%	399	419	-4.77%
40.50.4	264.65	134.54	96.71%	8,706.01	8,717.53	-0.13%	427	428	-0.23%
40.70.0	244.37	184.56	32.41%	8,546.13	8,592.64	-0.54%	431	419	2.86%
40.70.4	268.98	198.87	35.25%	8,717.16	8,717.53	0.00%	429	428	0.23%
40.90.0	245.36	209.02	17.39%	8,529.95	8,592.64	-0.73%	420	419	0.24%
40.90.4	270.98	224.82	20.53%	8,103.04	8,717.53	-7.05%	403	428	-5.84%
41.100.2	289.41	244.42	18.41%	10,054.34	10,056.59	-0.02%	477	471	1.27%
41.30.2	280.97	102.65	173.72%	9,173.49	10,056.59	-8.78%	421	471	-10.62%
41.50.2	287.73	158.69	81.32%	9,924.92	10,056.59	-1.31%	468	471	-0.64%
41.70.2	286.14	213.11	34.27%	9,997.24	10,056.59	-0.59%	470	471	-0.21%
41.90.2	288.25	243.96	18.15%	9,155.90	10,056.59	-8.96%	426	471	-9.55%
42.100.3	277.68	228.30	21.63%	10,351.95	10,410.35	-0.56%	499	485	2.89%
42.30.3	271.61	98.26	176.42%	10,384.46	10,410.35	-0.25%	479	485	-1.24%
42.50.3	274.48	150.73	82.10%	10,392.92	10,410.35	-0.17%	490	485	1.03%
42.70.3	276.15	203.04	36.01%	10,397.22	10,410.35	-0.13%	496	485	2.27%
42.90.3	271.53	227.72	19.24%	10,376.56	10,410.35	-0.32%	483	485	-0.41%

Results in Table 1 report that the MILP model was able to outperform the CT in all the studied instances, in terms of number of transfers. In average, the MILP model computed solutions with 63.95% more transfers than CT, and up to 176.42% for instance 42.30.3. Regarding the budgetary expenses, the MILP model managed to make a proper use of the resources. Schedules obtained with the MILP model have a smaller cost in 24 out of 25 instances (obtaining an average cost reduction of 2.21% and a maximum reduction of 12.42% for instance 40.100.4). In terms of the required number of buses, the solutions computed by the MILP model required 1.79% less buses on average and up to 12.62% less buses (for instance 40.100.4) than the current timetables applied in the city. These results confirm that the MILP model computed accurate and efficient schedules, both form the QoS and economic/resource utilization points of view.

Table 2 reports the average values of the three metrics used with instances grouped by the values of λ used to model different tolerance levels regarding the considered maximum waiting time W_b. This is a useful analysis to determine the capabilities of the proposed model to compute accurate solutions under tighter QoS thresholds for transfers. Figure 2 graphically summarizes the results.

Table 2: Average improvements of MILP solutions over CT for each value of λ

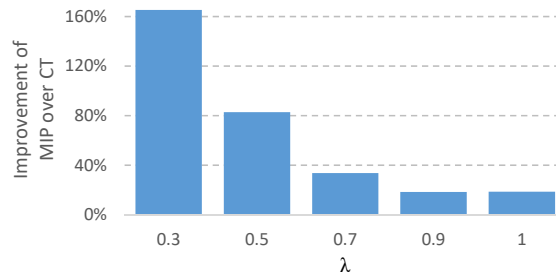| λ	average improvement (MILP over CT)		
	transfers	cost	# of buses
0.3	165.38%	-3.67%	-3.91%
0.5	83.00%	-0.82%	-1.10%
0.7	33.86%	-0.35%	0.94%
0.9	18.64%	-3.49%	-3.39%
1	18.85%	-2.71%	-1.49%

Fig. 2: Average improvements in the number of successful transfers of MILP solutions over CT for each value of λ.

Results in Table 2 indicate that, in terms of transfers, the MILP model was able to compute significantly better solutions than CT with smaller values of λ (Figure 2. The reason for this result is that the current timetables are not designed to promote or offer a better QoS to transfers. In addition, instances with a tighter threshold for waiting times pose a significantly more difficult challenge to practitioners to obtain manual solutions to the problem. The reason for this is that a smaller number of synchronizations will be considered successful since the time spent at the bus stop by the user waiting for the second bus exceeds the tolerance of the user. In this context, computer aided decision-making support tools, as the proposed MILP, contribute to successfully explore the solution space and obtain better solutions in these restricted instances.

Overall, results show that the computed solutions allow improving the QoS provided to passengers that perform transfers in the public transportation system of Montevideo. The QoS improvements are computed without increasing the overall operation cost of using additional resources.

5   Conclusions and future work

This article presented a MILP approach for bus timetabling to enhance multi-leg trips. The optimization proposes maximizing the number of successful transfers, while considering constraints on the QoS and the deployment cost.

The model was evaluated over a set of 25 real-world instances from the public transportation system in Montevideo, Uruguay, considering different numbers of bus lines and different threshold values for the maximum waiting time of users that transfer. The results evince that numerical solutions outperformed

the current timetables used in Montevideo in terms of the number of effective transfers (up to 176.42%), the total cost necessary to implement those schedules (up to 12.42%) and the number of buses to be used (up to 12.62%). Regarding transfers, the improvement of the numerically aided solutions over the manually crafted timetables increases as the problem becomes more restricted (smaller threshold value for the maximum allowable waiting time of users).

Overall, results show that schedules computed with the MIP model can efficiently use the available resources, since they have a larger number of successful transfers with similar budgets and a lesser number of running buses than the current–manually crafted–timetable.

The main lines for future work are related to include the cost to deploy the bus fleet as an optimization objective in a multi-objective approach, and including new technologies (i.e., electric buses) in the proposed model, with corresponding control variables to assess the convenience of using electric buses for some lines. Developing a more accurate QoS model for bus occupancy over direct travel is another line for future work.

References

1. Abbas, K., Abd-Allah, M.: Estimation and assessment of cost allocation models for main transit systems operating in cairo. Transport reviews **19**(4), 353–375 (1999)
2. Avenali, A., Boitani, A., Catalano, G., D'Alfonso, T., Matteucci, G.: Assessing standard costs in local public bus transport: A hybrid cost model. Transport Policy **62**, 48–57 (2018)
3. Benítez, G.: Progresividad y focalización en los subsidios del transporte público de Montevideo. Master's thesis, Universidad de la República, Uruguay (2020)
4. Ceder, A., Tal, O.: Timetable synchronization for buses. In: Lecture Notes in Economics and Mathematical Systems, pp. 245–258. Springer Berlin Heidelberg (1999)
5. Ceder, A., Wilson, N.: Bus network design. Transportation Research Part B: Methodological **20**(4), 331–344 (1986)
6. Cherwony, W., Gleichman, G., Porter, B., Hamilton, B.: Bus route costing procedures: a review. Urban Mass Transportation Administration of United States (1981)
7. Cherwony, W., Mundle, S.: Peak-base cost allocation models. Transportation Research Record **663**(663), 52–56 (1978)
8. Chu, J., Korsesthakarn, K., Hsu, Y., Wu, H.: Models and a solution algorithm for planning transfer synchronization of bus timetables. Transportation Research Part E: Logistics and Transportation Review **131**, 247–266 (2019)
9. Deakin, M., Al Waer, H.: From intelligent to smart cities. Intelligent Buildings International **3**(3), 140–152 (2011)
10. Fouilhoux, P., Ibarra, O., Kedad, S., Rios, Y.: Valid inequalities for the synchronization bus timetabling problem. European Journal of Operational Research **251**(2), 442–450 (2016)
11. Grava, S.: Urban Transportation Systems: Choices for Communities. McGraw-Hill (2002)
12. Hipogrosso, S., Nesmachnow, S.: Analysis of sustainable public transportation and mobility recommendations for montevideo and Parque Rodó neighborhood. Smart Cities **3**(2), 479–510 (2020)

13. Ibarra, O., Delgado, F., Giesen, R., Muñoz, J.: Planning, operation, and control of bus transport systems: A literature review. Transportation Research Part B: Methodological **77**, 38–75 (2015)
14. Ibarra, O., Rios, Y.: Synchronization of bus timetabling. Transportation Research Part B: Methodological **46**(5), 599–614 (2012)
15. Marquez, G.: Informe sobre tarifas y subsidios a usuarios del sistema de transporte público de pasajeros de Montevideo (2019)
16. Massobrio, R., Nesmachnow, S.: Urban mobility data analysis for public transportation systems: a case study in Montevideo, Uruguay. Applied Sciences **10**(16), 5400 (2020)
17. Massobrio, R., Nesmachnow, S., Muraña, J., Dorronsoro, B.: Learning to optimize timetables for efficient transfers in public transportation systems. Applied Soft Computing **119**, 108616 (2022)
18. Mehran, B., Yang, Y., Mishra, S.: Analytical models for comparing operational costs of regular bus and semi-flexible transit services. Public Transport **12**(1), 147–169 (2020)
19. Mishra, S., Mehran, B., Sahu, P.: Assessment of delivery models for semi-flexible transit operation in low-demand conditions. Transport Policy **99**, 275–287 (2020)
20. Nesmachnow, S., Baña, S., Massobrio, R.: A distributed platform for big data analysis in smart cities: combining intelligent transportation systems and socioeconomic data for Montevideo, Uruguay. EAI Endorsed Transactions on Smart Cities pp. 1–18 (2017)
21. Nesmachnow, S., Hipogrosso, S.: Transit oriented development analysis of parque rodó neighborhood, montevideo, uruguay. World Development Sustainability **1**, 100017 (2022)
22. Nesmachnow, S., Iturriaga, S.: Cluster-UY: collaborative scientific high performance computing in Uruguay. In: International Conference on Supercomputing in Mexico. pp. 188–202. Springer (2019)
23. Nesmachnow, S., Muraña, J., Goñi, G., Massobrio, R., Tchernykh, A.: Evolutionary approach for bus synchronization. In: Communications in Computer and Information Science, pp. 320–336. Springer International Publishing (2020)
24. Nesmachnow, S., Risso, C.: Exact and evolutionary algorithms for synchronization of public transportation timetables considering extended transfer zones. Applied Sciences **11**(15), 7138 (2021)
25. Risso, C., Nesmachnow, S.: Designing a backbone trunk for the public transportation network in Montevideo, Uruguay. In: Smart Cities, pp. 228–243. Springer (2020)
26. Rossit, D., Nesmachnow, S., Toutouh, J.: Multiobjective design of sustainable public transportation systems. CEUR Workshop Proceedings **2858**, 152–159 (2021)
27. Sinner, M., Weidmann, U., Nash, A.: Application of a cost-allocation model to swiss bus and train lines. Transportation Research Record **2672**(8), 431–442 (2018)
28. Taylor, B., Garrett, M., Iseki, H.: Measuring cost variability in provision of transit service. Transportation Research Record **1735**(1), 101–112 (2000)
29. Tolley, R. (ed.): Sustainable Transport. Elsevier (2003)
30. Toutouh, J., Nesmachnow, S., Rossit, D.: Generative adversarial networks to model air pollution under uncertainty. CEUR Workshop Proceedings **2858**, 169–174 (2021)
31. Wu, Y., Yang, H., Tang, J., Yu, Y.: Multi-objective re-synchronizing of bus timetable: Model, complexity and solution. Transportation Research Part C: Emerging Technologies **67**, 149–168 (2016)

Impact analysis of the implementation of V2G technology on electric distribution networks

Erick Delgado[1], Luis Medina[1], Miguel Davila-Sacoto[2][0000-0001-6318-2137], L.G. González[1][0000-0001-9992-3494], Luis Hernández-Callejo[2][0000-0002-8822-2948], and J.L. Espinoza[1][0000-0002-7450-2084]

[1] Electrical Engineering Department, University of Cuenca, 010104 Cuenca, Ecuador
[2] Agricultural and Forestry Engineering Department, University of Valladolid, 42004 Soria, Spain

erick.delgado@ucuenca.edu.ec
jose.medinam@ucuenca.edu.ec
miguelalberto.davila@estudiantes.uva.es
luis.gonzalez@ucuenca.edu.ec
luis.hernandez.callejo@uva.es
juan.espinoza@ucuenca.edu.ec

Abstract. This document presents an analysis of the impact of vehicle-to-grid (V2G) technology implementation in a distribution network, taking as reference an urban residential area of Cuenca (Ecuador), belonging to feeder, owned by Empresa Eléctrica Regional Centrosur (EERCS). A specialized software for distribution systems (CYME) provided by EERCS was used for this study. For the power flow simulations, the hourly demand over one day was considered. The analysis is focus on the distribution lines and distribution transformers load level, feeder demand, feeder losses and voltage level. For this, the use of the electric vehicle (EV) has been modeled and its main electrical parameters have been determined. The analysis is carried out based on 14 study scenarios, based on penetration level of EVs, behavior of electrical demand, type of EV and charging strategy. From the results obtained, it was possible to evaluate the behavior of the distribution network with V2G, and to compare between the scenarios proposed.

Keywords: Electric vehicle, Feeder, V2G, demand, loading.

1   Introduction

The concept of distributed generation refers to generating electricity close to loads, especially from renewable energy sources, since the resource is widely available, and due to technological advances, the market has greater access to renewable generation devices. Globally, the incursion of generation by renewable sources reached 2 537 GW in 2019, showing an increase of 176GW compared to 2018 [1], not only with large-scale projects, but also including micro-generation.

Similarly, the adoption of electric vehicles (EVs) has increased in recent years as an alternative to the use of internal combustion vehicles (ICEV), that use fossil fuels for their operation and also generate polluting gases. However, the EV is a high demand load, which can cause overloads in the electrical network, so it becomes necessary to manage the load and the development of new technologies that allow the working of the electrical network.

The vehicle-to-grid (V2G) technology that refers to the bidirectional energy transfer between the EV and the grid [2] is currently in the development and research stage, with some pilot projects being carried out such as Zem2All in Spain or Miraflori in Italy [3, 4], which seek the integration of EVs with renewable generation and the distribution electric network. electricity grid. However, various investigations have identified barriers to face in the implementation of V2G [5, 6], from the technological point of view requires further development in electricity networks, communication and control systems, energy conversion, battery degradation [7–10]; in the regulatory framework it is necessary to implement policies and incentives for the participation of EVs (such as energy storage systems) in the electricity market [11, 12].

V2G is shown as an alternative to the adoption of EVs, which remain inactive 96 % of the time [13], so in addition to the use for transportation could provide services to the grid, such as: frequency regulation, voltage regulation, integration with renewable energies, energy storage, among others [6, 14, 15].

The power flow can be unidirectional (G2V), from the grid to the EV or bidirectional (G2V/V2G) where the EV injects active power or reactive power into the grid [16–18]. Therefore, V2G requires a more complex structure for its operation, however, it can provide greater benefits to both users and the network, being necessary optimization algorithms focused on reducing costs and losses in the network and managing the charging and discharge of EVs [19–25].

Some studies have analyzed the impact of the charge of EVs on distribution networks [26–28], while in this research has been conducted a steady state analysis of the impact of V2G on distribution networks, focused on the loading of distribution transformers (DT), loading of the distribution network (primary and secondary), demand curve and losses of the primary network, as well as voltage levels.

2   Modeling and simulation

2.1   Components of the study

For the study has been selected an urban-residential area of the City of Cuenca (Ecuador) with an extension of 0.413 km^2, which is supplied by a distribution network at 22 kV in medium voltage (MV), and 220/240V in low voltage (LV), belonging to the 0324 feeder (numbering of the EERCS). In this area have been identified 42 DT that supply energy to 2182 customers, mostly residential, this information, as well as the model of the distribution network was obtained from the electric distribution company of the area. The typical demand curve of 0324 feeder for a working day (Monday-Friday) and semi-working day (Saturday) is shown in Fig. 1.

Fig. 1 0324 Feeder Demand

The vehicles selected for the study are: the KIA SOUL EV model with a capacity of 27 kWh and the BYD e5 with a capacity of 60.5 kWh, which are already in circulation in the country and are of type BEV (battery electric vehicles).

2.2   General considerations

1. The average travel of a particular vehicle in the city of Cuenca is approximately 36 km [29].
2. Considering the social behavior of the area, it is evident that the mobility requirements are given around 07h00 (work, education, etc.) and 18h00 (return home), so the following restrictions have been defined:

   — All EVs must be fully charged (100%) at 06h00.
   — At peak demand hours (18h00 to 22h00) you cannot charge the EV and only V2G can be done. Due to the capabilities of the EVs, the KIA Soul EV vehicle will perform V2G from 19h00 to 22h00 and the BYD e5 vehicle from 18h00 to 22h00.
   — From 22h00 to 06h00 the next day, you can only charge the EV.

3. The number of EVs in the study area is considered based on the estimate of the existing vehicle fleet in 2019.

Considering the population projection for 2019 in Cuenca according to INEC [30], and the relationship between urban and rural density, it has been estimated that the population in the urban area is 410 759 inhabitants (Hab_C).

Knowing that the area of the city (A_C) is 70.59 km² and the study area (A_E) is 0,413 km², you get 2 407 inhabitants in the study area (Hab_E) by the Eq. (1).

$$Hab_E = \frac{(A_E)(Hab_C)}{A_C} \tag{1}$$

The ratio Hab/Veh (Inhabitants / vehicle) is given by the 92 601 vehicles registered for the year 2019 in Cuenca Hab/Veh [31] and the number of inhabitants previously

obtained, resulting in 4,435 Hab/Veh while the ratio between inhabitant and customer in the study area (Hab/Cl) is 1.103. Relating these factors is obtained 4.02 Cl/Veh by Eq. (2).

$$\frac{Cl}{Veh} = \frac{Hab/Veh}{Hab/Cl} \qquad (2)$$

Finally, in the Eq. (3) the quantity of vehicles per DT (Veh_{Ti}), knowing the customers connected to each one $Veh_{Ti}(Cl_{Ti})$:

$$Veh_{Ti} = \frac{Cl_{Ti}}{Cl/Veh} \qquad (3)$$

Obtaining in the study area 539 vehicles (Veh_E), according to the Eq. (4).

$$Veh_E = \sum_{i=1}^{42} Veh_{Ti} \qquad (4)$$

2.3 Study scenarios.

The study scenarios have been raised based on 4 variables: type of EV, demand behavior in the electric network on working day or semi-working day, penetration level (10% or 25%), and load strategy with load management (WLM) or without load management (WOLM), they are shown in Table 1

Table 1 Study scenarios

Day →	Working day		Weekend	
Type of EV	WOLM	WLM	WOLM	WLM
KIA	3) 10%	5) 10%	7) 10%	9) 10%
	4) 25%	6) 25%	8) 25%	10) 25%
BYD	-	11) 10%	-	13) 10%
	-	12) 25%	-	14) 25%
Without EVs	1)		2)	

For each level of penetration (N_P) the EVs are calculated per DT (EV_{Ti}), this being an integer, using the Eq. (5).

$$EV_{Ti} = (N_P)(Veh_E) \qquad (5)$$

The time restriction for G2V/V2G are based on the premise that at peak demand hours the charging of EVs is undesirable and that electricity rates are lower outside

these hours, in terms of G2V/V2G power, the battery capacity of each EV and the time available for charging are consider. To do this, the following process is followed:

1. The energy consumption per km (C_{Ek}) is determined by Eq. (6) considering the capacity of the battery (C_B) and autonomy (Au).

$$C_{Ek} = {C_B 10^3}/{Au} \qquad (6)$$

2. With an average travel of 36 km (R_p), when returning home, the EV has a state of charge (SoC_r) and remaining energy (E_r) according to the Eqs. (7) and (8).

$$SoC_r = \left(1 - \frac{(R_p)(C_{Ek})}{C_B 10^3}\right) * 100\% \qquad (7)$$

$$E_r = (SoC_r)(C_B) \qquad (8)$$

3. The energy injected into the grid by each EV (E_{V2G}) is obtained with the Eq. (9) in the period (t_{V2G}) and power (P_{V2G}) determined is:

$$E_{V2G} = (P_{V2G})(t_{V2G}) \qquad (9)$$

4. So, the state of charge (SoC_{V2G}) and remaining energy (Er_{V2G}) after V2G are calculated using Eqs. (10) and (11) respectively.

$$Er_{V2G} = E_r - E_{V2G} \qquad (10)$$

$$SoC_{V2G} = \frac{Er_{V2G}}{C_B}(100\%) \qquad (11)$$

A 25% SoC_{min} has been proposed in order not to significantly affect the life of the battery.

5. Finally, the charging of the EV is achieved in a set time (t_{G2V}) at a charging power (P_{G2V}), by means of the Eq. (12).

$$t_{G2V} = \frac{C_B - Er_{V2G}}{P_{G2V}} \qquad (12)$$

The parameter values for each EV model are presented in Table 2.

Table 2 Technical parameters of EVs

Parameter	KIA		BYD
	WOLM	WLM	WLM
$C_B (kWh)$	27	27	60.5
$Au\ (km)$	200	200	400
$C_{Ek}(Wh/km)$	135	135	151.25
$R_p\ (km)$	36	36	36
$SoC_r\ (\%)$	82%	82%	91%

E_r (kWh)	22.14	22.14	55.055
P_{V2G} (kWh)	5.83	5.83	5.83
t_{V2G} (h)	2.64	2.64	4
E_{V2G} (kWh)	15.39	15.39	23.32
SoC_{V2G} (kWh)	25%	25%	52%
Er_{V2G} (kWh)	6.75	6.75	31.74
P_{G2V} (kW)	5.83	3.375	4.794
t_{G2V} (h)	3.47	6	6

2.4 Modeling of the distribution network and EVs

The parameters of the components of the distribution network: distribution lines, DT, protection devices, capacitor bank and loads, were provided by the distribution company in the CYME software.

The EVs were modeled as a BESS (Battery Energy Storage System). On the LV side of each DT a concentrated load of the corresponding clients and BESS is connected. The main parameters entered for the BESS are: charging and discharging power, charging performance and battery losses, efficiency and capacity of the converter.

The efficiency values are estimates based on measurements made in the Microgrid laboratory of the University of Cuenca in the KIA vehicle, and a similar behavior was assumed for the BYD EV model, they are summarized in Table 3.

Table 3 Efficiency of EVs components.

Parameter		KIA		BYD
		WOLM	WLM	WLM
Battery	*G2V/V2G efficiency (%)*	97.5	97.5	97.5
Converter	*G2V efficiency (%)*	87.4	77.22	83.53
	V2G efficiency (%)	87.4	87.4	87.4

The simulations were performed on a timely basis (24h) using Newton Raphson's method for power flows. To assign the load to each DT has been used the function of load distribution based on the energy consumption of each user and the demand measured at the beginning of the 0324 feeder, obtaining an approximation to the behavior of the electrical network.

3   Results and discussion

3.1   DT load level

The following analysis shows the behavior of the load level of DT #6452 with 50 kVA of nominal power. This equipment presented the highest load levels of the DTs analyzed. The 41 DTs had similar behavior, but with lower load levels.

When using KIA SOUL EV vehicles, it is observed in Fig. 2 that when introducing 56 and 137 EVs for the penetration scenarios of 10 % and 25 % respectively, the load level at 19h00 decreases to 42.80 % and 31.86 % respectively. First, with 10 % of EVs without load management, the DT has a load level of 87.66 % at 22h00 and 75.72 % at 00h00. For the same hours, but with 25 % of EVs, the DT #6452 is overloaded with levels of 121.10 % and 108.70 % respectively. On the other hand, load management turns out to be a great relief for the DT because the maximum load level is given at 00h00 reaching 80.86 % and 62.53 % for EV penetration levels of 25 % and 10 % respectively. Therefore, by 00h00 when performing load management with 25 % of EVs increases the load level of the DT by 5.14 % compared to the scenario without load management with 10 % of EVs (75.72 %).

When using the BYD EV model the load level of the DT #6452, it is observed that when performing V2G from 18h00 contributes to reduce the load level considerably for peak hours, however, this makes the BYD e5 EV require a greater load power compared to the KIA SOUL EV and despite the load management that is carried out, the load level of the DT in the early hours of the morning increases by approximately 15 % compared to the KIA SOUL EV vehicle.
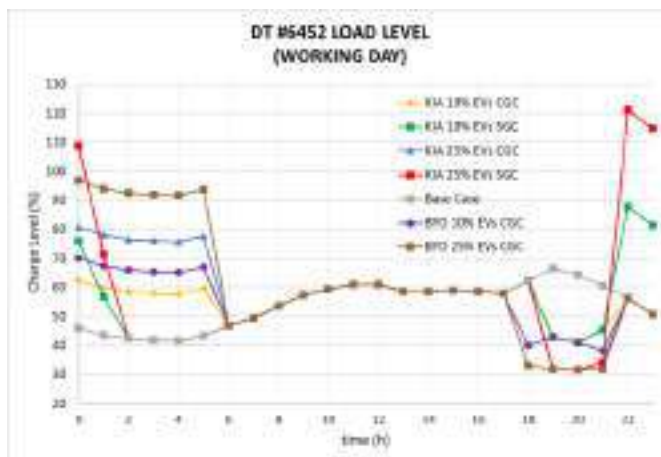

Fig. 2 DT #6452 load level for a working day

3.2   Feeder demand curve

When using KIA SOUL EV vehicles Fig. 3 shows that at the time of performing V2G (19h00-22h00) and when introducing 56 EVs (10 %) the peak demand of the entire 0324 feeder is eliminated and maintained for values below the demand of 18h00 (2 646.97 kW), on the other hand, a penetration of 137 EVs (25 %), causes a minimum of active power demand for the feeder 0324 at 20h00 (2 119.96 kW) and not at 21h00 where the base demand is lower, this because the KIA SOUL EV vehicle under the criteria established for this study can deliver energy to the grid only for 2h38 min. In turn, it is observed that without a charging strategy and only introducing 25 % of EVs in the assigned study area, the demand at 22h00 exceeds the peak demand of the base case, while with load management maintains active power values around 2 MW for the entire feeder, much lower than its peak in the base case of 2.9 MW.

The scenarios with BYD vehicles show that for the scenario of 10 % of EVs the peak demand is reduced to 2 626.52 kW with respect to the base case while in the scenario of 25 % of EVs the peak demand is reduced to 2 222.08 kW the smart load for this scenario does not exceed the base demand of 11h00 (2 487.78 kW) becoming the best of the scenarios presented for the 0324 feeder.

Fig. 3 Demand from 0324 Feeder on a Working Day

3.3   Feeder load level

Taking as a reference the results shown in the previous section, it can be considered that the most critical scenario is for the 25 % penetration of KIA SOUL EV vehicles, without load management at 22h00 (Scenario 4), so it is important to know the load level of the medium voltage network of the feeder in those conditions, in Fig. 4 case A scenario 4 it is observed that the main branch of the feeder has a load level between 20-30 %, and the secondary branches in their great majority maintain a load level between 0-5 %. On the other hand, for the base case (case A scenario 1) the load level of the main feeder section is between 10-20 % and the secondary branches mostly remain

between 0-5 %. This indicates that the effect of EV charging on the load level of medium voltage networks is very slight.

The load level of the feeder at the peak demand time (19h00), for scenarios 1 and 4 are shown in case B respectively, For the base case (Scenario 1), the main branch of the feeder has a load level between 20-30 % and the secondary branches remains between 0-5 % mostly, while for Scenario 4 the load level of the main branch of the feeder is reduced, which presents values between 10-20 % while the secondary branches do not present significant differences. That is to say that the relief of the load level of the medium voltage networks in the hours of V2G are very slight.
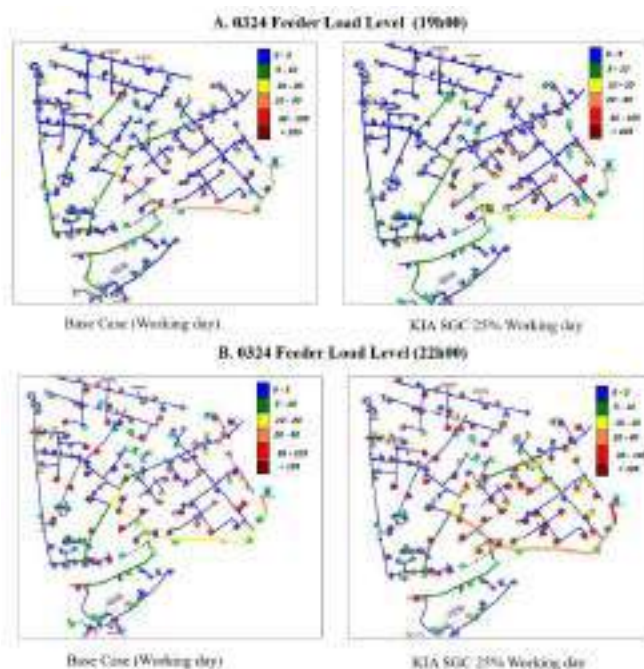

Fig. 4 0324 Feeder load level for base case and scenario 4: A. 19h00, B. 22h00.

3.4   Feeder losses

Table 4 shows an increase in losses of active and reactive power compared to the base case, this is normal due to the introduction of new load (EVs) in the feeder, however, this increase in active losses is very small compared to the number of EVs that is introduced, goes from 2.18 kWh/day for the KIA SOUL EV vehicle with a penetration of 10 % of EVs in a working day, which represents 0.167 %, and reaches values up to 38.20 kWh / day for the BYD e5 vehicle with a penetration of 25 % of EVs in a semi-working day that represents 3.058 %.

When comparing the active power losses for the same level of penetration and the same day of study, using KIA SOUL EV vehicles it is seen that applying load management the losses decrease significantly compared to the scenario without load management. With load management for 10 % penetration of EVs losses are reduced on average 2.73 times, while for a penetration of 25 % EVs losses are reduced on average 1.61 times.

Analyzing the losses of active power with load management and for the same level of penetration can be noticed a slight increase in losses in the semi-working day compared to the working day, because the base demand is higher in the early morning hours (00h00–04h00) for the semi-working day. Therefore, these results become a strong constraint if you want to perform a charging strategy that minimizes the losses of active power to the maximum in the feeder.

When comparing between the KIA SOUL EV vehicle and the BYD vehicle for the same day and the same penetration it can be observed that the losses are approximately 1.8 times more using the BYD vehicle than using the KIA SOUL EV vehicle. Reactive power losses for the analysis performed above follow the same behavior as active power losses.

Table 4 Active and reactive power losses of feeder 0324 on the day for the fourteen study scenarios.

| No.	Scenarios[1]	Difference from scenarios 1 and 2. P (%)	Difference from scenarios 1 and 2. Q (%)
1	Without EV/Weekday	0.00	0.00
2	Without EV/Weekend	0.00	0.00
3	KIA/WOLM/10%/Weekday	0.48	1.56
4	KIA/WOLM/25%/Weekday	2.44	8.06
5	KIA/WLM/10%/Weekday	0.17	0.59
6	KIA/WLM/25%/Weekday	1.36	4.61
7	KIA/WOLM/10%/Weekend	0.49	1.83
8	KIA/WOLM/25%/Weekend	2.34	8.70
9	KIA/WLM/10%/Weekend	0.19	0.76
10	KIA/WLM/25%/SL	1.64	6.15
11	BYD/WLM/10%/L	0.31	1.10
12	BYD/WLM/25%/L	2.59	8.72
13	BYD/WLM/10%/Weekend	0.47	1.78
14	BYD/WLM/25%/Weekend	3.06	11.45

---

[1] The scenarios are described with the following structure: EV Type/Charging Strategy/Penetration Level/Day.

3.5 Voltage levels

Voltage profiles considering BYD e5 vehicles are shown in Fig. 5 for 19h00., where they contribute to improving voltages in a similar way to that carried out in previous scenarios with the KIA SOUL EV, while in Fig. 48 for 00h00 the voltage profiles decreased with respect to the base case.
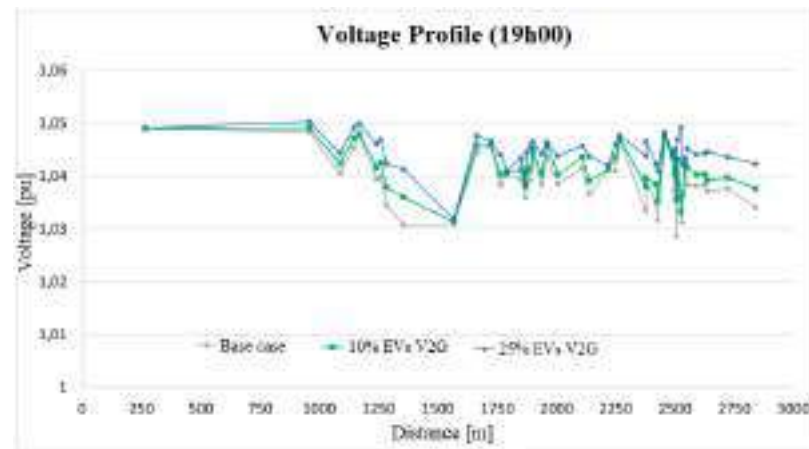
(a)
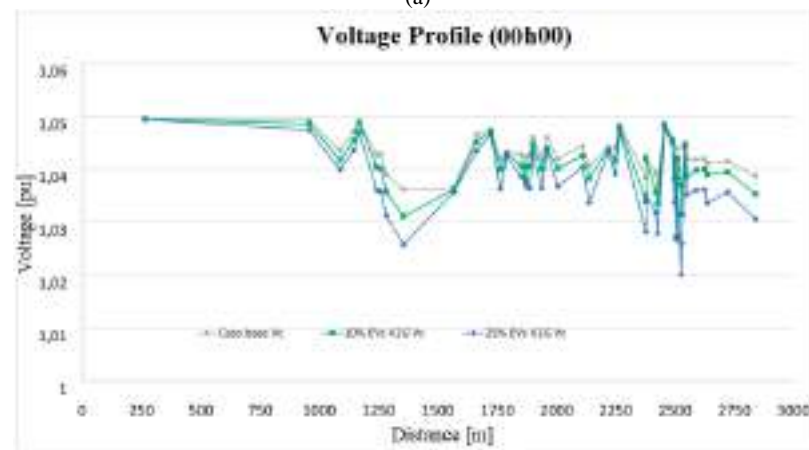
(b)

Fig. 5 Load profiles in Distribution Transformers (a) at 19h00 (b) at 00h00

The voltage values observed in the low voltage nodes of the DT in question without the presence of EVs are at adequate levels, within the limits established by the regulations in force in Ecuador (0.95 p.u – 1.05 p.u) [32], due to the compensation elements that the distribution network has; while, with the insertion of EVs in the study scenarios, voltage levels slightly increased in the hours of V2G and were slightly reduced in the hours of loading, these variations are in the order of 0.015 p.u, which is not representative.

4   Conclusions

Based on the results obtained, only with 10 % penetration of KIA SOUL EV type vehicles with load management was achieved to reduce the DT load level at the peak demand hour, without producing a higher demand in another period, which ratifies the importance of the charging / discharge power and the number of EVs connected.

When comparing the scenarios of a working day and semi-working day, the importance of analyzing the social behavior in the study area and the type of client (residential, commercial, urban, rural) is evident, since based on these variables, different strategies for the charging and discharge of the EVs should be proposed.

Because MV lines in a distribution network are planned in the long term, it is observed that the load level of both the main section and secondary branches is low, which is not a limitation for the penetration of EVs, however, the reduction in load level obtained by implementing V2G is not significant.

The effect of V2G on voltage levels was not representative, due to the modeling of EVs as an active power-only storage system. To achieve representative voltage compensation, it is necessary to model the power converter with the possibility of providing reactive power, however, in such a case, V2G should focus on sections of the low voltage distribution network that present low voltage levels.

References

1.　　IRENA: Estadísticas de Capacidad Renovable 2020.
2.　　Kempton, W., Letendre, S.E.: Electric vehicles as a new power source for electric utilities. Transp. Res. Part D Transp. Environ. 2, 157–175 (1997). https://doi.org/10.1016/S1361-9209(97)00001-1.
3.　　Real World Test of V2G Now Underway in Spain (w/videos).
4.　　The Vehicle-to-Grid pilot project has been inaugurated at Mirafiori | E-mobility | FCA.
5.　　Liu, B.C., Ieee, M., Chau, K.T., Ieee, F., Wu, D., Ieee, S.M.: Opportunities and Challenges of Vehicle-to-Home , Vehicle-to-Grid Technologies. 1–19 (2013).
6.　　Yilmaz, M., Krein, P.T.: Review of benefits and challenges of vehicle-to-grid technology. 2012 IEEE Energy Convers. Congr. Expo. ECCE 2012. 3082–3089 (2012). https://doi.org/10.1109/ECCE.2012.6342356.
7.　　Yamileth, N., Brizuela, M., Evangelina, J.: El esquema "Vehicle to grid" y los desafíos de su implementación en las actuales redes eléctricas. In: ESTUDIOS ESTRATÉGICOS DEL SECTOR ENERGÉTICO. pp. 332–358 (2017).
8.　　Dehaghani, E.S., Williamson, S.S.: On the inefficiency of vehicle-to-grid (V2G) power flow: Potential barriers and possible research directions. 2012 IEEE Transp. Electrif. Conf. Expo, ITEC 2012. (2012). https://doi.org/10.1109/ITEC.2012.6243446.
9.　　Noel, L., Zarazua de Rubens, G., Kester, J., Sovacool, B.K.: Vehicle-to-Grid. Vehicle-to-Grid. 65–89 (2019). https://doi.org/10.1007/978-3-030-04864-8.
10.　Dallinger, D., Krampe, D., Wietschel, M.: Vehicle-to-grid regulation reserves based on a dynamic simulation of mobility behavior. IEEE Trans. Smart Grid. 2, 302–313 (2011). https://doi.org/10.1109/TSG.2011.2131692.
11.　Castagneto Gissey, G., Dodds, P.E., Radcliffe, J.: Market and regulatory barriers to electrical energy storage innovation. Renew. Sustain. Energy Rev. 82, 781–790 (2018). https://doi.org/10.1016/j.rser.2017.09.079.
12.　Richardson, D.B.: Encouraging vehicle-to-grid (V2G) participation through premium tariff rates. J. Power Sources. 243, 219–224 (2013). https://doi.org/10.1016/j.jpowsour.2013.06.024.
13.　Kempton, W., Tomić, J.: Vehicle-to-grid power fundamentals: Calculating capacity and net revenue. J. Power Sources. 144, 268–279 (2005). https://doi.org/10.1016/j.jpowsour.2004.12.025.
14.　Lauinger, D., Vuille, F., Kuhn, D.: European Battery , Hybrid and Fuel Cell Electric Vehicle Congress A review of the state of research on vehicle - to - grid (V2G): Progress and barriers to deployment. Eur. Batter. , Hybrid Fuel Cell Electr. Veh. Congr. 1–8 (2017).
15.　Saini, S., Thakur, T., Kirar, M.: A Review of Electric Vehicles Charging Topologies, its Impacts and Smart Grid Operation with V2G Technology. SSRN Electron. J. (2020). https://doi.org/10.2139/ssrn.3575388.
16.　Distribution System V1G PEV Charging Impacts Report. (2018).
17.　Tan, K.M., Ramachandaramurthy, V.K., Yong, J.Y.: Integration of electric vehicles in smart grid: A review on vehicle to grid technologies and optimization techniques. Renew. Sustain. Energy Rev. 53, 720–732 (2016). https://doi.org/10.1016/j.rser.2015.09.012.

18.   Sovacool, B.K., Axsen, J., Kempton, W.: The Future Promise of Vehicle-to-Grid (V2G) Integration: A Sociotechnical Review and Research Agenda. Annu. Rev. Environ. Resour. 42, 377–406 (2017). https://doi.org/10.1146/annurev-environ-030117-020220.

19.   Parashar, S., Swarnkar, A., Niazi, K.R., Gupta, N.: Optimal integration of electric vehicles and energy management of grid connected microgrid. 2017 IEEE Transp. Electrif. Conf. ITEC-India 2017. 2018-Janua, 1–5 (2018). https://doi.org/10.1109/ITEC-India.2017.8333854.

20.   Bai, X., Qiao, W., Wei, H., Huang, F., Chen, Y.: Bidirectional coordinating dispatch of large-scale V2G in a future smart grid using complementarity optimization. Int. J. Electr. Power Energy Syst. 68, 269–277 (2015). https://doi.org/10.1016/j.ijepes.2014.12.072.

21.   Esmaili, M., Shafiee, H., Aghaei, J.: Range anxiety of electric vehicles in energy management of microgrids with controllable loads. J. Energy Storage. 20, 57–66 (2018). https://doi.org/10.1016/j.est.2018.08.023.

22.   Sortomme, E., El-Sharkawi, M.A.: Optimal combined bidding of vehicle-to-grid ancillary services. IEEE Trans. Smart Grid. 3, 70–79 (2012). https://doi.org/10.1109/TSG.2011.2170099.

23.   Sortomme, E., El-Sharkawi, M.A.: Optimal charging strategies for unidirectional vehicle-to-grid. IEEE Trans. Smart Grid. 2, 131–138 (2011). https://doi.org/10.1109/TSG.2010.2090910.

24.   Saboori, H., Jadid, S.: Optimal scheduling of mobile utility-scale battery energy storage systems in electric power distribution networks. J. Energy Storage. 31, 101615 (2020). https://doi.org/10.1016/j.est.2020.101615.

25.   Ortega-Vazquez, M.A.: Optimal scheduling of electric vehicle charging and vehicle-to-grid services at household level including battery degradation and price uncertainty. IET Gener. Transm. Distrib. 8, 1007–1016 (2014). https://doi.org/10.1049/iet-gtd.2013.0624.

26.   Liasi, S.G., Golkar, M.A.: Electric vehicles connection to microgrid effects on peak demand with and without demand response. 2017 25th Iran. Conf. Electr. Eng. ICEE 2017. 1272–1277 (2017). https://doi.org/10.1109/IranianCEE.2017.7985237.

27.   Oliinyk, M., Dzmura, J., Pal, D.: The impact of a electric vehicle charging on the distribution system. Proc. - 2020 21st Int. Sci. Conf. Electr. Power Eng. EPE 2020. 1–5 (2020). https://doi.org/10.1109/EPE51172.2020.9269213.

28.   Feng, K., Zhong, Y., Hong, B., Wu, X., Lai, C.S., Bai, C.: The Impact of Plug-in Electric Vehicles on Distribution Network. 2020 IEEE Int. Smart Cities Conf. ISC2 2020. 0–4 (2020). https://doi.org/10.1109/ISC251055.2020.9239073.

29.   Sarango, D., Moncayo, P.: Determinación del indicador kilómetros-vehículo recorrido (KVR) para la ciudad de Cuenca, (2016).

30.   Instituto Nacional de Estadísticas y Censos (INEC): Proyeccion Cantonal Total 2010-2020, (2016).

31.   EMOV: Rendición de Cuentas 2019.

32.   Agencia de regulación y control de energía y recursos naturales no renovables: Regulación ARCERNNR 002/20, (2020).

PVT systems in high summer temperature cities: technical feasibility

J. A. Aguilar-Jiménez [1,2,*], L. Hernández-Callejo [3,*], J. A. Suástegui-Macías [2], R. A. López-Meraz [4]

[1] Centro de Estudios de las Energías Renovables, Instituto de Ingeniería, Universidad Autónoma de Baja California, Blvd. B. Juárez s/n, 21280, Mexicali, BC, México.
[2] Facultad de Ingeniería, Universidad Autónoma de Baja California, Blvd. B. Juárez s/n, 21280, Mexicali, BC, México.
[3] Department of Agricultural Engineering and Forestry, University of Valladolid (UVA), Campus Universitario Duques de Soria, 42004 Soria, Spain.
[4] Unidad de Ingeniería y Ciencias Químicas, Universidad Veracruzana, Veracruz, México.
aguilarj30@uabc.edu.mx (J.A.A-J.); luis.hernandez.callejo@uva.es (L.H-C.)

Abstract. This work presents the study of a solar heating and electricity generation system using photovoltaic/thermal solar collectors, under a domestic consumption scenario. The climatic conditions where these systems are installed are of vital importance to determine their energy feasibility. In locations where ambient temperatures are high, the performance and operation of these technologies may be limited. In this study, the city of Mexicali, Baja California, Mexico, is considered as a case study due to its extreme environmental conditions, and is compared energetically with Mexico City, which has stable temperatures throughout the year. The TRNSYS program was used to develop a simulator to study the systems under typical weather conditions of each scenario and to determine the energy use that can be achieved. The results show that although Mexicali has a greater solar resource throughout the year, in Mexico City a greater use of these technologies is achieved due to the fact that a greater amount of heat is required for domestic water heating. This hybrid technology is limited in Mexicali because, due to its high environmental temperatures in summer, its operation is interrupted for a period of approximately 4 months, so its energy benefits are not exploited throughout the year, unlike in Mexico City.

Keywords: Solar energy, PVT collectors, Sustainability, Solar heating

1   Introduction

Replacing fossil fuels and moving towards an energy matrix based on renewable energies is one of the main actions to reduce the generation of greenhouse gases in order to mitigate the effects of climate change in the world. Countries are increasingly implementing energy policies to decarbonize their different sectors. The main sector generating polluting gases in the world is the energy sector, which accounts for 73.2% of total emissions. Within this sector, energy used in buildings accounts for 17.5% of all

pollutant emissions worldwide[1]. This forces the public and private sectors to seek technically and economically feasible solutions that promote the sustainable development of their activities. The different sectors demand electrical and thermal energy, and the fastest way to satisfy this need is with traditional energy sources, such as fossil fuels, which has repercussions on environmental pollution. Solar energy is a sufficiently mature technology to be able to meet the need for electrical and thermal energy.

Photovoltaic-thermal solar collectors (PVT) are a technology capable of satisfying the needs for electricity and heat simultaneously, with proven benefits [2]. The performance of PVT collectors is better than solar thermal and photovoltaic systems working separately [3], due to advantages such as collection area and overall energy conversion efficiency (thermal and electrical per collection area). However, one of the main problems of this technology is the price of the equipment [4]. Seeking to make these systems more energetically attractive and increase their applications, Ma *et al.* [5] proposed connecting a PVT collector and a solar collector in series to increase the heat transfer fluid outlet temperature. They found that the electrical efficiency of the system decreases little, but high quality thermal energy is obtained, so it can be an option for the domestic sector. Several studies show that the use of nanofluids in PVT collectors increases thermal efficiency [6, 7]. Herrando *et al.* analyzed the life cycle of PVT technology in an application to provide heat, cooling and electricity, compared to a traditional photovoltaic system, and concluded that over the lifetime of the project it can reduce CO2 emissions by 46% to 51% compared to a photovoltaic system alone. This allows for more sustainable technologies for the benefit of the planet. Therefore, the use of these heating and power generation technologies in the domestic sector is of vital importance to move towards global sustainability, especially in those scenarios where fossil fuels are used to meet domestic hot water (DHW) and electricity demands.

Factors such as ambient temperature, available solar radiation, application temperature and the local cost of energy are fundamental aspects in the decision making of this type of facilities. However, most of the studies of this type of technologies focus on the energy and/or economic part of similar locations, so it is necessary to focus on those regions where extreme climates can be contrasted, due to their high and low environmental temperatures, as well as their levels of solar radiation.

This work presents the energy analysis of a PVT collector system located in the city of Mexicali, Baja California, Mexico, which presents extreme weather conditions that affect the operation of the PVT collectors. It is compared energetically with the same PVT system but located in Mexico City, where ambient temperatures are more stable throughout the year and DHW requirements are higher. This study addresses the effect of locations with high ambient temperatures and their energy impact on PVT collectors, which has not been previously presented in the state of the art. The Mexicali scenario allows us to determine how much the systems are affected energetically, independent of the high solar resource present at the location.

2   System description

Fig. 1 shows the PVT collector system considered in this study. It consists of a field of collectors connected in series, which are responsible for converting solar radiation into photovoltaic and thermal energy simultaneously. In order to make better use of the solar thermal energy, a thermal storage tank connected directly to the solar collector field by means of a circulation pump is considered. The tank helps to be able to use solar thermal energy in periods when demand does not match availability. An arrangement of diverter and mixing valves allows the temperature of the water used for DHW to be regulated to avoid delivering higher temperatures to the users. There is also an auxiliary heating system to ensure that water is always supplied at the required temperature for DHW in the event that there is no solar resource and/or thermal energy stored in the tank.
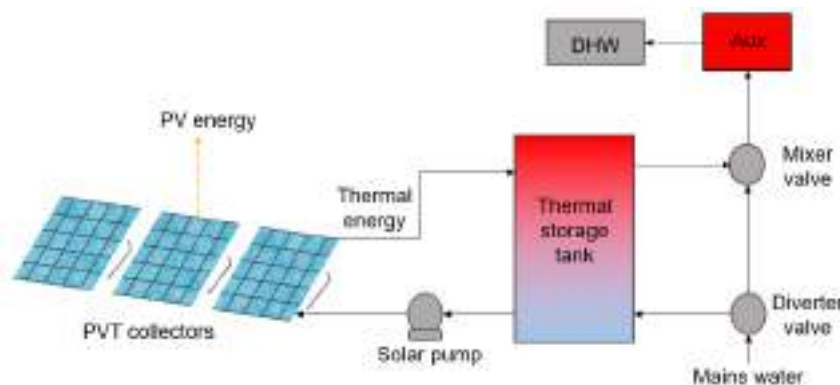
Fig. 1. Schematic diagram of the PVT collector system considered in this study.

Table 1 shows the characteristics of the PVT collector used. The characteristics correspond to the collector made by the Spanish company Abora Solar, model aH72SK [8]. The thermal storage tank has a volume of 200 L and is considered to be stratified in 3 temperature levels.

Table 1. Characteristics of the PVT collector [8]

Thermal data	
Aperture area	1.88 m^2
Optical efficiency (a_0)	0.7
First order heat loss coefficient (a_1)	5.98 $W/K/m^2$
Second order heat loss coefficient (a_2)	0 $W/K^2/m^2$
Working fluid	Water
Electrical data	
Photovoltaic cell type	Monocrystalline
Cells number	72

Nominal power	280 W
Module efficiency	17.8%
MPP voltage	39.86 V
MPP current	8.76 A
Open circuit voltage	48.61 V
Short circuit current	9.16 A
NOCT	45°C
V_{oc} thermal coefficient	-0.28 %/K
I_{sc} thermal coefficient	0.06 %/K
Power thermal coefficient	-0.36 %/K

3   Methodology

3.1   Simulator description

The simulation study was carried out using the TRNSYS® software [9] for the modeling of the system in general. This software has the advantage of having programmed models, called "types" of a large number of equipment, within which can be found photovoltaic modules, solar thermal collectors, storage tanks and other renewable technologies, to mention some. One of the main features of TRNSYS is that it uses a typical meteorological database (TMY) within its simulation process, where variations in radiation, wind speed, ambient temperature, loads, among many others, are contemplated, allowing the system to be studied under real operating conditions. The interface of the developed simulator is shown in Fig. 2.
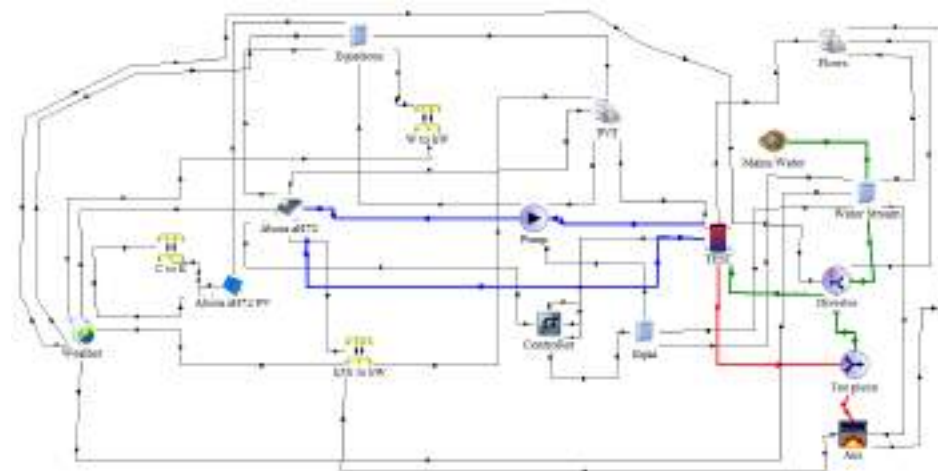

Fig. 2. PVT system simulator developed in TRNSYS.

The numerical validation of the simulator used in TRNSYS can be verified in the previous work of Aguilar-Jiménez *et al.* [2], as well as the mathematical models used for the calculation of efficiencies, energy and other variables considered in this study. For the simulation of the PVT module in TRNSYS, a combination of the flat plate solar collector and photovoltaic module types was considered, methodology proposed by Gagliano *et al.* [10].

3.2   Weather conditions

The city of Mexicali, Baja California, and Mexico City were considered in this analysis as scenarios for comparison. Both cities have different climatological conditions throughout the year. Mexicali is known for its extreme climate; in summer it can reach 50°C in the shade and in winter it can reach 0°C. Mexico City, on the other hand, has more stable weather conditions, with ambient temperatures that do not exceed 25°C. By considering both cities for comparison, it will allow to identify the climatological factors and their impact on energy production, both thermal and electrical, relating it to the heat needs for each scenario. Fig. 3 shows the (a) global solar radiation, (b) ambient temperature and (c) water temperature for both locations. Climatological information in TMY format was obtained from the Photovoltaic Geographical Information System database of the European Commission [11].

These cities were considered because of the different ambient temperatures that occur during the year. This is directly related to the energy needs for DHW and PVT collector operation. In Mexicali, especially in the summer period, ambient temperatures are so high, as shown in Fig. 3(b), that it is not necessary to heat water from the network to reach the required temperature. However, in Mexico City, water heating for DHW is required all year round. Considering the transition towards the use of sustainable technologies, such as renewable energies, PVT collectors should be energetically attractive for their implementation. In this study it was considered that when the water temperature of the network is higher than 32°C the solar heating system of the PVT collectors will not be used, since the water will be taken directly from the network for its normal use, as it is usually considered in the summer months in Mexicali. This makes the viability of this type of hybrid technology in cities with high ambient temperatures questionable.
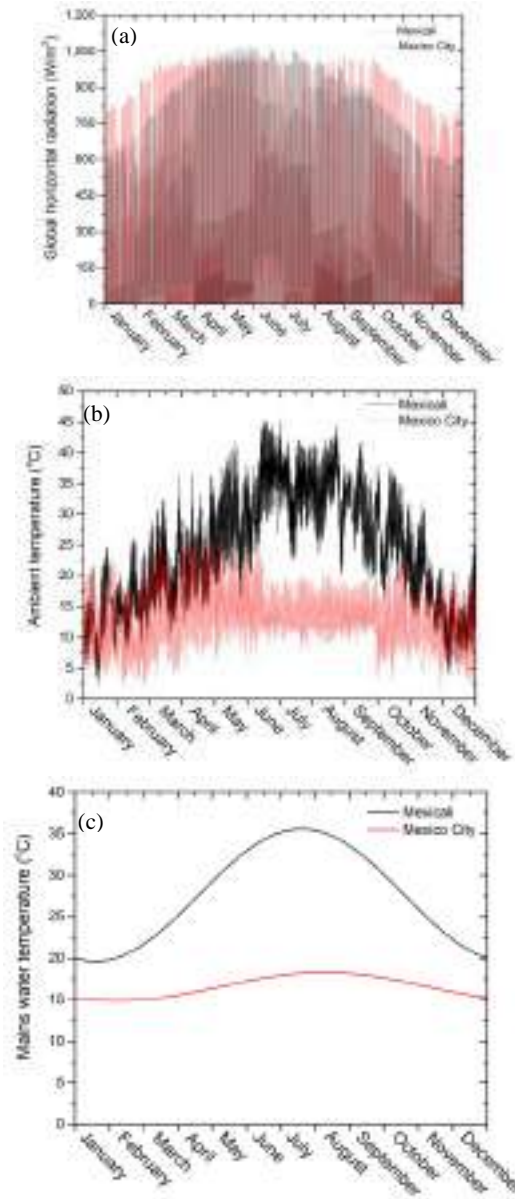
Fig. 3. Climatological conditions of Mexicali and Mexico City, showing (a) horizontal global radiation, (b) ambient temperature and (c) mains water temperature.

3.3   Water consumption profile

The hourly water consumption profile for DHW for both cities, specified in the standard EN 15,316:2007 [12], was used in this study and can be appreciated in the Fig. 4. The water flow required for 4 people was considered. The temperature of this water flow was considered at 45°C (set-point in the auxiliary system, with an efficiency of 0.9) except when the mains water temperature is higher than 32°C, under this scenario it will be taken directly at this temperature.
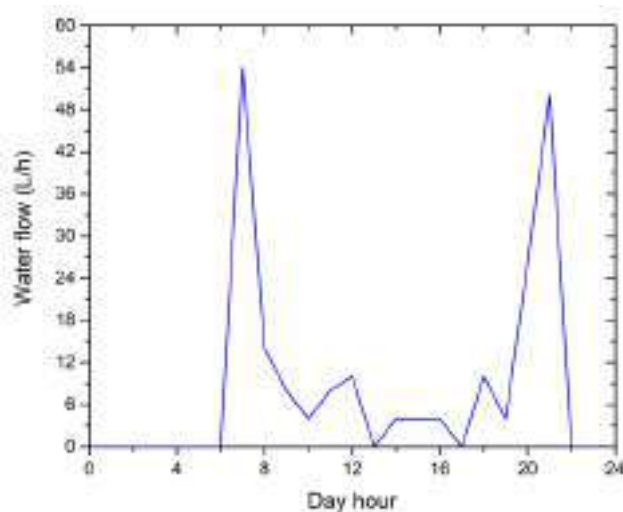

Fig. 4. DHW demand profile used in simulation.

4   Results

Fig. 5 shows the thermal energy required in both cities to satisfy the DHW demand, without considering the contribution of PVT collectors and only the water flow from the network. It shows that the thermal energy needs are considerably higher for Mexico City, with a total of 10,728 kWh per year, 102 % higher than Mexicali. This is due to the temperature of the water in the network, which is always lower in Mexico City, requiring more thermal energy to achieve the set-point temperature. It is important to note the time period between the months of May and September for Mexicali, since there is no need for water heating due to the water temperature of the mains water which is higher than 32°C. During these months in this city there is no need for water heating due to weather conditions. This is relevant for solar heating systems, regardless of whether they are PVT or only thermal collectors, since it is a period of approximately 4 months in which their operation is stopped.
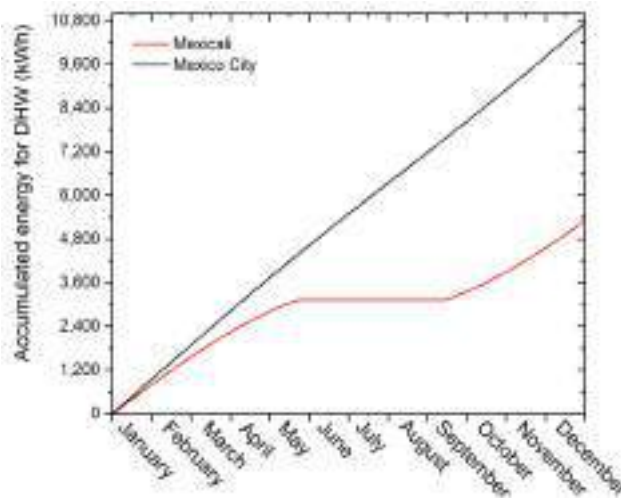
Fig. 5. Annual energy required for DHW without PVT collector input.

The effect of considering one or more PVT collectors to satisfy the thermal energy requirements for DHW, as well as useful heat generation, can be seen in Fig. 6. The higher amount of useful heat generation for PVT collectors located in Mexico City stands out for all the PVT collectors studied. These differences are related to the amount of heat required to satisfy the DHW; since a greater amount of heat is required in Mexico City, it is possible to take greater advantage of the heat generation by the PVT collectors. On the other hand, in Mexicali, due to high ambient and mains water temperatures, the heat generation that can be done by PVT collectors annually is lower, regardless of the fact that the solar resource in Mexicali is greater than that of Mexico City. With the demand profile considered and the environmental conditions presented, a PVT collector in Mexicali produces a total of 1,145 kWh of useful heat annually, 66% less than what it would generate located in Mexico City under the same water demand conditions. As the number of collectors increases the percentage increases. By using 6 PVT collectors, the useful heat generation in Mexico City is 72% higher than that produced in Mexicali. This is related to the greater use of the solar resource immediately and to the energy stored in the tank in Mexico City, since energy waste is reduced. In Mexicali, increasing the number of PVT collectors does not take full advantage of the heat that could be generated, since there is no relative need for water heating. Also, by stopping the operation of the collectors in Mexicali for approximately 4 months of the year, because no water heating is required, the useful heat is marginalized.
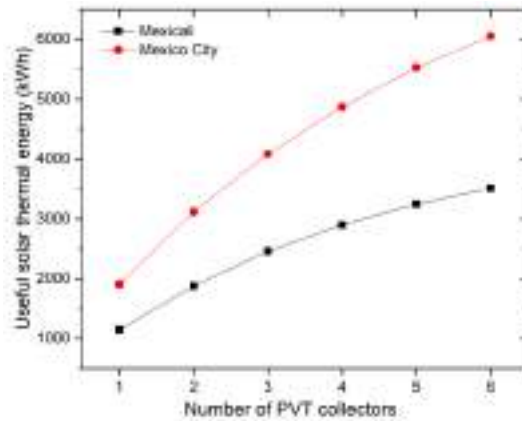
Fig. 6. Useful solar thermal energy per year as a function of the number of PVT collectors.

Although the useful heat generated with different PVT collectors is significantly higher for those located in Mexico City, the heat required by the auxiliary system is also higher, as can be seen in Fig. 7. The auxiliary heat required in Mexico City ranges from 101% to 117% higher than that required in Mexicali, when increasing from 1 to 6 PVT collectors. This represents thermal energy that has to be supplied by another energy source in a heater, most commonly those that use fossil fuels such as natural gas, liquefied gas or electric power from a thermal power plant. This does not go in the direction of sustainability. Although useful heat in Mexicali is significantly less than that generated in Mexico City, due to low DHW requirements, auxiliary heat needs are also low.

Fig. 7. Auxiliary energy required per year as a function of the number of PVT collectors.

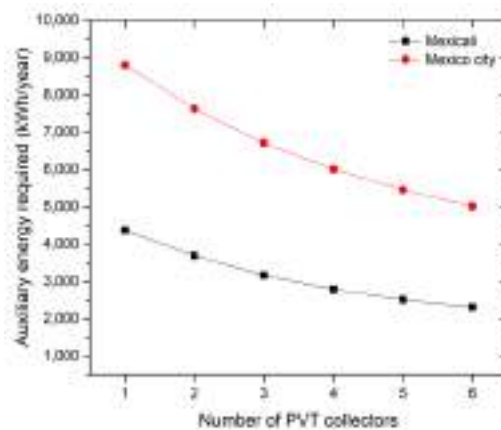Fig. 8 shows the solar fraction as a function of the number of PVT collectors. When only one PVT collector is installed in both locations, the percentage of solar contribution is similar, with 17% and 18% for Mexicali and Mexico City, respectively. However, as the number of collectors increases, the solar contribution to the DHW heat consumption tends to be higher for the system installed in Mexicali with 56 % compared to 53 % for Mexico City. The low solar contribution is notorious even with 6 collectors, this is mainly due to the time lag between the solar heat generation and the DHW consumption period. However, this solar fraction percentage can be raised by increasing the thermal energy storage volume. Increasing the number of PVT collectors to more than 6 would not contribute significantly to improve the solar fraction, since by comparing Fig. 6 and Fig. 7 it can be deduced that this increase encourages energy waste.
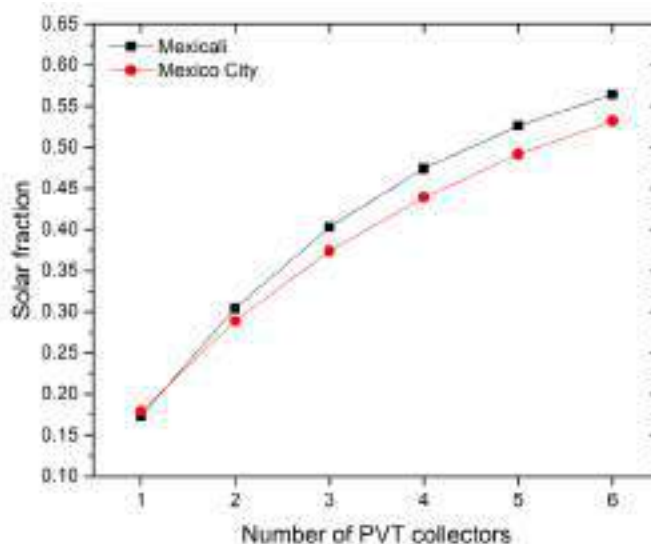
Fig. 8. Solar fraction as a function of the number of PVT collectors.

The electrical energy produced by the PVT collector system can be seen in Fig. 9. The generation is very similar and with a linear increase as a function of the number of collectors. Despite the fact that Mexicali has a greater annual solar resource, the effect of the operating temperature affects the electrical production. When one collector is considered, it generates 5% more electricity in Mexico City; when a system of 6 PVT collectors is considered, the electrical production is similar for both locations, with a total of 3,428 and 3,420 kWh per year for Mexicali and Mexico City, respectively.
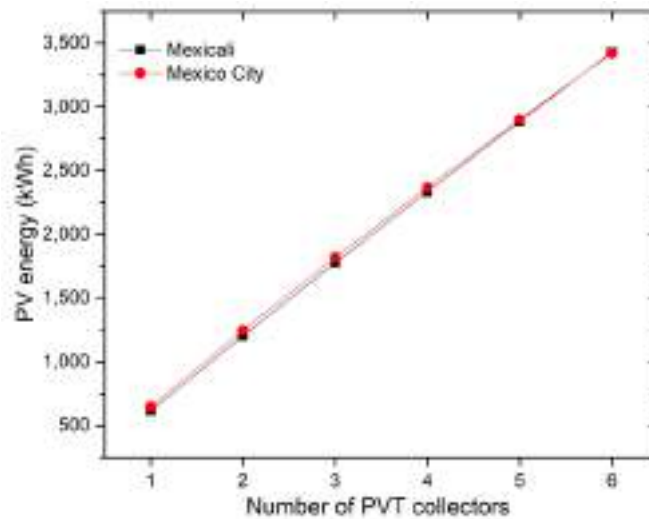
Fig. 9. Photovoltaic electric energy produced as a function of the number of PVT collectors.

5   Conclusions

In this work, the study of a PVT solar collector system to satisfy the DHW heat and electricity needs of the domestic sector was presented. Since environmental conditions are of utmost relevance to determine the feasibility of this type of technology, two cities with different characteristics were considered: Mexicali and Mexico City. The first is known for its extreme climate, with summers with temperatures that can reach over 50°C and winters with temperatures close to 0°C. The second presents more stable climatic conditions throughout the year. The two scenarios considered present differences that will cause operational dynamics specific to their location, directly impacting technical feasibility and energy attractiveness. For this study, TRNSYS software was used to carry out operational simulations under conditions typical of the system location. PVT systems with different number of collectors were considered to determine the effect on heat generation, auxiliary heat requirement and solar fraction. The results show that this type of sustainable equipment is of greater use in locations where heat requirements are high, since most of the heat generated by the collector would be used directly in the demand. In regions with warm climates, PVT collector operation is limited by operating and ambient temperatures. In the case of Mexicali, there is a period of approximately 4 months in which the solar thermal energy from the collector is not used because there is no need for hot water. The ambient and mains water temperature in these regions tends to favor the use of mains water at its original temperature, so these systems are not utilized all year round, diminishing their energy attractiveness.

Acknowledgments

References

1.   Ritchie, H., Roser, M., Rosado, P.: CO_2 and Greenhouse Gas Emissions. Our World in Data. (2020).
2.   Aguilar-Jiménez, J.A., Hernández-Callejo, L., Alonso-Gómez, V., Velázquez, N., López-Zavala, R., Acuña, A., Mariano-Hernández, D.: Techno-economic analysis of hybrid PV/T systems under different climate scenarios and energy tariffs. Solar Energy. 212, 191–202 (2020). https://doi.org/10.1016/j.solener.2020.10.079.
3.   Herez, A., el Hage, H., Lemenand, T., Ramadan, M., Khaled, M.: Review on photovoltaic/thermal hybrid solar collectors: Classifications, applications and new systems. Solar Energy. 207, 1321–1347 (2020). https://doi.org/10.1016/J.SOLENER.2020.07.062.
4.   Gorjian, S., Calise, F., Kant, K., Ahamed, M.S., Copertaro, B., Najafi, G., Zhang, X., Aghaei, M., Shamshiri, R.R.: A review on opportunities for implementation of solar energy technologies in agricultural greenhouses. J Clean Prod. 285, 124807 (2021). https://doi.org/10.1016/J.JCLEPRO.2020.124807.
5.   Ma, T., Li, M., Kazemian, A.: Photovoltaic thermal module and solar thermal collector connected in series to produce electricity and high-grade heat simultaneously. Appl Energy. 261, 114380 (2020). https://doi.org/10.1016/J.APENERGY.2019.114380.
6.   Diwania, S., Agrawal, S., Siddiqui, A.S., Singh, S.: Photovoltaic–thermal (PV/T) technology: a comprehensive review on applications and its advancement. International Journal of Energy and Environmental Engineering. 11, 33–54 (2020). https://doi.org/10.1007/S40095-019-00327-Y/TABLES/2.
7.   Hemmat Esfe, M., Kamyab, M.H., Valadkhani, M.: Application of nanofluids and fluids in photovoltaic thermal system: An updated review. Solar Energy. 199, 796–818 (2020). https://doi.org/10.1016/J.SOLENER.2020.01.015.
8.   Abora Solar, https://abora-solar.com/panel-solar-hibrido/, last accessed 2022/10/06.
9.   Klein, S.A., Beckman, W.A., Mitchell, J.W., Duffie, J.A., Duffie, N.A., Freeman, T.L., Mitchell, J.C., Braun, J.E., Evans, B.L., Kummer, J.P.: TRNSYS 17, (2009).
10. Gagliano, A., Tina, G.M., Aneli, S., Nižetić, S.: Comparative assessments of the performances of PV/T and conventional solar plants. J Clean Prod. (2019). https://doi.org/10.1016/j.jclepro.2019.02.038.
11. JRC Photovoltaic Geographical Information System (PVGIS) - European Commission, https://re.jrc.ec.europa.eu/pvg_tools/en/tools.html, last accessed 2022/11/27.

12.   BS EN 15316-3-1:2007 - Heating systems in buildings. Method for calculation of system energy requirements and system efficiencies. Domestic hot water systems, characterisation of needs (tapping requirements) (British Standard), https://webstore.ansi.org/standards/bsi/bsen153162007-1325671, last accessed 2022/11/27.

Estimación de la presión de falla en defectos por corrosión según ASME B31G para ductos de Transporte de Hidrocarburos utilizando Matlab

José Alberto Navarro Campos[1] [0000-0002-3367-0866] Jorge Mírez[1][0000-0002-5614-5853] Javier Elmar Franco[1][0000-0002-4712-0726] and Adrián Zapata Sernaque[1][0000-0002-5303-8286]

[1] Universidad Nacional de Ingeniería Lima, PERÚ
jose.a.navarrocampos@gmail.com
jmirez@uni.edu.pe
efrancog@uni.edu.pe
azapatas@uni.edu.pe

Resumen. El presente trabajo describe la metodología desarrollada en el estándar para determinación de la resistencia remanente en ductos corroídos - ASME B31G, para la determinación de la presión de falla en ducto con defectos por corrosión, basado en los resultados de una inspección en línea de integridad del ducto (medición de espesores) a través de una herramienta instrumentada. Los resultados de la inspección fueron reproducidos, mediante la creación de un código de programación en la herramienta informática Matlab para estimar la presión de falla y la presión de operación segura del ducto, los cuales fueron comparados con los resultados reportados por la empresa que desarrolló la inspección en línea. Lo estudiando es de interés de la industria de almacenamiento de combustibles, muy presente en la vida diaria de las Ciudades Inteligentes.

Palabras claves: Inspección, Ductos de petróleo, Presión de falla, Estándar ASME B31G.

1   Introducción

En la industria de almacenamiento de combustibles, es común que se utilicen los sistema de ductos para transferir los hidrocarburos líquidos desde buques hasta los tanques de almacenamiento, y como parte de las actividades de mantenimiento a los ductos de transporte de hidrocarburos, que trabajan a presiones de alrededor 100 psi, deben ser inspecciones para determinar si presentan defectos, principalmente del tipo corrosión, y comprobar si se encuentran aptos para continuar trabajando de manera segura, o determinar si existe la necesidad de reducir los parámetros de trabajo o deteniendo el equipo y reacondicionamiento, evitando lesiones al personal u otras personas, y accidentes ambientales inesperados [1]. Es por ello que, dentro de estas inspecciones se realiza la medición de espesores, para la determinación del espesor remanente de tubería a fin de identificar áreas donde existe defectos del tipo corrosión.

Los sistemas de tuberías en la industria del almacenamiento de combustibles es de gran alcance en el concepto de Ciudades Inteligentes – Rubro Energía.

Existen muchas maneras de inspección a fin de determinar el espesor remanente de tubería (por mencionar algunas, tenemos las ondas guiadas y la inspección en línea con herramienta instrumentada, etc.), herramientas que nos permiten identificar la ubicación del defecto y caracterizarlo determinando su valor de extensión del defecto así como su pérdida de espesor en dicha área.

Una vez identificado el defecto el operador de la instalación debe evaluar si la sección del ducto afectada es apta para continuar en servicio sin riesgo de falla en las zonas de corrosión identificadas por las herramientas antes señaladas.

Existen varias estándares con las cuales evaluar los defectos identificados, dentro de las más conocidas son: ASME B 31.4, API 579, ASME B31 G y DNV RP F101 [2-5]. En el presente trabajo, nos avocaremos al estándar ASME B31G, el cual sirve como una guía para la evaluación de la pérdida de metal en sistemas de tuberías presurizadas, el cual contiene cuatro niveles de análisis: Nivel 0, Nivel 1, Nivel 2 y Nivel 3, dependiendo de la cantidad de información disponible y el grado de refinamiento que se requiera en el análisis. Como está especificado en el ASME B31G, un Nivel 0 está basado en una evaluación bastante simple, mientras que un Nivel 1 incorpora un mayor nivel de detalle de manera de obtener una estimación más precisa de la presión de falla y un Nivel 2 y 3 ya requiere un análisis mucho más detallado del defecto.

El presente trabajo está basado en modelar, mediante la herramienta computacional Matlab, las ecuaciones utilizadas para el análisis de Nivel 1 en la determinación de la presión de falla de un defecto por corrosión. La información está basada en los resultados de la inspección de un ducto usando el método de inspección ultrasónica inteligente [6].

2   Estimación según ASME B31G usando Matlab

Basado en los datos geométricos obtenidos por la inspección en línea del tipo ultrasónica mediante herramienta instrumentada, realizada por la empresa que ejecutó los trabajos de medición de espesores [6], es de precisar que a fin de tener un punto de comparación, se tomó en cuenta los resultados del cálculo de la presión estimada de falla y presión estimada de operación segura reportados mediante el programa informático de APPLUS basados en el ASME B31 G, el cual consideró las características del ducto inspeccionado señaladas en la Tabla 1, así como con datos profundidad máxima y longitud máxima de cada defecto identificados durante las inspecciones.

La empresa que realizó la inspección reportó al operador del sistema de transporte una lista de defectos detectados tal como se muestra en la Tabla 2.

Tabla 1. Características del ducto.

Diámetro [pulg.]	Material	Espesor de pared [pulg.]	SMYS [Psi]	Factor de seguridad (SF)

| 34 | API 5L X42 | 0.5 | 42000 | 1.4 |

Tabla 2. Lista de defectos detectadas.

Defecto	Longitud [pulg.]	Profundidad [pulg.]	Presión estimada de falla [psi]	Presión operación segura [psi]
1	4.961	0.094	1230.000	878.600
2	2.165	0.094	1325.000	946.400
3	7.087	0.079	1240.000	885.700
4	12.205	0.102	1240.000	885.700
5	9.213	0.079	1221.000	872.100
6	4.016	0.079	1277.000	912.100
7	4.173	0.087	1270.000	907.100

Basándonos en la metodología para un nivel de inspección 1, señalado en el ASME B31G, la máxima presión a la cual un ducto puede trabajar de manera segura es estimada con las Ec. (1), (2) y (3):

$$M = (1 + 0.8z)^{1/2} \tag{1}$$

Para $z \geq 20$:

$$S_F = S_{Flow} \left[\frac{1-(\frac{2}{3})(\frac{d}{t})}{1- (\frac{2}{3})(\frac{d}{t})/M} \right] \tag{2}$$

Para $z \leq 20$:

$$S_F = S_{Flow} \left(1 + \frac{d}{t}\right) \tag{3}$$

donde: S_{Flow} es definido para acero al carbono simple que opera a temperaturas por debajo de 250 °F (120 °C), que corresponde a nuestro caso de análisis, y puede ser estimado mediante la Ec. (1). Además, z, es definido por la expresión L^2/Dt.

El estándar señala que, la presión estimada de falla P_F está definida por la expresión $2S_Ft/D$ y la presión de operación segura P_S está definida por P_F/SF.

Como se puede observar, el criterio de tolerancia estará supeditado a determinar los valores de presión de falla y presión de operación segura, luego de utilizar las Ec. (2) ó (3). Cabe precisar que, el ASME B31G recomienda un factor de seguridad SF mínimo igual a la relación de la presión de prueba hidrostática mínimo requerido para el tipo dado de construcción de tubería a la MAOP o MOP, pero por lo general, no menor de 1.25. Sin embargo a fin de poder tener un punto de comparación con los resultados de la empresa de inspección, utilizaremos el valor de factor de seguridad considerado por dicha empresa, es decir el valor de 1.4.

Por lo antes expuesto, procederemos a calcular estos valores, mediante la creación de un código utilizando la herramienta computacional Matlab y presentamos los pasos seguidos:

Paso 1. Los datos de caracterización del ducto bajo análisis, los cuales son constantes, se han introducido estos valores en nuestro editor creado en Matlab, según:

```
% Determinación presión de falla en defecto por corrosión según ASME B 31.G
% espesor nominal de la tubería
t = 0.5;
% Diámetro externo de la tubería
D = 34; % datos acorde tubería
% Caracterización de la tubería
smys = 42000;
SF_factordeseguridad = 1.4;
```

Paso 2. Se ingresa la data necesaria para cálculos, para lo cual se ha creado un archivo en Excel denominado "Data corrosion-ASME B 31G", conteniendo de manera agrupada toda la información necesaria para cálculos y se han utilizado los datos correspondientes a la columna 5 hasta la columna 11 según:

```
% Ingreso de data para cálculos
data = xlsread('Data corrosion-ASME B 31G','Hoja1','D5:I11');
```

Paso 3. Introducción de la data necesaria para cálculos, relacionados al defecto por corrosión tales como longitud del área afectada y la profundidad de corrosión, seguido procedemos a realizar los cálculos para cada par de datos, según:

```
% Ingreso de la información referida al defecto por corrosión
L = data(:,5);
z = ((L).^2./(D.*t));
% Cálculo de la tensión de falla por cada longitud de corrosión y su
% respectiva profundidad de corrosión
for d= data(:,6) %variable
  if  z <= 20;
  M_folias = sqrt(1 + (0.8 .* z));
  S_F= (1.1*smys).*((1-(2/3).*(d/t)) ./ ((1-(2/3).*(d/t)./M_folias)));
  else
  S_F = (1.1*smys).*(1 - (d./t));
  end
 end
```

Paso 4. Determinación de la presión de falla y la presión de operación segura, e inclusión de los resultados en el archivo Excel denominado Data corrosion-ASME B 31G, así como la creación de gráfica representativa, según:

```
% Determinación de la presión de falla y la presión de operación segura
P_F= 2 .* S_F .* t / D;
P_S= P_F ./ SF_factordeseguridad;
xlswrite('Data corrosión-ASME B 31G',P_F,'Hoja1','L5:L11');
xlswrite('Data corrosión-ASME B 31G',P_S,'Hoja1','M5:M11');
plot(data(:,6),P_F,'ro');
xlabel('Profundidad de corrosión [pulg.]');
```

ylabel('Presión de Falla [psi]');
title('Presión de Falla vs Profundidad de corrosión ducto 34 pulgadas');
grid;

Paso 5. Se realiza el análisis final, en donde los resultados de la ejecución del programa de Matlab son representados a través de una gráfica con los valores determinados, tal como se muestra en la Fig. 1, y la matriz de análisis mostrada en la Tabla 3. Los valores calculados a través de Matlab son introducidos en nuevas columnas del archivo Excel denominado Data corrosion-ASME B 31G,

Nomenclatura utilizada
D = Diámetro exterior específico del ducto
d = Profundidad de pérdida de metal
L = Longitud de pérdida de metal
M = Factor de abultamiento o Factor de Folias
MAOP = Máxima presión de operación permitida
MOP = Máxima presión de operación
P_F = Presión estimada de falla $2S_Ft/D$
P_S = Presión de operación segura P_F/SF
S_F = Nivel de tensión de falla estimada
SMYS = Tensión de fluencia mínima especificada a condiciones ambientales
t = Espesor de pared del ducto
$z = L^2/Dt$

Tabla 3. Resultados de cálculos con Matlab.

Defecto	Diámetro [pulg.]	Material	Espesor de pared [pulg.]	SYMS [psi]	Factor de seguridad (SF)	Longitud [pulg.]	Profundidad [pulg.]	Presión estimada de falla [psi] APPLUS	Presión operación segura [psi] APPLUS	Presión estimada de falla [psi] Matlab	Presión operación segura [psi] Matlab
1	34	API 5L X42	0.5	42000	1.4	4.961	0.094	1230.000	878.600	1299.039809	927.8855776
2	34	API 5L X42	0.5	42000	1.4	2.165	0.094	1325.000	946.400	1340.489908	957.4927917
3	34	API 5L X42	0.5	42000	1.4	7.087	0.079	1240.000	885.700	1290.014193	921.438709
4	34	API 5L X42	0.5	42000	1.4	12.205	0.102	1240.000	885.700	1232.81981	880.5855789
5	34	API 5L X42	0.5	42000	1.4	9.213	0.079	1221.000	872.100	1276.116616	911.5118687
6	34	API 5L X42	0.5	42000	1.4	4.016	0.079	1277.000	912.100	1320.715303	943.3680733
7	34	API 5L X42	0.5	42000	1.4	4.173	0.087	1270.000	907.100	1314.432455	938.8803251

3   Conclusión

Basados en la metodología del estándar ASME B31G utilizada, hemos determinado que los valores de presión de falla determinados con la herramienta computacional Matlab son bastante congruentes con los determinados por la empresa que realizó la inspección y detecto los defectos de corrosión, identificándose un error menor al 5 % tal como se muestra en la Tabla 4, y siendo que la presión de operación del ducto bajo análisis es de 100 psi, este valor se encuentra muy por debajo de la presión estimada de operación segura para las secciones identificadas con defectos y por tanto puede operar de manera segura.
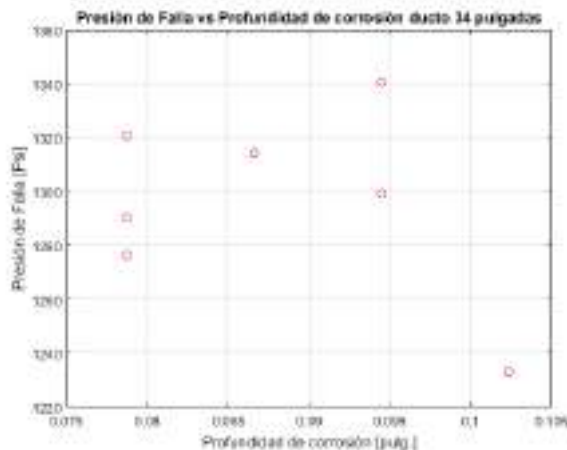
Fig. 1. Representación de los valores de Presión de falla para cada profundidad de corrosión detectada.

Tabla 4. Comparativa de resultados de cálculos con Matlab versus APPLUS

Defecto	Presión estimada de falla [psi] APPLUS	Presión operación segura [psi] APPLUS	Presión estimada de falla [psi] Matlab	Presión operación segura [psi] Matlab	Error respecto de los resultados de APPLUS
1	1230.000	878.600	1299.039809	927.8855776	5.61%
2	1325.000	946.400	1340.489908	957.4927917	1.17%
3	1240.000	885.700	1290.014193	921.438709	4.03%
4	1240.000	885.700	1232.81981	880.5855789	-0.58%
5	1221.000	872.100	1276.116616	911.5118687	4.51%
6	1277.000	912.100	1320.715303	943.3680733	3.42%
7	1270.000	907.100	1314.432455	938.8803251	3.50%

Referencias

1. Minescu, Mihail & Pana, Ion. (2012). The Equivalence of the Assessment Procedures API 579 and ASME B31G. Buletinul Universitatii Petrol - Gaze din Ploiesti - Technical Series. LXIV. 11-20.
2. ASME B 31.4 – 2019 – ASME Code for Pressure Piping, ASME B31, Pipeline Transportation Systems for Liquids and Slurries, November 2019.
3. API 579-1 / ASME FFS-1, Fitness-For-Service, June, 2016.
4. ASME B31G-2012, Supplement to ASME B31 Code for Pressure Piping, Manual for determining the Remaining Strength of Corroded Pipelines, October 2012.
5. Recommended practice Det Norske Veritas DNV-RP-F101 Corroded Pipelines, October 2010.
6. Final Report: Ultrasonic Inspection of the 34" Crude Oil Pipeline, Applus+ RTD-project number 1141-148874, 28-01-2022.

Minimización del requerimiento de almacenamiento de energía en parques eólicos a través del control del estado de carga del banco de baterías

Miguel Mendieta[1], Wilson Pavón[1], and Luis I. Minchala[2,3]

[1] Universidad Politécnica Salesiana, Cuenca, Ecuador
{mmendietas, wpavon}@ups.edu.ec
[2] Departamento de Ingeniería Eléctrica, Electrónica y Telecomunicaciones
Universidad de Cuenca
Ave. 12 de Abril y Agustín Cueva, Cuenca, Ecuador
[3] Grupo de investigación en conversión, almacenamiento y gestión de energía
Tecnologico de Monterrey
Ave. Garza Sada 2501, Monterrey, Mexico
ismael.minchala@tec.mx

Abstract. Este artículo presenta una metodología para reducir los requerimientos de almacenamiento de energía a través de baterías (BESS, por sus siglas en inglés) aplicada al suavizado de la variación de potencia de un parque eólico. Esta reducción se alcanza a través de la combinación en el funcionamiento de un sistema de gestión de energía (EMS, por sus siglas en inglés) con un BESS de tamaño optimizado. El cálculo de la capacidad del BESS se determina mediante el uso de un algoritmo evolutivo. El EMS despliega un sistema de control basado en retroalimentación del estado de carga (SOC-FB) para reducir las variaciones de potencia del parque eólico, mientras que el algoritmo de optimización determina el requisito mínimo del BESS para mantener la variación de potencia de acuerdo con una función de costo. Este enfoque se prueba utilizando datos reales de un parque eólico. Los resultados de la simulación muestran una reducción significativa de la variación de potencia en el caso de estudio, con una capacidad mínima del BESS.

Keywords: Battery energy storage system · Feedback control · Output fluctuation · Regulation state of charge · Wind power generation.

1 Introducción

El creciente desarrollo económico y la demanda de energía en las economías emergentes, sumado a la preocupación por el cambio climático [5], está impulsando el uso de energías renovables en muchos países a nivel mundial [14]. El estudio presentado en [5] prevé que América Latina duplicará su consumo eléctrico en los próximos veinte años. Parte de esa demanda será cubierta por energías renovables.

El uso de este tipo de fuentes de energía acarrea un enorme problema, y es que los recursos naturales presentan grandes niveles de variación a lo largo del día, lo que se traduce en picos y/o rampas de producción energética. Si estos picos no se controlan, perjudican el desempeño del sistema de generación y en consecuencia a los clientes conectados a la red de distribución [9] [1]. Por lo tanto, es necesario mantener la estabilidad de la energía producida por este tipo de sistemas [10].

Un sistema de almacenamiento de energía con baterías (BESS) puede proporcionar soluciones para la gestión de energía, permitiendo estabilizar y compensar las variaciones presentes en sistemas de energías renovables [10]. Con este fin, varios autores han estudiado y diseñado estrategias de control para mitigar las fluctuaciones de salida en plantas eólicas. Por ejemplo: el uso de un BESS para inyectar o absorber energía en momentos de alta a baja demanda, manteniendo la calidad del servicio requerido [11] [4]. En [16] se describen diferentes metodologías para la integración de un BESS, mejorando la eficiencia de la distribución de energía. La referencia [6] presentan un estudio detallado de la implementación de un BESS en una planta eólica de 30 MW, obteniendo una reducción significativa de grandes tasas de rampa positivas y negativas empleando un BESS de 15 MWh. En [3] se presenta un sistema híbrido, BESS y compresores de aire, para almacenar la energía excedente y entregarla cuando la demanda sea alta y/o suavizar la salida en caso de variaciones en una planta eólica. Por último, en [17] y [15] se presentan sistemas de suavizado de energía que combinan un BESS con controladores inteligentes que adaptan el sistema según las condiciones de la potencia generada en plantas eólicas.

El principal problema al trabajar con BESS en sistemas de gran potencia es que el nivel de carga de las baterías debe permanecer en un rango adecuado. Si la fluctuación de la producción en el parque eólico simplemente se suaviza con el BESS, sin regular el nivel de carga, ésta alcanzará su límite inferior cuando existan bajos niveles de generación o su límite superior al suavizar una gran variación de la producción de la planta eólica. Esto implica la necesidad de una gran capacidad energética, asociada a un coste monetario de valor proporcional, de un BESS si no existe un método de control para regular el nivel de carga [9].

Este trabajo presenta un sistema de suavizado para la energía de salida de una granja eólica empleando un BESS operado por un controlador basado en el estado de carga (SOC) conocido como SOC-FB (del inglés State-Of-Charge Feed Back) que se encarga de mantener el SOC de las baterías dentro de un rango adecuado de trabajo (del 0% al 100%). Se emplean datos reales de una granja eólica, que presentan grandes picos de producción debido a la ubicación geográfica de los aerogeneradores. El objetivo principal del sistema propuesto aquí es optimizar la magnitud de un BESS conectado a la salida de la granja eólica, de tal forma que la potencia de salida presente variaciones menores al 50% de su valor original, medidas a través de la desviación estándar de su derivada. Se emplea un algoritmo evolutivo para minimizar el valor de la desviación estándar de la derivada mediante una función de costo en la que se ponderan la derivada

de la salida y la capacidad de almacenamiento del BESS, obteniendo un valor óptimo de este último.

El documento se organiza de la siguiente manera. La sección II presenta el caso de estudio. La sección III presenta el controlador y algoritmo de optimización. La sección IV presenta resultados de simulaciones que se basan en datos experimentales. La sección V presenta las conclusiones del trabajo.

2   Caso de estudio

2.1   Granja eólica

Para realizar la presente investigación se toma como estudio una granja eólica compuesta por 26 aerogeneradores de 2 MW ubicados a lo largo de un perfil costanero, como se aprecia en la Fig. 1. En conjunto, los 26 aerogeneradores entregan un total de 52 MW de potencia instalada.
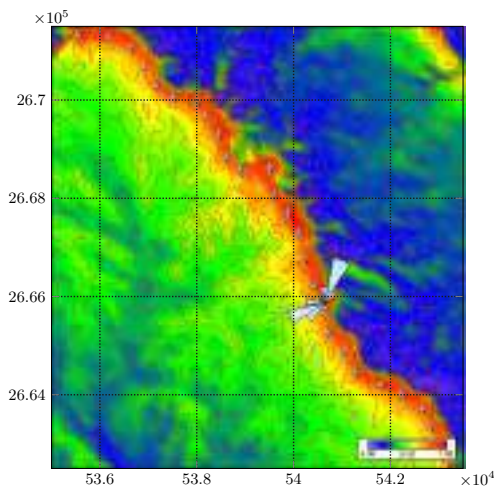
Fig. 1: Disposición geográfica de los aerogeneradoress

El modelo simplificado de los aerogeneradores se muestra en la Fig.2, donde se pueden distinguir las 4 regiones de operación de un aerogenerador. En la primera región, de baja velocidad, el aerogenerador está a la espera de que el viento supere la velocidad de corte, en este caso 3 m/s, para poder arrancar [8]. En la segunda región el aerogenerador comienza a funcionar; esta zona se encuentra limitada por la velocidad de corte y la velocidad nominal, que para este modelo es de 10 m/s. La tercera región, conocida como zona de potencia constante, se da cuando las velocidades del viento son lo suficientemente altas

como para que el aerogenerador deba limitar la potencia generada, asegurando que ésta no exceda las cargas eléctricas y/o mecánicas seguras. Finalmente, en la cuarta región, para proteger el aerogenerador de una sobrecarga estructural, éste debe retirarse del sistema de generación cuando el viento supera la segunda velocidad de corte [2], 25 m/s para el modelo en estudio.
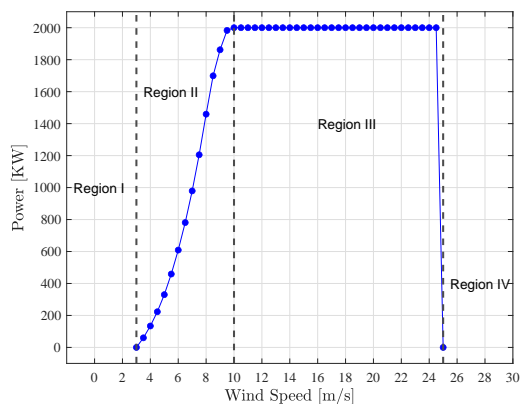
Fig. 2: Modelo simplificado del aerogenerador. Se incluye la etapa de conversión mecánica a energía eléctrica.

Los datos disponibles de la granja eólica consisten en un conjunto de mediciones de velocidad de viento, realizadas durante tres meses, obtenidas de tres torres equipadas con anemómetros, nombradas CB, NB y SE, ubicadas en las coordenadas geográficas (532851, 2670737), (540621, 2665887) y (542389, 2663778), respectivamente. Una porción de los datos se muestra en la Fig. 3.
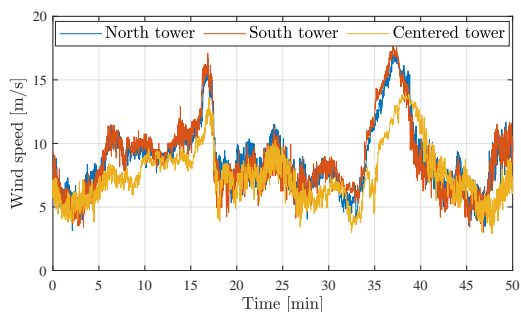
Fig. 3: Porción de datos de viento disponibles

El modelo de granja eólica propuesto genera predicciones de viento para los 26 aerogeneradores. Luego, se interpolan los datos predichos usando el modelo del aerogenerador de la Fig. 2, obteniendo valores de potencia generada para cada aerogenerador. Finalmente, la potencia total de la granja es la suma de estas potencias individuales.

Un análisis de la matriz de correlación de las tres mediciones de viento muestran que éstas se encuentran altamente correlaciones entre sí por lo tanto, para poder modelar el sistema es necesario implementar una simulación Montecarlo que permita obtener predicciones de viento, independientes, en base a las distancias de los aerogeneradores a los anemómetros. Se emplea la descomposición de *Cholesky*, que según [7] se usa generalmente en sistemas de predicción de viento, para correlacionar los datos predichos.

El modelo de la granja corresponde al siguiente algoritmo.

1. Se obtiene la matriz de covarianza $\mathbf{M}$ empleando un modelo polinomial con base en los datos de viento disponibles y la distancia entre los aerogeneradores.
2. Sobre $\mathbf{M}$ se aplica la descomposición de Cholesky, obteniendo la matriz $\mathbf{R}$, según la ecuación (1). Esta matriz será usada para entregar la correlación del sistema original a los datos predichos.

$$\mathbf{M} = \mathbf{R}^T \mathbf{R} \tag{1}$$

3. Se realiza la predicción de los datos de viento incidentes en cada aerogenerador usando un modelo ARMA (del inglés autoregressive–moving-average model) de los datos obtenidos por los anemómetros. Se emplea un vector de datos aleatorios para generar datos de viento no correlacionados entre sí, ecuación (2).

$$\mathbf{W}_p = ARMA[\mathbf{W}, \mathbf{W}_r] \tag{2}$$

donde, $\mathbf{W}_p$ son los datos de viento predichos, $\mathbf{W}$ son los datos de viento medidos por los anemómetros, y $\mathbf{W}_r$ son valores aleatorios.

4. Luego se realiza el ajuste de los datos predichos, agregando la covarianza deseada mediante la ecuación:

$$\mathbf{W}_n = \mathbf{W}_p \mathbf{R} \tag{3}$$

donde, $\mathbf{W}_n$ son los datos de viento ajustados.

5. $\mathbf{W}_n$ se utiliza como datos de entrada para interpolar la potencia producida por cada aerogenerador, $\mathbf{P}_n$, usando el modelo de la Fig. 2.
6. Finalmente, la potencia total de la granja eólica es la suma de las potencias obtenidas para cada torre, ecuación (4).

$$\mathbf{P}_T = \sum_{n=1}^{26} \mathbf{P}_n \tag{4}$$

La salida del modelo de la planta eólica se presenta en la Fig. 4, en donde además se muestra la derivada de la potencia generada por los 26 aerogeneradores. Un análisis de la Fig. 4 revela que la salida presenta grandes niveles de variación en períodos de tiempo relativamente cortos, llegando a existir diferencias de casi 50 MW, como se observa en el intervalo de los 1000 a 1100 minutos. Estas variaciones se pueden observar de mejor manera en la derivada de esta salida. Surge entonces la necesidad de suavizar la potencia generada con el objetivo de no provocar daños a los sistemas conectados a la granja eólica.
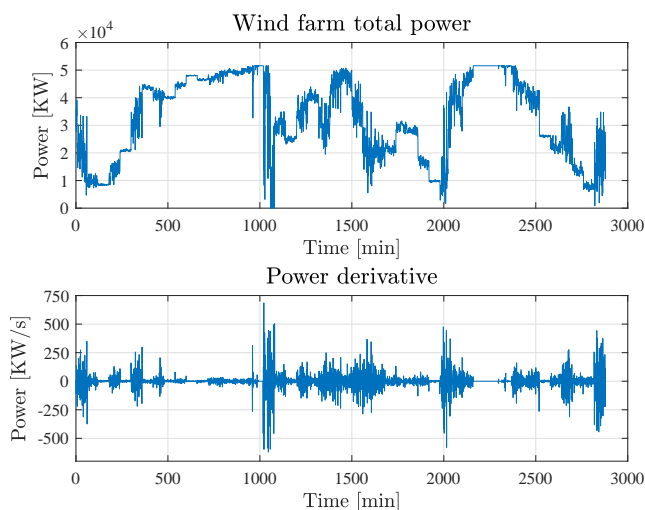
Fig. 4: Potencia de salida, y su derivada, del modelo de la planta eólica

3　Sistema propuesto

Con el objetivo de suavizar la potencia de salida de una planta de energía renovable, manteniendo el SOC de las baterías dentro del rango de funcionamiento, el sistema propuesto hace uso de un controlador basado en SOC-FB. Este controlador posee variables que, junto a la capacidad del BESS, deben ser determinadas y/o configuradas para un adecuado funcionamiento del sistema. Para esta última tarea se implementa un algoritmo evolutivo, llamado *Hybrid Differential Evolution Algorithm With Adaptive Crossover Mechanism*, disponible en [12], con el que se determina de manera óptima los parámetros del controlador y capacidad del BESS.

3.1   Esquema de control

El sistema de control a implementar fue adaptado de [9], éste tiene como objetivo suavizar la potencia de salida de una planta eólica a la vez que se mantiene el SOC de las baterías del BESS dentro de un rango de operación. El modelo de BESS implementado consiste en un sistema de baterías de flujo redox (conocida también como batería de vanadio) y el esquema de control adaptado a este problema se muestra en la Fig. 5, y a continuación se detalla su funcionamiento mediante el diagrama de flujo en Fig. 6.
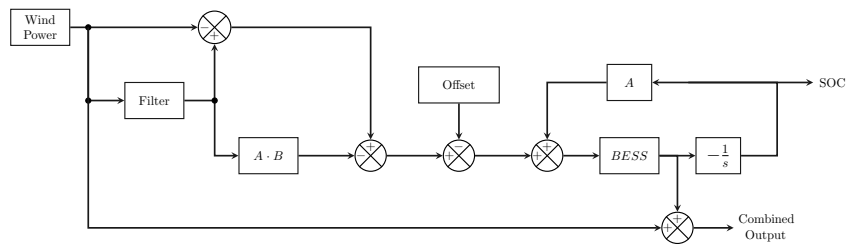
Fig. 5: Esquema de control SOC-FB

- En primer lugar, los datos de potencia generada por la granja eólica pasan a través de un filtro de retardo de primer orden con una constante de tiempo T (en segundos). La salida de este filtro recibe el nombre de *target output*.
- Con el objetivo de obtener la señal que debe ser producida/entregada por el BESS, el target output es restado de la salida de la planta. Esta salida recibe el nombre de referencia de potencia (PR).
- Luego, a PR se adiciona el SOC, generando la referencia final para el BESS (mediante el bucle de retroalimentación), asegurando de esta forma que el BESS no se cargue o descargue más allá de sus límites.
- La salida del BESS pasa por un bloque que permite el cálculo del SOC, que luego se retroalimenta para ser usado en la creación de la señal de referencia.
- Finalmente, se combinan la potencia generada por la planta y la salida del BESS para obtener la salida suavizada.

La aplicación del esquema de la Fig. 5 conlleva a la implementación de las variables indicadas en la Tabla 1, sujetas a las ecuaciones (5) - (9). La ecuación (5) representa el límite en donde el target output, salida del filtro con constante T, es alcanzable para una capacidad, E, de BESS dada ante una planta con una capacidad máxima C_{WF}. Así mismo, el valor de α, que debe ser obtenido de la ecuación (9), de allí la restricción de $0 < M < 0.5$ necesaria para mantener el rango de α en $0 < a < 1$.

$$T < \frac{E}{C_{WF}} \tag{5}$$
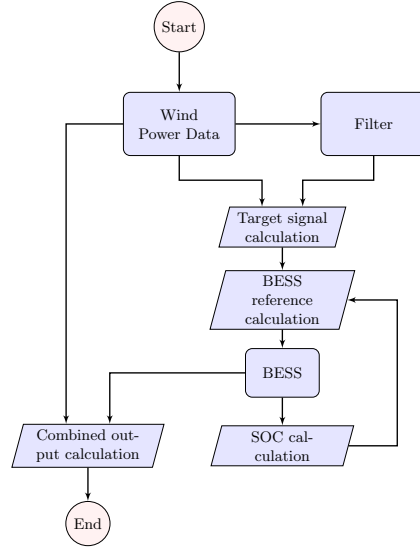
Fig. 6: Funcionamiento del esquema de control

$$A = \frac{1}{T} \tag{6}$$

$$B = \alpha T; \text{ con } 0 < a < 1 \tag{7}$$

$$Offset = A \cdot M \tag{8}$$

$$M = \frac{E - \alpha T C_{WF}}{2E}; \text{ con } 0 < M < 0.5 \tag{9}$$

3.2 Algoritmo de optimización

Uno de los objetivos de este proyecto es el dimensionamiento del BESS requerido para suavizar la potencia de salida. Adicionalmente, el controlador cuenta con dos parámetros principales: la constante de tiempo del filtro, T y el margen de offset M; variables de las que se derivan las restantes. Estas tres variables deben ser determinadas de tal manera que la salida sea óptima, reduciendo así la capacidad del BESS, y su coste asociado, y suavizando lo más posible la salida.

Para encontrar los valores antes mencionados se ha implementado el algoritmo evolutivo Hybrid Differential Evolution Algorithm With Adaptive Crossover Mechanism presentado en [13], que ya ha sido puesto a prueba en diversos problemas de optimización por los autores, encontrando soluciones dentro de los rangos reportados.

Tabla 1: Variables del esquema de control

Variable	Descripción	Unidades
E	Capacidad del BESS	MWh
C_{WF}	Capacidad de la granja eólica	MW
T	Constante de tiempo del filtro	Sec
A	Ganancia de retroalimentación	Sec^{-1}
B	Ganancia del target output	Sec
Offset	El offset y M (margen de offset) impiden que el SOC alcance sus límites operativos	MW
M		–
α	Coeficiente usado para mitigar las variaciones del target output	–

En términos generales, el diagrama de flujo de la Fig. 7 representa el funcionamiento del algoritmo evolutivo. A continuación, se detalla este algoritmo:

1. En primer lugar se generan los valores (dentro de los rangos dados) para las variables en estudio, en este caso E, T y M.
2. Los nuevos valores conforman el vector padre, que será usado para crear un vector mutante.
3. Se realiza el cruce entre el vector padre y el vector mutante aplicando algoritmos estadísticos para la creación de un vector hijo.
4. Se evalúa la función de costos para el vector padre e hijo.
5. Se seleccionan los valores que representen la mejor función de costos y se convierten en el nuevo vector padre.
6. Los pasos anteriores se repiten siempre que el número de generaciones no sea mayor al indicado como parámetro.
7. Al finalizar, el algoritmo devuelve los mejores valores encontrados.

La parte adaptativa del algoritmo se presenta cuando, luego de un determinado número de iteraciones, no puede encontrar un mejor resultado para la función de costos, entonces usando técnicas estadísticas crea un nuevo vector padre con el objetivo de salir de aquel mínimo local.

Para su aplicación en este proyecto el algoritmo fue adaptado con el fin de encontrar los valores óptimos de E, T y M, para ello fueron modificadas ciertas funciones del código principal para que sea compatible con el esquema de control, y fue implementada la siguiente función de costos:

$$f = m_d + \beta m_{BESS} \tag{10}$$

donde, m_d corresponde a un valor obtenido de la suma de los valores absolutos de los elementos de la derivada de la señal combinada (salida del sistema), m_{BESS}
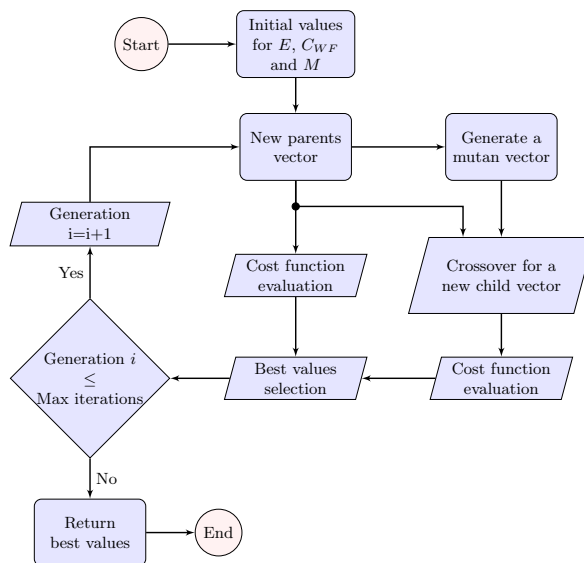
Fig. 7: Evolutionary Algorithm

representa la magnitud del BESS en MWh y β es una variable, en el rango $0 < \beta \leq 1$, que permite determinar si el algoritmo dará mayor o menor prioridad a la magnitud del BESS por sobre la suavidad de la señal de salida.

4   Resultados

Una primera prueba del sistema se lleva a cabo utilizando los datos de potencia generada mostrados en la Fig. 4 y los valores de la Tabla 2. Esta prueba se divide en dos partes: en la primera, se implementa únicamente el filtro para generar una señal deseada que se utiliza como referencia para el BESS. Es decir, no se implementa el controlador. En la segunda parte se adiciona el controlador, con el objetivo de observar el comportamiento de estos dos escenarios.

Tabla 2: Parámetros primera prueba

Variable	Magnitud
Capacidad de la granja eólica (C_{WF})	52 MW
Capacidad del BESS (E)	10 MWh
Constante de tiempo del filtro (T)	692 sec
Margen de offset (M)	0.3

En la Fig. 8a se muestra el resultado del primer escenario. Se observa como el SOC decae rápidamente, por lo que el BESS se queda sin energía, siendo entonces la salida del sistema igual a la potencia original de la planta. Esto ocurre debido a que los 10 MWh no son suficientes para compensar directamente los casi 30 MW que pierde inicialmente la potencia de salida de la planta.

Los resultados del segundo escenario de esta prueba se muestran en la Fig. 8b. Aquí el SOC se mantiene dentro de los límites de operación, entre 0% y 100%, lo que permite al BESS cargarse y descargarse cuando sea pertinente. Sin embargo, aún con el controlador no es suficiente para realizar un correcto suavizado de la potencia debido al bajo valor de la constante del filtro. Esto se refleja obteniendo la desviación estándar de la derivada de la potencia de salida de la planta original, 81.66, y la desviación estándar la derivada de la salida del sistema SOC-FB, que es de 42.08, representando más del 51%.
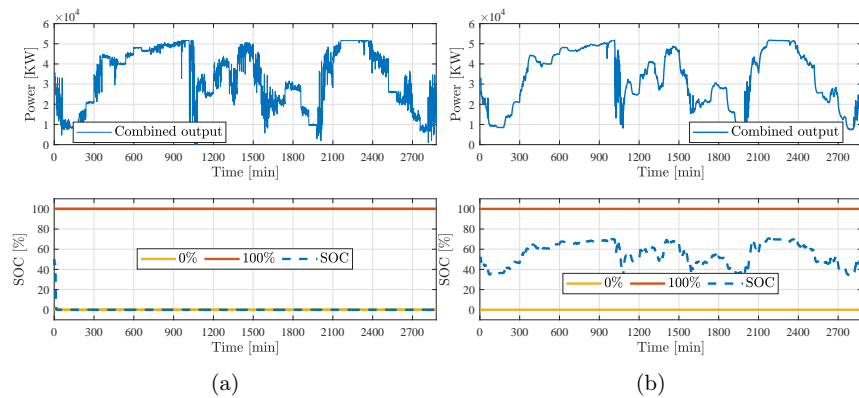
Fig. 8: Resultado del sistema a) sin controlador. b) con controlador SOC-FB

Una comparativa de los resultados de la primera prueba se presentan en la Fig. 9, donde se puede observar la salida del sistema en el intervalo de 0 a 1500 minutos. Aquí, la salida que no tiene controlador prácticamente se solapa con la potencia generada por la planta, es decir, no hay suavizado. La salida del sistema con SOC-FB presenta un suavizado, pero, aun así, no es mucha la diferencia con respecto a la potencia original, como muestran los valores de la desviación estándar, además de que no es capaz de seguir al 100% a la referencia debido a que el controlador debe mantener al SOC dentro de los límites operativos, evitando que el BESS libere demasiada energía.

De los resultados de la prueba anterior se hace evidente la necesidad de buscar los valores óptimos de las variables de E, M y T. Este problema se aborda en una segunda prueba, combinando ahora el sistema de control con el algoritmo Hybrid Differential Evolution Algorithm With Adaptive Crossover Mechanism.
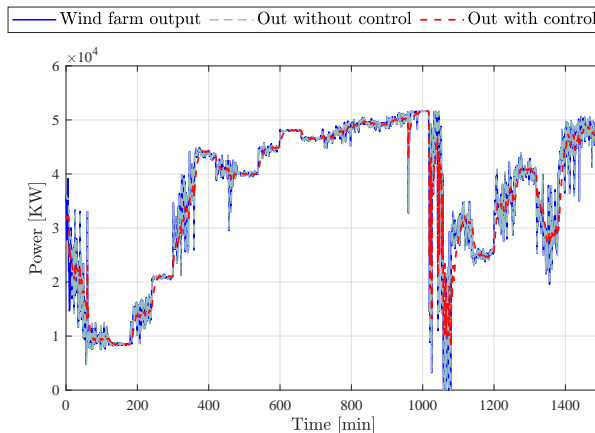
Fig. 9: Resultados de la prueba del sistema

Los rangos para los valores en donde se buscará la optimización se muestran en la Tabla 3, utilizando 100 generaciones.

Tabla 3: Rango de valores para la optimización

Variable	Rango
Capacidad del BESS (E)	1 MWh - 50 MWh
Constante de tiempo del filtro (T)	100 sec - 3460 sec
Margen de offset (M)	0.1 - 0.49

La ejecución del algoritmo entrega como resultado los valores: `E= 20 MW, T = 1325 s`, `M= 0.19`, presentando un valor relativamente bajo de E, esto debido a que mientras más alto sea β el algoritmo se enfocará más en reducir el valor del BESS. Los resultados de esta prueba se muestran en la Fig. 11a, con una desviación estándar de la derivada de la salida 27.14 (33% del valor original).

Para determinar el valor adecuado de β (coeficiente que determina la prioridad de la reducción del BESS) que entregue el mejor valor posible para el BESS, a la vez que se suaviza la potencia generada, se procedió a ejecutar simulaciones para diferentes valores de β, procediendo luego a analizar la derivada de la salida del sistema. En la Fig. 10 se muestran el mejor valor para el BEES y la desviación estándar de la derivada de la salida del sistema para cada valor de β. Se observa que alrededor del valor $\beta = 0.4$ se obtienen valores similares para estos estadísticos, más allá de éste la salida implicaría un mayor valor para el

BESS, lo que no justificaría su implementación, pues no tendría sentido poseer un BESS de 50 MWh en una planta de 52 MW.
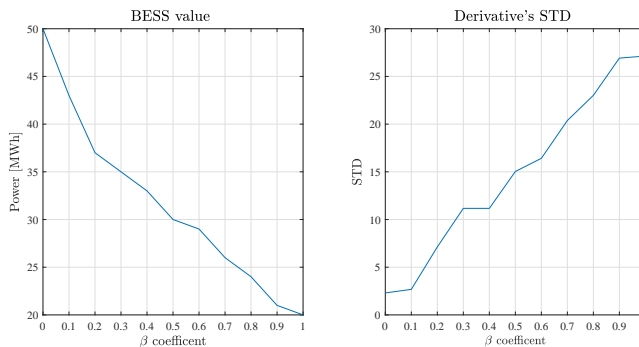
Fig. 10: Análisis de los resultados para diferentes β

Se concluye entonces que los valores óptimos para el sistema son: $\beta = 0.4$, $E = 33\ MWh$, $T = 2281$ y $M = 0.1$. Finalmente, en la Fig. 11b se muestra la salida del sistema para estos valores, en donde se tiene una variación máxima de aproximadamente 25 MW, en el intervalo de 1000 a 1100 minutos, contra los casi 52 MW que sufre la salida original de la planta, además la salida del sistema presenta una desviación estándar de 11.17 que representa menos del 13.77% del sistema sin controlador.
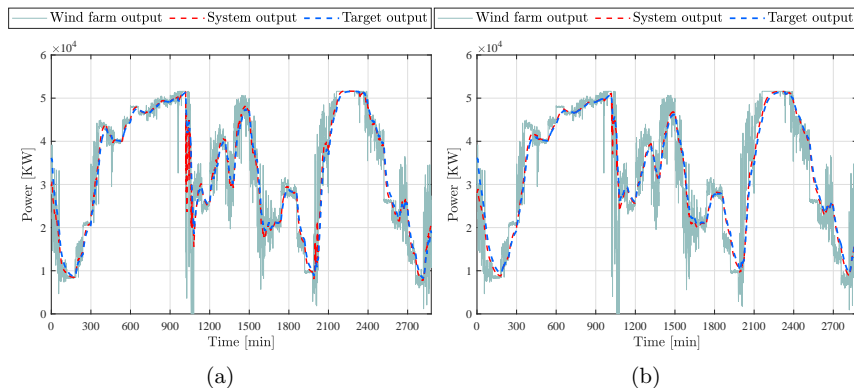
Fig. 11: Resultado de la optimización a) con $\beta = 1$. b) con $\beta = 0.4$

5   Conclusiones

La propuesta de dimensionamiento y gestión del almacenamiento de energía a través de baterías de este trabajo demuestra que es posible disminuir la variabilidad de la potencia en sistemas de generación de energía renovable que usan el viento como fuente primaria. Específicamente, el análisis crítico de la dimensión y operación del BESS en combinación con la estrategia de control SOC-FB reducen la variabilidad pico de la potencia en 86.32%, medido con respecto a la desviación estándar, en la granja eólica bajo estudio. Estos resultados soportan la hipótesis de que enfoques similares a los presentados en este trabajo ofrecen soluciones alternativas a los que basan la gestión de los sistemas renovables en esquemas de predicción complejos y altamente costosos. Finalmente, la metodología propuesta en este trabajo extiende las posibilidades de aplicación a otras tecnologías de almacenamiento de energía, como el almacenamiento de hidrógeno, aire comprimido, bombeo de agua, etc.

References

1. Abhinav, R., Pindoriya, N.: Grid integration of wind turbine and battery energy storage system: Review and key challenges. pp. 1–9 (2016), https://ieeexplore.ieee.org/abstract/document/7583998
2. Aerogenerador, U., Dspic, C., Frias, G., Catuogno, G.: Implementación de un seguidor del punto de máxima potencia en owntech-open source software defined power converter technology suit view project fault tolerant control in three and six-phase pm and synr machines view project (2018), https://www.researchgate.net/publication/325770833
3. Bitaraf, H., Rahman, S.: Reducing curtailed wind energy through energy storage and demand response. IEEE Transactions on Sustainable Energy **9**, 228–236 (1 2018). https://doi.org/10.1109/TSTE.2017.2724546
4. Borhan, H., Rotea, M., Viassolo, D.: Control of battery storage for wind energy systems. pp. 1342–1349 (2012)
5. Correa-Quezada, R., Tituaña-Castìllo, M.D.C., Río-Rama, M.D.L.C.D., Álvarez García, J.: Effects of increased renewable energy consumptionon electricity prices: Evidence for six south american countries. Energies **15** (1 2022). https://doi.org/10.3390/en15020620
6. Gevorgian, V., Corbus, D.: Ramping performance analysis of the kahuku wind-energy battery storage system (2013), www.nrel.gov/publications.
7. Huang, W.F., Sun, J.P.: Prediction of typhoon design wind speed with cholesky decomposition method. Structural Design of Tall and Special Buildings **27** (8 2018). https://doi.org/10.1002/tal.1480
8. Kathryn, E., Thomas, J., Thomas, N.: Wind farm control: addressing the aerodynamic interaction among wind turbines. pp. 2104–2109. IEEE (2009)
9. Katsuhisa, Y., Toshiya, N., Gentaro, K., Yoshihsa, U.: New control method for regulating state-of charge of a battery in hybrid wind power/battery energy storage system (2006), https://ieeexplore.ieee.org/abstract/document/4075924/
10. Khaki, B., Das, P.: Sizing and placement of battery energy storage systems and wind turbines by minimizing costs and system losses (2012)

11. Mohod, S.W., Hatwar, S.M., Aware, M.V.: Grid support with variable speed wind energy system and battery storage for power quality. vol. 12, pp. 1032–1041. Elsevier Ltd (2011). https://doi.org/10.1016/j.egypro.2011.10.135

12. Reynoso-Meza, G.: Hybrid differential evolution algorithm with adaptive crossover mechanism (2012), https://la.mathworks.com/matlabcentral/profile/authors/2438888

13. Reynoso-Meza, G., Sanchis, J., Blasco, X., Herrero, J.M.: Hybrid de algorithm with adaptive crossover operator for solving real-world numerical optimization problems. pp. 1551–1556 (2011). https://doi.org/10.1109/CEC.2011.5949800

14. Sadorsky, P.: Renewable energy consumption and income in emerging economies. Energy Policy **37**, 4021–4028 (10 2009). https://doi.org/10.1016/j.enpol.2009.05.003

15. Sattar, A., Al-Durra, A., Caruana, C., Debouza, M., Muyeen, S.M.: Testing the performance of battery energy storage in a wind energy conversion system. IEEE Transactions on Industry Applications **56**, 3196–3206 (5 2020). https://doi.org/10.1109/TIA.2020.2979792

16. Such, M., Hill, C.: Battery energy storage and wind energy integrated into the smart grid. 2012 IEEE PES Innovative Smart Grid Technologies (ISGT) pp. 1–4 (2012)

17. Yang, X., Yue, H., Ren, J.: Fuzzy empirical mode decomposition for smoothing wind power with battery energy storage system. vol. 50, pp. 8769–8774. Elsevier B.V. (7 2017). https://doi.org/10.1016/j.ifacol.2017.08.1735

Pump as Turbine in Small-Scale Hydro Generation

Vicente Leite [0000−0002−8790−519X]

Research Centre in Digitalization and Intelligent Robotics (CeDRI), Instituto
Politécnico de Bragança, Campus de Santa Apolónia, 5300-253 Bragança, Portugal
`avtl@ipb.pt`
https://cedri.ipb.pt

Abstract. The interest in small-scale hydropower generation (SSHG) has increased greatly, but its potential remains untapped, even in places where adequate infrastructure already exists. Many studies have highlighted the advantages of using pumps as turbines (PAT) and present this solution as the best for SSHG. However, pumps are not provided with technical characteristics in reverse mode. Several authors have presented suitable models for converting the best efficiency point of a pump when operating as a turbine and vice versa. Furthermore, PAT models have been also proposed to obtain their characteristic curves. This paper, presents a review of these methodologies and describes a step-by-step procedure that can be very useful to support small-scale hydropower designers to select the most suitable PAT for a given site, as well as for predicting the PAT performance curves. This procedure is applied in a case study, in which a PAT will be used to generate energy for self-consumption in a building.

Keywords: Pump as Turbine · PAT Characteristics · Small-Scale Hydropower · Case Study.

1 Introduction

Energy is a critical challenge that the world continues to face, today more than ever. Renewable energy has become a priority and conventional hydropower plants have the largest share [1] with well-known advantages and disadvantages. This is a well explored and mature technology. However, the potential for small-scale hydropower generation (SSHG) worldwide remains untapped and increasing attention is being paid to this energy resource [2]. Moreover, dealing with the very small still remains a challenge. The most significant one is the high cost of commercial turbines [1] and this has discouraged the exploitation of small water resources in the recent past [3]. An effective strategy to take advantage of SSHG is to use a Pump As Turbine (PAT) due to due to lower cost and higher availability [1, 4]. Indeed, cost savings can reach -74% at the expense of a slight reduction of -19% in the electrical power generated, compared with turbines designed for specific sites [2]. Furthermore, pumps are technologically simpler than conventional turbines and spare parts are widely available [4].

PATs can be used in many contexts such as in water distribution networks to replace pressure reducing valves [1, 3], in energy recover from rainwater [3], in pumped-hydro energy storage systems [5] or irrigation systems [2].

The main challenge to using PATs, is the lack of information since manufacturers do not provide the performances of their machines running in reverse mode of operation [2, 4]. For this reason, several authors have developed suitable prediction models of PAT characteristics. This is not a new topic [6, 7], but it has had a huge development in recent years [3, 8]. Basically, there are models that correlate the pump Best Efficiency Point (BEP) with the PAT one and models that predict the PAT characteristic curves. The former are based on conversion factors of the BEP between the modes of operation, as pump or as turbine [2, 3, 8–12]. In this way it is possible to select the most suitable pump for a given site and, on the other hand, knowing the BEP of a pump, to estimate the BEP of its operation as a turbine. To this end, different authors have proposed models based on polynomial expressions that predict the characteristic curves of head, power and efficiency as a function of flow [3, 9, 13, 14].

This paper presents a literature review of these models and a comprehensive application for SSHG using PATs. After this first section of introduction, section 2 describes, step-by-step, this methodology and section 3 presents the results of a case study with its application to a SSHG unit for self-consumption in the Ciência Viva Centre of Bragança, Portugal. Finally, the main conclusions are presented in section 4.

2   Methodology

The methodology used in this work is presented in Figure 1 and is described, step-by-step, in sections 2.1 and 2.2. The fundamental design criterion is to maximise the generated power per m^3 of water. Thus, a PAT is selected for a given site to operate at its BEP, even though it may generate greater power outside it. For this reason, the most relevant aspects related to the efficiency of the pump-motor set operating in generation mode (as a turbine) are briefly presented in the next paragraphs.
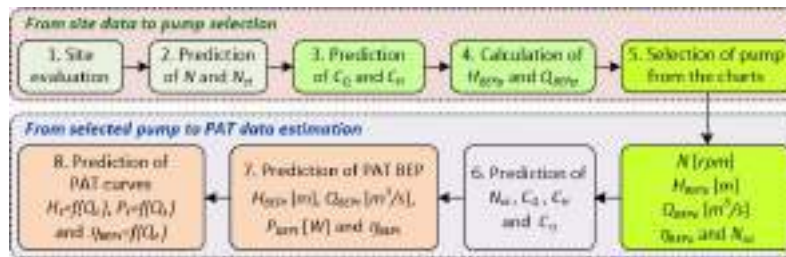

Fig. 1. Methodology used for selecting a pump and its characterisation as a PAT.

Hydraulic efficiency of well-designed turbines is in the range 80% to over 90%. In smaller systems, where PATs are a competitive alternative, it reduces to the range 60% to 80% and an efficiency around 70% can be expected [2]. Although the efficiency of a PAT is lower compared to conventional turbines [2], this is not true when compared to the efficiency in pump mode. Recent studies report that the maximum efficiency in pump and turbine modes is approximately the same [15]. With the experimental tests of 12 PATs reported in [3], it was possible to observe that the efficiency in turbine mode is greater than that in pump one for specific speeds between 15 and 65, and lower otherwise.

Usually, conventional centrifugal pumps are coupled with induction motors because they are widely spread due to their low cost and robustness. The induction machine is completely reversible and can suitably operate as a motor or as a generator without any modifications [16]. Its efficiency greatly depends on the efficiency class [17] and higher efficiency machines (i.e. IE3 and IE4) have greater efficiency in generator mode. On the contrary, low efficiency machines (i.e. IE1 and IE2) have greater efficiency in motor mode [16].

2.1 Design Methodology from Site Data to Pump Selection

Step 1 Site Evaluation

This first step basically consists of analysing the local energy potential and its context in terms of physical, technical and legal requirements. For a given site, the basic information required is the gross head (without considering any hydraulic losses) and flow rate. Equally important is to know its pattern throughout the year. With this site data, the hydraulic power, $P_h\,[W]$, is estimated by Equation (1):

$$P_h = \eta \times g \times \rho \times Q \times H \tag{1}$$

where η is the hydraulic efficiency, g is the gravity acceleration ($9.81\,m/s^2$), ρ is the water density ($1000\,kg/m^3$), $Q\,[m^3/s]$ is the flow rate and $H\,[m]$ is the gross head. In general, the head does not vary much and for small-scale hydro generation (SSHG), the annual yield will depend essentially on the time during which the flow is available. In this context, where the flow can vary significantly over time, the design becomes much more challenging. As for the overall efficiency, and for a first assessment, a value of 50% can be used, already considering all hydraulic losses (in pipe and PAT), and electric losses (in generator and other electric equipment and wiring).

Step 2 Predicting Rotational and Specific Speeds: N and N_{st}

The available head and expected flow at the site, determinate the theoretical BEP (Q_{BEPt}, H_{BEPt}) of the ideal PAT. In general, the shaft of a commercial pump is directly coupled to the shaft of a three-phase induction motor. This set operates at a rotation speed, $N\,[rpm]$, which depends on the number of pole pairs (pp) of the motor. This speed is close to the synchronous speed ($= 60f/pp$) which also depends on the grid frequency ($f = 50\,Hz$ or $60\,Hz$). Due to cost and manufacturing difficulties, most commercial induction motors are produced with

1, 2 or 3 pole pairs. This means that for a frequency of $50\,Hz$, the synchronous speed is 3000, 1500 and $1000\,rpm$, respectively. The shaft speed is a few per cent lower due to slip, which is inherent to the operation of asynchronous machines. For this reason, manufacturers present, in their centrifugal pumps catalogues, pump sets for 2900, 1450 and $960\,rpm$.

Using the rotational speed $N\,[rpm]$, together with the flow and head values in the BEP $\left(H_{BEPp}\,[m],\ Q_{BEPp}\,[m^3/s]\right)$, obtained from manufacturer catalogues, the specific speed of the pump can be calculated, as shown in Equation (2). In the same way, for a turbine (PAT), or for a given site (ideal PAT), the specific speed is given by Equation (3), knowing the flow rate $[m^3/s]$ and head $[m]$ available at the site BEPt.

$$N_{sp} = \frac{N\sqrt{Q_{BEPp}}}{H_{BEPp}^{0.75}} \tag{2}$$

$$N_{st} = \frac{N\sqrt{Q_{BEPt}}}{H_{BEPt}^{0.75}} \tag{3}$$

Step 3 Predicting Conversion Factors: C_Q and C_H

This step consists of estimating the conversion factors from the ideal turbine (site), obtained in the previous step, to the corresponding pump since manufacturers do not have the characterisation of their pumps in turbine mode. The head and flow conversion factors are defined by expressions (4) and correspond, respectively, to the ratio between the head in turbine mode ($H_{BEPt}=H_{site}$) and that in pump mode (H_{BEPp}), at the best efficiency point (BEP), and to the ratio between the flow in turbine mode ($Q_{BEPt}=Q_{site}$) and that in pump mode (Q_{BEPp}).

$$C_H = \frac{H_{BEPt}}{H_{BEPp}}, \quad C_Q = \frac{Q_{BEPt}}{Q_{BEPp}} \tag{4}$$

Predicting these conversion factors from the turbine mode to the pump mode and vice-versa has been the subject of much research work over the past decades. These studies resulted in proposals of different empirical methods, which predict the BEP of a PAT, from the pump characteristics available from manufacturers. Similarly, these methods also predict the BEP from PAT mode (head and flow of the site) to pump mode. Table 1 presents the expressions developed in recent studies and used in this work to predict these conversion factors.

Step 4 Predicting the Pump BEP: H_{BEPp} and Q_{BEPp}

In this step, the pump BEP (BEPp) is estimated from the BEP of the ideal turbine (BEPt=BEPsite) by using (5), obtained from coefficients (4), and using the expressions presented in Table 1.

$$H_{BEPp} = \frac{H_{BEPt}}{C_H}, \quad Q_{BEPp} = \frac{Q_{BEPt}}{C_Q} \tag{5}$$

Table 1. Expressions of head and flow conversion factors, from turbine to pump.

Authors	Calculation of C_H and C_Q (turbine $\rightarrow$ pump)
Barbarelli [9]	$C_H = -0.00003N_{sp}^3 + 0.0044N_{sp}^2 - 0.20882N_{sp} + 4.64293$ $C_Q = 0.00029N_{st}^2 - 0.02771N_{st} + 2.01648$ (with $N_{sp} = 0.9867N_{st} + 5.2818$)
Barbarelli [3]	$C_H = -0.0000237N_{st}^3 + 0.00331N_{st}^2 - 0.15047N_{st} + 3.68497$ $C_Q = 0.00026N_{st}^2 - 0.02302N_{st} + 1.88171$
Stefanizzi [10]	$C_H = -0.000023N_{st}^3 + 0.003206N_{st}^2 - 0.145781N_{st} + 3.604636$ C_Q not applied
Algieri [2]	$C_H = -0.000018N_{st}^3 + 0.002764N_{st}^2 - 0.134384N_{st} + 3.540085$ $C_Q = 0.00015N_{st}^2 - 0.0193N_{st} + 1.9011$
Pérez-Sánchez [8]	$C_H = \frac{1}{0.186314\,ln(N_{st})}$ and $C_Q = \frac{1}{0.210551\,ln(N_{st})}$

Step 5 Selecting a Pump from the Charts

Now, a standard pump must be selected from pump catalogues for the BEP predicted in the previous step (H_{BEPp}, Q_{BEPp}). Manufacturers offer charts for N=2900, 1540 and 960 rpm which allow to select the most suitable pump (50 Hz). Once the pump has been selected, the impeller diameter must be chosen, on another chart ($H - Q$), whose characteristic has the closest BEP to that obtained in the previous step. Normally, a larger diameter corresponds to a higher efficiency.

At the end of this step, the pump with a given impeller diameter is chosen, whose characteristics (BEP) are: N, H_{BEPp}, H_{BEPp}, and η_{BEPp}, as well as the specific speed, N_{sp}, using Equation (2).

2.2 Design Methodology from Pump to PAT Data Estimation

Step 6 Predicting Conversion Factors from Pump to Turbine: C_Q and C_H

Once a specific pump has been selected, its operation as a turbine has to be characterised since it is not provided by manufacturers. Over the last few years, many researchers have improved methods of predicting PAT characteristics. As with the conversion from site (turbine mode) to pump, many studies have presented conversion factors from pump to turbine. Some works use the same coefficients of step 3, others use different ones. Some of them are based on the pump efficiency at the BEPp [8, 12, 18], others use the specific speed [2, 3, 9, 10]. Table 2 presents the conversion factors used in this work.

Step 7 Predicting PAT BEP: H_{BEPt}, P_{BEPt} and η_{BEPt}

Now, once the conversion factors from pump to turbine mode have been predicted in previous step, the PAT BEP can be characterised through Equations (6) and (7).

$$H_{BEPt} = C_H H_{BEPp} \qquad (6)$$

Table 2. Expressions of head and flow conversion factors, from pump to turbine.

Authors	Calculation of C_H and C_Q (pump $\rightarrow$ turbine)
Yang [18]	$C_H = \frac{1.2}{\eta_{BEPp}^{1.1}}$ and $C_Q = \frac{1.2}{\eta_{BEPp}^{0.55}}$
Morabito [12]	$C_H = 5.1956\,N_{sp}^{-0.323}$ and $C_Q = 3.1276\,N_{sp}^{-0.219}$
Barbarelli [9]	$C_H = -0.00003N_{sp}^3 + 0.0044N_{sp}^2 - 0.20882N_{sp} + 4.64293$ $C_Q = 0.00029N_{sp}^2 - 0.02771N_{sp} + 2.01648$
Barbarelli [3]	$C_H = -0.0000237N_{st}^3 + 0.00331N_{st}^2 - 0.15047N_{st} + 3.68497$ $C_Q = 0.00026N_{st}^2 - 0.02302N_{st} + 1.88171$ (with $N_{st} = 0.9237N_{sp} - 2.6588$)
Stefanizzi [10]	$C_H = -0.000023N_{st}^3 + 0.003206N_{st}^2 - 0.145781N_{st} + 3.604636$ with $N_{st} = 0.9237N_{sp} - 2.6588$ C_Q not applied
Algieri [2]	$C_H = -0.000018N_{sp}^3 + 0.002764N_{sp}^2 - 0.134384N_{sp} + 3.540085$ $C_Q = 0.00015N_{sp}^2 - 0.0193N_{sp} + 1.9011$
Pérez-Sánchez [8]	$C_H = \frac{1.2337}{\eta_{BEPp}}$ and $C_Q = \frac{1}{0.825861\sqrt{\eta_{BEPp}}}$

$$Q_{BEPt} = C_Q\,Q_{BEPp} \qquad (7)$$

To complement this conversion it is also necessary to predict the efficiency of the PAT at the BEP from the pump data. Some studies reported that efficiency is lower in turbine mode than in pump mode, others referred that it is approximately the same [15] and others observed that is greater [3]. Table 3 presents the expressions used in this work to predict the efficiency in turbine mode. Some of them use the pump efficiency in BEPp [6], some use the specific speed [3, 19], and others uses both [7, 8, 20, 21].

Table 3. Expressions used to estimate efficiency in turbine mode (η_{BEPt}).

Authors	Calculation of η_{BEPt}
Alatorre-Frenk [6]	$\eta_{BEPp} - 0.03$
Gülich2008 [20]	$\left(1.16 - \frac{N_{sp}}{200}\right)\eta_{BEPp}$
Audisio [7]	$0.95\eta_{BEPp}^{0.7}\left[1 + \left(0.5 + ln(N_{sp})\right)^2\right]^{-0.25}$ with $N_{sp} = \frac{N\sqrt{Q[l/s]}}{1673\,H^{0.75}}$
Barbarelli [3]	$-0.00037N_{st}^2 + 0.02952N_{st} + 0.24326$
Novara [19]	$0.89 - \frac{0.024}{Q_{BEPt}^{0.41}} - 0.076\left(0.22 + ln\frac{N_{st}}{52.933}\right)^2$
Rossi [21]	$0.7933N_{sp} + 0.605\eta_{BEPp} - 0.09246N_{sp}^2 - 0.8254N_{sp}\eta_{BEPp} + 0.3936\eta_{BEPp}^2$ with $N_{sp} = \frac{\sqrt{Q}}{gH^{0.75}}$
Pérez-Sánchez [8]	$\eta_{BEPp}\sqrt{0.250976\,ln(N_{sp})}$

The predicted power of the PAT at BEP, P_{BEPt} [W], is calculated using Equation (1) as shown in Equation (8). The global efficiency of the set (PAT+ generator) is obtained by Equation (9), also considering the generator efficiency η_{BEPg}.

$$P_{BEPt} = \eta_{BEPt} \times g \times \rho \times Q_{BEPt} \times H_{BEPt} \tag{8}$$

$$P_{ele_{BEPt}} = \eta_{BEPg} \times P_{BEPt} \tag{9}$$

Step 8 Predicting PAT Curves: H_t, P_t and η_t

In the design of SSHG systems based on the use of PATs, it is not enough to estimate the BEP of the PAT, as described in the previous step. The BEP of the selected PAT may not exactly match the ideal BEP of the site and, furthermore, head and flow may vary over time. Thus, it is necessary to know the characteristic curves of the PATs, i.e. head (H_t), efficiency (η_t) and power (P_t) as a function of flow rate (Q_t). The usual way to get this information would be to ask the manufacturer. However, manufacturers also do not provide characteristic curves of their pumps running as turbines since this would require laboratory tests in turbine mode operation which would greatly increase their final cost [3]. Due to this, significant efforts have been made by several researchers to predict PAT performance curves, not only with theoretical approaches, but also with experimental work of pumps tested in turbine mode. Several methods have been developed over the past few years to predict head, efficiency and power characteristic curves of a PAT knowing its BEP [3, 8, 21]. Some of them report studies based on a database of 113 PATs [11]. Such methods are based on fixed-coefficient polynomials and use dimensionless parameters h, q, η and p which are obtained by dividing head (H_t), flow rate (Q_t), efficiency (η_t) and power (P_t) of the PAT, by the respective values at the BEP, as described by (10).

$$h = \frac{H_t}{H_{BEPt}}, \quad q = \frac{Q_t}{Q_{BEPt}}, \quad \eta = \frac{\eta_t}{\eta_{BEPt}}, \quad p = \frac{P_t}{P_{BEPt}} \tag{10}$$

The respective curves have the polynomial form described by Equation (11). The polynomials of h and p are of 2nd and 3rd order, respectively. Regarding efficiency, some authors have reported the respective curve with a 4th order polynomial [8], and others use the definition, $\eta_t = P_t/P_h$, to obtain the efficiency curve, according to the dimensionless equation (12) [3].

$$h, \eta, p = ... + a_2\, q^2 + a_1\, q + a_0 \tag{11}$$

$$\eta = p\,(hq)^{-1} \tag{12}$$

By way of example, the real curves corresponding to the dimensionless Equations (11) and (12) are written, respectively, by Equations (13) and (14). The real curves P_t and η_t are obtained in a similar way.

$$H_t = \left[a_2 \left(\frac{Q_t}{Q_{BEPt}} \right)^2 + a_1 \left(\frac{Q_t}{Q_{BEPt}} \right) + a_0) \right] H_{BEPt} \tag{13}$$

$$\eta_t = \left[\frac{P_t}{P_{BEPt}} \left(\frac{H_t}{H_{BEPt}} \frac{Q_t}{Q_{BEPt}} \right)^{-1} \right] \eta_{BEPt} \tag{14}$$

3   Results

3.1   Site Description

The PAT is to be installed in the Bragança Ciência Viva Centre, using the same infrastructures (pipe and powerhouse) of an existing turbine. This $15\,kW$ conventional turbine was installed just over 10 years ago, but the number of operating hours per year has been very low. This is mainly due to the required flow (over $160\,l/s$) is only available for a short period of the year. In addition, critical breakdowns have occurred, with long repair times and requiring specialised companies. The energy generated has been injected into the grid, according to the legislation at the time, published in 2007.

At the beginning, the selling price was rather high, relative to purchase price, due to the feed-in tariff incentive. Currently, the energy generated under those contracts is sold at a very low price, and many homeowners are changing to the current self-consumption legislation. In this new context, the energy generated is consumed in the house and the surplus is injected into the grid, in practice at zero cost.

In the case and according to the above mentioned, the goal is to make better use of the existing infrastructure and generate hydro energy that can be used for self-consumption in the building. It is worth pointing out that it is not necessary to build any additional infrastructure and the use of a PAT guarantees an effective solution, as it is low cost, widely available on the market, and whose installation, maintenance and replacement can be done by local companies. Furthermore, it does not require complex monitoring and control systems.

3.2   Design from Site Evaluation to Pump Selection

Step 1 Site Evaluation

The gross head available at the site is exactly $13\,m$. Assuming a head drop of $1\,m$ due to hydraulic losses in the pipe (curves and friction) and mainly due to the water shut-off valve, the useful head across the PAT will be $H_{site}{=}12\,m$, which corresponds to about 8% of head losses.

The load diagrams of the last year (September 2021 to August 2022) were analysed to obtain the average value of the minimum active power of the building. It was verified that it happens in the periods between 6 pm and 10 am (when the Ciência Viva Centre is closed).

The minimum values of active power, with a similar pattern, were recorded from September 9 to October 25, 2021, from February 19 to 23, 2022, and in the month of May 2022. In this month, the pattern of the minimum active power, recorded between days 1 and 10 and between days 17 and 19, are representative

of all the periods mentioned above. The average registered power (between 6 pm and 10 am) was $1750\,W$.

At this stage, the global efficiency is assumed to be 60% due to an expected PAT efficiency of 70% and generator efficiency of 85% as described in the beginning of section 2. Thus, for the head available, $H_{site}=12\,m$, and required electric power, $P_{ele}=1750\,W$, and according to Equation (9) the required flow is about $25\,l/s$. Even if it is a very low water flow, in the context of hydropower generation, this flow is not expected to be available throughout the year. Indeed, local observation experience in the context of other projects shows that, in a typical year, a flow of $25\,l/s$ will be difficult to guarantee during the summer months (July, August and September).

From the above, a PAT generating a power of about $1.8\,kW$ can operate 24 hours a day, for about 9 months, in a typical year. On the other hand, it should be noted that this power corresponds to the maximum value that the building can absorb, without having to send power back to the grid.

In summary, according to this first evaluation, an ideal PAT for the site, i.e. $H_t=12\,m$, and $Q_t=25\,l/s$, with an overall efficiency of 60%, will generate a power of about $1.8\,kW$, for 9 months per year, which corresponds to an annual yield of almost $12\,MWh$.

Step 2 Predicting Rotational and Specific Speeds: N and N_{st}

For the available head, there are pumps on the market with rotation speeds of 2900, 1500 and $960\,rpm$. However, the head of $12\,m$ is at the lower limit of $2900\,rpm$ pumps. On the other hand, calculating the specific speed, N_{st}, using Equation (3) for $N=2900$, 1540 and $960\,rpm$ results, respectively, 71.1, 35.6 and 23.5. It is worth noting that the experimental study reported in [3] proposed a correlation between the maximum efficiency, η_{max_t} and the specific speed N_{st} given by the equation shown in Table 3. Therefore, according to this equation ($\eta_{max_t} = -0.00037N_{st}^2 + 0.02952N_{st} + 0.24326$), η_{max_t} achieves its maximum for $N_{st}=40$ and η_{max_t} is above 80% for N_{st} in the range 30 to 50. Therefore, the most suitable rotation speed is, definitely $N=1450\ rpm$ giving a specific speed of $N_{st}=35.6$ which is not far way of the best value (40). On the other hand, it is inside the range 30 to 50, assuring an efficiency above 80%.

Steps 3 and 4 Predicting Pump BEP: H_{BEPp} and Q_{BEPp}

Table 1 has the expressions used to predict the head and flow rate conversion factors, C_H and C_Q, from turbine to pump. This corresponds to step 3 and the results are shown in Table 4. Using these conversion factors in step 4, according to Equations (5), the pump head and flow values at BEP are obtained. The results are also shown in Table 4.

Step 5 Selecting Pump from Charts

Now, a standard centrifugal pump is selected from the characteristic curves provided by the manufacturers. It was chosen the manufacturer KSB since there

Table 4. Values of head and flow rate conversion factors from turbine to pump.

Authors	$C_H(t \rightarrow p)$	$C_Q(t \rightarrow p)$	$H_{BEP_p}[m]$	$Q_{BEP_p}[m^3/s]$
Barbarelli [9]	1.41	1.37	8.5	0.0182
Barbarelli [3]	1.45	1.39	8.3	0.0180
Stefanizzi [10]	1.44	not applied	8.3	0.0196
Algieri [2]	1.45	1.40	8.3	0.0178
Pérez-Sánchez [8]	1.50	1.33	8.0	0.0188

is some information available in previous studies. From the characteristic curves for the desired rotation speed, N=1450 rpm, the pump whose BEP is closest to the one obtained in the previous step is selected, as illustrated in Figure 2(a). In this case, and at first sight, the choice is not very obvious. At this stage it should bear in mind that the pumps have their best efficiency in the upper part of their operating area. For this reason the 80-65-160 pump is selected. Next, the impeller diameter must be chosen, as illustrated in Figure 2(b). As can be seen, the desired BEP (P) is not far away from the BEP of the pump with a impeller diameter of 174 mm. In fact, this is the impeller diameter that allows the pump to achieve greater efficiency. If the 100-080-160 pump had been chosen, it would be concluded that its BEP occurs for lower head (7.3 m) and higher flow rate (31 l/s). Although this pump has a slightly higher efficiency at the BEP (85.8%), it would work with a lower efficiency due to the lower working flow. In this step, it may be necessary to perform a few iterations to identify the pump model and its impeller diameter that leads to the highest efficiency.

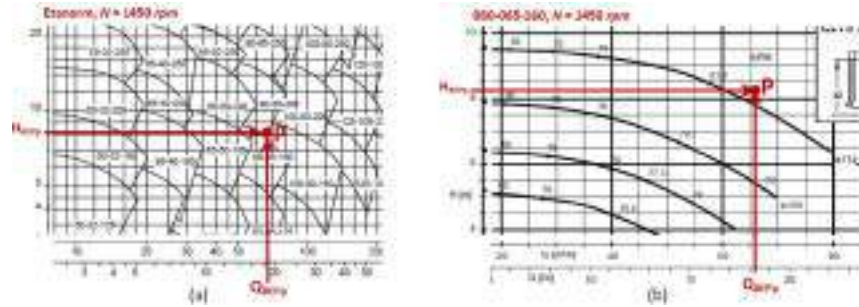**Fig. 2.** Selecting pump (a) and impeller diameter (b) from the characteristic curves.

The BEP of the selected pump is then obtained from Figure 2(b): H_{BEP_p}= 8.5 m, Q_{BEP_p}=57.5 m^3/h (16 l/s) and η_{BEP_p}=81.3%. At this stage it is recommended to consult the manufacturer's representative. They can usually give more precise information than is available in catalogues. In this case it was possible to

find out that rated rotation speed and motor efficiency are $1468\,rpm$ and 86%, respectively. Therefore, from Equation (2), the pump specific speed is $N_{sp}{=}37.3$. Table 5 summarises the characteristics of the selected pump (080-065-160, $\phi174$).

Table 5. Characteristics of the selected pump: 080-065-160.

H_{BEPp}	Q_{BEPp}	η_{BEPp}	N_{BEPp}	N_{sp}	Impeller diameter
$8.5\ m$	$57.5\ m^3/h$ ($16\ l/s$)	81.3%	$1468\ rpm$	37.3	$174\ mm$

3.3   Design from Selected Pump to PAT Data Estimation

This section presents the estimation of the pump data operating in turbine mode (PAT), based on the pump BEP obtained in the previous step (Table 5).

Steps 6 and 7 Predicting PAT BEP: H_{BEPt}, Q_{BEPt} and η_{BEPt}

The head and flow conversion factors, C_H and C_Q, from selected pump to turbine mode, are estimated in step 6, using the expressions presented in Table 2 and the respective values are presented in Table 6. Step 7 predicts the head and flow at BEP, in turbine mode, using the conversion factors presented in Table 6 in Equations (6) and (7). The efficiency, η_{BEPt}, was estimated using directly the expressions presented in Table 3 and the results are shown in Table 7.

Table 6. Values of head and flow rate conversion factors from pump to turbine.

Authors	$C_H(p \rightarrow t)$	$C_Q(p \rightarrow t)$	$H_{BEPt}[m]$	$Q_{BEPt}[m^3/s]$
Yang [18]	1.51	1.34	12.81	77.32
Morabito [12]	1.61	1.42	13.72	81.42
Barbarelli [9]	1.42	1.39	12.06	79.73
Barbarelli [3]	1.49	1.41	12.63	81.24
Stefanizzi [10]	1.47	not applied	12.51	74.58
Algieri [2]	1.44	1.39	12.23	79.93
Pérez-Sánchez [8]	1.52	1.34	12.90	77.22
Average	-	-	12.69	78.78

For the purposes of this work, the average values obtained by the different authors, are used for the pump operating point in turbine mode: $H_{BEPt}{=}12.7\,m$, $Q_{BEPt}{=}78.8\,m^3/s$ and $\eta_{BEPt}{=}78.5\%$. Using these results, the specific speed is calculated through Equation (3) which gives $N_{st}{=}32$. On the other hand, the power in turbine mode is calculated by Equation (8) that gives $P_{BEPt}{=}2097.2\,W$. Considering the efficiency of the three-phase induction motor, operating as a generator, equal to its efficiency as a motor (86%), the generated electric power will be, according to the Equation (9), $P_{ele_{BEPt}}{=}1803.6\,W$. These results are

Table 7. Values of efficiency at BEP in turbine mode (η_{BEPt}).

Authors	PAT efficiency (η_{BEPt})
Alatorre-Frenk [6]	78.3%
Gülich [20]	79.2%
Audisio [7]	81.7%
Barbarelli [3]	80.9%
Novara [19]	76.8%
Rossi [21]	75.3%
Pérez-Sánchez [8]	77.5%
Average	78.5%

summarised in Table 8 and correspond to the predicted BEP of the selected pump (Table 5) in turbine mode.

Table 8. Predicted BEP of the selected pump (080-065-160) in turbine mode.

H_{BEPt}	Q_{BEPt}	η_{BEPt}	η_{BEPg}	N_{BEPt}	N_{st}	P_{BEPt}	$P_{ele_{BEPt}}$
12.7 m	78.8 m^3/h (21.9 l/s)	78.5%	86%	1468 rpm	32	2097.2 W	1803.6 W

Step 8 Predicting PAT Curves: H_t, P_t and η_t

The PAT curves (H_t, P_t and η_t as a function of Q_t) were predicted using Equations (11) to (14) considering the BEPt described in Table 8. The coefficients of head curve (given by Equations (11) or (13)) and the power one (11) are presented in Table 9.

Table 9. Coefficients of head and power curves.

Authors	Head curve coeff.			Power curve coeff.			
	a_2	a_1	a_0	a_3	a_2	a_1	a_0
Pérez-Sánchez [8]	0.406	0.621	0.000	-0.333	2.190	-0.863	0.000
Barbarelli [3]	0.922	-0.406	0.483	0.040	1.185	-0.043	-0.183
Novara [11]	1.160	-0.746	0.586	0.000	1.248	0.074	-0.322
Pugliese [13]	0.950	-0.338	0.388	-0.012	1.495	-0.483	0.000
Fecarotta [14]	1.610	-1.410	0.805	0.000	1.850	-0.858	0.00567

Figure 3 shows the obtained head curves, H_t, using the polynomial expressions proposed by the different authors, and whose coefficients are in Table 9. The efficiency curves were obtained as proposed in [8] and [3] and are superimposed in Figure 3. According to [8], the efficiency curve was obtained using

polynomial Equation (11), with the following coefficients: a_4=-1.219, a_3=6.95, a_2=-14.578, a_2=13.231 and a_0=-3.383. The other efficiency curve was obtained using Equation (14) as in [3]. Figure 4 presents the power curves, P_t, as a function of flow, Q_t, using polynomial expressions whose coefficients are given in Table 9. The efficiency curves were also superimposed in this figure.
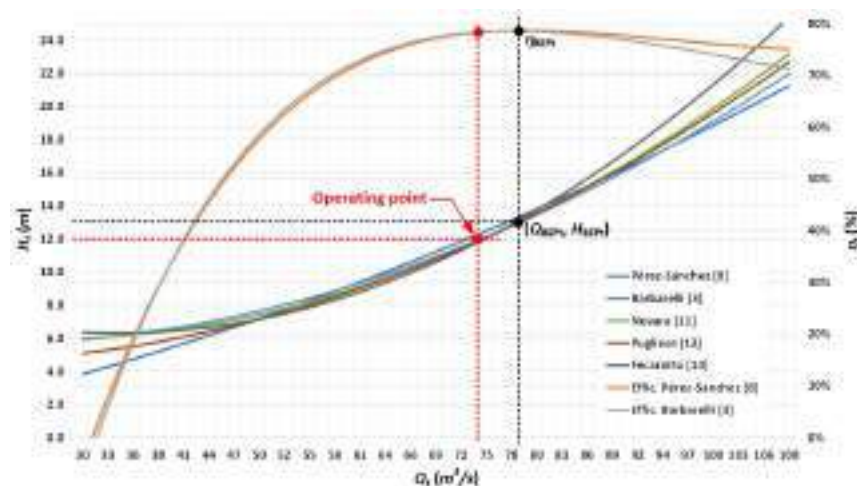

Fig. 3. Predicted curves of head and efficiency.

According to Figures 3 and 4, the PAT will operate at the site with an efficiency of 78.2%, which is very close to its maximum (78.5%). On the other hand, the mechanical power of the PAT will be 1834.1 W and, therefore, the electrical power will be 1.6 kW. These results are not much lower than the values in the BEP, shown in Table 8, respectively 2.1 kW and 1.8 kW. Considering 9 months of operation, the annual yield will be 10.2 MWh while an ideal PAT for this specific site would give 12 MWh, as described in step 1.

Additionally, the efficiency will be little affected, considering some uncertainty inherent to the curves, estimated by the different methods, since they are very close at the site operating point.

4   Conclusions

This paper has presented a comprehensive approach for small-scale hydropower designers, by providing a step-by-step procedure to select a pump and predict its performance as a turbine (Pump As Turbine - PAT) which is not provided by manufacturers. This procedure is based on recent studies that correlate the pump best efficiency point (BEP) with the one in turbine mode. For this purpose,
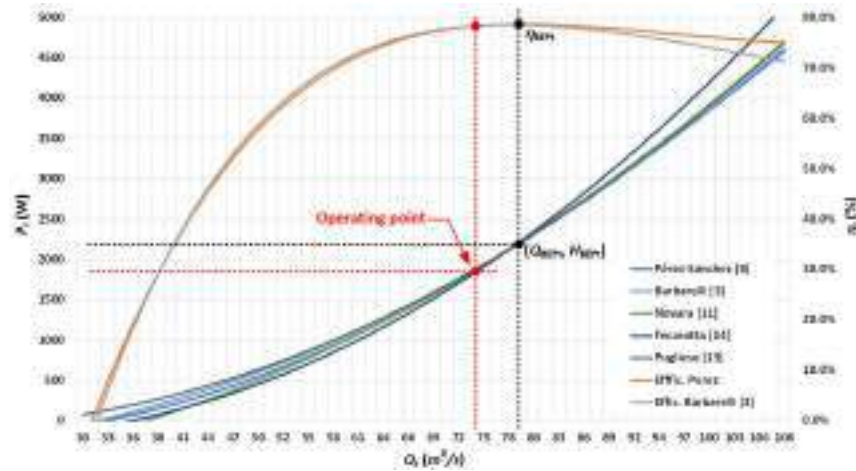
Fig. 4. Predicted curves of power and efficiency.

conversion factors obtained by several authors were used to select a suitable pump, considering the head and available (or required) flow in a given site. Then, for the selected pump, the corresponding BEP operating in turbine mode was estimated using similar conversion factors. The BEP of the chosen PAT rarely coincides with that of the site (head and flow). Thus, it is crucial to predict the PAT operating point at the site for the annual yield estimation. Because of this, the procedure uses models developed by several authors in order to predict the PAT performance curves, i.e. head, power and efficiency as function of flow.

This procedure was applied to select a PAT, to be installed in the Ciência Viva Centre of Bragança, Portugal, for self-consumption purposes, taking advantage of the existing infrastructures (pipe and powerhouse). Based on the head available $(12\,m)$ and the average value of the minimum power demanded by the building $(1.75\,kW)$, obtained by the analysis of its load diagrams, the required flow was determined $(25\,l/s)$ considering an expected efficiency of 60%. Based on the obtained results, and for the site head, the selected PAT will operate with $20.5\,l/s$ and generate an electric power of $1.6\,kW$, with a global efficiency of 67.3% (PAT efficiency of 78.2% and generator efficiency of 86%). From the knowledge of the site, the flow of $20.5\,l/s$ is expected to be available for a period of not less than 9 months per year. Thus, the energy generated annually will not be less than $10\,MWh$, and will be fully consumed in the building.

References

1. Ebrahimi, S., Riasi, A., & Kandi, A. (2021). Selection optimization of variable speed pump as turbine (PAT) for energy recovery and pressure management. Energy Conversion and Management, 227, 113586.
2. Algieri, A., Zema, D. A., Nicotra, A., & Zimbone, S. M. (2020). Potential energy exploitation in collective irrigation systems using pumps as turbines: A case study in Calabria (Southern Italy). Journal of Cleaner Production, 257, 120538.
3. Barbarelli, S., Amelio, M., & Florio, G. (2017). Experimental activity at test rig validating correlations to select pumps running as turbines in microhydro plants. Energy conversion and Management, 149, 781-797.
4. Amelio, M., Barbarelli, S., & Schinello, D. (2020). Review of Methods Used for Selecting Pumps as Turbines (PATs) and Predicting Their Characteristic Curves. Energies, 13(23), 6341.
5. Morabito, A., Spriet, J., Vagnoni, E., & Hendrick, P. (2020). Underground Pumped Storage Hydropower Case Studies in Belgium: Perspectives and Challenges. Energies, 13(15), 4000.
6. Alatorre-Frenk, C.; Ml, K.; Karin, A. Cost Minimisation in Micro-Hydro Systems Using Pumps-as-Turbines. Ph.D. Thesis, University ofWarwick, Coventry, UK, 1994.
7. Audisio, O. Bombas Utilizadas Como Turbinas; Universidad nacional del Comahue: Buenos Aires, Argentina, 2009.
8. Pérez-Sánchez, M., Sánchez-Romero, F. J., Ramos, H. M., & López-Jiménez, P. A. (2020). Improved planning of energy recovery in water systems using a new analytic approach to PAT performance curves. Water, 12(2), 468.
9. Barbarelli, S., Amelio, M., Florio, G., & Scornaienchi, N. M. (2017). Procedure selecting pumps running as turbines in micro hydro plants. Energy Procedia, 126, 549-556.
10. Stefanizzi, M., Torresi, M., Fortunato, B., & Camporeale, S. M. (2017). Experimental investigation and performance prediction modeling of a single stage centrifugal pump operating as turbine. Energy Procedia, 126, 589-596.
11. Novara, D., & McNabola, A. (2018). A model for the extrapolation of the characteristic curves of Pumps as Turbines from a datum Best Efficiency Point. Energy Conversion and Management, 174, 1-7.
12. Morabito, A., Steimes, J., & Hendrick, P. (2016). Pumped hydroelectric energy storage: A comparison of turbomachinery configurations. Sustainable Hydraulics in the Era of Global Change, 261-268.
13. Pugliese, F., De Paola, F., Fontana, N., Marini, G., & Giugni, M. (2018). Optimal Selection of Pumps As Turbines in Water Distribution Networks. Multidisciplinary Digital Publishing Institute Proceedings, 2(11), 685.
14. Fecarotta, O., Carravetta, A., Ramos, H. M., & Martino, R. (2016). An improved affinity model to enhance variable operating strategy for pumps used as turbines. Journal of Hydraulic Research, 54(3), 332-341.
15. Camilo Rosado, L. E., López-Jiménez, P. A., Sánchez-Romero, F. J., Conejos Fuertes, P., & Pérez-Sánchez, M. (2020). Applied strategy to characterize the energy improvement using PATs in a water supply system. Water, 12(6), 1818.
16. Nikolić, M., Mršević, D., Ristić, L., Čantrak, Đ., & Janković, N. (2021, March). Induction Machine Driven Pump Applied as Turbine in Micro-hydro Power Plants. In 2021 6th International Symposium on Environment-Friendly Energies and Applications (EFEA) (pp. 1-6). IEEE.
17. Deprez, W., Dexters, A., Driesen, J., & Belmans, R. (2006, September). Energy efficiency of small induction machines: comparison between motor and generator mode. In Proceedings of ICEM 2006: XVII International Conference on Electrical Machines (p. 6). IEEE.
18. Yang, S. S., Derakhshan, S., & Kong, F. Y. (2012). Theoretical, numerical and experimental prediction of pump as turbine performance. Renewable Energy, 48, 507-513.
19. Novara, D., & McNabola, A. (2018). The development of a decision support software for the design of micro-hydropower schemes utilizing a pump as turbine. Multidisciplinary Digital Publishing Institute Proceedings, 2(11), 678.
20. Gülich, J.F. Centrifugal Pumps; Springer: Berlin, Germany, 2008; Volume 2.
21. Rossi, M., Nigro, A., & Renzi, M. (2019). Experimental and numerical assessment of a methodology for performance prediction of Pumps-as-Turbines (PaTs) operating in off-design conditions. Applied Energy, 248, 555-566.

Seguimiento simplificado de consumos para reducción de gasto eléctrico

Jorge Gómez Sanz[1][0000−0003−4534−378X]

Facultad de Informática, Universidad Complutense de Madrid, 28040 Madrid, Spain
jjgomez@ucm.es
https: grasia.fdi.ucm.es jorge

Abstract. La gestión de energía se ha vuelto un objetivo estratégico que requiere una política con apoyo institucional. El control de gasto ya no se puede limitar a una comprobación de facturas cada mes. Por otro lado, ir más lejos requiere dotar de medios electrónicos para hacer un seguimiento de la lectura cuya instalación no es trivial. En este trabajo se presenta un enfoque intermedio que ha servido en la Universidad Complutense para empezar a implantar una política de gasto energético. Esta solución se apoya en la existencia de obligaciones por parte de las distribuidoras de energía de suministrar el consumo eléctrico hora a hora. Usando esta información, se propone un sistema basado en tecnologías abiertas para concienciar del consumo a los ocupantes de los centros y para habilitar que los gestores de dichos centros sepan qué está ocurriendo en el edificio. El sistema está desplegado actualmente en la Universidad Complutense de Madrid y ya ha servido para ahorrar 50MWh en total durante un mes en dos suministros.

Keywords: gestión de energía · monitorización del gasto

1 Introducción

Pese a los esfuerzos por crear un parque de energía renovable suficiente para las necesidades de la sociedad, la crisis en el suministro del gas de 2022, originado por la guerra de Ucrania, ha evidenciado deficiencias en el parque de producción eléctrica, especialmente el Europeo. Los altos precios de los mercados regulados han obligado a la emisión de normativa legal a nivel europeo que obligue a una reducción en el gasto y una mayor vigilancia. Esta orden llega en un momento en que la transición energética se estaba acelerando motivada, en la mayoría de los casos, por una mayor concienciación sobre la emergencia climática.

La acelerada instalación de placas fotovoltaicas no ha sido suficiente para satisfacer la demanda y, en parte, ello ha originado que los sistemas marginales de compra-venta de energía disparen el precio en el momento en que entraba en el mix energético el gas.

Al igual que en la emergencia climática, la política energética debería aplicar un enfoque de resiliencia. Asumiendo que es posible que nunca haya suficiente generación de energía renovable para la demanda actual, con los hábitos modernos, sería necesario aprender a vivir con menos energía.

En este enfoque hay que distinguir en los comportamientos entre un gasto necesario y un gasto innecesario. Por ejemplo, es necesario alimentar armarios frigoríficos para mantener muestras biológicas, pero no es necesario arrancar la climatización de madrugada para que el edificio esté fresco cuando empiece la jornada laboral.

Esta necesidad se ve obstaculizada por las limitaciones temporales de política de contratación pública. Esta política obliga a planificar con meses, alguna vez años, las actuaciones. Ello hace que los tiempos de reacción sean demasiado largos cuando se busca la solución fuera del ámbito institucional. La solución pasa por desarrollar fórmulas con los medios propios y conseguir el compromiso y apoyo de la institución para ello.

En este trabajo se muestra un desarrollo actualmente en ejecución que ha sido realizado con personal propio y sin invertir medios adicionales. Este desarrollo informa del consumo energético actual y pasado de diferentes formas. El trabajo ha permitido identificar excesos de consumo en varios centros y empezar a identificar qué consumos son justificables. En particular, la provisión de información sobre las tendencias e históricos, ha incentivado el estudio de la operación de los centros, llevando al ahorro de 30MWh en un mes.

Estos contenidos se organizan como sigue. La sección 2 presenta la arquitectura propuesta, cómo se recogen eventos de la simulación y se usan para entender qué actividad se usa. Los informes generados se explican en la sección 3. La sección 4 explica cómo se pueden usar estos informes para regular el consumo. La sección 5 presenta un caso práctico de ahorro. Se aporta una discusión sobre estos resultados y forma de gestión de la medida en la sección 7. Se presenta trabajo relacionado en la sección 6. El artículo termina con unas conclusiones.

2   Arquitectura propuesta

El sistema asume que existe una interfaz de programación que informa del consumo horario ofreciendo distintos informes en una única página web. El acceso a este consumo se hace con la colaboración de la distribuidora. Así, la distribuidora proporciona las curvas cuartorarias y horarias de consumo. En el momento actual, estos datos son suministrados por una entidad que hace de mediadora.

La arquitectura, ver figura 1, se despliega como un conjunto de componentes de un cluster kubernetes. Cada elemento es un pod, siguiendo la terminología kubernetes. Sus responsabilidades son las siguientes:

— El controlador web sirve los datos a través de un interfaz REST. Los datos se proporcionan en formato JSON. Los datos incluyen las medidas horarias empaquetadas según el informe que se quiera mostrar. Estos informes incluyen valores de referencia que distinguen el momento del año. Este componente está desarrollado en Java con SpringBoot.
— El controlador de datos descarga los datos del mediador con la distribuidora. Esta descarga se hace una vez a la hora para no saturar al proveedor y
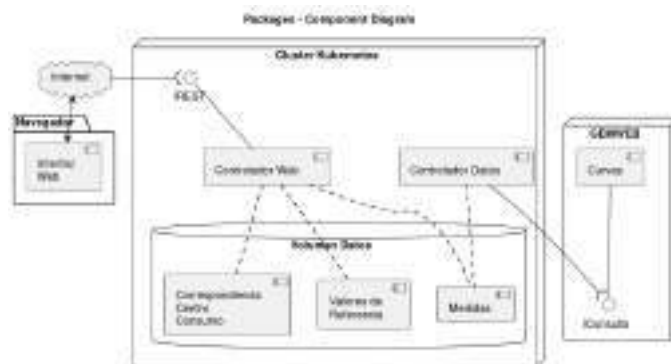
Fig. 1. Diagrama de despliegue de la arquitectura

　porque, para el formato de datos deseado, no proporciona datos con frecuencia mayor, sólo frecuencia horaria. Este componente está desarrollado en Java con SpringBoot.

− El volumen de datos almacena tanto las medidas como valores de referencia agregados. Los valores se obtienen de un estudio de la tendencia de cada centro y sirve a los gestores para saber si el consumo tiene sentido o no. Estos valores de referencia están sujetos a constante revisión. Para implementar el volumen de datos se ha usado MongoDB.

− C-EMWEB es el mediador con la distribuidora, que adquiere los datos y los incopora a su sistema. Su aplicativo ofrece una serie de informes tipo, pero no la opcion de tener informes dinámicos. En este caso, se aprovecha la API que ofrece para descarga de curvas horarias para transferir esa información y presentarla de forma más elaborada. La curva horaria incluye la hora de consumo y una cantidad de kWh.

　El sistema controla 40 suministros en la actualidad. El volumen de datos no es grande como para justificar una solución de canalice la ingesta de datos, como Kafka. Sólo ha sido necesario la incorporación de cachés en los controladores que proveen servicios REST para reducir el número de consultas a la base de datos.

　La interfaz de usuario renderiza los datos usando javascript y librerías plotly. La fuente de datos son objetos JSON que se incrustan en la página web en tiempo de servidor. Los datos extraídos a través de una interfaz web son incrustados en la página en el lado del servidor. Eso blinda toda la parte de kubernetes frente a intentos de asalto, pues no queda visible ni accesible a un atacante externo.

　El usuario que accede al entorno, se identifica y ese dato sirve para determinar el centro al que pertenece. La necesidad de requerir un usuario y contraseña junto a la incrustación de datos en el lado del servidor reducen la posibilidad de ataques al backend y la filtración de datos.

3   Informes generados

El sistema distingue tres tipos de usuarios: los habitantes del centro, los gestores del centro, y los gestores de la organización.

Los primeros acceden al sistema por motivos de conciencia medioambiental o por investigación/docencia. Las labores de concienciación y sensibilización en la Universidad Complutense son frecuentes y alcanzan a un número no menor a 300 estudiantes todos los años. Los estudiantes saben que reducir el gasto energético es parte de la estrategia para la descarbonización de la universidad. Si bien la energía que consume la Universidad es certificada en origen como 100% renovable, el uso de esa energía no tiene por qué estar exento de generación de carbono. Por ello, es importante siempre reducir el consumo. Por otro lado, la universidad tiene como misiones la docencia y la investigación. Los hábitos energéticos proporcionan datos relevantes para determinadas asignaturas o trabajos. Por ejemplo, asignaturas que ejemplifican machine learning. Así, habrá investigadores/docentes que se conecten a la interfaz y usen los controles de descarga de datos asociados a las gráficas que allí se muestren.

Los gestores del centro son los responsables de su operación. La gestión incluye la configuración de máquinas de refrigeración, activación de luces, calefacción y otra maquinaria. Por otro lado, también hay maquinaria destinada a la investigación, como armarios frigoríficos industriales para preservación de muestras biológicas. La actividad del edificio no debe ser interrumpida, pero las condiciones en que se desarrolla pueden ser revisadas. Por ejemplo, decidiendo activar la refrigeración una hora más tarde o apagarla una hora antes. También, trabajando con el régimen de las máquinas de climatización, reduciendo su actividad afectando lo imprescindible al confort de los habitantes del edificio. También actuando sobre instalaciones no controladas en el edificio, como aparatos de calefacción individuales no autorizados. Un aparato es difícil de detectar con este sistema, pero un número grande de ellos sí puede serlo. En este contexto, si una persona empieza usando este tipo de aparatos y lo comenta, eventualmente acaban siendo bastantes los que hacen lo mismo. Este incremento sí puede ser detectado.

Los gestores de la organización observan el consumo general para determinar el progreso de las medidas de contención del consumo. Desviaciones menores pueden ser ignoradas, pero grandes variaciones deberían estar justificadas. Por ejemplo, incrementos notables durante un fin de semana pueden explicarse con el desarrollo de procesos selectivos para la administración pública. Estos procesos hacen que los edificios tengan un régimen similar al de un día laborable.

La interfaz ofrece tres tipos de informe según el usuario. Todos los consumos se miden en kWh:

- A los habitantes del centro les ofrece: el consumo totalizado día a día los últimos 7 días, el consumo por hora las últimas 72 horas, el consumo totalizado por mes los últimos 3 meses y el consumo total en lo que va de año.
- A los gestores del centro se les ofrece: el consumo totalizado día a día los últimos 45 días, el consumo totalizado cada noche las últimas 15 noches, el

consumo totalizado por mes los últimos 7 meses y el consumo las últimas 72 horas. También tiene acceso a la información proporcionada a un habitante de un centro, pues el gestor del centro es también un habitante del centro.

– A los gestores del campus se les ofrece: el consumo totalizado día a día los últimos 45 días.
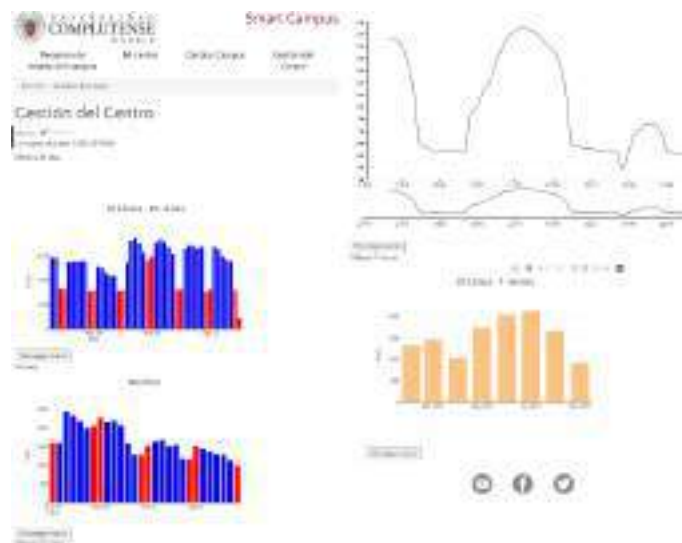
Fig. 2. Captura de un informe de gestor. La captura ha sido reorganizada para el formato de este documento

Para ilustrar estos informes, la figura 2 muestra una captura de pantalla de un informe de gestor de centro. El gestor puede revisar la tendencia los últimos días y también el consumo nocturno, durante el cual se supone que no hay actividad. Como se puede observar, el consumo nocturno es dispar tanto en laborable (columnas azules) como en fines de semana (columnas rojas). Esto señala a la conexión de aparatos durante la noche que podría evitarse. También se muestra un consumo irregular en los últimos meses no necesariamente conectado con la ola de calor que ha sucedido en 2022 durante los meses de junio, julio y agosto. El descenso del consumo en agosto se debe al cierre del edificio durante una semana. Pese a ello, se observa que agosto no descendió demasiado el consumo. Para el mes de septiembre no se disponían de datos completos a la hora de hacer esta captura.

4   Analizando el uso de la energía

Cada persona de la universidad, es informada de la cantidad de electricidad consumida en su centro. Esto debería crear una conciencia mayor acerca del uso que se hace de la energía.

Es necesario identificar valores de referencia. En el momento actual, se está centrando la atención en las franjas de baja actividad para reducir los consumos. Hay actividad que no debe ser afectada y por ello, es mejor trabajar primero en aquellos momentos del día donde se supone que hay que tener un consumo mínimo. Estos momentos son los festivos, días no laborables (sábados y domingos) y las noches. Las noches de los domingos deberían ser las franjas con menor actividad, y consumo, de toda la semana.

Buscando optimizar el resto de franjas, lo que se está transmitiendo es que hay que conseguir que en una noche de día laborable no se consuma más de lo que se consume una noche de festivo, salvo circunstancias excepcionales.

Los referentes históricos que se emplean no son los de años anteriores, sino los de días anteriores. Se presume que con los valores de los últimos días, 45 en el caso de gestores y 15 en el resto de casos, es suficiente para detectar la tendencia y decidir si la variación es significativa. Una variación de un megavatio hora de un día para otro es relevante, por ejemplo.

Transcurrido un año, se ofrece a los gestores información del consumo de su centro cada hora del día todo el año anterior usando un sistema complementario diferente al presentado (ver figura 3). Esto les permite contrastar el momento actual con el que consideran ellos adecuado el año anterior. También observar cómo evoluciona el gasto de su centro a lo largo de los meses y ser más conscientes del impacto de lo que se conecta.

Fig. 3. Informe anual de consumo del mismo centro que la figura 2

5   Un caso práctico

Usando la información proporcionada por el sistema y por los históricos, se hizo un ensayo en dos centros para verificar si se podían reducir los consumos. Con

la información suministrada se hizo un análisis para ver las causas de los días y horas afectados. En julio de 2022 se consumieron 286.361 kWh, mientras que en julio de 2021 se gastaron 367.387 kWh. Eso supone un ahorro de 81.026 kWh en un mes.

La actuación se limitó sólo a la gerencia del edificio y a la regulación de las actuaciones de consumo eléctrico (despachos y climatización). Se usó como referente para orientar sobre el efecto de la actuación la información similar a la de la figura 2.

Así pues, el efecto de la aplicación fue evidente. Hasta ese momento, para saber del consumo había que consultar manualmente facturas. Y estas facturas no informaban del consumo diario ni horario. Gracias a esta información, los responsables de los centros pudieron identificar la desviación, las horas en que se producía y actuar en consecuencia.

Se identificaron eventos en años anteriores que justificaron incrementos en el cosumo los fines de semana. No obstante, también se detectaron casos en los que se podía haber organizado mejor la activación de elementos en el edificio para consumir menos.

A futuros, se está organizando una guía para poder dirigir estas actuaciones con mayor criterio y poder continuar todo el año con estas reducciones de consumo.

Se había intentado conseguir la misma información mediante pinzas amperimétricas instaladas en los cuadros de luz, pero esta operación era más compleja porque había que apagar el centro para instalarlas, había dificultades en instalar puntos de comunicación para leer resultados y poco espacio para instalar la pinza. Otras soluciones eran posibles, pero se encontró que la lectura de las curvas de carga proporcionada por las empresas era un camino mucho más rápido sin necesidad de instalaciones.

También es menos preciso, pues el punto de consumo agrupaba más elementos de consumo ajenos al edificio en todos los casos. Por ejemplo, uno de los puntos de consumo analizados conectaba con tres infraestructuras adicionales, pero la optimización se limitaba a uno de ellos.

A futuros, hay que aspirar a los dos mecanismos, pues los medidores instalados localmente, como las pinzas amperimétricas, no son reconocidos por las compañías eléctricas. Las curvas de carga proporcionadas por ellas sí. Sin embargo, dichas curvas siempre llegan con retraso de horas o incluso días. Por ello, tener información en tiempo real es un buen complemento. Por un lado información aceptada por la compañía eléctrica, pero recibida con retraso y con imprecisión, y por otro lado información oficiosa, pero instantánea y con precisión.

6   Trabajo relacionado

La literatura recoge más trabajos similares, si bien la mayoría se limitan a instalar medidores locales, como los sistemas de bajo coste de [2] o [3].

Por otro lado, es cierto que incrementando la percepción de control por parte de los ocupantes de un edificio se consiguen reducciones en el consumo [5]. En

dicho experimento se instalaron medidores de forma extensiva para generar conciencia del consumo de cada aparato. En [4] también se informa de reducciones mediante la instalación de medidores para informar a los usuarios del consumo de la actividad. La diferencia con este trabajo es que la información se presenta vía web de forma diferenciada para los habitantes de las instalaciones. El coste de dicha instalación ha sido menor, y también se ha podido medir el efecto reductor en el consumo usando datos de dos años.

Los medidores vía web, como los propuestos aquí, también se han usado en [1], si bien la propuesta de este artículo es aún más barata, pues no requiere de la instalación de ningún medidor. Se basa exclusivamente en la proporcionada por la empresa distribuidora de electricidad.

7   Discusión

La operación de una instalación obedece a una rutina que suele estar salpicada de excepciones. En el caso de edificios públicos, los edificios pueden ser alquilados para otras actividades, como pruebas de selección de funcionarios o celebración de conferencias. Estos eventos modifican la rutina y hacen, generalmente, que se incremente el gasto.

Los valores históricos de años anteriores son relevantes en los informes, pero engañosos. Que el consumo un año sea inferior al anterior puede deberse a otros motivos: que no se esté celebrando una actividad programada que sí se hizo el año anterior, que los días festivos se desplacen a distintos días cada año, que la maquinaria no funcionase adecuadamente o que el tiempo metereológico fuera distinto (e.g. presencia/ausencia de olas de calor).

Por ello, sin descartar el mostrar valores históricos, como el informe de la figura 3, se prefiere trabajar en incluir valores concretos de referencia para ayudar a determinar de forma más absoluta e independiente de estos eventos. Además, ayuda a fijar un objetivo claro y constante para el gestor y los habitantes de la instalación, que es el mantener el consumo por debajo de un valor de referencia.

El fijar valores de referencia en este caso se está haciendo atendiendo a la estacionalidad y a las zonas horarias. No interesa en este momento un cálculo preciso de cuál sería el óptimo.

8   Conclusiones

Para desarrollar esto no hacen falta grandes medios: una base de datos mongodb sin optimizar y con índices básicos, un conjunto de componentes para recoger información de la distribuidora y ofrecerla a los usuarios.

En entornos donde no había nada antes y está legislado que las compañías eléctricas informen de las curvas de carga, es una opción fácil de implantar y de muy bajo coste el compilar dichas curvas y ofrecerlas a los responsables de los centros. Se asume que en los casos en que la electricidad se compra en el mercado indexado o bien está regulado por periodos o bien sea obligación el

informar de dichas curvas de carga, existirá dicho dato y se podrá incorporar de forma electrónica.

Reconocimientos

References

1. Moreira, L., Leitão, S., Vale, Z., Galvão, J.: Use of web based meters to improve energy efficiency and power quality in buildings. In: Doctoral Conference on Computing, Electrical and Industrial Systems. pp. 337–344. Springer (2015)
2. Nardello, M., Rossi, M., Brunelli, D.: A low-cost smart sensor for non intrusive load monitoring applications. In: 2017 IEEE 26th International Symposium on Industrial Electronics (ISIE). pp. 1362–1367. IEEE (2017)
3. Porcarelli, D., Balsamo, D., Brunelli, D., Paci, G.: Perpetual and low-cost power meter for monitoring residential and industrial appliances. In: 2013 Design, Automation & Test in Europe Conference & Exhibition (DATE). pp. 1155–1160. IEEE (2013)
4. Sirombo, E., Filippi, M., Catalano, A., Sica, A.: Building monitoring system in a large social housing intervention in northern italy. Energy Procedia **140**, 386–397 (2017)
5. Yearley, T., Hyde, K., Box, W.: Reducing building electricity use by increasing occupant perceived control. In: 29th Annual Association of Researchers in Construction Management Conference, ARCOM 2013. pp. 1275–1284 (2013)

The Impact of COVID-19 on Solar PV Electricity Generation and Consumption Patterns at CIC-IPN

P.J. Escamilla-Ambrosio [0000-0003-3772-3651], and M.G. Pulido-Navarro [0000-0002-5496-7044]

Centro de Investigación en Computación, Instituto Politécnico Nacional, Ciudad de México
07738, Mexico
pescamilla@cic.ipn.mx

Abstract. The COVID-19 pandemic has caused millions of morbidity and mortality cases across the world, forcing people to change their lifestyles and governments to take different measures to slow down its spread. As a result, electricity demand and consumption patterns across the different socioeconomic sectors were affected. This work presents a study investigating the impact of the COVID-19 pandemic on electricity consumption and generation at CIC-IPN, a research and academic unit in the north of Mexico City. Electricity consumption and on-site solar photovoltaic (SPV) electricity generation were assessed for three periods in the pandemic, pre-virtual activities, during-virtual activities, and post-virtual activities (activities in person), compared to electricity consumption prior to the pandemic, the year 2019. It is noted that the activation of the on-site SPV electricity generation plant took place while in the during-virtual activities period. Hence, generation and consumption patterns have also been compared before and after SPV electricity generation. The results show that electricity consumption declined during the virtual-activities period compared to the pre- and post-virtual activities periods. SPV electricity generation reduces electricity consumption from the state electricity company. The temporal analysis of the changing electricity consumption and generation patterns could provide helpful insight to decision-makers for targeted interventions.

Keywords: Electricity consumption, Solar photovoltaic, Electricity generation, COVID-19 impact.

1   Introduction

The coronavirus disease 2019 (COVID-19) pandemic has caused millions of morbidity and mortality cases across the world, forcing people to change their lifestyles and governments to take different measures to slow down its spread. Lockdown measures to prevent the spread of COVID-19 imposed by many countries led to sudden changes in socioeconomic habits which had direct effects on electricity systems. As a result, electricity demand and consumption patterns across the different socioeconomic sectors were affected. In this work a study, investigating the impact of the COVID-19 pandemic on electricity consumption and generation at Centro de Investigación en Computación del Instituto Politécnico Nacional (CIC-IPN), a research and academic unit in

the north of Mexico City, is presented. Understanding how efforts to limit exposure to COVID-19 have altered electricity demand provides insights not only into how dramatic restrictions shape electricity demand but also about future electricity use in a post-COVID-19 world and for on-site solar photovoltaic (SPV) electricity generation.

Electricity consumption and on-site SPV electricity generation were assessed for three time periods in the pandemic, pre-virtual activities, during-virtual activities, and post-virtual activities (activities in person), compared to electricity consumption prior to the pandemic, the year 2019. It is noted that the activation of the on-site SPV plant took place while in the during-virtual activities period. Hence, generation and consumption patterns have also been compared before and during the pandemic and before and after on-site SPV electricity generation.

Steep declines in electricity usage are associated with workday hourly load patterns that resemble pre-COVID weekend usage. Quantifying these impacts using a unified modeling framework is a crucial first step in understanding the impacts of crises like the pandemic and the associated societal response on electricity demand and consumption. The remaining of the paper is organized as follows, related research is presented as continuation of Section 1, together with the description of the SPV electricity generation plant installed at CIC-IPN; Section 2 presents the electricity consumption patterns for pre-virtual activities, during-virtual activities, and post-virtual activities (activities in person), and pre and post-activation of the SPV plant at CIC-IPN; Section 3 presents a brief discussion of patterns observed and comparisons; finally, Section 4 presents the conclusion and future work.

1.1　Related work

In [1] the authors describe how electricity demand dropped significantly on work activities during the COVID-19 pandemic period. This led to changes in the grid administration and electricity generation in a way that is unprecedented. The authors maintain that a study of this scenario will also be of great importance in the future transition to a greener energy. The data used in the study were taken from the national electricity company of Spain which has 44,000 km of power lines. For their research, they compare consumption electricity for two months of the years 2015 to 2019. The data taken were mainly from households in Spain, they compare previous years with the starting day of the lockdown and registered a reduction of 13.49% at the first weeks and continue to drop, reaching over 25%. As some industrial sectors were getting back to work, so demand started to rise. Also, it is noticed that peak consumption times changed reaching its peak between 14:00 and 15:00 hrs., whereas before the pandemic this peak was reached early in the morning, and by early afternoon this peak decreased showing that consumption was constantly being lower. For the industrial sector, such as hotels, offices, commerce, restaurants, health, education, etc., a decrease of the electricity demand also was noticeable due also to the fact that a great part of the afternoon activities for this sector were suspended, reaching a consumption decrease of more than 30%. As for the residential sector, they represent the 25% of total daily electricity consumption reaching sometimes up to 30%. During confinement this sector had an increase in electricity consumption as schools closed and many people did their job from home, while

others, unfortunately, lost their jobs. Hence, electricity consumptions at homes were distributed the whole day during lockdown instead of at peak times on the mornings and late afternoons.

In China regulations to control the pandemic disease were stricter with mandatory quarantines that led to a huge economic impact [2]. The electricity industry was one of the most affected by the effects of the pandemic, according to the International Energy Agency (IEA). The IAE found that the world's energy demand in 2020 sank by 6% compared with 2019, which represents a drop seven times higher than during the financial crisis of 2009. In [2], the authors analyzed the first two quarters of 2020-2021 in electricity production and consumption and how the pandemic affected the power industry in China. Comparing China's previous five years' energy production with 16 European countries, a drop of 9% in April 2020 was observed. Although there was a reduction in electricity consumption, electricity consumption from renewable energy grew around 3% in 2020, and by 2021 was expected to grow by 8%. For example, China's demand in February 2020 decreased by 10% compared to 2019 while in the United States showed almost the same reduction in May. As for Germany, France and the United Kingdom had a demand decreased of more than 15% from March to April, while Spain and Italy demand dropped by 25%. As the economy is recovering little by little also the renewable energy generation is growing as gas-fired plants dropped by 1.6% in 2020. For the same year, renewable-based energy generation increased by 3%.

According to [3], in what respects to Canada during the pandemic, this country also registered a drop in electricity demand. The authors went back for data of electricity demand up to 2016 to identify how the market in 2020 was affected for the pandemic. For example, during shutdown Ontario registered an electricity decline of 10% approximately, followed by other important cities such as Alberta, New Brunswick, and British Columbia, of 5%. The data obtained were analyzed also to include the changes in temperature compared to previous years. Also, were considered the different sources in the electricity generation. Comparing to the United States, during roughly the same period, electricity demand fell by 8%, while in European countries the electricity demand drop by 20% in France, 25% in Spain, and Italy registered a 28% fell. While Norway faced almost no reduction in electricity demand. In Canada, a grew in hydroelectric and wind electricity generation was reported and also generation from other fuels such as biomass, although the authors state that this change has nothing to do with the pandemic, they were changes programmed before 2019.

About Mexican electricity demand during the pandemic, it also registered a drop and brought along some reforms that brought back the control of energy generation to the Mexican state according to [4]. The authors also state that energy generation from renewable sources that represent about 60% of generation is mainly owned by private companies. Mexico exports crude oil and imports refined products from the United Sates which means that Mexico depends strongly on the economics of the US. This is why many changes have been implemented by the Mexican government, as to reduce the imports by generating their own products and turning to more eco-friendly power generation. Reduction in electricity generation in 2020 was about 1.9%, at the same period an increase on SPV generation was recorded, it went from 8.4 TWh to 13.5 TWh that represents a 61% rise. Wind sources also increased by 17%, hydroelectric sources

registered an increase of 14%, combined cycle source increased by 6%, nuclear power source remained the same, while internal combustion showed a reduction of 9%. Also turbogas sources had a reduction of 14% as did biomass with a reduction of 17%. Heavy oil sources also showed a reduction of 40% and also coal fired had a reduction of 42%.

According to [5], during the pandemic, solar energy production had a positive impact on the electricity demand as well as representing a positively impact on climate change. Global renewable generation capacity had an addition amounted to 2537 GW. Hydropower globally amounted a capacity of 1190 GW. Wind and solar energy amounted 623GW and 586GW, respectively. For bioenergy it was a total of 124 GW, as for geothermal generation accounted for 14 GW. The great buyers of solar photovoltaic systems are undeveloped countries even though they were worst hit by the pandemic, so governments should invest and give more facilities to private companies and other sectors in investing on this technology as to take advantage of their climate characteristics. The solar energy generation sector is highly dependent on Chinese supplies which had an impact production during the pandemic but has slowly recovered leading to a revival of this sector for energy generation.

In [6] the authors focused their study on the effect that the pandemic brought especially in the power generation by renewable sources. There was a reduction on electricity demand during lockdown and at the same time an increase on the electricity demand of energy from renewable sources. This brought along a reduction on gas emissions and a small decrease on electricity prices before the Ukrainian war. Since most people were forced to work from home during the pandemic, power system represented the main necessity for a functional society. Hence, the work in [6] presents an analysis on the development of the renewable energy technology, electric power and energy statistical data, as well as the challenges that this new technology has to face. Enhancing this new technology is a must and, due to the pandemic impacts, it has to adapt rapidly to changing situations. As some countries showed a reduction about 20% in electricity demand, this resulted in a less interest in investing in renewable energy production. Although little by little this situation has been turned around, and a new interest has emerged for countries to invest and support electrical energy markets and renewable energy sectors.

1.2   CIC-IPN and Solar Photovoltaic Plant

CIC-IPN is located at Av. Juan de Dios Bátiz s/n esq. Miguel Othón de Mendizábal, Col. Nueva Industrial Vallejo, Gustavo A. Madero, C.P. 07738, Mexico City, Mexico; see Fig. 1. In its infrastructure CIC-IPN has a building with a total constructed area of 9,768.8 m^2, the property is 25 years old, it houses a total population of 383 users, and a site computer center. The operation of the building is from Monday to Sunday, at a schedule of 07:00 am to 9:00 p.m., although it is an open-doors building for its users, that is, it is functional 24 hours a day, 365 days a year.

The SPV electricity generation plant installed at CIC-IPN [7], is located in north Mexico City, 19° 30' 11.1" North-latitude, 99° 08' 52.1" West-longitude, at 2,243 m altitude, see Fig.2. The SPV plant has 186 solar panels (Canadian Solar CS3U), connected to three inverters (each Fronius Symo, 22.7 KW) with a maximum power capacity of 66.96 kW.

Fig. 1. Location and view of CIC.

Fig. 2. SPV electricity generation system installed at CIC-IPN.

2   Electricity Consumption Patterns

In this section the impact of the COVID-19 pandemic on electricity consumption and generation at CIC-IPN, a research and academic unit in the north of Mexico City, is presented. Electricity consumption and on site SPV electricity generation were assessed for three time periods during the pandemic, pre-virtual activities, during-virtual activities, and post-virtual activities (activities in person), compared to electricity consumption prior to the pandemic, year 2019. In addition, as the activation of the on-site SPV plant took place while in the during-virtual activities period, generation and consumption patterns have also been compared for before and after SPV electricity generation.

At CIC-IPN there is installed an electricity consumption monitoring network as part of the SEEDS (acronym of the Spanish for Strategic System of Sustainability Evaluation and Performance) platform [7]. As part of this network, an electricity meter produces a consumption measurement every 10 minutes of the energy provided by Comisión Federal de Electricidad (CFE), the state electricity company [8]. Hence, the electricity consumption data from 01/Jan/2019 to 30/09/2022 is shown in Fig. 3. As can be seen in this figure, there are some gaps in the data, which correspond to dates where the communication with the server, where SEEDS resides, was interrupted. In any case, in the plot a clear change in the consumption patterns from pre-virtual activities, during-virtual activities, and post-virtual activities, can be observed. In the figure, the change in the consumption pattern when the SPV plant was activated, also can be observed.
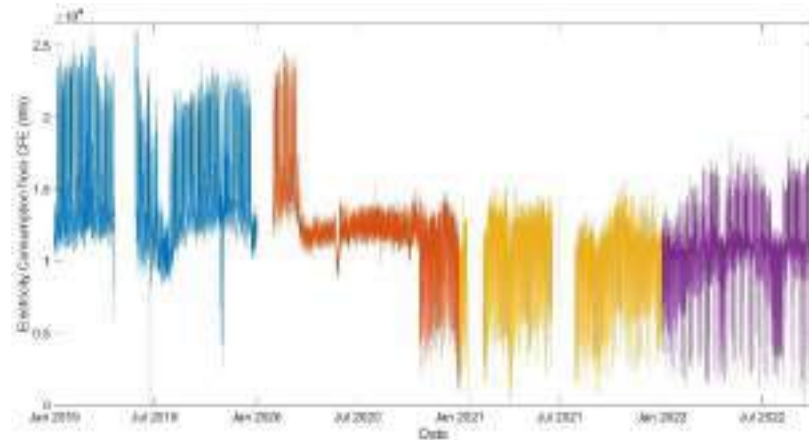
Fig. 3. Electricity consumption from CFE from 01/Jan/2019 to 30/09/2022 (note: the gaps are dates for which data communication was interrupted).

In Mexico City, at higher education units, the confinement started on 17/03/2020, date at which all activities became virtual, remaining as such up to 04/01/2022, date at which some administrative activities were reactivated to be in person, but teaching remained virtual. On 14/02/2022 some hybrid activities were allowed, meaning some administrative and teaching activities were in person and some virtual. It is up to 15/08/2022 when activities became fully in person. Furthermore, on 20/08/2020 the SPV electricity generation plant installed at CIC-IPN [7] was activated, and since then, is generating electricity, which is supplied to be consumed at CIC-IPN.

Fig. 4 presents a summary of the monthly electricity consumption from the years 2019-2022, as recorded by the monitoring network in the SEEDS platform.
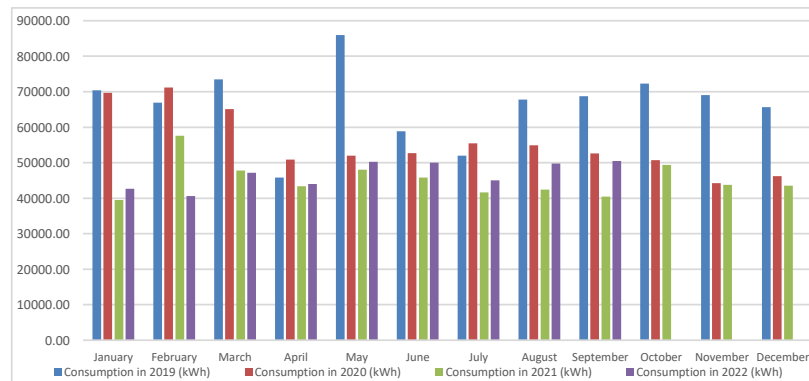
Fig. 4. Monthly electricity consumption from CFE for the years 2019-2022.

2.1 Electricity Consumption on Pre-Virtual Activities

The pattern of consumption before the pandemic and in pre-virtual activities can be observed in Fig. 5, where the electricity consumption from CFE for the month of March 2019 has been plot. It can be clearly observed the difference between week days and weekend days and working and outside of working hours consumption profiles. The electricity consumption in that month was 73509.85 kWh.
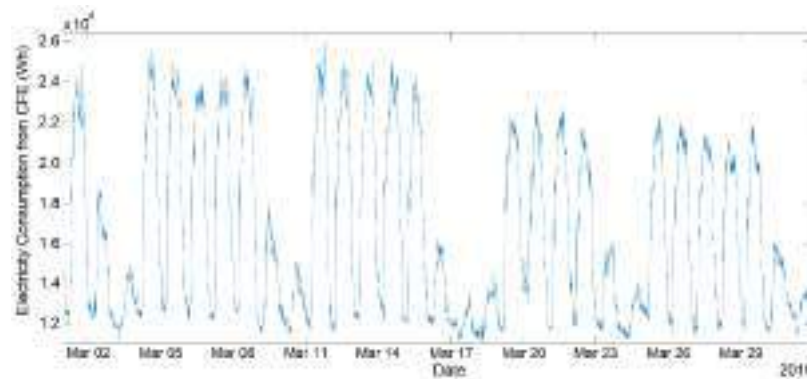
Fig. 5. Electricity consumption from CFE for the month of March 2019.

The same profile of consumption can be observed up to when the confinement was started, and all activities became virtual. At this point, a change in the consumption profile took place, as can be appreciated in Fig. 6, where the consumption for the month March 2020 is plot. Recall that the confinement started on March 17th, 2020. The electricity consumption from CFE in that month was 65070.77 kWh.
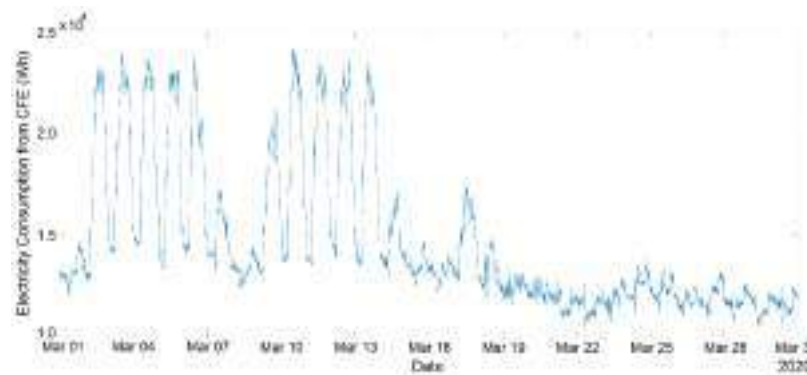
Fig. 6. Electricity consumption from CFE for the month of March 2020.

2.2   Electricity Consumption During Virtual Activities

Once the confinement started on March 17th, 2020, the profile of electricity consumption changed dramatically, as can be appreciated in Fig. 6 above. This pattern remained during most of the year 2020, at which most activities were carried out virtually. For example, Fig. 7 shows the electricity consumption profiles for the months of June and July of 2020. The electricity consumption in those months were 52714.84 kWh and 55462.55 kWh, respectively. Hence, this can be considered as the electricity consumption profile on virtual activities at CIC-IPN.

Most of the year 2020, the consumption profile remained the same as the one shown in Fig. 7. However, on October 20th, 2020, the SPV plant at CIC-IPN was activated, and with that the electricity consumption from CFE changed, as can be observed in Fig. 8. The electricity consumption from CFE in that month was 50720.88 kWh. It does not mean that the demand decreased, but instead the electricity generated by the SPV plan is now being supplied and consumed on-site.
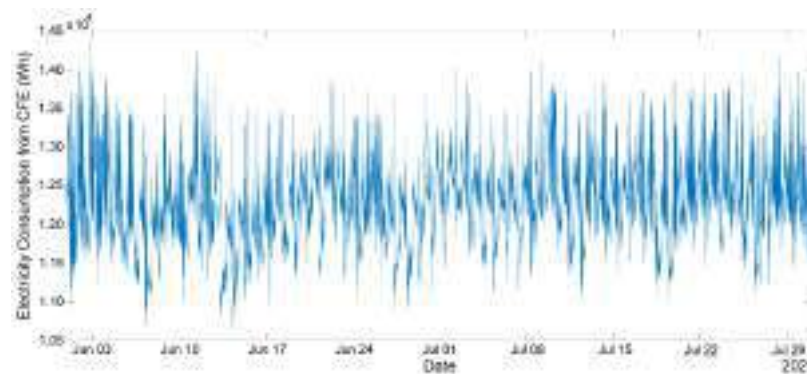
Fig. 7. Electricity consumption from CFE for the months of June and July 2020
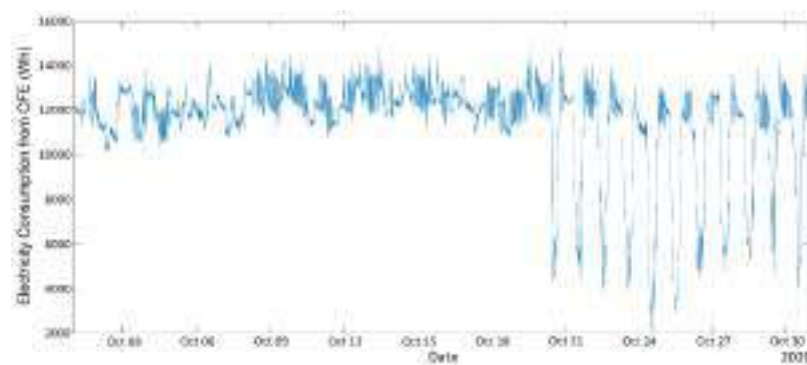
Fig. 8. Electricity consumption from CFE for the month of October 2020.

Once the SPV plant at CIC-IPN was activated and most of the activities continue being virtual, the same electricity consumption profile as the one for the month of March 2021, shown in Fig. 9, can be observed. The electricity consumption in that month was 47769.52kWh.
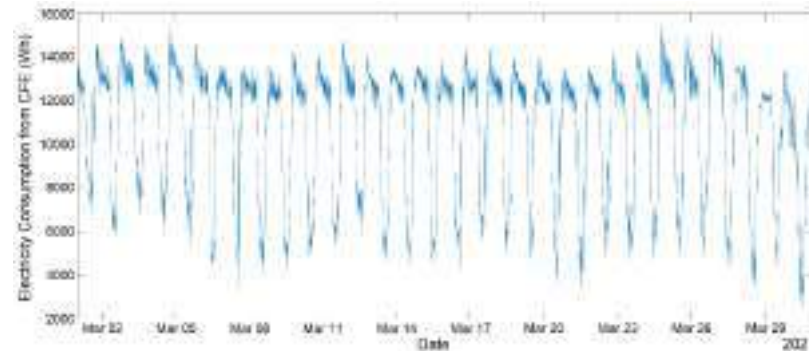
Fig. 9. Electricity consumption from CFE for the month of March 2021.

2.3   Electricity Consumption on Pos-Virtual Activities

As was mentioned before, on 14/02/2022 some hybrid activities were allowed, meaning some administrative and teaching activities were carried out in person and some virtual. Hence, the electricity consumption profile was again slowly changing, as can be appreciated in Fig. 10, where the electricity consumption profile for the month of March 2022 is plot. The electricity consumption in that month was 47162.52 kWh.
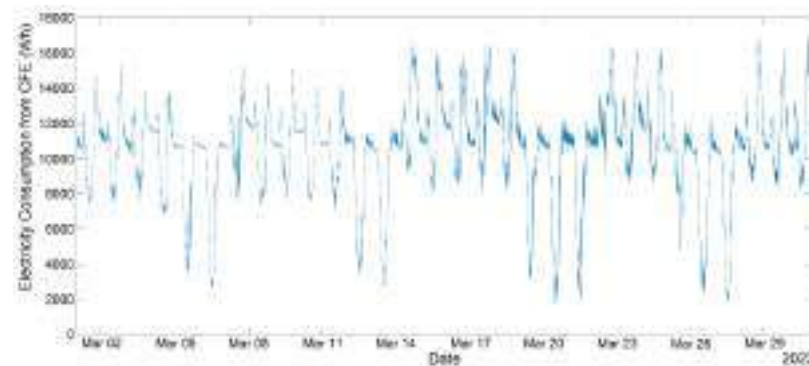
Fig. 10. Electricity consumption from CFE for the month of March 2022.

It was up to 15/08/2022 when activities became fully in person. Once again, at this point the consumption profile changed and is currently as the one observed in Fig. 11, where the electricity consumption profile for the month of September 2022 is plot. The electricity consumption in that month was 50500.70 kWh.
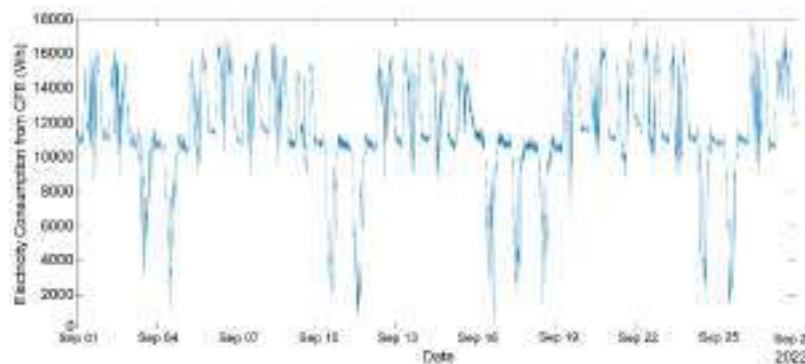
Fig. 11. Electricity consumption from CFE for the month of September 2022.

3   Discussion of Patterns Observed and Comparisons

From the sections presented before, it can be observed that the electricity consumption profile from CFE at CIC-IPN has had different changes. There are four electricity consumption profiles: 1) pre-pandemic and pre-virtual activities (2019), 2) during pandemic and virtual activities (2020), 3) during pandemic and virtual activities and SPV electricity generation (2021), 4) post-pandemic and in person activities and SPV electricity generation (2022).

In order to be fear in making comparisons of the different electricity profiles, Table 1 presents the electricity consumption from CFE from April to September on the years 2019, 2020, 2021 and 2022, which represent the profiles identified. Considering the averaged electricity consumption for the months considered, a 16% reduction in electricity consumption from CFE is observed in 2020, during virtual activities and during the pandemic, compared with the consumption for the same months in 2019, pre-virtual and pre-pandemic activities. If electricity consumption from CFE is compared of years 2020 and 2021, in 2021 a reduction of 18% is observed, this is due to the activation of the SPV electricity generation plant, while still in virtual activities and during the pandemic. Comparing electricity consumption from CFE in 2019 and 2021, in 2021 there is a 31% reduction, this is due to virtual activities and on-site SPV electricity generation and consumption. Once the activities are returning to be in person, if consumption of 2021 and 2022 are compared, there is an increase of 11% in 2022. However, if we compare consumption in 2019 and 2022, there is a 24 % reduction in consumption in

2022. It can be expected that, as activities return to be as normal as they were in pre-pandemic conditions, electricity consumption from CFE will return to have a similar profile as the one observed in 2019. However, a percentage of about 18% of the total electricity demand by CIC-IPN will continue to be provided by the on-site SPV electricity generation plant. This can be inferred from the situation observed in year 2021, during virtual activities, during pandemic and on-site SPV electricity generation. Fig. 12 plots the electricity consumed from CFE together with the electricity consumed from the on-site SPV plant at CIC-IPN for the years 2019 to 2022.

Table 1. Electricity consumption from CFE from April to September, 2019-2022.

Month	Consumption in 2019 (kWh)	Consumption in 2020 (kWh)	Consumption in 2021 (kWh)	Consumption in 2022 (kWh)
April	45852.60	50867.18	43371.69	44033.93
May	85999.78	52014.39	48061.50	50217.20
June	58871.98	52714.84	45802.28	49983.73
July	52008.66	55462.55	41661.53	45057.21
August	67767.51	54887.86	42394.53	49806.90
September	68705.77	52642.27	40469.10	50500.70
Mean	63201.05	53098.18	43626.77	48266.61
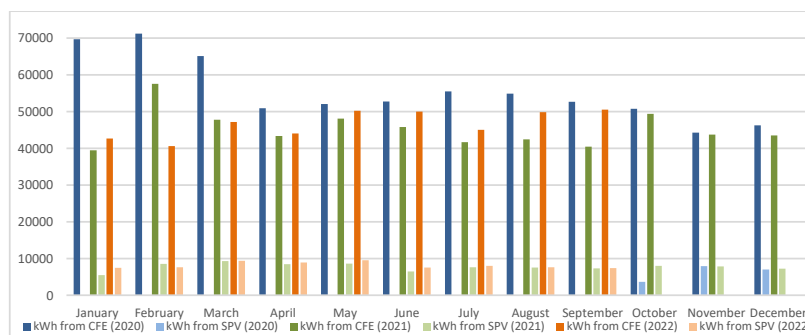
Fig. 12. Electricity consumption from CFE and from SFV plant for each month of 2020-2022.

4   Conclusions and Future Work

From the discussion presented before, it can be concluded that the measures taken due to the COVID-19 pandemic has affected the electricity consumption profiles of public buildings, including educational and research centers as is the case of CIC-IPN. Four electricity consumption profiles were identified: 1) pre-pandemic and pre-virtual activities (2019), 2) during pandemic and virtual activities (2020), 3) during pandemic and virtual activities and SPV electricity generation (2021), 4) post-pandemic and in person

activities and SPV electricity generation (2022). Hence, even activities are becoming in person, due to on-site SPV electricity generation, there is a reduction in electricity consumption from CFE, and this means economic savings and contribution to the reduction of CO2 emissions (indirectly) [7]. Notice that the total electricity consumption of the building of CIC-IPN is the sum of the electricity provided by CFE and the electricity generated on-site by the SPV plant. Hence, it may be expected that the demand when activities became totally in person and normal, will match that one in 2019, before the pandemic and before virtual activities. However, on-site SPV electricity generation will continue and it is expected to cover between 18% to 20% of the total electricity demand of CIC-IPN [7].

Further work includes applying clustering algorithms to group working hours and out of work hours, week and weekend days, for example.

In normal conditions, in the context of electricity usage in educational and research public buildings, the declines in electricity usage are associated with workday hourly load patterns that resemble pre-COVID weekend and holiday usage. Hence, it is relevant to quantify the impacts of crises like the pandemic using a unified modeling framework; this in order to understand the effects of the associated societal response on electricity demand in time of crisis.

References

1. Santiago, I.; Moreno-Munoz, A.; Quintero-Jiménez, P.; Garcia-Torres, F.; Gonzalez-Redondo, M. J. Electricity demand during pandemic times: The case of the COVID-19 in Spain. Elsevier, Energy Policy 148 (2021) 111964, available online: https://doi.org/10.1016/j.enpol.2020.111964.
2. Mastoi, M.S.; Munir, H.M.; Zhuang, S.; Hassan, M.; Usman, M.; Alahmadi, A.; Alamri, B. A Critical Analysis of the Impact of Pandemic on China's Electricity Usage Patterns and the Global Development of Renewable Energy. Int. J. Environ. Res. Public Health 2022, 19, 4608. https://doi.org/10.3390/ijerph19084608.
3. Leach, A.; Rivers, N.; Shaffer, B. Canadian Electricity Markets during the COVID-19 Pandemic: An Initial Assessment. Canadian Public Policy / Analyse de politiques, August 2020 doi:10.3138/cpp.2020-060.
4. Gonzalez-Lopez, R.; Ortiz-Guerrero, N. Integrated analysis of the Mexican electricity sector: Changes during the Covid-19 pandemic. Elsevier, The Electricity Journal 35 (2022) 107142. https://doi.org/10.1016/j.tej.2022.107142.
5. Das, K. Impact of covid 19 pandemic into solar energy generation sector. UPES, Uttarakhand, India. Electronic copy available at: https://ssrn.com/abstract=3580341.
6. Çelik, D.; Meral, M.E.; Waseem, M. The progress, impact analysis, challenges and new perceptions for electric power and energy sectors in the light of the COVID-19 pandemic. Sustainable Energy, Grids and Networks. 2352-4677/© 2022 Elsevier. https://doi.org/10.1016/j.segan.2022.100728.
7. Escamilla-Ambrosio, P. J., Ramírez-Salinas, M. A., Espinosa-Sosa, O., Gallegos-García, G., Morales-Olea, M., & Hernández-Callejo, L. IPN sustainability program: solar photovoltaic electricity generation and consumption reduction. In Ibero-American Congress of Smart Cities, pp. 109-120., Springer, Cham (2019).
8. https://www.cfe.mx/

Variable light intensity system for greenhouse applications

Halleluyah Kupolati[1][0000−0002−3018−9620], Luis
Hernandez-Callejo[2][0000−0002−8822−2948], and Victor
Alonso-Gomez[2][0000−0001−5107−4892]

[1] University of Pretoria, Hatfield, Pretoria, 0002, South Africa
u15078486@tuks.co.za
[2] Campus Universitario Duques de Soria, 42004, Spain
luis.hernandez.callejo@uva.es,victor.alonso.gomez@uva.es

Abstract. The use of artificial lighting for greenhouse applications has been proven to be necessary as a result of the increased demand for food resources around the world. For the full adoption of horticultural lighting, there is a need for the study of the effects of artificial lighting on the plants. A crucial part of the system is the LED driver, which is the system required to supply power to the LED array. According to literature, the most widely used light wavelengths are red, green, and blue wavelengths of light. Hence, a need for a multi-channel LED driver. This work outlines the design of a multi-channel LED driver with the use of a voltage pre-regulator and triple-channel linear current regulators. The results outlined are the light spectrum as observed through a spectrometer. The conclusion is that such a system has a relatively low cost but results in a slightly unstable light intensity.

Keywords: PAR (Photosynthetic Active Radiation) · PWM (Pulse Width Modulation) · DSP (Digital Signal Processor).

1 Introduction

In this section, the advancements and studies made regarding the effects of LED lights on plants are outlined. They are outlined with regards to the most preferrable light wavelengths by the plants, specifically the tomato plant which is the plant of subject of this thesis.

Although, LEDs have been in production since the 1960s, it was not until the 1990s where they had been developed to the point of their possession of the ability to emit high luminousity to the point of usefulness for the study of plant biology. LEDs have been shown to have the highest efficiency of all the artificial light sources such as incandescent light, and carbon arc lighting. Green plants have been studied and shown to be most responsive to red and blue lights on the PAR range. The LED presents the least complicated way to obtain red and blue lights separately. Additionally, due to the directly proportional relationship between diode forward current and light intensity, light intensity control of LEDs

is an uncomplicated process in comparison to the methods required to control fluorescent lights. UV lights consist of high frequency light particles that have been proven to exhibit bacteria eliminating qualities. This makes it an effective decontamination tool on surfaces, including those of fruits and vegetables, [1], [2]. Red blue(RB) light has been studied to observe its effect on fruit ripening [3], it was also found that melatonin played a crucial role in the ripening process. It was concluded that RB light regulation of melanin was a possibility, because the ripening process occurred faster under RB light than it did under white light.

According to [4], for tomato plants, temperatures of about 26C in combination with RB light are said to be optimal for increasing plant height. The plant height was found to be positively correlated with chlorophyll content in the plant. One of the general understandings of the effects of artificial lights on plant morphology is that high R:FR ratios could improve the defense system of plants as opposed to low R:FR ratios which induce a series of strong growth reactions in plants known as shade avoidance syndrome. However, it has been concluded that several unidentified agents affect tomato plant defense systems besides R:FR ratio of the light source being used, [5]. In the study of artificial light effects on tomato seedlings, blue and RB light have been shown to increase biomass accumulation and CO2 assimilation as opposed to monochromatic red light and white light. Additionally, there was observed to exist positive regulation of the photosynthesis of RB light treated seedlings, [6].

Monochromatic green light has been proven to have a positive effect on root development of tomato seedlings by driving photosynthesis. Additionally, it was shown that there was an increase in the activity of antioxidant enzymes, [7]. As the use of LEDs on plants to not pose safety problems to the plants as long as the emitted light is of appropriate intensity and within the PAR range, the point of concern is to understand its effect on plant growth regulators in order to promote technological development for tools to maximize the positive effects of artificial lighting on plants, [8]. The studies referenced in the preceding paragraphs indicates the effectiveness of various combinations of red and blue light wavelengths on plants.

Having giving a background to the study, the purpose of the paper is to outline the design and implementation of a multi-channel LED driver. The LED driver implements independent control for each channel using linear current regulation. The following sections are outlined for the paper: The design and implementation, the experimental procedure including the apparatus used, the results and discussion to outline the outcome and observations of the experiment, and lastly, the conclusion of the paper is given as to the future recommendations and the level of achievement of the objectives of the paper.

2   Design and Implementation

This section chronicles the design of the pre-regulator which is a voltage mode buck converter. The method chosen is the use of a PWM linear current regulator to realise a multi-channel LED driver.

Figure 1 indicates a representation of the hardware of the system in various blocks. Three blocks represent mechanical relays to switch between different power sources. The main section of the system is the power electronic converter, which in this case, is a buck converter. The converter operates under two different conditions; as a battery charger and a LED array supply. The system is designed to power 3 different coloured LEDs. A design challenge is to ensure the current in each channel i controlled separately in addition to providing the adequate voltage level. The block labelled variable current output and protection indicates the current control system required for driving the LEDs. The hardware of the system includes three parts; a source switching interface, a power electronic converter, and the sensor design required for closed loop control.

The target power rating for the system is 25W for each channel, however, due to financial constraints a lower output power for the LED is demonstrated in the results section of the report.
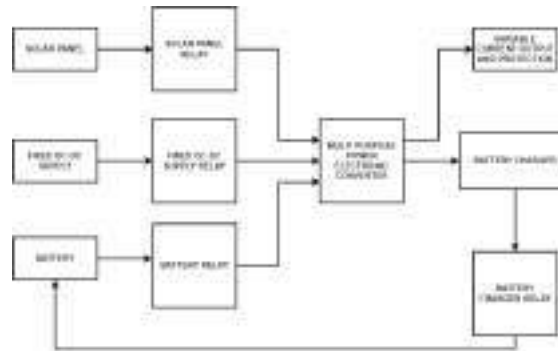
Fig. 1: Block diagram representation of the system hardware

The basic structure of the driver is shown in Figure 2 includes a buck converter and three MOSFETs for the purpose of individual current control of each LED channel.The red section represents the buck converter which serves as the voltage pre-regulator. The blue section represents the linear current regulators using MOSFETs. With regards to the design, the aspects of focus are the size of the inductor and capacitor of the system, which are calculated as follows,

$$\delta = \frac{i_L r_L + V_{out} + V_{fwd}}{V_{in} - V_{ce} + V_{fwd}} \qquad (1)$$
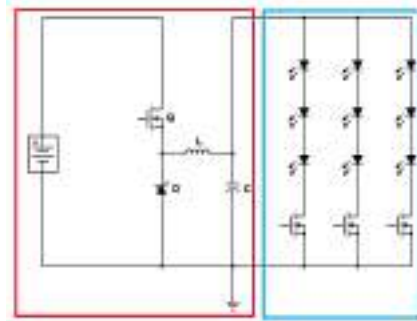
Fig. 2: Basic structure of the LED driver

$$L \geq \frac{(V_{in} - V_{ce} - i_L r_L - V_{out}) \times \delta}{\Delta_{L,pk-pk} f_{sw}} \tag{2}$$

$$C \geq \frac{\Delta I_{L,pk-pk}}{8\Delta V_{c,pk-pk} f_{sw}} \tag{3}$$

With regards to the mosfet and diode rating, the output and input voltage and current rating are considered; The system is designed to be powered from either a solar panel array, a fixed 48V DC power supply, or a 24V battery. Hence, the system is designed for a maximum of 48V for the input voltage. With regards to the output voltage, the battery charger system requires more power, voltage and current wise than the LED array. Hence, it is used as the reference for choosing the power components.

The concept behind including a battery charger is to account for instances where the grid, or solar power is unsuitable hence requiring a third power source.

A requirement for the battery is to power the LED array all through the night. Taking into account the worst case scenario of longer night times, the battery is required to operate for 10 hours. With a day light time of 14 hours, a current of at least 7A is required to charge the battery in the appropriate time.

Taking into account a worst case parasitic resistance for the inductor and the capacitor, the following parameters are used in the calculation of the minimum inductance and capacitance required.

$$V_{in} = 45 \ V, \ V_{out} = 29.4 \ V, \ \Delta V_{o,pk-pk} = 0.02 V_{o,ave} \ , \ \ \Delta I_{L,pk-pk} = 0.1 I_{L,ave}$$

$$V_{ce,sat} = 0.0552V, \ V_{fwd} = 0.95V, \ r_L = 100m, r_{esr} = 3m, I_{out} = 4A$$

Therefore

$$\delta = \frac{4 \times 0.1 + 29.4 + 0.95}{44 - 0.0552 + 0.95} = 0.6849$$

$$L \geq \frac{(44 - 0.0552 - 4 \times 0.1 - 0.95) \times 0.6849}{0.1 \times 4 \times 100000} = 242.2 \mu H$$

$$C \geq \frac{0.1 \times 4}{8{\times}0.02 \times 29.4 \times 100000} = 0.85 \mu F$$

3   Experimental Procedure

The following are the apparatus that were utilised to obtain the relevant results for the system:

- A C1880MA light spectrometer needed to view the spectral profile of the light produced by the LED array.
- An Arduino Uno which is used to obtain the information from the light spectrometer.
- The multi channel LED driver with the parts included in the parts list section.

The implemented LED driver shown in Figure 3a possesses three channels to enable connection to the 3 colored LED array, shown in Figure 3b. For light spectrum data collection, the light spectrometer shown in Figure 4b is placed in a dark enclosure such that the only light source received is from the LED array. It is subsequently connected to an arduino microcontroller as shown in Figure 4a that processes the data and sends the light spectrum information to a computer for the purpose of being saved as a txt file.

The following are the steps followed to obtain the light spectrum results:

1. The C1880MA light spectrometer is placed in an enclosed space with all the visible light removed.
2. The LED array is placed over the enclosed space such that the only source of light observed by the spectrometer is from the LED array.
3. The light spectrum is recorded to observe the baseline power level of the system.
4. The multi channel LED driver is connected to the LED array and turned on.
5. The light spectrum is recorded for different colour light intensity ratios.
6. The steps mentioned above are observed for the solar panel as a power source and a battery as the power source.

(a) The Implemented LED driver

(b) The RGB LED array
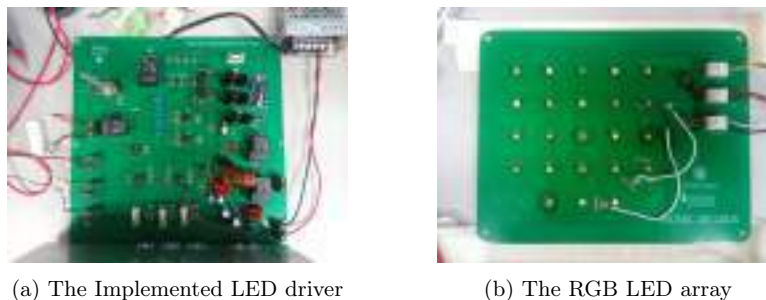
Fig. 3: Experimental circuit and LED array

(a) Arduino Uno to PC connection

(b) The C1880MA light spectrometer
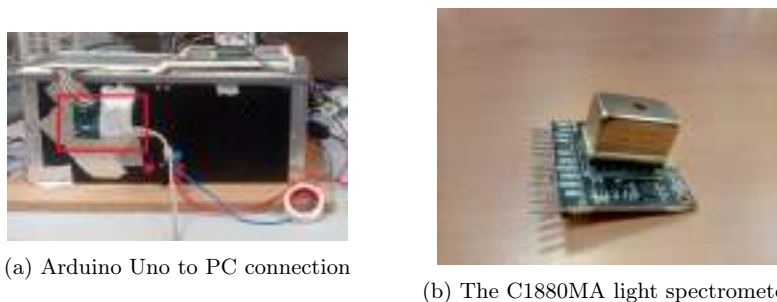
Fig. 4: Light spectrum data collection setup

4   Results and Discussion

In this section, the results obtained for the spectrum analysis are outlined and discussed. From the data, the red, green, and blue LEDs used represent wavelengths of 620-630nm, 530-535nm, and 440-455nm respectively. The goal was to obtain light spectrum profiles for 5 major scenarios, which are as follows; A light spectrum profile with the red wavelength light intensity proportionally larger than the 2 other wavelengths, a similar scenario for the blue and green wavelengths being dominant, as shown in Figure 5 , Figure 6, and Figure 7 respectively. A profile with relatively equal light intensities from the red and blue wavelengths as shown in Figure 8. Lastly, a profile with all 3 wavelengths present as shown in Figure 9. A point to note is that although the figures indicate a reading for the light intensity, the light spectrometer utilised is optimized for high accuracy wavelength measurements, with a trade-off of light intensity measurements of lower accuracy. Hence, the light intensity values indicated on the figures represent relative measurements only.

The profile is analyzed for a wavelength between 400nm and 700nm. This represents the PAR. The results shown are those of the spectrum profile. The individual red, green, and blue magnitude are adjustable. These are evident

from the series of results obtained of the profiles. For the study of the effects of artificial lights on plants. There are certain ratios that are taken note of. Varying ratios of red and blue light wavelengths are observed to be effective for plants. An effective system will signify one that can produce similar ratios that have been shown to produce effective plant growth results.

The method utilised was the use of linear current regulators to obtain average current control through the LED string. It appeared from the results that the frequency was not sufficiently high as a flicker was observed by the light spectrometer. The integration time of the sensor utilised had to be increased to stabilise the spectral power readings to obtain the required results.

From the results, the green component has a tendency to be overpowered by the red and blue wavelengths. Thus, highlighting the limitation of the system in studying the effects of green wavelengths on plants. Additionally, The relatively low green composition could be as a result of the positioning of the sensor.
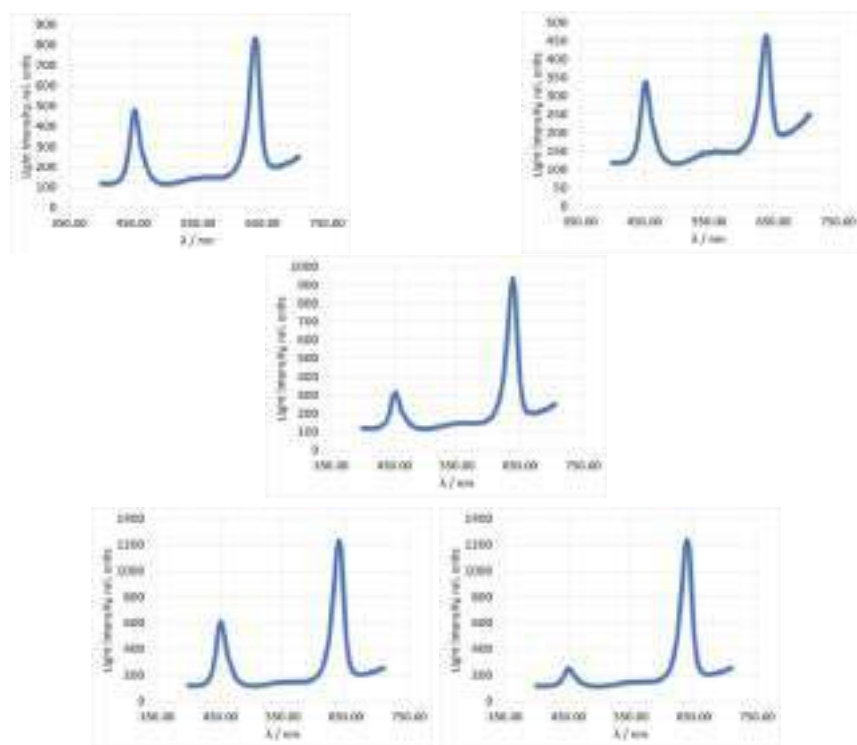
Fig. 5: Light spectrum with the dominant red wavelength
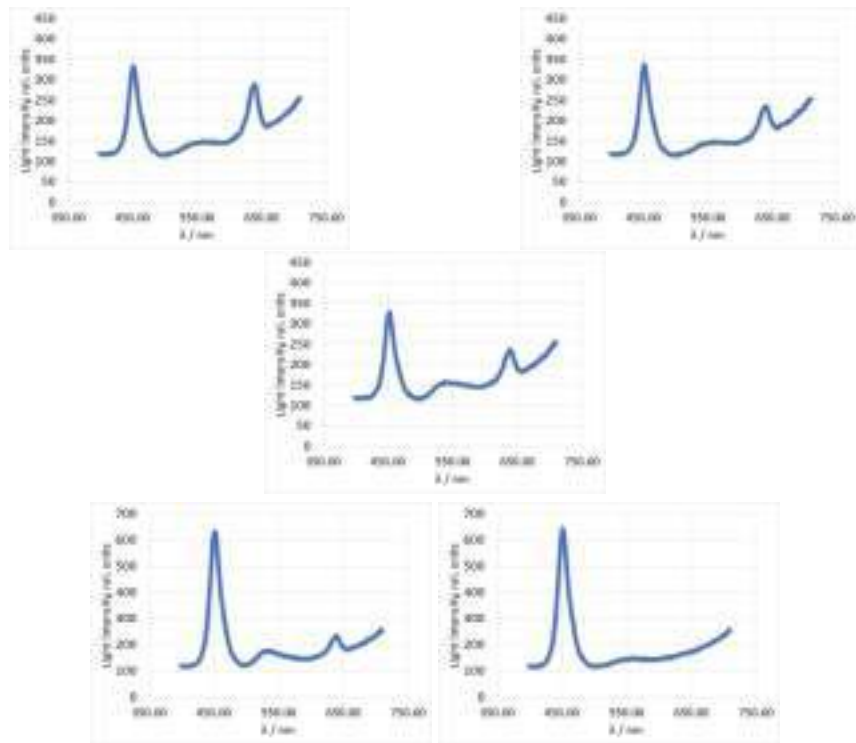
Fig. 6: Light spectrum with the dominant blue wavelength
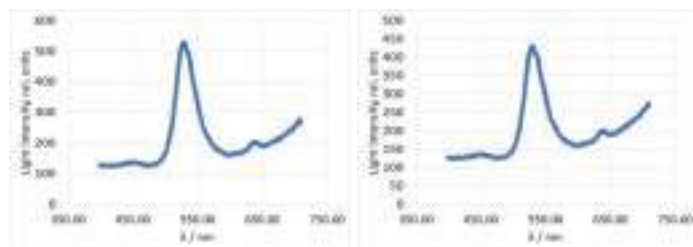
Fig. 7: Light spectrum with the dominant green wavelength
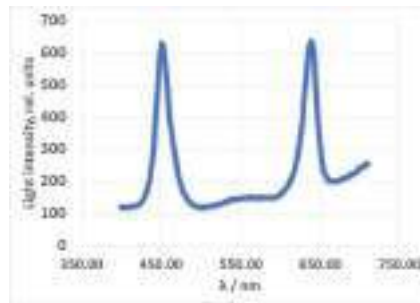
Fig. 8: Light spectrum with equal intensities for the red and blue wavelength
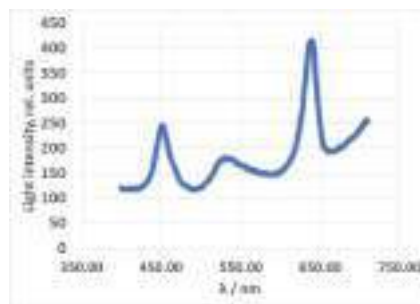
Fig. 9: Light spectrum with all three wavelengths present

5   Conclusion

With a knowledge of the importance of light quality for plant growth, the goal of the work was to develop a multi-channel LED driver for grow light applications for the end purpose of the study of the effects of artificial lights on vegetable plants to determine the best light spectral profile for favourable plant growth. To achieve this, the system developed needed to have the ability to emulate the light spectrum profiles that have been shown to have positive effects on select vegetable plants.

With the objective noted, an electronic system has been developed that varies the light intensity of an LED array with the ability to control each channel independently. The design of the system has been outlined in the preceding sections with special attention placed on the buck converter used as the pre-regulator. The results have shown that there is independent varied control of the light intensity, however, fluctuations were observed by the light spectrometer.

Future recommendations for the system are to do with the size and stability of the current which in turn affects light intensity. Possible improvements that can be made to the system are re-designing the linear current regulators section of the circuit to accommodate for continuous current on the output. Possible ways to achieve this are the look into current-sharing and single inductor, multiple output topologies for a reasonable trade-off between system size and stable output current readings for each channel. Additionally, the light spectrometer could be connected directly to the control unit for more precise control of the light intensity.

References

[1] S. Sethi, A. Joshi, and B. Arora, "Uv treatment of fresh fruits and vegetables," in *Postharvest disinfection of fruits and vegetables*, Elsevier, 2018, pp. 137–157.

[2] M. C. Lagunas-Solar, C. Pina, J. D. MacDONALD, and L. Bolkan, "Development of pulsed uv light processes for surface fungal disinfection of fresh fruits," *Journal of Food Protection*, vol. 69, no. 2, pp. 376–384, 2006.

[3] Y. Li, C. Liu, Q. Shi, F. Yang, and M. Wei, "Mixed red and blue light promotes ripening and improves quality of tomato fruit by influencing melatonin content," *Environmental and Experimental Botany*, vol. 185, p. 104 407, May 2021. DOI: `10.1016/j.envexpbot.2021.104407`. [Online]. Available: `https://doi.org/10.1016/j.envexpbot.2021.104407`.

[4] L. Kong, Y. Wen, X. Jiao, X. Liu, and Z. Xu, "Interactive regulation of light quality and temperature on cherry tomato growth and photosynthesis," *Environmental and Experimental Botany*, vol. 182, p. 104 326, Feb. 2021. DOI: `10.1016/j.envexpbot.2020.104326`. [Online]. Available: `https://doi.org/10.1016/j.envexpbot.2020.104326`.

[5] D. Meijer, M. Meisenburg, J. J. van Loon, and M. Dicke, "Effects of low and high red to far-red light ratio on tomato plant morphology and performance of four arthropod herbivores," *Scientia Horticulturae*, vol. 292, p. 110 645, Jan. 2022. DOI: `10.1016/j.scienta.2021.110645`. [Online]. Available: `https://doi.org/10.1016/j.scienta.2021.110645`.

[6] Y. Li, Z. Liu, Q. Shi, F. Yang, and M. Wei, "Mixed red and blue light promotes tomato seedlings growth by influencing leaf anatomy, photosynthesis, CO2 assimilation and endogenous hormones," *Scientia Horticulturae*, vol. 290, p. 110 500, Dec. 2021. DOI: `10.1016/j.scienta.2021.110500`. [Online]. Available: `https://doi.org/10.1016/j.scienta.2021.110500`.

[7] F. Li, Y. Li, S. Li, G. Wu, X. Niu, and A. Shen, "Green light promotes healing and root regeneration in double-root-cutting grafted tomato seedlings," *Scientia Horticulturae*, vol. 289, p. 110 503, Nov. 2021. DOI: `10.1016/j.scienta.2021.110503`. [Online]. Available: `https://doi.org/10.1016/j.scienta.2021.110503`.

[8] L. Xiao, T. Shibuya, K. Kato, M. Nishiyama, and Y. Kanayama, "Effects of light quality on plant development and fruit metabolism and their regulation by plant growth regulators in tomato," *Scientia Horticulturae*, vol. 300, p. 111 076, Jun. 2022. DOI: `10.1016/j.scienta.2022.111076`. [Online]. Available: `https://doi.org/10.1016/j.scienta.2022.111076`.

Biomethane production in isolated farms powered by solar energy: Anaerobic digestion/Solar hybridization technology

A. García Álvaro [1, 2], C. Ruiz Palomar [1, 2], L. Hernández-Callejo [3], V. Alonso Gómez [4], R. Muñoz Torre [1], D. Hermosilla Redondo [3,5], I. de Godos Crespo [1, 2]*

[1]University of Valladolid, Institute of Sustainable Process, Valladolid, Spain,

[2]Department of Chemical Engineering and Environmental Technology, University of Valladolid (UVA), Campus Universitario Duques de Soria, 42004 Soria, Spain.

[3]Department of Agricultural Engineering and Forestry, University of Valladolid (UVA), Campus Universitario Duques de Soria, 42004 Soria, Spain

[4]Department of Applied Physics, University of Valladolid (UVA), Campus Universitario Duques de Soria, 42004 Soria, Spain.

[5]Department of Forest and Environmental Engineering and Management, Universidad Politécnica de Madrid, José Antonio Novais 10, 28040 Madrid, Spain.

*Corresponding author

Abstract.

The sustainability of livestock production has been put in question due to the greenhouse gas emissions and pollution of soil and water. However, the implementation of renewable technologies in the farming practices such as anaerobic digestion and solar energy can overturn this situation.

In this work, an anaerobic digestion system for biogas production, under mesophilic conditions, fed with pig slurry and energetically covered with hybrid solar panels has been modeled. In this sense, the electrical requirements are covered by photovoltaic energy and thermal energy heats the digester to reach the mesophilic range (35ºC). The biogas generated in the process passes through an upgrading system to obtain high calorific content biomethane for as grid injection, vehicle fuel or electricity and heat generation. The system has been studied in five different climatic regions to see the effect of solar irradiation and temperature on the final biomethane production. The results demonstrate that slurry management is a viable alternative within the energy transformation framework of farms in isolated environments where solar irradiation convertible to energy is available.

Keywords: Anaerobic digestion, Biomethane, Energies hybridization, Rural areas, Solar energy, Waste to energy

1   Introduction

1.1 Decarbonization Economy - Biofuels and Renewable Technologies

Currently there is a high dependence on fossil resources to produce energy and raw materials, however, the rapid penetration of renewables in the energy sector makes electrification and renewable gases the main technologies for the decarbonization [1]

The technological development of electric renewable energies has allowed that, in many cases, they are currently the most competitive alternative to generate electricity, allowing a reduction in electricity costs for consumers [2] despite the obstacles of the diffusion of decentralized systems [3].

According to the last estimations, in 2050 more than half of the GHG emissions will be produced in the primary sector due to the special characteristics that make mitigation difficult [4]. By transforming the energy sector towards a renewable perspective based on the substitution of oil derivatives, environmental, social and economic benefits will be achieved. The main renewable sources that enable this transformation are biomass, solar energy, wind energy and biofuels such as bioethanol, biodiesel and biomethane [5]. In the case of biomass and biofuel, renewable feedstocks must be used to ensure sustainability, e.g., agricultural and forestry residues.

Anaerobic digestion is presented as a biological process that, under controlled conditions, the avoid the methane emission which has an effect about 80 times more harmful than CO_2 [6]. In addition, the process also produces biogas as a high value-added by-product and digestate

1.2. Rural development

In recent years, rural activities, whether agricultural or livestock, have faced different barriers to development and evolution. Understanding rural development as a process that seeks social change and sustainable economic growth for the permanent progress of the rural community, the ultimate goal is to improve the quality of life of these societies and conserve the environment [7].The significance of environmental protection has made renewable resources a strategic alternative to achieve sustainable development goals [8].

1.3. Technology hybridization

The lack of availability of these renewable energy resources throughout the complete year has led to research in the area of hybrid renewable energy systems [9].
Access to the grid is not always possible and the use of renewable energies does not always guarantee energy availability except in more complex installations. The possibility of mixing more than one renewable technology will allow a more constant energy generation optimizing the design and reducing costs [10].

This work presents a novel proposal for the hybridization of renewable energies in isolated areas where organic waste is produced and there is no access to the electricity grid. An anaerobic digester fed with pig slurry whose energy needs are obtained from the sunlight favoring a circular economy and decarbonization within the framework of rural development is proposed and modeled. For this purpose, different locations have been studied and the process has been simulated in each of them to see the differences in terms of biogas production and system efficiency.

2   Materials and Methods

2.1   System description

The scheme of the proposed system can be seen in Figure 1. The system consists of an anaerobic reactor and a set of Photovoltaic/Thermal (PV/T) modules connected to a battery system and a thermal energy storage tank respectively.

The anaerobic digester is the tank where the biological reactions of organic matter transformation of the substrate will be carried out. As a by-product, biogas is obtained, which will be passed through an upgrading equipment that will eliminate CO_2 and other undesirable elements to obtain biomethane.

The thermal energy captured by the module field is transferred to a thermal energy storage tank and a heat exchanger is used to heat the digester and the substrate.
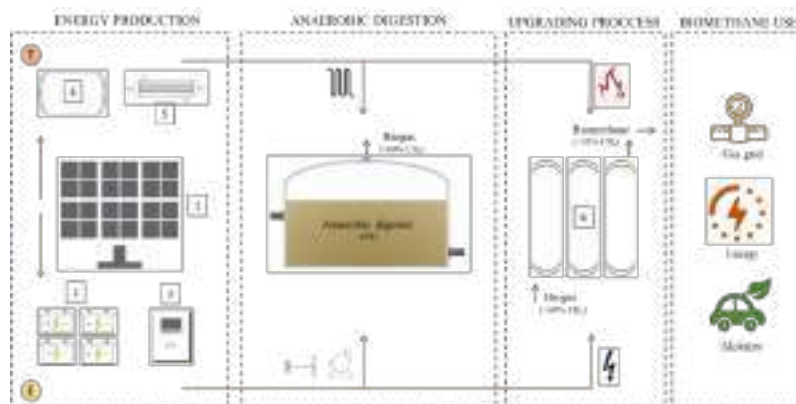
Figure 1. Schematic diagram of the Anaerobic digestion/Solar (AD/S) system studied

The electrical energy produced by the PV/T modules is fed to the junction box and protections, and then supplied to the load and/or battery system for the final use (substrate pumping, mixing and biogas upgrading). In periods of power lack, the upgrading process will be stopped to minimize power consumption while maintaining digester operation.

The simulated PV/T hybrid module was based on a commercial module with a maximum operating temperature of the PV/T collector is 80 ⁰C, and the set point of 30-45 ºC set is to control the inside of the anaerobic reactor, i.e., when the outlet temperature of the storage is lower than the set point, the system will turn on and raise its temperature to that level. In case the tank temperature conditions are below the set point, the system will be supported by a biogas boiler that will generate thermal energy.

2.2   Designed system

The slurry management of a 2,000 head pig farm is proposed. For this purpose, a cylindrical reactor of 4.5 m height and 9 m diameter has been designed with operating

parameters of a hydraulic residence time (HRT) of 25 days and a working temperature of 35 ℃ [11]. The characteristics can be seen in Table 1.

Pig slurry, as a substrate, can be very changing in composition and organic content. Representative average characteristics have been taken for any given pig farm [12].

The upgrading system chosen is the chemical absorption as it adapts very well to the energy model presented since its operation has an electrical consumption of 0.125 kWh/m^3 and a thermal consumption of 0.625 kWh/m^3 [13] with an efficiency of 97.3%.

The solar installation will be based on the installation of 150 hybrid solar panels with a surface area of 2 m^2 per unit and a thermal efficiency of 60% and electrical efficiency of 17% respectively compared to the theoretical photoelectric conversion efficiency of the photovoltaic subsystem and the thermal efficiency of the thermal utilization subsystem of the PVPT system of 26.7% and 68.4% [14].

Table 1. Characteristics of the proposed system

Anaerobic digester	
Work volume (m3)	700
Work temperature (℃)	35
HRT: Hydraulic Retention Time (days)	25
Substrate: Pig slurry	
Managed volume (m3/year)	11,500
Humidity (%)	95
Total Solids (kg/m3)	
Volatile Solids (kg/m3)	
Biogas upgrading technology: Chemical absorption	
Energy consumption	0.1-0.15 kWh/m3 and 0.5-0.75 kWh/m3 (heat) raw gas
Efficiency (%)	96.7-97.7
Solar system: Hybrid technology	
η_e thermal conversion efficiency (%)	60
η_{pv} photoelectric conversion efficiency (%)	17

2.3   Study localizations

In order to analyze the effect of the hybrid AD/S system under different climatic scenarios, where the solar resource and ambient temperature allow a comparison between different regions, five cities were selected for the study: Soria (Spain), (United States), (Denmark), (Brazil) and (China). All of them, regions with high swine activity [15].

The meteorological information for each city corresponds to a standard year. Table 2 shows the main characteristics of the regions analyzed. Since the five cities studied have different ambient temperatures and solar radiation, the thermal energy generation needs of the PV/T system to satisfy the demand of the anaerobic reactor will be different.

The annual thermal energy required for the reactor was calculated from the thermal energy that would be required to maintain the reactor and the input substrate at 35℃ throughout the year (Equation 1 to 3). Similarly, the electricity required for the system takes into account the reactor mixing and pumping needs, as well as biogas

purification. It is expected that in the winter months where irradiation and temperatures are lower, biomethane production will be limited since part of the biogas will be used to generate thermal energy.

$$Digester\ volume\ (m^3) = \frac{substrate\ V}{day}\left(\frac{m^3}{day}\right) * HRT\ (days) * 1.3\ (biogas\ factor) \qquad \text{eq. 1}$$

$$E_{Heat\ digester}\left(\frac{W \cdot h}{d}\right) = K\left(\frac{W}{m^{2 \cdot o}C}\right) * A(m^2) * \Delta(T_{ext} - T_{int})(^oC) * \frac{24h}{day} \qquad \text{eq. 2}$$

$$E_{Heat\ substrate}\left(\frac{W \cdot h}{d}\right) = Q\left(\frac{subst\ m^3}{day}\right) * \left(\frac{4.2\ MJ}{^oC \cdot m^3}\right) * \Delta(T_{ext} - T_{subst})(^oC) \qquad \text{eq. 3}$$

To show more fully the climate scenarios studied, Fig. 2a and b show the mean monthly ambient temperatures and irradiance for the five selected regions. This information has been generated with Solargis software. The ambient temperature, as well as the availability of the solar resource, determine the thermal energy requirements. In the same way, the software has determined the optimal tilt angle for the solar panels in each location.

It is observed that China, Soria, Denmark and Iowa have a similar pattern in temperatures throughout the year with hot summers and cold winters. In China the summers reach higher temperatures and in Iowa the winter temperatures are colder. The availability of sunshine in these four regions is different since Denmark has lower values, especially in winter while Soria has more irradiation throughout the year and especially in summer.

The case of Brazil has a different behavior with more constant temperatures and irradiation throughout the year.

Table 2. Cities selected for the study

	Soria (Spain)	Iowa (USA)	Odense (Denmark)	Santa Catarina (Brazil)	Laixi (China)
Latitude and longitude	41.7, -2.4	41.6, -91.7	55.3, 10.3	-26.9, -51.7	36.9, 120.5
Annual irradiation (MWh/m²)	1618.7	1492.0	1023.1	1760.0	1477.3
Average annual temperature (ºC)	11.4	10.1	9.1	16.7	13.0
Optimum inclination angle (º)	36	37	40	26	33
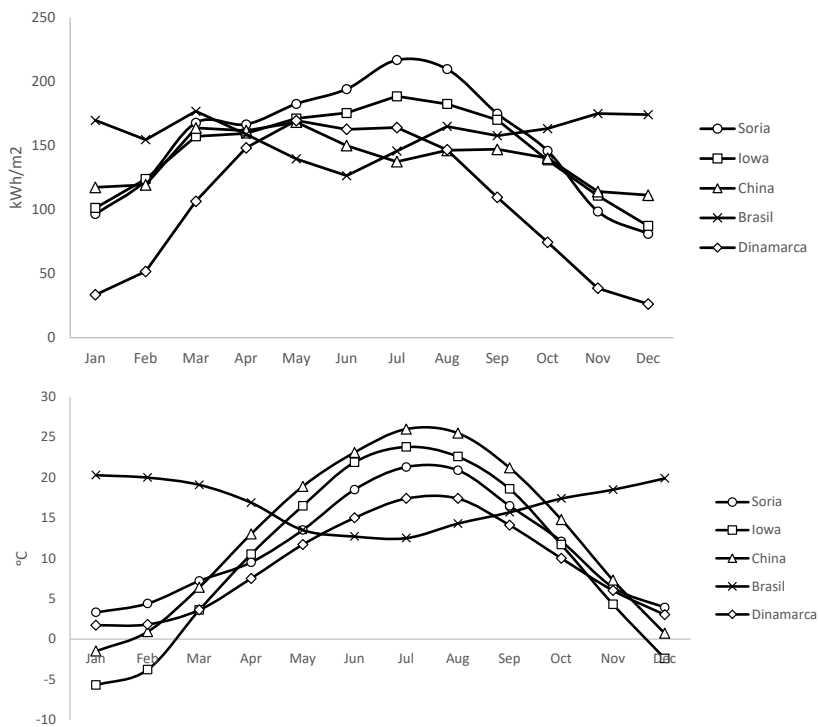
Figure 2. (a) Average temperature and **(b)** monthly ambient irradiation.

2.4 Data processing

The data generated has been processed and analyzed in the Microsoft Excel program.

3 Results and Discussion

3.1 Energy analysis. Energy requirements

According to the meteorological data available, monthly effective irradiance ranged between 148.2 and 201.4 kWh/m², while the temperature is between 24.9 and 26.09 ℃ Figure 3 presents the graphs of demand and electrical and thermal production of the system with monthly data. It can be seen how the adjustment in biomethane production has been more limited by the electrical part, especially in the winter months where irradiation is lower.

In the graphs on the right, the thermal production is not sufficient in the months of lower irradiation and lower temperatures. This difference is made up by the biogas that is not converted to biomethane and is transformed through the boiler into heat.

In the case of Denmark, in the most unfavorable months of irradiation, the system can not meet the required electrical demand, and this could lead to a loss of control of the anaerobic digestion process in the reactor.
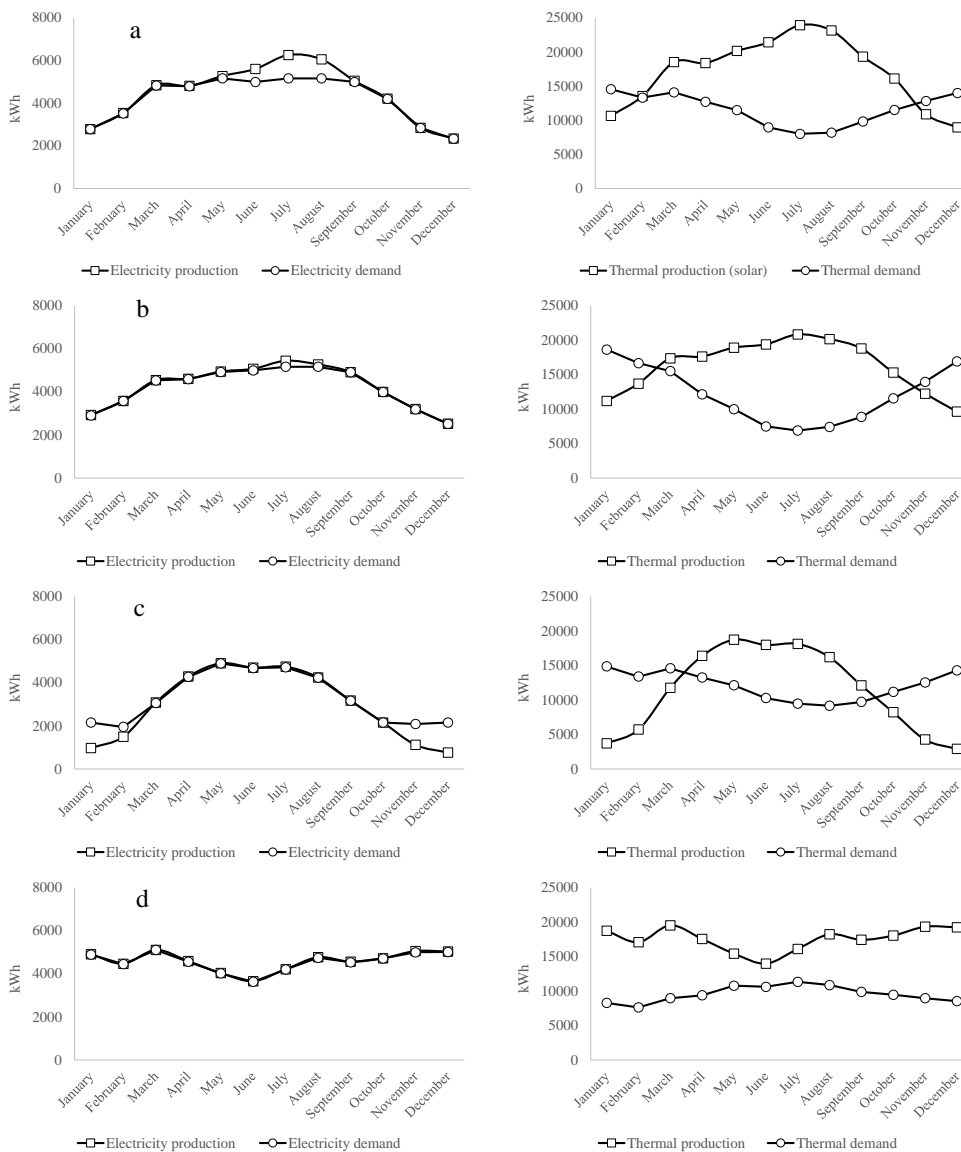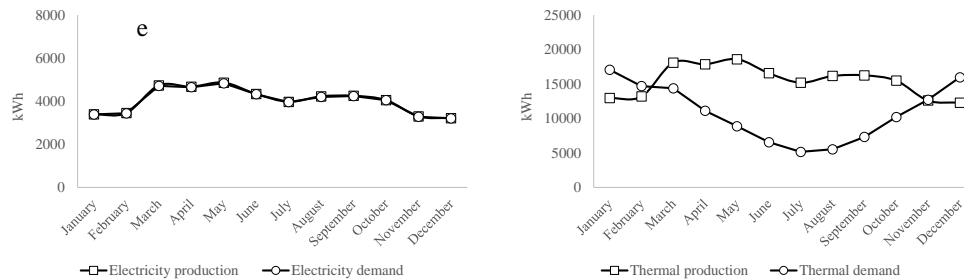
Figure 3. Thermal and electrical production and demand for the study locations: **a)** Soria; **b)** Iowa; **c)** Odense; **d)** Saint Catherine; **e)** Laixi

3.2   Biomethane productivity

The biomethane production study can be seen in Figure 4 where, as in the previous case, the winter months require the use of part of the biogas to ensure the operational viability of the system.
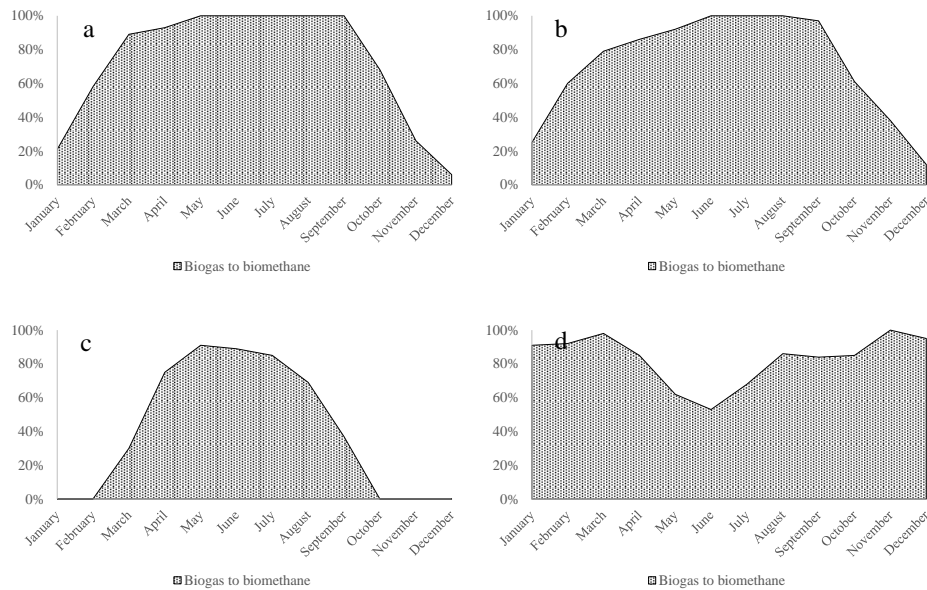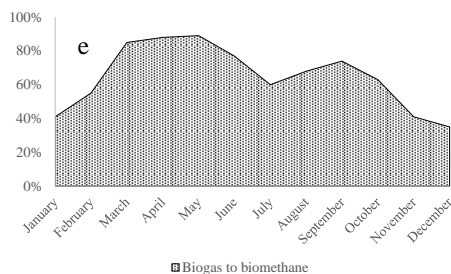
Figure 4. % of biogas destined for upgrading and generation of biomethane for the study locations: **a)** Soria; **b)** Iowa; **c)** Odense; **d)** Saint Catherine; **e)** Laixi

Table 3 shows the % of biogas used for biomethane for the whole year. Brazil has the highest production (83.25%) and Denmark the lowest due to the difference in climate (39.67%). The rest of the locations, being temperate climates, have an average production (64.67 - 71.75%).

Table 3. % of biogas destined for upgrading and generation of biomethane for the study locations: **a)** Soria; **b)** Iowa; **c)** Odense; **d)** Saint Catherine; **e)** Laixi

	Biogas to biomethane (%)
Soria (Spain)	71.75
Iowa (USA)	70.83
Odense (Denmarck)	39.67
Santa Catalina (Brazil)	83.25
Laixi (China)	64.67

4   Conclusions

Within the framework of rural development and the management of organic waste available from agricultural or livestock activity, the use of a hybrid system of anaerobic digestion and solar energy is presented as a viable alternative even in areas without access to the electricity grid.

The high temperatures and the availability of sunlight will favor this type of system in terms of energy efficiency and can optimize the production of biomethane, a substitute for natural gas.

Declaration of competing interest

The authors declare that they have no known competing financial interests or personal relationships that could have appeared to influence the work reported in this paper.

References

[1]   Ahlberg-Eliasson, K., Nadeau, E., Levén, L., Schnürer, A. (2017). Production efficiency of Swedish farm-scale biogas plants. Biomass and Bioenergy, 27–37. https://doi.org/https://doi.org/10.1016/j.biombioe.2016.12.002

[2]   Bajpai, P. Dash, V. (2012). Hybrid renewable energy systems for power generation in stand-alone applications: A review. Renewable and Sustainable Energy Reviews, 2926–2939. https://doi.org/https://doi.org/10.1016/j.rser.2012.02.009</div>

[3]   Burke, M. J., Stephens, J. C. (2018). Political power and renewable energy futures: A critical review. Energy Research ; Social Science, 78–93. https://doi.org/https://doi.org/10.1016/j.erss.2017.10.018

[4]   del Río, P. (2011). Analysing future trends of renewable electricity in the EU in a low-carbon context. Renewable and Sustainable Energy Reviews, 2520–2533. https://doi.org/10.1016/j.rser.2010.12.013

[5]   Dieter Deublein, & Angelika Steinhauser. (2008). Biogas frim Waste and Renewable Resources

[6]   European Parliament. (2018). Regulation (EU) 2018/1999. Governance of the Energy Union and Climate Action.

[7]   Food and Agriculture Organization os the United Nations. (2021). Meat market review 2020

[8]   Kallio, S., Siroux, M. (2022). Hybrid renewable energy systems based on micro-cogeneration. Energy Reports, 762–769. https://doi.org/https://doi.org/10.1016/j.egyr.2021.11.158

[9]   Mar, K. A., Unger, C., Walderdorff, L., Butler, T. (2022). Beyond CO2 equivalence: The impacts of methane on climate, ecosystems, and health. Environmental Science , 127–136. https://doi.org/https://doi.org/10.1016/j.envsci.2022.03.027</div>

[10]   MITECO. (2020). Estrategia de descarbonización a largo plazo 2050.

[11]   Ocon, J. D., Bertheau, P. (2019). Energy transition from diesel-based to solar photovoltaics-battery-diesel hybrid system-based island grids in the Philippines – Techno-economic potential and policy implication on missionary electrification. Journal of Sustainable Development of Energy, Water and Environment Systems, 139–154. https://doi.org/10.13044/j.sdewes.d6.0230

[12]   Sun, Q., Li, H., Yan, J., Liu, L., Yu, Z., Yu, X. (2015). Selection of appropriate biogas upgrading technology-a review of biogas cleaning, upgrading and utilisation. Renewable and Sustainable Energy Reviews, 521–532. https://doi.org/https://doi.org/10.1016/j.rser.2015.06.029

[13]   United Nations. (2021). Summary Progress Update 2021 : SDG 11 - Sustainable cities and communities

[14]   Wang, G., Wang, B., Yao, Y., Lin, J., Chen, Z., &; Hu, P. (2020). Parametric study on thermodynamic performance of a novel PV panel and thermal hybrid solar system. Applied Thermal Engineering, 115807. https://doi.org/https://doi.org/10.1016/j.applthermaleng.2020.115807

[15]   Yaqoot, M., Diwan, P., Kandpal, T. C. (2016). Review of barriers to the dissemination of decentralized renewable energy systems. Renewable and Sustainable Energy Reviews, 477–490. https://doi.org/https://doi.org/10.1016/j.rser.2015.12.224

Control Strategies in Microgrid Management: A state of Art

Oscar Izquierdo-Monge[1], Inés Fraile Martín[2], Paula Peña Carro[1], Gonzalo Manuel Martín Rodríguez[2], Ángel Zorita Lamadrid[3] and Luis Hernández Callejo[4]

[1] CEDER-CIEMAT, Autovía de Navarra A15 salida 56, 422290 Lubia (Soria), Spain.
[2] Universidad de Salamanca, Plaza de la Merced 18, 37008 Salamanca, Spain.
[3] ADIRE-ITAP. University of Valladolid, Paseo del Cauce 59, 47011 Valladolid, Spain.
[4] ADIRE-ITAP. University of Valladolid, Campus Duques de Soria, 42004 Soria, Spain.
oscar.izquiero@ciemat.es; inesfraile@usal.es; paula.pena@ciemat.es; gonmarro@usal.es;
zorita@eii.uva.es and luis.hernandez.callejo@uva.es.

Abstract: The imminent need to incorporate renewable energy sources (RES) as a useful solution to the scarcity of conventional resources and the environmental problems that they entail has motivated the development of new systems capable of producing, storing and serving energy based on demand, called microgrids (MGs). They are mainly made up of distributed generators (DGs) and energy storage systems (ESSs) and due to their great advantages, they are being implemented throughout the world and could be a great means for the development of RES. However, the intermittence of RES and general characteristics of MGs, constitute an important challenge for the scientific community in order to optimally manage the resources. For this, control strategies are being developed, putting attention in reducing operational costs, reducing damage in ESSs, insuring the stability of the system, etc. All this questions, the motivations that lead to develop a management system in each case and the solutions found so far are presented in this paper, as an overview of the progress achieved until now. Furthermore, a prediction about future trends in this field is done, based on the current situation and the estimations made on the energy future and the needs of communities in the coming years.

Keywords: energy management system, microgrid, optimization algorithms, control strategies

1   Introduction

Nowadays, the energy production is still related to great problems: the cost of the conventional energies together with the fact that they are running out, means that the exploitation of renewable energy sources (RES) will be simply necessary in the near future [1] and advanced strategies must be developed to take advantage of these resources.

Renewable sources produce energy from various natural phenomena [2]. Consequently, one of their main characteristics is that nature provides abundant supply

[3]. However, its production depends on climatic and economic conditions [4], so dealing with these drawbacks is an important challenge for the scientific community.

To this end, microgrids (MGs) are being developed as a good tool to alleviate the scarcity of conventional resources and to adapt energy development to the new circumstances.

An MG is a group of interconnected loads and distributed energy resources (DERs) [5], which are distributed generators (DGs) and distributed energy storage systems (ESSs). It can generate, distribute and regulate flow of electricity to costumers. It usually contains the Microgrid Central Controller (MGCC), smart switches, protective devices and automation systems [6] and it can operate in both connected and isolated modes [7].

Fig. 1. Scheme of a common MG [8].

Given the above, it is clear that MGs are commonly conformed by multiple devices so the information flow between all of them is complex. The optimal coordination of all the elements is necessary to provide quality energy to consumers. So, to this end, researchers are developing energy management systems (EMSs) whose general aim is to control the energy produced, stored and consumed [9] at any given time so that the system is never exposed to harmful conditions and user satisfaction is ensured.

When developing an EMS, investigators consider a great variety of goals among which are reducing the costs, enlarging the life of the ESSs and the DGs, improving the energy distribution and, definitely, optimizing the system operation while meeting the needs of consumers.

Knowing what progress has been made in recent years allows researchers to apply them to real world MGs around the globe and then, establish improvements in the strategies based on their own outcomes. This will favour the implementation of the MGs in the near future. So, the purpose of this paper is to present a summary of the control strategies that have been recently developed. Both the motivations that lead the authors to choose one or the other goals, and the variables that are considered in each case are analysed. Some relationships between different control strategies are

established and the results obtained by each author are shown. To end, a prediction about the possible future trends in EMSs is made according to the current scenario.

The paper is organised as follows: in Section 2, the criteria followed by researchers for managing MGs, together with the strategies developed so far, are presented. In Section 3, an estimation of the future perspectives in this field is made. Finally, the conclusions are given in Section 4.

2 Microgrids Management

The Energy Management System of a MG includes the basic functions like local generation and consumption control and ESSs management to reach multiple targets. The growing desire to improve the characteristics of future MGs carries a challenge for the development of control systems [10]. Some strategies are day-ahead and some are in real-time. In the first case, statical information is consider and methods to deal with uncertainties have to be incorporated, while in real-time models the information of power produced and demanded is updated in short periods of time and decisions can be made without unreliability. Traditional optimization methods cannot solve multi-objective systems, so intelligent multi-objective optimization methods are being developed to consider multiple system constraints. At the same time, researchers try to improve the computational viability of the processes.

Although EMSs are configurated according to multiple targets, there are two objectives that stand out as the most important: reducing MG costs and increasing the lifetime of the ESSs. Reducing grid dependency, smoothing the change between grid-connected and islanded modes, lessening the instability and maximising the power coming from RES are less common targets.

This section explains the objectives and the strategies developed so far in the field of MGs management.

2.1 Reducing the Operating Costs

Reducing the MG operating costs is the most common objective when talking about MG management. To reach this goal, multiple variables are considered.

Interaction with the main grid can maximize the profits when the excess of power produced by the MG is sell to the grid. It is usual to charge the ESSs when the power price is low and discharge them when the price rises. So, examining the possible variations in grid-price is one of the most used strategies. Finding the right storage size and location and decreasing the damage in ESSs are also contemplated. While the optimal ESSs' size can ameliorate the operating cost, the insufficient capacity can result in a cost increase of conventional fuel usage. Furthermore, as durability is increasing, it is not necessary an outlay of extra money to change the storage. Some authors have studied the impact of considering meteorological data as well as the repercussions of introducing RES' production estimations and the consumers' requirements in the final costs of the MG. All these questions are exposed in [8], [11]–[22] and the followed schemes and conclusions are presented now.

Fig. 2. Considerations taken by researchers when reducing the operational costs.

Authors address the issue of components durability in [11]. Different ways of managing a hydrogen storage based MG are examined in order to find the cheapest operational mode. The study contemplates the model predictive control (MPC); hysteresis band control strategy (HBCS), which is focused on the state of charge (SoC) of the batteries; equivalent consumption and minimization strategy (ECMS), whose main objective is to minimize the total fuel consumption; and state machine (SM), that controls charging/discharging periods. The results showed that the lowest cost is achieved by applying the HBCS strategy.

Finding the optimal battery energy system size and location is the point in [8], [14], [15]. The authors in [8] presents the modified shuffled frog leaping algorithm (MSFLA) in a day-ahead management strategy and the method is validated in three different scenarios for the SoC of the ESSs, while [14] proposes the Fuzzy Logic Wolf Optimization (FL-FWO) based metaheuristic method. Both strategies show advantages when compared to other optimization methods such as GA and the FL-FWO also reduced the consumption of fossil fuels in the system. Precisely, the GA is used in [15] considering PV power predictions in order to mitigate the effect of DGs intermittence. The simulation showed that the method reduces the cost of the MG as 24% relatively to the scenario in which optimal ESS installation, but no PV forecast were done. It also reduces the cost as 31% relatively to the case in which PV prediction was considered, but no optimal ESS implementation was done and it improves the power profile as 28% relatively to when none of the considerations were bore in mind. Results highlight the importance of choosing the right storage system in all the cases discussed.

Introducing weather forecasts and predictions about produced and consumed energy can optimize the operation of the MG. The effect of these considerations is shown in the following publications [13], [16]. Authors in [13] propose the hybrid economic model predictive control (HEMPC) approach for an islanded MG that can automatically connect to the main grid to sell the renewable energy surplus or to get power when the battery banks are in a lower level than desired. Weather forecasts and system constraints such as minimum disconnection/connection time and maximum connection frequency are contemplated to reach the connection/disconnection regulation from the utility grid. The control algorithm has been tested by simulations considering different meteorological scenarios. On the other side, in [16], a demand-side management (DSM)

formed by three stages is proposed for a grid-connected MG. It is in the first stage where real-time meteorological data is considered. At the end, the Quantum Particle Swarm Optimization is used together with the system constraints to reach the results.

Authors of [12], [22] estimate future loads. In [12], the electricity market price is considered together with the batteries' SoC to control the charging/discharging rate of the ESSs, as well as the power difference between load an RES. The fuzzy logic-based EMS proposed was experimentally validated on a real-world grid-connected MG in the energy storage test bed at Newcastle University, UK, resulting in a reduction of the average peak load and operating cost. To end, non-homogeneous loads in a population of 1000 consumers belonging to different social classes are considered in [22]. Here, authors propose a dynamic clustered community home energy management system (DCCHEMS) in conjunction with PSO to attain minimizing the costs and a flatter power demand. The results show that the costs were reduced by 4%.

Grid-connected MGs can sell power to the main grid when the power price is higher and can buy energy when necessary, obtaining benefits if the correct control strategy is introduced. This exchange is the motivation of the following methods, which consider the variable grid-price to manage the energy resources in the MG [17]–[21]. In [17] an EMS based on a regrouping particle swarm optimization (RegPSO), formulated over a day-ahead scheduling horizon, is developed. The objective function not only considers the quantity of power exchange with the main grid, but also considers the ESSs' characteristics. The RegPSO is compared to the genetic algorithm (GA) and shows better results in less computational time based on a real-world industrial MG in Beijing, China. In [18], it is sought that the fuel and electricity price fluctuations do not impact on the costs of the MG. The objective is minimizing the system levelized cost of energy (LCOE) according to the constraints. The environmental conditions are also considered making the strategy more feasible. In [20], the authors contemplate the costs paid to the main grid and try to minimize them through a two-stage planning framework of the battery ESS and micro-turbine (MT). The model is verified both in grid-connected and islanded mode and, at the same time, computational efficiency is improved. The intelligent controller based on artificial neural network (ANN) designed in [19] has also been validated in the two operational modes of the MG. The studied MG is a residential MG and the assumptions done in the development of the strategy are based on a single person behaviour. In every case, simulations in Matlab/Simulink have proved the validation of the control strategy with an accuracy of 95%, more than other methods to which the comparison is made in the paper. In [21], authors consider the energy cost profile, together with the future load behaviour to develop a MPC strategy which was validated by simulations and by laboratory experiments.

2.2   Ensuring the Optimal Operation of the Energy Storage Systems

ESSs have been shown to be a crucial element of the MGs. They play an essential role in maintaining the frequency and voltage stability when the MG works in the islanded mode [23] and contribute to constantly maintain the balance between energy produced and consumed establishing as a solution to smooth RES power fluctuations, reducing the necessity of conventional resources [24]. For all these reasons, EMSs have

been implemented to increase the lifetime of the ESSs. With an optimal control strategy, not only the lifetime of the ESSs can be extended, but the number of DGs can be decreased.

The ESSs can be damaged for multiple reasons. Rapid power fluctuations [25], overcharging or over discharging [26], grid faults, that destabilize the MG, and intermittence periods of charging and discharging are some of the inconveniences that researchers have to deal with.

Fig. 3. Criteria followed when optimizing the operation of the ESSs

Hence, authors propose multiple solutions. In [26], the energy sharing between the different ESSs in the MG is studied, as well as the SoC of the batteries, which is also analysed in [24], [27]–[29]. Investigators study how to prevent the systems from being overcharged or over discharged. To this aim, the multiple characteristics of each storage equipment (such as capacity, lifecycle, depth of discharge, charging/discharging rates, etc.) have to be considered. As the elevated number of switch ON/OFF leads to premature degradation of the ESSs, the aim of [31], [32] is to reduce the number of start/stop events ensuring the durability of the ESSs.

The SoC of the batteries is the main point in [26], while effective power sharing between the systems is also analysed. A virtual impedance control strategy for an islanded MG with hybrid ESS, consisting in batteries, which provides steady state power, and SCs that supports transient power fluctuations is proposed.

In [24], [27]–[29] authors study the charge/discharge rates of the battery energy storage systems (BESSs). In [24], the simulation based on real-world MG data shows that the proposed EMS can maintain the SoC of the batteries in a good range at any given time and in any situation. Furthermore, as an optimal management of batteries was done, the use of diesel generator was reduced while the lifetime of DGs was increased. In [27], a combined control scheme for the grid-connected ESS is presented. The strategy is composed of two stages: the power control mode for the charging or discharging condition, and the energy control mode for the stand-by condition. By selecting appropriate control parameters, the ESSs can be kept in safe ranges according to frequency limits without human intervention. In [28], the control of the charging/discharging rates is done by the integration of a smart controller for DC/DC converter. The main novelty of this solution is the integration of artificial neural network (ANN) for the estimation of the battery SoC. The stability of the system is ensured in order to reduce the damage caused in ESSs. In [29], Lyapunov

optimisation is used to satisfy the time-coupled constraints. To this end, a variable V algorithm is employed.

The studies [31], [32] show a way to reduce the number of switch ON/OFF. In [32], the study proposes a method in which the FC is operated at maximum efficiency power based on hysteresis band control (HBC) and it has been proved that it reduces the number of switch ON/OFF by 25%. In [31] a MPC methodology with a time horizon of a few seconds is exposed for optimizing the durability of the components in a grid-connected and hydrogen-based MG. As a short time horizon has been implemented, the system responds rapidly to possible disturbances and the model results in a good approach to reality. Both the aging of components and the operational constraints are considered as the method permits operations with high complexity. The MPC and hysteresis band (HB) are compared: the number of start/stop events is reduced by an additional 25% in MPC compared to HB.

2.3   Optimizing the Energy Distribution and Increasing the Production Coming from Renewable Energy Sources

Optimizing the energy distribution can make the MG a more sustainable and less expensive system as the power coming from renewable sources are maximizing. RESs bring great advantages that have been commented previously in this paper; but, due to their intermittence, it is necessary to develop a control strategy to ensure constant energy flow.

Fig. 4. Summary of the considerations made when designing control strategies for optimizing the energy distribution

In this case, the schemes are focused on the most suitable configuration of ESSs, so that RESs production is upgraded, and on the relation between the production costs of different DGs. All these questions are analysed in [33]–[35].

In [33], authors propose a sizing methodology for the RES components with various ESS scenarios with a techno-economic feasibility analysis. The aim is to maximize the RES utility while equating the cost to national tariff. To this end, the authors search the most suitable ESS configuration for a MG consisting in WT and PV. Thus, four scenarios are proposed and studied. The results showed that none of them achieve the target proposed above, so the final objective of the study is maximizing the fraction of RES with lower cost. The paper concludes that the optimal ESS for that MG is a hybrid storage formed by HFC and PHS. Furthermore, in [34] the multi-objective optimization algorithm of the Marine Predators Algorithm (MOEMPA) is proposed in order to

maximize the renewable factor so that emissions and costs are reduced at the same time. Authors proved its efficacy by comparing it to other multi-objective algorithms in the paper. Finally, in [35] the same goals are met by considering the equipment life of DERs, the physical limitations on the individual controllable resources and the frequency in which the MG operates, applying a MPC based optimal coordination (OC) strategy and studying the impact of different time steps in the results.

2.4　Stability of the Microgrid

Control policies to ensure the stability of the MGs are crucial to prevent the DGs from working in undesirable conditions. Thus, the instability of the system can lead to not secure the safe, continuous and maximized power production, so costumers will notice a lack of power and a decline in energy QoS. Furthermore, as DGs can suffer damage, they would have to be replaced increasing the operational costs.
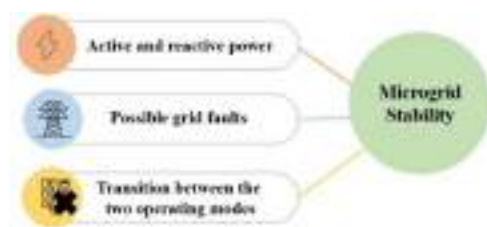
Fig. 5. Scheme that summarizes the objectives sought to ensure the stability of the MG.

Hence, researchers have studied the importance of regulating reactive power resources, such as micro-generators or static var compensator, to avoid voltage fluctuations caused by the intermittence of RESs. There must be control strategies that dispatch active and reactive power of each resource separately. It is sought that the DC link voltage remains constant. To this aim, the grid voltage converters should adjust the produced output power, balancing the required load power. When loads increase, the voltage decreases and control strategies must be developed to ensure the stability in this situation [37], [38]. The stability analysis has to be done in both grid-connected and islanded modes and even when the operating mode changes between them [9]. The instability of the grid-connected MG during grid faults is studied in [39]. Here, voltage faults are considered to be addressed as a priority. RES must be able to produce limited power as overcurrent problems caused by voltage sags can be prevented, but at the same time, their production must be maximized to make RES viable. Likewise, control algorithms must manage DC side voltage to save DGs converters from damage caused by the potential DC voltage increase during faults. Voltage unbalances at the point of common coupling (PCC) are studied in [40]. The destabilized line currents generated by unbalanced loads result in a PCC voltage containing negative-sequence components,

which affect induction motors and power electronic converters, so reliability of the system cannot be insured.

In [37], the online averaging fixed horizon control (AFHC) algorithm is developed to solve the MG energy distribution matter. This algorithm considers some uncertainties in renewable power production and load demands that are in line with the real situation, and makes it a better option in contrast to receding horizon control (RHC), that does not consider the uncertainties in data. The algorithm has been applied to a real-world MG in Heku town (Nantong city, Jianshu province, China). Simulations in Matlab has shown that the online model converges to the offline optimal solution. Thus, the necessity of considering both active and reactive power in MGs' management has been proved. In addition, the results showed that the algorithm achieves the objectives of smoothing the output of diesel power and optimizing energy. And, on the other hand, in [38] a real and reactive power dynamic management strategy is presented for a grid-connected MG, while power-sharing between the elements of the MG is insured. The adaptive fractional fuzzy sliding mode control (AFFSMC) is used to this end.

The transition from grid-connected mode to autonomous mode is smoothing in the control strategy proposed in [9]. Features of ESSs are taken into account to ensure the power flow and stability of the MG. Hence, the real-time MPC is used in this paper for controlling the MG managing power electronic devices including DC-DC converters and grid-connected inverters. The scheme is validated in different actual situations and proved its efficacy at regulating de DC bus voltage during instability periods.

In [39], the author aims to find the correct strategy to control the voltage unbalances during both nominal and faulty grid conditions. The paper presents a novel DC-link voltage stabilization algorithm based on the following conditions: DC-link voltage must be stable and controlled in all working regimes. Two situations are considered: One of them consists in one DC-DC converter and one inverter, while the other consists in multiple DC-DC converters connected to common DC-link. To this aim, a new DC-link voltage control has been developed based on new approaches. The amplitude of the currents injected into the grid is limited to a defined boundary during all regimes and oscillations in active and reactive power are eliminated.

Finally, in [40] authors purpose a novel strategy to mitigate the voltage unbalance at the point of common coupling (PCC) in an islanded MG. The study is based on PCC negative-sequence voltage feedforward. A virtual voltage source is added to the DG terminal at the negative-sequence. Then, the effective impedance between the distributed generation unit and the PCC can be reduced proportionally to the compensation coefficient. The impact of the DG equivalent output impedance is attenuated and the unbalanced voltage droop is compensated.

2.5   Reducing the Main Grid Dependency

The grid dependency is studied in [41], [42]. To this aim, Multi microgrids (MMGs) are being developed to facilitate the interaction between neighbouring MGs, regulating the resources without needing the main grid participation. Other authors try to reduce the energy import from the grid by optimizing the power resources.

A two-stage, day-ahead energy management strategy is proposed in [41]: at the first stage each MG is managed by its own system in a day-ahead strategy considering probabilistic data about DGs output and load demand, and share information with the EMS of the MMG. Then, at the second stage, the EMS coordinates the connected MGs. The proposed method is proved considering four interconnected MGs in four scenarios (different SoC and DGs in each one). It showed that the grid dependency was reduced to zero.

In [42], a day-ahead power management strategy for a Mega-scale grid-connected MGs is proposed in order to minimize the grid power import. The optimization model is solved using the ant colony optimization (ACO)-based metaheuristic approach, which has few parameters to update during the process compared to other methods previously studied. To prove its efficacy, it was applied to a real-world MG in Atlanta, GA, USA.

Fig. 6. Summary of the criteria taken into account to reach the MG independency.

3 Future Trends

Up to this point, some samples of the research carried out so far in the field of MG management have been presented, giving a general idea of the current situation in this field.

In this sense, we can make an estimate of the points on which research will focus attention in the coming years, considering the current reality of the energy market, the climate change and the progress made in recent years.

A brief summary of future objectives is presented below:

- The need to reduce the emission of GHG and other effects related to conventional energy sources served as a motivation to further implement RES in the last decades. Nowadays, fossil fuels are running out, so it is very likely that one of the main objectives will be to implement energy generation systems that come from inexhaustible sources to deal with the energy crisis. In addition, the avenues for studying storage systems are still open in order to put an end to the problem of the intermittence of these sources. In the design of control strategies, both the layout of the systems, and the best combination of sources and storage systems will be studied to achieve efficient systems, relegating conventional sources to the background. One of the technologies that is intended to be developed in the near future is the storage of Power to Gas (P2G), which generates hydrogen

through a hysteresis process from electricity. It would mean reducing costs and increasing capacity compared to conventional systems.

- One of the reasons for developing MG is to be able to work autonomously and researchers will mainly focus on them since they will take on importance in many industries, such as aerospace or marine [43].
- Management systems with short response times will be developed, so that the flow of information is evaluated almost constantly. This provides MGs with more reliability, since no information will be lost. It also helps to reduce potential damage in devices, since data about SoC of the ESSs and about the power produced and consumed is updated all the time and the systems will not work in undesirable circumstances.
- In this regard, researchers will design strategies to protect the data from cyberattacks and possible loss of information.
- Currently, an efficient flow of information is achieved through the installation of numerous sensors. EMSs will also focus on reducing these elements, achieving less complex and faster data transmission. The arrangement of sensors and protection elements of the MG will be studied [44].
- Until now, the mathematical models have been based, in general, on MGs simulations and, furthermore, they are operationally complex, obtaining with them results that do not sufficiently adjust to reality and that entail a great deal of computing time.

In short, the expectations for the future involve achieving the autonomous functionality of MGs through the small objectives discussed in this section. Another of the great goals will be to greatly increase the installed power from renewable energies.

For all this, research to design new security, storage, energy production and information transmission systems has been key up to now and will continue to be so in the coming years. The joint work of this part of the scientific community with those who study the most appropriate management systems in each case allows progress to be made in the development of MGs and smart grids, which have already established themselves as important systems in the field of energy.

4   Conclusions

An MG is a set of interconnected loads, generators and storage systems whose ultimate goal is to provide quality energy to consumers. Their characteristics have motivated their integration as environmentally friendly systems that, moreover, can be installed in remote areas and have proven to be useful in many sectors and industries.

But the fact that they are made up of so many different resources and the need to coordinate information between these systems, consumers and other external variables, constitutes a challenge for researchers.

Precisely, the main challenge of these systems is to develop energy management systems that meet the various needs in each case.

This paper attempted to provide a review of the state of the art in microgrids management. Considering MGs conformed by different DGs and ESSs, and meeting multiple objectives. The motivations that lead to study each case and the solutions proposed so far are presented. Although reducing operating costs and damage in ESSs are the most common goals within the scientific community, other targets such as maintaining the MG stability, maximizing the RES production and lessening the grid dependency have been also studied.

For all these objectives, different control strategies that meet multiple criteria have been successfully developed. When reducing de operational costs of the MG, authors consider the interaction between the MG and the main grid; the durability, size and location of the components, and meteorological data. The control strategies developed to reduce the damage in the ESSs focus on the specific characteristics of each system in order to maintain the optimal SoC and they also try to reduce the number of start/stop events when charging the batteries. The most suitable configuration of the resources is studied to optimize the energy distribution. On the other hand, researchers have paid attention to both active and reactive power when developing the EMS to insure the stability of the MG. Smoothing the change within grid-connected and islanded modes, and controlling the DC link voltage as it remains constant are the objectives in which researchers have focused on in this case. Finally, to reduce the grid dependency, MMGs are being studied and the optimization of energy production is indispensable to this aim.

The description of the strategies has been developed in the article and comparisons and relationships between some of them have been established.

To finish giving an overview of the issue, an estimate of future research has been made in the last section. Given the current climatic circumstances and the progress made so far in the study of MGs, it is expected that efforts will be made to achieve the autonomy of the systems and the implementation of clean energy sources. To do this, MG stability and resource security must be prioritized through better information flow, more effective sensor systems, more reliable weather forecasts, and other resources that are taken into account in the developing of future control strategies.

All of this will improve the working conditions of these systems that intend to be installed more and more all over the world, having demonstrated their qualities in recent years.

References

1. K. Abbasi, Z. Jiao, M. Shahbaz, and A. Khan, "Asymmetric impact of renewable and non-renewable energy on economic growth in Pakistan: New evidence from a nonlinear analysis," *Energy Exploration & Exploitation*, vol. 2020, no. 5, pp. 1946–1967, doi: 10.1177/0144598720946496.
2. A. Kwilinski and A. Kwilinski, "Mechanism of formation of industrial enterprise development strategy in the information economy," *Virtual Economics*, vol. 1, no. 1, pp. 7–25, Oct. 2018, doi: 10.34021/VE.2018.01.01(1).
3. Y. Zahraoui *et al.*, "sustainability Energy Management System in Microgrids: A Comprehensive Review," 2021, doi: 10.3390/su131910492.

4. A. Lavrik, E. Iakovleva, and A. Leskov, "Assessing the Solar Power Plant Efficiency Degradation Resulting from Heating," *Journal of Ecological Engineering*, vol. 19, no. 3, pp. 115–119, May 2018, doi: 10.12911/22998993/86149.

5. "doi:10.1016/j.tej.2012.09.013", doi: 10.1016/j.tej.2012.09.013.

6. S. Parhizi, H. Lotfi, A. Khodaei, S. Bahramirad, and A. Khodaei, "State of the Art in Research on Microgrids: A Review", doi: 10.1109/ACCESS.2015.2443119.

7. M. Farrokhabadi *et al.*, "Microgrid Stability Definitions, Analysis, and Examples IEEE PES Task Force on Microgrid Stability Definitions, Analysis, and Modeling," *IEEE TRANSACTIONS ON POWER SYSTEMS*, vol. 35, no. 1, p. 13, 2020, doi: 10.1109/TPWRS.2019.2925703.

8. N. Vu Quynh, | Ziad, M. Ali, M. M. Alhaider, A. Rezvani, and K. Suzuki, "Optimal energy management strategy for a renewable-based microgrid considering sizing of battery energy storage with control policies," 2020, doi: 10.1002/er.6198.

9. K. Kumar and S. Bae, "Dynamic power management based on model predictive control for hybrid-energy-storage-based grid-connected microgrids," *Electrical Power and Energy Systems*, vol. 143, p. 108384, 2022, doi: 10.1016/j.ijepes.2022.108384.

10. L. Meng, E. R. Sanseverino, A. Luna, T. Dragicevic, J. C. Vasquez, and J. M. Guerrero, "Microgrid supervisory controllers and energy management systems: A literature review," 2016, doi: 10.1016/j.rser.2016.03.003.

11. K. Kumar, M. Alam, V. Dutta, and (K Kumar, "Energy management strategy for integration of fuel cell-electrolyzer technologies in microgrid," 2021, doi: 10.1016/j.ijhydene.2021.07.203.

12. T. Teck Teo *et al.*, "Optimization of Fuzzy Energy-Management System for Grid-Connected Microgrid Using NSGA-II," *IEEE Trans Cybern*, vol. 51, no. 11, p. 5375, 2021, doi: 10.1109/TCYB.2020.3031109.

13. D. P. E. Silva, J. L. Félix Salles, J. F. Fardin, and M. M. Rocha Pereira, "Management of an island and grid-connected microgrid using hybrid economic model predictive control with weather data," 2020, doi: 10.1016/j.apenergy.2020.115581.

14. K. S. El-Bidairi, H. D. Nguyen, S. D. G. Jayasinghe;, and T. S. Mahmoud, *Multiobjective Intelligent Energy Management Optimization for Grid-Connected Microgrids; Multiobjective Intelligent Energy Management Optimization for Grid-Connected Microgrids*. 2018.

15. S. Rajamand, M. Shafie-khah, and J. P. S. Catalão, "Energy storage systems implementation and photovoltaic output prediction for cost minimization of a Microgrid," *Electric Power Systems Research*, vol. 202, Jan. 2022, doi: 10.1016/J.EPSR.2021.107596.

16. R. Seshu Kumar, L. P. Raghav, D. Koteswara Raju, and A. R. Singh, "Intelligent demand side management for optimal energy scheduling of grid connected microgrids," 2021, doi: 10.1016/j.apenergy.2021.116435.

17. A. T. Eseye, J. Zhang, D. Zheng, and H. Li, "Grid-price Dependent Optimal Energy Storage Management Strategy for Grid-connected Industrial Microgrids," *2017 Ninth Annual IEEE Green Technologies Conference (GreenTech)*, 2017, doi: 10.1109/GreenTech.2017.24.

18. J. Jiang *et al.*, "Optimal sizing, operation strategy and case study of a grid-connected solid oxide fuel cell microgrid," 2021, doi: 10.1016/j.apenergy.2021.118214.

19. H. Vaikund and S. S.g., "Cost mitigation strategy for microgrid using an advanced energy management system with an intelligent controller," *Electric Power Systems Research*, vol. 210, p. 108116, 2022, doi: 10.1016/j.epsr.2022.108116.

20. J. Qiu, J. Zhao, Y. Zheng, Z. Dong, and Z. Yang Dong, "Optimal allocation of BESS and MT in a microgrid; Optimal allocation of BESS and MT in a microgrid," *IET Gener. Transm. Distrib*, vol. 12, no. 9, pp. 1988–1997, 2018, doi: 10.1049/iet-gtd.2017.0717.

21. A. M. Mahfuz-Ur-Rahman, S. Member, M. Rabiul Islam, S. Member, K. M. Muttaqi, and D. Sutanto, "An Effective Energy Management With Advanced Converter and Control for a PV-Battery Storage Based Microgrid to Improve Energy Resiliency; An Effective Energy Management With Advanced Converter and Control for a PV-Battery Storage Based Microgrid to Improve Energy Resiliency," *IEEE Trans Ind Appl*, vol. 57, no. 6, p. 6659, 2021, doi: 10.1109/TIA.2021.3115085.

22. A. Abbasi *et al.*, "A Novel Dynamic Appliance Clustering Scheme in a Community Home Energy Management System for Improved Stability and Resiliency of Microgrids", doi: 10.1109/ACCESS.2021.3119538.

23. Y. Karimi, H. Oraee, M. S. Golsorkhi, and J. M. Guerrero, "Decentralized Method for Load Sharing and Power Management in a PV/Battery Hybrid Source Islanded Microgrid," *IEEE Trans Power Electron*, vol. 32, no. 5, p. 3525, 2017, doi: 10.1109/TPEL.2016.2582837.

24. K. Thirugnanam *et al.*, "Energy Management for Renewable Microgrid in Reducing Diesel Generators Usage With Multiple Types of Battery; Energy Management for Renewable Microgrid in Reducing Diesel Generators Usage With Multiple Types of Battery," *IEEE Transactions on Industrial Electronics*, vol. 65, no. 8, 2018, doi: 10.1109/TIE.2018.2795585.

25. R. A. Dougal, S. Liu, and R. E. White, "Power and Life Extension of Battery-Ultracapacitor Hybrids," 2002. doi: 10.1109/6144.991184.

26. W. Sufang, S. Wang, G. Liu, R. Liu, and S. Wen, "Energy Management and Coordinated Control Strategy of PV/HESS AC Microgrid During Islanded Operation", doi: 10.1109/ACCESS.2018.2887114.

27. M. Guan, "Scheduled Power Control and Autonomous Energy Control of Grid-Connected Energy Storage System (ESS) with Virtual Synchronous Generator and Primary Frequency Regulation Capabilities," *IEEE Transactions on Power Systems*, vol. 37, no. 2, pp. 942–954, Mar. 2022, doi: 10.1109/TPWRS.2021.3105940.

28. Y. Boujoudar, M. Azeroual, H. Elmoussaoui, and T. Lamhamdi, "Intelligent control of battery energy storage for microgrid energy management using ANN," *International Journal of Electrical and Computer Engineering (IJECE)*, vol. 11, no. 4, pp. 2760–2767, 2021, doi: 10.11591/ijece.v11i4.pp2760-2767.

29. S. Zeinal-Kheiri, S. Ghassem-Zadeh, A. M. Shotorbani, and B. Mohammadi-Ivatloo, "IET Renewable Power Generation Real-time energy management in a microgrid with renewable generation, energy storages, flexible loads and combined heat and power units using Lyapunov optimisation," 2019, doi: 10.1049/iet-rpg.2019.0297.

30. M. H. Nazari, M. Bagheri-Sanjareh, and S. H. Hosseinian, "A new method for energy management of residential microgrid for sizing electrical and thermal storage systems," 2021, doi: 10.1016/j.scs.2021.103482.

31. L. Valverde, C. Bordons, and F. Rosa, "Integration of Fuel Cell Technologies in Renewable-Energy-Based Microgrids Optimizing Operational Costs and Durability; Integration of Fuel Cell Technologies in Renewable-Energy-Based Microgrids Optimizing Operational

Costs and Durability," *IEEE TRANSACTIONS ON INDUSTRIAL ELECTRONICS*, vol. 63, no. 1, 2016, doi: 10.1109/TIE.2015.2465355.

32. K. Kumar, M. Alam, S. Verma, and V. Dutta, "Effect of hysteresis band control strategy on energy efficiency and durability of solar-hydrogen storage based microgrid in partial cloudy condition," 2020, doi: 10.1016/j.est.2020.101936.

33. L. Al-Ghussain, R. Samu, O. Taylan, and M. Fahrioglu, "Sizing renewable energy systems with energy storage systems in microgrids for maximum cost-efficient utilization of renewable energy resources," 2020, doi: 10.1016/j.scs.2020.102059.

34. D. Yousri *et al.*, "Managing the exchange of energy between microgrid elements based on multi-objective enhanced marine predators algorithm," *Engineering Journal*, pp. 8487–8505, 2022, doi: 10.1016/j.aej.2022.02.008.

35. E. Mayhorn, L. Xie, and K. Butler-Purry, "Multi-Time Scale Coordination of Distributed Energy Resources in Isolated Power Systems," *IEEE Trans Smart Grid*, vol. 8, no. 2, 2017, doi: 10.1109/TSG.2016.2547342.

36. M. Savaghebi, A. Jalilian, J. C. Vasquez, and J. M. Guerrero, "Autonomous Voltage Unbalance Compensation in an Islanded Droop-Controlled Microgrid," *IEEE TRANSACTIONS ON INDUSTRIAL ELECTRONICS*, vol. 60, no. 4, 2013, doi: 10.1109/TIE.2012.2185914.

37. H. Zou *et al.*, "Online Energy Management in Microgids Considering Reactive Power; Online Energy Management in Microgids Considering Reactive Power," *IEEE Internet Things J*, vol. 6, no. 2, 2019, doi: 10.1109/JIOT.2018.2876245.

38. R. Sedaghati and M. R. Shakarami, "A novel control strategy and power management of hybrid PV/FC/SC/ battery renewable power system-based grid-connected microgrid," 2018, doi: 10.1016/j.scs.2018.11.014.

39. I. Isakov and I. Todorovic, "Power production strategies for two-stage PV systems during grid faults," *Solar Energy*, vol. 221, pp. 30–45, 2021, doi: 10.1016/j.solener.2021.03.085.

40. J. Luo, N. Haiji Wang, and N. Liyuan Liu, "Paper Adaptive Voltage Unbalance Compensation Based Control Strategy for Islanded Microgrid," *IEEJ Trans*, vol. 16, pp. 1470–1478, 2021, doi: 10.1002/tee.23450.

41. S. Iqbal and K. Mehran, "A Day-Ahead Energy Management for Multi MicroGrid System to Optimize the Energy Storage Charge and Grid Dependency-A Comparative Analysis," 2022, doi: 10.3390/en15114062.

42. H. Wu, H. Li, and X. Gu, "Optimal Energy Management for Microgrids Considering Uncertainties in Renewable Energy Generation and Load Demand", doi: 10.3390/pr8091086.

43. J. Maurilio Raya-Armenta, N. Bazmohammadi, J. Gabriel Avina-Cervantes, D. Sáez, J. C. Vasquez, and J. M. Guerrero, "Energy management system optimization in islanded microgrids: An overview and future trends," 2021, doi: 10.1016/j.rser.2021.111327.

44. O. Ouramdane, E. Elbouchikhi, Y. Amirat, and E. S. Gooya, "Optimal Sizing and Energy Management of Microgrids with Vehicle-to-Grid Technology: A Critical Review and Future Trends," 2021, doi: 10.3390/en14144166.

IoT platform for monitoring nutritional and weather conditions of avocado production

Pedro Moreno-Bernal[1][0000−0002−2811−5331], Paris Arizmendi-Peralta[2],
J. Alberto Hernández-Aguilar[2][0000−0002−5184−0005],
Sergio Nesmachnow[3][0000−0002−8146−4012],
J. del Carmen Peralta-Abarca[1][0000−0003−2995−9277], and
J. Guadalupe Velásquez-Aguilar[1][0000−0002−5708−5688]

[1] Facultad de Ciencias Químicas e Ingeniería,
Universidad Autónoma del Estado de Morelos, México
{pmoreno, carmen.peralta, jose_hernandez, jgpeva}@uaem.mx
[2] Facultad de Contaduría, Administración e Informática,
Universidad Autónoma del Estado de Morelos, México
paul.arizmendi@uaem.edu.mx
[3] Universidad de la República, Uruguay
sergion@fing.edu.uy

Abstract. Agricultural productivity is crucial to supply the current food demand. However, food production requires facing technological challenges to achieve the level of demand production. In this context, Internet of Things technology is used for efficient farming processes. This article proposes an Internet of Things platform for collecting and processing soil nutrients and weather data of crop avocados in an orchard. Data were collected every 300 seconds for 24-hour monitoring of the avocado trees. Experimental validation recorded 8 832 data for monitoring soil nutrients and weather variables of an avocado orchard in the Northeast of Morelos, Mexico. Results demonstrate that the proposed IoT platform can effectively monitor agriculture information in the context of smart farming.

Keywords: Smart farming, avocado production, Internet of Things

1　Introduction

The world population is growing with considerable acceleration, i.e., it is expected to increase from 7.7 billion in 2020 to 9.7 billion people in 2050 [21]. The demographic growth implies an increase in food consumption in the following years. Therefore, food consumption will demand an increment in agricultural productivity. Food productivity requires technological challenges to achieve the level of production needed to satisfy the predicted world food demand [8]. However, excessive crop production implies a deterioration of soil by chemical nutrients and pesticides, water dearth, terrain deforestation, greenhouse gas emissions producing scarceness of natural resources and contamination.

Recently, the Industry 4.0 revolution has extended as an integral part of social and technological changes under the paradigm of smart cities [15,22]. In this context, agriculture must provide practical solutions to benefit food consumption demand by incorporating technology based on Industry 4.0. in a sustainable manner. Sustainable agriculture refers to the cycle of producing, harvesting, and distributing all related to farming without waste. Today, agriculture uses advanced technology to increase productivity by optimizing resources in a controlled and measurable way[1]. This way, smart farming combines sustainable agriculture and the Information and Communication Technologies [14]. In particular, the Internet of Things (IoT) and sensor technology are vital for increasing productivity in smart farming. IoT technologies permit the migration from traditional agriculture to smart farming, i.e., automatization, control systems, supervision, and monitoring of farming performance. Furthermore, the combination of IoT with artificial intelligence and big data approaches helps estimating future production and increase crop productivity for immediate human needs [7].

This article proposes an IoT platform for collecting and processing data of soil nutrients and weather conditions in the context of smart farming. The proposed approach applies the Message Queue Telemetry Transport (MQTT) protocol-based smart farming solution to send data of soil nutrients and weather variables from an orchard of avocado trees to a cloud MQTT server by an IoT device. Furthermore, a specific design of the proposed IoT platform is presented for monitoring avocado tree nutrients using soil NPK RS485 sensors and Arduino Mega 2560 microcontroller hardware. The proposed IoT platform sends data to a remote MQTT server through 4G LTE band support using a GSM/GPRS module (SIM808) hardware. Experimental evaluation is performed by collecting data every 300 seconds for 24-hour monitoring. Results demonstrate that the proposed IoT platform can monitor farming information in the considered scenario in the Northeast of the State of Morelos, Mexico.

The article is structured as follows. Section 2 describes the application of IoT in agriculture and smart farming. Section 3 describes the proposed IoT platform for the studied orchard of avocado trees. Section 4 reports and discusses the evaluation results. Finally, Section 5 presents the conclusions and formulates the main lines for future work.

2　Agriculture and smart farming

This section describes agriculture production and the model of smart farming. The section also reviews the related works about relevant technologies applied in the context of smart farming.

2.1　Agriculture production

Food production and supply systems are categorized into primary agriculture, i.e., cropping, livestock, horticulture, and fisheries; food processing and packing; commerce and transportation; and household consumption [16]. Nevertheless,

food production depends on the sustainability of farming production systems and natural resources. This way, agricultural production includes all farming operations from land preparation to land development, e.g., tillage, sowing, fertilizing, pest control, and harvest, continuing with transportation and trade. However, increasing agricultural production involves land wear by the excessive application of agrochemicals, e.g., fertilizers, soil ameliorants, and pesticides [10]. In this sense, automatization and technological control systems based on IoT, computational intelligence, and sensors are necessary to improve and optimize agricultural production and supply procedures. Post-hoc optimization methods take advantage of data collected using IoT and sensors, to design improved plans to assist production [6,5]

2.2　Smart farming

Smart farming applies computational intelligence, Information and Communication Technologies, and sensor technologies to agriculture. The most relevant technologies applied in smart farming involve satellite and aerial imagery, agricultural robots, IoT devices with sensor nodes, and Unmanned Aerial Vehicles [4,9]. As a result, smart farming scales agricultural production, reducing the workforce and enabling overcoming challenges in food production demands [12]. Technological resources in farms are applied in the diverse phases of the production process, i.e., nutrient and soil monitoring, growing plants monitoring, irrigation, fertilizer, pest control, and harvesting. This way, relevant data to collect are soil nutrients, soil PH, electrical conductivity, temperature, luminosity, moisture, and pressure for better farm production management. Essentially, the main objective of smart farming is to reduce agricultural cost production, minimizing crop waste while still maintaining end product quality.

2.3　Related Works

Producers, governments, and academia are exploring innovative manners to increase farming production. Recent related works propose different methodologies using IoT technologies for efficient farming processes. A brief review of related works is presented next.

Gomes et al. [3] proposed a system to gather data from the soil probe using an IoT platform for farm water management. The IoT device collected data and displayed information in a dashboard monitoring. Several sensor nodes were connected to the IoT platform, including the temperature and humidity DHT22 sensor, ambient light BH1750 sensor, geospatial position Venus GPS device, the ground temperature DS18B20 sensor, and the soil moisture CSMv1.2 sensor. A Raspberry Pi-2 module received signals from sensor nodes through the I2C interface and GPIO serial bus. Cloud Applications used were Fiware IoT, Fiware Orion, MongoDB, Draco, MySQL, and Grafana. Results showed that the IoT platform analyzed data in the cloud. Then, processed data were sent as input in a physical system based on a Programmable Logic Controller for the irrigation system, decreasing the impact on water management.

Serikul et al. [17] proposed a smart capsule prototype to monitor humidity in paddy bags stored on a warehouse. The prototype used an ESP8266 microcontroller and an SHT21 humidity sensor. Data collected was sent to a Blynk server through a Wi-Fi network and a mobile application. The investment in the hardware prototype was 300 USD. Results showed effective monitoring of humidity at each smart capsule in real-time. Smart capsules application was suitable for humidity controlling in paddy bags helping to prevent excessive humidity.

Trilles et al. [20] proposed an IoT platform for monitoring wine production in a smart farming context. The studied IoT platform was evaluated for scalability, stability, interoperability, and reusability. Computer paradigms used were microservices and serverless computing. The technological architecture proposed (SEnviro Connect) was validated for wine production in Spain. Experimental results showed that concerning scalability, the microservices architecture evaluated requires only a single server to ensure scalability and stability with 0% losses of throughput rates upper than 2400 msg/sec. The CPU and memory consumption were lower and stable. The proposed architecture based on Docker containers offered horizontal scalability and reusability. Platform validation was carried out over 140 days during vineyard season in 2018, monitoring five *SEnviro* nodes.

Ahmed et al. [2] proposed an IoT-based control system for advancement in the agriculture and farming of rural areas. The proposed architecture connected rural farms using IoT of low cost. The architecture combined one WiLD network and a set of 6LoWPAN to enable Wireless Sensor Network (WSN). The 6LoWPAN-based wireless sensor and actuator network were used in the farm domain for sensing and actuating multiple operations. The performance of the proposed approach was analyzed in two phases. First, the individual performance of the proposed WSN and WiLD network were studied, and second, the performance of the overall framework using results achieved in the first phase was evaluated. The cross-layer-based MAC and routing solution for IoT achieved better energy, delay, and throughput performance. The proposed solution, combined with the WiLD network, reduced delay and improved throughput performance for end-mile connectivity concerning connected rural farms by IoT devices.

Muangprathub et al., [11] proposed the design and development of a control system based on WSN to manage crops grown by monitoring data via smartphone and a web application. The proposed control system included IoT hardware, a web application, and a mobile application. An IoT hardware device was used as a control box connected to WSN to collect data on the crop. Soil moisture sensors were used to monitor the field. The web application was designed and implemented to analyze the details of crop data, i.e., temperature, humidity, and soil moisture. The control of crop watering was managed through a smartphone application. The control crop system was implemented and tested in Makhamtia District, Thailand. The results showed that the appropriate temperature for increased productivity of homegrown vegetables and lemons was between 29 °C and 32 °C. Moreover, suitable humidity for high productivity of lemons was within 72–81%. Also, the soil moisture content was maintained appropriately for vegetable growth, reducing costs and increasing agricultural productivity.

Suhag et al. [19] proposed a framework for IoT-based soil nutrition. The proposed approach used several sensors to collect plant-related data through the proximal soil sensor. Data collected were sent by the IoT device to a mobile application. The hardware component was included in polyhouse farming. Results showed that the appropriate temperature for increased productivity of sugar cane was between 20 °C and 35 °C, for rice was between 15 °C and 25 °C, and for wheat between 11 °C and 25 °C.

The related works allowed identifying a growing interest in IoT-based platforms for increasing agriculture productivity in the context of smart farming. In this line of work, this article contributes to smart farming with an IoT platform for monitoring soil nutrients and weather conditions for avocado production in the Northeast of the state of Morelos, Mexico. Next section describes the implementation of the proposed IoT platform to monitor soil nutrients and weather conditions is described.

3   IoT platform for monitoring avocado production

This section describes the proposed IoT platform for monitoring avocado production.

3.1   Internet of Things

The IoT paradigm has developed as an essential component of the transformative era of technological changes in smart and rural cities. IoT is defined as the interaction of the physical and digital worlds through various sensors and actuators [23]. IoT is a paradigm of embedded computing and networking capabilities in any conceivable object with capacities to modify its state [13]. In this context, IoT refers to devices and appliances connected to a network collaboratively to execute a task with high intelligence through embedded sensors, actuators, processors, and transceivers [18].

The basic architecture for IoT considers three layers: perception layer, network layer, and application layer. However, additional layers are required to properly consider all the aspects involved in realistic and research applications [18]. The five-layer architecture includes additional layers: the network layer is separated into transport and processing layers, and a new business layer is included to manage the deployed the IoT platform. The five layers are:

1. *Perception Layer.* The perception layer is the physical layer, and it provides the function of converting analog signals into digital form and vice versa. In addition, this layer is responsible for sensing and gathering information about the environment through sensors and actuators. Sensors are used to detect environmental changes by physical parameters such as humidity or temperature to transform them into electric signals. Actuators allow the transforming of an electrical signal into physical actions through a machine or device.

2. *Transport Layer.* The transport layer is responsible for transport communications between smart components of the IoT network, including network devices and computers. This layer transmits sensor data collected from the perception layer to the processing layer through wireless sensor networks such as 3G/4G/5G, LAN, Bluetooth, RFID, and NFC.

3. *Processing Layer.* The processing layer stores, analyses, and processes a large volume of data from the transport layer. Technologies used in the processing layer are cloud computing, distributed computing, databases, and big data.

4. *Application Layer.* The application layer provides services to the end-user. IoT applications are deployed in smart cities, smart homes, smart health, and smart farming.

5. *Business Layer.* The business layer manages service applications based on IoT through business and profit models.

3.2 The proposed IoT platform for monitoring crop avocado information

Overall structure of the system. Based on the first three layers of the five layer architecture for IoT, the proposed IoT architecture is divided into three stages. The first stage corresponds to collecting data from soil nutrient sensors and weather conditions through the IoT device as a monitoring station. The collected information contains the following data: date/hour, soil temperature, area temperature, soil moisture, lumens, nitrogen (N), phosphorus (P), and potassium (K) of two avocado trees. One avocado tree is fertilized, and the other consumes natural soil nutrients. The second stage sends information collected from the IoT device every 300 seconds to an MQTT server. A local storage device is used to record data as backup. In the last stage, data cleaning is performed using a Python script for future analysis.

Hardware components. The hardware components of the proposed IoT platform include:

- *Main board*: Arduino MEGA 2560 board (voltage: 5V)
- *4G LTE Network*: GSM/GPRS/SIM808 module (voltage: 3.4V∼4.4V)
- *Soil nutrients*: Soil NPK generic sensor (voltage: 12V)
- *Communication* RS-485 to TTL module (voltage: 3.4V∼4.4V)
- *Temperature sensor*: DS18B20 (voltage: 3V∼5.5V)
- *Soil moisture*: HD–38 sensor (voltage: 3.3V∼12V)
- *Lumens*: Photoresistor sensor (voltage: 5V)

All these components are integrated in an easy-to-deploy platform, adapted to be used in any agricultural facility. The proposed IoT platform is energy efficient: the estimated overall power consumption of the deployed infrastructure is just ∼365mA (0.0438kWh). The overall cost of the built platform is approximately 250 USD.

Software components. The proposed IoT platform for monitoring crop avocado information is implemented using MQTT and Arduino libraries. The MQTT broker is available by a Mosquitto server on a cloud host with a public IP address. The main function of the MQTT broker is filtering incoming messages from the IoT device client into the MQTT topic `huitzilac`. Then, a Python script is executed to save data in a CSV file on a local storage disk. Once the data are saved, a data cleansing process is performed to process the gathered data, in order to verify the coherency and redundancy of the stored information, for future analysis.

Fig. 1 describes the proposed IoT architecture for monitoring the nutrients and weather conditions of avocado production. The main hardware components and software products are identified.
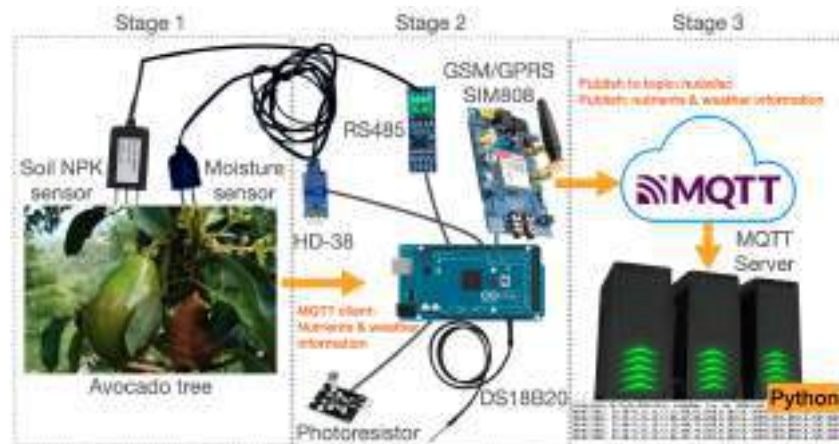
Fig. 1: Diagram of the proposed IoT platform for monitoring crop avocado information

Fig. 2 presents photographs of the real deployment (in production) of the proposed IoT platform for monitoring crop avocado information in Huitzilac, Morelos. The photograph in Fig. 2(a) shows the Soil NPK sensor in one of the avocado trees being monitored. The photograph in Fig. 2(b) presents the IoT device. The photograph in Fig. 2(c) shows the metal shield protection of the IoT device placed on the avocado orchard. Finally, the photograph in Fig. 2(d) shows the Soil NPK sensor wrapped into a plastic shield to protect it from rodents and external factors. The deployed IoT platform allowed gathering relevant data about the avocado crop.

The proposed IoT platform aims to collect and generate a database of avocado crops comparing nutrients by fertilization and without fertilization to study machine learning techniques to predict avocado production.

(a) Avocado tree with Soil NPK sensor   (b) IoT device

(c) Shield protection of the IoT device   (d) Soil NPK sensor

Fig. 2: IoT platform for monitoring crop avocado information

The following section analyzes the experimental results of the proposed IoT platform for monitoring avocado information.

4 Experimental validation and discussion

This section describes the experimental validation of the proposed IoT platform and the specific data processing methods. The main results from the collected information are reported and discussed.

4.1   Development and execution platform

The control and processing software of the IoT device was coded in Arduino employing TinyGSMClient, PubSubClient, ArduinoRS485, ThreeWire, RtcDS1302, OneWire, DallasTemperature, Wire, SPI, and SD libraries.

The experimental evaluation was performed using an Intel Xeon E5-2650 (16 cores, 32 threads) processor at 2.0 GHz, 32 GB of RAM, and the Debian 4.19 Linux operating system.

4.2   Studied area

The area considered for the case study is described next.

The avocado orchard "La Ceiba" is located in the municipality of Huitzilac, in the Northeast of the state of Morelos, México (UTM coordinates 19.008174,-99.268800).

The terrain has an altitude of 2 273 MSL. The weather has an average temperature between 14 °C and 22 °C throughout the year. The avocado orchard is divided into four zones, and the zone in production was used for the validation of the proposed IoT platform.

The production zone contains ten-year-old avocado trees. The other zones have young trees without production. The study area is fertilized every four months. This way, two avocado trees are studied through the soil nutrients. One avocado tree is fertilized with an average of 21.77 grams per tree (g/t) of N, 4.7 g/t of P, and 39.16 g/t of K. The other avocado tree studied is not fertilized.

Fig. 3 shows the geographic location of the avocado orchard studied. The image was taken from Google Earth, and used only for academic purposes, according to the "fair use" copyright.

Fig. 3: Geographic location of the avocado orchard

For the case study presented in this article, the proposed IoT platform for monitoring crop avocado information was set to collect, process, and store soil nutrients and weather data every 300 seconds during 58 days, from August 05 to September 30, 2022.

4.3   Data cleaning process

The cleaning process prepares the data gathered by the proposed IoT device for analysis by removing or modifying erroneous records.

Raw data are emitted by the Arduino control program of the IoT device. These data are an ASCII-encoded, stored in a file, with fields delimited by commas (CSV format). Data cleaning involves identifying duplicate data, correcting spelling and syntax errors, and correcting empty fields and negative or null values. Data errors occur when the IoT device has a power supply interruption by an external factor in the rural area or when environmental conditions affect the sensors producing a piece of erroneous lecture information. Fig. 4 shows collected data by the IoT device in raw format.

Fig. 4: Data in raw format

Then, the data cleaning process verifies the coherence and redundancy of data. Several options for actions are performed if there is missing data, e.g., normalize by scaling to a range by approximating upper and lower bounds on data or approximate uniformly in a range. The previous data can be copied if there is no considerable variation in values. The missing value can be omitted, but having different information for subsequent models is preferable. Fig. 5 shows the data after the cleaning process.

4.4   Results and discussion

This subsection presents and discusses the results of the proposed IoT platform for monitoring crop avocados. Fig. 6 shows the information collected and sent to the cloud by the IoT device. The notification of data stored locally in a

Fig. 5: Data after cleaning process

storage device is presented in Fig. 6a. In turn, Fig. 6b shows the notification of information sent through the data network received by the MQTT server.

(a) Data stored locally

(b) Data received by MQTT server

Fig. 6: Information collected by the IoT device

The IoT device for monitoring crop avocado trees collects data on soil temperature, weather temperature, soil moisture, and lumens. Also, it collects the soil NPK data of two avocado trees. Table 1 reports the maximum, minimum, and average values of data collected by the IoT platform. The average soil temperature value was 15.57°C, and the weather temperature was 14.57°C, considering an average temperature in the zone between 14°C and 22°C during the year, helping maintain healthy roots and flowering. The average soil moisture value was 75% (scale from 0 to 100) during the rainy season. The average amount

of visible light collected by a photoresistor sensor was 980 lumens during the rainy season. From the two monitoring avocado trees, the average N value of the fertilized tree (Sensor A) was 18405 mg/kg compared with the non-fertilized tree (Sensor B), which had an average value of 129 mg/kg. The average K value for sensor A was 14394 mg/kg compared with sensor B was 2150 mg/kg. Finally, the average P value for both sensors was 8694 mg/kg.

Table 1: Maximum, minimum and average values of data collected by the IoT platform

#	Variable	minimum	Maximum	average
1	Soil temperature	12.88 °C	17.69 °C	15.57 °C
2	Weather temperature	8.63 °C	20 °C	14.69 °C
3	Soil moisture	21%	100%	75%
4	Lumens	0	25 550	980
5	N sensor A	26 870 mg/kg	28 673 mg/kg	18 405 mg/kg
6	K sensor A	6 535 mg/kg	28 744 mg/kg	14 394 mg/kg
7	P sensor A	8 659 mg/kg	8 703 mg/kg	8 694 mg/kg
8	N sensor B	0 mg/kg	159 mg/kg	129 mg/kg
9	K sensor B	2 050 mg/kg	2 587 mg/kg	2 150 mg/kg
10	P sensor B	8 659 mg/kg	8 703 mg/kg	8 694 mg/kg

The graphics in Fig. 7 show the maximum, minimum, and average values of soil temperature, weather temperature, soil moisture, lumens, and soil nutrients of two avocado trees.

Regarding soil temperature and weather temperature, both showed a steady behavior. The average value was 15 °C for both temperatures. Soil moisture sensors returned raw values that must be appropriately calibrated by establishing a range for dry and wet values. The Arduino-based soil moisture sensor ranges from 0 to 1023; therefore, collected data were converted into a percentage output, to get values from 0 to 100. Fig. 7c shows the normalized values for soil moisture behavior. The graphic reporting lumens shows an incorrect behavior during two days, when the photoresistor sensor did not collect data. Finally, Fig. 7e shows the differences in the behavior of NPK nutrients for sensor A (SA) and sensor B (SB). The average N value for sensor B represents 0.7% of the average N value of sensor A, and the average K value for sensor B represents 14.9% of the average of nutrient K for sensor A. However, both sensors have the same average value for the nutrient P; probably due to the properties of the soil in the studied area.

Summarizing, the experimental validation results demonstrate that the information collected by the proposed IoT platform was coherent and valid for

(a) Soil temperature

(b) Weather temperature

(c) Soil moisture

(d) Lumens
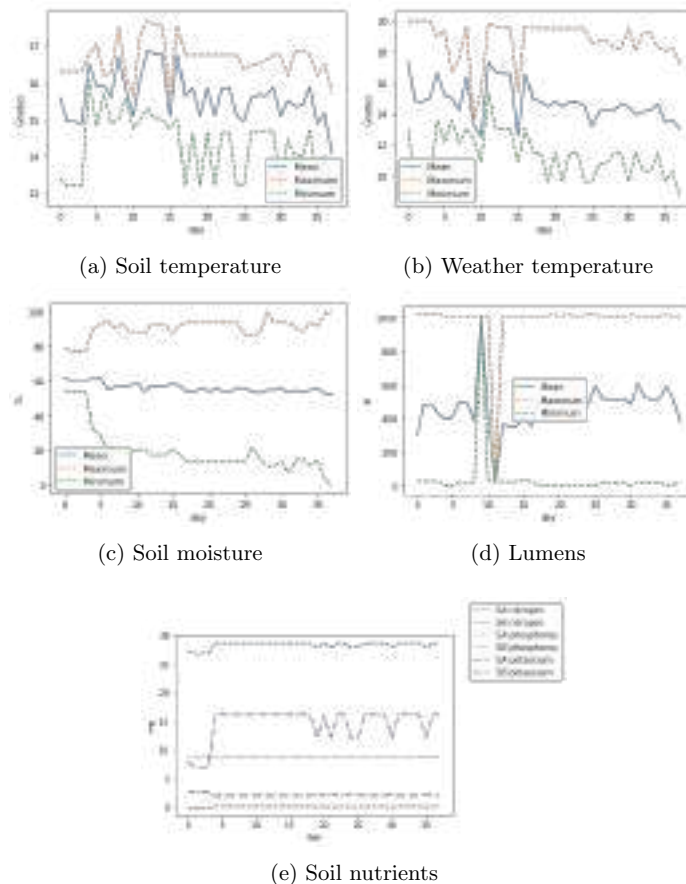
(e) Soil nutrients

Fig. 7: Soil nutrients and weather variables

monitoring crop avocado orchards. The system showed a correct stability and robustness, collecting and processing significant information every 300 seconds.

5   Conclusions and future work

This article presented an IoT platform for monitoring the nutritional and weather conditions of crop avocados in an orchard in the context of smart cities, particularly for smart farming applications.

The proposed IoT platform combines cloud computing and open hardware using sensors to collect and clean data for relevant analysis in smart farming. First, the platform collects nutritional and weather conditions from an IoT device

over the MQTT protocol to the Mosquitto broker; then, data is saved in a CSV file to be cleaned using a spreadsheet reader.

The experimental validation recorded 8832 data from August 05 to September 30, 2022. The main results indicate that the proposed IoT platform effectively collects and processes nutritional and weather data every 300 seconds.

The main lines for future work are oriented to extend the proposed system to compute essential indicators and statistics of smart farming applications, i.e., vegetables, citrus, fruits, and exotic plants. Also, the data collected by the proposed IoT platform will be used to study machine learning techniques to predict avocado production in the studied orchard. In turn, the data collected by the IoT platform can be used for analysis through computational intelligence techniques to improve farming production and supply systems for increasing agriculture productivity in the context of smart farming.

References

1. Acharya, B., Garikapati, K., Yarlagadda, A., Dash, S.: Internet of things (IoT) and data analytics in smart agriculture: Benefits and challenges. In: Abraham, A., Dash, S., Rodrigues, J., Acharya, B., Pani, S. (eds.) AI, Edge and IoT–based Smart Agriculture, pp. 3–16. Intelligent Data-Centric Systems, Academic Press (2022)
2. Ahmed, N., De, D., Hussain, I.: Internet of things (IoT) for smart precision agriculture and farming in rural areas. IEEE Internet of Things Journal **5**(6), 4890–4899 (2018)
3. Alves, R., Souza, G., Maia, R., Tran, A., Kamienski, C., Soininen, J., Aquino, P., Lima, F.: A digital twin for smart farming. In: IEEE Global Humanitarian Technology Conference. pp. 1–4 (2019)
4. Bacco, M., Barsocchi, P., Ferro, E., Gotta, A., Ruggeri, M.: The digitisation of agriculture: a survey of research activities on smart farming. Array **3–4**, 100009 (2019)
5. Bayá, G., Canale, E., Nesmachnow, S., Robledo, F., Sartor, P.: Production optimization in a grain facility through mixed-integer linear programming. Applied Sciences **12**(16), 8212 (2022)
6. Bayá, G., Sartor, P., Robledo, F., Canale, E., Nesmachnow, S.: A case study of smart industry in Uruguay: Grain production facility optimization. In: Smart Cities, pp. 101–115. Springer International Publishing (2022)
7. Bhardwaj, H., Pradeep, T., Aditi, S., Uttam, S.: Artificial intelligence and its applications in agriculture with the future of smart agriculture techniques. In: Pradeep, T., Kaur, G. (eds.) Artificial Intelligence and IoT-Based Technologies for Sustainable Farming and Smart Agriculture, pp. 25–39. IGI Global (2021)
8. Colizzi, L., Caivano, D., Ardito, C., Desolda, G., Castrignano, A., Matera, M., Khosla, R., Moshou, D., Hou, K., Pinet, F., Chanet, J., Hui, G., Shi, H.: Introduction to agricultural iot. In: Castrignano, A., Buttafuoco, G., Khosla, R., Mouazen, A., Moshou, D., Naud, O. (eds.) Agricultural Internet of Things and Decision Support for Precision Smart Farming, pp. 1–33. Academic Press (2020)
9. Garate, B., Díaz, S., Iturriaga, S., Nesmachnow, S., Shepelev, V., Tchernykh, A.: Autonomous swarm of low-cost commercial unmanned aerial vehicles for surveillance. Programming and Computer Software **47**(8), 558–577 (2021)

10. Maraseni, T., Cockfield, G.: Including the costs of water and greenhouse gas emissions in a reassessment of the profitability of irrigation. Agricultural Water Management **103**, 25–32 (2012)
11. Muangprathub, J., Boonnam, N., Kajornkasirat, S., Lekbangpong, N., Wanichsombat, A., Nillaor, P.: Iot and agriculture data analysis for smart farm. Computers and Electronics in Agriculture **156**, 467–474 (2019)
12. Navarro, E., Costa, N., Pereira, A.: A systematic review of iot solutions for smart farming. Sensors **20**(15) (2020)
13. Peña-López, I.: The Internet of things. Tech. rep., ITU Internet Reports (2005)
14. Pretty, J.: Agricultural sustainability: Concepts, principles and evidence. Philosophical transactions of the Royal Society of London **363**, 447–465 (2008)
15. Rossit, D.A., Toncovich, A., Rossit, D.G., Nesmachnow, S.: Flow shop scheduling problems in industry 4.0 production environments: Missing operation case. In: Handbook of Smart Materials, Technologies, and Devices, pp. 1–23. Springer International Publishing (2021)
16. Safa, M.: Measuring and auditing on-farm energy use. In: Sims, R.E. (ed.) Energy-Smart Farming: Efficiency, Renewable Energy and Sustainability, pp. 8–35. Burleigh Dodds Science Publishing (2022)
17. Serikul, P., Nakpong, N., Nakjuatong, N.: Smart farm monitoring via the blynk iot platform : Case study: Humidity monitoring and data recording. In: 16th International Conference on ICT and Knowledge Engineering. pp. 1–6 (2018)
18. Sethi, P., Sarangi, S.: Internet of things: Architectures, protocols, and applications. Journal of Electrical and Computer Engineering **2017**, 25–32 (2017)
19. Suhag, S., Singh, N., Jadaun, S., Johri, P., Shukla, A., Parashar, N.: Iot based soil nutrition and plant disease detection system for smart agriculture. In: 10th IEEE International Conference on Communication Systems and Network Technologies. pp. 478–483 (2021)
20. Trilles, S., González-Pérez, A., Huerta, J.: An iot platform based on microservices and serverless paradigms for smart farming purposes. Sensors **20**(8) (2020)
21. United Nations Department of Economic and Social Affairs, Population Division: World population prospects 2022: Summary of results (2022)
22. Ustundag, A., Cevikcan, E.: Industry 4.0: Managing The Digital Transformation. Springer International Publishing (2018)
23. Vermesan, O., Friess, P., Guillemin, P., Gusmeroli, S., Sundmaeker, H., Bassi, A., Jubert, I., Mazura, M., Harrison, M., Eisenhauer, M., Doody, P.: Internet of things strategic research roadmap. In: Internet of Things – Global Technological and Societal Trends. vol. 1, pp. 9–52 (2011)

Sustainable House Manufacturing for Smart Matching Cities

Paolo Piantanida[1], Claudia Pilar[2], Valentina Villa[1], Antonio Vottari[1]

[1] DISEG-Politecnico di Torino, 10129 Torino, Italy
[2] FAU-Universidad Nacional del Nordeste, 3500 Resistencia, Argentina
paolo.piantanida@polito.it

Abstract. In bottom-up approach to the smart city, the construction of the house and its related land consumption is the fundamental cell for governing urban development and its sustainable relationship with society and the rural area. Given the situation in northern Argentina, the research outlines a construction system based on the sustainable wood supply chain, with industrialized production of wood wafer panels and the proposal of a deconstructible house whose elements can be transported by truck. Sustainability of the building system is achieved through the use of wood from rotational forests and the proposed re-purposing of river and rail transport, while building sustainability is pursued through the integrated use of photovoltaics, heat pump, rainwater and surface geothermal energy. The designed dwelling envelope results B rated, according to the IRAM 11605 Argentine standard and the "Minimum Quality Standards for Social Housing".

Keywords: prefabricated building wood components, energy efficiency, rainwater usage.

1   Introduction

«A smart city should above all be a human city. […] Today, digital platforms are key components of all these urban systems but I don't believe they are the real answer. What would help is to imagine the city differently in a more radical way» stated Carlos Moreno in an interview in 2019 [1]. If we consider how the urban metabolism is affected by supply and waste of construction materials before any building goes into service, we can argue the sustainability impact of construction phase is not negligible, even if the present standard and law context does not seem to care a lot, while building energy efficiency is much more under (sometimes strict) regulations.

In this context, the Authors investigated in the last years how to improve the city metabolism and sustainability by a bottom-up approach, that is, working on the basic bit the urban fabric is made of: housing.

First, smart buildings must be brilliantly managed and produced in a sustainable way. Second, a really smart location of smart buildings (and homes) is a matter of urban planning, of a radical change in the conception of the city. Third, collaborative networking, IoT, and big data management etc. are critical, but they are the rails to guide

change, not the engine and the fuel for it. Confident in these three criteria, the research team began working on the first assumption.

Sustainable houses should adapt to the local availability of energy, e.g., solar energy and rainwater, by integrating into the area network: reducing energy demand for HVAC systems and managing rainwater could be a brilliant way to physically integrate the building into the urban organism; furthermore, learning from nature, a sustainable housing system should be located where humans carry out their main activities (unlike human behavior, it is not common to travel far to work in nature) and thus, in principle, houses could be moved according to the supply of work. In this way, clogged streets, traffic jams, and peak hours of public transportation could be relieved, the city would become more human-scale, and, ideally, people would choose to travel primarily for leisure. Moreover, relocation for work would not necessarily imply abandoning an empty building "shell" to seek or build another one elsewhere. The result would be a dynamic city not only in the metabolism of energy and networked resources, but also in the texture of the building fabric.

This paper presents a proposal for a sustainable housing construction/deconstruction system suitable for the forest resources of Argentina and Latin America. The system is designed to meet the energy integration needs mentioned above, and its production is aimed at fostering the demand for local labor force, avoiding its relocation.

Based on the forestry situation in Argentina, we propose a possible way to locally industrialize the prefabrication of the main components for such type of building system, comparing the expected performance with the requirements of Argentine social housing legislation and some case studies of prefabricated housing.

2　　Argentina's forestry and wood supply chain current situation

Argentina has 33 million hectares of native forests and about 1 200 000 hectares of production forests (the latter with a growth of 40 000 hectares per year) and it's one of the most productive countries in Latin America in the forestry sector.

Wood production yearly rates of Argentine forests, mainly pine and eucalyptus, range between 35 m^3 and 45 m^3 per hectare and are about 6-10 times higher than production rates recorded in European and North American forests [2]. This is made possible by favorable climatic conditions and soil quality enjoyed by Argentina's forests (which allow above-average growth rates), most of which belong to the green lung of Gran Chaco in *Nordeste Argentino* (NEA), which is the second largest tropical forest in Latin America after Amazon rainforest. According to *Ministerio de Agroindustria* data released in 2015, 85% of country's total wood production is concentrated precisely in *Nordeste*, whose main provinces are Misiones, Corrientes and Entre Ríos.

Despite the enormous potential related to continuous availability of raw material, Argentine wood supply chain has several problems basically related to infrastructural deficiencies and high costs for logistics (timber storage and transportation). This is caused by the large distance between NEA forests and main commercial ports in the central provinces of Santa Fe, Córdoba, and Buenos Aires. At present, connection between production centers and ports (foreign market) or distribution centers (domestic

market) is only possible by tractor trailers that travel along existing road networks, resulting in poor sustainability and disadvantages in terms of time, cost, personnel employment for transportation, and increased pollution.

Fig. 1. Map of production forests in *Nordeste Argentino* (NEA) and Table of hectare distribution of production forests broken down by provinces. [3]

A significant abatement of transportation charges and environmental footprint could result from the use of alternative infrastructure or the smart rehabilitation of decommissioned ones.

In the first case, thanks to the presence of Paranà and Uruguay rivers (which connect the NEA with areas where actually ports and distribution centers take place), river transport could be a promising alternative, so much that Argentine government already attempted to encourage the birth of this network in the 1990s, through the construction of some river ports. However, the lack of agreements with neighboring countries, which share the river basin, has not so far allowed for a consolidation of this transport network.

In the second case, an important alternative to the road network could come from the use of the current rail network, with an upgrading of *Nordeste Argentino* local network and its connections to central areas. Argentina's current forestry situation is thus divided between infrastructural deficiencies and new prospects for more economically and environmentally sustainable models.

3   A more sustainable wood supply chain

The housing needs due also to manpower relocation and the forestry situation previously described suggest a systemic approach to the whole wood supply chain, in order to better express social, economic benefits and sustainable development.

The housing issue can be addressed not only by improving subsidized housing, but also by increasing the income of those who, today, find it difficult to access the housing resource: both of these objectives can favorably dovetail with the development of forest

resource, providing that its use is tied to rotational plantations in order to reverse the current deforestation trend.

A sustainable forest management in the NEA would complement the traditional agricultural economy, also by involving the natives in occupations and incomes that would result from a responsible management of rotational plantations, without imposing extraneous working models to local cultures. There are many abandoned industrial areas in Chaco, usually relics related to industrial exploitation of agricultural resources, e.g., the production of various seed oils for food use. These areas are often close to river routes or railroad networks and their redevelopment could allow the settlement of new activities related to timber processing from rotational forests wood into building components, in order to increase employment and local professional qualifications in a social process that is aimed at the placement of both young recent graduates and skilled unemployed people in the world of work.

Abandoned industrial sites cover more than 80 hectares of land in Chaco area and they include some large warehouses used until the second half of the 20th century: most of those are in disrepair, but about one-third are reusable through modest rehabilitation works (mainly roof and facility renovation). Road, rail and energy network are still potentially efficient.

The historical industrial heritage reuse and recovery is a proactive activity that tends to enhance the history of a territorial area: the feasibility of industrial redevelopment and reactivation is based both on the advantage provided by reuse of existing facilities in term of environmental, social and economic sustainability, and also on new opportunities of education and training dissemination powered by the new industry demand. In contexts of relevant economic fragility, such as the city of Resistencia in Chaco, the synergy between education-training-cultivation-production-construction is a particularly essential condition for the feasibility and sustainability of this systemic approach.

The restart of Chaco industry is also a favorable condition for the enhancement of more sustainable transportation systems alternatives to road. The rail network was initially sized and articulated to serve factories that have now disappeared: for this reason, its reactivation and coordination with the rest of the Argentine rail system does not require large resources, but rather a new connected and smart management system (e.g., rail freight convoys with electric locomotives should travel only when the sun provides sufficient energy through photovoltaic farms: timber has no deadline and no hurry) and provides, on the other hand, an additional factor for the development of employment and social welfare. The river network can be managed almost in the same way.

Using alternative and more sustainable methods to transport building components constitutes an added value compared to the raw material alone, lowering the unit selling price thanks to a less impact handling charges and favoring the spread of the product. The latter, consisting of building envelope elements, has in turn the potential to be a driver of a wood construction market that, in Argentina, can still grow a great deal and will increasingly need skilled figures (from designers to assemblers). This will have a positive spin-off in local employment opportunities and in the quality of available housing. Not only jobs, then, but also increased income to facilitate access to housing and its increased quality, also far from urban areas, where the complexity of access routes may make transportation of prefabricated building components less immediate. The

systemic approach to the wood supply chain, moreover, has positive spillover effects on satellite activities: from service and network providers, to equipment maintainers, railroaders, seafarers, etc., which is a significant multiplier of investment, public or private, in this sector. However, this is limited by the low uptake of wood construction with industrialized components (e.g., panels), which today is still conditioned by certain regulatory preconceptions.

4   A look to the current social housing regulations in Argentina

Over the past two decades, Argentina has completed a series of regulatory efforts to improve habitability and thermo-hygrometric comfort of social housing, along with an increasing attention and care for environmental sustainability.

From 2000 to 2019 there have been a series of regulations with technical prescriptions to increase requirements for thermal quality, use of renewable energy, and procedures and technical specifications have been introduced for the evaluation, diagnosis and certification of constructions according to sustainability criteria established by Argentine legislation [4].

Secretaría de Vivienda del Ministerio de Infraestructura y Vivienda de la Nación, together with *Ministerio de Ambiente y Desarrollo Sustentable y el Ministerio de Energía* have produced in 2018 the "Handbook of Sustainable Building" [5]: this guide (regarding Site, Integral Design, Energy, Water, Urban Agriculture, Building, and Best Practices) proposes an assessment tool called "traffic light" which emphasizes for each topic the distinction of desirable versus undesirable variables and effects. The tool also incorporates the concepts of flexible and accessible design in addition to the need to carry forward building design by contemplating future plans for redevelopment, deconstruction and recycling.

Among the possible technological solutions for construction, one of the main aspects that limited (and partially still hinders) wood construction is the fact that it was considered by Argentine regulations to be an "unconventional" system. For this very reason, any use of it required the development of a "Certificate of Technical Aptitude" (CAT) to be submitted to the *Secretaría de Vivienda*, for which it was necessary to complete numerous tests, trials and produce a thorough technical report.

Since 2018, however, Resolution 3-E-2018 of the Ministry of Housing and Habitat [6] has finally recognized the wood frame construction system as "traditional": thanks to this recognition, the wood house sector has benefited from a major regulatory update and a significant incentive that greatly favors this system over others. The growing awareness and concern for environmental issues, coupled with the abolition of CAT, have created favorable conditions for rethinking the wood supply chain in the construction industry, also in terms of sustainability and social spinoff.

Considering energy saving strategy, the "Minimum quality standards for Social housing" [7] stated the value of "K" (thermal transmittance) for the exterior wall and roof must be equal to or lower than the maximum established in Table 1 of IRAM 11605 standard (1996 edition) for level B, i.e., 0.6 to 1 W/m²K for walls and 0.52 to 0.83 W/m²K for roofs (depending on the local climate).

5　　Housing sustainable rethinking

Some best practices on wood housing in Argentina can be traced among recent social housing developments.

In the city of Virasoro (province of Corrientes), 320 km far from the capital, 11 social housing units of 70 m² each were built in 2015: the prototype was designed by the Corrientes Housing Institute (INVICO) and consists of a one floor building with dining/living room, a kitchen, a bathroom, two bedrooms and two covered loggias (Fig. 2). This plan setting derives from the traditional local housing model. These houses were built with wood-frame technology and insulated infills, pitched roofing, interior sheathing of gypsum board, and exterior cladding of painted wood; windows and doors are made of aluminum frame. The constructions rest on a raised and ventilated basement in order to avoid contact between wooden elements and soil moisture. Each dwelling was built in 29 working days by four carpenters, an electrician and a plumber and 14.15 m³ of lumber was used [8].

Fig. 2. Floor plan, elevation and photographs of the construction phases of INVICO's *viviendas sociales* at the Virasoro locality. [© INVICO (drawings) and Erick Kennedy (photographs)]

Similarly, in Entre Ríos Province, twelve houses were built between 2014 and 2015 in the Chaco neighborhood of the city of Chajarí, each one of 67 m². In 2016, eight more houses of 62 m² each were built in the La Florida neighborhood. Also in the province of Entre Ríos, in the city of Concordia, another 250 houses are being built in the Agua Patito neighborhood, in order to be able to relocate families who lived in the

flooded areas: these are 48 m² homes, each of which used 3.6 m³ of wood for the load-bearing structure in addition to 65 m² of facade cladding made of horizontal solid wood slats laid in "American style", 170 m² of interior matchboarding, and 30 boards of 9 mm thick phenolic plywood.

6   Toward a prototype of a locally produced system for wooden houses

As anticipated in § 3, this research investigated the possibility of local production of sandwich panels, framed elements and complements to promote the integral use of wood resource and, at the same time, to improve local housing conditions, enhancing skills and availability of local workforce, as well as responding to the needs of Argentine housing emergency, especially in the North, also conditioned by the persistent difficulty in accessing housing credit [9].

Below are described the first results obtained in the design of the technological system, which is first and foremost oriented toward simplifying the manufacturing process, lowering construction and handling costs, and favoring simple and flexible floor plans.

This flexibility and simplicity appeared to be a necessary condition to allow the declination of the proposed model according to the various cultural, social and climatic instances that are a very true expression of the local tradition: in fact, the diffusion of a "new" building system cannot be associated with the imposition of a new way of living, but rather the system itself should be naturally metabolized by the socio-cultural context of reference, which can "appropriate" it in the ways and with respect to local customs. The sustainable city can be made of sustainable technology, but it can not be made of sustainable buildings that are empty and rejected.

For this reason, the example of conceptual application of the system is intentionally inspired by the traditional *vivienda rural* that is typical of the northern subtropical region of Argentina (fig. 4). The so-called *casa rural* was born in close contact with the territory and its climate, so much that home is a simple shelter from bad weather and only destined for basic functions such as sleeping, cooking, and even giving refuge to domestic animals. As a result, the *vivienda* has no definite boundaries, there is no clear or fixed separation between inside and outside, and it is not even possible to "crystallize" certain functions within it. The functional scheme is therefore an open and dynamic model always connected to the outdoor, both to extend the living function to the outside environment and to allow further additions through aggregation of the same model, which is developed on a single floor usually elevated above the ground in order to prevent possible river flooding. The *galería* is the recurring element: a central aggregative space, covered but not enclosed, in which all the social activities of daily life take place. On this *galería* insist the *habitación*, which consists of bedrooms, the only enclosed spaces of the dwelling. Technological and planimetric linearity together with the use of natural materials (mainly wood) allow the implementation of a series of bioclimatic principles to which these Argentine rural houses conform, achieving favorable interior microclimates thanks, for example, to natural ventilation and shading control

(think of the opposing openings of the central *galería*, or shading and evapotranspiration cooling given by dense surrounding vegetation). Two rural homes are illustrated in Fig. 3 [10, 11].

The proposed technological system is based on locally producible elements: 2 or 4 cm thick wood planks measuring 132×52 cm (and also 17 or 10 cm to allow better utilization of the log), while the processing waste is used to produce wood wool that can form thermal insulation of the infill and bracing panel.

Specifically, "wafer" panels are conceived with solid perimeter frames suitable for tongue-and-groove joining, consisting of boards 4 cm thick on the outside and 2 cm thick on the inside. The thickness of the gap is governed by the thickness of the frame, which can be 2, 4, or 6 cm. In the most thermally favorable case (6 cm cavity filled with wood wool), the resulting panel has a thickness of 12 cm and a thermal transmittance of less than 0.5 W/m²K (which meets the B level required by the "Minimum Quality Standards for Social Housing") i.e., four times more favorable than the more usual hollow brick wall of similar thickness (2 W/m²K) compared to which it would also be much lighter (30 kg versus 60 kg for an equal area of hollow brick wall). Smaller panels have corresponding lower performance, lower mass and lower manufacturing cost.

Fig. 3. Argentina subtropical area: typical rural housings (Carli C L, [10])

In order to contain costs and simplify the whole process, the proposed system allows the construction of e.g. an entire house through the use of the same multi-layer wood panel. This logic of unification and simplification facilitates both the manufac-

turing, which is faster and more sustainable (less waste), as well as warehouse management, and the construction phase, with greater simplicity of supply and speed of assembly. The size of the panel also favors quick assembly (no winches or cranes are needed and everything can be completed by a couple of workers), resulting in lower costs for both site management and components procurement [12, 13].

All the elements of which the multilayer panel is made of are illustrated and catalogued in Table 1.

From the cut of the C element of which the multi-layer wood panel is composed, it is possible to make additional solid wood elements, which are depicted and catalogued in Table 2 below, again with an approach to simplifying production and limiting material waste. The latter are used to assemble the portals with a structural function, suitably braced by the multi-layer wood panel, which combines the bracing function with that of external closure: the same panel is, moreover, used to make the entire envelope of the house (floor, external walls, roofing) and any partitions with its lesser thicknesses.

Table 1. Multi-layer wood panel manufacturing steps: (a) from the logs of the production forests, all the necessary material, including wood fiber for the insulation panel, is obtained in the supply chain and waste minimized; (b) (c) exploded views of the panel (see element list in the lower part of the table); (d) complete multi-layer wood panel

(a)   (b)   (c)

(d) wooden wafer panel
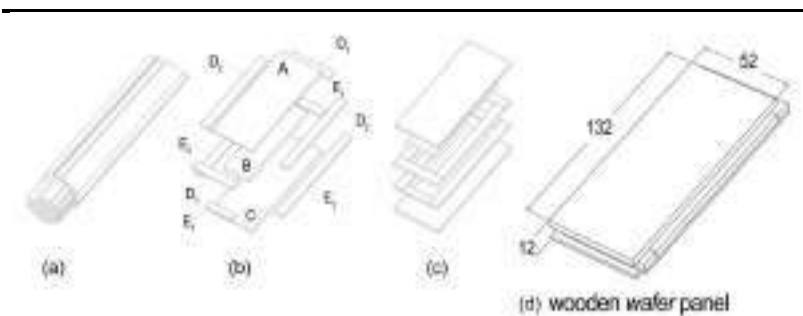
wooden wafer panel function:	bracing and infill panel (floor, vertical and roof envelope)		
cod.	dim. LxDxH [cm]	material	No. of panels needed:
A	132x52x2	solid wood	Floor: 90
B	112x32x6	wood wool	Vertical envelope: 168
C	132x52x4	solid wood	Roof: 126
D_1	52x10x4 (No. 2)	solid wood	**Total: 384***
D_2	112x10x4 (No. 2)	solid wood	
E_1	32x10x2 (No. 2)	solid wood	*No. of wafer panels needed to build the proposed dwelling model
E_2	132x10x2 (No. 2)	solid wood	

The inner side of the building envelope can also be completed with electricals, fittings, piping etc., also to enable building's energy self-sufficiency (e.g., photovoltaics, thermal solar panels) and finishing materials (plasterboard, matchboarding, flooring,

etc.) even at a later stage, because as supplied the assembled system allows immediate use of the volumes as soon as the windows and doors are placed. This also makes it usa-ble in cases of immediate relief or for the construction of temporary buildings (ex-hibi-tion stands, mobile construction sites, etc.). Furthermore, the reiteration of the elementary cell can give rise to multi-family buildings, small schools, clinics, service centers, etc.

   The small size of the elements of which the system is composed allows them to be transported even by common vans, facilitating their distribution even in the most de-centralized rural areas that could achieve a sustainable housing development and bene-fit from the "connected society" distributed chances: all the elements for this dwelling, repeating the traditional rural houses scheme of two compartments and central gallery, can be transported with a couple of trips of a tractor-trailer: it is a matter of transporting about 40 tons of material with a footprint of about 50 m^3.

   On the other hand, the intrinsic characteristics of the system, in accordance with the requirements of the mentioned "Manual of Sustainable Construction" make it easily de-constructible and transportable elsewhere, as well as fully reusable and recyclable, with the exception of only the pair of masonry baffles that are needed for the interface of the house with the ground. De-constructability and transportability, due to dry assembly and the small size of the elements that make up the system, is also advantageous in terms of reliability of investment for the house: in the case of relocation, the *vivienda* can be moved elsewhere, without the need to be resold on site, perhaps in a market condition where demand is weak and the price would not be adequate for the original resource commitment. So doing, the soil usage is almost reversible and the ghost house phenomenon avoided.

Table 2. List of the additional solid wood elements for house portals (they are all obtained by appropriate cutting of the "C" elements)

	cod.	dim. LxDxH [cm]	Function: structural portals
	C_1 (C/3)	132x17x4	
	C_2 (C_1/2)	66x17x4	
	C_3 (C_2/2)	33x17x4	

7   Sustainability and house energy equipment

The energy transition asks people to change the model of production and consuming to achieve a Positive Anthropogenic Impact (PAI) on the environment. Therefore, policies are required for the efficiency of consumption, production, transmission and distribution of energy and the increase in the production mix from renewable sources, considered to have a low climate impact. All buildings contribute to the city's sustainability, and the wafer wood panel building system is no exception; this is why the proposed house design was geared toward reducing energy needs and environmental impact, both in the manufacturing and construction process and during its life.

In facts, as elementary bit of the city fabric, the wafer wood panel house is in close relationship with its physical and social neighborhood, connected with the district network systems and relied also upon Energy Communities (i. e. a socio-economic model consisting in a consortium of users, focused on the decentralization and local exchange of energy, according to the principles of circularity, and aimed to self-produce from renewable sources, consume and manage energy through one or more local energy plants, in order to achieve energy self-sufficiency). It is not a matter of connection only, but also of the way of connection.

Smart cities are made of smart behaviors of each member: a building can not take whatever it needs at any time, and so the first rule should be to reduce as much as possible the energy footprint on the town.

For this reason, electrical, HVAC, and plumbing systems are integrated into the same design and such as to decrease the house's energy footprint to city grids (see Fig. 4): on sunny hours, the rooftop generates electricity through a photovoltaic-battery-inverter system; during rainy days, the rooftop collects rainwater that the downspouts do not convey into the city sewer system (avoiding its overloading), but take it to a large underground reservoir, where it can be used in the part exceeding the minimum operating level in the tank for toilet flushing but mostly stored as a closed-loop heat sink to feed the water-to-water heat pump. During dry periods, the heat-pump uses water stored in the reservoir as a closed water loop and "thermal flywheel" to exchange energy to the ground [14].

In daylight hours, the system will operate almost off-grid, while the closed loop of rainwater for the heat pump is made to facilitate energy exchange to the ground as well. Any PV production during stand-by periods of the heat pump will be sold via smart connection to an energy community through the city grid or stored in battery packs.

The Argentine Board of Construction (Cámara Argentina de la Construcción) has estimated [15] that the average electricity requirement (Heat Pump excluded) of sustainable social housing is about 1.5 MWh per year. A photovoltaic array of 1.16 kWp can generate about 1.6 MWh/year in Buenos Aires and 2 MWh/year in Mendoza, being sufficient for the general electricity demand, while the photovoltaic capacity would have to be about 4 or 3 times higher to cover the heat pump needs as well.
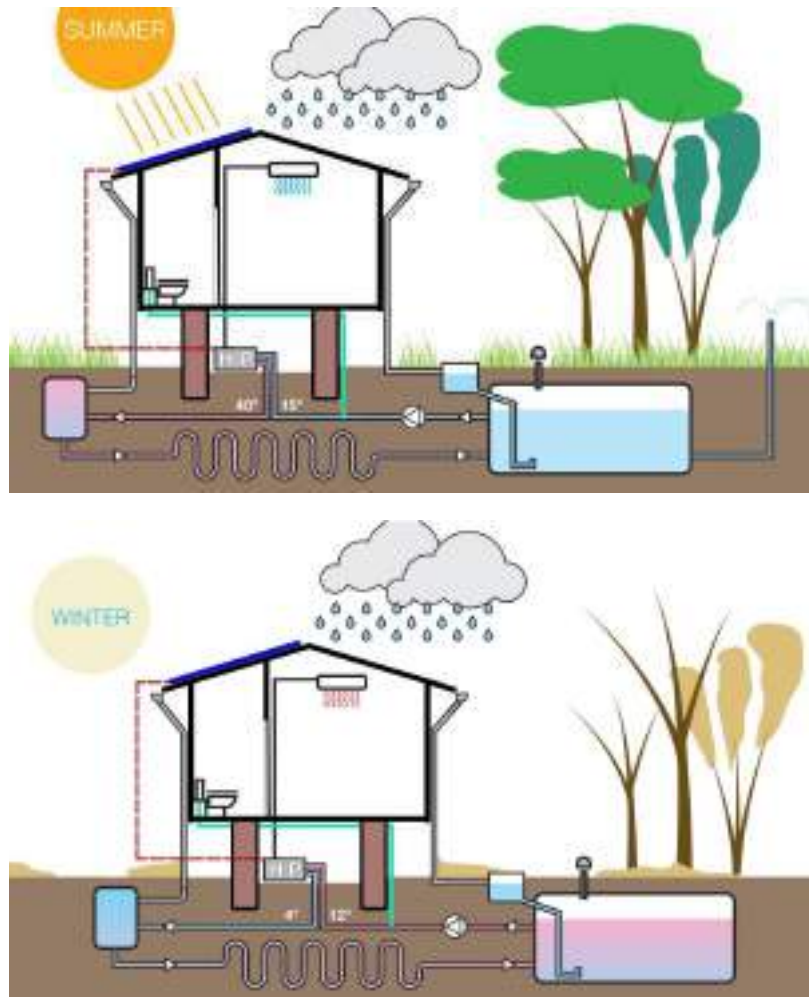
Fig. 4. Scheme for energy and HVAC system in the proposed prefabricated wood dwellings (summer and winter operation).

Fig. 5. Monthly simulation for a 1.16kWp PV system in Buenos Aires (1650 kWh/year (±10).

8　Conclusions

The energy transition asks people to change the model of production and consuming to achieve a Positive Anthropogenic Impact (PAI) on the environment. Therefore, policies are required for the efficiency of consumption, production, transmission and distribution of energy and the increase in the production mix from renewable sources, considered to have a low climate impact. All buildings contribute to the city's sustainability, and the wafer wood panel building system is no exception; this is why the proposed house design was geared toward reducing energy needs and environmental impact, both in the manufacturing and construction process and during its life: the de-constructible house can also be enlarged or reduced in size according to users' needs and can be disassembled, moved, and assembled elsewhere, reducing the impact of abandoned houses.

In facts, as elementary bit of the city fabric, the wafer wood panel house is in close relationship with its physical and social neighborhood, connected with the district network systems and relied also upon Energy Communities (i. e. a socio-economic model consisting in a consortium of users, focused on the decentralization and local exchange of energy, according to the principles of circularity, and aimed to self-produce from renewable sources, consume and manage energy through one or more local energy plants, in order to achieve energy self-sufficiency). It is not a matter of connection only, but also of the way of connection. Smart cities are made of smart behaviors of each member: a building cannot take whatever it needs at any time, and so the first rule should be to reduce as much as possible the energy footprint on the city grid and the waste of embedded energy. Considering the possibility of volunteers to assemble/disassemble the house, the cost is competitive with that of conventionally built houses; but the main purpose of the proposed system is to enable mobility-reuse of building components: the same costs can thus be amortized two or three times.

Fig. 6. 3D modelling of the proposed wafer wood panel rural house.

References

1. Meeting With Carlos Moreno: Human Smart Cities, https://www.moreno-web.net/meeting-with-carlos-moreno-human-smart-cities, last accessed 2022/10/06.
2. Broza D, Rossit Da, Rossit Di, Cavallín A, The Argentinian forest sector: opportunities and challenges in supply chain management. Uncertain Supply Chain Management 6, pp. 375–392 (2018).
3. Ministerio de Hacienda, Presidencia de la Naciòn, Subsecretarìa de Programaciòn Micro-econòmica, Secreterìa de Politica Econòmica. Informes de Cadenas de Valor. Forestal, paper y muebles (2019).
4. Ministerio del Interior, Obras Públicas y Vivienda de la Nación. Resolución 9-E: Estándares mínimos de calidad para viviendas de interés social. Secretaría de Vivienda y Hábitat. Buenos Aires (2017).
5. Ministerio del Interior, Obras Públicas y Vivienda de la Nación. Manual de la Vivienda Sustentable. Subsecretaría de Desarrollo Urbano y Vivienda. Buenos Aires (2018).
6. Secretaría de vivienda y hábitat. Resolución 3-E-2018. Ministerio del interior, obras públicas y vivienda. Buenos Aires, República Argentina (2018).
7. Norma IRAM 11605, Accondicionamento térmico de edificios condiciones de habitabilidad en edificios. Valores máximos de trasmitancia térmica en cerramientos opacos (1996).
8. Pilar C, Vallejos, S. y Kennedy, E. Casos de construcción de viviendas en entramado de madera de bosques implantados en Corrientes. Congreso Regional de Tecnología en la Arquitectura. Mar del Plata, Argentina (2019).
9. Argentina lanza un programa de crédito para construir miles de viviendas nuevas, https://el-pais.com/economia/2012/06/13/actualidad/1339544540_890839.html, last accessed 2022/10/06.
10. Carli C L, La Casa. El Espacio y la Distancia. Las nuevas teorias. Editor literario César Luis Carli, 1° ed. Ilustrada, Santa Fe (2017).
11. Sartorio R, Siniak M, Investigación sobre la vivienda rural en el nordeste de la República Argentina y propuesta para el déficit actual, Informes de la Construcción. Vol. 36, n.° 361, junio (1984).
12. Bagnato F., Processi edilizi in autocostruzione assistita. Una risposta al problema abitativo delle fasce deboli, Iiriti Editore, Reggio Calabria (2002).
13. Grahame A, McKean J, Walter Segal: Self-Built Architect. Lung Humphries, London (2021).
14. Rollin K, Ground Source Heat Pumps. A Low-Carbon Energy Technology. Energy Resources. 12 (1), 10-19 (2010).
15. Silvina Carrizo S, Azqueta P, Strier, Gil S, Vivienda social sostenible, Cámara Argentina de la Construcción, CABA (AR) (2021).

Lean Office approach for *muda* identification in the admission process of university students

Jesús del Carmen Peralta-Abarca [1][0000−0003−2995−9277],
Pedro Moreno-Bernal [1][0000−0002−2811−5331],
Sergio Nesmachnow [2][0000−0002−8146−4012], and
Viridiana Aydeé León-Hernández [1][0000−0002−5070−9320]

[1] Facultad de Ciencias Químicas e Ingeniería,
Universidad Autónoma del Estado de Morelos, México
{carmen.peralta, pmoreno, vleon}@uaem.mx
[2] Universidad de la República, Montevideo, Uruguay
sergion@fing.edu.uy

Abstract. The new model of industry 4.0 boosts productivity in modern life, as an essential part of social and technological changes under the paradigm of smart cities. As a part of social changes, universities restructured their ability to trace internal processes through smart campuses, using Information and Communication Technologies and industrial improvement methodologies. Lean principles are used for process improvement through *muda* elimination and value generation in office tasks. This article introduces a Lean Office methodology for the admission process of incoming students in a public university in Mexico. Ishikawa and Pareto diagrams are applied to analyze and identify *muda* in the admission procedure, reducing the time delays in the admission form exchange subprocess.

Keywords: Lean Office, process improvement, industry 4.0, university

1 Introduction

In recent years, the Industry 4.0 revolution has advanced as an essential part of social and technological changes under the paradigm of smart cities [10,13]. As part of the social changes, universities have restructured their ability to track their internal processes on smart campuses, to the benefit of students and their community. A smart campus is related to internal communications, Internet of Things (IoT), Big Data, and data governance [3]. Local communications networks are used to provide connectivity and services, impacting daily user experience. [14].

Universities are essential in civil societies for learning and higher education. Nonetheless, universities worldwide needed to restructure their internal processes after the COVID-19 pandemic, complementing the smart campus digitalization. In this context, a smart campus must provide practical digital applications

based on information and communication technologies and process improvement methodologies for better school services management.

Methodologies for process improvement in engineering increase productivity and help boosting business goals. Several process improvement methodologies, including Six Sigma, Total Quality Management, Toyota Production System (TPS), Kanban, Kaizen, Lean Manufacturing, have been proposed as decision-making methodologies for industrial processes, and selecting the best approach for a particular process is essential to improve its productivity and efficiency. Each methodology assists the process improvement step by step, to deliver better products and services. Methodologies use tools like diagrams, flowcharts, etc., to detect and evaluate defects or inconsistencies in a particular process. Particularly, Lean Manufacturing principles have been extended to non-manufacturing areas, e.g., services and offices, receiving the Lean Office (LO) name [15,18]. The lean concept emerged from TPS, based on making work more satisfying by eliminating *muda* or converting it into value [6]. Muda represents all waste created by human activities absorbing resources without creating value [16]. Everything a client refers to, in terms of satisfying his needs at any specific moment, generates value for the product or service. The LO concept comprises the application of lean thinking principles in administrative areas to eliminate muda in processes and information flows [4,12]. In this context, information management identifies opportunities for improving the management of information sources and information systems infrastructure, adding value to the information provided to the customer [5].

This article proposes the application of a LO methodology to the admission process for incoming students in a public university, particularly for the admission form exchange subprocess. A specific case study is analyzed, for the 2019–2020 admission process to Universidad Autónoma del Estado de Morelos (UAEM), Mexico. The annual admission process for new students requires carrying out a series of personal procedures in the admission services offices of the institution. However, during the COVID-19 pandemic, the subprocess for exchanging the admission form could not be performed in person, and a migration to web forms based on LO principles was adopted.

The main contribution of this article is the implementation of LO tools to identify muda by ranking the significant non-value added activities in the admission process. Several muda are detected, including redundant activities that are performed in different subprocesses, causing waiting times to applicant; low efficiency in customer service tasks due to limited computer equipment resources; and error-prone office and support activities because of the lack of trained personnel. The causes identified in each stage are integrated into an optimization plan to conduct a standardized process. Results demonstrate that LO tools identified the major waste that impacts waiting times in the different stages of the admission form exchange subprocess.

The article is structured as follows. Section 2 describes the admission process for incoming students and reviews related works. Section 3 describes the proposed methodology for the admission form exchange subprocess and the LO

tools used. Section 4 presents and discusses the results for the case study. Finally, section 5 presents the conclusions and formulates the main lines for future work.

2   The admission process of university students

This section describes the admission process for incoming students to UAEM. Also, the section reviews the related works about LO principles applied for processes that require substantial time improvements and waste elimination.

2.1   Admission process before the COVID-19 pandemic

Every year, UAEM calls for the admission of new students interested in joining middle and higher education educational programs. According to the Quality Plan of the Department of Admission and Revalidation, the admission process starts with the planning. Later, the call for admission is published on official and local media. Then, an admission deadline is established for the applicants to exchange the pre-registering admission form for an official admission sheet.

The institutional admission process is carried out by the admission services area of the school services offices of UAEM. Usually, the admission process presents contretemps due to failures in personnel management, the digital database system, and the lack of communication and visual support instructions. These deficiencies generate inconveniences and complaints from applicants, who expect the process to be carried out as efficiently as possible. Besides, the current admission process represents a problem for the organization because UAEM has the ISO 9001 certification; therefore, the admission process must maintain a quality standard as a part of the organizational processes

The admission form exchange subprocess comprises seven stages. First, the call for admission is published in local media. Second, the pre-register stage permits candidates to fill out a form to provide personal information, i.e., identity card (INE) and a certificate of high school studies. Third, the registration fee is published for applicants to pay the admission charges before the fifth stage. Fourth, applicants proceed to the admission services office to validate the information on the pre-register form by presenting authentic documents. Then, the admissions services office takes a photo of the applicant to include on the pre-register form. Fifth, the admission form exchange process is carried out by the admission services office, to exchange the pre-register form for an admission sheet. Sixth, applicant are appointed on a date to take the admission exam. Finally, the results are published in local media to show the lists of accepted candidates for the different educational programs, in accordance with the procedure established in the Manual of Processes and Operating Procedures of UAEM.

2.2   Related Works

Research in smart campuses uses ICT to provide intelligent process systems that support digital applications for better management. Smart campus applications

use Big Data, IoT, and mobile devices as tools for managing internal processes. Current works propose different methodologies for better and more efficient processes in the context of the smart industry, smart campus, and smart cities. A review of related works is presented next.

Chen and Cox [2] applied Lean Manufacturing concepts in an office environment. The authors proposed a systematic procedure for Lean practitioners to conduct Lean events in their office environment. The proposed LO method incorporates the knowledge of several articles, books, and successful Lean events for many study cases. The proposed systematic procedure transforms the office environment into Lean Office customer-triggered working processes. As a result, results were faster and more systematic tasks, tracking-reducing costs due to reduced non-value-added activities.

Sabur and Simatupang [11] applied Lean principles in the service support of a manufacturing company to increase customer satisfaction on order acceptance to achieve the targeted customer response time. Lean tools were applied on the office floor of the company, particularly in handling the administration of customer order acceptance. The causes of the treated problem were the lack of practical business orientation and an integrated system for information and data sharing. Value stream mapping (VSM) was used to identify waste using solution maps. Also, the standardization of processes was applied for better time response. The solutions were based on analyzing future VSM by changing the priorities. The proposed solution point targeted 40-hour customer response may be achieved in 37 hours 22.2 minutes.

Monteiro et al. [9] applied LO tools to improve opportunities for raw materials management of a logistics department in shop-floor operations. Lean tools identified waste by lacking information integration and visibility on managing raw materials, producing low data processing efficiency. 5S, Poka-Yoke mechanism, standard work, and visual management were used as Lean tools to identify waste and generate value opportunities. Results obtained were transparency on processes, better task definition of priorities to perform, better organization and work management. The *open points* and *production losses*, and both reduced their processing time by 84% and 66%, respectively. Also, standardization and a clear definition of stakeholders responsibilities allowed significant reductions in process lead time equivalent to $645/year of saving for the company.

Magalhães et al. [8] applied LO tools, i.e., electronic standardization and critical performance indicators, in the administrative processes of an undergraduate/postgraduate office of the Department of Production and Systems at the University of Minho, Portugal. Lean techniques were applied in an administrative environment allowing the development of skills at a professional level and professional teamwork. Electronic standardization was applied to six educational projects and it was implemented successfully. Personal computers and network drives reorganization reduced 84% of the file search time, impacting students registration and project management. Also, student searching was reduced by 69% of search time, impacting input times and information handling, equivalent to 12 hours/year of saving for the Department of Production and Systems.

The related works allowed identifying several proposals showing a growing interest in LO tools. The optimization of the design of administrative processes is part of strategic management toward a productive process. In this sense, organizations seek to improve their operations in an efficient and productive way. Organizations review their administrative processes through the identification of waste in workflows to eliminate them. This work contributes to a LO methodology for the admission process of incoming students in UAEM. The benefits of the proposed methodology include significant reductions in time delays in the admission form exchange subprocess. Next, the implementation of LO tools to identify *muda* by ranking the significant non-value added activities in the admission process is described.

3 Lean Office for the admission process of incoming students

This section describes the proposed LO methodology of the admission form exchange subprocess and the LO tools used.

3.1 Lean Office

The LO concept came from TPS, which originated in the Japanese automotive industry after World War II. Japan started to work in automobile production, but the lack of resources prevented efficient and dynamic production models. The need to have a production model adapted to the Japanese requirements generated the Just in Time (JIT) concept. The main goal of JIT is to increase production efficiency through waste disposal within the production environment [6]. Womack et al. [17] called this production system Lean Thinking. The word Lean become a way to define TPS in practice. The lean principle starting point is to recognize a small fraction of time and effort in an organization that it can become valuable. For example, the customer capacity provided the right time at an appropriate price, as defined in each case by the customer. It applies to everything the client refers to in terms of satisfying their needs; at that moment, value is generated for the product or service given value to the different processes in a company. Currently, the Lean philosophy is applied through its different aspects defined by the organizations: Lean Manufacturing for the productive sector, LO for office and service environments, Lean Construction for environments and sectors related to construction, and Lean Health for the health sector. The Lean aspects share the mentality of quality principles to optimize work, improve results and establish continuous improvement within the organization [1].

In practice, the significant waste of LO is the time of activities, lack of standardization, generating batch and unorganized documents, careful data entry and information, and document report unstructured correctly. Once waste is identified, it is necessary to implement LO tools to analyses the value in the office to eliminate or reduce wastes. Likewise, root-cause Ishikawa diagrams help to create and classify ideas or hypotheses concerning the root causes of a problem

in a graphical manner. Another useful technique is Pareto analysis. Pareto diagrams help to prioritize tasks highlighting which actions are proposed to solve each problem. In addition, VSM and programs like 5S are used to standardize the new value achieved to stabilize the new process. Finally, it is necessary to stimulate continuous cycle improvements in the LO deployment process for higher performance.

3.2   LO tools for admission form exchange subprocess

Locher [7] recommended performing an observation of the current process to identify, differentiate and detect opportunities for improvement that allow an objective evaluation from the perspective of the LO. Therefore, in the proposed approach the admission process is analyzed in two stages. The first stage follows the four basic steps [stabilize, standardize, make visible, and continuous improvement] to apply the lean methodology. If a process is unstable, the focus on adopting the methodology depends on the starting point, e.g., an unstable, irregular, and unacceptable process must be stabilized. Then, the stabilized process is initialized in the standardization stage. Later, a standardized process must be visible inside the organization for a correct following. Finally, the process improvement must be in continuous way. In this context, the first action is searching for instability or unacceptable activities in the admission process. The implementation of the four phases for the stabilizing stage is described in the following paragraphs.

Identification of essential activities. Critical activities and procedures of the admission process are used to identify possible *muda*. The Quality Plan of the Department of Admission and Revalidation defines five essential activities for the support staff. However, the process quality manual does not identify the specific activities, so they are not considered standardized elements. Table 1 shows the essential activities and the corresponding procedures related to the admission form exchange subprocess.

Table 1: Procedures carried out during each activity of the admission process

	Activity	Procedure
1	Reception of documents	Gathering documents from applicants
2	Detailed data review	Careful review of data in documents of the applicant
3	Photography	Save applicant photograph in a digital database
4	Applicant registration	Store applicant information in a local database
5	Print	Print and deliver admission form

Process organization. The applicant goes to the admission services office to deliver the admission form. Subsequently, the documents of the applicant are collected and reviewed according to the activities in Table 1. If all the documents

are correct, the applicants can exchange their admission form for an admission sheet that endorses them as candidates.

Table 2 describes the activities developed at the admission form exchange subprocess phases to identify possible *muda* in practice, according to the Quality Plan of the Department of Admission and Revalidation.

Table 2: Admission form exchange subprocess activities performed in a module

#	Phase	Activity
1	Applicants reception	Arrange and review documentation (INE, admission token and charge voucher)
2	Documents preparation	Staple the admission form and fee voucher.
3	Documents reception	Review personal information, i.e., INE, admission form, and charge voucher. If there is a mistake in personal information, the staff comments on the mistake to alert and be corrected in phase 4.
4	Detailed revision	Inspect carefully the personal information to identify any mistakes from the receptionist staff. The difference from the past module is careful verification. Also, this phase prepares the applicant for a photo in phase 3.
5	Take a photo	Take a photo if the personal information is valid. Subsequently, the photo is uploaded to the Documentation Management and Scholar Control System (SADCE).
6	Assignment	Staff assigns and sends the applicant to the data capture phase.
7	Data capture	Data capturer staff collate personal documents with data captured in SADCE. Then, two filters are applied to find any mistake notifying the applicant if it is necessary to make any correction or continue the process. If the information is correct, the applicant signs a printed admission sheet.
8	Deliver admission sheet	Applicant collects its print admission sheet. The printed admission sheet indicates the date, place, campus location, and degree bachelor of interest.
9	Critical information	The staff in this phase explains to the applicant important information about campus location, exam date and provides a study guide for the admission exam.

Muda is identified in phases one, two, six, and nine of Table 2. The phases are not standardized processes yet. Phase nine is an activity recently implemented in the admission form exchange subprocess. In practice, the staff roles are not clearly defined, impacting the development of the admission process and generating possible *muda*.

Muda identification. *Muda* detected in the admission process includes redundant activities that are performed in different subprocesses, causing waiting times to applicants; suitable communication and collaboration of personnel; bottleneck by cross information; low efficiency in service attention by limited computer equipment resources; and error-prone office and support activities because of the lack of trained personnel. Table 3 summarizes the detected *muda* for admission form exchange subprocess.

Table 3: Detected activities do not generate value

Muda	*Identification*	*Problems*
Waiting times: time delays at previously activities for next step.	A document preparation bottleneck in phase 2. A prolonged recess times in activities. A failure of computer system.	Unoptimized activities in phase 2 generate time delays. Lack of trained personnel. Lack of computer system support and maintenance.
Unused talent: do not exploit the experience, knowledge, and creativity of the staff.	Limited collaboration between support staff. The lack of cross-training in support staff.	The coordinator does not take advantage of the support staff ideas to implement them. Lack of training for job roles.
Movements: unnecessary movements by staff.	Unnecessary movement generated in activities.	Lack of communication when the applicant makes a mistake in registering personal information on the admission form or when the applicant decides to switch from the initial academic program selected during the admission form exchange subprocess.

Identification of opportunities for improvement. The improvements allow redesigning the current process, considering the information presented in Tables 2 and 3. The improvement activities proposed for the admission form exchange subprocess are described in Table 4. Those activities identified as *muda* and the not standardized phases are merged or eliminated to achieve a better efficiency in the admission process.

Table 4: Improvement activities proposed for the admission form exchange subprocess

Activities	Improvement
Documents reception	Provide precise and simplified instructions about the admission form exchange. Improve the delivery of documents in phase 2: prepare the stapling documents by cropping the admission form by half. Allow student access in blocks of 16 individuals to avoid congestion.
Documents review and validation	Provide the first filter to detect mistakes or inconsistencies in record information. Documents detailed review; personal information must coincide with the admission form recorded. Specify and comment as mistake correction the error of the registration form or when the applicant decides to switch from the initial academic program selected. Provide precise instructions to the applicant or clarify doubts for next steps.
Detailed review information	Delete this module. The labor of this module must be reassigned as an duty for instructors.
Photo	Increase the number of photographic equipment and personnel.
Data capture registration	Implement a visual control system for applicants can identify which data capture staff was assigned. Reduce the number of applicant teams by 15%; there is an excess.
Print	Assign trays to classify admission forms by venue and incoming exam date; give recommendations by blocks of applicants.

Once the unacceptable activities for stabilizing stage are identified, a problem cause-effect analysis based on Ishikawa diagram was carried out to define possible causes of the problem. The criteria considered for the cause-effect analysis based on 'why questions' about the possible causes of the problem:

1. Why is this a factor that causes the problem?
2. Why does that factor directly produce the problem?
3. If it is a direct cause, why has it not been eliminated to correct the problem?
4. Why is it not considered a feasible solution?
5. Why can not it assess if the solution worked?
6. Why is the solution a lower-cost solution?

Figure 1 presents a qualitative analysis applying an Ishikawa diagram. The analysis shows that continuous and frequent complaints are generated by time delays in activities at each phase impacting the value flow of the admission form exchange subprocess.
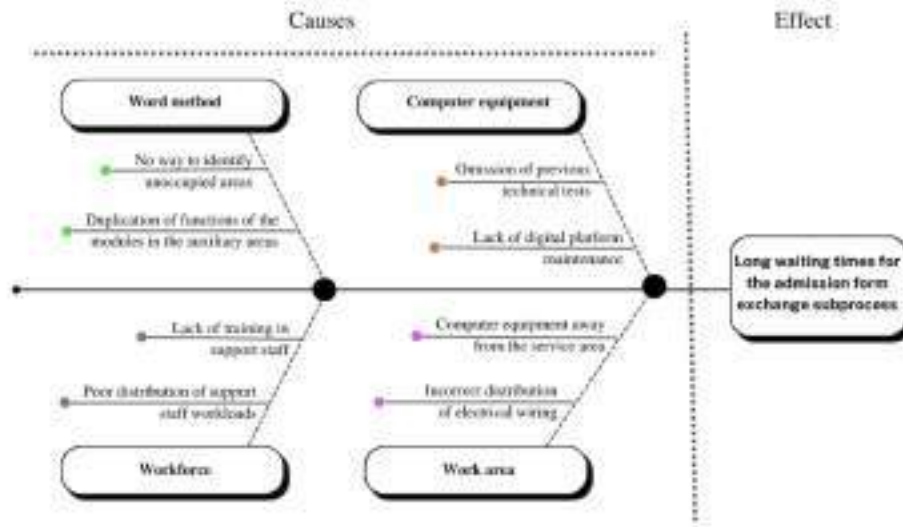
Fig. 1: Ishikawa diagram for the admission form exchange subprocess

Once the main problems that affect the admission form exchange subprocess have been identified, an improvement analysis was applied through Lean tools. LO tools helps to develop ideas that can be implemented to increase the value flow through continuous improvement of the admission process. Next section describes and discusses the results of the improvement analysis using LO for admission form exchange subprocess.

4   Results and discussion

This section describes the results of the LO approach to identify *muda* for the admission form exchange subprocess, and a specific case study is described for the 2019–2020 admission process of UAEM.

4.1   Studied case

The analysis of the admission was carried out in person, to learn about the current procedures of the admission form exchange subprocess operated during the 2019–2020 period. UAEM carried out the admission process simultaneously in four locations (campuses). Information from the North campus, located in Cuernavaca, Morelos, was considered, since this campus has a higher demand for admission (12 395 applicants in 2020). The college tuition in the North campus is 5 075 new students to be accepted into the university for the 2020–2021 term.

4.2   Results and discussion

The admission form exchange subprocess was analyzed using the *muda* identification method, and Ishikawa and Pareto diagrams. These tools help understanding processes failures and the relations between the facts and the possible causes. Lean tools provide a perspective on the analyzed process that will propose improvements to deploy for process higher performance. The score to qualify each cause considers a scale between 1 and 3. Value 3 is equivalent to a more significant benefit, and value 1 to a lower benefit. The evaluated criteria and their respective solutions are listed on Table 5.

Table 5: Evaluated criteria and their respective solutions

#	*Causes*	*Solution*
1	Lack of activities distribution of the process	Merge phase 2 with the documents reception
2	Lack of visual support communication	Apply Kanban to the LO process
3	Lack of maintenance to the computer system	Provide technical support and maintenance to the computer system.
4	Omission of previous computer system technical tests	Carry out preliminary simulations of the process
5	Poor planning of personnel management	Implement Heinjunka to level the LO process
6	Poor management of staff during the process	Implement cross-training based on the Pull LO System
7	Distribution of communication network by cable	Restructure the communication network installation
8	Poor distribution of computer equipment	Redistribution of the computer equipment for data capturer staff

Table 6 shows the assessment analysis of the criteria evaluated: problem factor (PF), direct cause (DC), solution (SL), feasible (FE), measurable (ME), and low cost (LC). The causes with the most benefit score are "Poor planning of personnel management" and "Poor management of staff during the process", and the cause with the lower benefit score is "Distribution of communication network by cable". The number of failures was measured during the in-person evaluation, and the number of events was counted.

Table 6: Assessment analysis of the criteria evaluated

# Cause	Criteria						Total
	PF	DC	SL	FE	ME	LC	
1	3	2	3	2	1	3	**13**
2	3	2	3	3	2	2	**14**
3	3	3	3	1	3	1	**14**
4	3	2	2	3	1	2	**12**
5	2	3	3	3	1	3	**15**
6	2	3	3	3	1	3	**15**
7	1	1	3	1	1	1	**8**
8	2	2	3	2	1	3	**13**

Figure 2 shows the critical phases of the admission form exchange subprocess reported by the admission services area. Critical phases presented failures in the activities developed in the admission process. The main failures identified are:

1. Staff carelessness when receiving documents
2. Reception staff carelessness due to lack of care in receiving documents
3. Reception staff carelessness in comparing the recorded admission form with information of the applicant
4. Photo equipment failure to take the photo
5. Printer failure

Fig. 2: Critical phases of the admission form exchange subprocess

The main failures detected in the admission process were not consecutive and occasionally a failure occurs due to factors unrelated to the process. The failures in sectors such as offices are not continuous, unlike failures in the manufacturing sector, which are consecutive. In this way, failures were measured to prioritize tasks that could assist in solving the main failures. In addition, Pareto analysis was performed to identify the frequency that a failure occurs in the admission process. Table 7 shows the frequency of failures in the admission form exchange subprocess.

Table 7: Frequency of failures that occurs in the admission form exchange subprocess

#	Failure	Frequency	Sum	Share	Sum
1	Digital database failure	135	135	34.09%	34.09%
2	Reception carelessness	99	234	25.00%	59.09%
3	Detail review careless	72	306	18.18%	77.27%
4	Printer failure	60	366	15.15%	92.42%
5	Entrance carelessness	30	396	7.57%	100.00%
	Total	**396**	**N/A**	**100.00**	

Figure 3 shows the Pareto chart of the frequency of failures in the admission form exchange subprocess.
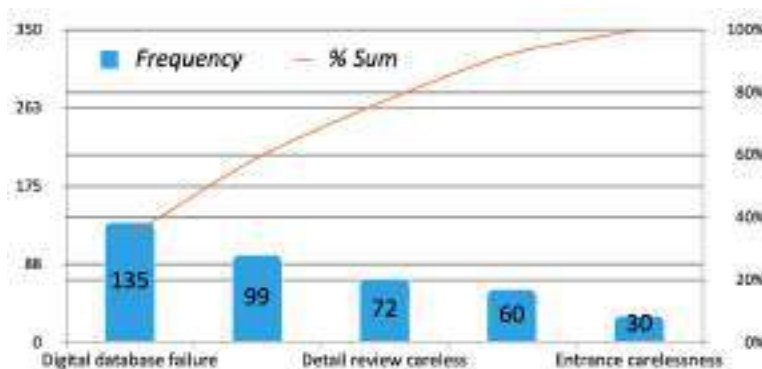
Fig. 3: Pareto chart of failures frequency in the admission process

Figure 3 shows that failures #1, #2, and #3 in table 7 produce 80% of the problems in the admission form exchange subprocess. The analysis carried out using the Ishikawa diagram (Figure 1) identifies that there is *i)* excess of time in the detailed review of the applicant information, *ii)* the phase does not have a sufficient number of cameras to satisfy all the demand in a reasonable time, *iii)* the Data Capture phase is deficient and confusing for applicants, and *iv)* the digital database usually has problems accessing concurrently, generating access time delays in next activities.

5 Conclusions and future work

This article presented a Lean methodology for *muda* identification in the admission form exchange subprocess of new university students in the smart campus context. The proposed Lean methodology combines Lean tools to identify mistakes generated in the admission process of UAEM, a case study in Mexico. The Lean methodology employed analysis tools, i.e., Ishikawa and Pareto diagrams.

The Lean tools helped understand process failures to improve the admission process. The main failures detected in the admission form exchange subprocess are: *i)* time excess on document detailed review activities, *ii)* high demand on photo taking in function with the number of photo equipment, *iii)* confusion by applicants to find the data capture staff location, and *iv)* concurrent access problems to the computer system. Also, the admission form exchange subprocess lacks standardization of subprocesses. Even though there is a standardized operation manual, the subprocesses are neglected. The methodology validation focused on evaluating the time saving of the admission form exchange subprocess by employing *muda* identification. The college tuition offered was of 5 075 new students to be accepted into the university for the 2020–2021 term. The number of applicants was 12 395 in 2020. The computed results indicate that the proposed Lean methodology is efficient for *muda* identification and for agile improvements for the admission form exchange subprocess in reasonable time.

The main lines for future work are oriented to extend the proposed Lean methodology to apply essential indicators, statistics, and Lean tools such as Failure Mode and Effect Analysis and Andon. In addition, those tools would be valuable for relevant research, such as standardizing processes through Digital Lean Manufacturing and Industry 4.0. Also, the proposed Lean methodology must be extended for the income educational offer for new students on all university campuses.

References

1. Bhamu, J., Singh, K.: Lean manufacturing: literature review and research issues. International Journal of Operations & Production Management **34**(7), 876–940 (2014)
2. Chen, J., Cox, R.: Value stream management for lean office—a case study. American Journal of Industrial and Business Management **2**, 17–29 (2012)
3. Cheong, P., Nyaupane, P.: Smart campus communication, internet of things, and data governance: Understanding student tensions and imaginaries. Big Data & Society **9**(1) (2022)
4. Greef, A., Romanel, F., Do Carmo, M.: Lean Office: Operação, Gerenciamento e Tecnologias. Atlas Editora (2012)

5. Hicks, B.: Lean information management: Understanding and eliminating waste. International Journal of Information Management **27**(4), 233–249 (2007)

6. Liker, J.: The Toyota Way: 14 Management Principles From the World's Greatest Manufacturer. McGraw-Hill Education (2003)

7. Locher, D., Benavent, E.: Lean office: Metodología Lean en servicios generales, comerciales y administrativos. Profit Editorial (2017)

8. Magalhães, J., Alves, A., Costa, N., Rodrigues, A.: Improving processes in a postgraduate office of a university through lean office tools. International Journal for Quality Research **13**, 797–810 (2019)

9. Monteiro, J., Alves, A., Carvalho, M.: Processes improvement applying lean office tools in a logistic department of a car multimedia components company. Procedia Manufacturing **13**, 995–1002 (2017)

10. Rossit, D.A., Toncovich, A., Rossit, D.G., Nesmachnow, S.: Flow shop scheduling problems in industry 4.0 production environments: Missing operation case. In: Handbook of Smart Materials, Technologies, and Devices, pp. 1–23. Springer International Publishing (2021)

11. Sabur, V., Simatupang, T.: Improvement of customer response time using lean office. International Journal of Services and Operations Management **20**(1), 59–85 (2015)

12. Tapping, D., Shuker, T.: Value Stream Management for the Lean Office: Eight Steps to Planning, Mapping, & Sustaining Lean Improvements in Administrative Areas. Taylor & Francis (2018)

13. Ustundag, A., Cevikcan, E.: Industry 4.0: Managing The Digital Transformation (2018)

14. Van Deursen, A., Mossberger, K.: Any thing for anyone? a new digital divide in internet-of-things skills. Policy & Internet **10**(2), 122–140 (2018)

15. Wang, J.: Lean Manufacturing: Business Bottom-Line Based. CRC Press, 1 edn. (2010)

16. Womack, J., Jones, D.: Lean Thinking: Banish Waste And Create Wealth In Your Corporation. Simon & Schuster UK (2013)

17. Womack, J., Jones, D., Roos, D.: La máquina que cambió el mundo: La historia de la Producción Lean, el arma secreta de Toyota que revolucióno la industria mundial del automóvil. Profit Editorial (2017)

18. Yokoyama, T., Oliveira, M., Futami, A.: A systematic literature review on lean office. Industrial Engineering & Management Systems **18**, 67–77 (2019)

Analyzing the feasibility of the use of computational analysis in lighting improvement projects: The case of the Aerospace Engineering School of UPM (Spain)

Álvaro Pérez-Rees[1][0000-0001-7388-7894], Daniel Alfonso-Corcuera[1,2][0000-0002-1080-0840] and Santiago Pindado[1,2][0000-0003-2073-8275]

[1] Departamento de Sistemas Aeroespaciales, Transporte Aéreo y Aeropuertos, ETSI Aeronáutica y del Espacio, Universidad Politécnica de Madrid, Pza. del Cardenal Cisneros 3, 28040 Madrid, Spain

[2] Instituto Universitario de Microgravedad "Ignacio Da Riva" (IDR/UPM), ETSI Aeronáutica y del Espacio, Universidad Politécnica de Madrid, Pza. del Cardenal Cisneros 3, 28040 Madrid, Spain

`alvaro.prees@alumnos.upm.es`

Abstract. This paper analyzes the feasibility of using simulation software for the application of lighting improvements in university buildings, specifically in the case of the Aerospace Engineering School (*Escuela Técnica Superior de Ingeniería Aeronáutica y del Espacio* – ETSIAE) of the *Universidad Politécnica de Madrid* (UPM). The paper analyzes the effects of a project to change the lighting fixtures in several classrooms. An analysis of the lighting in the students' workstations was carried out by means of in situ measurements and simulations, taking as a reference the data prior to the change, using the DIALUX® software. The simulations were able to relatively predict the evolution of the lighting characteristics of the classrooms after the renovation project.

Keywords: Lighting, lighting simulation, illuminance, DIALux, educational building.

1   Introduction

The quantity and quality of lighting is a vital aspect of building construction. In the literature, there are numerous examples of the impact that poor lighting can have on the mood and productivity of workers or occupants of a building [1–4]. There are also several studies that highlight the importance of good visual comfort conditions in academic institutions of all types [5–18]. Although visual comfort can be influenced by other factors, it depends mainly on lighting [18, 19].

There is a vast literature that relates illuminance levels and their uniformity to the quality of illumination [17, 20–22]. Similarly, there is also a large literature that studies the negative impact of glare on perceived lighting quality and performance [1, 23, 24]. Finally, another of the most frequently analyzed aspects is the importance of correct

color rendering by artificial light sources [25–28]. Based on the above, the UNE-EN 12464-1:2012 standard, which regulates lighting projects in workspaces, with the aim of guaranteeing acceptable lighting quality, takes as indicators

- the average horizontal illuminance values,
- the horizontal illuminance uniformity,
- the color rendering index of the installed luminaires, and
- the values of the Universal Glare Rating (UGR).

Fig. 1. Aerial view of the *Escuela Técnica Superior de Ingeniería Aeronáutica y del Espacio* (ETSIAE). Source: *Universidad Politécnica de Madrid*.

This paper continues the work previously carried out on the study of the lighting characteristics at the Aerospace Engineering School (*Escuela Técnica Superior de Ingeniería Aeronáutica y del Espacio* – ETSIAE) of the *Universidad Politécnica de Madrid* (UPM) [29], in which a detailed study of the lighting characteristics of typical classrooms in different buildings of the ETSIAE was carried out (see Fig. 1). In this study, through an extensive measurement campaign, the illuminance values of the different type classrooms were obtained. Using the data obtained and by modeling the installed luminaires, a model of the classrooms was made using the DIALux® software, studying the impact of different measures to reshape the lighting installation in order to adapt the work areas to the requirements established in the UNE-EN 12464-1:2012 standard (see Table 1).

This work proposed a methodology based on representing through software, and taking into account the measured data, the lighting characteristics of the spaces in order to be able to propose improvement measures.

Table 1. Required lighting quality indicator values of mean perpendicular illuminance E_m, maximum UGR value, uniformity factor U_o, and chromatic reproduction R_a for working areas according to UNE-EN 12464-1:2012 for classrooms [30].

Type	E_m [lx]	UGR_L	U_o	R_a
Classroom	300	19	0.60	>80

In 2021, and based on the previous work [29], the luminaires of the ETSIAE were updated. As a consequence, some luminaires were completely replaced, while in other cases, only the lamps were replaced.

Based on the above, it was proposed to analyze, based on the methodology proposed in [29], the effects that these changes had had on the lighting characteristics of the studied classrooms.

This paper is divided as follows. First, the methodology used for the study is analyzed, considering the simulations performed using the DIALux® software, as well as the campaign of real illuminance measurements. Second, the results of the study are discussed. Finally, a series of conclusions are presented.

2   Materials & methods

To verify that the standard requirements are met, a measurement campaign has been carried out in 4 classrooms of ETSIAE (see Fig. 2), which were selected in previous work [29] as representative of the different types of poorly illuminated classrooms prior to the luminaire update. This was done by selecting for each classroom size type (see Table 2) the classroom which obtained the worst illuminance measurement results, and for which extensive analysis was performed prior to the luminaire update.

Table 2. Detail on the classrooms selected as representative of poorly illuminated classrooms.

Classroom	Capacity (students)	Surface (m^2)
A-005 (medium size)	99	103,53
A-016 (small size)	28	31,20
A-038 (big size)	115	111,59
B-306 (average classroom building B)	96	86,94

In this campaign, the perpendicular illumination has been measured both in tables and blackboards in the classrooms themselves and also a simulation has been made in DIALux® to verify that the UGR did not exceed the maximum allowed, to make this simulation as accurate as possible the luminaries were measured in the laboratory to adjust the polar curves of the LED tubes simulating them being installed in the current luminaries of building A, the process concluded with an adjusted model of the .ldt archives that the software DIALux® uses; although it regulates the polar curves it does not alter the glare, only the width and shape of the light beam.
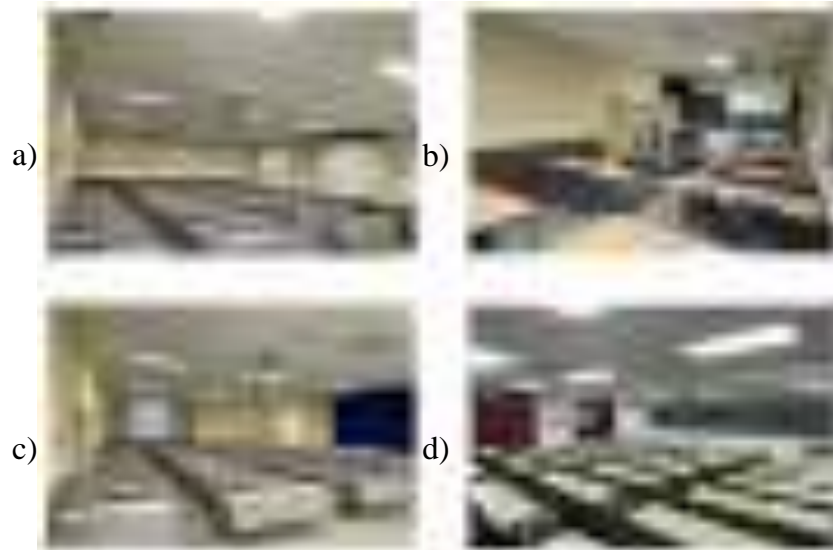
Fig. 2. Images of the four classes studied: a) A-005; b) A-016; c) A-038 & d) B-306.

2.1 SIMULATION

Once the rooms representative of the ETSIAE classrooms were selected, their lighting situation was represented as accurately as possible using DIALux® simulation software. Due to the data collected in the testing campaign, the simulations were carried out taking into account precise details from:

- the geometry of the classes;
- the actual layout of the luminaires, which was reproduced;
- the arrangement of desks, chairs, blackboards, and elements that affect lighting, and the textures of the walls and floor; and
- the degradation of the luminaires, which was implemented by dimming the wattage to account for soiling due to age, dust or any other defects that the reflector may have on its surface, parameters which were estimated.

This was done to reproduce both the geometry and the lighting conditions of the classrooms as accurately as possible in the subsequent simulation. For the geometry and disposition of luminaires, physical measurements were performed.

Within the group of classrooms studied, it should be noted that in each building a different technology has been implemented, in building A LED tubes have been chosen,

while in building B the choice has been LED screens, Figure 3 shows the comparison of classroom A-005 and its simulation with DIALux®.

Fig. 3. Comparison between a real image (left) of the A-005 classroom and its simulation in DIALUX® (right).

2.2   Classroom measurements

A CEM-DT 1308 luxmeter was used to take the measurements at the different points on the tables and the blackboards of the horizontal illuminance. These measurements were carried out on consecutive days, specifically on June 7 and 8, 2022, between 21:00 and 23:00. The time of the day was selected to reproduce the conditions of [29] in which, to evaluate the most unfavorable conditions, illuminance was measured after sunset and with the classroom curtains covering the windows (when possible). For the desks, a set of 7 representative points was measured for each desk position (see Fig. 4). For the blackboards, measurements were made at each 1 m on the mean height line.
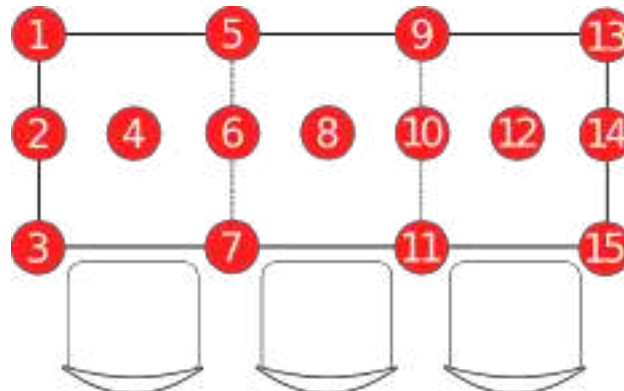
Fig. 4. Diagram of the position and distribution of the points selected for horizontal illuminance measurements on the classroom desks.

3   Results & discussion

This study aims to analyze the quality of lighting in the *Escuela Técnica Superior de Ingeniería Aeronaútica y del Espacio* (ETSIAE) at the *Universidad Politécnica de Madrid* (UPM). The reason was the poor lighting that the school had in recent years, especially in the evenings, and since a change of luminaires was made at the beginning of the year, its impact was studied. The work was carried out:

— by measuring the illuminance of representative classrooms of this faculty, and
— by simulation.

With the simulation in DIALux® and the measurements taken in the classrooms, conclusions can be drawn about which technology is the most appropriate for a university teaching building and the degree of compliance with the standard, especially regarding the glare levels. Table 3 shows the lighting and glare values of the simulation carried out with DIALux® for the different classrooms.

Table 3. Data obtained with DIALUX® simulations and measured in the classrooms showing the maximum, minimum and average perpendicular illuminance E_{max}, E_{min} and E_{av} and the maximum UGR values for the working planes.

Classroom	Model	E_{max}(lx)	E_{av} (lx)	E_{min} (lx)	*UGR*
A-005	Measured	154	116	62	
	DIALux	141	117	89	17.0
A-016	Measured	165	104	40	
	DIALux	152	109	74	21.0
A-038	Measured	156	116	60	
	DIALux	152	118	81	17.0
B-306	Measured	1256	954	604	
	DIALux	1248	951	668	20.2

As can be seen in Table 3 classroom B-306 is the only one that meets the minimum lighting requirements of UNE-EN 12464-1:2012, although it exceeds the maximum illumination and UGR values. However, the classrooms in building A do not meet the minimum lighting requirements, being well below the target value, although they do meet the UGR requirement in 2 of 3 classrooms. The classroom that does not meet the UGR requirement (A-016) has a different configuration of the lamps, which leads to higher glare on some desks.

As can be seen in Table 3, the measured values and those from the DIALux® simulation are practically identical, which shows that if the wear and tear of the reflectors is correctly adjusted in the software, a faithful representation of reality can be obtained, which also suggest the use of this software to evaluate the different possible alternatives to improve the lighting performance of buildings.

The results indicate a poorly illumination in one of the buildings and an excessive glare in the other, which proved that the LED tubes are not the correct technology to be used in this type of buildings, and to improve the current situation, three possible solutions are suggested:

— Connect a dimmer to reduce the power of LED screens without having to replace them with another model, with the objective of reducing the maximum brightness of the lamp to not exceed 1000 lx, and reducing the glare below 19.
— Place a diffuser that reduces glare on the LED screens to reduce the UGR so that it does not exceed a value of 19.
— Replace the LED tubes in building A with the LED screens that are being used in building B.

4. Conclusions

As it has been shown in the previous section, none of the classrooms meet the basic standards of illumination and glare, although this would be easily achieved with the implementation of the solutions previously stated. These poor results also put into perspective the poor conditions under which students take classes at night, which might affect their performance.

DIALux® EVO software was used to analyze the current situation of the illumination conditions in classrooms. Comparison with results from physical measures indicate that using lighting simulation software not only can correctly predict and represent the lighting performance in buildings but also suggest its use to evaluate measures to improve the actual lighting conditions.

Future work that follows this study should focus on:

— Including daylight in the lighting analysis, as some classrooms might have glare problems at certain periods of the day.
— Include the energy consumption of luminaires in order to find the most sustainable solution, given that the current situation in Europe shows the need to reduce energy consumption in the short term.
— Establish methods to quantify and apply the wear and tear of the reflectors in the simulations.

Finally, the importance of this study must be emphasized, as it reveals a serious problem that could also exist at other UPM schools and faculties and at other Spanish universities.

References

1. Hwang T, Jeong TK (2010) Effects of Indoor Lighting on Occupants' Visual Comfort and Eye Health in a Green Building. https://doi.org/101177/1420326X10392017 20:75–90. https://doi.org/10.1177/1420326X10392017

2. Juslén H, Tenner A (2005) Mechanisms involved in enhancing human performance by changing the lighting in the industrial workplace. Int J Ind Ergon 35:843–855. https://doi.org/10.1016/J.ERGON.2005.03.002

3. Weston HC (1935) The Relation between Illumination and Industrial Efficiency. 1.-The Effect of Size of Work. The Relation between Illumination and Industrial Efficiency 1-The Effect of Size of Work

4. Konstantzos I, Sadeghi SA, Kim M, et al (2020) The effect of lighting environment on task performance in buildings – A review. Energy Build 226:110394. https://doi.org/10.1016/J.ENBUILD.2020.110394

5. de Giuli V, Zecchin R, Corain L, Salmaso L (2014) Measured and perceived environmental comfort: Field monitoring in an Italian school. Appl Ergon 45:1035–1047. https://doi.org/10.1016/J.APERGO.2014.01.004

6. Winterbottom M, Wilkins A (2009) Lighting and discomfort in the classroom. J Environ Psychol 29:63–75. https://doi.org/10.1016/J.JENVP.2008.11.007

7. Mott MS, Robinson DH, Walden A, et al (2012) Illuminating the effects of dynamic lighting on student learning. Sage Open 2:1–9. https://doi.org/10.1177/2158244012445585

8. Samani SA, Samani SA (2012) The Impact of Indoor Lighting on Students' Learning Performance in Learning Environments: A knowledge internalization perspective

9. Barrett P, Davies F, Zhang Y, Barrett L (2015) The impact of classroom design on pupils' learning: Final results ofaholistic, multi-level analysis. Build Environ 89:118–133. https://doi.org/10.1016/J.BUILDENV.2015.02.013

10. Bluyssen PM, Zhang D, Kurvers S, et al (2018) Self-reported health and comfort of school children in 54 classrooms of 21 Dutch school buildings. Build Environ 138:106–123. https://doi.org/10.1016/J.BUILDENV.2018.04.032

11. M Hui SC, Y Cheng KK (2008) Analysis of effective lighting systems for university classrooms

12. Wang R, He X-Y, Liu S, et al (2017) Investigation and analysis on the illumination of the university classroom. 430–438. https://doi.org/10.2991/ICMMCT-17.2017.92

13. Yang Z, Becerik-Gerber B, Mino L (2013) A study on student perceptions of higher education classrooms: Impact of classroom attributes on student satisfaction and performance. Build Environ 70:171–188. https://doi.org/10.1016/J.BUILDENV.2013.08.030

14. Castilla N, Llinares C, Bravo JM, Blanca V (2017) Subjective assessment of university classroom environment. Build Environ 122:72–81. https://doi.org/10.1016/J.BUILDENV.2017.06.004

15. Castilla N, Llinares C, Bisegna F, Blanca-Giménez V (2018) Affective evaluation of the luminous environment in university classrooms. J Environ Psychol 58:52–62. https://doi.org/10.1016/J.JENVP.2018.07.010

16. Ricciardi P, Buratti C (2018) Environmental quality of university classrooms: Subjective and objective evaluation of the thermal, acoustic, and lighting comfort conditions. Build Environ 127:23–36. https://doi.org/10.1016/J.BUILDENV.2017.10.030

17. Tahsildoost M, Zomorodian ZS (2018) Indoor environment quality assessment in classrooms: An integrated approach. J Build Phys 42:336–362. https://doi.org/10.1177/1744259118759687

18. Yang W, Moon HJ (2019) Combined effects of acoustic, thermal, and illumination conditions on the comfort of discrete senses and overall indoor environment. Build Environ 148:623–633. https://doi.org/10.1016/J.BUILDENV.2018.11.040

19. Wu H, Wu Y, Sun X, Liu J (2020) Combined effects of acoustic, thermal, and illumination on human perception and performance: A review. Build Environ 169:. https://doi.org/10.1016/J.BUILDENV.2019.106593

20. Leccese F, Salvadori G, Rocca M, et al (2020) A method to assess lighting quality in educational rooms using analytic hierarchy process. Build Environ 168:. https://doi.org/10.1016/J.BUILDENV.2019.106501

21. Bellia L, Spada G, Pedace A, Fragliasso F (2015) Methods to evaluate lighting quality in educational environments. Energy Procedia 78:3138–3143. https://doi.org/10.1016/J.EGYPRO.2015.11.770

22. Yacine SM, Noureddine Z, Piga BEA, et al (2017) Towards a new model of light quality assessment based on occupant satisfaction and lighting glare indices. Energy Procedia 122:805–810. https://doi.org/10.1016/J.EGYPRO.2017.07.408

23. Konstantzos I, Tzempelikos A (2017) Daylight glare evaluation with the sun in the field of view through window shades. Build Environ 113:65–77. https://doi.org/10.1016/J.BUILDENV.2016.09.009

24. Petherbridge P, Hopkinson RG (2016) Discomfort Glare and the Lighting of Buildings. http://dx.doi.org/101177/147715355001500201 15:39–79. https://doi.org/10.1177/147715355001500201

25. Hopkinson RG, Petherbridge P, Longmore J (1966) Daylight in architecture

26. Kim W, Jeong TK (2011) The scope of the glare light source of the window with non-uniform luminance distribution. Indoor and Built Environment 20:54–64. https://doi.org/10.1177/1420326X10389269/SUPPL_FILE/IBE396935.PDF

27. Plympton P, Conway S, Epstein K (2000) Daylighting in Schools: Improving Student Performance and Health at a Price Schools Can Afford.

28. Nazzal AA (2005) A new evaluation method for daylight discomfort glare. Int J Ind Ergon 35:295–306. https://doi.org/10.1016/j.ergon.2004.08.010

29. Zamarreño-Suárez M, Alcala-Gonzalez D, Alfonso-Corcuera D, Pindado S (2020) Measuring the Lighting Quality in Academic Institutions: The UPM

Energy efficiency in buildings: Experimental test about the thermal behaviour of mortars with different additives

Jorge López-Rebollo[1][0000-0002-6230-3889], Natalia Nuño Villanueva[1][0000-0001-7022-119X], Ignacio Martín Nieto[1][0000-0003-3984-7228], Cristina Sáez Blázquez[2][0000-0002-5333-0076] , Susana Del Pozo[1][0000-0003-4869-3742] and Diego Gonzalez-Aguilera[1][0000-0002-8949-4216],

[1] Department of Cartographic and Land Engineering. University of Salamanca, Higher Polytechnic School of Ávila, Hornos Caleros, 50, 05003, Ávila, Spain.
jorge_lopez@usal.es; id00816629@usal.es; nachomartin@usal.es; s.p.aguilera@usal.es; daguilera@usal.es
[2] Department of Electric, System and Automatic Engineering, Universidad de León, León, Spain.
u107596@usal.es

Abstract. This study focuses on the search for building materials modified in such a way that their thermal properties are adapted to sustainable energy applications. Several materials with different thermal properties are proposed as additives to modify the thermal conductivity of mortar. Initially, tests are carried out to determine the thermal conductivity of all the manufactured mixtures, analysing the influence of each of the additives. In this sense, materials that show extreme thermal behaviour (crystallised gypsum with higher conductivity and polyester fibres with lower conductivity) can improve the conductivity or isolation of a construction, depending on the need of each case. The samples with the selected additives were subjected to heating-cooling tests using a low-cost solar simulator in order to analyse their behaviour using a thermographic camera. After comparing its thermal performance with that of a reference mortar (without additives), it was concluded that differences of up to 30% in final temperature variation can be achieved by using this kind of additives. Without being a definitive study, this contribution allows drawing promising conclusions for the construction industry, showing new development possibilities and future lines of research for new sustainable materials in the construction sector.

Keywords: Thermal properties, Sustainable material, Solar simulator, Additive mortar.

1 Introduction

The effects of climate change are becoming more and more compromising even in our urban environments [1]. The possibilities of mitigating its undesired effects can no longer depend solely on the implementation of emission reduction policies; it is necessary to adopt coordinated measures on many other fronts of action.

One of the unwanted effects of this climatic emergency that we are beginning to suffer is the creation of heat islands that significantly alter the environmental stability of these urban environments [2]. The forms of mitigating this undesired effect go through the reasonable programming of urban spaces. Initially, the inclusion of green areas has been shown to be one of the fundamental favourable factors, lately, the inclusion of mitigation measures in the building construction procedures have also been considered. On the other hand, the current energy crisis makes it necessary to implement saving measures in urban environments, which will also result in a reduction in greenhouse gas emissions. Ideally, a combination of measures to mitigate unwanted effects with energy saving measures could even be proposed, such as the approach of systems for the use of residual heat stored by the heat island effect for energy purposes.

This work aims to study the thermal behaviour of different additives for building materials, which allow them to perform a second function (in addition to its structural nature), related to energy efficiency and mitigation of the heat island effect. For this to occur, it is necessary to look in two different directions, on the one hand, in some locations, it will be preferable for the material to conduct and/or store heat more efficiently while in other locations the opposite effect will be desired. In this way, some building structures can be set up to reduce the heat island effect where necessary, and others to take advantage of this waste heat and distribute it efficiently. Traditionally, the thermal properties improvement in mortars has been tested from the thermal conductive point of view [3], this research includes thermographic analyses that have been used in thermal tests with other materials with promising results [4]. In this sense, it is proposed to apply active thermography by means of a solar simulator in such a way that the different composition of the materials causes alteration of the thermal diffusivity and heat flow [5]. These differences can be captured by a thermographic camera, which allows full field analysis unlike point contact sensors.

As consequence, an experimental campaign is carried out on mortars with different additives using conductivity and thermographic test to analyse their thermal behaviour. After this Introduction, Section 2 describes these materials and techniques employed. In Section 3, the experimental results for each test are shown and a discussion of these results is given. Finally, in Section 4, a series of conclusions are drawn about the suitability of a series of compounds in thermal mortar mixtures that will allow the development of future research on the way to introduce these elements in the usual processes of the construction industry.

2   Materials and methods

This work focuses on the use of additives particularly selected to alter the thermal properties of mortars. When the additives for this preliminary study were selected, the following factors were taken into account:

- Thermal conductivity, the property of selected additives capable of altering in one way or another the thermal behaviour of the resulting building material. It oversees conferring the desired energetic behaviour to the mixture.

- The availability of additives, so that their possible integration into manufacturing processes does not pose a logistical and economic problem.
- No reactivity of the additives with the mixture in the setting process, thus ensuring that the mechanical properties of the final product are maintained.

Once the additives materials for the mixtures had been selected, the samples were prepared for the subsequent tests. Respecting the setting period, thermal tests were carried out on the samples, consisting of thermal conductivity tests using the needle probe method [6], as well as reflectivity and thermal distribution tests by means of a thermographic camera [7] on the samples that have shown the most promising results in the conductivity test. **Fig. 1** shows a schematic diagram of the workflow followed.
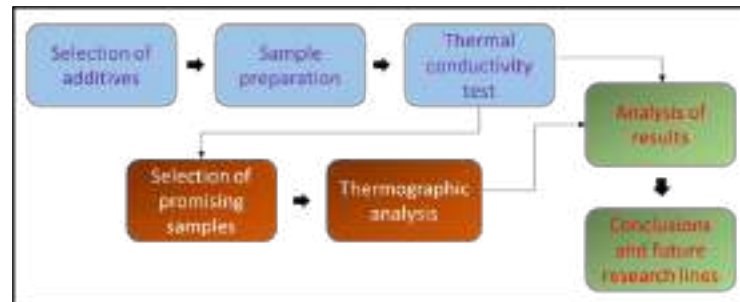
Fig. 1. Workflow diagram.

2.1   Materials for the additive mortars

Due to the importance given to the building materials in construction as stated in the introduction in terms of temperature efficiency, it is valid to assume that a change in the characteristics in the base of those materials such as bricks and mortar could make a significant change in its behaviour. In this line of research, the mortar will be the focus of study since it is widely used and it can be mixed with different additives in order to increase or decrease its resistance to temperature.

In order to select the additives some key factors have been determined such as it ease of obtaining, the possibility of giving the additive a second life reusing them for this objective or if any additive happens to exist in different forms (e.g. dust or liquid) each of them has to be studied in order to determine if it could present any differences; additionally, the additives selected cannot currently be used commercially.

Consequently, five different additives have been chosen (**Fig. 2**): polyester fibres, polystyrene, graphite, gypsum powder and crystallised gypsum. All of them relatively easy to access and possible reuse in the construction industry.

Fig. 2. Different additives selected to be used in the mortar mix. From left to right: polyester fibres, polystyrene, graphite, crystallised gypsum and gypsum powder.

In the case of the polyester fibres, the factors that determined their selection are based on their easy access and possible reuse, since bags made of polyester are usually used in construction, as an example, the sample used for this research was obtained by ripping said bags and obtaining the fibres. Polystyrene shares the key factors of polyester fibres as it is commonly used as packaging from which the sample was extracted. Graphite is a mineral used in various industries such as the pharmaceutical industry, construction or even electric industry used in electrodes, so it would be another use to which it could be applied, given its easy access. Gypsum is one of those materials that could be presented in different form, in this research its crystalline and powder form have been considered since the crystallised gypsum is its base mine form whereas the powder form is the gypsum form that has been processed. The gypsum powder is extensively used in construction as a paste for trim, as a bonding and joint paste or for artistic purposes, so it is already present on the construction sites and could be pre-used for the mortar.

For the purpose of the decision in the quantity of the additive that has to be added in the mortar, given the nature of the form of the additives presented in **Fig. 2**, the measurement of the additive has to be in % volume since if it was by weight additives such as polystyrene would exceed the amount of mortar used per sample. The following **Table 1** presents a summary of the additives. The inaccuracy in the measurement is due to the complexity of measuring the additives, in addition it should be considered that this study seeks to locate general behaviours, and in no case has it exceeded 5% by volume in order not to alter the mechanical properties of the final mortar.

Table 1. Summary table of additives, its thermal conductivity (λ) and their percentage by volume used.

	Polyester (fibres)	Polystyrene	Graphite	Gypsum (crystal)	Gypsum (powder)
λ (W/m·K)	0,038 [8]	0,035 [9]	130 [10]	0,56 [9]	0,30 [9]
% Volume	$\leq 5\ \%$	$\leq 5\ \%$	$\leq 5\ \%$	$\leq 5\ \%$	$\leq 5\ \%$

Once the additives have been selected and the quantity is decided, it is important to determine the base mortar mixture on which they will be added. For this study, the

mortar will consist of natural siliceous aggregates, Portland cement and water in a proportion of 3:1:0,5 respectively. The characteristics of the components of the mortar mixture are as follows:

- The cement used corresponds to white Portland cement with limestone (EN 197-1:2011 [11]) with a resistance of compression of 42,5N by AXTON.
- The selected natural aggregates are siliceous sand treated with a test sieve (UNE 7050-3 [12]) of 2mm (**Fig. 3**).
- The sample water is non-aggressive according to UNE 83952 [13].

Fig. 3. Detail of the sieve used and the difference in the sand processed.

In order to optimise the material for the samples, the mortar dosage consisted of 600g of natural aggregates, 200g of Portland cement and 100g of water. A volume of 5% has been estimated for the additive concerning the whole sample volume by using a cubic measurement container with an edge of 3.5 cm.

The moulds with dimensions of 160 x 40 x 40 mm described in the UNE-EN 196-1 standard [14] were used for the manufacture of the samples. The curing conditions were respected by keeping the samples in the moulds for the first 24 hours and subsequently the specimens were kept in water at a temperature of 20±2 ºC.

A total of 18 samples were manufactured, so that three specimens were obtained for each of the six mixtures (5 additives and reference mortar). One of these specimens was used for the thermal conductivity tests and another one was used for the heating-cooling tests. The remaining specimen was kept for safety and for future research.

2.2   Thermal conductivity test

Thermal conductivity parameter was measured in laboratory thanks to the thermal properties of the TEMPOS analyser used. The device (commercially by "DECAGON") complies with the ISO 2008 standards and the ASTM 5334 and IEEE 442 and is designed for taking accurate readings of thermal conductivity, thermal resistivity, specific heat, and thermal diffusivity of materials [15].

Depending on the material and the specific parameter to measure, different specific needles are used, generating discrete amount of heat to virtually eliminate the moisture movement (or free convection in the case of liquids) that could influence the reading

The basis of measuring of this devise is the infinite line heat source theory, in which thermal conductivity is calculated from monitoring the dissipation of heat in the needle probe. Heat is injected to the needle for an established heating time th, and temperature

is then measured in the monitoring needle during heating and for an extra time equal to *th* after heating. Equation 1 describes how the temperature during heating is obtained [16].

$$T = m_0 + m_2 t + m_3 lnt \qquad (1)$$

Where m_0 is the ambient temperature during the heating stage; m_2 is the rate of background temperature drift; and m_3 is the slope of a line relating temperature rise to logarithm of temperature.

The model during cooling is described in Equation 2.

$$T = m_1 + m_2 t + m_3 ln \frac{t}{t-t_h} \qquad (2)$$

The thermal conductivity of the sample is finally obtained from Equation 3, which also considers the heat flux *(q)*.

$$k = \frac{q}{4m_3} \qquad (3)$$

In this research, RK-3 sensor was used to carry out the thermal conductivity measurements with TEMPOS device. This sensor is specifically designed for solid and rocky materials and its main specifications are included in **Table 2**.

Table 2. Specifications of the single needle RK-3 used with TEMPOS analyser.

RK-3 needle – TEMPOS	
Size	3.9 mm diameter x 60 mm length
Range	Resistivity: 17 – 1000ºC·cm/W Conductivity: 0.1 – 6 W/(m·K)
Accuracy	Conductivity: ±10% from 0.1 – 6 W/(m·K)

2.3 Thermographic analysis

The thermal behaviour has been monitored with a thermographic camera after heating the specimens with a low-cost solar simulator.

Specifically, a FLIR T540 thermographic camera with built-in RGB sensor and a 42º lens (FOV of 42º x 32º) capable of capturing 30 fps has been used. It is a device that offers a resolution of 464 x 348 pixels in the TIR and 5 MPx in the VIS spectrum. In addition, it has a laser sensor that allows knowing, prior of acquisitions, the distance between the camera and the object to perform autofocus. It has a thermal sensitivity of <30 mK at 30°C and it is calibrated for use within the temperature range of -20 to 120°C.

Regarding the lighting system, a 250W metal arc halide lamp from Philips was chosen. **Table 3** shows the main features of this lamp. This type of lamps is one of the most used to simulate the heating produced by solar rays [17, 18].

Table 3. Features of the Philips metal halide arc lamp.

Parameter	Value
Product name	HPI-T Plus 250W/645
Nominal luminous flux	19500 lm
Colour temperature	4500 K
Length	255 mm
Diameter	47 mm

Fig. 4. Low-cost solar simulator device.

Finally, this lamp was installed on a platform designed ad-hoc to form the low-cost solar simulation system (**Fig. 4**). This system is composed of a ballast to regulate the continuous flow of the arc as well as to provide the appropriate voltage to the lamp, a support for the lamp with an aluminium plate to concentrate the radiation, the metal halide lamp, and the sample tray. Solar simulators are devices capable of approximately simulating, by means of artificial light, the natural light of the sun. In this study, the uniformity and temporal stability of the luminous flux received by the samples is guaranteed because they were always located in the same place with respect to the lamp, in addition to the fact that the heating-cooling tests were carried out under the same conditions (same turn-on and turn-off duration for all simulations). Regarding the optical spectrum, metal halide lamps have a spectral coverage close to the global solar radiation spectrum.

3   Experimental results and discussion

3.1   Thermal conductivity test

Test setup

When performing the thermal conductivity test with the already described TEMPOS analyser, samples were radially drilled for the introduction of RK-3 needle. The contact between the needle and the material is ensured by inserting thermal grease in the mentioned hole.

Before the measuring process, RK-3 sensor was accordingly calibrated with the specific sample supplied by the manufacturer. Once calibrated, three measurements (of around 10 minute each) were carried out on each mixture to evaluate possible measuring uncertainties and errors. A total of 18 measurements were made on the performed samples (3 thermal conductivity tests on the 6 mixtures).

It must be also mentioned that ambient temperature was kept as constant as possible at 25ºC during the measurement process to obtain the most accurate data possible. In this sense, to minimize these sources of error, about 15 minutes for samples and needle to equilibrate with the ambient temperature before taking measurements and around 15 minutes between readings for temperatures to equilibrate. In the following **Fig. 5** it is possible to observe the laboratory measuring with TEMPOS analyser and RK-3 sensor.

Fig. 5. Process of samples measuring in laboratory with TEMPOS analyser.

Thermal conductivity test results

The following results presented in **Table 4** and **Table 5** are obtained by measuring the three samples individually. The mean ($\bar{X}$) and the standard deviation (δ) was also calculated.

Table 4. Results of the thermal resistance of the samples.

Sample	Thermal resistance (ºC·cm/W)			$\bar{X}$	δ
Mortar	173	159	183	171.67	12,055
Polyester	276	241	264	260.33	17,786
Polystyrene	106	112	111	109.67	3,21
Graphite	125	104	122	117	11,358
Gypsum (C)	96.7	80.1	111	95.93	15,464
Gypsum (P)	205	225	247	225.67	21,008

Table 5. Results of the thermal conductivity of the samples.

Sample	Thermal conductivity (W/m·K)			$\overline{X}$	δ
Mortar	0,579	0,6275	0,5465	0,5843	0,041
Polyester	0,3626	0,4156	0,3783	0,3855	0,027
Polystyrene	0,941	0,894	0,9014	0,9121	0,025
Graphite	0,799	0,96	0,8226	0,8605	0,087
Gypsum (C)	1,034	1,249	0,899	1,0607	0,177
Gypsum (P)	0,4879	0,4449	0,4044	0,4457	0,042

Consequently, compared to the reference mortar with 0,58W/m·K, materials with higher thermal conductivity and lower thermal conductivity have been obtained. As for the material with higher thermal conductivity, the gypsum in its crystalline form, has a value of 1,06W/m·K, which represents an increase of 0,476W/m·K with respect to the reference mortar. On the other hand, the mortar with polyester fibres with 0,39W/m·K shows a decrease of 0,199W/m·K in its thermal conductivity properties. These variations can also be observed in their thermal resistance where the polyester sample presents an increase of 89ºC·cm/W and the gypsum in its crystalline form presents a decrease of 76ºC·cm/W, both referred to the reference mortar.

The other additives have also modified the thermal properties but to a lesser extent. On the one hand, it could be expected that the sample with polystyrene would reduce the conductivity given its low value, similar to polyester fibres. However, this sample has obtained a higher thermal conductivity than the reference mortar, which could be explained from the point of view of the shape of its particles and their interaction with the mortar. On the other hand, graphite originally has a high conductivity. Mortar with this additive has increased the final value, but to a lesser extent than other additives. Finally, the powdered gypsum (which had a slightly lower value than the mortar) slightly reduced the conductivity of this mixture.

Considering the margin of error of the measuring device and given that the aim of this study is to locate general behaviours, it was decided to select the two samples with the most extreme behaviours: crystallised gypsum and polyester fibres. Nevertheless, the results obtained from the three measurements show that they are consistent and have allowed us to obtain a valid approximation for the thermal conductivity of each of the samples.

3.2   Thermal behaviour

Test setup

The thermal behaviour study was carried out with the three samples selected after conductivity tests. In this way, the materials with the highest (mortar with crystallised gypsum) and lowest (mortar with fibres) thermal conductivity were selected, in addition to the reference mortar. Considering that the original samples of 160 x 40 x 40 mm were divided into two for the two types of tests, the dimensions of the samples for the thermal test were 80 x 40 x 40 mm, with the illumination being applied on the side with the larger dimensions.

The tests for each material were carried out individually, placing the samples in such a way that the illumination had a vertical incidence on the surface to be studied, with a distance of 0.5 m. The camera was placed at the same distance with the least possible inclination to avoid errors in the measurement.

In order to guarantee the same initial conditions in each test, the samples were kept isolated until they were placed under the solar simulator. In this way, the initial temperature of each sample was 25°. To ensure that the illumination was stable and to avoid deviations during heating, the lamp was turned on for 10 minutes until the sample was placed. Once the sample is placed, the thermographic image acquisition stars during the heating stage, with a duration of 15 minutes. Once this time has elapsed, the solar simulator is switched off and the cooling stage begins, maintaining image acquisition for an additional 30 minutes. No additional device was used during this stage, so the sample was cooled by natural convection. Although the ambient temperature remained stable during the whole process, the heating of the solar simulator device itself can cause slight variations in the ambient temperature, so that slight oscillations can occur during the cooling of the samples.

Regarding the acquisition of thermographic images, a frequency of 1 fps was used, since counting heating and cooling, a total of 2700 images were acquired (45 min).

For each of these images, in order to study if there were significant differences between the inside and outside of the sample due to edge effects three Region Of Interest (ROI) were selected (**Fig. 6**): i) full sample, corresponding to the entire study surface; ii) edges, corresponding to the outer region with a width of 10 mm; and iii) centre, corresponding to the inner area with dimensions of 60 x 20 mm.
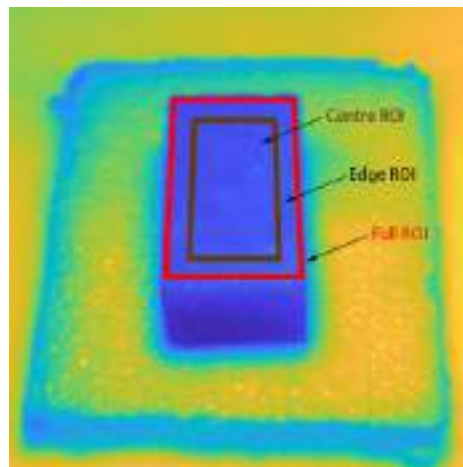
Fig. 6. Selected Regions Of Interest for thermal analysis.

Thermal results

The tests were analysed using two different approaches. On the one hand, the temperature evolution curve was analysed, both in the heating and cooling phases in order to study the differences in the behaviour of each material. On the other hand, the ROIs described above were studied to determine the possible influence of edge effects and effectiveness of the heating device.

Heating and cooling curves

The heating and cooling curves (**Fig. 7**) were obtained for each of the samples. For this purpose, the mean value of the full ROI was calculated for each of the thermal images to eliminate point errors or defective pixels. Then, a moving average filter was applied to eliminate anomalous values caused by erroneous frames. This filter allows a smoother curve to be obtained while reducing noise due to camera sensitivity.
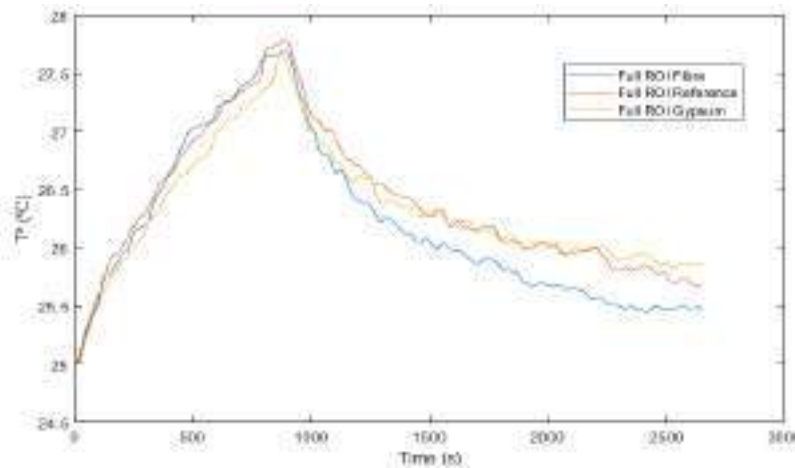
Fig. 7. Heating and cooling curves of thermal tests.

Once the curves were plotted, the values corresponding to the end of heating and cooling were extracted. These values correspond to the maximum temperature increase and the final temperature variation of the sample (**Table 6**). These values, together with the graph, allow a better analysis of the heating and cooling processes.

Table 6. Maximum temperature increase and final temperature variation for each material.

Sample	Maximum temperature increase (ºC)	Final temperature variation (ºC)
Fibre	2.69	0.46
Reference	2.78	0.66
Gypsum	2.65	0.85

With regard to heating, the curves for each of the materials are practically similar, reaching a similar maximum temperature increase. The slight differences in this value are barely significant (0.1ºC) and may be due to causes associated with the measurement process, such as the sensitivity of the camera or the slight thermal oscillations caused by natural convection. In this sense, it must be considered that the heating is produced by radiation and that only surface heating is produced because the time is not very long, so it is difficult for the difference in conductivity to have an influence.

In the case of the cooling phase, significant differences can be seen, both in the curves shown in Fig. 2 and in the final values shown in **Table 6**. In this case, there is a difference of 0.4ºC between the fibre sample and the crystallised gypsum sample, corresponding to those with the lowest and highest conductivity respectively. The reference sample is practically equidistant between the two. Due to the fact that the heating is carried out by radiation and in a short period of time as mentioned above, there is mainly surface heating, which means that the difference in conductivity does influence the final temperature of the sample in this case. In the case of the mortar with fibre, as it has a lower conductivity, the heating is only superficial without heating the whole sample, which causes a greater reduction in temperature during the cooling phase. On the other hand, the sample corresponding to the mortar with crystallised gypsum can heat up inside due to the higher conductivity, not only being a superficial heating. In this case, the heating of the whole sample causes the final surface temperature to be higher.

In this sense, it would be interesting to know the internal temperature of the sample for a more exhaustive analysis in order to check these hypotheses and to analyse the thermal profile at different depths to determine the influence of conductivity. In the same way, heating for a longer time and reaching a higher temperature should also show differences in the heating phase, which in this case did not exist.

Nevertheless, the results obtained show significant differences in the behaviour of materials with additives to modify their thermal conductivity. Thus, thermal conductivity has a notable influence especially in the cooling phase, since if we observe the surface temperature values at the end of the whole process, the sample with fibre has reduced its temperature by 30% with respect to the reference sample, while the sample with crystallised gypsum has increased its temperature by 29%.

Edge effect analysis

The analyses described above for the full ROI were performed for each of the ROIs shown in **Fig. 6** in order to determine whether the heating of the sample was homogeneous and to detect possible edge effects. The results for the temperature increase after the heating phase are shown in **Table 7** and the results for the final temperature variation after the cooling phase are shown in **Table 8**.

Table 7. Maximum temperature increase for each ROI.

Sample	Full ROI	Centre ROI	Edge ROI
Fibre	2.69	2.70	2.68
Reference	2.78	2.79	2.76
Gypsum	2.65	2.65	2.64

The results show a similar behaviour during the heating phase as the difference between the centre and edge region does not exceed 0.03ºC in any case. This indicates that during heating, edge effects are not visible, as these small differences fall within logical values attributable to the sensitivity of the camera. Nevertheless, it is true that in all cases the centre temperature is equal to or higher than the edge temperature, so it would be interesting to carry out an analysis with a longer heating time and higher maximum temperatures to check whether these effects are visible in this case. In any case, it seems reasonable to assume that the heating of the solar simulator is homogeneous, since the temperature of the sample does not show spatial irregularities.

Table 8. Final temperature variation for each ROI.

Sample	Full ROI	Centre ROI	Edge ROI
Fibre	0.46	0.50	0.41
Reference	0.66	0.72	0.61
Gypsum	0.85	0.89	0.80

In the case of the results for the final temperature, differences can be seen between the temperatures corresponding to the central region and the edge region, while the temperatures for the full ROI are logically situated between the two. In this case, the differences reach 0.1ºC, so that the edge ROI cools more than the centre ROI in all cases. These results show the need to consider both regions for more detailed studies, and it would be interesting to study the thermal profile as mentioned above to determine from what distance the edge ceases to have an influence. In this sense, it would be advisable to work with larger sample sizes in order to make a more detailed analysis taking full advantage of the resolution of the thermal sensor.

4　Conclusions

This work consists of a preliminary study to investigate the possibilities of using additives in the manufacture of mortar in order to adapt its thermal properties to the needs of use in applications in the construction and building sector where materials with a specific thermal behaviour are required. The use of materials with adjusted thermal properties can be an advantage in terms of sustainability and energy efficiency, as well as the consequent cost savings in construction materials and during the useful life of the infrastructures.

The additives used for the manufacture of the mortar showed that they were able to modify the thermal properties of the final mix. In this sense, it was determined that the additives with the greatest influence were polyester fibres and gypsum in its crystallised form. The former achieved the greatest reduction in thermal conductivity, as the thermal conductivity of this material is very low. The second achieved the highest value for thermal conductivity among the mixtures manufactured, even though its value is similar to that of the mortar.

Regarding the other additives, the addition of polystyrene caused an increase in thermal conductivity, even though this material has a very low value; graphite caused an increase in thermal conductivity, although to a lesser extent considering its high value; finally, the mixture with powdered gypsum slightly reduced the thermal conductivity, its value also being slightly lower than the reference value.

The heating-cooling tests carried out with a low-cost solar simulator made it possible to analyse the thermal behaviour of the two materials with extreme behaviour and compare it with that of the reference. In this respect, no significant differences were found in the heating phase, but differences were found in the cooling phase caused by the difference in conductivity. The mixture with fibres acted as an insulator and caused the surface temperature at the end of the test to be lower than the mixture with crystallised gypsum, which ended with a higher temperature than the previous and reference samples.

Finally, an attempt was made to analyse the possible influence of the edge effect to find out the factors that may affect the results and try to find the best configuration for future tests. The results showed that the heating device produced a homogeneous heating and hardly affected the spatial distribution of temperatures. Nevertheless, there was a higher cooling at the edges of the sample, which will require increasing the sample size and differentiating between the two areas in future tests.

The results obtained highlight the influence of the additives tested on the thermal behaviour of the mortar. These results are a starting point for further research to facilitate their incorporation in the construction industry. The application of the studied materials with lower conductivity as cladding in buildings could result in a decrease in their temperature during the cooling periods (night) and the consequent decrease in the heating-cooling sequence by starting at a lower initial temperature, thus contributing to the reduction of the heat island effect in cities. On the other hand, the use of materials with a higher conductivity becomes more interesting in uses where a material that favours heat transfer is needed, such as geothermal installations or heat exchanger walls.

In both cases, it can be considered that the work yields promising results for the sector that motivate the continuation of this line of research. Future work will focus on carrying out more exhaustive analyses of the behaviour of these materials, carrying out tests with different configurations. In this sense, it will be interesting to check their behaviour over longer heating-cooling times, and it will also be possible to carry out thermal profile studies to analyse temperatures at different depths.

References

1. Medved, S. Urban Environment and local climate. In Building Physics (pp. 453-472). Springer, Cham (2022).
2. Halder, B., Bandyopadhyay, J., & Banik, P. Evaluation of the climate change impact on urban heat island based on land surface temperature and geospatial indicators. International Journal of Environmental Research, 15(5), 819-835 (2021).
3. Corinaldesi, V., Mazzoli, A., & Moriconi, G. Mechanical behaviour and thermal conductivity of mortars containing waste rubber particles. Materials & Design, 32(3), 1646-1650 (2011).
4. Lizaranzu, M., Lario, A., Chiminelli, A., & Amenabar, I. Non-destructive testing of composite materials by means of active thermography-based tools. Infrared Physics & Technology, 71, 113-120 (2015).
5. Maldague X. Theory and practice of infrared technology for nondestructive testing. 2001.
6. Yun, T. S., Jeong, Y. J., Han, T. S., & Youm, K. S. Evaluation of thermal conductivity for thermally insulated concretes. Energy and Buildings, 61, 125-132 (2013).
7. Holland, S. D., & Reusser, R. S. Material evaluation by infrared thermography. Annual Review of Materials Research, 46, 287-303 (2016).
8. «Fibras poliester no tejidas». https://ceimat.es/es/productos/producto-2. Last accessed 2022/09/23.
9. «Catalogo de Elementos Constructivos CAT-EC-v06.3_marzo_10.pdf». http://www.anape.es/pdf/Catalogo%20de%20Elementos%20Constructivos%20CAT-EC-v06.3_marzo_10.pdf . Last accessed 2022/09/23.
10. «Propiedades», GAB Neumann GmbH. https://www.gab-neumann.com/Grafito-impermeable-Propiedades. Last accessed 2022/09/23.
11. AENOR. UNE-EN 197-1. Cement - Part 1: Composition, specifications and conformity criteria for common cements. Madrid, Spain (2011).
12. AENOR. UNE 7050-3. Test sieves. Technical requirements and testing. Part 1. Test sieves of metal wire cloth. Madrid, Spain (1997).
13. AENOR. UNE 83952. Concrete durability. Water for mixing and aggresives waters. Determination of the pH. Potentiometric method. Madrid, Spain (2008).
14. AENOR. UNE-EN 196-1. Methods of testing cement - Part 1: Determination of strength. Madrid, Spain (2018).
15. Decagon Devices. KD2 Pro Thermal Properties Analyzer Operator's Manual; Decagon Devices, Inc.: Pullman, WA, USA (2016).
16. Sáez Blázquez, C., Farfán Martín, A., Martín Nieto, I., Carrasco García, P., Sánchez Pérez, L. S., & González-Aguilera, D. Efficiency analysis of the main components of a vertical closed-loop system in a borehole heat exchanger. Energies, 10(2), 201 (2017).
17. Tawfik M, Tonnellier X, Sansom C. Light source selection for a solar simulator for thermal applications: A review. Renewable and Sustainable Energy Reviews. 90:802-13 1364-0321 (2018).
18. Colarossi D, Tagliolini E, Principi P, Fioretti R. Design and validation of an adjust-able large-scale solar simulator. Applied Sciences. 11:1964 (2021).

The role of small cities in achieving carbon neutrality

Co-creating carbon neutral cities: a case study of transition management in small European cities

María Dolores Cadarso[1][0000-0002-9850-1406]

Pablo de Frutos[2][0000-0002-8206-984X], Marcia Eugenio[3] [0000-0002-7907-9780]

Universidad de Valladolid, Campus Duques de Soria, 42004, España
[1]lola.cadarso@cesefor.com
[2]pablof@ea.uva.es [3]marcia.eugenio@uva.es

Abstract. Cities are key players in the transition to sustainability, and more and more local leaders are now working towards sustainable and climate-neutral cities. In order to achieve this, new participatory processes have been developed as innovative governance mechanisms. In the city of Soria (Spain), with less than 50,000 inhabitants, the City Council has promoted the participatory process Soria 2030, based on the transition management approach at the urban scale. We present the Soria 2030 process to impulse local change to sustainability through empowerment of city actors. This paper focuses on determining the obstacles that may have hindered the potential of this process and its extrapolation to other similar cities. For this purpose, the participatory mechanism and the main implementation gaps in the co-creation process identified by [1] are analyzed. We identified key factors that have positively influenced participation, such as the members of the work team engagement scale, as well as the methodology and tools used by the project coordinating team. Obstacles that limited the organizations' willingness to participate have also been identified, such as summer calendar and deadlines. Due to the requirements of the health crisis context, most meetings were virtual, which entailed the use of multiple digital tools, for which it would be worth exploring in the future whether the use of such tools has contributed to improving the co-creation process of the local working group.

Keywords: Sustainability transitions, Urban low-carbon development, Urban climate governance

1   Introduction

Metropolitan governance has become one of the key issues for the development of the New European Urban Agenda. Cities play a key role in economic and demographic growth, but so far they have not been able to respond to expectations about improving the living conditions of their inhabitants [2, 3]. As cited in [4], within the fields of collaborative governance of the 'right to the city¨ [2-3, 5] and the role of citizen-ship in designing the city [6]; there are academic contributions that point to the high degree of

conflict between the actors that are part of the urban transformation process, for example [7], where the authors looked at the right of the city symbol in civil society in Cape Town, hugely divide across racial and class lines). The complexity of achieving a balance between meeting the needs of the population, the productive sectors and ensuring long-term sustainability falls under what sustainability researchers called persistent problems [8, 9]. This type of problems is often called "wicked" [10]. Some authors point out that in order to address municipal management focused on achieving sustainability in the future, it is necessary to incorporate new approaches and methodologies that overcome what has so far been the role of planning, the results of which have not been up to the task of sustainability [11]. The challenge for governments is, firstly, to recognize that business organizations, civil society, groups and citizens have a role in the pursuit of sustainability and, secondly, to have sufficient capacity for effective and efficient coordination, steering and reorientation [11]. Furthermore, governance for sustainability entails sensitizing all institutions to achieve social change [11]. One approach that fosters reflective governance is transition management [10-12-13, 14]. This approach has received attention both in the public policy field, see [15, 16] and in the social science field under the concept of transitions, see [12-17-18, 19].

The European Commission has gradually given greater importance to the urban sphere in its programs and policies. There is now a growing concern for integrated sustainable urban development, both in its environmental and social aspects [20]. Cities have become one of the central axes of its cohesion policy, and are accompanied by instruments and initiatives such as community-led local development mechanisms, integrated territorial investments, or the Urban Innovative Actions and the URBACT program, where metropolitan areas appear specifically as eligible subjects to present projects (more details in [21], as cited in [20]). URBACT helped to strengthen relationships between cities and EU institutions and was initially conceived as a learning networking experience to produce and exchange usable knowledge [21].

Several projects have been carried out over the years, such as the MUSIC project [1](2010-2015), funded by Interreg IVB, which used transition management in the urban context to catalyze and regulate carbon and energy reduction in urban policies, activities and the built environment in five pioneering European cities (Dutch Research Institute for Transition, 2014). Inspired by the concept of the "living lab"[22] as a user-centered open innovation ecosystem, [23] presented "Urban Transition Labs" (UTL) as settings in which real life trajectories of sustainable development in cities are deployed and observed at the same time, in collaboration between actors and researchers. UTL is considered a hybrid, flexible and transdisciplinary platform that provides space and time for learning, working as an incubator for transformative urban innovation and adding an additional dimension to the local urban governance approach, but not replacing it, with the aim of supporting sustainable development in cities. The UTL concept was developed at its first experimentation in the EU MUSIC project and first impressions on the barriers and facilitators of this first experience where shared by [23].

---

[1] EU MUSIC project: Mitigation in Urban areas: Solutions for Innovative Cities

Two EU-funded projects were developed by EIT Climate-KIC2: Pioneer Cities and Transition Cities: The Pioneer Cities project (2012-2013) highlighted the role of the urban scale in facilitating transitions and collected information on low-carbon innovation projects underway in partner cities. In 2014, the follow-up Transition Cities project was set up to refine the methodology and develop approaches to identify pilot projects and replicate the projects in new cities by developing case studies of lessons and experiences learned from the projects [24]. These authors illustrated the practical applicability of the UTL concept in European cities by analyzing these last two projects as case studies, identifying five barriers that limited their implementation [24]. They concluded that, in order to maximize the practical utility of the approach, it should be kept in mind that the processes are difficult to manage, with a variety of actors involved [25], and recommended to focus on key elements to meet initial expectations and avoid frustration. In this study, the funded projects were focused on short-term results, which led to disorganized decision-making, and different stages were carried out in parallel due to restricted time frames and financial budgets. Also, in the framework of multilevel governance, lack of knowledge may be a barrier worthy of further research. In conclusion, they advise paying attention to the difficulties and conflicts that arise during the project implementation phase to lead a better understanding of whether removing them may help to convert "shallow" processes into real transitions [24].

In recent years, Urban Living Labs (ULL) have become spaces for experimenting with co-creation processes, as a format for collective urban governance and experimentation towards to urban sustainable living. Living labs can promote a more proactive and co-creative role of users in the research and innovation process of smart city solutions [26]. The co-creation pathways and different mechanisms of shared governance in 3 European projects: CLEVER Cities, Sharing Cities, and SUNEX, have been analyzed by [1], identifying the key principles that allow consolidating models for the co-creation of urban planning policies. The importance of embedding co-creation principles is discussed to create more participative and realistic ULL. "Co-creation changes the innovation game from designing for people to designing with people" as cited in [1] (p. 4-5). Among the key dimensions, they identify: geographical embeddedness (the context), experimentation and learning approach, participation and end-user involvement as partnership (see [23]), and temporal approach.

The city of Soria has also considered tackling this challenge from a cross-cutting perspective, through a participatory process to build with the community and local stakeholders the Soria 2030 Roadmap, with the main lines of action to guide the city towards climate neutrality. The participatory process is largely based on the *transition management approach* [10], acting as a strategic governance tool to induce a transition towards sustainability. The aim of this paper is to evaluate the participatory process, carried out over nine months in the context of a small city in a particularly depopulated territory in Europe, to assess the possibility of extrapolating it to other small European cities.

---

[2] Climate-KIC (Knowledge and Innovation Community). Private innovation partnership focused on climate innovation to mitigate and adapt to climate change. More information on KIC's activities is available at www.climate-kic.org

2   Analysis of the case

2.1   Presentation

The participatory process Soria 2030 was born because of an agreement between the Soria City Council and the Cesefor Foundation with the main objective of developing a Soria 2030 Roadmap to free the city from carbon dioxide emissions by 2030. The Roadmap will become in the new Sustainable Energy and Climate Action Plan of the city (new SECAP of the Covenant of Mayors) and the instrument to be submitted to the EC Mission 100 carbon neutral cities by 2030 - by and for the citizens. This initiative differs from those mentioned above in the European projects Pioneer Cities and Transition Cities, composed of medium-sized to large conventional cities [24]. The Cesefor Foundation has coordinated the participatory process from its inception in 2020 until the end of the first phase in November 2021 with the approval of the Roadmap.

2.2   Research methodology

The empirical analysis of the case benefits from access to first-hand information, as the researcher has contributed to coordinating and dynamizing the whole process as Cesefor staff. The use of participatory action research (participative-research and action methodology) (PAR) as a social research process and a social intervention process, is configured as a space-time spiral, as cited in [27]; which helps citizens to define their needs and define lines of change, generating a process of exchange and collective construction of knowledge. PAR seeks to unite the field of research with that of action, promoting the participation of citizens in general and their most active sector in particular through local organizations, in all phases of the research, in order to enhance the value of popular and institutional knowledge and skills related to the environment [27]. From the point of view of the methodology proposed, the researcher, who is part of the team that stimulates energises the participatory process and who also plays a multidisciplinary technical support role, has been an active knowledge builder and not merely a neutral data collector [28]. She has become transformed in the process she has researched, acquiring new knowledge thanks to the space for co-creation generated in the working group. It has gone from a study model as an element to be observed (as in classical research) to considering it as an active subject capable of transforming itself in the researched process.

Data has been collected through multiple techniques and instruments, such as participant observations in the working meetings (attendance and active participation), documentary analysis, forms and proposals sent through the web platform and email. Through participatory observation, social action could be recorded and documented *in vivo*, as was the case in the empirical analysis [24], conducted through the observations and working groups that took place throughout the Transition Cities project (2014-2016), rather than relying on interviews, where data must be reconstructed from the narratives, interpretations or comments of the interviewees.

For the analysis, we use the framework of "Urban Transition Labs" described by [23], and also used by [24] and [1], on the basis that co-creation processes through these

urban laboratories aim to develop revolutionary solutions in urban sustainability and sustainable development, taking into account collaboration, communication and transparency between all relevant actors, organization, planning and monitoring of activities and outcomes of the processes, their commitment and long-term projection.

2.3　　Research questions and starting hypothesis

The article focuses on determining the obstacles that may have hindered the potential of the participatory process and hinder its extrapolation to other cities with similar characteristics. To this end, it analyses the type of participation mechanism used and the main implementation gaps in the co-creation process indicated by [1], focusing on the nature of the stakeholders that have been part of the working group (Task Force), the activities carried out throughout the different working meetings, the commitment of the team to develop lines of action that contribute to achieving the objectives in a time horizon beyond the short term.

The hypothesis of the study is that the participatory methodology of Soria 2030 encourages the responsible participation and commitment of citizen organizations to identify, through joint production, the lines of action that will drive the ecological transition for the city, generating transformative changes.

2.4　　Working team and selection of actors

In the case of the Soria 2030 process, the transition team in charge of supervision is formed by the Soria City Council and the Cesefor Foundation, the latter being the co-ordinating and dynamizing body of the project. After an initial diagnosis of the context of the city of Soria, as in the case study of [23], the space for co-creation of the participatory process was organized collaboratively, i.e. the closed virtual platform for the working group where each member could incorporate their proposals, comments and assessments, the number of virtual and/or face-to-face sessions or meetings to be held, the objective and work plan were determined. A study was also carried out to select and convene the local actors who should be involved and form part of the working group [14, 29], as cited in [24] and the team in charge of guiding the sessions and supervising the process was determined.

The selection of participants was based on an 'actor analysis' by mapping potential stakeholders according to their competences, interests, informational and transformative power [23]. An initial group of 'core' pioneers was selected, defined as visionary individuals or organizations (who have a link to the city in question) who are able and willing to engage in a creative process of innovative thinking regarding a desirable long-term future for a sustainable city. Participants should have an explicit ambition for sustainable innovation and the most important societal perspectives relevant to sustainability development and the subject under study should be represented [10]. Throughout the process, the addition of new actors was considered to reinforce the transition process [23, 30].

As "the capacity to address urban sustainability challenges relies on multi-level governance structures, as well as the development of different modes of governance (Garcia, 2006)" as cited in [1], (p. 2), municipal governments must work together with stakeholders and local communities to build partnerships, attract resources, design plans and demonstration projects to accelerate the adoption of long-term sustainable measures [31-32, 33].

In the case of Soria, the organizations that were invited to participate in the task force were: nine from the civil and social sphere; three from the economic sphere; four from the educational, cultural and research field; four from the environmental sphere; and five from the government field.

Thus the "transition arena" was gradually set up, with a working group made up of these organizations that share the project's objective, and a group of experts in the different issues to be worked on (Think Tank), who guide and advise the core team.

This kind of process in comparison to more usual projects approaches, entails the introduction of a radically new co-creation space to the usual model carried out by municipal governments (city councils), by passing the rigidity, control and command attitudes from politics and administrations, strict planning without room for creativity and manoeuvre, and leaving room for reflection, reconsideration and mutual learning, [23].

The structure of the participatory process has been flexible and adapted to the suggestions of the participating organizations (in terms of inviting new members, the need to increase the number of meetings due to the interest of the topic to be discussed, etc.). In addition, members of the Think Tank expert group have been invited to contribute their vision and suggestions at the working group meetings to enlighten participants and encourage participatory learning.

2.5   Goal development: Visioning and development of driving actions for change

The process of developing visions that represent the desired future state in each of the domains being worked on allows creating a shared definition of the problem to be addressed, identifying long-term goals, outlining the trajectory of change and building coalitions (i.e. gaining stakeholder support), [10, 25]. The involvement of local change agents is also likely to increase the success of project visualization [23]. A shared vision connects and engages actors with different backgrounds and interests, and this vision is employed to engage the community, [19]. Starting from the inspiring vision, strategies to achieve the desired future situation were outlined. This back-casting exercise, (see [23, 34], has resulted in the strategic transition path that includes the actions of the Roadmap.

In Soria, throughout the participatory process, inspiring visions of the city in 2030 were provided in the different areas worked on ("Built Environment", "Mobility and Transport", "Responsible Food Production and Consumption", "Energy", "Water and Waste" and "Governance"), and the changes and actions needed to make this future a reality were identified and evaluated.

For this purpose, tools provided by EIT Climate-KIC have been widely applied in systemic innovation and transition management combined with other project management and innovation instruments. These are adaptable and flexible methods to address the challenges and issues of climate change through envisioning activities, as well as cooperative learning methods, peer-to-peer activities and horizontal working formats that aim to enhance the development and skills of participants in the field of climate change, both professionally and organizationally. Twelve working group meetings were held (10 virtual, 2 face-to-face) involving the working group organizations as well as other invited parties.

2.6　　Experimentation and implementation of the Roadmap

The transition management approach emphasizes the need and importance of small-scale experiments, because of their potential to develop new solutions and facilitate learning processes [35, 36], as cited in [24]. In the framework of the Soria 2030 process, several pilot experiments have been set up, such as bike rides to school in certain educational centers; a line of sustainable and innovative street furniture through signage designed and built thanks to the collaboration of the Integrated Vocational Training Center Pico Frentes and the Cesefor Foundation, with 100% PEFC-certified pine wood from Soria, such as the "Soria in 15 minutes" sign that promotes active mobility in the city; the pedestrianization of streets, spaces in the city center; incentive policies to promote recycling in catering establishments, etc. After the approval of the Roadmap, the Soria 2030 project promotes its implementation in the city by the City Council, through consortiums and associations. The Soria 2030 Roadmap itself establishes that the local administration must lead the ecological transition, leading by ex-ample. In this sense, more concrete alliances are sought with the organizations in the working group and other stakeholders, as well as funding through national and European calls for projects. The City Council participates in the Climate Projects of the Carbon Fund for a Sustainable Economy (FES-CO2) in conjunction with the Science Park Foundation of the University of Valladolid (UVa) as part of its objective to comply with the 2030 Agenda and to promote sustainable development. As a promoter of the Soria 2030 initiative, it plans to implement Green Public Procurement to improve the competitiveness of organizations and private bidders and to develop accompanying, awareness-raising and reinforcement actions for all publics. It has also obtained an al-location of European funds to reduce the impact of the carbon footprint through the BRERA project - Well-being, restoration, resilience and adaptation. Soria 2030, with the aim of "renaturing the city" and materializing the driving action 1 of the Roadmap (Improving resilience and increasing carbon sinks). This project, developed together with the Cesefor Foundation and the Natural Heritage Foundation of Castilla y León, includes interventions that will increase green areas, guaranteeing their accessibility and distribution to be implemented before 2025, and implies an increase in the absorption capacity of 24.25 tCO2eq. On the other hand, and before December 2024, it will carry out the Zero Emissions Urban Center project, also financed by the European Union with Next Generation EU funds, implementing a low-emission zone in the city center, pacifying stretches of surrounding streets and extending a dissuasive car park, as a result of the proposals of

the Soria 2030 project. These two projects have been expressly endorsed by the members of the Soria 2030 working group through support letters.

The City Council has developed the Local Action Plan of the Soria Urban Agenda, which includes the initiatives underway (including the Soria 2030 project itself) and constitutes a commitment to the future to continue advancing towards the ten strategic objectives of the Spanish Urban Agenda and the Sustainable Development Goals of the 2030 Agenda. In the participatory process with citizens and local organizations, a working group made up of local organizations has been set up, inviting the Soria 2030 working group and other organizations, mainly from the social sphere, to participate in the working meetings. The Soria Urban Agenda, which has already been approved by the City Council Plenary in September 2022, will facilitate access to national and European funding sources and to continue promoting the development of a more economically attractive, socially cohesive, sustainable and environmentally friendly city.

2.7   Results

Four gaps in the theoretical framework of co-creation and practical experience.
We identify the challenges faced by the project examining the experience of shared governance, studying the four main implementation gaps in the theoretical framework of co-creation and the practical experience in the urban laboratory, as identified by [1]:

Firstly, co-creation is based on collaboration between all relevant stakeholders: a) The success of the participatory process of urban regeneration depends substantially on the inclusion of stakeholders throughout the process of planned projects [1]. Stakeholders can be defined as individuals or organizations with a vested interest in the initiatives or activities being undertaken and may be affected by the issues at stake [37].

In this case, and as previously described in point 2.4, the selection of participants was based on a "stakeholder analysis" by mapping potential stakeholders according to their competences, interests, informative and transformative power, finally convening different organizations from the civil and social sphere, the economic sphere, the educational, cultural and research sphere, the environment and government field.

Of the convened organizations that agreed to be part of the project, only one expressly indicated its wish to leave the group after several working meetings, considering the project to be too idealistic.

b) The success of co-creation tools, planning and implementation of any co-creation process that includes co-design and co-implementation phases, depends on the model's specification of stakeholder's level of participation as well as their commitment and participation in the process timeline. We look at the stakeholders' level of participation and engagement scales model categorized as non-participatory (level of engagement: inform and consult) and participatory (level of commitment: involve, collaborate, empower) engagement approaches [1]. While non-participatory methods are very one-sided, participatory methods are more two-sided, meaning collaboration with others to generate change, and in the higher-level stakeholders are fully involved.

From the outset, it was indicated to the organizations in the working group that the Soria 2030 participatory process, as in the ULLs, pursued a high level of participatory engagement with the intention of involving, asking for collaboration and empowering

organizations from all fields, bringing together science, policy, business and civil society (see [38]) to create together the Soria 2030 Roadmap. Throughout the process, participatory co-creation activities were carried out using the practical tools outlined in 2.5. supported by EIT Climate-KIC in accordance with available technologies and the cur-rent health situation.

Secondly, open and clear communication between the different members of the working group is required. To this end, the Soria 2030 project established a communication channel to disseminate the results to citizens through the project's website, and a private platform was created for the members of the working group. Likewise, virtual meetings were held using digital tools to promote communication, transparency and feedback among participants.

Thirdly, participants need to take ownership of the process and express their commitment in the long term. In this case, the participatory process for the elaboration of the Soria 2030 Roadmap has lasted 9 months, which has required a continuous coordination and commitment among the members of the working group. As detailed in the following paragraphs, attendance has decreased during the holiday periods (in summertime) (see Table 1).

Fourthly, the success of the results of the co-creation process can be deduced from the solutions and strategies that were co-created, which confirm a new solution jointly created through the shared process. In relation to this point, the Soria 2030 Roadmap approved by local organizations and unanimously in the Soria City Council Plenary in November 2021, is the innovative and strategic result of the co-creation process, with the main lines of action to decarbonize the city by 2030.

Endogenous variables studied in the participatory process. The analysis carried out on the participation of organizations within the Soria 2030 project has yielded the following results: The endogenous variables studied were attendance at the working meetings held (10 virtual, 2 face-to-face); proposals sent by the organizations via the platform or e-mail; number of e-mails sent by the organization to the coordinating entity; and active oral participation of the organization (number of minutes and oral interventions) in 6 virtual meetings.

Table 1 below displays the dates and attendance data of the organizations from the different areas at the working meetings held (10 virtual, 2 face-to-face). The data have been obtained from recordings and reports for internal use by the coordinating body.

Table 1. Attendance at working meetings held (10 virtual, 2 face-to-face)

Organization	Built Environment		Mobility and transport		Responsible food production and consumption			Energy		Water and reuse		Soria 2030 Roadmap
	11.1	14	20+	11.1	21.8	4.7	10.7	10.8	38.8	44	74.9	11.41
Total	11	11	11	11	16	11	4	4	7	7	11	19
Social	4	4	1	1	4	4	1	1	1	2	4	4
Economic	7	7	1	1	2	1	1		1		1	1
Environment	1	1	1	1	5	1	1	1	2	1	1	1
Education	1	2	1	1	2	2	1			1	1	1
Government	1	1	1	1	1	2	1	1	1	1	1	1
%	76.30%	76.90%	41.90%	41.90%	58%	48%	52%	18%	39%	54%	48%	79%

The number of attendees has varied significantly over the months of 2020 and 2021. In the first meetings held virtually in the "Built Environment" and "Mobility and Transport" areas, the number of attendees was high: on 18 March, thirteen organizations representing seventy-six percent of those convened attended the meeting; on 8 April, fifteen organizations attended, representing approximately seventy-nine percent of those convened; on 29 April and 13 May, thirteen organizations attended (approximately sixty-two percent of those convened). The next meeting on 21 June was in person, in the Alameda space in the city centre, and even considering health restrictions (one organization from the economic sphere expressly refused to attend the meeting in person for health reasons), fourteen participants attended, representing fifty-six percent of the organizations convened. In July and August, participation dropped considerably, reaching a low of four participants (sixteen percent of those convened) at the virtual meeting on 12 August. From the meeting of 7 October onwards, the number of participants increased again considerably, reaching forty-eight percent of those convened, and finally, on 11 November, with the approval of the Soria 2030 Roadmap, nineteen organizations attended the face-to-face event held in the afternoon at the Palacio de la Audiencia, that is, seventy-six percent of those convened, and the other sixteen percent expressly indicated that they agreed with the approval of the document and justified their absence.

As can be seen in the data collected by the researcher (Table 2) through the virtual platform set up for this purpose for each member of the working group, where the participants were able to include, comment on and evaluate the proposals generated, and by means of e-mails: The largest number of proposals sent by the organization through the web platform and email correspond to the "Built Environment" axis. The axis with the lowest number of ideas received was Energy (developed during the month of August, coinciding with the decrease in the participation of the working group due to the summer period).

Table 2. Proposals sent by platform or email.

Organizations N=24	Built Environment	Mobility and transport	Responsible food production and consumption	Energy	Water and waste	Transversal	Total Proposals submitted
	92	68	81	15	40	11	275
Social	11	11	26	5	13	16	96
Economic	4	4	5	4	1	4	17
Educational	8	8	2	0	4	8	8
Government	15	41	1	1	2	1	81
Environment	42	2	36	5	30	8	105

Of the 24 organizations that have participated in the process, (discounting the activity of the organization that has coordinated and dynamized the whole participatory process), the environmental organizations are the ones that have contributed with the greatest number of ideas, and specifically one of them has sent the greatest number of proposals (105 responses, representing 38.2% of the total without counting Cesefor).

Table 3 shows the number of emails sent by the organizations to the coordinating body. The same environmental organization that has sent the most proposals (see pre-

vious paragraph) is also the one that has sent the largest number of emails to the coordinating body (23 emails representing 25.8% of the total number of emails sent by the organizations to the coordinating foundation).

Table 3. Number of e-mails sent by organizations in different fields to the coordinating body

Organizations	Sent by Coordinator	Received by Coordinator	% Sent	% Received
Total	601	89	100	100
Social	231	20	38	22.5
Economic	69	19	11.5	21.3
Educational	134	15	22.3	16.9
Government	107	10	11.8	11.2
Environment	70	25	11.6	28.1

The researcher also analyzed the active participation of those attending the virtual meetings through their oral interventions (number of minutes and number of oral interventions). The data obtained were collected from internal recordings of six of the virtual sessions (Table 4).

Table 4. Active oral participation (minutes and speaking interventions) in 6 meetings

Organization	Responsible land production and consumption		Energy		Water and waste		Oral participation (minutes)	Interventions (number)
	3-7	22-7	11-0	20-2	0-0	7-18		
Social	10	11	80	16	12	11	70	20
Economic	-	9	-	9	-	-	38	6
Educational	1	20	-	-	-	-	11	1
Environment	7	40	9	11	18	7	81	17
Environment	8	19	9	22	79	11	68	50

Three organizations have contributed with their active participation to the development of the agenda during the whole period of work. The first one is a civil organization (neighbourhood association), with a representative between 30 and 60 years old, which has actively participated in all the meetings of the working group (obtaining a 5 on the likert scale for its communicative activity) and which has sent thirty-five percent of all the proposals obtained (Table 2).

The second organization that has contributed extensively to the development of the participatory process belongs to the political sphere and has participated in 11 of the 12 meetings convened, sending 22.2% of the total number of proposals to the work platform, and has obtained a score of 4 on the likert scale with which the researcher has perceived the leadership.

The third organization is from the environmental field, has obtained a scale 3 in the perception of communicative leadership carried out by the researcher, has participated in 10 of the 12 meetings that have taken place and has been the organization that has sent the most proposals and mails.

3   Discussion

The Soria 2030 project has provided data that have made it possible to identify positive factors that have influenced the participatory process, such as the willingness and commitment of the organizations involved, as well as a barrier that has limited the group's activity, namely the working hours during the summer months.

As pointed out by [1], the creation of multi-level governance systems for sustainable urban development is not an easy task and yet it is important, because sustainable development does not depend only on one measure or activity, but on a set of actions. Collaborative governance has been the subject of debate by opening up the process to multiple actors and delving into the role of scientists, policy makers, urban planners and citizens to converge on a common vision for the future, work together and collaborate to co-produce knowledge that responds to the needs and challenges facing cities [39, 40].

In collaborative processes, the different interests of the actors involved in any urban sustainability problem, as well as their lack of awareness, values and priorities lead to less sustainable choices. In this regard, it has been observed in the Transition Cities project meetings that there existed a fragmentation between the different initiatives proposed and the plans that existed in the cities [24]. This gap was not due to a lack of knowledge on the part of the main actors, but to other reasons, such as previous experiences of collaboration between local organizations, political leadership preferences, existence of approved sustainability plans, funding and resources, inflexible silo thinking, among others. To avoid these problems, organizations belonging to the task force should work together with other stakeholders and the local community [31-32, 33].

The affinity of the objectives of each organization in the working group with the objectives of the Soria 2030 project has been essential in relation to their commitment and degree of participation. In this sense, when selecting the stakeholders, the aim was to bring together a group of "ambassadors" inspired to go beyond current interests and daily routines. These ambassadors of the "transition arena" [10, 41] belong to the various spheres mentioned above (civil, social, economic, educational, research, environmental, government).

However, as we have seen in the previous section 2.7, throughout the Soria 2030 participatory process, there was one economic organization that expressly and voluntarily abandoned the participatory process, considering it to be unrealistic. Specifically, it pointed out that the ideas put forward in the meetings basically consisted of putting flowers and trees in all the streets ("there are things that are very idealized but not real"). It would be legitimate to ask, for future discussions, whether the representative should have submitted such a decision to an internal vote within his own organization. In this case, and similar to the experience described in [24], the interests and expectations of the organization did not coincide with the objectives of the Soria 2030 project, which had been established and indicated from the beginning. Apart from this anecdote, the Soria 2030 process went smoothly without detecting any extraordinary discrepancies among the members of the working group, who worked actively and jointly generating a space for participation and co-creation of high-quality knowledge that culminated in

the approval of the Soria 2030 Roadmap by the local organizations and unanimously in the City Council Plenary.

As indicated in the results, the Soria 2030 project has adopted a participatory approach that is more bilateral than non-participatory approaches, where members have collaborated with each other to bring about change (section 2.7). According to [1], "well-planned and inclusive engagement leads to better outcomes at all levels", (p. 8). The recent shift towards community empowerment is reflected in co-creation processes where local knowledge is shared by the community that is involved in the problem to solve processes from the outset [1, 42].

In this sense, the Soria 2030 process has been an inclusive process that has used communication and dissemination channels with the objective of "Leaving no one behind", indicating that all members play an important role. This premise has strengthened the commitment and empowerment of all actors. Furthermore, contracting an organizing entity that guarantees neutrality and transparency in communication can keep stakeholder participation active, as pointed out [1]. In this case, the Cesefor Foundation has dynamized and coordinated the participatory process by enabling communication channels between the members of the working group.

Furthermore, among the findings and discussions of [1], it is also indicated that co-creation processes require flexible leadership and governance. In the Soria 2030 project, the City Council is the driving force behind the project (the driving body of the project) and is committed to act as a driver of change and transition towards sustainability. Regarding the flexibility in the expected timeframe to implement the project, due to the COVID-19 health crisis, in the framework of CLEVER Cities, the City Council decided to delay the planned activities by a few months and the co-implementation and co-development plans were readapted to these circumstances [1].

However, the Soria 2030 process has not been fully flexible in the timeframe and has not allowed for changes in the timeline, similar to other piloting processes that were also inflexible, such as Transition Cities [24]. To facilitate the piloting process of that project, funding was provided to cities to carry out pilot projects and replicate the scheme elsewhere. All experiments were to be undertaken and completed within twelve months and preference was given to pilots in more than one city at the same time. The administrative rigidity imposed generated frustration and confusion among project partners and city stakeholders. The experience gained in the case study suggested that the transition required more time than the projects offered [24].

In the case of the Soria 2030 project, time has also been a limiting factor for participatory activity, as the results show an objective decrease in the number of members attending the working meetings during the months of July and August (Table 1). It would be interesting to investigate in future studies whether the level of participation during these months decreased only due to scheduling issues (as several organizations indicated that they could not attend the working group meetings due to holidays or summer work schedule) or due to the nature of the topics discussed ("Energy" and "Water and waste"). In this regard, it should be added that the main organizations affected were from the economic and educational and research fields, and they expressly indicated to the coordinating group that they could not be available to collaborate in the participatory process (via email), claiming that they were on holiday or that they had

changed their working hours in the summer and could not attend the meetings in the afternoons.

The inflexibility of the process was due to the need to have it completed to draw up the Soria 2030 Roadmap on time and to be able to present the candidacy of the city of Soria to EC Mission 100 carbon neutral cities by 2030 - by and for the citizens. If there had not been an urgent deadline and the co-creation period had been more flexible, the participatory process could have been delayed for a few months to ensure greater attendance of the parties involved, offering them the opportunity to participate in the meetings and in the co-creation process by sharing their knowledge and experiences.

Even considering the time restrictions imposed, which led to a decrease in the number of participants during the months of July and August, transformative proposals were generated and reflected in the Soria 2030 Roadmap document.

In any case, if the participatory process had been postponed for a few months, strong and continuous coordination would have been necessary to keep the co-creation process and the interest of all parties alive; because shared governance processes are frequently abandoned by stakeholders, depending on different factors [1, 43].

Co-management and governance of cities in transition to carbon neutrality, including shared cities or green transitions, are still in a phase of experimentation of policies and practices in the context of sustainable cities and communities [1-44, 45].

This study reaffirms the importance and necessity of including co-creation processes to create successful participatory and realistic pathways, according to [1-23, 46].

4   Conclusion

This article has focused on identifying the way in which the participatory process has been carried out and on evaluating, based on the results obtained, whether this process could be replicated in other cities of similar size with the same probabilities of success. To this end, the Soria 2030 process has also been compared with other processes developed in the framework of European programs that have followed similar approaches.

Co-creation processes in urban regeneration produce multiple benefits if they are properly integrated into public decision-making routines and a common long-term vision is achieved among working group members. In addition, the processes must be context-specific and flexible, using mutually reinforcing elements (from long-term envisioning to experimentation); they are therefore the opposite of quick-win approaches and visible short-term results.

The co-creation process carried out in Soria 2030 has been considered an innovative process for stakeholders, who have felt empowered and have contributed to achieving a shared governance model. Through their participation, they have developed a sense of identification and belonging with the proposed solutions [1-46, 47]. A specific asset of the project is that stakeholders have seen it as a positive and desirable project (not just another obligation) according to report results, whereby most organizations have moved from 'having to' to 'wanting to' participate in urban design and planning [48] as cited in [23]. With the aim of achieving ambitious targets and for any attempt to replicate the model in another city, it is important to find actors who are already adopting

new or alternative ways of thinking and doing, who are actively engaged in the participatory process and want to participate in the working groups, among other factors [41].

According to [23], the Urban Transition Lab approach within a context of transition management, can be applied to urban contexts if they are carefully tailored to the needs and characteristics of each city. It needs space, time and the necessary empowerment tools to be able to develop its essentials. It entails a tailor-made conception aligned with differences in city structures and have to be adapted to urban conditions, structures and situations [23, 49].

The global pandemic of COVID-19 has meant a shift from traditional methods of participation to more innovative digital solutions (meetings via virtual platforms and digital tools such as mentimeter or google form). These tools have now been incorporated into everyday life in combination with traditional techniques.

It would be interesting, on the one hand, to analyze the impact and effectiveness of these new instruments in subsequent studies. The research also leaves other questions open windows open, such as exploring the degree of commitment of the organizations in the working group as other pilot projects and more concrete actions to be developed in the framework of the Soria 2030 project are implemented.

Reference

1. Mahmoud, I.H., Morello, E., Ludlow, D., Salvia, G.: Co-creation Pathways to Inform Shared Governance of Urban Living Labs in Practice: Lessons From Three European Projects. Front. Sustain. Cities. 3, 1–17 (2021). https://doi.org/10.3389/frsc.2021.690458.

2. Marcuse, P.: From critical urban theory to the right to the city. City. 13, 185–197 (2009). https://doi.org/https://doi.org/10.1080/13604810902982177.

3. Harvey, D.: Rebel cities. From the Right to the City to the Urban Revolution. Verso, London (2012).

4. Mireles, A., Benavides-Rincón, G., Garrido, A.: Urban social movements as a critical agent for city planning: Towards a sustainable development of the Deusto Ribera and Zorrotzaurre by 2030 [El movimiento social urbano como agente crítico para la planificación de ciudad: Hacia un desarrollo sostenible de la Ribera de Deusto y Zorrotzaurere al 2030]. Obets. 15, 589–624 (2021). https://doi.org/10.14198/OBETS2020.15.2.08.

5. Castells, M.: The city and the grassroots. A Cross-Cultural Theory of Urban Social Movements. Edward Arnold, London (1983).

6. Leontidou, L.: Urban Social Movements in "Weak" Civil Societies: The Right to the City and Cosmopolitan Activism in Southern Europe. Urban Stud. 47, 1179–1203 (2010). https://doi.org/https://doi.org/10.1177/0042098009360239.

7. Diani, M., Ernstson, H., Jasny, L.: '" Right to the City "' and the Structure of Civic Organizational Fields : Evidence from Cape Town. Voluntas. 29, 637–652 (2018).

https://doi.org/10.1007/s11266-018-9958-1.

8.   Loorbach, D., Rotmans, J.: Managing transitions for sustainable development. In: Olsthoorn, X., Wieczorek, A. (ed.) Understanding industrial transformation: views from different disciplines. pp. 187–206. Springer, Dordrecht (2006). https://doi.org/https://doi.org/10.1007/1-4020-4418-6_10.

9.   Sánchez, A.T.: Pertinence of transition approach of urban water management in Latin America [Pertinencia del enfoque de la transición en la gestión del agua urbana en Latinoamérica]. Ateliê Geográfico J. 10, 7–20 (2016). https://doi.org/https://doi.org/10.5216/ag.v10i2.37923.

10.   Loorbach, D.: Transition Management: New Mode of Governance for Sustainable Development. International Books, Utrecht (2007).

11.   Jorge, A., Monedero, C.: Scenario's method for the foundation of a management model for the transition towards sustainable development of Caroní municipality, Bolivar state, Venezuela. [El método de escenarios en la construcción de un modelo de gestión de la transición hacia la sustentabilidad del municipio de Caroní, estado Bolívar, Velenzuela]. Terra. Nueva Etapa. 33, 13–50 (2017).

12.   Rotmans, J., Kemp, R., van Asselt, M.: More Evolution than Revolution: Transition management in public policy. Foresight. 3, 15–31 (2001). https://doi.org/https://doi.org/10.1108/14636680110803003.

13.   Voß, J.-P., Bauknecht, D., Kemp, R.: Reflexive Governance for Sustainable Development. Edward Elgar, Cheltenham (2006). https://doi.org/10.4337/9781847200266.

14.   Kemp, R., Loorbach, D., Rotmans, J.: Transition management as a model for managing processes of co-evolution towards sustainable development. Int. J. Sustain. Dev. World Ecol. 14, 78–91 (2007). https://doi.org/10.1080/13504500709469709.

15.   Organization for Economic Cooperation and Development: Towards Green Growth: A Summary for Policy Makers. OECD, Paris (2011).

16.   United Nations Environment Programme: Towards a Green Economy: Pathways to Sustainable Development and Poverty Eradication - A Synthesis for Policy Makers. UNEP, St-Martin-Bellevue (2011).

17.   Frantzeskaki, N., Loorbach, D.: Towards governing infrasystem transitions: Reinforcing lock-in or facilitating change?. Technol. Forecast. Soc. Change. 77, 1292–1301 (2010). https://doi.org/10.1016/j.techfore.2010.05.004.

18.   Grin, J., Rotmans, J., Schot, J.: Transitions to Sustainable Development: New Directions in the Study of Long Term Transformative Change. Routledge., New York (2010). https://doi.org/https://doi.org/10.4324/9780203856598.

19.   Smith, A., Stirling, A., Berkhout, F.: The governance of sustainable socio-technical transitions. Res. Policy. 34(10), 1491–1510 (2005). https://doi.org/10.1016/j.respol.2005.07.005.

20.   Tomàs, M.: European policies and metropolitan governance: an unresolved matter [Políticas europeas y gobernanza metropolitana: una asignatura pendiente]. Gestión Y Análisis Políticas Públicas. 53–64 (2018). https://doi.org/10.24965/gapp.v0i20.10489.

21.   González Medina, M., Fedeli, V.: Exploring European urban policy: Towards an EU-national urban agenda? Gestión y Análisis Políticas Públicas. 14, 8–22 (2015).

22.   Chesbrough, H.W.: Open Innovation: The New Imperative for Creating and Profiting

from Technology. Harvard Business School Press, Boston (2003).

23. Nevens, F., Frantzeskaki, N., Gorissen, L., Loorbach, D.: Urban Transition Labs: Co-creating transformative action for sustainable cities. J. Clean. Prod. 50, 111–122 (2013). https://doi.org/10.1016/j.jclepro.2012.12.001.

24. Nagorny-Koring, N.C., Nochta, T.: Managing urban transitions in theory and practice: The case of the Pioneer Cities and Transition Cities projects. J. Clean. Prod. 175, 60–69 (2018). https://doi.org/10.1016/j.jclepro.2017.11.072.

25. Rotmans, J., Loorbach, D.: Complexity and transition management. J. Ind. Ecol. 13, 184–196 (2009). https://doi.org/10.1111/j.1530-9290.2009.00116.x.

26. European Commission: Analysing the potential for wide scale roll out of integrated Smart Cities and Communities solutions. Office for Official Publications of the European Communities, Luxembourg (2016).

27. López Medina, J.M., Matarán Ruiz, A., Manuel Jerez, E., González Arriero, C., Fayos Oliver, C., et al.: Socio-Ecological transitions in metropolitan urban areas: (re)building neighborhoods on a human scale [Transición socioecologica en ámbitos urbanos metro-politanos: (re)construyendo barrios a escala humana]. Rev. Econ. Crítica. 17, 136–154 (2014).

28. Ramos Muslera, E.A.: Participatory methodologies from the Sociopraxic perspective [Las metodologías participativas desde una perspectiva sociopráxica]. Encrucijadas. Rev. Crítica Ciencias Soc. 4, 115–132 (2012). https://doi.org/https://recyt.fecyt.es/in-dex.php/encrucijadas/article/view/78880.

29. Loorbach, D., Rotmans, J.: The practice of transition management: Examples and lessons from four distinct cases. Futures. 42, 237–246 (2010). https://doi.org/10.1016/j.futures.2009.11.009.

30. Reed, M.S., Graves, A., Dandy, N., Posthumus, H., Hubacek, K., Morris, J., et al.: Who's in and why? A typology of stakeholder analysis methods for natural resource management. J. Environ. Manage. 90, 1933–1949 (2009). https://doi.org/10.1016/j.jen-vman.2009.01.001.

31. Evans, J.: Governing Cities for Sustainability: A Research Agenda and Invitation. Front. Sustain. Cities. 1, (2019). https://doi.org/10.3389/frsc.2019.00002.

32. Mccormick, K.: Cities, Nature and Innovation: New Directions. Lund University (2020).

33. UN-HABITAT: The New Urban Agenda. (2020).

34. Robinson, J., Burch, S., Talwar, S., O'Shea, M., Walsh, M.: Envisioning sustainability: Recent progress in the use of participatory backcasting approaches for sustainability research. Technol. Forecast. Soc. Change. 78, 756–768 (2011). https://doi.org/10.1016/j.techfore.2010.12.006.

35. Porter, N., Claassen, M., Timmermans, J.: Transition experiments in Amsterdam: Conceptual and empirical analysis of two transition experiments in the WATERgraafsmeer program. Technol. Forecast. Soc. Change. 90, 525–537 (2015). https://doi.org/10.1016/j.techfore.2014.02.010.

36. Kivimaa, P., Hildén, M., Huitema, D., Jordan, A., Newig, J.: Experiments in climate governance: A systematic review of research on energy and built environment transitions. J. Clean. Prod. 169, 17–29 (2017). https://doi.org/10.1016/j.jclepro.2017.01.027.

37. Aligica, P.D.: Institutional and Stakeholder Mapping : Frameworks for Policy Analysis and Institutional Change. Public Organ. Rev. 6, 79–90 (2006). https://doi.org/10.1007/s11115-006-6833-0.

38. Bulkeley, H., Coenen, L., Frantzeskaki, N., Hartmann, C., Kronsell, A., Mai, L., et al.: Urban living labs: governing urban sustainability transitions. Curr. Opin. Environ. Sustain. 22, 13–17 (2016). https://doi.org/10.1016/j.cosust.2017.02.003.

39. Ahern, J., Cilliers, S., Niemelä, J.: The concept of ecosystem services in adaptive urban planning and design: A framework for supporting innovation. Landsc. Urban Plan. 125, 254–259 (2014). https://doi.org/10.1016/j.landurbplan.2014.01.020.

40. Raymond, C.M., Frantzeskaki, N., Kabisch, N., Berry, P., Breil, M., Nita, M.R., et al.: A framework for assessing and implementing the co-benefits of nature-based solutions in urban areas. Environ. Sci. Policy. 77, 15–24 (2017). https://doi.org/10.1016/j.envsci.2017.07.008.

41. Roorda, C., Wittmayer, J., Henneman, P., van Steenbergen, F., Frantzeskaki, N., Loorbach, D.: Transition Management in the Urban Context: Guidance Manual. DRIFT, Erasmus University Rotterdam, Rotterdam (2014).

42. Rock, J., McGuire, M., Rogers, A.: Multidisciplinary Perspectives on Co-creation. Sci. Commun. 40, 541–552 (2018). https://doi.org/10.1177/1075547018781496.

43. Fors, H., Hagemann, F.A., Sang, Å.O., Randrup, T.B.: Striving for Inclusion-A Systematic Review of Long-Term Participation in Strategic Management of Urban Green Spaces. Front. Sustain. Cities. 3, 572423 (2021). https://doi.org/10.3389/frsc.2021.572423.

44. Loorbach, D., Wittmayer, J., Shiroyama, H., Fujino, J., Mizuguchi, S.: Governance of Urban Sustainability Transitions: European and Asian Experiences. Springer, Tokio (2021). https://doi.org/10.1007/978-3-030-67130-3_7.

45. Davies, C., Lafortezza, R.: Transitional path to the adoption of nature-based solutions. Land use policy. 80, 406–409 (2019). https://doi.org/10.1016/j.landusepol.2018.09.020.

46. Agrawal, A.K., Kaushik, A.K., Rahman, Z.: Co-creation of Social Value through Integration of Stakeholders. Procedia - Soc. Behav. Sci. 189, 442–448 (2015). https://doi.org/10.1016/j.sbspro.2015.03.198.

47. Ramaswamy, V., Ozcan, K.: What is co-creation? An interactional creation framework and its implications for value creation. J. Bus. Res. 84, 196–205 (2018). https://doi.org/10.1016/j.jbusres.2017.11.027.

48. Meijer, A.J., Lips, M., Chen, K.: Open Governance: A New Paradigm for Understanding Urban Governance in an Information Age. Front. Sustain. Cities. 1, (2019). https://doi.org/10.3389/frsc.2019.00003.

49. Madlener, R., Sunak, Y.: Impacts of urbanization on urban structures and energy demand: What can we learn for urban energy planning and urbanization management? Sustain. Cities Soc. 1, 45–53 (2011). https://doi.org/10.1016/J.SCS.2010.08.006.

Effect of sustainable Local Energy Communities on low voltage distribution networks

Samuel Borroy[1][0000-0002-2412-576X], Daniel Marquina[1][0000-0001-8151-0974], Andres Llombart[1][0000-0001-6350-4474] and Luis Hernandez-Callejo[2][0000-0002-8822-2948]

[1] Fundacion CIRCE, Parque Empresarial Dinamiza, Avenida Ranillas 3-D, 1st Floor, 50018 Zaragoza, Spain
[2] ADIRE-ITAP, Departamento Ingeniería Agrícola y Forestal, Universidad de Valladolid, 47002 Valladolid, Spain
sborroy@fcirce.es

Abstract. The energy trends and the international objectives in terms of sustainability and efficiency implies an expected growth in electrification and in renewable generation penetration, presenting future scenarios in which actors such as distributed energy resources, storage and active consumers can play a key role in the energy transition. The objective of this paper is to explore the impact that the irruption and proliferation of figures such as Local Energy Communities (LEC) can represent for distribution networks, analyzing especially the effect of their integration on indicators related to voltage profiles and maximum power flows. The study presented follows a methodology based on quasi-dynamic simulations performed on different scenarios considering the evolution of electric demand and both Business As Usual and LEC-based low voltage networks, which allow quantifying the defined indicators, thus understanding the technical impact of the integration of LEC in distribution systems.

Keywords: Local Energy Communities, Sustainability, Energy Transition, Voltage levels, Overloads, Technical losses.

1　Introduction

The fulfillment of European and global objectives focused on alleviating energy dependence on fossil fuels and mitigating the effects of climate change, implies an evolution of the energy model towards sustainable energy consumption, produced from renewable energy sources, while maintaining (and improving) current levels of quality, continuity, and reliability.

These objectives present an ambitious scenario for the energy sector, since quantitatively they imply for the European Union to achieve a penetration of renewable energies of 32% by the year 2030. The green pact focused on sustainable development, the "Green Deal", proposes to achieve "*a pan-European integrated energy system that is low in carbon, secure, reliable, resistant, accessible, cost-efficient that supplies all of society and paves the way for a fully carbon neutral economy by 2050, maintaining and expanding industrial leadership in energy systems during the energy transition* " [1].

In this context, electricity arises as one of the critical energy vectors of this transition, thus being the electrification of society, together with the increase in renewable generation, one of the keys for the emissions reduction pursued by the aforementioned objectives. In its report "*Net Zero by 2050. A Roadmap for the Global Energy Sector*", the international energy agency forecasts that "*The global demand for electricity more than doubles between 2020 and 2050*" [2]. To be able to meet this increase in demand, electrical systems will have to evolve significantly, both in production capacity and in evacuation, transmission, and distribution infrastructures.

A crucial and transversal element for such scenario is the price of electricity, whose high values currently reached, together with the technological development experienced by renewable generation sources and storage systems, have highlighted intensive scenarios in sustainable self-consumption from renewable generation.

Local Energy Communities (hereinafter, LEC) represent a further step in this context. They were born with the main objective of obtaining a collective benefit from the same renewable generation facilities, providing energy efficiency services and their scope includes the supply, consumption, aggregation and storage of energy and potentially its distribution, as well as the provision of recharging services for electric vehicles or other energy services. From a regulatory point of view, LEC are in an incipient phase and dependent on a regulatory framework not yet fully developed, but their evolution and penetration are intuited to be of great relevance in the near future [3].

From the point of view of electricity networks, a scenario of proliferation of LEC based on renewable generation can be translated technically as an increase in the penetration of dispersed generation units in the distribution network, especially in low voltage (LV), as well as other energy vectors such as storage systems and manageable loads (e.g., electric vehicles). This energy transition poses multiple challenges for electricity networks, which must be able to integrate new generation based on non-manageable primary resources, combining large-scale renewable energy plants with the mentioned growing presence of distributed renewable generation sources [4]. This is a challenging scenario, since distribution networks were originally designed to unidirectionally distribute electricity supplied by large generation plants based on predictable and manageable generation sources and synchronous connection. Consequently, the network evolves towards a bidirectional, distributed and variable system. In addition to this integration of generation sources, the new paradigm includes changes such as the active participation of demand, considering figures such as the aggregator, the prosumer, or LEC [5].

However, in addition to implying a challenge, this new paradigm based on the integration of new actors in the system such as LEC, together with the development of Smart Grids technologies that make it possible, represents an opportunity for the evolution of electrical systems towards the achievement of the previously mentioned objectives [6]. The intelligent integration of distributed resources in electricity networks can play a determining role in making feasible the electrification of society, linked to the energy transition and sustainability, by optimizing the use of transmission and distribution infrastructures [7], [8], [9]. Likewise, the coordinated control of these resources and demand management, including aggregation, should contribute to increase the overall flexibility of the system, thus reducing the impact of the variability of the

primary resource associated with renewable generation [10]. Different research projects tackle challenges and work in the development of technology solutions aimed at enhancing the integration of LEC in energy systems. In this sense, this work has been carried out in the framework of Horizon 2020 ACCEPT project [11], which aims to develop solutions to increase opportunities for integrating LEC.

Technical literature explores in detail specific problems and challenges brought by the connection of distributed energy resources, as well as different solutions for improving the behaviour of these actors and thus enhancing their integration of the network, as is explained in references included above. However, studies analyzing quantitatively the effect of an adequate connection of dispersed resources in distribution networks are hard to find. The objective of the work presented in this paper is to explore the impact that the irruption and proliferation of actors such as LEC can have on electrical systems, analyzing especially their contribution to a sustainable electrification of society as well as the increase of penetration of renewable energies. Particularly, this study analyzes qualitatively and quantitatively, in terms of voltage levels, overloads and technical losses, the effect of the penetration of LEC in network scenarios considering electric demand growth. This paper is organized as follows: Section 2 describes the methodology followed in the study, including simulation tools and test cases definition, focusing on benchmark networks, load and generation profiles and scenarios definition. Section 3 presents the results obtained in terms of the impact of PV based LEC integration in the LV distribution network. Finally, Section 4 summarizes the main conclusions of the study and introduces further working lines.

2   Methodology

In order to achieve the objectives mentioned in the introduction, several simulation analyses based on the comparison of different scenarios, with and without the integration of LEC, have been performed, obtaining quantitative results of KPIs (Key Performance Indicators). Three main indicators have been selected to quantify the technical impact of the integration of LEC from the point of view of the distribution network:

- Voltage levels of the nodes of the network, considering both maximum and minimum values.
- Load levels of the different line sections of the network, with special focus on the relative values regarding nominal levels.
- Technical losses due to the load flows through the different elements of the network.

These indicators have been selected since voltage profiles and load levels of network infrastructure are variables highly representative of the status of a power system considering steady state conditions. In addition, technical losses are considered due to their close impact on efficiency and sustainability. Furthermore, the selected parameters are highly impacted by electric demand growth and distributed generation penetration, which are key factors of the scenarios related to the energy transition.

Next, in the following subsections, the simulation tools used, and the building of the test cases and scenarios is described.

2.1　Simulation methods

The calculation of the indicators which will be used to quantify the effect of the penetration of distributed energy resources is based on the analysis of the Power System operation under steady-sate conditions, that is, considering the operation under stable regime and with no faults or short-circuits in any active section of the network. Under such assumptions, load flow calculations are the ones more suitable for the study. Thus, load profiles and generation profiles evolution along the day are studied. The time scale of the variations is typically minute(s)-based, rather than millisecond scale. Therefore, series of load flow simulations are performed in order to obtain the values of the state variables along the considered period of time (in this study a complete day period is analyzed).

The simulations performed to conduct the described load flow analyses are executed using PowerFactory DIgSILENT [11] software, in which the benchmark network and the cases studies explained in the following subsections have been modelled. Quasi-Dynamic Simulation toolbox have been used mainly to obtain the results presented in section 3.

2.2　Test cases

A benchmark network has been modelled in PowerFactory DIgSILENT in order to be used as a base where loads and PV units are modelled considering different levels of demand evolution and generation penetration, thus defining the set of scenarios analyzed in the present study, as it is detailed next.

Benchmark network.

The scenarios analyzed in the study presented in this paper are implemented on the network *IEEE European Low Voltage Test Feeder* [13], a reference network developed by the IEEE working group of the Distribution System Analysis Subcommittee of the Power Systems Analysis, Computing, and Economics (PSACE) Committee, with the purpose of providing a benchmark for researching LV feeders common in Europe.

The LV test feeder is a radial distribution feeder connected to the medium voltage (MV) system through a transformer at substation. The transformer steps the voltage down from 11 kV to 416 V. The three-phase transformer at substation has a rated MVA of 0.8, rated voltages of 11/0.416 kV, and a delta/grounded-wye connection. The resistance and reactance of the windings are 0.4% and 4%, respectively.

The LV feeder includes the connection of loads at different nodes implementing a one-minute time resolution over 24 hours for time-series simulation. For scenarios considering the integration of local energy communities, PV units connected at demand nodes have been modeled, using real generation profiles based on data from south Spain units. In the following subsections the load and generation modeling as well as the scenarios definition are explained. Fig. 1 shows the one-line diagram of the network used as benchmark.
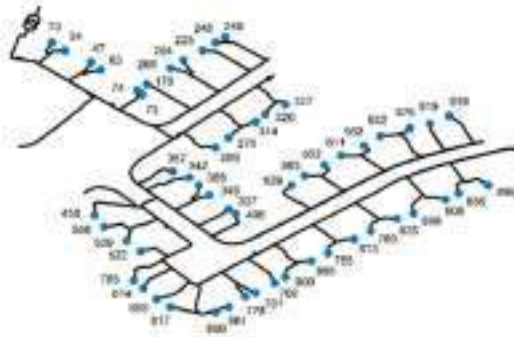
Fig. 1. One-line diagram of the European LV test feeder.

Load profiles.

As it is introduced in the benchmark network description, each node of the IEEE European LV test feeder includes a load which represents the demand connected at such point of the network. A single-phase connection is considered for each load, as it is common for LV feeders, specially in urban areas (different phase for each load is considered, providing a balanced system from the MV/LV transformer perspective).

Each load is modeled considering base power, power factor and load shape with a one-minute time resolution. Fig. 2 a) shows the demand curve of one of the loads initially included in the IEEE benchmark network. The figure shows that demand has relevant peaks at early moments of the morning and also late in the afternoon, being this type of profile the common behaviour of several loads included in the IEEE test case. As it is explained next, these initial profiles are adapted for the study.

For the scenarios based on the integration of LEC, PV units are modeled considering real generation profiles from installations located in the south of Spain (measured in June), as it has been introduced above. Therefore, it is considered pertinent to compare the load profile included in the benchmark case with that of the Spanish system. Fig. 2 b) shows the electricity demand curve in Spain of a weekday in June 2022, provided by REE, TSO of Spain [14], being the peak of demand at 13:45 h. As it can be observed, the type of profile of the electric demand in the Spanish case and the one of the loads initially included in the IEEE test feeder are significantly different.

Thus, considering that for the sake of consistency of the analysis, it is desirable that the behaviour of the loads of the analyzed benchmark network is comparable with that of the demand in the Spanish system (as it is the case of PV generation), some modifications were made in each individual load model, adapting the temporary profile and keeping nominal power values in similar ranges to original models. A scaling curve has been calculated as a factor of the Spanish load shape related to the total original demand curve of the LV test feeder and has been applied to the model of each load. Additionally, a selection of the most relevant loads, for their impact in the total demand, have been adapted manually to integrate their peak hours in the typical peak periods of the Spanish case. The resulting total demand of the feeder is shown in Fig. 3.
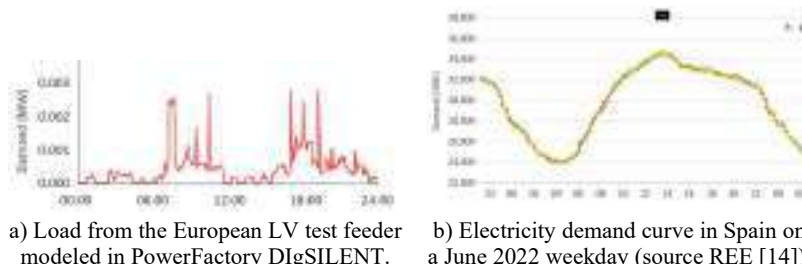
a) Load from the European LV test feeder modeled in PowerFactory DIgSILENT.

b) Electricity demand curve in Spain on a June 2022 weekday (source REE [14]).
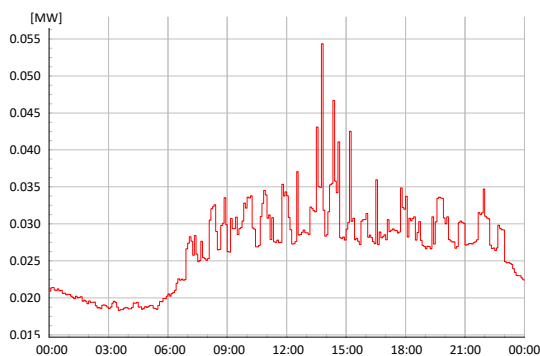
Fig. 2. Load profiles comparation.

Fig. 3. Total electricity demand curve in European LV test feeder with adapted load profiles.

Generation profiles.

The integration of LEC is modeled through the connection of distributed generation units, based on PV units, in the demand nodes. These modules are modeled in Power-Factory DIgSILENT taking into account nominal power and daily generation profiles (based on real data taken form PV installations).

Once generation profiles are defined, the quantification of the nominal power to be considered for each node is undertaken. For such purpose, the magnitude of the total electric consumption at each node where the PV generation is connected is taken into account. Thus, the nominal power of each converter associated to PV connection is defined as a fraction of the maximum demand of the affected node, being the chosen criterion 50% of the maximum power demanded (maximum value between 13:45 h and 14:45 h). Finally, since PV connection is assumed to be mainly for self-consumption purposes, the topological connection of generation units at each node replicates that of the loads, thus being single-phase connected in the same phases than electric loads.

Scenarios.

The methodology followed in the present study is based in the comparison of different indicators (introduced in the methodology section) between several scenarios considering the evolution of the electric demand as well as different levels of penetration of LEC based on the connection of PV units. Regarding the evolution of electric demand, the link between sustainability and the electrification of society mentioned in the introduction is taken into account, therefore a growing evolution of electricity consumption is considered, as explained below.

Depending on the consideration of the integration of LEC the scenarios for this study are classified as Business As Usual (BAU) scenarios and LEC scenarios, according to the following criteria:

- BAU Scenarios. These scenarios consider a conventional network with radial operation, being all the demand fed by the high voltage network. Under this assumption, in base case scenario the demands are based on nominal values included in the IEEE European LV test feeder (including the load profiles adaptations explained) while for the other scenarios several variations of the total demand at each node of the network are taken into account, based on the growth in energy demand forecast by the international energy agency that is noted in the introduction. Table 1 summarizes the characteristics of BAU scenarios, based on demand increase regarding base case:

Table 1. BAU scenarios description.

	BAU Scenario					
	Base Case	120% demand	140% demand	160% demand	180% demand	190% demand
Demand increase regarding Base Case	NA	20%	40%	60%	80%	90%

Note that all the BAU scenarios consider the same load profiles explained previously.

- LEC Scenarios. These scenarios consider the integration of PV units in the demand nodes, thus emulating the behaviour of sustainable LEC. In this case, following the same criteria of BAU scenarios, and pursuing the feasibility of comparing scenarios, the same variation of nominal power of PV generation is considered to define the scenarios. Table 2 summarizes the description of LEC scenarios, considering that in base case scenario the demands are based on nominal values included in the IEEE European LV test feeder (including the load profiles adaptations explained) and the connection of PV units at each demand node (with the assumptions explained in the Generation profiles subsection) is included.

Table 2. LEC scenarios description.

	BAU Scenario					
	Base Case	120% demand & PV	140% demand & PV	160% demand & PV	180% demand & PV	190% demand & PV

| Demand increase regarding Base Case | NA | 20% | 40% | 60% | 80% | 90% |
| PV generation units nominal power increase regarding Base Case | NA | 20% | 40% | 60% | 80% | 90% |

Note that all the LEC scenarios consider the same load and generation profiles.

3   Results

Quasi-Dynamic simulations, whose approach is introduced in section 2.1, performed in PowerFactory DIgSILENT, allows obtaining relevant results regarding voltage levels, load levels and technical losses, which are useful to understand the technical impact on LV distribution networks of the penetration of LEC based on PV generation.

The obtained results can be studied focusing the analysis on the nodes of the network (the test network contains around 900 nodes) and on the line sections (similar number of circa 900 line sections). The description of the type of results provided by quasi-dynamic simulations selected for analysis are summarized in Table 3 and Table 4:

Table 3. Node voltage results description.

Umin (%)	Umax (%)	Uavg (%)
Minimum voltage magnitude obtained at any node of the network for a minute-based load flow for a 24h period	Maximum voltage magnitude obtained at any node of the network for a minute-based load flow for a 24h period	Average voltage magnitude obtained for a minute-based load flow for a 24h period

Table 4. Line sections power flow results description.

Max Load (%)	Total Losses (kWh)
Maximum power flow through any line section obtained for a minute-based load flow for a 24h period	Total energy losses in the line section obtained considering the whole 24h load flow simulation. Specific total daily losses value per line section and total network losses value are calculated

The following subsections present the results obtained for the different scenarios.

3.1   BAU Scenarios

This section summarizes the results of quasi-dynamic simulations performed in the BAU scenarios described in section 2.2. Due to the huge number of results obtained, graphics presenting the extreme values, relevant to extract conclusions, are shown.

Nodes voltages.

Table 5 shows a summary of the results for voltage values obtained for each scenario.

As it can be observed, minimum voltage values decrease with the increase of the demand, being in the last two scenarios below 93% of nominal voltage, which is commonly the minimum operation voltage allowed by regulation.

Table 5. Node voltage results for BAU scenarios.

Scenario	Umin (%)	Umax (%)	Uavg (%)
base case	98.30%	103.96%	102.08%
120% demand	96.96%	103.95%	101.67%
140% demand	95.50%	103.94%	101.26%
160% demand	93.84%	103.93%	100.85%
180% demand	91.73%	103.93%	100.41%
190% demand	89.72%	103.92%	100.19%

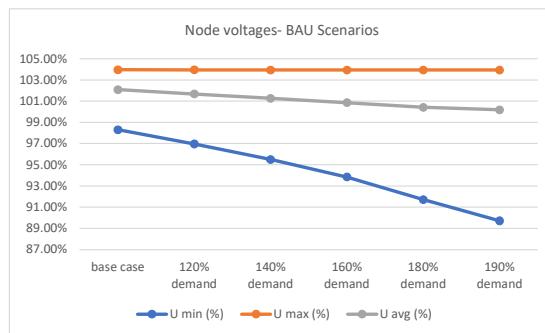Fig. 4 shows graphically the results, presenting the described trend.

Fig. 4. Node voltage results for BAU scenarios.

Fig. 5 presents the results shown by PowerFactory DIgSILENT for the most restrictive scenario (190% demand), representing voltage levels through a heatmap.
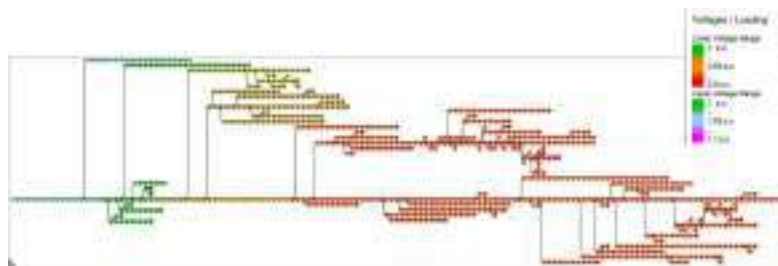

Fig. 5. Voltage heatmap in PowerFactory DIgSILENT for the most restrictive BAU scenario.

Line sections power flows.

Following the same structure than in the presentation of node results, Table 6 shows a summary of the results for power flows in line sections for each scenario.

Table 6. Line section power flows results for BAU scenarios.

Scenario	Max Load (%)	Total Losses (kWh)
base case	99.17%	21.18
120% demand	125.09%	31.32
140% demand	155.13%	43.91
160% demand	192.23%	59.34
180% demand	246.56%	78.42
190% demand	311.21%	90.79

Fig. 6 shows graphically the results and Fig. 5 presents the results shown by Power-Factory DIgSILENT for the most restrictive scenario (190% demand).
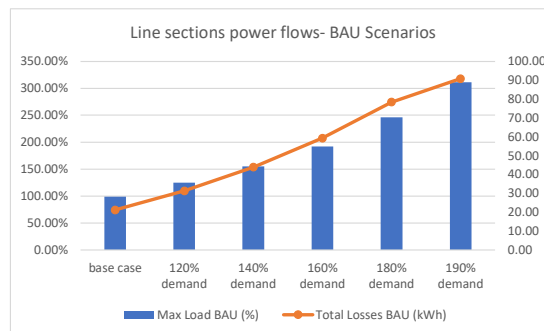

Fig. 6. Line sections power flows results for BAU scenarios.
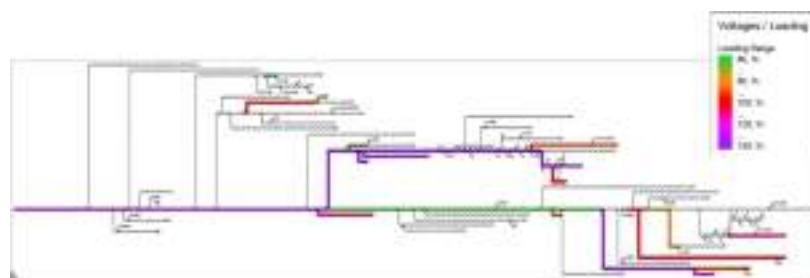

Fig. 7. Loading heatmap in PowerFactory DIgSILENT for the most restrictive BAU scenario.

As it can be observed, load ratio increases dramatically with demand scenarios, being above nominal values just from 120% demand scenario. Next section will show the effect of the connection of distributed PV close to the consumption points.

3.2   LEC Scenarios

Results of quasi-dynamic simulations performed in the LEC scenarios. Presentation of results follows the same structure as in previous section for BAU scenarios.

Nodes voltages.

Table 7 and Fig. 8 show a summary of the results for voltage values obtained for each scenario, presenting the same parameters than the ones included in BAU scenarios report.

Table 7. Node voltage results for LEC scenarios.

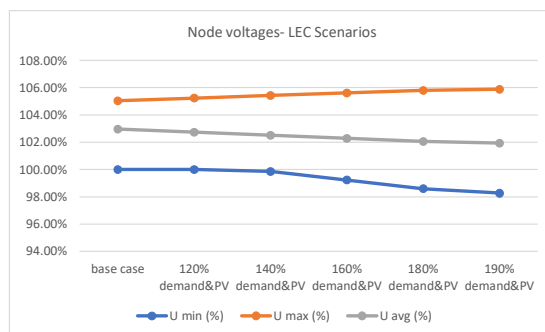| Scenario	Umin (%)	Umax (%)	Uavg (%)
base case	100.00%	105.04%	102.96%
120% demand&PV	100.00%	105.24%	102.74%
140% demand&PV	99.86%	105.43%	102.51%
160% demand&PV	99.23%	105.61%	102.29%
180% demand&PV	98.59%	105.79%	102.05%
190% demand&PV	98.26%	105.88%	101.93%

Fig. 8. Node voltage results for LEC scenarios.

It can be appreciated that the connection of PV units close to demand nodes, with the level of penetration associated to each scenario as described in section 2.2, allows avoiding voltage decreases below 98% of nominal values, thus fulfilling minimum operation voltages requirements. Likewise, maximum voltages are always kept below 106% of nominal voltage, therefore not exceeding maximum operation voltage allowed

(typically 107%). Fig. 9 completes the graphic report presenting the results shown by PowerFactory DIgSILENT for the most restrictive scenario.
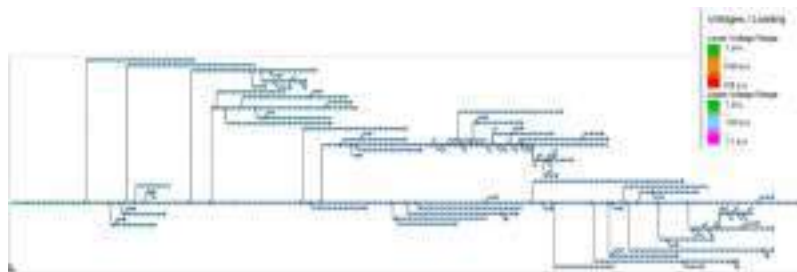

Fig. 9. Voltage heatmap in PowerFactory DIgSILENT for the most restrictive LEC scenario.

Line sections power flows.

The summary of the results for power flows in line sections for each scenario is presented in Table 8 and in Fig. 10, replicating the parameter selection shown for BAU scenarios.

Table 8. Line section power flows results for LEC scenarios.

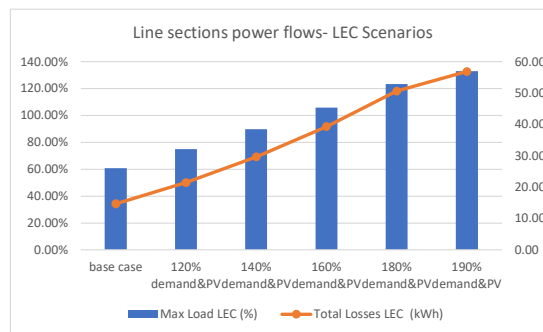| Scenario	Max Load (%)	Total Losses (kWh)
base case	60.72%	14.69
120% demand&PV	74.77%	21.44
140% demand&PV	89.73%	29.61
160% demand&PV	105.84%	39.29
180% demand&PV	123.41%	50.58
190% demand&PV	132.89%	56.88

Fig. 10. Line sections power flows results for LEC scenarios.

Fig. 11 presents the results shown by PowerFactory DIgSILENT for the most restrictive scenario (190% demand&PV).
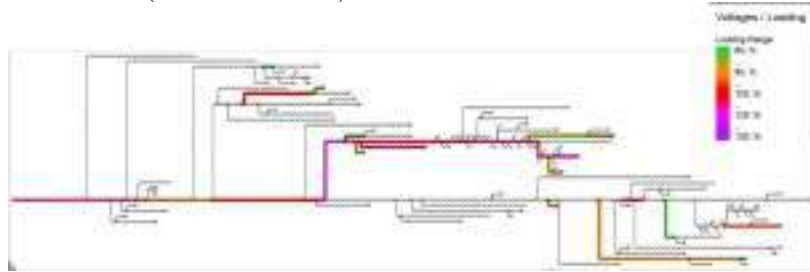

Fig. 11. Line sections power flows heatmap in PowerFactory DIgSILENT for the most restrictive LEC scenario.

Results show that the integration of PV based LEC helps to reduce both overloads and technical losses. Nevertheless, scenarios considering a higher growth rate for demand still present overloads even with PV penetration (although significantly less severe than in BAU scenarios). Further studies including a more detailed tuning of the penetration level of generation and, specially, the integration of more advanced Smart Grids functionalities will help to enhance the behaviour of the network.

For the sake of clarity and to assist in drawing conclusions, results for BAU and LEC scenarios are explicitly compared in next subsection.

3.3   Comparison of scenarios

In the following figures the results for node voltages and line section power flows, for BAU and LEC scenarios are compared quantitatively and graphically.

Nodes voltages.

Table 9 presents a comparison of voltages obtained for BAU scenarios and LEC scenarios, focusing of minimum values, which have turned out to be the most relevant, according to the results of the simulations, as it is explained in section 3.1. To clarify the comparison of scenarios, last column of the table presents the difference between highest voltage drop in BAU case and highest voltage drop in LEC case, for each demand scenario. Fig. 12 shows graphically these results. Both the table and the graphic show explicitly the improvement on minimum voltage levels which involves the integration of LEC, which increases with the growth of the demand.

To complete the vision of voltage levels, Fig. 13 presents maximum and minimum voltage values for BAU and LEC scenarios.

Table 9. Node voltage results comparison (BAU vs LEC scenarios).

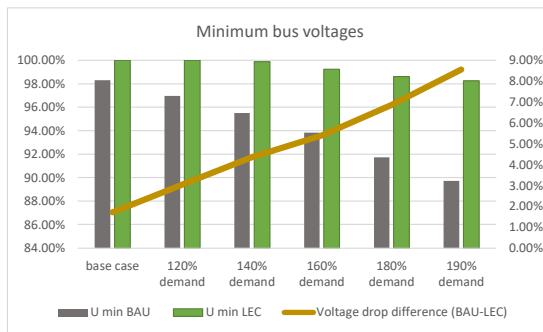| Scenario	Umin BAU (%)	Umin LEC (%)	Voltage drop difference (BAU-LEC)
base case	98.30%	100.00%	1.70%
120% demand	96.96%	100.00%	3.04%
140% demand	95.50%	99.86%	4.36%
160% demand	93.84%	99.23%	5.39%
180% demand	91.73%	98.59%	6.86%
190% demand	89.72%	98.26%	8.54%

Fig. 12. Minimum voltage results comparison for BAU and LEC scenarios. Secondary axis (right) quantifies the voltage drop difference (BAU-LEC).

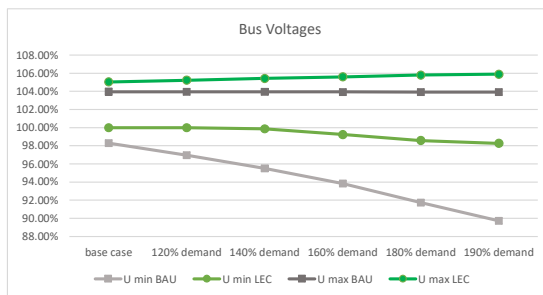**Fig. 13.** Voltage results comparison for BAU and LEC scenarios.

Line sections power flows.

Table 10 presents the maximum load values for each scenario comparing BAU and LEC cases. Fig. 14 shows graphically these results.

Table 10. Maximum load flow comparison for BAU and LEC scenarios.

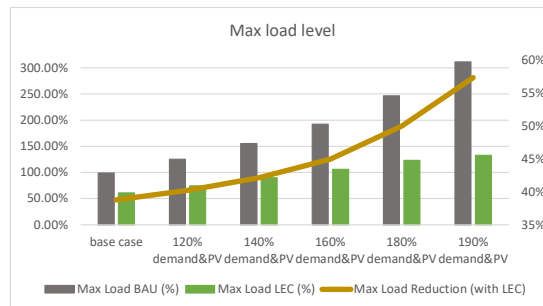| Scenario	Max Load BAU (%)	Max Load LEC (%)	Max Load Reduction (with LEC)
base case	99.17%	60.72%	39%
120% demand	125.09%	74.77%	40%
140% demand	155.13%	89.73%	42%
160% demand	192.23%	105.84%	45%
180% demand	246.56%	123.41%	50%
190% demand	311.21%	132.89%	57%

Fig. 14. Maximum load results comparison for BAU and LEC scenarios. Secondary axis (right) quantifies the reduction of maximum load values provided by the integration of PV based LEC.

Table 11 presents total technical losses values in kWh for each scenario comparing BAU and LEC cases. Fig. 15 shows graphically the same results.

Table 11. Technical losses comparison for BAU and LEC scenarios.

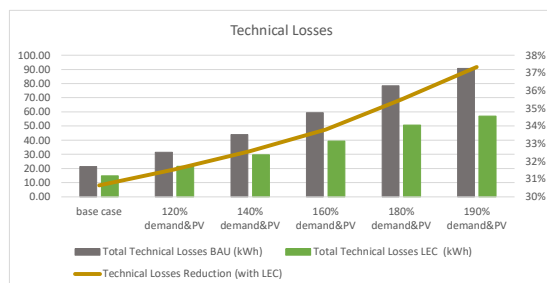| Scenario	Total Technical Losses BAU (kWh)	Total Technical Losses LEC (kWh)	Technical Losses Reduction (with LEC)
base case	21.18	14.69	31%
120% demand	31.32	21.44	32%
140% demand	43.91	29.61	33%
160% demand	59.34	39.29	34%
180% demand	78.42	50.58	35%
190% demand	90.79	56.88	37%

Fig. 15. Technical losses results comparison for BAU and LEC scenarios. Secondary axis (right) quantifies the reduction of losses provided by the integration of PV based LEC.

4   Conclusion

The effect in LV distribution networks of the integration of sustainable LEC, based on the connection of PV units close to the demand nodes, is analyzed in this paper. For such purpose the quantification of voltage and load-based variables is carried out comparing different scenarios with and without LEC. As it has been detailed in the paper, the enhancement observed in the scenarios which consider sustainable LEC integration is remarkable.

The study takes a representative LV network as a basis to build significant scenarios in terms of load profiles, generation profiles and evolution of electric demand. Each scenario acts as a testbed where quasi-dynamic load flow simulations are performed, obtaining minute-based voltage and power flow values throughout day-long power flow analyses. The gathering and comparing of the results obtained for all the scenarios analyzed allows quantifying the impact of the connection of PV based LEC.

In terms of voltage profiles, it is observed that the growing evolution of electric demand might involve minimum voltage limits violation in BAU cases, while for the same evolution of demand, voltages are kept within healthy limits in all cases considering the connection of PV based LEC. The improvement in voltages profiles in LEC cases with respect to BAU scenarios reaches out more than 8.5%.

The results regarding the impact on maximum load levels and technical losses are also relevant. The simulations show that in BAU scenarios the increase of demand can involve high levels of overloads for some line sections in some high-demand periods, while in LEC scenarios the maximum load values decrease dramatically (the reduction in maximum power flowing LV line sections ranges from 39% to 57% with the connection of PV units). It is also remarkable, specially considering sustainability purposes, the reduction in technical losses achieved through the connection of LEC, which reaches a decrease of 37% in LEC scenarios.

In light of the quantitative results obtained in this study, it is concluded that LEC based on the integration of distributed generation from renewable sources can play a key role in meeting sustainability objectives, facilitating the electrification of society and the penetration of renewable energies.

Taking these conclusions as starting point, further analyses in this field will explore the maximization of the positive impacts of the integration of LEC and the reduction of potential risks, considering more complex structures of sustainable LEC integrating additional elements aligned with Smart Grids paradigm, such as storage systems, diverse renewable generation sources or electric vehicles with V2G capabilities.

Acknowledgments

References

1. European Green Deal. European Commission
2. IEA (2021), "Net Zero by 2050", IEA, Paris https://www.iea.org/reports/net-zero-by-2050
3. J. Eichman, M. Torrecillas Castelló and C. Corchero. "Reviewing and Exploring the Qualitative Impacts That Different Market and Regulatory Measures Can Have on Encouraging Energy Communities Based on Their Organizational Structure". Energies 2022, 15(6), 2016
4. José Luis Ruiz Duarte and Neng Fan. "Operation of a Power Grid with Embedded Networked Microgrids and Onsite Renewable Technologies". Energies 2022, 15(7), 2350
5. Moiz Masood Syed and Gregory M. Morrison. "A Rapid Review on Community Connected Microgrids". Sustainability 2021, 13(12), 6753
6. Sabrina Lee Chartier, Vinod Kumar Venkiteswaran, Shriram S. Rangarajan, Edward Randolph Collins and Tomonobu Senjyu. "Microgrid Emergence, Integration, and Influence on the Future Energy Generation Equilibrium—A Review". Electronics 2022, 11(5), 791
7. P. Pijarski, P. Kacejko and M.Wancerz. "Voltage Control in MV Network with Distributed Generation—Possibilities of Real Quality Enhancement". Energies 2022, 15(6), 2081
8. Prashant, A. Shahzad Siddiqui, Md Sarwar, A. Althobaiti and S. S. M. Ghoneim. "Optimal Location and Sizing of Distributed Generators in Power System Network with Power Quality Enhancement Using Fuzzy Logic Controlled D-STATCOM". Sustainability 2022, 14(6), 3305
9. Md Masud Rana, Mohamed Atef, Md Rasel Sarkar, Moslem Uddin and GM Shafiullah. "A Review on Peak Load Shaving in Microgrid—Potential Benefits, Challenges, and Future Trend". Energies 2022, 15(6), 2278
10. Gregorio Fernández, Noemi Galán, Daniel Marquina, Diego Martínez, Alberto Sanchez, Pablo López, Hans Bludszuweit and Jorge Rueda. "Photovoltaic Generation Impact Analysis in Low Voltage Distribution Grids". Energies 2020, 13(17), 4347
11. Accept Horizon 2020 project. https://cordis.europa.eu/project/id/957781
12. DIgSILENT PowerFactory. https://www.digsilent.de/en/
13. The IEEE European Low Voltage Test Feeder. https://cmte.ieee.org/pes-testfeeders/
14. REE. Real-time demand and generation. https://www.ree.es/en/activities/realtime-demand-and-generation

Energy and economic analysis of renewable energy-based isolated microgrids: Case study Bigene, Guinea-Bissau

J. A. Aguilar-Jiménez [1,2,*], L. Hernández-Callejo [3,*], V. Alonso-Gómez [4], A. García-Álvaro [3], R. Maján-Navalón [5,*]

[1] Centro de Estudios de las Energías Renovables, Instituto de Ingeniería, Universidad Autónoma de Baja California, Blvd. B. Juárez s/n, 21280, Mexicali, BC, México.
[2] Facultad de Ingeniería, Universidad Autónoma de Baja California, Blvd. B. Juárez s/n, 21280, Mexicali, BC, México.
[3] Department of Agricultural Engineering and Forestry, University of Valladolid (UVA), Campus Universitario Duques de Soria, 42004 Soria, Spain.
[4] Department of Applied Physics, University of Valladolid (UVA), Campus Universitario Duques de Soria, 42004 Soria, Spain.
[5] Asociación Tierra sin Males, Soria, Spain.
aguilarj30@uabc.edu.mx (J.A.A-J.); luis.hernandez.callejo@uva.es (L.H-C.); raulmn89@gmail.com (R.M-N.)

Abstract. In order to reach a larger population with access to electricity, it is necessary to implement different strategies, alternative to centralized electrification and grid extension. The installation of isolated microgrids using renewable energies has greatly increased and promises to be one of the most attractive option to bring energy to the most difficult accessible regions. This paper presents the energy and economic study of a system for the electrification of the isolated community of Bigene, Guinea-Bissau, by means of a microgrid using different generators and energy storage. The relationship between generation-storage capacity and its effect on variables such as auxiliary energy requirements, energy waste, initial investment and cost for the energy generated during the useful life of the project is analyzed. The results show that the capacity of the generators and energy storage to be installed depend on factors external to the energy analysis, such as the availability of financial capital and pollutant gas emissions to be avoided, since the initial investment cost of the energy storage system has a negative impact on the economic feasibility, making the prolonged use of fossil fuels more financially attractive.

Keywords: Microgrid, Renewable Energy, Solar Energy, Isolated Community.

1   Introduction

Bringing electricity service for the majority of the world's population that need it is a major challenge. Despite a global electricity access rate of 90.5 % by 2020 [1], there are countries with very low values, most of which are located on the African continent. The Sub-Saharan African countries presented in the same year an average access to electricity of 48.4 %, in contrast to 100 % of the countries of the European Union. This

becomes an issue of vital importance, in which the efforts of public and private institutions must contribute with new projects and technologies, seeking to reduce this huge gab that is the access to basic electricity services in a sustainable way.

Different strategies have been implemented to bring electricity to the entire population. In most cases, it has been decided to extend the transmission lines to carry the energy from the large generation centers to each consumer. However, sometimes the remoteness of the consumption centers made it impossible to extend the grid due to economic reasons. In addition, in other cases, the geographical location of the users, such as in mountains or difficult access areas, made it technically impossible to install transmission lines. In order to solve this problem, it was proposed to bring generators to the consumption centers so that the energy would be produced in the same place as the user, eliminating the costs and energy losses related to the extension of the electric grid. Based in these strategies, the microgrid model was initiated. The Institute of Electrical and Electronics Engineers (IEEE) defines microgrid as *"a group of interconnected loads and distributed energy resources with clearly defined electrical boundaries that acts as a single controllable entity with respect to the grid and can connect and disconnect from the grid to enable it to operate in both grid-connected or island modes"* [2]. Based on the above, a microgrid can be composed of different generators, including renewable energies, promoting sustainable decentralized electrification. In the past, due to the low cost of fossil fuels, it was common to install an electric power generator based on diesel or gasoline combustion. However, nowadays, and due to the problems of environmental pollution and climate change, traditional generators have been largely replaced by generator based on renewable energies. This allows the electricity produced in the consumption centers to come from a clean and free source, taking advantage of the natural resources present in the region. This, together with the lower costs of renewable technologies, makes it an economically and sustainably attractive option for rural electrification [3].

Several rural electrification projects have been developed under the concept of the community microgrid, defined as a system that *"(…) is connected with its community through physical placement and can be owned by said community or other part"* [4], using renewable energies as the main driving force. In Puertecitos, Baja California, Mexico, an isolated microgrid was installed in a fishing community with a high level of social marginalization [5, 6]. The system was sized to meet basic needs, such as food preservation, comfort and education. Due to the extreme climatic conditions, where summers are very hot and winters have low temperatures, the electricity demand profile contrasts between the different seasons of the year. A 55 kW photovoltaic (PV) module system, a 5 kW wind turbine, a 75 kVA diesel generator as auxiliary, and a 522 kWh lead-acid battery energy storage were chosen. The microgrid cannot fully meet demand during the summer, when air conditioning equipment is needed, so the diesel generator is used for short periods of time to cover the energy shortage. During the winter there is a large amount of wasted energy because energy demand is very low compared to generation capacity. In Huatacondo, in the Atacama Desert, Chile, a microgrid isolated from the power transmission system was installed to provide electricity service for 24 hours continuously [7]. The system incorporates 22.5 kW of PV technology, 3 kW of

wind power, a 140 kWh battery bank and a 120 kVA diesel generator. Another microgrid installed in Chile, in the town of Ollagüe in the Antofagasta region, incorporates 200 kW PV power, 30 kW of wind energy, 410 kVA of diesel generation, 752 kWh of energy storage, and two parabolic dish solar collectors to provide hot water for the local school [7]. In many regions of the world, low-capacity microgrids have been installed for rural electrification, using renewable energies as a basis, in order to improve the living conditions of marginalized communities [8–10].

The high cost of isolated microgrids remains an impediment to their implementation in poor communities [11]. Therefore, the correct sizing of the equipment is of great importance during planning. This work presents the energy and economic analysis for the implementation of a microgrid for the isolated community of Bigene, Guinea-Bissau, an African country, which has a high rate of social marginalization. The microgrid is based on the use of renewable technologies and an energy storage system using batteries. Through the use of energy simulation software, it is possible to establish the expected energy demand and the sizing of an energy generation system that is sensitive to local environmental conditions, such as solar photovoltaic energy. An auxiliary power generation system using diesel combustion is also considered for periods when there is no stored energy. The study includes the analysis of the generation-storage capacity relationship and its effect on variables such as auxiliary energy requirements, energy waste, initial investment and cost for the energy generated during the useful life of the project. With the above, it is intended to establish the criteria for decision making regarding the capacity of the system to be installed, considering different factors, such as the availability of financial capital and emissions of polluting gases, among others.

2   System description

The sustainable electrification system consists of a photovoltaic module field responsible for generating electrical energy by means of solar energy. The energy produced is fed to the inverter/controller which, depending on the electricity demand of the community and the state of the battery system, determines whether it satisfies the electrical requirements and/or stores energy. An auxiliary power system based on a diesel generator is available to meet demand during periods when there is insufficient solar resource or stored energy. The proposed independent microgrid will be distributed by electrical transmission lines from the plant to the different consumers (loads). The schematic diagram of the system is shown in Figure 1. Wind energy was not considered in this system because the location does not have adequate wind speeds for its utilization.
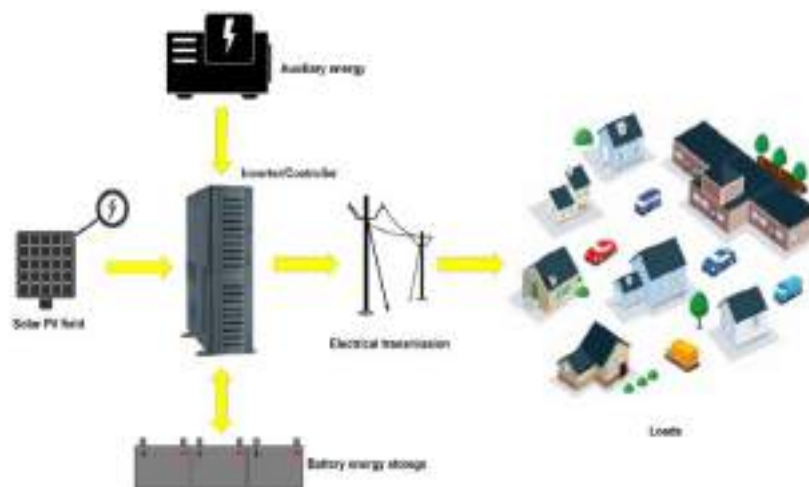
Fig. 1. Schematic diagram of microgrid for rural electrification.

3   Methodology

The isolated community of Bigene (12.44 N, 15.54 W) is located in the region of Cacheu, in the African country of Guinea Bissau; it has a high social marginalization due to the lack of basic services, such as electricity and drinking water. Microgrids based on renewable energies are an excellent option to improve living conditions and promote sustainable economic development in this type of communities [6].

3.1   Load profile

Given the current conditions of no access to electricity, it is necessary to estimate electricity consumption profiles based on the essential requirements of this kind of population, to enable the sizing of the renewable energy system. In this community there are different types of buildings, so a consumption profile was established for each user, in which houses, businesses, schools and hospitals are considered. The equipment considered within the loads are shown in Table 1. The amount and energy consumption of each equipment are different depending on the user, so Figure 2 shows the daily load established per user and the total load of the community. The users are 500 homes, 25 businesses, 1 hospital and 3 schools.

Table 1. Equipment considered for each user connected to the microgrid.

Equipment	Home	Business	Hospital	School
Light	4 x 10 W	5 x 10 W	50 x 10 W	10 x 10 W
Fridge	1 x 600 W	4 x 600 W	3 x 600 W	1 x 600 W

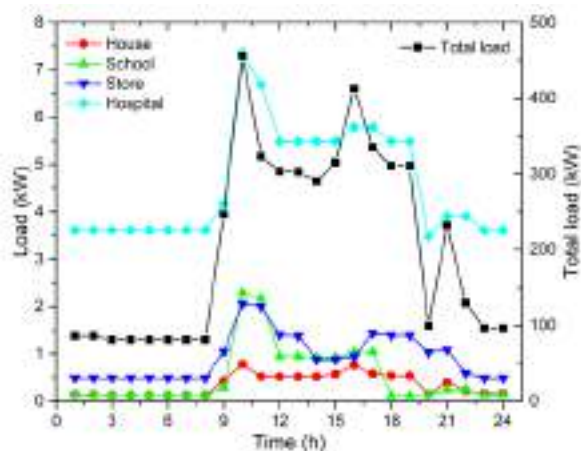| TV	1 x 60 W	1 x 60 W	5 x 60 W	2 x 60 W
Blander	1 x 500 W	-	-	-
Fan	2 x 200 W	2 x 200 W	10 x 200 W	4 x 200 W
Computer	-	1 x 600 W	2 x 60 W	2 x 600 W
Electric motor	-	1 x 1,000 W	-	-
Constant load	-	-	1 x 3,000 W	-

Fig. 2. Load profile of different users during a day.

For homes, equipment was considered for food preservation and preparation, lighting and entertainment, while for businesses, a computer and a 0.6 kW electric motor were added so that specialized activities can be carried out. For schools, a greater number of computers and televisions are contemplated for use in teaching. For the hospital alone, a constant load of 3 kW is considered in addition to the equipment, to be used for specialized systems that need to be on 24 hours a day. This results in a demand profile with an approximate peak of 450 kW in the morning and another of 400 kW after 16:00, mainly due to the number of domestic users.

3.2 Climatological conditions

The demand profile shown in Figure 2 is considered a repetitive profile throughout the year, mainly due to the fact that Bigene has template climatic conditions, with an average ambient temperature of approximately 25 °C, with no noticeable variations throughout the year, as shown in Figure 3. In different scenarios, when the demand profile differs in the seasons of the year, the sizing of the system may be affected, since the energy requirements would determine different optimal capacities of the system, i.e., it could be oversized or undersized for certain periods, increasing energy waste and auxiliary energy. Figure 4 shows the global solar radiation available in the study region.

Being close to the equator, it has stable radiation levels during most of the year, with maximums of up to 1,000 W/m², which is an indication that it is a good solar resource for electricity production. This climatological information was acquired using Meteornorm software.
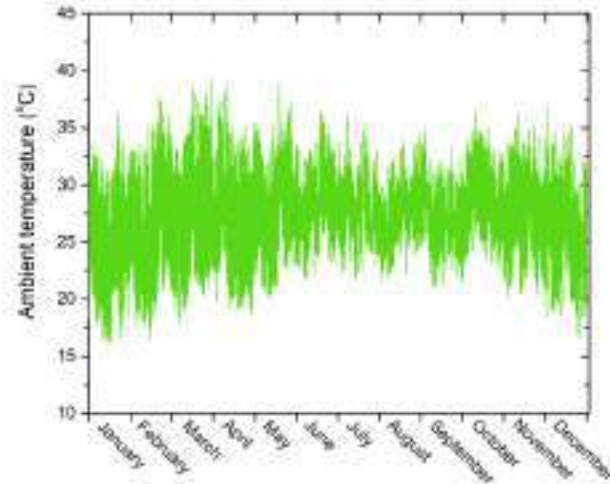

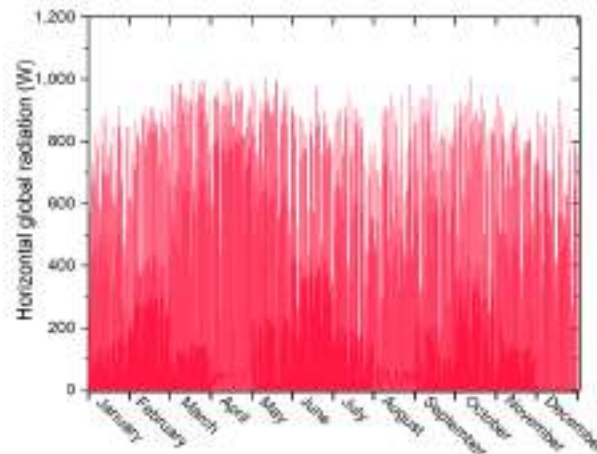**Fig. 3.** Yearly ambient temperature of Bigene, Guinea Bissau.

Fig. 4. Annual global horizontal radiation of Bigene, Guinea Bissau.

For the development of the simulation, TRNSYS software was used and hourly studies were carried out during an entire operating year. A database of climatological data

typical of the region was considered, as well as energy generation and storage equipment available in the market. Table 2 shows the characteristics of the equipment used in the microgrid simulation.

Table 2. Characteristics of the main equipment used in the simulation.

PV module manufacturer	Yingli Solar
Model	YGE 72 cells
Power	330 W
Batteries manufacturer	BSB
Capacity per battery	1650 Ah
Voltage	2 V
Charging efficiency	0.9
Inverter efficiency	0.9
Diesel generator efficiency	0.35

With the climatic characteristics of the region and the particularities of the equipment, it is possible to carry out studies that allow an optimal sizing of the microgrid, considering the most economically acceptable ratio between the wasted energy and the extra energy generated by the auxiliary system. For the presentation of the results, the annual totals of energy generation, consumption, storage and waste were made.

3.3   Economical analysis

The energy results shown in the previous section help to understand the behavior of the microgrid according to the system capacity. However, decision making should not be based solely on the optimal ratio between wasted energy and extra auxiliary energy required. The economic factor, in conjunction with the above, determines the appropriate capacity with the optimal cost-benefit ratio.

For the comparison, the Levelized Cost Of Energy (LCOE) was used, which is the economic valuation of the cost of the electricity generation system that includes all the costs over the project life, which was considered as 25 years for both, and was calculated based on [12], as follows:

$$LCOE = \frac{ATE\ (USD)}{E_{gen}\ (kWh)} \tag{1}$$

where E_{gen} is the energy that will be produced during the operational lifetime. ATE is the annual total expenditures over the entire operational lifetime and are comprised of the investment expenditures and the operating costs accumulating over the operational lifetime [13], and it is calculated as:

$$ATE\ = CAPEX + O\&M \tag{2}$$

where $CAPEX$ is the capital cost of the system and $O\&M$ are the operating and maintenance expenses over the life of the project, which are calculated according as follows:

$$O\&M = \sum_{i=1}^{plant\ life} O\&M(i) \qquad (3)$$

where $O\&M(i)$ are the operation and maintenance costs during the ith year of operation. An $O\&M(i)$ expense of 2% of CAPEX was assumed for the two systems and an annual inflation rate (ir) of 5% [12]. Then, the $O\&M(i)$ is calculated as:

$$O\&M(i) = 0.02 \times CAPEX \times (1 + ir)^{i-1} + R(i) \qquad (4)$$

$R(i)$ corresponds to the eventualities that may arise during the operation of the system in terms of spare parts or changes of individual equipment due to their useful life. For all capacities, an expense of 30% of the cost of the inverter every 10 years, and for the PV-Battery system the change of the battery bank every 4 years, were considered based on the manufacturer's guarantees for this type of equipment, as well as on the authors' experience with the Puertecitos microgrid [6]. The cost of the diesel generator is equivalent to one with a capacity of 460 kW, which is the highest instantaneous demand during the year. The cost estimates of the equipment of both systems are presented in Table 3.

Table 3. Cost estimation of microgrid system.

Initial investment			Annual cost	
PV module	400 USD/kW	O&M(i)	2%	
Inverter	190 USD/kW	Inflation rate	5%	
Lead-acid battery	520 USD/kAh	Diesel	0.3025 USD/kWh*	
Balance of Plant	248 USD/kW		Replacement costs	
Diesel generator	180,000 USD	Inverter	30% of price every 10 years	
		Batteries	Every 4 years	

   * The kWh cost of diesel was calculated based on the price per liter of fuel (1.145 USD/L), its calorific value (1 L= 9.9611 kWh) and the efficiency of the direct combustion generator (0.38). A 1.5% annual increase in fuel cost was considered.

4   Results

4.1   Energy analysis

To perform the energy analysis of the microgrid in Bigene, parametric studies were carried out with different values of photovoltaic and battery storage capacity, observing the effect on energy production, storage and loss, as well as quantifying the energy requirements through the auxiliary generator. Figure 5 shows the annual energy contribution of the PV system and the battery system to the community's demand as a function of the installed capacity. Up to 600 kW of PV power, the increase in the size of the

energy storage system does not have a significant impact on the contribution of renewable energy to the demand, mainly because all of the energy produced by the PV system is consumed, leaving no part for storage. As the PV capacity increases, the energy production is sufficient to meet the instantaneous demand and direct an amount to the battery storage for later use. This results in a better use of the solar resource and, therefore, a greater contribution of renewable energies.
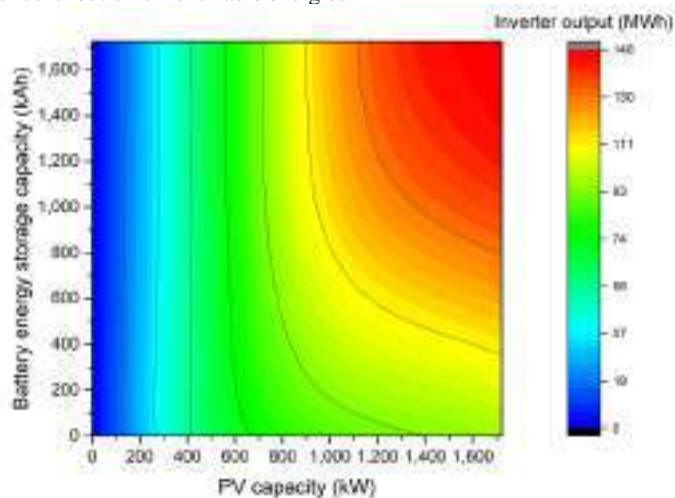

Fig. 5. Effect of varying PV capacity and battery system size on annual energy contributed to demand only by PV modules and/or stored.

However, it has to be taken into account that the electricity demand profile of the community does not coincide in its entirety with the energy production profile of the PV system. Depending on the scenario, at sometimes it may be possible that the PV power is greater than the community's demand and the storage system is at its maximum capacity, so that excess energy would be lost. Figure 6 shows the effect of PV system size and battery bank on energy losses. There are a large number of combinations that do not allow energy to be wasted. However, as the size of the PV system increases, the capacity of the battery system becomes vitally important. The expected annual energy consumption for the Bigene community is 153 MWh; a PV capacity of 1,700 kW with a battery bank of less than 100 kAh represents losses of up to 93% of the community's annual consumption. This is why the proper sizing of microgrids based on renewable energies is so important, having to determine the optimal ratio between energy losses and required auxiliary energy.
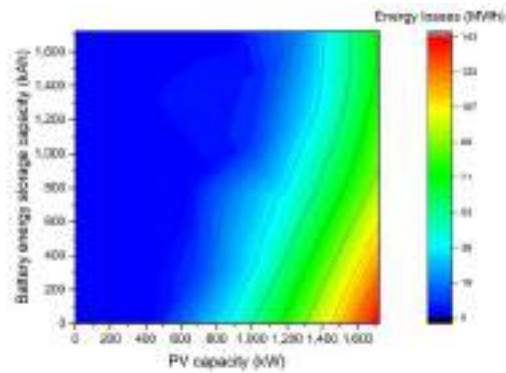
Fig. 6. Variation in PV system and battery system size and its effect on annual energy losses.

Figure 7 shows the annual need for auxiliary power (diesel generator) according to the size of the microgrid. Without PV system and battery bank, the total energy provided by the diesel generator is 153 MWh, which is the annual energy requirement of the study community. As the PV capacity increases, the fossil fuel contribution is reduced proportionally, with no effect on the capacity of the battery bank, since all the energy is used to meet the demand. From about 600 kW of PV capacity, excess solar energy production aided by energy storage tends to reduce auxiliary power requirements. However, a microgrid with high PV capacity and energy storage is needed to almost completely eliminate the need for fossil fuels. With the maximum system values analyzed in this work, a 97 % share of renewable energies was achieved, the remaining 3 % having to be produced with fossil fuels or some other source of generation.

Fig. 7. Annual auxiliary power requirement according to microgrid capacity.

4.2   Economical comparison

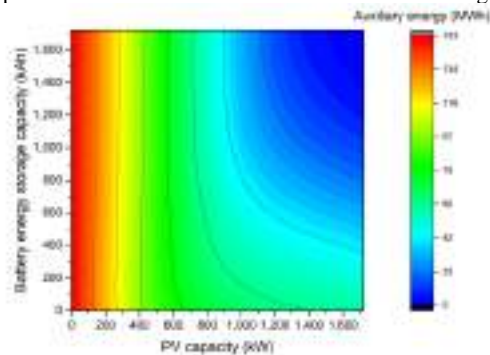Figure 8 shows the annual cost of fossil fuel required to meet the community's energy needs as a function of PV capacity and battery bank. Up to a maximum of $46,200 USD in expenses in the first year of operation is required if the microgrid were to be powered solely by diesel. As PV capacity brings clean energy, these values tend to decrease, regardless of battery bank capacity. From 600 kW, and more noticeably after 900 kW of PV capacity, it is possible to store energy for later consumption, implying a reduction in fossil fuel costs.
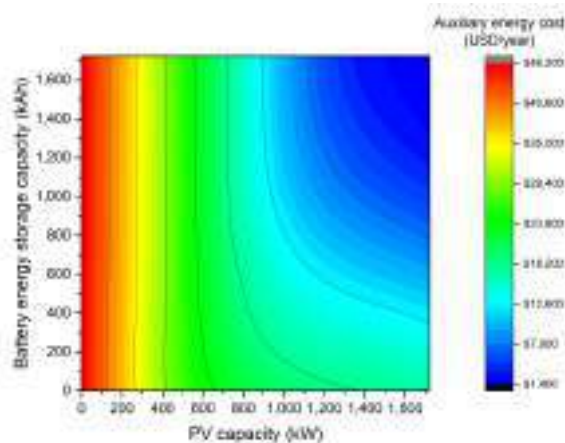
Fig. 8. Variation of the annual cost of auxiliary energy required to meet the demand, according to the capacity of the microgrid.

Considering the equipment costs shown in Table 3, as well as the price of fuel and replacements, Figure 9(a) and Figure 9(b) present the CAPEX and O&M values as a function of the microgrid capacity. The lowest initial investment is found when considering that only the diesel generator will be installed, with a cost of $180,000 USD. When the capacity of renewable technologies increases, the initial investment increases greatly, with the cost of the battery bank being slightly more representative than the cost of the PV system. However, when O&M costs are considered over the useful life of the system (considered to be 25 years), the trend changes drastically. The increase in PV capacity is not representative of the O&M compared to the increase in battery bank capacity, mainly due to the cost of replacing it with a new storage system, considering a useful life of four years. This means that, during the 25-year duration of the project, it is necessary to replace the battery bank six times due to its short useful life. This greatly impacts the costs during operation, since the price of this equipment is the highest of all the components that make up the microgrid. On the other hand, when the PV capacity increases, the electrical inverter also increases, but its specific cost is not as high as that of the energy storage, and its replacement is every ten years only in damaged parts.
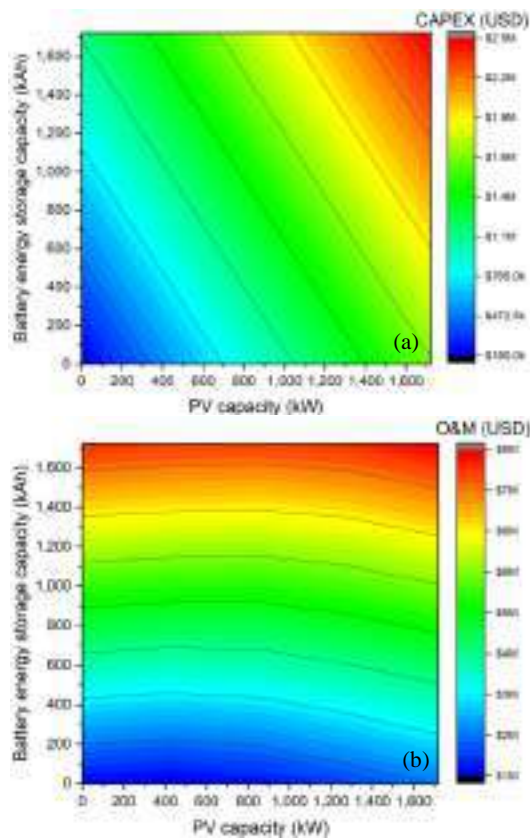
Fig. 9. Variation of (a) initial investment (CAPEX) and (b) O&M during system lifetime, as a function of PV capacity and energy storage capacity.

Finally, Figure 10 shows the LCOE as a function of the size of the microgrid. With this, it can be determined, in economic terms, which of the capacity combinations is more attractive. It can be seen that the lowest lifetime energy costs are found with low or no energy storage capacity, due to its high initial investment cost and short lifetime. As the size of the PV system increases, the LCOE decreases, concluding that PV technology does contribute to lowering the cost of energy. The calculated LCOEs are in the range of $0.43-2.77 USD/kWh, where the lowest values correspond to fossil fuel-only electrification, mainly due to its low initial investment cost and low fuel price. It can be predicted that, as the cost of fossil fuel increases and better and more economical options for energy storage systems become available, the LCOE will tend to decrease with respect to the increased renewable energy usage.

With Figure 10, decisions can be made regarding the selection of equipment capacity, taking into consideration the previous results, such as energy losses and CAPEX. However, the results of this study do not determine an optimal PV-storage capacity ratio for the Bigene microgrid, since the final selection must take into account factors such as resource availability for the initial investment, reduction of greenhouse gas pollution and the nature of the project (social or for-profit), to mention a few. For example, if the aim is to reduce the economic expense due to the use of auxiliary energy, the most convenient would be to increase the PV generation capacity while maintaining an energy storage capacity in the range of 800-1,000 kAh, according to the results shown in Fig. 8.
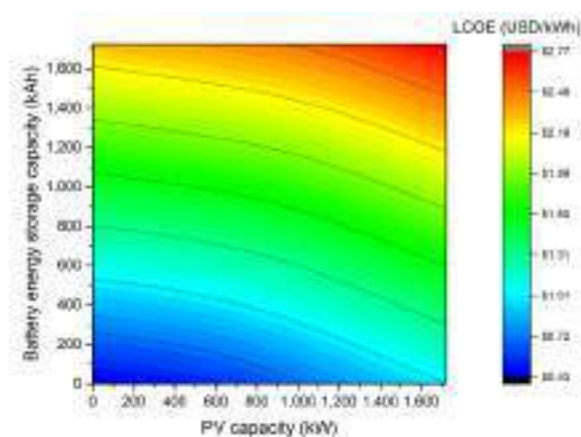
Fig. 10. LCOE as a function of PV capacity and energy storage.

5　　Conclusions

This paper presented the energy and economic analysis of a microgrid based on the isolated community of Bigene, Guinea-Bissau, as a case study. The microgrid incorporates as generation equipment PV modules and a diesel auxiliary system, as well as an energy storage system. An electricity demand was established for different users, including homes, businesses, schools and hospitals, which focused on covering basic needs depending on the type of user. A microgrid simulator was developed and the generation-storage capacity relationship was analyzed and its effect on variables such as auxiliary energy requirements, energy waste, initial investment and the cost of energy generated during the useful life of the project. The results show that the storage system is the main component of the microgrid that affects the cost of energy due to its high initial price and short useful life, forcing it to be replaced up to six times during the total life of the project. The PV system contributes to reducing the cost of energy because, unlike batteries, it is an economical technology, requires low maintenance and has a long useful life. The calculated LCOEs are in the range of $0.43-2.77 USD/kWh,

where the lowest values correspond to fossil fuel-only electrification, mainly due to its low initial investment cost and low fuel price. This study helps decision making when selecting the appropriate energy generation-storage ratio, taking into consideration other factors, such as initial investment capacity, reduction of greenhouse gas pollution, and the nature of the project (social or for-profit).

Acknowledgments

References

1. The World Bank: Access to electricity, https://data.worldbank.org/indicator/EG.ELC.ACCS.ZS.
2. IEEE Power and Energy Society: IEEE Standard for the Testing of Microgrid Controllers. (2018).
3. Hirsch, A., Parag, Y., Guerrero, J.: Microgrids: A review of technologies, key drivers, and outstanding issues. Renew. Sustain. Energy Rev. 90, 402–411 (2018). https://doi.org/10.1016/j.rser.2018.03.040.
4. Warneryd, M., Håkansson, M., Karltorp, K.: Unpacking the complexity of community microgrids: A review of institutions' roles for development of microgrids. Renew. Sustain. Energy Rev. 121, 109690 (2020). https://doi.org/10.1016/j.rser.2019.109690.
5. Aguilar-Jiménez, J.A., Velázquez-Limón, N., López-Zavala, R., González-Uribe, L.A., Islas, S., González, E., Ramírez, L., Beltrán, R.: Optimum operational strategies for a solar absorption cooling system in an isolated school of Mexico. Int. J. Refrig. 112, 1–13 (2020). https://doi.org/10.1016/j.ijrefrig.2019.12.010.
6. Aguilar-Jiménez, J.A., Velázquez, N., Acuña, A., Cota, R., González, E., González, L., López, R., Islas, S.: Techno-economic analysis of a hybrid PV-CSP system with thermal energy storage applied to isolated microgrids. Sol. Energy. 174, 55–65 (2018). https://doi.org/10.1016/J.SOLENER.2018.08.078.
7. Jiménez-estévez, B.G., Navarro-espinosa, A., Palma-behnke, R.: Achieving Resilience at the Distribution Level. IEEE Power Energy Mag. 64–73 (2017). https://doi.org/10.1109/MPE.2017.2662328.
8. López-González, A., Domenech, B., Gómez-Hernández, D., Ferrer-Martí, L.: Renewable microgrid projects for autonomous small-scale electrification in Andean countries. Renew. Sustain. Energy Rev. 79, 1255–1265 (2017).

https://doi.org/10.1016/j.rser.2017.05.203.

9.　Valer, L.R., Manito, A.R.A., Ribeiro, T.B.S., Zilles, R., Pinho, J.T.: Issues in PV systems applied to rural electrification in Brazil. Renew. Sustain. Energy Rev. 78, 1033–1043 (2017). https://doi.org/10.1016/j.rser.2017.05.016.

10.　Gaona, E.E., Trujillo, C.L., Guacaneme, J.A.: Rural microgrids and its potential application in Colombia. Renew. Sustain. Energy Rev. 51, 125–137 (2015). https://doi.org/10.1016/j.rser.2015.04.176.

11.　Shakya, B., Bruce, A., MacGill, I.: Survey based characterisation of energy services for improved design and operation of standalone microgrids. Renew. Sustain. Energy Rev. 101, 493–503 (2019). https://doi.org/10.1016/j.rser.2018.11.016.

12.　Patil, V.R., Biradar, V.I., Shreyas, R., Garg, P., Orosz, M.S., Thirumalai, N.C.: Techno-economic comparison of solar organic Rankine cycle (ORC) and photovoltaic (PV) systems with energy storage. Renew. Energy. 113, 1250–1260 (2017). https://doi.org/10.1016/j.renene.2017.06.107.

13.　Kost, C., Mayer, J.N., Thomsen, J., Hartmann, N., Senkpiel, C., Philipps, S., Nold, S., Lude, S., Saad, N., Schlegel, T.: Levelized Cost of Electricity Renewable Energy Technologies. Fraunhofer Institut for Solar Energy Systems ISE, Freiburg, Germany (2013).

Analysis of the Use of Active Technologies to Convert Traditional Buildings into Net Zero Energy Buildings Using Building Energy Modeling

David Zabala-Pedraza[1] [0000-0002-8034-8140], Ricardo Peña-Guzman[1] [0000-0003-2758-1856], Diego Morales-Polanco[1] [0000-0002-0094-2183], Genesis Sanchez-Sosa[1] [0000-0003-1004-1183], Arismendy Del Orbe[1] [orcid.org/0000-0002-6639-5960], Jose Duran[1] [0000-0001-6505-5182], Nabil Sbriz[1] [0000-0001-5131-6505], Miguel Aybar-Mejía[1] [0000-0002-4715-3499], Deyslen Mariano-Hernández[1] [0000-0002-4255-3450]

[1] Área de Ingeniería, Instituto Tecnológico de Santo Domingo.
Santo Domingo, Dominican Republic.
deyslen.mariano@intec.edu.do

Abstract. Buildings as consumers of electrical energy worldwide have drawn the attention of researchers. To ensure comfort and effective management of the planet's resources, it has tried to continue developing ways to implement buildings with almost zero consumption. Building energy modeling is a very multipurpose tool for energy efficiency. This tool can help to build energy managers make decisions regarding the technology that could be implemented to reduce electricity consumption. Considering this, the objective of this article is to present a methodology to analyze the implementation of different active technologies in traditional buildings using building energy modeling to be converted into net zero buildings. To carry out this analysis, OpenStudio software was used to learn how implementing different active technologies could help reduce electricity consumption. The PV*SOL software was also used to analyze a photovoltaic system that covers the demand of the building. The results showed that not all active technologies alone could bring reductions in all building subsystems but that combining them with advanced technologies would be necessary.

Keywords: Net zero energy building, renewable energy, energy efficiency, building energy modeling, sustainable building.

1　Introduction

The predicted increment of energy requests drives the need to limit buildings' energy utilization. As per the EIA (Energy Information Administration), the building sector (non-residential and residential buildings) represented 40% of the total final energy utilized in 2021 [1]. The pace of energy-efficient improvement is meager, about 1-2% in the U.S. and Europe, with average energy intensity decreases of under 15%. These parameters can be attributed to an absence of information about cost-ideal retrofit strategies, low energy costs, and the powerlessness to thoroughly measure the ad-

vantages of energy retrofitting [2]. Thus, the idea of Net Zero Energy Building (NZEB) has surfaced in the plan of building energy efficiency policies in numerous nations to tackle the rising pattern of energy use in buildings [3].

NZEB use renewable energy and energy efficiency to produce as much energy as they use throughout the year. By producing their renewable energy, NZEB lower operating and maintenance costs, help the climate, and increment versatility during blackouts [4]. Sun-powered prosumer buildings are acquiring popularity and are introduced as net-zero or positive energy structures. Building energy managers anticipate that NZEB should significantly decrease the energy utilization of renewable energy sources and energy efficiency [5]. To accomplish a Net Zero result, choosing energy-efficient technologies and picking stable energy sources is essential [6].

New choice-making tools, such as Building Energy Modelling (BEM), are required to enhance the overall performance of buildings [7]. BEM is a cycle to foresee the energy demand of a building through virtual experience. Building energy investigation through virtual experience commonly occurs because of the quest for energy efficiency. BEM applied to exist buildings assists with investigating retrofit opportunities at minimal price and without intercession [8]. Energy simulations are a fundamental method for helping building-correlated activities and relate to the whole life of a building, from design to everyday building operations and end-of-life procedures [9].

Recent studies using BEM have shown how to improve energy efficiency in buildings. For example, Nabil et al. [10] developed an energy model applying efficiency measures in insulation materials for windows, roofs, and walls. Fazelpour et al. [11] simulated a green roof and a double-skin facade to optimize the building design in different climates to reduce energy consumption. Caponetto et al. [12] analyzed different performances of green building techniques and contrasted them with commonly adopted technology. Webb [13] proposed a fur-perfusion façade compared with other building envelope energy efficiency or upgrades to reduce energy consumption. Guo et al. [14] assess the effect of climatic circumstances and building structures on the passive ventilation of medium-sized exercise rooms in subtropical regions.

As seen in the literature review, there are recent studies on building modeling to support building energy performance-related choices. However, most studies focus on passive technologies, omitting active ones to transition from traditional buildings to sustainable ones, such as NZEB. This paper aims to present a methodology to analyze the incorporation of active technologies in traditional buildings using BEM to convert them into NZEB.

2   Building Energy Model Development

2.1   Case of Study

For this research, a building located on a university campus was selected. Once the building was selected, a survey of the physical characteristics of the building was made. With the characteristics of the building, a digital twin was created to implement improvements to reduce electrical energy consumption. After creating the digital twin with the improvements, the original model was compared to the model with the improvements made. Within the Instituto Tecnológico de Santo Domingo campus, the Ercilia Pepín (EP) Building was selected (see Fig. 1). The EP Building has 1,180.24 square meters distributed on three levels, one of which is underground. In the basement, there are classrooms and research laboratories; on the first level, there are administrative offices and recreation space for students, while on the second level, there are administrative offices and classrooms.

For the simulation of the building, the OpenStudio software was used. OpenStudio is a cross-platform assortment of programming tools developed by the U.S. Department of Energy to help with whole-building energy modeling utilizing EnergyPlus and high-level daylight analysis utilizing Radiance [15].

Fig. 1. View of EP Building.

2.2   Energy Model with an Unconditioned Envelope

The first step was to model the building considering only its physical structure, without considering loads and consumption. To model the building, its measurements were taken using a laser distance meter because the architectural plans of the building were not available. In the survey carried out, the distribution of the building was rec-

orded. The distance between walls, the ceilings, and the location of the windows in contact with the outside was measured. Fig. 2 shows the obtained result from the model.

For this model, only the windows that have contact with the outside were considered because the interior windows do not generate a significant difference in the simulation of the building model. In addition, the student recreation space was modeled as a window with airflow, so it will not generate conflicts in the model.
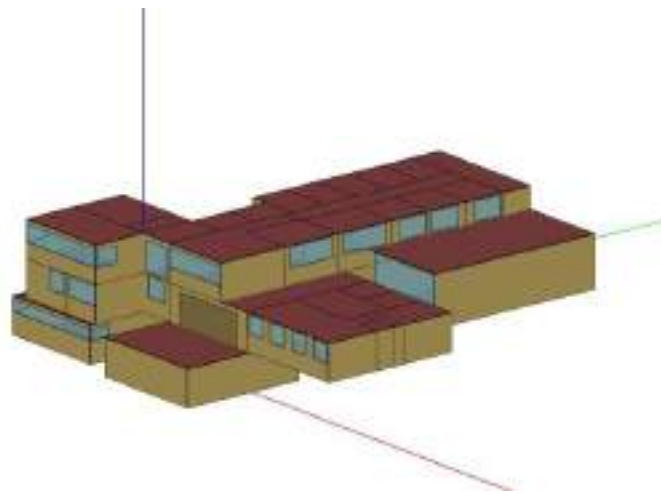
Fig. 2. Building energy model with unconditioned envelope.

2.3   Loads and Consumption Details

The determination of the energy demand of the building was carried out through OpenStudio because the building does not have local electricity metering. To complete the model of the building, it was necessary to define the spaces based on the different electrical and thermal loads that act on them. Detailing these loads implied that during the information collection stage, each space's electrical and lighting devices, the number and flow of people, the work schedule, the behavior of people concerning the equipment during the day, and activities carried out in the office.

The load definition of this model was classified based on three types of loads: People, lights, and electric equipment. People definitions correspond to the loads that people generate in a given area with their presence, which were defined by the maximum number of people passing through the area during the day, the heat contributed to the environment by the presence of people, and the rate of carbon dioxide generation per person.

Lights definitions correspond to the loads represented by the lighting. Which were defined by the consumption of maximum power (W) for lighting elements corresponding to each zone, the heat that the lights emit to contribute to the ambient temperature in the form of thermal radiation, and the heat with which lights contribute to the ambient temperature in the form of visible radiation. Electric equipment definitions are represented by electrical equipment, defined by the consumption of maximum power (W) corresponding to the set of electrical elements in the area. The heat that the equipment emits contributes to the ambient temperature in the form of thermal radiation, the humidity generated by the equipment's temperature increase, and the loss of energy generated by converting one type of energy into another.

2.4   Loads Schedules

For each zone, a set of schedules have been defined that work as multipliers for the different loads. Depending on the types of cargo that we are using to define the spaces, each series of itineraries has:

- A schedule defines the behavior of the corresponding load of people. Based on the number of people and on the activities that these people are carrying out.
- A schedule that defines the hourly behavior of the lighting elements based on the equipment that is working and how long they are on.
- A schedule that defines the behavior of electrical equipment using the same principle applied to lighting loads.
- A schedule that defines the behavior of unwanted air infiltration.

For the named schedules, the values in the different hours oscillate between 0 and 1. These parameters were defined this way since they function as multipliers of the maximum load. These parameters were defined this way since they function as multipliers of the maximum load. These reflect the fraction of the maximum load that works, a part of the time, within each hour. The corresponding scheduled activities that people carry out are based on the estimation of the metabolic rate (W/person) generated by people according to the activities they perform within the area of the building in which they are located. The reference values of these estimates were obtained and can be seen in Table 1.

Table 1. Metabolic rates for various activities.

Activity	Activity Level w/ Person EnergyPlus Schedule Value	Activity Level W/m2	Metabolic Rates
Resting			
Sleeping	72	40	0.7
Reclining	81	45	0.8
Seated, quiet	108	60	1
Standing, relaxed	126	70	1.2

Activity	Activity Level w/ Person EnergyPlus Schedule Value	Activity Level W/m2	Metabolic Rates
Walking (on a level surface)			
3.2 km/h (0.9 m/s)	207	115	2
4.3 km/h (1.2 m/s)	270	150	2.6
6.4 km/h (1.8 m/s)	396	220	3.8
Office Activities			
Reading, seated	99	55	1
Writing	108	60	1
Typing	117	65	1.1
Filling, seated	126	70	1.2
Filling, standing	144	80	1.4
Walking about	180	100	1.7

2.5   Air Infiltration and Types of Spaces

The types of space define the profile of an area concerning its energy behavior. They are composed of itineraries corresponding to the space and the definition of untreated/conditioned air infiltration. The type of space encompasses what is known as the outdoor air design specification. Those values were selected according to the American Society of Heating and Air-Conditioning Engineers (ASHRAE) Standards 62.1 and 62.2. The design infiltration flow rate was selected by considering the OpenStudio default value.

To define the spaces, the union was made between the software's physical model and the different areas' energy characteristics. Each space was linked to a thermal zone, a type of space, a default structural configuration, and a default schedule. Since the types of spaces only contain the schedule and the infiltration behavior, the loads corresponding to each area were also added.

3   Active Technologies Implementation

3.1   OpenStudio Measures

Once the energy model of the EP building was made, the OpenStudio measures were used. Measures are scripts developed in the Ruby programming language and are a unique feature of OpenStudio. The measures are used to implement transformations corresponding to energy efficiency measures [16]. The measures applied to the original model were obtained from the Building Component Library of the National Renewable Energy Laboratory (https://bcl.nrel.gov, accessed on 02 October 2022).

For the selection of the measures that were used, the ASHRAE Advanced Energy Design Guides (AEDG) were taken into consideration. AEDG is a set of distributions intended to give suggestions for accomplishing energy savings over the base code

prerequisites of ANSI/ASHRAE/IES Standard 90.1. From the different guides provided by ASHRAE, the AEDG for small to medium office buildings [17] was taken as a reference. This guide was selected because the spaces of the EP building are occupied mainly by administrative offices. The measures used to improve the original building model were the following and were used as shown in Table 2:

- *Add a Daylight Sensor at the Center of Spaces with a Specified Space Type Assigned (DS)*. Add daylighting controls to spaces with space types allocated with names containing the string in the contention.
- *Reduce Nighttime Lighting Loads (NLL)*. Turn off lights at night without affecting the daily operation of building occupants.
- *AEDG Small To Medium Office Electric Equipment Controls (EEC)*. This feature lessens the values related to electric equipment timetables to simulate decreases due to equipment controls. This strategy includes occupancy-based outlets or adapters.
- *Reduce Nighttime Electric Equipment Loads (EEL)*. Turn equipment off at night without affecting the daily operation of building occupants.

Table 2. List of the measures used in each of the areas.

Zone	DS	NLL	EEC	EEL
Bathrooms – Levels 1 & 2	✓	✓		
Classrooms – Level 2			✓	
Halls – Levels 1 & 2	✓	✓		
Laboratories – Basement			✓	
Lobby – Level 1			✓	
Offices – Levels 1 & 2		✓	✓	✓
Recreation Zone – Level 1	✓	✓	✓	

3.2 Renewable Energy Integration

As the integration of renewable energy is necessary to convert a traditional building into an NZEB, the installation of photovoltaic (PV) panels in the EP Building was analyzed. For the analysis of the PV installation, the PV*SOL software was used. PV*SOL is a tool that simulates a PV system's performance. Among its main characteristics, the 3D shading analysis stands out, allowing it to represent the shadows produced by the elements close to the installation [18]. Since the roof of the building is not available, the placement of the PV system in an area destined for parking next to the building was analyzed (see Fig.3).

Fig. 3. Photovoltaic System Location.

The number of photovoltaic modules for the selected area gave a total of 354 modules with a peak power generated of 83.19 kWp, multiplied by 4.5 hours, which is the number of effective hours of sunshine determined by the software for the Dominican Republic, a total of 374.355 kWh was obtained of energy produced during the day.

Although the area close to the available building allowed the installation of more PV panels, it was only considered in the designated areas because a balance was sought between the energy generated and the space used to place the system. In this sense, the following general characteristics were considered for the installation of the system:

- The building has an estimated daily consumption of 325.98 kWh on working days, specifically from Monday to Saturday, while for Sundays and holidays, a consumption of 89.86 kWh was taken.
- For the software simulation, a three-phase system with a line to neutral voltage of 120 V was installed; this system has a configuration connected to the network with electrical consumers and injection of the surplus.
- The losses assigned by wiring were configured with a parameter of 1.5% because the solar panels and the inverter are not far from the power point of the building.
- The module used to perform this simulation was the Sunman MF235M with a power of 235 W; this was chosen due to its high efficiency.
- The PV panels were placed on a 2.7-meter platform related to a roofing project for a parking area.
- The PV panels would be installed on a metal structure that allows the vehicles to be covered from the sun and provides them with an 18° inclination facing south.

4   Results and Discussion

When obtaining the results of the original and improved models, a comparison was made between the consumption (kBtu) of the different loads, as seen in Table 3. Within the data obtained, it is highlighted that the load of the lighting equipment presented a slight increase in the improved model. This increase is due to the limitation that the daylight sensor measure can turn on the lighting when there is partial cloudiness, causing greater lighting consumption. However, since lighting does not represent less than 5% of the total consumption, the improved model obtains better results.

Table 3. Annual overview between original model vs. improved model.

Loads	Original Model (kBtu)	Original Model (%)	Improved Model (kBtu)	Improved Model (%)
Cooling	1,139,741	77.5	1,110,984	78.93
Interior Lighting	58,092	3.95	60,158	4.28
Interior Equipment	272,753	18.55	236,433	16.79

Fig. 4 shows that the measures reduced the total electricity consumption from more than 8,000 kWh/month to less than 7,500 kWh/month. However, it can be seen that the energy used by the lighting equipment increased since the simulation conditions foresee that most of the lighting load is off at night. As control equipment was added, these generated a slight increase in consumption.

Fig. 4. Monthly overview of electricity consumption before and after measures.

The building used for the case study is located in a country with a tropical climate, with only demand for cooling. Fig. 5 shows that after applying the measures, there was a reduction in the cooling load of the building. With the use of electrical controls, the operating time of the cooling equipment is reduced, which translates into a decrease between 2 MBtu and 2.5 MBtu of the cooling load.
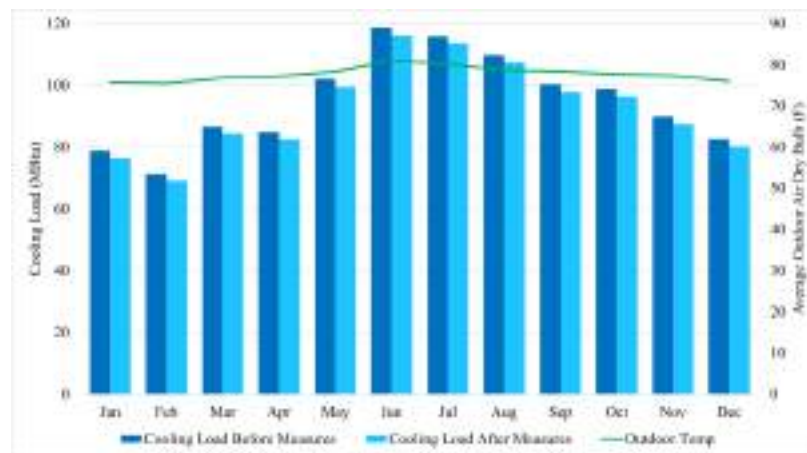
Fig. 5. HVAC monthly load profiles before and after measures.

Table 4 shows the monthly energy produced by the solar panels, data that was obtained from the simulation of the photovoltaic system with the help of PV*SOL. The monthly electrical energy consumption of the building is also presented after implementing the improvements and the energy surplus that would result if the climatic conditions allowed the energy production estimated by the software.

Table 4. Monthly overview of power generation, building consumption, and excess power.

Month	Power Generation (kWh)	Building Consumption (kWh)	Excess Power (kWh)
January	11,537.4	7,355.0	4,182.4
February	11,779.9	6,695.3	5,084.6
March	14,878.3	7,595.8	7,282.5
April	16,059.7	6,826.5	9,233.2
May	17,610.2	7,582.6	10,027.6
June	17,122.5	7,268.6	9,853.9
July	16,074.8	7,116.9	8,957.9
August	15,780.2	7,582.5	8,197.7

Month	Power Generation (kWh)	Building Consumption (kWh)	Excess Power (kWh)
September	13,014.1	7,093.2	5,920.9
October	12,256.4	7,339.3	4,917.1
November	11,020.3	7,306.5	3,713.8
December	10,716.5	7,161.9	3,554.6

With the recent growth in the use of electric vehicles in the country, the university is planning the installation of chargers for electric vehicles. Therefore, the excess energy of the PV systems is injected into the grid and used for electric vehicle chargers.

5　　Conclusions

The case study presented in this research highlights the opportunity created by using building energy modeling tools to plan the implementation of net zero energy buildings in existing buildings without the need to make a significant investment or halt building operations. In addition, these tools allow for analyzing the implementation of active technologies to achieve optimal results in terms of resource management, efficiency, and comfort, such as natural light sensors, night lights shutdown, automatic on and off of lights, and electrical equipment.

Among the results, it should be noted that saving measures does not always positively impact consumption. Even when implemented, combining them with other technologies is sometimes necessary to obtain the desired results. In this case, an increase of 0.33% in the consumption of lighting equipment could be observed. However, since lighting does not have an impact like the other systems, this increase did not affect the overall electric consumption of the optimized model. The implementation measures only considered control restriction, which in this case, due to the shape of the building, was not as beneficial as expected.

Finally, it should be noted that in the improved model presented, the simulation of the building's operation did not consider holidays or vacation periods. In addition, for this model, the cooling loads were simulated as electrical equipment. Therefore, in future research, it could be interesting to see the effect of these exceptions on the behavior of the building's electrical consumption.

References

1.　　EIA (2022) Consumption & Efficiency - U.S. Energy Information Administration (EIA). https://www.eia.gov/consumption/. Accessed 27 September 2022
2.　　Szcześniak JT, Ang YQ, Letellier-Duchesne S, Reinhart CF (2022) A method for using street view imagery to auto-extract window-to-wall ratios and its relevance for urban-level daylighting and energy simulations. Build Environ 207:108108. https://doi.org/10.1016/j.buildenv.2021.108108

3. Omrany H, Chang R, Soebarto V, et al (2022) A bibliometric review of net zero energy building research 1995–2022. Energy Build 262:111996. https://doi.org/10.1016/j.enbuild.2022.111996
4. U.S. Department of Energy (2015) Zero Energy Buildings: Hub. https://www.energy.gov/eere/buildings/zero-energy-buildings-resource-hub. Accessed 27 September 2022
5. Kilkis B (2022) Net-zero buildings, what are they and what they should be? Energy 256:124442. https://doi.org/10.1016/j.energy.2022.124442
6. Dhakal R, Sedai A, Paneru S, et al (2021) Towards a Net Zero Building Using Photovoltaic Panels: A Case Study in an Educational Building. Int J Renew Energy Res 11:879–889. https://doi.org/10.20508/ijrer.v11i2.12044.g8209
7. Faure X, Johansson T, Pasichnyi O (2022) The Impact of Detail, Shadowing and Thermal Zoning Levels on Urban Building Energy Modelling (UBEM) on a District Scale. Energies 15:1525. https://doi.org/10.3390/en15041525
8. De Oliveira ACF, Carmo CST do, Cruz AS, Faisca RG (2021) A case study to explore the synergy between HBIM and BEM for maintenance of historical buildings. Int J Build Pathol Adapt. https://doi.org/10.1108/IJBPA-03-2021-0033
9. Chiesa G, Fasano F, Grasso P (2021) A New Tool for Building Energy Optimization: First Round of Successful Dynamic Model Simulations. Energies 14:6429. https://doi.org/10.3390/en14196429
10. Meftah Nabil, Mahri Zine Labidine (2022) Application Efficiency Measures Through TRNSYS Software on Algerian Building to Save Energy. J Adv Res Fluid Mech Therm Sci 93:160–172. https://doi.org/10.37934/arfmts.93.2.160172
11. Fazelpour F, Bakhshayesh A, Alimohammadi R, Saraei A (2022) An assessment of reducing energy consumption for optimizing building design in various climatic conditions. Int J Energy Environ Eng 13:319–329. https://doi.org/10.1007/s40095-021-00461-6
12. Caponetto R, Di Mari C, Giuffrida G, Nocera F (2022) Analysis of the environmental, economic, thermal and energy performances of green building technologies. Renew Energy Power Qual J 20:84–89. https://doi.org/10.24084/repqj20.226
13. Webb M (2022) Biomimetic building facades demonstrate potential to reduce energy consumption for different building typologies in different climate zones. Clean Technol Environ Policy 24:493–518. https://doi.org/10.1007/s10098-021-02183-z
14. Guo W, Liang S, He Y, et al (2022) Combining EnergyPlus and CFD to predict and optimize the passive ventilation mode of medium-sized gymnasium in subtropical regions. Build Environ 207:108420. https://doi.org/10.1016/j.buildenv.2021.108420
15. Alliance for Sustainable Energy OpenStudio. https://openstudio.net/. Accessed 1 October 2022
16. Brackney L, Parker A, Macumber D, Benne K (2018) Building Energy Modeling with OpenStudio
17. ASHRAE (2019) Advanced energy design guide for small to medium office buildings : achieving zero energy. ASHRAE, Atlanta, GA.
18. PVSOL (2022) PV*SOL – Plan and design better pv systems with professional solar software | PV*SOL and PV*SOL premium. https://pvsol.software/en/. Accessed 2 October 2022

Expanded Realities for Smart Inclusive Education

A. A. Navarro-Newball[1][0000−0002−4231−8661], M.V. A Sierra G.[1][0000−0001−6331−4435], J.C. Martínez[1][0000−0001−8606−7107], J.J. Betancourt[1][0000−0003−2832−4261], K. Ramírez[1][0000−0002−4397−429X], A. Velásquez[1][0000−0002−9505−089X], V. Quinto[1][0000−0003−4551−020X], J.M. Cardona[1][0000−0002−9734−4699], A.E. Calderón[1][0000−0002−6137−0836], G. Restrepo[2][0000−0001−6315−5905], A.D. Castillo[3][0000−0002−4581−0811], E. Asprilla[3][0000−0001−8089−358X], A. Portilla[3][0000−0003−1365−2107], L.L. Serrano[4][0000−0002−3319−0184], F. A. Rodríguez[4][0000−0002−6275−3839], and E. Peñaloza[5][0000−0001−9278−3281]

[1] Pontificia Universidad Javeriana Cali, Cali, Colombia
{anavarro,martinv.sierra,jcmartinez,juanjo44,r4m1r2z,avelasquez09,valeriaquinto,
juancard997,cafe}@javerianacali.edu.co
[2] Université de Sherbrooke, Sherbrooke, Canada
gerardo.restrepo@usherbrooke.ca
[3] Instituto Para Niños Ciegos y Sordos del Valle del Cauca, Cali, Colombia
{andres.castillo,elizabeth.asprilla,anita.portilla}@ciegosysordos.org.co
[4] Universidad Autónoma de Bucaramanga, Bucaramanga, Colombia
{lserrano735,frodriguez757}@unab.edu.co
[5] Universidad del Norte, Barranquilla, Colombia
erpenaloza@uninorte.edu.co

Abstract. Education in so called Smart Cities should be smart and inclusive. Smart Education can refer to learning in the digital age and should provide personalised learning anytime and anywhere. The idea is to foster the 21st century skills. However, sometimes inclusiveness in Smart Education is difficult to achieve. There is a need to provide a common learning environment where students with diverse backgrounds and abilities learn together. We describe some systems supported by Expanded Realities (XR) aimed at achieving this inclusivity. XR has shown to motivate learners and could be a tool for Smart Inclusive Education. Moreover, we consider that XR tools should be adaptive to be smart and inclusive. First, we explain our method and review related work. Next, we device a procedure to understand our inclusive XR tools requirements. Then, we present our XR developments. A preliminary evaluation with five children, chosen because they represented a range of different conditions, showed that these systems may positively impact the learning and development of sensorially diverse children coming from diverse backgrounds. To perform this evaluation we asked the children simple questions about what they had experienced and the language therapists about enhancements. The idea is that these systems will serve all who need them and will remain at our XR lab for sensorially diverse children, to our knowledge, the first of its kind in Latin America.

Keywords: Smart Education · Inclusion · Expanded Realities

1   Introduction

"Interactivity (virtual relationships) must live together with the interaction (physical and personal relationships) and be at the service of all people, considering that we all have limitations." [18] (p. 219). For example, designing for extreme users, or edge users of an interface, can deliver innovative, universal access, and inclusive solutions [3]. However, challenges using mainstream technologies remain, such as: a need to overcome time consuming and error-prone interactions; a lack of services for customizing technology; and a need to put an extra physical or cognitive effort [3]. Moreover, accessibility is not only related to physical diversity needs, meaning a variety in physical characteristics, or cognitive diversity needs, meaning different styles of problem solving. Indeed, it can also be related to social and cultural matters [18] when it refers to technological devices and services that are not accessible by people with socio-cultural diversity such as income, geography, or politics. One example of this is Brand Bullying phenomena [18]. Bill Gates stated [10] (p.238) as cited by [18], that technology should be the servant and not the master. In this sense, technology should be invisible and perfectly blended [18].

At the same time, access to knowledge seems to be a continuous problem. "Knowledge, represented electronically, could be moved around the globe at the speed of electrons," [13]. In fact, evolution of society and technological advance is continuously affecting the way people learn [20]. Thus, in a smart society knowledge sharing becomes fundamental [21]. For example, corporate knowledge management simplifies knowledge extraction [21] and digital technologies can allow the public comprehend matters as specific as whatever happened to the Spanish Art during the civil war [1]. For instance, specific or general knowledge affecting both, a few employees in an enterprise or a vast number of people who wants to gain cultural information are relevant to make the transition that the smart society of a smart city requires. Previously we have proposed XR tools to aid education (smart books) and tourism (smart avatars), which are mechanisms that can be used to promote knowledge [12, 16].

We believe, XR technologies (augmented - AR, mixed - MR and virtual reality -VR) can foster Smart Inclusive Education. All kind of inclusions are important; thus, we start describing our related work, which uses XR for socio-cultural inclusion. At this point, we raise some questions related to cognitive and physical diversity inclusion to invite the reader to reflect on these matters. We continue with a literature review and propose a procedure to create smart inclusive XR systems. Then, we present the advances of our project for aiding the development of sensorially diverse children. Our goal is to provide hints on how to create inclusive XR systems and the benefits these systems may bring.

1.1   Related work

Our previous work was briefly described [20] in a poster session at the International Conference on XR and Visualization (IXRV) 2019. Here, the idea of the project was to favour citizenship and pride on the population from Tumaco, a

town from the Colombian Pacific coast that has been affected by conflict and violence. We planned to do it through music using a traditional musical instrument (the marimba) as a tangible interface which is augmented using XR. Figure 1A shows the architecture for the implementation. Here, each key has a hit sensor and a XR marker, the sensor sends signals to an Arduino microcontroller. Then, the Arduino sends a Bluetooth signal to an Android phone which can be placed in a cardboard. The phone detects the XR markers on the marimba keys and presents the user with augmented musical notes that challenge the player. Figure 1B shows the game mechanics, a user testing the system and the phone's augmented view. Here (left), a musical note is represented by a double circle while a marimba key is represented by a button. The game board is visualised and augmented in front of the user and above the marimba. The idea is that the player must hit the key at the right moment when the musical note falls on the marimba key (similar to Guitar Hero). Additionally, there is a play mode where the user can hit the keys and learn about the Tumaco's culture. Due to the pandemic period, we only were able to make a preliminary validation of the system among five users. We made them use the marimba and asked them a set of questions. We used scale from 1 to 5, where 5 is most positive evaluation, and one final open question: (1) The instructions for using the system are clear and intuitive?; (2) Do you consider the use of the proposed system interesting?; (3) Did you feel comfortable using the system?; (4) Did you enjoy the activity?; (5) What senses do you think you connected in the interaction? (Sight, Smell, Taste, Touch, Hearing); (6) What aspects would you improve of the system (open)?

According to the results obtained, we found that users considered the use of the proposed system attractive (75% of participants), interesting (100%), easy to use (75%) and with a 100% of enjoyment of the activity. They also managed to identify the immersion using the senses of hearing (75% of participants), touch (50%), and sight (100%) in the interaction. Aspects to improve in the adaptation characteristic of the system were identified, particularly for people with vision problems. For example, we could enhance colour contrast, enhance the view of the musical notes, or associate a number to both the marimba keys and the musical notes. This experiment raised some further questions: (1) Having been able to test the marimba with Tumaco's inhabitans, which have much less access to technology, would we have gotten the same responses regarding easiness of use?; (2) Having been able to test the system with sensorially diverse people, would users have felt the same levels of sensory immersion?; (3) How can we make these kind of systems more inclusive? We still believe the marimba project offers great opportunities for social, cognitive, and sensory inclusion. Additionally, it could be a successful gadget to promote our Pacific coast culture worldwide. This system opens a whole range of possible exploration and can be included as one of the tools to experiment in our current project (Section 4). Still, a lot of research is required to fully answer the questions raised. Additionally, we are aware we have to consider interface adaptability.
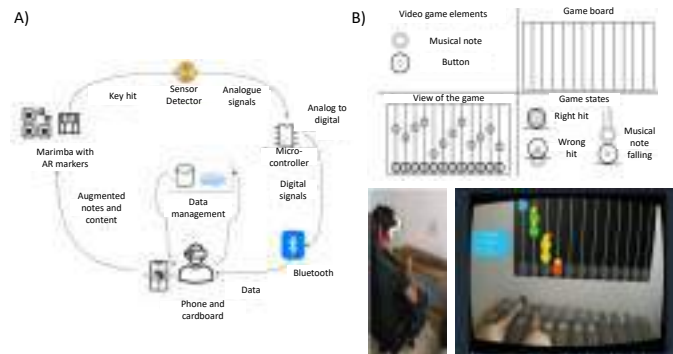
Fig. 1. XR marimba. Video available at: https://youtu.be/94tD29lRIJg

2 Literature review

The search for information was carried out systematically using the PRISMA method [24]. The articles were obtained mainly from IEEE Xplore, ACM Digital Library and ScienceDirect. Other articles were obtained from Internet searches and those endorsed by research and/or university institutions were selected. For the inclusion and exclusion criteria, we used the guide "Guidelines for Performing Systematic Literature Reviews in Software Engineering" [11]. The criteria included: (1) Publication time between 2011 and 2022; (2) Written in English; (3) The main search topic is Adaptive Interface (AIF); (4) Describe the AIFs relationship with sensory diversity to identify how different users use them; (5) Finding General Purpose Literature about AIFs to identify their applications in different contexts; (6) Exclude articles describing sensory diversity but not covering AIFs; (7) Exclude articles shorter than five pages; (8) Exclude not endorsed articles. Additionally, we proposed the following questions to guide the search: How much progress has been made in the development of AIF from 2011 to 2021? In which countries, research centres and universities have studies of AIF been carried out? What types of research are being done on AIF? What kind of limitations have been encountered during the development of AIFs? Which of the systems developed using AIFs can be improved? What are the most commonly used types of AIFs? What are the basic requirements for the development of AIFs? What are the techniques used for the evaluation of AIFs? With the information found during this process, relevant words were identified which were used in the different databases to obtain the articles discussing AIFs as related to XR and/or impairment (diversity). Then, different search strings were created and combined with the main text "Adaptive Interface" in each of the different electronic databases using the Boolean operators AND and OR. Some exmples include: "Adaptive interface" OR "Augmented reality", "Adaptive interface" OR "Virtual reality", "Adaptive interface" OR "Mixed reality", "Adaptive interface" OR "Virtual Continuum", "Adaptive interface" OR "Visual impairment", "Adap-

tive interface" OR "Hearing impairment", "Adaptive interface" AND "Augmented reality", "Adaptive interface" AND "Virtual reality", "Adaptive interface" AND "Mixed reality", "Adaptive interface" AND "Virtual Continuum", "Adaptive interface" AND "Visual impairment", "Adaptive interface" AND "Hearing impairment." The total number of articles found during the search in the electronic databases was 7.32.724. Once we applied the protocol with the criteria of inclusion and exclusion, research questions, questions with relevant words, search strings and filters on the information found, a total of 31 articles remained. We studied the titles and abstracts, and 14 articles were studied in depth.

From the review, we can observe that adaptation can be possible in different manners. Technological devices that provide computer accessibility to people who have a physical disability in their upper limbs or who have some difficulty using their hands can be achieved using adaptable glasses [2]. It is also possible to help people with vision problems to find objects within an unfamiliar indoor environment. This can be achieved with a mobile orientation aid capable of changing its own parameters to better adapt to the strengths and limitations of perception that users may have [15]. Brain-computer interfaces (BCI) can aid adapting haptic assistance for people going through a virtual maze or aid piercing the liver with a needle in tumour biopsy simulation [14]. Here, the haptics comes from the liver's resistance and is adapted according to the user's input. Moreover [8], intracortical BCI can decode the expected movement of neuronal activity at the time of controlling an external device, such as a robotic arm. Here, adaptation is achieved through the Multiple Offset Correction Algorithm. In contrast, tactile sensations and haptics do not necessarily require BCI devices. It can be suggested [23] that visual sensory inputs can provoke experiences in the tactile sense. Here, interactive visual stimuli take advantage of tactile perceptual information to improve the understanding of a product with respect to its attributes. Also, a haptic magnetic levitation device [28] can serve to provide a precise and immersive increase in the perception of tissue stiffness. For example, haptic devices are used to capture the perception of tissue stiffness during the palpation training performed by surgeons to improve their diagnostic abilities. Additionally, a rehabilitation system [17] can be adapted to the psychophysiological state during robotic rehabilitation therapies of patients who have suffered a stroke. This system relies on VR and robotics and aims at regaining motricity. Finally, innovative technologies such as smart fabrics (e-Textiles) [7] can be explored in terms of tactile interaction for the visually impaired. Indeed, research into smart fabrics and conductive materials has been due to their attractive visual properties but their tactile properties have been little explored.

On the other hand, starting from interactive narrative creation tools which allow creators adapt diverse content [22], there are also systems which focus on narrative and rely on sensors to adapt to the users. The Virtual Jump Simulator [5] describes a VR system that simulates a parachute jump. The simulation begins with a physical jump from a ramp one meter high from the ground where the person is stabilised in a horizontal flight position during the free fall. After a certain time, the opening of the parachute is mechanically simulated, and

the VR recreates the descent environment. During the virtual fall, audio-visual content is presented to tell integrated stories. Here, a Kinect sensor scans the user's body. Oculus Story Studio [10] explores immersive narrative cinematic techniques. Here, the user is immersed inside an engaging emotional narrative. Also, there are systems [4] that propose an adaptive application layer which includes a communication protocol for multimedia applications that incorporate all, haptic, visual, auditory, and odour data for non-dedicated networking environments. Finally [30], It is important to compare the level of experience and satisfaction of users when using different immersive technologies as some studies suggest that AR and VR can be effective in immersive storytelling.

Adaptive systems are those that can detect deviations between their runtime behaviour and their requirements [1], especially when their operation does not meet one or more of their requirements. When there is a deviation in functioning, adaptive systems can analyse changes and decide with or without human assistance, how to adjust their behaviour. To make the adjustments, these systems go through different adaptations that change their configurations, to finally restore compliance with the requirements. However [1], requirements engineering for adaptive software systems is not standard because at the time of design it is not possible to know all the changes that may occur in the requirements and conditions presented by the environment, therefore, the specification will not include how the system should respond to changes at run time. This is unlike standard requirements engineering, where the requirements do not seek to change the system's operation during runtime, but it should be considered in the design of an adaptive system for people sensorially diverse, so that it meets the requirements of each person. Overall, having awareness of the technological advances, particularly those related to XR, the idea is to propose a procedure to properly identify requirements and develop adaptive systems for sensorially diverse users in the development of XR systems.

3   A procedure for identifying requirements in an adaptive interface for XR based Smart Inclusive Education

We propose a procedure for identifying AIFs' requirements, to improve the usability of XR Smart Inclusive Education applications. Aspects such as the cost, the environment and the type of users are also considered. The cost, because not everyone can have access to high-cost devices. The environment, because elements such as noise, temperature, light conditions, the space required for the mobility of the user and distractions may interfere in the use of XR systems. The type of users, because they are the ones who finally will use the application and the functionality should consider cognitive, psychological restrictions, the capacity of attention and concentration to perform tasks, the need or not to manipulate objects, and the age group to which they belong. Moreover, the design should consider if the user is a person with some special condition, or if the user presents some type of sensorial diversity such as hearing impairment or visual impairment, among others. During a XR experience, the quality of the senso-

rial interactions captures the users' attention aiding learning, understanding, attraction, operability, and conformity of use [27].

AIFs main feature is their adaptability. They can adapt to the needs and preferences of the users and environments. However, it is difficult to adapt to all of the needs for each specific user, or even for a certain finite number of users. XR configurations can be infinite depending on what is needed, according to the level of realism, immersion and interaction that is required to achieve within a smart inclusive XR experience. We propose a procedure bearing in mind the importance of the design of AIFs and the development of applications based on the recommendations by Jakob Nielsen [19]. To give an idea, we mention some considerations that may influence the requirements as we follow the procedure. For example, there are some related to the type of application (desktop, mobile, Web, native); others related to the level of immersion (level of realism, 3D graphics, 2D graphics, 360 images or videos); others related to the space and field of view (a big room is required, a wide field of view is important); others related to multisensoriality (requires tactile, hearing, smell, haptic, kinesthetics, taste); others related to the type of interaction (through motion sensors, gloves, vests, speech, CAVEs, head mounted displays, projections); others related to comfort (wear on gadgets or tracking free users with free hands and free head); others related to portability (the application needs to work in multiple devices); others related to collaboration (metaverse); others related to performance (it is important to track users' neuropsychological reactions using BCI devices); others related to limitations and advantages of certain technologies as related to the users; others related to cost (whether or not the cost of the hardware and software is a limitation); finally, other related to adaptability of the interface(is it required?).

Nowadays the development of XR applications has been extended to many areas of knowledge as XR is a technology that allows users to have interactivity in real time and enable them to perform experiments in virtual environments with different levels of realism and immersion. According to the considerations discussed, we propose to follow the procedure of the diagram presented in Figure 2, which associates user's XR requirements with usability heuristics. Here, we focus on some issues that may be relevant for the design of XR applications. Considerations will limit the kind of devices or platforms to be used. Then, at each stage we should verify the heuristic principles against potential requirements.

4   Prototype implementations at the Institute for Blind and Deaf Children of Valle del Cauca

Now we show two examples of interactive systems built for the Institute for Blind and Deaf Children of Valle del Cauca. With these systems in which XR is used, we seek to expand the narratives that have been developed by language therapists. The main objective that the institute has with the use of these systems is to study the effects on language development for visually and hearing diverse children while stimulating multiple senses. The Institute for Blind and Deaf Chil-

Fig. 2. A procedure based on heuristics. Items to consider in each step are given as examples in possible XR configurations.

dren of Valle del Cauca in Cali, Colombia works on the rehabilitation of children with conditions of low visual capacity that belong to the following functional groups: hemianopsias, blurry vision without visual field reduction, central visual field alteration and peripheral visual field reduction (Figure 34). Also, they work in the rehabilitation of children with low hearing conditions. Narration is one of the methods professionals from the institute use to support rehabilitation. Narration is acquired parallelly with language development during the early years of life and favours language learning [25]. It requires children to acquire the ability to structure and combine simple phrases to produce a discourse that leads to the use of more complex syntactic structures. This ability is an early indicator of the presence of language disorders and language learning difficulties [20]. The "Colombia-Québec collaborative project: Narrative, VR, Sensorial Impairment" seeks to develop interactive XR narratives about four Colombian animals to help develop language, cognitive and motricity skills in children while they gain awareness of endangered animals. Next, we present our advances on narratives about one of these animals, the cotton top tamarin. These XR systems were developed while we were reflecting about the procedure we suggested (Figure 2). For instance, we checked to what extend these systems were inclusive, but did not use the procedure during the whole development.

4.1 Puzzles and masks in AR

For the Cotton top tamarin, we developed two AR systems. The first system allows the superposition of tamarin's masks and can be adjusted for two types

Fig. 3. AR and Visual diversity. A) From normal vision to the left to blurred vision to the right. Field alterations are in the middle. B) Facial filters that can be displayed in different places. C) Puzzle, pieces and one augmented piece.

of conditions of low visual ability, to show the interactive elements to the child. Figure 3B shows the five possible places where the masks can be placed. In this example, according to the diversity of visual field that the children have, they can see the masks in their visible region, while the application is responsible for detecting the face of the children. Here, the appearance of a mask can be controlled by adapting the interface according to the child's field of view and the mask may appear at five different locations on the screen for the child to see. Additionally, different images are also evaluated to determine which contrast is better. Finally, we implemented a game within the filter where the children need to blink every time two masks of the tamarin coincide in space (which we found could be a good motility excercise, as explained later). The second system overlays augmented information on the cotton top tamarin as the children solve a puzzle (Figure 3C). We used the Spark AR tool for the creation of an AR filter for the masks. The application was deployed as an Instagram filter and can run on different operating systems. Figure 4A shows there are two layers, the Client Layer, and the Services Layer. These are connected through an event handler; thus, following the event-driven microservices architecture. The Client Layer consists of a component and an embedded database from Spark AR. The Services Layer includes connection with the database, as well as the processing of faces where the masks will be overlaid. These connections are made with Spark AR services through Instagram, thus reducing the load of the application on the device. To communicate the Client Layer with the Service Layer, we created an event handler. This handler is a finite state machine.

Regarding the puzzle, we used the Unity game engine to implement a game tree search and Vuforia for marker (piece) training. When the children begin with the first piece of the puzzle, they have five possibilities to choose, since the puzzle frame comes empty. The children choose a piece and must place it in the right place. When they place it correctly, the application shows augmented information. Figure 4B shows an example of the game tree when the children take the head of the tamarin as the first piece. Then, they take the tail at the

second level. Here the tree branches to head, chest, and paws. The entire tree is not shown for space reasons. There are five levels of interaction. On the fifth level the puzzle should be complete. There are 120 ways the children can complete the puzzle. The AR application does not have a graphical user interface. However, the camera activates detection of the puzzle at different stages and audio visual content is overlaid on the puzzle.

These systems comply with some usability heuristics as proposed in our procedure. For example, "Match between the System and the Real World", since it is easily noticeable that it is a puppet monkey mask that the children want to put on top of their face. "Control and Freedom," since the puzzle is put together by the children in any order. "Consistency and Standards," since the puzzle is made with pieces that fit properly to put together the figure. "Recognition instead of Remembrance," since each piece of the puzzle has a shape that makes the children easily recognise where it should be located. "Flexibility and Efficiency of Use," since the mask can be placed on one of five possible locations to allow the visibility of the children according to their sensory condition. "Aesthetic and Minimalist Design," since the mask is not larger than the image of the person to whom it is put and by the different contrast colours it is noticeable that the scene is composed of two objects (face image and mask). "Recognise, Diagnose, Recover Errors," since if the mask appears at a point where the children cannot see it, it can be changed to one of the other four available locations that correspond to the children visual field; also, if one piece of the puzzle does not fit with another, the children can change it for another that does fit. Among requirements found following the procedure are: (1) run in an Android mobile device; (1) display messages with sound, text and images; (2) use contrasting colours; (3) favour tactile interaction (puzzle); (4) allow visualisation of masks in different positions (masks).
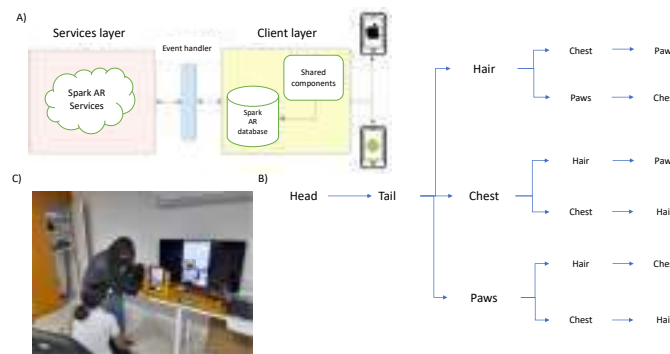

Fig. 4. Details on AR apps. A) System architecture's layers. B) Puzzle's game tree. C) Tests at the institute.

5   Evaluation

On June 24/2022, we carried out and evaluation with five children of the Institute (7 to 9 years old, mixed genders); two with hearing diversity, two with visual diversity and one with full visual and hearing capacity (Figure 40). Children were chosen by the language therapist to account for diverse conditions. We tested the AR masks' filter and the puzzle. At the end, with the help of the professionals from the Institute we observed the children and asked them: "What did you learn?" (Table 1). Additionally, we asked one professional of the institute to provide and opinion.

We got the following comments from the professionals at the institute, regarding the masks: "It is very interesting, the possibility of the spoken text. The activity with the masks caught children's attention more, because the colours, the transformation, the movement, and the interaction allow to maintain the motivation." "The live masks (3D) are preferable, since the tamarin looks more colourful than with the flat ones and generate more interest." "The live mask by its size manages to give the possibility of identification of the animal and details of its face. For the observer is very impressive the projection on the TV. We really liked the image of the face of the children with the mask." "On the faces of the children highlights more the black-white contrasts, as well as the combination with yellow." "The option to move the eyes allows to be used as an exercise for ocular motility for the training of gaze position in eccentric fixation." "It could be left as further work that every time the child recognises a characteristic of the monkey, the child generates a typical sound of it. For example, fright, joy, exaltation and the child can discover it as a riddle." "The option could be given for the child to imitate the movement of the monkey's eyes (close, open, move them up or to the sides)."

We got the following comments from the professionals at the the institute, regarding the puzzle: "Although the children are of an average age, many of them required help to put together the puzzle so I suggest the whole picture to be presented on the screen first, then removed and ask the child to put it together." "Also every time a piece is placed correctly, a sound of the animal could be generated and at the end of the figure, a question that leads the child to investigate, expand the information or give possible suggestions about the conservation." "I could not understand the objective of the geometric figures, was it to measure the visual capacity of the children with the faded image in the background figure?, or the level of attention?"

The tests brought out interesting outcomes. For example, we were not expecting that the blinking game had additional functionality beyond motivation and entertainment. Also, we found that the interaction with the proposed prototypes needs professional guidance from the language therapist which can complement the interaction asking related questions to the children. Another option is automating the questioning mechanism, but that has been left as further work. An important matter is that the shape and colours of the art pieces representing the tamarin may affect the way children perceive and learn about it. In contrast, augmented content, particularly in the puzzle, should support gaining insight

about the animal and its anatomy. Nevertheless, there was high motivation from the children who got some information about the tamarin. After interacting with the two systems, they seemed to have learnt that tamarins are endangered (even comparing them with polar bears), small, with a long tail and a bird like sound.

Table 1. Evaluation and results

Child	Masks' observations	Puzzle's observations	What did you learn?
1 - Hearing problems	The child started interacting alone with the tool.	Required help. Associated the augmented content with the anatomy.	"It's an animal, it's light, it's small, it has a long tail, it doesn't talk but it sounds like a little bird."
2 - Hearing problems	The child liked to see a mask of the tamarin.	Required no help. Did not associated the content with the tamarin.	"It is a large animal, has a long tail, is black and white, lives in a dangerous place."
3 - Sees better through one eye	The child states that the masks do not look like the tamarin. Prefers black and white contrast.	Required help. Liked the changes in the augmented visual content.	"It lives in the jungle, it is black and white, it is small, its tail is long, I do not remember the sound. I have to take care of them."
4 - Retinal involvment. Attention deficit	The child leaned over, got very close to the camera, had fun and liked the filter.	Required no help. Associated the augmented content with the anatomy.	"It is white and with black, and white dots, has a long tail. It's like a polar bear. It sounds like a bird and a monkey."
5 - No condition	The child knew the tamarin. considers the mask to be similar and had fun.	Required no help. Liked the augmented content. Dis not pay attention to sound.	"It is small, it is black and white, it makes like squeals of bats. It has a long tail. I have to take care of them.

6 Conclusions and further work

We proposed a procedure that is directly related to the revision of the Nielsen heuristics. We consider these universal heuristics as a good starting point for the design of Smart Inclusive Education using XR. Thus, following them in order, but in the XR context, can provide answers to the questions raised in Section 1.1. However, it is necessary to check the type of conditions described in Section 3. Then, it is important to follow the procedure step by step, but with an

inclusive perspective (Figure 2). We sought to associate the procedure with usability heuristics to make applications designed and developed considering the best usability practices recognised in the technological framework of software applications, to improve their quality, and especially, the quality of user interfaces. With the contribution of the recommendations and the procedure proposed in this research work for the design and development of adaptive interfaces, especially for XR environments, it is sought that in the future these interfaces will detect the changes that may occur in the context of use, that the adaptations are applied according to the changes that are detected and the needs that users may have, thus becoming full Smart Inclusive Education tools.

Even though we did not use the procedure to guide the whole application development, we found that the proposed XR applications aligned to some extent to it. Much more inclusion and adaptation could have been achieved have we followed it. However, everything was under development at the same time. Despite this, one of the ways to make a more inclusive world for people with sensorial diversity is to make new technologies include them in their consumption process. Therefore, we consider that working for children with conditions of low visual and hearing capacity was a way to achieve this purpose. The tests showed great potential in both applications (masks and puzzle). It could be suggested that, according to the tests carried out, there is a relation between XR and learning and the development of cognitive skills in sensorially diverse people towards a smart inclusive education, but to confirm this we require more tests. However, this is evidenced in the responses of the participants in the tests, as well as the fact that they mention that there are not many animals like this (tamarin) and that they must be taken care of.

References

1. Arevalo-Arboleda, J.I., Moreno-Sanchez, I., Navarro-Newball, A. A., Contreras-Roldan, V.E.: Usability and narrative geolocation for the monitoring of spanish artistic heritage. ARTE INDIVIDUO Y SOCIEDAD **33**(4), 1117–1135 (2021). https: doi.org https: dx.doi.org 10.5209 aris.7029S

2. Bender Machado, M., Dias Rodrigues, A., Bender Machado, M., Kruger da Costa, M., Cunha Cardoso, R., Souza Medeiros Quadros, P.L., Ferreira Xavier, K., Peroba, J., Aires Tavares, T.: An adaptive hardware and software based human computer interface for people with motor disabilities. IEEE Latin America Transactions **17**(09), 1401–1409 (2019). https: doi.org 10.1109 TLA.2019.8931132

3. Contreras, V.E., Gómez, G., Navarro-Newball, A. A.: Towards the gamification of assistive technology for professionals with severe impairments. In: 2019 International Conference on VR and Visualization (ICVRV). pp. 176–179 (2019). https://doi.org/10.1109/ICVRV47840.2019.00041

4. Eid, M., Cha, J., El Saddik, A.: Admux: An adaptive multiplexer for haptic–audio–visual data communication. IEEE Transactions on Instrumentation and Measurement **60**(1), 21–31 (2011). https://doi.org/10.1109/TIM.2010.2065530

5. Eidenberger, H., Mossel, A.: Indoor skydiving in immersive virtual reality with embedded storytelling. In: Proceedings of the 21st ACM Symposium on Virtual Reality Software and Technology. p. 9–12. VRST '15, Association for Computing Machinery, New York, NY, USA (2015). https://doi.org/10.1145/2821592.2821612, https://doi.org/10.1145/2821592.2821612

6. Gates, B.: The Road Ahead; Revised edition. Penguin Books (1996)

7. Giles, E., van der Linden, J.: Using etextile objects for touch based interaction for visual impairment. In: Proceedings of the 2014 ACM International Symposium on Wearable Computers: Adjunct Program. p. 177–183. ISWC '14 Adjunct, Association for Computing Machinery, New York, NY, USA (2014). https://doi.org/10.1145/2641248.2641351, https://doi.org/10.1145/2641248.2641351

8. Homer, M.L., Perge, J. A., Black, M.J., Harrison, M.T., Cash, S.S., Hochberg, L.R.: Adaptive offset correction for intracortical brain–computer interfaces. IEEE Transactions on Neural Systems and Rehabilitation Engineering **22**(2), 239–248 (2014). https://doi.org/10.1109/TNSRE.2013.2287768

9. Jureta, I.J., Borgida, A., Ernst, N. A., Mylopoulos, J.: The requirements problem for adaptive systems. ACM Trans. Manage. Inf. Syst. **5**(3) (sep 2014). https://doi.org/10.1145/2629376, https://doi.org/10.1145/2629376

10. Kang, E.: Imago. In: Proceedings of the 14th ACM International Conference on Multimedia. p. 1031–1032. MM '06, Association for Computing Machinery, New York, NY, USA (2006). https://doi.org/10.1145/1180639.1180866, https://doi.org/10.1145/1180639.1180866

11. Kitchenham, B., Charters, S.: Guidelines for performing systematic literature reviews in software engineering **2** (01 2007)

12. Kolivand, H., Prakash, E., López, M., Hernández, D., Navarro-Newball, A. A.: Reimaging the book ... again! a new framework for smart books using digital twins technology. In: Nesmachnow, S., Hernández Callejo, L. (eds.) Smart Cities. pp. 233–245. Springer International Publishing, Cham (2021)

13. Koutras, N.: Building Equitable Access to Knowledge Through Open Access Repositories. Advances in Library and Information Science. IGI Global (2020)

14. Lécuyer, A., George, L., Marchal, M.: Toward adaptive vr simulators combining visual, haptic, and brain-computer interfaces. IEEE Computer Graphics and Applications **33**(5), 18–23 (2013). https://doi.org/10.1109/MCG.2013.80

15. Lock, J.C., Gilchrist, I.D., Gilchrist, I.D., Cielniak, G., Bellotto, N.: Experimental analysis of a spatialised audio interface for people with visual impairments. ACM Trans. Access. Comput. **13**(4) (oct 2020). https://doi.org/10.1145/3412325, https://doi.org/10.1145/3412325

16. López, M.C., Hernández, D., Navarro-Newball, A. A., Prakash, E.C.: VIA: A virtual informative assistant for smart tourism. In: Nesmachnow, S., Hernández Callejo, L. (eds.) Smart Cities. pp. 15–30. Springer International Publishing, Cham (2022)

17. Morales, R., Badesa, F.J., Garcia-Aracil, N., Aranda, J., Casals, A.: Evaluación en un paciente con ictus en fase crónica de un sistema autoadaptativo de neurore-

habilitación robótica. Rev. Iberoam. Autom. Inform. Ind. RIAI **12**(1), 92–98 (Jan 2015)

18. Navarro Newball, A. A., Moreno Sánchez, I.: Redefinición de las tic en el museo: del discurso invasivo al inclusivo. Complutum **26**(2), 219–228 (2015). https: doi.org http: dx.doi.org 10.5209 rev_CMPL.2015.v26.n2.50432, http: revistas.ucm.es index.php CMPL issue archive

19. Nielsen, J.: Usability Engineering. Morgan Kaufmann Publishers Inc., San Francisco, CA, USA (1993)

20. Norbury, C.F., Bishop, D.V.M.: Narrative skills of children with communication impairments. International Journal of Language & Communication Disorders **38**(3), 287–313 (2003). https: doi.org https: doi.org 10.1080 136828031000010833, https: onlinelibrary.wiley.com doi abs 10.1080 136828031000010833

21. Usman, M. A., Mohd Noah, S. A., Saad, S.: Ontology-based knowledge management tools for knowledge sharing in organization; a review. IEEE Access **10**, 43267–43283 (2022). https: doi.org 10.1109 ACCESS.2022.3163758

22. Ustrin, I., Frey, J., Gauchard, J.R.: Interactive narrative in virtual reality. In: Proceedings of the 17th International Conference on Mobile and Ubiquitous Multimedia. p. 463–467. MUM 2018, Association for Computing Machinery, New York, NY, USA (2018). https: doi.org 10.1145 3282894.3289740, https: doi.org 10.1145 3282894.3289740

23. Overmars, S., Poels, K.: Online product experiences: The effect of simulating stroking gestures on product understanding and the critical role of user control. Computers in Human Behavior **51**, 272–284 (2015). https: doi.org https: doi.org 10.1016 j.chb.2015.04.033, https: www.sciencedirect.com science article pii S0747563215003209

24. Page M.J. et al.: The prisma 2020 statement: an updated guideline for reporting systematic reviews. TBMJ (Clinical research ed.) **372**(71) (2021). https: doi.org 10.1136 bmj.n71

25. Portilla, A.Y., Almanza, V., Castillo, A.D., Restrepo, C.: El desarrollo de las habilidades narrativas en niños: una revisión sistemática de la literatura. Revista de Investigación en Logopedia **11**(2), e67607 (abr 2021). https: doi.org 10.5209 rlog.67607, https: revistas.ucm.es index.php RLOG article view 67607

26. Pucciarelli, M., Cantoni, L.: Mobile Access to Knowledge, pp. 71–76 (01 2012)

27. Segura Ruiz, M.Y., Osorio Diaz, R.: Usabilidad en aplicaciones de realidad virtual inmersiva accesible e inclusiva multi-escenario: Caso práctico. Investig. Innov. Ing. **9**(3), 82–92 (Dec 2021)

28. Tong, Q., Yuan, Z., Liao, X., Zheng, M., Yuan, T., Zhao, J.: Magnetic levitation haptic augmentation for virtual tissue stiffness perception. IEEE Transactions on Visualization and Computer Graphics **24**(12), 3123–3136 (2018). https: doi.org 10.1109 TVCG.2017.2772236

29. Valencia C, L.M., Cardona A, J.M., Navarro-Newball, A. A.: Interactive computer-based system to promote the exploration of Tumaco's culture. In: 2019 International Conference on VR and Visualization (ICVRV). pp. 281–282 (2019). https: doi.org 10.1109 ICVRV47840.2019.00070

30. Verhulst, I., Woods, A., Whittaker, L., Bennett, J., Dalton, P.: Do vr and ar versions of an immersive cultural experience engender different user experiences? Computers in Human Behavior **125**, 106951 (2021). https: doi.org https: doi.org 10.1016 j.chb.2021.106951, https: www.sciencedirect.com science article pii S0747563221002740

El desarrollo de ciudades inteligentes desde la mirada de los criterios ASG y el enfoque de Sustentabilidad Corporativa en el sector industrial.

Figueroa-Negrete Angeles Dennis[1][0000-0002-7083-1526], Gallegos-Hernández Karen[1][0000-0001-6377-4597], León-Hernández Viridiana Aydeé[1][0000-0002-5070-9320] y Torres-Salazar María del Carmen[1][0000-0002-2119-8998]

[1] Facultad de Ciencias Químicas e Ingeniería (FCQeI), Universidad Autónoma del Estado de Morelos (UAEM), Cuernavaca, Morelos 62209, México

vleon@uaem.mx

Resumen: Las Ciudades Inteligentes (CI) representan un valioso elemento de aportación hacia las metas de Desarrollo Sustentable (DS) a través de las interrelaciones de sus dimensiones y partes interesadas, considerando que su aplicación debe cubrir las necesidades de la calidad de vida de la ciudadanía actual y de las futuras generaciones. Una parte fundamental de las ciudades es el sector industrial, que ha enfrentado mayores retos al implementar la sustentabilidad, por lo que se han desarrollado estrategias que contribuyen a este propósito como son los criterios ASG (Ambiente-Social-Gobernanza) y la Sustentabilidad Corporativa (SC). En este estudio se identifican los elementos que constituyen individualmente los conceptos de CI, criterios ASG y de SC, al mismo tiempo que se explora mediante el análisis comparativo su relación entre sí. Se encontró que existe correspondencia entre los conceptos, por lo que se concluye que las prácticas ambientales y sociales de la SC se encuentran alineadas a los criterios ASG y dimensiones de CI, proponiéndose como alternativa al sector industrial para su contribución a la construcción de Ciudades Inteligentes y Sustentables.

Palabras clave: Ciudades Inteligentes y Sustentables, Criterios ASG, Sustentabilidad Corporativa.

1 Introducción

Las ciudades son responsables de más del 70 % de las emisiones mundiales de carbono y de entre el 60 % y el 80 % del consumo de energía [19]. El rápido proceso de urbanización ha entrañado nuevas dificultades, que van desde la movilidad y transporte hasta el impacto ambiental y la desigualdad social. Los nuevos modelos de gestión urbana denominados Ciudades Inteligentes y Sustentables, resultan ser un factor cen-

tral como estrategia para garantizar un mejor nivel de vida de la sociedad, sin seguir comprometiendo la sustentabilidad del ambiente.

Una Ciudad Inteligente y Sustentable es una ciudad innovadora que utiliza las tecnologías para mejorar la calidad de vida de las personas, la eficiencia de las operaciones, los servicios urbanos y la competitividad, al tiempo que satisface las necesidades económicas, sociales, ambientales y culturales de las generaciones presentes y futuras.

En 2015, la Organización de las Naciones Unidas (ONU) aprobó la Agenda 2030 sobre el Desarrollo Sustentable, una oportunidad para que los países y sus sociedades emprendan un nuevo camino para mejorar la vida de todos, sin dejar a nadie atrás. La Agenda se integra de 17 Objetivos de Desarrollo Sustentable (ODS). El desarrollo de comunidades inteligentes y sustentables puede mejorar la calidad de vida de los habitantes de estas zonas y contribuir al logro de los ODS [18].

En el caso del ODS-9 *Industria, innovación e infraestructura*, la ONU [18] destaca la importancia de construir infraestructuras resilientes, promover la industrialización inclusiva y sustentable; asi como del fomento a la innovación. Para ello es posible establecer la normatividad que regule y garantice la gestión sustentable de los proyectos e iniciativas empresariales.

Respecto al ODS-11 *Ciudades y comunidades sustentables*, se reconoce que las ciudades y las áreas metropolitanas son centros neurálgicos del crecimiento económico, ya que contribuyen al 60 % aproximadamente del PIB mundial. Sin embargo, también representan alrededor del 70 % de las emisiones de carbono mundiales y más del 60 % del uso de recursos [17], lo cual está empeorando la contaminación del aire y el crecimiento urbano incontrolado.

En cuanto al ODS-13 *Acción por el Clima*, la ONU señala que el cambio climático está afectando a todos los países de todos los continentes al alterar las economías nacionales. Una de las aristas importantes recae en el sector industrial, en donde se reconoce que los efectos por el cambio climático en términos ambientales plantean riesgos importantes asi como nuevas oportunidades para la competitividad, el crecimiento y el desarrollo de sus industrias, convirtiendo así; el desafío climático en una oportunidad de mercado [18].

En este sentido, las industrias pueden ser parte de la solución al comprometerse a eliminar las emisiones de carbono de sus operaciones y cadenas de suministro, mejorando su eficiencia energética, reduciendo la huella de carbono de sus productos, servicios y procesos, aumentando la inversión en el desarrollo de productos y servicios innovadores e inclusivos, climáticamente inteligentes y con bajo nivel de emisión de carbono [19].

De acuerdo con algunos autores [20,21], ponen de manifiesto la adopción de un enfoque que priorice en los criterios ASG (Ambientales, Sociales y de Gobernanza) en la atención a los efectos del cambio climático y su relación con el mundo industrial. Cuando una industria incorpora prácticas con los criterios ASG en sus procesos, tiene

un impacto directo en su creación de valor, generando confianza y buena reputación dentro y fuera de la organización. Pero, más allá de ello, de acuerdo con la Asociación Nacional de Agentes de Valores y Cotización Automatizada (NASDAQ, por sus siglas en inglés), un programa sólido de ASG puede dar acceso a grandes grupos de capital, a construir una marca corporativa más fuerte y a promover, en el largo plazo, un crecimiento sustentable que beneficie a las industrias y a la comunidad [15].

Bajo este panorama, surge la necesidad de identificar los elementos que posibiliten mejorar la gestión empresarial, de manera que su impacto sea tanto positivo como de beneficio económico y social; además de contribuir a la sustentabilidad de una ciudad inteligente.

2   Referentes Teóricos

2.1 Desarrollo Sustentable

El crecimiento de las actividades productivas de los distintos sectores ha generado un aumento de la contaminación, evidenciando las presiones que se ejercen sobre el ambiente, ocasionando un problema global que trasciende hacia distintos ámbitos de lo social, académico y político.

El pronunciamiento de las nuevas acciones a tomar por parte de los gobiernos con el propósito de analizar, criticar y replantear las políticas de desarrollo económico globalizador fue señalado en la publicación de las Naciones Unidas en el Informe Brundtland donde se habla del Desarrollo Sustentable (DS), dando su definición más popular "la satisfacción de las necesidades de la generación presente sin comprometer la capacidad de las generaciones futuras para satisfacer sus propias necesidades" [27].

La definición anterior tiene amplitud para abordarla, Lélé [12] explica que su uso depende de la connotación (respecto al desarrollo y lo sustentable), el significado y la condición, de donde sugiere que brotan dos líneas principales: la primera, sobre el crecimiento sustentable, y la segunda, hacia la sustentabilidad ecológica. Por esta razón, Barret [3] argumenta que la toma de decisiones de una política social o económica debe planificarse considerando sus implicaciones sobre el planeta, tanto como su capacidad de proporcionar recursos.

Aunque su interpretación ha dado lugar a un sin fin de discusiones, es bien sabido que existe un común denominador en este tema, los tres pilares clásicos: personas (sociedad), planeta (ecología) y prosperidad (economía). Agregando a lo anterior, diferentes autores y organizaciones han considerado que es necesaria la adición de una cuarta dimensión, la institucional, con la intención de proveer cohesión entre los pilares por medio de mecanismos políticos y de gestión, acuerdos, liderazgo responsable y el involucramiento activo de los sectores públicos y privados [2].

Linnenluecke [13] señala la necesidad de impulsar el desarrollo económico de forma sustentable y avanzar en la atención integral del tema ambiental. Por ello, es

esencial que su interpretación adopte una visión holística y no solamente enfatizar la eficiencia de los gobiernos o corporaciones.

2.2 Ciudades Inteligentes

La Ciudad Inteligente (CI), en un sentido amplio, se refiere a aquellas urbes que ponen al ser humano al centro del desarrollo y la planificación, estableciendo de esa manera una visión a largo plazo [5].

La esencia de las CI radica en mejorar la calidad de vida para los residentes y ciudadanos, aumentar la competitividad económica para atraer a la industria y al talento, proveer un enfoque consciente de la sustentabilidad ambiental, además de planificar y suministrar recursos que cuenten con estrategias específicas para que puedan lograr la sustentabilidad con una visión a largo plazo.

Para Cabello [6], una ciudad bien diseñada, compacta, transitable y con un buen sistema de transporte público reduce la huella de carbono per cápita y facilita el logro de los ODS 2030. También reflexiona sobre el uso de tecnologías como fuente de innovación y la necesidad de gobernanza como un factor elemental e integrado a la planificación y administración de una ciudad para su conversión a inteligente.

En la opinión de Sikora [24], las dimensiones de las CI son: 1. *Smart governance*, para la construcción de políticas abiertas y transparentes en función de la tecnología para conseguir calidad y eficiencia en sus servicios; *2. Smart mobility*, mejora la movilidad y accesibilidad en la ciudad; 3. *Smart environment*, gestiona la eficiencia y sustentabilidad de recursos como energía, agua, medio ambiente urbano y gestión de residuos; 4. *Smart economy*, desarrolla la economía y competitividad con base en la innovación; incrementa la calidad de vida de las personas; 5. *Smart people*, potencia el capital social y humano de la ciudad; 6. *Smart living*, incrementar la calidad de vida de las personas que forman parte de la ciudad.

Aunado a lo anterior, Cabello [6] propone seis características de una ciudad inteligente: genera integración, optimiza recursos, utiliza indicadores de desempeño, da atención a los ciudadanos, tiene eficiencia de procesos y participación ciudadana. Haciendo énfasis en que todas las soluciones deben pensarse estratégicamente, alinearse con los objetivos y necesidades de cada ciudad, debe ser sistemática, monitoreada y medible (Ver Fig. 1).

Algunos ejemplos de CI en México son: Ciudad de México, Guadalajara, Monterrey, Aguascalientes y Querétaro [2].
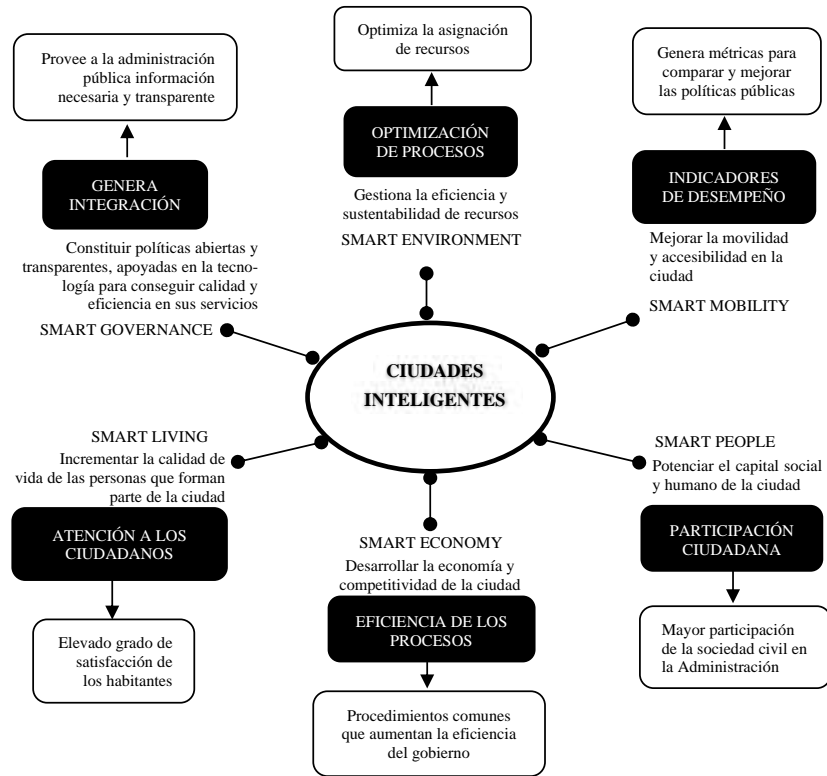
Fig. 1. Dimensiones y características de las ciudades inteligentes. Fuente: Elaboración propia adaptado de Cabello y Sikora [6,24].

2.3 Sustentabilidad Corporativa

La introducción del concepto de Desarrollo Sustentable (DS) en las corporaciones significó un gran desafío, pues influyó en el mejoramiento de las condiciones de bienestar social y humano, asimismo, la disminución del impacto ecológico aunado a la globalización tuvo como respuesta la estandarización de criterios tecnológicos, calidad de productos, uso de materias primas y la aplicación de nuevos enfoques gerenciales, tomando como punto de referencia el deterioro ambiental. Resalta entonces, que la economía es la que depende de los sistemas ecológicos y sus interacciones [3,13].

El origen del concepto de Sustentabilidad Corporativa (SC) está vinculado a la definición de DS, tiene principios en la teoría de las partes interesadas[1] y está estrechamente relacionado con la Responsabilidad Social Corporativa [9,25]. En el sector industrial y en el mundo laboral, las esferas del DS deben trabajar en conjunto vinculando las mejores acciones de productividad con mejores condiciones laborales e integradas con buenas prácticas ambientales [16].

Trabajar a favor del DS no solo significa compensar parcialmente las externalidades negativas de la industria a través de proyectos filantrópicos o efectos perjudiciales considerados colaterales, sino que deben ir más allá de la comprensión del terreno ambiental; en otras palabras, buscar el equilibrio entre las dimensiones de la sustentabilidad. Una industria se considera sustentable cuando su comportamiento se define por la prosperidad económica, la calidad, el respeto con el entorno y la justicia social [23].

Cuando las industrias realizan actividades y estrategias sustentables obtienen múltiples beneficios a largo plazo, lo que les permite mejorar su imagen de marca y obtener ventajas reputacionales así como reforzar la confianza por parte de la sociedad, ahorrar costes, aumentar la satisfacción de los empleados y mejorar la atracción de talento, así como impulsar la innovación de sus productos y servicios, acceder a nuevos recursos de financiación y mejorar las relaciones con los grupos de interés [4].

Para Szekely y Knirsch [26] el significado de sustentabilidad en las industrias se entiende como el mantenimiento y la expansión del crecimiento económico, el valor para los accionistas, el prestigio, la reputación corporativa, las relaciones con los clientes y la calidad de los productos y servicios, así como la adopción y búsqueda de prácticas comerciales éticas, la creación de empleos sustentables, la creación de valor para todas las partes interesadas y la atención de las necesidades de los desatendidos. La SC es un enfoque que persigue la creación de valor a largo plazo para los accionistas mediante el aprovechamiento de oportunidades y la gestión eficaz de los riesgos inherentes al desarrollo económico, ambiental y social [22].

La adopción de los principios de SC genera una cultura organizacional basada en criterios de ASG que provoca cambios en los valores y las creencias de los empleados en todos los niveles de la industria, considerando también a agentes internos y externos. En un nivel fundamental, la incorporación de la SC requiere de un cambio de concepción de la interdependencia de los sistemas humanos y ecológicos, pues interrelaciona simultáneamente cada uno de los componentes por medio del Gobierno Corporativo (GC) [8,13].

---

[1] Por partes interesadas o *stakeholders* debemos entender como un individuo o un grupo de individuos que pueden afectar o verse afectados en el logro de los objetivos empresariales [9]. De esta forma tanto una persona, un grupo, una organización, una institución o el entorno, pueden ser considerados como grupos de interés actuales o potenciales de una empresa.

2.4 Criterios ASG

El modelo Ambiente-Social-Gobernanza (ASG) para el DS aplicado a nivel industrial es de reciente creación y es utilizado en varios contextos, como en la evaluación de riesgos, en la inversión responsable, en los reportes de responsabilidad empresarial y en la evaluación de la sustentabilidad de los negocios. Este modelo integra la eficacia administrativa, la cultura, la ética, la estructura de gobierno y los perfiles competitivos [20,21].

La incorporación de los criterios ASG responde a principios y prácticas que permiten tanto el control como la clasificación del desempeño que facilita el desenvolvimiento de las industrias, más allá de la maximización de sus ingresos. Aborda por igual factores de conciencia social sobre el cambio climático, nuevas búsquedas de inversionistas en temas de innovación e impacto social, además de regulaciones a fin de cumplir con la transparencia. En consecuencia, la toma de decisiones supone que las industrias valoran cada vez más un impacto positivo y real a nivel socioambiental, así como aquellos que mejoren el GC dentro de la propia industria [11,15].

En cuanto a los ejes conceptuales de los criterios ASG, la "A" referente al criterio ambiental, cuyo objetivo es generar prácticas sustentables encaminadas a mitigar el impacto de la industria sobre el ambiente, gestionar los impactos ambientales directos e indirectos por parte de la organización, reducir las emisiones de gases de efecto invernadero y contribuir hacia una economía de carbono neutral, entendiendo que las actividades de las organizaciones dependen de la salud de los ecosistemas mundiales.

La "S" apelando al criterio social, hace alusión a las relaciones de la industria con la comunidad, incluyendo a los empleados, proveedores, clientes, y en general cualquier persona que se pueda ver impactada por sus operaciones. Dentro de dicho criterio, se evalúa la reputación e impacto que ha generado la industria respecto de la comunidad, las organizaciones con las que trabajan y las personas involucradas en el desarrollo del objeto social y se vincula con la gestión de las personas que forman parte o tienen relación con las organizaciones.

Finalmente, la "G" referente al criterio de gobernanza que integra el compromiso de las organizaciones con el buen gobierno, la eficacia en la administración, la cultura y el comportamiento de la industria, los códigos éticos y de conducta, así como la transparencia y anticorrupción. De este modo, la gobernanza se materializa en la gestión de la organización, al mismo tiempo que los altos directivos se relacionan con las partes interesadas. En esos términos, las actividades que demuestran este criterio son: el direccionamiento estratégico, la dirección y administración de la industria, la revelación de información y rendición de cuenta, la arquitectura de control y administración de riesgos, y la integración de elementos de sustentabilidad en la toma de decisiones [10,28].

3   Justificación

En los últimos años el tema de Ciudades Inteligentes (CI) ha fortalecido su vínculo con el término de Sustentabilidad, formando una relación más estrecha entre las CI y sus factores de desarrollo en el mundo industrial [1]. Desde la perspectiva de Carvalho [7], una CI es un ecosistema regional inteligente, que incluye varias partes interesadas que se interconectan para formar redes de colaboración (empresas, ciudadanos, organizaciones públicas, infraestructuras culturales, económicas y sociales), creando un entorno dinámico a fin de mejorar la calidad de vida de la población, desarrollar negocios y proyectos sociales inteligentes e innovadores.

Sin duda esta definición se encuentra fuertemente ligada al concepto de Desarrollo Sustentable, por lo que resulta inevitable imaginar que una ciudad sin industrias sustentables logre ser inteligente; no obstante, para que una industria sea sustentable debe contar con estrategias transversales en todos sus niveles de estructura organizacional vistas desde un enfoque de Sustentabilidad Corporativa (SC), a través de las prácticas ambientales y sociales de las organizaciones sin omitir su relación con las partes interesadas.

Bajo esta óptica, desarrollar Ciudades Inteligentes y Sustentables requiere de la planeación de proyectos enfocados a atender aspectos que beneficien a la población en su calidad de vida, a través de una gestión eficiente de políticas, transporte y conectividad, capital ambiental, competitividad económica y otros aspectos sociales considerando los criterios ASG.

3.1 Objetivo

Dar cuenta de la identificación de las relaciones y condiciones necesarias entre las dimensiones que integran una Ciudad Inteligente y los criterios ASG mediante el enfoque de Sustentabilidad Corporativa en el sector industrial.

4   Metodología

4.1 Enfoque y Fases

El enfoque de la investigación es de carácter interdisciplinar, empleando una metodología analítica-descriptiva, cuya finalidad es comparar y discutir los conceptos de CI y su relación con los criterios ASG desde el enfoque de SC a través de la recopilación de información localizada en diversos sistemas de información, investigaciones, estudios y reportes ya existentes en el campo.

Fases de la investigación:

a) Selección de investigaciones: se llevó a cabo la selección de investigaciones pertinentes al tema que aportarán elementos esenciales.
b) Análisis comparativo de investigaciones por dimensiones de CI y criterios ASG: construcción del análisis comparativo de autores empleando un cua-

dro de doble entrada para identificar similitudes y diferencias entre las investigaciones.

c) Interpretación del análisis comparativo y descripción analítica.

5   Resultados y Conclusiones

5.1 Análisis de criterios y dimensiones de ASG-CI

Desde la perspectiva de algunos autores, en el tema de CI se deben considerar seis dimensiones a cumplir: *smart environment, smart living, smart mobility, smart people, smart economy y smart governance*. Estas dimensiones señalan el propósito que se requiere para lograr la conversión de una ciudad, sin embargo, las acciones concretas que se lleven a cabo dependen de las circunstancias de cada una.

Las dimensiones que caracterizan una CI [6] pueden relacionarse a nivel industrial, extrapolando los elementos que integran dichas dimensiones. Del mismo modo, las industrias hacen uso de estrategias de gobernanza para mejorar sus relaciones tanto a nivel interno como con sus partes interesadas cumpliendo así con los criterios de ASG.

Del contraste realizado en el cuadro de doble entrada donde se relacionaron los criterios ASG y las dimensiones de las CI, se demuestra la compatibilidad e interrelación de los aspectos que presenta cada concepto. En la Tabla 1 se muestran los resultados del análisis realizado.

Tabla 1. Relación de contraste de criterios ASG y dimensiones CI. Fuente: Elaboración propia adaptado de Sikora [24].

CRITERIOS ASG	DIMENSIONES DE CI
AMBIENTE	
Política ambiental Consumo energético Consumo de agua Generación de residuos Emisiones de Gases de Efecto Invernadero (GEI)	*Smart Environment*
SOCIAL	*Smart Living*
Política social Diversidad Monitoreo de satisfacción, salud, seguridad y bienestar de los colaboradores	*Smart Mobility* *Smart People*
GOBERNANZA	
Órganos de Gobierno Evaluaciones de riesgos ASG Política de gobernanza Cumplimiento regulatorio	*Smart Governance* *Smart Economy*

5.2 Descripción de las dimensiones de CI en relación con criterios ASG

En la Tabla 2, se observa el análisis comparativo de los indicadores de CI propuestos en distintos casos de estudio realizados por Alvarado y Miranda [2,14], considerando las dimensiones propuestas por Sikora. Al contrastar los criterios ASG, se puede comprobar que las dimensiones de CI junto con sus indicadores pueden contribuir a la evaluación de criterios ASG incluso en un contexto industrial.

En cuanto a los indicadores que señalan los autores es importante destacar que, aunque los temas corresponden a los criterios, aún quedan áreas de oportunidad que deben ser atendidas. A pesar de que el criterio ambiental se aborda con amplitud, es evidente que los criterios de gobernanza y social necesitan profundizar en sus pará-metros de evaluación para que estos sean integrales.

Tabla 2. Indicadores de CI con respecto a criterios ASG. Fuente: Elaboración propia adaptado de Alvarado y Miranda [2,14].

ENFOQUE ASG	CIUDADES INTELIGENTES		
	Dimensiones de CI	Miranda *et al* (2018)	Alvarado (2020)

AMBIENTE	*Smart Environment*	Descargas residuales
		Índices de sustentabilidad ambiental
		  Calidad del aire
		  Manejo de residuos
		  Energía
			Gestión de residuos sólidos urbanos
			
			  Disposición de RSU
			  Separación de RSU
			Ahorro de energía
			  Iluminación en hogares
			  Calentamiento de agua
			  Uso de energía renovable
			Contaminación-aire
			  Monóxido de carbono
			  PM10 mg/m^3
			  PM2.5 mg/m^3
			  Dióxido de nitrógeno mg/m^3
			  Aguas residuales tratadas

SOCIAL	*Smart Living*	Índice de calidad de vida
		  Salud
		  Educación
		  Seguridad y protección
		  Espacio público
		  Acceso a cultura
			Educación
			  Nivel de educación
			  Nivel de alfabetización
			Salud
			  Mortalidad infantil
			  Esperanza de vida

	Smart Mobility	Infraestructura de vivienda
		Infraestructura social
		Infraestructura de comunicacio-nes
		Movilidad urbana
		
		Forma urbana
			Disponibilidad técnica
			  Acceso a internet
			
			  Fibra óptica
			  Acceso WIFI público
			
			Uso de tecnologías TIC
			  Teléfonos móviles
			  Smartphones
			  Computadoras
			Uso individual
			  Uso de internet
			  Social networking
			Uso público y commercial
			  E-gobierno
			  Comercio electrónico
			  Banca electrónica

	Smart People	Características de la población Equidad e inclusión social	Inclusión social

GOBERNANZA	*Smart Economy*	Unidades económicas	Productividad		
		Tamaño de empresa y actividad económica	Producto interno bruto per cápita		
			Competitividad		
			Nivel de educación terciaria		
			Propiedad intelectual		
			Empleo basado en el conocimiento		
	Smart Governance	Gobernanza y legislación urbana			
		Participación y rendición de cuentas			
		Capacidad institucional y finanzas municipales			
		Gobernanza de la urbanización			

5.3 Interrelación de criterios y dimensiones desde la Sustentabilidad Corporativa

Al igual que en los contrastes anteriores, se analizaron la compatibilidad del concepto de SC con los criterios de ASG y las dimensiones CI a fin de hacer una propuesta de implementación en el sector industrial, en donde, se asuma el cumplimiento de los criterios ASG y las dimensiones de las CI posibilitando la atención al DS (Ver Tabla 3).

De la Tabla 3 se destaca la interrelación entre las dimensiones de SC, las dimensiones de CI y los criterios ASG. Ejemplo de ello se observa en la categoría de las prácticas ambientales (agua, suelo, atmósfera-energía) de la SC, que corresponden con la dimensión *Smart environment* de las CI y el factor ambiental de los criterios ASG. Esta correspondencia está presente en cada elemento que integra a la SC, CI y los ASG.

Las prácticas ambientales y sociales tanto internas como externas bajo el enfoque de SC se proponen como imprescindibles, de este modo, el sector industrial da cumplimiento a los términos del DS. En consecuencia, las industrias pueden contribuir a la consolidación de una ciudad inteligente, y al mismo tiempo sustentable.

Tabla 3. Indicadores de CI con respecto a criterios ASG. Fuente: Elaboración propia adaptado de Sikora [24].

CRITERIOS ASG	DIMENSIONES DE CI	SUSTENTABILIDAD CORPORATIVA			
		Dimensiones de análisis	Categorías de análisis	Internos	Externos
Ambiental	*Smart Environment*	Prácticas ambientales	Agua	Análisis de agua	Análisis de agua residual
				Reducción de consumo	Tratamiento de agua residual
				Captación de agua pluvial	Reutilización de agua tratada
			Suelo	Gestión de residuos	Tratamiento de residuos
				Reducción de residuos	Obras de restauración
				Reutilización de residuos	
			Atmósfera-energía	Análisis de emisiones	Obras de restauración
				Eficiencia de uso de	Captura de carbono

Social	Smart Living	Prácticas sociales	Cultura organiza-cional	energía	
				Uso energías renova-bles	
				Emisiones GEI	
				Prácticas laborales	Participación en campañas sociales
	Smart People			Valores y ética	Comunicación al exterior
	Smart Economy		Gobernan-za	Cumplimiento legal	Responsabilidad externa
				Desempeño empresa-rial	Relación con partes interesa-das
Gobernanza	Smart Mobility			Relaciones internas	
	Smart Governance		Comunidad	Desarrollo con el entorno	Inclusión
				Compromiso social	Imagen corporativa

6　Conclusiones

La construcción de Ciudades Inteligentes debe ajustar su aplicación de manera estricta a las necesidades de la calidad de vida de la ciudadanía actual y de las futuras generaciones, impulsando las estrategias necesarias para abordar a profundidad cada una de sus dimensiones. En este sentido es indispensable generar información y bases de datos lo más completas posibles a fin de que apoyen a la toma de decisiones de los gobiernos o directivos según sea el caso.

Los conceptos de CI, ASG y SC están estrechamente relacionados a través de los términos del DS; el papel de la gobernanza es el elemento clave para la articulación de las prácticas ambientales y sociales en las industrias, refiriéndose en concreto a la Sustentabilidad Corporativa.

Dar cuenta de la identificación de las relaciones y condiciones necesarias entre las dimensiones que integran una CI ponen de manifiesto la necesidad de adopción de un enfoque que priorice los criterios ASG (Ambientales, Sociales y de Gobernanza) en la atención a los efectos del cambio climático y su relación con el mundo industrial. Cuando una industria incorpora prácticas con los criterios ASG en sus procesos, tiene un impacto directo en su creación de valor, generando confianza y buena reputación dentro y fuera de la organización.

El reto además del desarrollo de CI es contar con industrias que asuman su responsabilidad al contribuir con el DS de las ciudades.

7　Referencias

1. Abdala, L., Schreiner, T., da Costa, E., Dos Santos, N.: Como as cidades inteligentes contribuem para o desenvolvimento de cidades sustentáveis?: Uma revisão sistemática de literatura. International Journal of Knowledge Engineering and Management. 3, 98-120 (2014). doi: 10.47916/ijkem-vol3n5-2014-5
2. Alvarado, R.: Ciudades inteligentes y sostenibles: una medición a cinco ciudades de México. Estudios sociales: Revista de alimentación contemporánea y desarrollo regional. 30, 2-28 (2020). doi: 10.24836/es.v30i55.860

3. Barrett, J., Scott, A.: The Ecological Footprint: A Metric for Corporate Sustainability. Corporate Environmental Strategy. 8, 316–325 (2001). doi: 10.1016/s1066-7938(01)00132-4

4. Berns, M., Townend, A., Khayat, Z., Balagopal, B., Reeves, M., Hopkins, M. S., Kruschwitz, N.: Sustainability and Competitive Advantage. MIT Sloan Management Review. 51, 19-26 (2009).

5. Bouskela, M., Casseb, M., Bassi, S., De Luca, C., Facchina, M.: La Ruta hacia las Smart Cities: Migrando de una gestión tradicional a la ciudad inteligente. Banco Interamericano de Desarrollo, Washington D. C. (2016) doi: 10.18235/0000377

6. Cabello, S.: El camino de desarrollo de las ciudades inteligentes. Una evaluación de Bogotá, Buenos Aires, Ciudad de México y Sao Paulo. Comisión Económica para América Latina y el Caribe, Santiago (2022).

7. Carvalho, L.: Entrepreneurial Ecosystems: Lisbon as a Smart Start-up City. IGI Global (2017). doi: 10.4018/978-1-5225-5646-6.ch053

8. Carro, J.: La cultura organizacional y su influencia en la sustentabilidad empresarial. La importancia de la cultura en la sustentabilidad empresarial. Estudios Gerenciales. 33, 352-365 (2017). doi: 10.1016/j.estger.2017.11.006

9. Freeman, R.: Strategic management: A stakeholder approach. Pitman Publishing, Boston (1984).

10. Henisz, W., Koller, T., Nuttal, R.: Five ways that ESG creates value, https://www.mckinsey.com/~/media/McKinsey/Business%20Functions/Strategy%20and%20Corpo-rate%20Finance/Our%20Insights/Five%20ways%20that%20ESG%20creates%20value/Five-ways-that-ESG-creates-value.ashx

11. Kocmanová, A., Dočekalová, M.: Construction of the economic indicators of performance in relation to environmental, social, and corporate governance (ESG) factors. Acta Universitatis Agriculturae et Silviculturae Mendelianae Brunensis, 60, 195-206 (2013). doi: 10.11118/actaun201260040195

12. Lélé, S.: Sustainable development: A critical review. World Development. 19, 607-621 (1991). doi: 10.1016/0305-750X(91)90197-P

13. Linnenluecke, M., Griffiths, A.: Corporate sustainability and organizational culture. Journal of World Business. 45, 357-366 (2010). doi: 10.1016/j.jwb.2009.08.006

14. Miranda, R., Calderón, J., Rosas, F.: Evaluación de Toluca, ciudad inteligente y sustentable. Universidad Nacional Autónoma de México y Asociación Mexicana de Ciencias para el Desarrollo Regional A.C, México (2018).

15. National Association of Securities Dealers Automated Quotation (NASDAQ): Strong ESG Practices Can Benefit Companies and Investors: Here's How, https://www.nasdaq.com/articles/strong-esg-practices-can-benefit-companies-and-investors-2019-03-13

16. Organización Internacional del Trabajo (OIT): Empresas sostenibles, https://www.ilo.org/wcmsp5/groups/public/---ed_emp/--ed_emp_msu/documents/publication/wcms_185282.pdf

17. Organización de las Naciones Unidas (ONU): Nueva Agenda Urbana. Habitat III, https://habitat3.org/wp-content/uploads/NUA-Spanish.pdf

18. Organización de las Naciones Unidas (ONU): La Agenda 2030 y los Objetivos de Desarrollo Sostenible: una oportunidad para América Latina y el Caribe. Naciones Unidas, Santiago (2018).

19. Organización de las Naciones Unidas (ONU): World Cities Report 2022 United Nations Human Settlements Programme (UN-Habitat), https://unhabitat.org/wcr/

20. Plasencia, J., Marrero, D., Bajo, A., Nicado, M.: Modelos para evaluar la sostenibilidad de las organizaciones. Estudios Gerenciales. 34, 63-73 (2018). doi: 10.18046/j.estger.2018.146.2662

21. Rahdari, A., Anvary, R.: Design in a general set of sustainability indicators at the corporate level. Journal of Cleaner Production. 118, 1-15 (2015). doi: 10.1016/j.jclepro.2015.05.108

22.   ROBECO: Corporate   Sustainability   Assessment, https://www.robeco.com/es/fortalezas/inversion-sostenible/redes-de-sostenibilidad.html

23. Searcy, C.: Corporate sustainability performance measurement system: a review and research agenda. Journal of Business Ethics. 107, 239-253 (2012). doi: 10.1007/s10551-011-1038-z

24. Sikora, F.: Factores de desarrollo de las ciudades inteligentes. Revista Universitaria de Geografía. 26, 135-152 (2017).

25.   Swarnapali,   R.:   Corporate   sustainability: a   literature   review, http://repository.rjt.ac.lk/bitstream/handle/123456789/1471/RMNCS3.pdf?sequence=1

26. Szekely, F., Knirsch, M.: Responsible leadership and corporate social responsibility: Metrics for sustainable performance. European Management Journal. 23, 628-647 (2005). doi: 10.1016/j.emj.2005.10.009

27. World Commission on Environment and Development (WCED): World commission on environment and development: our common future, https://digitallibrary.un.org/record/139811

28. Xie, J., Nozawa, W., Yagi, M., Fujii, H., Managi, S.: Do environmental, social, and governance activities improve corporate financial performance? Business Strategy and the Environment. 28, 286-300 (2018). doi: https://doi.org/10.1002/bse.2224

Urban wind energy potential assessment and key factors that influence in the energy harnessing in the Dominican Republic: A case study

Alexander Vallejo[1,2], Candida Casilla[2], Idalberto Herrera[1] and Carlos Pereyra[1,2]

[1] Instituto Tecnológico de Santo Domingo, Santo Domingo, Dominican Republic
[2] Instituto Especializado de Estudios Superiores Loyola, San Cristóbal, Dominican Republic
avallejo@ipl.edu.do

Abstract. This article presents the urban wind potential that exists in the provinces of the Dominican Republic through free access data provided by numerical weather prediction and geographical information systems. Then, a hybrid SWOT–AHP analysis was conducted to qualitatively determine the factors that influence urban wind energy, such as strengths, weaknesses, opportunities and threats, and the weighting of these through expert judgments, quantifying the prioritized factors. The results show that the average consolidated urban wind speed is 3.66 m/s at 10 m height, and the predominant direction is 86°. Adopting the parameters of the Weibull distribution, an annual energy produced (AEP) of 1,145 kWh/y is estimated. Assuming that ten 2-blade Darrieus H-type VAWTs are installed in each province, the global AEP is 423,936 kWh/y. Applying the hybrid analysis with the combination of the factors, the results indicate that the strengths and opportunities represent 0.716. and the weaknesses and threats are 0.284. The most important SWOT factors of each category were i) low emission of greenhouse gasses (internal), ii) low energy sale price of surplus energy to the grid (internal), iii) use of public policies (external) and iv) bureaucracy and slow processes in public companies related to permits (external).

Keywords: Urban Wind Energy, GIS, SWOT Analysis, AHT Analysis, Wind Harnessing.

1   Introduction

The growth in energy demand and care for the environment call for appropriate solutions to achieve a balance that guarantees sustainable development. Renewable energies promise to contribute from a technological perspective to mitigate the carbon footprint. Solar photovoltaic and wind farms are the two technologies that have shown the greatest growth in recent years due to their considerable reduction in production costs. The levelized price of electricity from wind and solar PV fell by 70% and 89% in the last decade [1]. These technologies can be harnessed through small scales. With the integration of small renewable energy systems for self-production, considerable benefits

can be obtained in terms of reduced electricity tariff costs, reduced generation costs and carbon footprint.

The Caribbean countries have a small economy that supports a population of 42 million inhabitants, 89.6% of which are in the Greater Antilles. These are: Cuba, the Dominican Republic, Haiti, Puerto Rico and Jamaica. The rest corresponds to the countries that make up the Lesser Antilles [2]. According to the World Bank [3], the Dominican Republic has had sustained economic growth in the last 25 years, its economy had a great expansion in the years prior to COVID-19; between 2015 and 2019 the annual GDP growth rate averaged 6.1%.

PV energy in the Dominican Republic has grown exponentially since 2012, when 1.58 MW of installed capacity spread over 112 clients; and as of August 2022, it amounts to 243.30 MW corresponding to a population of 10,190 clients (Net Metering Documents - National Energy Commission, 2022). This scheme consists of a net metering model in which users who install this technology in their homes or businesses are compensated. However, there are no records of urban wind energy, although there are records of projects that are part of isolated systems, where there is photovoltaic solar energy, bioenergy, and mini hydro. Sporadically, few small wind turbines integrated into houses can be visualized in the National District and in Baní, but they are not registered in the net metering program.

The purpose of this research is to evaluate the wind potential in all urban areas of the 32 cities of the Dominican Republic through Numerical Weather Prediction tools. Then, to identify the internal and external qualitative factors that influence the development of urban wind energy technology dissemination through strengths, weaknesses, opportunities, and threats (SWOT) analysis. Finally, the conversion of the qualitative factors into quantitative ones through the analytic hierarchy process (AHP) analysis tool.

1.1   The role of urban wind energy in the energy transition

As urban areas are constantly growing and this leads to an energy demand increase in the same proportion, urban wind energy is an alternative to produce clean, safe and environmentally friendly source [4]. This type of energy can contribute to decarbonization, as it can be integrated into existing buildings and produce energy close to the center of consumption. There is great potential in urban wind energy to be harnessed in buildings [5]. Urban wind energy depends considerably on the orography of the site because obstacles can cause turbulence in the wind flow [6].

In 2021 the worldwide installed capacity of small wind turbines amounted to 40 MW, where the leading countries were Denmark, Italy, United Kingdom, Germany and China, respectively [7]. In tropical countries there is a marked absence of research on urban wind energy as well as experiments of small turbine performance at such latitude according to [8]. Recently [9] conducted research evidencing the absence of these studies in the tropics and the need to consider atmospheric events that can put these distributed energy systems at risk. SWT systems are classified as close to buildings, integrated into existing buildings and fully designed into the architecture of new buildings [10],

and these can be positioned in highways, rail tracks, between or around high-rise buildings, and others [11].

1.2   Aim and Structure of the article

The objective of this research is divided into two phases: the first phase consists of identifying the urban wind potential in the 32 provinces of the Dominican Republic through the open access databases of the Geographic Information Systems provided by NASA's Prediction of Worldwide Energy Resource (POWER) meteorological data [12]. The second phase is to quantify the internal and external factors that influence the urban wind energy harnessing in the DR through the qualitative and quantitative tools SWOT and AHP, respectively, presented for other energy systems by [13], [14].

This article is structured as follows: Section 2 presents the method and methodological approach for each phase. Section 3 presents the qualitative and quantitative results of each phase. Section 4 follows with a discussion. Finally, in Section 5, the conclusions are presented.

2   Method

This section is divided into two parts, one is the assessment of urban wind potential and the other is the qualitative-quantitative factor analysis using SWOT/AHP tools. The methods for each subsection are described below.

2.1   Analysis of urban wind power in the Dominican Republic

Urban wind can be harnessed through the installation of small building-integrated turbines. A great effort has been made in the last decades to harness urban wind and improve energy efficiency [15]. Recently [9] presented a six main steps methodology to characterize urban wind energy in two highly populated cities in the DR. The steps are: (1) site selection, (2) resource prospecting/analysis, (3) turbine selection, (4) estimation of currently produced energy, (5) environmental evaluation and (6) resilience assessment. The main objective of this prospecting work is to provide a guide to determine the best urban sites in the Dominican Republic for energy utilization through small wind turbines. The selection of the sites is made by taking the main towns (head municipalities) of each of the 32 provinces of the Dominican Republic according to the source [16].

Several methods for urban wind prospecting for energy purposes are reported in the literature, where commonly one can find on-site measurement, Numerical Weather Prediction, wind tunnel, computational fluid dynamics simulation and analytical methods. Most of the time, two or three of the above methods are combined for purposes of validating the results [17]–[19]. For reasons of resource availability (time and money) this research will adopt the Numerical Weather Prediction (NWP) method for site selection and energy potential identification (step 2). NWP is a good starting point for large-scale identification of urban potential through Meso-scale Weather Models [8].

Normally NWP programs are at heights of 50 m and above, so they are not suitable for micro-scale assessment, unless corrected with adjustment factors, as these consider a very broad resolution of the phenomenon produced by the wind flow [20]. In this context, computer programs called Geographic Information Systems (GIS) are now widely used to describe certain features at a site by combining digital maps and related information of interest to the researcher [18]. From wind atlases, the average wind speed at 10 m height can be obtained through the application of the wind profile equations, both logarithmic and exponential above and below, respectively, the urban canopy building according to [4].

Using the NASA Prediction of Worldwide Energy Resource (POWER) open-access database, wind meteorological variables will be determined for the 32 provinces of the Dominican Republic. Table 1 shows the variables adopted in this initial study. The period analyzed corresponds to monthly values from January 2011 to December 2021 (11 complete years). The location in each of the cities corresponds to the central positioning of the most urbanized town. In some cases, for very rural cities, the location of the town was confirmed through Google Maps [21].

Table 1. Main meteorological parameters.

Acronyms	Descriptions
PC	Precipitation Corrected (mm/day)
SP	Surface Pressure (kPa)
RH2M	Relative Humidity at 2 Meters (%)
WD10M	Wind Direction at 10 Meters (°)
WS10M	Wind Speed at 10 Meters (m/s)

Small wind turbines (SWTs) are aerodynamic machines, which have the purpose of converting wind energy into electricity. Electricity production depends mainly on the speed cube, the swept area and air density [22]. There is a wide variety of SWT designs and types. The main SWT designs that predominate in the industry are horizontal axis turbines (HAWTs) and vertical axis turbines (VAWTs) [18], [23], [24]. The most suitable type depends on the cut-in wind speed, flexibility in installation and operation, height-limit and aesthetic integration in the urban built environment [25]. VAWTs are frequently adopted in urban environments because they are omnidirectional, however HAWTs should be oriented perpendicular to the wind flow [11], [26]. For step 3 of this case study, a 2-bladed Darrieus H-type VAWT is going to be selected, which is a good performing turbine in urban sites according to [10]. It has main parameters such as a rotor diameter of 1 m, a rotor height of 5 m, and a rotor swept area of 5 m2, symmetric NACA0018 airfoil blade cross-section and 0.3 solidity, Cut-in and Cut-out wind speed of 2 and 24 m/s, respectively.

To determine the energy production during a period, the operating hours during that interval, which is usually one year, must be simulated. For this purpose, various probability distributions are used, such as the Weibull, Rayleigh, and Lognormal distributions. The Weibull distribution is the most widely accepted due to its flexibility and simplicity [27]. Weibull distribution with the shape factor equal to 2 is known as Rayleigh Distribution [28].

The parameters that define the Weibull distribution are the shape parameter k, which controls the width of the distribution and the scale parameter c, which controls the mean wind speed. Both parameters can be estimated by the maximum likelihood method, which is the most used [29]. The wind speed and the shape parameter are directly proportional, the estimation of the density distribution can be very inconsistent for low speeds, in the order of 2 m/s [27]. In Eq. 1, Weibull Distribution is presented, where k is the shape factor and c is the scale factor in m/s. The parameters k and c control the width of the distribution and average wind speed defined in Eq. 2, where V_{avg} is the average wind speed, respectively.

$$p(V_{avg}) = \left(\frac{k}{c}\right) * \left(\frac{V_{avg}}{c}\right)^{k-1} e^{-\left(\frac{V_{avg}}{c}\right)^k} \tag{1}$$

$$c = \frac{V_{avg}}{\sqrt{\pi}} \tag{2}$$

Once identified the site selection and urban wind energy assessment, is important calculate the Annual Energy Production (AEP). The methodology proposed by Rezaeiha [10], is adopted to estimate the AEP in Eq 3. Where 8,760 are the hours during a year, $P(V_{avg}; c; k)$ is the probability of a given speed based on the Weibull distribution, and $P\left(V_{avg_z}\right)$ is the power produced by the wind turbine at that speed at a given height. The power extracted by the wind turbine is described according to Eq. (4). Where: A is the rotor area, C_P is the power coefficient of the rotor, V_{avg} is the mean wind speed for a given height and ρ is the air density.

$$AEP_z = 8,760 * \int_0^{8,760} P\left(V_{avg_z}; c; k\right) * P\left(V_{avg_z}\right) dv \tag{3}$$

$$P(V_{avg_z}) = 0.5 * C_P * \rho * A * V_{avg_z}^{\ 3} \tag{4}$$

Finally, there are the steps to identify the site, evaluate the resource potential, select a turbine according to the resource conditions and finally, estimate Annual Energy Production.

To determine the urban wind profile the most adopted expression is Hellman's exponential law that correlates the wind speed at two different heights. Eq. (5) shows the expression of Hellman's law, where v is the velocity at height H, v_0 is the speed to the height H_0 (at 10 m height) and α is the friction coefficient or Hellman exponent. This expression explores the effect of wind speed in relation to height. The friction coefficient assumed was 0.30 for small towns with some trees and shrubs [30].

$$\frac{v}{v_0} = \left(\frac{H}{H_0}\right)^{\alpha} \tag{5}$$

2.2   SWOT/AHP analysis

SWOT analysis is often used as a strategic planning method to evaluate Strengths (S), Weaknesses (W), Opportunities (O), and Threats (T) involved in a process or project [31]. The four categories of SWOT analysis present the internal (strengths and weaknesses) and external (opportunities and threats) factors, as well as the positive and negative ones, respectively. SWOT analysis is a strategic tool for identifying key factors

in a qualitative manner. This depends largely on the criteria, experience and judgments of the experts interviewed or evaluated [32], [33].

In this research, interviews and online surveys were conducted through Google Form with 25 professionals and academic experts in areas related to sustainable development, electricity markets and climate change in the Dominican Republic. Sixteen responses were received from the total requests, as shown in Table 2. Based on literature from previous very similar studies such as ref. [14], and brainstorming, the 19 factors for the SWOT categories were identified. In addition, 10 new factors emerged in the interview process, which were integrated into the existing factors. After weighting and thorough review to avoid redundancy, the list was reduced to 16 factors, four for each category as shown in Table 3.

Table 2. Expertise of the sample of experts.

Expertise	Number	Background	Number
Research and Education	5	O&M Manager	1
Energy Manager	5	Business Development	1
Executive Director	4		

Table 3. Summary of SWOT factors.

	Positive	Negative
	Strengths	**Weakness**
Internal	S1: Low greenhouse gasses emission.	W1: Long period of recovery of the investment.
	S2: Availability of urban sites (buildings or public spaces).	W2: Sale price of energy to the grid is less than the purchase price ($sale < $purchase).
	S3: Possibility for self-generation.	W3: Negative impact on human life.
	S4: Sale energy surplus.	W4: Negative impact on wildlife.
	Opportunities	**Threats**
External	O1: Taking advantage of public policies and regulations.	T1: Bureaucracy and slow procedures.
	O2: Decarbonization of the matrix.	T2: Conflicts with protected areas.
	O3: New business model, such as electric mobility (new service companies).	T3: Resistance of the population.
	O4: New business model, such as electric mobility (new service companies).	T4: Lack of identification of wind potential.

As SWOT does not provide information on relative importance among the factors in the SWOT groups or categories, it was complemented with an AHP analysis to establish the order of prioritization for decision making towards the key factors [33].

AHP analysis is a quantitative analytical tool used to establish a local and group weighted weight to the factors obtained through the SWOT analysis. AHP is a systematic technique for organizing and analyzing complex criteria for decision making through multilevel comparison and criticality by their weighted weight [34]. The AHP is based on the average value method, in the end each value of the factors of the SWOT

analysis corresponds to the priority level ¨p¨ of the same set of "n" elements (0 < p < 1). The main steps are as follows:

— Averaging the results obtained in the surveys. First calculate the probability of each factor according to the comparison of the results obtained in the SWOT analysis categories.
— Establish the relative priority of the SWOT analysis categories.
— Overall comparison of all factors on the basis of the 9-point scale recommended by Thomas Saaty [35].

3   Results and discussion

Table 4 shows the average meteorological information for 11 years of data collection (2010 - 2021). There is no correlation between Precipitation Corrected (mm/day), Surface Pressure (kPa), and Relative Humidity at 2 Meters (%) with Wind Speed at 10 Meters (m/s), in all cases it was less than 20%. The provinces with the highest wind potential at 10 m height were Monte Cristi (6.63 m/s), El Seibo (5.21 m/s), La Altagracia (4.83 m/s), La Romana (4.83 m/s), and Puerto Plata (5.13 m/s), respectively. The other 27 provinces have an average speed of 3.35 m/s, with a minimum of 2.19 m/s (Monte Plata) and a maximum of 4.50 m/s (Pedernales). Table 4 shows the energy density obtained through the Weibull frequency distribution for each province's average speed and energy production with the small wind turbine selected for this study. Deeming 10 small wind turbines installed per provinces, the energy produced annually is 423,936 kWh/y.

Table 4. Meteorological information from POWER to the DR.

Cities	PC (mm/day)	SP (kPa)	RH at 2 m (%)	WD at 10 m (°)	WS at 10 m (m/s)	AEP for one SWT (kWh/yr)
Azua	2.01	95.58	75.90	86.32	3.97	1,464
Bahoruco	2.02	96.75	70.30	117.44	3.15	722
Barahona	3.11	97.67	81.29	92.01	4.12	1,638
Dajabón	1.72	98.01	71.75	59.67	3.93	1,416
Distrito Nacional	2.04	100.05	76.59	79.94	3.41	919
Duarte	2.22	100.66	77.87	86.82	3.46	964
El Seibo	3.14	101.04	78.77	82.48	5.21	3,162
Espaillat	2.09	98.33	76.86	88.22	2.72	461
Hato Mayor	2.43	100.40	76.86	81.82	3.29	828
Hermanas	2.09	98.33	76.86	88.22	2.72	461
Independencia	2.02	96.75	70.30	117.44	3.15	722
La Altagracia	2.42	100.80	73.27	80.59	4.83	2,587
La Estrelleta	1.79	95.72	66.63	79.91	2.57	385
La Romana	2.42	100.80	73.27	80.59	4.83	2,587
La Vega	1.90	91.61	78.65	90.10	3.02	632
María Trinidad Sánchez	2.22	100.66	77.87	86.82	3.46	964
Monseñor Nouel	1.90	91.61	78.65	90.10	3.02	632
Monte Cristi	2.09	101.40	79.62	73.36	6.63	5,197
Monte Plata	1.91	99.72	74.91	84.18	2.19	236
Pedernales	2.66	97.39	75.42	95.34	4.50	2,121
Peravia	2.01	95.58	75.90	86.32	3.97	1,464

Cities	PC (mm/day)	SP (kPa)	RH at 2 m (%)	WD at 10 m (°)	WS at 10 m (m/s)	AEP for one SWT (kWh/yr)
Puerto Plata	2.32	100.67	79.79	89.98	5.13	3,045
Samaná	2.43	100.40	76.86	81.82	3.29	828
San Cristóbal	2.04	100.05	76.59	79.94	3.41	919
San José de Ocoa	2.01	95.58	75.90	86.32	3.97	1,464
San Juan	1.81	91.20	70.85	99.45	3.20	761
San Pedro de Macorís	2.09	100.94	74.94	81.96	4.07	1,572
Sánchez Ramírez	1.91	99.72	74.91	84.18	2.19	236
Santiago	2.09	98.33	76.86	88.22	2.72	461
Santiago Rodríguez	1.84	97.09	71.31	78.34	3.83	1,313
Santo Domingo	2.04	100.05	76.59	79.94	3.41	919
Valverde	1.84	97.09	71.31	78.34	3.83	1,313
Average	**2.15**	**98.12**	**75.42**	**86.13**	**3.66**	**1,145**

Fig. 1 shows the political map with the urban wind potential at 10 m height for the Dominican Republic in the 32 provinces. This information has a high positive correlation with the wind map, in which the provinces of Monte Cristi, La Altagracia and Pedernales have the highest wind potential [36]. This is the first approximation step to determine the urban wind potential at the national level with data from wind atlases, which must be validated through on-site measurement to consider the effects of land roughness [29]. Fig. 2 shows the monthly evolution of wind speed for all provinces where a higher intensity can be observed in winter-summer, with a predominant direction from the Northeast. Fig. 3 shows the one-year frequency distribution of wind speeds and the Annual Energy Production (AEP) for the consolidated mean wind speed of 3.66 m/s, the shape factor k=2, and the scale factor c=4.13 m/s. The AEP is 1,142 kWh/yr for each small wind turbine.
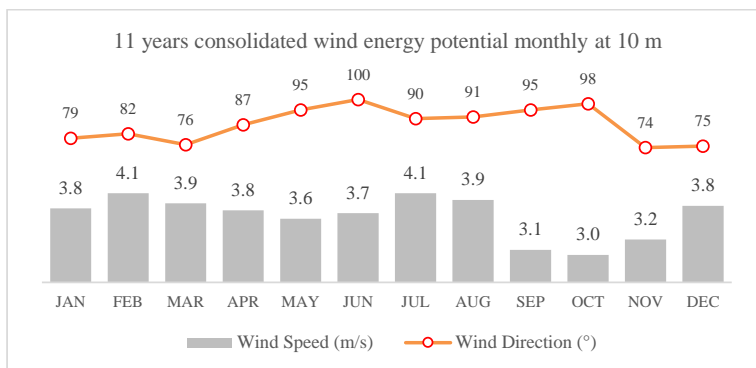

Fig. 1. Urban wind map of the Dominican Republic.

Fig. 2. 11 years (2010 – 2021) consolidated wind energy potential monthly at 10 m.
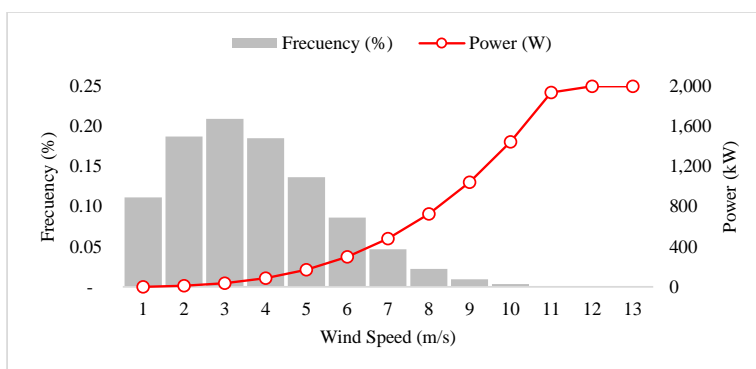

Fig. 3. Urban wind energy harnessing consolidated at 10 m.

Adopting the classification of Poor, Marginal, Good to Very Good and Exceptional to classify the proposed wind speed based on records at 10 m height [37], the province of Monte Cristi was identified as Good to very Good (5.4 - 6.7 m/s). With marginal potential are the provinces of El Seibo, Puerto Plata, La Altagracia and La Romana (4.5 - 5.4 m/s). The rest of the 27 provinces are considered to have poor potential (<4.5 m/s). No provinces were identified in the Exceptional category (>6.7 m/s).

To explore the effect of wind speed in relation to height on the wind speed in accordance with Hellman's exponential law, Fig. 4 shows the wind profile for i) the average of the 32 provinces, ii) the four provinces with marginal potential, and iii) the province with a Good to very good potential.
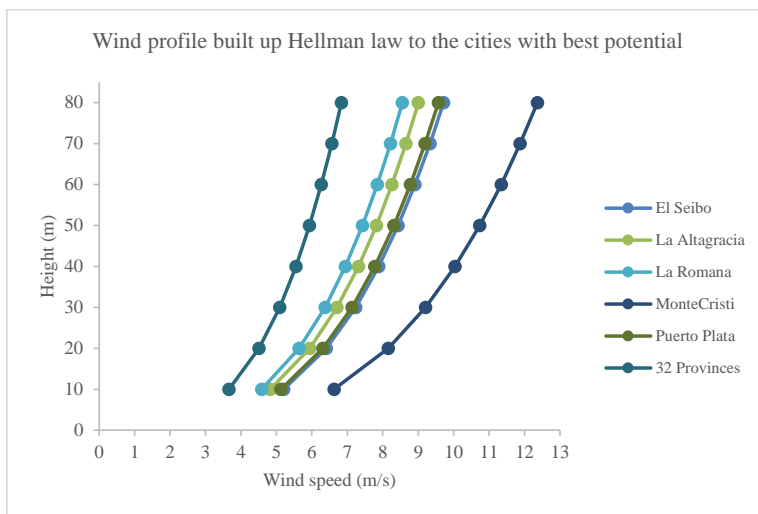
Fig. 4. Wind profile built up Hellman law to the cities with best potential.

Four factors were obtained for each SWOT category. This analysis provides us with the qualitative part of these factors; however, to facilitate understanding and decision making based on the given factors, the SWOT analysis was converted into a quantitative AHP analysis. Table 5 shows that the experts assigned prioritization to the categories of strengths (0.574), weaknesses (0.240), opportunities (0.142) and threats (0.044). The factors with the highest weighting for each category are Low greenhouse gas emissions (strength), low energy sale price (weakness), taking advantage of existing policies (opportunities), and bureaucracy and slow processes (threat). This indicates that the preference for reducing greenhouse gasses and contributing to the decarbonization of the energy matrix is key for the experts. In the same way, eliminating the obstacles of public procedures to take advantage of the benefits of existing regulations is a key factor to be overcome.

Table 5. SWOT factors and relative priorities of urban wind energy exploitation in the DR.

SWOT Categories	SWOT factors	Factor priority	Overall priority
Strengths 0.574	S1: Low greenhouse gasses emission.	0.465	0.267
	S2: Availability of urban sites (buildings or public spaces).	0.425	0.244
	S3: Possibility for self-generation.	0.081	0.046
	S4: Sale energy surplus.	0.029	0.017
Weaknesses 0.240	W1: Long period of recovery of the investment.	0.246	0.059
	W2: Sale price of energy to the grid is less than the purchase price.	0.599	0.144
	W3: Negative impact on human life.	0.060	0.014
	W4: Negative impact on wildlife.	0.095	0.023

SWOT Categories	SWOT factors	Factor priority	Overall priority
Opportunities 0.142	O1: Taking advantage of public policies and regulations.	0.455	0.064
	O2: Decarbonization of the matrix.	0.303	0.043
	O3: New business model, such as electric mobility (new service companies).	0.085	0.012
	O4: New business model, such as electric mobility (new service companies).	0.157	0.022
Threats 0.044	T1: Bureaucracy and slow procedures.	0.465	0.020
	T2: Conflicts with protected areas.	0.425	0.019
	T3: Resistance of the population.	0.081	0.004
	T4: Lack of identification of wind potential.	0.029	0.001

Fig. 5 shows graphically the factor scores through the quantitative AHP analysis. The most voted by far are the strengths (internal) and opportunities (external) represent 0.716 according to the experts' judgment. This indicates that there is a remarkable interest in harnessing urban wind for energy purposes as the strengths have a prioritization of 0.574. The author recommends further research with the objective of stratifying the provinces where there is a higher potential with high rates of urbanization. SWTs can be integrated into existing buildings in metropolises, however, they can be in urban public environments, such as parks, roads, and if necessary, in rural locations. Other factors considered by the experts are the possible integration into microgrids, production outside sunlight hours, and the contribution of society to the energy transition.

The overall negative factors are of the order of 0.284 (internal and external), which may affect the dissemination of this technology in a systematic way. As for the weaknesses, the experts indicated as class factors the selling price of surplus energy under the net metering program and the long payback period of the investment. Other external factors, such as threats, are the bureaucracy in the public processes for dealing with permits and the lack of sites identified as good to excellent for the use of wind energy potential. Other factors that naturally became known are related to the vulnerability of these energy systems to atmospheric events (hurricanes), certified labor for installation, O&M, and integration with energy storage.
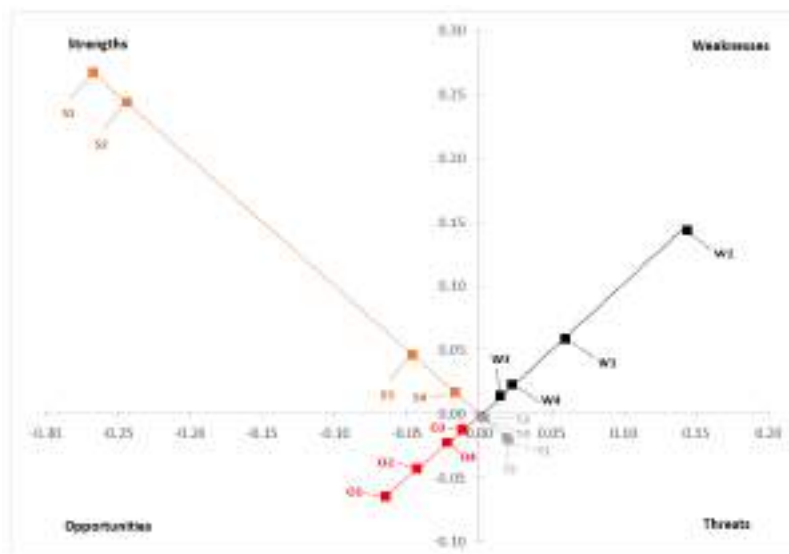
Fig. 5. Graphical representation of the SWOT/AHP analysis.

4   Conclusions

Urban wind energy has a great potential to be harnessed close to the area of demand, it is not dependent on sunlight, and it can be an alternative to be optimally combined with other energy sources. This research was conducted in the framework of two phases, which were: to identify the urban energy potential in the main cities of the 32 provinces of the Dominican Republic, and to identify the key factors that influence the dissemination and systematic use of this energy source through a SWOT/AHP analysis.

The analysis consisted of the evaluation of the wind energy potential in the 32 provinces of the Dominican Republic and it utilized open access data from NASA Prediction of Worlwide Energy Resource (Power) for the period 2010-2021, with monthly measurements. After analyzing the main meteorological parameters, we have a consolidated mean wind speed of 3.66 m/s, mean wind direction of 86°, relative humidity of 75.82 % and atmospheric pressure of 98.12 kPa. There is no significant correlation between wind speed and the other meteorological parameters, globally. In the Dominican Republic, the provinces with the greatest urban wind potential are Monte Cristi, El Seibo, La Altagracia, La Romana and Puerto Plata, with average wind speeds at 10 m of 6.63, 5.21, 4.83, 4.83 and 5.13 m/s, respectively. The predominant wind direction is northeast, between 60° – 90°.

For the average speed of the 32 provinces (3.66 m/s) the annual energy production is 1,145 kWh/year with a vertical shaft turbine with good performance in urban

environments. Assuming the installation of 10 SWT in each province the annual energy produced is 423,936 kWh/year.

Through 16 interviews with professional experts from the energy sector and academia, the key internal and external factors that influence the use of urban wind energy were identified through SWOT analysis. The qualitative factors were then quantified through AHP analysis. The four SWOT's categories weighted are 0.574, 0.240, 0.044, and 0.142, respectively, where it is observed that strengths and opportunities represent 0.716. and weaknesses and threats 0.284. The most important SWOT factors in each category were I) low greenhouse gas emissions (Strengths), ii) low price for selling surplus energy to the grid (Weaknesses), iii) taking advantage of public policies (Opportunities), and iv) bureaucracy and slow processes in public companies regarding permits (Threats).

It is recommended to extend this study to provinces that can be identified with good to moderate potential and that are relatively more urbanized. In addition, take into consideration the threats of hurricanes in the Dominican Republic to increase the resilience of these distributed generation systems.

References

[1] "Levelized Cost Of Energy, Levelized Cost Of Storage, and Levelized Cost Of Hydrogen," *Lazard.com*, Oct. 01, 2022. http://www.lazard.com/perspective/levelized-cost-of-energy-levelized-cost-of-storage-and-levelized-cost-of-hydrogen/ (accessed Oct. 01, 2022).

[2] R. Vélez, "Las economías de la zona del Caribe en el contexto de la Revolución Tecnológica," *Études Caribéennes*, no. 42, Art. no. 42, Apr. 2019, doi: 10.4000/etudescaribeennes.15177.

[3] Banco Mundial, "República Dominicana: panorama general," *World Bank*, Apr. 10, 2021. https://www.bancomundial.org/es/country/dominicanrepublic/overview (accessed Apr. 10, 2021).

[4] Q. Wang, J. Wang, Y. Hou, R. Yuan, K. Luo, and J. Fan, "Micrositing of roof mounting wind turbine in urban environment: CFD simulations and lidar measurements," *Renew. Energy*, vol. 115, pp. 1118–1133, Jan. 2018, doi: 10.1016/j.renene.2017.09.045.

[5] T. Simões and A. Estanqueiro, "A new methodology for urban wind resource assessment," *Renew. Energy*, vol. 89, pp. 598–605, 2016, doi: https://doi.org/10.1016/j.renene.2015.12.008.

[6] J. Fields, F. Oteri, R. Preus, and I. Baring-Gould, "Deployment of Wind Turbines in the Built Environment: Risks, Lessons, and Recommended Practices," NREL/TP--5000-65622, 1260340, Jun. 2016. doi: 10.2172/1260340.

[7] "Distributed Wind Market Report: 2022 Edition," *Energy.gov*, Sep. 10, 2022. https://www.energy.gov/eere/wind/articles/distributed-wind-market-report-2022-edition (accessed Sep. 10, 2022).

[8] Y. Toparlar, B. Blocken, B. Maiheu, and G. J. F. van Heijst, "A review on the CFD analysis of urban microclimate," *Renew. Sustain. Energy Rev.*, vol. 80, pp. 1613–1640, Dec. 2017, doi: 10.1016/j.rser.2017.05.248.

[9]   A. Vallejo-Díaz, I. Herrera-Moya, A. Fernández-Bonilla, and C. Pereyra-Mariñez, "Wind energy potential assessment of selected locations at two major cities in the Dominican Republic, toward energy matrix decarbonization, with resilience approach," *Therm. Sci. Eng. Prog.*, vol. 32, p. 101313, Jul. 2022, doi: 10.1016/j.tsep.2022.101313.

[10]   A. Rezaeiha, H. Montazeri, and B. Blocken, "A framework for preliminary large-scale urban wind energy potential assessment: Roof-mounted wind turbines," *Energy Convers. Manag.*, vol. 214, p. 112770, Jun. 2020, doi: 10.1016/j.enconman.2020.112770.

[11]   Z. Tasneem *et al.*, "An analytical review on the evaluation of wind resource and wind turbine for urban application: Prospect and challenges," *Dev. Built Environ.*, vol. 4, p. 100033, Nov. 2020, doi: 10.1016/j.dibe.2020.100033.

[12]   "POWER | Data Access Viewer," Sep. 20, 2022. https://power.larc.nasa.gov/data-access-viewer/ (accessed Sep. 20, 2022).

[13]   T. Brudermann, C. Mitterhuber, and A. Posch, "Agricultural biogas plants – A systematic analysis of strengths, weaknesses, opportunities and threats," *Energy Policy*, vol. 76, pp. 107–111, Jan. 2015, doi: 10.1016/j.enpol.2014.11.022.

[14]   T. Kiunke, N. Gemignani, P. Malheiro, and T. Brudermann, "Key factors influencing on-shore wind energy development: A case study from the German North Sea region," *Energy Policy*, vol. 165, p. 112962, Jun. 2022, doi: 10.1016/j.enpol.2022.112962.

[15]   T. F. Ishugah, Y. Li, R. Z. Wang, and J. K. Kiplagat, "Advances in wind energy resource exploitation in urban environment: A review," *Renew. Sustain. Energy Rev.*, vol. 37, pp. 613–626, Sep. 2014, doi: 10.1016/j.rser.2014.05.053.

[16]   "Provincias Dominicanas," Sep. 24, 2022. https://dominicana.gob.do/index.php/e-municipios/e-localidades/2014-12-16-20-41-38 (accessed Sep. 24, 2022).

[17]   A. Al-Quraan, T. Stathopoulos, and P. Pillay, "Comparison of wind tunnel and on site measurements for urban wind energy estimation of potential yield," *J. Wind Eng. Ind. Aerodyn.*, vol. 158, pp. 1–10, Nov. 2016, doi: 10.1016/j.jweia.2016.08.011.

[18]   A. Gagliano, F. Nocera, F. Patania, and A. Capizzi, "Assessment of micro-wind turbines performance in the urban environments: an aided methodology through geographical information systems," *Int. J. Energy Environ. Eng.*, vol. 4, no. 1, p. 43, Nov. 2013, doi: 10.1186/2251-6832-4-43.

[19]   F. Toja-Silva, T. Kono, C. Peralta, O. Lopez-Garcia, and J. Chen, "A review of computational fluid dynamics (CFD) simulations of the wind flow around buildings for urban wind energy exploitation," *J. Wind Eng. Ind. Aerodyn.*, vol. 180, pp. 66–87, Sep. 2018, doi: 10.1016/j.jweia.2018.07.010.

[20]   R. Byrne, N. J. Hewitt, P. Griffiths, and P. MacArtain, "An assessment of the mesoscale to microscale influences on wind turbine energy performance at a peri-urban coastal location from the Irish wind atlas and onsite LiDAR measurements," *Sustain. Energy Technol. Assess.*, vol. 36, p. 100537, Dec. 2019, doi: 10.1016/j.seta.2019.100537.

[21]   "Google Maps," *Google Maps*, Sep. 21, 2022. https://www.google.com/maps/@18.4507649,-69.9193002,15z (accessed Sep. 21, 2022).

[22]   K. Dai, A. Bergot, C. Liang, W.-N. Xiang, and Z. Huang, "Environmental issues associated with wind energy – A review," *Renew. Energy*, vol. 75, pp. 911–921, Mar. 2015, doi: 10.1016/j.renene.2014.10.074.

[23]   I. Paraschivoiu, "Wind Turbine Design: With Emphasis on Darrieus Concept - Ion Paraschivoiu," *Polytechnic International Press, Canada*, 2002.

https://books.google.com.do/books?hl=es&lr=&id=sefVtnVgso0C&oi=fnd&pg=PR13&ots=HmDYuSgz1d&sig=8Ef1nSjDDSp1SDRWbmPZiX_F_Go&redir_esc=y#v=onepage&q&f=false (accessed Jul. 17, 2020).

[24] T. Stathopoulos *et al.*, "Urban wind energy: Some views on potential and challenges," *J. Wind Eng. Ind. Aerodyn.*, vol. 179, pp. 146–157, Aug. 2018, doi: 10.1016/j.jweia.2018.05.018.

[25] A. Kc, J. Whale, and T. Urmee, "Urban wind conditions and small wind turbines in the built environment: A review," *Renew. Energy*, vol. 131, Jul. 2018, doi: 10.1016/j.renene.2018.07.050.

[26] D. Micallef and G. Van Bussel, "A Review of Urban Wind Energy Research: Aerodynamics and Other Challenges," *Energies*, vol. 11, no. 9, Art. no. 9, Sep. 2018, doi: 10.3390/en11092204.

[27] M. R. Islam, R. Saidur, and N. A. Rahim, "Assessment of wind energy potentiality at Kudat and Labuan, Malaysia using Weibull distribution function," *Energy*, vol. 36, no. 2, pp. 985–992, Feb. 2011, doi: 10.1016/j.energy.2010.12.011.

[28] *IEC 61400-2:2013*. 2013. [Online]. Available: https://webstore.iec.ch/publication/5433

[29] B. R. Karthikeya, P. S. Negi, and N. Srikanth, "Wind resource assessment for urban renewable energy application in Singapore," *Renew. Energy*, vol. 87, pp. 403–414, Mar. 2016, doi: 10.1016/j.renene.2015.10.010.

[30] F. Bañuelos-Ruedas, C. Angeles-Camacho, and S. Rios-Marcuello, "Analysis and validation of the methodology used in the extrapolation of wind speed data at different heights," *Renew. Sustain. Energy Rev.*, vol. 14, no. 8, pp. 2383–2391, Oct. 2010, doi: 10.1016/j.rser.2010.05.001.

[31] F. Yavuz and T. Baycan, "Use of Swot and Analytic Hierarchy Process Integration as a Participatory Decision Making Tool in Watershed Management," *Procedia Technol.*, vol. 8, pp. 134–143, Jan. 2013, doi: 10.1016/j.protcy.2013.11.019.

[32] P. Kotler, R. Berger, and N. Bickhoff, *The Quintessence of Strategic Management*. Berlin, Heidelberg: Springer, 2016. doi: 10.1007/978-3-662-48490-6.

[33] A. Posch, T. Brudermann, N. Braschel, and M. Gabriel, "Strategic energy management in energy-intensive enterprises: a quantitative analysis of relevant factors in the Austrian paper and pulp industry," *J. Clean. Prod.*, vol. 90, pp. 291–299, Mar. 2015, doi: 10.1016/j.jclepro.2014.11.044.

[34] Z. Ilham *et al.*, "Analysing dimensions and indicators to design energy education framework in Malaysia using the analytic hierarchy process (AHP)," *Energy Rep.*, vol. 8, pp. 1013–1024, Nov. 2022, doi: 10.1016/j.egyr.2022.07.126.

[35] T. L. Saaty, "Axiomatic Foundation of the Analytic Hierarchy Process," *Manag. Sci.*, vol. 32, no. 7, pp. 841–855, Jul. 1986, doi: 10.1287/mnsc.32.7.841.

[36] D. Elliott *et al.*, "Wind Energy Resource Atlas of the Dominican Republic," NREL/TP-500-27602, 15000080, Oct. 2001. doi: 10.2172/15000080.

[37] S. AL-Yahyai, Y. Charabi, A. Gastli, and S. Al-Alawi, "Assessment of wind energy potential locations in Oman using data from existing weather stations," *Renew. Sustain. Energy Rev.*, vol. 14, no. 5, pp. 1428–1436, Jun. 2010, doi: 10.1016/j.rser.2010.01.008.

Classification of polyethylene terephthalate bottles in a recycling plant

[1]Diego Alberto Godoy [0000-0002-7445-7375], [2]Enrique Marcelo Albornoz [0000-0002-7044-020X],
[1]Ricardo Selva [0000-0002-4843-1243], [1]Nicolas Ibarra [0000-0003-4654-8410], [1]Cesar Gallardo [0000-0002-3227-487X]

[1] Centro de Investigación en Tecnologías de la Información y Comunicaciones (CITIC).
Universidad Gastón Dachary, Av. López y Planes 6519, 3300 Posadas - Argentina
[2] Instituto de investigación en Señales, Sistemas e Inteligencia Artificial - sinc(i), CONICET-UNL

diegodoy@citic.ugd.edu.ar,emalbornoz@sinc.unl.edu.ar,
Ricardosel@gmail.com, Niicoibarra1@gmail.com,
cesar.cgallardo@gmail.com

Abstract. One of the more serious problems that the planet faces is the pollution, which exposes its integrity and the living beings that inhabit it at risk. Pollution is a constantly growing problem due to the increase in population and large companies, and it contributes to the detriment of people's health and the environment. The advancement of technologies, and in particular of intelligent systems, allows automating and optimizing many processes that are usually carried out manually and very expensive. The artificial intelligence systems allow the redistribution of efforts and resources, increasing productivity. In this work, an approach to the detection of different types of recyclable plastic waste that arrive at a recycling plant using a convolutional neural network is presented. Several models were evaluated for this task and the YOLOv5 achieved the best results. Preliminar results show a confidence of up to 65% on images taken from the recycling plant in the city of Posadas, Misiones (Argentina).

Keywords: Convolutional Neural Networks, Waste Classification, Computer Vision.

1   Introduction

For many years now, the world has been challenged by problems that compromise the environment, such as the deterioration of the ozone layer [1], massive deforestation of trees, poaching of animals, or environmental pollution. The latter has several classes such as contamination of the soil, water, air, radioactive, acoustic, or chemical contamination. In addition to the environmental pollution, this causes dangerous and serious illnesses, and also in the worst cases, death [2]. Recycling is the method through which it is possible to reuse raw materials and one of its most relevant impacts is to help curb exploitation of natural resources. For example, recycling paper

and cardboard helps reduce deforestation and chemical pollution of the air and rivers, and consequently helps preserve the environment [3]. In this sense, garbage recycling is of vital importance for our environment. However, some aspects must be taken into account before thinking of a solution. According to studies carried out by the organization Natural Resources Defense Council (NRDC) [4] in Latin America, if the garbage were properly separated before reaching the municipal dump, an average of almost 92% could be recycled, but since citizens do not usually differentiate their waste, it is only possible to recycle 30%. In 2020, the city of Posadas produced an average of 8,000 tons of waste per month [5] which is equivalent to approximately 266 tons per day. Taking into account the mentioned percentage, it is probably that less than 80 tons were processed per day. This number is constantly growing due to the trend of increasing population and large companies in recent years in Posadas. The recycling process is carried out through a waste collection plant located in the municipal green center in the City of Posadas, being a part of the Integral Management of Urban Solid Waste (GIRSU).

The main problem is social, although there is a city ordinance corresponding to the proper separation of waste in the city of Posadas [6], people are not used to making an adequate differentiation of garbage and usually mix organic and inorganic waste. This is the reason why most of the daily garbage cannot be recycled, since organic waste decomposes and makes waste that could be recycled useless. This has a direct impact on GIRSU, since before the classification process of a particular type of waste (such as plastic, cardboard, etc.), a manual pre-sorting process is needed to assess which waste can be recycled.

To automate the classification process, it is necessary to emulate the complex human task of image recognition. In addition, for the GIRSU scene, the system is immersed in a fast and continuous process where the elements are presented in different positions, sizes, colors, and overlap with other elements. In order to simplify the processing, some mechanical systems could be used to isolate the elements avoiding irregularities and classify them. It is important to note that the conveyor belt does not stop and large volumes of waste must be processed in a very fast manner.

The computer vision techniques, that include digital image processing and neural networks, can support the identification of waste automatically. However, it is necessary to establish a set of restrictions and conditions on certain waste classification operations, considering how waste arrives at GIRSU today. The approach presented in this work focuses on the classification of polyethylene terephthalate (PET) bottles (crystal, green and light blue).

2   Related Works

In [7] the classification of waste is addressed using Machine Learning using Google Cloud Platform, Microsoft Azure, and a model designed by the authors. The main described problem is the lack of any treatment or management process for the inevitable massive generation of garbage by people in cities. The objective was to develop an API based on computer vision techniques supported by Cloud services that allows

the recognition of waste and determines the belonging of an element to the group of recyclable waste. Two approaches are taken for the waste sorting process. The first is based on Auto Machine Learning, which together with cloud services allows automatically designing of a Machine Learning model for a given dataset. Specifically, Cloud Vision API and AutoML (which are Google Cloud Platform products), and Custom Vision (which is a Microsoft Azure product) were used. The second is based on the manual design of a computer vision model using convolutional neural networks and Transfer Learning, which allows taking a previously trained model and adapting it to a particular problem. Various experiments were performed combining architectures such as VGG16, VGG19, and MobileNet while tuning hyperparameters such as the number of epochs and batch size.

The used dataset has 2527 waste images and it is freely available online at [8]. This dataset is made up of 501 images of glass, 594 of paper, 403 of cardboard, 482 of plastic, 401 of metal, and 137 of non-recyclable waste. For the tests, the images were taken on a white background with both artificial and natural light. The size of each image is 512 x 384 pixels. The devices used to take the images were: Apple iPhone 7 Plus, Apple iPhone 5S, and an Apple iPhone SE. The results obtained were 76% correct for the model designed by the authors, while 93% and 98% correct with cloud tools. Both the source code of the experiments carried out as well as the complete results can be found at [9].

Different from the aforementioned work, Deep Learning was used to identify recycled waste in the Municipal Green Center. For the training of the neural network, 300 images of each type of residue will be used, while for the tests, 100 images of each one. In both training and testing processes, photographs will be taken with a GoPro camera.

In [10], authors propose the automatic classification of plastics, glass bottles, and cans using the SSD-Mobilenet[11] convolutional neural network. The motivation of this work was the great generation of waste on the beaches, where most of the waste is recyclable but people have no interest or knowledge to throw the waste in the corresponding container. The corpus contains 317 images of 3 types of waste: plastic bottles, glass bottles, and metal cans; including a wide variety of brands for each type. For plastic bottles, 31 different brands were used; 19 brands for glass bottles, and 18 for cans. The labeling of the dataset and the training of the model was carried out in a computer: Intel Core i7-6700 CPU, 8 GB RAM, with a GEFORCE GTX 1070 TI 8 GB GDDR5 GPU. In the test phase, a Raspberry Pi with a camera was used. For each type of waste, 5 experiments with 20 images in each were done. The results show for metal cans a success rate of 86%, a success rate of 95% for plastic bottles, and a success rate of 82% for glass bottles.

In this case, the waste includes plastic bottles, glass bottles, and metal cans, while in our approach different types of plastics will be identified: green PET, crystal PET, light blue PET, and blown plastic. In addition, they used an average of 300 images per type of waste, while in our work 400 images per type of waste are used and the classes are more similar between them. In our approach, the labeling phase is also done.

3   Methodology

In this section the Crisp-DM methodology is introduced, and it was selected because it is widely used in data mining projects in multiple industries [12].

3.1   DATA MODEL ANALYSIS

In the first phase, the aim was to understand and determine what types of images were the best input to reach a suitable prototype. These images should be as realistic as possible and appropriately reflect the scenario and conditions where the prototype will work. For this purpose, the authors captured and labeled photos in the GIRSU plant. Additionally, images from other available waste datasets were used, as Bottles and cans images [13], and Garbage Classifications [14] datasets.

Available datasets
Two available datasets were used to perform the image survey: Bottles and Cans Images [13] and Garbage Classification [14]. On these, there is a great variety of PET crystal, light blue, green, and blown arranged on white backgrounds that serve as a starting point to provide the network with knowledge about the data that must be identified. Some examples can be found in figure 1.

Fig. 1. Examples of images from Garbage database [14].

Acquired data
Our own database is formed by images captured in the municipal green center, and images taken at the author's homes where the PETs were set in situations that simulate the application scenario. Some examples are shown in figure 2.

Fig. 2. Examples of images taken at home and in the GIRSU plant.

3.2   DATA PREPARATION

At this point, the available datasets were ready to use but our own database needed to be labeled. After that, the sets for experiments were defined.

Images labeling

In this process, each image is associated with a label that represents it. In this way, all the data will be suitable to perform the training or test phase. Here, Roboflow [15] was used as a labeling tool.

Datasets definition

In this phase, with uniform labeled images, different subsets of images were formed that will have different purposes: training, validation, and test. The validation set is very useful to avoid overtraining [16]. The training and validation sets were randomly selected while the test set contains only examples of the real scenario.

Table 1. Distribution of image sets. An image can have more than one object.

	Number of images	%	Labels	Labels per class	% of each class in the dataset
Training	635	69	Light blue	357	43.97
			Crystal	393	48.4
			Green	62	7.64
Validation	257	28	Light blue	107	33.75
			Crystal	182	57.41
			Green	28	8.83
Test	25	3	Light blue	4	11.76
			Crystal	27	79.41
			Green	3	8.82
Total	917	100			

3.3   MODEL EXPLORATION

In this stage, different CNN approaches were evaluated in order to obtain the best implementation for the prototype. It is important to note that all the CNN were pre-trained and here, the transfer learning technique was used. In this scheme, the weights of the CNN are set and it is not necessary to train the network from scratch. In Table 1 is possible to observe an important unbalance of the data with respect to the classes. In this sense, it appropriated the use of metrics that consider the unbalanced among classes, and thus avoid an erroneous interpretation of the performance of the system. This means that the global metric must take into account the performance of the system for each class. To achieve this, the unweighted average recall (UAR) is used and it is computed as the average of all recalls per class (see equations 1 to 4).

$$recall_{\ light\ blue} = \frac{number\ of\ hits\ in\ detecting\ a\ light\ blue\ class}{total\ number\ of\ images\ of\ light\ blue\ class} \tag{1}$$

$$recall_{\ crystal} = \frac{number\ of\ hits\ in\ detecting\ a\ crystal\ class}{total\ number\ of\ images\ of\ crystal\ class} \tag{2}$$

$$recall_{\ green} = \frac{number\ of\ hits\ in\ detecting\ a\ green\ class}{total\ number\ of\ images\ of\ green\ class} \tag{3}$$

$$UAR = \frac{recall_{light\ blue} + recall_{\ crystal}\ recall_{\ green}}{3} \tag{4}$$

The analyses were performed checking the UAR obtained on the validation set in order to select the best model for this domain. The results can be seen in Table 2, while in figure 3, the evolution of the metrics with respect to the number of epochs is presented.

Table 2. Best results using 25 training epochs as maximum.

CNN	Execution time(min)	Best Epoch	UAR (val)	UAR (test)
ALEXNET	3.0	6	0.87	0.71
GOOGLENE	3.3	13	0.56	0.30
INCEPTION	3.0	3	0.33	0.34
RESNET18	3.0	15	0.87	0.79
VGG16	9.6	6	0.87	0.79
YOLO V5	6.2	18	0.84	**0.85**
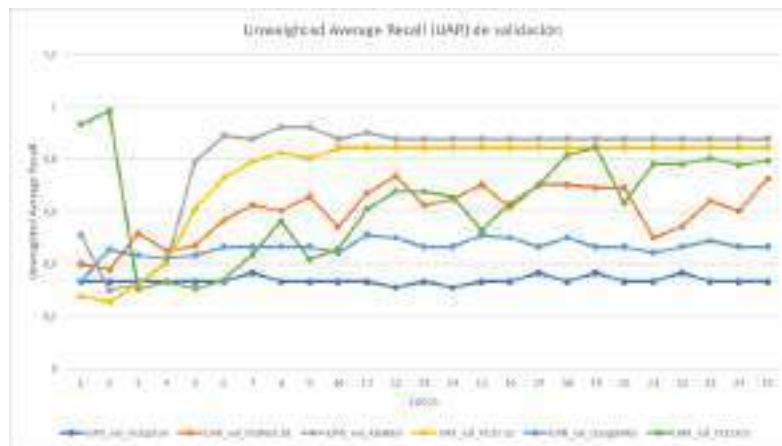
Fig. 3. Validation accuracy progress over 25 epochs (training phase).

4　　Prototype Architecture

The proposed prototype was implemented in Python using PyTorch, and includes the best trained model obtained in the previous stage. In figure 4, the prototype workflow can be seen. The input images are taken from a database or from the camera, and feed the CNN which gives as a result the class to which the PET belongs.
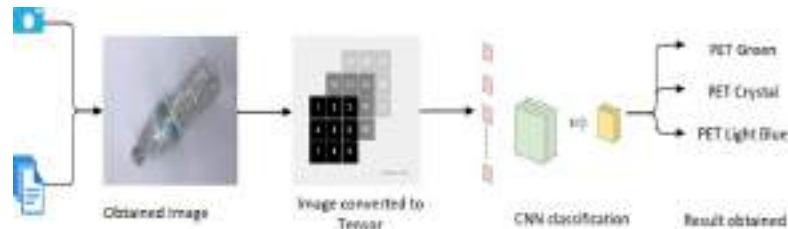
Fig. 4. Prototype workflow

4.1   **Input data**

The prototype can take images from different sources, such as video or surveillance cameras, where snapshots are taken at certain pre-established time intervals; or from stored images in jpg, jpeg, or png format. These images are transformed into Pytorch Tensors [16] for further processing in the next stage.

4.2   **Inference**

It is done through the Python programming language using the Pytorch library and the YOLOv5 convolutional neural network. The model is already trained, and the inference is the operation that allows to classify the test images taken from the application scenario.

5   TESTING SCENARIOS

5.1   Bottles classification: lab test

In initial laboratory tests, the different PET (crystal, green and light blue) were used. These were put on clean surfaces, with a white background and the photos were captured close to the PET (see figure 5). This was done to evaluate the feasibility of the project. The results demonstrate a very appropriate initial approach evaluating the metrics obtained.

Fig. 5. Examples of images used in lab test.

5.2   Bottles classification: clean environment

In a second instance, different scenarios presented in figures 6 and 7 have been evaluated, where it is evident that the prototype is capable of identifying the elements. In the figure on the left, confidence is relatively low and it could be attributed to the size of the element, although it can be observed empirically that the model is capable of identifying the glass PET bottles that were on the floor and the tabletop. In the figure on the right, the network recognizes the element with a confidence of 51% and it could be reached because of the orientation of the element. These results show that it is possible to recognize the recyclable waste on remote surfaces and with a computationally complex scenario.
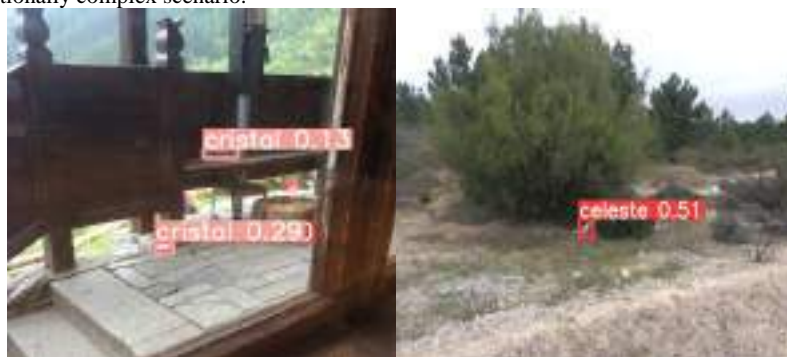
Fig. 6. Distant bottles with no close or overlapped objects.

Fig. 7. Distant bottles with waste around them.

5.3   Bottles classification: complex scenario

We defined the complex scenario when the images are as those show in figures 8 and 9, where the bottles are not only scattered on the green floor, but can be confused with the green glass and glass PET bottles, can be overlapped and occluded, even with other waste. Taking into account the metrics in the figure 8 and 9, where the average confidence is about 23%, it is possible to say that the results are promising to identify waste in noisy environments.

Fig. 8. Complex scenario for green and crystal PET.

Fig. 9. Distant bottles with waste around them.

It is important to highlight these results because the used images have similar characteristics as the goal scenario where the waste is scattered on a surface with other elements around it, for example, other waste that is not within the scope of this project. On the other hand, in some cases the obtained confidences are relatively low with respect to the previous proofs. Therefore, even though the metrics are not high enough to think about implementation, they could be a starting point to the future work due to the feasibility of the prototype.

5.4   Bottles classification: goal scenario

The images presented in figure 10 were taken on the conveyor belt of the recyclable waste plant. These show some confidence results and indicate that it is possible to recognize the desired elements with a good rate. The best results are associated with different PETs bottles forms. It would be possible to take advantage of this by using a hierarchical classification scheme in future work, where in a first step a coarse classification is performed and then, a specific PET classification is done.

Fig. 10. Bottles at closer distance, in a conveyor belt with waste around.

6   CONCLUSION AND FUTURE WORKS

An approach to PET classification in a conveyor belt at a recyclable waste plant was designed and implemented. Pre-trained CNNs were used to reduce time and resources to build the image classification prototype. After the experiments, the YOLOv5 was chosen because it achieved the best results, as can be seen in table 2. It also has the advantage of being able to detect and classify different class objects in the same image. However, like any prediction model, it can be affected by factors such as the brightness of the environment, the partial or complete capture of the object, the overlap between bodies, or the focus and distance from them. These circumstances can confuse the model generating erroneous results, such as false positives, wrong classes, or low success percentages. At the same time, the prototype presents the possibility of improving the outcomes by providing, exhaustively, inputs that reflect all the conditions and circumstances that could be found when carrying out an evaluation. In addition, this prototype is a first step in the development of a fully automated waste classification system, which would mean a reduction in the time of exposure of workers to harmful substances and an increase in the productivity of the beneficiary entity.

As future work the real photo set and the augmented data need to be emphasized to get a better trained model, as well as to allow a bigger number of epochs in the training. An issue to analyze in future works is to apply image processing techniques to improve the learning performance of the network, even super-resolution techniques. Also, a new design of the model, maybe using hierarchical structures in order to reach better results, is contemplated. In addition, the implementation of the prototype in a real environment, such as the recycling plant in the Municipal Green Center is agreed.

References

1. C. Romo-Gómez, C.: Actividades antrópicas: deterioro de la capa de ozono estratosférico. Boletín Científico de Ciencias Básicas e Ingenierías del ICBI 7(13), 1–5

2. Arcos Medina, G., Arcos, A., Oñate Andino, M., Danilo, P., Jerves Cobo, R.: Simulación para Estimación de Muertes por Cáncer de Pulmón por Contaminación Ambiental de PM2.5. (2018)

3. Citlalic Gonzales Martinez, A.: Costos y beneficios ambientales del reciclaje en México. Una aproximación monetaria. (2001)

4. Moyer, E.: Día del Reciclaje: ¿Qué tanto se recicla en América Latina? In: NRDC. (Accessed 2018) Available at: https://www.nrdc.org/es/experts/erika-

5. moyer/dia-reciclaje-tanto-recicla-america-latina

6. Municipalidad de Posadas: Servicio de Recolección general de Residuos Sólidos Urbanos. In: Desarrollo Sustentable. (Accessed 2018) Available at:

7. https://posadas.gov.ar/sustentable/servicio-de-recoleccion-general-de-residuos-solidos-urbanos/

8. Honorable Concejo Deliberante de la Ciudad de Posadas: Ordenanza VI - N 29., Posadas (2021)

9. Castrillon Medina, M.: REDO: Sistema de reconocimiento de desechos reciclables. (2019)

10. Thung, G., Yang, M.: Dataset of images of trash; Torch-based CNN for garbage image classification. In: Github. (Accessed 2017) Available at: https://github.com/garythung/trashnet

11. Castrillon Medina, M.: Sistema de reconocimiento de desechos reciclables. (Accessed 2019) Available at: https://github.com/ManuCastrillonM/redo

12. Sorawit, T., Kittiya, T., Prajaks, J.: Valuable Waste Classification Modeling based on SSD-MobileNet. (2021)

13. Howard, A., Zhu, M., Chen, B., Kalenichenko, D., Wang, W., Weyand, T., Andreetto, M., Hartwig, A.: MobileNets: Efficient Convolutional Neural Networks for Mobile Vision. (2017)

14. Schröer, C., Kruse, F., MarxGómez, J.: A Systematic Literature Review on Applying CRISP-DM Process Model. (2021)

15. Kaggle: Starter: Bottles and Cans Images. In: Kaggle. (Accessed July 14, 2020) Available at: https://www.kaggle.com/code/kerneler/starter-bottles-and

16. -cans-images-aa8808c7-4

17. cchangcs: Garbage Classification. In: Kaggle. (Accessed 2018) Available at:

18. https://www.kaggle.com/datasets/asdasdasasdas/garbage-classification

19. Roboflow: Roboflow - Give your projects the power to see objects in images and videos. (Accessed 2022) Available at: https://roboflow.com/
20. Bishop, C. M., & Nasrabadi, N. M. (2006). Pattern recognition and machine learning (Vol. 4, No. 4, p. 738). New York: springer.
21. Paszke, Adam, Sam Gross, Francisco Massa, Adam Lerer, James Bradbury, Gregory Chanan, Trevor Killeen, et al. Pytorch: An Imperative Style, High-Performance Deep Learning Library. (2019)

Study of the inactivation of *Escherichia coli* strain vs. native bacteria during UV disinfection treatment with a flow-trough reactor

Duque-Sarango, Paola[1,3 [0000-0003-4484-7273]]; Romero-Martínez, Leonardo[2 [0000-0002-4599-1907]]; Pinos, Verónica[3 [0000-0001-8278-5873]]; Sánchez, Esteban[4 [0000-0002-8206-386X]]; Samaniego, Esteban[3[0000-0002-8728-491X]]

[1] Universidad Politécnica Salesiana. Grupo de Investigación de Tecnología Ambiental (INBIAM). Campus El Vecino. Calle Vieja 12-30 y Elia Liut. Cuenca, Ecuador.
[2] Universidad de Cádiz. Departamento de Tecnologías del Medio ambiente. Instituto Universitario de Investigación Marina (INMAR). Campus de Excelencia Internacional del Mar (CEI·MAR). Centro Andaluz Superior de Estudios Marinos (CASEM). Campus de Puerto Real. 11510 – Puerto Real, Cádiz, España.
[3] Universidad de Cuenca. Departamento de Recursos Hídricos y Ciencias Ambientales. Ecocampus Balzay. Av. Victor Manuel Albornoz, Cuenca, Ecuador.
[4] Universidad de Cuenca. Departamento de Ingeniería Civil. 010203 Cuenca, Ecuador
pudque@ups.eu.ec

Abstract. The reuse of effluents from wastewater treatment plants is a reality in several countries due to water scarcity. To ensure its quality, tertiary disinfection treatments are needed. The present work aims to evaluate the efficacy of ultraviolet (UV) disinfection systems for the elimination of fecal bacteria in effluents from urban wastewater treatment plants. Kinetic modeling was used to study the influence on the inactivation of *Escherichia coli* considering different UV doses, origin of the bacteria (native or standardized lyophilized strain), and the response to post-treatment at 24 hours under light and dark conditions. In the adjustment of the experimental inactivation values with non-linear regression techniques, the linear mathematical model with tail was chosen as it showed better statistical fit. The evaluation showed that between the two *E. coli* variants tested, the native bacterium presented higher UV resistance and was also affected by reactivation to a lesser extent, with respect to the *E. coli* ATCC 8739 strain. In other words, although the inactivation dose for both bacteria was similar, the recovery of damage from photoreactivation effects was higher in the native species. Therefore, the necessary dose of inactivation was determined by UV technology, which was equal to 15 mJ cm^{-2} for a reduction of 5 $\log_{10}$ for both the *E. coli* strain and the native type, without considering reactivation processes, while the maximum percentage of photoreactivation detected was 6% achieved by native *E. coli* treated with 5.88 mJ cm^{-2}.

Keywords: Wastewater reuse, ultraviolet disinfection; photoreactivation; *Escherichia coli*

1   Introduction

The present world is intimidated by the problem of water scarcity that is to be addressed immediately. So, it is wise to treat wastewater to meet the massive need for drinking water for the fast-growing population. The continuous growth of population and urban development, stupendous growth of industries, and increased food production culminate in water resources. This jeopardizes the health and safety of the global population in the spheres of both short- and long-term impact and the remedial measures adopted to eradicate poverty by simultaneously maintaining the balance of our unique ecosystems. The estimated amount of untreated wastewater disposal is 30% based on the existing data related to the high, upper and lower-middle-income countries, reporting 62% and 72%, respectively, and in low-income countries reporting 92%. Another survey analysis has reported that the discharge of untreated wastewater amounts to 90% [1].

A paradigm shift and higher-order thinking are crucial in encountering current and evolving challenges in urban water management. waste management concepts in urban planning processes are capable of bringing several key advantages. A Smart City is a city committed to its environment, both environmentally and in terms of the cultural and historical elements, and where the infrastructure is equipped with the most advanced technological solutions to facilitate citizen interaction with urban elements.

The increasing demand for water contrasts with the alarming scarcity of available water sources worldwide. An alternative to this demand is the reuse of wastewater effluents [2]. In fact, in recent years, several guidelines regulating the reuse of treated wastewater have been published, such as the Guidelines for the Safe Use of Wastewater, Excreta and Graywater [3] and the EPA Guidelines for the Reuse of Treated Wastewater in the Agricultural Sector [4]. In the latter, depending on the water use, it is established that the presence of fecal coliforms should be non-detectable or up to a permissible concentration of 200 CFU/100 mL, depending on the intended use [5].

Bacteria can be divided into two main groups according to the chemical and physical properties of their cell walls by means of the Gram staining technique. Gram-negative bacteria have a cytoplasmic membrane, a thin peptidoglycan layer and an outer membrane containing lipopolysaccharide. Meanwhile, Gram-positive bacteria have only a cytoplasmic lipid membrane and the peptidoglycan layer is thicker than that of Gram-negative bacteria. Therefore, these bacteria are much more difficult to destroy [2]. *E. coli* is the most commonly used indicator of fecal contamination in the analysis of water and wastewater. E. coli is commonly used to indicate the presence of fecal contamination in water and, by extension, the possible presence of pathogenic microorganisms [6]. Therefore, to make appropriate water management decisions, survival rates of E. *coli* in water must be known [7].

For the above reasons, it is essential to implement disinfection treatments. The disinfection of water is based on the extraction, deactivation, or elimination of pathogenic

microorganisms, as well as possible toxins that may have unpinned, can be applied by physical and/or chemical methods. As an alternative to traditional disinfection, ultraviolet disinfection processes (UV) have been developed based on the use of radiation emitted at wavelengths within the germicidal range (UV-C, 200-320 nm) [8], [9]. UV radiation inactivates microorganisms mainly through photochemical damage caused directly to nucleic acids [10]. Treatment proposals should consider that bacteria present in natural environments develop a certain resistance to disinfection processes [11], [12], and in addition, it is known that many microorganisms have the ability to repair damage induced by UV radiation [9]. Two repair mechanisms are reported. One is light-independent, which is termed dark repair [13] and the other is photoreactivation, where UV-induced DNA lesions can be repaired using near ultraviolet light energy (310 - 480 nm) and the enzyme photolyase [14]. This problem has received considerable attention because it can influence the efficiency of UV disinfection a few hours after treatment.

Therefore, it would be useful to establish the necessary inactivation doses for native species indicative of contamination as an indicator of the effectiveness of the treatment, analyzing characteristics of greater or lesser resistance to irradiation and lesser or greater influence of photoreactivation. This would allow reporting the necessary doses of inactivation by UV technology for future applications of UV disinfection in wastewater reuse, highlighting here that it is necessary to consider studies with species native to the area and the application of UV disinfection technology in developing countries.

Here, the present work focusing on the kinetic analysis of the inactivation of two groups of *E. coli*: strain ATCC 8739 and native isolates, to report the necessary inactivation doses and the influence of photoreactivation. This work provides insights into treatment levels needed for bacterial disinfection with UV light.

2   2. Materials and Methods

2.1   2.1 Inactivation tests

In the present study we worked with two types of microorganisms: 1) *E. coli* strain ATCC 8739 acquired from the Spanish Type Culture Collection (CECT) in lyophilized format and 2) native *E. coli* bacteria isolated from the effluent of the Ucubamba wastewater treatment plant in the city of Cuenca-Ecuador.

The bacteria were reactivated in 50 mL of Tryptic Soy Broth (TSB) culture medium (Sigma-Aldrich) for 24 h at 37ºC. Subsequently, a subculture was performed by depositing 1 mL of the culture in 50 mL of TSB medium. After another 24 h, the subculture was centrifuged at 3000 rpm for 10 min; after discarding the supernatant, the sediment obtained was washed with peptone solution (10%) and added to 50 mL of distilled water with phosphate buffer at pH 7.20, obtaining the bacterial inoculum in exponential growth phase [15]. The inoculum was added to a drum with 20 L of distilled water

buffered to pH 7.20, obtaining concentrations between 105 and 106 CFU/mL. To determine the bacterial concentration after the treatments, the membrane filtration method was applied with subsequent incubation on chromogenic selective agar. Sterile 0.45 μm square membrane filters (Pall Corporation, NY, USA) were used to obtain the appropriate number of CFU. Decimal serial dilutions of each sample were seeded in triplicate. Merck Coliform Agar Acc. Chromocult® was used as selective medium, deposited in Petri dishes. The samples were incubated at 37 °C for 24 h; after this time, the developed CFU were counted and those corresponding to plates with a number of CFU between 20 and 150 were considered as valid dilutions. Sterile conditions were controlled by blank sample plates during the microbiological analysis process.
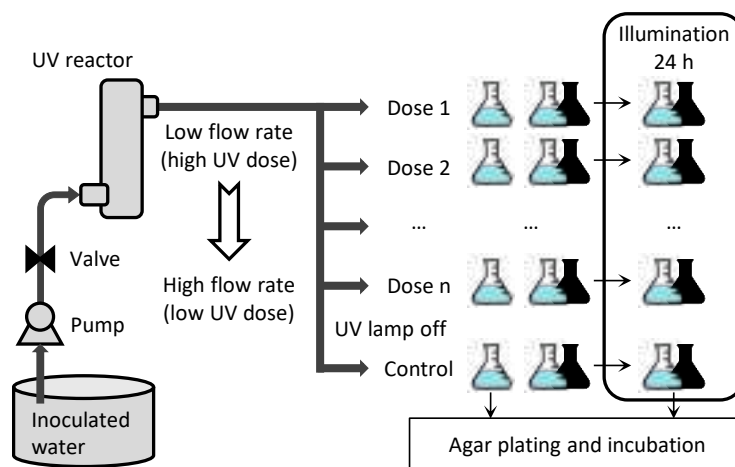
Fig. 1. Scheme of the laboratory plant and experimental procedure.

The UV treatment was applied by means of a continuous flow reactor of annular type, built at laboratory scale. This reactor has a low-pressure mercury UV lamp (Phillips 1GPM - in/out 1/4"), with a power of 6 W, and monochromatic emission at 254 nm, connected by a system of hoses and valves in order to manipulate the reactor inlet flow rate and the working flow rate in front of the UV lamp, obtaining different doses by exposure time (Fig 1). The UV dose (D) was applied in a single exposure (Eq. 1), as a function of mean intensity (Im) and Theoretical Retention Time (*TRT*) according to USEPA specifications [6], using a geometric radiation dispersion model for ring reactors, which was validated by biodosimetry in previous studies (Eq. 2) [16]. TRT was calculated as the quotient between the volume of water exposed to UV light (*VR*) and the flow rate (*Q*). The flow rate values were in the range of 60 to 720 Lh^{-1}, corresponding to a *TRT* of 3.06 to 0.26 s and doses of 26.5 and 2.2 mJcm^{-2} respectively.

$$D = TRT.Im \qquad (1)$$

$$D = \frac{VR}{Q} * \frac{P_{254}*TQ^e}{2L\pi^2*(rR^2-rQ^2)} \iint_{rQ}^{rR} \frac{TW^{r-rQ}}{r} * dx \, dy \tag{2}$$

Where:

P_{254}: Lamp power at 254 nm, in new lamps 1/3 power.
e: Quartz thickness (mm).
L: Lamp length (cm).
rR: Reactor radius (cm).
rQ: External radius of the quartz sheath (cm).
TQ: % Transmittance at 254nm of the quartz (usually 0.94).
TW: % Transmittance at 254nm of the treated water.

The inoculated matrices were pumped in a single pass from the 20 L tank through the reactor at different flow rates (60 to 720 Lh^{-1}). Three samples per flow rate were collected in sterile 250 mL flasks. The contents of one of the three flasks were directly subjected to the procedure to determine the bacterial concentration immediately after UV irradiation (day 0). The other two flasks were used for reactivation tests in light and dark. For this purpose, these were incubated for 24 h in a growth chamber (Binder KBWF Series brand) illuminated at 36 µEinstein m^{-2} s^{-1} and at 20 °C. One of the flasks was covered with aluminum foil to prevent light from entering (1 day dark), while the other remained uncovered (1 day light). After incubation, the contents of both flasks were subjected to the bacterial concentration determination procedure described above.

2.2　2.2 Analysis of results

The effectiveness of disinfection was determined by calculating the logarithmic reduction in the survival of microorganisms: log (N/N_0). Where N_0 and N is the number of colonies (CFU/mL) before and after UV irradiation. The Geeraerd and Van Impe inactivation model-fitting tool (GInaFiT) was used to describe the inactivation processes of $E.\ coli$ [17]. The R^2 values of the regression between the values determined by the model versus the experimental values were used. This was used to obtain the kinetic parameters of inactivation, and finally to determine the dose required to reduce the initial concentration by two (D_2) and three orders of magnitude (D_3) as an estimator of treatment efficacy.

To evaluate the effect of photoreactivation, the photoreactivation percentage was calculated, defined as follows [18]:

$$Percentage\ photoreactivation\ (\%) = \frac{N_p-N}{N_0-N} \times 100\% \tag{3}$$

Where: N_p = bacterial concentration of the photoreactivated sample (CFU/mL), N = bacterial concentration immediately after UV disinfection (CFU/mL), N_0 = bacterial concentration before UV disinfection (CFU/mL). This concept illustrates the percentage of photoreactivated bacteria among the bacteria affected by UV irradiation.

3   Results and Discussion

The inactivation results of the studied bacteria did not fit with linear mathematical models. The bacterial inactivation obtained presented curvilinear shapes, with tail phenomena, Fig. 2 shows the inactivation curves of the two groups of E. coli bacteria, plotting Log (S) versus UV dose applied. In all cases they showed inactivation kinetics according to a log-linear model with tail (Eq. 4), where S: survival; S_0: survival in the absence of irradiation; S_{res}: residual survival; k: inactivation rate; and D: UV dose [19]. The R^2 values show good prediction results for the model with values above 0.9 in most cases (Table 1).

$$S = (S_0 - S_{res})\, e^{-k \cdot D} + S_{res} \tag{4}$$

From the results, it was found that in both groups of *E. coli*, the inactivation values increase as the dose increases, in a linear manner up to a certain dose, followed by an asymptotic trend from a certain UV dose, this can be attributed to the fact that the model represents the inactivation based on a linear kinetics of first order with a residual population of resistant character that does not undergo drastic changes in its composition, i.e., it is not affected beyond the experimental doses [19]. Therefore, a certain UV dose will be required to be applied for the inactivation rate to reach its maximum value, which for the case of treatment without incubation approximately 15 mJ cm^{-2} is needed for a reduction of 5 log10 in both cases.

Under the effects of incubation in light and dark, the UV doses change depending on the subsequent treatment. In the samples incubated for 24 h in darkness, it is observed that survival is slightly lower than in the non-incubated samples. This difference is mainly observed in the *E. coli* strain (ATCC 8739). While survival in the samples incubated for 24 h exposed to light is in both cases higher than in the non-incubated samples, it stands out mainly in the native *E. coli*.
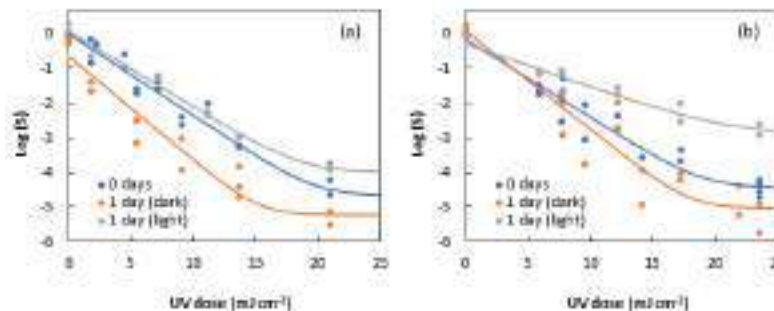

Fig. 2. Inactivation curves of the different *E. coli* strains for different post-treatment conditions. a) *E. coli* (ATCC 8739) b) *E. coli* (wild)

The inactivation kinetic parameters allow quantification of the treatment effect on the different strains and under the different post-treatment conditions (Fig. 3). The inactivation rates (k) of log-linear with tail in both *E. coli* decreased with increasing UV intensities in all assays. With respect to the non-incubation assays (day 0), this rate was found to be similar, with values of 0.54 and 0.52 cm^2 mJ^{-1} for *E. coli* (ATCC 8739) and *E. coli* (wild-type), respectively. This value is higher because of incubation in darkness (day 1 dark) and is lower after 24 h incubation in light (day 1 light) for the two types of *E. coli*.

The Log (S_0) values of the incubated samples represent the effect of incubation on the survival of the organisms, without considering the effect of UV treatment. The values range from -0.65 to 0.08, indicating that incubation alone has no effect on survival in general.
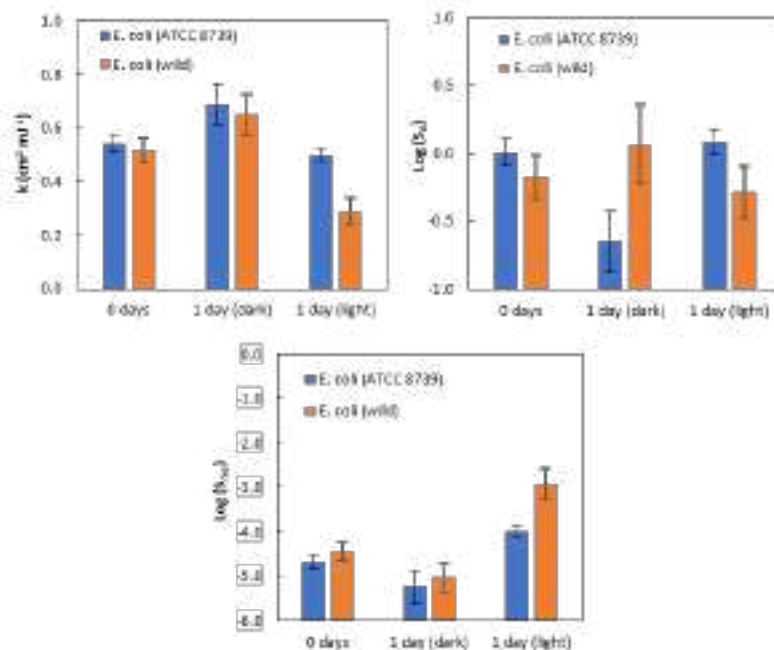
Fig. 3. Kinetic parameters of inactivation for *E. coli* in different post-treatment conditions: a) inactivation rate b) Log of survival in the absence of irradiation and c) Log of residual survival.

The log-linear with tail model also estimates the logarithm of residual survival (log S_{res}) that characterizes the inactivation tail kinetics. That is, if minimum counts are desired, it is not necessary to prolong a treatment beyond the indicated doses because additional inactivation would not be achieved [20]. As a result, it was found that without

incubation (day 0) the values are around -4.5 log CFU/mL for both cases. This is not altered by the effect of incubation in darkness, while incubation in light causes the effect to increase around -4 and -3 log CFU/mL for *E. coli* (ATCC 8739) and *E. coli* (wild) respectively.

The percentage of photoreactivation decreased with the UV dose applied (Fig 4). In the case of *E. coli* ATCC 8739, once the 2 orders of magnitude reduction are achieved with a dose of 8.51 mJ cm^{-2}, there is a risk that 0.67 % of the initial bacterial concentration will be reactivated at 24 h after the inactivation treatment. It is more critical for native *E. coli*, since once reduced by 2 orders of magnitude with a dose of 8.13 mJ cm^{-2}, 3.79 % of the initial bacterial concentration would be reactivated within 24 hours. The maximum percentage of photoreactivation detected was 6% achieved by native *E. coli* treated with 5.88 mJ cm^{-2}.
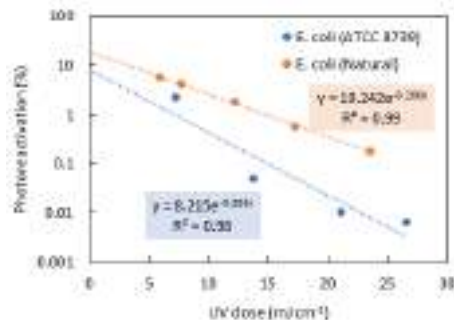
Fig. 4. Relationship between the percentage of photoreactivation and UV dose for *E. coli* bacterial strains tested.

Regarding photoreactivation profiles, survival in samples incubated for 24 h exposed to light is in all cases higher than in non-incubated samples. Since in a tailed log-linear model the efficiency results from the combination *Sres* and *k*, a new parameter including the effect of both is needed, D_4 being normally used for this purpose [9]. In the present study, D_4 reduction was not reached in all cases and therefore D_2 and D_3 values is used for the comparison of results (Table 1), and is around 8 mJ cm^{-2}, similar for both groups of bacteria when reactivation processes are not taken into account. On the other hand, D_2 values increase in samples incubated in light, indicating that photoreactivation has an important effect on treatment efficacy, the most notable increase occurring for native *E. coli* equal to 14 mJ cm^{-2}.

Table 1. D_2 and D_3 values obtained for the different *E. coli* strains for different post-treatment conditions, and percentage of variation with respect to non-incubated samples. NR (not reached)

Organism	Treatment	R^2	$D_2 \pm$ SE (mJ cm^{-2})	$D_3 \pm$ SE (mJ cm^{-2})
E. coli (ATCC 8739)	0 days	0.972	8.5 ± 1.0	12.8 ± 1.3
	1 day (dark)	0.937	4.5 ± 1.4	7.8 ± 1.8
	1 day (light)	0.990	9.6 ± 0.9	14.4 ± 1.2
E. coli (wild)	0 days	0.935	8.1 ± 1.5	12.6 ± 2.0
	1 day (dark)	0.882	7.3 ± 2.1	10.8 ± 2.6
	1 day (light)	0.922	14.0 ± 5.6	NR

Summarized data in the literature for UV-C treatment of several kinds of aqueous matrixes using a collimated beam reactor equipped with a low-pressure Hg lamp indicated a D_4 ranging from 6.5 up to 19 mJ cm^{-2} for E. coli, for both the same strain used in this study and wild types[21] [22]. In the present study, elimination was not achieved at a D_4 dose, a difference with respect to other studies may be due to the configuration of the reactor; with respect to the size and treatment flow rate experienced, which conditions the exposure time necessary to achieve the same UV dose, as well as the distribution of UV-C light intensity throughout the volume of water exposed, these phenomena could explain the different disinfection kinetics observed.

4   Conclusions

By means of the disinfection profiles obtained experimentally, a comparative evaluation of the treatment applied by means of a continuous flow reactor on the bacteria studied was achieved. When comparing *E. coli* ATCC 8739 vs. native *E. coli*, the native strain is more difficult to inactivate if the photoreactivation processes are taken into account. This indicates that the determination of photoreactivation using pure cultures of *E. coli* in the laboratory could possibly underestimate the real risk of microorganisms in wastewater if they are exposed to light after UV treatment.

The inactivation rates obtained after the fitting of the bacteria inactivation results with mathematical models highlighted the differences between the behavior of E. coli ATCC 8739 vs. native E. coli. The inactivation rate of E. coli ATCC 8739 was substantially higher in all the studied treatments. Therefore, the necessary dose of inactivation was determined by UV technology, which was equal to 15 mJ cm^{-2} for a reduction of 5 log10 for both the E. coli strain and the native type, without considering reactivation processes, while the maximum percentage of photoreactivation detected was 6% achieved by native E. coli treated with 5.88 mJ cm^{-2}.

The method used, including the photoreactivation procedure, can be used to assess the microbiological quality of UV-disinfected water. The increased UV dose should be

taken into account during the design of UV disinfection when UV disinfected water is discharged into open receiving systems, such as rivers or lakes, where they are exposed to light conditions, which may favor photoreactivation processes.

References

[1]   T. Sato, M. Qadir, S. Yamamoto, T. Endo, and A. Zahoor, "Global, regional, and country level need for data on wastewater generation, treatment, and use," *Agric Water Manag*, vol. 130, pp. 1–13, Dec. 2013, doi: 10.1016/J.AGWAT.2013.08.007.

[2]   J. Rodríguez-Chueca, M. P. Ormad, R. Mosteo, and J. L. Ovelleiro, "Kinetic modeling of Escherichia coli and Enterococcus sp. inactivation in wastewater treatment by photo-Fenton and H2O2/UV–vis processes," *Chem Eng Sci*, vol. 138, pp. 730–740, Dec. 2015, doi: 10.1016/J.CES.2015.08.051.

[3]   "Guidelines for Water Reuse | US EPA." https://www.epa.gov/water-reuse/guidelines-water-reuse (accessed Aug. 29, 2022).

[4]   "Guidelines for Water Reuse - Google Books." https://books.google.es/books?hl=en&lr=&id=_aPXo-asZqoQC&oi=fnd&pg=PA1&dq=Guidelines+for+water+reuse.+Technology+Transfer+and+Support+Division,+National+Risk+Management+Re-search+Laboratory&ots=6ZoUERx2fy&sig=RL-AAyeuMUx4ygyPQvv3KCEGzFo&redir_esc=y#v=onepage&q=Guide-lines%20for%20water%20reuse.%20Technology%20Trans-fer%20and%20Support%20Division%2C%20National%20Risk%20Manage-ment%20Research%20Laboratory&f=false (accessed Aug. 29, 2022).

[5]   "OMS | Informe sobre la salud en el mundo 2004 - cambiemos el rumbo de la historia," *WHO*, 2013.

[6]   D. M. USEPA, *Municipal Wastewater Disinfection*. 1986.

[7]   J. Marugán, R. van Grieken, C. Sordo, and C. Cruz, "Kinetics of the photocata-lytic disinfection of Escherichia coli suspensions," *Appl Catal B*, vol. 82, no. 1–2, pp. 27–36, Jul. 2008, doi: 10.1016/J.APCATB.2008.01.002.

[8]   W. Kowalski and W. Kowalski, "Pulsed UV Systems," in *Ultraviolet Germi-cidal Irradiation Handbook*, Springer Berlin Heidelberg, 2009, pp. 383–398. doi: 10.1007/978-3-642-01999-9_16.

[9]   W. A. M. Hijnen, E. F. Beerendonk, and G. J. Medema, "Inactivation credit of UV radiation for viruses, bacteria and protozoan (oo)cysts in water: A review," *Water Research*, vol. 40, no. 1. Elsevier Ltd, pp. 3–22, 2006. doi: 10.1016/j.wa-tres.2005.10.030.

[10]   H. P. von Sonntag, C., & Schuchmann, "UV disinfection of drinking water and by-product formation- some basic considerations," *Aqua- Journal of Water Supply: Research and Technology*, vol. 41(2), 67-, 1992.

[11]   C. von Sonntag, H. S.-A.-J. of W. S. R. and, and 1992Sign in, "UV disinfection of drinking water and by-product formation- some basic considerations.".

[12] Y. Ramos and G. Alonso, "Evaluación de la resistencia a agentes desinfectantes de bacterias aisladas de ambientes naturales," *Revista de la Sociedad Venezolana de Microbiología*, vol. 31, no. 2, pp. 130–137, 2011, Accessed: Aug. 24, 2022. [Online]. Available: http://ve.scielo.org/scielo.php?script=sci_arttext&pid=S1315-25562011000200009&lng=es&nrm=iso&tlng=es

[13] C. Jungfer, T. Schwartz, and U. Obst, "UV-induced dark repair mechanisms in bacteria associated with drinking water," *Water Res*, vol. 41, no. 1, pp. 188–196, Jan. 2007, doi: 10.1016/J.WATRES.2006.09.001.

[14] K. Tosa and T. Hirata, "Photoreactivation of enterohemorrhagic Escherichia coli following UV disinfection," *Water Res*, vol. 33, no. 2, pp. 361–366, Feb. 1999, doi: 10.1016/S0043-1354(98)00226-7.

[15] A. J. Verhulst, A. M. Cappuyns, E. van Derlinden ., K. Bernaerts, and J. F. van Impe, "Analysis of the lag phase to exponential growth transition by incorporating inoculum characteristics," *Food Microbiol*, vol. 28, no. 4, pp. 656–666, Jun. 2011, doi: 10.1016/J.FM.2010.07.014.

[16] J. Moreno-Andrés, L. Romero-Martínez, A. Acevedo-Merino, and E. Nebot, "UV-based technologies for marine water disinfection and the application to ballast water: Does salinity interfere with disinfection processes?," *Science of The Total Environment*, vol. 581–582, pp. 144–152, Mar. 2017, doi: 10.1016/J.SCITOTENV.2016.12.077.

[17] A. H. Geeraerd, V. P. Valdramidis, and J. F. van Impe, "GInaFiT, a freeware tool to assess non-log-linear microbial survivor curves," *Int J Food Microbiol*, vol. 102, no. 1, pp. 95–105, Jun. 2005, doi: 10.1016/J.IJFOODMICRO.2004.11.038.

[18] K. G. Lindenauer and J. L. Darby, "Ultraviolet disinfection of wastewater: Effect of dose on subsequent photoreactivation," *Water Res*, vol. 28, no. 4, pp. 805–817, Apr. 1994, doi: 10.1016/0043-1354(94)90087-6.

[19] A. H. Geeraerd, C. H. Herremans, and J. F. van Impe, "Structural model requirements to describe microbial inactivation during a mild heat treatment," *Int J Food Microbiol*, vol. 59, no. 3, pp. 185–209, Sep. 2000, doi: 10.1016/S0168-1605(00)00362-7.

[20] A. Izquier and V. M. Gómez-López, "Modeling the pulsed light inactivation of microorganisms naturally occurring on vegetable substrates," *Food Microbiol*, vol. 28, no. 6, pp. 1170–1174, Sep. 2011, doi: 10.1016/J.FM.2011.03.010.

[21] T. P. Coohill and J. L. Sagripanti, "Overview of the Inactivation by 254 nm Ultraviolet Radiation of Bacteria with Particular Relevance to Biodefense," *Photochem Photobiol*, vol. 84, no. 5, pp. 1084–1090, Sep. 2008, doi: 10.1111/J.1751-1097.2008.00387.X.

[22] G. D. Harris, V. D. Adams, D. L. Sorensen, and M. S. Curtis, "Ultraviolet inactivation of selected bacteria and viruses with photoreactivation of the bacteria," *Water Res*, vol. 21, no. 6, pp. 687–692, Jun. 1987, doi: 10.1016/0043-1354(87)90080-7.

Impact of Power Ramps of Photovoltaic Systems on the Electricity Grid. Case Study: Girasol Solar Park

Aybar-Mejía, Miguel [1][0000-0002-4715-3499], Santos, Darwin [1][0000-0001-9090-4414], Contreras-Álvarez, Adellin-Anderson [1][0000-0002-7248-6498], Rosario-Weeks, Dinelson [1][0000-0002-8091-6697], Smith, Mischael [1][0000-0001-7427-6286], Jiménez Matos, Elvin [1][0000-0002-0031-6772], Mariano-Hernández, D. [1][0000-0002-4255-3450] and Báez-Santana, Rene [1][0000-0002-6664-5237]

[1] Área de Ingenierías, Instituto Tecnológico de Santo Domingo, 10602, Santo Domingo, Dominican Republic
miguel.aybar@intec.edu.do

Abstract. The implementation of renewable energies in different countries has in-creased considerably over the years. Due to the absence of inertia and constant fluctuations derived from the variability of the renewable energy source, high levels of uncertainty have been generated. The continuous changes evident in the output power of photovoltaic generation plants are mostly the product of climatic externalities, known as power ramps. These constant changes impact the electrical parameters of the electrical grid. Considering the power ramps' negative impact on grid stability, this research pro-poses a methodology to soften the effects of the immense power ramps that occur daily in solar parks. To validate this methodology, the Girasol solar park in San Cristobal, Dominican Republic, was used as a case study. To determine the feasibility of using the BESS, a comparative technical analysis of the alternatives currently used was carried out; simulations were also carried out using the PowerFactory DIgSILENT engineering software to study the effects of the implementation of BESS in the case of mentioned study. The results of the different models using the DIgSILENT simulation software showed that using a 40 MW auxiliary battery storage system would help maintain the system frequency (59.92 Hz) at stable levels for drops of up to 46.7 MW/min. The proposed storage system improves the transition of the power ramps of the photovoltaic park.

Keywords: Power ramp, photovoltaic systems, solar parks, active power, electrical grid.

1   Introduction

The objectives of a people-centered smart city are sustainability, quality of life, and economic growth, while an electric utility aims to provide affordable, reliable, and environmentally responsible energy [1]. Electrical power is essential for developing social activities [2]. Different technology have been developed to reduce the environmental damage provided by conventional electricity generation methods that enable the implementation of technologies to massify the use of renewable resources [3].

One of them is obtaining electrical energy through the photovoltaic (PV) solar source, a power generation technology that uses solar radiation to generate electricity [4] due to the massification of these technologies to interconnect to the electric network.

The energy that comes from the sun is affected by fluctuations due to factors such as climate, temperature, impurities, and other situations that can then be reflected in the generation's behavior as a function of time (MW/h) [5]. This behavior implies that when there are variations in the electricity generation process, sudden rises and falls of electrical power generated are created; these variations are known as power ramp rates [6]. The power ramps of PV systems develop problems with the grid's frequency. Typically, PV generation fluctuations are caused by a cloud that interrupts the passage of solar radiation, reducing the level of energy generated, which causes drops in the grid frequency [7].

PV systems generate active power in direct current, and inverters convert that energy to alternating current [8], [9]. Power electronics enable inverters to develop current advances and delays concerning voltage, producing reactive power [10]. Fluctuations in power generation vary the levels that reach the inverters, so reactive power drops generate drops in voltage levels [11]. The mechanisms have been proposed to counteract reductions in electricity generation so that the frequency can be maintained under the regulatory framework, avoiding emergency levels and, therefore, the entry of generators and other backup machines [12].

This paper's objective is to present a methodology to mitigate the power ramps generated in solar parks due to the stochasticity of the solar resource that affects the generation of active power through the analysis and simulation of storage systems integrated into PV parks. The main contributions of this paper in this field of research are:

• Critical analysis of the different system applications to mitigate the power ramps generated in the PV systems connected to the grid when climatological or technical variations occur and affected de stability of the power grid.
• Analysis of regulations in countries with technical and geographical similarities to know which strategies to use to mitigate the power ramps that solar parks can exert on the stability of the electricity system.
• A methodology to mitigate the impact of power ramps generated in grid-connected PV systems through storage system integration using DIgSILENT software.

This paper begins by presenting the methodology used in Section 2. Power ramps in photovoltaic systems are presented in Section 3. Then, continue with the case study presented in Section 4. The results and discussion are presented in Section 5. Finally, Section 6 presents the conclusions and future work.

2   Methodology

The methodology used in this article consisted of the following steps:

- Collected the existing data on power ramps registered in the database of the electric transmission company.
- Analysis of the statistics of the maximum fall power registered in the case study.
- Evaluate the existing regulations in countries where the power ramp of PV installations interconnected to the grid is regulated.
- Select the electrical variables that produce power ramps in solar parks connected to a specific point of the electrical network.
- Simulation of scenarios based on the selected electrical variables to compare the behavior of the power ramp of the solar park in the electrical network before and after the proposed solution.
- Analysis of the results applying the proposed solution to mitigate the power ramps in the case study.

3 Power Ramp in Solar Parks

Energy production through PV panels is not exempt from factors such as an intermittent primary resource; it is impossible to control its magnitude, recurrence, or constancy, causing large fluctuations within the system [13]. These fluctuations in power production generate a series of disturbances in the attenuation within the generation curve, known as a power ramp [14]. Power ramps cause problems in the correct functioning of the grid, considering the installed capacity of PV generation since it is directly proportional to the magnitude of the change within the system [15]. The power ramps can be classified into ascending and descending ramp.

The reduction of the power generated within the PV systems leads to effects such as a decrease or increase in frequency, which can trigger the protection system case not being controlled immediately. Such disconnection of the electricity supply is undesirable as it leads to an interruption for consumers [16].

In the process where the continuous power is changed to alternating power by the PV systems, there is a reduction in the operating energy production, causing a voltage drop. To compensate for the voltage drop, it is necessary to generate reactive power to control the voltage within the process at the time of disturbances [17].

Due to the high penetration of renewable energies in some countries, the impact of the power ramp caused by PV systems began to be a point of study [18]–[21]. Some of the measures that regulate power ramps in some countries are presented in Table 1. However, the regulations regarding the power ramps are minimal.

Table 1. Power ramp regulations in some countries.

Country	Deviation Margin	Regulations
Germany	±10%/min	EON
Ireland	±10%/min	EirGrid
Puerto Rico	±10%/min	PREPA
Hawaii	2MW/min - 1MW/min	HECO

Different methods can be used to mitigate the power ramps and keep them within limits indicated by the regulations, as mentioned earlier. When implementing the strategies, the methods are dynamically implemented during the transition period. [22]. The advantage and limitations of the most used methods worldwide [23]–[26] for mitigating power ramps are presented in Table 2.

Table 2. Advantages and limitations of most used methods to mitigate power ramps.

Methods	Advantage	Limitations
Energy storage systems	Quick response when the controller requires them to act.	High economic investment.
An increase in the reserves of electrical power generated	Power reserves counteract deficits at critical moments.	Limited in the percentage of generation, and expanding that percentage requires a very high economic cost.
Active power reduction	Allows bidirectional control of the behavior of power ramps.	High economic costs.
Disconnecting loads	It gives authorization to the system to stabilize the appropriate parameters.	Does not supply continuity service.

Within the methods mentioned earlier, energy storage systems have presented the most significant advantages, such as grid stability, renewable energy reserves, and environmental protection [27], [28]. There are different energy storage systems [29]–[31], which are presented with advantages and limitations in Table 3.

Table 3. Advantages and Limitations of different types of energy storage systems.

Method	Advantage	Limitation
Mechanical	Rapid dynamic response.	Energy capacity is limited to the size and dimensions of the storage equipment.
Battery-based	Supplies the necessary power reliably; Long service life.	The capacity will be based on the type of material used.
Thermal	Response of great capacity, effectively supplying the high demands.	It has a delayed response time.

While it is true that each of the methods for the solution the power ramp has its advantages and disadvantages, the literature verifies how the authors have a marked tendency to use battery bank for the solution of the problem [32]-[33].

4   Case Study

4.1   General Description

As a case study, the Girasol solar park in San Cristobal, Dominican Republic, was selected (see Fig. 1) as the largest photovoltaic power plant (Girasol Solar Park) in the country and the Antilles. Property of the Empresa Generadora de Electricidad de Haina, S.A. (EGE HAINA) The solar park has a surface of 220 hectares and 268,200 panels of 445/450 Wp. Contains 268,200 photovoltaic modules, 8,490 Strings, 532 In Parallel Connection, 28 power inverters. It has a total installed capacity of 120 MWp with an annual production of 240,000 MWh. It has a solar position tracker system that rotates 104º over 12 hours to use the sun better. Fig. 2 presents the interconnection of the photovoltaic park and the national grid.

Fig. 1. Girasol solar park view. Source: Egehaina.
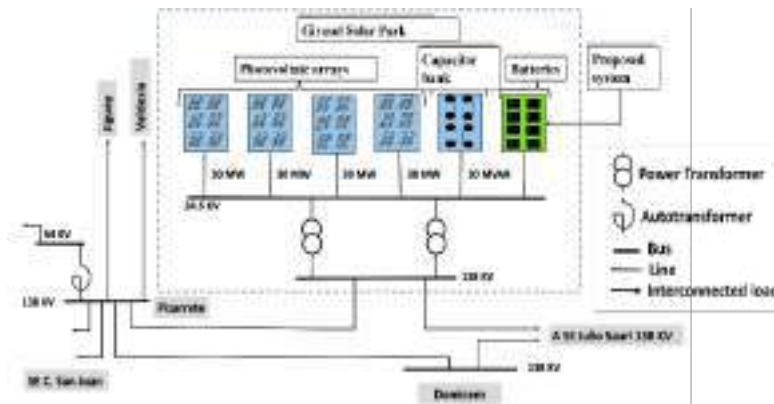
Fig. 2. Diagram of the solar park interconnected to the national grid.

Fig. 3 shows the interconnection diagram of the southern area of the interconnected electrical system and the Girasol photovoltaic park.
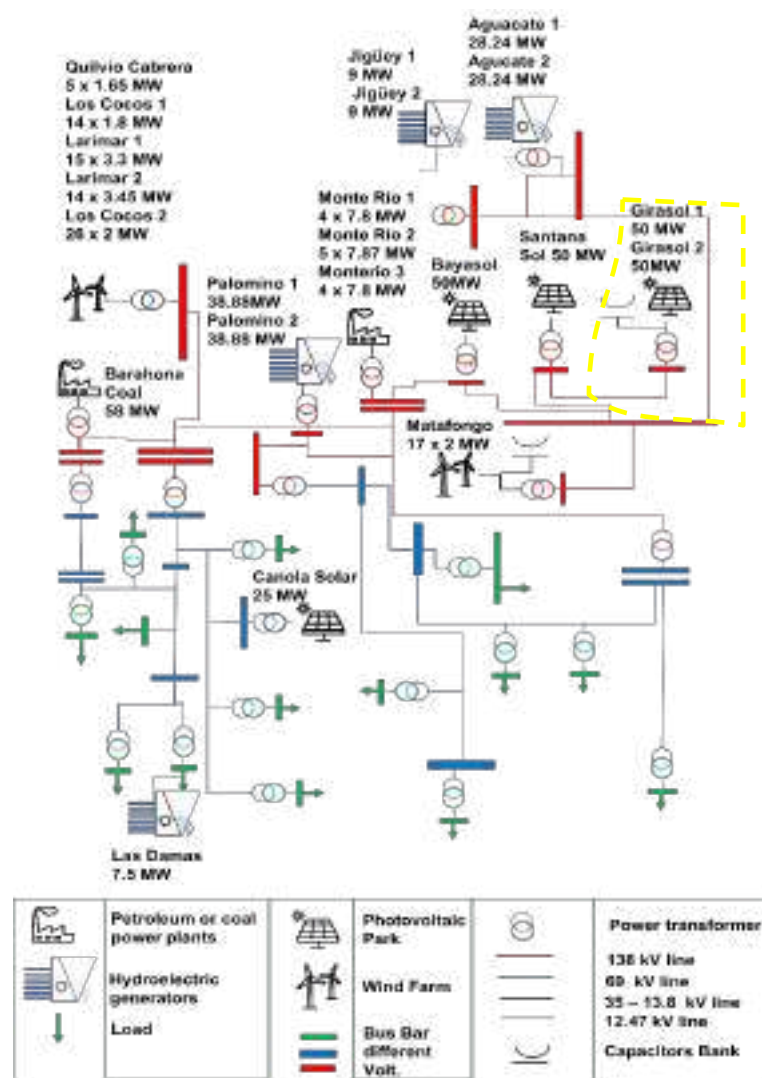
Fig. 3. Diagram of the southern zone of SENI

4.2   Ramps Statistics

The groups of ramps that were analyzed to determine the capacity of the storage system to be used for the Girasol solar park can be seen in Table 4. 92.4% of the ramps range from -10 to 10 MW/min. To determine the energy capacity of the storage system that the Girasol solar park needs to implement, the regulations of Puerto Rico were considered due to its similar conditions to those of the Dominican Republic. Puerto Rico regulations establish a minimum ramp change of +/- 10MW/min, so the solar system must maintain 10MW power close to its rated capacity.

Table 4. Statistics of the average number of power ramps in the Girasol Solar Park. Data registered in the energy control center of the Empresa de Transmisión Eléctrica Dominicana (ETED). Data Collection 1/11/2021 to 30/06/2022 time-averaged to 10 second intervals.

Ramps Groups (MW/min)	Number of Events	Total Registered Events (%)
-50 to -40	10	0.02
-40 to -30	69	0.11
-30 to -20	384	0.61
-20 to -10	1940	3.12
-10 to 0	26969	43.15
0 to 10	30800	49.28
10 to 20	1800	2.99
20 to 30	377	0.60
30 to 40	69	0.11
40 to 50	11	0.02

Equation (1) from [21] was used to determine the storage system's capacity. The nominal capacity of the park is 100 MW, assuming that 10% of the capacity is what can be reduced at any moment. Considering that the minimum allowed power drop is 50MW according to regulations of other countries. A 40 MW storage system would be necessary to attenuate the power ramp.

$$P_{Grid}(t) = P_{Grid}(t - \Delta t) + min[P_{PV}(t) - P_{PV}(t - \Delta t), \Delta P_{RR}] \qquad (1)$$

$$P_{BAT}(t) = 90\ MW - 50\ MW$$

$$P_{BAT}(t) = 40\ MW$$

Where,
PGrid(t) = Minimum power of the previous case,
ΔP_{RR} = Photovoltaic power limited to the maximum allowable variation,
PPV = Output power of the photovoltaic plant at a given moment,

Δt = Rate of time of the series of production data analyzed,
PBAT = Battery power

5 Simulation

The DIgSILENT computer tool was used to simulate the behavior of the photovoltaic park, the proposed storage system, and the flow of energy in the grid due to its great capacity for analysis before large nodes within the same system. In addition, it allows power variations in the desired periods, achieving a perfect simulation of the incidents or factors that cause power ramps. Table 5 presents the leading software used for this type of analysis:

Table 5. and disadvantages of different software according to some authors.

Autor	Software	Advantages	Limitations
[34]	DIgSILENT	Analyzes large power systems without any difficulty	High runtime in simulations
[34]	DIgSILENT	Allows manipulation of existing blocks	Limitations when simulating rotary machines
[35]	PSS/E	Allows project automation thanks to its scheduling	Difficult compression by an untrained user
[36]	PSS/E	Presents a simulation time compared to other software.	Little variety among modeled elements
[36]	Simulink	It gives the ease of modeling power systems	It is very slow from 1000 buses
[37]	Simulink	Gives the option of communication between different software	This does not allow carrying out a study of load flow

5.1 Scenario Process

The Organismo Coordinador del Sistema Eléctrico Nacional Interconectado de la República Dominicana (OC-SENI) gives access on its website to the diagrams of the Dominican electrical system in the DIgSILENT Power Factory software, so the simulations were carried out with this data, adapting a battery system in the Gira-sol solar park for the simulation in question.

The simulations of the situation of the Girasol solar park with the storage system and without it were carried out according to the regulatory standards of power ramps in photovoltaic systems, which Puerto Rico (PREPA) established for its photovoltaic

systems, this is because in the Dominican Republic it does not have a regulation of these.

Scenarios simulated (11:00 am – 2:00 pm) where exist much solar generation in the park. Therefore, the inertia of the electrical grid decreases since solar generation displaces conventional generation machines (gas and steam turbines), which produces variations in the system's frequency. The data on the power ramps were obtained from the Energy Control Center (CCE) database of the Dominica Electric Transmission Company ETED; power plant dispatches were simulated from the Girasol solar park with and without batteries to see how the frequency varies in the system.

6   Results and Discussion

Ten scenarios with different conditions regarding the ramp's power, the ramp, the direction of the ramp, and whether the photovoltaic system has BESS were performed. Each of these scenarios presented how the ramp power affected the frequency's stability, as seen in Table 6.

Table 6. Simulated Power Ramp Scenarios.

Scenario	Ramp (MW)	Ramp Direction	BESS	BESS Capacity (MW)	Frequency (Hz)
1	10	Descent	OK	40	60
2	20	Descent	OK	40	60
3	30	Descent	OK	40	60
4	46.7	Descent	-	-	59.85
5	46.7	Descent	OK	40	59.92
6	47	Descent	-	-	59.87
7	50	Descent	OK	40	59.95
8	60	Descent	OK	40	59.97
9	80	Descent	OK	40	59.95

The development of the simulations showed that with a power ramp of 46.7 MW, the system experiences a frequency deviation with values below 59.90 Hz, representing the action of the primary frequency regulation and the other regulation steps to stabilize the frequency values to their appropriate range. Below are some scenarios to see the power ramp with or without a battery, three scenarios were selected that generalize the system condition.

Scenario 3. It shows a decrease or decrease in the generation of 30 MW in the Girasol solar park (see Fig. 4). The frequency does not perceive any effect since it has a storage system, and 30 MW is less than the maximum power of the battery. The genera-

tion drop is below what is being solved by the battery, so this variation becomes imperceptible to the frequency, remaining at its nominal value, 60 Hz.
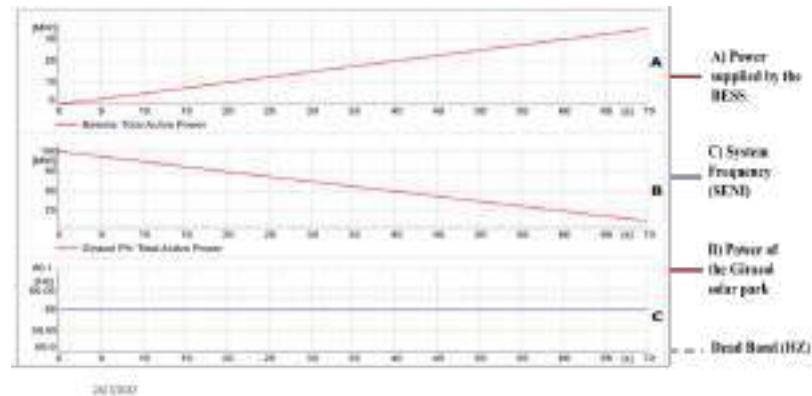

Fig. 4. Power Ramp of 30 MW with the energy storage system.

Scenario 4. It shows the frequency behavior at the time of a sudden drop of 46.7 MW in the system (see Fig. 5). It is well observed that the initial frequency of 60 Hz presented a deviation of descent up to 59.84283 Hz. The frequency drop occurred in an estimated time of 70 seconds.
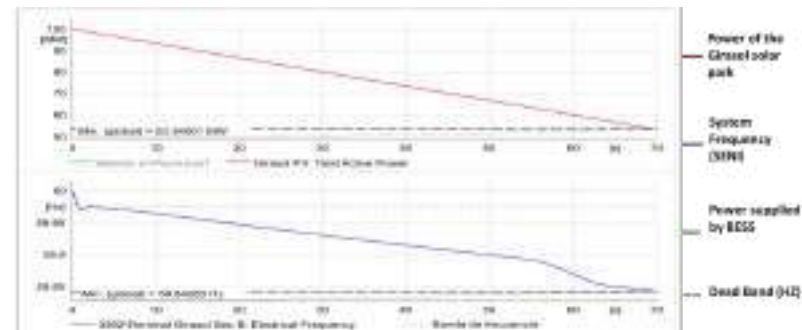

Fig. 5. Power Ramp of 46.7 MW without an energy storage system.

Scenario 9. It shows a generation increase of 50 MW after the photovoltaic system has experienced a power decrease in a generation (see Fig. 6). At first, it is observed that before this event, the batteries are subjected to curability, reaching their maximum point of 40 MW in 97.95 seconds. During this time, the frequency begins to change from the output of service of the battery product has reached its maximum charge point. The storage system will try to absorb the most significant amount of energy for its load. However, when it comes to its limit of approximately 50 seconds, it will let the power continue to rise.
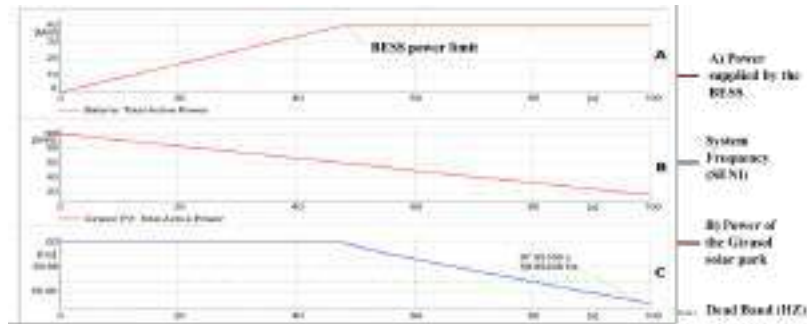
Fig. 6. 50 MW incremental power ramp with the storage system.

6.1   Cost

Based on the prices of different storage systems, when checking them on their commercial systems, a weighted initial and variable cost is projected as a capital cost of $37,577,490 operation/maintenance annual cost of $81,030.

The investment would be amortized according to the effects of the diversions of electricity generation through photovoltaic systems for the programmed generation. Similarly, this would reduce the cost of operating the electrical system due to the reduced dispatch of thermal power plants to supply the energy that was not provided every hour by photovoltaic sources.

7   Conclusion

Power ramps fluctuations of PV power output are produced by the fluctuations of the irradiance receive in the Panel. There are different types of methods for the attenuation of power ramps. The storage system begins to gain more ground for regulating power ramps. Due to the response time being more dynamic to disturbances that can occur in the design, this type of technology is experiencing a price reduction in the Levelized Cost of Energy due to the development of new materials used for chemical storage.

For more integration of solar photovoltaic technologies in the grid and considering that the changes in the power ramps created disturbances that affected the grid's stability. The development of power ramp policies and regulations in photovoltaic systems connected to the grid from the Dominican Republic o another country with island characteristics that are not interconnected to other electrical networks must be developed.

After analyzing the different scenarios, it was possible to visualize that a battery bank with a capacity of 40 MW is ideal for solving the problem because it can thoroughly cushion the ramps up and down in the Girasol solar park. The results of the simulations showed that when a ramp of power is presented without BESS, the fre-

quency experiences a deviation with values less than 59.90 Hz, which, if several solar parks experience these changes, can affect the system's stability.

In future works, economic studies must be carried out on the incentives and penalties for installing the battery bank in PV systems connected to the grid under different conditions, in the case of the Dominican Republic. These studies allow the development of regulations to regulate the renewable electricity market.

Acknowledgment

References

1. Deloitte Development LLC, "Renewables (em)power smart cities," Deloitte Insights, 2019.
2. J. L. Paixao, A. R. Abaide, and P. G. A. Filho, "Impact evaluation of the photovoltaic generation input on a concessionaire's network," *SBSE 2018 - 7th Brazilian Electr. Syst. Symp.*, pp. 1–6, Jun. 2018, doi: 10.1109/SBSE.2018.8395937.
3. H. Awijen, F. Belaïd, Y. Ben Zaied, N. Hussain, and B. Ben Lahouel, "Renewable energy deployment in the MENA region: Does innovation matter?," *Technol. Forecast. Soc. Change*, vol. 179, p. 121633, Jun. 2022, doi: 10.1016/J.TECHFORE.2022.121633.
4. P. A. Juá Stecanella, D. Vieira, M. V. Leite Vasconcelos, and A. L. de Ferreira Filho, "Statistical analysis of photovoltaic distributed generation penetration impacts on a utility containing hundreds of feeders," *IEEE Access*, vol. 8, pp. 175009–175019, 2020, doi: 10.1109/ACCESS.2020.3024115.
5. L. R. Visser, E. M. B. Schuurmans, T. A. AlSkaif, H. A. Fidder, A. M. van Voorden, and W. G. J. H. M. van Sark, "Regulation strategies for mitigating voltage fluctuations induced by photovoltaic solar systems in an urban low voltage grid," *Int. J. Electr. Power Energy Syst.*, vol. 137, p. 107695, May 2022, doi: 10.1016/J.IJEPES.2021.107695.
6. A. Atif and M. Khalid, "Saviztky-Golay Filtering for Solar Power Smoothing and Ramp Rate Reduction Based on Controlled Battery Energy Storage," *IEEE Access*, vol. 8, pp. 33806–33817, 2020, doi: 10.1109/ACCESS.2020.2973036.
7. Q. Peng, "Coordination of Virtual Inertia Control and Frequency Damping in PV Systems for Optimal Frequency Support," *CPSS Trans. Power Electron. Appl.*, vol. 5, no. 4, pp. 305–316, Dec. 2020, doi: 10.24295/CPSSTPEA.2020.00025.
8. H. Hafdaoui, E. A. K. Boudjelthia, A. Chahtou, S. Bouchakour, and N. Belhaouas, "Analyzing the performance of photovoltaic systems using support vector machine classifier," *Sustain. Energy, Grids Networks*, vol. 29, p. 100592, Mar. 2022, doi:

10.1016/J.SEGAN.2021.100592.

9.   X. Li and S. Wang, "A review on energy management, operation control and application methods for grid battery energy storage systems," *CSEE J. Power Energy Syst.*, vol. 7, no. 5, pp. 1026–1040, Jun. 2019, doi: 10.17775/CSEEJPES.2019.00160.

10.   L. P. Sampaio, P. J. S. Costa, and S. A. O. da Silva, "Modified zeta inverter intended for single-phase grid-tied photovoltaic system," *Sustain. Energy Technol. Assessments*, vol. 52, p. 102076, Aug. 2022, doi: 10.1016/J.SETA.2022.102076.

11.   P. A. Anju and B. J. Mampilly, "Voltage regulation with smart loads in distribution system under high penetration of renewable energy," *2018 Int. Conf. Control. Power, Commun. Comput. Technol. ICCPCCT 2018*, pp. 512–518, Dec. 2018, doi: 10.1109/ICCPCCT.2018.8574284.

12.   J. Ma, H. Ye, Z. Li, P. Han, and X. Wang, "Design and Application of a Photovoltaic-Energy Storage Joint System with Active Frequency Regulation Capability," *Proc. 15th IEEE Conf. Ind. Electron. Appl. ICIEA 2020*, pp. 1193–1197, Nov. 2020, doi: 10.1109/ICIEA48937.2020.9248270.

13.   R. B. Bollipo, S. Mikkili, and P. K. Bonthagorla, "Hybrid, optimization, intelligent and classical PV MPPT techniques: Review," *CSEE J. Power Energy Syst.*, vol. 7, no. 1, pp. 9–33, Jan. 2020, doi: 10.17775/CSEEJPES.2019.02720.

14.   A. Ali *et al.*, "Investigation of MPPT Techniques under Uniform and Non-Uniform Solar Irradiation Condition-A Retrospection," *IEEE Access*, vol. 8, pp. 127368–127392, 2020, doi: 10.1109/ACCESS.2020.3007710.

15.   S. Sreekumar, S. Yamujala, K. C. Sharma, R. Bhakar, S. P. Simon, and A. S. Rana, "Flexible Ramp Products: A solution to enhance power system flexibility," *Renew. Sustain. Energy Rev.*, vol. 162, p. 112429, Jul. 2022, doi: 10.1016/J.RSER.2022.112429.

16.   E. A. Voloshin, A. A. Voloshin, R. S. Maksimov, D. S. Bondar, and S. S. Usachev, "Development the algorithm for control the consumed load due to the combined action of adaptive underfrequency load shedding and changing the power frequency," *2019 2nd Int. Youth Sci. Tech. Conf. Relay Prot. Autom. RPA 2019*, Oct. 2019, doi: 10.1109/RPA47751.2019.8958215.

17.   A. Makibar, L. Narvarte, and E. Lorenzo, "Contributions to the size reduction of a battery used for PV power ramp rate control," *Sol. Energy*, vol. 230, pp. 435–448, Dec. 2021, doi: 10.1016/J.SOLENER.2021.10.047.

18.   M. S. Md Said and M. Z. Mohd Tohir, "Characterisation of thermal runaway behaviour of cylindrical lithium-ion battery using Accelerating Rate Calorimeter and oven heating," *Case Stud. Therm. Eng.*, vol. 28, p. 101474, Dec. 2021, doi: 10.1016/J.CSITE.2021.101474.

19.   M. Saleh, Y. Esa, and A. A. Mohamed, "Communication-Based Control for DC Microgrids," *IEEE Trans. Smart Grid*, vol. 10, no. 2, pp. 2180–2195, Mar. 2019, doi: 10.1109/TSG.2018.2791361.

20.   S. Maleki and M. T. Hagh, "Review of PV Power Ramp Rate Control Methods and Their Requirements," *SVU-International J. Eng. Sci. Appl.*, vol. 2, no. 2, pp. 14–25, 2021, doi: 10.21608/svusrc.2021.83458.1011.

21.   A. Makibar, L. Narvarte, and E. Lorenzo, "On the relation between battery size and PV power ramp rate limitation," *Sol. Energy*, vol. 142, pp. 182–193, 2017, doi:

https://doi.org/10.1016/j.solener.2016.11.039.

22. S. Sukumar, M. Marsadek, K. R. Agileswari, and H. Mokhlis, "Ramp-rate control smoothing methods to control output power fluctuations from solar photovoltaic (PV) sources—A review," *J. Energy Storage*, vol. 20, pp. 218–229, Dec. 2018, doi: 10.1016/J.EST.2018.09.013.

23. B.-I. Craciun, T. Kerekes, D. Sera, R. Teodorescu, and U. D. Annakkage, "Power Ramp Limitation Capabilities of Large PV Power Plants With Active Power Reserves," *IEEE Trans. Sustain. Energy*, vol. 8, no. 2, pp. 573–581, Apr. 2017, doi: 10.1109/TSTE.2016.2612121.

24. E. Garabitos Lara and F. Santos García, "Review on viability and implementation of residential PV-battery systems: Considering the case of Dominican Republic," *Energy Reports*, vol. 7, pp. 8868–8899, Nov. 2021, doi: 10.1016/J.EGYR.2021.11.208.

25. Z. Hongxia, T. Yuqing, and C. Deying, "Application of solar photovoltaic generation in the world," *MATEC Web Conf.*, vol. 108, p. 14006, May 2017, doi: 10.1051/MATECCONF/201710814006.

26. A. K. S. S. K. Sudhakar, "Solar energy policy of India: An overview," *CSEE J. Power Energy Syst.*, p. 14, 2020, doi: 10.17775/cseejpes.2020.03080.

27. N. Sabeh, "Rooftop Plant Production Systems in Urban Areas," in *Plant Factory*, T. Kozai, G. Niu, and M. Takagaki, Eds. San Diego: Elsevier, 2016, pp. 105–111.

28. E. Scolari, L. Reyes-Chamorro, F. Sossan, and M. Paolone, "A Comprehensive Assessment of the Short-Term Uncertainty of Grid-Connected PV Systems," *IEEE Trans. Sustain. Energy*, vol. 9, no. 3, pp. 1458–1467, Jul. 2018, doi: 10.1109/TSTE.2018.2789937.

29. Y. J. Chae and J. I. Lee, "Thermodynamic analysis of compressed and liquid carbon dioxide energy storage system integrated with steam cycle for flexible operation of thermal power plant," *Energy Convers. Manag.*, vol. 256, p. 115374, Mar. 2022, doi: 10.1016/J.ENCONMAN.2022.115374.

30. L. Changshi, "Reliable and precise evaluation energy-transfer and efficiency of super-capacitors," *Renew. Sustain. Energy Rev.*, vol. 151, p. 111566, Nov. 2021, doi: 10.1016/J.RSER.2021.111566.

31. J. W. Zhang, Y. H. Wang, G. C. Liu, and G. Z. Tian, "A review of control strategies for flywheel energy storage system and a case study with matrix converter," *Energy Reports*, vol. 8, pp. 3948–3963, Nov. 2022, doi: 10.1016/J.EGYR.2022.03.009.

32. C. G. Haba, "Monitoring photovoltaic parks for damage prevention and optimal operation," *2017 11th Int. Conf. Electromechanical Power Syst. SIELMEN 2017 - Proc.*, vol. 2017-January, pp. 321–326, Nov. 2017, doi: 10.1109/SIELMEN.2017.8123340.

33. V. Papadopoulos, J. Desmet, J. Knockaert, and C. Develder, "Improving the utilization factor of a PEM electrolyzer powered by a 15 MW PV park by combining wind power and battery storage – Feasibility study," *Int. J. Hydrogen Energy*, vol. 43, no. 34, pp. 16468–16478, Aug. 2018, doi: 10.1016/J.IJHYDENE.2018.07.069.

34. S. A. Shezan *et al.*, "Effective dispatch strategies assortment according to the effect of the operation for an islanded hybrid microgrid," *Energy Convers. Manag. X*, vol. 14, p. 100192, 2022, doi: https://doi.org/10.1016/j.ecmx.2022.100192.

35. H. Alipour and A. Ghadimi, "Optimization of lead-free perovskite solar cells in normal-

      structure with WO3 and water-free PEDOT: PSS composite for hole transport layer by SCAPS-1D simulation," *Opt. Mater. (Amst).*, vol. 120, p. 111432, 2021, doi: https://doi.org/10.1016/j.optmat.2021.111432.

36. S. Ullah, A. M. A. Haidar, and H. Zen, "Assessment of technical and financial benefits of AC and DC microgrids based on solar photovoltaic," *Electr. Eng.*, vol. 102, no. 3, pp. 1297–1310, 2020, doi: 10.1007/s00202-020-00950-7.

37. K. Y. Yap, J. M.-Y. Lim, and C. R. Sarimuthu, "sps," *Int. J. Electr. Power Energy Syst.*, vol. 132, p. 107180, 2021, doi: https://doi.org/10.1016/j.ijepes.2021.107180.

Solar energy integration to achieve the Net-Zero Standard in Educational Buildings.

Esteban Zalameal[1], Alfredo Ordoñez[1], Boris Orellana[1], Juan Hidalgo[1]

[1]Architecture and Urbanism Department, Cuenca University

ABSTRACT

In the near future it is essential that cities and buildings become energy neutral and fed with renewables in order to reach low impact sustainable cities. This is essential in developing countries where the largest increases in energy consumption are expected, but there are natural resources that allow Net Zero buildings. This research is an initial step towards analyzing the Net Zero feasibility in the Architecture Department buildings of the University of Cuenca, as a case sample of educational building located next to the equator and in the highlands of the Andes mountains. In this research we had just determined the photovoltaic (PV) potential to reach the actual energy requirement, to do so, we had virtually constructed the building facilities and obtained the building energy requirements, considering full power requirements measured before the COVID restrictions. We had determined, considering architectural restrictions, that the 88,6 % of the 2019 energy requirements could be solved with solar PV and the financial analysis also reveals that it is a profitable strategy. Next steps are determining the real performance of the PV technology, and measure the comfort levels, in order to foresee the total requirements, to reach the Net Zero Energy standard.

Keywords:
Net Zero Energy Buildings; Energy Efficiency; Solar PV; Educational Buildings.

INTRODUCTION

Cities consume about 65% of the energy human requirement, also promoting 70% of greenhouse gases and associated effects (IRENA, 2016). In Cuenca, Ecuador, the city where this research takes place, the massive introduction of energy efficiency and self-supply measures in urban areas is essential to reduce the impact and environmental degradation. These urban areas are located in Ecuador very next to the equator line, at medium altitude above sea level, in a valley between the Andes Mountain range (between 2300 m above sea level and 2700 m above sea level). This implies that despite being located in the torrid-tropical zone of the planet, there is no excessively hot climate, rather it is under a temperate climate, with few hours in specific days when the temperature could reach close to 30 º C (not depending on seasonal periods), and others when the temperature is close to 0 ºC, in the early morning for a few hours. This climate condition implies very particular urban and building energy requirements, where buildings and indoor spaces do not require heating and air conditioning systems. The analysis of this climate condition is very appropriate, considering that in the South America region, there are several cities under the similar condition as Cuenca, like Bogota or Quito, capital cities, but, there are several mid-size cities and countless small towns and populated areas, special implications that had been analyzed by the authors in previous research (Zalamea-león and Barragán-escandón, 2021).

Due to economic and population growth in developing countries located in South America, this is a region with the highest growth in energy requirements as a consequence, the energy consumption grew from 2,200 KBEP per year (thousands of barrels of oil equivalent) to more than 2,700 KBEP between 2009 and 2015 (Barragán-Escandón, 2018) showing an average 3% annual growth. The building sector around the world is essential to achieve energy neutral communities, reducing energy consumption as well as

environmental impact associated (Skaar *et al.*, 2018), in addition, it is considered that shortly, individual buildings and typologies will be where to focus to solve these concerns. The built environment as human creations could contribute also accordingly to their characteristics to contribute to energy requirements. Buildings can supply energy to cities and communities (Disch, 2010; Powerhouse co., 2020). For this purpose, it is very important to have a thorough knowledge of possibilities and technologies to achieve neutral and positive energy buildings locally (Net-Zero Buildings and Plus-Energy Buildings) which implies building that reach comfortable standards and that obtain energy from in site renewable sources, then architects and urban designers are key towards this goal (Wall *et al.*, 2012).

The design process of buildings in the early stages is very important to achieve high energy standards. The process also requires figuring out the reliability of tools for environmental indoor simulation and prediction of energy self-supply capabilities. To start firstly is required to determine the energy required to achieve any energy standard, then, it is required to consider different requirements to achieve the Net Zero Standard, in different locations and building typologies.

In Ecuador since 2018, there is a regulation extended to permit to building owners to install small distributed generation systems connected to the grid and achieve an energy self-supply in buildings through a micro-red connection in each power network(ARCONEL, 2018). This regulation that has been actualized recently (ARCERNNR, 2021a), this permits to achieve energy self-supply without power surpluses exceeding's recognition, but the surpluses remain after two years as credit, then the exceeding are reset in zero, the local utility never financially reward to the generator owner.

Any energy simulation from intermittent energy sources that is performed, no matter how accurate has been built, because of the different inputs and climate incidence and the model inaccuracy as a consequence of the impossibility to consider all the variable aspects, then the simulated results will differ in more or less from real measurements and outputs, but we do not know to what extent. Then, the only alternative is programing the simulation model as the best and precise definition following the real model. Then, to have the climate data for the simulation tool, the information must be taken on-site, to run the simulation afterward, so it is possible to determine the tool's accuracy.

Under the background mentioned, this work proposes a methodological process to evaluate in a bi-directional way, different predictive tools to figure out the feasibility of this kind of software to predict energy performance of power generation through PV technology, these compared to the reality. This research is the starting point for detecting the real accuracy of PV simulation tools, then, after the PV installation proposed in this research, there will be an instance when the installation will be monitored conjunctly with indoor thermal performance and real outdoor climate conditions, comparing simulations with real data. This research then is a basis for achieving energy-neutral buildings and then establishing the potential of existing simulation tools to detect the capacity of PV technology, which is the possibility of in site renewable in the equatorial region right now, considering the fast technology development and the higher potential compared to other alternatives. This meant in the long run that PV due to fast cost reduction and increased efficiency, the versatility of power to supply all building demands, it is now the best technology that prevails in regions with high solar incidence, surpassing other alternatives for in-site self-energy supply (International Energy Agency, 2021; Weiss and Spörk-Dür, 2019).

STATE OF THE ART

In the last two decades, several research approaches to decipher cities as energy sources by themselves had been performed. The research about urban energy capability started at the begging of this century with the methodological process to decipher irradiation availability on urban fabric surfaces, detecting the solar incidence and irradiation availability as Campagnon proposed with Radiance lightning software (Compagnon, 2004). Other different methodological processes had been implemented also to figure out the solar potential of an entire country or city, through satellite information as performed by Izquierdo and others in Spain, so determining the overall solar availability of entire regions (Izquierdo *et al.*, 2008). Then other

tools had been applied for detecting spatial fabric information and color and light automatic detection with image analysis (Bergamasco and Asinari, 2011; Travesset-Baro *et al.*, 2021) or roof geometrical construction (Araya-Muñoz *et al.*, 2013). Complementary, at the same time, other methodological processes for achieving Net-Zero energy buildings were performed in different climate conditions and different building typologies(Feng *et al.*, 2019; Voss and Musall, 2012).

But the background research does consider the detected energy requirements, for individual buildings, before the energy supply capability, it is required to implement low energy requirements, then energy self-supply capability. So there has been an evolution of building energy standards accordingly to energy efficiency and energy capability of self-supply, first as Passivhaus standard described in Germany at the end of the last century was emplaced, where certain basic requirements must be met to guarantee high interior comfort and, secondly, to lower energy consumption. To reach the standard, the criteria observed must consider air conditioning only with external airflow, solar passive capture or solar blockage if required, to limit the minimum temperature of the interior envelope surface, overheating, avoiding the risk of condensation effect, limit the interior airspeed so as not to have a negative sensorial effect, control air tightness reducing infiltration, and as a consequence of all these only passive strategies, to achieve a reduced energy consumption(Hatt *et al.*, 2012). Then, a second standard intends to trigger buildings that do not pollute with greenhouse gasses emanations as a result of their energy requirements (Net-Zero Buildings) and then buildings that generate as much energy as they consume for their operation requirements (Net-Zero Energy Buildings) (Torcellini *et al.*, 2006). The next standard corresponds to buildings with negative energy consumption or, to that extend, buildings with an energy capability to achieve an energy production higher than their energy requirement, called ads Plus Energy Buildings, a concept raised by Rolf Disch (Disch, 2010). This kind of buildings makes it possible to reach energy-neutral communities, by directing those surpluses that could satisfy other urban energy requirements (Amado *et al.*, 2017; Marique and Reiter, 2014). The recent energy standard for building corresponds to the Powerhouse buildings. This is theoretically the highest standard and corresponds to buildings with the capability to generate as much energy as that equivalent to that necessary throughout the entire life cycle required by the building. This implies that the building does integrate energy efficiency measures jointly with renewable energies that provide energy surpluses that allow recovering the energy required for the process of manufacturing materials, the energy required during the building process, and disposal of the building as I waste, considering a useful life of sixty years(Powerhouse co., 2020).

Each climate condition supposes different requirements for building performance accordingly to energy consumption. Then, local analysis is required for detecting the best strategies for achieving building energy self-sufficiency. Architectural and energy simulator tools include the capability to predict the environmental quality and energy requirement on buildings, through simulations in the architectural design process as predictive tools. Energy efficiency strategies as well clean energy technologies for self-supply, especially under equatorial middle altitude mountain context, where normally there is no heating or cooling requirement for indoor condition. Computers have incorporated tools for building and renewable energy integrated design. Currently, almost all architectural projects follow their design process in CADs (Computer Collaborated Design) through BIM (Building Information Modeling) which are specialized platforms for building design process (Ghaffarianhoseini *et al.*, 2017). In addition, there are specialized tools to perform simulations of comfort levels, which in the design process, foresee, among other aspects: passive and active strategies pertinent to being incorporated into a building. Before digital technology, the possibility of bioclimatic analysis in architecture was based on the background and knowledge of the designer, in an intuitive application of experience, mostly in a near context: Accessibility or solar blocking, ventilation, insulation levels or levels of tightness, acoustics, etc. Nevertheless, architects are less associated with energy simulation tools, and these are integrated in energy software as Ecodesigner and Design Builder, or specialized tools for only decipher renewables integrated to buildings as SAM software. Currently, the development of a more sophisticated computer processor, complemented with more powerful tools for building modeling, makes it possible to forecast comfort and energy parameters in response to climate, accordingly shape, materiality, setting regarding the environmental context and the overall performance of the building as consequence (García Álvarado and González, 2014).

However, simulations usually are not contrasted with reality. Comparisons have been made between types of software (Attia *et al.*, 2009; Horvat and Dubois, 2012; Lobos *et al.*, 2014) but not between software and real conditions, that is, a comparison with survey data obtained from a weather station. Therefore, using the equipment and capacities available at the Faculty of Architecture and Urbanism buildings (blocks built with a precise functional program, installed a weather station, environmental measurement equipment, modeling software) it is possible to carry out this research, simulating levels of environmental comfort and integration of renewable energies, in order to check the reliability of the software against reality.

MATHODOLOGICAL APPROACH

This research project proposes to determine the different parameters and requirements to get a university-level educational Net Zero Energy Building. To do so it is required to get the energy supply within-site renewables. Previously, extensive analysis had found that the main energy source available in Cuenca, Ecuador, to obtain in-site clean energy is solar by far (Barragán Escandon, 2018). This is a starting point considering operational energy consumptions that have been determined just before the COVID pandemic period, when these buildings were being used to their full capacity. The energy demands of the year 2019 were taken as the base energy requirement. This has been obtained through the energy bills that are publicly available thanks to the fact that the electrical utilities in Ecuador are state-owned, and the bills are freely available online (Empresa Eléctrica Regional Centro Sur C.A., 2022).

Then, according to the energy requirement, a PV system integrated into the buildings in the System Advisor Modeling software of the NREL is constructed accordingly (NREL, 2019). This free online software does have the capability of static simulations to determine the performance of specific solar products. In concordance con PV products available in Ecuador, and in concordance with an aspectual expression of PV products and its visual impact, Trinasolar Vertex S Black Structured PV Half Cell (Vertex DE09-05, 2022) has been considered to determine the required dimension to achieve a close PV requirement. The initial PV requirement is dimensioned considering a close demand next to 90 %, considering that actual regulation does not allow power exceeding the grid on annual consumption [9], so to approve the energy production do require this margin to ensure avoiding possible surpluses.

In concordance to the initial analysis, climate data from the NREL available for SAM is obtained, through a free download process. After performing a simple solar availability through a recent solar potential accordingly to slope and orientation, it is possible to predict initially the area requirement for solar surface required (Zalamea-león and Barragán-escandón, 2021). With the simulations, it has been observed that accordingly to orientation parameters, when the tilt is lower than 22 º, the power capability is only reduced maximum in 6,1 % compared to the best orientation compared with worst orientation (260,09 KWh/year by m^2 of PV installed orientated toward the east versus 244,41 KWh/year by m^2 of PV installed oriented toward West-South). Then, for the solar plant, it has been considered to set the PVs oriented towards the four cardinal orientations, to achieve higher power production in different hours in different arrays as described by Hachem (Hachem, 2012). To deploy the PV arrays towards different orientations in the future will be very useful to further research.

With these simulations of PV performance, the next work after the installation of the PV arrays and the connection to the grid is the reliability and deviation of the tools for simulation. It is foreseen that in the future climate information will be taken from the climatic station that is already installed and functional on the roofs of the buildings of the Faculty of Architecture. So, with this information, and PV power output and programing software for PV simulation like SAM or DesignBuilder software, that is available in the Cuenca University, it will be possible to perform a comparison of these tools with real performance of this solar equipment.

This research in part of overall research that will compare different levels of building indoor comfort parameters and in-site renewable production, comparing real data of performance with software simulations through virtual building construction in comparative precise best similarity with indoor spaces in the three blocks of the Faculty of Architecture and Urbanism (FAUC) of the Cuenca University, climatic files constructed from data taken from a climatic station located in the FAUC three-block building roof while the

levels of thermal comfort of 18 interior spaces of permanence for students (temperature and CO_2 detection). The climate data will be collected on-site when the PV plant will be generating power. These climate data afterward could be converted through Meteonorm software, in files .csv, .epw or .tm2 to run in the simulation software like Archicad's Ecodesigner (Graphisoft@, 2021) and Designbuilder software (Design Builder Software, 2020). This process is expected to detect real performance data for the requirements to achieve the Net Zero standard.

It is necessary to consider PV performance and the indoor environmental characteristics under an equatorial context. This particular context has been determined as a particular region with ideal characteristics to achieve a huge impact in self-energy supply for buildings and communities, the high irradiation, relative low seasonal fluctuations, and the minimal thermal requirements for achieving internal comfort, makes it possible to integrate and feed an important energy fraction of building and urban energy requirements with relatively reduced PV installations (Zambrano-Asanza *et al.*, 2019). So, detecting the energy capability of individual buildings typologies and introducing the technology observing its real performance is the first step to achieving neutral energy communities taking advantage of the enormous opportunity thanks to the excellent local conditions as explained previously.

RESULTS

ARCHITECTURAL AND ENERGY CAPABILITY INTEGRATION

The energy requirements for the Architecture Department buildings analyzed are determined by power requirements. These buildings contain spaces for permanence uses such as classrooms, laboratories, offices, and others, which due to the prolonged use of users require adequate habitability and comfort conditions, in these spaces, there are 3483.40 m^2; complementarily, there are circulation and complementary areas like bathrooms, storage, and support in general, they are also interior spaces, but with less demand in environmental comfort since they are not permanence spaces. In total, the buildings of the complex have 4418,16 m^2. Accordingly, to the climatic conditions described before, the building complex analyzed currently consumes only electricity. There is no heating or hot water requirements, so the energy demands correspond mainly to artificial lighting, electronic equipment such as computers, projectors, and support equipment for computational systems. In addition, the Architecture Department buildings includes a carpentry workshop that also requires electrical consumption for mechanical equipment for woodwork and wooden board cutting. Table 1 is expressed the energy consumption in 2019, just before the COVID pandemic event. This consumption implies a requirement index of 30.5 KWh/m^2 in a year, much lower than the measurements performed in other educational buildings under seasonal climate, where the energy requirement oscillates between 55 KWh /m^2 yearly to 195 KWh /m^2 yearly, depending if the climate corresponds to north or south Europe context (Marrone *et al.*, 2018). In this table, it is possible to observe that contrary to what is expected and happens in buildings located in seasonal locations, the power consumption increases during months with academic activity, without any correspondence to climate variations.

TABLE 1: Energy consumption and spent in power bill, in the School of Architecture of Cuenca University

Montly power bills ($)													
Utility Ac	Department	Jan	Feb	Mar	Apr	May	Jun	Jul	Aug	Sep	Oct	Nov	Dec	TOTAL
	Architecture													

Montly Power Consumption (kWh)	

Utility Ac	Department	Jan	Feb	Mar	Apr	May	Jun	Jul	Aug	Sep	Oct	Nov	Dec	TOTAL
	Architecture													
										KWh Average costo (Kwh) USD				

Then charging this consumption as expected demands in the SAM simulator software, we proceed to dimension the PV system required to reach 90% of a full year consumption as said before, to adjust to the approval norm of the local distribution utility.

In the SAM simulator, the integration of 228 PV units is found to achieve close to the required power output, deployed in the three built blocks accordingly to the roof availability as shown in Figure 1. In Figure 2 it is shown an aerial view of the PV arrangement on the roofs. To avoid the accumulation of dirt and dust, it is necessary to tilt the PVs, therefore they are placed with a 15-degree slope, which has been shown to minimally reduce production since the best theoretical performance next to the equator is horizontally to capture more direct solar incidence. Buy sloped arrangement maximizes cleaning due to the high and constant levels of rainfall in the area.

FIGURE 1: PV Arrangement of 228 PV units of 385 Wp deployed accordingly to roof availability
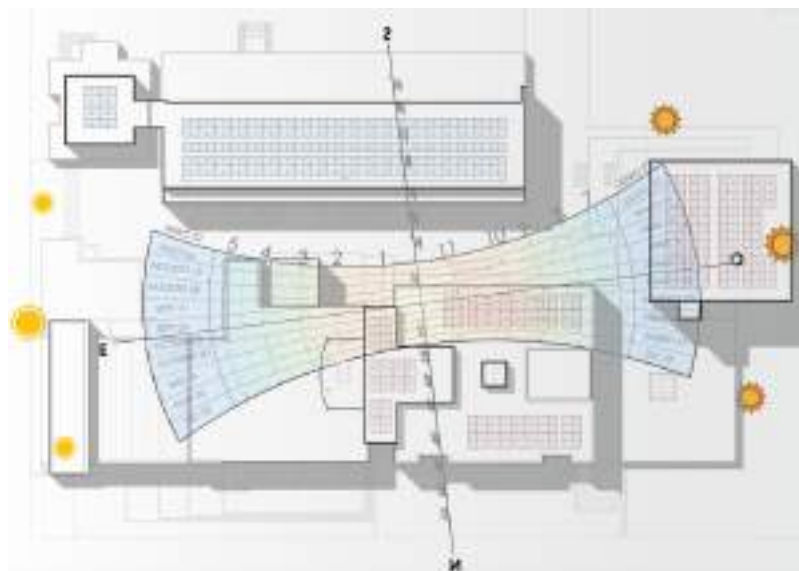
FIGURE 3: Aerial view of the PV deployment of 228 PV units of 385 Wp accordingly to architectural criteria

The Architecture Department buildings had been cataloged as "patrimonial value" so, any intervention must consider a low impact and be reversible intervention. In consequence, the PV arrangement has been performed considering under Kaan and Reijenga conceptualization (Kaan and Reijenga, 2004) accordingly to PV solar integration architectural integration guidelines, Under this concepts we had deployed the PV as trying to make invisible the PV array, from the ground perspective that has been which has been classified as Level 1, according to those authors. The PV arrays are visible from the sky, so the PV arrays are arranged symmetrically paired with each other in pairs, as well these had been arranged also symmetrically accordingly to the roof configuration. The PVs selected also are all black type, that fits better over the old-dark grey concrete roof, so the product selected is DE05-09 full black product from Trina solar (Vertex DE09-05, 2022). The arrangement of the PV arrays is close to the four cardinal points, with a 7 ° deviation, as a consequence of the deviation of the roofs and buildings. The energy output as consequence will be very close by the unit as if the PVs were exactly arranged facing the cardinal points directly. As a consequence of special availability and visual coupling, 60 PV units were arranged facing East, 60 West, 54 to North and 54 to South as observed in Figure 2.

PV POTENTIAL AND FINNANCIAL RESULTS

With the PV installation proposed, it is possible to reach 119563 KWh annually from 134954.64 KWh consumption 2019, corresponding to 88,6 %. This generation does oscillate monthly according to irradiation availability as well as the monthly consumption, in Figure 3 it can be observed. It shows that in the months with higher irradiation, on September or December 1000 KWh of exceeding's, in June and July with low irradiation, in addition to PV generation, about 5,000 to 4,000 KWh additional power from the grid are required, in months where these buildings are fully operational.

FIGURE 4: Monthly power consumption recorded in the year 2019 versus PV potential
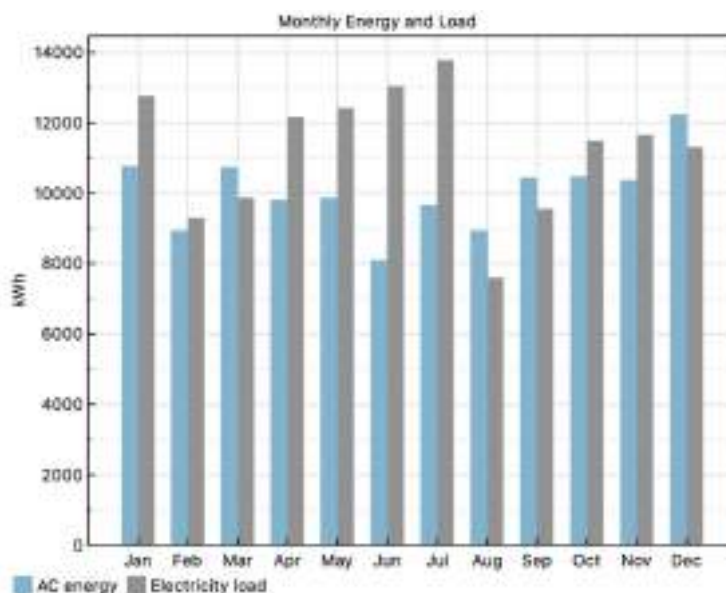
In addition, and as a complementary result of the SAM simulation, the software makes a financial estimate, to perform this, it has been considered and simulated the energy costs jointly with the costs of the PV installation. After a revision about the retail prices from a local installer (Heliostrategiaecuador, 2021), where the system is budgeted by the PV systems proposed, the solar products, and the planned arrangement system, a market cost of about 1.20 USD per Wp is obtained. This price and an annual efficiency reduction of 0.5% are also taken into account, typically reduction for PV technology along the 25 years of useful life. The financial results show a payback of 7.9 years period. Therefore, the result shows that a bit more than 17 years of "free" electricity is obtained as a net benefit. The price by KWh purchased from the utility by the university is 0.082 dollars, 25% less than the residential cost, this price is also 41.5% cheaper than the real estimated cost of production is around $ 0,098 KWh USD without considering that the Hydro had been built by public founding; then, when real prices including the generation system, it has been determined the real power retail price in the country about USD 0,14 in the region (ARCERNNR, 2021b). Then, solar energy self-supply meant savings to the public accounts, and an interesting alternative to all public buildings, not only to promote private investment in self-provisioning electricity, it also saves public spending. Figure 5 reflects the annual investment recovery. The overall cost of the PV plants is USD 115,150.00. This investment has a recovery period of 12,8 years if the electricity prices is maintained. But considering only a 1 % increase, very low as expected (It has been about 37 % annual average from 2014 until 2019 accordingly to world bank, from USD 0,079 average cost in 2014 to USD 0,119 en 2019), it would be reduced to 12,3 annual payback period, and it would be much higher if continue the recent price trends, affected by energy requirement and global warming effects.

FIGURE 5: Annual investment recovery, considering not power retail price increase.

CONCLUSION

This research is the first step to determine the requirements for reaching Net_zero Energy standard in the Architecture Department buildings of the Cuenca University, as a representative case of the educational building. Firstly, it has been determined that, in the 1076,35 m^2 of overall flat regular roof, in this available space accordingly to architectural impact, shadowing and maintenance aspects, it was possible to integrate 228 Vertex All Black Trinasolar Product, of 380 Wp each, which implies an available PV area for solar production of 438,3 m^2. In consequence, implies an available PV surface of 40,7 % occupancy rate. Also it expresses that in this typology in this context, according to the case analyzed, it is required about 0,01 m^2 with this per square meter of PV solar capture to get close to the energy requirement, with the PV efficiency proposed (around 20 %).

With this PV system proposed, it has the potential of covering the 88,6 % of the 2019 power consumption. This dimension supposes close to the overall energy requirement, considering there is not any type of fuel consumption currently.

The next step is to determine the interior comfort level. Even there are no HVAC systems integrated into this building, it is a requirement, and considering that in cities in this altitude and latitude, very favorable climatic conditions are observed that suppose the non-installation of this equipment, this also supposes that there are times when conditions out of thermal comfort conditions. To achieve the standard requirements will be performed in the next research. The overall 100 % reduction could be achieved by improving actual luminaries from fluorescent lightning to led lightning and analyzing complementary other equipment that could be a high requirement. Additionally, it is necessary to determine if there are moments outside the comfort requirements, then, if it is possible to integrate strategies to and closely analyze other equipment that makes it possible to reduce consumption, additionally, determine if there are moments outside the comfort requirements, if possible applying conditioning measures with passive strategies, to achieve the overall Net Zero Energy requirements, without including active energy consumer strategies.

NEXT RESEARCH

REFERENCES

Amado, M., Poggi, F., Amado, A.R. and Breu, S. (2017), "A cellular approach to Net-Zero energy cities", *Energies*, Vol. 10 No. 11, available at:https://doi.org/10.3390/en10111826.

Araya-Muñoz, D., Carvajal, D., Sáez-Carreño, A., Bensaid, S. and Soto-Márquez, E. (2013), "Assessing the solar potential of roofs in Valparaíso (Chile)", *Energy and Buildings*, Vol. 69, pp. 62–73.

ARCERNNR. (2021a), "Resolucion Nro. ARCERNNR 001/2021", *ARCERNNR*, available at: https://www.controlrecursosyenergia.gob.ec/wp-content/uploads/downloads/2021/03/Resolucion-ARCERNNR-001-2021.pdf (accessed 24 September 2021).

ARCERNNR. (2021b), *ACTUALIZACIÓN DEL ANÁLISIS Y ELÉCTRICA APROBADO CON PERIODO : ENERO ECONÓMICA Y TARIFAS DEL SECTOR ELÉCTRICO*, available at: https://www.controlrecursosyenergia.gob.ec/wp-content/uploads/downloads/2021/07/informe_actualización_análisis_costos_spee_2021_aprobada.pdf.

ARCONEL. (2018), "Resolución Nor. ARCONEL -042/18", *ARCONEL*.

Attia, S., Beltrán, L., De Herde, A. and Hensen, J. (2009), *"ARCHITECT FRIENDLY": A COMPARISON OF TEN DIFFERENT BUILDING PERFORMANCE SIMULATION TOOLS.*

Barragán-Escandón, E. (2018), *EL AUTOABASTECIMIENTO ENERGÉTICO EN LOS PAÍSES EN VÍAS DE DESARROLLO EN EL MARCO DEL METABOLISMO URBANO: CASO CUENCA,*

ECUADOR, Universidad de jaen, available at: http://ruja.ujaen.es/handle/10953/936.

Barragán Escandon, A. (2018), *EL AUTOABASTECIMIENTO ENERGÉTICO EN LOS PAÍSES EN VÍAS DE DESARROLLO EN EL MARCO DEL METABOLISMO URBANO: CASO CUENCA, ECUADOR*, Universidad de Jaén, available at: http://ruja.ujaen.es/handle/10953/936.

Bergamasco, L. and Asinari, P. (2011), "Scalable methodology for the photovoltaic solar energy potential assessment based on available roof surface area: Further improvements by ortho-image analysis and application to Turin (Italy)", *Solar Energy*, Elsevier Ltd, Vol. 85 No. 11, pp. 2741–2756.

Compagnon, R. (2004), "Solar and daylight availability in the urban fabric", *Energy and Buildings*, Vol. 36, pp. 321–328.

Design Builder Software. (2020), "DesignBuilder".

Disch, R. (2010), "PlusEnergy - The Manifesto".

Empresa Eléctrica Regional Centro Sur C.A. (2022), "Consulta y pago de Planillas – Centrosur", *CENTROSUR*, available at: https://www.centrosur.gob.ec/consulta-de-planillas/ (accessed 4 January 2022).

Feng, W., Zhang, Q., Ji, H., Wang, R., Zhou, N., Ye, Q., Hao, B., *et al.* (2019), "A review of net zero energy buildings in hot and humid climates: Experience learned from 34 case study buildings", *Renewable and Sustainable Energy Reviews*, Elsevier Ltd, Vol. 114 No. July, p. 109303.

García Álvarado, R. and González, A. (2014), "Condiciones de forma y desempeño energético de viviendas unifamiliares en el centro-sur de Chile", *Revista INVI*, Universidad de Chile. Facultad de Arquitectura y Urbanismo. Instituto de la Vivienda, Vol. 29 No. 80, pp. 111–141.

Ghaffarianhoseini, A.A., Tookey, J., Ghaffarianhoseini, A.A., Naismith, N., Azhar, S., Efimova, O. and Raahemifar, K. (2017), "Building Information Modelling (BIM) uptake: Clear benefits, understanding its implementation, risks and challenges", *Renewable and Sustainable Energy Reviews*, Vol. 75 No. December 2016, pp. 1046–1053.

Graphisoft@. (2021), "Archicad 24", available at: https://www.graphisoft.es/archicad/ (accessed 21 February 2021).

Hachem, C. (2012), *Investigation of Design Parameters for Increased Solar Potential of Dwellings and Neighborhoods*, Concordia University.

Hatt, T., Saelzer, G., Hempel, R. and Gerber, A. (2012), "Alto confort interior con mínimo consumo energético a partir de la implementación del estándar ' Passivhaus ' en", pp. 123–134.

Heliostrategiaecuador. (2021), "La energía solar a tu alcance", available at: https://heliostrategiaecuador.com (accessed 18 December 2021).

Horvat, M. and Dubois, M.C. (2012), "Tools and methods for solar design - An overview of IEA SHC Task 41, Subtask B", *Energy Procedia*, The Authors, Vol. 30, pp. 1120–1130.

International Energy Agency. (2021), *Renewables*, Paris, available at: https://iea.blob.core.windows.net/assets/5ae32253-7409-4f9a-a91d-1493ffb9777a/Renewables2021-Analysisandforecastto2026.pdf.

IRENA. (2016), *Renewable Energy in Cities*, Abu Dhabi, available at: http://www.irena.org/-/media/Files/IRENA/Agency/Publication/2016/IRENA_Renewable_Energy_in_Cities_2016.pdf.

Izquierdo, S., Rodrigues, M. and Fueyo, N. (2008), "A method for estimating the geographical distribution of the available roof surface area for large-scale photovoltaic energy-potential evaluations", *Solar Energy*, Vol. 82 No. 10, pp. 929–939.

Kaan, H. and Reijenga, T. (2004), "Photovoltaics in an architectural context", *Progress in Photovoltaics: Research and Applications*, Vol. 12 No. 6, pp. 395–408.

Lobos, D., Wandersleben, G. and Castillo, L.S. (2014), "Mapeo de Interoperabilidad entre BIM y BPS Software (Simulación Energética) para Chile Mapping the Interoperability between BIM and Energy Simulation Software for Chile", Vol. 1 No. June 2016, available at:https://doi.org/10.5151/despro-sigradi2013-00.

Marique, A.-F. and Reiter, S. (2014), "A simplified framework to assess the feasibility of zero-energy at the neighbourhood/community scale", *Energy and Buildings*, Vol. 82, pp. 114–122.

Marrone, P., Gori, P., Asdrubali, F., Evangelisti, L., Calcagnini, L. and Grazieschi, G. (2018), "Energy benchmarking in educational buildings through cluster analysis of energy retrofitting", *Energies*, Vol. 11 No. 3, pp. 1–20.

NREL. (2019), "System Advisor Model", *U.S. Department of Energy*, Golden, CO, available at: https://sam.nrel.gov (accessed 12 June 2018).

Powerhouse co. (2020), "Powerhouse Brattørkaia", available at: https://www.powerhouse.no/en/about-us/ (accessed 23 April 2021).

Skaar, C., Labonnote, N. and Gradeci, K. (2018), "From Zero Emission Buildings (ZEB) to

Zero Emission Neighbourhoods (ZEN): A Mapping Review of Algorithm-Based LCA", *Sustainability*, Vol. 10 No. 7, p. 2405.

Torcellini, P., Pless, S., Deru, M. and Crawley, D. (2006), "Zero Energy Buildings: A Critical Look at the Definition", *ACEEE Summer Study Pacific Grove*, p. 15.

Travesset-Baro, O., Vilella, M. and Borges, P. (2021), "Hacia la autosuficiencia energética en las ciudades. análisis del potencial solar fotovoltaico a escala urbana en el Principado de Andorra", *CienciAmérica*, Vol. 10 No. 3, p. 25.

Vertex DE09-05. (2022), "Trinasolar", *Trinasolar Vertex S*, available at: https://www.trinasolar.com/es/product/VERTEX-DE09.05 (accessed 4 January 2022).

Voss, K. and Musall, E. (2012), "Net zero energy buildings: International projects of carbon neutrality in buildings", edited by Hellsterm, C., Ahrend, K. and Rackwitz, J., DETAIL Green Books, Munich, December.

Wall, M., Munari Probst, M.C., Roecker, C., Dubois, M.C., Horvat, M., Jørgensen, O.B. and Kappel, K. (2012), "Achieving solar energy in architecture - IEA SHC Task 41", *Energy Procedia*, Elsevier B.V., Vol. 30, pp. 1250–1260.

Weiss, W. and Spörk-Dür, M. (2019), *Solar Heat Worldwide. Global Market Development and Trends in 2018*, *Solar Heat Worldwide Report*, Vol. 1, available at: http://www.iea-shc.org/solar-heat-worldwide.

Zalamea-león, E. and Barragán-escandón, A. (2021), *Arquitectura, Sol y Energía*, 1st ed., Cuenca, available at: https://dialnet.unirioja.es/servlet/libro?codigo=850885.

Zambrano-Asanza, S., Zalamea-León, E.F., Barragán-Escandón, A., Parra-González, D., Barragán-Escandón, E.A. and Parra-González, A. (2019), "Urban photovoltaic potential estimation based on architectural conditions, production-demand matching, storage and the incorporation of new eco-efficient loads", *Renewable Energy*, Elsevier Ltd, Vol. 142, pp. 224–238.

ACKNOWLEDGEMENTS

Partial photoluminescence imaging of silicon solar cells

Alberto Redondo Plaza [1] [0000-0002-2109-5614], Víctor Alonso Gómez [1] [0000-0001-5107-4892], and Luis Hernández Callejo [1] [0000-0002-8822-2948]

[1] Universidad de Valladolid, Campus Universitario Duques de Soria, 42004 Soria, Spain.
A.R.P. alberredon@gmail.com
V.A.G. victor.alonso.gomez@uva.es
L.H.C. luis.hernandez.callejo@uva.es

Abstract: Solar energy is one of the main renewable sources that could improve the sustainability of a city. Here, solar module inspection techniques play an important role in order to detect several failures that appear throughout the photovoltaic module lifespan. One of the most used and useful techniques is luminescence, which is based on silicon emission capture. The present article shows a luminescence technique called partial photoluminescence. It is based on lighting one region of the solar cell and capturing the luminescence signal in the rest of the area. This allows capturing the luminescence emission in a dark environment, which is advantageous because the luminescence emission is much lower than solar radiation. The partial photoluminescence images have a similar quality to conventional electroluminescence images, although partial photoluminescence images require higher exposure times. The technique has been implemented in the laboratory. Nevertheless, it could be adapted in order to achieve solar module images in the field using sunlight as the excitation source.

Keywords: Photovoltaic, Inspection techniques, Electroluminescence and Photoluminescence

1 Introduction

Since the beginning of the century, the population that lives in urban areas has increased considerably, forecasting that more than 2.5 billion people will live in urban areas by 2050 [1]. That means that the growth of energy consumption in the cities that will lead to different challenges related to the city's sustainability. Here city-integrated renewable energy could increase energy independence and reduce greenhouse emissions in cities, transforming urban environments into sustainable and self-sufficient places.

Solar energy is one of the most important sources that cities could use due to its low cost, facility installation, and great potential. City-integrated photovoltaics has the potential of satisfying much of the city's electricity demand, being able to generate more than 60% [1] of the electrical needs.

One of the main objectives of solar energy research and development is a continuous cost reduction that allows solar energy to be competitive against fossil fuels. Therefore, maintenance plays an important role in solar energy [2]. The most used inspection and

characterization techniques for photovoltaic field applications are visual inspections, current-voltage measures, thermography imaging, and luminescence imaging [3]. Those techniques can detect several failures that appear throughout the solar module lifespan.

Luminescence imaging is a technique that allows the characterization and inspection of silicon samples, an element by which most commercial photovoltaic cells are manufactured. This technique is based on the silicon electromagnetic radiation capture, getting images that show high added value information about the solar cell performance. Luminescence images are a great tool for fault detection in photovoltaic modules such as cracks, microcracks, finger failures, potential induced degradation (PID), bypass diode failure, mechanical load failures, humidity corrosion, shunt faults, or series resistance failures [3].

The luminescence radiation can be generated by current injection in the photovoltaic module (Electroluminescence) or an optical excitation with a proper light source (Photoluminescence). Moreover, luminescence radiation has an emission peak at 1150 nm and can be captured with two different varieties of sensors: the Charged Coupled Device (CCD) and the Complementary Metal Oxide Semiconductor (CMOS) [4].

The intensity of luminescence emission is much less than the intensity of the solar emission, hindering image acquisition in high-irradiance environments. Therefore, luminescence images have traditionally been taken at night, which is not optimal from a plant operational point of view. To make possible electroluminescence (EL) and photoluminescence (PL) with high irradiance levels possible, a bias switching method has been developed [5]. This method is based on the acquisition of a couple of pictures where the luminesce emission is high and null respectively. Then a proper picture subtraction allows the removal of the background signal and obtains pictures that only show the luminescence emission.

Another disadvantage of the luminescence technique is the need for an external energy source like a power supply in EL or a lighting device in PL. However, solar power plants may have bidirectional inverters [6] that allow the current injection in the photovoltaic array, leading to the EL effect. On the other hand, PL images can be generated using an excitation source such as sunlight [7]. Furthermore, a sophisticated method called DaySy [8] (Day Light Luminescence System Testing) was presented which enables EL and PL solar modules characterization in bright daylight.

Another possibility in luminescence is the non-homogeneous lighting techniques, where only a fraction of the solar cell is illuminated [9]–[11]. Those kinds of PL images may differ from conventional PL images with uniform illumination [12] because lateral currents appear in partial illumination. When non-homogeneous illuminated PL images are interpreted, it must consider the effect of those lateral currents as well as the relative position of the solar cell and the illuminated and captured area. Nonetheless, those kinds of techniques, especially line scan imaging [9], [10], are useful to detect broken fingers or series resistance failures, being more accurate than conventional EL and PL images. Line scan imaging is used by manufacturers for modules fault detections and characterization. This technique is based on a line scan camera, in which the sensor is reduced to a single line of pixels. The illumination source for excitation can also be reduced to a line. One of the main advantages of PL line scan imaging is that it avoids electrical

contacts, something that can increases complexity, risk of mechanical damage and can have a negative impact on production throughput.

When the excitation light is the focus in one region of the solar cell, the conductor structures allow the induced voltage spreads throughout the cell, leading photoluminescence effect on the entire surface of the solar cell. The technique shown in the present paper is based on this effect. So, half of the solar cell is illuminated while the PL emission in the other half is captured in a dark environment, avoiding the use of algorithms for the excitation light subtraction and the need of a line scan camera. The second section of the paper shows the implemented methodology technique and the devices used. The third section collects the results and finally, the conclusion and future work are presented in the fourth section.

2   Materials and methods

The present technique has been implemented in a laboratory using an artificial excitation light. However, the technique could be adapted for taking luminescence images in the field using sunlight as an excitation source.

As can be seen in Fig. 1 the experimental device built allows half of the solar cell is illuminated by an infrared LED array while in the other solar cell half the photoluminescence emission is captured in a dark environment. A removable opaque sheet splits the solar cell allowing the darkness in the capture area of the device.
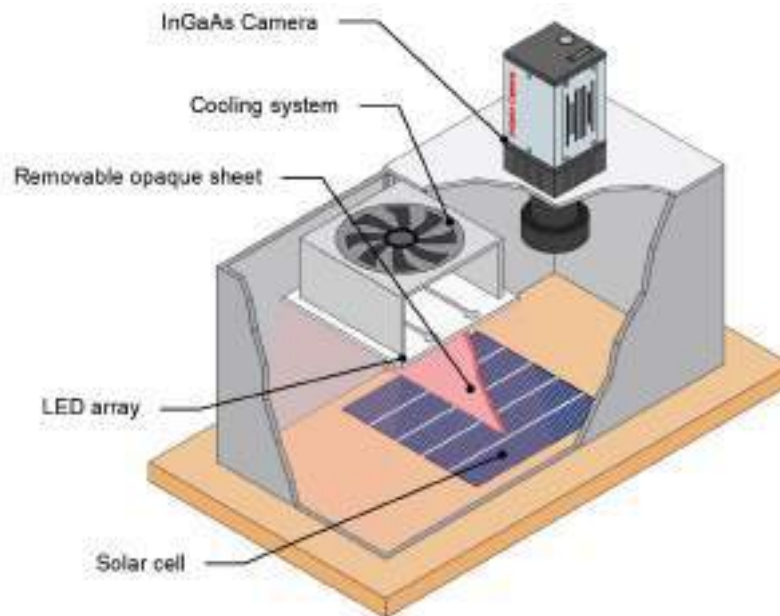
Fig. 1: Experimental device for the partial photoluminescence image acquisition.

The LED array is made up of 42 infrared LEDs (OSLON SFH 4715) with a peak wavelength of 860 nm. The LED array has also been calibrated with the purpose to know the equivalent irradiance that the solar cell is going to receive. The images of the solar cells were obtained with the Hanamatsu InGaAs camera (C12741-03). The use of this kind of camera allows a faster image acquisition than CDD cameras and it is also not sensitive to visible and excitation wavelengths, which reduces its sensitivity to the background signal. Finally, the solar cells tested are polycrystalline silicon cells (IM156B4) with 8.99 A short circuit current and 0.638 V open circuit voltage.

As mentioned in the introduction, the luminescence relative intensity has a peak wavelength at 1150 nm, out of the visible range. The used InGaAs camera has a maximum quantum efficiency from 1000 to 1600 nm, which makes it ideal for luminescence emission capture (see Fig. 2). The choice of the lighting source wavelength plays an important role because it must be matching with the quantum efficiency of the solar cell that is going to be tested. As the Fig. 2 shows the infrared emission of the LED used is matching with the quantum efficiency of the polycrystalline solar cells. This will allow the luminescence effect.
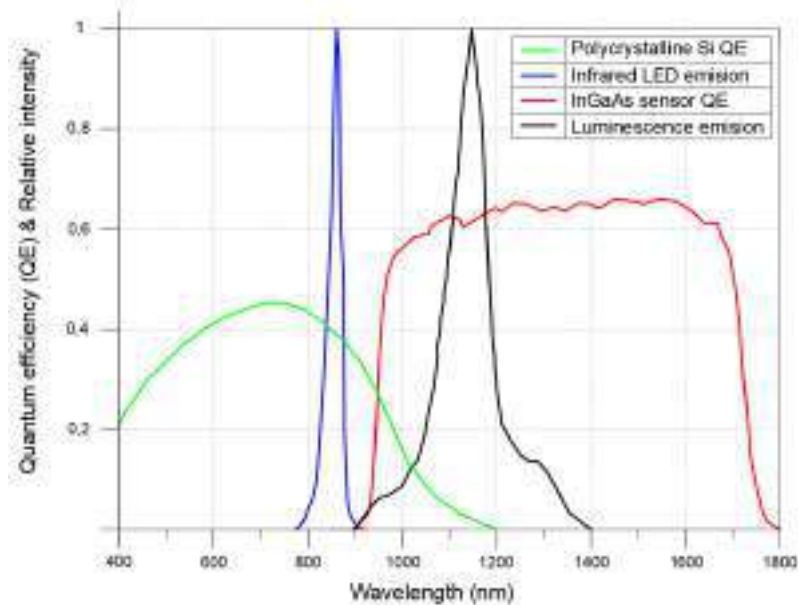
Fig. 2: Polycrystalline silicon solar cells quantum efficiency, InGaAs camera quantum efficiency, infrared LED array relative intensity and luminescence emission relative intensity.

The methodology of the implemented technique is schematized in Fig. 3. The steps necessary for the partial PL image acquisition are shown below.

1. The capture of the first solar cell half. Here, two pictures are taken:
   a. Image in lighting: A picture is taken when the LED array is on and consequently the PL emission is maximum. This picture captures the PL emission and the background signal.
   b. Image in darkness: A picture is taken when the LED array is off, and the PL emission is null. This picture just captures the background signal.
2. Image subtraction: Both pictures are subtracted with the purpose of removing the background signal and getting a better-quality picture that just shows the PL emission.
3. Image processing: The image obtained is processed to correct the optical effect that is generated due to the camera lens.
4. Replicate the above steps with the second half of the solar cell.
5. Images combination: A manual combination of the two solar cell images allows one to get an image of the full solar cell area that can be compared with conventional PL or EL images. This steps just includes the union of both images and brightness matching.
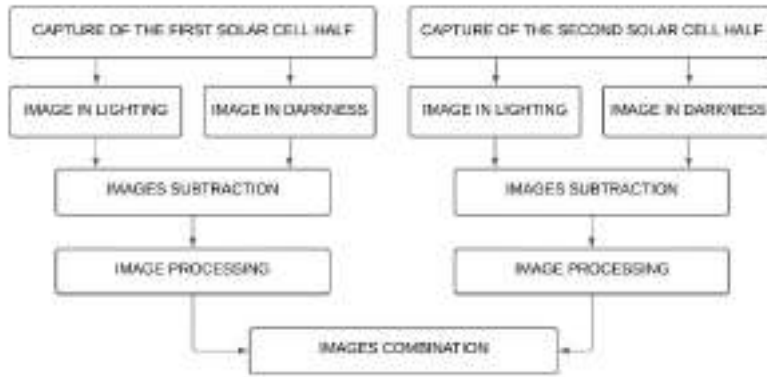
Fig. 3: Schematic of partial photoluminescence imaging methodology

Equivalent circuit models define the entire I-V curve of a cell, module, or array for a given set of operating conditions. One of the most used equivalent circuits for electrical performance simulation is the one diode model [13]. Based on this model, it has been possible to simulate the performance of a partially illuminated cell using its equivalent circuit (see Fig. 4.). This circuit is the result of the parallel association of two solar cells modeling using the one diode model. One of the solar cells lacks a current source trying to emulate the portion of the solar cell that does not receive light.

The current through the diodes can be interpreted as the photoluminescence signal intensity. As can be seen in Fig. 4 the intensity increases exponentially whit the operational solar cell voltage. In order to achieve the largest PL intensity emission and get high-quality pictures with the shortest possible exposure times, the solar cells have been tested in an open circuit.
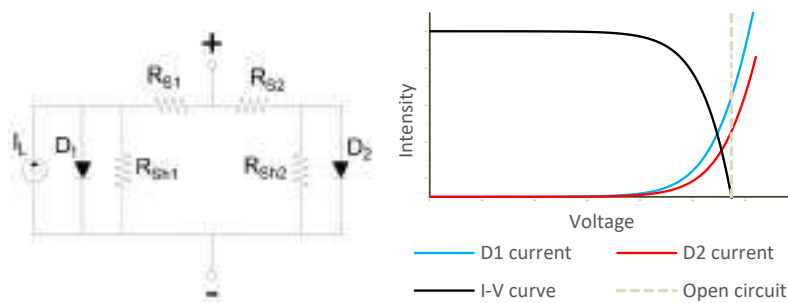
Fig. 4: Partially illuminated solar cell electrical modeling

During the experimental process different solar cells have been tested. Moreover, pictures of the same cell have been taken in different conditions, modifying exposure time, irradiance, and percentage of the illuminated solar cell.

3   Results

As mentioned above different pictures of the same solar cell have been taken in different conditions, where two correlations have been observed. On the one hand, for the same exposure time there is a correlation between the irradiance and the PL emission; the greater irradiance, the greater the PL signal captured. On the other hand, for the same exposure time there is a correlation between the percentage of solar cells illuminated and the PL emission; the greater irradiance, the greater PL signal capture. Therefore, for high-quality image acquisition is essential to adjust the exposure time according to the percentage of solar cell illuminated and irradiance.

In order to achieve the maximum PL signal, it may seem optimal to light 50% of the solar cell surface and capture the PL emission on the other 50% surface. However, this causes problems in the union area of both images due to the excitation light passing through the opaque sheet that split the lighted area from the acquisition image area. This light could mask possible defects in the middle of the solar cell. So, it is needed to reduce the lighted area and increase the capture area. This reduces the PL signal intensity but allows for the removal of the area affected by the excitation light in the image combination step. Therefore, it has been considered that the best choice is a configuration where the 40% of the solar cell surface is lighted and the other 60% is captured by the InGaAs camera.

Fig. 5 shows partial PL images of the same solar cell under different irradiance and lighted area. All the PL images show the potential for characterization and fault detection in solar cells. However, an increment of the irradiance and lighted area allows for an increase in the PL intensity emission and reduces the exposure time. The partial PL images taken show similar results to conventional EL images. Nevertheless, conventional EL needs lower exposure times, allowing faster data acquisition.
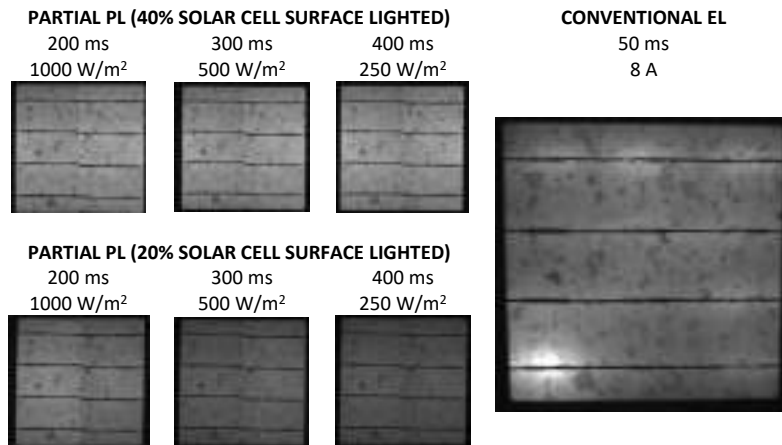
PARTIAL PL (40% SOLAR CELL SURFACE LIGHTED)

200 ms	300 ms	400 ms
1000 W/m²	500 W/m²	250 W/m²

CONVENTIONAL EL
50 ms
8 A

PARTIAL PL (20% SOLAR CELL SURFACE LIGHTED)

200 ms	300 ms	400 ms
1000 W/m²	500 W/m²	250 W/m²

Fig. 5: Partial PL images under different irradiance, lighted area, and exposure time

Partial PL images, as well as conventional EL images, are able to detect different kinds of failures in solar cells. The first row of Fig. 6 shows partial PL solar cell images with several failures while the second row shows the same solar cell images using a conventional EL technique acquisition.

A)   B)   C)   D)   E)
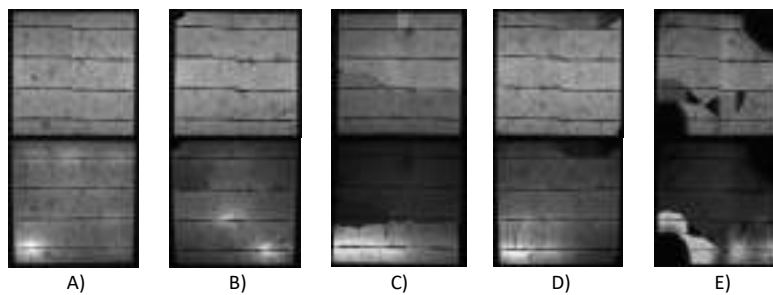
Fig. 6: Partial PL images (1000 W/m², 200 ms exposure time and 40% of illuminated cell surface) and conventional EL images (8 A and 50 ms exposure time)

4   Conclusions and future work

The present work shows the viability of a PL image technique acquisition, where one region of the solar cell is lighted while the PL emission in the rest of the solar cell area is captured in a dark environment. The main advantage of this technique is that it

does not need the use of algorithms in order to remove the background signal. None-theless, partial PL images, besides needing higher exposure times than conventional EL images, require the acquisition of two pictures and a combination process. The quality of the partial PL images is like EL images, which means that the partial PL technique is an effective tool to detect failures in solar cells.

After several tests, it has been determined that the best configuration is lighted the 40% of the solar cell and capture the PL emission in the other 60% area. This allows the removal of the area affected by the excitation light and maximizes the PL signal emission, which leads to a lower exposure time. The partial PL technique is able to get high-quality pictures under different irradiance conditions, from 250 to 1000 W/m2. Therefore, although the technique shown in this article has been carried out in a labor-atory, the technique could be adapted in order to get photovoltaic module measures in the field using sunlight as the excitation source. This would have two great advantages. On the one hand, it is possible to get daylight luminescence images without the need to use techniques to remove the background signal. On the other hand, while conventional EL and PL images need external energy sources like power supplies or homogeneous lighted devices respectively, partial PL is able to achieve pictures using the sunlight as an excitation source.

The main disadvantage detected is that de combination process, which has been done manually, requires a lot of time. Therefore, future works will focus on improving the combination process in order to automate it. In this sense, it will be essential a proper design of the process in order not to increase the computational costs compared to con-ventional EL Moreover, the device will be adapted to make possible solar cells images acquisition in the field

References

[1]   D. M. Kammen and D. A. Sunter, "City-integrated renewable energy for urban sustainability", Accessed: Aug. 15, 2022. [Online]. Available: https://www.sci-ence.org

[2]   L. Hernández-Callejo, S. Gallardo-Saavedra, and V. Alonso-Gómez, "A review of photovoltaic systems: Design, operation and maintenance," *Solar Energy*, vol. 188, pp. 426–440, Aug. 2019, doi: 10.1016/J.SOLENER.2019.06.017.

[3]   Marc Köntges *et al.*, "Review of Failures of Photovoltaic Modules," 2014.

[4]   M. H. Ulrike Jahn *et al.*, "Review on Infrared and Electroluminescence Imag-ing for PV Field Applications," 2018.

[5]   M. Guada *et al.*, "Daylight luminescence system for silicon solar panels based on a bias switching method," *Energy Sci Eng*, vol. 8, no. 11, pp. 3839–3853, Nov. 2020, doi: 10.1002/ESE3.781.

[6]   J. Ballestín-Fuertes *et al.*, "Novel Utility-Scale Photovoltaic Plant Electrolumi-nescence Maintenance Technique by Means of Bidirectional Power Inverter Controller," *Applied Sciences 2020, Vol. 10, Page 3084*, vol. 10, no. 9, p. 3084, Apr. 2020, doi: 10.3390/APP10093084.

[7]　　R. Bhoopathy, O. Kunz, M. Juhl, T. Trupke, and Z. Hameiri, "Outdoor photo-luminescence imaging of photovoltaic modules with sunlight excitation," *Progress in Photovoltaics: Research and Applications*, vol. 26, no. 1, pp. 69–73, Jan. 2018, doi: 10.1002/PIP.2946.

[8]　　L. Stoicescu, M. Reuter, and J. H. Werner, "DaySy: Luminiscence imaging of PV modules in daylight ," *29th European Photovoltaic Solar Energy Conference Exhibition*, pp. 2553–2554, 2014.

[9]　　M. Juhl *et al.*, "Module Inspection Using Line Scanning Photoluminescence Imaging," *32nd European Photovoltaic Solar Energy Conference and Exhibition*, 2016, doi: 10.4229/EUPVSEC20162016-5BV.1.12.

[10]　Z. Iskra, M. K. Juhl, J. W. Weber, J. Wong, and T. Trupke, "Detection of Finger Interruptions in Silicon Solar Cells Using Line Scan Photoluminescence Imaging," *IEEE J Photovolt*, vol. 7, no. 6, pp. 1496–1502, Nov. 2017, doi: 10.1109/JPHOTOV.2017.2732220.

[11]　National Renewable Energy Laboratory and S. Johnston, "Contactless electroluminescence imaging for cell and module characterization," Dec. 2015. doi: 10.1109/PVSC.2015.7356423.

[12]　D. B. Sulas, S. Johnston, and D. C. Jordan, "Comparison of photovoltaic module luminescence imaging techniques: Assessing the influence of lateral currents in high-efficiency device structures," *Solar Energy Materials and Solar Cells*, vol. 192, pp. 81–87, Apr. 2019, doi: 10.1016/J.SOLMAT.2018.12.022.

[13]　D. T. Cotfas, P. A. Cotfas, and S. Kaplanis, "Methods to determine the dc parameters of solar cells: A critical review," *Renewable and Sustainable Energy Reviews*, vol. 28, pp. 588–596, Dec. 2013, doi: 10.1016/J.RSER.2013.08.017.

Analyzing the influence of the building energy demand in the final design of shallow geothermal systems

Cristina Sáez Blázquez[1,2 0000-0002-5333-0076], Ignacio Martín Nieto[2 0000-0003-3984-7228], Natalia Nuño Villanueva[2 0000-0001-7022-119X], Miguel Ángel Maté-González[2,3 0000-0001-5721-346X], Arturo Farfán Martín[2 0000-0002-1506-1207] and Diego González-Aguilera[2 0000-0002-8949-4216]

[1]Department of Electric, System and Automatic Engineering, Universidad de León, León, Spain
[2] TIDOP Group, Department of Cartographic and Land Engineering, University of Salamanca, Higher Polytechnic School of Avila, Avila, Spain
[3]Department of Topographic and Cartography Engineering, Higher Technical School of Engineers in Topography, Geodesy and Cartography, Technical University of Madrid, Mercator 2, 28031 Madrid, Spain
csaeb@unileon.es/u107596@usal.es

Abstract. The correct design of a low enthalpy geothermal system is a priority to ensure the expansion of this renewable energy in the alarming world energy panorama. In this sense, the present research has analyzed how the estimation of the initial energy demand of a space plays a fundamental role in the corresponding geothermal design. Thus, the main tools used in Spain (location of the study case) in the calculation of the energy demand have been used for then designing the shallow geothermal system. Results show that the official tools (HULC and CE3X) provide lower energy demand values and adjusted to the construction conditions of the building that allow the optimization of the geothermal well field. On the contrary, simpler, and more intuitive applications (regular spreadsheets and GES-CAL software) assume a higher value of heating energy demand, which in turn implies an oversizing of the geothermal scheme. Even though all the procedures ensure to cover the energy requirements of the building, the most precise tools manage to reduce the initial investment of the system and its operating costs, in addition to reducing the global CO_2 emissions because of the lower power of the associated geothermal heat pump.

Keywords: energy demand, shallow geothermal energy, HULC, CE3X, GES-CAL.

1 Introduction

Climate change and its devastating effects are pushing the energy sector towards a transition to cleaner technologies with lower CO_2 emissions. However, the world energy supply is still highly dependent on fossil fuels (~80% of primary energy),

which translates into unacceptable levels of Greenhouse Gases (GHG) emissions and other environmental impacts [1-2].

The European Union (EU) is committed to reducing the global GHG emissions by 20% from the 1990 levels by 2020 and around 80–95% by 2050 [3]. In this context, increasing the penetration of renewables is mandatory for ensuring the future decarbonized energy system. Contributions are required from the different energy consuming sectors, but specially from the building one, which represents in the EU 40% of the total final energy use, meaning 36% of the global CO_2 emissions [4]. The principal legislation in the European Union for the energy efficient buildings together with the International Energy Agency (IEA) promote the implementation of heat pumps and renewable energy for the heating and cooling sectors [5-6].

In this sense, Geothermal Energy (GE) is a non-carbon source of renewable energy that constitutes an ideal solution for reducing the dependence on fossil fuels using the available heat stored in the ground, ground water, or surface water [7]. Deep geothermal resources based on hot-water and steam are currently exploited for producing electricity, whereas shallow geothermal heat pump systems mean a mature technology for space heating and cooling and the production of Domestic Heat Water (DHW).

Regarding the emission of CO_2 and energy efficiency, geothermal heat pumps rank higher than all fossil fuel-based boilers and the air source systems [8-10]. However, and despite advances in this renewable energy have led to the increase in the energy efficiency and its expansion through the global heating/cooling energy sector, geothermal energy is not as widespread as other renewable energies such as solar or wind.

This fact derives in part from the lack of knowledge about this energy by the general user but also from certain wrong practices carried out in the different phases of a shallow geothermal project. These actions lead to failures during the operation of the installation, compromising its correct operation throughout the initially projected useful life of the systems.

In the above context, one of the fundamental steps when starting this type of project is the evaluation of the energy consumption of the particular building. Different research has addressed the application of software to simulate the energy behavior such as TRNSYS, Energy Plus or ESPr which are useful to provide an estimation of how the building behaves from the energy point of view [11].

In the case of Spain, the practical calculation of the heating and/or cooling energy demand has been usually performed using tools that complies the Technical Code for Building [12] and are freely available for technicians and users (LIDER and CALENER) [13]. With the transposition of the EU Directive 2012/27/EU to Spanish regulations based on the Royal Decree 235/2013, that ratifies the process for certifying the energy performance of buildings [14], the two applications tools were unified into a single unified software called the "Herramienta Unificada LIDER CALENER" or LIDER-CALENER Unified Tool, usually known as "HULC".

Beyond this official application, different tools based on a more simplified procedure are frequently used for estimating the energy demand, especially in single-family buildings. These tools provide faster but less accurate results that frequently lead to errors in the future calculation of the heating and cooling system. This is especially

influential in the design of shallow geothermal systems and the well field, where the differences in the estimated initial energy demand make the final scheme approached vary to a high degree (depending on the magnitude of the installation).

Based on the above reasons, this research deals with the calculation of the heating energy demand of a specific building through the use of different tools and applications usually implemented with this purpose. From this calculation, the design of a low enthalpy geothermal system will be addressed for evaluating the influence of the different energy demand procedures in the final design of the system.

2   Materials and method

2.1   Description of the case under study

Following the objective set in this research, a single-family building located in the region of Ávila (central Spain), is considered. It is a three-story building consisting of a basement, a ground and a first floor together with a unhabitable rooftop level, built in the year 2020. Dimensions of each floor are presented in the following Figure 1. Additionally, Table 1 includes the surface and height of each of the mentioned levels.
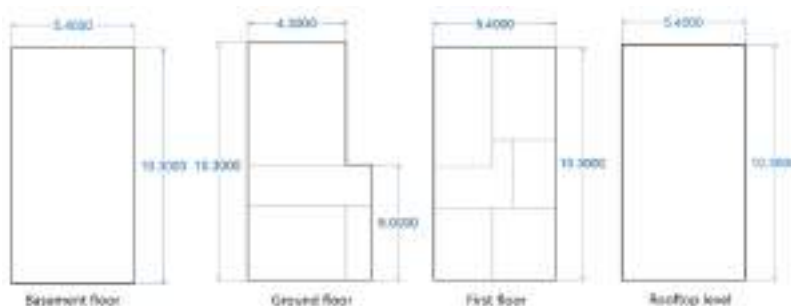
Figure 1. Description of the floors that make up the single-family building. *Dimensions are expressed in meters.

Table 1. Geometrical information of the building included in the study.

House level	Surface (m^2)	Height (m)
Basement floor	55,62	2,70
Ground floor	49,79	3,00
First floor	55,62	3,00
Rooftop level	55,62	0,83

The total useful living surface of the single-family house is of 161,03 m^2 and the estimated daily use of Domestic Hot Water (DHW) is of 140 l/day, since the building is constituted by five bedrooms [15].

Considering the location of the building in a region characterized by cold, dry winters and mild summers, only heating energy needs are taken into account in this research. On top of the above, for the subsequent calculation of the heating energy demand, the surface and orientation of each façade and the surface of windows placed on them must be also known. In this way, Table 2 includes all this information.

Table 2. Orientation and surfaces of façades and windows.

Façade	Surface (m^2)	Windows (m^2)	Windows (%)
North	42,62	6,02	14,12
South	44,01	9,69	22,02
East	73,71	----	----
West	89,61	----	----

To end the description of this section, it is also convenient to define the geological environment in which the building under study is located. This information, presented in Figure 2, will be necessary throughout the design process of the shallow geothermal system selected as a means of heating solution.
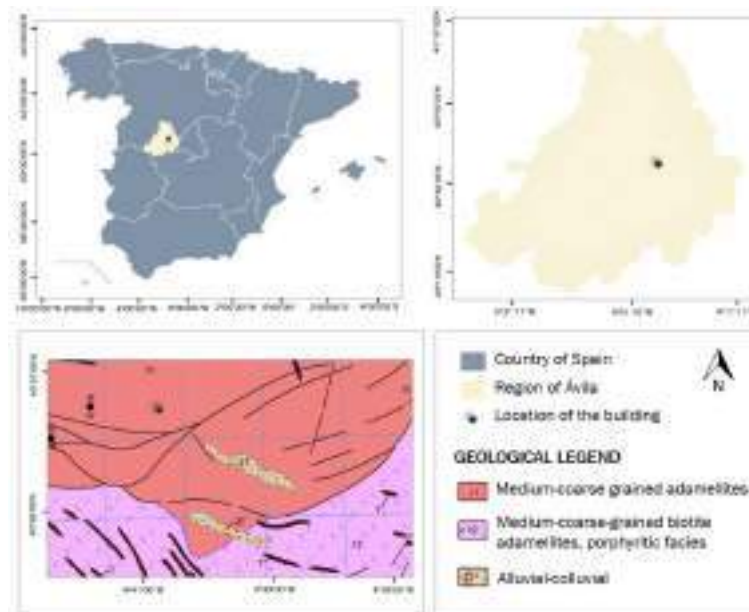
Figure 2. Location of the building under study and geology of the environment.

2.2   Calculation of the energy demand

As mentioned in the introductory section, the calculation of the heating energy demand of a given building can be made from different perspectives and approaches that can significantly alter the final result of the selected heating/cooling system.

The following subsections describe the most frequent procedures used in this sense and which will be considered in this research.

Regulated spreadsheets

One of the simplest and most widely used procedures for estimating the energy demand is the use of programmed spreadsheets designed in accordance with the specific regulations in force. The purpose of this kind of tools is to determine in quick and approximate way the annual and monthly energy demand of a building. This method allows to analyze visually and intuitively the sensitivity of each possible variable on the energy behavior of the building in very early phases of the design, where only geometry is available.

The specific tool used in the present research follows the monthly method prescribed in the standard regulation UNE-EN ISO 52016-1 [16]. During its use, a series of numerical values (surface, height, percentage of openings and surface of each façade) are introduced and the climatic zone where the building is located is selected. Once all these information is given, different options can be evaluated based on the following variables of:

- Gains: contribution of heat in W/m^2 that supposes the use of the building.
- Inertia: represents the internal thermal mass of the building expressed in kg/m^2.
- Ventilation: indicates the number of renewals per hour.
- U_o: represents the average thermal transmission coefficient (including integrated thermal bridge) expressed in $W/m^2 \cdot K$.
- U_v: average thermal transmission coefficient (considering the average frame and glass) expressed in $W/m^2 \cdot K$.
- g: represents the modified solar factor of the glass.
- Sup: linear thermal bridge formed by the intersection between façades and roofs expressed in $W/m \cdot K$.
- Iner: linear thermal bridge constituted by the intersection between façades and intermediate slabs expressed in $W/m \cdot K$.
- Infer: linear thermal bridge formed by the intersection between façades and floors expressed in $W/m \cdot K$.

Figure 3 shows the graphical interface of the tool that has been used in this research.

Figure 3. Graphical interface of the spreadsheet considered for the energy analysis of this work.

CE3X

CE3X is an official tool promoted by the Ministry for the Ecological Transition and the Demographic Challenge for the certification of the energy efficiency of buildings. This program, developed by Efinovatic and the National Center for Renewable Energies (CENER), allows the certification of any type of building in a simplified way to obtain any rating from «A» to «G» but also provides a final value of the heating and/or cooling energy demand [17].

The CE3X tool can be downloaded on the official page of the Ministry for the Ecological Transition and the Demographic Challenge, as well as a document with the main instructions for its use.

The program is based on the comparison of the building object of the certification and a database conceived for each of the representative climatic zones. The database is sufficient broad to cover any case of the Spanish building stock. When the user enters the data of the object building, the program parameterizes these variables and compares them with the characteristics of the cases collected in the database. In this way, the software searches for the simulations with characteristics most similar to those of the target building and interpolates the heating and cooling demands with respect to them, thus obtaining the heating and cooling demands of the target building. In function of the degree of knowledge of the thermal characteristics of the building and installations the procedure of CE3X establishes different levels of data entry, in:

    a) Default values.
    b) Estimated values.
    c) Known values (tested/justified).

Throughout the use of the program, information (in the mentioned levels) is entered regarding administrative data, general data, thermal envelope, and heating and/or cooling installations. Figure 4 presents the main window of the CE3X tool.
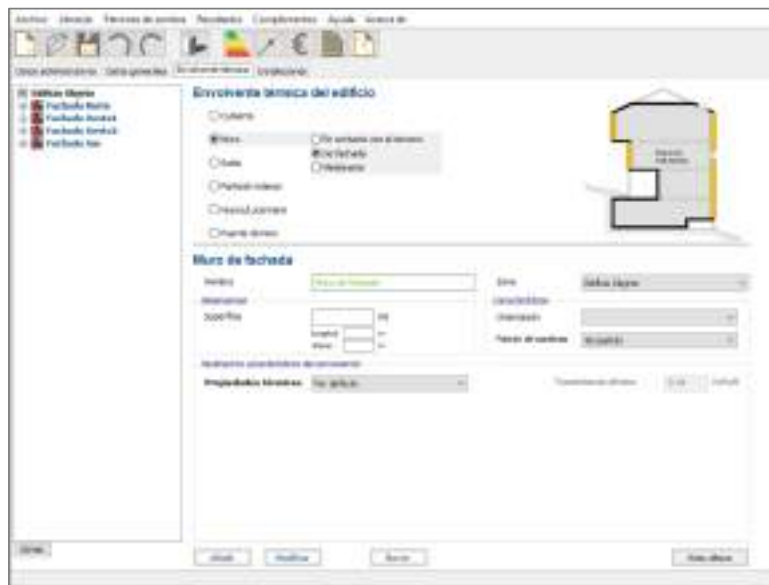

Figure 4. Main window of CE3X tool.

HULC

In Spain, LIDER was the computer application used a few years ago to comply with the general verification of the Energy Demand Limitation requirement established in the Basic Document of Habitability and Energy of the Technical Building Code (CTE-HE1) [18]. As of 2016, it was unified with CALENER (that considers the use of the energy systems) to create HULC (Leader-Calener Unified Tool), whose use is mandatory to carry out official energy efficiency certificates.

The tool includes all the updates of the Technical Building Code and is commonly used by professionals when evaluating whether all the legally established energy saving requirements are met on a particular building. In fact, it is applied both to carry out certifications and verifications.

The design of this tool is specifically created so that the energy certification of a residential building can be assessed visually and clearly. In addition, energy demand

is also provided by the software both for heating and cooling mode, so this module will be applied for the present research.

The first step when using the program is to introduce the general and administrative data and standard information of the building and energy sources considered, allowing differentiating between the electrical energy generated and the produced self-consumed energy.

After entering all these data, it is necessary to define the envelope and the workspace to model the system. Throughout this stage, it is possible to introduce the specific plans of the building (as in the case of this work) or to design it directly on the program. Once the constructive solutions adopted in the building have been defined and the corresponding thermal bridges are calculated, the tool allows to determine if the building meets the energy demands limited by the Technical Building Code [19]. Next, the energy installations of the building can be defined to obtain the global results according to demand, consumption, and CO_2 emissions.

In the following Figure 5 it is possible to observe the workspace of HULC in which the building under study has already been designed.
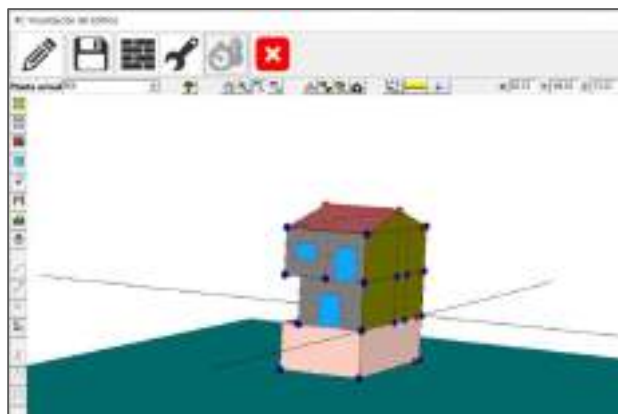
Figure 5. Workspace in HULC once built the single-family house used as study case.

GES-CAL

GES–CAL software has been developed by researchers from the TIDOP Research Group (University of Salamanca) for the modelling and design of shallow geothermal systems [20]. The tool is specially conceived for being used in the region of Ávila (location of the case under study) and, beyond the geothermal calculation of the system, the energy demand can be also estimated by one its initial modules. For this reason, GES-CAL has been included in this research for both the calculation of the heating energy demand of the building and the corresponding design of the geothermal system.

The tool is mainly constituted by five modules, starting by a brief description of the software, and following by the introduction of initial data of the building (in

which the energy demand is estimated), the design of the geothermal solution and a final economic and environmental analysis. The initial module conceived for the energy demand allows to introduce the specific value (if known) or to automatically calculate it from easily available information of the space (specification of demand, surface, height, year of construction and orientation), complying the procedures specified at the regulation ISO 52016-1:2017 [16].

Once detailed or calculated the building energy demand, it is possible to define the main characteristics of the closed-loop geothermal system (heat pump parameters, ground thermal properties, and configuration of the geothermal installation) so GES-CAL software finally calculates the design parameters of the geothermal well field, such as the total pipe and drilling length and the schema of the system. After this stage, the software suggests several possible designs so the user can select one of the proposed solutions to ultimately obtain the well field schema besides an economic and environmental analysis of the geothermal system.

In the following Figure 6 the initial window of GES-CAL software is shown, highlighting the energy demand calculation module.
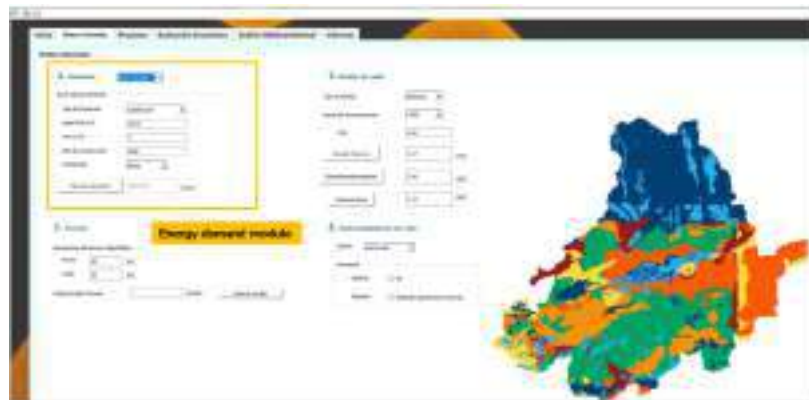
Figure 6. Initial window of GES-CAL software in which the energy demand calculation module is included.

3 Results

3.1 Heating energy demand

After the application of each of the procedures described in the previous section, the values of the heating energy demand associated with the conditions of the building included as case study are obtained. From these values (presented in Table 3), the following subsection will address the design of the shallow geothermal system from each one of them.

Table 3. Results of the heating energy demand of the building obtained by the tools considered in this research.

Application	Heating demand (kWh/m²·year)	Heating demand (kWh/year)
Spreadsheet	243,43	39199,00
CE3X	134,50	21658,53
HULC	95,97	15454,05
GES-CAL	214,75	34581,51

It should be noted that, of all these procedures, the regulated spreadsheet (the one that is only conceived for the calculation of the space energy use) also provides a graph of the evolution of this energy demand throughout the entire period of the year, differentiating the contribution of the main factors that are considered in the procedure. This graphic can be observed in the following Figure 7.
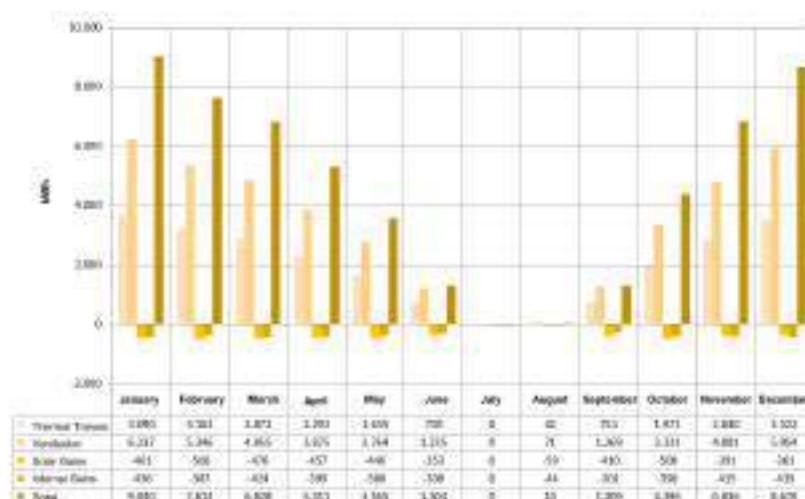
Figure 7. Evolution of the heating energy demand for the single-family house obtained with the regulated spreadsheet.

3.2 Geothermal design

As already explained, GES-CAL software has also been used for the dimensioning of the geothermal system that will cover the energy needs of the building. As it is a program specifically designed for its use in the province of Ávila, calculations will be precise and based on empirically obtained terrain thermal properties.

When proceeding to the geothermal design with this tool, the same initial data about the geothermal system are used (Polyethylene doble-U vertical heat exchangers of 32 mm, standard geothermal grout, heat pump with Coefficient of Performance (COP) of 4, and granite environment with thermal conductivity of 2.9 W/mK), only varying the value of the heating energy demand obtained by each of the evaluated procedures.

Table 4 includes the main parameters that characterize the geothermal system obtained with GES-CAL for each of the assumptions.

Table 4. Parameters of the geothermal design performed with GES-CAL software.

Application	Heating demand (kWh/year)	Heat pump power (kW)	Number of boreholes	Total drilling length (m)
Spreadsheet	39199,00	7,84	2	117
CE3X	21658,53	5,41	1	69
HULC	15454,05	4,55	1	50
GES-CAL	34581,51	7,20	2	109

4   Discussion

4.1   Tool reliability

As can be seen in the results of the energy demand associated with the building under study (Table 4), there are significant variations between each of the procedures used in this research.

Observing the aforementioned Table 4, HULC and CE3X programs (official tools of the Ministry for the Ecological Transition and the Demographic Challenge) provide the lowest values of heating energy demand required by the building, and this is especially evident in the case of HULC software. This program is undoubtedly the most precise solution and the one that best adjusts to the real construction conditions of the building. In effect, the tool allows defining its envelope and optimizing its energy requirement based on the materials used in its construction. The large amount of information that HULC allows to enter about gaps, construction solutions, thermal bridges, etc. as well as the exact definition of its geometry mean that the final result of its energy demand can be adjusted to the maximum, constituting a reliable value and in accordance with the particular conditions of the building.

Regarding CE3X program, it is considered a version prior to HULC, where the constructive conditions of the building are also taken into account, but without reaching the level of detail that HULC allows. Although both tools comply with the provisions of the Technical Building Code, CE3X cannot adjust the results to the same degree as HULC, which makes the energy demand more conservative and somewhat higher than that obtained with HULC.

Beyond these two official tools, the regulated spreadsheet and GES-CAL program provide the highest values of energy demand. This is due to the lower robustness of

these applications, which, even based on specific UNE regulations, are simple solutions that only take into account general geometric parameters of the building and therefore cannot adjust the value of energy demand so as not to compromise the future operation of the selected energy system.

4.2   Economic and environmental evaluation

As a consequence of the differences in the energy demand values obtained from each methodology, the geothermal design is also different in each case. Thus, both the power of the heat pump and the total length of drilling is much lower with the results of CE3X and especially of HULC. In the same way, GES-CAL and the spreadsheet whose energy demand values are higher, require a geothermal well field with a higher drilling length (and number of boreholes) as well as a greater power in the geothermal heat pump. All this means that, although with these last two applications, the building's energy needs would be totally covered, the oversizing that this entails, causes higher initial investment and annual operating cost. In addition, derived from the greater power of the heat pumps, CO_2 emissions directly associated with their operation are inevitably higher. The following table 5 collects all this economic and environmental information of each assumption.

Table 5. Economic and environmental results for each solution.

Application	Initial investment (€)	Annual cost (€/year) *	CO₂ emissions (kg/year)
Spreadsheet	21958,81	3386,88	3498,51
CE3X	17954,93	2337,12	1932,98
HULC	16335,86	1965,60	1379,27
GES-CAL	20957,78	3110,40	3086,35

* Considering an electricity prize of 0,18 €/kWh and a heat pump operation of 2400h/year.

Finally, the following Figure 8 shows the evolution of the economic comparison considering the initial investment of each solution and the annual operating costs in terms of Net Present Value (NPV) with a discount rate of 0.18 during an estimated useful life of 30 years.
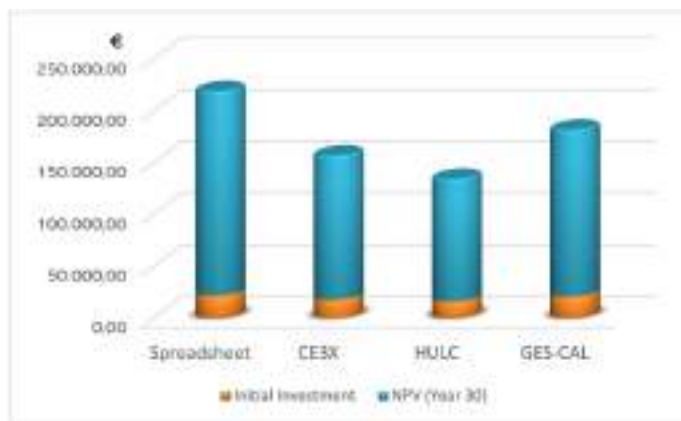
Figure 8. Economic evaluation based on the initial investment and the annual operation costs in terms of NPV.

5   Conclusions

The objective of this work has been to evaluate the influence of the energy demand on the final shallow geothermal design. For this, different tools, frequently used in the calculation of the energy requirements of a space in Spain (location of the building under study), have been used.

As the results obtained with each methodology demonstrate, those applications in which the degree of detail of the building and its constructive solutions is high, allow to maximize the adjustment of the value of energy demand required by the building.

Therefore, the geothermal design can also be optimized, reducing the initial investment of the system and the operating costs associated with the operation of the geothermal heat pump (also reducing the emission of CO_2). All this becomes more evident in the 30-year global economic comparison, where it has been possible to observe how the most robust tool (HULC) allows savings of around 40% compared to the simplest procedure, the spreadsheet used in the study.

Lastly, it should be noted that all the procedures used provide energy demand values that guarantee that the heating energy system will meets the needs of the buildings, but in the case of the simplest tools, these values are oversized with the economic that this fact entails.

Future research lines will be aimed at including alternative simulation tools and additional study cases in other conditions and climates that allow to evaluate in a more detailed way the suitability of each solution.

References

1. Wolf, C., Klein, D., Richter, K., & Weber-Blaschke, G. Environmental effects of shifts in a regional heating mix through variations in the utilization of solid biofuels. Journal of Environmental Management, 177, 177-191 (2016).
2. Günther, M., & Hellmann, T. International environmental agreements for local and global pollution. Journal of Environmental Economics and Management, 81, 38-58 (2017).
3. Langsdorf, S. EU Energy Policy: from the ECSC to the Energy Roadmap 2050. Green European Foundation: Brussels, Belgium (2011).
4. Fertner, C., & GROßE, J. Compact and resource efficient cities? Synergies and trade-offs in European cities. European Spatial Research and Policy, 23(1), 65-79 (2016).
5. Clarke, L., & Sahin-Dikmen, M. Unions and the green transition in construction in Europe: Contrasting visions. European Journal of Industrial Relations, 26(4), 401-418 (2020).
6. International Energy Agency. Directorate of Sustainable Energy Policy. Transition to sustainable buildings: strategies and opportunities to 2050. Organization for Economic (2013).
7. Noorollahi, Y., Shabbir, M. S., Siddiqi, A. F., Ilyashenko, L. K., & Ahmadi, E. Review of two-decade geothermal energy development in Iran, benefits, challenges, and future policy. Geothermics, 77, 257-266 (2019).
8. Sarbu, I., & Sebarchievici, C. (2014). General review of ground-source heat pump systems for heating and cooling of buildings. Energy and buildings, 70, 441-454 (2014).
9. Blázquez, C. S., Borge-Diez, D., Nieto, I. M., Martín, A. F., & González-Aguilera, D. Technical optimization of the energy supply in geothermal heat pumps. Geothermics, 81, 133-142 (2019).
10. Blázquez, C. S., Borge-Diez, D., Nieto, I. M., Martín, A. F., & González-Aguilera, D. Multi-parametric evaluation of electrical, biogas and natural gas geothermal source heat pumps. Renewable Energy, 163, 1682-1691 (2021).
11. Pérez-Andreu, V., Aparicio-Fernández, C., Martínez-Ibernón, A., & Vivancos, J. L. Impact of climate change on heating and cooling energy demand in a residential building in a Mediterranean climate. Energy, 165, 63-74 (2018).
12. The Technical Building Code; Ministry of Development and the Spanish Research Scientific Council (CSIC): Madrid, Spain, (2006).
13. Torra i Guarch, O. Estudio de la mejora de la eficiencia energética en los edificios de oficinas mediante el software HULC (2019).
14. Royal Decree 235/2013, of 5th April, Agreeing to the Procedure Basic for the Certification of the Energy Efficiency of Buildings. Available online: https://www.boe.es/buscar/pdf/2013/BOE-A-2013-3904-consolidado.pdf (accessed on June 2022).
15. Grandío Rodríguez, J. M. Modificación del código técnico de la edificación 2019. Parte 2. *DePlano*, (43), 5-17 (2020).
16. Energy performance of buildings - Energy needs for heating and cooling, internal temperatures and sensible and latent heat loads - Part 1: Calculation procedures (ISO 52016-1:2017) (Endorsed by Asociación Española de Normalización in December of 2017.)
17. Ruiz-Checa, J. R., Cristini, V., Higón, J. L., & López, J. A. Identification and analysis of passive energy resources applied in constructions of "La Mancha" region, Spain. Vernacular Architecture: Towards a Sustainable Future, 649-654 (2014).

18. Documento Básico-HE, HE1, Condiciones para el control de la demanda energética (2022).
19. Sobaler-Rodríguez, J., Villar-Burke, R., Sorribes-Gil, M., & Jiménez-González, D. Transmitancia térmica de la envolvente y cumplimiento del DB-HE 2019 para un bloque de viviendas. Informes de la Construcción, 74(565), e433-e433 (2022).
20. Blázquez, C. S., Nieto, I. M., Mora, R., Martín, A. F., & González-Aguilera, D. GES-CAL: A new computer program for the design of closed-loop geothermal energy systems. Geothermics, 87, 101852 (2020).

Operation Analysis of the Electrical System in Areas with Growth of Tourist Complexes. Case Study: Enriquillo Region, Dominican Republic

Miguel Aybar-Mejía[1][0000-0002-4715-3499], Randy Andrés[1][0000-0001-7965-416X], Alam Cabral-Soto[1][0000-0002-3093-5910], Carlos Montás[1][0000-0002-8632-08944], Wilmer-Johann Núñez-García[1][0000-0001-5841-7309], Elvin Arnaldo Jiménez Matos[1][0000-0002-0031-6772],   and Deyslen Mariano-Hernández [1][0000-0002-4255-3450],

[1] Área de ingenierías, Instituto Tecnológico de Santo Domingo (INTEC), Dominican Republic.
miguel.aybar@intec.edu.do

Abstract. The growing integration of tourist areas and complexes increases the demand for electrical power systems. This increased demand may represent a vulnerability to voltage and frequency stability in electrical networks, where these parameters are essential for an optimal and continuous electrical energy supply. The Dominican Republic has begun a process of tourist expansion in areas that were previously not commercially exploited. This article analyzes power systems in response to the growth of tourist areas in the poles with abundant generation and low demand, taking the Enriquillo Region, Dominican Republic, as a case study. For this investigation, actual data from load profiles of the area were used, with which Quasi-Dynamic and RMS/EMT simulations were carried out in the DIgSILENT software. The results show that the electrical system benefits stability and national standards.

Keywords: Stability analysis, Electrical Grid, Electrical Demand, Electrical Energy, Power System Stability.

1 Introduction

Today the demand for electrical energy experiences drastic increases [1]. Electricity is the heart of modern societies and economies, so its evolution brings with it the growth of power systems. Communities are expected to continue to increase the demand for electricity thanks to rising household incomes and the growing order for and purchase of electrical devices across various applications, such as electric vehicles becoming more prevalent daily in homes or workplaces [2]. This situation leads the electrical power system to work to the limit; therefore, to have a reliable, stable, and quality system that meets society's present and future demands. The electrical power systems are responsible for providing the necessary electrical energy with the highest possible quality standards to consumers.

For this reason, the stability of an electrical power system is critical [3, 4]. Tourism worldwide is one of the sectors that contributes the most to the economy of many countries. According to [5], the tourism sector contributes 270 million jobs, directly

and indirectly, in addition to contributing more than 4.5 billion US dollars to the world's gross domestic product, a number given in 2020 by the World Travel and Tourism Council. Only in North America, Central, and South America 69.7 million tourist arrivals were registered for this year, an amount affected by the current global situation regarding SARS-CoV-2, while in 2019, there were 219.3 million tourist arrivals [6]. The previous puts into perspective the relevance of the tourism sector in America, for which nations' interest in promoting this sector can be understood and developed.

The growth in demand due to the increase in the tourism sector in different countries causes electrical distribution networks to work at or very close to their maximum capacity, producing power and energy losses in the system [7]. Similarly, it compromises the stability of the network, reducing its security and reliability.

Considering those mentioned earlier, the objective of this article is to present a methodology for analyzing the impact caused by the increase in electricity demand due to the tourism sector. The Enriquillo Region, located in the southwestern Dominican Republic, was used as a case study.

2   Methodology

First, the necessary technical information was collected, which was obtained from the Dominican Electric Transmission Company (ETED), the electric power distribution company Edesur and the National Energy Commission (CNE). The technical information on the generation technologies, transmission lines, and users connected to the grid was obtained from ETED and Edesur. It was used to define the characteristic load profiles of the southern and hotel zones, while the data obtained from the CNE disclosed the system's trend.

The simulation defined two power demand profiles; the first profile was that of the southern zone. All measurement points were considered used for the coordinate organism (OC-SENI) to establish present and future data. The second profile was that of the tourist areas and complexes, which served as a reference to simulate the behavior of the tourist sector. For the current load profiles, the electrical energy consumption obtained from the measurement points of the selected areas was used, estimating the average of the hours of all the days of the month to get the average behavior of a year. For future demand profiles, data on demand growth were used in the scenario forecast by the CNE until 2032.

Quasi-Dynamic simulation and RMS/EMT simulation were then performed in DIgSILENT. Quasi-Dynamic simulation works well for planning studies where long-term load and generation profiles are established and network evolution is modeled using variations and expansion stages [8]. The Quasi-Dynamic simulation was used to see the system's development during the analysis period, measuring variables such as line currents, line load, solar, wind, hydro, and conventional generation, and active, reactive, and apparent power in lines [9]. Regarding the RMS/EMT simulation, it was used to observe the system's behavior in the following situations: output of a generator with the capacity to activate the load shedding system and input of the most significant load in a bus of the system. The bus bars' electrical frequency and voltage be-

`

havior were measured to validate if they were within the stability margins. Finally, the results were analyzed, describing the behaviors in the simulations, and their relevance was verified in terms of the adverse effects they could produce on the electrical power system. Fig. 1 shows the methodology used for the study.
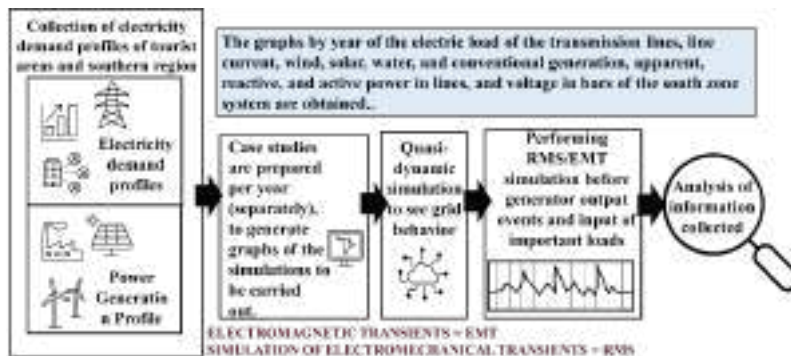

Fig. 1. Methodology used.

3   Stability in Electrical Grid

According to [8], stability in an electrical grid [10] is the ability to return to a stable state after a disturbance. There are three types of stability: angular, frequency, and voltage. Each of them has a different impact on the electrical power system. Fig. 2 shows the classification of stability of angle, frequency, and electrical voltage in power systems according to international standards [11]:
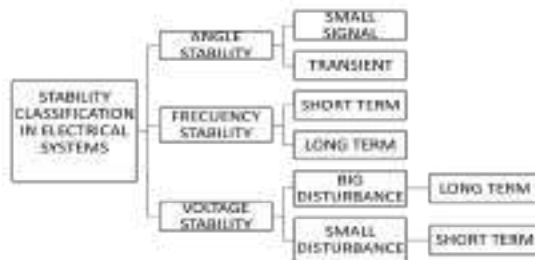
Fig. 2. Power system stability classification scheme.

Stability can be divided by periods; in each of these, specific effects are presented in the power system. These effects vary by period or deadlines and are divided into:

• Transitional stability: The study time is less than ten (10) seconds, and tends to happen significant disturbances, derives from a first oscillation, and is aperiodic.
• Medium-term stability: The study time is up to several minutes, large voltage and frequency excursions occur, fast and slow dynamics, and severe disorders.
• Long-term stability: The study time is up to several minutes, dynamic low ones occur, and the system's frequency becomes uniform.
• Stability of significant disturbance voltage: it occurs in "switches" events, the Ultc (Ultra Loaded Transformer Changer) dynamics, and loads coordination of controls and protection.

Maintaining voltage and frequency stability in electrical power systems has been one of the significant challenges of electrical engineering. Some studies that analyze how to maintain the stability of the power system using voltage and frequency variables as indicators of energy service quality are shown in Table 1.

Table 1. Study on voltage and frequency stability in electrical power systems.

Ref.	Contribution	Limitation
[12]	FACTS control application to improve the stability of the electrical grid voltage.	Does not cover frequency stability.
[13]	The control scheme for an MV-HVDC power system to improve stability.	The study only focused on a multi-dimensional droop-based control strategy.
[14]	The effect of voltage variation on frequency control through phase loop dynamics was analyzed.	A unique problem arises in the frequency control structure when the voltage varies suddenly.
[15]	It proposed a control for voltage and frequency called Automatic Voltage Regulator, which can be considered a solution to tuning frequency.	Unable to keep voltage and frequency balanced when connected to the grid.
[16]	It proposed a simple frequency controller that uses the inverter's output current as feedback to adapt its frequency.	Existing schematics only focus on power and having a good transient response.
[17]	Provides an introduction to the grid's control and stability of integrating renewable energies.	The study was not detailed in the context of the electricity market.

Due to the increase in demand, electrical distribution networks are forced to operate at or near-maximum capacity, which causes power and energy losses in the system, affecting the grid's stability and reducing its security and reliability [7].

Voltage stability refers to the ability of a system to maintain steady-state voltage while balancing active power. Voltage stability may be required depending on significant and small disturbances. Major disturbances occur when there are faults in the transmission lines, significant load increases, distant generation plants, and insufficient compensation of reactive power, while small disturbances happen when there are incremental variations in load. Additionally, depending on the duration of the disturbance, these can be classified as short-term or long-term disturbances. Short-term disturbances involve the dynamics of the load elements in several seconds, while long-term disturbances are produced for several minutes [18].

Frequency stability refers to the ability of the system to maintain the balance of active power between generation and demand, and its objective is to keep the system fre-

`

quency at its nominal value. Frequency stability may be required in cases such as transient instability and small disturbances. Transient instability occurs when the fault cannot be cleared quickly, and an imbalance between the mechanical and electrical torque of the generator happens. Small disturbances happen when there is little availability in transmission lines to transport the electrical energy, resulting in a voltage collapse and instability to the steady state phase angle [19].

The NERC (North America Reliability Corporation) [20] presented the voltage stability control policy addressing voltage and frequency stability regulations.

4   Case Study

The Enriquillo Region is in the southwestern area of the Dominican Republic, formed by the provinces of Barahona, Pedernales, Independencia, and Bahoruco. The space occupied by these four provinces is 6,961.43 km². The Enriquillo Region has five wind generation plants in two of its four areas, which are the case of Barahona and Pedernales. Barahona has three plants with a total installed capacity of 149.80 MW. At the same time, Pedernales has two plants with a total installed capacity of 33.45 MW. Additionally, Barahona has a photovoltaic generation plant with an installed capacity of 25 MW, a thermal generation plant with an installed capacity of 51.80 MW, and a hydroelectric generation plant with an installed capacity of 7.50 MW (see Fig.3). Fig. 4 shows the configuration of the grid in the simulated southern zone [21].
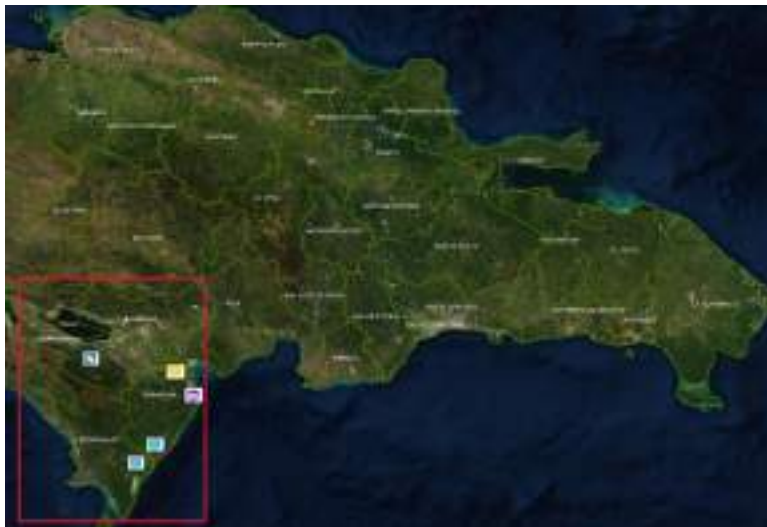
Fig. 3. Location of the Enriquillo Region, Dominican Republic. Source:
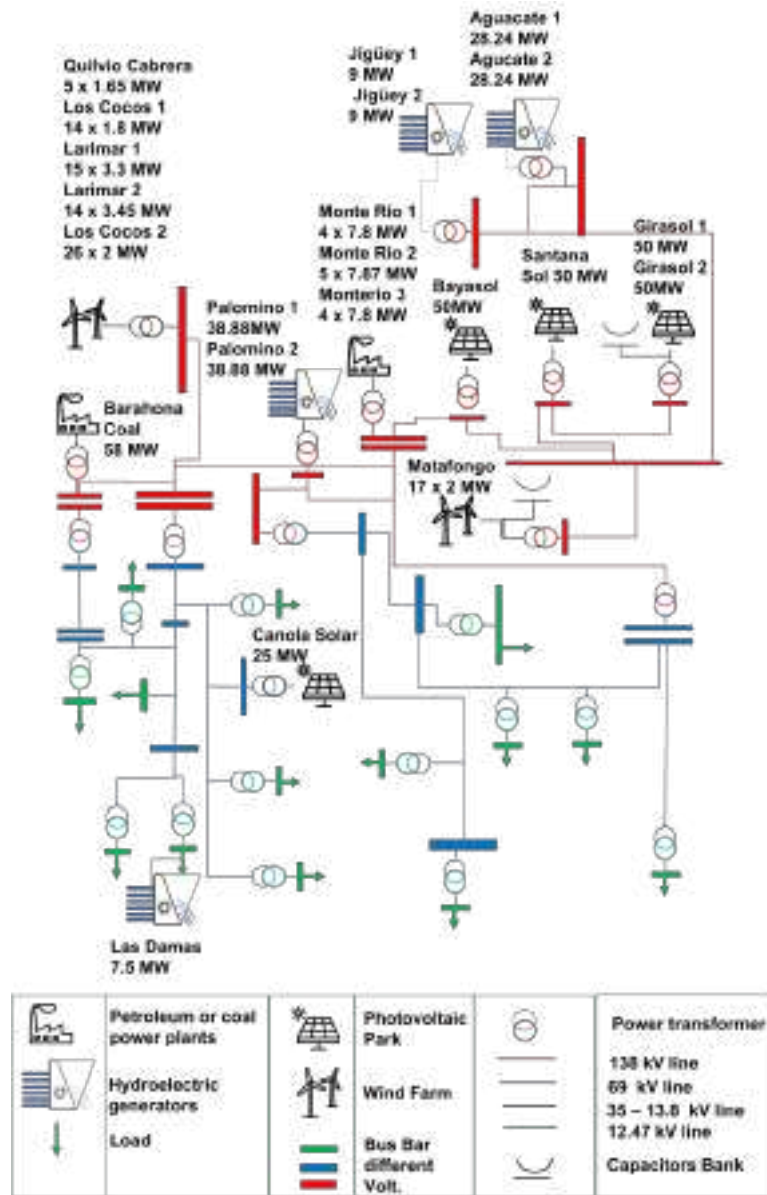https://www.mapas.cne.gob.do/.

Fig. 4. Grid section of the southern zone.

Fig. 5 shows the average monthly demand southern zone registered for 2020, and Fig. 6 shows the generation curve by technology for the same area and same year. These data were essential for the simulation and scenarios presented in the result and discussion section.
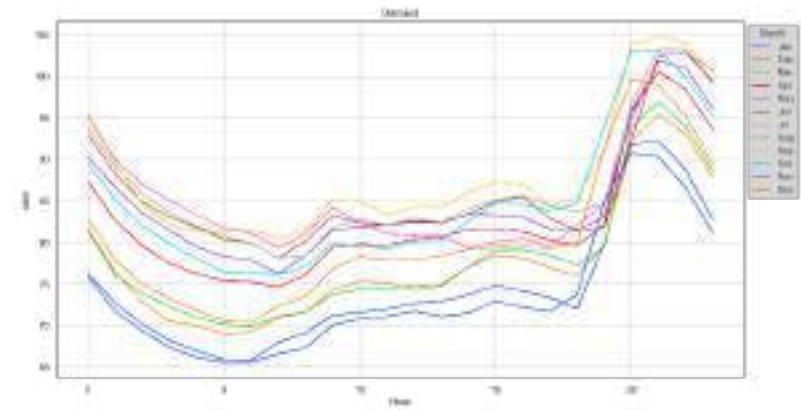

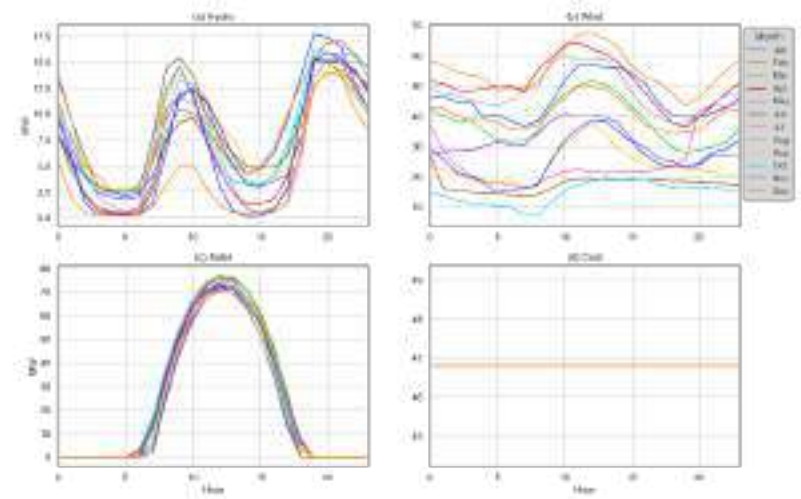**Fig. 5.** Average monthly demand southern zone.

Fig. 6. Generation curve by technology (a) Hydro, (b) Wind, (c) Solar Photovoltaic, (d) Coal-Power Plant.

The regulations for the primary frequency regulation are explained in Regulation of Law No. 125-01 [22]. Table 2 shows a comparison of international frequency stability standards and the Dominican Republic:

Table 2. Comparison of regulations on frequency stability.

Parameter	NERC	Dominican Republic
Active power between 1.5-10% of its value	✓	✓
Frequency insensitivity between 10-30 mHz	✓	✓
Dead band between 0-500 mHz	✓	
Frequency drop between 2-12%	✓	✓
Maximum justified delay (2 sec)	✓	
Activation time (30 sec)	✓	
Distribute hydroelectric units for regulation		✓

In resolution SI-060-2015-MEM, CC4.1.1 [23], it is explained that the regulation of voltages in 69 kV, 138 kV, or greater bus bars, and generators, must remain within the range of $\pm$ 5%.

The power demand data per province are determined as the average of the maximum, average, and minimal demand in the daily dispatch program (PDD) [24]. The average power demand in the Enriquillo region in 2019 for the following provinces was Barahona 30.49 MW, Pedernales 1.97 MW, and Bahoruco 10.03 MW. The average power demand is from 11 a.m. -2 p.m. because, in this area, there are many solar photovoltaic components, and the grid is stressed more since the low demand is also affected by homes that install photovoltaic systems, which impacts the power demand.

According to [25], this area will have an annual growth of 3.41%, the demand for electricity from 2021 to 2032. The analysis of the long-term demand for the period 2021 to 2024 was based on a single demand scenario with the annual energy projection obtained from the historical data of the actual demand supplied and forecast models based on Box-Jenkins.

In the expansion plan of the electric transmission system, 2021 – 2035 [26] is explained that there will be a proliferation of non-conventional renewable energies in the electric power system without a specific insertion plan. This proliferation of non-conventional renewable energies causes much uncertainty about the definition of the optimal growth of transmission networks. Due to the uncertainty caused, various scenarios in the areas most likely to carry out projects with more significant renewable potential are analyzed, as well as the development of thermal generation projects in the vicinity of ports. This projection of power generation is why the country's future demand from 2017 to 2030 presents two possible scenarios:

Low growth. This scenario is based on the trend of the demand for electrical energy, which presents an average annual increase of 3.41%.

High Growth. This alternative possibility considers a higher growth of the economic development of the country and a decrease in the energy not supplied, which grants a supply level of 100% by 2028.

`

5   Results and Discussion

In the Quasi-Dynamic simulation, the following behaviors were identified:
Transmission lines reduced their load capacity by approximately 2.99%, which can be extrapolated to all the regional lines. The evolution of the transmission line with the highest average load in the period established analysis can be seen in Table 3. This behavior contributes to a longer useful life of the lines, alleviates network congestion, allows for lower operating costs, improves network reliability in the event of breakdowns or maintenance on adjacent lines, and reduces losses [17].

Table 3. Transmission line evolution with a higher average load.

Years	Load (%)	Current (kA)
2021	31.022	0.152
2022	30.193	0.148
2023	29.435	0.144
2024	28.745	0.141
2025	28.196	0.138
2026	27.781	0.136
2027	27.501	0.135
2028	27.348	0.134
2029	27.324	0.135
2030	27.428	0.135
2031	27.664	0.137
2032	28.031	0.139

Table 4 shows that both the highest and lowest voltage bus bars reduce their level to more central values in the range allowed by the regulations. Adjustment of the voltages above the acceptable range towards the safe area is achieved ten years after the start of the study (2030).

Table 4. Evolution in bus bars of lower and higher average stress.

Years	Bar with lower average tension	Bar with higher average tension
2021	1.007	1.082
2022	1.007	1.079
2023	1.006	1.075
2024	1.006	1.071
2025	1.005	1.068
2026	1.005	1.064
2027	1.005	1.060
2028	1.004	1.056
2029	1.004	1.052
2030	1.003	1.047
2031	1.003	1.043
2032	1.003	1.037

The RSM/EMT simulation was performed assuming a failure at the AES Andres power plant, which supplies 300 MW to the electrical grid through two plants of 196.80 MW and 121.32 MW representing 10% of the demand of the electrical system [27].

The simulation was carried out in a period of 20 seconds where, at the first second of starting, the electricity generator failed; the behavior of the system frequency can be visualized in the established period; this process was carried out for each year from 2021 to 2032. Fig. 7 compares the system's response in 2021 and 2032, the ones with the greatest and least impact, respectively.

Similarly, it can be seen how the frequency of the system reaches lower values in 2021 before the output of the power plant, reaching values of 59,135 Hz, while, in 2032, minimum values of 59,165 Hz are reached, which represents an average difference of 0.0233% during the analysis period. After 3 seconds of analysis, the primary regulation raising the frequency to 59,768 for 2021 and 59,165 for 2032 presented a faster response in the latter. It should be noted that the frequency does not reach nominal values due to the lack of modeling of the secondary regulation, an area that can be expanded in future research.

It is worth mentioning that the results obtained are shown to be outside the acceptable frequency ranges in the system operating conditions scenario and that in the event of transients or faults that affect frequency stability, the primary regulation must come into play within 30 seconds of the event occurred without leaving the established limits, which is fulfilled in the established analysis. These operating conditions show that even if a significant generator trips, the frequency can fluctuate and recover according to established regulations.
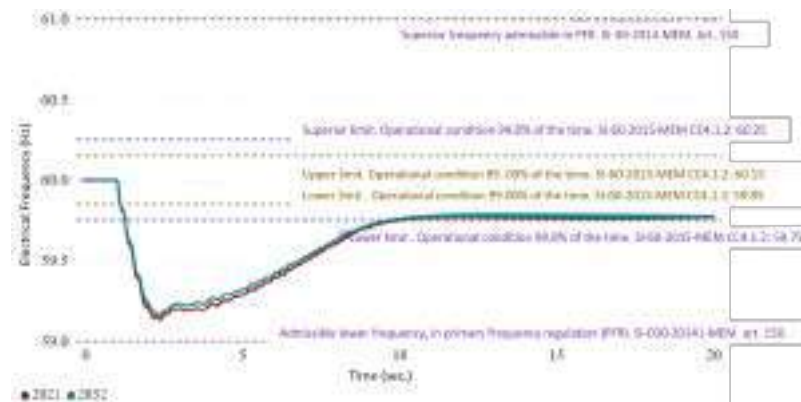

Fig. 7. Electric frequency comparison slack bus between the years 2021 and 2032.

In the RSM/EMT simulation, the behavior of the electrical system in the region was analyzed in the face of the unexpected entry of a large load in the Pedernales area, which has the highest average annual demand for electricity. Fig. 8 compares voltages in the system when a large power demand load enters during the analysis period.
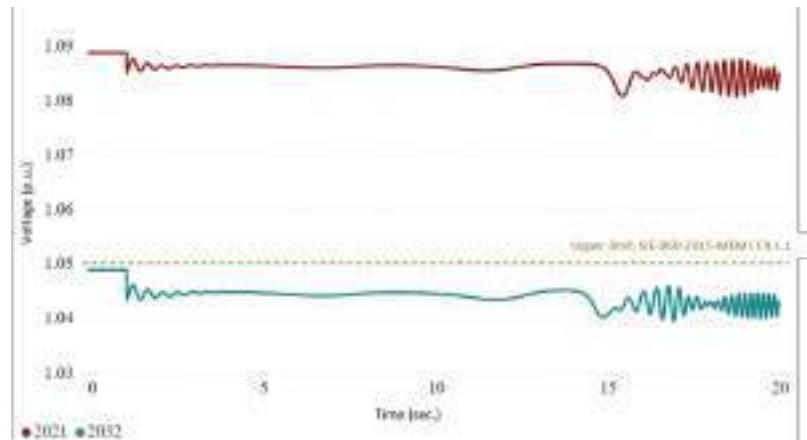
Fig. 8. Comparison of voltages in the system when a large load enters between 2021 and 2032.

The voltage in the treated bus bar is above the upper limit of the norm, this being 1.05 p.u., while in 2032, it is within the allowed range. In both scenarios, the voltages in the bus bars, before the entry of the most critical load in the Pedernales bus bar, oscillate, tending to more noticeable and more significant fluctuations in 2021, while in 2032, there are more damped oscillations (see Fig. 9).
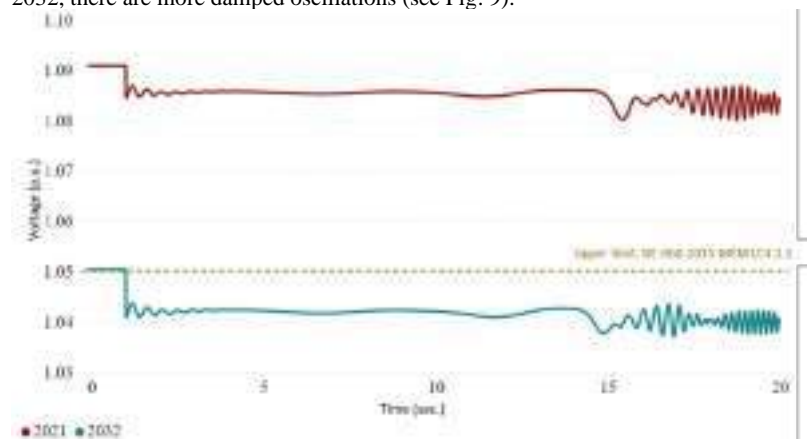

Fig. 9. Comparison of tensions in the Pedernales bus bar before entering a large load.

Fig. 10 shows a behavior similar to that in the bus bar. Both in 2021 and 2032, it is observed that both voltages are identified above the allowed limits before the event. When the input event occurs, the voltage in 2021 remains outside the range, while in 2032, the behavior does not happen, implying that the introduced load is key to maintaining the voltage within the established range by the norm. In both cases, the same

thing happens as in the previous point; oscillations occur that are later corrected, with the one in 2021 being more pronounced.

In the same way, an apparent variation of the electrical frequency is identified now of introducing the load in the Pedernales bus bar. For 2021 and 2032, oscillations are observed in the system. The apparent difference is that in 2021, there is a more pronounced disturbance in the frequency compared to 2032. It can also be observed as the frequency regulation starts working faster in 2032, 15 seconds after the event occurred. In both cases, the frequency remains within the standard's range based on frequency, so this event does not compromise the electrical system.
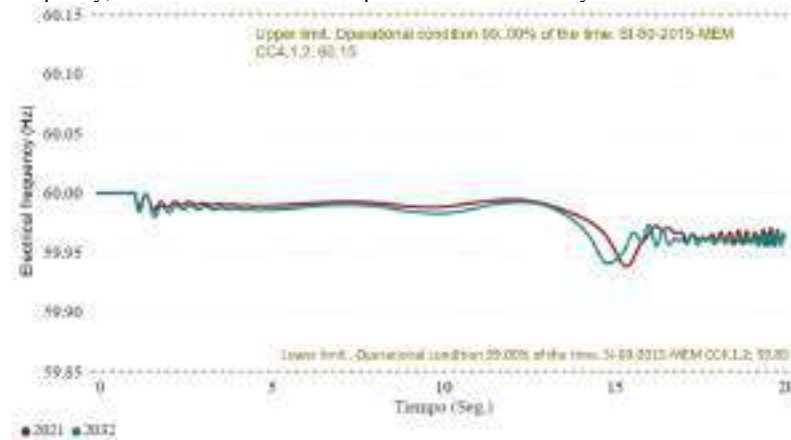
Fig. 10. Frequency comparison in the system, load input in Pedernales 2021 and 2032.

6   Conclusion and Future Works

The control stability of an interconnected electrical system of a country at the voltage and frequency level is a common problem that can be evaluated depending on the power system's complexity. The electrical demand that the tourist infrastructure can produce due to the growth of this sector in different regions of any country can affect the stability parameters of the power system, which can reduce the quality of energy service.

With the acquisition of data from the case study, it was possible to compare and evaluate the behavior of the current and projected energy demand due to growth according to the trend scenario of the electric power transmission company. It was also possible to simulate the necessary scenarios to carry out a technical analysis that reveals the system's behavior in the face of certain events.

The results of the simulations affirm that within the study time, the current system has sufficient capacity for the insertion of electrical demand from our tourist facilities that are to be incorporated in the southern part of the country as a new tourism strategy that is to be developed. In addition, there is no need to implement techniques and/or methods for controlling voltage and frequency in the electrical network. With the

Quasi-Dynamic simulation, it was possible to demonstrate that several parameters, as the years go by with the estimated growth, manage to go from states out of range to within range. The RMS/EMT simulation verified that in the face of events, such as the output of a critical generator and the entry of a large load, the system does not present complications that put its continuous operation at risk.

For future work, it is recommended to carry out a stability study considering the intermittence of the connected renewable energies to see how this affects the system's stability. In addition, perform scenarios where unscheduled outputs of the generation plants are contemplated to see the voltage and frequency profiles of the bus bars. Finally, implement a secondary regulation system during the simulation of the generation profiles in the system.

References

1. Li X., Ge Y.Y., Mao X., et al.: Improved Energy Structure Prediction Model Based on Energy Demand Forecast. 2nd IEEE Conf Energy Internet Energy Syst Integr EI2 2018 - Proc 1–5. https://doi.org/10.1109/EI2.2018.8582170 (2018).
2. Patil S., Deshmukh SR.: Development of control strategy to demonstrate load priority system for demand response program. 5th IEEE Int. WIE Conf. Electr. Comput. Eng. WIECON-ECE2019-Proc1–6.https://doi.org/10.1109/WIECON- CE48653.2019.9019950 (2019).
3. Outlook World Energy Electricity.: World Energy Outlook 2019 – Analysis - IEA. In: Int. Energy Agency (2019).
4. Patel T., Parmar M.:(Special Issue for ITECE 2016) Power System Stability and Control. Int. J. Adv. Res. Eng. Sci Technol 5 (2017).
5. Orús A.: El turismo en el mundo - Datos estadísticos | Statista (2021).
6. Statista: Llegadas de turistas internacionales a América 1990-2020 | Statista (2021).
7. Jorge Eduardo Játiva Sierra: Impacto De La Generación Distribuida En La Estabilidad Del Voltaje En Los Sistemas De Distribución (2020).
8. GmbH Di. Quasi-Dynamic Simulation - DIgSILENT. https://www.digsilent.de/en/quasi-dynamic-simulation.html. Accessed 2022/11/3.
9. Organismo Coordinador del Sistema Eléctrico Nacional Interconectado de la República Dominicana (CO-SENI): Operación del Sistema Eléctrico Nacional Interconectado de la República Dominicana (SENI). In: Report. https://www.oc.do/Informes/Operación-del-SENI/Análisis-Operativo/EntryId/182308 (2022).
10. Arenas A., Mediavilla P., Gracía F., Garcés P.: Estabilidad en los Sistemas Eléctricos de Potencia con Generación Renovable. Organización Latinoamérica Energía 1–28 (2013).
11. Hatziargyriou N., Milanovic J., Rahmann C., et al.:Definition and Classification of Power System Stability – Revisited & Extended. IEEE Trans Power Syst 36:3271– 3281. https://doi.org/10.1109/TPWRS.2020.3041774 (2021).
12. Adetokun B., Muriithi C.: Application and control of flexible alternating current trans mission system devices for voltage stability enhancement of renewable-integrated power grid: A comprehensive review. Heliyon 7:7. https://doi.org/10.1016/j.heliyon.2021.e06461 (2021).
13. Gu M., Meegahapola L., Wong K.L.: Coordinated Voltage and Frequency Control in

Hybrid AC/MT-HVDC Power Grids for Stability Improvement. IEEE Trans Power Syst 36:635–647. https://doi.org/10.1109/TPWRS.2020.2983431 (2021).

14. Mukherjee N., De D., Nandagaoli N.: Effect of sudden variation of grid voltage in primary frequency control application using converter based energy storage systems for weak grid systems. In: 2017 19th European Conference on Power Electronics and Applications (EPE'17 ECCE Europe). IEEE, p P.1-P.10 (2017).

15. Antonello Monti, Federico Milano, Ettore Bompard X.G.: Classical grid control: Fre quency and voltage stability. In: Press A (ed) Converter-Based Dynamics and Control of Modern Power Systems, Elsevier. Joe Hayton, India, p 360 (2021).

16. Ojo Y., Benmiloud M., Lestas I.: Frequency and voltage control schemes for three- phase grid-forming inverters. IFAC-PapersOnLine 53:13471–13476. https://doi.org/10.1016/j.ifacol.2020.12.713 (2020).

17. Yan L., Xiaohui Q., Yongning C., et al.: Study on Requirement of Control and Stability with Renewable Energy Generation Grid Integration. In: 2019 IEEE 8th International Conference on Advanced Power System Automation and Protection (APAP). pp 26–30 (2019).

18. Hatziargyriou N., Milanovic J., Rahmann C., et al.: Definition and Classification of Power System Stability – Revisited & Extended. IEEE Trans Power Syst 36:3271–3281. https://doi.org/10.1109/TPWRS.2020.3041774 (2021).

19. Fernández-Guillamón A., Gómez-Lázaro E., Muljadi E., Molina-García Á.:Power systems with high renewable energy sources: A review of inertia and frequency control strategies over time. Renew Sustain Energy Rev 115:109369. https://doi.org/https://doi.org/10.1016/j.rser.2019.109369 (2019)

20. World Energy Council W.E.C.: Voltage Stability Criteria. (1998).

21. Organismo Coordinador del Sistema Eléctrico Nacional Interconectado de la República Dominicana (CO-SENI): UNIFILAR Sistema Eléctrico Nacional Interconectado de la República Dominicana (SENI) https://www.dropbox.com/sh/rhs9u44j7z79u1k/AACEZm9U25eOQNY-XQiDQZMZa/UNIFILAR SENI?dl=0&subfolder_nav_tracking=1. Accessed 2020/11/09.

22. Superintendencia de Electricidad (SIE): Reglamento para la Aplicación de la Ley General de Electricidad Número 125-01. 314 (2012).

23. Superintendencia de Electricidad (SIE): RESOLUCION SIE-060-2015-MEM. Santo Domingo, Distrito Nacional (2015).

24. Organismo Coordinador del Sistema Eléctrico Nacional Interconectado de la República Dominicana (CO-SENI) Informe anual de operaciones y transacciones económicas 2020.

25. Roa L., Ogando L., LastNameSimó A., et al.: Organismo Coordinador Del Sistema Eléctrico Nacional Interconectado De La República Dominicana Para: AGENTES DEL MEM Preparado por: Gerencia de Operaciones OC-SENI. Santo Domingo (2020).

26. Departamento de Análisis y Planeación del Sistema, de Transmisión.: ETED – Planificación Estratégica Institucional - Planificacion Estratégica 2021-2035. Santo Domingo (2020).

27. Superintendencia de Electricidad (SIE).: Resolución SIE-002-2017-RCD, Autorización de trasnferencia de conseción definitiva para la explotación obra de generación eléctrica "Central AES Andrés" de 300 MW (2017).

`

Harmonic impact of Electric vehicles in Electrical Distribution Systems with high photovoltaic penetration

Miguel Davila-Sacoto[1][0000-0001-6318-2137], L.G. González[2][0000-0001-9992-3494], Luis Hernández-Callejo[1][0000-0002-8822-2948], Óscar Duque-Perez[3][0000-0003-2994-2520], Ángel L. Zorita-Lamadrid[3][0000-0001-7593-691X], and J.L. Espinoza[2][0000-0002-7450-2084]

[1] Department of Agricultural and Forestry Engineering, University of Valladolid, Duques de Soria University Campus, 42004 Soria, Spain
[2] Department of Electrical Engineering, University of Cuenca, Central Campus, 010104 Cuenca, Ecuador
[2] Department of Electrical Engineering, University of Valladolid, School of Industrial Engineering, 47011 Valladolid, Spain

```
miguelalberto.davila@alumnos.uva.es M.D.-S.
    luis.gonzalez@ucuenca.edu.ec L.G.G
   luis.hernandez.callejo@uva.es L.H.-C.
      oscar.duque@eii.uva.es O.D.-P.
        zorita@eii.uva.es A.L.Z.-L.
   juan.espinoza@ucuenca.edu.ec J.L.E.
```

Abstract. The integration of electric vehicles and the charging stations associated with their operation requires an exhaustive analysis of the impacts on the electrical network. In the case of grids with high photovoltaic penetration, the scenario is complicated due to the effects of the variation of the solar resource and the connection times of the vehicles that respond to the preferences of the users. In the present study, an analysis of the impact of harmonics generated by electric vehicle charging stations in different scenarios of photovoltaic penetration in a electrical distribution system is carried out by obtaining the harmonics in direct current and alternating current charging stations with different brands of electric vehicles. Results of magnitudes of 5th and 7th harmonics higher than 30% are obtained and the effect of the variation of current and voltage in the final users and in the substation transformer is shown.

Keywords: Electric Vehicle, Photovoltaic generation, Microgrid, Distribution System, Harmonics.

1   Introducción

The adoption of electric vehicles (EVs) has experienced considerable growth over the last 5 years, so the integration of these types of loads into electrical distribution systems requires an in-depth analysis of their effects on the network. The connection of EVs to the network increases the harmonic distortion of voltage and current, and in general decreases the useful life of the distribution transformers due to the increase in temperature [1]. On the other hand, the inverters of photovoltaic (PV) systems connected to the grid are also a source of harmonic distortion that can reach up to 5.59 % for the third harmonic and 14.65 % for the fifth harmonic [2], which added The effect of electric vehicles in a network with high PV penetration can cause problems in microgrids. In addition, a high penetration of EVs can cause problems in the network in terms of power quality, which can lead to inconveniences of service interruption, voltage and current variations and harmonic distortion [3]. For this reason, the integration of EVs to systems dependent on PV generators must be properly planned to avoid unwanted operation of the distribution system.

Several related studies have been carried out on the impact of EVs in electrical distribution systems both on the penetration side of EVs and the PV system [3]–[7], however, there are few case studies that carry out a integration of technologies in a microgrid. In the proposed study, the harmonic effects of EV charging stations in a microgrid with high penetration of PV energy are presented, considering cases of peak demand and valley demand. For this, the measurement of the power quality of fast charging stations in direct current and slow charging in alternating current in the charging process of KIA and BYD brand vehicles was carried out to obtain the real harmonic values. The simulation of the system was performed in OpenDSS and the IEEE European Low Voltage Test Feeder case was used for its validation.

2   Methodology

To obtain the electrical parameters of this study, a methodology based on measurement in real charging conditions of different brands of electric vehicles and charging stations was carried out. In addition, the modeling of charging stations and electric vehicles was executed as a storage element and as a source of harmonic generation. Finally, a standard electrical network model was used to perform the simulations.

2.1   Electric Vehicle and Charging Stations

The EVs are modeled according to the OpenDSS storage elements and are distributed in different phases of the system and as a harmonic current source. The equivalent circuit of the EV (see Fig. 1) is modeled as an RL load with series and parallel components [8].
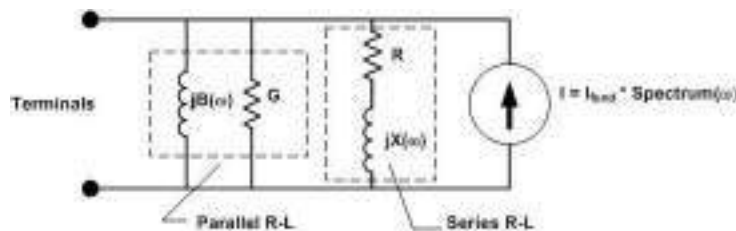
Fig. 1. Harmonic model for electric vehicles.

For the acquisition of real data of current harmonics, tests were carried out in the Microgrid Laboratory of the University of Cuenca using a Fluke 435 II power quality analyzer. The measurements were carried out in a BYD model T3 vehicle and in a KIA Soul model vehicle, a generic slow charge electric vehicle charging station or electric vehicle supply equipment (EVSE) and a Circontrol Raption 50 model fast direct current charging station. The results of current harmonics (magnitude and angle) are shown in Table 1 and are compared with those obtained in similar studies.

Table 1. Current harmonics for different electric vehicles and charging stations.

Har-monic order	Pa-rame-ter	Electric vehicle charger [6]	Nissan Leaf [5]	BYD slow AC charge	Kia slow AC charge	BYD fast DC charge	kia fast DC charge
1	Mag.	100	100	100	100	100	100
	Angle	305	-26	136	143	8.6	28.6
3	Mag.	9.20	25.00	9.91	6.31	2.40	6.22
	Angle	120.00	-94.00	98.00	102.00	6.50	32.00
5	Mag.	62.20	17.00	8.47	1.15	1.73	14.55
	Angle	255.00	-96.00	120.00	131.00	7.20	36.00
7	Mag.	41.80	14.20	8.11	0.83	2.14	5.61
	Angle	332.00	-72.00	146.00	153.00	6.80	31.00
9	Mag.	1.48	9.69	7.30	0.49	1.13	4.34
	Angle	357.00	-68.00	152.00	161.00	5.70	34.00
11	Mag.	7.08	5.04	6.92	0.64	2.45	5.06
	Angle	358.00	-49.00	168.00	182.00	5.60	35.00

In addition, the efficiency of both the charging station and the vehicle's internal converter was measured, that is, the input power of the station and the power directly at the EV battery terminals were measured. (see Fig. 2). The equipment used for sampling was a Fluke 435 II for AD parameters and a Hioki PW3337 for DC parameters. The experiment was carried out in the microgrid laboratory of the University of Cuenca [9].
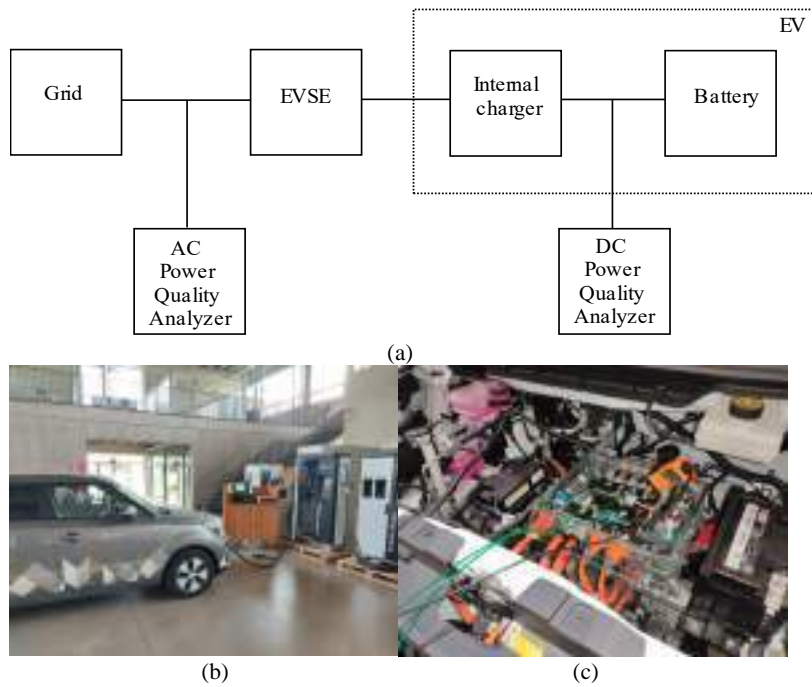
(a)

(b)   (c)

Fig. 2. Measurement of parameters of the electric vehicle and the charging station: (a) Equipment connection diagram; (b) Overview of the experiment; (c) Connection of probes to the battery of the electric vehicle.

The efficiency of the EVSEs was analyzed in both alternating current and direct current charging modes (see Table 2).

Table 2. Current harmonics for different electric vehicles and charging stations.

EV	Charge mode	Charge Power	Efficiency
BYD T3	AC Slow	5.6 kW	92.90 %
BYD T3	DC Fast	50 kW	94.60 %
KIA Soul	AC Slow	5.6 kW	89.80 %
KIA Soul	DC Fast	50 kW	91.70 %

2.2   Application Scenario in a Low-Voltage Network Feeder

To verify the impact of harmonics and efficiency of the charging stations, a simulation was carried out in OpenDSS and Matlab of the IEEE European Low Voltage Test Feeder which is a model commonly used in microgrids, analyzing two cases of PV generation location: (1) 14 distributed PV systems of 5kW and 14 EVSEs of 7.2 kW each, and (2) 1 central PV system of 70 kW and 14 EVSEs of 7.2 kW (see Fig. 3). The harmonic spectrum of table 1 was assigned to each case. The values were selected for illustrative purposes and the simulation can be downloaded from https://github.com/davilamds/harmonicsevpv .
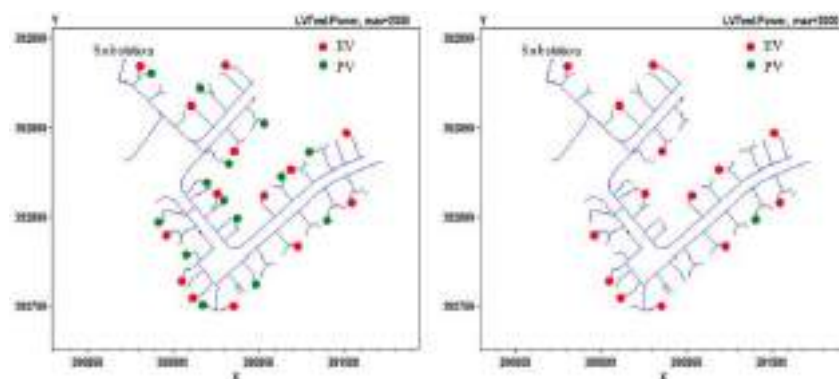
Fig. 3. Test cases: (a) distributed EV and PV; (b) distributed EV single PV.

The following scenarios were analyzed:
- Base case;
- EVs connected without PV generation, without harmonics;
- Connected EVs, distributed PV generation, without harmonics (Case 1);
- Connected EVs, single PV generation, no harmonics (Case 2);
- Connected EVs, distributed PV generation, with harmonics (Case 1);
- Connected EVs, single PV generation, with harmonics (Case 2).

The response of the substation, the voltage and the current in terminals of the client 349 were analyzed.

3   Results

In the first instance, the power of the station transformer was analyzed in the scenarios described in section 2. As can be seen in the Figure 4, the power of the substation transformer varies as the EVs are added to the network and when considering the effect of the harmonics injected by the loads and the EV-SEs. The lowest power value occurs in

Case 2 without harmonics, however, when harmonics are injected into the network, the maximum power value of all scenarios is obtained. The harmonics, by causing a high current and saturating the system's conductors, cause the effect of power injection by the PV generation to be less. It is also observed that the situation worsens when there is only one PV generation in the distribution system.
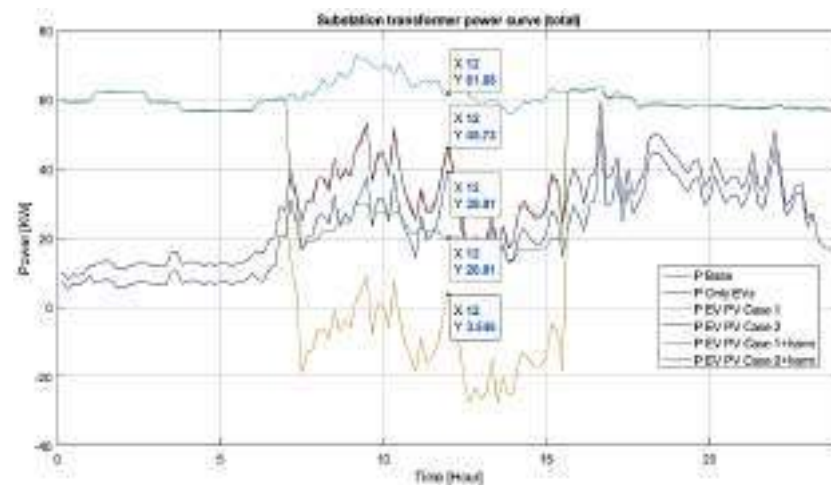

Fig. 4. Substation transformer Power curve for different scenarios

When checking the voltage and current in the connection bars of one of the clients, it is observed that the impact of the harmonics is considerable. In the case of voltage (see Fig. 5a), the harmonics cause a voltage variation for both case 1 and case 2 of PV generation. In case 1, an increase in tension of 1.2 % is observed, while in case 2 a decrease of 0.56 % is observed in measurements at noon.

On the other hand, the current (see Fig. 5b) increases both in case 1 and in case 2 during the operation of the system in general, however, at the moments of connection of the EVs, the cases with harmonics cause a decrease in the current in terminals of the client of 25.97 %.
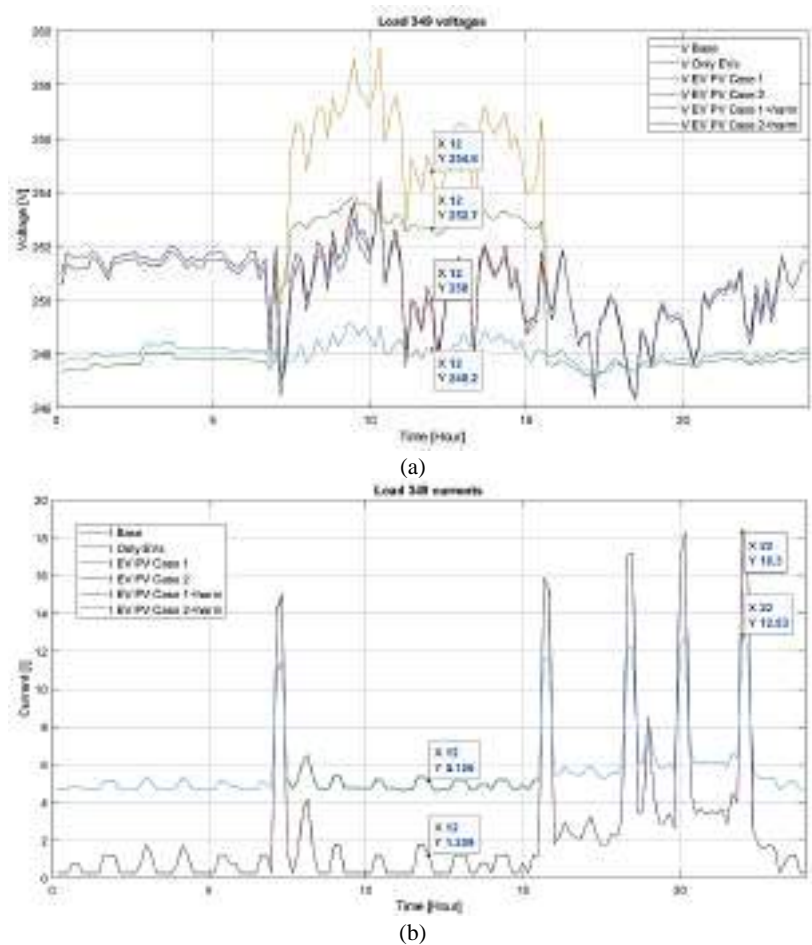
(a)

(b)

Fig. 5. Behavior of the 349 load in different scenarios: (a) Voltage; (b) Current.

Table 3 shows the maximum and minimum power values of the substation transformer and the voltage and current at the customer's terminals. It is observed that the scenario that requires the highest power from the transformer is case 2 with harmonics in both maximum and minimum power during the 24-hour period. Regarding the voltage, the cases with harmonics do not have a considerable effect, however in the current the highest values are maintained at the minimum of case 2 with harmonics.

Table 3. Maximum and minimum values of Power, Current and Voltage of the analyzed scenarios.

Case		Transformer Power [kW]	Load Voltage [V]	Load Current [I]
Base	max	51.45	254.11	18.31
	min	5.24	246.45	0.23
Only Evs	max	59.35	254.08	18.30
	min	7.96	246.31	0.23
EV PV Case 1	max	59.35	259.39	18.30
	min	-27.68	246.31	0.23
EV PV Case 2	max	59.35	254.48	18.30
	min	7.96	246.31	0.23
EV PV Case 1 + Harmonics	max	63.86	253.87	12.83
	min	13.54	246.99	4.63
EV PV Case 2 + Harmonics	max	72.81	249.14	12.83
	min	55.74	246.90	4.57

Reviewing only the harmonics injected into the network during the 24 hours (see Fig. 6a), it is observed that there is a predominance of harmonics 5 and 7, which corresponds to the high magnitude found in laboratory measurements. Also, if the evolution of the 5th harmonic is observed during the day (see Fig. 6b), it is determined that the high magnitudes coincide with the connection of the EVs to the system, causing values higher than 30 % with respect to the harmonic in periods without connection of EVs.
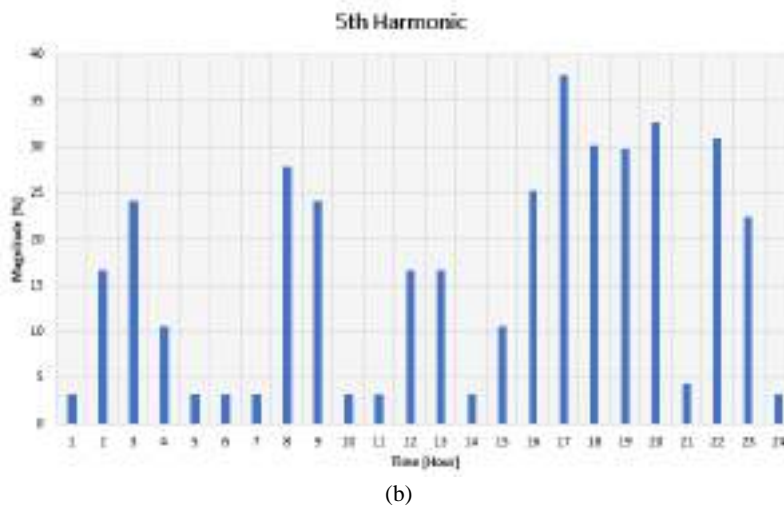

(a)

(b)
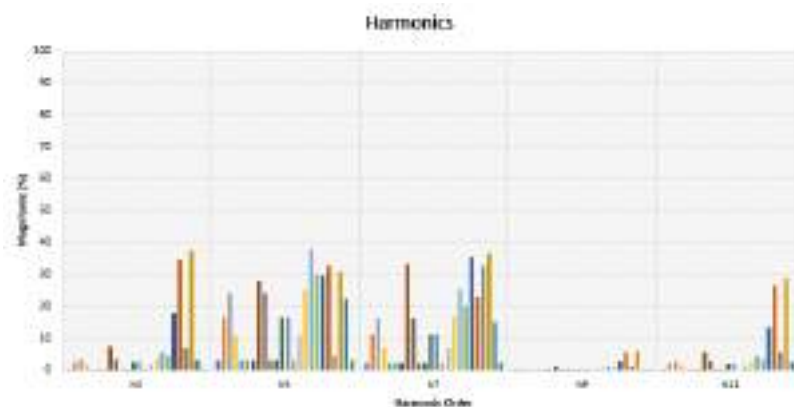
Fig. 6. Harmonic behavior: (a) 5th harmonic; (b) 7th harmonic.

4   Conclusions

This study presents the impact of harmonics caused by electric vehicle charging stations in an electric power distribution network with a high penetration of photovoltaic generation. Two specific cases of photovoltaic penetration were analyzed, the first with distributed generation and the second with centralized generation. It was observed that the harmonics cause an important variation in the current and voltage in the terminals of the final users and in the power of the transformer of the substation of the IEEE case analyzed. Magnitudes of the 5th harmonic greater than 30 % were observed, which is above known norms. In addition, and as an input for this study, the magnitude and angle values of harmonics for charging stations and electric vehicles were obtained by measuring directly at the battery terminals, thus achieving the consideration of the entire energy conversion system. of both the station and the electric vehicle.

Future Work

The harmonics model used must be expanded to values for each minute and the impact on the distribution system analyzed. It is also required to analyze the impact of the efficiency of the charging stations in the system.

Acknowledgement

References

1. D. Alame, M. Azzouz, and N. Kar, "Assessing and mitigating impacts of electric vehicle harmonic currents on distribution systems," Energies, vol. 13, no. 12, 2020, doi: 10.3390/en13123257.
2. N. Phannil, C. Jettanasen, and A. Ngaopitakkul, "Power quality analysis of grid connected solar power inverter," in 2017 IEEE 3rd International Future Energy Electronics Conference and ECCE Asia (IFEEC 2017 - ECCE Asia), Jun. 2017, pp. 1508–1513, doi: 10.1109/IFEEC.2017.7992269.
3. X. Wang, H. He, F. Sun, X. Sun, and H. Tang, "Comparative Study on Different Energy Management Strategies for Plug-In Hybrid Electric Vehicles," Energies, vol. 6, no. 11, pp. 5656–5675, Oct. 2013, doi: 10.3390/en6115656.
4. Anita Gusai, "Harmonic Analysis in PV Connected Power System," Int. J. Eng. Res., vol. V9, no. 08, pp. 474–477, 2020, doi: 10.17577/ijertv9is080179.
5. A. Aljanad and A. Mohamed, "Harmonic Impact of Plug-In Hybrid Electric Vehicle on Electric Distribution System," Model. Simul. Eng., vol. 2016, 2016, doi: 10.1155/2016/5968943.
6. M. A. S. Masoum, P. S. Moses, and S. Deilami, "Load management in smart grids considering harmonic distortion and transformer derating," Innov. Smart Grid Technol. Conf. ISGT 2010, pp. 1–7, 2010, doi: 10.1109/ISGT.2010.5434738.
7. P. T. Staats, W. M. Grady, A. Arapostathis, and R. S. Thallam, "A statistical method for predicting the net harmonic currents generated by a concentration of electric vehicle battery chargers," IEEE Trans. Power Deliv., vol. 12, no. 3, pp. 1258–1264, 1997, doi: 10.1109/61.637002.
8. R. Dugan, "OpenDSS Level 2 Training Getting Started : Installation & Basic Usage," no. April, 2009.
9. J. L. Espinoza, L. G. Gonzalez, and R. Sempertegui, "Micro grid laboratory as a tool for research on non-conventional energy sources in Ecuador," in 2017 IEEE International Autumn Meeting on Power, Electronics and Computing (ROPEC), Nov. 2017, vol. 2018-Janua, no. Ropec, pp. 1–7, doi: 10.1109/ROPEC.2017.8261615.

Super resolution generative adversarial network for velocity fields in Large Eddy Simulations

Maximiliano Bove[0000−0002−8065−4308],
Sergio Nesmachnow[0000−0002−8146−4012], and Martín Draper

Universidad de la República, Uruguay
{mbove,sergion,mdraper}@fing.edu.uy

Abstract. This article presents an approach for generating synthetic velocity fields in Large Eddy Simulations. This is a relevant problem, considering the high computational effort required to simulate turbulent flows with fine resolution. The proposed approach applies a Generative Adversarial Network, considering relevant information about horizontal slices of turbulent velocity fields. The approach is evaluated on a real-world case study: augmenting the resolution of horizontal velocity fields downstream of a wind turbine. The main results indicate that the proposed approach is able to generate high resolution images of horizontal velocity fields given a low resolution counterpart, without the need for explicitly performing computationally expensive Large Eddy Simulations.

Keywords: velocity fields, superresolution, Large Eddy Simulations, GANs

1   Introduction

Several well-known methods have been proposed for modeling turbulent flows, within the area of Computational Fluid Dynamics (CFD) [19]. Although turbulent flows respond to Navier-Stokes equations, there is no general analytical solution for them so far. Numerical methods allow approximating solutions to Navier-Stokes equations applied to turbulent flows, but the computational resources needed for realistic engineering applications are usually excessively large, especially for very turbulent flows [30]. Methods like Large Eddy Simulation (LES) are responsible for solving only the low-frequency turbulent scales (large vortices) and evaluating the effects of small scales without having to solve them explicitly [5,20]. LES provides a compromise between the computational cost and the resolution accuracy of the turbulent scales in the studied phenomenon [2].

A viable alternative to solve the turbulent flows problem using less computational resources consists in augmenting the resolution of CFD simulations using synthetic data. Synthetic data generation refers to the process of creating new data by applying a systematic and programmatic method [3]. The main idea is to use both real and synthetic data when obtaining new data is not practical or even not possible. The (new) synthetic data must approximate accurately the distribution of real data, and even incorporate realistic features to the datasets.

The super resolution problem refers to reconstructing or recovering high resolution details from low resolution data, usually to overcome the limitations of physical systems. This is a very important problem in image processing [13,14] but it is also applied in signal and multimedia processing, astronomy, privacy and security, remote sensing, etc. Obtaining such super resolution dataset from low-resolution samples is a challenging problem, for which several computational algorithms have been proposed. Among them, Generative Adversarial Networks (GANs) have shown very good problem solving capabilities, computing accurate results, especially in image generation and recovery tasks [26].

In this line of work, this article presents an approach for the generation of synthetic velocity fields in LES. A specific GAN is applied to generate high fidelity (resolution) horizontal velocity fields slices (images) of a portion of the flow downstream of a wind turbine. The applied GAN is trained with low and high fidelity single channel images of velocity fields horizontal planes at hub height of a a wind turbine. The main goal is learning to generate new synthetic high resolution slices, using as input a low resolution slice computed using LES simulations. The main results of the research is the acquired capability of the trained GAN to generate high resolution turbulent flow images. In turn, the generated images have good similarity metrics, when compared with the original images from LES simulations. Overall, the article contributes with a methodology for generating synthetic velocity fields in LES and the evaluation of the proposed methodology in a real case study, relevant for the study of renewable energies.

The article is organized as follows. Next Section presents the main concepts about GANs and a description of the problem solved. Section 3 reviews relevant related works. Section 4 presents the applied methodology and implementation details. The experimental evaluation of the proposed resolution approach is described in Section 5. Finally, Section 6 presents the conclusions of the research and formulates the main lines for future work.

2   Generative Adversarial Networks

A generative model is a statistical tool that allows modeling the joint probability distribution $p(X, Y)$ relating a given observable variable X (input or data instance) and a target variable Y (output) [16]. Generative machine learning is a branch of computational intelligence including methods that are able to generate new instances of data, by learning the joint probability $p(X, Y)$ to describe the process of generating new datasets [4].

GANs use adversarial artificial neural networks (ANNs) for generating new data [7]. A GAN consists of two ANNs competing and cooperating: the *generator* and the *discriminator*. Both ANNs apply an adversarial learning approach to optimize their parameters in order to generate accurate synthetic data.

The generator ANN (g) specializes on learning how to create synthetic data samples x', taking as input random vectors from a latent space z. The generator is characterized by the equation $g(z) = x'$. The main goal of the generator is to approximate the distribution of true data, by considering the information about

the problem provided by the discriminator. The discriminator ANN specializes on learning how to distinguish real data samples x (from a training dataset) from the synthetic samples x' created by the generator. Both ANNs are trained simultaneously and following an adversarial approach: the discriminator tries to learn the real data distribution for a proper evaluation of new synthetic data and the generator seeks to generate images that deceive the discriminator, by generating data samples that the discriminator cannot label as real or synthetic. A well-designed training process converges to a generator ANN that approximates the real data distribution, thus generating high-quality synthetic data samples.

Recent articles have demonstrated that GANs are useful tools for many applications that require generating synthetic data, especially in multimedia processing, healthcare, time series analysis, and other areas [11,17,23,24]. This article applies a GAN-based approach for generating synthetic velocity fields in LES. The generator learns to upsample an image while maintaining its quality, applying several transformations via specific ANN layers (residual and convolutional networks). Instead of taking random noise as input, the GAN takes an image and increases its resolution. The discriminator evaluates both the original high resolution image and the synthetic image created by the generator. Through a succession of convolutional layers, the discriminator outputs a binary result that indicates whether the input image is real or synthetic. The discriminator is trained by comparing its output with the ground truth. In the resulting adversarial game, the generator tries to create super resolution images indistinguishable from the original image and the discriminator attempts to discriminate the high resolution image from the super resolution image.

3   Related work

The super resolution problem has been successfully addressed using GAN in many application areas, including computer vision, image synthesis and translation, video generation, and also fluid dynamic problems [26].

Ledig et al. [9] proposed Super Resolution GAN (SRGAN) for the super resolution problem on images. SRGAN included a supervised training method, applying a generator conditioned on a low resolution image. In turn, new components were included to complement the adversarial loss used for training: a perceptual loss from a pre-trained classifier and a regularization loss to promote the creation of spatially coherent images. SRGAN was able to create photo-realistic images, upscaling four times the input image.

Xie et al. [29] applied a generative model to synthesize multi dimensional physics fields. A conditional GAN was proposed to infer 3D volumetric data and generate realistic high-resolution flow data. A data augmentation phase was included, guided by physics information to avoid overfitting. The approach was validated over a 3D plume scenario and simulations augmented with additional turbulence. The GAN generated stable and realistic details, properly benefiting from coherent, physical information. The method was robust for realistic models of physical phenomena, but required a moderate execution time for training in 2D and a large execution time (many days) for the full 3D models.

Werhahn et al. [28] proposed Multi-Pass GAN, a method for sampling volumetric functions using GANs. A decomposition was applied to divide the problem into simpler subproblems. Two GANs were applied: one for upscaling and the other for refining the volume, using two-dimensional slices. Two components are included in the loss function for spatial and temporal supervision. The method was validated on realistic buoyant smoke motion scenarios, including colliding smoke plumes. The approach was able to compute significant upscaling factors for volume, while showing a better computing performance than the models proposed by Xie et al., i.e., five days using a single GPU.

Subramaniam et al. [22] proposed Turbulence Enrichment residual block neural network (TEResNet) and Turbulence Enrichment GAN (TEGAN) applying physics-based data-driven and the SRGAN approach, for studying turbulent phenomena. TEResNet is formed by the residual network generator of TEGAN, trained without the adversarial approach. The validation of the proposed methods was performed on an incompressible forced isotropic homogeneous turbulence problem in a 3D periodic domain, considering as input data a low resolution turbulent flow. The evaluation studied different loss functions and physics-based terms. TEGAN obtained the best results, being able to enrich low resolution fields and recover a large portion of the missing finer scales.

Li and McComb [10] applied Physics-Informed Generative Adversarial Networks (PIGANs) for super resolution multiphase fluid simulations. A variant of the adversarial generative approach in SRGAN was proposed to reconstruct fluid phase fraction at a higher resolution. The proposed model incorporates a physics-informed term in the loss function. Accurate results were reported, outperforming other non-learning upsampling approaches in terms of accuracy and detail preservation. Even though the proposed model computed accurate results, a comparison with a traditional SRGAN suggested that using physic information does not allow to significantly improve the results.

The analysis of related works indicates that there is still room to contribute in this line of research, by proposing and studying generative models for super resolution in the context of CFD.

4 Super resolution GAN for velocity fields in LES

This section describes the methodology applied for the generation of velocity fields in LES using GANs.

4.1 Resolution approach

Overall description. The strategy for solving the problem consists of taking high-resolution images and applying a random image cropping of a defined size (96×96 for images from the DIV2K dataset and 32×32 for the UxLES dataset). Each image is flipped horizontally and rotated an angle of 90° (clockwise), with a probability of 0.5. Then, images are scaled down using a bicubic kernel in order to have low resolution images $4\times$ smaller (i.e., 24×24 or 8×8 depending on the

dataset). After that, the high resolution image is normalized with a mean of 0.5 and a standard deviation of 0.5 ($[0, 1]$ range) on each channel. Similarly, the low resolution image is normalized with a mean of 0 and a standard deviation of 1 ($[0.5, 0.5]$ range). The resulting images stored in a tensor are then used to define the training and validation sets for the proposed GAN.

Both the generator and the discriminator in the proposed GAN are trained with the goal of obtaining super resolution images that the discriminator is not able to distinguish from the original high resolution images. The details of the applied generator and the discriminator are presented in the next subsection.

4.2 Architecture of the applied ANNs

The proposed GAN is based on deep residual networks (ResNet) [8], which have shown very good capabilities for image recognition and image processing tasks. The main details of the architectures are described next.

Residual Networks. The decision of using the ResNet structure is based on the need of properly dealing with the information degradation. ResNet is able to handle the difficulties of propagating the information from the superficial layers to the deepest layers of the model. Additional features are included, namely skip-connections and batch normalization, to mitigate the effect of internal covariate shift, i.e., the change in the distribution of network activations due to the change in network parameters during training.

Generator. Instead of using a random latent space, as usually applied in GANs, the generator receives a low resolution image as input and processes it using a Convolutional Neural Network (CNN). The CNN architecture consists of a single convolutional layer with kernel size $k = 9$, number of feature maps $n = 64$, and stride $s = 1$ (k9n64s1). The activation function is a channel-wise Parametric ReLU (PReLU), which overcomes the shortcomings of the traditional ReLU activation function and considers different slopes for each exit channel. Then, $B = 16$ residual blocks are defined. Each block consists of a CNN, followed by batch normalization (BN) to standardize the inputs of a layer for each mini-batch, to stabilize the learning process and reduce the required number of training epochs. The final components of each block are a PReLU activation, a CNN, BN, and the sum of the input of the block (using the skip connection). Following the B residual blocks, a new CNN, BN, and a skip-connection from the start of the block series is applied to avoid loss information during the B blocks. The scale up is performed in two successive $2\times$ factor increases after applying a CNN having a number of output channels four times greater than the input, and then performing a PixelShuffler. PixelShuffler is used to convert the depth (channel) into the 2D space (height and width), to upsample the images, i.e., distributing the increase in the width and height of the image ($C \cdot 4 \times H \times W \to C \cdot H \times 2 \times W \times 2$). This step is performed twice, to obtain an increase of four times of the original resolution. Finally, a CNN with 3 output channels corresponding to the RGB colors is added. A diagram of the generator is presented in Fig. 1(a).

Discriminator. The discriminator receives a high resolution image (either real or synthetic) as input. The architecture of the discriminator includes a CNN with LeakyReLU activation, followed by seven blocks composed by a CNN, BN, and LeakyReLU, with successive increases in kernel size and alternating with stride 1 or 2. After that, the discriminator applies a linear ANN with LeakyReLU and finally another linear ANN with sigmoid activation. The discriminator returns the probability that the two input images are identical, according to the learned criteria. A diagram of the discriminator is presented in Fig. 1(b).
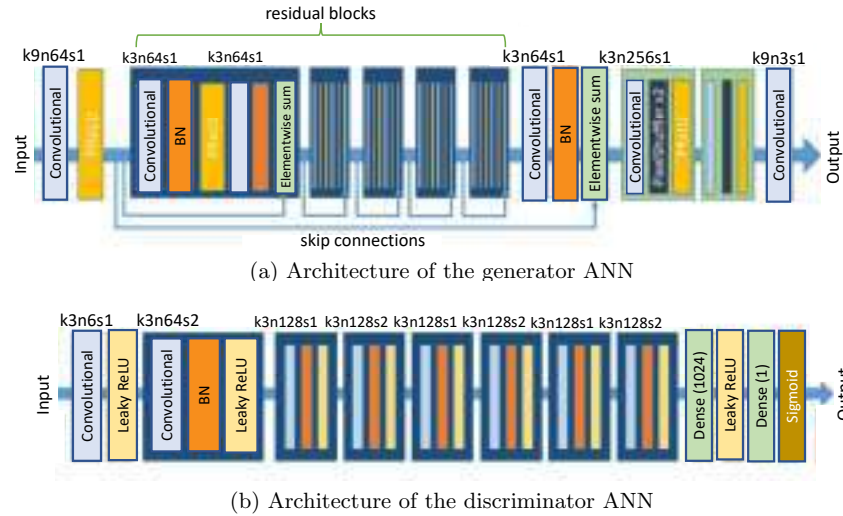

(a) Architecture of the generator ANN

(b) Architecture of the discriminator ANN

Fig. 1: Architecture of generator and discriminator (based on Ledig et al. [9])

4.3   Loss functions

Commonly used loss functions for GAN training (Mean Squared Error (MSE) or Peak Signal-to-Noise Ratio (PSNR)) do not capture relevant differences in velocity fields per se, because they are defined as a mere pixel difference [9].

The loss function for training the generator is the sum of two components: the content and the adversarial terms. For the content term, the loss function based on MSE is replaced by a specific loss function computed from the feature maps of a VGG network ($l_{VGG/i.j}^{SR}$). The content term is defined in Eq. 1, where $W_{i,j}$ and $H_{i,j}$ are the dimensions of the fetaure maps defined by the VGG network.

$$l_{VGG/i.j}^{SR} = \frac{1}{W_{i,j}H_{i,j}} \sum_{x=1}^{W_{i,j}} \sum_{y=1}^{H_{i,j}} (\phi_{i,j}(I^{HR})_{x,y} - \phi_{i,j}(G_{\theta_G}(I^{LR}))_{x,y})^2 \qquad (1)$$

The proposed content term evaluates the differences between the features of the super resolution image generated by VGG and the features of the original high resolution image. Specifically, the proposed VGG loss is based on the ReLU activation layers of the VGG19 ANN.

Regarding the adversarial term of the loss function, the following ideas are applied. The main goal of the generator is to deceive the discriminator, trying to generate synthetic super resolution images indistinguishable from real high resolution images. Thus, the output of the discriminator of the synthetic super resolution image is maximized, since the main goal is for the discriminator to output the value one for synthetic super resolution images. For a better convergence, the opposite value of the discriminator output is minimized (Eq. 2).

$$l_{GEN}^{SR} = \sum_{n=1}^{N} -\log D_{\theta_D}(G_{\theta_G}(I^{LR})) \tag{2}$$

Despite MSE not being fully adequate to evaluate the differences of the synthetic and the real image, an empirical evaluation demonstrated that the best training results are obtained when adding the MSE loss, defined in Eq. 3.

$$l_{MSE}^{SR} = \frac{1}{r^2 WH} \sum_{x=1}^{rW} \sum_{y=1}^{rH} (I_{x,y}^{HR} - G_{\theta_G}(I^{LR})_{x,y})^2 \tag{3}$$

Then, terms are added to define the global loss function, applying a suitable rescaling of the the content loss and the adversarial loss, for the three considered functions to have the same order of magnitude. The content loss is rescaled by a factor of 6×10^{-3} and the adversarial term is rescaled by a factor of 1×10^{-3}.

5   Experimental analysis and discussion

This section reports the experimental analysis of the proposed GAN for the generation of velocity fields in LES.

5.1   Methodology

Development and execution platform. The proposed GAN was developed in Python using the open source machine learning framework PyTorch [18], and the albumentations and matplotlib libraries. The developed code is publicly available at https://github.com/maxibove13/SRGAN. The experimental analysis was performed on the high performance computing platform of National Supercomputing Center (Cluster-UY), Uruguay [15].

GAN training and validation. A k-fold cross validation was applied for validating the proposed method, for efficiently using the available data. k-fold cross validation [6] overcomes the reduction of data samples when using training, validation, and testing datasets, to lowering the risk of overfitting. It does not require a test dataset, since the model is evaluated on a subset of the training set.

The applied k-fold cross validation first divided the dataset in 89% of the samples for training and 11% for validation. Then, the training set was divided in k subsets (folds). Subsequently, the model was trained k times, leaving out

from the training a different subset of the k folds each time. Thus, the evaluation metrics were computed for the k training instances, averaged, and considered for hyperparameter tuning. After determining suitable values for the hyperparameters, the final version of the model was trained with all the training set, including all folds. The performance of the model on unseen data was evaluated with the (previously separated) testing set.

The Adam optimizer was used for training the ANNs, with learning rate 1×10^{-4} and $\beta \in \{0.9, 0.999\}$. A batch size of 16 was selected, and the training was stopped after 160 epochs. A parallel implementation was developed, using four worker processes to generate and process batches in parallel.

Evaluation metrics. PSNR and Structural Similarity Index Measure (SSIM) [27] are used to assess the quality of the generated images. PSNR is an expression for the ratio between the maximum possible signal power and the power of the distorting noise. This ratio is computed in decibel form and it tends to infinity when the images are identical. SSIM is a perception based model, in which image degradation is considered as the change of perception in structural information. This metric extracts three key features of an image: luminescence, contrast and structure. SSIM ranges from 0 to 1; two identical images have an SSIM of 1. [21]. Both metrics were calculated on the first channel over the entire image.

5.2   Problem instances

The problem instances used in this research consider data from two repositories. The first repository is the DIVerse 2K (DIV2K) dataset [1], including high quality resolution images used in image super resolution challenges. The dataset includes 900 generic photographs with resolution 462×510 pixels. Low resolution images from DIV2K (i.e., Train Data Track 1) were used for training and validation of the proposed approach. DIV2K is publicly available at https://data.vision.ee.ethz.ch/cvl/DIV2K. A 4× bicubic downscaling was applied.

The second repository is the UxLES dataset, consisting of 1609 images of a real CFD problem. Images correspond to the first component (Ux) of the velocity field of an LES simulation around a wind turbine (dimension 64×64) obtained using the heterogeneous computing CFD-LES code caffa3d [12,25]. Fig. 1a shows the entire horizontal domain of the simulation with the selected plane indicated as a black dashed line and the wind turbine in the thick black line. A close up is shown in Fig. 1b. Images in the UxLES dataset were obtained from the velocity vector using colormap jet and adjusting the color scale to cover all the Ux velocity changes throughout the dataset. The applied color scale is defined within the range 2 to 12 m/s. Points with a speed of 2 m/s are represented with a color with RGB encoding [0,0,1] and points with a speed of 12 m/s are represented with a color with RGB encoding [1,0,0]. Despite having the same number of points, the data points are not equally spaced. Thus, the image is not square (Fig.1c). Therefore, images were resized to a 64×64 pixel size to use usual ANN architectures. A 4× downscaling was applied.

The UxLES dataset is publicly available at shorturl.at/hjsv1. Fig.2 presents two sample images in the UxLES dataset.
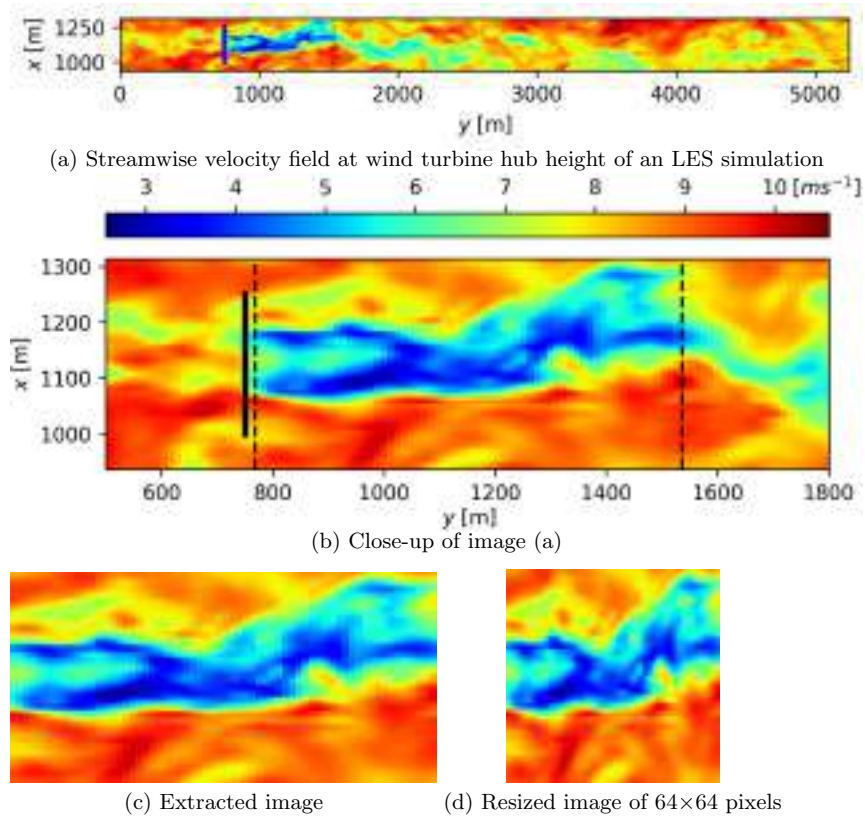
(a) Streamwise velocity field at wind turbine hub height of an LES simulation

(b) Close-up of image (a)

(c) Extracted image

(d) Resized image of 64×64 pixels

Fig. 1: Data from the UxLES dataset

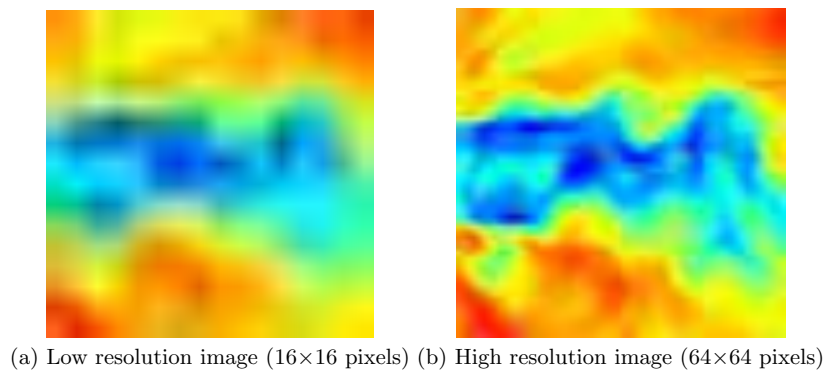(a) Low resolution image (16×16 pixels) (b) High resolution image (64×64 pixels)

Fig. 2: Two sample images in the UxLES data set.

5.3   Results and discussion

This section reports the results of training and validation experiments.

Training stage. Fig. 3 presents the evolution of the adversarial losses (the generator loss, the discriminator loss for real images and the discriminator loss for synthetic images) over epochs for the UxLES dataset. The adversarial loss evolution shows an stable training despite the large variance of the losses, specially of the generator. This variance represents the *minmax* adversarial game of alternated gradient reductions.
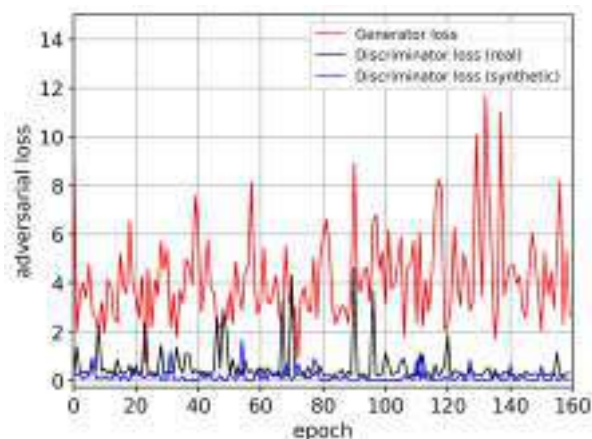

Fig. 3: Adversarial loss for the generator and discriminator through epochs.

Fig. 4 reports the MSE and VGG losses evolution for training. They behave in a similar way, with a sharp decreasing slope for the first 40 epochs, and then reach an asymptote that caps the reduction of these losses.
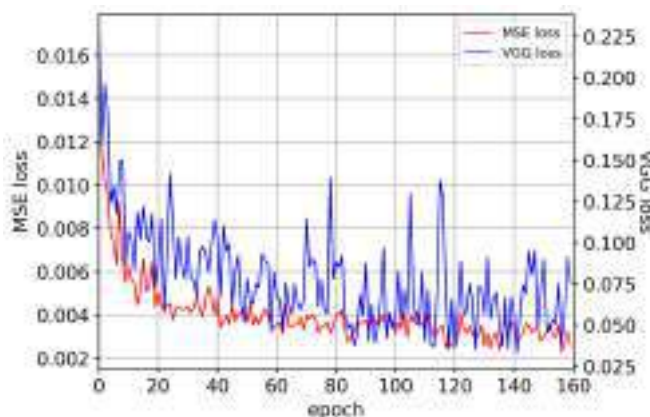

Fig. 4: Generator losses: MSE and VGG through epochs.

As expected, both the MSE and VGG components of the generator loss diminish considerably as the epochs pass. MGE and VGG are associated with the similarity between the original and the generated image, and particularly help to achieve better PSNR results (i.e., greater dB).

Fig. 5 reports the evolution of the PSNR and SSIM metrics along epochs during training. Both PSNR and SSIM metrics increase along the epochs, showing an improvement of the quality of the synthetic image over learning iterations. Both improve fast on the first 20 epochs, but then the learning pace slows down up to a point on which more iterations do not improve the quality of the generated images or the improvement is marginal; this occurs after 100 epochs.
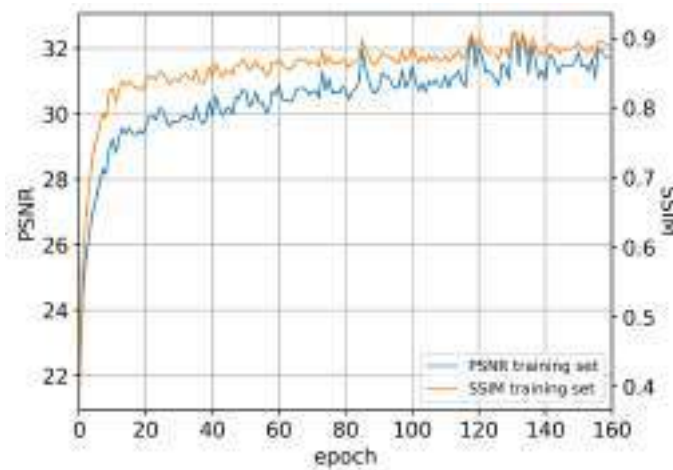

Fig. 5: PSNR and SSIM metrics on training data through epochs.

Validation stage. Regarding the considered performance metrics, the model reached a mean of 32.50 db for PSNR and 0.93 for SSIM, with a relatively low variance of 0.73 and 0.01 respectively.

Fig. 6(a) compares four random samples of the testing dataset of the LR, SR and HR images. The coordinate axes on each image are expressed as a ratio between the position and the diameter of the wind turbine. Fig.6(b) depicts the error (difference) between the synthetic (SR) and the real (HR) velocity fields (images) in ms^{-1} for the same random testing samples.

The obtained results proved to be satisfactory, by judging not only the objective metrics PSNR and SSIM, but also applying a subjective visual inspection of the quality of the generated images. It is noteworthy that the lack of diversity of the considered UxLES dataset helps the model to improve its performance. However, this property is not necessarily an indication of a poor quality dataset, because for many specific applications the dataset is still useful.
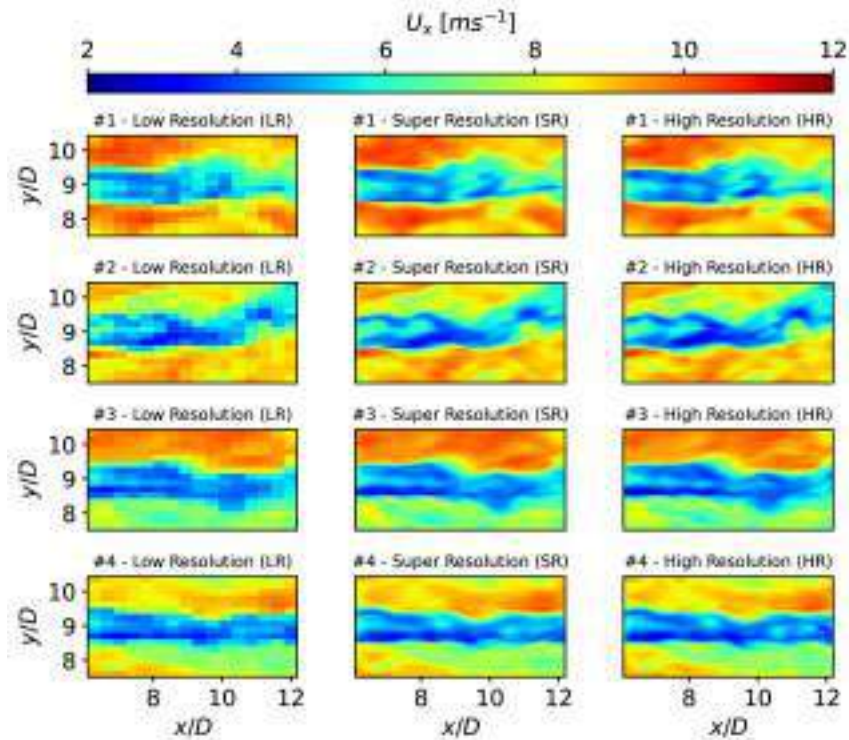
(a) Comparison between LR, SR and HR images rescaled and resized to the original value of the velocity planes.
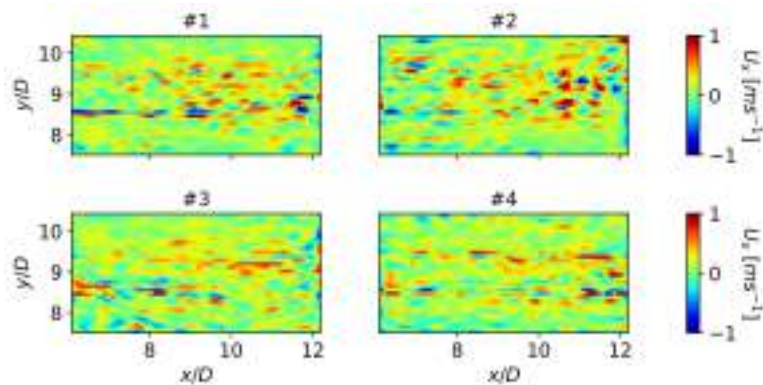
(b) Error between SR and HR images measured as the difference in ms^{-1}.

Fig. 6: Visual comparison of a $4\times$ upscale using the trained SRGAN. From left to right: low resolution image, super resolution image and high resolution image. The images are scaled to the original velocity values, and the coordinates are expressed as a ratio of the wind turbine diameter.

Computational efficiency analysis. A LES simulation like the one used to trained and validate the proposed GAN approach demands five days of computing time in a HP ProLiant DL380 G9, with Intel Xeon Gold 6138 processors (18 cores), to simulate a 1.1 h period. Considering that a coarse (LR) LES simulation requires half the computational cost of a fine (HR) one, the proposed approach implies a reduction of the computational cost by 2.5 days for each horizontal plane of a fine simulation. This reduction is most beneficial for some applications, like micrositing of wind turbines or analysis of operating wind farms, where tenths or even hundreds of fine grid simulations are needed. In these applications, using a surrogate model based on GANs might imply a potential reduction in computing times in the order of weeks, thus highlighting the importance of the proposed approach.

6   Conclusions and future work

This article presented an approach for the generation of synthetic velocity fields in LES. Particularly, the proposed approach applies a Generative Adversarial Network to increase the resolution of horizontal slices of turbulent velocity fields.

The proposed GAN learned structural information from high resolution velocity fields and applied the learned knowledge to infer (generate) new high resolution velocity slices when a low resolution one is given as input.

The proposed approach was evaluated on a real-world case study: augmenting the resolution of horizontal velocity fields downstream of a wind turbine. Results showed an stable and converging training process of the proposed GAN. In turn, the objective metrics PSNR and SSIM considered in the evaluation exhibited a relatively good similarity between the super resolution generated image (slice of horizontal velocity field) and the high resolution used as a reference baseline. Besides, a subjective visual inspection showed a strong similarity between the synthetic and the real images.

The reported research is a first step on the application of computational intelligence methods for generating velocity fields in Large Eddy Simulations. The obtained results encourage the application of GANs (and other deep Learning techniques) as surrogate models in order to reduce the cost of performing complex CFD simulations.

The main lines for future work are related to develop a full approach for generating images to characterize the three velocity components of turbulent velocity fields and generalizing the methodology for a more diverse dataset that includes other type of flows. The proposed approach can also be integrated with the formalism of Physics-Informed Neural Networks, in order to give the model the ability to evaluate if the generated image is physically possible.

References

1. Agustsson, E., Timofte, R.: NTIRE 2017 challenge on single image super-resolution: Dataset and study. In: The IEEE Conference on Computer Vision and Pattern Recognition Workshops (2017)

2. Breton, S., Sumner, J., Sørensen, J., Hansen, K., Sarmast, S., Ivanell, S.: A survey of modelling methods for high-fidelity wind farm simulations using large eddy simulation. Philosophical Transactions of the Royal Society A: Mathematical, Physical and Engineering Sciences **375**(2091), 20160097 (2017)
3. El Emam, K., Mosquera, L., Hoptroff, R.: Practical Synthetic Data Generation. O'Reilly Media, Inc. (2020)
4. Foster, D.: Generative Deep Learning. O'Reilly Media, Inc. (2019)
5. Fröhlich, J., Rodi, W.: Introduction to large eddy simulation of turbulent flows (2002)
6. Fushiki, T.: Estimation of prediction error by using k-fold cross-validation. Statistics and Computing **21**(2), 137–146 (2011)
7. Goodfellow, I., Pouget, J., Mirza, M., Xu, B., Warde, D., Ozair, S., Courville, A., Bengio, Y.: Generative adversarial nets. In: Advances in neural information processing systems. pp. 2672–2680 (2014)
8. He, K., Zhang, X., Ren, S., Sun, J.: Deep residual learning for image recognition. In: IEEE Conference on Computer Vision and Pattern Recognition (2016)
9. Ledig, C., Theis, L., Huszar, F., Caballero, J., Cunningham, A., Acosta, A., Aitken, A., Tejani, A., Totz, J., Wang, Z., Shi, W.: Photo-realistic single image super-resolution using a generative adversarial network. In: IEEE Conference on Computer Vision and Pattern Recognition (2017)
10. Li, M., McComb, C.: Using physics-informed generative adversarial networks to perform super-resolution for multiphase fluid simulations. Journal of Computing and Information Science in Engineering **22**(4) (2022)
11. Machín, B., Nesmachnow, S., Toutouh, J.: Multi-target evolutionary latent space search of a generative adversarial network for human face generation. In: Genetic and Evolutionary Computation Conference (2022)
12. Mendina, M., Draper, M., Kelm, A., Narancio, G., Usera, G.: A general purpose parallel block structured open source incompressible flow solver. Cluster Computing **17**(2), 231–241 (2014)
13. Milanfar, P.: Super-resolution imaging. CRC press (2017)
14. Nasrollahi, K., Moeslund, T.B.: Super-resolution: a comprehensive survey. Machine vision and applications **25**(6), 1423–1468 (2014)
15. Nesmachnow, S., Iturriaga, S.: Cluster-UY: Collaborative Scientific High Performance Computing in Uruguay. In: Torres, M., Klapp, J. (eds.) Supercomputing, Communications in Computer and Information Science, vol. 1151, pp. 188–202. Springer (2019)
16. Ng, A., Jordan, M.: On discriminative vs. generative classifiers: A comparison of logistic regression and naive Bayes. In: Conference on Neural Information Processing Systems (2002)
17. Pan, Z., Yu, W., Yi, X., Khan, A., Yuan, F., Zheng, Y.: Recent progress on generative adversarial networks (GANs): A survey. IEEE Access **7**, 36322–36333 (2019)
18. Paszke, A., Gross, S., Massa, F., Lerer, A., Bradbury, J., Chanan, G., Killeen, T., Lin, Z., Gimelshein, N., Antiga, L., et al.: Pytorch: An imperative style, high-performance deep learning library. Advances in neural information processing systems **32** (2019)
19. Pope, S.: Turbulent flows. Cambridge University Press (2000)
20. Sagaut, P.: Large eddy simulation for incompressible flows: an introduction. Springer Science & Business Media (2006)
21. Sara, U., Akter, M., Uddin, M.: Image quality assessment through FSIM, SSIM, MSE and PSNR—a comparative study. Journal of Computer and Communications **7**(3), 8–18 (2019)

22. Subramaniam, A., Wong, M.L., Borker, R.D., Nimmagadda, S., Lele, S.K.: Turbulence enrichment using physics-informed generative adversarial networks (2020), https://arxiv.org/abs/2003.01907 [June 2022]

23. Toutouh, J., Esteban, M., Nesmachnow, S.: Parallel/distributed generative adversarial neural networks for data augmentation of COVID-19 training images. In: High Performance Computing, pp. 162–177. Communications in Computer and Information Science, Springer International Publishing (2021)

24. Toutouh, J., Nesmachnow, S., Rossit, D.G.: Generative adversarial networks to model air pollution under uncertainty. In: International Workshop on Advanced Information and Computation Technologies and Systems, CEUR Workshop Proceedings, vol. 2858, pp. 169–174. CEUR (2020)

25. Usera, G., Vernet, A., Ferré, J.: A parallel block-structured finite volume method for flows in complex geometry with sliding interfaces. Flow, Turbulence and Combustion 81(3), 471–495 (2008)

26. Wang, L., Chen, W., Yang, W., Bi, F., Yu, F.R.: A state-of-the-art review on image synthesis with generative adversarial networks. IEEE Access 8, 63514–63537 (2020)

27. Wang, Z., Bovik, A.C., Sheikh, H.R., Simoncelli, E.P.: Image quality assessment: from error visibility to structural similarity. IEEE transactions on image processing 13(4), 600–612 (2004)

28. Werhahn, M., Xie, Y., Chu, M., Thuerey, N.: A multi-pass GAN for fluid flow super-resolution. Proceedings of the ACM on Computer Graphics and Interactive Techniques 2(2), 1–21 (2019)

29. Xie, Y., Franz, E., Chu, M., Thuerey, N.: tempoGAN. ACM Transactions on Graphics 37(4), 1–15 (2018)

30. Zhiyin, Y.: Large-eddy simulation: Past, present and the future. Chinese journal of Aeronautics 28(1), 11–24 (2015)

BB-PLC over LV networks – a step forward towards Smart Grid implementation

Jon González-Ramos [1][0000-0001-9221-6957], Itziar Angulo [1][0000-0002-7855-3516], Amaia Arrinda [1][0000-0001-6058-1837], Igor Fernández [1][0000-0002-9312-5886], David de la Vega [1][0000-0003-4811-4173] and Alexander Gallarreta [1][0000-0002-5336-8824]

[1] University of the Basque Country (UPV/EHU), Bilbao Bizkaia 48013, Spain
jon.gonzalezr@ehu.eus

Abstract. This article reviews the current state of the art of Broadband Power Line Communications (BB-PLC) over the Low Voltage (LV) grid. First, the evolution of BB-PLC is summarized, including the past, present, and future of the technology. Second, the main opportunities and applications are gathered, including smart metering, smart city services, control of distributed generation, and Electric Vehicles (EVs). Then, the challenges that BB-PLC should face are presented, highlighting the need of characterizing the grid as a transmission medium in terms of grid access impedance, attenuation, and Non-Intentional Emissions (NIEs), as well as the cybersecurity issues that should be taken into consideration. Finally, the current state of the already rolled out BB-PLC pilot projects is described.

Keywords: Low Voltage Grid, Broadband Power Line Communications, Smart Grids.

1   Introduction

The Smart Grid (SG) concept is bringing a great revolution, mainly in the distribution and customer domains, due to the fact that it allows consumers to be more involved in the operation of the power system [1], [2]. The development of the SGs means the end of the classic production-distribution-generation model of the electrical grid, evolving into a distributed, flexible and efficient model. In this way, it is paving the way for the integration of Distributed Energy Resources (DERs), the management of Electric Vehicle (EV) charging, and the increasing energy demand response [3]-[6]. Moreover, it is also leading to a reduction of the losses and illegal usage of the transmission and distribution lines, as well as an easy operation of the grid and automated monitoring [5], [7].

In this context, communications are critical and essential for the proper operation and performance of the SGs [8]. As described in section 5, some Distributed System Operators (DSOs) have selected Power Line Communications (PLC) as the alternative for the development of new SG applications, because of the advantages it offers com-

pared to other communication technologies. First, as the electrical grid is already deployed, additional infrastructure costs are avoided; and, second, coverage problems that may occur in wireless communications are prevented. Finally, they also provide the DSOs the opportunity to have control of their own data without relying on third parties [9].

Several DSOs have already deployed Narrowband Power Line Communications (NB-PLC) technologies worldwide for applications such as telemetry, monitoring of the devices connected to the power grid, and signal quality analysis [10]-[13]. Nevertheless, future SG applications imply more demanding requirements (higher data rate and lower latency), which cannot be accomplished with NB-PLC. For this reason, some DSOs are considering the deployment of Broadband Power Line Communications (BB-PLC), also known as Broadband over Power Lines (BPL), in the Low Voltage (LV) distribution grid.

This paper gives an overview of the current state of the art of BB-PLC over the LV grid. In section 2, the evolution of BB-PLC technologies is presented, whereas section 3 gathers the main opportunities and applications of BB-PLC over the LV grid. Section 4 summarizes the challenges that should be faced by BB-PLC and, finally, in section 5, the current state of BB-PLC is included, highlighting some of the pilot projects carried out up to date.

2　　　Past, present, and future of BB-PLC

BB-PLC refers to PLC systems operating in the frequency range of about 1 MHz to 30 MHz and beyond, with a signal bandwidth of tens of MHz and with data rates ranging from several Mbps to hundreds of Mbps.

The origins of BB-PLC date back to the late 1990s. In a context of deregulation of the telecommunication and energy markets in Europe, electric power utilities considered providing additional consumer services through their power lines, including Internet access by means of BB-PLC systems as an alternative to Digital Subscriber Lines (DSL) systems. However, the high costs and growing Electromagnetic Compatibility (EMC) issues prevented the technology from a more successful deployment. Therefore, in early 2000, the interests of the industry focused on the use of BB-PLC for in-home communication and multimedia applications [14], [15].

In parallel, at the beginning of the 2010s, several industry alliances and standards developing organizations started defining a new generation of PLC systems operating at frequency bands below 500 kHz. These NB-PLC systems are currently widely deployed in the LV grid worldwide, especially for smart metering purposes in Europe [14]. Some examples of these NB-PLC technologies are PoweRline Intelligent Metering Evolution (PRIME) [16], G3-PLC [17], Meters and More (M&M), CX1, and Open Smart Grid Protocol (OSGP). In all cases, these technologies turn into technical standards accepted by standardization bodies such as the ITU or the IEEE.

However, as more applications of the SG concept are becoming a reality (integration of DERs, EVs, security issues, etc.), a more reliable communication network with higher data rates and lower latency is needed. As a first step, some DSOs are already

using BB-PLC systems over the Medium Voltage (MV) grid for backhauling traffic without the need for fiber optics or wireless communications [14], [18]. But more demanding requirements in terms of security, speed, latency, and coverage also apply to the communications over the LV grid in order to obtain an enhanced control of this distribution segment. In this context, the concept of BB-PLC over the LV network resurges, but not as a technology to offer Internet access to subscribers, but as a communication network for SG applications [18]. In Fig. 1, the evolution of BB-PLC technologies is gathered.

Fig. 1. Evolution of BB-PLC technologies: past, present and future.

Finally, in Table 1, a comparison of the characteristics of NB-PLC and BB-PLC technologies is gathered, including the main applications and advantages and disadvantages.

Table 1. Comparison of the characteristics of NB-PLC and BB-PLC technologies.

Technology	NB-PLC	BB-PLC
Frequency band	3-500 kHz	1.8-250 MHz
Modulation	Orthogonal Frequency Division Multiplexing	Orthogonal Frequency Division Multiplexing
Bitrate	500 kbps	1.5 Gbps (indoor)
Applications	• Smart metering • Electrical signal Quality • Remote monitoring	• Smart metering • Smart city services • Distributed generation • Integration of EVs • Energy demand response • High data rate
Advantages	• Low power consumption • Long distances	• Low latency • Higher complexity of the hardware
Disadvantages	• Low data rates • High latency • High Non-Intentional Emissions	• No regulation • High attenuation • High Non-Intentional Emissions

3   Opportunities and applications of BB-PLC over LV grids

BB-PLC offers high-performance features (high data rate, availability and bandwidth, and low latency) [18] and, thus, some utilities are considering the use of this technology to develop SGs applications and services that are not feasible with NB-PLC. First, it provides information about the voltage levels, phase angles, harmonics, and temperature, as well as offers connectivity for other applications. Second, as it supports interoperability with NB-PLC technologies, it allows utilities to benefit from BB-PLC by making use of the communications infrastructure already deployed [18].

The benefits previously mentioned allow BB-PLC to fulfill the requirements needed for many applications, such as smart metering, smart city services, grid automation, or EVs integration, among others [3].

3.1   Smart metering

The PRIME alliance has already defined three use cases related to smart metering based on BB-PLC. The first use case is based on deploying BB-PLC Smart Meters (SMs) and BB-PLC concentrators for telemetry services. In this way, a complete BB-PLC metering chain is established, where the SM acts as the end point and the data concentrator as the controller. The second use case considers the coexistence between BB-PLC and NB-PLC technologies. This would allow utilities to take advantage of the NB-PLC SMs, installing BB-PLC concentrators and gateways. Finally, BB-PLC SM gateways for voltage sensing purposes are being considered, allowing detection of problems in the grid, reducing investments in equipment, in addition to enabling a better quality of service (QoS), and reducing the overall CO_2 footprint. Up to now, as described in section 5, some field trials have been developed by several European utilities regarding these use cases [18].

3.2   Smart city services

Moreover, BB-PLC enable multiple services regarding smart city services, such as the control of lights and traffic signaling, as well as the parking and traffic flow [3]. In some European countries, the urban lighting is already controlled by BB-PLC systems, allowing the monitoring of the status of the street lamps, in addition to setting up an alarm system for error detection [3], [20]. This means a considerable reduction in the power energy consumption.

3.3   Control of distributed generation

Distributed generation is a particular example of grid automation and focuses on the continuous communication between the Distribution Energy Resources (DERs) and the power grid [3]. In this way, photovoltaic panels (PVs), wind turbines, natural-gas-fired, fuel cells, biomass combustion systems, waste incineration systems, and EVs, can constantly be connected to the grid as distributed generation sources [3]. BB-PLC allow

the control and monitoring of the energy injected into the grid so that complete and detailed information is obtained. In the case of the PV panels, the tilt of the panel can also be controlled by BB-PLC remotely, in order to maximize the sun exposure.

3.4   Integration of EVs

Finally, concerning EVs, BB-PLC also fulfills the technical requirements specified, first, for the communication between several EVs in the same parking space, so that they behave as a collaborative community of consumers with a common power management system. Second, in bad coverage conditions, it allows communication between EVs as a Local Area Network (LAN) for transmitting the data to the backbone network [3].

4   Challenges of BB-PLC over LV

4.1   Characterization of the LV grid as a transmission medium

The electrical cables are not originally designed for data transmission [21], [22], and, thus, communications are considerably affected in terms of impedance variations, attenuation or transmission losses, and noises due to Non-Intentional Emissions (NIEs) [9], [22]-[24]. Therefore, a proper and detailed characterization of the LV grid as a transmission medium is needed in order to optimize the opportunities offered by the electrical distribution grid.

The characteristics of the LV grid for the frequencies beyond traditional harmonics are difficult to predict, as they show a frequency and time-dependent behavior [23], [25]. The characterization of the grid is an extremely complex study since it depends on a very large number of factors: grid topology, type of cable, type of electrical and electronic equipment connected to the grid, and its operating regime [3], [26]. In addition, due to the fact that such complex grid models for the frequency bands of interest are not available, it is not possible to simulate different grid topologies and conditions. Therefore, empirical studies are needed, based on laboratory and field trials that characterize representative environments and that allow obtaining typical values for PLC design, planning, or performance evaluation [27], [28].

4.2   Design of new BB-PLC protocols

The lack of knowledge of the channel characteristics poses two different scenarios in the design and development of BB-PLC technologies in the LV grid. First, an adaptation of the indoor BB-PLC standards to the outdoor channel can be considered. For instance, the PRIME alliance has selected G.hn [29], a technology originally designed for in-home communications, as their preferred solution for the BB-PLC applications over the LV grid [18]. This technology, detailed in a set of standards [29]-[34], is based on Orthogonal Frequency Division Multiplexing (OFDM) and low-density parity-check (LDPC) codes as forward error correction (FEC). In the MAC layer, Time

Division Multiplexing (TDMA) is used. In order to optimize the performance of the communications system, transmission parameters such as the number of carriers, carrier spacing, modulation, etc., are to be modified and adapted to the new transmission environment.

Second, the design of completely new and innovative BB-PLC technologies is also considered as an option, since indoor and outdoor PLC channels are not expected to have similar transmission characteristics.

In this context, the need to characterize the LV grid as a transmission medium is an essential factor for the proper development of BB-PLC, regardless of whether an existing standard is adapted or new technologies are developed.

4.3   Cybersecurity issues

The increasing amount of data transmitted over PLC systems in recent years, mainly due to the deployment of SMs, turns cybersecurity into a key aspect in the maintenance of the confidentiality and integrity of the information propagated through the LV grid. Vulnerabilities in the transmissions can expose not only the consumers, since private information regarding the periods when they are out of home are transmitted, but also the DSOs, due to the data related to the grid power quality that is sent through the cables [3].

Up to now, some studies have been carried out analyzing the Physical Layer Security (PLS) of wireless, PLC, and hybrid wireless/PLC channels. The theoretical results lead to conclude that the wireless fading channels show considerably higher secrecy rates than the PLC channels [35]. Hybrid wireless/PLC technologies, in turn, offer increased secrecy for low data rate applications [36], mainly when coding diversity is applied [37].

Finally, it is important to mention that in BB-PLC technologies, due to the higher frequency range of operation, the radiation of the transmitted signal is significantly higher than in NB-PLC [3]. This implies that an intruder can easily access the signal without necessarily accessing the power cable, which could jeopardize the proper performance of the energy system or which could imply that a third party disposes of sensitive information.

5   Current state of BB-PLC pilot projects

In recent years, several European DSOs have started with the rollout of BB-PLC pilot projects over the LV grid. In 2019, the first full implementation of BB-PLC with approximately 100000 devices connected to the grid was performed by E.ON, a German utility. It is worth mentioning that they are planning an expansion of the BB-PLC infrastructure based on G.hn [18], [38].

In Spain, Iberdrola has also opted for G.hn as the BB-PLC technology for the development of new SG applications [18], [38], rolling out several pilot projects throughout the country. According to [38], in 2019, 2 small pilot networks with 20 BB-PLC devices were carried out.

A deployment of Advanced Metering Infrastructure (AMI) based on BB-PLC is described in [39]. This pilot project, developed in 2012 for 17000 customers in both residential and commercial zones in the LV grid in Doha (Qatar), uses BB-PLC in order to communicate the data concentrator and the data center.

In Mannheim (Germany), an intelligent and real-time energy communication platform was established by means of BB-PLC technologies for the increase of energy efficiency and the integrity of renewable energies. In this way, three smart grid applications in the smart city environment were implemented: management of the energy demand, analysis of the power grid, and price communication to the smart home [40].

Finally, a group of Swiss utilities developed a platform for the monitoring and active control of the distribution grid considering three alternatives: fibre optics, GPRS/UMTS, and BB-PLC [41]. Although no specific details of the deployment of BB-PLC devices are mentioned, the good potential of BB-PLC for future SG applications is highlighted.

6   Conclusions

In order for the Smart Grid concept to become a reality, utilities need high-speed, real-time, two-way communications networks to be deployed over their distribution sections. In this context, developing BB-PLC networks over the LV segment becomes an appealing option for DSOs in terms of costs and network ownership, as well as providing enough data rate to develop applications beyond those envisaged today.

Although the experience with NB-PLC systems might be valuable in the evolution towards BB-PLC systems, there is still a lot of work to be done to obtain the needed maturity for massive roll-outs, mainly in three aspects: characterization of the transmission medium, design of communication protocols, and cybersecurity issues.

References

[1]   Seijo Simó, Miguel & López, Gregorio & Matanza, Javier & Moreno, Jose. (2016). Planning and Performance Challenges in Power Line Communications Networks for Smart Grids. International Journal of Distributed Sensor Networks. 2016. 10.1155/2016/8924081.

[2]   Ekanayake J, Liyanage K, Wu J et al (2012) Smart grid, technology and applications. Wiley, NY.

[3] González-Ramos, J.; Uribe-Pérez, N.; Sendin, A.; Gil, D.; de la Vega, D.; Fernández, I.; Núñez, I.J. Upgrading the Power Grid Functionalities with Broadband Power Line Communications: Basis, Applications, Current Trends and Challenges. *Sensors* **2022**, *22*, 4348. https://doi.org/10.3390/s22124348.

[4] Mlýnek, P.; Rusz, M.; Benešl, L.; Sláˇcik, J.; Musil, P. Possibilities of Broadband Power Line Communications for Smart Home and Smart Building Applications. Sensors **2021**, 21, 240.

[5] I.Colak, "Introduction to smart grid," *2016 International Smart Grid Workshop and Certificate Program (ISGWCP)*, 2016, pp. 1-5, doi: 10.1109/ISGWCP.2016.7548265.

[6] H. Gharavi and R. Ghafurian, "Smart Grid: The Electric Energy System of the Future [Scanning the Issue]," in *Proceedings of the IEEE*, vol. 99, no. 6, pp. 917-921, June 2011, doi: 10.1109/JPROC.2011.2124210.

[7] Taha, Mohammed. "Advantages and recent advances of smart energy grid" *Bulletin of Electrical Engineering and Informatics*, Vol. 9, 5, 2020.

[8] D. Baimel, S. Tapuchi and N. Baimel, "Smart grid communication technologies- overview, research challenges and opportunities," 2016 International Symposium on Power Electronics, Electrical Drives, Automation and Motion (SPEEDAM), 2016, pp. 116-120, doi: 10.1109/SPEEDAM.2016.7526014.

[9] Uribe Pérez, N. Análisis de la capacidad de PRIME para gestión de red en entornos con generación distribuida y sistemas de almacenamiento. Doctoral Thesis. Spain, 2017.

[10] Slacik, J.; Mlynek, P.; Rusz, M.; Musil, P.; Benesl, L.; Ptacek, M. Broadband Power Line Communication for Integration of Energy Sensors within a Smart City Ecosystem. Sensors 2021, 21, 3402.

[11] Mlynek, P.; Misurec, K.; Kolka, Z.; Slacik, J.; Fujdiak, R. Narrowband Power Line Communication for Smart Metering and Street Lighting Control. IFAC-Pap. 2015, 48, 215–219.

[12] Llano, A.; De La Vega, D.; Angulo, I.; Marron, L. Impact of Channel Disturbances on Current Narrowband Power Line Communications and Lessons to Be Learnt for the Future Technologies. IEEE Access **2019**, 7, 83797–83811.

[13] Elfeki, I.; Jacques, S.; Aouichak, I.; Doligez, T.; Raingeaud, Y.; Le Bunetel, J.-C. Characterization of Narrowband Noise and Channel Capacity for Powerline Com-munication in France. Energies 2018, 11, 3022.

[14] Lutz Lampe, Andrea M. Tonello, Theo G. Swart, "Power Line Communications: Principles, Standards and Applications from Multimedia to Smart Grid, Second Edition. ", Ed. John Wiley & Sons, Ltd., 22 April 2016.

[15] S. Galli, A. Scaglione, and Z. Wang, For the grid and through the grid: The role of power line communications in the smart grid, Proc. IEEE, 99(6), 998–1027, Jun. 2011.

[16] PRIME Alliance, "PRIME v1.4 White Paper", PRIME Alliance, Brussels, 2014.

[17] G3-PLC Alliance, "Narrowband OFDM PLC specifications for G3-PLC networks", G3-PLC Alliance, Paris, 2015.

[18] Segalotto, J.-F. Towards a Truly Smart Grid—The Case for Broadband over Power Line. IDC White Paper, PRIME Alliance. August 2021.

[19] PRIME Alliance. Available online: https://www.prime-alliance.org/ (accessed on 21 February 2022).

[20] Hashiesh, Fahd and Pavel Soukal. "A Proposed Broadband Power Line Communication System for Smart Grid Applications in a Typical Egyptian Network." (2009).

[21] G. Hallak and G. Bumiller, "Time variant voltage and current modeling correspond-ing to access impedance measurements," 2018 IEEE International Symposium on Power Line Communications and its Applications (ISPLC), 2018, pp. 1-6, doi: 10.1109/ISPLC.2018.8360226.

[22] M. Antoniali and A. M. Tonello, "Measurement and Characterization of Load Im-pedances in Home Power Line Grids," in IEEE Transactions on Instrumentation and Measurement, vol. 63, no. 3, pp. 548-556, March 2014, doi: 10.1109/TIM.2013.2280490.

[23] A. Majumder and J. Caffery J, "Power line communications," in *IEEE Potentials*, vol. 23, no. 4, pp. 4-8, Oct.-Nov. 2004, doi: 10.1109/MP.2004.1343222.

[24] J. Anatory, N. Theethayi, R. Thottappillil, M. M. Kissaka and N. H. Mvungi, "The Influence of Load Impedance, Line Length, and Branches on Underground Cable Power-Line Communications (PLC) Systems," in *IEEE Transactions on Power Delivery*, vol. 23, no. 1, pp. 180-187, Jan. 2008, doi: 10.1109/TPWRD.2007.911020.

[25] Ferreira, Hendrik & Grove, H.M. & Hooijen, O. & Vinck, Jan. (1996). Power line communications: an overview. 558-563 vol.2. 10.1109/AFRCON.1996.562949.

[26] I. Fernández, A. Arrinda, I. Angulo, D. De La Vega, N. Uribe-Pérez and A. Llano, "Field Trials for the Empirical Characterization of the Low Voltage Grid Access Impedance From 35 kHz to 500 kHz," in IEEE Access, vol. 7, pp. 85786-85795, 2019, doi: 10.1109/ACCESS.2019.2924253.

[27] CENELEC. CLC/TR 50627; Study Report on Electromagnetic Interference between Electrical Equipment/Systems in the Frequency Range below 150 kHz; CENELEC SC 205A Mains Communicating Systems. CENELEC: Brussels, Belgium, 2015.

[28] International Electrotechnical Commission. IEC/TR 60725:2012: Consideration of Reference Impedances and Public Supply Network Impedances for Use in Determin-ing Disturbance Characteristics of Electrical Equipment Having a Rated Current ≤ 75 A Per Phase; International Electrotechnical Commission: Geneva, Switzerland, 2012.

[29] ITU-T Rec. G9978; Secure Admission in a G.hn Network. 2018. Available online: https://www.itu.int/rec/T-REC-G.9978-201802-S/es (accessed on 22 February 2022).

[30] ITU-T Rec. G9960; Unified High-Speed Wire-Line Based Home Networking Transceivers—System Architecture and Physical Layer Specification. 2018. Available online: https://www.itu.int/rec/T-REC-G.9960-201811-I/en (accessed on 22 February 2022).

[31] ITU-T Rec. G9961; Unified High-SpeedWireline-Based Home Networking Transceivers—Data Link Layer Specification. 2018. Available online: https://www.itu.int/rec/T-REC-G.9961 (accessed on 22 February 2022).

[32] ITU-T Rec. G9962; Unified High-Speed Wire-Line Based Home Networking Transceivers—Management Specification. 2018. Available online: https://www.itu.int/rec/T-REC-G.9962/en (accessed on 22 February 2022).

[33] ITU-T Rec. G9963; Unified High-Speed Wireline-Based Home Networking Transceivers—Multiple Input/Multiple Output Specification. 2011. Available online: https://www.itu.int/rec/T-REC-G.9963-201112-S (accessed on 22 February 2022).

[34] ITU-T Rec. G9964; Unified High-SpeedWireline-Based Home Networking Transceivers—Power Spectral Density Specification. 2011. Available online: https://www.itu.int/rec/T-REC-G.9964-201112-I/en (accessed on 22 February 2022).

[35] Pittolo, A.; Tonello, A.M. Physical layer security in PLC networks: Achievable secrecy rate and channel effects. In Proceedings of the 2013 IEEE 17th International Symposium on Power Line Communications and Its Applications, Johannesburg, South Africa, 24–27 March 2013; pp. 273–278.

[36] Camponogara, A.; Poor, H.V.; Ribeiro, M.V. The Complete and Incomplete Low-Bit-Rate Hybrid PLC/Wireless Channel Models: Physical Layer Security Analyses. IEEE Internet Things J. 2019, 6, 2760–2769.

[37] Salem, A.; Hamdi, K.A.; Alsusa, E. Physical Layer Security Over Correlated Log-Normal Cooperative Power Line Communication Channels. IEEE Access 2017, 5, 13909–13921.

[38] Enabling decarbonization through self-regulating energy systems, Corporate Presentation, CORINEX. Available online: https://uploads-ssl.web-flow.com/62337650701b6f122d6b4d65/62753d15c0efab5dd909a5ed_Corinex%20Corpo-rate%20Deck.pdf (accessed on 04 October 2022).

[39] G. Abdulla, "The deployment of advanced metering infrastructure", *2015 First Workshop on Smart Grid and Renewable Energy (SGRE),* 2015, pp. 1-3, doi: 10.1109/SGRE.2015.7208738.

[40] Moma—Smart City Mannheim Research Project. Available online: https://www.ppc-ag.de/wp-content/uploads/media/PPC-Case-Study-MOMA-16-2026-2E.pdf (accessed on 04 October 2022).

[41] Brenzikofer, Alain & Müller, Florian & Ketsetzis, Alexandros & Kienzle, Florian & Mangani, Marco & Eisenreich, Marc & Farhat, Yamshid & Bacher, Rainer. (2016). GridBox pilot project: A platform for monitoring and active control of distribution grids. Computer Science - Research and Development. 10.1007/s00450-016-0308-5.

Energy management of the CEDER's smart microgrid with different battery technologies

Oscar Izquierdo-Monge[1], Marcos Martínez Gurría[1], Paula Peña Carro[1]

[1] CEDER-CIEMAT, Autovía de Navarra A15 salida 56, 422290 Lubia (Soria), Spain. O.I-M: oscar.izquiero@ciemat.es; M.M.G: marcosmg9703@gmail.com; P.P.C.: paula.pena@ciemat.es;

Abstract: With the rise in the use of renewable energy, microgrids have played a very important role in their generation. To store all that energy, batteries have been the most used storage system. This paper proposes a management of the energy consumption of the Centre for the Development of Renewable Energy (CEDER), using both lithium-ion and lead-acid batteries. This management of both batteries is done by computer and is capable of controlling the energy that can be charged or discharged in periods of 15 minutes. With this optimization in the use of our batteries, it has been possible to reduce energy consumption from 90 to 200 kWh approximately, depending on the case study that is carried out.

Keywords: Microgrid, storage system, battery, energy management.

1   Introduction

Microgrids are self-sufficient, low voltage power systems. They include energy generating resources, energy storage systems (ESS) and loads and can operate both plugged (grid connected) and unplugged (islanded mode) from the main grid. Energy generation by renewable energy resources can be of different types, being photovoltaic and wind the most common forms of generation.

   As microgrids carry an economical save and a more stable grid, the power generation comes from intermittent sources such as solar photovoltaic (PV) and wind, added to variations in grid tariffs and load demands. They are special or customized power networks that can be constructed with various control and topology approaches, depending on the goals and needs of researchers and developers [1]. Due to the implementation in recent years of renewable resources in order to minimize greenhouse gas emissions, a new scenario has been launched where sustainable energy systems have become essential. Here is where microgrids have took an important role, as a viable alternative to carbon oxides (COx) emitting energy systems, being able to manage frequency regulation, peak shaving and energy arbitrage [2].

   The vast majority of microgrids work with alternating current (AC), since most of the loads networks require AC supply because it can be easily and efficiently step down or step up through a transformer. However, direct current (DC) microgrids have been launched lately, as efficiency of power conversion is normally higher in DC systems,

and it is mainly affected by the technology of the primary source and the AC and DC load ratios [3, 4].

In the implementation of both AC and DC microgrids, it is necessary to carry out a previous plan and analyze various factors such as location or design solutions to local parameters such as energy tariffs, abundance of renewable fuel sources, and properties of the demand curves. In [5], numerical simulations with IEEE 33-bus distribution test system were made to study different cases and zones where the optimal centralized microgrid topology with its optimal installed distributed energy resources can be located. In [6], an improved algorithm called Improved Arithmetic Optimization Algorithm (IAOA) is presented where different designs of new renewable energy systems are studied, including PV, wind turbine, diesel generator and battery system.

Microgrids have become a popular solution for isolating deployments of renewable generation facilities to avoid the problem of network destabilization. Load fluctuations in a microgrid are managed with information technology and high-speed control [7]. Thus, an energy management system (EMS) is essential for an optimal use of these distributed energy resources in intelligent, secure, reliable, and coordinated ways. The EMS of a microgrid encompasses both supply and demand side management, while satisfying system constraints, to realize an economical, sustainable, and reliable operation of the microgrid [8]. EMS optimization methods are mainly split into three kinds namely computational intelligence, mathematical programming, and hybrid techniques [9]. Some optimization techniques in EMS of microgrids, including Artificial Intelligence (AI), conventional and metaheuristic-based techniques, are presented in [10]. To ensure the efficient operation, an optimal energy management system is proposed for resource scheduling and for optimal operation of PV, wind or tidal microgrid utilization in [11].

In order to adequately support intermittent power generation, storage technologies are vital. The energy demand is not constant throughout the day or during the year, as there are peak and valley demands that arise due to the needs at each moment and climatic effects [12]. Storage systems buffer energy variations and compensate for renewable intermittency, mitigate load uncertainties and improve the stability of the entire microgrid. The presence of energy storage in the microgrid also improves its efficiency by managing energy flow and reducing operating losses [13].

The main techno-economic characteristics of renewable technologies that are important to manage are nominal power, specific energy, specific power, efficiency, useful life, cycle times and capital cost, that is the most studied in the establishment of microgrids [14]. The cost of storage devices is still very high at present, existing methods for sizing of storage and resources are usually based on hourly solar insolation, wind speed and load data [15]. In [16], to solve the planning of the microgrid, the useful life of the battery energy storage system (BESS) and the degradation of capacity are considered. To consider the latter elements, an improved perspective is proposed to calculate the optimal size, technology, depth of discharge (DOD) and year of replacement of BESS; all by using the Mixed Integer Linear Programming (MILP) method.

Many forms of microgrid energy storage have been implemented, for example mechanical energy storage, which includes both pumped hydro energy storage systems (PHES) and flywheels. These systems have high prices that are difficult to recover, a long useful life, and some risks such as the uncertainty of the price of electricity [17],

[18]. Other energy storage systems such as electrical energy storage with capacitors or thermal energy have less use, although they provide flexibility, since, with proper management, microgrids adapt better to sources and demands over a wider current range [19, 20].

Due to the advantages of cost-effective performance, unaffected by the natural environment, convenient installation, and flexible use, the development of electrochemical energy storage has entered the fast lane nowadays [21].

Storing electrochemical energy has become vital in the development of renewable energies in microgrids, covering a wide range of batteries that convert the chemical energy contained in its active materials into electric energy by an electrochemical oxidation-reduction reverse reaction. Electrochemical technologies are competitive and available in the market, as well as having an acceptable degree of cost-effectiveness, good power and energy densities, and maturity, also battery technology choice is usually defined by the economic capacity of the donor or investor [2, 22]. Some of the services that can be provided by battery systems are frequency regulation, voltage regulation, demand response and congestion management [23].

Lead-acid and lithium-ion batteries dominate the electrochemical energy storage market. Both of them are the most popular options for incorporation into microgrids. Since its inception, lead-acid batteries have been widely used in microgrids, due to their great profitability and technological reliability [24]. On the other hand, the operating conditions of a microgrid can cause moments of stress that are incompatible with the manufacturer's specifications, leading to a decrease in useful life as well as the constant need to replace battery banks [25]. Periodic equalization charges must be applied to the bank to mitigate the degradation process [26]. They are usually used as starter batteries in vehicles or as a storage method in microgrids, especially in emerging countries, since they are characterized by their low cost and ease of manufacture [27]. Even though lead-acid batteries present problems due to their low energy density or their low energy to weight ratio, they still have the capacity to supply microgrids with large currents maintaining a relatively high power density [28].

The other most established form of battery energy storage on the electric market is the lithium-ion battery. Lithium-ion battery is a promising electrical storage technology because of its high energy density and coulombic efficiency. However, the power variation frequency of this battery is very small, and the charging and discharging duration is long [29]. The higher energy density and volumetric power make them a suitable choice to produce small units with small size, nevertheless they are extensively applied in renewable energy grid systems and microgrid systems, as they can be considered an ideal energy storage element due to their long life, environmental impact and safety [30, 31].

Lithium iron phosphate (LFP) batteries might be the most widely used lithium-ion battery today. They are in high demand due to their low raw material cost, low toxicity, environmentally friendly, excellent safety properties, cyclic performance and long lifespan, which makes them easily applicable in microgrids [32].

The present study aimed to analyze how the use of batteries, both lead-acid and lithium-ion, affects both the elimination of energy consumption peaks and the reduction of consumption in different periods of time in CEDER microgrid. For this, the batteries mentioned above were discharged simultaneously, varying their power setpoint for a

more efficient use. In addition, the lead-acid batteries were charged in periods of energy surplus thanks to the microgrid energy generation systems.

The paper is organised as follows: in Section 2, an overview of CEDER is introduced, with its forms of energy generation, loads and storage systems. In Section 3, the practical case study with the use of batteries is presented. It ends with the conclusions in Section 4.

2   Overview of CEDER microgrid

2.1   Microgrid

The Centre for the Development of Renewable Energy (CEDER) has a smart microgrid, which is operated and administrated in real time. The CEDER's microgrid is underpinned a 45 kV power line and serves a 45/15 kV (1 000 kV) substation.

From this substation, medium-voltage power is distributed via an underground network of eight transformer substations, which adjust the power to low-voltage, three-phased supply delivering 400 V. The contracted power is 135 kV.

The network can operate as a ring, enabling a medium-voltage perimeter some 4200 metres long, and as a radial network (see Fig.1). All of the components that comprise the systems for distributed generation, distributed electricity storage and loads are connected at low voltage.
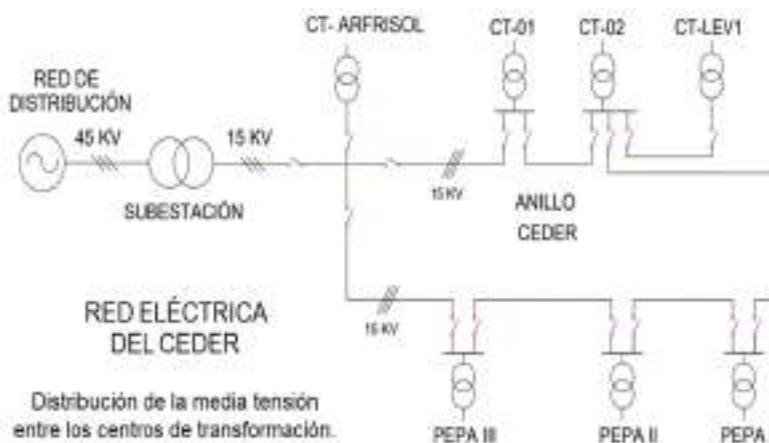

Fig.1. Medium-voltage distribution between transformation centres.

Generation systems

The following elements of distributed generation constitute the grid at CEDER:

- Wind-energy systems: There are 4 small wind turbine connected to the microgrid (total installed power 61.2 kW):

    - ATLANTIC AOC: 50 kW (diameter 15 m downwind).

    - ENNERA: 3.5 kW (Ø 4.36 m upwind).

    - ENNERA WINDERA S: 4.2 kW (Ø 4.36 m upwind).

    - RYSE E5: 3.5 kW (Ø 4.3 m upwind).

- Photovoltaic systems: There are eight different photovoltaic systems connected to the microgrid. All these systems are south orientated. Five of them are installed in the rooftops and three are on the ground (total installed power 126.8 kW)

    - Building E01: there are 80 single-crystal silicon solar panels, with 150 W power each. They are distributed in 5 arrays, connected in parallel. Each array is constituted by 16 panels connected in series, providing a total power of 12 kW.

    - Building E03: There are 54 photovoltaic panels with a total power of 12.6 kW.

    - Building E09: The installation consists of 238 de thin-film panels (97 W each), divided into 17 arrays of 14 panels, providing 23.2 kW.

    - LECA building: There are two different systems:

        - LECA 1: 63 polycrystalline photovoltaic modules (310 W each), providing a total power of 19.5 kW.

        - LECA 2: 63 polycrystalline photovoltaic modules (310 W each), providing a total power of 19.5 kW.

    - PEPA III: The installation consists of 24 polycrystalline panels (210 W each), divided into 4 arrays of 6 panels, providing a total of 5 kW.

    - Hydraulic turbine Area: The installation consists of 64 single-crystal panels (250 W each) providing a total of 16 kW.

    - PEPA II: The installation consists of 54 polycrystalline panels (410 W each), providing a total of 22.1 kW.

- Reversible hydraulic system comprising a Pelton turbine: 60 kW.

- Diesel engine generator: 100 kVA.

Storage systems

In a microgrid, it is essential to achieve some balance in power. Thus, it is necessary that the distributed generation elements are compatible with distributed electricity

storage. For this purpose, CEDER's microgrid integrates different storage technologies. This makes the centre a flexible environment for demand management:

- Mechanic storage: It is connected to the hydraulic system and consists of a pumping system with the following elements:

  - 4 centrifugal pumps of 7.5 kW each.
  - 3 water-storage tanks:
    - Primary tank ~ 500 m^3 located in LEVI.
    - Upper tank ~ 1500 m^3 placed 16 m below the primary tank.
    - Bottom tank ~ 1900 m^3 placed 70 m below the upper tank.

- Electro-chemical storage: There are 3 storage systems connected to the microgrid, we will see in next chapter.

Loads

Loads are the elements that enable CEDER's day-to-day operation, i.e. the various buildings and equipment (motors, lighting, boilers, laboratories, etc.) that make up the Centre and require energy in order to function. In terms of demand, CEDER offers a number of different consumption profiles, similar to those that can be found in an industrial environment, a services environment and even a domestic environment.

Management system

The management system at CEDER's microgrid consists of:

- ❑ **Communications bloc**: based on NodeRED. It integrates the different communication protocols of the generation, storage and consumption systems at CEDER (Modbus, MQTT, HTTP, etc.).

- ❑ A **database** (MariaDB) for data storage and its later analysis and treatment.

- ❑ An **EMS** with a Human-Machine Interface via HomeAssistant. This enables researchers to monitor all the elements that comprise the microgrid in real-time and to command or program different kinds of energetic strategies.

Figure 2 shows the interrelationships between the different elements that make up the monitoring and control system of CEDER's smart microgrid.
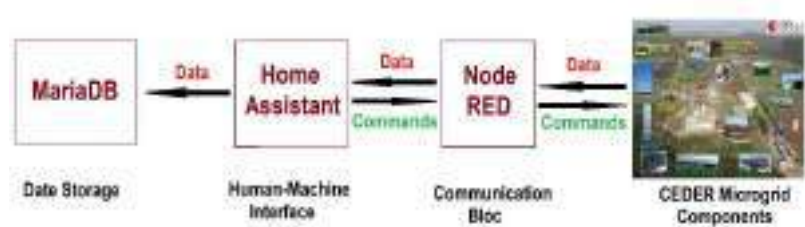
Fig.2. Elements of CEDER microgrid control system.

2.2 Electro-chemical storage systems

This section presents the different battery-based energy storage systems connected to the CEDER microgrid.

- **P.E.P.A. I battery system:** comprised of 120 sets of 2 V (240 V) Tudor 7EAN100T (Classic OPzS 1080) lead-acid batteries, with a capacity of 1,080 Ah over 120 hours (C_{120}).
  It is connected to the microgrid via a 50 kW DC/AC inverter with an isolation transformer and an inductance.

- **P.E.P.A. II battery system**: comprised of 120 sets of 2 V (240 V) Tudor 5EAN70T (Classic OPzS 765), lead-acid with a capacity of 765 Ah. P.E.P.A. II is connected to the microgrid via a 20 kW inverter (see Figure 5).
  It is connected to the microgrid via a 20 kW DC/AC inverter with an isolation transformer and an inductance.

Lithium Iron Phosphate Batteries (LFP): The system comprises two racks of 14 modules, with 196 cells per module, each of 3.2 V and 50 Ah. This is connected to the microgrid via a 30 kW inverter.

3   Battery management

In this study, three cases are proposed to be analysed for a reduction in the centre's energy consumption. For which, both P.E.P.A. I and P.E.P.A.II lead-acid batteries will be used. In turn, we will also use lithium-ion batteries. For this, three ways of reducing energy expenditure in different periods of time are analysed. In the first case, the influence of battery discharge at a time of peak energy consumption of approximately two hours is studied. Subsequently, a longer period of 8 hours is analysed on a day where consumption was relatively high throughout the day. It ends with a study on the impact of the use of batteries in 5 hours, in a morning where there was an expense of almost 80 kW during that period of time. The three forms of energy reduction are presented below, differing in the power at which the batteries are discharged and the time of said discharges. Table 1 shows the maximum power provided by lead-acid batteries and LFPs for each period of time.

Table 1. Battery discharge at different power settings.

Time	PEPA I (kW)	PEPA II (kW)	LFP (kW)
2 h	31	15	12
5 h	18	11	4
8 h	15	8.2	2.8

　　The data in the following graphs was collected in periods of 15 minutes, which gives us a relatively realistic view of the energy that is generated and consumed throughout the day. The consumption without the use of batteries are represented in red, while the new consumption with the use of batteries are represented in blue.

　　The first case to analyse was the elimination of peaks of high-energy consumption for two hours and 45 minutes (see Figure 3). The selected day is February 28, when the electrical cost reached up to 110 kW for two periods of approximately 15 minutes each if the batteries had not been used.
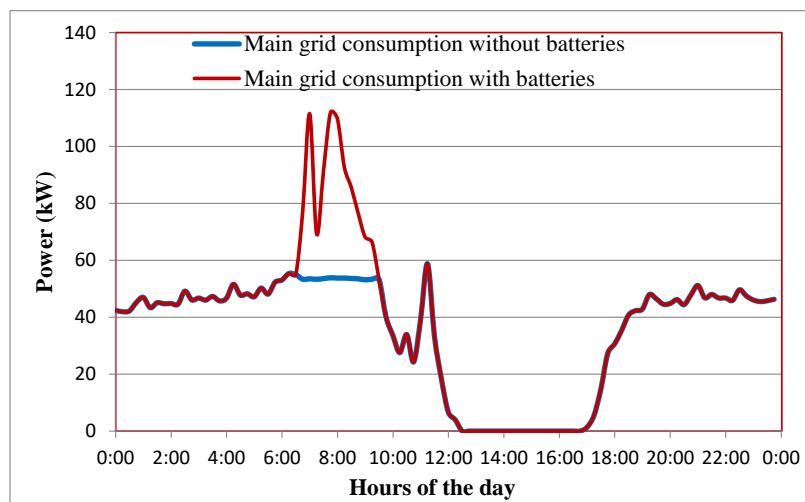

Fig. 3. Consumption reduction of 2 h.

　　To reduce this high-energy use, the batteries were discharged at the same time, varying the discharge power of each one of them every 15 minutes. This way, the new consumption that we achieve with the use of the batteries is as linear as possible. The batteries have been discharged for 165 minutes, where they have delivered 58 kW in some periods of 15 minutes, since together they can supply 58 kW for 2 hours constantly. With this discharge of the three batteries simultaneously, it has been possible to maintain an electrical network consumption of approximately 53 kW, mitigating such high peaks in energy consumption.

　　In the following case (see Figure 4), the study focuses on reducing the use of network energy for a longer period of time, 8 uninterrupted hours. The selected day is February 14, the day on which there was a higher consumption than usual, of more than 40 kW from 4:00 a.m. to 12:00 noon, having even 125 kW in one period of 15 minutes.
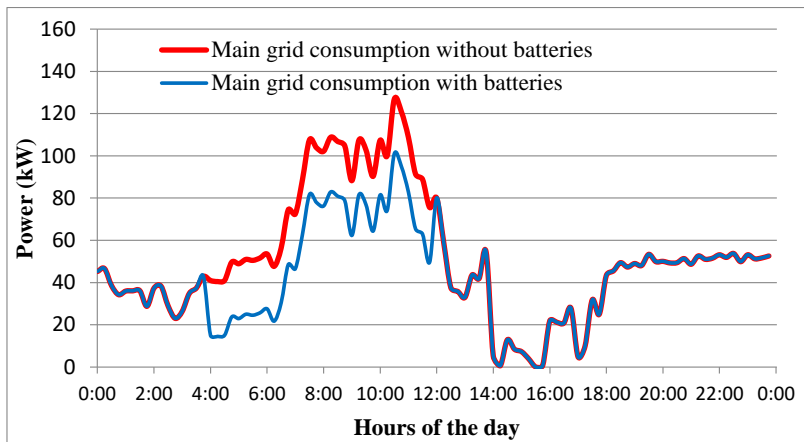
Fig. 4. Consumption reduction of 5 h.

In this period of 8 hours, the batteries used are the same as before, knowing that they together deliver 26 kW for 8 hours of power drops. With this correct use of the batteries, a total of 208 kWh was reduced, where half of the total battery discharge time occurs in the phases where electricity was more expensive.

The last case study deals with mitigating energy expenditure in a time period of 5 hours and 15 minutes (see Figure 5), where a combination of the previous cases was analysed. For this, the action time of the batteries was 315 minutes, where they were asked for up to a maximum of 36 kW, since at certain times the discharge value was changed to have a relatively linear consumption. The total energy saving was 150 kWh, also in periods where the energy cost was higher.
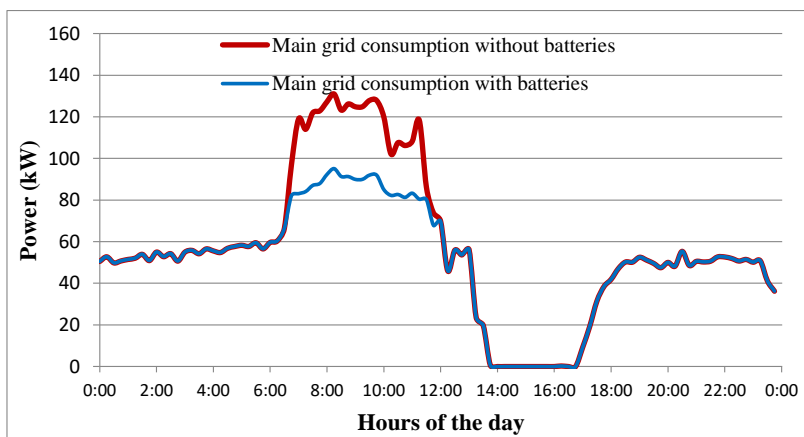

Fig. 5. Consumption reduction of 8 h.

In all three cases, the generation of energy, which includes the contribution of the batteries, never exceeds the total consumption of the centre, so it is not discharged into the distribution network. In our case, all these battery discharges start in the morning, approximately when the working day begins, and finish in all three cases before 2:00 pm, when the working day ends. This is because it is easier to manage the discharge of the batteries through the computer during the working day. It would be interesting to discharge the batteries in periods when energy is more expensive, between 6:00 pm and 9:00 pm, when the price reaches its maximum, saving money on the electricity bill.

Just as the batteries are discharged to reduce the energy consumption of the CEDER, they also have to be previously charged, this study is explained below.

The batteries are charged using surplus energy from CEDER's own microgrid. The days selected for battery charging were days that we knew would be hot, which would ensure a high energy production by the photovoltaic panels, having a surplus of energy. The objective of this study is to charge the batteries at different power settings during these periods of excess energy, the control and change of these settings will be by computer, varying them so that we can have different ways of charging the batteries depending on the needs from the centre.

To characterize the battery charge, P.E.P.A. I lead-acid batteries are used, which have a 50 kW inverter. The previously mentioned power setpoints will be 10 kW and 30 kW. Firstly, it is evaluated how the charge of the batteries affects 10 kW. In the graph (see Figure 6), the discharge to the network if the batteries had not been used is represented in blue, while the real case of the discharge to the network with the use of batteries is represented in red. The time during which energy is poured into the network is approximately 8 hours in total. In turn, the charge of the batteries, which are capable of receiving 10 kW constantly for approximately 8 hours, is represented in yellow. By charging these batteries at a power of 10 kW it has been possible to stop pouring and take advantage of a total of 78 kWh.
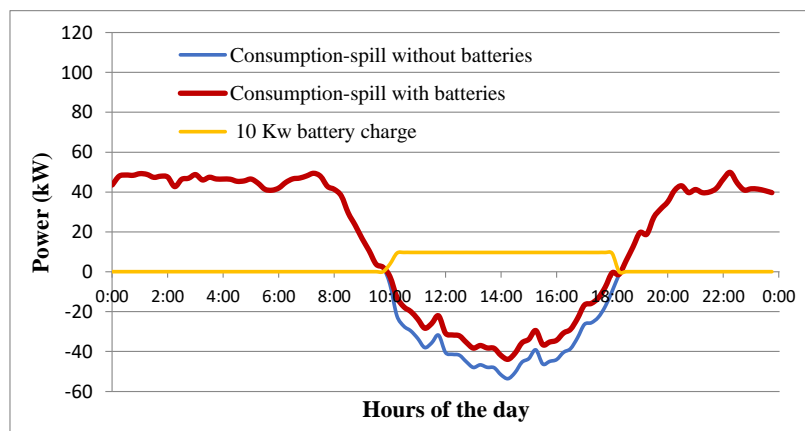

Fig.6. Load study at 10 kW.

The following graph (see Figure 7) shows how the battery charge affects a power of 30 kW on the CEDER microgrid. The batteries are charged for 3 hours and 30 minutes and can store up to 100 kWh in that period of time. The consumptions with and without batteries are represented with the same colors as before, as well as the energy charged by the batteries, which is the yellow line. In this case, the battery charge is programmed in such a way that the charge setpoint is regulated, so that it is not necessary to go to the electrical network and have the minimum economic cost.
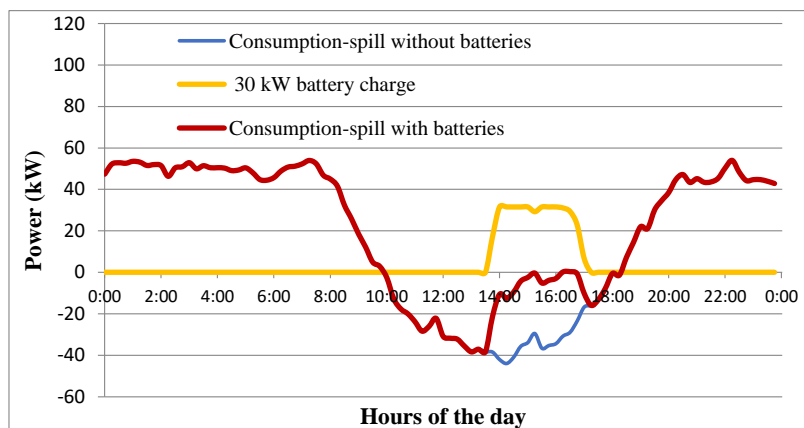

Fig.7. Load study at 30 kW.

4   Conclusions

In this paper, we have tried to analyze the effect that the use of lead-acid and lithium-ion batteries would have simultaneously to reduce the electrical consumption of the CEDER. For this, it has been studied how both batteries behave both in discharge and in charge.

Given the intermittence in the generation of energy from the microgrid and the constant variation in the consumption of the CEDER itself, the energy produced and consumed must be computer controlled. The discharge and charge of the batteries were controlled by a computer in order to reduce both consumption peaks and lower but longer energy consumption over time. With this optimization and good maintenance of the batteries, it will be possible to use the energy in a more intelligent way, saving on the electricity bill and not pouring as much energy into the main grid. In all three cases of reduction of energy consumption, electricity consumption has been minimized thanks to the batteries. It has been possible to reduce 93 kWh, 150 kWh and 208 kWh for the cases of 2 hours, 5 hours and 8 hours, respectively. As mentioned above, this has been done by varying the battery discharge instructions by means of a computer,

although more energy could have been saved if the batteries had been discharged simultaneously to their maximum power in each period of time studied.

As for battery charging, the choice of sunny days for a large energy generation, especially photovoltaic energy, makes it possible to fill the batteries and also not pour so much electricity into the distribution network, being exempt from possible sanctions.

References

[1] M. Debouza, A. Al-Durra, T. H. M. EL-Fouly, and H. H. Zeineldin, "Survey on microgrids with flexible boundaries: Strategies, applications, and future trends," *Electric Power Systems Research*, vol. 205, no. January, p. 107765, 2022, doi: 10.1016/j.epsr.2021.107765.

[2] D. Q. Oliveira *et al.*, "A critical review of energy storage technologies for microgrids," *Energy Systems*, no. 0123456789, 2021, doi: 10.1007/s12667-021-00464-6.

[3] E. Planas, J. Andreu, J. I. Gárate, I. Martínez De Alegría, and E. Ibarra, "AC and DC technology in microgrids: A review," *Renewable and Sustainable Energy Reviews*, vol. 43, pp. 726–749, 2015, doi: 10.1016/j.rser.2014.11.067.

[4] K. Gandhi and S. K. Gupta, "Operational strategies and electricity market structure of microgrid: A critical review," *Renewable Energy Focus*, vol. 39, no. December, pp. 163–171, 2021, doi: 10.1016/j.ref.2021.09.001.

[5] A. Albaker, M. Alturki, R. Abbassi, and K. Alqunun, "Zonal-Based Optimal Microgrids Identification," *Energies (Basel)*, vol. 15, no. 7, 2022, doi: 10.3390/en15072446.

[6] İ. Çetinbaş, B. Tamyürek, and M. Demirtaş, "Sizing optimization and design of an autonomous AC microgrid for commercial loads using Harris Hawks Optimization algorithm," *Energy Convers Manag*, vol. 245, 2021, doi: 10.1016/j.enconman.2021.114562.

[7] S. Obara, S. Fujimoto, K. Sato, and Y. Utsugi, "Planning renewable energy introduction for a microgrid without battery storage," *Energy*, vol. 215, p. 119176, Jan. 2021, doi: 10.1016/J.ENERGY.2020.119176.

[8] M. F. Zia, E. Elbouchikhi, and M. Benbouzid, "Microgrids energy management systems: A critical review on methods, solutions, and prospects," *Appl Energy*, vol. 222, no. March, pp. 1033–1055, 2018, doi: 10.1016/j.apenergy.2018.04.103.

[9] S. Leonori, A. Martino, F. M. Frattale Mascioli, and A. Rizzi, "Microgrid Energy Management Systems Design by Computational Intelligence Techniques," *Appl Energy*, vol. 277, no. June, p. 115524, 2020, doi: 10.1016/j.apenergy.2020.115524.

[10] G. Sidarth, M. Seyedmahmoudian, E. Jamei, and B. Horan, "Role of optimization techniques in microgrid energy management systems — A review," *Energy Strategy Reviews*, vol. 43, no. June 2021, p. 100899, 2022, doi: 10.1016/j.esr.2022.100899.

[11] M. F. Zia, M. Nasir, E. Elbouchikhi, M. Benbouzid, J. C. Vasquez, and J. M. Guerrero, "Energy management system for a hybrid PV-Wind-Tidal-Battery-

based islanded DC microgrid: Modeling and experimental validation," *Renewable and Sustainable Energy Reviews*, vol. 159, no. January, p. 112093, 2022, doi: 10.1016/j.rser.2022.112093.

[12] L. C. S. Rocha, P. Rotella Junior, G. Aquila, and K. Janda, "Utility-scale energy storage systems: World condition and Brazilian perspectives," *J Energy Storage*, vol. 52, p. 105066, Aug. 2022, doi: 10.1016/J.EST.2022.105066.

[13] S. Dhundhara, Y. P. Verma, and A. Williams, "Techno-economic analysis of the lithium-ion and lead-acid battery in microgrid systems," *Energy Convers Manag*, vol. 177, pp. 122–142, Dec. 2018, doi: 10.1016/J.ENCONMAN.2018.09.030.

[14] W. Wang, B. Yuan, Q. Sun, and R. Wennersten, "Application of energy storage in integrated energy systems — A solution to fluctuation and uncertainty of renewable energy," *J Energy Storage*, vol. 52, p. 104812, Aug. 2022, doi: 10.1016/J.EST.2022.104812.

[15] J. Das, "Spectrum analysis for deterministic storage sizing in an isolated microgrid," *Mater Today Proc*, vol. 58, pp. 359–366, 2022, doi: 10.1016/j.matpr.2022.02.269.

[16] M. Amini, A. Khorsandi, B. Vahidi, S. H. Hosseinian, and A. Malakmahmoudi, "Optimal sizing of battery energy storage in a microgrid considering capacity degradation and replacement year," *Electric Power Systems Research*, vol. 195, p. 107170, Jun. 2021, doi: 10.1016/J.EPSR.2021.107170.

[17] H. Kikusato *et al.*, "Flywheel energy storage system based microgrid controller design and PHIL testing," *Energy Reports*, vol. 8, pp. 470–475, 2022, doi: 10.1016/j.egyr.2022.05.221.

[18] L. M. Abadie and N. Goicoechea, "Optimal management of a mega pumped hydro storage system under stochastic hourly electricity prices in the Iberian Peninsula," *Energy*, vol. 252, p. 123974, Aug. 2022, doi: 10.1016/J.ENERGY.2022.123974.

[19] F. Carducci, A. Giovannelli, M. Renzi, and G. Comodi, "Improving flexibility of industrial microgrids through thermal storage and HVAC management strategies," *Energy Procedia*, vol. 142, pp. 2728–2733, Dec. 2017, doi: 10.1016/J.EGYPRO.2017.12.217.

[20] J. J. Caparrós Mancera *et al.*, "Experimental analysis of the effects of supercapacitor banks in a renewable DC microgrid," *Appl Energy*, vol. 308, no. December 2021, 2022, doi: 10.1016/j.apenergy.2021.118355.

[21] Q. Zhang, W. Pei, and X. Liu, "Advances in Electrochemical Energy Storage Systems," *Electrochem*, vol. 3, no. 2, pp. 225–228, 2022, doi: 10.3390/electrochem3020014.

[22] M. Moncecchi, C. Brivio, S. Mandelli, and M. Merlo, "Battery energy storage systems in microgrids: Modeling and design criteria," *Energies (Basel)*, vol. 13, no. 8, pp. 1–18, 2020, doi: 10.3390/en13082006.

[23] I. S. Freitas Gomes, Y. Perez, and E. Suomalainen, "Coupling small batteries and PV generation: A review," *Renewable and Sustainable Energy Reviews*, vol. 126, no. March, p. 109835, 2020, doi: 10.1016/j.rser.2020.109835.

[24] J. Carroquino, C. Escriche-Martínez, L. Valiño, and R. Dufo-López, "Comparison of economic performance of lead-acid and li-ion batteries in standalone

photovoltaic energy systems," *Applied Sciences (Switzerland)*, vol. 11, no. 8, 2021, doi: 10.3390/app11083587.

[25] J. M. Lujano-Rojas, R. Dufo-López, J. L. Atencio-Guerra, E. M. G. Rodrigues, J. L. Bernal-Agustín, and J. P. S. Catalão, "Operating conditions of lead-acid batteries in the optimization of hybrid energy systems and microgrids," *Appl Energy*, vol. 179, pp. 590–600, Oct. 2016, doi: 10.1016/J.APENERGY.2016.07.018.

[26] K. Santos-Pereira, J. D. F. Pereira, L. S. Veras, D. L. S. Cosme, D. Q. Oliveira, and O. R. Saavedra, "The requirements and constraints of storage technology in isolated microgrids: a comparative analysis of lithium-ion vs. lead-acid batteries," *Energy Systems*, 2021, doi: 10.1007/S12667-021-00439-7.

[27] P. B. L. Neto, O. R. Saavedra, and L. A. de Souza Ribeiro, "A Dual-Battery Storage Bank Configuration for Isolated Microgrids Based on Renewable Sources," *IEEE Trans Sustain Energy*, vol. 9, no. 4, pp. 1618–1626, 2018, doi: 10.1109/TSTE.2018.2800689.

[28] C. Zhang, Y. L. Wei, P. F. Cao, and M. C. Lin, "Energy storage system: Current studies on batteries and power condition system," *Renewable and Sustainable Energy Reviews*, vol. 82, no. October 2017, pp. 3091–3106, 2018, doi: 10.1016/j.rser.2017.10.030.

[29] D. Li, S. Guo, W. He, M. King, and J. Wang, "Combined capacity and operation optimisation of lithium-ion battery energy storage working with a combined heat and power system," *Renewable and Sustainable Energy Reviews*, vol. 140, no. November 2020, p. 110731, 2021, doi: 10.1016/j.rser.2021.110731.

[30] M. Gutsch and J. Leker, "Global warming potential of lithium-ion battery energy storage systems: A review," *J Energy Storage*, vol. 52, no. PC, p. 105030, 2022, doi: 10.1016/j.est.2022.105030.

[31] Y. Wang *et al.*, "Environmental impact assessment of second life and recycling for LiFePO4 power batteries in China," *J Environ Manage*, vol. 314, p. 115083, Jul. 2022, doi: 10.1016/J.JENVMAN.2022.115083.

[32] P. Ayuso, H. Beltran, J. Segarra-Tamarit, and E. Pérez, "Optimized profitability of LFP and NMC Li-ion batteries in residential PV applications," *Math Comput Simul*, vol. 183, pp. 97–115, May 2021, doi: 10.1016/J.MATCOM.2020.02.011.

Power quality improvement techniques in SmartGrids

Daniel Alcala-González[1*] M. Isabel Más-López [2], Eva M. García del Toro [1], Sara García-Salgado [1]y Santiago Pindado[3]

[1] Departamento de Ingeniería Civil, Hidráulica, Energía y Medio Ambiente, ETSI Caminos Canales y Puertos Universidad Politécnica de Madrid, Alfonso XII, 3, 28014 Madrid, Spain; d.alcalag@upm.es, evamaria.garcia@upm.es, sara.garcia@upm.es

[2] Departamento de Matemática e Informática Aplicadas a las Ingenierías Civil y Naval, ETSI Caminos Canales y Puertos Universidad Politécnica de Madrid, Alfonso XII, 3, 28014 Madrid, Spain
mariaisabel.mas@upm.es

[3] Instituto Universitario de Microgravedad "Ignacio Da Riva" (IDR/UPM), ETSI Aeronáutica y del Espacio, Universidad Politécnica de Madrid, Pza. del Cardenal Cisneros 3, 28040 Madrid, Spain
santiago.pindado@upm.es

Abstract. The increase in the installation of renewable energy sources in electric power systems has changed the behavior of power distribution networks, creating a new scenario with respect to the performance of protection devices, such as fuses or overcurrent relays. Distributed Generation (DG) can cause delays in the performance of these devices as a result of short circuits and the consequent loss of power supply to the subscribers. For this reason, this work shows improvement techniques for the response of the protection devices that entails an implicit improvement in the quality of electricity supply in distribution networks with the presence of DG that make up the SmartGrid.

Keywords: Distributed Generation, Protection Coordination, Smartgrid, Quality of supply.

1   Introduction

Distributed Generation (DG) based on renewable energy sources has caused an important change in the traditional energy supply model in distribution networks. This new paradigm has brought the generation of electrical energy closer to the user, in contradiction with the traditional generation in centralized plants [1,2]. Therefore, it is necessary to implement electrical systems with an infrastructure that allows energy to be distributed and available to users in optimal conditions for its use [3].

Although the presence of DG in power grids can be beneficial [4,5], it produces a structural transformation, not behaving as a classical radial distribution network. Reverse

power flows can occur both in steady state and in the presence of faults [6-10]. The impacts that DG can have on these distribution networks will depend, among other aspects, on the type of generation, technology used, installed power and location in the network [11-15].

Different problems may arise with the increase of DG within electrical networks, for example harmonic distortion, frequency drop and network stability and reliability [16-20]. One of the most relevant problem is the coordination of expulsion fuses and protection relays . The traditional protection system was designed for unidirectional power distribution. However, this new situation has been changed by the increasing presence of these decentralized renewable energy sources [21], also taking into account other ways to reduce the energy production of traditional energy sources that have a negative impact on the climate (e.g., the use of electric vehicles as energy sources [22-27]). Consequently, distribution networks with DG, such as photovoltaic generation, located at different grid locations, can lead to a mismatch in the coordination between protection devices [28-36].

For all the above reasons and with the aim of ensuring a good quality of power supply, achieving an adequate functionality of the protection devices and a more sustainable energy network, different novel methods that avoid untimely tripping and ensure an effective coordination between protection devices, and thus improve the quality of power supply in the distribution networks of SmartCities, are shown in this work.

This paper is organized as follows. Section 2 describes the methodology and the network used to analyze the coordination, while the results are included in Section 3. Finally, the conclusions are summarized in Section 4.

2 Methodology

2.1 Improved fuse protection response

The tripping curve of protection fuses is an inverse time-current characteristic curve. It is a straight line I^2t *log-log*, where I is the tripping current and t is the tripping time, usually expressed for minimum fuse melting and total clearing times. From the fuse characteristic in the *log-log curve*, it is possible to approximate it to a second-order polynomial function. However, the fuse performance curve can be approximated to a straight line so the general equation describing the fuse characteristic curve can be expressed as the following equation [37-43]:

$$\log(t) = m \log(I) + n \qquad (1)$$

where m and n are the parameters of the selected tripping curve [41, 42].

The fuse tripping characteristic curve is shown in Figure 1, and it is characterized by two limit curves:

- The minimum melting curve (as the lower limit), which detects the minimum overcurrent that causes the initiation of fusing of the link.
- The full opening curve (as an upper limit), which indicates the complete melting of the fuse and the opening of the circuit.
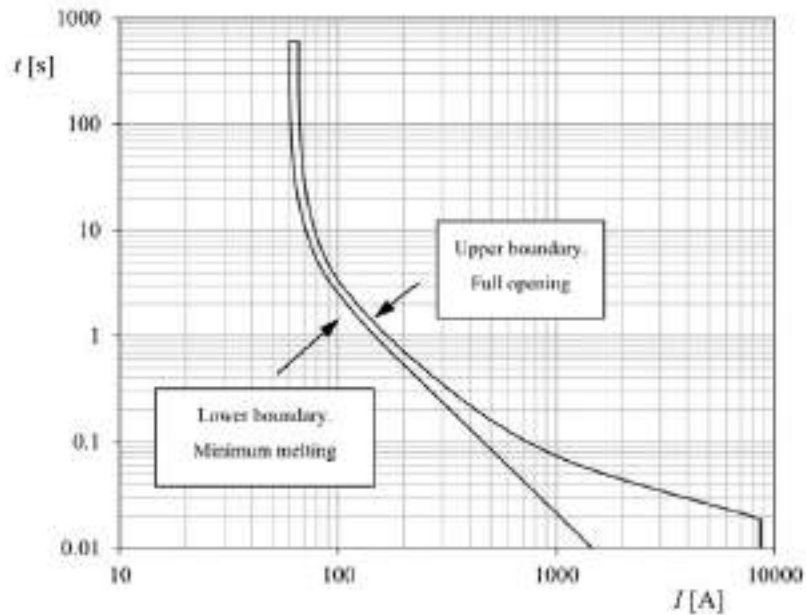

Fig. 1. Fuse actuation characteristic (*cut-out*).

The operation of these devices can be seen in Figure 2, which shows a classic coordination between them in electrical networks without the presence of DG. The diagram included in this figure shows a radial network in which F1 is the fuse protecting the main line and F2 the one protecting the secondary line. The criteria for correct coordination between fuses are as follows:

- For faults on the main line, fuse F2 will not detect any fault current, with fuse F1 acting as the main protection.
- For branch faults, F2 will act as main protection and F1 as backup protection.
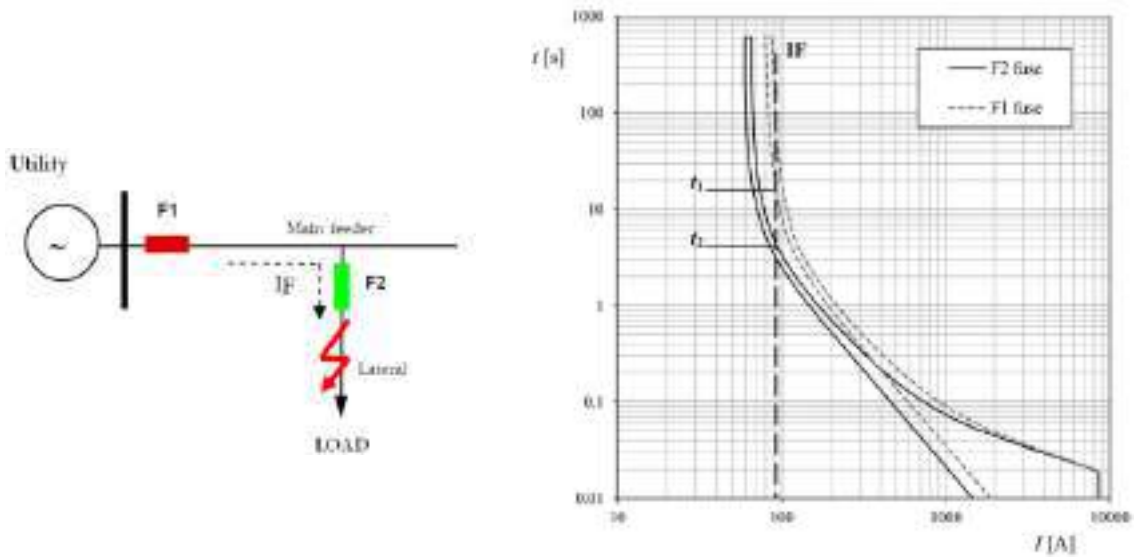
Fig. 2. Classic coordination between protection fuses in radial distribution networks without DG (Left) Diagram of a radial distribution network without the presence of DG (Right) Operating characteristic curves of F1 and F2 protection fuses

In the presence of DG, the value of the current shown in Figure 2 can vary, thus causing untimely tripping and/or delay of the device to clear the fault. At this regard, Pindado et al [44] proposed a new method of selecting protection fuses to avoid these impacts, achieving a more sustainable electrical network while maintaining the functionality of the protections. This procedure was based on a new mathematical modeling of the tripping curves of the upper envelope (*ES*) and lower envelope (*EI*) of the fuses to be coordinated. For the upper envelope, two mathematical expressions are proposed (equation 2), as a function of the current, *I*, in relation to a given value, *I**:

$$\frac{1}{t_{ES}} = \begin{cases} \sum_{i=0}^{N_1} \beta_i I^{\frac{i}{2}}; I < I^* \\ \sum_{i=0}^{N_2} \beta_i I^{\frac{i}{2}}; I > I^* \end{cases} \tag{2}$$

For the lower envelope it is expressed by equation 3:

$$\frac{1}{t_{EI}} = \sum_{i=0}^{N} \beta_i I^{\frac{i}{2}} \qquad (3)$$

In equations 2 and 3, t_{ES} and t_{EI} represent the total operating time corresponding to the upper envelope curve of the fuse acting as the main protection, and the minimum melting time corresponding to the lower envelope curve of the fuse acting as the backup protection, respectively. $\beta_{1,i}$ and $\beta_{2,i}$ are characterization parameters of the upper boundary curve of the fuse acting as the main protection. β_i are the characterization parameters of the lower boundary curve of the fuse acting as backup protection.

The coordination criterion of the protection fuses can be expressed as shown in the following equation:

$$t_{EI} = K\left(t_{ES} + CTI\right) \qquad (4)$$

where *CTI* is the coordination time interval (200-300 ms) [32,33], and *K* is a proportionality constant.

2.2 Improved coordination of overcurrent relays

Overcurrent relays (OCR) are currently the most widely used overcurrent protection devices at line outlets [45,46], used as main and backup protection. With respect to its operation, the OCR should act as primary protection by eliminating faults occurring in the zone under its supervision. Only in the event that the primary protection fails to operate, the backup protection should initiate tripping.

A typical electrical distribution network may consist of hundreds of equipment protection relays. Each relay in the system must be coordinated with the adjacent equipment protection relay. If the backup protection is not well coordinated, a coordination failure may occur. Therefore, the coordination of the backup protections is a major concern in the network protection system [45,47]. Generally, the coordination of protections can be performed by topology [48,49], by optimization methods [50,51], or by expert methods [52]. Topological analysis is used for relay tuning in multiterminal networks, whereas graph theory and functional approximation techniques are used to provide the best solution, which does not need to be the optimal one. In optimization methods, some researchers [50, 53] used nonlinear programming techniques to determine the optimal relay settings, subject to constraints due to coordination and limits of the relay settings themselves. Bedekar et at [54-55] proposed the large-M method to find the optimal value of the time multiplier setting (TMS) of the OCR, where the set values of the plug setting are assumed to be known and fixed.

Alcala-Gonzalez et al [56] developed a unified protection system that offered dual functionality. It was shown that the system was able to optimize the relay settings for each network situation, and the OCR coordination problem in the distribution system

with the presence of DG was defined as an optimization problem with constraints, whose objective function is shown in equation 5:

$$min \ \frac{\alpha}{(k_{i,j})^{\beta}-1} \sum_{i=1}^{n}\left(\sum_{j=1}^{m} \text{TMS}_{i,j} - \text{TMS}_{i+1,j+1}\right) \quad\quad (5)$$

where α and β are the OCR shape constants according to Table 1, $k_{i,j}$ is the ratio between the short-circuit current, I_{CC}, and the relay setting current, I_{ar}, with respect to relay I with fault in section j, and *TMS* is the time multiplier setting.

Table 1. Parameters α y β IEC [55].

Curve	α	β
Time inverse	0.14	0.02
Very inverse	13.5	1
Extremely inverse	80	2

3   Results

The relay performance has been tested for different DG penetration levels, different types of short-circuit faults (single-phase to ground and three-phase), and different fault zones (main feeder and lateral faults).

For the implementation of the techniques described in the previous sections, the IEEE 13 network was used, as shown in Figure 3. As it can be observed, the distribution network was divided into 4 different protection zones.
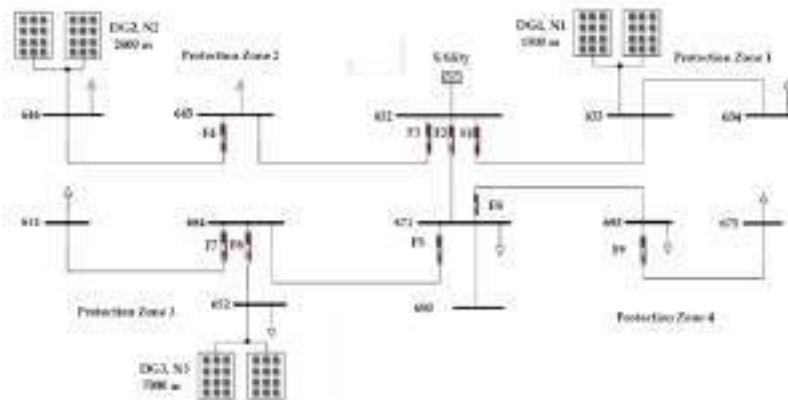
Fig. 3. IEEE 13-bus test feeder used to test the performance of the proposed improvement techniques [44].

The case studies were designed for three different DG locations in the network (bus/nodes 633, 646 and 652) and different DG power penetration levels, namely 25%, 50%, 75% and 100% [56]. They were simulated with Power Factory's DIgSILENT© software [57], since this electrical system simulation software has a specific library for electrical protection. The DG locations in the distribution network are shown in Table 2, together with the distance to the electrical substation (S) in each case.

Table 2. DG location and distance to the substation.

Bus	Distance (m)	Description
Bus 633 (N1)	1500	Nearby to Substation
Bus 646 (N2)	2400	Medium distance to Substation
Bus 652 (N3)	7000	Far to Substation

A nominal voltage of 20 kV was considered for the cases analyzed, being the overhead cable made of reinforced aluminum 47-AL1/8ST1A (see Table 3 for the main characteristics, according to EN 50182 [58]). The total load considered was 3.83 MW, consisting of several three-phase loads distributed according to the information included in Table 4.

Table 3. Conductor characteristics 47-AL1/8ST1A.

Electrical resistance to 20ºC [$\Omega \cdot km^{-1}$]	0.614
Electrical reactance at 20ºC [$\Omega \cdot km^{-1}$]	0.41
Max. short circuit current [kA]	0.202

Table 4. Characteristics of the loads considered as a function of the bus (see Figure 3).

Location	Load Type	Power (MW)
Nudo 634	Type Y	1.5
Nudo 611	Type Y	0.056
Nudo 645	Type Y	0.056
Nudo 646	Type D	0.5
Nudo 652	Type Y	1
Node 671	Type D	0.385
Nudo 675	Type Y	0.281
Nudo 692	Type D	0.056

The supplier's standards [59] and the recommendations of IEC 60787 [60] were considered for the selection of the size of the expulsion fuses. In addition, two complementary criteria were established: the rated current of the fuse must be above the maximum expected load current of the generator with a sufficient margin (125% load), and the fuse must not trip at the generator switching currents [42]. The results of the simulations performed can be found in [44].

Figure 4 shows the results obtained from the simulation of the IEEE 13-bus power system, fuses F3 (E13) and F4(E10) that tripped for a current I = 87.2 A with poor coordination between them (i.e., the time between the upper envelope curve of fuse F4, t_{ES}, and the lower envelope curve of fuse F3, t_{EI}, is lower than the coordination time interval, CTI = 0.3 s). This lack of coordination could be mitigated by replacing one of the fuses.
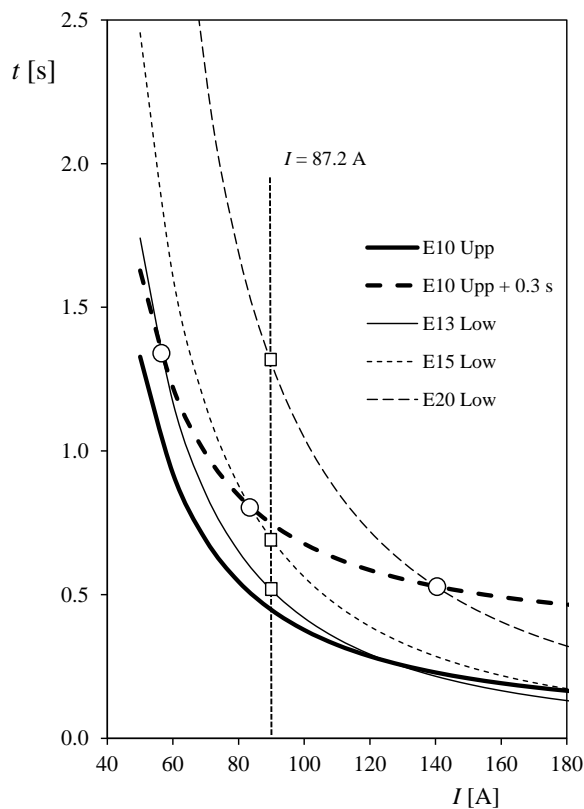
Fig. 4. Fuse selection to avoid uncorrected coordination detected when considering the PV nodes where the DG sources are installed.

Figure 4 shows the upper curve of fuse F4 (SMD-50 E10) and the lower curve of fuse F3 (SMD-50 E13). It can be observed that the current intercepts the curve of fuse F3 at a point (indicated by a square) located below the curve corresponding to fuse F4 plus a CTI = 0.3 s (which implies a lack of coordination).

If fuse F3 was replaced by the next fuse in the family, characterized by a higher rated current (SMD-50 E15), the situation was not solved, since at a current I = 87.2 A the lower curve of the fuse had a lower tripping time than that indicated by the upper curve of fuse F4 plus a CTI = 0.3 s (also indicated by a square in Figure 4). The problem was finally solved by selecting an SMD-50 E20 for fuse F3.

In Figure 4 it can also be seen how the tripping time of its lower curve at I = 87.2 A (indicated by a square), was off by more than 0.3 s relative to the upper curve of the SMD-50 E10.

With respect to the performance of the OCRs, the values of the a and TMS constants and the top relay actuation times for the rest of the scenarios are shown in [56].

The plots of classical coordination versus linear programming coordination in the case of more severe three-phase short circuits are shown in Figure 5. It can be seen that the response of the main and backup OCR protection devices was significantly optimized with the method proposed in this work.
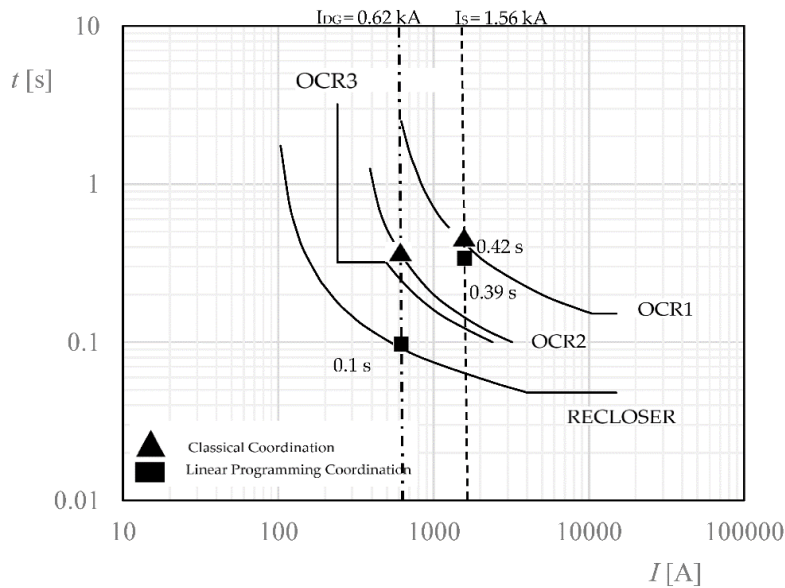
Fig. 5. Short circuit in F2 with a DG1 penetration level of 17%. Classical versus linear programming.

4   Conclusions

Different novel methods that avoid untimely tripping and ensure an effective coordination between protection devices, and thus improve the quality of power supply in the distribution networks of SmartCities, are shown in this work.

Regarding the coordination of fuses in power grids with the presence of photovoltaic technology DGs, the behavior of fuses in the power supply system of 13 IEEE bus with DG has been studied with DIgSI-LENT©, considering different levels of power

penetration and power distribution between the three bus nodes where the DG sources were installed (at short, medium and long distances from the substation), in order to study the widest range of possibilities. The most relevant results of this work are:

- The effect of photovoltaic DG on fuse coordination in an electrical network similar to that present in small rural villages were tested. The results indicated that inadequate coordination could occur in the fuses (correctly selected in the absence of DG).
- A new and simple way to simulate fuse operation was described.
- Thanks to the new fuse modeling developed, criteria for selecting new fuses in electrical networks that can ensure correct coordination between them were described.

On the other hand, and with regard to the response of the OCR adjusted by programming versus classical coordination, it can be concluded that, in all the cases studied, the system proved to be able of adapting the trip parameters of the relays protecting the faulted line section according to the operating conditions of the system at the time of the fault. The results showed that the protection coordination proposed in this work was able to reduce the operating times of the relays by more than 80% compared to classical coordination, resulting in a more reliable operation of a DG network.

References

1. Paithankar YG, Bhide SR. Fundamentals of power system protection. PHI Learning Pvt. Ltd; 2011.
2. Jennett K, Coffele F, Booth C. Comprehensive and quantitative analysis of protection problems associated with increasing penetration of inverter-interfaced DG. 11th IET Int. Conf. Dev. Power Syst. Prot. (DPSP 2012). 23-26 April 2012, Birmingham. Conf. Publ., 2012. https://doi.org/10.1049/cp.2012.0091.
3. Cidrás J, Miñambres JF, Alvarado FL. Fault Analysis and Protection Systems. Analysis and Operation. Electr. Energy Syst. Anal. Oper., 2009, p. 303–54.
4. Liu Z, Wen F, Ledwich G. Potential benefits of distributed generators to power systems. DRPT 2011 - 2011 4th Int. Conf. Electr. Util. Deregul. Restruct. Power Technol., IEEE; 2011, p. 1417–23. https://doi.org/10.1109/DRPT.2011.5994118.
5. Chamandoust H, Hashemi A, Derakhshan G, Abdi B. Optimal hybrid system design based on renewable energy resources. IEEE Proc. 2017 Smart Grid Conf. SGC 2017, vol. 2018-Janua, 2018, p. 1–5. https://doi.org/10.1109/SGC.2017.8308878.
6. Bastiao F, Cruz P, Fiteiro R. Impact of Distributed Generation on Distribution Networks. 5th Int. Conf. Eur. Electr. Mark. 28-30 May 2008, Lisboa, 2008. https://doi.org/10.1109/TDC-LA.2008.4641762.
7. Hsu CT, Tsai LJ, Cheng TJ, Chen CS, Hsu CW. Solar PV generation system controls for improving voltage in distribution network. ISNE 2013 - IEEE 2nd Int. Symp. Next-Generation Electron. 2013. Febr. 25-26 , Kaohsiung, Taiwan, IEEE; 2013, p. 486–9. https://doi.org/10.1109/ISNE.2013.6512404.

8. Zheng S, Xu ZH, Liu JJ, Fu Q. The Application of Electronic Communication Relay Protection in Distribution Network with Distributed Generation. Adv Mater Res 2014;1070–1072:938–42. https://doi.org/10.4028/www.scientific.net/amr.1070-1072.938.

9. Li Y, Ren H, Zhou L, Wang F, Li J. Inverse-time protection scheme for active distribution network based on user-defined characteristics. 2017 IEEE PES Innov. Smart Grid Technol. Conf. Eur. ISGT-Europe 2017 - Proc., vol. 2018- Janua, 2017, p. 1–6. https://doi.org/10.1109/ISGTEurope.2017.8260253.

10. Zhang Y, Song X, Li J, Gao F, Deng Z. Research on Voltage Rise Risk Assessment Model and Method for Distribution Network with Distributed Generation. 2nd IEEE Conf. Energy Internet Energy Syst. Integr. EI2 2018 - Proc., IEEE; 2018, p. 1–5. https://doi.org/10.1109/EI2.2018.8582001.

11. Deng W, Pei W, Qi Z. Impact and improvement of distributed generation on voltage quality in micro-grid. 3rd Int. Conf. Deregul. Restruct. Power Technol. DRPT 2008, 2008, p. 1737–41. https://doi.org/10.1109/DRPT.2008.4523687.

12. Kulkarni SN, Shingare P. A review on power quality challenges in renewable Energy grid integration. Int J Curr Eng Technol 2011;6:1573–8. https://doi.org/10.14741/ijcet/22774106/6.5.2016.14.

13. Hakimi SM, Moghaddas-Tafreshi SM. Optimal planning of a smart microgrid including demand response and intermittent renewable energy resources. IEEE Trans Smart Grid 2014;5:2889–900. https://doi.org/10.1109/TSG.2014.2320962.

14. Sandhu M, Thakur T. Issues, Challenges, Causes, Impacts and Utilization of Renewable Energy Sources - Grid Integration. J Eng Res Appl 2014;4:636–43.

15. Ehsan A, Yang Q. Optimal integration and planning of renewable distributed generation in the power distribution networks: A review of analytical techniques. Appl Energy 2018;210:44–59. https://doi.org/10.1016/j.apenergy.2017.10.106.

16. Abdul Kadir AF, Mohamed A, Shareef H. Harmonic impact of different distributed generation units on low voltage distribution system. 2011 IEEE Int. Electr. Mach. Drives Conf. IEMDC 2011, IEEE; 2011, p. 1201–6. https://doi.org/10.1109/IEMDC.2011.5994774.

17. Antonova G, Nardi M, Scott A, Pesin M. Distributed generation and its impact on power grids and microgrids protection. 2012 65th Annu. Conf. Prot. Relay Eng., IEEE; 2012, p. 152–61. https://doi.org/10.1109/CPRE.2012.6201229.

18. Bignucolo F, Cerretti A, Coppo M, Savio A, Turri R. Impact of distributed generation grid code requirements on islanding detection in LV networks. Energies 2017;10. https://doi.org/10.3390/en10020156.

19. Senarathna TSS, Udayanga Hemapala KTM. Review of adaptive protection methods for microgrids. AIMS Energy 2019;7:557–78. https://doi.org/10.3934/energy.2019.5.557.

20. Adefarati T, Bansal RC. Reliability assessment of distribution system with the integration of renewable distributed generation. Appl Energy 2017;185:158–71. https://doi.org/10.1016/j.apenergy.2016.10.087.

21. Barik MA, Pota HR. Complementary effect of wind and solar energy sources in a microgrid. 2012 IEEE Innov. Smart Grid Technol. - Asia, ISGT Asia 2012, IEEE; 2012, p. 1–6. https://doi.org/10.1109/ISGT-Asia.2012.6303325.

22. Clement-Nyns K, Haesen E, Driesen J. The impact of vehicle-to-grid on the distribution grid. Electr Power Syst Res 2011;81:185–92. https://doi.org/10.1016/j.epsr.2010.08.007.

23. López MA, Martín S, Aguado JA, De La Torre S. V2G strategies for congestion management in microgrids with high penetration of electric vehicles. Electr Power Syst Res 2013;104:28–34. https://doi.org/10.1016/j.epsr.2013.06.005.

24. García-Villalobos J, Zamora I, San Martín JI, Asensio FJ, Aperribay V. Plug-in electric vehicles in electric distribution networks: A review of smart charging approaches. Renew Sustain Energy Rev 2014;38:717–31. https://doi.org/10.1016/j.rser.2014.07.040.

25. López MA, De La Torre S, Martín S, Aguado JA. Demand-side management in smart grid operation considering electric vehicles load shifting and vehicle-to-grid support. Int J Electr Power Energy Syst 2015;64:689–98. https://doi.org/10.1016/j.ijepes.2014.07.065.

26. Tan KM, Ramachandaramurthy VK, Yong JY. Integration of electric vehicles in smart grid: A review on vehicle to grid technologies and optimization techniques. Renew Sustain Energy Rev 2016;53:720–32. https://doi.org/10.1016/j.rser.2015.09.012.

27. Galiveeti HR, Goswami AK, Dev Choudhury NB. Impact of plug-in electric vehicles and distributed generation on reliability of distribution systems. Eng Sci Technol an Int J 2018;21:50–9. https://doi.org/10.1016/j.jestch.2018.01.005.

28. Margossian H, Capitanescu F, Sachau J. Distributed generator status estimation for adaptive feeder protection in active distribution grids. 22 nd Int. Conf. Electr. Distrib. Stock. 10-13 June 2013, 2013.

29. Margossian H, Capitanescu F, Sachau J. Feeder protection challenges with high penetration of inverter based distributed generation. IEEE EuroCon 2013, Zagreb. 1-4 July 2013, 2013, p. 1369–74. https://doi.org/10.1109/EUROCON.2013.6625157.

30. Neshvad S, Margossian H, Sachau J. Topology and parameter estimation in power systems through inverter-based broadband stimulations. IET Gener Transm Distrib 2016;10:1710–9. https://doi.org/10.1049/iet-gtd.2015.1163.

31. Margossian H, Sachau J, Deconinck G. Short circuit calculation in networks with a high share of inverter based distributed generation. 2014 IEEE 5th Int. Symp. Power Electron. Distrib. Gener. Syst. PEDG 2014, IEEE; 2014, p. 1–5. https://doi.org/10.1109/PEDG.2014.6878629.

32. Dewadasa M, Ghosh A, Ledwich G. Fold back current control and admittance protection scheme for a distribution network containing distributed generators. IET Gener Transm Distrib 2010;4:952–62. https://doi.org/10.1049/iet-gtd.2009.0614.

33. Dewadasa M, Ghosh A, Ledwich G. Protection of distributed generation connected networks with coordination of overcurrent relays. IECON Proc. (Industrial Electron. Conf. 10 Nov. 2011, Melb., IEEE; 2011, p. 924–9. https://doi.org/10.1109/IECON.2011.6119434.

34. Sa'ed JA, Favuzza S, Ippolito MG, Massaro F. An investigation of protection devices coordination effects on distributed generators capacity in radial distribution systems. 4th Int Conf Clean Electr Power Renew Energy Resour Impact, ICCEP 2013 2013:686–92. https://doi.org/10.1109/ICCEP.2013.6586928.

35. Fani B, Bisheh H, Sadeghkhani I. Protection coordination scheme for distribution networks with high penetration of photovoltaic generators. IET Gener Transm Distrib 2018;12:1802–14. https://doi.org/10.1049/iet-gtd.2017.1229.

36. Brahma SM, Girgis AA. Microprocessor-based reclosing to coordinate fuse and recloser in a system with high penetration of distributed generation. Proc. IEEE Power Eng. Soc. Transm. Distrib. Conf., IEEE; 2002, p. 453–8. https://doi.org/10.1109/pesw.2002.985041.

37. Nojavan, M.; Seyedi, H.; Mahari, A.; Zare, K. Optimization of Fuse-Recloser Coordination and Dispersed Generation Capacity in Distribution Systems. Majlesi J. Electr. Eng. 2014, 8, 15–24.

38. Yousaf, M.; Mahmood, T. Protection coordination for a distribution system in the presence of distributed generation. Turkish J. Electr. Eng. Comput. Sci. 2017, 25, 408–421, doi:10.3906/elk-1408-27.

39. Chaitusaney, S.; Yokoyama, A. Reliability analysis of distribution system with distributed generation considering loss of protection coordination. In Proceedings of the 2006 9th International Conference on Probabilistic Methods Applied to Power Systems, PMAPS; 2006.

40. Braga, G.; Zanin Bertoletti, A.; Peres de Morais, A.; Ghendy Cardoso, J. Curve Fitting Analysis of Expulsion Fuse Links through the Cross-Validation Technique. In Proceedings of the 2018 IEEE PES Transmission & Distribution Conference and Exhibition - Latin America (T&D-LA); IEEE: Lima, Peru, 2018; pp. 1–5.

41. Fazanehrafat, A.; Javadian, S.A.M.; Bathaee, S.M.T.; Haghifam, M.R. Maintaining the recloser-fuse coordination in distribution systems in presence of DG by determining DG's size. In Proceedings of the IET 9th International Conference on Developments in Power Systems Protection (DPSP 2008); 2008; pp. 132–137.

42. Anderson, P. *Power system protection*; Wiley, 1998;

43. Viawan, F.A.; Karlsson, D.; Sannino, A.; Daalder, J. Protection scheme for meshed distribution systems with high penetration of distributed generation. In Proceedings of the 2006 Power Systems Conference: Advanced Metering, Protection, Control, Communication, and Distributed Resources; 2006; pp. 99–104.

44. S. Pindado, D. Alcala-Gonzalez, D. Alfonso-Corcuera, E. M. García del Toro, and M. I. Más-López, "Improving the Power Supply Performance in Rural Smart Grids with Photovoltaic DG by Optimizing Fuse Selection," Agronomy, 2021

45. Warrington, A.R.V.C. Protective Relays: Their Theory and Practice, Wiley, J., York, S.N., Eds.; Springer: Cham, Switzerland, 1969.

46. Paithankar, Y.G. Transmission Network Protection: Theory and Practice; Routledge: Oxfordshire, UK, 1997.

47. Noghabi, A.S.; Sadeh, J.; Mashhadi, H.R. Considering different network topologies in optimal overcurrent relay coordination using a hybrid GA. IEEE Trans. Power Deliv. 2019, 24, 1857–1863.

48. Knable, A. A standardized approach to relay coordination. IEEE Winter Power Meet. 1969, 69, 58.

49. Jenkins, L.; Khicha, H.; Shivakumar, S.; Dash, P. An application of function dependencies to the topological analysis of protection schemes. IEEE Trans. Power Deliv. 1992, 7, 77–83.

50. Urdaneta, A.J.; Nadira, R.; Perez Jimenez, L.G. Optimal coordination of directional overcurrent relays in interconnected power systems. IEEE Trans. Power Deliv. 1988, 3, 903–911.

51. Chattopadhyay, B.; Sachdev, M.S.; Sidhu, T.S. An on-line relay coordination algorithm for adaptive protection using linear programming technique. IEEE Trans. Power Deliv. 1996, 11, 165–173.

52. So, C.W.; Li, K.K. Time coordination method for power system protection by evolutionary algorithm. IEEE Trans. Ind. Appl. 2000, 36, 1235–1240.

53. Laway, N.A.; Gupta, H.O. A method for adaptive coordination of overcurrent relays in an interconnected power system. In Proceedings of the Fifth International Conference on Developments in Power System Protection, York, UK, 30 March–2 April 1993; pp. 240–243.

54. Bedekar, P.; Bhide, S.; Kale, V. Optimum time coordination of overcurrent relays in distribution system using big-m (penalty) method. WSEAS Trans. Power Syst. 2019, 4, 341–350

55. IEC 61850-SER; Communication Networks and Systems in Substations. All Parts. IEC Std: Geneva, Switzerland, 2005.

56. D. Alcala-Gonzalez, E. M. García del Toro, M. I. Más-López, S- García-Salgado and S. Pindado, "Linear Programming Coordination for Overcurrent Relay in Electrical Distribution Systems with Distributed Generation" Applied Sciences, 2022.

57. Razavi, S.E.; Rahimi, E.; Javadi, M.S.; Nezhad, A.E.; Lotfi, M.; Shafie-khah, M.; Catalão, J.P.S. Impact of distributed generation on protection and voltage regulation of distribution systems: A review. Renew. Sustain. Energy Rev. 2019, 105, 157–167.
58. UNE-EN 50182:2002/AC:2013: Conductores para líneas eléctricas aéreas. Conductores de alambres redondos cableados en capas concéntricas;
59. Iberdrola MT 2.13.40: Criterios de selección y adaptación del calibre de los fusibles de MT para Centros de Transformación; 2003;
60. Commission, I.-I.E. IEC 60783. Application guide for the selection of fuse-links of high-voltage fuses for transformer circuit applications; 1983.

Open-software microgrid alarm system: A case study of CEDER microgrid

Óscar Izquierdo Monge[1], Alberto Redondo Plaza[2], Paula Peña Carro[1], Gonzalo Martín Jiménez[1], Ángel Zorita Lamadrid[2], Luis Hernández Callejo[2]

[1] CEDER-CIEMAT, Autovía de Navarra A15 salida 56, 422290 Lubia (Soria), Spain.
[2] Universidad de Valladolid, Campus Universitario Duques de Soria, 42004 Soria, Spain.
oscar.izquierdo@ciemat.es; alberredon@gmail.com;
paula.pena@ciemat.es; gonzalo.martinjimenez@ciemat.es;
zorita@eii.uva.es; luis.hernandez.callejo@uva.es.

Abstract: Nowadays microgrids (MGs) are becoming tools that can improve the reliability, stability, and supply quality of the electrical system. In addition, MG are also able to help the integration of renewable technologies for electrical applications. The present paper shows the implementation of a mobile alarm system to optimize the MG maintenance. The novelty of the system is that it is based on open-source software, Node-RED, Homme Assistant and Telegram. The system has been tested in the CEDER microgrid (MG) and it is able to detect faults in the several devices that make up the MG like generation units, storage systems or loads. When a fault is detected, the system sends a Telegram text message to the MG operator or maintenance crew mobile phones so that they can fix the problem as soon as possible. The software implemented can also manage the MGs periodic preventive maintenance sending periodic messages in order to remind the maintenance crew the preventive maintenance task that must be done.

Keywords: Alarm system, microgrids, maintenance

1   Introduction

Nowadays the consumption of electricity has become a necessity around the world. This means that the electric energy demand increases every year due to the population increase and the economy's growth. In the present, more than 70% [1] electric energy production in the word comes from non-renewable sources. Non-renewable technologies can be related to a high-level greenhouse gases emission, which produce the global warming, one of the biggest problems that current society faces. Renewable technologies for electricity generation are an alternative to traditional energy sources with a competitive generation cost.

The constant growth of the different renewable energy systems and its integration into the different sorts of grids have a significant impact on the electric system performance. Because of the electricity grid requirements, the integration of the different

technologies of renewable electricity generation presents a challenge in the grids control and operation. This is because of the common yield variation that present technologies like photovoltaic or wind energy [2].

MGs can be considered as independent distribution networks that are made up by different units of distributed generation, loads and often storage elements as well. Therefore, MGs can provide a tool able to improve the reliability, stability, and supply quality of the electrical system [3], [4], solving the main problems related to the increasing implementation of renewable technologies for electrical applications.

Unlike conventional networks, MGs lack rotating inertia in the system. This and the fact that the MG generators are frequently fed by renewable energy source, lead to the need of developing MGs control systems. The most common control strategy is a hierarchical control strategy based on three levels [5]. The primary controller is a local control system that is responsible for ensuring a proper sharing among the different generators that make up the MG and allow each generator to operate autonomously. The secondary controller is used in order to achieve the global controllability of the MG. For this secondary controller a MG central controller is needed. This MG central controller can also include a tertiary controller, which is responsible for the purchase and sale operations between the MG and the distribution network [5]–[8]. Moreover, the distribution networks can be able to communicate with the MG central controller and give it energy dispatch orders. In this way, the control capacity offered by the MGs to distribution networks is one of the keys that allows the integration of renewable technologies, which are based on distribution generation.

The implementation of a control system in a MG needs the use of a programming language based on C++, Python, MATLAB y LabVIEW [9]–[11]. The use of these programs requires advanced knowledge of programming and paid license.

Most MGs that use this kind of control hierarchy include in their programming a decision-making system, which is able to perform control actions on the different elements of the MG. They include the off or on of the generation units, actuation on the switches or storage system loading and unloading. However, it is unusual that the system is able to notify the maintenance crew or the persons in charge of the MG control and monitoring [12].

Therefore, it is possible to classify the monitoring MGs system into two categories. The first one includes monitoring systems that don't include an alarm system while the second one includes monitoring systems that are able to notify the different persons in charge of the MG. Next, some of the monitoring systems that include an alarm system are shown.

One possibility is a system that has a datalogger and a local server that file data in a database [13]. The program also does an analysis in order to update the linkage and detect failures in the different units that make up the MG. If one of the values that the system is able to monitor is different from the previously defined nominal values, the system sends a notification email to the desired users.

Other possibility is a monitoring system based on Smart Meters and a Supervisory Control and Data Acquisition (SCADA) [14]. In this case, the periodicity of data acquisition can be from minutes to hours. This data acquisition is complemented with an alarm system that can be configured so that it notifies the users registered in the control

system. The Smart Meters can be configured in order to visualize data and to send notifications. The system is also able to be programmed so that the recorded fault can be manually solved with the support of one of the users or automatically solved thanks to a previous programming. Some "social SCADAs" [15] have been implemented in s MGs. This SCADA has got a simple interface, what allows that people without technical knowledge can understand the system performance. This SCADA is also able to send notifications to the user so that they perform maintenance tasks like battery bank maintenance.

An alarm system can also be achieved using a Matlab/Simulink program [16]. The program compiles a protocol of different logic equations whose result determinate if the MG is working properly or if it has one or some failures. The failure must persist for a certain time until the system sends the failure notification. This allows that a temporary failure in the communication system can be differentiated from a failure in the MG.

It is also possible to develop an intelligence remote monitoring system based on Web [17]. This use B/S architecture (browser/server architecture) to realize real-time monitoring and adjusting the value of the environment factor data. In addition to monitoring environmental parameters, the system can send alarms when some parameter is outside its thresholds values, which can be defined previously.

Finally, the monitoring and alarm system can also be based in a smartphone application supported by a Raspberry Pi 3 and the cloud platform [18]. This smartphone application allows to the user who are register in it the live data visualization. Moreover, the user can send control orders to the different devices connected and receive notification about the MG performance. With a proper setup, this system also allows plug in or out the MG loads and generators.

The MGs alarm systems can be supplemented with a MG alarm processing method based on equipment fault prediction and improved support vector machine learning [19]. This system allows to improve the alarm processing speed and fault detection accuracy.

The development of an alarm system in a MG is a good tool that could improve the MG performance and optimize the maintenance tasks, maximizing the renewable energy yield and increasing the availability and the sturdiness of the MG. In fact, a proper alarms system allows to leave out the continuous surveillance, which could save a lot of time and money.

In this paper a MG alarm system is presented. The alarm system has been implemented in the CEDER MG and it is based on open-source software: Home Assistant, NodeRed and Telegram. The second section of this paper describes the CEDER MG features while the third section shows the alarm system performance and the sort of alarms implemented. Finally, the conclusions of this mobile system are shown in fourth section.

2   CEDER microgrid description

CEDER is the place where the mentioned alarm system has been implemented. This center belongs to CIEMAT. It is located in Lubia, in the province of Soria (Spain), with a built-up area of 13,000 m² in three distinct areas, out of a total of 640 ha (see Fig. 1).

Fig. 1. CEDER location and distribution.

CEDER has a smart electrical MG which is used or modified in order to do researching activities. The CEDER MG is connected to a 45 kV distribution network and a 1,000 kVA electrical transformer reduces the voltage to feed a 15 kV close-ring grid. This close-ring grid has 8 transformation centers that reduce the voltage to 400 V. All the loads, generators and storage systems are connected to this transformation centers. The several elements that make up the CEDER MG are detailed below.

2.1 Distributed generation

The different electrical generation systems are spread over the 640 ha that make up the CEDER and all these generators are connected to the MG in low voltage (400 V). Depending on their renewable character and manageability, generation systems can be divided into the following groups:

- Non-controllable renewable:

    - Photovoltaic: 8 photovoltaic plants with 123.5 kW of total capacity.
    - Wind energy: 4 wind turbines with 61.2 kW of total capacity.
  - Controllable renewable:
    - Hydraulic turbine with 50 kW of total capacity.
  - Non-renewable:
    - Diesel generator with 100 kVA.

2.2 Storage systems

CEDER MG has several energy storage systems that are essential in order to achieve balance between generation and consumption. They avoid the energy injection into the utility grid and allow to store the excess energy for a later use, when the load is greater than the generation. The different CEDER storage systems are detailed below:

- Mechanical storage:
  - Hydraulic pumping system: 4 pumps with 7 kW each one.
  - Water tanks (3 tanks, 2000 m3 and 70 m unevenness).
- Electrochemical storage:
  - Lead-acid battery I: 120 cells with 2 V 1,080 Ah. Inverter 50 kW.
  - Lead-acid battery II: 120 cells with 2 V 765 Ah. Inverter 20 kW.
  - Lead-acid battery III: 120 cells with 2 V 650 Ah. Inverter 5 kW.
  - Lithium-ion battery: 2 racks with 14 modules and 14 cells per module (LFP). Each cell has 3,2 V and 50 Ah. Inverter 30 kW.

2.3 Loads

The several loads that make up the CEDER MG are connected into the low voltage grid. In order to measure the energy consumption, there is a main smart meter in the point of common coupling between the MG and the distribution network. In addition, each transformer center has a grid analyzer (PQube) that can measure the quality and energy consumption.

2.4 Management system

The management system at CEDER's microgrid consists of:

- **Communications bloc**: based on NodeRED. It integrates the different communication protocols of the generation, storage and consumption systems at CEDER (Modbus, MQTT, HTTP, etc.).

- Database: it is based on a database management system called MariaDB. The latter is a relational database that allows us to storage data per second in real-time thanks to programmed events and calculations (minute average or 15-minute average, as the ones used by the energy distribution company that supplies CE.D.E.R.) through the corresponding queries.
  This is important because, in addition to monitoring in real-time to make immediate decisions, it is of great interest to storage and analyse the data in order to stablish management strategies in the medium and long-term.

- **Energy Management System** (EMS) with a human-machine interface based on the Home Assistant software (see Fig. 11). This software allows monitoring all the necessary data from the equipment connected to the microgrid in real-time and giving instructions to each one. Furthermore, it is accessible from every point of the CE.D.E.R. communication network (meaning it is decentralized) and it can be accessed remotely with a smartphone application.

To achieve this, it is essential to connect all the elements of the microgrid as well as the management system to CE.D.E.R.'s data network. In this case, the equipment is connected to an Ethernet data network.

Cybersecurity is closely linked to the microgrid's management and control software. Due to the number of devices, entry points and protocols used, there is a bigger area susceptible to cyberattacks.

The modern cybersecurity market does not have the capacity to manage accurately such display for the entire power grid yet. Because of the latter, a member of the project is developing a security framework to provide a set of defensive measures in network attacking scenarios.

All of the above means that the operating mode and the cybersecurity system preparation is based on vulnerability evaluation and attack scenarios. The aim is to design a smart network architecture against malware. At the same time, the security performance will be analysed to reduce the impact of human errors and spear phishing campaigns.

3   Mobile Alarm System

3.1   Implementation of the alarm system

Home Assistant is an open-source software, developed in Python and generally used for home automation applications. However, it is a robust solution, economically affordable and with great potential for monitoring and managing MGs in real-time. Home Assistant allows connecting with all the elements in a MG (generation sources, storage systems and loads) using different communication protocols, developing SCADAs for the operation of each one and its integration in a single Human Machine Interface (HMI) to operate the MG [20]. Node-RED is an open-source tool developed in JavaScript for wiring together hardware devices, APIs and online services. It provides a browser editor which makes it easy to connect flows using several nodes. Telegram is an open source, cross-platform instant messaging software and application service that provides end-to-end encrypted calls.

Node-RED has a Telegram integration that allows to send text messages to the mobile phone of the MG supervisor. This enables to instantly inform them of all the issues in the MG so that they can take the appropriate actions for its operation or program the necessary maintenance tasks. In order to do this alarm system, the MG monitoring and control system needs to be developed using Home Assistant [20].

It is necessary to create a telegram bot. Hence, it is needed to follow the following steps:

1. Install Telegram application and run it.
2. Search BotFather, which is a bot that allows to create new bots and change the configuration of our own bots.
3. Start a conversation with BotFather and send him the command "/newbot". This allows to create a new bot, which must have a name and username. When the bot is created, a token is generated. This token must be included in the Home Assistant configuration file.
4. Then, it is needed to achieve the identifying numbers of each mobile phone that are going to communicate with the MG control system and receive the several alarms. For this, it is necessary to start a conversation with the bot IDBot and send it the command "/getid". This step must be done in all the mobiles phones that are going to receive the MG alarms or notifications.
5. Integrate telegram in Nod- RED. Install the additional node "node-red-contrib-telegrambot". The additional node can be installed from the Nodered interface in the "Manage Palette". Then it is needed to include the name of the bot and the API key in the Nodered configuration nodes.
6. Finally, the several alarms can be programed using the Node-RED browser-based editor. In this case two additional nodes are used: "node-red-contrib-telegrambot" and "node-red-contrib-home-assistant-websocket". The second one allows to integrate Home-assistant into Node-RED.

A simple example of one alarm is shown below (see Fig. 2). This nodes configuration allows to detect a fault in one of the solar plants. The configuration detects when one solar inverter doesn't produce energy while the solar irradiance is high enough to do it. When this fault is detected the system sends a text message alarm.

Fig. 2. Example of a corrective maintenance alarm configuration.

The first node is a "trigger node" and it checks the value of the inverter power. When the power is less than 0 W for 20 minutes the node triggers a flow that is sent to the next node. The configuration of this node must include the Homme Assistant server and the name of the entity that is wanted to check (see Fig. 3).

Fig. 3. Trigger node configuration.

The second node is a "conditional node", and it checks if the measured irradiance is high enough to allow generation. Hence, if the inverter power is less than zero for 20 minutes and solar irradiance is higher than 50 W/m^2 a flow is sent to the third node. The configuration of this node must include the Homme Assistant server and the name of the entity that is wanted to check (see Fig. 4).

Fig. 4. Conditional node configuration.

The configuration of the next node, "function node", must include the Telegram user ID of the person who is going to receive the alarm and the message text (see Fig. 5).

Fig. 5. Function node configuration.

The last node is a "Telegram sender node" and it allows the communication between Node-RED and Telegram. This node must include the bot username and the bot token which has been generated in the bot creation bot process Fig. 6.

Fig. 6. Telegram sender node configuration.

This system also allows to program a node configuration to send alarms when a periodic preventive task must be done (See Fig. 7). One possibility is a configuration that sends a periodic alarm, in this case an alarm every 180 days. Meantime, the other possibility is a configuration that sends an alarm each year in a determinate day and hour, in this case an alarm at 7:30 every 15th of April. The first configuration could fit better with tasks that have to be done two or more periodic times per year while the second one fits better with the tasks that have to be done once per year or the tasks that have to be done in a determinate moment of the year, like starting the electrical heater in the hydraulic turbine (before the frost period).
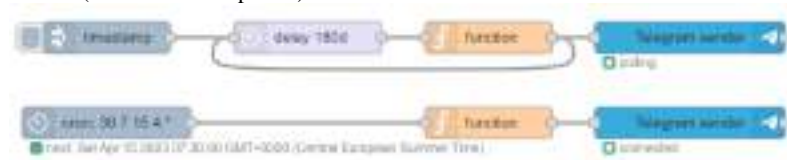

Fig. 7. Examples of preventive maintenance alarms.

Furthermore, the system can be configured so that it sends different alarms to different persons. The main operator of the MG receives all the alarms that the system detects while each member of the maintenance crew just receives the alarms of the facilities for which they are responsible.

3.2   System performance and sorts of alarms

There are many types of alarms that can be defined to notify the different failures that can occur during the normal MG performance. Not all the failures require the same type of response. The performance of the alarm system and the several sorts of alarms are shown below (see Fig. 8). When one of the monitored parameters is outside of its normal range and this parameter remains outside of its normal for a determinate time, the system sends the alarm message. This allows to differentiate a failure in the MG from a momentary communication failure. Depending on whether the parameter failure prevents the normal MG performance, the alarms can be classified as corrective maintenance alarm or informative alarms. Finally, the system sends periodic alarms to the person in charge of the several preventive maintenance task. If the conditions don't allow to do the maintenance, the system waits until the conditions allow to do it and send the alarm message.
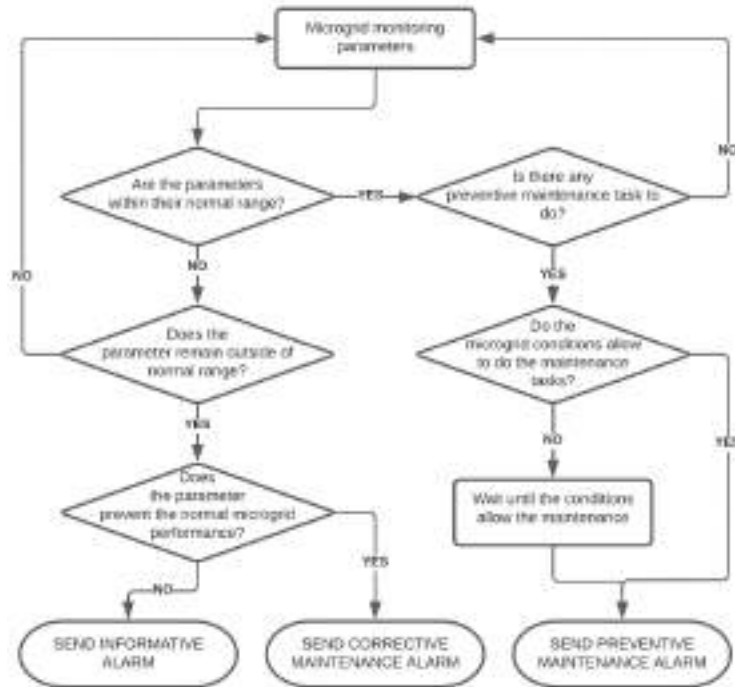
Fig. 8. Mobile alarm system performance.

Corrective maintenance alarms: These sorts of alarms don't let a normal MG perfor-mance and need the intervention of the maintenance crew so that they fix the detected failure. Among them we find the followings alarm:

- Differential or magnetothermic trip switch: when the power measured by one of the network analysers is zero during a determinate quantity of time, the system detects it and sends a message to the maintenance crew so that they fix it.
- Photovoltaic fault: If there is an irradiation higher than a determinate value and one of the inverters doesn't produce power while the other produces it, the system detects it and sends a message to the maintenance crew so that they fix it.
- Wind turbine failure: If there is a wind speed higher than the cut-in wind speed and the power of the wind turbine is zero, the system detects it and sends a message to the maintenance crew so that they fix it.
- Failure in the energy storage system when generation is greater than consump-tion.
- Motor protection trip switch.
- Lead-acid battery faults.

Some alarms are detected during normal operation as these cause a change in one of the parameters that are checked. On the other hand, other failures cannot be detected until the generation or storage units start to work. In both situations, a member of the maintenance crew must go to the place where the failure occurred.

Preventive maintenance alarms: In a MG with several generation and storage units, regular maintenance tasks must be done in order to avoid breakdowns or a premature degradation of the storage system. So, several alarms can be programmed to remind the maintenance crew that they have to perform these tasks. Among them we find the followings alarms:

- Visual and thermographic inspections of the inverters and the distribution boards.
- Solar module thermographic inspection by DRON.
- Wind turbines visual inspections.
- Check the hydraulic circuit and tanks leaks.
- Check the level of the electrolyte and measure his density in the different lead acid cells.
- Check the voltage of the battery cells.
- Turn on an electric heater in the pumps and hydro turbine so that the water doesn't freeze.

Moreover, it could be other preventive maintenance task whose performance is only possible in determinate conditions. For example, the maintenance task that must be done inside the tank only can be done when the level of the tank is lower than 30 cm. So, the system can be programmed to send the alarms when the conditions allow to do maintenance tasks.

These sorts of alarms let a normal MG performance but need that a member of the maintenance crew must go to the place where the unit that need a maintenance task is placed. However, some of them can be automatically solved. For example, it isn't recommended that the diesel generator isn't off more than 7 days. So, if its revolutions per minute are zero for one week, the system detects it, sends an alarm to the maintenance crew and starts the diesel generator for 10 minutes.

Informative alarms (Management alarms): These sorts of alarms give information about the performance of the MG. This information can be useful for the maintenance crew:

- Wind speed higher than a determinate value.
- The tilt angle of the photovoltaic modules should be changed to maximize the production: this task must be done manually, so the system sends several alarms throughout the year showing the optimized tilt angle depending on the month.
- Low tank level.
- Low battery in the storage system.

4   Conclusions

This paper shows the viability of developing an alarm system based on Node-RED, Home Assistant and Telegram that allows to improve the performance of a MG and optimize the maintenance of the several devices that make up the MG.

The system is able to detect faults in the different units of generation, storage and loads, what enables to maximize the renewable fraction energy consumption and improve the MG reliability. The system can also manage the preventive maintenance of the different devices that make up the MG sending alerts to the maintenance crew about the periodic maintenance task that must be done. Other informative alarms that are interesting to the MG operator or maintenance crew can be programed using the presented system.

The implemented system has demonstrated to be a robust solution with great potential for managing the several alarms in a MG. Moreover, the alarm system is based on open-source software, while other monitoring and alarm systems require paid license. This means that the alarm system presented could be an economically affordable solution for most of the MGs. Finally, the Node-RED browser editor allows to program several alarms without the need of an advanced knowledge about programing.

The alarm system implementation in the CEDER MG has improved the performance of the MG. The programed corrective alarms have achieved a quick fault detection in the several generators, what means a higher energy yield and less energy consumption from the distribution network. The alarm system implemented has also enabled to leave out the continuous monitoring and save microgrid operator time.

References

[1]   "Data & Statistics - IEA." https://www.iea.org/data-and-statistics (accessed Feb. 21, 2022).

[2]   M. Sechilariu, "Intelligent energy management of electrical power systems," *Applied Sciences (Switzerland)*, vol. 10, no. 8, Apr. 2020, doi: 10.3390/APP10082951.

[3]   N. Anandan, P. Sheeba, S. Sivanesan, S. Rama, and T. T. Bhuvaneswari, "Wide area monitoring system for an electrical grid," in *Energy Procedia*, 2019, vol. 160, pp. 381–388. doi: 10.1016/j.egypro.2019.02.171.

[4]   M. Aybar-Mejía, J. Villanueva, D. Mariano-Hernández, F. Santos, and A. Molina-García, "A review of low-voltage renewable microgrids: Generation forecasting and demand-side management strategies," *Electronics (Switzerland)*, vol. 10, no. 17, Sep. 2021, doi: 10.3390/electronics10172093.

[5]   Tine L. Vandoorn, Juan C. Vasquez, Jeroen De Kooning, Josep M. Guerrero, and Lieven Vandevelde, "Microgrids - Hierarchial control and an overview of the control and reserve managemenet strategies," *IEEE INDUSTRIAL ELECTRONICS MAGAZINE*, vol. 7, no. 4, pp. 42–55, 2013, doi: 10.1109/MIE.2013.2279306.

[6] S. Saponara, R. Saletti, and L. Mihet-Popa, "Hybrid micro-grids exploiting renewables sources, battery energy storages, and bi-directional converters," *Applied Sciences (Switzerland)*, vol. 9, no. 22. MDPI AG, Nov. 01, 2019. doi: 10.3390/APP9224973.

[7] I. Sadeghkhani, M. E. H. Golshan, A. Mehrizi-Sani, and J. M. Guerrero, "Low-voltage ride-through of a droop-based three-phase four-wire grid-connected microgrid," *IET Generation, Transmission and Distribution*, vol. 12, no. 8, pp. 1906–1914, Apr. 2018, doi: 10.1049/iet-gtd.2017.1306.

[8] T. Kull, B. Zeilmann, and G. Fischerauer, "Modular model composition for rapid implementations of embedded economic model predictive control in microgrids," *Applied Sciences (Switzerland)*, vol. 11, no. 22, Nov. 2021, doi: 10.3390/app112210602.

[9] L. Meng, M. Savaghebi, F. Andrade, J. C. Vasquez, J. M. Guerrero, and M. Graells, "Microgrid central controller development and hierarchical control implementation in the intelligent microgrid lab of Aalborg University," in *Conference Proceedings - IEEE Applied Power Electronics Conference and Exposition - APEC*, May 2015, vol. 2015-May, no. May, pp. 2585–2592. doi: 10.1109/APEC.2015.7104716.

[10] D. Weber, S. Heid, H. Bode, J. H. Lange, E. Hullermeier, and O. Wallscheid, "Safe bayesian optimization for data-driven power electronics control design in microgrids: From simulations to real-world experiments," *IEEE Access*, vol. 9, pp. 35654–35669, 2021, doi: 10.1109/ACCESS.2021.3062144.

[11] M. Hosseinzadeh and F. R. Salmasi, "Robust optimal power management system for a hybrid AC/DC micro-grid," *IEEE Trans Sustain Energy*, vol. 6, no. 3, pp. 675–687, Jul. 2015, doi: 10.1109/TSTE.2015.2405935.

[12] A. Jahic, M. Eskander, and D. Schulz, "Charging schedule for load peak minimization on large-scale electric bus depots," *Applied Sciences (Switzerland)*, vol. 9, no. 9, May 2019, doi: 10.3390/app9091748.

[13] E. Augustins, D. Jaunzems, C. Rochas, and A. Kamenders, "Managing energy efficiency of buildings: analysis of ESCO experience in Latvia," *Energy Procedia*, vol. 147, pp. 614–623, Aug. 2018, doi: 10.1016/J.EGYPRO.2018.07.079.

[14] W. Aslam, M. Soban, F. Akhtar, and N. A. Zaffar, "Smart meters for industrial energy conservation and efficiency optimization in Pakistan: Scope, technology and applications," *Renewable and Sustainable Energy Reviews*, vol. 44. Elsevier Ltd, pp. 933–943, 2015. doi: 10.1016/j.rser.2015.01.004.

[15] R. Palma-Behnke, D. Ortiz, L. Reyes, G. Jiménez-Estévez, and N. Garrido, "A social SCADA approach for a renewable based microgrid - The Huatacondo project," *IEEE Power and Energy Society General Meeting*, 2011, doi: 10.1109/PES.2011.6039749.

[16] J. Kennedy, P. Ciufo, and A. Agalgaonkar, "Intelligent load management in microgrids," *IEEE Power and Energy Society General Meeting*, 2012, doi: 10.1109/PESGM.2012.6345729.

[17] J. Zhuang, G. Shen, J. Yu, T. Xiang, and X. Wang, "The Design and Implementation of Intelligent Microgrid Monitoring System Based on WEB," *Procedia Comput Sci*, vol. 107, pp. 4–8, Jan. 2017, doi: 10.1016/J.PROCS.2017.03.047.

[18] Aznor Hanah, Rohani Farook, Shamsul Jamel Elias, M R A Rejab, M Fairuz M Fadzil, and Zulkifli Husin, "IoT Room Control And Monitoring System Using Rasberry Pi," *2019 4th International Conference and Workshops on Recent Advances and Innovations in Engineering (ICRAIE)*, pp. 1–4, 2019, doi: 10.1109/ICRAIE47735.2019.9037759.

[19] H. Zheng *et al.*, "A microgrid alarm processing method based on equipment fault prediction and improved support vector machine learning," *J Phys Conf Ser*, vol. 1639, no. 1, p. 012041, Oct. 2020, doi: 10.1088/1742-6596/1639/1/012041.

[20] O. Izquierdo-Monge *et al.*, "Conversion of a Network Section with Loads, Storage Systems and Renewable Generation Sources into a Smart Microgrid," *Applied Sciences 2021, Vol. 11, Page 5012*, vol. 11, no. 11, p. 5012, May 2021, doi: 10.3390/APP11115012.

Flexibility Management System for Executing Energy Program with Distributed Resources

Jose-Fernando Forero-Quintero[1][0000−0001−5930−4226],
Roberto Villafafila-Robles[1][0000−0003−4372−2575], Daniel
Montesinos-Miracle[1][0000−0003−3983−0514], and Sara
Barja-Martinez[1][0000−0003−4126−8858]

Centre d'Innovació Tecnològica en Convertidors Estàtics i Accionaments
(CITCEA-UPC), Department d'Enginyeria Elèctrica, Universitat Politècnica de
Catalunya, (UPC). Av. Diagonal 647, Pl. 2. 08028, Barcelona, Spain
https://www.citcea.upc.edu/

Abstract. The energy transition is impulsing multiple challenges in the power system's technical and economic areas. The stochastic behavior of renewable energy generates high uncertainty levels, which only can manage through the development of flexibility capacities from demand response or generation-side. Energy management systems have been raised to optimally schedule prosumer's power dispatch with hourly timeframes or every minute. During this energy planning, a real-time control management system is needed to handle deviations, cost overruns, risks, loss of quality, supply reliability, and identify economic opportunities to reduce electricity bill. This paper endeavors to present a flexibility management system for executing an energy program of distributed energy resources based on a power re-dispatching and unit re-commitment module using an adaptive auto-regression algorithm as a forecasting module. The conclusions drawn from this study demonstrate that the proposed flexibility management system can control real-time dispatch profitably and optimally.

Keywords: Flexibility Management, Energy Program, Cost Overrun.

Abbreviations:
AMI Advanced Metering Infrastructure
ARA Adaptive Auto-regression Algorithm
BBSA Binary Backtracking Search Algorithm
BRP Balance Responsible Party
CBA Cost-Benefit Analysis
DER Distributed Energy Resources
DSO Distributed System Operator
EMS Energy Management System
EV Electric Vehicle
FLEMS Flexibility Management System
GA Genetic Algorithm
POI Point of Interconnection
PV Photovoltaic Panel

Ech_B^{bat}	Efficient factor for charging of battery
$Edis_B^{bat}$	Efficient factor for discharging of battery
SOC_{min}^{bat}	Minimum SOC for period t
SOC_{max}^{bat}	Maximum SOC for period t
Rch_{bat}	Power ramp rate for charging of battery
$Rdis_{bat}$	Power ramp rate for discharging of battery
Pch_t^{bat}	Battery energy charging
$Pdis_t^{bat}$	Battery energy discharging
P_{PV}	PV production
$P_t^{,PV}$	Predicted PV production
Cur_t^{PV}	Solar curtailment
$Cur_{t,tolerable}^{PV}$	Solar curtailment limit value
V_t^{AMI}	Inverter voltage measured by AMI
$Vmax_{t,nom}$	Maximum inverter voltage at rated power
$Vmin_t$	Inverter voltage at minimum active power
$Pnom_t^{PV}$	PV rated active power
$Pmin_t^{PV}$	Minimum PV active power
Rch_{EV}	Power ramp rate for charging of EV
$Rdis_{EV}$	Power ramp rate for discharging of EV
$\sigma(Ibat_t^{SOCt})$	Severity factor for battery aging
$Ibat_t^{nom}$	Nominal charging and discharging current of battery
Ah_t^{bat}	Total aging effect caused by cycling
X	Battery market price
$Clife_t$	Battery life cycle
$Ppoi_{t,s}$	Forecasted power at POI for time t done at time s
$Ppoi_{s-n+1}$	Measured power at POI for time s-n+1
$Ppoi_{s-n+1,s-n}$	Forecasted power at POI for time s-n+1 done at time s-n
$Ppoi_{t,s}^{FLEMS}$	Forecasted demand at POI estimated by FLEMS
X_t^{buy}	Electricity retail price
$Ppoi_{t,s-1}^{EMS}$	Forecasted power at POI for time t done at period s-1 estimated by EMS.
C_{flex}^{FLEMS}	Flexibility costs calculated by FLEMS

1　Introduction

The growth of Distributed Energy Resources (DER), mainly from Renewable Energy Sources (RES) in power systems, is turning flexibility into an essential element for a feasible, safe, and reliable electrical supply [1, 2]. Traditionally, flexibility was provided by conventional generators, which possess flexible power output to preserve the balance between generation and consumption. Demand-side flexibility is getting lots of attention owing to an increasing storage devices

(electric vehicles and fixed residential batteries), flexible loads, and control and communication devices in power systems. All above-mentioned are modifying the traditional end-users into prosumers [3].

Prosumers and microgrids are transforming into an efficient solution to integrate DER and RES, as well as manage and control the increased flexibility from the demand-side [4]. For flexibility services and optimal dispatch, a management and control system is necessary to accomplish the energy commitments at reduced costs and preserve the acceptable quality of electricity supply. Energy Management System (EMS) has been tested successfully by [5, 6], which establish an optimal dispatch of DER assets during a given period time. Besides, during this same period time, EMS could properly execute flexibility requests from external agents such as Distributed System Operator (DSO), Balance Responsible Party (BRP), aggregators, or end-users. Along with EMS, a real-time management system is needed to manage power output, and unexpected events, as well as execute voltage/frequency, real/reactive power control, and flexibility services outside of EMS control, according to the power system's needs.

To define real time management system, authors have developed some algorithms to manage real-time energy dispatch in power systems. Firstly, Binary Backtracking Search Algorithm (BBSA) is implemented to give an optimal schedule for home devices to limit the total demand and schedule the operation of home appliances at specific times during the day [3]. BBSA is based on producing a trial population that evolves using two new mutation and crossover operators. Adaptive Auto-regression Algorithm (ARA) is also used as a real-time predictive controller [6, 8], where forecasted values are generated for the next period time (1 minute), using coefficients found by optimizing the model on the training date from past series values. Thirdly, two-stage stochastic programming with a scenario reduction method based on mixed-integer linear optimization classifies the decision variables into two groups [9]. First, the decision maker takes some action in the first stage, after which a random event occurs, affecting the outcome of the first-stage decision. Then, a recourse decision will be made in the second stage that compensates for any undesirable effects that might have been experienced due to the first-stage decision. Additionally, a Genetic Algorithm (GA) is implemented to determine the optimal settings by minimizing the cost functions in a power system with distributed energy resources [10, 11]. In the end, power re-dispatching and unit re-commitment use hill climbing (optimal local values) iteration to correct voltage and current violations [8, 10]. These solutions should be validated by an optimizer solver and report the updated data.

On the other hand, although diverse projects are proposing short-term control schemes, those are oriented towards distribution networks with real-time monitoring and control schemes from DSO, local flexibility market, or centralized aggregator point of view. In general, these works is neglecting the management of energy planing in real-time and its deviations during its executing from prosumer or end user perspectives. Therefore, this article's close-to-real-time management system, named Flexibility Management System (FLEMS), is a challenge still unsolved [7]. This paper focuses on developing a FLEMS that

can efficiently manage power dispatch in real-time, persevering the generation and consumption balance and quality of electricity services, as well as managing flexibility requests assigned to FLEMS by EMS. FLEMS and EMS should be adequately coordinated and guarantee an unfailingly minimum quality of service in electricity supply. The remainder of the paper is organized as follows: Section 2 describes the FLEMS framework. Section 3 exposes the mathematical formulation problem. A case study and its results are presented in Section 4. In the end, conclusions are outlined in Section 5.

2   System Description

The proposed FLEMS is based on the INVADE H2020 project [12, 13]. The system is initially composed of a connected-to-grid prosumer with an electric vehicle residential charging station, photovoltaic panel, and battery as flexible assets. The architecture is completed with an EMS as a high-level energy manager, which generates the prosumer's optimal dispatch according to an optimization process with economic and technical variables. Additionally, an aggregator or DSO could generate flexibility requests handled by EMS and FLEMS. As shown in Figure 1, FLEMS also receives real-time measurements, which adjusts the optimal dispatch through new set-point profiles of the prosumer's flexible assets.

Fig. 1. Control Scheme of Power System with Distributed Resources

2.1 Flexible Assets Models

This section formulates the flexible assets models applied to the formulation of the FLEMS. Once models have been drawn, FLEMS's power management strategy proceeds.

Battery model : In order to represent an accurate model, efficient factor for charging η_{ch}^{bat} and discharging $\eta_{dis,B}^{bat}$ energy has been involved. The State of Charge (SOC) of the battery (SOC_t^{bat}) must be between a minimum SOC_{min}^{bat} and maximum SOC_{max}^{bat} limit value. Besides, the power ramp rate for charging Rch_{bat} and discharging $Rdis_{bat}$ for period t must be taken into account to preserve the battery lifetime.

$$SOC_t^{bat} = SOC_{t-1}^{bat} + Ech_t^{bat} * \eta_{ch}^{bat} - \frac{Edis_t^{bat}}{\eta_{dis}^{bat}} \tag{1}$$

$$SOC_{min}^{bat} \leq SOC_t^{bat} \leq SOC_{max}^{bat} \tag{2}$$

$$Ech_t^{bat} \leq Rch_{bat} \tag{3}$$

$$Edis_t^{bat} \leq Rdis_{bat} \tag{4}$$

Where, Ech_t^{bat} and $Edis_t^{bat}$ are energy charging and discharging for battery, respectively.

Detachable and reducible photovoltaic panel model : For this PV model, the energy production (P_t^{PV}) for a period t must be between 0 and predicted production ($P_t^{,PV}$). FLEMS can charge the predicted values if solar curtailment (Cur_t^{PV}) rises to limit values ($Cur_{tolerable}^{PV}$). Equations 5 and 6 express those as mentioned earlier.

$$0 \leq P_t^{PV} \leq P_t^{,PV} \tag{5}$$

$$Cur_t^{PV} \leq Cur_{tolerable}^{PV} \tag{6}$$

Solar curtailment is determined using the Volt-Watt curve of panels, where voltage variations at inverters express the solar curtailment due to volt-watt control to accomplish set-point profiles from the PV controller. The mathematical formulation is drawn in equation 7 based on [14, 15]:

$$Cur_t^{PV} = \sum_{t=1}^{T} \frac{V_t^{AMI} - Vmax_{nom}}{Vmin - Vmax_{nom}} * (Pnom^{PV} - Pmin^{PV}) \tag{7}$$

Where, V_t^{AMI} is the voltage measured by Advanced Metering Infrastructure (AMI), $Vmax_{nom}$ is the maximum voltage at which PV system produces its rated power $Pnom^{PV}$. $Vmin$ is voltage at which the system generates its minimum active power $Pmin^{PV}$.

Electric vehicle controllable and interruptible model : This EV model allows to control and interrupt charging sessions, shaping the final charging profile according to the energy needs of the prosumer. The charging and discharging power (P_t^{EV}) must be between 0 and maximum value (P_{max}^{EV}). Besides, the energy charging Ech_t^{EV} and discharging $Edis_t^{EV}$ of EV for period t must be less than maximum power ramp rate for charging Rch^{EV} and discharging $Rdis^{EV}$. Those indexes are considered to preserve the EV-battery lifetime.

$$0 \leq P_t^{EV} \leq P_{max}^{EV} \tag{8}$$

$$Ech_t^{EV} \leq Rch^{EV} \tag{9}$$

$$Edis_t^{EV} \leq Rdis^{EV} \tag{10}$$

2.2   Flexibility Management System

The FLEMS proposed in this article aims to manage the prosumer's energy program in a close-to-real-time framework. The FLEMS structure is shown in Figure 2. Initially, FLEMS has an activation module where real-time power measurements and control signals from EMS are received. The activation module aims to establish the initial conditions, such as SOC Residential Battery and EV Battery, and EV charging session, of the prosumer's flexible assets and calculate reference values from EMS optimal dispatch, e.g. prosumer's forecasted cost of electricity, forecasted energy consumption, and forecasted inflexible consumption. During the energy program, the activation module supervises the energy exchanges with the grid to prevent exceeding the maximum power agreed with DSO or fixed by EMS, as well as to ensure that the prosumer does not discharge energy to the grid at any time. It has defined a tolerance range of 5% concerning limit values to complete the above.

Subsequently, FLEMS diagnoses the power absorbed from network by prosumer. This short-term forecasting allows determining if the present deviations could generate unacceptable economic losses for end-user or aggregator, if the aggregator is in charge of the energy management of the prosumer's installation. It can be seen in Figure 2 that FLEMS receives energy set-point profiles from EMS, resulting from an optimization carried out by EMS for the present period of time. Additionally, FLEMS receives as an input the real-time measurements of the main variables of the system, such as PV production, consumption, and state of charge of residential battery and EV battery, among others. FLEMS performs its predictive processes to optimize the cost overrun due to deviation in uncontrollable variables such as PV production, inflexible consumption, or unplanned events such as EV disconnection or network failure. FLEMS generates or modifies the flexible assets' set-point profiles from EMS in a close-to-real-time timeframe.

According to the above-mentioned, FLEMS uses an ARA to forecast the energy exchanges with the grid in a short time period. This short-term prediction

generates information to be evaluated in Cost-benefit Analysis (CBA) module. CBA module optimizes the real-time power dispatch reducing the cost overrun of the prosumer, augmenting the generation of renewable energy resources, and minimizing the flexibility services cost. According to CBA and taking into account the flexibility requirements accepted by EMS, a power re-dispatching and unit re-commitment module assign the final set-point profile to the prosumer's devices, depending on the current flexibility request if they have been accepted previously. Each control signal will be valid until the predicted values return to accepted ranges and the activation signal is disabled.
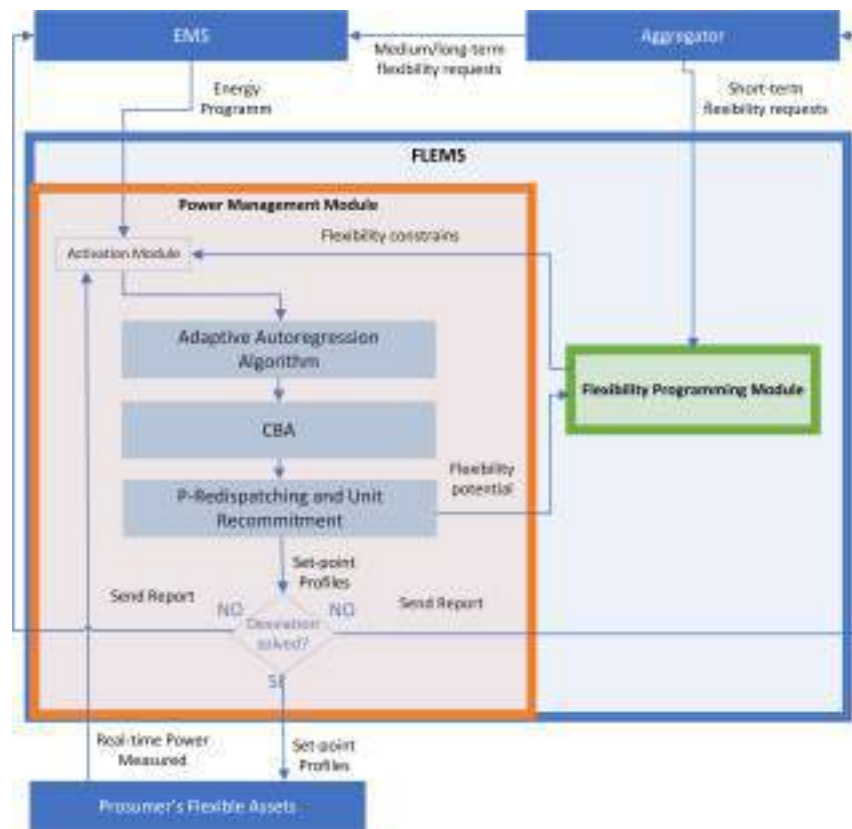

Fig. 2. Flexibility Management in Power System with Distributed Energy Resources

Power Management Strategy: The management strategy developed by the power management module is initially executed by FLEMS employing the in-

formation provided by EMS (every 15 minutes). As mentioned, EMS generates set-point profiles for prosumer flexible assets according to the planning horizon. These values represent a local optimum, which establishes an overall referent cost for flexible assets, inflexible load and energy purchases from grid. FLEMS's power management strategy is based on electric parameters at the Point of Interconnection (POI) and AMI in order to control solar curtailment. First, FLEMS seeks that prosumer is not discharging to the grid, and therefore, flexible assets will be activated depending on their cost models. The above happens until when exchanged power between prosumer and grid comes to zero. In the same way, if exchanged power exceeds subscribed or predefined maximum power, fixed and mobile battery (electric vehicle charging station), as well as flexible load are managed to reduce the energy demand. A deviation tolerance range is defined concerning the power control signal generated by EMS, given that a significant deviation could generate both opportunity loss or large imbalances. Once more, FLEMS manages flexible assets to overcome this undesired situation.

Supposing the above deviations remain in time. FLEMS generates a report, which could be sent to EMS, aggregator, and DSO, reporting the situation or future events according to its predictive models. Conversely, the normal operation of the prosumer continues until EMS updates the power control signals for the next period. Considering that the uncertainty in power systems is increasing in the same proportion as the renewable energy penetration level, short-time control systems are desired to maintain the stability and reliability of the electricity supply.

2.3 Cost Functions of Flexible Assets

The FLEMS attempts to incorporate cost models related to energy assets to make proper decisions to reduce the energy cost for prosumers. This section presents cost models used in this study, leaving the potential benefits of close-to-real-time energy management for future work.

Battery costs : The cost related to residential battery usage is listed as follows:

– Cost of Discharging and Charging: The operating cost of the battery can be defined as a continuous convex quadratic function [9, 10], where charging and discharging powers are used to calculate the operating cost. Equations 11, 12, and 13 describe this function cost:

$$Cch_t^{bat} = a_c * (Pch_t^{bat})^2 + c \tag{11}$$

$$Cdis_t^{bat} = a_d * (Pdis_t^{bat})^2 + c \tag{12}$$

$$Cope_t^{bat} = Cch_t^{bat} + Cdis_t^{bat} - Cope_t^{bat,EMS} \tag{13}$$

– Aging for cycling: Withing the energy storage system operation, aging cost has generally been reflected in various studies, but this phenomenon has high relevance to the battery's useful life. FLEMS pretends to manage deviation in a close-to-real-time period through flexible assets, so the aging cost must be defined. In equations 20, 21, and 22, a mathematical formulation for aging cost for cycling is drawn for period t [16]. This model uses a severity factor $(\sigma(Ibat_t^{SOCt}))$ to measure the impact of any cycle (charging or discharging) on battery lifespan, according to standard conditions ($Ibat_t^{nom}$). Ah_t^{bat} represents the total aging effect caused by cycling over a period of time T. X and $Clife_t$ depict the battery market price and life cycle, respectively.

$$Cag_t^{bat} = X_{bat} * \frac{Ah_t^{bat}}{Qbat_t^{bat} * Clife_t^{bat}} - Cag_t^{bat,EMS} \tag{14}$$

Where,

$$Ah_t^{bat} = \frac{1}{T} * \int_0^T \sigma(Ibat_t^{SOCt}) * Ibat_t^{nom} \, dt \tag{15}$$

$$\sigma(Ibat_t^{SOCt}) = \frac{\int_0^T Ibat_t \, dt}{\int_0^T Ibat_t^{nom} \, dt} \tag{16}$$

Photovoltaic panel model costs : For detachable and reducible PV model, costs are incurred when there is solar curtailment due to forecasting deviations. Curtailment solar was defined in equation 7.

Electric vehicle costs : In the same sense as the stationary battery, EV battery has operation cost and aging costs associated with unusual cycling.

– Cost of Discharging and Charging:

$$Cch_t^{EV} = a_c * (Pch_t^{EV})^2 + c \tag{17}$$

$$Cdis_t^{EV} = a_d * (Pdis_t^{EV})^2 + c \tag{18}$$

$$Cope_t^{EV} = Cch_t^{EV} + Cdis_t^{EV} - Cope_t^{EV,EMS} \tag{19}$$

– Cost of Discharging and Charging:

$$Cag_t^{EV} = X_{EV} * \frac{Ah_t^{EV}}{Qev_t^{EV} * Clife_t^{EV}} - Cag_t^{EV,EMS} \tag{20}$$

Where,

$$Ah_t^{EV} = \frac{1}{T} * \int_0^T \sigma(Iev_t^{SOCt}) * Iev_t^{nom} \, dt \tag{21}$$

$$\sigma(Iev_t^{SOCt}) = \frac{\int_0^T Iev_t \, dt}{\int_0^T Iev_t^{nom} \, dt} \tag{22}$$

3   Mathematical Problem Formulation

The close-to-real-time energy program execution problem of the power systems with distributed resources is addressed in two steps. First, an activation module is carried out. This module consists in real-time forecasting, which is undertaken with ARA. Together with forecasted values, indicators are established to measure the excessive deviations, cost overruns, as well as economic opportunities such as high renewable energy generation or attractive electricity prices. FLEMS should be activated in such situations. Once the activation signal is produced, a CBA is performed to determine the set-point profile of the prosumer's assets within of specific period of time, depending on the prosumer's behavior (economy or reliability followers). Finally, if the deviations and limit values can not be solved with FLEMS' resources, a report is sent to EMS, aggregator, or DSO to notice the current situation.

3.1   Close-to-Real-Time Power Forecasting Problem

The close-to-real-time power forecasting problem is defined as follows: for managing the energy program execution, FLEMS must predict the net prosumer demand on a certain rolling horizon base time, near to the actual value. FLEMS defines this timeframe according to complexity, according to complexity, communication, and processing system constraints and variability of the consumption and generation of the power system. The rolling horizon base time could be fixed or variable, but it will be constant for the present paper. The fast forecasting technique selected in this document is ARA. ARA has a rapid execution time, adaptive and trainable to the historical data of prosumers. Equation 23 shows the ARA's mathematical formulation according to [6, 8]:

$$Ppoi_{t,s}^{,} = Ppoi_{t,s-1}^{,} * \frac{1}{min(n,s)} * \sum_{n=1}^{min(n,s)} \frac{Ppoi_{s-n+1}}{Ppoi_{s-n+1,s-n}^{,}} \qquad (23)$$

Where, $Ppoi_{t,s}^{,}$ is forecasted power at POI at time t done at time s based on n previous time intervals, $Ppoi_{s-n+1}$ is measured value of power at POI and $Ppoi_{s-n+1,s-n}^{,}$ is forecasted power at POI done at time s-n. The number of past values used to forecast the next future value depends on the training data of the power system. According to [6] and [8], a third grade (n=3) was estimated for a residential prosumer.

3.2   Energy Program Execution Problem through Cost Analysis

Energy Program Execution Problem is solved through Cost Analysis. This cost analysis is performed to minimize the costs associated with the analysis period, which is the period at which FLEMS estimated the power in the POI $Ppoi_{t,s}^{,FLEMS}$. First, the prosumer's energy cost is found using the energy tariff of the Spanish market, PVPC (Precio Voluntario para el Pequeño Consumidor) X_t^{buy}. Energy cost predicted by EMS must be subtracted from total cost in order

to find cost overrun by deviations $Ppoi_{t,s-1}^{;EMS}$. In the same sense, flexible costs are computed as the difference between the cost incurred by FLEMS' management of the energy program and reference values from EMS in terms of the costs of the energy program. For instance, EMS schedules the electric vehicle charging session from 03:30 to 05:30. EV operation cost and aging costs are estimated and valid within of energy program. This energy program is optimal according to EMS criteria. If the FLEMS acts on the EV during this period, the operating and aging costs must consider that the EMS has previously optimized them. In this way, flexibility costs C_{flex}^{FLEMS} have been calculated for the period of FLEMS execution and management.

$$min \sum_{t=1}^{T} ((Ppoi_{t,s}^{;FLEMS} - Ppoi_{t,s-1}^{;EMS}) * X_t^{buy} + C_{flex}^{FLEMS} \qquad (24)$$

With,

$$C_{flex}^{FLEMS} = Cope_t^{bat} + Cag_t^{bat} + Cur_t^{EV} + Cope_t^{EV} + Cag_t^{EV} \qquad (25)$$

Where X_t^{buy} is the retail price for energy purchases, C_{flex}^{FLEMS} is the flexibility cost calculated by FLEMS, and $Ppoi_{t,s-1}^{;EMS}$ is forecasted demand at POI estimated by EMS.

4   Case Study

In order to demonstrate the suitability of FLEMS, a prosumer with an EV's charging station, residential battery, photovoltaic panel, and flexible loads is selected as a case study. Real-time demand, EV's consumption, and PV generation data have been obtained by DataPort Inc. Street 2022 for prosumers located in Austin, Texas [17]. The present case study encompasses a horizon of 15 minutes, divided into 10-second time intervals, starting on January 14th of 2018 at 17:00. As was mentioned before, FLEMS works in an economic follower mode, in consequence, deviations will be transferred to the next 15-minutes period time. Previously, the energy program was held by EMS, according to [5]. Figure 3 exposes prosumer consumption every 15 minutes, starting on January 13th of 2018 at 17:00, and set-point profiles for prosumer's assets found by EMS. These set-points are input data for FLEMS's activation module. For a better understanding, negative values express demand or consumption, and positive values represent electricity input to the system.

On the other hand, prosumers define some indicators related to their preferences regarding acceptable cost overrun, maximum and minimum range for POI power, and maximum solar curtailment. Also, economic variables related to the storage system must be declared. These parameters can be seen in Table 1. EMS determined the prosumer's energy program for a rolling horizon for the next 24 hours. From 17:00 to 17:15 on January 14th, neither the projected battery nor

Table 1. FLEMS initiation parameters.

Parameters	Values
Tolerable cost overrun	1€
Maximum Range for POI power	95%
Minimum Range for POI power	5%
Penalty for Exceeding Max Power	1.4064 €/kWh
a_B^c	2
a_B^d	2
c_B	5
PVPC	0.04 €/kWh
Max Power at POI	2.6 kW
Min Power at POI	0 kW

EV battery will be discharged or charged during this period. At the same time, solar output is expected to be 600W, forecasted consumption from grid will be 350W and inflexible load is awaited at 950W along of 15 minutes. Figure 4 shows the set-point profiles of prosumer's flexible assets under FLEMS's management over 15 minutes divided into 10-second periods.
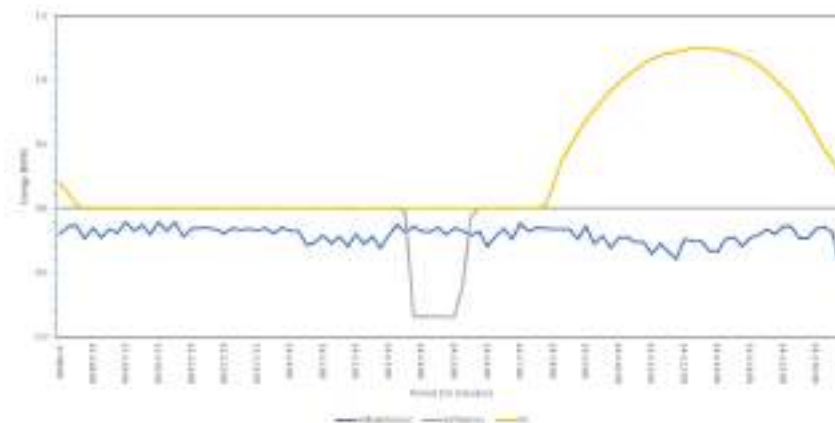

Fig. 3. Prosumer consumption and PV generation. Source: Pecan Street Inc. Dataport 2022

First, there is a solar curtailment due to a deviation from the EMS forecast. This solar curtailment is detected through the AMI-voltage-based method, as mentioned in section 2.3 above. FLEMS adjusts the solar panel control signal to allow more solar output. Subsequently, FLEMS manages an unscheduled electric vehicle charging session, modeling a rare behavior of a prosumer when it has arrived home at a random time. The additional charging of the electric vehicle
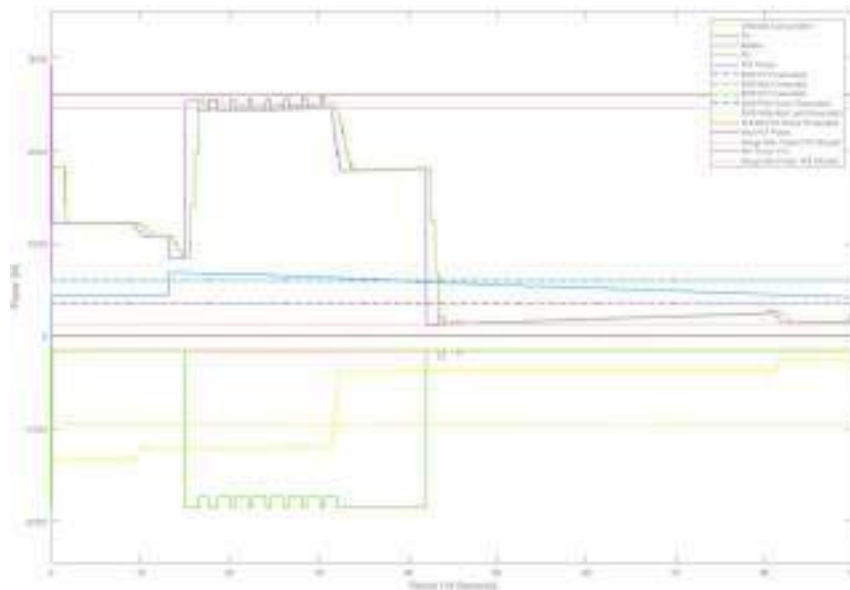
Fig. 4. Close-to-real-time execution of energy program under FLEMS from 17:00 to 17:15 of January 14th in 10-second periods.

increases the energy drawn from the grid at the POI to the maximum allowable power range. Before the maximum power is likely reached, FLEMS manages flexible assets to temporarily reduce the energy transfer to the EV battery. FLEMS acts until period 32, when the power at POI is less than the maximum allowed values. Finally, the unexpected charging session of the electric vehicle is terminated in period 42. FLEMS manages a deviation of the power absorbed from the grid at the POI by activating the fixed battery connected to the prosumer's installation. The battery is charged according to the allocated power necessary for the power at the POI to be higher than the minimum allowed range. Both the reduction of the EV charging session and activation of the battery for charging or discharging is determined by cost functions in Equations 24 and 25.

Economical Analysis: As mentioned before, FLEMS attempts to reduce the cost overrun and, consequently, the prosumer's electricity bill. From EMS, the total cost is estimated according to the optimization of the power dispatch. For the case study, this cost is 0,32 €. If FLEMS is not activated, the total cost increases to 0.96 €, according to the real-time variation of solar production and consumption recorded in DataPort Inc. Street 2022 for the prosumer selected. Due to the activation of FLEMS to increase solar production and manage flexible assets to cope with deviations, the total cost has been reduced to 0.86€.

Therefore, cost overruns due to deviations have been reduced by 10.4%. The evolution of the electricity cost can be seen in Figure 5.
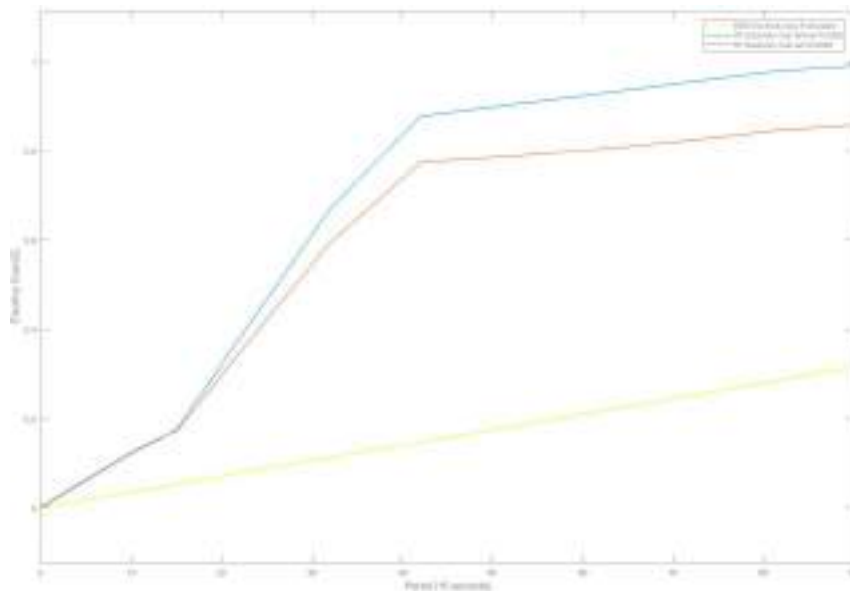

Fig. 5. Evolution of cost overrun under FLEMS from January 14th 17:00 to 17:15 in 10-second periods

5   Conclusions

According to the results, the proposed flexibility management system performs as expected. Firstly, the solar curtailment is reduced through FLEMS's management of solar production when it is higher than the forecasted value by EMS. On the other hand, FLEMS manages distributed and flexible resources to assure the optimal dispatch within the allowed range, as well as reduce the prosumer's electricity bill through maximizing PV production and establishing the set-point profiles for flexible assets in order to minimize the cost overruns by deviations. FLEMS initiation parameters should be studied in depth in future work to find possible findings for a more appropriate FLEMS design according to the flexible assets, distributed resources, flexibility potential, and power system. For flexibility services, such as reactive power supply, voltage and frequency regulation, operative reserves, and inertia, among others, and their remuneration system will be handled in future works on FLEMS.

References

1. Ali, M., Ghazvini, F., Steen, D., Tuan, L A.: A Close-to-Real-time Energy Management System for Smart Residential Buildings. CONFERENCE 2019 IEEE Milan PowerTech, 2019, pp. 1–6, doi10.1109/PTC.2019.8810885.
2. Yuhji, M. Seiya, E, Yu, N. Yoshiaki, S. Ryoichi, K. Yasumasa, F: Investigating the economics of the power sector under high penetration of variable renewable energies. Applied Energy Journal **1**(267), 113956 (2020).
3. Ahmed M.S., Mohamed A., Khatib T., Shareef H., Homod R., Ali J.A.: Real time optimal schedule controller for home energy management system using new binary backtracking search algorithm. Energy and Buildings Journal **1**(138), vol. 138, 215–227 (2017). doi.org/10.1016/j.enbuild.2016.12.052.
4. Netto, R., Ramalho, G., Bonatto, B., Carpinteiro, O., Zambroni A. C., Oliveira, D., Braga, R.: Real-Time Framework for Energy Management System of a Smart Microgrid Using Multiagent Systems. Energies Journal **3**(11), vol. 11, 656, (2018). doi: 10.3390/en11030656.
5. Barja, S. Lloret, P. Olivella, P. Villafafila, R: Centralized flexibility services for distribution system operators through distributed flexible resources. A: Ibero-American Congress of Smart Cities. pp. 507–519. (2019). ISBN 978-958-5583-78-8.
6. H. Chen, R. Xiong, C. Lin and W. Shen: Model predictive control based real-time energy management for hybrid energy storage system. CSEE Journal of Power and Energy Systems **4**(7), vol. 7 862–874 (2021). doi: 10.17775/CSEEJPES.2020.02180.
7. Chee, L. Iromi U. Ranaweera and Ole-Morten, M. Lars, N S: A real-time energy management system for smart grid integrated photovoltaic generation with battery storage. Renewable Energy Journal **1**(130), 774–785, (2019).
8. Elkazaz, M., Sumner, M., Thomas, D.: Real-Time Energy Management for a Small Scale PV-Battery Microgrid: Modeling, Design, and Experimental Verification. A: Energies Journal. **14**(12), 2712 (2019).
9. Mo, X., Zhu J., Chen J., Guo, Y., Xia, Y., Liu, M.: A Stochastic Spatiotemporal Decomposition Decision-Making Approach for Real-Time Dynamic Energy Management of Multi-Microgrids. IEEE Transactions on Sustainable Energy Journal **2**(210), 821–833 (2021).
10. Nemati, M., Braun, M., Tenbohlen, S.: Optimization of unit commitment and economic dispatch in microgrids based on genetic algorithm and mixed integer linear programming. Applied Energy Journal **1**(210), 944–963 (2018).
11. Elsied M., Oukaour A., Youssef T., Gualous H., Mohammed O.: An advanced real time energy management system for microgrids. Energy Journal **11**(114), 742–752 (2016).
12. INVADE H2020 Project Grant Agreement 731148. 2017. url: https ://h2020invade.eu (visited on 10/20/2017).
13. Bendato, I. Bonfiglio, A. Brignone, M. Delfino, F. Pampararo, F. Procopio, R: A real-time Energy Management System for the integration of economical aspects and system operator requirements: Definition and validation. Renewable Energy Journal **3**(102), 406–416 (2017).

14. Emmanuel, M., Giraldez, J., Gotseff, P. and Hoke, A.: Estimation of solar photo-voltaic energy curtailment due to volt–watt control. IET Renewable Power Generation Journal **1**(14), 640–646, (2020). https://doi.org/10.1049/iet-rpg.2019.1003

15. J. A. Azzolini, M. J. Reno and K. A. W. Horowitz: Evaluation of Curtailment Associated with PV System Design Considerations. 2020 IEEE Power & Energy Society General Meeting (PESGM), 2020, pp. 1–5. doi: 10.1109/PESGM41954.2020.9281427.

16. Jingda, W. Zhongbao, W. Weihan, L. Yu, W. Yunwei, L. Dirk, U S: Battery Thermal-and Health-Constrained Energy Management for Hybrid Electric Bus Based on Soft Actor-Critic DRL Algorithm. IEEE Transactions on Industrial Informatics Journal **6**(17), 3751–3761 (2021).

17. DataPort Data Base. https://dataport.cloud/. [Online; accessed 07-September-2022]. 2018.

Synthetic Dataset of Electroluminescence images of Photovoltaic cells by Deep Convolutional Generative Adversarial Networks

Héctor Felipe Mateo Romero[1], Miguel Angel González Rebollo[1], Valentín Cardeñoso-Payo[1], Victor Alonso Gomez[1], Hugo Jose Bello[1], Alberto Redondo Plaza[1], and Luis Hernandez Callejo[1]

University of Valladolid, Spain,
H.F.M.R. `hectorfelipe.mateo@uva.es`
M.A.G.R. `mrebollo@eii.uva.es`
V.C.P. `valen@infor.uva.es`
V.A.G. `victor.alonso.gomez@uva.es`
H.J.B. `hugojose.bello@uva.es`
A.R.P. `alberredon@gmail.com`
L.H.C. `luis.hernandez.callejo@uva.es`

Abstract. This article presents a different way of obtaining images of solar cells using Artificial Intelligence techniques such as Generative Adversarial Neural Networks(GANs). This will improve the maintenance of Photovoltaic Systems in different places like Smart Cities. The original data has been obtained manually and preprocessed to create better images. The GAN architecture used is known as Deep Convolutional GAN since it performs better than other GANs. The synthetic images were labeled and analyzed to ensure their quality.

Keywords: Generative Adversarial Neural Networks, Photovoltaics, Artificial Intelligence, Synthetic Data, Electroluminescence

1 Introduction

A smart city [1] can be defined as an urban area highly developed in terms of infrastructure, communications, and sustainability. These cities need high amounts of electricity. Two factors are increasing the importance of renewable energies: the rise in the cost of traditional energies and the effects that fossil fuels have on the environment. Solar energy is one of the most important sources due to its facility being installed in different places such as rooftops.

The maintenance of the solar panels is not a trivial issue [2]. Their performance depends on different conditions, which makes necessary a mechanism to control and optimize the production. Solar modules are also vulnerable to phenomena that can reduce or even nullify the production of one cell or even the whole module in the worst cases. This is usually dealt with human labor, checking each module in a certain time.

Artificial intelligence is also applied to deal with this kind of problem. The problem is that AI models need a lot of amounts of data to train [7]. This problem is more critical in this area since it is not easy to obtain the data.

To solve this problem, we present a new approach: we will use Artificial Intelligence, Generative Adversarial Networks (GANs), to generate new data. This article offers a synthetic dataset ready to be used with models, the images will have associated a value according to their performance. This dataset can also be used alone to analyze characteristics, defects, or properties of cells.

GANs have been used in other works to generate synthetic data [3]. They have been applied to PV systems for solving others problems[4]. They also have been used to generate EL images of PV cells[5, 6] but these images were created for fault detection, they do not provide information about the IV curve or the power.

In Section 2 the Generative Adversarial Networks are explained, in Section 3 the methodology that was followed to generate the dataset is commented and in Section 4 we present the synthetic dataset. Finally, we present our conclusions in Section 5.

2　Generative Adversarial Networks

Generative Adversarial Networks (GANs) are an emerging technology that has been mainly applied to semi-supervised and unsupervised learning. A GAN can be defined as a pair of networks competing against each other [8], one of the networks is known as the Generator, which tries to create realistic new data, and the other one is the discriminator which has to decide which data is real and which data has been forged.

A key feature of these systems is that the generator network does not have access to real data. Its only feedback about the results of the forgery comes from the discriminator. The discriminator has access to both real and fake data. The loss is computed based on the number of times that the discriminator is deceived by the fake data. This loss is also provided to the generator to improve the quality of the forged images (see Fig. 1).
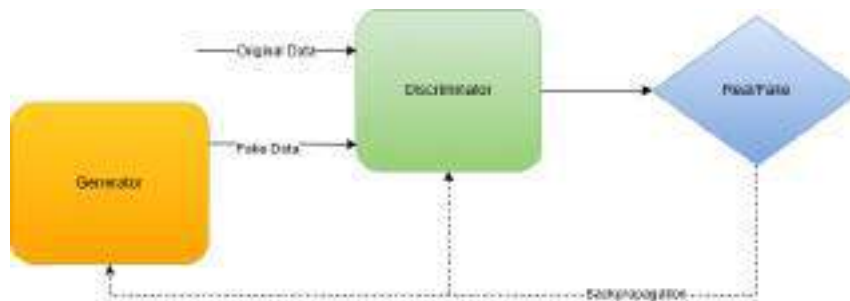

Fig. 1: Diagram of a GAN

The networks working as generators and discriminators are usually implemented by deep Feedforward Networks but there are also more complex architectures based on convolutional or other kinds of layers. These advanced architectures and layers can improve the quality of the forged data.

Deep Convolutional GAN

One of the most interesting improvements of the basic GAN is the Deep Convolutional GAN[9]. Its contributions consisted of a set of constraints on the conventional Convolutional GANs to provide more stable training in almost every setting. The most important guidelines were the utilization of batch normalization in both the generator and discriminator and the removal of fully connected hidden layers.

Another key aspect of the article is the usage of convolutional transposed layers(fractional-stridden) instead of stridden convolutional layers. This is applied to the generator network to increase the size of the images.

3 Methodology

The creation of the synthetic dataset has been a complex process due to the nature of the problem. The gathering of the original data has been realized with a manual process and the data needed different methods of preprocessing. Finally, the labeling of the synthetic images has been done based on the IV curve of the original data.

3.1 Data gathering

The first part of every research is obtaining data. There are some public datasets available in the bibliography but they are not suitable for this problem since they lack of the Intensity-Voltage (IV) curve that is associated with each PV cell. For the measurements for the IV curve, a device we have used the device with the capacity of measuring the IV curve of a single PV cell [11]. The images of the PV cells were obtained with the electroluminescence (EL) camera Hamamatsu InGaAs C12741-03. It is known that this technique is highly effective for detecting defects on PV modules or cells [10]. and it is widely used in other works related to PV systems. In the Fig.2 different photographs of the device and the camera are presented.
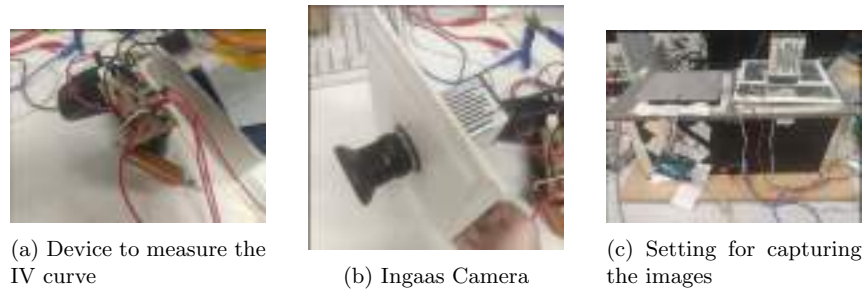
(a) Device to measure the IV curve

(b) Ingaas Camera

(c) Setting for capturing the images

Fig. 2: Devices used to obtain the data
.

The cells were shadowed with different artificial defects, in order to improve the amount of data. The shadows were created aiming to imitate different defects or problems found on solar farms.

(a) Shadow/Defect 0: Original Image

(b) Shadow/Defect 1: Long Horizontal Line

(c) Shadow/Defect 2: Long Vertical Line

(d) Shadow/Defect 3: Big Central Circle

(e) Shadow/Defect 4: Small Central Circle

(f) Shadow/Defect 5: Two small circles in the corners

(g) Shadow/Defect 6: Big circle in one corner

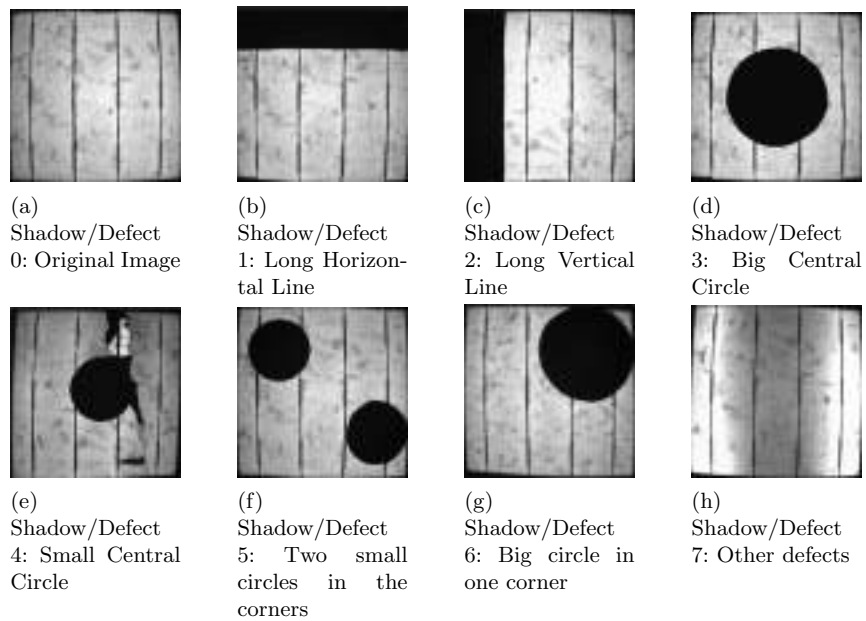(h) Shadow/Defect 7: Other defects

Fig. 3: Different Techniques to photography modules
.

We obtained 602 different images with their corresponding IV curves.

3.2 Image Preprocessing

The obtained images suffered from different problems:

- Dead pixels and luminous noise: The camera has some dead pixels due to its usage, there is also a bit of luminous noise produced by leaks in the insulation of the device. These two phenomena are harmful to the quality of the images even though they are almost not visible to the human eye, so it is important to remove or reduce their presence. To solve this problem, we captured an image before giving power to the PV cell for performing the EL image. This enabled us to perform a subtraction of the noise from each captured image.
- Images with poor lighting: Most of the libraries and programs have problems understanding the scale of the histogram of an image, not knowing with the value is supposed to be white. We can see in Fig. 4a4b how the channels of the images only occupy a tiny fraction of all of the possible values. To fix this problem we have performed a min-max standardization, subtracting the minimum value and dividing the maximum value found in the image. The resulting image can be seen in Fig. 4c and Fig. 4d.
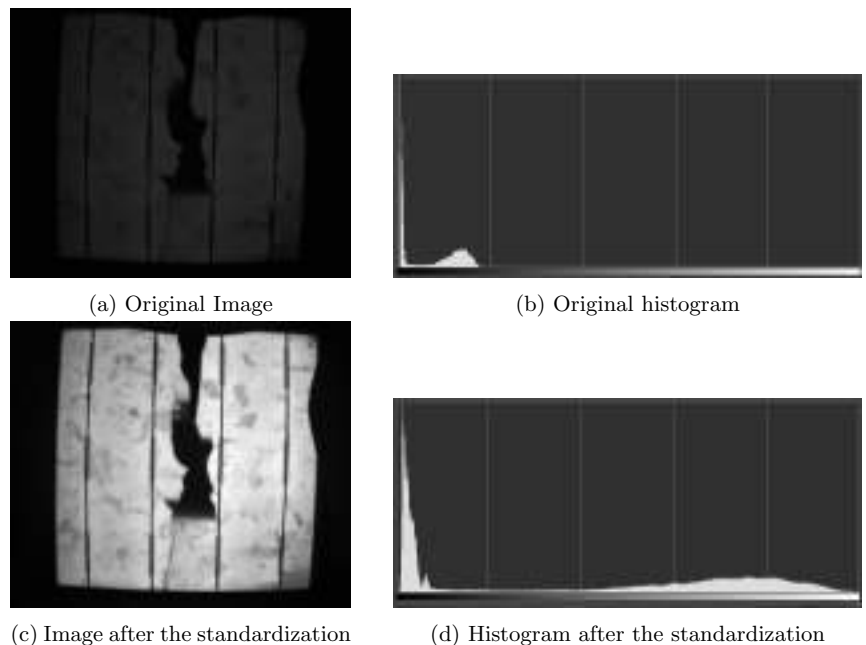

(a) Original Image

(b) Original histogram

(c) Image after the standardization

(d) Histogram after the standardization

Fig. 4: Image before and after applying the fix in the color
.

– Black surrounding Areas: As it can be seen in Fig.4c, the cells are surrounded by a black area, this is caused due to the lens of the camera since it is also capturing the walls of the insulated area. The issue was solved by performing a change of perspective. First of all, we applied different filters to remove the details and obtain the maximum contour polygon of the cell. After that, we performed a Hough Transform to find the corners of the cell. In some cells, we needed to make minor fixes before the transformation due to their defects or black areas. The results of the transformation can be seen in Fig.5
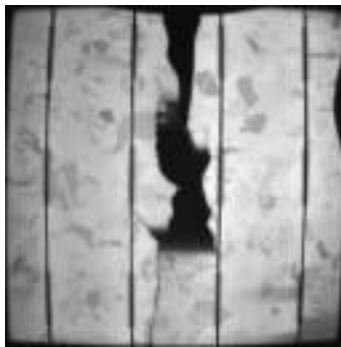

Fig. 5: Cell after removing the black contour

Since the process was applied to every image, we obtained 602 processed images.

3.3　Creation of the synthetic images

As commented before, we have used Deep Convolutional Generative Adversarial Network. The model is composed of two different networks: generative and discriminator.

The architecture of the generative network can be seen in Fig.7. The input of this network is a random noise with a Normal distribution and produces an image of the desired size. In Fig.6 we can see the output before and after the training. The network has Convolutional Transpose Layers of different sizes to improve its generative properties. It also uses Batch Normalization [13] and the Leaky Relu function [14]. Other important parameters can be found in Table 1.

(a) Output image before training
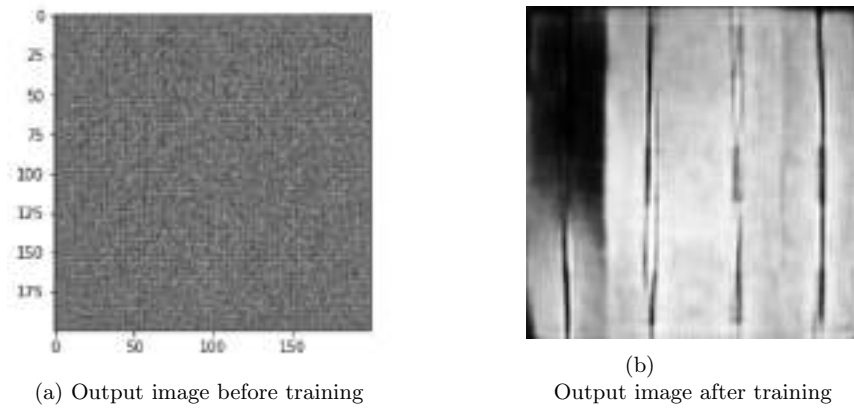
(b)
Output image after training

Fig. 6: Differences in the output images before and after the training
.
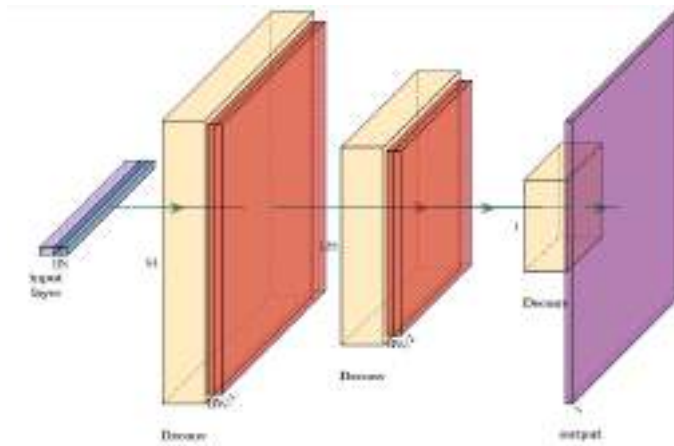

Fig. 7: Architecture of the generator network

Activation Function	Loss Function	Learning Rate	Epochs	Batch Size	Output Size
Leaky Relu	Cross Entropy	$5 * 10^{-5}$	800	4	200x200

Table 1: Hyperparameters for the generator network

The architecture of the discriminator network can be seen in Fig.8. The input is an image of the desired size. The single output determines if the image is a real cell or a fake image. The network uses convolutional layers to find the patterns and features of the images. It also uses dropout and batch normalization to improve its generalization capacities. Other important parameters can be found in Table 2.
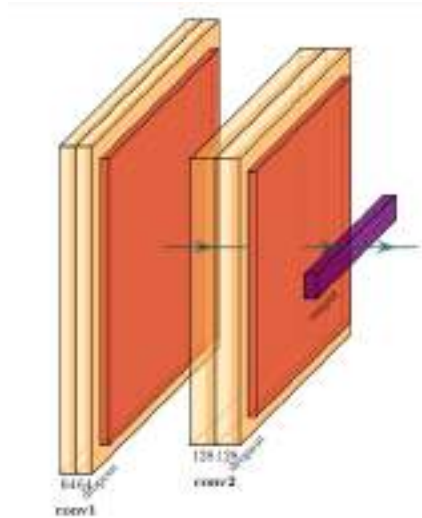
Fig. 8: Architecture of the discriminator network

Activation Function	Loss Function	Learning Rate	Epochs	Batch Size	Input Size
Leaky Relu	Cross Entropy	$5 * 10^{-5}$	800	4	200x200

Table 2: Hyperparameters for the discriminator network

The training of both networks was performed simultaneously. We used all the images for training the GAN. The training loop starts with the generator being provided for seed as input. The generator produces a cell from that seed. After that, the discriminator is used to classify real images and fake images. The loss is computed for each of the networks, based on the results of the discriminator. In Fig. 9 we can observe the evolution of the loss in both networks. In the first epochs, the loss of the discriminator is high, until it learns to detect the real images. At that moment the loss of the generator reaches its peak since almost

any fake image is being classified as real. After that, the generator improves steadily its images reaching its lower loss near epoch 400. During that time the performance of the discriminator worsens since it gets difficult to differentiate between real and fake images. It reaches its highest loss near epoch 400.

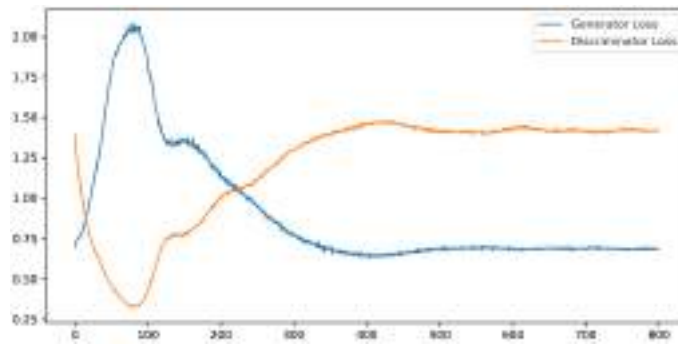Fig. 9: Evolution of the loss of generator and discriminator

The training took 2 hours and 41 minutes with a CPU AMD Ryzen 7 5800H, 16 GB of RAM, and a GPU Nvidia Geforce GTX 1650.

After the training, the generator network is used to generate 10000 images. Each image is produced by a different random seed. In Fig. 10 we can see some of the generated images.
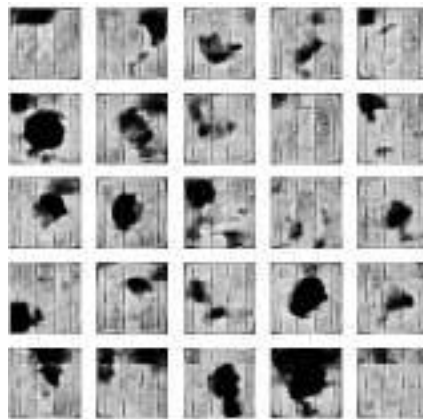

Fig. 10: Multiple generated images

3.4   Labeling

The process of labeling the synthetic images was not trivial. The main problem was related to the nature of the labels of the original images. The labels are based on the energetic production of the cells which is measured with the IV curve. Synthetic cells are not physical cells, so it is not possible to measure their curves. To solve this problem we have created a regression model based on Random Forest (RF) [12]. The tuning of the hyperparameters has been done of this RF with GridSearchCV using the Sklearn library We can see the results of the optimization for RF in Table 3. The RF model is trained with the complete original dataset (602 images).

n_estimators	max_depth	min_samples_split	min_samples_leaf	min_weight_fraction_leaf
200	10	1	1	0

Table 3: Best hyperparameters found for Random Forest: n_estimators $\in$ $[20, 500]$, max_depth $\in [0, 10]$, min_samples_split $\in [1, 10]$,min_samples_leaf$\in$ $[1, 10]$,min_weight_fraction_leaf $\in [0, 0.8]$

The training data of this model was composed of different features extracted from the original 604 images (Table 4) and was divided into training and validation (66%/33%), we decided to use only two different sets due to our limitation in data. The target variable was the power produced by each cell, standardized between 0 and 1.

mean	median	mode	variance	std	
roughness	blacks	burned whites	others	peaks_number	20
peaks distance	peak 0 height	peak 0 width	peak 1 height	peak 1 width	

Table 4: Features for Random Forest Regressor

The model performed a Mean Absolute Error (MAE) of 0.041 and a Mean Squared Error (MSE) of 0.0038 in the validation dataset. The predictions of the generated dataset can be seen in Fig.11. Finally, the images were divided in two according to their power (class $0 > 0.8$ and class $1 <= 0.8$). 6963 images were classified as class 0 and 3037 as class 1.
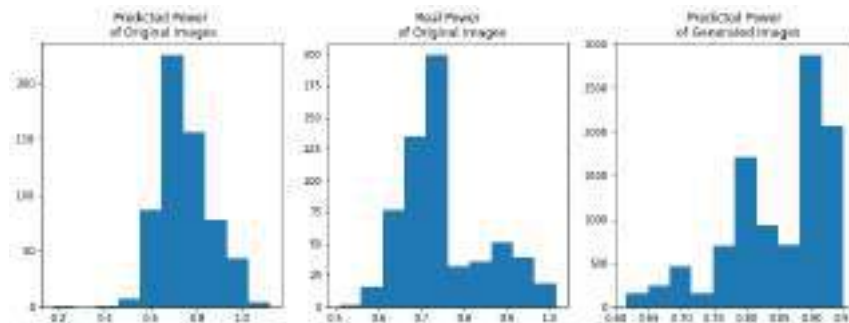
Fig. 11: Histogram of predicted labels of the generated dataset

4   Results

The dataset is divided into two folders according to each class: class 0 represents the images that have a relative power output of at least 0.8. As we have said before the dataset is divided into 6963 of class 0 and 3037 of class 1. The cells in the class are producing enough electricity even if some of them have some kinds of defects (Fig.12a). class 1 represents the images that have a relative power output of less than 0.8. The cells in that class are underperforming due to their defects (Fig.12b).
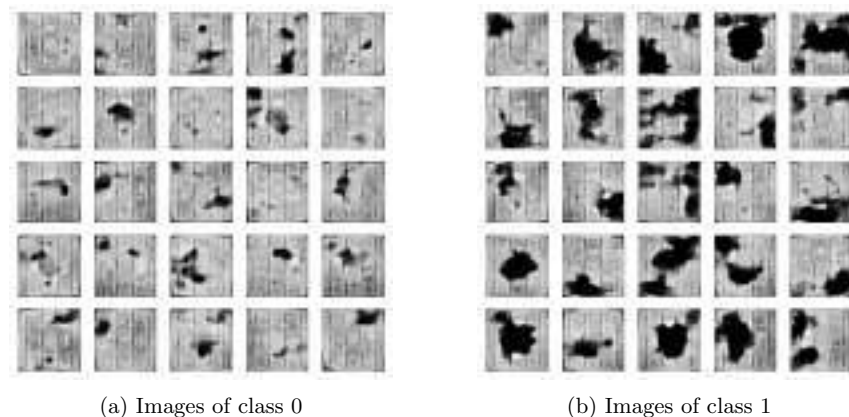
(a) Images of class 0

(b) Images of class 1

Fig. 12: Different generated images of both classes.

We can also observe that the generated images present different defects from the original images. This improves the diversity of defects in the datasets. Even

if the images seem to be quite different than the original we can observe that the average of all of the histograms of the images for each class presents a similar structure. The images of class 0 (Fig. 13a) mostly present gray-white colors but in some cases present minor defects that are reflected in the peaks of the black areas. The images of class 1 (Fig. 13b) present a high amount of black pixels due to their high amount of shadows or defects. The generated images have a peak with a higher height than the peak found in the original images but in contrast, the peak in the original images is wider.

(a) Histogram of the images of class 0   (b) Histogram of the images of class 1
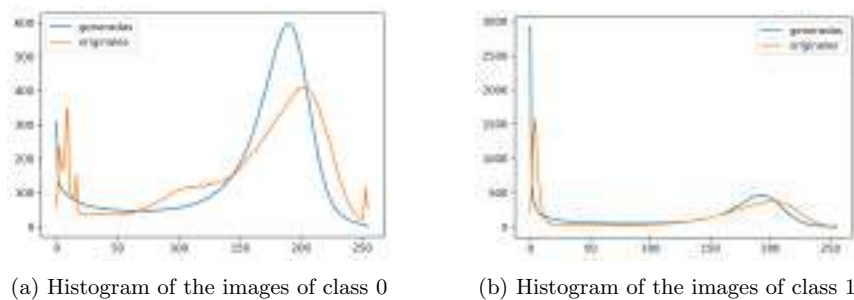
Fig. 13: Different generated images of both classes.

In Fig. 14 we can see a generated cell with its histogram and an original cell with present a similar defect. We can observe that their histogram is also similar, they present the same amount of peaks and are in a similar position.

(a) A defective synthetic cell with its histogram
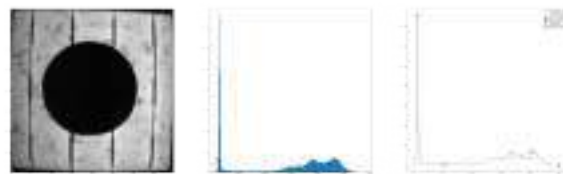
(b) A defective original cell with its histogram

Fig. 14: Comparison of a defective synthetic cell and a defective original cell

In Fig. 15 we can also observe it with the synthetic cells that have almost no defects and an original without them either. Their histogram is also quite similar since their most important peak is placed around the same area.
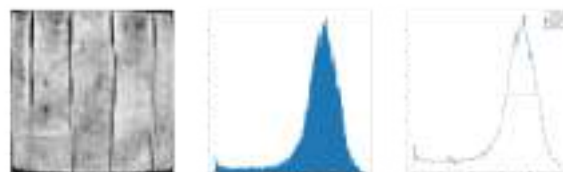
(a) A defective synthetic cell with its histogram
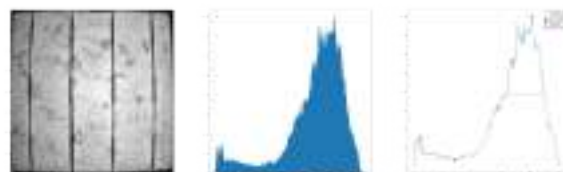
(b) A defective original cell with its histogram

Fig. 15: Comparison of a defective synthetic cell and a defective original cell

The dataset can be downloaded from https://github.com/hectorfelipe98/ Synthetic-PV-cell-dataset. We also provide a file that relates each image with its label and its output power.

5   Conclusions and future work

This work has shown that it is possible to create new PV datasets using the newest Artificial Intelligence Techniques. The process is not straightforward since it needs different techniques to prepare the data. The labeling of the new images is a complex process since it is not possible to ask a domain expert.

The obtained images present more kinds of defects than the originals. This can be used to train models to improve their generalization capacity.

In future research work, we will try to improve the original dataset, creating new kinds of shadows or defects and trying to make the data more realistic. Another important aspect to improve are the processes to prepare the data, in order to obtain better images. Finally, new architectures or models need to be tested to improve the generation of the images.

6   Acknowledgements

References

1. Kim, JungHoon Smart city trends: A focus on 5 countries and 15 companies CITIES Volume 123 Article Number 103551 Year 2022 https://doi.org/10.1016/j.cities.2021. 103551
2. Luis Hernández-Callejo, Sara Gallardo-Saavedra, Víctor Alonso-Gómez, A review of photovoltaic systems: Design, operation, and maintenance, Solar Energy, Volume 188, 2019, Pages 426-440, ISSN 0038-092X, https://doi.org/10.1016/j.solener.2019. 06.017.
3. Creswell, A., White, T., Dumoulin, V., Arulkumaran, K., Sengupta, B.; Bharath, A. A. (2017). Generative Adversarial Networks: An Overview
4. Schreiber, J., Jessulat, M., Sick, B. (2019). Generative adversarial networks for operational scenario planning of renewable energy farms: A study on wind and photovoltaic. Lecture Notes in Computer Science (Including Subseries Lecture Notes in Artificial Intelligence and Lecture Notes in Bioinformatics),11729 LNCS, 550–564. https://doi.org/10.1007/978-3-030-30508-6_44
5. Shou, C., Hong, L., Ding, W., Shen, Q., Zhou, W., Jiang, Y., Zhao, C. (2020). Defect detection with generative adversarial networks for electroluminescence images of solar cells. Proceedings - 2020 35th Youth Academic Annual Conference of Chinese Association of Automation, YAC 2020, 312–317. https://doi.org/10.1109/ YAC51587.2020.9337676

6. Luo, Z., Cheng, S. Y.; Zheng, Q. Y. (2019). GAN-Based Augmentation for Improving CNN Performance of Classification of Defective Photovoltaic Module Cells in Electroluminescence Images. IOP Conference Series: Earth and Environmental Science (1), 012106. https://doi.org/10.1088/1755-1315/354/1/012106

7. Du, Xuedan, Cai, Yinghao, Wang, Shuo, Zhang, Leijie IEEE 2016 31ST YOUTH ACADEMIC ANNUAL CONFERENCE OF CHINESE ASSOCIATION OF AUTOMATION (YAC) Page 159-164 Published 2016

8. Goodfellow, Ian, Pouget-Abadie, Jean and Mirza, Mehdi and Xu, Bing and Warde-Farley, David and Ozair, Sherjil and Courville, Aaron and Bengio, Y.. (2014). Generative Adversarial Networks. Advances in Neural Information Processing Systems. 3. 10.1145/3422622.

9. Alec Radford, Luke Metz, Soumith Chintala: Unsupervised Representation Learning with Deep Convolutional Generative Adversarial Networks. ICLR 2016

10. Sara Gallardo-Saavedra, Luis Hernández-Callejo, María del Carmen Alonso-García, José Domingo Santos, José Ignacio Morales-Aragonés, Víctor Alonso-Gómez, Ángel Moretón-Fernández, Miguel Ángel González-Rebollo, Oscar Martínez-Sacristán, Nondestructive characterization of solar PV cells defects by means of electroluminescence, infrared thermography, I–V curves and visual tests: Experimental study and comparison, Energy, Volume 205, 2020, 117930, ISSN 0360-5442, https://doi.org/10.1016/j.energy.2020.117930.

11. Morales-Aragonés, J.I.; Gómez, V.A.; Gallardo-Saavedra, S.; Redondo-Plaza, A.; Fernández-Martínez, D.; Hernández-Callejo, L. Low-Cost Three-Quadrant Single Solar Cell I-V Tracer. Appl. Sci. 2022, 12, 6623. https://doi.org/10.3390/app12136623

12. Ho, T. K. (1995). Random decision forests. In Proceedings of 3rd international conference on document analysis and recognition (Vol. 1, pp. 278–282).

13. Sergey Ioffe and Christian Szegedy ICML'15: Proceedings of the 32nd International Conference on International Conference on Machine Learning - Volume 37 July 2015 Pages 448–456

14. Andrew L., Awni Y. Hannun and Andrew Y. Computer Science D Empirical Evaluation of Rectified Activations in Convolution Network https://arxiv.org/pdf/1505.00853.pdf

15. Nitish Srivastava, Geoffrey Hinton, Alex Krizhevsky, Ilya Sutskever, Ruslan Salakhutdinov Dropout: A Simple Way to Prevent Neural Networks from Overfitting Journal of Machine Learning Research 2014

Distribution of Police Patrols as a Covering Problem in Smart Cities: Fuengirola Use Case

Jamal Toutouh[1][0000−0003−1152−0346], Francisco Chicano[1][0000−0003−1259−2990], and Rodrigo Gil-Merino[2][0000−0001−7376−4499]

[1] Universidad de Málaga, Málaga, Spain
{jamal,chicano}@uma.es
[2] Universidad de León, León, Spain
rgilmerino@unileon.es

Abstract. Security and emergency services are among the biggest concerns for both authorities and citizens. Better adapting those services to inhabitants is a key goal for smart cities. All emergency services have their own peculiarities, and in particular, the control of police patrols in urban areas is a complex problem connected to the dynamic vehicle routing and traveling salesman problems. We propose in this paper two bi-objective integer linear programming formulations for the police patrol routing problem, which differs from the vehicle routing and travelling salesman problems in which not all the nodes in the city must be served, and there is no "depot". The first formulation is more precise but computationally costly, and the second one is a relaxation that standard integer linear programming solvers can easily solve. The experimental analysis shows that the complete Pareto front can be computed for the relaxed formulation, providing valuable information to solve the precise formulation in future work. In particular, we analyze the number of patrols and the length of the routes they traverse.

1 Introduction

Smart cities try to improve their functioning using information and communication technologies [2]. Consequently, there are many ways of making a city smart [4]. In general terms, the smartness of a city should translate into more and better-personalized services for its inhabitants. Among these services, security in cities is probably one of the biggest concerns for both authorities and citizens. To increase security and how the urban population perceives security, emergency services must be well coordinated in order to prevent crime, minimize arrival times to crime spots, and effectively attend to emergencies and disasters. The most visible corp in terms of security in cities is the fleet of police patrols, and optimizing the use of these police resources to serve citizens better is one of the ways of making a city smarter.

The control of police patrols in urban areas is a complex problem of increasing difficulty with cities' growth. Two main issues must be considered in patrol routes: on the one hand, effective positioning of patrols might prevent crime

in conflicting areas and assist communities more efficiently; on the other hand, emergencies stochastically appear and must be responded to on real-time bases, leaving unattended areas during certain periods. Strategies to solve these issues are included in the concept of the police patrol routing problem (PPRP) [10].

Studies on the PPRP are very limited. The PPRP has many similarities with the vehicle routing problem (VRP) [9], which is a generalization of the traveling salesman problem (TSP) [8]. There exist many variants of the VRP [5,14,19], and it is usual to find in the literature a treatment of the PPRP as a dynamical vehicle routing problem (DVRP) [13], a VRP that evolves in time. Nevertheless, the police patrol problem has its own characteristics, making it a significantly different problem by itself. In particular, the existence of stochastic events, in the form of emergencies and disasters, forces the police patrols to be reactive, suspend current tasks, minimize their reaction times towards demanding spots and resume daily tasks once the emergency finishes.

Police patrol emergencies are conceptually different from emergency calls received by other emergency services, such as ambulances and fire-trucks. In these last services, vehicles attend the emergencies from their depots and return when they are over without altering prefixed routes. Some authors have tried to solve these kinds of problems by treating them as the maximal expected coverage relocation problem [12], where the aim is to maximize the coverage of an urban area by allocating waiting sites for emergency vehicles. In this scheme, the city is divided into blocks in which waiting emergency vehicles have a driving time until the emergency spot to be minimized.

This work aims to propose PPRP as a covering problem in the context of smart cities: a fixed number of police patrols are distributed in an urban region in such a way that they cover the maximum possible conflicting areas and, at the same time, the total cost of deploying the patrols is minimized. We use the total length of the routes traversed by the patrols as a proxy for the cost since this length is directly related to fuel consumption and greenhouse gas emissions. Thus, PRPP is addressed as a multi-objective optimization problem by using mathematical programming. Specifically, a variant of the ε-constraint method, called *hybrid method* by Ehrgott [11], is used to compute the set of *efficient* solutions that represent different trade-offs between the objectives. The problem is addressed over three instances defined using real data from the city of Fuengirola (Spain).

The main contributions of this paper are: *a)* providing two new formulations of the PPRP problem as a covering problem, *b)* using a multi-objective exact method to address one of the formulations of PPRP, and *c)* solving the PPRP problem on a real-world instance.

This paper is organized as follows: the next section mathematically describes the police patrol routing problem as a covering problem; Section 3 reviews related work in the context of smart city problems; Section 4 details the proposed methodology, algorithm and experimental setup used to solve the problem; Section 5 discusses the results and the solutions found; and finally, Section 6 draws the main conclusions and ideas for future work.

2   The Police Patrol Routing Problem

We model a city with a graph $G = (V, E)$, where V is the set of nodes, representing junctions of streets, and $E \in V \times V$ is the set of edges of the graph representing the streets. The graph is vertex- and edge-weighted. The weights associated with the nodes, denoted with w_i with $i \in V$, represent the number of events associated with the node. These weights are computed based on the historical data recorded in the city. In particular, historical data provides events that occurred at different streets (edges), and the events are assigned to the closest node. The weight w_i is the number of events for which i is the closest node in the map. The weights associated with the edges (streets), denoted with c_e with $e \in E$, represent the length of the street. The *successor* and *predecessor* functions of G, denoted with $N^+ : V \mapsto 2^V$ and $N^- : V \mapsto 2^V$, are defined as follows:

$$N^+(i) = \{j \in V | (i, j) \in E\} \tag{1}$$

$$N^-(i) = \{j \in V | (j, i) \in E\} \tag{2}$$

A solution x to the PPRP is a set of cycles in graph G with each cycle representing the route of one patrol. We will assume a maximum of P patrols that will be denoted with numbers 1 to P. We will use the notation $[n]$ to denote the integer numbers from 1 to n. Thus, the patrols will have labels in the set $[P]$. The goals of PPRP are to maximize the sum of the weights of the visited nodes and minimize the distance traveled by all the patrols to visit those nodes. By maximizing the sum of weights, we are providing a better service quality; while minimizing the length of the routes, we reduce the cost of the solution and the pollution due to police vehicles. Since we have a limited number P of patrols, reducing the lengths of the routes and covering all the nodes of the graph are conflicting objectives. Thus, we formulate the problem as a bi-objective problem.

In the following, we propose two formulations for the problem. The first is more precise but also more complex, and solving it requires more computational power. The second is a relaxation of the first formulation and can be solved efficiently using exact methods but assumes an unlimited number of patrols.

2.1   Precise Formulation

Before presenting the formulation we will present the variables used in it. Let $x_{p,e}$ be a binary variable that is 1 when patrol p traverses edge e and zero otherwise, and let y_j be a variable that is 1 when node j is covered by at least one route and 0 otherwise. We will use variables l and u to represent the lower and upper bounds for the length of the routes. We will also introduce variables $z_{p,j}$ and $d_{p,j}$ to avoid several cycles associated with the same patrol. We can formalize the PPRP with the following bi-objective mixed integer linear program:

$$\min \sum_{e \in E} c_e \sum_{p=1}^{P} x_{p,e}, \quad \max \sum_{i \in V} w_i y_i, \tag{3}$$

subject to:

$$\sum_{i \in N^-(j)} x_{p,(i,j)} = \sum_{k \in N^+(j)} x_{p,(j,k)} \ \ \forall j \in V, \forall p \in [P], \tag{4}$$

$$\sum_{i \in N^-(j)} x_{p,(i,j)} \le 1 \ \ \forall j \in V, \forall p \in [P], \tag{5}$$

$$\sum_{i \in V} d_{p,i} = 1 \ \forall p \in [P], \tag{6}$$

$$z_{p,j} \ge z_{p,i} + 1 + |V|(x_{p,(i,j)} - d_{p,j} - 1) \ \ \forall (i,j) \in E, \ \forall p \in [P], \tag{7}$$

$$y_j \le \sum_{i \in N^-(j)} \sum_{p=1}^{P} x_{p,(i,j)} \ \ \forall j \in V, \tag{8}$$

$$l \le \sum_{e \in E} c_e x_{p,e} \ \ \forall p \in [P], \tag{9}$$

$$\sum_{e \in E} c_e x_{p,e} \le u \ \ \forall p \in [P], \tag{10}$$

$$u - l \le \alpha u, \tag{11}$$

$$x_{p,e} \in \{0,1\} \ \ \forall e \in E, \ \forall p \in [P], \tag{12}$$

$$d_{p,j} \in \{0,1\} \ \ \forall j \in V, \ \forall p \in [P], \tag{13}$$

$$0 \le y_j \le 1 \ \ \forall j \in V, \tag{14}$$

$$z_{p,j} \ge 0 \ \ \forall j \in V \ \forall p \in [P], \tag{15}$$

$$u, l \ge 0. \tag{16}$$

Equation (3) expresses the two objectives, which is minimizing the sum of the lengths of the routes and maximizing the sum of the weights of the nodes covered by the routes. Observe that even if y_j is continuous, it can only take values 0 or 1 due to constraint (8) and the second objective in (3). The family of constraints (4) force the patrols to pass through a node and not stop on it. Equations (5) prevents a patrol from visiting the same node twice. Together, Eqs. (4) and (5) force the patrols to follow cycles in the graph. But there could be more than one cycle associated to one patrol, which is not realistic. To solve this issue we add Equations (6) and (7). We adapted here the sub-tour elimination equations traditionally used in the ILP formulation of the Vehicle Routing Problem (VRP) formulation [1]. In this case, the main difference is that we do not have a designated depot (as it happens in VRP). Thus, we add a new variable $d_{p,j}$ that is 1 when patrol p uses node j as a depot and is 0 otherwise. Equation (6) ensures that only one depot per patrol exists. Equations (7) ensure that the cycle associated with each patrol is connected. One criticism of the adopted approach is that routes in real life do not need to be cycles in the city. There can be nodes visited more than once in a route because it could be convenient due to the existing road graph. In that case, our model is still valid, but we need to pre-process the underlying graph. Instead of using the real roads in the city as edges, we produce a complete graph where the nodes are those with nonzero

weights, and the edges represent the shortest path from one node to another. That is, each edge in this second graph corresponds to a complete path in the original road graph. We defer to future work the analysis of this approach.

Equation (8) ensures that y_j is zero if there is no route visiting node j. Otherwise, y_j will be 1 due to the second objective, as pointed out above. Equations (9) and (10) introduce the constraints for the lower and upper bound variables l and u, respectively. These variables are used in Equation (11) to put some limits to the difference between the lengths of the patrol routes. With this constraint, we want to allow the decision-maker to fix the maximum difference in the length of the routes followed by the different patrols. The parameter α provides a convenient parameter to tune this difference. If $\alpha = 0$, all routes should have the same length, which could be impossible for some graphs. If $\alpha = 1$, the routes can have any length. A value between 0 and 1 for α will set the difference between the longest and the shortest route to a fraction of the longest route. The decision-maker can use low values for α, if it is important that the routes do not differ too much in length. This parameter is related to "fairness". Finally, Equations (12), to (16) establish the domain of the variables.

2.2　Relaxed Formulation

The precise formulation is equivalent to solving several VRPs simultaneously. We ran out of computational resources when performing preliminary experiments on this formulation. Since VRP is NP-hard, solving precise formulation will require using heuristics when the instances are medium to large. In this section, we propose a relaxed ILP formulation that can be solved exactly using ILP solvers in a reasonable time and can provide valuable information to guide the use of heuristics and the precise formulation. In this relaxed formulation, we assume that $\alpha = 1$ and omit the corresponding constraints for the lower and upper bounds, Equation (11).

Let x_e be a binary variable that is 1 when one of the patrols traverses edge e and 0 otherwise. The relaxed formulation of the PPRP is as follows:

$$\min \sum_{e \in E} c_e x_e, \quad \max \sum_{i \in V} w_i y_i, \tag{17}$$

subject to:

$$\sum_{i \in N^-(j)} x_{(i,j)} = \sum_{k \in N^+(j)} x_{(j,k)} \ \ \forall j \in V \tag{18}$$

$$y_j \leq \sum_{i \in N^-(j)} x_{(i,j)} \ \ \forall j \in V \tag{19}$$

$$x_e \in \{0,1\} \ \ \forall e \in E \tag{20}$$

$$0 \leq y_j \leq 1 \ \ \forall j \in V \tag{21}$$

In this relaxed formulation, the number of patrols is unbounded. One solution provided by this formulation will be composed of a set of cycles covering nodes in the graph, which will be given by the variables x_e. We use again variables y_j to represent the visit of at least one patrol to node j. Given the values of x in one solution, it will be possible to provide a lower bound to the number of patrols required to implement that solution. The minimum number of patrols will be the number of connected components in the subgraph induced by the set of edges $E' = \{e \in E | x_e = 1\}$. We can also compute some statistics regarding the lengths of the routes associated with those patrols. The computation of the Pareto front for this relaxed model will provide an "optimistic" Pareto front; that is, no solution to the precise formulation can dominate any solution in the Pareto front of the relaxed formulation. The solutions in the front also represent real solutions for the case in which the number of patrols is not bounded, and there is no constraint related to the lengths of the routes.

3 Related work

Literature on smart cities includes many research studies on addressing optimization problems with the aim of improving inhabitants' life. These optimization problems deal with real-world environments, and, in general, their objective functions are noisy and/or are based on simulations. Besides, these optimization problems comprise substantial search spaces and/or consider several (not easy to meet) constraints. These specific characteristics make these problems hard to solve (most of them are NP-hard problems) [17,18]. Therefore, heuristics and metaheuristics (e.g., evolutionary computation, EC) emerged as effective and efficient tools to compute good solutions requiring bounded computational resources. Besides, mathematical programming techniques (e.g., integer linear programming, ILP) have become very popular in addressing such problems in the last few years.

Many studies in the literature focus on the use of heuristics and metaheuristics to address smart city problems. For example, different EC methods were coupled with machine learning approaches to build accurate models for road traffic mobility [21] and car parking availability [3] prediction. The first study applied EC to address feature selection, and the second used EC to optimize the hyperparameters and architecture of a neural network. A heuristic algorithm was designed to address communication among vehicles and road infrastructure elements to improve security and efficiency in urban road transportation [20]. The authors proposed a communication algorithm based on swarm intelligence in which each node in the network takes the routing decisions in order to optimize its own and the neighborhood nodes' throughput.

Many real-world smart city problems are multi-objective because they consider several (often conflicting) objectives (e.g., when dealing with public transportation: the quality-of-service and economic cost). For example, multi-objective EC algorithms were analyzed for the efficient design of the vehicle charging infrastructure [6]. The authors considered two conflicting objectives:

the quality-of-service regarding charging time and distance to the charging station and the economical cost of the charging station installation [7].

In recent years, mathematical programming methods are gaining prominence. Thus, several studies in the literature apply mathematical programming techniques to solve problems in the domain of smart cities. A mono-objective variant of the problem of designing the vehicle charging infrastructure was addressed by using ILP [17]. The exact approach improved the results provided by a genetic algorithm (GA). Other authors applied ILP to find the best location for parking lots [15]. This research aimed to minimize the vehicles' travel time for finding a parking lot near the users' destination. Multi-objective mixed-ILP was proposed to deal with the problem of rescheduling trains to serve passengers from delayed high-speed railway trains [23]. The objectives of this problem were to maximize the number of expected transported passengers and minimize the number of extra trains and operation-ending time of all extra trains.

PPRP problem is a variant of VRP. Some studies use mathematical programming to address VRP (and variants) in smart cities literature. The ε-constraint method was applied to optimize the delivery service provided by unmanned aerial vehicles (UAV) [24]. The problem was addressed as a multi-objective nonlinear programming problem established by taking the minimum total flight distance and the highest average customer satisfaction as the objective functions. The proposed method improved the results computed by a GA. A combination of the ε-constraint method and the modified column-and-constraint generation algorithm was proposed to deal with the efficient urban waste collection [25]. The authors defined a bi-objective problem to minimize the worst-case total collection cost and the environmental disutility, considering service demands uncertainty and traversing costs uncertainty on roads. Another variation of the urban waste collection problem was proposed by considering three objectives: minimizing the average required collection frequency of the containers, minimizing the installation cost of bins, and minimizing the average distance between the users and the bins [18]. The authors applied the augmented ε-constraint method and the Page-Rank heuristic. The results show the proposed approaches' competitiveness for constructing a set of candidate solutions that considers the different trade-offs between the optimization criteria.

4   Methodology

In multi-objective optimization problems, there is usually no single solution that optimizes all the objectives at the same time. Instead, we are interested in finding a set of the so-called *efficient solutions*, with the property that it is not possible to improve one objective without worsening another one. Let d be the number of objectives in our multi-objective problem, we say that a solution x is *efficient* if there is no solution y such that $f_i(y) \leq f_i(x)$ for all $i \in [d]$ and $f_j(y) < f_j(x)$ for at least one $j \in [d]$. The set of all efficient solutions of a multi-objective problem is called *efficient set*, and the image of that set is called *Pareto front*. Each d-dimensional point in the Pareto front is called *non-dominated point*. There can

be more than one efficient solution mapped to a single non-dominated point. In those cases, we are interested in finding only one of those efficient solutions. In the following subsections, we first present the algorithm used to find the Pareto front (and one efficient solution per non-dominated point). We also explain the experimental setup used in this work to illustrate how the problem can be solved in a real scenario. To the best of our knowledge, the formulation of the problems used here is novel, and thus, there are no algorithms to compare in the literature. Furthermore, since we use an exact algorithm, the optimality of the solutions is ensured, and the only comparison we can do with potential previous algorithms is related to the time required to solve the problem.

4.1   Algorithm

In this work, we are interested in finding the complete Pareto front of the relaxed formulation of the PPRP. In order to compute the front, we use a variant of the ε-constraint method, called the *hybrid method* by Ehrgott [11, p. 101], that optimizes a weighted sum of the objectives to ensure that the solutions found by the ILP solver are always efficient. Algorithm 1 shows the Hybrid method adapted to the bi-objective case we face. We assume that f_1 and f_2 are to be minimized. If one of the objectives is to be maximized (as it happens with the second objective in Eq. (17)) we can multiply it by -1. The method transforms the bi-objective problem into a set of single-objective problems where the goal is to minimize $f_2(x) + \lambda f_1(x)$, with λ a constant. The value of λ must be small enough not to lose any non-dominated point in the Pareto front, but large enough to ensure that all the solutions found are efficient[3]. In addition to the constraints of the problem, that we represent with the expression $x \in X$, the method adds a new constraint on f_1: $f_1(x) \leq \varepsilon$. This constraint is the key to obtaining all the efficient solutions even if the Pareto front is concave. The value ε is reduced by an amount δ along the search to find all the non-dominated points. In the beginning, ε must be large enough to find the non-dominated point with a minimum at f_2 value (and maximum at f_1 value). The value of δ should be small enough not to jump over any solution in the Pareto front. The algorithm ends when the problem is unfeasible, or ε reaches a minimum value ε_s. We use this limit in ε to be able to compute only one part of the Pareto front. This is useful when the decision maker has a clear idea of the range of values to consider. It is also especially useful to parallelize the computation of the whole Pareto front.

In our case, we use $\lambda = 0.0001$, since we computed the two lexicographic optimal solutions of the Pareto front and found that this value is small enough not to lose any efficient solution. Our first objective, f_1, is the sum of the weights of the visited nodes multiplied by -1, and f_2 is the sum of the lengths of the routes traversed by the patrols. We use the sum of weights as f_1 because the weights are integers and, thus, a value of $\delta = 1$ ensures that we do not miss any efficient solution. The length of the routes traversed by the patrols take, in

---

[3] In theory, for any value of $\lambda > 0$ the solution found is efficient, but in practice numerical errors in floating point operations can result in non-efficient solutions.

Algorithm 1: Hybrid method [11, p. 101]

Data: $\lambda, \delta, \varepsilon_0, \varepsilon_s$
Result: Pareto front, PF

1 $\varepsilon \leftarrow \varepsilon_0$;
2 $PF \leftarrow \emptyset$;
3 while $\exists x \in X$ *with* $f_1(x) \leq \varepsilon$ *and* $\varepsilon > \varepsilon_s$ **do**
4 $\quad x^* \leftarrow \underset{x \in X, f_1(x) \leq \varepsilon}{\arg\min}\ f_2(x) + \lambda f_1(x)$;
5 $\quad PF \leftarrow PF \cup \{(f_1(x^*), f_2(x^*)\}$;
6 $\quad \varepsilon \leftarrow f_1(x^*) - \delta$;
7 return PF

---

general, fractional values. If we would choose the length of routes as f_1, then finding the appropriate value for δ would have been more involved.

4.2 Experimental Setup

The experimentation was performed over three instances based on a realistic scenario defined in Fuengirola, a low-medium-sized city in the south of Spain. Fuengirola covers an area of 10.37 square kilometers and nowadays it has more than 82 000 inhabitants. The information about the events was provided by Fuengirola's City Police and the geographical data was obtained from Open Street Maps [16].

The instances have been defined as connected graphs in which the edges represent the roads, and the nodes encapsulate the number of events that occurred in their immediate area. During the period considered in our study (from January 1st, 2017 to December 31st, 2017), there were 2764 events that are distributed in 948 different nodes in the graph. We call this instance real. Due to data privacy issues, we cannot publish more details of the realinstance, and for this reason, we generated two synthetic additional problem instances based on the real one. In one of them, called shuffled, the weights of the nodes are randomly shuffled and then re-assigned to different nodes; the set of events is the same, but not their node in the graph. This instance contains 2764 events distributed in 473 different nodes. In the third instance, called sampled, we recover the original empirical distribution and generate a new set of weights according to this statistical distribution; the set of events is different, and so the place where they took place, but the statistical properties remain the same. This last instance has 2329 events distributed in 469 different nodes. Fig. 1 illustrates the map of the shuffled instance. The size of the nodes represents the number of events that occurred at that node in the considered period. The weight of an edge is the distance between the two nodes connected by that edge.

The experiments were run in the Picasso supercomputing facility of the University of Málaga with 126 SD530 servers with Intel Xeon Gold 6230R (26 cores each) at 2.10GHz, 200 GB of RAM and an InfiniBand HDR100 network. In order

to speed up the execution, we run several instances of the hybrid method, each computing in one part of the Pareto front. In order to speed up the computation of the whole Pareto front, we split the whole range of values for f_1 in the Pareto front in 30 intervals and run 30 instances of Algorithm 1 in parallel per problem instance. Each algorithm instance used different values for ε_0 and ε_s to avoid overlapping the computed solutions. The range of values for f_1 was computed based on the objective values of lexicographic optima (efficient solutions with minimum f_1 and minimum f_2 values).

The source code was written in Python using the Pyomo 6.2 library[4] to create the ILP model and Gurobi 9.5.1 as ILP solver. All the source code, data (except for the real instance) and results can be found in Zenodo [22].

5   Results and Discussion

In this Section, we present the results of the application of the hybrid method described in Subsection 4.1 to the three instances considered: `real`, `shuffled` and `sampled`. Since we are using a deterministic exact algorithm, we only performed one run of it. Different runs could differ in runtime, but we are not interested here in the analysis of runtime. However, we can say that the computation in parallel of the 30 algorithm instances to get the whole Pareto in front of the three problem instances took no more than 4 minutes in the Picasso supercomputing facility. This means that computing the whole Pareto front using one single machine with a sequential approach should not require more than 120 minutes (2 hours). This time is considered small compared to the lifetime of the solution, which is in the order of days. The Pareto front could be computed during the night because the routes have to be planned daily. We defer to future work on applying *anytime muti-objective algorithms*, which are specially designed to find a set of well-spread solutions in the objective space at any point during the search. These algorithms are especially useful when the runtime is an important parameter.

Fig. 2 shows the Pareto fronts of the three instances of PPRP. Table 1 presents the main metrics of the computed Pareto fronts: the relative hypervolume and the number of solutions in the frong. Focusing on Fig. 2, we observe that there are no big gaps in the front in any instance, in spite of the fact that the problem is combinatorial. For the `real` and `shuffled` instances, the front is wider in the x axis because these instances contain more events. However, we noticed that not all the events can be covered. In particular, for the `real` instance, the maximum number of events covered was 2756 (out of 2764). In the case of the instances `shuffled` and `sampled`, the maximum number of events covered were 2692 and 2292, respectively, out of 2764 and 2329. The reason for not covering some of the events has to do with the connectivity of the graph. The uncovered events must be in nodes that form isolated, strongly connected components of the graph, and it is not possible to form a cycle. There can be two

---

[4] https://pyomo.readthedocs.io/en/stable/

Fig. 1: Graph representing an efficient solution for the `shuffled` instance with 1900 events covered.

reasons for this to happen. First, the node is really disconnected from the traffic network (for example, a fire in the countryside), and it makes no sense to visit that node with a police car. Second, it could also be an artifact due to errors in the map used for the computations or a cut of a road at an extreme of the map. In this case, we could fix the problem by correcting the map and adding the missing edges. We defer to future work a detailed analysis of the uncovered events and their potential solution.

(a) `real`　　　　(b) `shuffled`　　　　(c) `sampled`
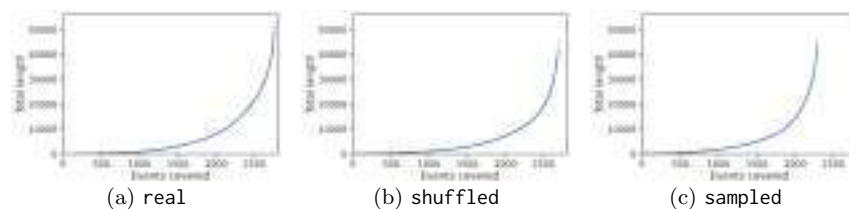
Fig. 2: Pareto fronts of the instances.

Table 1: Hypervolume and number of solutions of the computed Pareto fronts.

Metric	real	shuffled	sampled
Relative hypervolume	0.874	0.879	0.872
Number of solutions	2038	2345	2148

Now we will analyze in more detail the features of the efficient solutions found by the hybrid method. In all the cases, we will use the number of events covered as an index of the efficient solution (we could also use the length of the routes). Fig. 3 illustrates the minimum number of patrols required to implement the

efficient solution. We should say that efficient solutions could exist with fewer patrols than the ones plotted in the figure because we are not minimizing the number of routes in our relaxed formulation of the problem. Furthermore, it is always possible in a real situation to cover several routes with one single patrol by asking the patrol to alternate between the different routes (increasing the length of the routes). Thus, what we see in the figure is the minimum number of patrols required to implement *the* particular efficient solution found by the solver assuming that patrols are not allowed to alternate between routes. This number is related to the effort in personnel and vehicles required by the municipality to provide a good service to the citizens. We see that for a city like Fuengirola, this number could be as high as 300.

(a) real   (b) shuffled   (c) sampled
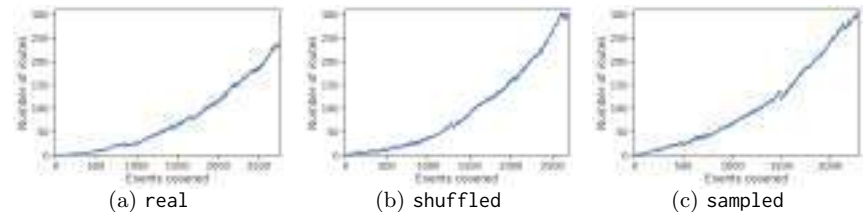
Fig. 3: Number of routes computed according to the number of covered events.

Fig. 4 shows statistics about the length of the routes followed by the different patrols. We plot the quartiles 1, 2 (median) and 3 of the set of routes corresponding to each efficient solution. This information is again indexed by the number of events (x axis). Ideally, these routes should be as short as possible to visit the conflicting points more frequently. We can see that for the efficient solutions found, these distances do not exceed 100 meters in the median. We can also appreciate these short routes in the representation of a solution in Fig. 1. These short routes explain the high number of vehicles required by the efficient solutions. In a real scenario, with a limited number of vehicles (around tens), this number should be much higher. Considering this more realistic scenario implies solving the precise formulation of PPRP, which we defer to future work.

(a) real   (b) shuffled   (c) sampled

Fig. 4: Length of the routes given the events covered.

We are also interested in analyzing the difference between the length of the routes. In the precise formulation, we can limit this difference using the α parameter, but in the relaxed formulation, there is no limit to the difference. Thus, we want to analyze how different these routes are. This is a measure of "fairness" for the patrols. Ideally, all the patrols should have 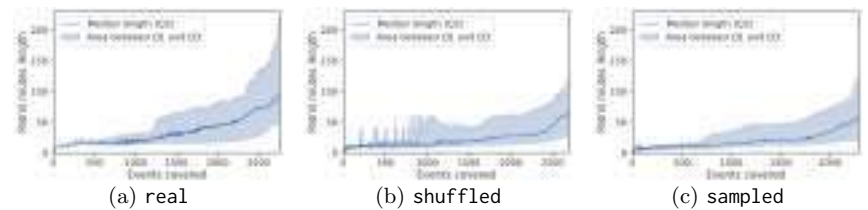routes with the same length since the length of the route is directly related to the cost of covering the routes (fuel consumption and greenhouse gas emissions). We plot in Fig. 5 the interquartile range (IQR) of the length of the routes divided (normalized) by the median length. We can see that this measure of fairness has no clear trend (as it happens with the previous features). An interesting observation in the three instances is that the normalized IQR has a peak between 1000 and 1500 events covered (depending on the instance). Definitely, the underlying graph has an influence on the routes that are possible and could explain part of the behaviour that the normalized IQR exhibit for the efficient solutions. We defer to future work a detailed analysis and the optimization of the distance between route lengths.

(a) `real`   (b) `shuffled`   (c) `sampled`
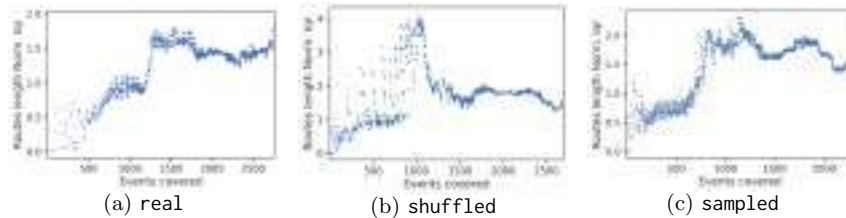
Fig. 5: Normalized interquartile range of the routes length given the events covered.

6   Conclusions

This paper presents two bi-objective formulations for the PRPP problem. One is precise but computationally costly to solve, while the second is a relaxed formulation that is easy to solve using standard exact methods. The problem has been formulated as a covering problem in the road graph of a city. The edges of the graph describe the streets, and the weight of the nodes represents the number of events. Thus, the police patrols have to visit (cover) the areas (nodes) with the highest number of events. Three instances of the problem have been generated based on real data from the city of Fuengirola (Spain). The relaxed formulation has been solved over the three instances to analyze the feature of the solutions that can be obtained for the problem. The results obtained show that the complete Pareto front of the relaxed formulation can be obtained in a few minutes. The analysis of this relaxed formulation provides valuable information to solve the precise formulation in a future work. In particular, we have an "optimistic" Pareto front, which informs about the range of values expected in the precise formulation. We also have an idea of the minimum number of patrols

required to reach the minimum length of the routes. The analysis of the lengths of the proposed routes provides information regarding the difference between the proposed routes. This will be useful to set the values for parameter α in the precise model.

Future work can focus on solving the precise formulation. This will probably require the use of a combination of exact methods (like ILP solvers) and heuristics (the so-called *matheuristics*). The information gained from solving the relaxed formulation in this paper will be very valuable in selecting the algorithms and parameters to solve the precise formulation. We also plan to do a deeper analysis of the difference in the lengths of the routes traversed by the patrols. We can consider dynamism as part of the problem formulation. In this case, one patrol must cover emergencies, and the other ones have to re-schedule their routes to maximize the coverage of the conflicting points. Another future line of research is the design of specific algorithms and operators to solve this problem.

References

1. Achuthan, N., Caccetta, L.: Integer linear programming formulation for a vehicle routing problem. European Journal of Operational Research **52**(1), 86–89 (1991). https://doi.org/10.1016/0377-2217(91)90338-V

2. Batty, M., Axhausen, K.W., Giannotti, F., Pozdnoukhov, A., Bazzani, A., Wachowicz, M., Ouzounis, G., Portugali: Smart cities of the future. The European Physical Journal Special Topics **214**(1), 481–518 (2012)

3. Camero, A., Toutouh, J., Stolfi, D.H., Alba, E.: Evolutionary deep learning for car park occupancy prediction in smart cities. In: International conference on learning and intelligent optimization. pp. 386–401. Springer (2018)

4. Camero, A., Alba, E.: Smart city and information technology: A review. Cities **93**, 84–94 (2019). https://doi.org/10.1016/j.cities.2019.04.014

5. Christofides, N.: Vehicle routing. The traveling salesman problem (1985)

6. Cintrano, C., Toutouh, J.: Multiobjective electric vehicle charging station locations in a city scale area: Malaga study case. In: EvoApps (part of EvoStar). pp. 584–600. Springer (2022)

7. Cintrano, C., Toutouh, J., Alba, E.: Citizen centric optimal electric vehicle charging stations locations in a full city: case of malaga. In: Conference of the Spanish Association for Artificial Intelligence. pp. 247–257. Springer (2021)

8. Dantzig, G., Fulkerson, R., Johnson, S.: Solution of a large-scale traveling-salesman problem. Journal of the Operations Research Society of America **2**(4), 393–410 (1954). https://doi.org/10.1287/opre.2.4.393

9. Dantzig, G.B., Ramser, J.H.: The truck dispatching problem. management. Science **6**(1), 80–91 (1959)

10. Dewinter, M., Vandeviver, C., Vander Beken, T., Witlox, F.: Analysing the police patrol routing problem: A review. ISPRS International Journal of Geo-Information **9**(3) (2020). https://doi.org/10.3390/ijgi9030157

11. Ehrgott, M.: Multicriteria Optimization (2. ed.). Springer (2005). https://doi.org/10.1007/3-540-27659-9

12. Gendreau, M., Laporte, G., Semet, F.: The maximal expected coverage relocation problem for emergency vehicles. Journal of the Operational research Society **57**, 22–28 (2006)

13. Khouadjia, M.R., Sarasola, B., Alba, E., Talbi, E.G., Jourdan, L.: Metaheuristics for dynamic vehicle routing. In: Metaheuristics for Dynamic Optimization, pp. 265–289. Springer (2013)

14. Laporte, G.: The vehicle routing problem: An overview of exact and approximate algorithms. European Journal of Operational Research **59**(3), 345–358 (1992). https://doi.org/10.1016/0377-2217(92)90192-C

15. Mukherjee, T., Gupta, S., Sen, P., Pandey, V., Karmakar, K.: Go-park: A parking lot allocation system in smart cities. In: Singh, M., Gupta, P.K., Tyagi, V., Flusser, J., Ören, T. (eds.) Advances in Computing and Data Sciences. pp. 158–166. Springer Singapore, Singapore (2018)

16. OpenStreetMap contributors: Planet dump retrieved from OpenStreetMap. https://www.openstreetmap.org (2017), Accessed: 2021-12-20

17. Risso, C., Cintrano, C., Toutouh, J., Nesmachnow, S.: Exact approach for electric vehicle charging infrastructure location: a real case study in málaga, spain. In: Ibero-American Congress of Smart Cities. pp. 42–57. Springer (2021)

18. Rossit, D.G., Toutouh, J., Nesmachnow, S.: Exact and heuristic approaches for multi-objective garbage accumulation points location in real scenarios. Waste Management **105**, 467–481 (2020)

19. Toth, P., Vigo, D.: Vehicle Routing. Society for Industrial and Applied Mathematics, Philadelphia, PA (2014). https://doi.org/10.1137/1.9781611973594

20. Toutouh, J., Alba, E.: A swarm algorithm for collaborative traffic in vehicular networks. Vehicular Communications **12**, 127–137 (2018)

21. Toutouh, J., Arellano, J., Alba, E.: Bipred: A bilevel evolutionary algorithm for prediction in smart mobility. Sensors **18**(12), 4123 (2018)

22. Toutouh, J., Chicano, F., Gil-Merino, R.: Code and datasets for the paper "distribution of police patrols as a covering problem in smart cities: Fuengirola (spain) use case". Zenodo https://doi.org/10.5281/zenodo.7153528

23. Wang, W., Bao, Y., Long, S.: Rescheduling urban rail transit trains to serve passengers from uncertain delayed high-speed railway trains. Sustainability **14**(9) (2022)

24. Xiong, M., Fei, H., Yan, W.: Research on distribution path of multi-target urban uav (unmanned aerial vehicle) based on epsilon-constraint method. In: 2021 International Conference CISAI. pp. 632–637 (2021). https://doi.org/10.1109/CISAI54367.2021.00127

25. Xu, K., Zheng, M.M., Liu, X.: A two-stage robust model for urban food waste collection network under uncertainty. In: 2021 IEEE International Conference on Industrial Engineering and Engineering Management (IEEM). pp. 824–828 (2021). https://doi.org/10.1109/IEEM50564.2021.9672895

Artificial intelligence for automatic building extraction from urban aerial images

Lucas González[1][0000−0003−2306−7382], Jamal Toutouh[2][0000−0003−1152−0346], and
Sergio Nesmachnow[1][0000−0002−8146−4012]

[1] Universidad de la República, Uruguay
lucas.gonzalez.petti@fing.edu.uy, sergion@fing.edu.uy
[2] Universidad de Málaga, Málaga, Spain
jamal@uma.es

Abstract. Cartographic information is key in urban city planning and management. Deep neural networks allow detecting/extracting buildings from aerial images to gather this cartographic information. This article explores the application of deep neural networks architectures to address automatic building extraction. The results reported that UNet-based architectures provide the most accurate predictions.

Keywords: building detection, artificial neural networks, deep learning

1　Introduction

Cartographic information is an essential tool for urban decision-makers. It plays a key role in urban city planning, citizen welfare, and resources management [5]. ·[5]. High-resolution remote sensing images are now easier and cheaper to acquire using satellites and unmanned aerial vehicles. Thus, cartographic information can be obtained from aerial and satellite images by applying computer vision and artificial intelligence, at limited costs [22].

Land cover and land use classification is a fundamental task in remote sensing. The main goal of land cover and land use classification is to assign a category label to each pixel of an image [9]. It provides the opportunity to get cartographic information and to monitor the evolution of the regions easily [2]. New applications have emerged using this technology, such as precision agriculture [21] and population density estimation [4]. This article focuses on a specific application, the automatic building detection/extraction from optical remote sensing images.

For more than two decades, significant research has been carried out on automatic building extraction. However, incomplete cue extraction, sensor dependency of data, and scene complexity are hindering the success of automatic building extraction and modeling [9]. Nowadays, the most popular methods to address automatic building detection are based on deep learning (DL) using deep neural networks (DNN). DL allows DNNs to learn representations of data samples with several levels of abstraction [6]. DL overcomes the main challenges in the literature on automatic building detection.

This article focuses on DL for automatic building extraction (or detection). Three different DNNs are evaluated: fully convolutional neural networks (FCNs), residual neural networks (ResNet), and UNet. Specifically, the `FCN-ResNet50`, `UNet-ResNet101`, and `UNet-ResNeXt50` architectures are evaluated over the Inria Aerial Image Labeling Dataset (IAD) [14]. The IAD dataset includes aerial images from different regions representing various types of urban areas.

The main results of the research indicate that the proposed models were able to learn building extraction tasks in different building composition contexts. Additionally, better performance was observed in models that were trained with larger image cutouts. Overall, this article contributes to the proposal of a methodology for building identification using FCN and the evaluation of the proposed methodology in a real case study. The research was developed in the context of the SaniBID project, from the Inter-American Development Bank.

The article is organized as follows. Next section describes the problem solved and reviews relevant related works. Section 3 introduces the network architectures analyzed applied to address building extraction. The experimental evaluation is reported in Section 5. Finally, section 6 presents the conclusions and formulates the main lines for future work.

2   Problem definition and literature review

This section describes the addressed problem and reviews relevant related works.

2.1   The automatic building detection problem

The easy acquisition of high-resolution remote sensing images has promoted the emergence of remote sensing studies and applications. Remote sensing methods apply classification at the pixel level to extract/detect artificial objects, such as buildings, roads, and vehicles, to perform mapping and to build cartographic data. One of the most salient applications is automatic building extraction.

Given an aerial/satellite source image, the general idea behind the automatic building extraction is to obtain a 2D labeling output matrix (i.e., a binary image) with the same scale in which the pixels represent whether the corresponding pixel in the source image belongs to a building or not. In general, the 2D labeling output is obtained according to a 2D building class probability matrix. Fig. 1 illustrates an example of the workflow of how a CNN is applied to automatic building extraction. The white pixels in the output indicate that the corresponding pixel in the input image belongs to a building.

In some locations, the shapes and colors of buildings and the objects in their surrounding (such as tanks, lakes, and plants) are very similar, making the automatic building extraction task extremely challenging. As the sensors are able to retrieve more accurate data with higher resolution (such as multispectral images), the applied models get more clues for recognizing the building regions. These models require higher computational resources to deal with such higher information.
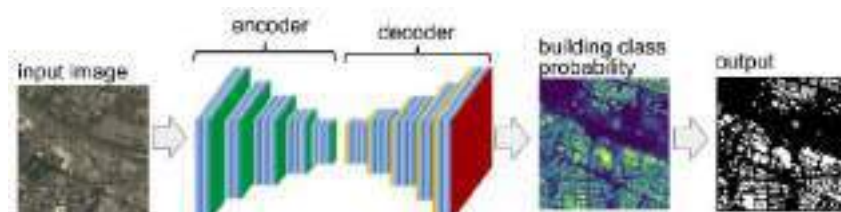
Fig. 1: CNN architecture with encoder and decoder networks applied to automatic building extraction.

The progress of DL has motivated several authors to address the computer vision problem behind automatic building extraction using DNNs. At the same time, machine learning (ML) methods were adopted to deal with the same problem by principally applying feature learning methods.

2.2 Related work

DNNs have shown they are able to learn features describing buildings and map them onto output layers. The output layers of the DNNs represent the probability that a given pixel in an image belongs to a building. The learning methods applied by DNNs are improving their efficacy and efficiency thanks to the development of modern parallel computing processors and graphics processing units. Different annotated aerial high-resolution image datasets have been collected, contributing to the continuous improvement of the accuracy and quality of the results because the training process may use more data.

Variations of convolutional neural networks (CNNs) are the most commonly applied DNNs in building extraction literature. CNNs have been shown to be highly competitive in computer vision tasks, such as large-scale image recognition, object detection, and semantic segmentation [23]. A representative set of these DNNs are FCNs, DeepLab, Pyramid Scene Parsing Network or Pyramid Scene Parsing Network, LinkNet, ResNets, ResNetXt, and UNet [15].

UNet-based DNNs have been the most promising models for building extraction. Two comparative studies [8,10] evaluated UNet against LinkNet on building extraction over the Planet dataset, which covers different areas of Russia. Both studies concluded that UNet provides more competitive results than LinkNet. UNet was also applied over the SpaceNet dataset by Khryashchev et al. [11]. The authors modified the original UNet architecture by including two separate encoders to accept two separate inputs from the same geographical area: an RGB image and an infrared (IR) image. The proposed approach improved the results provided by the original UNet for the regions studied. The same approach (using two separate UNet encoders) was used over Inria Aerial Image Labeling Dataset (IAD) [20]. In this case, the authors evaluated this approach by applying different loss functions during the training process. The experimental analysis did not provide statistical results on which loss function provided the best performance.

A general problem when dealing with building extraction is that the buildings can be located close to each other and be merged into one single object after segmentation (extraction). A variation of UNet was proposed by Pasquali et al. [18] to deal with this problem. The authors proposed using two encoders, one specialized in detecting the buildings and the other in detecting the separation between buildings. The experimental results show that the proposed approach was able to extract the buildings while detecting their boundaries.

Li et al. [12] analyzed five modifications to the UNet architecture (adding and removing layers) to check which modifications showed the best accuracy and were the most computationally efficient. Besides, UNet has been studied over several types of imagery databases, for example, a combination of aerial imagery with data from geographic information systems [17], a high-resolution imagery dataset [1], and a very ultra-high-resolution imagery dataset captured by unmanned aerial vehicles.

This article analyzes different DNNs whose architectures combine UNet and ResNet. In literature, an approach based on this combination, a UNet-ResNet architecture, adapted the UNet to jointly accept different data types such as IR imagery, RGB satellite imagery, and others. Xu et al. [25] proposed this approach to extract buildings on multispectral imagery from Vaihingen and Potsdam, Germany. The method was compared with other remote sensing algorithms, a FCN and a CNN combined with Random Forest. Experimental results showed that UNet-ResNet was better than the other methods in terms of accuracy and F1 score.

The main contribution of the research reported in this article over the previous approach is that the proposed models only use as input RGB images because the other type of data used to address the analyzed problem, e.g., IR imagery or normalized differential vegetation index, is not always available.

3   Deep neural networks considered in the study

This section describes the three main DNNs architectures applied for the automatic building detection problem.

3.1   Residual neural networks

The depth of DNNs is an important factor for their performance and it has proven to be one of the main parameters that allows learning of increasingly complex functions. However, increasing the number of layers brings the main problem of vanishing gradient, which prevents the network weights to be updated, i.e., no learning is being performed [15]. ResNet was developed to mitigate the gradient vanishing problem shown by very dense CNNs. The main idea of ResNet is to introduce skip connections among residual units, which bypass one or more layers (see Fig. 2). Skip connections allow the gradient to flow backward through the shortcut created between layers, from later layers to initial filters [7].
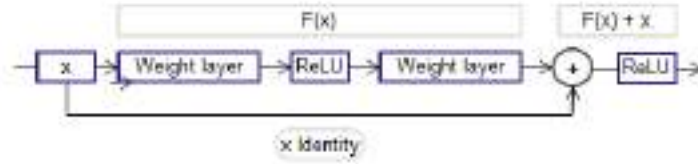
Fig. 2: Basic diagram of a residual unit.

Several variants of ResNet have been proposed, e.g., ResNet34, ResNet50, and ResNet101. The number in the name, i.e., 34, 50, and 101, indicate the number of layers of the network. These CNNs have one MaxPool layer at the beginning and one AveragePool layer at the end, and convolution layers.

Subsequently, the ResNeXt architecture [24] was proposed as an extension to ResNet. ResNeXt applies the "split-transform-merge" paradigm to replace the standard residual blocks. Instead of performing convolutions on the entire input mapping (i.e., using a unique convolution block), the block input is projected onto a set of lower-dimensional representations (channels) to which convolutional filters are applied separately to finally merge the results (i.e., generating multiple convolution paths to different convolution blocks, which outputs are merged by adding them together). In ResNetXt, all the convolution paths have the same topology. The number of paths is a hyperparameter itself called cardinality (C).

Fig. 3 compares a residual block of ResNet50 and one of ResNeXt with C=32. The input of the ResNeXt block is divided into 32 channels of dimension 4 ("split"). Then, the convolutions are performed in each of the paths separately ("transform"). Finally, the channels are added together ("merge"). ResNeXt applies skip connections as in the case of ResNet.

(a) ResNet50   (b) ResNeXt with C=32
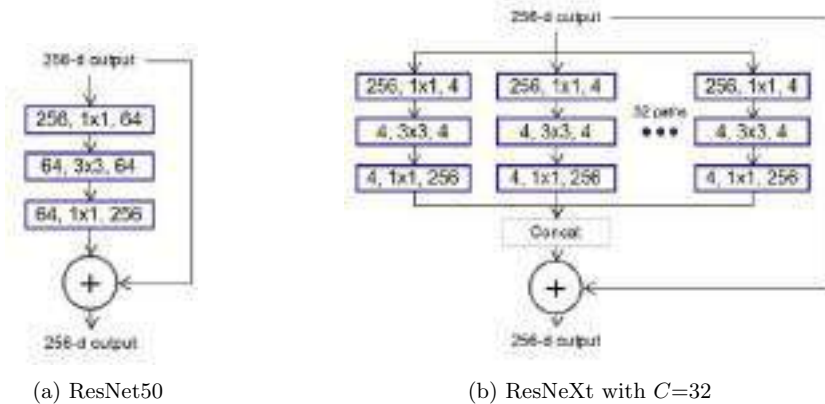
Fig. 3: ResNet50 residual block and ResNeXt block (C=32). Each layer is represented as (number of input channels, kernel size, number of output channels).

3.2   Fully convolutional neural networks

CNNs perform well in addressing image classification, i.e., labeling input images with a unique category. However, CNNs lack the notion of locality mainly because they use fully connected layers in the output. FCNs were proposed to keep the locality concept in learning, required to deal with image segmentation (i.e., the task of labeling individually each pixel of the input image) [13].

FCNs replace fully connected layers in the output with 1×1 convolutional layers. After performing the CNN downsampling operations to the input image, adding the new 1×1 convolutional layers allows upsampling to calculate the pixelwise output (label map). Thus, the classification output and the input image have a one-to-one correspondence at the pixel level: the channel dimension at any output pixel holds the classification results for the input pixel at the same spatial position.

The main advantages of using FCN over CNN are: a) FCNs are better suited to perform image segmentation, and b) FCNs do not necessarily have to receive inputs whose dimensions are of a fixed size.

3.3   UNet

The UNet architecture is based on FCN and it was introduced to address image segmentation task in the field of bio-medicine [19]. The main idea is to have a new ANN trained with few images (and making use of data augmentation) able to be used for image segmentation.

The UNet architecture consists of a contraction path (encoder) and an expansive path (decoder). The encoder is similar to that of FCN architecture and its objective is to capture the context in the image, while the decoder has the function of specifying the location of the elements. The contracting path is more or less symmetric to the expansive path, which yields a U-shaped architecture.

The main benefits of UNet over other ANNs architectures are: a) it has a simple structure built by using convolutional, ReLu activation function, and max pooling layers, and b) it exhibits very competitive performance in segmentation tasks by requiring a little amount of training data (i.e., labeled images).

4   Experimental setup

This section introduces the ANN architectures analyzed, the dataset used to define the problem instances, the evaluation metrics, the hardware platform used to run the experiments, and the software libraries to develop the code.

4.1   Evaluated ANNs architectures

The experimental analysis performed in this study considered more than one single ANN architecture. The idea is to find the best-suited architecture for the building segmentation problem. Among an initial list of candidate architectures

and after performing preliminary experiments, three architectures performed better than the other ones and they were selected to address the problem. These architectures are defined by combining the architectures introduced in Section 3 (i.e., ResNet, ResNeXt, FCN, and UNet). These architectures are:

- `FCN-ResNet50`, a FCN with a ResNet50 as the backbone (i.e., encoder);
- `UNet-ResNet101`, a UNet with a ResNet101 as the backbone;
- and `UNet-ResNeXt50`, a UNet with a ResNeXt50 as the backbone.

The three models were trained by using the same main hyper-parameters: 40 training epochs, learning rate of 8×10^{-5} and Dice Loss as the loss function.

4.2   Problem instance

The experimental evaluation was carried out over the IAD dataset [14]. IAD includes color aerial imagery covering a total area of $810\,\mathrm{km}^2$, divided into $405\,\mathrm{km}^2$ for the training set and 405 km^2 for the testing set. The data covers different regions in the USA and Austria: San Francisco, Chicago, Kitsap County, Bellingham, and Bloomington in the USA; Vienna and Innsbruck in Austria. These regions represent different types of urban areas, from small cities to megacities.

The dataset was constructed by combining public domain images and the official location of public domain buildings from the cadaster. The dataset contains three color bands (Red, Green, and Blue) orthorectified images with a resolution of 1000×1000 pixels and a spatial resolution of 0.3 meters per pixel.

As the ultimate goal of the IAD dataset is to evaluate building remote sensing techniques, the semantic segmentation of the images considers two different labels: building and no-building. Including data (images) from several types of cities allows this dataset to evaluate the generalization capabilities of the segmentation algorithms. Thus, the training and test sets do not overlap, i.e., include images from different cities. For example, the images of Chicago are included in the training set (and not in the test set), and the images of San Francisco are included in the test set (and not in the training set).

The training dataset contains 180 color image frames of size 5000×5000 pixels, covering an area of 1500×1500 meters each. The regions included are Austin, Chicago, Kitsap County, West Tyrol, and Vienna. The test dataset has also 180 images and covers Bellingham, Bloomington, Innsbruck, San Francisco, and East Tyrol. Fig. 4 shows two examples of the images contained in the IAD dataset and their corresponding reference data.

In the proposed experimental evaluation, the automatic building extraction was addressed over IAD (defining an instance named `IAD`). In order to evaluate the impact of the size of the dataset images on the accuracy of the evaluated methods, four additional datasets (instances) were defined by cropping the original IAD images. Four derived instances were defined:

- `IAD1000`: including 1000×1000 pixels images,
- `IAD1250`: including 1250×1250 pixels images,
- `IAD1666`: including 1666×1666 pixels images,
- and `IAD2500`: including 2500×2500 pixels. images.

<div align="center">(a) Chicago   (b) Chicago   (c) Kitsap County   (d) Kitsap County</div>
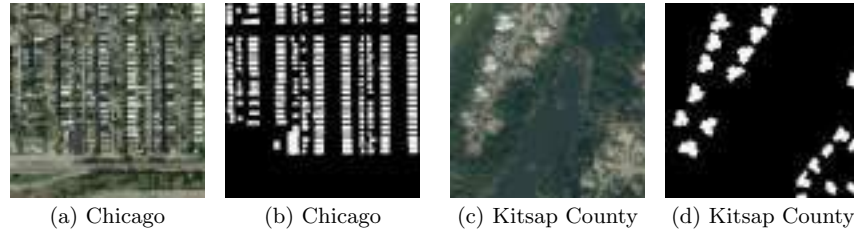
Fig. 4: IAD images (a and c) and their corresponding reference data (b and d).

4.3 Performance metric

The metric used to evaluate the proposed models is Intersection over Union (IoU). IoU is a standard performance metric used for comparing the similarity between two arbitrary shapes, which is useful for image segmentation problems. Given an input image, IoU provides a measure of the similarity between the predicted region by using an ANN and the input image ground truth.

IoU is defined as the size of the intersection divided by the size of the union of the two regions (Equation 1, where X is the actual class mapping of an image (given by the ground truth) and Y is the predicted map by the ANN). IoU is a normalized measure, invariant to the scale of the problem under consideration.

$$IoU = \frac{|X \cap Y|}{|X \cup Y|} \tag{1}$$

4.4 Development and execution platform

The proposed approach was developed in Python using PyTorch and Segmentation Models PyTorch libraries. OpenCV and Albumentation [3] were used for image manipulation and data augmentation. The experimental evaluation was performed on the high performance computing infrastructure of National Supercomputing Center (Cluster-UY), Uruguay [16].

5 Experimental evaluation and discussion

This section describes the main results by reporting IoU and discussing the quality of the predictions.

5.1 Quantitative analysis: IoU results

Table 1, summarizes the IoU results for the three evaluated architectures (i.e., `UNet-ResNet101`, and `UNet-ResNeXt50`) and the five instances (i.e., `IAD1000`, `IAD1250`, `IAD1666`, `IAD2500`, and `IAD`). Besides, the table presents the mean and standard deviation (std) values for all the architectures and all the instances. When evaluating IoU, the higher the better the results.

dataset	architecture			mean	std
	FCN-ResNet50	UNet-ResNet101	UNet-ResNeXt50		
IAD1000	0.8469	0.8802	0.8694	0.8694	0.0139
IAD1250	0.8666	0.8611	0.8771	0.8683	0.0066
IAD1666	0.8782	0.8534	0.8816	0.8711	0.0126
IAD2500	0.9181	0.9057	0.9102	**0.9113**	0.0051
IAD	0.8965	0.9177	0.8965	0.9036	0.0100
mean	0.8813	0.8836	**0.8869**		
std	0.0245	0.0248	0.0146		

Table 1: IoU values obtained for each dataset derived from IAD.

Results of the evaluated models depend on the size of the images in the instances. According to the results in Table 1, UNet-ResNeXt50 is the most competitive ANN architecture taking into account the mean and the standard deviation IoU values. The mean IoU achieved by UNet-ResNeXt50 is the highest one (i.e., it was the model that has best learned to identify buildings from aerial images). Besides, its standard deviation is the lowest, meaning that it was the most robust method. Even though, UNet-ResNeXt50 provided the best IoU values only for two instances, the IAD1250 and IAD1666.

The second most competitive architecture was UNet-ResNet101, which provided the second-best mean IoU value. rngot the best results for the IAD1000 and IAD instances, i.e., for the instances that have the smallest and the biggest images, respectively. FCN-ResNet50 was able to provide the most competitive results only for the IAD2500.

Thus, the results in Table 1 show that in general the ANN architectures that are based on UNet provide better results than the one based on FCN. This is because UNet is an evolution of FCN that provides enhancements that make it better suited for image segmentation tasks such as in the building extraction from aerial images. Likewise, the results show that the use of ResNeXt as a backbone can improve the results compared to the use of the basic ResNet.

5.2 Qualitative results analysis: output labeling map results

In order to perform a qualitative analysis, four areal images from the testing dataset of IAD were selected to compute the labeling map by using the three studied architectures. Figs. 5–8 present the areal image, the ground truth (i.e., true labeling map), and the output labeling maps for each one of the models.

Fig. 5 corresponds to an areal image from a rural area where there are just a few small buildings. In general, the three models provided similar results. They were able to extract the buildings, differentiating them from the vegetation and the roads. Focusing on UNet-ResNeXt50, the right side of the image in Fig. 5e that the model was able to extract different buildings that were not found by the other models. These different buildings are seen on the original aerial image in Fig. 5a, but the map in Fig. 5a labels all of them as one unique building.

(a) Input image   (b) Label map

(c) FCN-ResNet50 output   (d) UNet-ResNet101 output   (e) UNet-ResNeXt50 output
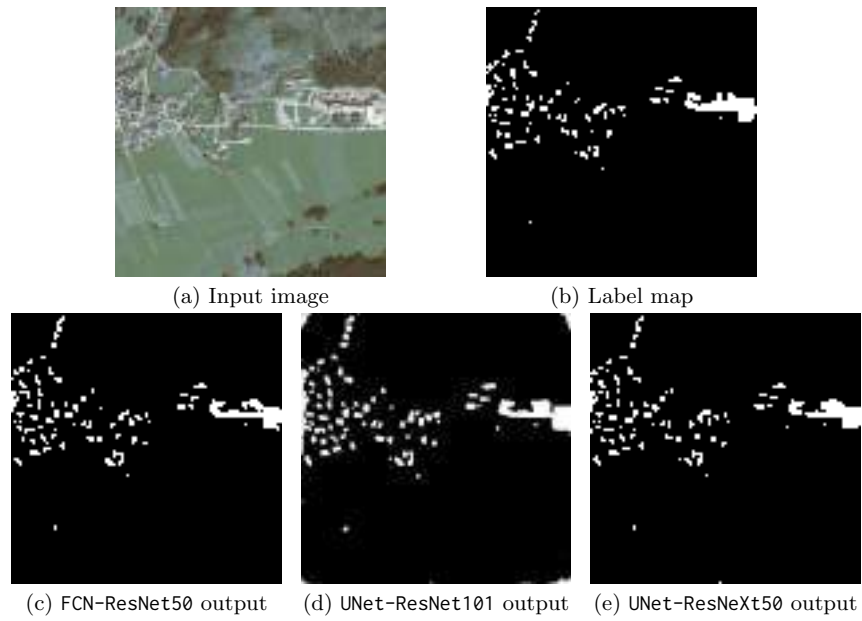
Fig. 5: Image `tyrol-w322500_2500` from `IAD2500` results.

(a) Input image   (b) Label map

(c) FCN-ResNet50 output   (d) UNet-ResNet101 output   (e) UNet-ResNeXt50 output
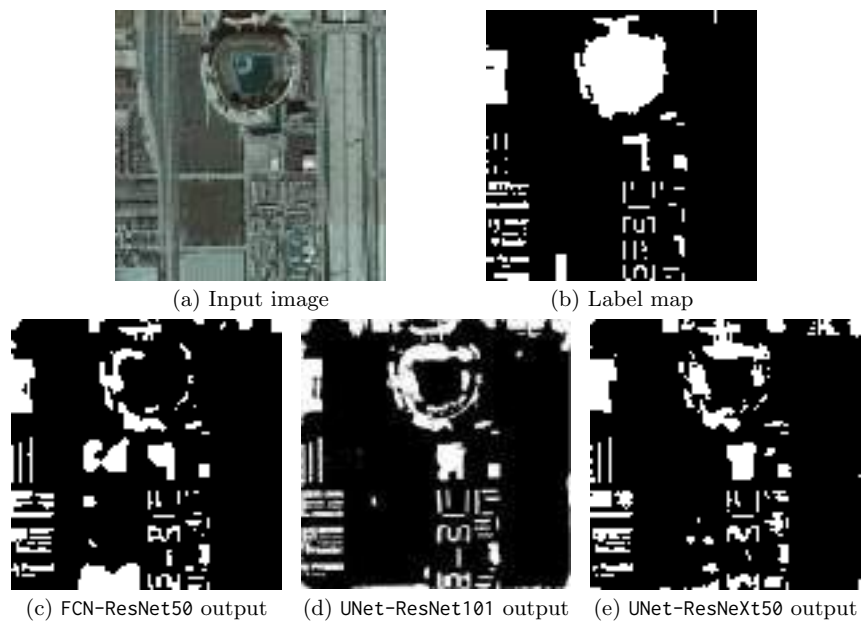
Fig. 6: Image `chicago312500_2500` from `IAD2500` results.

Figs. 6 and 7 represent areas with an increasing number of buildings in the suburbs of Chicago. In the results shown in Fig. 6, `FCN-ResNet50` provided the least competitive results because the output labeling map includes several false positives (i.e., several white shapes in the output labeling map that in the real image do not correspond to any building). The other two models got pretty similar results. However, the shapes of the buildings extracted by `UNet-ResNet101` match better with the ground truth shapes than the shapes computed by`UNet-ResNeXt50`. It is remarkable that the three models were able to extract buildings with special shapes like the baseball stadium, where the predictions were able to distinguish the playing field from the stands.

(a) Input image　　　　　　　　　　(b) Label map

(c) `FCN-ResNet50` output　(d) `UNet-ResNet101` output　(e) `UNet-ResNeXt50` output
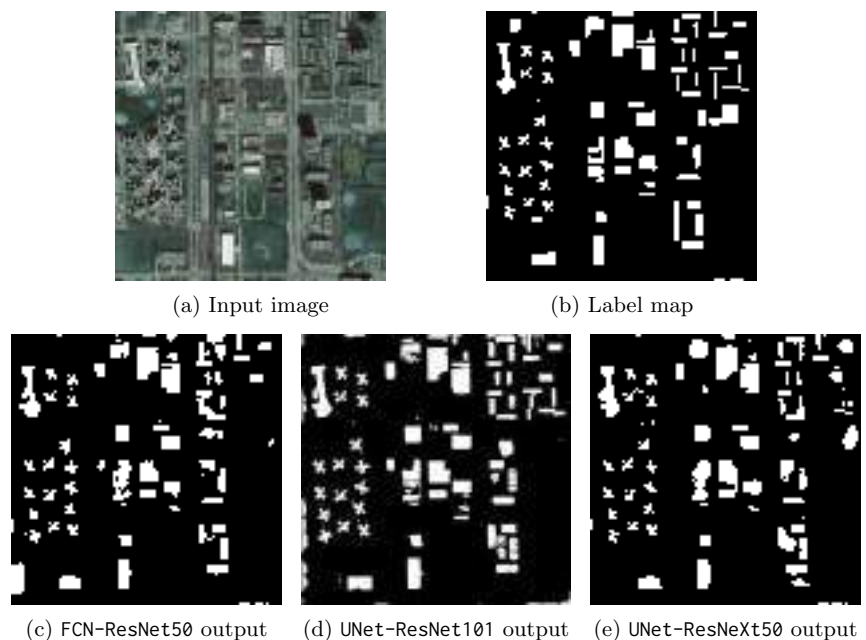
Fig. 7: Image `chicago322500_2500` from `IAD2500` results.

The area represented in Fig. 7 includes buildings of different shapes, including cross-shaped buildings. In general, all the evaluated models were able to predict all the buildings, regardless of the shape. The results show that `UNet-ResNet101` provided the best results. `UNet-ResNet101` was able to extract all the buildings while getting a negligible number of false positives. `FCN-ResNet50` and `UNet-ResNeXt50` were able to extract almost all buildings, but the shapes do not fit the ground truth in Fig. 7b as well as the shapes extracted by the `UNet-ResNet101`.

(a) Input image

(b) Label map

(c) FCN-ResNet50 output (d) UNet-ResNet101 output (e) UNet-ResNeXt50 output
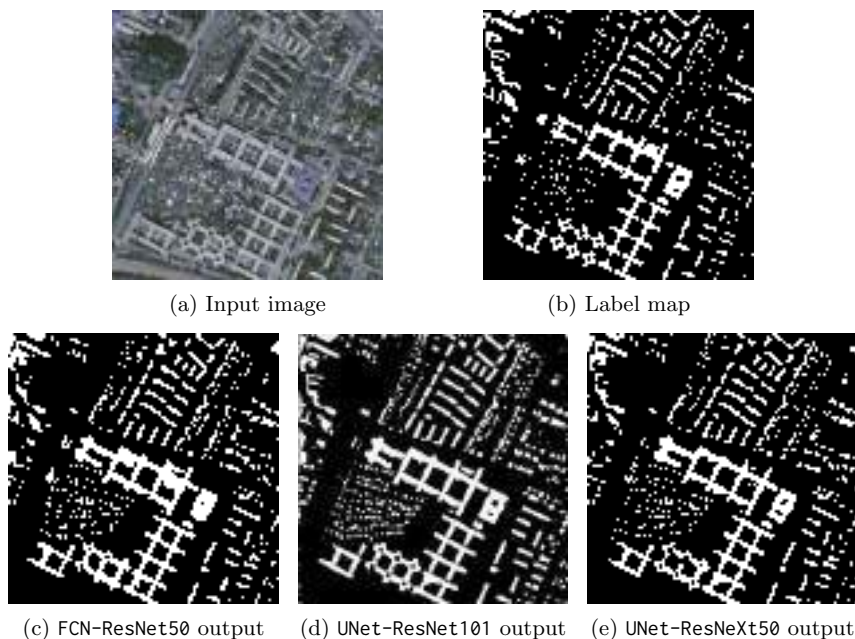
Fig. 8: Image vienna32250_0 from IAD2500 results.

The aerial image in Fig. 8 is taken from an urban area with a high density of buildings and several roads in Vienna. In turn, it includes buildings of different sizes (ranging from small houses to big condos). The results provided by the three models show that they were able to extract the buildings distinguishing them from other types of infrastructures included in the image and the roads. Besides, the three models correctly labeled buildings of any size. In this case, it is pretty difficult to select which architecture got the most competitive results because the output labeling maps are close.

Summarizing, the qualitative results are in line with the quantitative results discussed in Section 5.1. The accuracy of the results of the networks build using a UNet architecture (i.e., UNet-ResNet101 and UNet-ResNeXt50) is better than the network based on FCN.

6 Conclusions and future work

This article presented a study of different architectures of deep neural networks in the task of buildings extraction.

Based on the related works, the FCN, ResNet, UNet architectures and their combinations were selected for the analysis. Special emphasis was placed on exploring the network encoder, using the ResNet architecture and its variants

for that purpose. Besides the experiments made for the mentioned architectures, the effect of different image sizes in training was explored. Four datasets were constructed from the standard IAD dataset, and for each of them the three candidate models were trained if the size of training images had an impact on performance.

From the considered architectures, a better performance from those based on UNet was computed, compared to the FCN variants. Regarding the size of the training images, for the studied dataset a tendency to better performance was detected over the models trained with larger images.

The results obtained in the experimental evaluation suggest that it is feasible developing automatic strategies for building detection using deep neural networks. Results from these strategies are valuable inputs for addressing more complex tasks such as population estimation or planning wastewater treatment in urban areas.

The main lines for future work are related to extending this study to datasets constructed from cities with dissimilar characteristics, e.g., to model scenarios with a poor urban development where buildings patterns are not regular, and introducing automatic methods for the calibration of certain hyperparameters of the studied neural networks, such as the learning rate and the cost function.

References

1. Ahmed, N., Mahbub, R.B., Rahman, R.M.: Learning to extract buildings from ultra-high-resolution drone images and noisy labels. International Journal of Remote Sensing **41**(21), 8216–8237 (2020)
2. Asokan, A., Anitha, J.: Change detection techniques for remote sensing applications: a survey. Earth Science Informatics **12**(2), 143–160 (2019)
3. Buslaev, A., Iglovikov, V., Khvedchenya, E., Parinov, A., Druzhinin, M., Kalinin, A.: Albumentations: Fast and flexible image augmentations. Information **11**(2) (2020)
4. Doda, S., Wang, Y., Kahl, M., Hoffmann, E., Taubenböck, H., Zhu, X.: So2sat pop–a curated benchmark data set for population estimation from space on a continental scale. arXiv preprint arXiv:2204.08524 (2022)
5. Donnay, J., Barnsley, M., Longley, P.: Remote sensing and urban analysis: GIS-DATA 9. CRC Press (2000)
6. Goodfellow, I., Bengio, Y., Courville, A.: Deep learning. MIT press (2016)
7. He, K., Zhang, X., Ren, S., Sun, J.: Deep residual learning for image recognition. In: IEEE Conference on Computer Vision and Pattern Recognition. pp. 770–778 (2016)
8. Ivanovsky, L., Khryashchev, V., Pavlov, V., Ostrovskaya, A.: Building detection on aerial images using u-net neural networks. In: 24th Conference of Open Innovations Association. pp. 116–122 (2019)
9. Jahan, F., Zhou, J., Awrangjeb, M., Gao, Y.: Fusion of hyperspectral and lidar data using discriminant correlation analysis for land cover classification. IEEE Journal of Selected Topics in Applied Earth Observations and Remote Sensing **11**(10), 3905–3917 (2018)

10. Khryaschev, V., Ivanovsky, L.: Urban areas analysis using satellite image segmentation and deep neural network. In: E3S Web of Conferences. vol. 135, p. 01064. EDP Sciences (2019)

11. Khryashchev, V., Larionov, R., Ostrovskaya, A., Semenov, A.: Modification of u-net neural network in the task of multichannel satellite images segmentation. In: East-West Design & Test Symposium. pp. 1–4 (2019)

12. Li, W., He, C., Fang, J., Zheng, J., Fu, H., Yu, L.: Semantic segmentation-based building footprint extraction using very high-resolution satellite images and multi-source gis data. Remote Sensing **11**(4), 403 (2019)

13. Long, J., Shelhamer, E., Darrell, T.: Fully convolutional networks for semantic segmentation. In: Proceedings of the IEEE Conference on Computer Vision and Pattern Recognition (CVPR) (June 2015)

14. Maggiori, E., Tarabalka, Y., Charpiat, G., Alliez, P.: Can semantic labeling methods generalize to any city? the inria aerial image labeling benchmark. In: IEEE International Geoscience and Remote Sensing Symposium. pp. 3226–3229 (2017)

15. Minaee, S., Boykov, Y., Porikli, F., Plaza, A., Kehtarnavaz, N., Terzopoulos, D.: Image segmentation using deep learning: A survey. IEEE Transactions on Pattern Analysis and Machine Intelligence **44**(7), 3523–3542 (2022)

16. Nesmachnow, S., Iturriaga, S.: Cluster-UY: Collaborative Scientific High Performance Computing in Uruguay. In: Supercomputing, Communications in Computer and Information Science, vol. 1151, pp. 188–202. Springer (2019)

17. Pan, Z., Xu, J., Guo, Y., Hu, Y., Wang, G.: Deep learning segmentation and classification for urban village using a worldview satellite image based on u-net. Remote Sensing **12**(10), 1574 (2020)

18. Pasquali, G., Iannelli, G., Dell'Acqua, F.: Building footprint extraction from multispectral, spaceborne earth observation datasets using a structurally optimized u-net convolutional neural network. Remote Sensing **11**(23), 2803 (2019)

19. Ronneberger, O., Fischer, P., Brox, T.: U-net: Convolutional networks for biomedical image segmentation. In: Medical Image Computing and Computer-Assisted Intervention. pp. 234–241 (2015)

20. Sedov, A., Khryashchev, V., Larionov, R., Ostrovskaya, A.: Loss function selection in a problem of satellite image segmentation using convolutional neural network. In: Systems of signal synchronization, generating and processing in telecommunications. pp. 1–4 (2019)

21. Sishodia, R., Ray, R., Singh, S.: Applications of remote sensing in precision agriculture: A review. Remote Sensing **12**(19), 3136 (2020)

22. Weng, Q., Quattrochi, D.A.: Urban remote sensing. CRC press (2018)

23. Wurm, M., Stark, T., Zhu, X., Weigand, M., Taubenböck, H.: Semantic segmentation of slums in satellite images using transfer learning on fully convolutional neural networks. ISPRS Journal of Photogrammetry and Remote Sensing **150**, 59–69 (2019)

24. Xie, S., Girshick, R., Dollár, P., Tu, Z., He, K.: Aggregated residual transformations for deep neural networks. In: 2017 IEEE Conference on Computer Vision and Pattern Recognition (CVPR). pp. 5987–5995 (2017)

25. Xu, Y., Wu, L., Xie, Z., Chen, Z.: Building extraction in very high resolution remote sensing imagery using deep learning and guided filters. Remote Sensing **10**(1), 144 (2018)

Detecting air conditioning usage in households using unsupervised machine learning on smart meter data

Rodrigo Porteiro[1][0000−0001−7793−1645] and
Sergio Nesmachnow[2][0000−0002−8146−4012]

[1] UTE
rporteiro@ute.com.uy
[2] Universidad de la República, Uruguay
sergion@fing.edu.uy

Abstract. This article presents an unsupervised machine learning approach for the problem of detecting use of air conditioning in households, during the summer. This is a relevant problem in the context of the modern smart grid approach under the paradigm of smart cities. The proposed methodology applies data analysis, a thermal inertial model for estimating the temperature inside a household, statistical analysis, clustering, and classification. The proposed model is validated on a real case study, considering households with known use of air conditioning in summer. In the evaluation, the proposed classification methodology reached an accuracy of 0.897, a promising result considering the very small cardinality of the set of households. The proposed method is valuable since it applies an unsupervised approach, which does not require large volumes of labeled data for training, and allows determining characteristics in the electricity consumption patterns that are useful for categorization. In turn, it is a non-intrusive method and does not require investing in the installation of complex devices or conducting consumer surveys.

Keywords: unsupervised learning, data analysis, residential electricity consumption

1 Introduction

Currently, electricity utilities have advanced strongly in the deployment of various smart devices that assist monitoring and decision making. Final consumers have taken a very active role, given that there is greater knowledge of their behavior and their use of the electrical resource [23]. For utilities, it is essential to analyze the large amount of data gathered by using smart devices, to add value to the electricity business. In the residential sector, the existence of smart meters is crucial to improve management and profit. At the same time, it makes it possible to carry out commercial policies in which the consumer is a key player and feels part of the improvements.

Usually, utilities only consider the benefits obtained by being able to operate the smart meter remotely when analyzing the technical requirements of the smart meter to be deployed. For example, the benefits to obtain consume measurements without the presence of an employee in the field, to the detect blackouts remotely, or to perform remote power cuts in case of unpaid bills. For this reason, many electric utilities do not properly plan the selection of smart meters considering the benefit they will generate when analyzing the measured data. One of the features of smart meters that is not properly valued is the measurement frequency. Many of the tools that can be developed using consumption data require a high granularity in the values measured from smart meters. Another technical feature of smart meters usually underestimated for the creation of these tools, is the measurement of harmonics.

A very useful approach for building a detailed profile of consumers is to detect which electrical devices are in use. The literature shows that for obtaining a very precise disaggregation of the electrical appliances uses from smart meter data, very high measurement frequency and harmonic measurement are needed [9,10]. If the smart metering infrastructure is already deployed additional devices would need to be installed in households. However, this type of intrusive intervention is not always financially profitable and is often frowned upon by clients.

This article addresses the problem of detecting the use of air conditioning in summer, using the existing infrastructure of the Uruguayan electricity company (UTE). The company deployed smart meters on residential consumers, so replacing them would be very expensive. The meters are not capable of measuring harmonics, and have a quarterly consumption measurement frequency. However, despite the technological limitations, it is feasible to detect air conditioners using the available information and climate data. Detecting the use of this type of device, which is intensive in the summer, allows designing appropriate energy efficiency policies and commercial products, to optimize the electrical system and reduce the cost for the company, for consumers, and for the country [2,12].

An unsupervised machine learning algorithm is proposed to detect the use of air conditioning in summer. Given a household, the proposed methodology applies urban data analysis [15] over consumption measurements, and temperature and irradiance measured at the nearest weather station. An approximation of the internal temperature of the household is then obtained a simplified model of thermal inertia for a standard Uruguayan residential building. Thus, a function is obtained that approximates the internal temperature from the external temperature and the irradiance. With the fifteen-minute data on consumption and internal temperature, consumption measurements less than 10% of the average consumption are excluded, as a criterion to consider the moments in which there is activity in the household. The resulting data is classified into two sets using the k-means clustering algorithm, only considering its temperature. A set of consumptions for low temperatures and another one for high temperatures are obtained. The average consumption is calculated for each set and if the difference between these values is greater than a threshold value, the consumer in the studied household is classified as an air conditioning user.

A practical validation of the proposed methodology is presented for a case study with a set of 29 households for whom the use of air conditioning in summer is known. The main results of the research applying the proposed methodology to this set, yields an accuracy of 0.897. This result is promising, especially considering that the study could only be carried out on a very small set of households due to lack of labeled consumers. The proposed method is valuable since it applies an unsupervised approach, which does not require large volumes of labeled data for training and it is non-intrusive. Thus, it is a viable alternative to intrusive methods, which require replacing the currently installed smart meters with more sophisticated ones (a very costly task in economical terms). In turn, having labeled data to use supervised learning or to validate the presented algorithm requires conducting surveys that demand a hard and expensive task. Therefore, the proposed methodology has the advantage that it can be applied immediately using the current installed infrastructure, without incurring in significant investments costs.

The article is organized as follows. Section 2 describes the problem addressed in this article and reviews related works. Section 3 describes the proposed approach, including a description of data sources, the process of data preparation and the definition of the classification algorithm. Details of the developed implementation are provided in Section 4. Section 5 present the experimental evaluation of the proposed approach and discusses the obtained results. Finally, Section 6 present the conclusions of the research and formulates the main lines for future work.

2   Problem definition and literature review

This section describes the general problem addressed problem and reviews relevant related works.

2.1   General problem: Energy disaggregation

Traditionally, electricity companies have mainly worked using static information from consumers. The only source of data that dynamically linked consumers to the company was the measurement that a company official obtained monthly from traditional meter. Nowadays, the massive deployment of smart meters has allowed companies in the energy sector to know in greater detail the behavior of consumers, regarding energy use. It is possible to detect various details regarding the behavior of consumers with greater or lesser accuracy, depending on the technical specifications of the smart meters deployed.

If smart meters with high metering frequency and harmonic measurement are available, it is possible to successfully address the overall problem of energy disaggregation. It consists of identifying the individual consumption of different household appliances, using only aggregate measurements of all the measured variables. Many studies have analyzed the problem of energy disaggregation using smart meters with advanced technological features.

2.2　Problem description: detection of air conditioning usage

The addressed problem is detecting the use of air conditioners in summer, from smart meters with a measurement frequency of fifteen minutes and without measuring harmonics. Air conditioner is the only electrically-intensive device to lower the temperature of households in the summer. It is highly correlated with climatic variables and allows addressing the classification problem without the need to have labeled consumers or to have more advanced measurement devices. Then, the solution proposed is considered non-intrusive.

The input data consist of electricity consumption curves with quarterly frequency, the geographical location of the consumer, and weather information to approximate the temperature inside the household. One of the hypotheses assumed is that the only electrical device for thermal comfort in summer with a relevant consumption is the air conditioner. Other thermal conditioning devices for the summer have negligible power consumption respect to air conditioners. For example, the average power of fans is 50W and coolers 100W, compared to 1000W to 2000W for air conditioner. The other hypotheses is that its use is strongly correlated with the internal temperature of the household.

2.3　Related work

The application of energy disaggregation tools to the residential sector has developed strongly after the high penetration of smart meters in electrical systems. The addressed problem is to estimate the consumption of each of the electrical devices in the household, considering as input the overall energy consumption. When disaggregation is coarse-grained, the main objectives are related to provide more information to consumers on energy bills, or even offer specific commercial products depending on the type of use. When the disaggregation problem is solved in real time, the main applicability is to identify problems such as electrical losses in the household, detection of overloads, and other relevant issues.

Non-intrusive load monitoring (NILM) and the dissagregation problem in households were introduced by Hart [11], as an alternative to existing intrusive, hardware-based monitoring approaches. The main advantages of NILM is that it does not require installing specific devices, but makes use of existing smart meters, focusing on more sophisticated software for data analysis. Hart also introduced the binary (ON/OFF) variant of the dissagregation problem and proposed the principle of continuity switch, i.e., assuming that in a given small time interval, few appliances change their status (from ON to OFF or vice versa).

Many recent articles have dealt with NILM as a learning problem, applying computational intelligence to solve it, both in supervised and unsupervised fashion. Supervised approaches (e.g., Bayesian learning, neural networks (ANN), patterns similarity) make use of specific datasets of electricity consumption of each device and the aggregate household consumption signal. Unsupervised approaches (e.g., Hidden Markov Models, HMM) seek to learn the ON/OFF state of devices from the aggregate consumption, without explicit knowledge about the consumption of each device [4].

Kelly and Knottenbelt [13] studied ANNs for the NILM problem, using the UK-DALE dataset, which includes the electricity consumption of appliances (fridge, washing machine, dishwasher, kettle, and microwave) in five houses in the UK. A denoising autoencoder ANN computed the best results, outperforming over a long short-term memory (LSTM) and a rectangles ANN. Kolter and Johnson [14] introduced the REDD dataset to study a HMM for the NILM problem. Mixed results were computed over two weeks of data from five households (64.5% accuracy on the training set and just 47.7% in the evaluation test).

Our previous articles [6,7] studied the dissaggregation of electricity consumption in residential buildings and proposed a method based on detecting similarities in the electricity consumption patterns from previously recorded labeled datasets. The method was evaluated over four different problem instances that model real household scenarios, reporting accurate results regarding standard prediction metrics.

Computational models are also very valuable for energy demand management and demand response [16,17]. Our previous articles [19,20] applied computational methods for defining a thermal index associated with an active demand management that interrupts domestic electric water heaters. Specific models using Extra Trees Regressor and a linear model were defined for water utilization and water temperature considering continuous power consumption measurements of water heaters, and Monte Carlo simulations to compute the proposed index. The approach was evaluated using real data from the ECD-UY dataset, Uruguay [8]. The thermal discomfort index correctly modeled the impact on temperature, providing accurate inputs for demand response and load shifting. Data analysis and computational intelligence techniques were also applied for the characterization and forecasting of short term electricity consumption on industrial facilities [21,22]. The model was validated for an industrial park in Burgos (Spain), the total electricity demand for Uruguay, and demand from a distribution substation in Montevideo (Uruguay).

3 The proposed approach for the detection of air conditioning usage in summer

This section describes the data sources, the methodology to approximate indoor temperature, the data preparation and the methodology applied for the detection of air conditioning usage in summer.

3.1 Data sources

The consumption data used in this article was provided by the Uruguayan National Electricity Company (UTE). It corresponds to "Total household consumption" and "Disaggregated electricity consumption by appliance", two of the three subsets included in the ECD-UY dataset [8]. The Total household consumption set gathers data of quarterly total consumption from 110953 households and

Disaggregated electricity consumption by appliance contains data of 9 households with minutal measures and dissagegated consumption by appliance. These sets have measurements from January 1, 2019 to November 2, 2020. In turn, data obtained from 20 additional households from known consumers was used for validation. The overall dataset includes 29 labeled households (19 use air conditioning in the summer and 10 do not).

To approximate the temperature of the household, which is the variable that has the strongest correlation with the use of air conditioning, climate information on temperature and solar irradiance was used. The data used was obtained manually from Uruguayan Institute of Meteorology (INUMET), disaggregated by weather station. Only data from January 1, 2019 to November 2, 2020 were considered, to match with the consumption data. Therefore, the horizon of data analyzed in this article is determined by these dates.

Likewise, both the consumption and the climate information contains the location of the measurement, which allows households to be associated with the climate data obtained from the nearest station.

3.2 Approximation of the internal temperature of the household from the external temperature and solar irradiance

An approximation of the temperature inside each household is needed for the proposed model. The proposed approach consists in estimating the inside temperature from the curve of the outside temperature and the external solar irradiance.

The thermal inertia that occurs inside the household is considered. The most relevant factors to model this effect are the construction material, the number of windows, and the insulation. Cengel et al. [5] showed that the heat flux is proportional to the magnitude of the temperature gradient, and opposite in sign. This article only requires an approximation of the internal temperature, and for this purpose a simplified model, proposed by Absi et al. [1] is used.

The model by Absi et al. assumes that the effect of the walls of a house produces two transformations in the external temperature curve: a delay (thermal lag) and an attenuation in the amplitude of the curve. Fig. 1 shows that the amplitude of the indoor temperature (A_{ind}) is smaller than the amplitude of the external temperature (A_{ext}). It also shows that indoor temperature is lagged by $\beta \times w_{irr}$, the thermal lag considering the irradiance.

According to the aforementioned model, these parameters depend on the wall material, the wall thickness, and the solar irradiance. Intuitively, the flow of heat from outside to inside is more delayed (thermal lag) and also the indoor thermal amplitude decreases when thicker and more robust walls are used, and the lower the solar irradiance. For instance, if the wall is extremely thin, the indoor temperature and the external temperature are almost equal. This model provides a rough simplification of the real temperature dynamics, which is appropriate for the proposed case study, especially considering that there is not enough information about households to estimate the internal temperature using a more complex model.
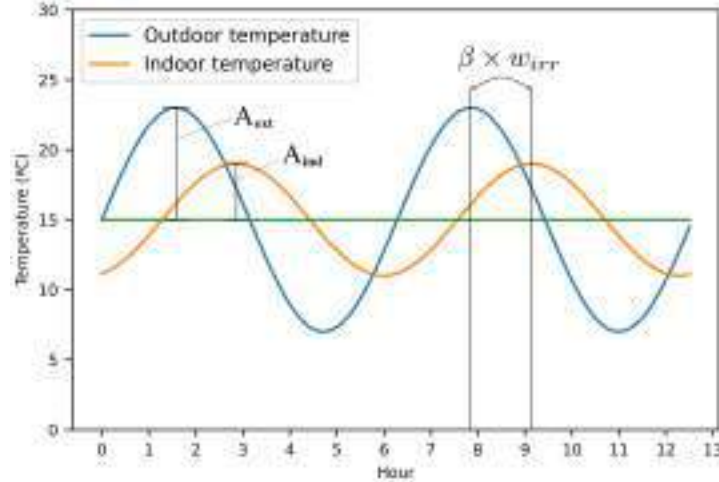
Fig. 1: Amplitude variation and thermal lag of indoor and outdoor temperature.

The internal temperature is represented as a function of the external temperature and the irradiance, according to the formulation in Eq. 1.

$$T_{ind}(t) = (T_{ext}(t - \beta \times w_{irr}) - \overline{T}_{24}(t))\rho \times w_{irr} + \overline{T}_{24}(t) \tag{1}$$

In Eq. 1, the function $T_{ind}(t)$ is the indoor temperature at time t and the function $T_{ext}(t)$ is the external temperature at time t. The function $\overline{T}_{24}(t)$ is the external average temperature of the last 24 hours, used as a baseline to estimate the amplitude. Then, $\beta \times w_{irr}$ is the thermal lag and the parameter $\rho = A_{ind}/A_{ext} \times w_{irr}$ captures the amplitude reduction. Finally, $w_{irr} = 1$ when irradiance is 0 and a maximum value when irradiance reach its maximum. So β and ρ are the thermal lag and the amplitude reduction factor when solar irradiance is 0.

3.3   Data preparation

The objective of preparing the data is to obtain a historical bivariate series for the summer, in the considered analysis horizon. The first variable of the series represents the electricity consumption of the considered household and the second variable is an approximation of the internal temperature. First, since the temperature and irradiance data are hourly, they are converted to quarterly simply by using the hourly value. There are no missing values in either the consumption data or the climate data.

To generate the series of indoor temperatures, the parameters β, ρ and w_{irr} must be estimated. β, ρ and w_{irr} are estimated by measuring real temperature curves in three types of buildings (considering the most used construction materials in Uruguay: brick, concrete and wood [3]. First, measures were performed during the night, so $w_{irr} = 1$ (since there is no irradiance).

According to Eq. 1, $\beta \times w_{irr}$ is the thermal lag between indoor and outdoor temperature, considering irradiance. The lag is calculated using the measured curves at night (i.e., the difference between T_{ext} and T_{ind} along the x-axis). Then, setting $w_{irr} = 1$, the value of β is determined. Analogously, $\rho \times w_{irr} = A_{ind}/A_{ext}$; A_{ind} and A_{ext} are measured, and $w_{irr} = 1$ at night, so, the value of ρ is determined.

Then, fixing β and ρ, the value of w_{irr} is estimated for a completely clear day using Eq. 1, so the maximum w_{irr} is determined (w_{irr}^{max}). All estimations are performed using real indoor and external temperature measures. To compute Eq. 1 for an intermediate value of irradiance I_{real}, w_{irr} must be calculated for I_{real}, proportionally. So $w_{irr} = I_{real} \times (w_{irr}^{max} - 1)/(I_{max} - 1)$, where I_{max} is the maximum irradiance measured in a clear day.

Once the three relevant parameters of the temperature model are estimated, the indoor temperature series is obtained from the outdoor temperature series and irradiance series applying Eq. 1. This procedure is performed for each household, using weather data of the closest meteorological station. Fig. 2 presents the internal temperature curves for the same external temperature and solar irradiance, depending on the type of construction.
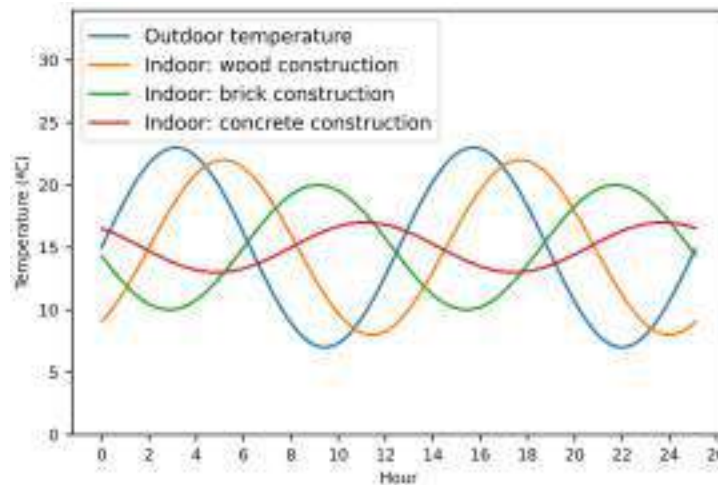
Fig. 2: Indoor temperature curves for wood, brick and concrete constructions.

The graphic in Fig. 2 shows that brick constructions present a thermal inertia between wood and concrete constructions. In the proposed study, since there is no information on the construction material of each household, the set of parameters estimated for a brick construction was used, considering that it represents a non-extreme thermal inertia. Also, brick is widely used in Uruguay, due to solidity and durability [3].

Finally, on the bivariate series with quarterly values, the data that do not correspond to the summer months (December, January, February, and March) are excluded. Then, the maximum consumption for the resulting data is obtained, and all data with consumption less than 10% of the maximum are excluded from the series, considering that in those cases there is no activity in the household.

3.4 Unsupervised machine learning classification algorithm

The unsupervised classification algorithm must take into account the high correlation between the consumption of the household and its internal temperature when there is activity in it. In the preparation of data, very low consumption was excluded, to focus on the correlation between consumption and temperature in the case of activity in the household. It is important to consider that if there is any device with relevant consumption not associated with thermal conditioning, it will not present a strong correlation with temperature.

The proposed algorithm consists of performing the following seven steps, including data preparation:

1. Construction of the indoor temperature curve of the analyzed household, using the technique described in Section 3.2 applied to the meteorological data of the nearest station. As a result, a bivariate quarterly series is obtained with consumption and indoor temperature variables.
2. From the series obtained, entries with consumption less than 10% of the maximum of the series are excluded.
3. A clustering is performed applying k-means, with $k = 2$ in the temperature variable. Thus obtaining a set of consumption values for low temperatures (L) and another set of consumption values for high temperatures (H).
4. A clustering is performed applying k-means, with $k = 2$ in the consumption variable for the set L (obtaining two classes, L_L and L_H).
5. A clustering is performed applying k-means, with $k = 2$ in the consumption variable for the set H (obtaining two classes, H_L and H_H).
6. $center_L = (T_L, E_L)$ is defined as the center of L_H and $center_H = (T_H, E_H)$ as the center of the cluster H_H
7. if $E_H/E_L \geq \Theta$, then the consumer is classified as user of air conditioning, otherwise it is classified as non-user of air conditioning. Parameter Θ must be calibrated considering the average increase in quarterly consumption when the air conditioning is on. The calibration methodology is described in the Section 5.3.

Figure 3 presents the main steps specified in the previous paragraph. In Fig. 3a, the original data for a consumer is presented (step 1). Fig. 3b shows the data after excluding low consumptions (step 2). Fig. 3c presents the data after step 3, the class L in blue and the class H in orange. Finally, in Fig. 3d, all four classes are presented: L_L, L_H, H_L and H_H after step 6. The blue cross is $center_H = (T_H, E_H)$ and the orange cross is $center_L = (T_L, E_L)$. In this case, the value of E_H is significantly greater than the value of E_L, so with a value of Θ barely greater than 1, the condition $E_H/E_L \geq \Theta$ would be met and the consumer would be classified as an air conditioning user.

(a) Original data.   (b) Low consumptions excluded.

(c) Temperature clustering.   (d) E_H and E_L calculation.
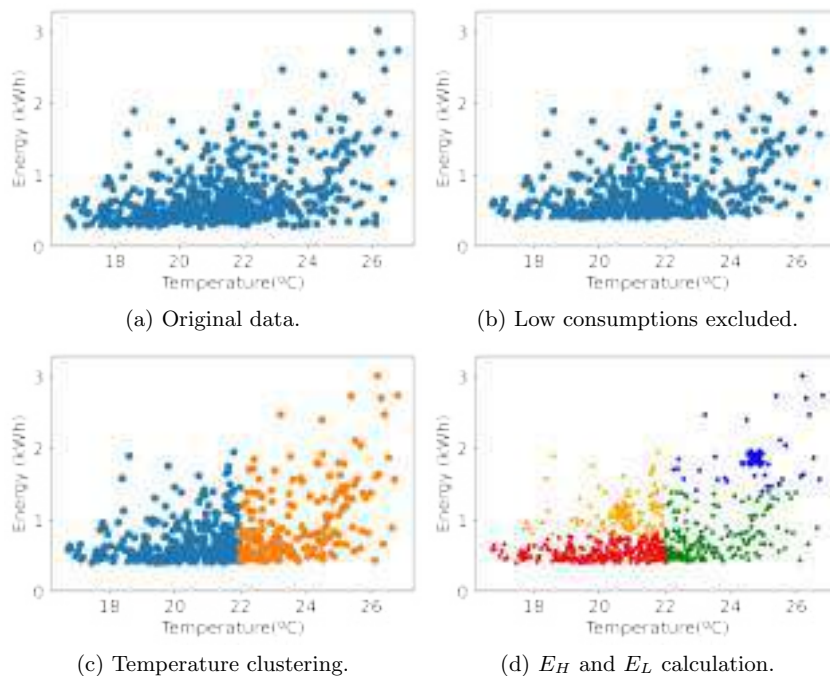
Fig. 3: Main steps of the proposed classification algorithm.

The rationale behind the proposed algorithm for classification is that if there is indeed an intensive electrical use associated with thermal comfort, consumption at high temperatures tends to be greater that consumption at low temperatures. By separating the consumption by temperature (low and high) into two sets, and then taking the averages of the highest consumption of those sets, if the value associated with high temperatures is significantly higher than that associated with low temperatures, this is due to the use of air conditioning, since no other thermal conditioning device for summer consumes a significant amount of energy. However, if the averages are similar, there is not statistical significance in the reported eleectricity consumption values with respect to the indoor temperature and the consumer is classified as a non air-conditioning user.

4   Implementation

This section presents the implementation details of the proposed solution.

4.1   Implementation details

The implementation of the proposed classification algorithm involved four stages, which are described next.

Construction of the indoor temperature curve. The geographical coordinates of each consumer and the weather stations available were processed to find the closest station for each household. The curves of temperature and hourly solar irradiance are obtained from the corresponding station. Next, both curves are converted from hourly to quarterly, assigning each 15-minute time step the value of the corresponding hour. Finally, Eq. 1 is applied using the calibrated parameters to obtain the indoor temperature series. A new quarterly bivariate series S, is constructed with consumption and indoor temperature variables.

Selection of relevant consumption entries. To properly capture the correlation between electricity consumption and internal temperature, the periods of time when there is activity in the household must be considered. To determine those periods, the method excludes entries from the series S with low consumption. Any entry with a consumption less than 10% of the maximum consumption existing in the considered time horizon is excluded from the series.

Classification by indoor temperature. To perform the classification according to the indoor temperature, the *Keras* library is used to apply the the k-means algorithm, using two clusters ($k = 2$). The resulting clusters represent consumptions with low temperatures, and consumptions with high temperatures.

Classification by consumption. For each cluster found according to the indoor temperature, the k-means algorithm is applied again for classification according to the consumption variable, using two clusters ($k = 2$). The resulting clusters correspond to lower consumptions and higher consumptions values.

4.2　Final classification

After determining the indoor temperature curve, the selection of relevant consumption entries, the classification by indoor temperature, and the classification by consumption, four sets are obtained. They represent:

1. Samples that have high consumption with high temperatures;
2. Samples that have low consumption with high temperatures;
3. Samples that have high consumption with low temperatures; and
4. Samples that have low consumption with low temperatures.

Sets 2 and 4 are ignored, because the focus is analyzing high consumptions depending on the temperature. The consumption average is calculate for sets 1 and 3. If the quotient between the average obtained for set 1 and the average obtained for set 2 is greater than a specified threshold Θ, the consumer is classified as user of air conditioning in the summer. The value of Θ must be estimated in such a way that it correctly considers the difference in consumption at high and low temperatures. In Section 5.3, a value of Θ appropriate for Uruguayan households is estimated.

5   Experimental analysis and discussion

This section presents the experimental analysis and discussion of the results.

5.1   Development and execution platforms

The proposed solution was implemented on Python. Many scientific libraries and packages were used to handle data, fit the models and visualize results, including Pandas and Matplotlib and Numpy. The experimental evaluation was performed on the high performance computing infrastructure of National Supercomputing Center (Cluster-UY), Uruguay [18].

5.2   General considerations

The labeled data set, consisting of 29 users, was used for the analysis. In any case, for the calibration of the theta parameter, information from these users was not used, since in this way supervision would be introduced into the algorithm and, given the small amount of available data, this strategy would not have statistical support. For this reason, in this experimental analysis, the set of 29 consumers is used to evaluate the proposed unsupervised methodology but not for designing it. The vast amount of unsupervised data was used to perform an exploratory analysis to design the algorithm.

5.3   Parameter calibration

To calibrate the parameter Θ, the maximum consumption of the considered household is considered. If it is a consumer that has a relatively low average consumption for the residential sector, the consumption of air conditioning will be relevant. However, if the household has a high base consumption, when turning on an air conditioner, the relative increase in consumption may be small. Therefore, if the parameter Θ is adjusted for households with high average consumption, it will be suitable for households with low consumption. Taking into account that the average energy consumed by an air conditioner in fifteen minutes on extreme situation is 300Wh (standard power is $1200W$), and assuming an average intense consumption in peak hours of $1000Wh$, an appropriate value for theta would be $\Theta = 1300/1000$. But the costumer does not use the air conditioner in all extreme temperature situations. Therefore, a conservative Θ value could be estimated if it is assumed that on average 1 out of 10 times the costumer uses the air conditioner. Then, the average increase in consumption would be $300 {}^{1}\!/ 10 = 30$, so $\Theta = 1300/1270 = 1.0237$. This value is the one used for the experimental analysis and subsequent evaluation.

5.4   Analysis of the proposed methodology

To validate the proposed methodology, two analysis are presented. On the one hand, to calculate the precision of the algorithm in the set of 29 labeled household data. On the other hand, apply the proposed classification algorithm to the

complete set of non-labeled households of the data from ECD-UY and observe the percentage of households that results classified in the category of air conditioning use in summer. The purpose of estimating the number of households that use air conditioning in summer is to compare this value with the continuous survey of households carried out by the National Statistics Institute. To classify the unlabeled data, a sample of 1000 households is randomly taken. In both lines, the procedure described in the Section 3.4 is applied to the analyzed set.

5.5   Validation results on labeled data

To validate the results of the application of the algorithm on the labeled data and considering that the sample is balanced, the accuracy metric is used. The result obtained on the set of 29 households is an accuracy of 0.897.

All 16 households were correctly classified as users of air conditioning in summer. However, of the 12 who were classified as not using air conditioning in the summer, 3 were misclassified. This shows that there were no false positives and also allows us to conclude that in order to improve the algorithm it is necessary to avoid the occurrence of false negatives. These considerations are preliminary, due to the small size of the sample used.

5.6   Validation results on unlabeled data

According to the continuous household survey, by 2021, 53% of households have at least one air conditioner. When applying the developed algorithm to the sample of 1,000 non-labeled households, 497 households were classified as users of air conditioning in summer. Bearing in mind that most households that have air conditioning use it in summer, since there are no equivalent alternative thermal conditioning devices in this season (as is the case in winter), the result obtained of 49.7% is reasonable. This result is preliminary since there are no labels and it could happen that, although the total percentage is reasonable, many were misclassified. In any case, it could have happened that this analysis invalidated the algorithm if the percentage obtained was very different from the one shown by the survey.

6   Conclusions and future work

This article presented an unsupervised algorithm to detect the use of air conditioning in households, during summer. The proposed approach is valuable because it can be implemented in Uruguay with the existing infrastructure, without incurring large investment costs. The unsupervised algorithm applies the urban data analysis approach. First, it applies a filter by electricity consumption, then a chain of clustering, and finally estimates an indicator related to the variation in consumption with respect to temperature. As a result, the proposed algorithm classifies each consumer as a user (or not) of air conditioning in summer.

The proposed detection methodology was evaluated on a real case study considering data from 29 households in Montevideo, Uruguay. The unsupervised algorithm obtained an accuracy of 0.897 in the considered dataset. This is a promising result, considering the very small cardinality of the set of households.

The main lines of future work are related to improving the accuracy of the air conditioner detection tool, eventually using supervised learning. For this approach, communication with consumers (for example, through a mobile app) would be needed to allow a progressive labeling of households. Another line of future work consists of detecting the use of devices in real time, using the information from various sources and big data analysis.

Acknowledgments

References

1. Absi, R., Marchandon, S., Bennacer, R.: Thermal-electrical analogy and inertia for thermal performance of building envelops. In: MATEC Web of Conferences. vol. 330, p. 01037 (2020)
2. Al-Qawasmi, A., Tlili, I.: Energy efficiency and economic impact investigations for air-conditioners using wireless sensing and actuator networks. Energy Reports **4**, 478–485 (2018)
3. Arias, C., Mujica, F., Nicola, C., Menini, A.: Tendencias de diseño, sector materiales de construcción (2019), cámara de Industrias de Uruguay/INEFOP
4. Bonfigli, R., Squartini, S., Fagiani, M., Piazza, F.: Unsupervised algorithms for non-intrusive load monitoring: An up-to-date overview. In: 15th International Conference on Environment and Electrical Engineering (2015)
5. Cengel, Y., Cimbala, J., Turner, R.: Fundamentals of Thermal-Fluid Sciences (SI units). McGraw Hill (2012)
6. Chavat, J., Graneri, J., Nesmachnow, S.: Household energy disaggregation based on pattern consumption similarities. In: Smart Cities, pp. 54–69. Springer International Publishing (2020)
7. Chavat, J., Nesmachnow, S., Graneri, J.: Non-intrusive energy disaggregation by detecting similarities in consumption patterns. Revista Facultad de Ingeniería Universidad de Antioquia (2020)
8. Chavat, J., Nesmachnow, S., Graneri, J., Alvez, G.: ECD-UY, detailed household electricity consumption dataset of uruguay. Scientific Data **9**(1) (2022)
9. Chiang, J., Zhang, T., Chen, B., Hu, Y.: Load disaggregation using harmonic analysis and regularized optimization. In: IEEE Asia Pacific Signal and Information Processing Association Annual Summit and Conference. pp. 1–4 (2012)
10. Devarapalli, H., Dhanikonda, S., Gunturi, S.: Non-intrusive identification of load patterns in smart homes using percentage total harmonic distortion. Energies **13**(18), 4628 (2020)

11. Hart, G.: Nonintrusive appliance load monitoring. Proceedings of the IEEE **80**(12), 1870–1891 (1992)
12. Hu, M., Xiao, F.: Price-responsive model-based optimal demand response control of inverter air conditioners using genetic algorithm. Applied energy **219**, 151–164 (2018)
13. Kelly, J., Knottenbelt, W.: Neural NILM: Deep Neural Networks Applied to Energy Disaggregation. In: 2nd ACM International Conference on Embedded Systems for Energy-Efficient Built Environments. pp. 55–64 (2015)
14. Kolter, J., Johnson, M.: Redd: A public data set for energy disaggregation research. In: Workshop on Data Mining Applications in Sustainability. pp. 59–62 (2011)
15. Massobrio, R., Nesmachnow, S.: Urban Mobility Data Analysis for Public Transportation Systems: A Case Study in Montevideo, Uruguay. Applied Sciences **10**(16), 1–20 (2020)
16. Muraña, J., Nesmachnow, S., Iturriaga, S., de Oca, S.M., Belcredi, G., Monzón, P., Shepelev, V., Tchernykh, A.: Negotiation approach for the participation of datacenters and supercomputing facilities in smart electricity markets. Programming and Computer Software **46**(8), 636–651 (2020)
17. Muraña, J., Nesmachnow, S.: Simulation and evaluation of multicriteria planning heuristics for demand response in datacenters. Simulation p. 003754972110200 (2021)
18. Nesmachnow, S., Iturriaga, S.: Cluster-UY: Collaborative Scientific High Performance Computing in Uruguay. In: Supercomputing, Communications in Computer and Information Science, vol. 1151, pp. 188–202. Springer (2019)
19. Porteiro, R., Chavat, J., Nesmachnow, S.: A thermal discomfort index for demand response control in residential water heaters. Applied Sciences **11**(21), 10048 (2021)
20. Porteiro, R., Chavat, J., Nesmachnow, S., Hernández-Callejo, L.: Demand response control in electric water heaters: Evaluation of impact on thermal comfort. In: Smart Cities, pp. 74–89. Springer International Publishing (2021)
21. Porteiro, R., Hernández-Callejo, L., Nesmachnow, S.: Electricity demand forecasting in industrial and residential facilities using ensemble machine learning. Revista Facultad de Ingeniería Universidad de Antioquia (2020)
22. Porteiro, R., Nesmachnow, S., Hernández-Callejo, L.: Short term load forecasting of industrial electricity using machine learning. In: Smart Cities, pp. 146–161. Springer International Publishing (2020)
23. Zafar, R., Mahmood, A., Razzaq, S., Ali, W., Naeem, U., Shehzad, K.: Prosumer based energy management and sharing in smart grid. Renewable and Sustainable Energy Reviews **82**, 1675–1684 (2018)

IDE Y MOVILIDAD SOSTENIBLE: ESTADO DEL ARTE EN IBEROAMÉRICA

Teresa Batista[1], Carlos Grande[2], Carmen Vásquez[3], Leonardo Suárez[4], Luís Manuel Navas[5], Rodrigo Ramirez[6], Rhonmer Pérez[3], Renato Andara[3], Carla Fajarda[3]

[1] Universidad de Évora, Portugal
[2] Universidad Centroamericana José Simeón Cañas, El Salvador.
[3] Universidad Nacional Experimental Politécnica Antonio José de Sucre, Venezuela
[4] Universidad Técnica Nacional, Costa Rica
[5] Universidad de Valladolid, España
[6] Universitat Carlemany, Andorra

mtfb@uevora.pt

Abstract. En general, por sus características, las infraestructuras de datos espaciales (IDE) son la mejor opción tecnológica para compartir datos geográficos en la web. Permiten sintetizar, calcular y analizar datos espaciales a través de servicios web interoperables. Es la forma más efectiva de tener un sistema distribuido y flexible basado en estándares (OGC, W3C o ISO) y tecnología de código abierto. En este marco, la información geográfica es fundamental para planificar, gestionar y controlar la movilidad. Indicadores como el número de vehículos por unidad de superficie, la concentración de emisiones gaseosas o la población residente, son indicadores geográficos básicos para planificar la movilidad sostenible. El objetivo de este artículo es investigar el estado del arte sobre la importancia de las IDE para apoyar la planificación y gestión de una movilidad cada vez más sostenible en Iberoamérica.

Keywords: Movilidad sostenible, RITMUS, IDE, Portugal, Ibero América.

1   Introducción

La información, entendida como el conjunto organizado de datos tratados, es el insumo básico necesario para el desarrollo de las actividades que, como sociedad, realizamos en busca del crecimiento y del bienestar. Así, la necesidad de contar con información suficiente para la toma de decisiones y la gestión de programas, proyectos y actividades en general se torna fundamental en la sociedad actual y futura. Actualmente, contar con información que tenga las características necesarias para que se puedan tomar

decisiones de manera adecuada es uno de los desafíos más importantes. Una de las características más importantes es disponer de información con los datos abiertos y aprovechables a las necesidades de la sociedad.

Para que los datos se consideren abiertos, cualquier persona u organización puede acceder a ellos, utilizarlos o compartirlos cuando están en línea. Según el Banco Mundial [1], para considerar que los datos son abiertos, se deben cumplir dos (2) aspectos:

a) Estar en un sitio web de acceso público o en condiciones de libre acceso y con restricciones mínimas y, además, en términos técnicos.

b) Estar a disposición del público, en formato electrónico, en lenguaje informático, sin contraseñas ni cerramientos (*firewalls*) para que los usuarios puedan acceder y utilizar la información.

Los datos abiertos se convertirán en información y conocimiento y su éxito radica en el impacto que tienen en la sociedad al permitir que los gobiernos, las personas y las empresas interactúen [2]. Se utiliza una gran cantidad de datos en áreas diversas como cartografía, catastro, estadísticas, presupuestos y ejecución de fondos públicos, registros comerciales, legislación, transporte, comercio, salud, educación, seguridad, medio ambiente, resultados electorales y compras públicas, entre otros.

El principal problema que se produce en el uso de datos abiertos es que las licencias bajo las que se almacenan a menudo no son accesibles para uso público y pueden estar incompletas o repartidas en varias secciones o en varios sitios web. Los datos pueden aparecer como no disponibles, no actualizados, sin información sobre la frecuencia de la actualización o en formatos no legibles o reutilizables. El acceso a los datos también puede tener un coste, lo que contribuye a aumentar la brecha digital [3]. Éstos aspectos afectan las características de los datos abiertos al limitar la realización de los posibles beneficios sociales y económicos que ofrecen.

Otros problemas que interfieren en el acceso a los datos abiertos son la integración de datos de diferentes fuentes, arreglos y tecnologías [4], causando problemas de interoperabilidad entre diferentes entidades y usuarios, especialmente los que se puedan generar en datos geoespaciales o cartográficos [5]. La necesidad de integrar datos geoespaciales a través de las fronteras nacionales, plantea retos sobre cómo superar las barreras técnicas y organizativas, entre las diversas agencias cartográficas, debido, a que en los primeros esfuerzos utilizaron tecnologías heterogéneas y desarrollaron una cierta cultura entre los usuarios. Resultando que los recursos técnicos de la comunidad de usuarios, junto con la forma en que se proporcionan los datos desde una perspectiva técnica, son cruciales para la (re) usabilidad potencial de los datos en cualquier nivel.

Existen algunos ejemplos prácticos de compatibilidad de información geográfica y alfanumérica a diferentes niveles, de los que destacamos en Iberoamérica el proyecto Observatorio Territorial y Ambiental Alentejo-Extremadura Centro (OTALEX C) [6]. Este proyecto hizo la compatibilidad de información geográfica y alfanumérica, proveniente de diferentes entidades, niveles de administración del territorio (local, regional y nacional) y países (Portugal y España) y desarrolló una infraestructura de datos espaciales transfronterizos (IDE) entre las regiones de Alentejo y Centro de Portugal y Extremadura de España [7].

La movilidad debe ser vista más allá de los desplazamientos. Estas forman parte de la vida de las ciudades, impactando en su desarrollo y competitividad. Además, las políticas existentes de protección del ambiente y la necesidad de reducir las emisiones de

gases de efecto invernadero y otros efectos, impulsan a que esta movilidad debe ser sostenible y, en este marco, se forma la Red Iberoamericana de Transporte Urbano y Movilidad Sostenible (RITMUS) [8]. El objetivo de este artículo es investigar el estado del arte sobre la importancia de las IDE para apoyar la planificación y gestión de una movilidad cada vez más sostenible en Iberoamérica. El cual se encuentra estructurado en las secciones relacionadas con la movilidad en el mundo y sus impactos sociales y ambientales, RITMUS, y las IDE y su apoyo en la movilidad urbana. La metodología utilizada es revisión de la literatura existente, de documentos oficiales y diversos sitios web sobre la apertura de los datos. Se muestran los resultados relacionados con las iniciativas de construcción de las IDE en la región, la información necesaria para la movilidad y, finalmente, a cuáles datos realmente es posible acceder.

La movilidad es uno de los derechos fundamentales de la sociedad, aspecto que se ha contemplado en la mayoría de las constituciones o cartas magnas de los países. Sin embargo, ese derecho ha acentuado las innegables diferencias económicas, sociales y ambientales en nuestro planeta. El acceso a la movilidad digna significa, en casi todos los casos, la posibilidad de contar con beneficios vinculados al desarrollo social, económico y ambiental, entre otros, y en general con aspectos positivos relacionados con el futuro libre de nuestra sociedad [9].

Merecen especial atención los aspectos relacionados con la salud, la seguridad y el bienestar donde la movilidad tiene un impacto decisivo [10]. No tener una movilidad eficiente y sostenible no sólo puede ser visto como una violación de un derecho fundamental, sino que también significa diferencias entre sociedades o comunidades que pueden estar relacionadas con numerosas situaciones negativas derivadas de ello. Sería imposible enumerar todos los problemas e impactos que genera la movilidad deficiente, sin embargo, se sabe que esto retrasa y pone en riesgo el desarrollo y el bienestar de la sociedad.

Si a lo anterior se suma, que la movilidad en nuestro planeta se ha centrado efectivamente en el uso indiscriminado de combustibles fósiles [11], se puede concluir que es deber de nuestra sociedad desarrollar sistemas sostenibles que minimicen su impacto en el medio ambiente y que busquen desarrollar prácticas beneficiosas para el mismo.

El uso de fuentes, tecnologías y herramientas que garanticen la movilidad sostenible, es uno de los pilares fundamentales sobre los que se construye un modelo de movilidad necesario para nuestro futuro inmediato.

1.1　La movilidad urbana sostenible

La movilidad urbana sostenible es el eje central de la Red Iberoamericana de Transporte Urbano y Movilidad Sostenible (RITMUS), compuesta por 91 investigadores de 20 grupos de 14 países iberoamericanos: Argentina, Brasil, Colombia, Costa Rica, Cuba, Ecuador, El Salvador, España, Guatemala, Honduras, México, Panamá, Portugal y Venezuela. Esta red se creó en 2018, en el marco del Programa Iberoamericano de Ciencia y Tecnología para el Desarrollo (CYTED) y su objetivo general es desarrollar una red de entidades dedicadas a la I+D+i, empresas, administraciones y otros interesados, para el análisis en la región Iberoamericana de fuentes de energía, tecnologías e infraestructuras relacionadas con la movilidad, así como asistir a las estructuras de planificación y gestión del transporte, en la transferencia de conocimiento e innovación que permitan un transporte más eficiente, sostenible, seguro y equitativo.

Según Naciones Unidas, en el año 2018, el 55% de los habitantes del planeta vive en zonas urbanas. El número de megaciudades (con más de 10 millones de habitantes) está creciendo rápidamente. Existe un enorme auge de ciudades intermedias latinoamericanas, con expansiones desproporcionadas y desordenadas, debido a los crecientes movimientos migratorios, provocados tanto por crisis económicas, como por conflictos internos y externos [12]. Hay una necesidad urgente de mejorar la movilidad, especialmente en las economías emergentes, los países y regiones en desarrollo como China, India, América Latina (AL), África. Por otra parte se espera que las ventas de automóviles se dupliquen de 2010 a 2025 [13]. La dependencia del sector del transporte de los combustibles fósiles y la creciente motorización de las ciudades hace que sea responsable del 25% del consumo energético mundial y del 25% de las emisiones de Gases de Efecto Invernadero (GEI) [14].

Los altos niveles de urbanización, el crecimiento acelerado de las áreas urbanas y su altísima motorización, han provocado problemas de congestión, accesibilidad a mejores oportunidades laborales, medio ambiente, salud, seguridad y otros. En este contexto, la movilidad urbana sostenible tiene como objetivo:

- Disminuir el calentamiento global y minimizar el cambio climático.
- Mejorar la calidad del aire en las zonas urbanas y la calidad de vida de los ciudadanos.
- Reducir el consumo de energía y la dependencia de combustibles fósiles.
- Reducir riesgos y accidentes.
- Contribuir al acceso universal al mercado laboral y la participación en la vida social activa.
- Reducir la congestión en las ciudades.

Se tiene especial énfasis en las ciudades intermedias, que se consideran más vulnerables a los efectos del transporte y la movilidad inadecuados. La movilidad urbana es mucho más que sistemas de transportes, se trata de personas y su entorno. AL se destaca por sus altos índices de viajes motorizados y niveles de congestión. Existen ciudades emblemáticas reconocidas por sus niveles de sustentabilidad, entre ellos se encuentra la ciudad de Curitiba en Brasil, que engloba varias prácticas de movilidad (individual, colectiva y urbana) debidamente articuladas que sirven de modelo a nivel regional y global, por su contribución a la sostenibilidad del entorno urbano.

La demanda de información geográfica se ha incrementado en varios ámbitos de la movilidad urbana, gracias a la evolución de las tecnologías y, sobre todo, de la IDE, entendida como el conjunto de tecnologías, políticas, estándares y recursos humanos para adquirir, procesar, almacenar, distribuir y mejorar la difusión de información geográfica.

En general, por sus características la IDE es la mejor opción tecnológica para compartir datos geográficos en la web. Permiten sintetizar, calcular y analizar datos espaciales a través de servicios web interoperables. También es la forma más efectiva de tener un sistema distribuido y flexible basado en estándares (OGC, W3C o ISO) y tecnología de código abierto. Están formados por tres (3) componentes: (a) un visor de datos (visor de mapas), (b) un catálogo de metadatos y (c) un catálogo de nombres de lugares. Los sistemas de información geográfica local se comunican a través de servicios de mapas web (WMS), servicio de catálogo web (CSW) y servicios de características web (WFS). La información geográfica es fundamental para planificar, gestionar y controlar la movilidad. Indicadores como el número de vehículos por unidad de superficie, la

concentración de emisiones gaseosas o la población residente, son índices geográficos básicos para planificar y gestionar la movilidad sostenible.

En AL se destacan dos (2) áreas principales de uso de las IDE. La primera es el Catastro Multifinalitario, que sirve como fuente de información para soporte de decisiones en el contexto de la Gobernanza Inteligente, específicamente en la información temática sobre movilidad urbana y sus redes de rutas de transporte, medición de tiempos y volúmenes de personas por viaje, entre otros. Además, el segundo se refiere a las ciudades inteligentes (s*mart cities*) y la movilidad inteligente (s*mart mobility - SM*) [16].

Según Uteng, et al, [16], aunque el término no sea consensual, teniendo al menos 23 definiciones de SM identificadas, se puede generalizar los conceptos de Sistema de Transporte Inteligente (ITS), Transporte Inteligente (TI) y Movilidad como Servicio (MaaS), que están vinculados a bases de datos robustas, integrando organizaciones de diferentes niveles de administración territorial, empresas y ciudadanos.

La mayoría de los datos necesarios para planificar y gestionar la movilidad urbana son capturados y gestionados de diversas formas por los gobiernos centrales y locales. El informe del Banco Interamericano de Desarrollo (BID) propone cuatro (4) indicadores para evaluar el estado de los datos abiertos en todo el mundo. Ellos son: (a) el Barómetro de Datos Abiertos (BDA), (b) el Índice Global de Datos Abiertos (GODI), (c) el Inventario de Datos Abiertos (ODIN) y (d) y el índice OECD OURdata [17]. De su análisis, se desprende que los indicadores de AL están siempre por debajo de los estándares europeos.

Según Ballari, et al, [18], advierten sobre la heterogeneidad de la situación dentro de AL, en comparación con Europa. Esto como resultado que Europa asume estándares rigurosos como ISO 19100 e ISO 19115. Los autores también destacan a México, Brasil y Colombia como países emergentes en el desarrollo de la IDE, por el contrario, El Salvador aparece con resultados modestos en los índices de 2017.

Es importante resaltar cómo cada uno de ellos tiende a vincularse con Big Data, Web Cloud e Inteligencia Artificial, designada como cuarta fase de implementación del IDE en todo el mundo. Es en esta etapa, que se amplía el ámbito de posibilidades para recuperar datos de buena calidad a partir del suministro de información de los usuarios de diferentes sistemas de movilidad. En este sentido, es relevante hablar de la tendencia, aún incipiente, de la Información Geográfica Voluntaria (IGV) y su impacto en hacer cada vez más robusta la base de datos para la toma de decisiones en AL, luego de la actualización de la normativa [19].

En Europa, concretamente en Lisboa, Portugal, se está desarrollando con la implementación de una manera más avanzada con Voluntary Geo-Dynamic Information (VGDI), con lo cual se demuestra su gran potencial en la determinación patrones de movilidad individual [20], uno de los principales desafíos en la evaluación de la accesibilidad como medida de sostenibilidad de la movilidad urbana [21].

2　　Resultados

Los resultados se obtienen a partir de la revisión de la literatura existente, de documentos oficiales y diversos sitios web sobre la apertura de los datos. Se analizaron en total 16 artículos, sobre los cuales se muestran los resultados relacionados con las iniciativas de construcción de las IDE en la región, la información necesaria para la movilidad y la que realmente es accesible. Se utilizaron palabras claves para la selección de los

artículos como: "Spatial Data Infrastructure" "Transport" "Urban Mobiliy" en el buscador EBSCO, con el fin de homogenizar la búsqueda de los investigadores, posteriormente se compartieron los artículos seleccionados para eliminar la posibilidad de seleccionar repetidos.

Una alternativa de solución a la carencia de disponibilidad de información espacial, necesaria para llevar a cabo los procesos de planificación y desarrollo, puede ser cubierta con IDE. Éstas pueden ser consideradas para la toma de decisiones a nivel local, nacional o regional y ser enfocadas en aspectos económicos, estadísticos, demográficos, entre otros. El objetivo es lograr un desarrollo sostenible aplicando políticas de estandarización, interoperabilidad y accesibilidad de las tecnologías y datos geográficos digitales para gestionar la información geoespacial [22].

En el recuento histórico, la construcción de las IDE en AL tiene más de quince (15) años de esfuerzo. En este marco es oportuno destacar varias iniciativas, que se muestran en la Tabla 1, relacionadas con la integración de las IDE en Iberoamérica.

Tabla 1. Iniciativas de construcción de las IDE en Iberoamérica

Acrónimo	Nombre	URL
IGN	Red Interamericana de Datos Geoespaciales	http://www.ign.es
SIRGAS	Sistema de Referencia Geocéntrico para las Américas	http://www.sirgas.org/es/
R3IGeo	Red Iberoamericana de Infraestructuras de Información Geográfica	http://www.r3igeo.org/
PC-IDEA	Infraestructura de Datos Espaciales de las Américas	http://www.cp-idea.org/
GeoSur	Programa GeoSUR	http://www.geosur.info/geosur/index.php/en/
GSDI	Infraestructura Global de Datos Espaciales	http://gsdiassociation.org/
IPGH	Instituto Panamericano de Geografía e Historia	http://www.ipgh.org/

Entre las iniciativas que se muestran en la Tabla 1, el Banco de Desarrollo de América Latina persigue el objetivo de promover el desarrollo de IDE en la región a través del Programa GeoSUR. Este Programa posee un punto de entrada a los datos espaciales publicados por agencias de AL y provee capacitación para fortalecer sus servicios de mapas web y habilidades asociadas para las agencias geográficas nacionales de la región. Por otra parte, la R3IGeo es un geoportal que permite el acceso a los datos, metadatos, servicios e información de tipo geográfico de sus países miembros. Entre sus productos figuran la localización, visualización, descarga y transformación de datos geográficos. Para los países integrantes de la red y, conforme a sus respectivas regulaciones, al menos los servicios de visualización y localización son gratuitos. Son miembros de esta Infraestructura:

- Las Infraestructuras Nacionales de Datos Espaciales de los países miembros de la Red.
- La Infraestructura de Datos Espaciales de las Américas (PC-IDEA)
- La Infraestructura del Instituto Panamericano de Geografía e Historia (IPGH) para apoyar el desarrollo de los datos espaciales.
- La Infraestructura de Datos Espaciales de España (IDEE)
- La Infraestructura de Datos Espaciales de Portugal (SNIG).

En cuanto a los países de Iberoamérica con IDE desarrollados figura España, con altos avances en este tipo de infraestructuras y pioneros tanto local como internacional [23]. En la tabla 2 y 3 se muestran, los 16 artículos en análisis, clasificados en otras regiones del mundo e Iberoamérica, respectivamente, y la información referente a la caracterización de los artículos en cuanto al tipo de IDE o SIG que conforman determinados países o regiones.

Tabla 2. Artículos consultados

Año	Región/país o ciudad	Palabras clave	Tipo de investigación	Referencia
2019	Finlandia, Holanda, Noruega y España	OpenELS, Geospatial Linked Data, INSPIRE, Spatial Data Infrastructure, SDI	Documental	[1] [5]
2019	Reino Unido	Urban big data infrastructure, Urban analytics Spatial, urban indicators Small area assessment, Spatial big data	Documental	[2] [24]
2019	Gran Bretaña	Urban big data infrastructure, Urban analytics Spatial, urban indicators Small area assessment, Spatial big data	Documental	[3][25]
2019	India	Cloud computing, SDI, Geographical Indications, Overlay analysis	Documental	[4][26]
2019	Estado de Maharashtra (India)	Spatial data infrastructure (SDI), Geospatial big data, Fog computing, Cloud computing, Geo-health big data, Malaria	Construcción de Prototipo	[5][27]
2020	Ghent, Belgica	Traffic management as a service, Traffic management, Urban mobility, Smart city, Data integration, Data visualization	Proyectiva, Construcción de Prototipo Traffic Management as a Service (TMaaS)	[6][28]
2019	Alabama, USA	Google maps, Transportation infrastructure, traffic analysis, isochrone map, geographic information systems	Proyectiva. Construcción de Prototipo Transportation Analysis Tool.	[7][29]
2019	Yangon City, Myanmar, Japón	Geospatial dashboard, IoT, big data analytics, geovisualisation, disaster management	Proyectiva. Construcción de Prototipo	[8][30]

Tabla 3. Artículos consultados

Año	Región/país o ciudad	Palabras clave	Tipo de investigación	Referencia
2017	Diversas regiones, resaltando Ciudades de España.	IDE, ciudad inteligente, sostenibilidad, sensores	Documental	[9][31]
2015	España	Ciudades inteligentes (*smart cities),* SIG, GIS, Sistemas de Información Geográfica, Ordenación del territorio, Planificación urbana, Espacio urbano, Aplicaciones	Documental	[10] [32]
2014	Ecuador	Infraestructuras de Datos Espaciales, Sistemas de Información Geográfica, Ontologías, Planeación Territorial, Sensor Ciudadano	De campo	[11] [33]
2014	LATAM	Tendencias, dispositivos móviles, crowdsourcing, información geográfica voluntaria, sensores, Latinoamérica	Documental	[12] [18]
2013	Cuba	Análisis de redes viales; bases de datos espaciales; camino mínimo; datos espaciales; sistemas información geográfica	De campo	[13] [34]
2013	España	*Smart Cities*, IDEZar	Documental	[14] [23]
2012	Colombia	Datos espaciales, infraestructura, preferencias, transporte público, sistema de información, Bogotá	Documental	[15] [35]

En la siguiente tabla, dedicada al tema de bases de datos y dispositivos tecnológicos para la movilidad urbana, se han enfocado los recursos existentes y los deseados y se plantearon propuestas, la mayoría de ellas en torno a tres (3) temas: (a) apertura en la recopilación y difusión de datos a través de sistemas abiertos, (b) generación de cultura y educación para mejorar la movilidad urbana y (c) actualización y aplicación de normas. De la consulta de expertos de RITMUS en materia de movilidad se ha recopilado la información necesaria a la gestión de la movilidad sostenible [8].

En la Tabla 4 se puede observar que para la movilidad sostenible es necesario tipos de información en formatos *raster*, servicios de mapas, vectorial, sistemas de información y alfanumérico para mapas en sus diferentes tipos (ortofotomapas, imágenes satelitales, límites administrativos, red de vías, personas y ciclovías, red de transporte público, control del tráfico, datos de tránsito en tiempo real, seguridad vial y planes y otros, los cuales han sido agrupados en la siguiente Tabla 5 en cuatro (4) clases. Estas clases son información de base, infraestructura para la movilidad, datos operacionales y, planificación y gestión.

Tabla 4. Información geográfica necesaria para la movilidad sostenible

Clase de información	Tipo de información	Formato	Fuentes de datos de Europa (Portugal e España)
Información de base	Ortofotomapas	Raster	CNIG España; Direção Geral do Território (DGT) Portugués
	Imágenes de satélite	Raster	Landsat, IKONOS, Quikbird??, Sentinel
	Modelo Digital del Terreno	Raster	www.igeo.pt; www.cing.es
Infraestructuras para la movilidad	Mapa base con limites administrativos; localidades; hidrografía; relevo; toponimia	Serviço de mapas	bingmaps; institutos geográficos nacionales
	Red viaria (auto-rutas, rutas e otras vías)	Vectorial	openstreetmap, entidades nacionales; regionales y locales
	Red ferrocarril (electrificado o a combustible)	Vectorial	openstreetmap, entidades nacionales; regionales y locales
	Vías perdónales y ciclo vías	Vectorial	openstreetmap, entidades nacionales; regionales y locales
	Interfaces (parajes y centrales de transporte; otros)	Vectorial	municipios
	Señalética de tránsito, vertical y horizontal; Semáforos	Vectorial	municipios
Dados operacionales	Sentido de las vías	Alfanumérica	openstreetmap; google drive, otros
	Cualidad y conservación de la vía	Alfanumérica	municipios
	Visibilidad de la vía	Vectorial	análisis espacial
	Dados de tránsito en tiempo real	Vectorial	sensores e Información Geográfica Voluntaria (IGV)
	Rutas dos transportes públicos	Vectorial	empresas de transportes e Autoridades de transportes (SIGGESC - Portugal)
	Información sobre transporte al ciudadano	Sistemas de información	Paineles informativos
	Seguridad de la vía (indicador)	Alfanumérica	Autoridades de seguridad
Planificación y gestión	Planes de ordenación del espacio urbano	Vectorial	municipios
	Puntos negros en la movilidad	Vectorial	Autoridades de seguridad/policía

Clase de información	Tipo de información	Formato	Fuentes de datos de Europa (Portugal e España)
	Planos de movilidad sostenible	Vectorial	Autoridades de Transporte
	Nº de usuarios /residentes/turistas/otros	Alfanumérica	empresas de transportes e Autoridades de transportes (SIGGESC - Portugal)
	Movimientos pendulares	Alfanumérica	empresas de transportes e Autoridades de transportes (SIGGESC - Portugal)

La información geográfica es uno de los pilares de la movilidad sostenible, sin la cual no es posible gestionar carreras y flujos de personas. Actualmente, la mayoría de las infraestructuras de datos espaciales tienen acceso a información de base territorial. Este es el caso de las infraestructuras de datos geográficos nacionales en España y Portugal, donde la información es proporcionada por diferentes entidades nacionales, regionales y locales.

En la Tabla 5 se muestra la información accesible, clasificada en estadísticas, movimientos pendulares y tipos de transporte para la movilidad sostenible.

Tabla 5. Información accesible

Clase de Información	Indicadores
Estadísticas censitarias relacionadas con a movilidad	Número de residentes
	Número de visitantes
Movimientos pendulares	Cuantas personas se mueven al día
	Lugar de destino y sentido
	Razones de la Movilidad (ocupacional, personal o de retorno)
	Grupos etarios
	Lugar, destino y tipo de transporte de persona con necesidades especiales
Tipos de transporte	Tipo de Movilidad: Activa (caminata, bicicleta y otros), Transporte público (autobús, metro, ferrocarril y otros) y vehículo privado (automóvil, motocicleta y otro)
	Forma de organización/gestión do transporte
	Gobernanza do transporte
	Intermodalidad
	Tipo de combustible e emisiones de gases de efecto invernadero y material particulado

3   Conclusiones

Según la investigación de las IDE entre Europa y América Latina, se encuentra una situación de contrastes. Europa es una región con una directriz clara a partir de la implementación de la normativa ISO19100 e ISO19115 y la normativa europea INSPIRE, en contraste con una región latinoamericana marcada por la desigualdad entre países y al interior de ellos, por una profunda brecha tecnológica aún no superada.

Ante esta situación la IGV y la IGDV se constituyen como verdaderas herramientas que pueden potenciar la generación de nuevas fuentes de información de manera más dinámica, producto de la participación ciudadana, sin embargo, Latinoamérica se enfrenta nuevamente ante un reto de diseñar normativas acordes a los requerimientos de la utilización de la información personal.

Las fases de implementación de IDE propuestas por Ballari, et al, son un estándar de evaluación de la situación de ambas regiones y representan un campo de profundización de cara al establecimiento de programas y metas conjuntas, para la mejora de la ejecución de las IDE en Latinoamérica.

Los datos abiertos abren posibilidades para mejorar, la gobernanza y la calidad de vida de la sociedad en general. Se abren opciones para mejorar la movilidad sostenible y plantear soluciones eficientes, por medio de mapeos, plataformas o sitios web que satisfagan las demandas de información de la sociedad, para la mejora de la toma de decisiones.

Agradecimientos

Referencias

[1]   "Aspectos fundamentales de los Datos Abiertos | Data." http://opendatatoolkit.worldbank.org/es/essentials.html (accessed Nov. 18, 2022).

[2]   F. G. Figueroa Garza, M. A. Vázquez Zacarías, and Á. F. Salazar González, "De datos, diseño y ciudades inteligentes," *Vinculatégia EFAN*, vol. 5, no. 1, pp. 788–797, Jul. 2019, Accessed: Nov. 18, 2022. [Online]. Available: http://www.web.facpya.uanl.mx/vinculategica/vinculategica_5/70.-Figueroa_Garza.pdf.

[3]   M. C. Vera Martinez and M. C. Martinez Rodriguez, "Hacia un diseño de políticas públicas de datos abiertos de medio ambiente," *Cad. Gestão Pública e Cid.*, vol. 25, no. 82, 2020, doi: 10.12660/cgpc.v25n82.80506.

[4]   A.-B. Sabino, P. Reis-Martins, and M. Carranza-Infante, "Experiencias y retos del uso de datos de aplicaciones móviles para la movilidad urbana," *Rev. Arquit.*, vol. 22, no. 1, 2019, doi: 10.14718/revarq.2020.3039.

[5]   S. Ronzhin *et al.*, "Next Generation of Spatial Data Infrastructure: Lessons from Linked Data implementations across Europe ," *Int. J. Spat. Data*

Infrastructures Res., vol. 14, pp. 83–107, 2019, doi: 10.2902/1725-0463.2019.14.art4.

[6]   T. Batista *et al.*, "IDE-OTALEX C. The First Crossborder SDI between Portugal and Spain: Background and Development Grande Rota do Montado View project IDE-OTALEX C. The First Crossborder SDI between Portugal and Spain: Background and Development," *J. Earth Sci. Eng.*, vol. 3, pp. 393–400, 2013, doi: 10.17265/2159-581X/2013.06.006.

[7]   "OTALEX C." http://www.ideotalex.eu/OtalexC/ (accessed Nov. 18, 2022).

[8]   RITMUS-CYTED, "Tercer Simosio Internacional RITMUS de Movilidad Urbana Sostenible," Antiguo Cuscatlán, La Libertad, El Salvador, 2019.

[9]   G. N. Barón, "La transición urbana y social hacia un paradigma de movilidad sostenible," *Cuad. del Cent. Estud. en Diseño y Comun. Ensayos*, no. 80, pp. 152–172, Aug. 2020, doi: 10.18682/CDC.VI80.3701.

[10] Y. N. Saldeño-Madero and R. A. Blanco-Rodríguez, "Movilidad y espacio público: condiciones para el bienestar de las personas que laboran en Chapinero, Bogotá, Colombia," *Rev. Salud Pública*, vol. 20, no. 5, 2018, doi: 10.15446/rsap.v20n5.60995.

[11] Ipcc, *Cambio climático 2007: Informe de síntesis*. 2007.

[12] M. Jans B., "Movilidad urbana: en camino a sistemas de transporte colectivo integrados," *AUS*, no. 6, pp. 6–11, 2009, doi: 10.4206/aus.2009.n6-02.

[13] I. Tapia Ramírez, "La rivalidad estratégica entre China y EE. UU. en el área de la energía," in *Energía y Geoestrategia 2020*, Madrid, España: Instituto Español de Estudios Estratégicos, 2020, pp. 39–104.

[14] H. Terraza, D. R. Blanco, and F. Vera, "De Ciudades Emergentes a Ciudades Sostenibles; comprendiendo y proyectando las metrópolis de siglo XXI," Santiago de Chile, 2016. Accessed: Nov. 18, 2022. [Online]. Available: https://publications.iadb.org/publications/spanish/document/De-ciudades-emergentes-a-ciudades-sostenibles.pdf.

[15] "RED IBEROAMERICANA DE MOVILIDAD Y TRANSPORTE URBANO SOSTENIBLE (RITMUS) | CYTED. Programa Iberoamericano de Ciencia y Tecnologia para el Desarrollo." https://www.cyted.org/es/ritmus (accessed Nov. 18, 2022).

[16] T. P. Uteng, Y. J. Singh, and O. H. Hagen, "Social sustainability and transport: Making 'smart mobility' socially sustainable," in *Urban Social Sustainability: Theory, Policy and Practicepolicy*, 1st ed., R. Shirazi and R. Keivani, Eds. Springer, 2019, pp. 59–77.

[17] A. Muente-Kunigami and F. Serale, *Los datos abiertos en América Latina y el Caribe*. New York, 2018.

[18] D. Ballari, L. Vilches, D. Randolf Perez, D. Pacheco, and V. Fernández, "Tendencias en infraestructuras de datos espaciales en el contexto latinoamericano," *MASKANA, I+D+ingeniería*, vol. 5, no. 5, pp. 177–184, 2014, Accessed: Aug. 23, 2020. [Online]. Available: https://publicaciones.ucuenca.edu.ec/ojs/index.php/maskana/article/view/565.

[19] A. I. Hernández Magaña and F. N. Güiza Valverde, "Información Geográfica Voluntaria (IGV), estado del arte en Latinoamérica," Sep. 2016. Accessed:

Aug. 23, 2020. [Online]. Available: https://www.revistasipgh.org/index.php/rcar/article/view/426.

[20]   C. Aubrecht, D. Özceylan Aubrecht, J. Ungar, S. Freire, and K. Steinnocher, "VGDI – Advancing the Concept: Volunteered Geo-Dynamic Information and its Benefits for Population Dynamics Modeling," *Trans. GIS*, vol. 21, no. 2, pp. 253–276, 2017, doi: 10.1111/tgis.12203.

[21]   C. Zegras, "Mainstreaming sustainable urban transport: putting the pieces together," in *Urban Transport in the Developing World, A handbook of Policy and Practice*, H. T. Dimitriou and R. Gakenheimer, Eds. Edward Elgar Publishing, 2011, pp. 548–588.

[22]   J. Suniaga, "Promoting the development of Spatial Data Infrastructure in Latin America and the Caribbean.," 2016, Accessed: Nov. 18, 2022. [Online]. Available: https://conf.gsdi.org/index.php/conferences/gsdi15/paper/view/81.

[23]   M. J. Pérez Pérez, J. López-de-Larrínzar, M. J. Fernández-Ruiz, V. Morlán-Plo, P. Rodrigo-Cardiel, and M. Usón Montesinos, "Infraestructuras de dados espaciales como eje central del desarrollo de las smart cities," *IV Jornadas Ibéricas Infra-estruturas Dados Espac.*, 2013.

[24]   O. C. D. Anejionu *et al.*, "Spatial urban data system: A cloud-enabled big data infrastructure for social and economic urban analytics," *Futur. Gener. Comput. Syst.*, vol. 98, 2019, doi: 10.1016/j.future.2019.03.052.

[25]   O. C. D. Anejionu, Y. Sun, P. (Vonu) Thakuriah, A. McHugh, and P. Mason, "Great Britain transport, housing, and employment access datasets for small-area urban area analytics," *Data Br.*, vol. 27, 2019, doi: 10.1016/j.dib.2019.104616.

[26]   R. Kumar Barik *et al.*, "Geocloud4GI: cloud SDI model for geographical indications information infrastructure network," *Springer*, pp. 215–224, 2019, doi: 10.1007/978-3-030-03359-0_10.

[27]   R. K. Barik, H. Dubey, K. Mankodiya, S. A. Sasane, and C. Misra, "GeoFog4Health: a fog-based SDI framework for geospatial health big data analysis," *J. Ambient Intell. Humaniz. Comput.*, vol. 10, no. 2, 2019, doi: 10.1007/s12652-018-0702-x.

[28]   C. Van Gheluwe, I. Semanjski, S. Hendrikse, and S. Gautama, "Geospatial Dashboards for Intelligent Multimodal Traffic Management," 2020, doi: 10.1109/PerComWorkshops48775.2020.9156231.

[29]   M. Mcleroy, B. Hallihan, B. Wright, and T. Atkison, "Sustainable Mobility: Developing a Web-Based Software Suite for Transportation and Traffic Analysis using Google Maps," in *Proceedings of the International Conference on Software Engineering Research and Practice (SERP)*, Aug. 2019, pp. 29–35.

[30]   K. K. Lwin, Y. Sekimoto, W. Takeuchi, and K. Zettsu, "City Geospatial Dashboard: IoT and Big Data Analytics for Geospatial Solutions Provider in Disaster Management," 2019, doi: 10.1109/ICT-DM47966.2019.9032921.

[31]   S. Y. Velazco, A. Abuchar Porras, G. A. Alzate, A. A. Porras, and G. A. Alzate, "Las infraestructuras de datos espaciales como apoyo al desarrollo de la ciudad inteligente," *Redes Ing.*, pp. 74–83, May 2017, doi:

10.14483/2248762X.11994.

[32]   E. Bustillo Holgado and P. Rodríguez Bustamante, "Los Sistemas de Información Geográfica y las ciudades inteligentes," *Polígonos. Rev. Geogr.*, no. 27, 2015, doi: 10.18002/pol.v0i27.3283.

[33]   V. M.-C. de C. y T. ESPE and undefined 2014, "Mejorando la Usabilidad en las Plataformas de Infraestructura de Datos Espaciales," *journal.espe.edu.ec*, Accessed: Nov.   18,   2022.   [Online].   Available: https://journal.espe.edu.ec/ojs/index.php/cienciaytecnologia/article/view/90.

[34]   E. Sánchez-Ansola *et al.*, "Una mirada al análisis de redes de transporte en Cuba desde el punto de vista de los datos.," *Lámpsakos*, no. 10, pp. 21–33, Dec. 2013,   Accessed: Sep.   19,   2020.   [Online].   Available: https://www.funlam.edu.co/revistas/index.php/lampsakos/article/view/918.

[35]   D. F. Pajarito Grajales and J. N. Pérez Castillo, "Propuesta para el sistema de información al usuario de transporte público de Bogotá combinando preferencias y datos espaciales básicos," *UD y la geomática*, no. 6, pp. 3–10, Dec. 2012, doi: 10.14483/23448407.4405.

Synthesized data generation for public transportation systems

Federico Gómez and Sergio Nesmachnow[0000−0002−8146−4012]

Universidad de la República, Uruguay
fgomez@fing.edu.uy,sergion@fing.edu.uy

Abstract. This article presents a proposal for generating synthesized data for public transportation systems. This is a relevant problem whose solution assists the planning and operation of Intelligent Transportation Systems. The proposed methodology applies a conditional Generative Adversarial Network approach, considering relevant real information about trips performed by citizens. A practical validation is presented for a real case study in the public transportation in Montevideo, Uruguay. The main results indicate that the proposed approach is able to generate accurate synthesized data.

1   Introduction

Mobility and urban transportation are fundamental components of the functional dimension of a city, which together with other relevant factors (land use, urban planning, etc.) determines the way in which citizens perform their daily activities [1].

The analysis of urban mobility data is crucial to help public administrations and policy makers to improve public transportation systems [15]. The emergence of data-driven approaches led to an improved transportation paradigm, known as Intelligent Transportation Systems (ITS). ITS are innovative systems that, by integrating synergistic technologies, allows providing services to both traffic management operators and citizens. Their main goal is to develop coordinated and integrated mobility means that in turn are smarter, safer, efficient, and provide a better user experience [24].

Synthesized data generation refers to the process of creating a repository of data by applying a systematic and programmatic method [3]. Synthesized data complement real data in those situation where real-life or experimental gathering is not practical or even not possible. Synthesized data allows performing more accurate analysis to better understand underlying processes, a critical component for self-driven data science [8]. The most desired properties of synthesized data are they must follow or accurate approximate the distribution of real data, have the same type of features than real data, randomness should be controlled and noise must be injected if needed. In particular, synthesized data are crucial for developing computational intelligence and machine learning methods to solve complex problems.

Synthesized mobility data are very useful for planning and operation within ITS. Retrieving real high-quality mobility data is a hard task, mainly due to privacy issues related to gathering and managing sensitive data about citizens. In addition, the real mobility time series gathered by ITS usually have missing data due to several reasons, including missing, malfunctioning, and low maintenance of the gathering devices/sensors and intermittent communications between devices/sensors and the central server. Thus, synthesized mobility data are useful for characterizing mobility patterns, detecting anomalies and unusual mobility patterns, and also for performing simulations of different realistic scenarios. Some interesting studies that benefit from the availability of both real and synthesized mobility data are public transportation network design, analysis and improvement of the quality of service and user experience, determining stress conditions and other traffic-related situations such as predicting traffic jams, analyzing speed of vehicles, detecting special incidents, and performing traffic engineering and traffic operation tasks [17]. Overall, accurate (real and synthesized) mobility data provide useful insights about traffic and citizens movement patterns, which are important inputs for nowadays ITS.

In this line of work, this article presents an approach applying Generative Adversarial Networks (GANs) for the generation of synthesized mobility data for ITS. A specific conditional network architecture is studied and implemented and a practical validation is presented for a real case study, the ITS for public transportation in Montevideo, Uruguay. The main results of the research indicate that the proposed conditional GAN is able to generate accurate synthesized mobility data, according to the statistical analysis and metrics studied.

Overall, this article contributes with the proposal of a methodology for synthesized public transportation data generation based on GANs and the evaluation of the proposed methodology in a real case study, considering real data from the public transportation system in Montevideo, Uruguay.

The article is organized as follows. Next section presents the main concepts about GANs. Section 3 presents a description of the problem solved and reviews relevant related works. Section 4 describes the case study, the public ITS in Montevideo, Uruguay. The applied methodology and implementation details is presented in Section 5. The experimental evaluation of the proposed generative approach is reported in Section 6. Finally, section 7 presents the conclusions of the research and formulates the main lines for future work.

2　Generative Adversarial Networks

A generative model is a statistical tool that allows modeling the joint probability distribution $p(X, Y)$ relating a given observable variable X (input or data instance) and a target variable Y (output) [20]. Generative machine learning is a branch of computational intelligence including methods that are able to generate new instances of data, by learning the joint probability $p(X, Y)$ to describe the process of generating new datasets [5].

GANs are a type of generative machine learning methods that use adversarial artificial neural networks (ANNs) for generating new data [6]. A GAN consists of two ANNs working in competition and cooperation: the *generator* and the *discriminator*. Both ANNs apply and adversarial learning approach to optimize their parameters in order to generate accurate synthesized data.

The generator ANN (g) specializes on learning the way of creating synthesized data samples x', taking as input random vectors from a latent space z. The generator can be characterized by the equation $g(z) = x'$. The main goal of the generator is to approximate the distribution of true data, by considering the information about the problem provided by the discriminator. In turn, the discriminator ANN specializes on learning how to distinguish real data samples x (taken from a training dataset) from the synthesized samples x' created by the generator. Both ANNs are trained simultaneously and following an adversarial approach: the discriminator tries to learn the real data distribution for a proper evaluation of new synthesized data and the generator seeks to generate images that deceive the discriminator, by generating data samples that the discriminator cannot label as real or synthesized. A well-designed training process converges to a generator ANN that approximates the real data distribution, thus generating high-quality synthesized data samples.

Recent articles have demonstrated that GANs are very useful tools for many applications that propose/require generating synthesized data, especially in multimedia processing, healthcare, time series analysis, and other areas [12,21,25,26]. Fig. 1 presents a schema of a GAN.
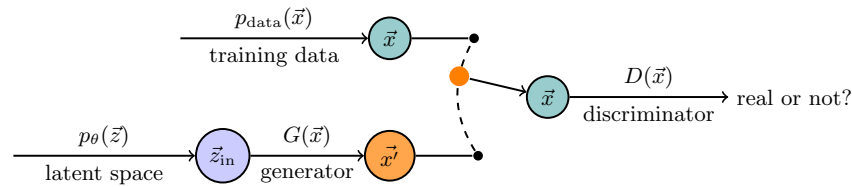

Fig. 1: Schema of a GAN

3 Problem definition and literature review

This section describes the addressed problem and reviews relevant related works.

3.1 Problem description

The addressed problem concerns the generation of synthesized data for mobility and transportation systems. Passenger mobility information is very relevant for management and quality of service assessment of public transportation, infrastructure planning, and other relevant issues to provide an enhanced and smart mobility [23].

In the real world, it is very common that the available data are not enough for a proper analysis, mainly because they are incomplete (e.g., the time series has gaps due to logging errors), they are obtained from different sources that are not always directly combinable (e.g., GPS traces, ticket sales, mobility data from third parties such as the applications from Google or Waze, mobile phones location data, etc.), or even because relevant information is not recorded (such as alighting points for trips performed in bus). Therefore, the generation of synthesized mobility data is an important line of research.

Special care must be taken to apply systematic methodologies that allow generating good quality data, which capture with the greatest possible precision the distributions and characteristics of the real data.

3.2   Related work

Several recent articles from Jauhri et al. have studied the problem of generating mobility data in urban areas. In 2020, Jauhri et al. [10] applied GANs for creating a model to generate synthesized mobility data for real world cases considering ride-sharing/hailing services from four cities in the USA (San Francisco, Los Angeles, New York, and Chicago) considering different temporal and spatial quantization of raw ride request data. The proposed GAN was able to learn the spatial and temporal variability of mobility patterns, according to the validation analysis performed considering the fractal dimensionality and the densification power law quantitative characterizations. A specific application of the generated data was also presented, namely the dynamic vehicle placement problem, to place in real time idle vehicles near possible future pickup locations. Results using the synthesized dataset maintained the same pattern than when using the real dataset. After that, Jauhri and Shen [9] applied the analysis for the characterization of human mobility considering data from twelve cities. The authors proposed a framework including a stochastic graph model and GANs for data augmentation to preserve the geographical and temporal characteristics observed in real data. The analysis included a formal characterizations of mobility applications (ride pooling and vehicle placement) and how to apply augmented datasets to analyze different mobility scenarios to be applied in real cities.

Saxena and Cao [22] propose a model based on a deep GAN for learning feature representations on spatio-temporal urban mobility data. Two computational intelligence models were applied: i) a deep GAN for feature learning, managing correlations, semantic variations, and irregularities in mobility data, and ii) a fusion module to combine multiple data sources with heterogeneous formats (e.g., weather data, information about points of interest, etc.), that help improving inference results. The proposed approach was validated on two real-world case studies, considering six months of the Yellow Taxi dataset and one month of the CitiBike trip dataset, both collected in New York, USA. An exhaustive comparison with 14 state-of-the-art statistical and leaning methods was performed, using the generated datasets for demand prediction. The proposed GAN-based approach computed the best Mean Square Error (RMSE) and Mean Absolute Error (MAE) results among the 15 studied methods.

Some recent articles have focused on protecting the privacy of mobility data. Liu et al. [11] proposed the TrajGAN framework, which applies GANs for privacy protection of trajectory data. The proposed model incorporates a geo-privacy protection layer for trajectory data and a traditional GAN architecture for generating synthetic trajectories that preserve the main features of real data. Authors described the main challenges for generating individual trajectories (i.e., with similar properties to each individual) and aggregated trajectories that approximate overall statistics of the training dataset, including the use of dense representations of trajectories as a fixed-length vector of numbers. Several validation metrics were proposed for both road- and place-based trajectories, including segment usage distribution and temporality, transportation mode, speed, time in transit, activity space, mobility motivations (for individual trajectories) and user distribution, driving behavior, temporal semantics of points of intrest, trip-length distribution, and OD matrix comparison (for aggregated trajectories).

Yin and Yang [28] also addressed the problem of generating synthesized trajectories that properly protect the information of users, using GANs. The proposed GAN was evaluated on two real world mobile datasets: MoMo Mobile App Dataset, a mobile SC networking application in China containing GPS data (fields: user ID, timestamp, latitude, and longitude) and San Francisco Cabs Dataset, containing mobility trajectories of taxi cabs in San Fancisco, USA (fields: cab ID, timestamp, latitude, and longitude.) Authors performed a comparison with differential privacy (DP), a privacy preservation method based on adding noises into aggregated mobility data. Results showed that the proposed method was able to improve over the differential privacy approach, considering metrics related to data usefulness and robustness against attacks.

Other articles have focused on important related problems, for which generation/data augmentation approaches using GANs have been proposed. New synthesized data are useful for predicting the location of specific vehicles or individuals; performing crowd flow prediction, i.e., forecasting in-out flows on a given urban area [27]; and generating realistic trajectories for vehicles or fleets of vehicles. Furthermore, these specific problems are related to higher important issues such as air quality and pollution, public services and public resources (e.g., water, electricity, etc.) utilization, public health and the spreading of diseases, among others. The main challenges related to generation of mobility data to be applied to these problems are capturing the dynamic of mobility patterns, and learning the spatial-temporal correlations between data.

4   Case study: the public transportation system in Montevideo, Uruguay

The Metropolitan Transportation System (STM) is a program whose objective is the integration of the public transportation of Montevideo and the metropolitan area into a common system. The system is aimed at improving mobility throughout the department of Montevideo and nearby population conglomerates.

STM proposed important investments in road infrastructure for public transportation. A significant modification of STM was including the use of new technologies that allow a more efficient, rational and safe public transportation. In turn, the system provides effective control and enhanced convenience for users, through routes and costs according to their specific needs. A conceptual diagram of the STM is presented in Fig. 2.
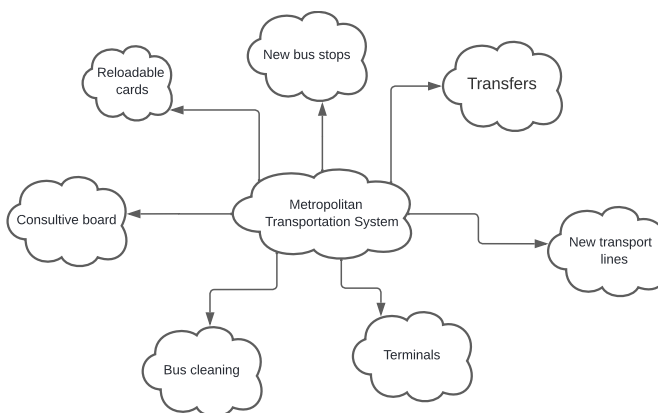

Fig. 2: Conceptual diagram of the STM (Montevideo)

One of the most relevant changes in STM was the incorporation of a smart card to pay for trips [13]. The smart card is an important technological tool to have control and knowledge about the trips or transfers for citizens of Montevideo and suburban areas [19]. Previous works from our research group [2,4,7,13,14,15,16] proved that is possible to process the data of millions of trips using the STM card crossing various sources (geospatial data, bus information, etc.) and conducting a data cleansing process to maintain integrity between them. As a result, a set of tabular data of user trips was obtained.

Travel records are divided into categories of users, namely: public transportation employees, teachers, retirees, minors, common users, among others. It was recently identified that the records of users who are public transportation employees are underrepresented, because the trips described do not faithfully represent the movement routine in the city of said users. This under-representation has a negative impact on the statistical indicators that are obtained from the original travel data. To address the presented issue, this article proposes applying a methodology for building at a more complete version of the trip data for transportation employees by generating synthesized data, based on the original data set for all users. In particular, we are interested in the trips made by the employees of the transport companies, therefore, the false sample must be filtered by that value. Filtering the sample allows us to focus on those rows that interest us to make a better statistical study.

5   A conditional tabular GAN for synthesized data generation for the STM

This section describes the data source and the methodology applied for synthesized data generation for the STM using a GAN approach.

5.1   Data sources

The main source of data is the repository of urban mobility data for the public transportation systems in Montevideo, Uruguay, developed by our group [13]. It consists of tabular data in csv format. Data for a total number of 289 271 trips were reported, from trips paid using a smart card.

Relevant information considered in the analysis includes attributes that identify users, the bus lines (to know the route each passenger takes), the number of tickets paid using the smart card in each transaction, and the company operating each line. These attributes are categorical in the set and correctly describe the mobility patterns of users. In turn, geographical data sources (e.g., shapefiles containing the route of the considered bus lines) are used to properly locate bus lines and selecting relevant case studies for the analysis.

5.2   Overall description of the methodology

The applied methodology consists of eight activities, organized in three phases, as described next.

Phase 1: Data analysis and preprocessing. The first phase included two activities: statistical analysis of source data and grouping. The statistical analysis of source data studied the main features of the available data, including the number of lines and users of the STM, ticket types, user category and number of passengers. If necessary, attributes (or columns) of the sample that are not relevant for the proposed study (such as date and time of the trip, or patronymic data of the passengers) are eliminated. After that, the available data were grouped according to the type of user (i.e., transportation employees) to identify the most demanded lines in the city. Studying the composition of origin–destination for user trips in Montevideo is relevant from the study. From a quantitative point of view, it is recommended groping the individual records into groups of users to determine their proportion over the total number of trips and to account for all the different lines. For example, there should not be a majority of trips associated with lines in the metropolitan area, since they are the least requested trips. Furthermore, it should be analyzed whether the number of lines used by a group of users is representative of their usual trips.

Another relevant analysis is the identification of underrepresented sets. The statistical analysis detected that few information is available in the repository for some user categories. Some data are incomplete or do not represent the daily nature of the trips of those users. Identifying underrepresented categories is crucial, as they are the target categories for data augmentation using GANs.

Phase 2: Resolution. The resolution phase included three activities: selection of the GAN model and architecture, training, and generation of synthesized data. From the analysis, a conditional GAN for modeling and generating tabular data (CTGAN) was selected. CTGAN is specialized on the generation of tabular data. CTGAN has been applied to generate high-quality synthesized tables, including discrete and continuous variables. This property is very relevant for the reported research, to correctly generate new data based on the real samples available.

The applied CTGAN was trained considering relevant accuracy metrics and controlling overfitting. Finally, the CTGAN was applied to generate synthesized data from the real samples, with the main goals of respecting the distribution, proportions and fidelity of the original data.

Phase 3: Validation. The last phase included activities to analyze the quality of the generated data. First, specific metrics were applied to evaluate the distributions and features of the generated data and two-dimensional graphics were used to study the correlation with the attributes of real data. After that, cross-validation was applied combining the generated data with other sources of geographical information, to analyze the bus lines and passengers routes. Finally, visualization tools were used to generate maps for a proper visual evaluation of the generated data. Fig. 3 describes the activities in phases 2 and 3.
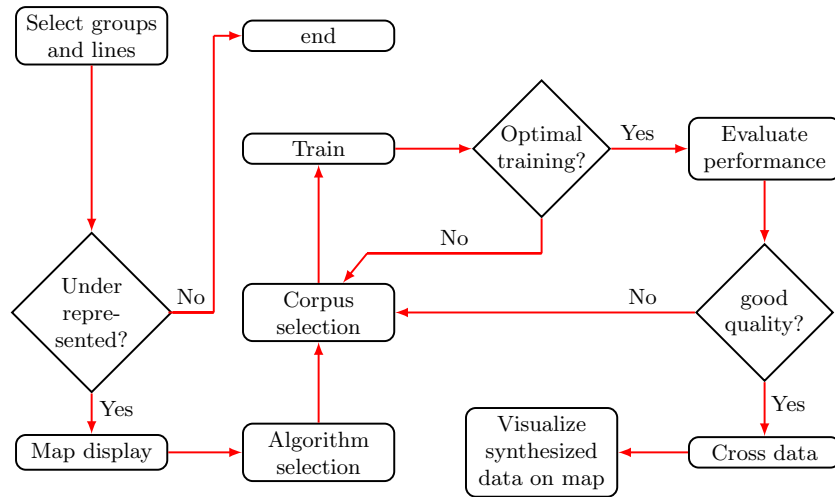

Fig. 3: Activities in the resolution and validation phases

5.3 The proposed GAN for synthesized data generation

The proposed approach consists in generating synthesized mobility data based on the information from all trips of the user groups. A supervised learning approach is applied, based on structured data. To properly capturing the class information associated with the groups of users in the considered problem, a conditional GAN is applied. The diagram of a conditional GAN is presented in Fig. 4.

$$p_{\text{data}}(\vec{x})$$
training data
$$p_{\text{data}}(\vec{y})$$
training data
$$p_\theta(\vec{z})$$
latent space
$$G(z_{in}, \vec{y'})$$
generator
$$D(\vec{x}, \vec{y})$$
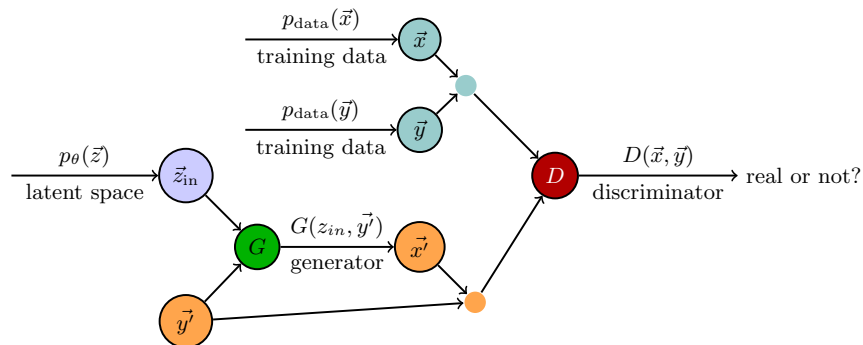discriminator → real or not?

Fig. 4: Schema of a conditional GAN

The applied CTGAN uses the training-by-sampling approach and conditional generators to resample the training data, so that all categories in discrete variables have a fair chance of being included in the sample that GAN learns from.

6 Experimental analysis and discussion

This section describes the experimental evaluation of the proposed CTGAN approach. The obtained results are reported and discussed.

6.1 Development and execution platform

The proposed CTGAN was developed in Python3, following the replicable research approach. Specific libraries and packages were applied for processing geographic information (Geopandas) and for statistical analysis (scikit-learn). The library CTGANSynthesizer was used for the implementation and the table_evaluator library was applied to evaluate the correlations between the real samples and the synthesized data. The experimental analysis was performed on the high performance computing platform of National Supercomputing Center (Cluster-UY), Uruguay [18].

6.2 Problem instances

The considered instances correspond to trip records of a particular month (April 2021). This month was selected since it is a representative month for bus trips, with a normal demand of mobility and activities in the city. Each instance was built considering a representative sample of trips, respecting the proportions of trips performed on each line. The proposed CTGAN was trained with this subset, which comprise about a fifth of the records in the complete repository.

Information in the considered problem instances includes:

– Type of the trip (TT): This attribute refers to the user category. The user category has the following values: common users (US), student (ST), institutional (OG), retired (RT), and transportation (TR).
– User group (UG): This attribute groups users according to the fare of the ticket. The considerd groups are one hour (1H), two hours (2H), student A (STA), student B (STB), retired A (RTA), retired B (RTB).
– Number of passengers (NP): This attribute indicates the number of tickets paid in each smart card transaction (between one and seven).
– Description of the company (CD): This attribute is the name of the transportation company that operates the line.
– Code of the line (CL): This attribute is a numerical code that allows linking the line with geographical data.

6.3   Results and discussion

This subsection reports and discusses the results of the experiments performed to analyze the similarity and correlation between synthesized and real data.

CTGAN training. The CTGAN was trained for 10 epochs, considering the loss functions defined for both the generator and discriminator. The training process was performed over a training dataset, defined by the following five categorical attributes: trip type, user group, number of passengers, company, and line, which define the characteristics of the passengers using each line. Fig. 5 presents the evolution of the discriminator and generator loss in training experiments.
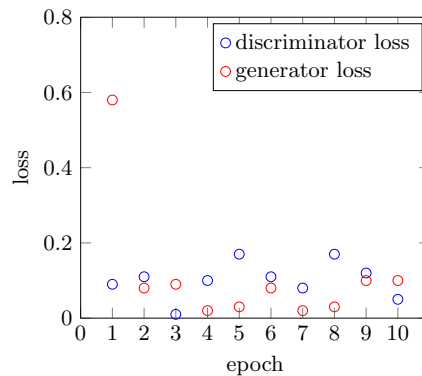

Fig. 5: Evolution of the discriminator and generator loss in training experiments

Results in Fig. 5 show that the generator loss reduced and that the loss of the discriminator and the loss of the generator have rather similar values after epoch 2. This results indicate that the generator is sufficiently well trained to generate sinthetized data samples that are able to deceive the discriminator. Overall, the training was performed in an average execution time of ten minutes.

CTGAN validation. The main goal of the validation experiments is to analyze the similarities of the synthesized data generated using the proposed CTGAN with samples of the real data. Three samples are considered in validation analysis, including 10000, 50000, and 100000 records. The table_evaluator library is applied to compute similarity metrics between synthesized and real data.

Modal partition. The first study evaluates the modal partition of the categorical variables in the artificial set, compared with the ones in the real data. This analysis allows detecting if the proportions/relative distributions of each attribute are respected in the generated data. Fig. 6 presents an example of the obtained results, regarding mode partition of the user category field. In turn, Fig. 7 presents the mode partition of tickets type for both real and synthesized data.
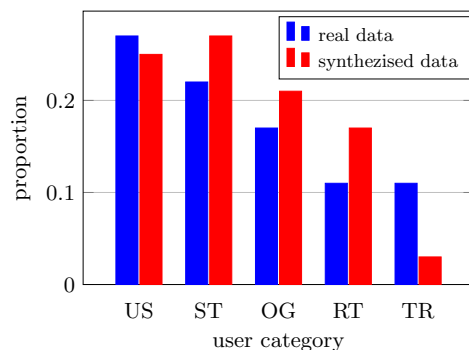
Fig. 6: Modal partition of user categories

The graph bar in Fig. 6 shows that the synthesized data has a similar distribution (modal partition) for the different user categories. Some deviations are detected in medium-valued categories (ST, OG, and RT), where the proposed CTGAN generated larger values than real data. Deviations are below 5% in those cases. A similar situation is observed for ticket type RTB in Fig. 7.
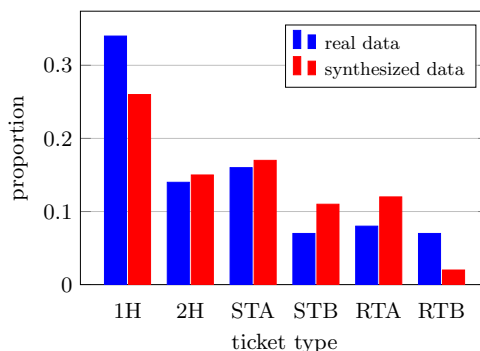

Fig. 7: Modal partition of ticket types

Number of passengers. Fig. 8 compares the real and synthesized data regarding another relevant attribute for travel demand characterization: the number of passengers for each smart card transaction.
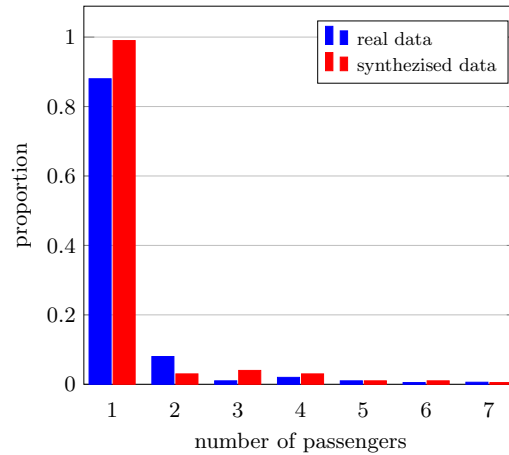

Fig. 8: Modal partition of number of passengers

The most relevant results from Figs. 6–8 are related to the most important categories (type of travel, group of users and quantity of tickets), which accounts for the larger proportion in previous analysis. These categories are considered for the analysis of correlations in both real and synthesized data.

Analysis of correlations. Table 1 reports a statistical analysis of three samples of the generated synthesized data filter by code line. Values reported in the table are computed from the synthetic report by table_evaluator. The computed statistical estimators are the mean coefficient of correlation between synthesized and real data, the similarity score and the number of rows duplicated between synthesized and real data.

Table 1: Statistical analysis for three samples of the generated synthesized data

instance	size	mean correlation	similarity score	duplicated rows
sample 1	10000	0.8001	0.8004	(9669,8990)
sample 2	50000	0.9394	0.6505	(49649,48012)
sample 3	100000	0.8154	0.7405	(99649,96815)

Results in Table 1 suggest that the proposed CTGAN approach was able to generate accurate synthesized samples, with up to 0.94 of mean correlation and up to 0.80 similarity score with real data.

The heatmaps in Fig. 9 graphically report the correlation between attributes for representative real and synthesized data samples.

	TT	UG	NP	CD	CL
TT	1.0	0.9	0.2	0.1	0.2
UG	0.8	1.0	0.2	0.1	0.1
NP	0.1	0.0	1.0	0.1	0.0
CD	0.0	0.0	0.0	1.0	0.2
CL	0.1	0.0	0.0	0.2	1.0

(a) Correlation for a real sample

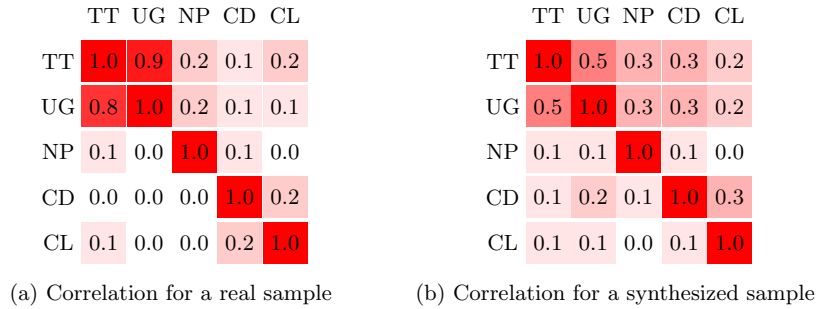|	TT	UG	NP	CD	CL
TT	1.0	0.5	0.3	0.3	0.2
UG	0.5	1.0	0.3	0.3	0.2
NP	0.1	0.1	1.0	0.1	0.0
CD	0.1	0.2	0.1	1.0	0.3
CL	0.1	0.1	0.0	0.1	1.0

(b) Correlation for a synthesized sample

Fig. 9: Heatmaps of correlation between columns

The correlation heatmaps in Fig. 9 summarizes the main results in the correlation matrix. Heatmaps show a similar pattern for both real and synthesized sample, suggesting that the generated data properly captures the distribution and correlations of existing real data.

Summarizing, the computed results show that there is a great similarity between the real and synthesized data samples. This result suggests that it is possible to consider the generated samples as valuable data augmentation sets to compute accurate statistics about the STM utilization.

7   Conclusions and future work

This article presented a study applying a GAN approach for generating synthesized data for public transportation systems.

A CTGAN neural network was applied to properly model tabular data from ticket sales of ITS. The model was trained with real data from the case study considered in the validation experiment: the public transportation system in Montevideo, Uruguay.

The main results indicated that the proposed CTGAN was able to generate accurate synthesized mobility data, according to the statistical analysis of correlations and the graphical analysis of distributions. Accurate values were obtained for the metrics used to analyze the results: up to 0.94 of mean correlation and up to 0.80 similarity score with real data. Summarizing, the computed results show that there is a great similarity between the real and synthesized data samples. This result suggests that The generated synthetic datasets are valuable inputs for data augmentation to be used for computing relevant metrics and statistics about the public transportation system in Montevideo.

The main lines for future work are related to expand the proposed methodology to better capturing the main features and attributes of real public transportation data, by applying other GAN models or other generative approaches.

References

1. Cervero, R., Guerra, E., Al, S.: Beyond Mobility. Island Press/Center for Resource Economics (2017)
2. Denis, J., Massobrio, R., Nesmachnow, S., Cristóbal, A., Tchernykh, A., Meneses, E.: Parallel computing for processing data from Intelligent Transportation Systems. In: 10th Int. Supercomputing Conf. in Mexico. pp. 1–15 (2019)
3. Emam, K.E., Mosquera, L., Hoptroff, R.: Practical Synthetic Data Generation. O'Reilly Media, Inc. (2020)
4. Fabbiani, E., Nesmachnow, S., Toutouh, J., Tchernykh, A., Avetisyan, A., Radchenko, G.: Analysis of mobility patterns for public transportation and bus stops relocation. Programming and Computer Software **44**(6), 508–525 (2018)
5. Foster, D.: Generative Deep Learning. O'Reilly Media, Inc. (2019)
6. Goodfellow, I., Pouget-Abadie, J., Mirza, M., Xu, B., Warde-Farley, D., Ozair, S., Courville, A., Bengio, Y.: Generative adversarial nets. In: Advances in neural information processing systems. pp. 2672–2680 (2014)
7. Hipogrosso, S., Nesmachnow, S.: Analysis of Sustainable Public Transportation and Mobility Recommendations for Montevideo and Parque Rodó Neighborhood. Smart Cities **3**(2), 479–510 (2020)
8. James, S., Harbron, C., Branson, J., Sundler, M.: Synthetic data use: exploring use cases to optimise data utility. Discover Artificial Intelligence **1**(1) (2021)
9. Jauhri, A., Shen, J.P.: Real-world data driven characterization of urban human mobility patterns. Tech. rep., Mobility21, Carnegie Mellon University, USA (2021)
10. Jauhri, A., Stocks, B., Li, J.H., Yamada, K., Shen, J.P.: Generating realistic ride-hailing datasets using GANs. ACM Transactions on Spatial Algorithms and Systems **6**(3), 1–14 (2020)
11. Liu, X., Chen, H., Andris, C.: trajGANs: Using generative adversarial networks for geo-privacy protection of trajectory data. In: Location Privacy and Security Workshop. pp. 1–7 (2018)
12. Machín, B., Nesmachnow, S., Toutouh, J.: Multi-target evolutionary latent space search of a generative adversarial network for human face generation. In: Genetic and Evolutionary Computation Conference (2022)
13. Massobrio, R., Nesmachnow, S.: Urban Mobility Data Analysis for Public Transportation Systems: A Case Study in Montevideo, Uruguay. Applied Sciences **10**(16), 1–20 (2020)
14. Massobrio, R., Nesmachnow, S., Tchernykh, A., Avetisyan, A., Radchenko, G.: Towards a cloud computing paradigm for big data analysis in smart cities. Programming and Computer Software **44**(3), 181–189 (2018)
15. Massobrio, R., Nesmachnow, S.: Travel time estimation in public transportation using bus location data. In: Smart Cities, pp. 192–206. Springer International Publishing (2022)
16. Massobrio, R., Pías, A., Vázquez, N., Nesmachnow, S.: Map-Reduce for Processing GPS Data from Public Transport in Montevideo, Uruguay. In: Simposio Argentino de Grandes Datos, 45 Jornadas Argentinas de Informática. pp. 41–54 (2016)
17. Nesmachnow, S., Baña, S., Massobrio, R.: A distributed platform for big data analysis in smart cities: combining intelligent transportation systems and socioeconomic data for montevideo, uruguay. EAI Endorsed Transactions on Smart Cities **2**(5), 153478 (2017)
18. Nesmachnow, S., Iturriaga, S.: Cluster-UY: Collaborative Scientific High Performance Computing in Uruguay. In: Torres, M., Klapp, J. (eds.) Supercomputing,

Communications in Computer and Information Science, vol. 1151, pp. 188–202. Springer (2019)

19. Nesmachnow, S., Risso, C.: Exact and evolutionary algorithms for synchronization of public transportation timetables considering extended transfer zones. Applied Sciences **11**(15), 7138 (2021)

20. Ng, A., Jordan, M.: On discriminative vs. generative classifiers: A comparison of logistic regression and naive Bayes. In: Conference on Neural Information Processing Systems (2002)

21. Pan, Z., Yu, W., Yi, X., Khan, A., Yuan, F., Zheng, Y.: Recent progress on generative adversarial networks (GANs): A survey. IEEE Access **7**, 36322–36333 (2019)

22. Saxena, D., Cao, J.: Multimodal spatio-temporal prediction with stochastic adversarial networks. ACM Transactions on Intelligent Systems and Technology **13**(2), 1–23 (2022)

23. Shi, R., Steenkiste, P., Veloso, M.: Generating synthetic passenger data through joint traffic-passenger modeling and simulation. In: Zhang, W., Bayen, A.M., Medina, J.J.S., Barth, M.J. (eds.) 21st International Conference on Intelligent Transportation Systems. pp. 3397–3402 (2018)

24. Sussman, J.: Perspectives on Intelligent Transportation Systems (ITS). Springer Science + Business Media (2005)

25. Toutouh, J., Esteban, M., Nesmachnow, S.: Parallel/distributed generative adversarial neural networks for data augmentation of COVID-19 training images. In: High Performance Computing, pp. 162–177. Communications in Computer and Information Science, Springer International Publishing (2021)

26. Toutouh, J., Nesmachnow, S., Rossit, D.G.: Generative adversarial networks to model air pollution under uncertainty. In: International Workshop on Advanced Information and Computation Technologies and Systems, CEUR Workshop Proceedings, vol. 2858, pp. 169–174. CEUR-WS (2020)

27. Wang, S., Miao, H., Chen, H., Huang, Z.: Multi-task adversarial spatial-temporal networks for crowd flow prediction. In: Proceedings of the $29^{t}h$ ACM International Conference on Information & Knowledge Management. ACM (2020)

28. Yin, D., Yang, Q.: GANs based density distribution privacy-preservation on mobility data. Security and Communication Networks **2018**, 1–13 (2018)

Big data analysis for delay estimation
of public transportation systems

Santiago Guridi[0000−0002−4448−0435], Santiago Olmedo[0000−0002−4500−8028], and
Sergio Nesmachnow[0000−0002−8146−4012]

Universidad de la República, Uruguay
santiago.guridi,santiago.olmedo,sergion@fing.edu.uy

Abstract. This article presents a proposal applying big data analysis
and parallel computing for delay estimation of public transportation sys-
tems. This is a relevant problem to assist the planning and operation of
Intelligent Transportation Systems to provide a better quality of service
to passengers. The proposed methodology applies parallel computing for
processing large volumes of data to estimate the punctuality or delay
of buses in main avenues, using relevant real information about ticket
sales. A practical validation is presented for a real case study in the pub-
lic transportation in Montevideo, Uruguay. The main results indicate
that the proposed approach is able to efficiently compute delay metrics.

Keywords: public transportation, quality of service, urban data analysis

1　Introduction

Mobility is a key concept within the paradigm of smart cities, and a pillar of
sustainable urban development [2]. Public transportation is crucial in the struc-
ture of modern cities, directly impacting in terms of efficiency and sustainability.
Public transportation is considered significantly more energy efficient than other
transportation modes, and also offers competitiveness versus private transporta-
tion, when efficient travel times, direct routes or few transfers, and high service
frequency are provided [14]. Furthermore, public transportation allows reducing
pollutant emissions, diminishing the number of vehicles in the roads and crowd-
ing/traffic jams, build cleaner, greener communities, and is more affordable.

Although the ratio between travel times of public transportation and private
transportation varies depending on several factors, the concerns of users about
travel time on public transportation is less when the travel time is reasonably
predictable. Thus, the analysis of urban mobility data is crucial to help admin-
istrations and public transportation companies to provide a better quality of
service (QoS) and travel experience [17].

The emergence of data-driven approaches led to the paradigm of Intelligent
Transportation Systems (ITS). Conceived as innovative systems that integrates
synergistic technologies, ITS allows developing valuable services to improve pub-
lic transportation operation and provide useful information to passengers [22].

ITS make use of large volumes of data collected by different types of sensors and devices (passenger counters, GPS devices, video cameras, ticket vending machines, etc.). The development of smart tools that use data collected by the ITS infrastructure has increased in recent years, allowing citizens to interact with transportation systems and improve their travel experiences. These tools are based on efficient and accurate data processing, posing an interesting challenge from the technological point of view. In this context, parallel/distributed computing has emerged as a useful solution to process large volumes of data to be used in applications by citizens and authorities alike.

This article proposes a thorough analysis of the delays in public transportation systems. A urban data analysis approach [15] is proposed for computing the delays between scheduled times and real times. Considering the large amount of data processed and the number of costly operations needed to compute the proposed metrics, high performance computing techniques are used to achieve the results reasonable execution times. A specific case study is studied: the public transportation system in Montevideo. Results are analyzed in the context of the city and the metropolitan area, focusing on the most important streets and avenues. Several relevant metrics are computed, including the delays between scheduled times and real times, the difference between delays on weekdays and weekends, the difference between the delays in rush hours and quiet hours, the difference between the delays for each of the main streets a given bus line where it operates, and the percentage of trips that have a meaningful delay. The analysis focuses on the bus stops with the higher demand of trips, from the most important streets and avenues in the city.

The main results of the research indicate that the performance of the public transportation system improved in the last five years. The computed delays are rather low, less than 14% of the frequency in rush hours. Few trips (1.2%) have a significant delay. These results allow concluding that delays are not the main issue about the local public transportation system in Montevideo, but other concerns [11]

Overall, this article contributes with the proposal of a methodology for the applications of high performance computing techniques in the context of big data analysis for delay estimation. It also contributes to the evaluation of the proposed methodology in a real case study, considering real data from the public transportation system in Montevideo, Uruguay.

The article is organized as follows. Section 2 describes the problem addressed in this article and reviews related works. Section 3 describes the case study, the public ITS in Montevideo, Uruguay. The applied methodology and implementation details is presented in Section 4. The experimental evaluation of the proposed approach is reported in Section 5. Finally, section 6 presents the conclusions of the research and formulates the main lines for future work.

2   Problem definition and literature review

This section describes the addressed problem and reviews relevant related works.

2.1   Delay estimation in public transportation systems

The addressed problem concerns the assessment of punctuality of bus lines to the planned schedules and evaluate their deviations, especially tardiness, when trips or lines suffer a systematic delay. Several static metrics have been proposed to evaluate the performance of public transportation systems (e.g., service coverage, frequency, and travel time). Other relevant dynamic metrics, such as delay identification and estimation, are useful for performance evaluation, since they are often more related to the QoS perceived by users [24].

Delay estimation is utterly relevant for transportation administrators and users. On the one hand, a proper performance evaluation of the public transportation system allows implementing active management and proactive operation techniques. On the other hand, the ability to be punctual when covering routes is crucial for service reliability, which is directly related to user satisfaction.

Municipal administrations and public transportation companies provide citizens with theoretical timetables, defining the time of day in which each bus line must arrive/pass through the different stops. The information is public and easy to access, so people can use it to plan their trips, to reach the corresponding stop a few minutes earlier than the theoretical information establishes. In practice, due to many factors, bus trips may have a delay with respect to the predefined schedule. Delays are often caused by variations in traffic and passengers demand, external factors such as weather conditions or street repairing, etc.

The problem proposes applying big data analysis for computing the deviation from the theoretical timetables from information gathered about ticket sales, lines and paths of the public transportation system, and GPS locations of bus stops. The proposed approach is validated for a case study defined over the public transportation system of Montevideo, Uruguay, analyzing the speed and delay over several main avenues of the city road network.

2.2   Related work

Big data analysis have been largely applied to study the travel behavior of citizens and to evaluate the QoS provided to users [28,26].

An important topic refers to the different sources of information for the analysis of public transportation systems. Automated vehicle location (AVL) and automated passenger counting systems (APC) systems are two of the main sources to get vehicle mobility information (e.g., GPS coordinates, speed), but several other important sources are often available, such as cell phone information (providing GPS and WiFi signals), web logs and social media (providing user identification, incident reports, comments, etc.). Crowdsourced data are also very useful, e.g., from mobile apps and traffic/surveillance cameras.

Regarding QoS analysis, Chen et al. [4] applied big data analysis on Hadoop to predict traffic speed using historical ITS data, weather conditions, and special events. The model was evaluated on a real scenario in California, USA, obtaining

high accuracy and improved performance when executed on a cluster of computers. Xia et al. [27] developed a distributed version of the kNN algorithm in Hadoop for forecasting public transportation traffic flow. GPS data from over 12000 taxis in Beijing were used for evaluation. The main results indicated that the distributed KNN reduced the mean absolute error up to 11.5% on average over other kNN-based methods, while achieving well computational efficiency. Erhardt et al. [6] studied performance metrics, including level-of-service, reliability, and crowding, using big data from AVL and APC systems.

Other relevant developments include web-based applications using large volumes of data to assist public transportation operators to monitor the QoS of the system [1], algorithms for building origin-destination matrices to improve operation [9], and systems that use mobile phone data for proposing route modifications and optimization for bus services, to improve user satisfaction [3].

Several articles have focused on big data analysis to identify delays in public transportation. Khiari et al. [13] applied big data from AVL and APC and machine learning for defining schedules and suggesting route improvements. The approach was successfully evaluated on Sweden. Ingvardson et al. [12] applied big data analysis of smart card trips to compute the distributionss of passenger arrival and waiting time for train stations in Copenhagen, Denmark. Gröflin et al. [8] used big data crawling from the web to analyze and detect trams or buses that experienced a delay of a minute or more in the public transportation system of Basel, Switzerland. Rahman et al. [21] used GPS data to determine if buses are on time by computing the distance between the GPS transmitted on each bus and the upstream GPS receiver. The method estimated intervals considering the uncertainty of (future) bus arrival times, given that early and late buses have their own deviations. Szymański et al. [23] used GPS data to develop a spatio temporal characterization of delays in the public transportation system of Wrocław, Poland. The proposed approach applied hierarchical clustering to identify six different types of delays. Wang et al. [25] studied the impacts of winter weather on bus travel time in cold regions of China.

In Uruguay, several works from our research group [5,7,10,15,16,17,18] have applied data analysis for processing trips data through the smart card used in the public transportation system of Montevideo. The general approach consisted on combining data from multiple sources (geospatial data, static information about lines and bus stops, timetables, data from GPS records, and in-situ surveys), applying a data cleansing process to maintain integrity, and develop specific algorithms for the specific goals of each research, such as the construction of origin-destination matrices [16], the evaluation of sustainable mobility [10], the calculation of relevant metrics about public transportation use [17], etc.). Our previous work [18] addressed the problem of processing large volumes of historical GPS data from buses to compute quality-of-service metrics for urban transportation systems. We designed and implemented a solution to distribute the data processing in a distributed computing infrastructure. The solution was evaluated for a case study, using historical data from the ITS in Montevideo, Uruguay. The proposed solution scaled properly when processing large volumes

of input data. The study evaluated the QoS of bus lines in Montevideo and identified problematic locations.

3　Case study: the public transportation system in Montevideo, Uruguay

The case study addressed in this article of big data analysis for delay estimation is the public Metropolitan Transportation System (STM) in Montevideo, Uruguay. The STM integrates the public transportation of Montevideo and the metropolitan area into a common system.

STM introduced the use of new technologies, allowing a more efficient and safe public transportation. A relevant technology introduced by the STM was incorporating a smart card to pay for trips [15]. This technology allows gathering important data and extract useful knowledge about the trips or transfers for citizens of Montevideo [20]. The analysis of smart card data gathered by the STM allows computing several relevant indicators for properly dimensioning, operating, and improving the QoS provided to citizens. The automatic processing of large volumes of STM data has allowed developing relevant studies, such as building origin-destination matrices, establishing travel demand characterization, performing socio-demographic mobility analysis, etc.

Previous articles from our research group [5,7,15,16,17,18] studied the STM and proposed processing trip data from smart card records for specific analysis. Several other sources of data, including geospatial data, information on lines and bus stops, socio-demographic information, among others, were also used.

4　Delays of the public transportation in Montevideo

This section describes the data sources and the methodology applied for delay estimation of public transportation systems.

4.1　Data sources

The data collections used in the analysis were gathered from The National Catalog of Open Data of Uruguay who allows accessing to open data from public institutions, academia, civil society organizations, and private companies in the country. The data collections used included"

- Bus tickets sold in specific months, gathered from the use of the STM. Several field are included in this collection, the most relevant for this research are: *ftripId*, that identifies a specific trip within a specific month; *DateTime*, date and time when the ticket was sold; *OriginStop*, origin bus stop; *Company*, company that the bus belongs to; *Line*, bus line; and *Variant*, line variant.
- Bus stops information. It has static information about bus stops, the most important metadata for this collection is as follows: *stopUbicCode*, that identifies a bus stop; *Street* and *Corner*, giving the geographical location of the stop.

- Planned schedule for lineal trips. The metadata for these collections is as follows: *dayType*, a numerical value, meaning 1: working day, 2: Saturday, and 3: Sunday; *variantCode*, identifies a line variant; *stopUbicCode*, identifies a bus stop; *hour*, time at which the bus passes by the stop;
- Planned schedule for circular trips, including the meta-attribute *cod_circular* (circular trip code) and all attributes of lineal trips.

4.2   A parallel algorithm for delay estimation

The proposed algorithm for processing big data from trips performed in the public transportation system in Montevideo is described in Algorithm 1.

Algorithm 1 Trips processing

1: avenues_list ← get_avenues()
2: bus_stops_with_counter ← get_bus_stops_avenue(avenues_list)
3: busiest_bus_stops ← get_busiest_bus_stops(bus_stops_with_counter)
4: scheduled_times_busiest_stops ← get_schedule(busiest_bus_stops)
5: estimate_frequency(scheduled_times_busiest_stops)
6: trips ← read_monthly_trips_dataset()
7: **for** *number_process* in range(*number_processes*) **do**
8:     processes.append(compute_delay(trips,scheduled_times_busiest_stops, queue)))
9: **end for**
10: **for** *p in processes* **do**
11:     p.start()
12: **end for**
13: final_dictionary ← empty_dictionary
14: **for** *p in processes* **do**
15:     final_dictionary ← final_dictionary.append(p.get(queue))
16: **end for**

Algorithm 1 was applied for computing the delay for a set of relevant avenues, specified in a configuration file. The configuration file also allows defining relevant variables in the algorithm. The main features of the proposed processing algorithm are described in the following paragraphs.

Parallel calculation. Considering the large volume of data to be processed (i.e., more than 25 millions of tickets are sold each month), parallel computing techniques were used for an efficient calculation of relevant metrics in different scenarios. Since the delay for each trip can be calculated independently of the others, the parallel calculations were straightforward. The data parallel approach consisted in splitting the set of tickets sold among the processes available for computation. The tickets sold each month were divided in order and assigned to each process. Each process was assigned a subset of the monthly tickets and performed the algorithms independently (i.e, they do not share information to other processes). Each process returns a dictionary with the mean delay for each

of the assigned tickets. After each process completes its task, the dictionaries are joined to obtain one data structure with the results of the entire month. All the functionalities related to parallel computing were implemented and successfully accomplished by using the multiprocessing library from Python.

Processing logic. The first step is gathering the avenues to be considered in the calculation. The get_avenues function reads a configuration file and returns the avenues to be processed (line 1). Then, the get_bus_stops_avenue function is applied. It receives a list with the avenues to be processed and returns a dictionary containing the bus_stops on relevant avenues, with the following format:

``bus_stop_code'': {``tickets_sold'', ``main_st'', ``secondary_st''}.

The procedure for filtering the entire set of bus stops to get the ones located on the given avenues is described in Algorithm 2.

Algorithm 2 Function get_bus_stops_avenue

Input: avenues_list: list of relevant avenues for the calculation
Output: dictionary with the bus stop code as the key and, the tickets sold, the street that it lies on and the secondary street as values
1: bus_stops ← read_bus_stops_dataset()
2: filtered_bus_stops_by_avenue ← join bus_stops with avenues_list by *street*.
3: final_dictionary ← empty dictionary
4: **for** *bus_stop in filtered_bus_stops_by_avenue* **do**
5:     final_dictionary[bus_stop[code]] ← [0, bus_stop[main_st], bus_stop[secondary_st]]
6: **end for**
7: trips ← read_monthly_trips_dataset()
8: **for** *trip in trips* **do**
9:     current_bus_stops_code ← assign the bus stop code for the current trip
10:     final_dictionary[current_bus_stops_code][1] += 1
11: **end for**
12: **return** final_dictionary.

Algorithm 2 reads the bus stops and join them with avenues_list, by the street field. Then, iterates over the monthly trips, computing the number of tickets sold in each bus stop in the considered month. After that, the main algorithm applies the function get_busiest_bus_stops. For each avenue, the bus stops are ordered by tickets sold, in descending order. The N (variable defined by NUMBER_OF_BUS_STOPS in the configuration file) bus stops with the most tickets sold are stored for each avenue. The delay of a trip is computed on the busiest bus stops in an avenue, since many bus stops lie close to each other and several have a low flow of passengers. Nevertheless, the NUMBER_OF_BUS_STOPS variable allows performing the computation for any given number of bus stops.

Ater that, using the previously built dictionary, the get_schedule function (line 4) returns a dictionary with the scheduled weekly trips for the busiest bus stops, with the following format:

``bus_stop_code": { ``bus_line'': { [``day_type'', ``scheduled_time'',
``main_street'', ``secondary_st''] } }.

Then, the frequency (i.e., the time between two consecutive trips of buses operating the same line) is estimated (line 5), by applying Algorithm 3.

Algorithm 3 Function estimate_frequency

Input: dictionary with the scheduled weekly trips for the busiest bus stops
Output: dictionary with the scheduled weekly trips for the busiest bus stops expanded with a field for each bus line in a bus stop, representing the time between two consecutive trips of buses operating the same line on the same bus stop.
1: **for** $scheduled\_time = 1, 2, \ldots$ **do**
2:     select the closest 3 scheduled times to scheduled_time
3:     frequency $\leftarrow$ calculate the average differences of the 4 times.
4:     add a column to the corresponding scheduled_time with the frequency
5: **end for**

The frequency of each bus line is relevant to match each ticket sold with a scheduled trip. Algorithm 3 selects, for each scheduled time for a bus line in a bus stop, the closest three scheduled times and computes the average difference.

Then, Algorithm 3 adds a field to the correspondent bus_line and bus_stop with the estimated frequency. The returned dictionary has the following format:

``bus_stop_code'': { ``bus_line'': { [``day_type'', ``scheduled_time'',
                ``main_street'', ``secondary_st'', ``estimated_frequency''] } }

The next stage of the main algorithm is the computation of delays (lines 7–9). This task is performed by each process executing in parallel, over a fraction of the monthly tickets sold. The specific computation is performed by function compute_delay, whose pseudocode is presented in Algorithm 4.

Algorithm 4 Function compute_delay

Input: trips: the dataset with the monthly trips
Input: scheduled_times_busiest_stops: dictionary with the scheduled weekly trips for the busiest bus stops
Output: dictionary with the delay for each trip
1: result $\leftarrow$ empty dictionary
2: **for** $ticket\_sold$ in trips **do**
3:     **if** $ticket\_sold$.bus stop() is in scheduled_times_busiest_stops **then**
4:         **if** $ticket\_sold$.bus line() is in scheduled_times_busiest_stops **then**
5:             **for** $time$ in scheduled_times_busiest_stops[bus_stop][bus_line] **do**
6:                 delay $\leftarrow$ compare_with_frequency(time,ticket_sold[time], bus_frequency)
7:                 result $\leftarrow$ add_delay_to_dictionary(delay)
8:             **end for**
9:         **end if**
10:     **end if**
11: **end for**

Algorithm 4 computes the delay for each ticket sold and stores the mean of the delays in a nested dictionary identified by day of the week, time of the day, bus stop, and bus line. It iterates over all tickets sold and filters by bus stop and bus line. Then, the time of the day and day of the week are compared between the ticket sold and the scheduled information. The delay is computed by function compare_with_frequency, presented in Algorithm 5.

Algorithm 5 Function compare_with_frequency

    Input: scheduled_time, real_time, bus_frequency.
    Output: computed delay.
1: **if** $scheduled\_time[day\_week]$ $equals$ $real\_time[day\_week]$ **then**
2:    delay = real_time[hour] − scheduled_time[hour]
3:    **if** $delay > (2/3) \times frequency$ or $delay < -frequency \times (1/3)$ **then**
4:       **return** none
5:    **else**
6:       **return** delay
7:    **end if**
8: **end if**

One of the main challenges detected was matching the time each ticket was sold with the scheduled time for the trip of the corresponding line. The main issue is how to determine if the bus is arriving early for the next scheduled trip or if it is arriving late for the last trip.

The following approach was adopted to deal with the previously commented issue. First, a comparison is performed to determine if the day of the week matches the day the ticket was sold and the day of the scheduled time. If that is the case, the delay is computed by computing the time the ticket was sold minus the time the trip was scheduled. Then, if the bus is arriving later than $2/3 \times frequency$ or arriving earlier than $1/3 \times frequency$, it means than the tickets sold do not correspond to the considered scheduled time. The threshold considered for the computation (1/3) is a parameter read by the algorithm that is editable by the user in the configuration file.

4.3 Methodology for the statistical analysis

The experimental results presented in Section 5 were calculated from the dictionary returned by Algorithm 4, which has the following format:

   "street_avenue": { "day_week": { "time_of_the_day": { "bus_stop" "bus_line": { ["delay", "number_of_trips"] } } } }.

Rush hours vs. quiet hours. It is evaluated if "time_of_the_day" belongs to a rush hour or quite hour. Then, ["delay", "number_of_trips"] is inserted in a dictionary with the following format, where hour_type was either rush_hour or quite_hour:

"street_avenue": { "hour_type": : { ["delay", "number_of_trips"] } }

From this dictionary, the average delay is computed as delay / number_of_trips.

Weekdays vs. weekends. It is evaluated if "day_week" belongs to a weekday or weekend. Afterwards, ["delay", "number_of_trips"] was attached to a dictionary with the following format, where day_type was either weekday or weekend:

"street_avenue": { "day_type": : { ["delay", "number_of_trips"] } }

The average delay is computed as delay / number_of_trips.

Delays of specific bus lines. This method received as input bus_line_to_be_considered. It evaluates if bus_line is equal to bus_line_to_be_considered. Next, ["delay", "number_of_trips"] was inserted in a dictionary with the following format:

"street_avenue": { "bus_line_to_be_considered": : {["delay", "number_of_trips"]}}

The average delay is computed as delay / number_of_trips.

Percentage of significant delays in avenues. This method receives as input the value significant_delay, i.e., a threshold to check if a delay is significant or not. It evaluates if the delay is greater than the threshold. If it is the case, the trip is inserted in a dictionary with the following format:

"street_avenue": { ["trips_with_significant_delays", "number_of_trips"] }

The percentage of significant delays in a given avenue is calculated as trips_with_significant_delays / number_of_trips.

5   Experimental analysis and discussion

This section reports the experimental evaluation of the proposed big data analysis approach for delay estimation in public transportation systems.

5.1   Development and execution platform

The proposed big data processing algorithm was implemented using Python, considering the availability of high-level libraries whose implementations allow efficient data processing. The applied libraries include:

− *Multiprocessing*, a module that allows creating and managing child processes in Python.
− *NumPy*, a fundamental package for scientific computing in Python. It is a Python library that provides a multidimensional array object, several derived objects (such as masked arrays and matrices), and an assortment of routines for fast operations on arrays.
− *Matplotlib*, a comprehensive library for creating static, animated, and interactive visualizations in Python.
− *Datetime*, a module that supplies classes for manipulating dates and times.

- *Itertools*, a module that standardizes a core set of fast, memory efficient tools that are useful by themselves or in combination. Together, these modules form an iterator algebra, making it possible to compactly and efficiently construct specialized tools in pure Python.
- *JSON*, a lightweight data interchange format inspired by JavaScript object literal syntax.

The experimental analysis was performed on a HPE Proliant server with Xeon Gold 6138 processor, 40 cores and 120 GB of RAM memory. from the high performance computing platform of National Supercomputing Center (Cluster-UY), Uruguay [19]. The source code and results are available on github.com/flacoski/Montevideo-bus-stops-delay.

5.2   Validation results

This subsection reports and analyzes the main results and indicators computed in the validation experiments of the proposed approach for delay estimation in the public transportation system of Montevideo. Sample results are reported for trips performed in May 2002 in important avenues of Montevideo: a) Avenues 18 de Julio, 8 de Octubre and Camino Carrasco (bus line 109), and b) Avenues Luis Alberto de Herrera, Boulevard Artigas, Boulevard España (bus line 181).

Rush hours vs. quiet hours. The first step was determining the rush hours for the public transportation in the considered month. The histogram showed three peaks: the morning peak (7:00–9:00), the midday peak (12:00–14:00) and the evening peak (16:00–18:00). Early morning hours were excluded from the analysis due to the almost zero demand. Table 1 reports the average delay for each of the listed avenues in rush hours and quiet hours, the average frequency of bus lines traveling in each avenue, and the percentage value of delays.

avenue	delay		average frequency	percentage	
	rush hours	quiet hours		rush	quiet
18 de Julio	116.91	115.77	842.86	13.9%	13.7%
8 de Octubre	111.38	95.17	883.63	12.6%	10.8%
Camino Carrasco	95.60	77.69	913.59	10.5%	8.5%
Luis Alberto de Herrera	79.34	66.21	608.66	13.0%	10.9%
Boulevard Artigas	91.48	85.33	691.85	13.2%	12.3%
Boulevard España	92.77	75.17	882.77	10.5%	8.5%

Table 1: Average delays for rush and quiet hours (in seconds)

Results in Table 1 indicate that the average delays of the public transportation in Montevideo are quite reasonable for a city with medium-high traffic. The computed delays are below two minutes in the six main avenues analyzed. Delays are between 8.5% and 13.9% of the average frequency of bus lines traveling through the studied avenues. These values are manageable for citizens and demonstrate a reasonable punctuality and quality of service.

Results also show that rush hours have a slightly longer delay. In the best case (18 de Julio) the difference between delays in rush hours is is just 1.14 s. The worst case is Boulevard España, with a difference of 17.6 s. In any case, differences are not significant, suggesting a steady behavior and correct efficiency of the studied bus lines.

Weekdays vs. weekends. Table 2 reports the computed delays in weekdays and weekends, and the reference average frequencies. Results show that the av-

avenue	delay		average frequency	percentage	
	weekend	weekdays		weekend	weekdays
18 de Julio	115.51	115.11	1051.88	11.0%	10.9%
8 de Octubre	101.32	110.50	1081.22	9.4%	10.2%
Camino Carrasco	84.96	111.97	1154.76	7.4%	9.7%
Luis Alberto de Herrera	71.91	74.91	707.75	10.2%	10.6%
Boulevard Artigas	87.59	75.44	847.61	10.3%	8.9%
Boulevard España	83.72	70.95	956.66	8.8%	7.4%

Table 2: Average delays for weekdays and weekends (in seconds)

erage delay is larger on weekdays than on weekends, most notable on Camino Carrasco and 8 de octubre. In turn, Boulevard Artigas and Boulevard España have higher delays on weekends, mainly due the high traffic on those avenues (e.g. Boulevard España is located near the seafront, which is a busy promenade on weekends). Delays on the other avenues have a non significant difference between weekdays and weekends.

Delays of specific bus lines. A specific analysis was performed to compute the delay on trips of line 109 (Plaza Independencia, in downtown, to Parque Roosevelt, in the East of the city) and line 181 (Paso Molino, Northwest of the city to Pocitos in the South). These are two representative lines that connect the most populated neighborhoods in the city. Table 3 reports the delays for the two studied lines, considering trips in rush hours on weekdays.

line 109			line 181		
avenue	delay	frequency	avenue	delay	frequency
18 de Julio	134.81	804.55	Luis Alberto de Herrera	53.24	384.83
Camino Carrasco	105.85	915.67	Boulevard Artigas	60.39	378.97
8 de Octubre	93.09	936.53	Boulevard España	57.52	372.65

Table 3: Average delays computed for lines 109 and 181 (in seconds)

Results show that bus line 109 is significantly more delayed in the whole trip than bus line 181. Also, 18 de Julio is the avenue where line 109 spends the longest time on average, mainly due to the high traffic on that way. Figs. 1–2 show the bus stops with most delay on each avenue for line 109.

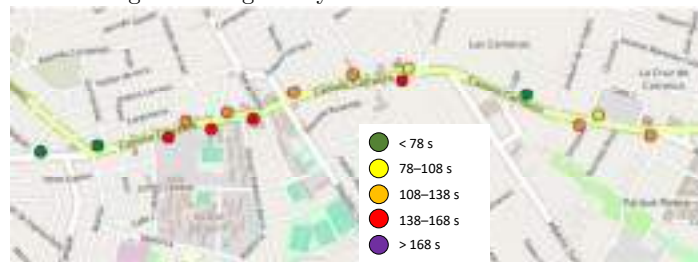Fig. 1: Average delays of line 109 in 18 de Julio

Fig. 2: Average delays of line 109 in Camino Carrasco

In both 18 de Julio and Camino Carrasco, the highest delays are concentrated in the central part of the avenues. In 18 de Julio, the westernmost section (where bus line 109 starts of finishes its trips) reports lower delays.

Figs. 3–4 show the bus stops with most delay on each avenue for line 181. In the three studied avenues, line 181 has low and evenly distributed delays. Differences between bus stops are not significant.
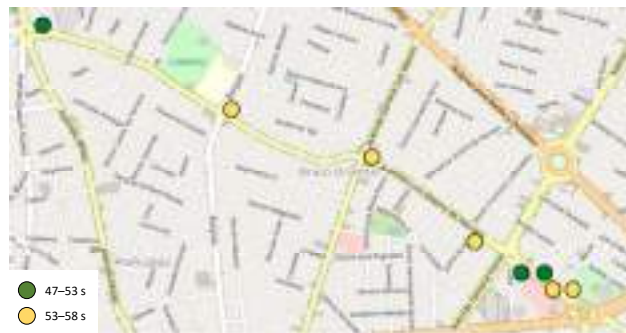
Fig. 3: Average delays of line 181 in Luis Alberto de Herrera

Significant delays in avenues. This analysis studied the tardiness of bus lines with a *significant* delay, defined as those buses that pass five minutes after or three minutes before the theoretical timetable. The considered threshold for defining a significant delay are parameters for the algorithm. The chosen values are based on the average waiting time for users of direct and transfer trips [20], and represent unacceptable thresholds for the QoS offered to citizens.

(a) Boulevard España   (b) Boulevard Artigas

Fig. 4: Average delays of line 181 in Boulevard España and Boulevard Artigas

Low overall percentages of significant delays were obtained. 18 de Julio and Boulevard Artigas have the higher number of delayed trips (1.2%). The other studied avenues have less than 0.5% trips with significanl delay.

6   Conclusions and future work

This article presented a big data, urban analysis approach for computing the delay of public transportation systems. A specific case study was addressed: the public transportation system in Montevideo, Uruguay.

The analysis focused on the bus stops with the higher demand in the most important avenues of the city. Low delays were computed, less than 14% of the frequency in rush hours, and few trips (1.2%) have a significant delay. These results allow concluding that, nowadays, delays are not the main issue about the local public transportation system in Montevideo.

The main lines for future work include computing disaggregated statistics, for a more precise characterization of the STM, and analyzing specific situations such as winter months and the comparison of pre- and post-COVID pandemic.

References

1. Anwar, A., Odoni, A., Toh, N.: BusViz: Big data for bus fleets. Transportation Research Record **2544**(1), 102–109 (2016)
2. Barrionuevo, J., Berrone, P., Ricart, J.: Smart cities, sustainable progress. IESE Insight **14**(14), 50–57 (2012)
3. Berlingerio, M., Calabrese, F., Di Lorenzo, G., Nair, R., Pinelli, F., Sbodio, M.: Allaboard: a system for exploring urban mobility and optimizing public transport using cellphone data. In: 93rd Annual Meeting Transportation Research Board (2014)
4. Chen, X., Pao, H., Lee, Y.: Efficient traffic speed forecasting based on massive heterogenous historical data. In: IEEE International Conference on Big Data. pp. 10–17 (2014)
5. Denis, J., Massobrio, R., Nesmachnow, S., Cristóbal, A., Tchernykh, A., Meneses, E.: Parallel computing for processing data from Intelligent Transportation Systems. In: 10th Int. Supercomputing Conf. in Mexico. pp. 1–15 (2019)

6. Erhardt, G., Lock, O., Arcaute, E., Batty, M.: A big data mashing tool for measuring transit system performance. In: Springer Geography, pp. 257–278 (2016)
7. Fabbiani, E., Nesmachnow, S., Toutouh, J., Tchernykh, A., Avetisyan, A., Radchenko, G.I.: Analysis of mobility patterns for public transportation and bus stops relocation. Programming and Computer Software **44**(6), 508–525 (2018)
8. Gröflin, A., Weber, M., Guggisberg, M., Burkhart, H.: Traffic flow measurement of a public transport system through automated web observation. In: 2017 11th International Conference on Research Challenges in Information Science (2017)
9. Hanft, J., , Iyer, S., Levine, B., Reddy, A., , and: Transforming bus service planning using integrated electronic data sources at NYC transit. Journal of Public Transportation **19**(2), 89–108 (2016)
10. Hipogrosso, S., Nesmachnow, S.: Analysis of Sustainable Public Transportation and Mobility Recommendations for Montevideo and Parque Rodó Neighborhood. Smart Cities **3**(2), 479–510 (2020)
11. Hipogrosso, S., Nesmachnow, S.: A practical approach for sustainable transit oriented development in montevideo, uruguay. In: Smart Cities, pp. 256–270 (2022)
12. Ingvardson, J., Nielsen, O., Raveau, S., Nielsen, B.: Passenger arrival and waiting time distributions dependent on train service frequency and station characteristics: A smart card data analysis. Transportation Research Part C: Emerging Technologies **90**, 292–306 (2018)
13. Khiari, J., Moreira, L., Cerqueira, V., Cats, O.: Automated setting of bus schedule coverage using unsupervised machine learning. In: Advances in Knowledge Discovery and Data Mining, pp. 552–564 (2016)
14. Lunke, E., Fearnley, N., Aarhaug, J.: Public transport competitiveness vs. the car: Impact of relative journey time and service attributes. Research in Transportation Economics **90**, 101098 (2021)
15. Massobrio, R., Nesmachnow, S.: Urban Mobility Data Analysis for Public Transportation Systems: A Case Study in Montevideo, Uruguay. Applied Sciences **10**(16), 1–20 (2020)
16. Massobrio, R., Nesmachnow, S., Tchernykh, A., Avetisyan, A., Radchenko, G.: Towards a cloud computing paradigm for big data analysis in smart cities. Programming and Computer Software **44**(3), 181–189 (2018)
17. Massobrio, R., Nesmachnow, S.: Travel time estimation in public transportation using bus location data. In: Smart Cities, pp. 192–206. Springer International Publishing (2022)
18. Massobrio, R., Pías, A., Vázquez, N., Nesmachnow, S.: Map-Reduce for Processing GPS Data from Public Transport in Montevideo, Uruguay. In: Simposio Argentino de Grandes Datos, 45 Jornadas Argentinas de Informática. pp. 41–54 (2016)
19. Nesmachnow, S., Iturriaga, S.: Cluster-UY: Collaborative Scientific High Performance Computing in Uruguay. In: Supercomputing, Communications in Computer and Information Science, vol. 1151, pp. 188–202. Springer (2019)
20. Nesmachnow, S., Risso, C.: Exact and evolutionary algorithms for synchronization of public transportation timetables considering extended transfer zones. Applied Sciences **11**(15), 7138 (2021)
21. Rahman, M., Wirasinghe, S., Kattan, L.: Analysis of bus travel time distributions for varying horizons and real-time applications. Transportation Research Part C: Emerging Technologies **86**, 453–466 (2018)
22. Sussman, J.: Perspectives on Intelligent Transportation Systems. Springer (2005)
23. Szymanski, P., Zolnieruk, M., Oleszczyk, P., Gisterek, I., Kajdanowicz, T.: Spatiotemporal profiling of public transport delays based on large-scale vehicle position-

ing data from GPS in Wrocław. IEEE Transactions on Intelligent Transportation Systems **19**(11), 3652–3661 (2018)

24. Trépanier, M., Morency, C., Agard, B.: Calculation of transit performance measures using smartcard data. Journal of Public Transportation **12**(1), 79–96 (2009)

25. Wang, Y., Bie, Y., An, Q.: Impacts of winter weather on bus travel time in cold regions: Case study of harbin, china. Journal of Transportation Engineering, Part A: Systems **144**(11) (2018)

26. Welch, T.F., Widita, A.: Big data in public transportation: a review of sources and methods. Transport Reviews **39**(6), 795–818 (2019)

27. Xia, D., Wang, B., Li, H., Li, Y., Zhang, Z.: A distributed spatial–temporal weighted model on mapreduce for short-term traffic flow forecasting. Neurocomputing **179**, 246–263 (2016)

28. Zheng, X., Chen, W., Wang, P., Shen, D., Chen, S., Wang, X., Zhang, Q., Yang, L.: Big data for social transportation. IEEE Trans. Intell. Transport. Syst. **17**(3), 620–630 (2016)

Big Data trends in the analysis of city resources

Regina Gubareva[1][0000−0003−2081−6771] and Rui Pedro
Lopes[1,2][0000−0002−9170−5078]

[1] Research Center in Digitalization and Intelligent Robotics (CeDRI), Instituto
Politécnico de Bragança, Portugal
[2] Institute of Electronics and Informatics Engineering of Aveiro (IEETA), University
of Aveiro, Portugal
{regina.gubareva,rlopes}@ipb.pt

Abstract. The operation and management of a municipality generate
large amounts of complex data, enclosing information that is not easy
to infer or extract. Their analysis is challenging and requires specialized
approaches and tools, usually based on statistical techniques or on ma-
chine learning and artificial intelligence algorithms. These Big Data is
often created by combining many data sources that correspond to differ-
ent operational groups in the city, such as transport, energy consumption,
water consumption, maintenance, and many others. Each group exhibits
unique characteristics that are usually not shared by others. This paper
provides a detailed systematic literature review on applying different al-
gorithms to urban data processing. The study aims to figure out how
this kind of information was collected, stored, pre-processed, and ana-
lyzed, to compare various methods, and to select feasible solutions for
further research. The review finds that clustering, classification, correla-
tion, anomaly detection, and prediction algorithms are frequently used.
Moreover, the interpretation of relevant and available research results is
presented.

Keywords: big data · smart city · resources consumption.

1   Introduction

The smart city concept is popular and common in scientific literature, charac-
terizing a healthy environment that improves the quality of life and well-being
of citizens [10]. Due to the diversity of services, resources, and projects, smart
cities manage huge amounts of data, typically within the Big Data concept.
One can argue what are the minimum conditions and characteristics for a city
to become "smart". However, since nowadays most operations are controlled via
comprehensive information and communication technologies, the need to collect,
store, integrate, process, and analyze data is prevalent and important in most
cities. Over the past ten years, the number of sensors and metering devices has
been increasing geometrically. The intention to control and understand every-
thing surrounding us became a significant step in the development of technolo-
gies of environmental sensors: smart houses, smart cities, smart devices, IoT,

and many others. Legacy information is also laying around, in spreadsheets or databases, which can be valuable if correctly accessed and integrated. Citizens and institutions also make use of social networks to convey opinions, criticism, or information about resources, services, or events. The essential questions are how to use this data and how to extract practical and meaningful information from all these measurements. Big data is a set of technologies for processing large amounts of data. It refers not only to the amount of information but also to the data rate, meaning the multiple streams of data that should be processed in real-time. Moreover, large examples of data usually enclose hidden, potentially valuable, patterns. Several unique phenomena associated with high dimensionality, including noise accumulation, spurious correlation, and random endogeneity, make traditional statistical procedures difficult to use. In the Big Data era, large sample sizes allow us to better understand heterogeneity by shedding light on research such as examining the relationship between specific covariates and rare outcomes.

This work is developed within the project "PandIA - Management of Pandemic Social Isolation Based on City and Social Intelligence", which focus on providing detailed information, such as resource consumption trends, estimation of people in each area or household, a heat map of suspected outbreaks, and others to health and municipal authorities and to emergency personal. For that, it uses information from several sources, including pathogen characteristics, infection statistics, municipal information, social networks, and hospital information and statistics. The work described in this paper uses a systematic literature review to understand the nature and purpose of the data generated and collected in the context of a city. It aims to understand what types of data are usually considered, how they what collected, what algorithms are used, and for what purposes. We look for evidence and best practices for using city information in Big Data settings, the impact, and results. The authors do not set out to compare the algorithms with mathematical certainty, we just review various approaches and provide rough estimates of effectiveness. The article should give a base understanding of what to do with smart city data. Broadly speaking, the purpose of this paper is to systematize the basic principles of digital data handling in the formation and development of smart cities. The review summarizes the research being done for the last five years. The literature is categorized according to the algorithms used, the approach to handling data, the nature of data, and the results of the data processing.

The paper is structured in four sections, starting with this introduction. Section 2 describes the methodology followed in this study. The Result and Analysis follow, with the results and associated discussion and it finishes in section 4 with some conclusions.

2   Methodology

The main objective of this literature review is to try to understand the data structure and nature, their sources, the processes of collecting and storing, the

algorithms and tasks these are developed to do, and, finally, the purposes or intentions of the results. This literature review follows the approach suggested by Materla, Cudney, and Antony [11] and by Subhash and Cudney [14], including three phases: planning, operation, and dissemination (Figure 1).
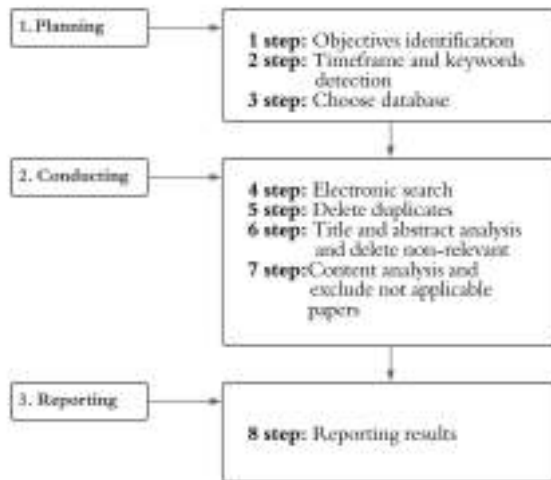

Fig. 1. Phases of the systematic literature review.

To guide the search, a set of research questions was considered:

1. What is the format, structure, and context of the data each paper uses?
2. What algorithms are used for urban data handling?
3. What is the complexity of each algorithm?
4. What are the results achieved after the analysis and what do they mean?

The papers were searched in Scopus and IEEEXplore. These databases were selected because they provide a wide set of areas and the key terms provide an initial focus on the main objective of this work. A total of 230 papers were identified in the first run (Table 1).

Only the papers retrieved from Scopus and IEEEXplore published between January 1st, 2015, and December 31st, 2020, whose text was available in the institutional repositories were considered. Moreover, papers without a peer review process and written in a different language than English were also excluded. After removing the duplicate entries, the total number of papers was 208.

Some guidelines were defined for the title, abstract, and text analysis. After a primary assessment, a detailed analysis of conformity to a chosen theme was made. The title's meaningfulness, associated with the abstract description helped

Table 1. Search terms and the number of papers retrieved

Database	Search term	Results
Scopus	TITLE ("big data" AND ("urban data" OR "smart city" OR "geo data" OR "social network" OR "predictive maintenance" OR "algorithms"))	123
IEEEXplore	(("Document Title": "big data") AND ("Document Title": "urban data" OR "Document Title": "smart city" OR "Document Title": "geo data" OR "Document Title": "social network" OR "Document Title": "predictive maintenance" OR "Document Title": "algorithms"))	107
	Total	230

with this. Next, the text was skimmed to assess if all the information needed could be found. So, in summary, the papers were analyzed according to the following steps:

1. Searched articles were limited to the predefined time frame (2016-2021)
2. Papers with non-relevant titles, abstracts, and keywords were excluded
3. Text that did not mention the required subjects was excluded

After analysis of the title, abstract, and text, 196 more papers were excluded for being out of the scope of this work. A total of 12 papers remained for the analysis (Table 2).

Table 2. The results of the search by journals

Phase	Scopus	IEEEXplore	Total
search	123	107	230
del. duplicates	114	94	208
title	42	36	78
abstract	11	8	19
content	7	5	12

3 Analysis and Discussion

The analysis process started with the characterization of the selected references. Content analysis followed, to assess the context and definition of self-study and the purpose of the work described in the paper.

3.1 Characterization

In total, papers from 9 countries were found. Spain has 3 papers and China 2 papers. For United Arab Emirates, Denmark, Malaysua, South Korea, Taiwan, India and Greece, a single paper was found. It should be highlighted that the countries' distribution does not connect with cities' development in these regions.

The distribution by year reveals a peak number of papers in 2018, with 7 papers. The lowest amount of research is observed in 2019 (a single paper), which can reflect the exploration of new approaches in the area. The remaining years

(2017 and 2016, two papers were accounted). Despite considerable attention from the scientific community to the issue of the impact of such a resource as digital data on the development of modern socio-economic systems, including cities, this area is only beginning to develop, and the understanding of the use of data as a tool for the development of smart cities remains limited in the scientific literature. In general, it can be noted that research is increasingly focused on the use of digital data as a new socio-economic phenomenon, and attempts are made to conceptualize, classify and evaluate the role of different types of data in socioeconomic processes. In most cases, such studies are related to the use of big data in certain areas of the urban environment, such as transportation, public safety, and environmental protection. At the same time, the literature lacks studies of a general systemic nature on the use of big data for smart cities regardless of the field of application.

3.2   Data types and sources

The smart city concept implies integrating multiple information and communication technologies for city infrastructure management: transport, education, health, systems of housing and utilities, safety, etc. Municipal governments collect numerous heterogeneous information, and an "urban data" term can mean various datasets: data from video surveillance cameras, traffic, air quality, energy and water consumption, and images for smart recognition. Therefore for this study, the essential is to recognize and classify different datasets utilized in considered resources.

Trilles et al. describe a methodology of (big) data process produced by sensors in real-time [15]. It assumes that it works with different sensor data sources with different formats and connection interfaces. Wireless sensor networks (WSN) are used for monitoring the physical state of the environment: air pollution, forest fire, landslide, and water quality. Although the system proposed by the authors is designed to process all data types, the WSNs mainly produce numerical data like water level, and the gas concentration in the air, mainly classified as quantitative information. An efficient method to derive spatio-temporal analysis of the data, using correlations was proposed by [3]. The authors use data from Bluetooth sensors installed in light poles. The data was collected from the road sensors in the city of Aarhus in Denmark. The measurements are taken every 5 minutes and the dataset includes a timestamp, location information, average speed, and a total of automobiles at the time of commit. The data were classified as numerical as there are no text, images, sound, or video information.

Bordogna et al. used in their paper big mobile social data, which included users-generated, geo-referenced and timestamped contents [4]. The content means text data that users posts in modern emerging social systems like Twitter, Facebook, Instagram, and so forth. Hereby, the dataset can be classified as heterogeneous by way of containing the text of social network posts and numerical data of location and time. Wang et al. considered another approach to analysis and evaluated the effectiveness of deep neural networks [16]. The aim of their paper was the monitoring and control of local HIV epidemics. The collection includes

statistics on the number of morbidities, mortality, and mortality by region, age, sex, and occupation. The type of data is categorized as text and numerical.

The researchers from Spain, Pérez-Chacón et al., proposed a methodology to extract electric energy consumption patterns in big data time series [12]. The study used the big data time series of electricity consumption of several Pablo de Olavide University buildings, extracted using smart meters over six years. Karyotis et al. presented a novel data clustering framework for big sensory data produced by IoT applications [9]. The dataset was collected from an operational smart-city/building IoT infrastructure provided by the Federated Interoperable Semantic IoT/cloud Testbeds and Applications (FIESTA-IoT) testbed federation. The array is heterogeneous and represents measurements of different types: temperature, humidity, battery level, soil moisture, etc.

Azri et al. presented a technique of three-dimensional data analytics using a dendrogram clustering approach [2]. It is assumed that the algorithm can be applied to large heterogeneous datasets gathered from sensors, social media, and legacy data sources. Alshami et al. tested the performance of two partition algorithms K-Means and Fuzzy c-Mean for clustering big urban datasets [1]. Compared techniques can be applicable to huge heterogeneous datasets in various areas like medicine, business, biology, etc. In the paper, the authors utilized urban data from various data sources, such as the Internet of Things, LIDAR data, local weather stations, and mobile phone sensors.

Chang et al. developed a new iterative algorithm, called the K-sets+ algorithm for clustering data points in a semi-metric space, where the distance measure does not necessarily satisfy the triangular inequality [6]. The algorithm is designed for clustering data points in semi-metric space. To understand what semi-metric space is, it is necessary to briefly consider the concept of metrics in space. The metric is the mapping for some set $d : X \times X \to R$, for which the axioms of non-degeneracy and symmetry have to be satisfied but not necessarily the triangle inequality. If the distance between different points can be zero, the metric is semi-metric. The method was evaluated with two experiments: community detection of signed networks and clustering of real networks. The dataset included 216 servers in different locations, and the latency (measured by the round trip time) between any two servers of these 216 servers is recorded in real-time.

Chae et al. have compared the performance of the deep neural network (DNN), long-short-term memory (LSTM), and the auto-regressive integrated moving average (ARIMA) in predicting three infectious diseases [5]. The study uses four kinds of data to predict infectious diseases, including search query data, social media big data, temperature, and humidity. Data related to malaria, chickenpox, and scarlet fever, for 576 days, were considered. As a result, the data is partly numerical and partly text. The research of Chen et al. focuses on multisource urban data analysis [7]. The points of interest are geographical, street view, road map, and real-estate data. The record comprises the road network of the city, longitude, latitude, name, and functionality of a structure in the

urban environment, and imagery of locations. Obviously, the dataset is ranked as heterogeneous.

Simhachalam and Ganesan presented a multidimensional mining approach in a successive way by finding groups (clusters) of communities with the same multi-dynamic characteristics [13]. The data refers to the statistics of population, migration, tax capacity, dwellings, employment, and commuters.

The majority of the studies assume heterogeneous nature data. There are two research papers with only numerical data and one of the papers investigates image data processing. Text and numerical data are dominant and they are collected from multiple sources (Table 3).

Table 3. Data types and sources.

Paper	Data	Category
[15]	data from different sensors	heterogeneous
[3]	traffic data collected from the road sensors in the city: geographical location, time-stamp, average speed, and total of automobile	numerical
[4]	social networks posts, timestamp, geo-location	heterogeneous
[16]	10-year historical HIV incidence data: the number of morbidity, morbidity, mortality and mortality by region, age, sex, occupation	heterogeneous
[12]	electricity consumption for 6 years for several buildings	numerical
[9]	big sensory data, measurements of different types: temperature, humidity, battery level, soil moisture	heterogeneous
[2]	smart city data	heterogeneous
[1]	data from the Internet of Things, LIDAR data, local weather stations, mobile phones sensors	heterogeneous
[6]	locations and the latency (measured by the round trip time) between any two data points	heterogeneous
[5]	search query data, social media big data, temperature, and humidity	heterogeneous
[7]	geographical data, points of interests data(longitude, latitude, name, and functionality of a structure in the urban environment), street view data, real estate data, mobile phone location data, social network data, micro-blog data, taxi GPS trajectory data, taxi profile data	heterogeneous
[13]	the measurements of the blood tests as the corpuscular volume of test substances and the number of half-pint equivalents of alcoholic beverages drunk per day	numerical

3.3   Algorithms

In general, 12 different approaches to big municipal data processing were considered. The methods can be divided into groups depending on the manner of information handling: clustering, classification, correlation, deep neural network, frameworks, and community detection. Figure 2 illustrates the proportion between different techniques. The most popular approach is clustering, various algorithms of clustering utilized in 5 considered studies.

The approach followed by [15] includes three layers: content layer, services layer, and application layer. The content layer includes sensor network data sources, and the services layer provides database connection, transformations of data, and communications protocols for real-time data handling and processing. The last layer implies client application. The service layer implements the
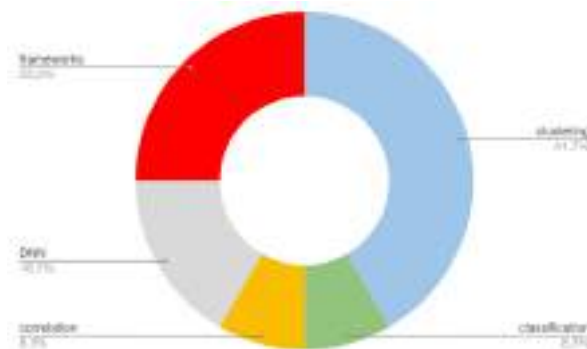
Fig. 2. Methods of urban data analysis

Cumulative SUM (CUSUM) algorithm of anomaly detection. The method considers the set of observations following a normal distribution. For each collection of measurements, the cumulative sum is calculated. When the score overcomes the threshold, the algorithm detects anomalies. If the parameter exceeds the threshold, the anomaly will be due to the increase (up-event), and if the sum is greater than the threshold, it will be due to the decrease (down-event). Different data types from multiple sources are processed by a special wrapper and transformed into standard form. Transformed observation is encoded in line according to Open Geospatial Consortium (OGC) standard for Observations and Measurements.

The unique method used in [3] tried to apply correlation methods to urban data analysis. They suggested an efficient method to derive spatio-temporal analysis of the data, using correlations, with Pearson and Entropy-based methods and compares the results of both algorithms. Pearson's coefficient characterizes the presence of linear dependence between two values. The weakness of Pearson correlation is poor accuracy when variables are not distributed normally. Mutual information is the statistical function of two random variables, which describes the quantity of information of one random value in another. The constraint of mutual information is that it has a higher processing complexity than Pearson correlation. The technique continuously calculates the average correlation for sensory road data divided into two sectors until the data runs out. Different types of correlation were tested.

The Long short-term memory (LSTM) neural network models, auto-regressive integrated moving average (ARIMA) models, generalized regression neural network (GRNN) models, and exponential smoothing (ES) models to estimate HIV incidence in Guangxi, China, and explore which model is the best and most precise for local HIV incidence prediction were used by[16]. ARIMA is the model used for time series forecasting. LSTM is a recurrent neural network, characterized by the ability to learn long-term dependencies. In this study, several

models were built. The model with the lowest mean square error (MSE) was considered the optimal model. GRNN is a feed-forward neural network, which estimates values for continuous dependent variables. The principal advantages of GRNN are fast learning and convergence to the optimal regression surface as the number of samples becomes very large. GRNN is particularly advantageous with sparse data in a real-time environment because the regression surface is instantly defined everywhere, even with just one sample. The method is usually used for functions' approximation, so it can provide very high accuracy, but for huge samples is computationally expensive. ES model is one of the simplest and most widespread practices of series alignment. The method can be presented as a filter that receives the original series members as the input, and the output forms the current values of the exponential average.

The patterns in data related to electricity consumption were searched in [12]. The methodology describes all stages of data processing: data collection, cleaning, transformation, index analysis, clustering, and results. The first stage aims to pre-process the data so that they can be clustered. The second phase consists of obtaining the optimal number of clusters for the dataset by analyzing and interpreting various cluster validation indices. Next, k-means is used for clustering and, finally, retrieves the centroids for each cluster. The processing is done in Apache Spark and the algorithms include big data clustering validity indices (BD-CVIs) and k-means.

The community detection algorithm Girvan–Newman GN) [8] algorithm was modified for big data clustering of IoT sensors by [9]. Their method organizes complex data in blocks, called communities or modules, according to certain roles and functions, organized in a multi-graph. The problem is to find in a given multi-graph a partition of vertices where the objective function is minimized. To achieve this, the graph edges are deleted iterative, depending on the value of the metric. The Edge-Betweenness Centrality (EBC) is the most common metric used, but the computation for this is time-consuming. The authors suggested a new measure approximating EBC, which capitalizes on hyperbolic network embedding and can be considered as the "hyperbolic" analog of EBC. This measure is denoted as Hyperbolic Edge Betweenness Centrality (HEBC), and it is computed by utilizing the hyperbolic node coordinates assigned to the embedded nodes. The novel metric enhances the performance without harming accuracy.

The other technique of data organizing and processing proposed by [2] implies 3D data analytics using a dendrogram (hierarchical) clustering approach. 3D data represents a structure of information that combines, simultaneously, the classification and clustering tasks. The organized data is mapped to a tree structure and retrieved by tree traversal algorithms. Dendrogram clustering is a method of merging objects into bunches. In the study, the bottom-up algorithm of clustering is utilized, which means that each item in a class is assigned to a single cluster. Then combine the clusters until all objects are merged together. An important parameter is a distance between objects in a class. The metric shows a quantitative assessment of the items' similarity ratio according to different criteria. The given research does not provide a selection of the spe-

cific parameter, although the choice of metric occurs in the second step of the method. The ability to retrieve information and the efficiency of the structure were measured. In general, the technique demonstrates a good characteristic of information extraction but not the most attractive performance parameters.

Other clustering algorithms, Fuzzy c-Mean (FCM) and K-Means were tested by [1]. The k-Means algorithm is one of the simplest methods but at the same time the most inaccurate. The main idea is that at each iteration, the center of mass is recalculated for each cluster obtained in the previous step, then results are partitioned into clusters again under new centers. The algorithm ends when the cluster is not changed in iteration. The fuzzy c-Mean method allows for obtaining "fuzzy" clustering of large sets of numerical data and makes it possible to correctly identify objects at the boundaries of clusters. However, the execution of this algorithm requires serious computational resources and the initial setting of the number of clusters. In addition, ambiguity may arise with objects remote from the centers of all clusters.

A new approach for clustering data points was designed by [6]. In essence, the method is an extension of the K-set clustering algorithm for semi-metric space. The problem with the K-sets approach is that the triangle distance is not non-negative. Thus the K-sets algorithm may not converge at all and there is no guarantee that the output of the K-sets algorithm is clustering. For solving this difficulty, the definition of triangle distance was adjusted, so that the non-negativity requirement could be lifted. The experimental results confirm the proficiency of the method for the geographic distance matrix and the latency matrix. The deep neural networks for the prediction of infectious diseases were used in [5].

A visual analysis framework for exploring and understanding heterogeneous urban data was presented by [7]. A visually assisted query model is introduced as a foundation for interactive exploration coupled with simple, yet powerful, structural abstractions and reasoning functionalities.

One more clustering method is used by [13]. Fuzzy c-Means (FCM), k-means (KM), and Gustafson–Kessel (GK) clustering algorithms are implemented. According to the paper, the most accurate and effective algorithm is k-means clustering, but the other methods have their own advantages and show higher correctness in certain cases.

3.4   Algorithm assessment

The algorithms described above have characteristics of performance and scalability that should be understood. Table 4 gives a comprehensive description of the complexity and accuracy of the considered algorithms. For many, it was not easy to evaluate the complexity since the time depends on the characteristics of the machine. Therefore we provide only rough estimates, and all presented assessments are for worst-case values.

The K-sets+ algorithm yields the highest performance from all cluster algorithms. The time complexity is linear $O((Kn + m)I)$, where I is the number of iterations. The other method with linear time is Fuzzy c-mean with $O(nCI)$,

Table 4. Algorithms assessment

Algorithm	Purpose	Complexity	Accuracy	Ref
CUSUM algorithm	anomaly detection	O(n)	—	[15]
Mutual information and Pearson correlation	find correlation between sensory data	$O(n^3)$	+	[3]
LSTM	predict diseases	$O(w)$	85%+	[16]
ARIMA	predict diseases	—	80%	[16]
GRNN	predict diseases	—	76%	[16]
ES	predict diseases	—	74%	[16]
K-means clustering	to extract electric energy consumption patterns	$O(n^2)$	78%	[12]
modification of Girvan-Newman algorithm	community detection	$O(n^2)$	65%-100%	[9]
Dendrogram clustering	produce hierarchical tree structure for data for data retrieval and analytics	$O(n^3)$	—	[2]
K-Means	clustering	$O(n^2)$	87,94%	[1, 12]
Fuzzy c-Mean	clustering	$O(nCI)$	81,91%	[1]
K-sets+	clustering in metric space	$O(Kn + m)$	95%	[6]
DNN	predicting infectious diseases	$O(wnk)$	77%	[5]
VAUD	spatio-temporal data visualisation	—	78,6%+	[7]
K-Means	clustering	70,22%	60,41%-87,94%	[13]
Fuzzy c-Means (FCM)	clustering	68,54%	56,25%-81,91%	[13]
Gustafson–Kessel (GK)	clustering	60,68%	66,19%-95,83%	[13]
Similarity-Matrix-based Clustering	trip clustering	$O(n^3)$	—	[4]

where C - number of clusters, I - number of iterations. If we compare the exponent for these two approaches, the apparent fact is that the K-sets+ gives a little advantage. Considering the accuracy, K-sets+ has 95% as the worst result. The Fuzzy c-Means algorithm gives the complexity on average 81,97%. It is noteworthy that the Girwan-Newman modification provides 100% accuracy for most datasets and only 50% in the case of outliers. It could be used for a dataset with low sparseness if high accuracy is required. The dendrogram clustering method is slower than the others but can produce a hierarchical tree structure for data. K-means clustering is the simplest method but has a quadratic complexity and an accuracy of not more than 88% for different input data.

The deep learning algorithms were compared by the set of parameters: MSE, Root-Mean-Square Error (RMSE), Mean Absolute Error (MAE), and Mean Absolute Percentage Error (MAPE). From the results given by the authors, it follows that the most accurate algorithm is LSTM, but at the same time, the slowest. The fastest method is ES, but with the worst accuracy. All deep learning algorithms were used for predicting diseases. The accuracy of the ES and GRNN model was relatively poor [16]. The ARIMA model has several requirements: the time series should be stationary with steadily changing differences, and only linear relationships could be captured [16]. The DNN and LSTM models were observed to be sensitive to decreasing trends and increasing trends, respectively [5]. It is worth noticing that the time complexity for the deep neu-

ral network is hard to evaluate with O notation. The authors provide real-time results, according to the considered research the fastest model is ES, and the slowest is LSTM.

The CUSUM algorithm is time linear complexity. The solution is straightforward and fast but has limitations that must be taken into account, such as the consideration that all the series must follow a normal distribution and a series of observations cannot have trends [15]. VAUD presents the visualization of heterogeneous urban data. The approach is based on queries to the database, hence the time complexity can not be estimated. The data gathered from mobile phones and stored in one database combines different queries and different results are obtained. The accuracy on average for queries is 76%.

One of the widespread statistical methods applied to big data is correlation. In the listed papers, there is one algorithm that considered the correlation applied to smart city data. The study compared two types of methods: Pearson correlation and Mutual information. The time complexity for both is a cube. But Pearson correlation can discover the linear distribution of data, and mutual information can discover dependencies in more general data distribution cases. However, if an application prioritizes real-time response over accuracy, Pearson correlation will be suitable as it will only give a few false negatives. In other scenarios with different types of data streams (temperature, pollution, etc.), it is better to use mutual information without a priori knowledge of the potential correlations because we do not know the percentage of cases where Pearson correlation will fail to detect the correlations [3].

The assessment of time and accuracy of all proposed algorithms demonstrate that if our purpose is prediction, the best variant for us is deep neural networks like LSTM. For effective clustering, the K-sets+ or Fuzzy c-Means algorithms are the most powerful. If it is necessary to obtain additional analysis, it is possible to find the correlation. Considering the context of municipal data the frameworks are beneficial, as they assume all stages of data processing from storage to visualizing.

3.5 Processing outcomes and purpose

The anomaly detection by CUSUM algorithm of the[15], creates the warning message for the client side in the case of rare events. Each event contains a sensor identifier (sender field) and the identifier of the particular observation that has caused the event (identifier field). An event dashboard visualizes this data. The panel shows all sensing nodes of a network on a map using markers. Inside each marker, the amount of events that have been detected for this particular sensing node appears. If this node triggers an event, the marker turns red, if not the marker remains blue.

The analyses based on the correlation and mutual information were used to monitor the traffic of the city. Three sets of experiments have been performed. In the first one, the performance of Pearson correlation and mutual information was compared [3]. The results were visualized on Google Maps. It can be concluded

that the Pearson correlation is effective for the linear distribution of data, and mutual information is vital for nonlinear dependencies but requires more time.

The results obtained by [16] are predictions of HIV disease for two years. Each compared algorithm has its metrics. For example, ARIMA includes a moving average process, an auto-regressive moving average process, an auto-regressive moving average process, and an ARIMA process according to the different parts of the regression and whether the original data are stable. To evaluate data accuracy, they compared with original information about HIV cases for 2015 and 2016 years. The same type of outcomes data demonstrates the [5]. They compared the same parameters for LSTM, DNN, and ARIMA to evaluate infectious disease prediction correctness. All cluster algorithms give the same result as a count of clusters and their accuracy.

The electricity consumption data were clustered into 4 and then into 8 groups in [12]. The outcomes are presented as diagrams. The clusters are categorized depending on buildings, seasons of the year, and days of the week.

The modification of the Girvan-Newman method with a novel metric provided by [9], was applied to multidimensional data obtained from an operational smart-city/building IoT infrastructure. The authors presented an accuracy evaluation, modularity, and time comparison of HGN and GN, comparing the execution time of GN and HGN algorithms for graphs with known communities and modularity comparison for 5, 10, 20, 30, and 60-minute sampling. Given that statistics demonstrate the computational efficiency and that algorithm can give accurate outcomes.

The cluster visualization into dendrograms, as tested on the information about 1000000 buildings was presented by [2]. Response time analysis was provided as well, which exhibits that response time for the proposed method is 50-60% faster than non-constellated data.

4   Conclusion

The aim of the article was to figure out what is the trend in the city's infrastructure data processing. The authors were interested in consumption data of electricity, water, heat, data of city traffic, and the methods for creating predicting models, clustering, and classifying. Increasingly, big data are seen as a key resource for the development of the urban environment, which presents opportunities for the optimization of economic processes, the creation of innovations in the social sphere, formation of new management models. The literature review serves as a foundation for future work in resource expenditures data analysis and urban management system creation.

The article presents a detailed analysis of the twelve papers from the last five years. The authors considered the techniques of urban data processing. The input and output data, assessments of algorithms' effectiveness, and methods description are provided. The inspection gives the following results: 1 algorithm of correlation, 2 algorithms of classification, 1 method of anomaly detection, 2 approaches for data visualization, 5 algorithms of predicting, and 6 methods for

data clustering. A disproportion between the number of reviewed articles and the number of techniques dues to the fact that more than one method in each research was provided.

The input and output data vary depending on the method and purposes of the research. Predominantly heterogeneous data sources are considered. In one case the images are exploited and in two cases the numerical information is leveraged. The heterogeneous data mean that the information of different bases is used: images, text, and numerical. The video or sound data is not used in reviewed papers. The major part of the investigation offers a clustering model in the capacity of output results. The second place in prevalence is frameworks. The remaining outcomes can be divided between deep neural networks, classification, and correlation models.

The most interesting approach is the leverage of LSTM. Based on surveyed articles LSTM gives the highest accuracy of prediction and is the fastest solution in comparison with similar solutions. The forecasting of social phenomena based on city data is the most desirable result. Although, in the context of the modern situation is a still challenging task, as the whole pipeline of the assembly, processing, and analysis is important. As the given review demonstrates, different data are necessary for various problems, different algorithms give diverse findings. The dilemma of the practical benefits and standardization in smart city data is still open.

Acknowledgments

References

1. Alshami, A., Guo, W., Pogrebna, G.: Fuzzy partition technique for clustering Big Urban dataset. pp. 212–216 (2016). https://doi.org/10.1109/SAI.2016.7555984
2. Azri, S., Ujang, U., Abdul Rahman, A.: Dendrogram clustering for 3D data analytics in smart city. vol. 42, pp. 247–253 (2018). https://doi.org/10.5194/isprs-archives-XLII-4-W9-247-2018, issue: 4/W9
3. Bermudez-Edo, M., Barnaghi, P., Moessner, K.: Analysing real world data streams with spatio-temporal correlations: Entropy vs. Pearson correlation. Automation in Construction **88**, 87–100 (2018). https://doi.org/10.1016/j.autcon.2017.12.036
4. Bordogna, G., Cuzzocrea, A., Frigerio, L., Psaila, G.: An effective and efficient similarity-matrix-based algorithm for clustering big mobile social data. pp. 514–521 (2017). https://doi.org/10.1109/ICMLA.2016.188
5. Chae, S., Kwon, S., Lee, D.: Predicting Infectious Disease Using Deep Learning and Big Data. International Journal of Environmental Research and Public Health **15**(8), 1596 (Jul 2018). https://doi.org/10.3390/ijerph15081596, http://www.mdpi.com/1660-4601/15/8/1596
6. Chang, C.S., Chang, C.T., Lee, D.S., Liou, L.H.: K-sets+: A linear-Time clustering algorithm for data points with a sparse similarity measure. pp. 1–8 (2018). https://doi.org/10.1109/UIC-ATC.2017.8397636

7. Chen, W., Huang, Z., Wu, F., Zhu, M., Guan, H., Maciejewski, R.: VAUD: A Visual Analysis Approach for Exploring Spatio-Temporal Urban Data. IEEE Transactions on Visualization and Computer Graphics **24**(9), 2636–2648 (Sep 2018). https://doi.org/10.1109/TVCG.2017.2758362, conference Name: IEEE Transactions on Visualization and Computer Graphics

8. Girvan, M., Newman, M.E.J.: Community structure in social and biological networks. Proceedings of the National Academy of Sciences **99**(12), 7821–7826 (Jun 2002). https://doi.org/10.1073/pnas.122653799

9. Karyotis, V., Tsitseklis, K., Sotiropoulos, K., Papavassiliou, S.: Big data clustering via community detection and hyperbolic network embedding in IoT applications. Sensors (Switzerland) **18**(4) (2018). https://doi.org/10.3390/s18041205

10. Kwon, O., Kim, Y., Lee, N., Jung, Y.: When Collective Knowledge Meets Crowd Knowledge in a Smart City: A Prediction Method Combining Open Data Keyword Analysis and Case-Based Reasoning. Journal of Healthcare Engineering **2018** (2018). https://doi.org/10.1155/2018/7391793

11. Materla, T., Cudney, E.A., Antony, J.: The application of Kano model in the healthcare industry: a systematic literature review. Total Quality Management & Business Excellence **0**(0), 1–22 (May 2017). https://doi.org/10.1080/14783363.2017.1328980, https://doi.org/10.1080/14783363.2017.1328980

12. Pérez-Chacón, R., Luna-Romera, J., Troncoso, A., Martínez-Alvarez, F., Riquelme, J.: Big data analytics for discovering electricity consumption patterns in smart cities. Energies **11**(3) (2018). https://doi.org/10.3390/en11030683

13. Simhachalam, B., Ganesan, G.: Performance comparison of fuzzy and non-fuzzy classification methods. Egyptian Informatics Journal **17** (Nov 2015). https://doi.org/10.1016/j.eij.2015.10.004

14. Subhash, S., Cudney, E.A.: Gamified learning in higher education: A systematic review of the literature. Computers in Human Behavior **87**, 192–206 (Oct 2018). https://doi.org/10.1016/j.chb.2018.05.028

15. Trilles, S., Belmonte, O., Schade, S., Huerta, J.: A domain-independent methodology to analyze IoT data streams in real-time. A proof of concept implementation for anomaly detection from environmental data. International Journal of Digital Earth **10**(1), 103–120 (2017). https://doi.org/10.1080/17538947.2016.1209583

16. Wang, G., Wei, W., Jiang, J., Ning, C., Chen, H., Huang, J., Liang, B., Zang, N., Liao, Y., Chen, R., Lai, J., Zhou, O., Han, J., Liang, H., Ye, L.: Application of a long short-term memory neural network: a burgeoning method of deep learning in forecasting HIV incidence in Guangxi, China. Epidemiology and Infection **147**, e194 (2019). https://doi.org/10.1017/S095026881900075X

Walking Accessibility to the Public Transport Network in Montevideo, Uruguay

Sara Perera[1][0000−0002−4228−3657], Renzo Massobrio[1,2,3][0000−0002−0040−3681], and Sergio Nesmachnow[1][0000−0002−8146−4012]

[1] Facultad de Ingeniería, Universidad de la República, Montevideo, 11300, Uruguay
{sara.perera,renzom,sergion}@fing.edu.uy
[2] Transport & Planning Department, Delft University of Technology, Delft, 2628 CN, the Netherlands
[3] Departamento de Ingeniería Informática, Universidad de Cádiz, Puerto Real, 11519, Spain

Abstract. Public transport plays a key role in expanding the distances that people can travel using active modes of transport. Studying walking accessibility to public transportation systems is highly relevant, since the walk to stops/stations can be particularly challenging for children, the elderly, citizens with disabilities, and for the general population during bad weather conditions or in pedestrian-unfriendly cities. This work presents a study on walking accessibility for the public transport system in Montevideo, Uruguay. The proposed methodology combines information of the bus stops and lines that operate in the city, the road infrastructure, and demographic information of the city to compute walking accessibility indicators to the public transport system. The results of the analysis suggest that over 95.5% of the population can access at least one stop when walking up to 400 meters. However, these values are not evenly distributed among the population, with young citizens and men showing lower levels of coverage compared to their counterparts.

Keywords: accessibility · walking · public transport.

1   Introduction

The organization of transport systems condition the mobility of people, limiting their ability to participate in society and generating different forms of social exclusion [2]. In particular, geographic exclusion consists in the lack of auto-mobility and access to public transport systems. The importance of ensuring mobility for non–automobile users to reach destinations beyond normal walking range is key for the mitigation of this type of exclusion.

Public transport systems complement the use of active modes of transport (e.g., walking, cycling) by extending their range. Thus, an increase in the use of public transport can deliver significant health benefits, as this mode almost always includes a stage with physical activity [14]. In particular, studying walking accessibility to public transport is relevant since the majority of users access

networks in this manner. Passengers make their route choice based on the entire trip, including entering and exiting the public transport network [3], and tend to have an aversion towards long walks. However, passengers accept longer access and egress distances to/from the public transport network when the characteristics of the transport service (e.g., speed and frequency) improve [3]. Moreover, time is valued differently by passengers on each part of the trip. It is estimated that passengers value walking time up to 1.65 times more compared to in-vehicle time [1]. Therefore, a reduction in access times would render a greater reduction in the perceived total travel time for passengers.

This work presents a study on walking accessibility from a potential mobility approach using Montevideo, Uruguay, as a case study. The main objective is to provide accessibility indicators for Montevideo's public transport bus network that measure how easy/hard is for citizens in different parts of the city to access the public transport system by walking. For this purpose, several sources of information are combined, including bus lines, bus stops, road infrastructure and population distribution in the city. Through a geospatial analysis, three accessibility indicators are computed. The results obtained are inline with figures reported by the transit authorities while also allowing for a finer-grain analysis throughout the city.

The remainder of this article is organized as follows. First, Section 2 provides a review of relevant literature on the subject. Next, Section 3 presents the methodology to compute the accessibility indicators. Then, Section 4 presents the case study and discusses the results of the indicators. Finally, Section 5 summarises the main outcomes and potential lines of future work.

2   Related work

Studies of walking as a mean of access to public transport networks are classified into two approaches: studies of observed mobility and studies of potential mobility. Observed mobility studies seek to accurately measure the distance or time walked by users to access a public transport network. Most related works with this approach are based on survey information, where passengers declare their point of origin and point of entry to the public transport network [4,5,13].

In contrast, the research reported in this article is categorized in the literature of potential mobility. One of the most widespread methods to capture the potential mobility of individuals is related to the concept of accessibility [6]. In general, accessibility indicators are based on identifying the number of opportunities that an individual has under certain cost parameters associated with the transited networks (e.g., time, distance). Studying walking accessibility to public transport networks implies considering each stop in the system as an opportunity and walking through the road infrastructure as the access method. The standard procedure consists in evaluating the coverage of the transport network through the proportion of the population that is able to access the network by walking up to a certain distance threshold.

An interesting approach was proposed by Langford et. al, which studied the accessibility to the public transport system of South Wales, UK [10]. The authors introduced an accessibility measure based on enhanced *floating catchment* techniques, which capture many detailed aspects of accessibility. The method is a particular case of a gravitational model used to measure spatial interaction. Using information about public transport schedules and stop locations, the authors calculated a walking accessibility indicator to the transport system through geospatial analysis tools. The proposed indicator incorporates aspects of proximity, frequency, demand and availability of the public transport service. The authors concluded that their approach provides considerably more analytical detail than traditional approaches based on calculating the percentage of population covered using Euclidean buffers and area-ratio overlays.

When calculating the distance people walk to access public transport, several approaches exist in the literature to measure the distance from the point of origin to the point of entry to the transport system. The standard procedure in most recent works seems to be to use the shortest distance traveled through the road network from origin to the stop/station of entry [4,5,13]. Many guidelines in the literature suggest using a threshold distance of 400 meters [4,13]. However, the origin of this value is unclear; although it might be related to the work of Neilson and Fowler [4]. Several works have shown that this assumption is quite realistic on average. A study done in The Hague, Netherlands, suggests that the median distance walked as a feeding method for the public transport system is 380 meters [13]. Similarly, for Sydney, Australia, the median walking distance was estimated to be 364 meters for the bus system [4]. Nevertheless, both works highlight that these median values indicate that exactly half of the respondents travel beyond the 400 meters threshold used as a rule of thumb.

For the specific case study used in this work—Montevideo, Uruguay—there are no prior studies on walking accessibility to public transport to the best of our knowledge. Some previous works have addressed accessibility to employment opportunities [8], to hospitals [9] and to education centers [7] using public transport, but were not focused on the access/egress to the public transport network. Also, a household mobility survey was conducted in 2016 to obtain a large-scale image of the mobility in the city, considering all modes of transportation and incorporating the metropolitan area of the city [11]. In this survey, participants were asked to provide rough estimates of their walk to stops for those trips involving public transport. Lastly, some figures have been suggested by the transport authorities in the press stating that nearly 97% of Montevideo's population is covered by the public transport network when considering a walking threshold of 400 meters [12]. These figures confirm that Montevideo's city planners also assume a fixed distance of 400 meters—as guidelines in the literature suggest—and provide a reference accessibility value for comparison.

3   Methodology

This section describes the methodology applied to calculate the indicators of walking accessibility to public transport systems. The workflow is based upon the reviewed literature albeit slightly adapted to the specific case study addressed in this work.

The following data sets are needed to compute the walking accessibility to public transport indicators:

 – Zoning of the studied area
 – Road network of the studied area
 – Population of each zone
 – Geographical location of stops
 – List of public transport lines that operate on each stop

Indicators are based on a service area (sa) geospatial analysis. This method consists in delimiting the portion of the road network (RN) from which the stop can be reached within a fixed walking distance threshold (d). An example of service area calculation is shown in Fig. 1. The road network is displayed in grey, the stop is marked with a blue dot, and an example service area for the stop is defined in orange. Since bus stops are located in the sidewalk, it is necessary to first project them to the nearest point in the road network.

For notation purposes we will define the service area for a bus stop s_i, given the road network RN and a threshold walking distance d as:

$$SA_i = sa(s_i, RN, d) \tag{1}$$

As outlined in the review of related works, there seems to be a consensus among city planners of using $d = 400$ meters as the walking distance threshold to access public transport networks.

Then, to calculate accessibility indicators in an aggregated way, a zoning of the area of study must be provided. Depending on the nature of the analysis, coarser or finer zonifications may be considered. Since the road network itself can be used as the delimitation of the zones, it is advisable to take a small buffer for each zone in order to consider roads right in the edge of the zone. Fig. 2 shows an example of a zone that correspond to a block; the buffer plotted in orange allows considering the portion of road that delimits the zone within it. Without this buffer, no portion of the road network would be considered to be inside the zone.

Given a pre-defined set of zones $z_1, z_2, ..., z_n$, the portion of the road network within each zone is considered as $rn_1, rn_2, ..., rn_n$. Thus, a formulation is given in Eq. 2, where $\cap$ is the geospatial intersection operation and $b(z_j, B)$ is the resulting polygon of applying a geospatial buffer operation of B units to zone z_j.

$$rn_j = RN \cap b(z_j, B) \tag{2}$$

Thus, with the previous formulations, the definition of whether a stop s_i covers a zone z_j can be defined:

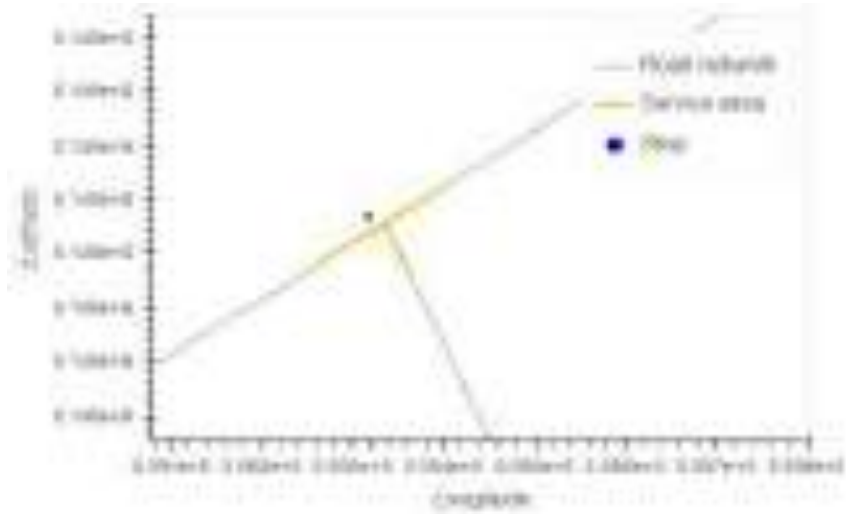$$s_i \text{ covers } z_j \iff rn_j \cap SA_i \neq \emptyset \tag{3}$$

Fig. 1. Service area analysis example

Fig. 2. Zone with buffer example

Also, given the aforementioned road network portions and the service area of each stop, the overlap between these can be computed to determine the coverage c_j at the zone level:

$$c_j = (SA_1 \cup SA_2 \cup ... \cup SA_n) \cap rn_j \qquad (4)$$

Summarizing, three accessibility indicators at the zone level are defined:

1. **Number of bus stops covering each zone at d $\leq$ 400 meters:** corresponding to the number of bus stops that comply with Eq. 3

2. **Number of bus lines covering each zone at d $\leq$ 400 meters:** calculated as the count of different bus lines that operate on bus stops that comply with Eq. 3

3. **Percentage of population within the zone covered by at least one bus stop at d $\leq$ 400 meters:** assuming a uniform spatial distribution of the population in the road segments of each zone, coverage can be estimated through Eq. 4

4   Case study: Montevideo, Uruguay

This section presents the results of the analysis of walking accessibility to the public transport network in Montevideo, Uruguay.

4.1   City and public transport system overview

Montevideo is the capital and most populated city of Uruguay. It is situated on the southern coast of the country. It has a population of 1,3 million, which constitutes 40% of Uruguay's total population. The size of Montevideo is 201 km^2 and therefore, has roughly 6.5 thousand inhabitants per km^2. It is a sparsely populated urban area compared to other large cities in Latin American.

The Statistics National Institute (INE) has divided the Uruguayan territory for statistical purposes. Three levels of division are considered:

– Section: Montevideo is divided into 27 Sections, according to the limits established in the 1963 Census. Sections are shown in Fig. 3 with dark blue lines.
– Segment: each Section is subdivided into Segments, which consist of a set of blocks. Montevideo is comprised of 1 063 Segments, which are marked in blue in Fig. 3.
– Zone: is the smallest identifiable zoning defined by INE. Each Segment is divided into several Zones. In densely populated parts of the city Zones usually coincide with a single block. In more rural areas, Zones correspond to portions of territory defined by natural or artificial limits (e.g., watercourses, highways, local roads, railways). Fig. 3 shows the 13 608 Zones of Montevideo in sky blue.
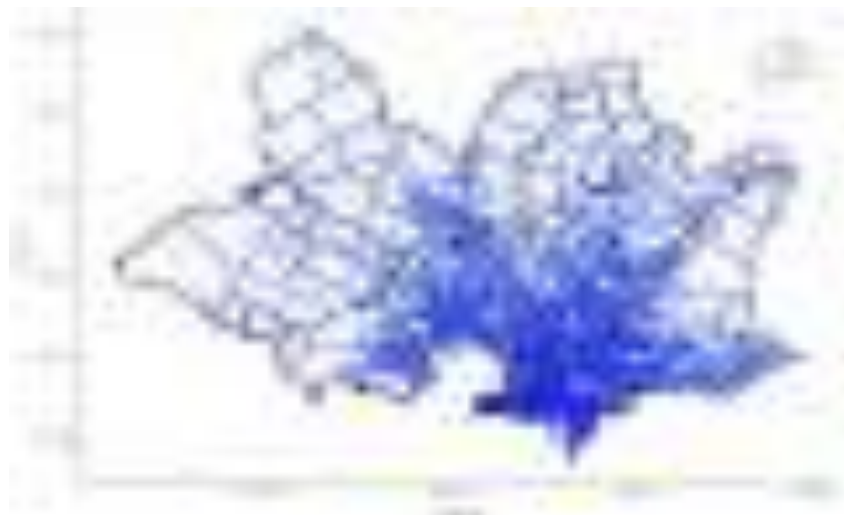
Fig. 3. Division of Montevideo in Sections, Segments, and Zones.

In this work Zones are used to compute the walking accessibility indicators, which are the finer-grain zoning division available for the city.

The public transport system in Montevideo is based on buses. Public transport plays an important role in the city. Results from the Mobility Survey of the Metropolitan Area of Montevideo 2016 show that bus trips represent 25% of all trips [11]. Fig. 4 outlines the road network, bus lines and bus stops of Montevideo. It is easy to distinguish the central parts of the city as the density of bus stops increases and most lines converge to it.

4.2   Software and tools

Service area analysis was made with QGIS through its algorithm provider using the function *service area*. Similarly, the buffer of Zones was carried out using the vector spatial analysis tool of QGIS. On the other hand, the computation of the accessibility indicators were made through Jupyter Notebooks, which offer a programming ecosystem that integrates data, code and results. Geospatial information was handled through the *Pandas* and *Geopandas* libraries and visualizations were created using the *Bokeh* library.

4.3   Data sources and data cleansing

The main data sources were obtained through the open data catalog of the Municipality of Montevideo. All data sets obtained from this source were downloaded on 3/18/2022. The datasets used correspond to the bus lines and bus

Fig. 4. Montevideo: road network and public transport system

stops of the public transport system, the road network of Montevideo, and the population data from the 2011 census for the three existing zoning levels: Section, Segment and Zone.

Bus stops and bus lines Cleaning the bus lines and stops data comprised a series of consistency checks. A first approach with the data was enough to rule out a line that is active only during the Carnival season in Montevideo and was therefore removed from the lines and stops data set. Another verification carried out was through a full join between the data set of lines and the data set of stops, to check that all lines have associated stops and that all stops have at least one corresponding bus line. As a result of this analysis, one line was removed because it did not have corresponding stops in the set of bus stops. Finally, all the bus stops that were located outside of Montevideo were removed and the lines that operate beyond the department were cut short. In conclusion, the remaining data set of bus lines has 634 different lines; and the set of bus stops is comprised of a total of 4 643 unique stops.

Montevideo road network The cleansing process of the Montevideo road network consisted simply in correcting invalid geometry errors using the predefined Check Validity function provided by the QGIS topology checker plugin.

4.4   Accessibility indicators

The three accessibility indicators were computed according to the methodology, using the finest zoning available for the city, and considering a buffer of 10 meters for each Zone as described in the methodology.

The first indicator shows the number of bus stops that cover each Zone considering a walking distance of 400 meters or less. Results are shown in the map of Fig. 5, where darker shades of blue indicate a higher number of bus stops reachable from the Zone. The city center (south central area in the map) can be easily distinguished given the higher density of bus stops. Some peripheral Zones also stand out, since Zones in the periphery are larger in area and thus may have access to a higher absolute number of bus stops.
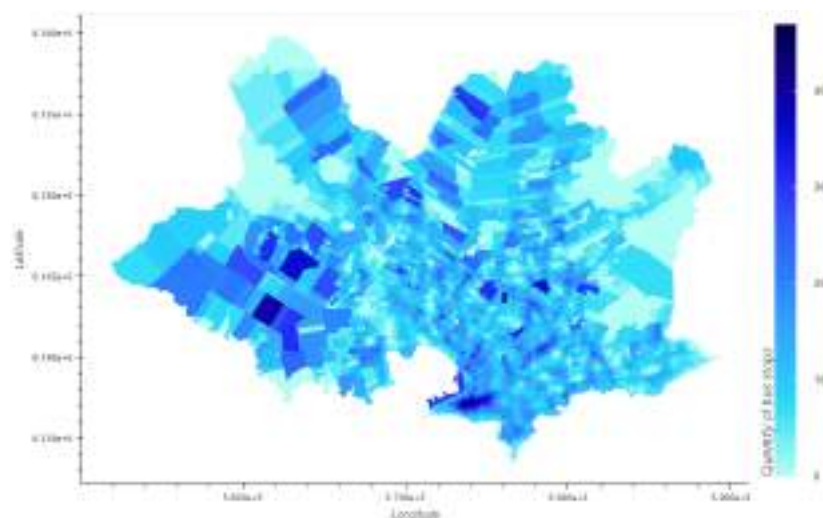
Fig. 5. Number of bus stops accessible when walking up to 400 meters per Zone

The mean number of bus stops accessible by a given Zone is 9.2; whereas the median is 9.0. A histogram of the distribution of the number of bus stops is presented in Fig. 6. The *saw-tooth* shape of the distribution can be explained by the fact that bus stops tend to be placed on each side of the road to service both directions of bus lines. Thus, it is more likely to reach an even number of bus stops (i.e., for inbound and outbound bus lines).

Next, we calculate the second accessibility indicator, i.e., the number of bus lines that are accessible for each Zone when considering a walk of 400 meters or less. Results are shown in the choropleth map in Fig. 7, where darker colors indicate that a larger number of lines are accessible for that Zone.
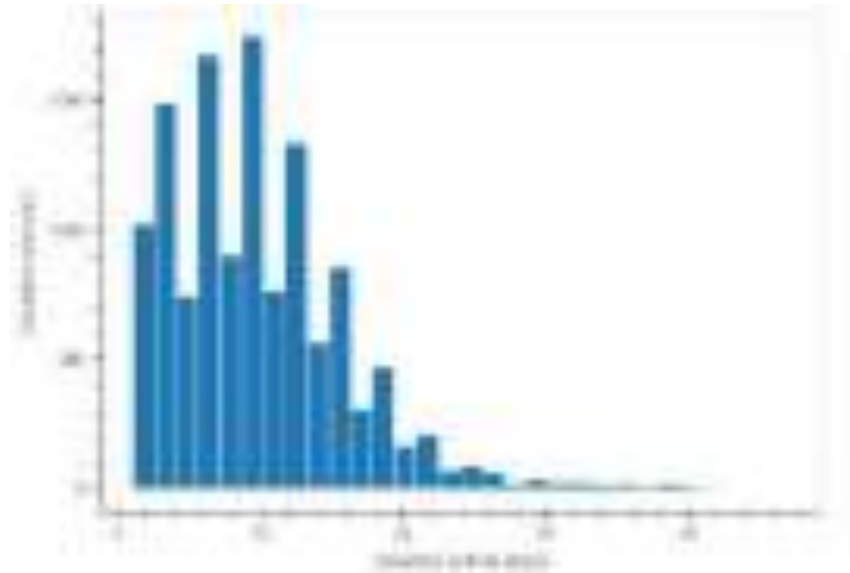
Fig. 6. Distribution of the number of bus stops accessible when walking up to 400 meters
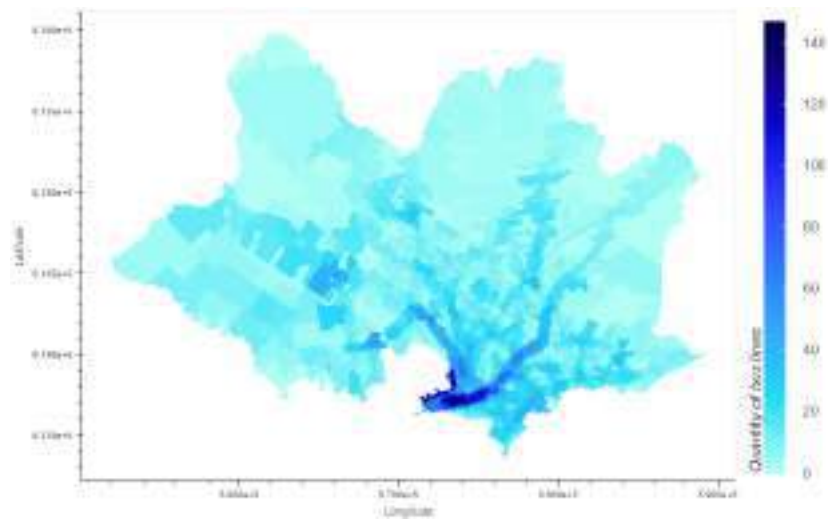

Fig. 7. Number of bus lines accessible when walking up to 400 meters per Zone

The city center in this map stands out compared to other areas since many different bus lines converge to it. Also, the main arteries of the city (going East and North from the city center) can be distinguished because of the density of bus lines that operate over those main roads. Moreover, comparing Fig. 5 with Fig. 7, a softening of peripheral areas can be appreciated, suggesting that while some Zones in the periphery access a large number of stops, these stops provide service to a small number of bus lines. The mean number of lines is 16.7 and the median is 10.0. The distribution of the number of bus lines accessible is shown in the histogram in Fig. 8.
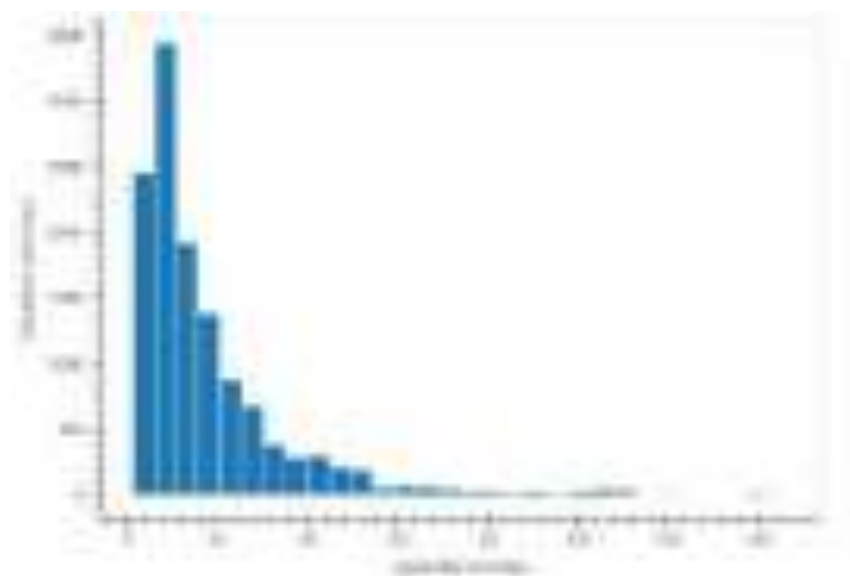
Fig. 8. Distribution of bus lines accessible when walking up to 400 meters

The third and last accessibility indicator illustrates the percentage of population of each Zone covered by the union of service areas. Results are shown in Fig. 9. Key results are that the mean coverage is 94.1% and the median is 100%. An histogram of the distribution of coverage is shown in Fig. 10 and shows that, for most Zones, 100% of their population have access to a bus stop walking 400 meters or less. Given the assumption that the population is evenly distributed on the road network, the percentage of Montevideo's population covered by at least one bus stop at 400 meters or less is 95,5%. When considering the population split by gender, women (95.7%) present a slightly higher percentage of coverage than men (95.3%). In regards to age, young citizens (0 to 14 years old) present the lowest levels of accessibility with a coverage of 93.9% whereas senior citizens present the best values of accessibility with 95.6%.
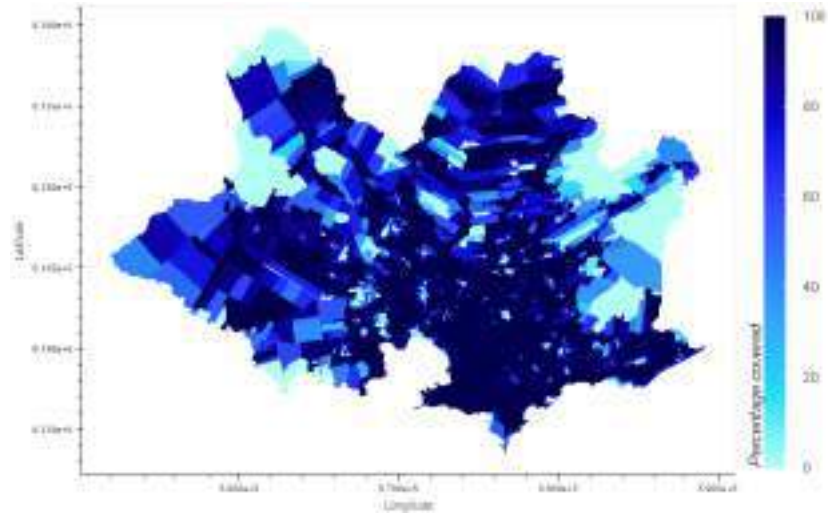
Fig. 9. % of population with access to a bus stop when walking up to 400 meters per Zone
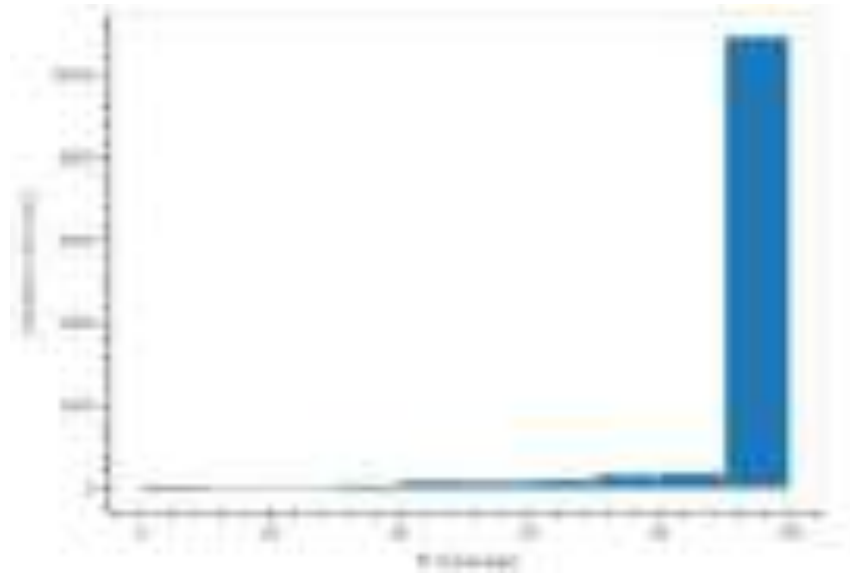

Fig. 10. Distribution of the % of population with access to a bus stop when walking up to 400 meters

5   Conclusions and future work

This work presented a study on walking accessibility to public transport systems using Montevideo, Uruguay, as a case study. As public transport in Montevideo is based on buses, the main data sets considered are bus stops and lines. The analysis was performed using the smallest zoning available for the city which is roughly equivalent to blocks in densely populated areas of the city. Through a service area analysis using geospatial tools we estimated the coverage of Montevideo's public transport bus network. The implemented methodology accounts for the actual walk that passenger do through the road network, improving other simpler estimations based on straight line distances and buffer areas.

The main finding of the analysis is that 95,5% of Montevideo's population can access at least one bus stop when walking up to 400 meters. However, when considering the number of different bus lines that operate on these stops, results show that areas in the outskirts of the city have access to fewer bus lines compared to downtown areas. The results are in-line with figures reported by transport authorities in the press (around 97% of coverage). The overestimation in coverage can be explained by the simpler approach used by the authorities (i.e., straight line buffer areas) compared to the more precise approach proposed in this work based on service areas. Additionally, results showed that the walking accessibility is unequal when considering gender and age, with young citizens (0 to 14 years old) and men showing lower levels of coverage compared to their counterparts.

The main lines of future work include incorporating line schedules in order to analyze how accessibility indicators and coverage vary throughout the day. Also, we propose to compare the computed indicators against the results from a household mobility survey conducted in 2016. Finally, the results of this study could be used as input to address many different optimization problems, such as, bus stop (re)location, network redesign, and expanding the catchment areas of current bus stops by including facilities for other active modes (e.g., shared bikes) to be used as a feeding method for the public transport system.

References

1. Abrantes, P.A., Wardman, M.R.: Meta-analysis of UK values of travel time: An update. Transportation Research Part A: Policy and Practice **45**(1), 1–17 (2011)
2. Audirac, I.: Accessing transit as universal design. Journal of Planning Literature **23**(1), 4–16 (2008)
3. Brand, J., Hoogendoorn, S., van Oort, N., Schalkwijk, B.: Modelling multimodal transit networks integration of bus networks with walking and cycling. In: 2017 5th IEEE International Conference on Models and Technologies for Intelligent Transportation Systems (MT-ITS). pp. 750–755 (2017)

4. Daniels, R., Mulley, C.: Explaining walking distance to public transport: The dominance of public transport supply. Journal of Transport and Land Use **6**(2), 5–20 (2013)
5. García-Palomares, J.C., Gutiérrez, J., Cardozo, O.D.: Walking accessibility to public transport: an analysis based on microdata and GIS. Environment and Planning B: Planning and Design **40**(6), 1087–1102 (2013)
6. Hansen, W.G.: How accessibility shapes land use. Journal of the American Institute of planners **25**(2), 73–76 (1959)
7. Hernandez, D.: Uneven mobilities, uneven opportunities: Social distribution of public transport accessibility to jobs and education in montevideo. Journal of Transport Geography **67**, 119–125 (2018)
8. Hernandez, D., Hansz, M., Massobrio, R.: Job accessibility through public transport and unemployment in latin america: The case of montevideo (uruguay). Journal of Transport Geography **85**, 102742 (2020)
9. Hernández, D., Rossel, C.: Unraveling social inequalities in urban health care accessibility in montevideo: A space-time approach. Journal of Urban Affairs **0**(0), 1–16 (2022)
10. Langford, M., Fry, R., Higgs, G.: Measuring transit system accessibility using a modified two-step floating catchment technique. International Journal of Geographical Information Science **26**(2), 193–214 (2012)
11. Mauttone, A., Hernández, D.: Encuesta de movilidad del área metropolitana de Montevideo. principales resultados e indicadores (2017)
12. Pablo, M.: LadoB - ¿Cómo se transporta Montevideo? Entrevista a Pablo Menoni. TV Ciudad (July 2022), Available online: https://www.youtube.com/watch?v= nU6gZKqi_k8. Last accessed: 2022-10-03
13. Rijsman, L., van Oort, N., Ton, D., Hoogendoorn, S., Molin, E., Teijl, T.: Walking and bicycle catchment areas of tram stops: factors and insights. In: 2019 6th International Conference on Models and Technologies for Intelligent Transportation Systems (MT-ITS). pp. 1–5 (2019)
14. van Soest, D., Tight, M.R., Rogers, C.D.: Exploring the distances people walk to access public transport. Transport reviews **40**(2), 160–182 (2020)

Analysis of public transportation in Montevideo, Uruguay during the COVID-19 pandemic

Andrés Collares[1], Diego Helal[1],
Sergio Nesmachnow[1][0000−0002−8146−4012], and
Andrei Tchernykh[2][0000−0001−5029−5212]

[1] Universidad de la República, Uruguay
{andres.collares,diego.helal,sergion}@fing.edu.uy
[2] CICESE Research Center, Ensenada, Baja California, México
chernykh@cicese.edu.mx

Abstract. This article presents the analysis of the demand and the characterization of mobility using public transportation in Montevideo, Uruguay, during the COVID-19 pandemic. A urban data-analysis approach is applied to extract useful insights from open data from different sources, including mobility of citizens, the public transportation system, and COVID cases. The proposed approach allowed computing significant results to determine the reduction of trips caused by each wave of the pandemic, the correlation between the number of trips and COVID cases, and the recovery of the use of the public transportation system. Overall, results provide useful insights to quantify and understand the behavior of citizens in Montevideo, regarding public transportation during the COVID-19 pandemic.

Keywords: public transportation, COVID-19 pandemic, urban data analysis, mobility patterns

1 Introduction

Mobility was significantly affected by the COVID-19 pandemic. Although all transportation means were affected worldwide, the impact was even more notable on public transportation. Despite the different sanitary measures taken by governments and local administrations, the number of trips on public transportation significantly reduced during the COVID-19 pandemic, mainly because citizens perceived a high risk of contagion when sharing a mobility mean [31].

The reduction on the number of trips was notable, reaching values over 90% during the hard restrictions, especially in countries that adopted lockdown as countermeasure. Trips on public transportation have not fully recovered, even in countries that have significantly lowered the contagion levels [9,19,28].

The analysis of urban mobility data is crucial to help administrations and policy makers to improve public transportation systems [23]. Data analysis has been even more important as a tool to study and characterize the mobility patterns

of citizens during the COVID-19 pandemic. A proper analysis via relevant indicators helps the authorities to identify citizens who are forced to move despite sanitary measures, understand their behavior, and adequately size the public transport system in this type of special situation, according to their needs.

In this line of work, this article presents a study to analyze the demand and characterize the mobility patterns of citizens using the public transportation system in Montevideo, Uruguay, during the COVID-19 pandemic. A urban data-analysis approach is applied to process and analyze available open data about trips performed in the public transportation system, geographical data, and statistics about the COVID-19 pandemic in Uruguay.

The main results indicate that the reduction of trips in public transportation was 71.4%, lower than the reductions reported in similar case studies. In turn, a negative correlation was detected between the use of the public transportation system in Montevideo and confirmed COVID-19 cases in Uruguay. A characterization identifies that neighborhoods with the higher correlation have lower levels of sociodemographic index, suggesting that low income citizens were the most forced to use public transportation. Finally, the analysis of the recovery of trips in public transportation indicate that citizens returned to use public transportation at a fast pace, significantly faster than in other capital cities. Overall, the study provides useful insights to understand the mobility patterns and the use of public transportation in Montevideo during the COVID-19 pandemic.

The article is organized as follows. Section 2 presents a description of the problem solved and reviews relevant related works. Section 3 describes the case study, the public ITS in Montevideo, Uruguay. The applied methodology and implementation details is presented in Section 4. The experimental evaluation of the proposed approach is reported in Section 5. Finally, section 6 presents the conclusions of the research and formulates the main lines for future work.

2   Problem definition and literature review

This section describes the addressed problem and reviews relevant related works.

2.1   Problem description

The proposed problem is characterizing the use of public transportation during the COVID-19 pandemic in Montevideo, Uruguay. The main goal is to quantitatively evaluate the reductions of the use of public transportation after the national sanitary emergency was declared, characterize the mobility patterns during the different stages and waves of the pandemics, and how citizens returned to use public transportation when the sanitary conditions improved.

The problem is relevant considering two distinctive aspects of the case study addressed, in Montevideo, Uruguay, which are commented next.

On the one hand, in Montevideo there is a natural tendency of citizens to shift to public transportation and more sustainable transportation modes [15,16], but this tendency significantly reverted during the COVID-19 pandemic when

citizens decided to shift to car for commuting because of the perceived or suspected risk of shared transportation means as a vector for the spread of the virus, considering the practically impossibility of observing the recommended social distance. This fact is not new; as safety is one the main concerns that affect and determine the mobility behavior of citizens [5].

On the other hand, the model followed by the Uruguayan government to deal with the COVID-19 pandemic was different than in other countries. Instead of promoting a lockdown, the 'responsible freedom' (*libertad responsable*) model was adopted. The model was based in a voluntary quarantine, without limiting people mobility (i.e., people were never mandated to stay at home). A meticulous tracking of infected people was implemented, complemented by randomized COVID-19 testing and promoting the use of face masks, publicity campaigns to promote social distance and social responsibility, and a reasonable reduction of social activities. The model was successful to keeping infections controlled, even at zero during several days in the first few months of the pandemics. During the first eight months of the pandemic, active cases did not exceed a threshold of 200 [30]. The first wave of COVID-19 was this way postponed until mid-2021, when the influence of tourism and the fully recovered social activities played a role to help spreading the virus. The situation normalized in August 2021, until the second wave (Omicron strain) stroked the country in the summer of 2022. However, vaccination developed at a fast pace (more 50,000 shots per day) and the country was among the top of the list in terms of percentage of vaccinated population in the world [8]. The situation returned to normality in March 2022. The end of the sanitary emergency was officially declared on April 5th, 2022.

2.2   Related work

Studies on the demand of public transportation during the COVID-19 pandemic in Europe, North America, and Asia concluded that the number of trips significantly reduced. The behavior of citizens varied depending on the type of lockdown implemented and also other cultural factors [10]. A reduction of 50% was reported in Australian cities [4], 60% in Stockholm, Sweden [17], and 80% (peak of 90%) in Budapest, Hungary [6]. Significant differences for the reduction of public transportation were reported in Poland, depending on the level of confinement [33]. Reductions between 50% to 85% were reported for Warsaw, later confirmed by an average of 70%, according to an online survey questionnaire [18]. The reduction was up to 90% in Gdansk, but 75% of the interviewed persons planned to return using public transportation when the sanitary situation improved [28]. In the Netherlands, reductions on public transportation usage up to 90% were reported, based on the analysis of data from 2500 Dutch citizens [9]. In all reviewed cases, the use of public transportation accounted for the largest decrease, when compared with other mobility means, such as private vehicles.

Similar reductions were reported in North America. Lui et al. [19] studied the impacts of the pandemic on public transportation demand for more than 100 cities in USA. Results shown that communities with higher proportions of essential workers and vulnerable populations had higher demand levels during

COVID-19. A similar situation was detected for the public transportation systems in Toronto and Vancouver, Canada. Palm et al. reported that 63% of citizens stopped using public transportation during the first stage of the COVID-19 pandemic. During the second wave of the COVID-19 pandemic, 70% of citizens that stopped using public transportation returned [27].

In Latin European countries, where the behavior of citizens is more similar than in our Latin American cities, different considerations were analyzed. Carteni et al. [7] found a high correlation between COVID-19 contagion and the number of trips performed on public transportation 22 days before, during the second wave (without vaccination). In Spain, Rodríguez et al. [29] developed characterized the impact of the COVID-19 pandemic on public and private mobility in Fuenlabrada. The reductions at the peak of the pandemic were significant, 95% for public mobility and 86% for private mobility. Similar results were computed for the city of Santander by Aloi et al. [1], who also studied the impact on NO_2 emissions and traffic accidents. The average overall mobility reduced 76%, the demand of public transportation reduced up to 93%. In turn, NO_2 emissions and traffic accidents reduced up to 60%–67%. Awad et al. [3] studied the users behavior regarding public transportation and shared mobility in Spain. Results revealed that although the use of public transportation reduced significantly, citizens were still willing to use public transportation, as long as proper sanity measures are implemented without increasing the ticket prices.

Few articles have studied the impact of the COVID-19 pandemic in public transportation in Latin America. Andara et al. [2] presented a study of the impact of the COVID-19 pandemic on mobility in eight major cities in Latin America. The study focused on developing descriptive statistical models for the variation of motorized mobility in the period from March to September 2020. Traffic congestion and urban transportation were analyzed via regression models. The main results indicated that private mobility recovered faster than public transportation. Authors concluded that public transportation did not accounted as a relevant factor in the spread of the pandemic in the studied cities.

Gramsch et al. [13] analyzed the impact on public transportation of the dynamic lockdown strategy in Santiago, Chile. The main results reported a reduction of 72% on the demand for public transportation when strict lockdown measures were adopted, and a reduction of 12% when the dynamic lockdown strategy was applied. The study also detected a short-term effectiveness of lockdowns to reduce mobility. The implemented lockdowns had a greater impact on the demand for public transportation in municipalities with a larger elderly population and high-income households.

No studies have been published about the use of public transportation during the COVID-19 pandemic in Uruguay. This article contributes in this line of work, by applying a data analysis approach to characterize mobility in the public transportation system of Montevideo during the COVID-19 pandemic.

3　Case study: the public transportation system in Montevideo, Uruguay

The public transportation system in Montevideo is within the Metropolitan Transportation System (STM), a program designed to integrate all public transportation of Montevideo and nearby locations and conglomerates.

The STM comprises 145 main lines, more than one thousand line variants, and five thousand bus stops, remarkable large numbers for a city like Montevideo. Fig. 1 presents the bus stops of the public transportation system in Montevideo.

Fig. 1: Bus stops of the public transportation system in Montevideo

Among several features oriented to develop a more efficient, rational and safe public transportation, STM introduced a relevant technological improvement: contact-less smart cards to be used by passengers to pay for tickets, without using physical money [21]. Each smart card is linked to the identity of the owner, and the collected data are crucial to analyze the system performance, to determine the mobility patterns of citizens, and to identify issues that affect the quality of service offered to citizens.

The information about trips, collected by STM, is crucial to know relevant data, such as origin stop, destination, travel demand, bus line, date and time of travel, type of ticket or category of user, etc. These data allow computing important indicators, identify mobility patterns, and categorize the mobility demands. Previous research efforts from our research group [11,12,15,21,22,23,24] processed records of trips in the public transportation of Montevideo, and also crossing with other data sources (geospatial data, information on lines, etc.).

4　Analysis of COVID-19 and mobility information

This section describes the data source and the methodology applied for the analysis of public transportation in Montevideo during the COVID-19 pandemic.

4.1　Data sources

The processed data to solve the problem was obtained from open data repositories provided by the Uruguayan government, under the National Open Data Catalog . Several data collections are free and fully available. In particular, the catalog includes data on trips made by bus, from the STM. The dataset of trips contains all the trips made on the lines of the public transportation system in Montevideo, including information on companies, lines, date and time, ticket categories and other relevant information, such as the origin bus stop for each trip and the payment method (smart card or cash). The information available for public transportation trips has data from November 2019 to June 2022.

Geographical information was obtained from shapefiles containing the location of bus stops in Montevideo and shapefiles containing the polygons of neighborhoods in Montevideo. In turn, free access data provided by the Uruguayan Interdisciplinary Group for COVID-19 Data Analysis (GUIAD-COVID-19) were also used. The extracted data from this dataset was the number of registered COVID-19 cases per day and department [14].

4.2　Overall description of the methodology

The applied methodology included three stages: data pre-processing, data processing applying parallel computing, and analysis of results.

Data pre-processing. The data preprocessing stage included data cleansing and also associating the geographical location (neighborhood) to each registered ticket sale from the trips dataset. The shapefiles containing the location of bus stops in Montevideo was crossed with the shapefile containing the polygons of neighborhoods in Montevideo, to be used in the aggregation of results. The open-source cross-platform desktop geographic information system application QGIS was used for this task. A manual classification was performed for those bus stops that are located outside Montevideo. They were categorized as 'Canelones East' or 'Canelones West', according to their geographical location (Canelones is the department surrounding Montevideo).

Parallel processing. A large volume of data was available to process in the proposed study. The size of the corresponding datasets for the analyzed period (2019–2022) was over $73\,$GB. In addition, there is a large flow of parallelizable operations, that fit on the using the MapReduce parallel computing paradigm. Examples of those operations are the grouping of data according to day and neighborhood (in order to analyze the daily mobility by neighborhood), the transformation of each trip into an integer for counting the number of trips that occurred each day, the grouping by day and user category, and the grouping by day and bus line.

Analysis of results and metrics. The final stage involved the computation of relevant metrics for the analysis and the application of statistics and time series analysis over the computed results.

4.3　Resolution strategy

The parallel algorithm for data processing was developed in several stages:

1. An algorithm was implemented to compute the number of trips per day. The main goal was to find out how the start date of the pandemic and the declaration of the sanitary emergency impacted on the mobility patterns of citizens and determine the reduction of public transportation usage. For the implementation, the data about trips was separated by day to perform a parallelization of the computation and then a reduce operation was applied to group by day.
2. A second algorithm was implemented to calculate the correlation between reported COVID cases and mobility patterns of citizens.
3. In addition, an analysis of the mobility patterns of citizens during the COVID pandemic by neighborhood, bus line, and user category was carried out. Trip data was grouped by day and neighborhood, by day and line number, and by day and user category. The main goal was determining which category of users most needed to use public transportation, through the value of the correlation between COVID cases and trips for each case.
4. Finally, the recovery of citizens mobility in the city during the COVID pandemic was studied. The analysis studied the dates on which citizens returned to 'normal' levels of public transportation use, by analyzing how the monthly average of daily trips varied over time.

4.4　Implementation details

The developed algorithms were implemented using the Scala programming language [26] and the Hadoop MapReduce framework [32]. The MapReduce framework adapts very well to the characteristics of the data processing problem and Scala offers a flexible and robust development and interoperability. Both are popular options in the field of big data.

The Hadoop Distributed File System (HDFS) was used for data storage. HDFS is a fault-tolerant system that uses data replication and was designed to be used as the storage system of Hadoop. Using HDFS allows for a robust and efficient design. On the one hand, if a processing node goes down, the data will be available on the other configured nodes. HDFS is optimized to store large amounts of data and maintain multiple copies to ensure high availability and fault tolerance. On the other hand, HDFS provides a very efficient access to data, granting a large bandwidth, so that MapReduce applications can efficiently process large volumes of data. It also uses the write-once-read-many storage model, so input data is written once and can be read as many times as needed.

The analysis of processed data and results was performed in Python, using the Pandas and Matplotlib libraries.

5　Experimental analysis and discussion

This section reports the results of the experimetnal analysis of COVID-19 and mobility information from the public transportation system in Montevideo.
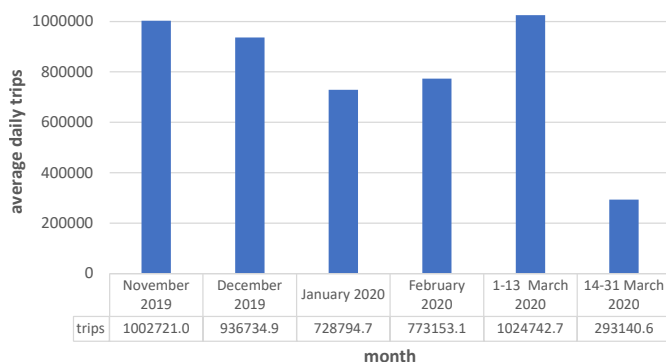
5.1 Development and execution platform

The proposed big data processing approach was developed in Scala and Hadoop. The experimental analysis was performed on a HPE Proliant server with Xeon Gold 6138 processor, 40 cores and 120 GB of RAM memory. from National Supercomputing Center (Cluster-UY), Uruguay [25]. The amount of physical memory was set to 4 GB for the map processes and 8 GB for the reduce processes.
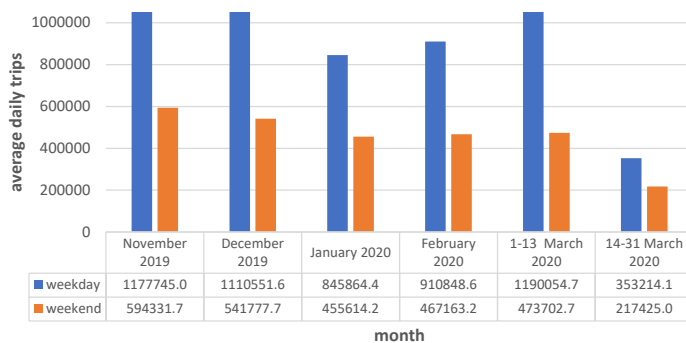
5.2 Validation results

The computed results are reported and discussed in the following paragraphs.

Effect of the declaration of sanitary emergency. Fig. 2 presents a comparison of the average number of trips performed on the STM before and after the sanitary emergency was declared in Uruguay.

	November 2019	December 2019	January 2020	February 2020	1-13 March 2020	14-31 March 2020
trips	1002721.0	936734.9	728794.7	773153.1	1024742.7	293140.6

month

(a) Average of daily trips (November 2019–March 2020)

	November 2019	December 2019	January 2020	February 2020	1-13 March 2020	14-31 March 2020
weekday	1177745.0	1110551.6	845864.4	910848.6	1190054.7	353214.1
weekend	594331.7	541777.7	455614.2	467163.2	473702.7	217425.0

month

(b) Average of daily trips for weekdays and weekends (November 2019–March 2020)

Fig. 2: Comparison of average daily trips pre- and post-declaration of the sanitary emergency in Montevideo, Uruguay

The valley at the beginning of the year in Fig. 2 is seasonal: January and February are the holiday months, whereas most education activities (school, high school, university) started on March, 2nd, 2020. In a normal situation, bus trips peak in March, with a similar average than in November.

Fig. 2(a) clearly shows the reduction on bus trips from the day when the sanitary emergency was declared (March, 13rd). The overall reduction was 71.4% with respect to the number of daily trips in 1–13 March. A different situation occurred for weekdays and weekends. In weekends, the reduction of trips was 54.1%, mainly because a significantly lower of bus trips are performed on weekends. Therefore, the reduction due to the COVID pandemic had a less significant impact. Fig. 2(b) reports the analysis, separating weekday trips and weekend trips. The graph bar shows that the number of weekend trips reduced to approximately one half of the trips, considering the average trips in weekends from March 1–13. The reported reductions on trips performed in public transportation are lower than other reported cases for similar cities in Europe and America. This result suggest that the risk perceived by citizens regarding trips in public transportation was lower than in other countries.

The use of public transportation steadily increased since the first week after the declaration of sanitary emergency. The evolution is reported and analyzed in the next paragraph.

Trips and COVID cases. Fig. 3 presents the evolution of the number of trips from May 2020 to May 2002 in the public transportation system on Montevideo, and the number of confirmed COVID cases, according to GUIAD-COVID-19 and the Public Health Ministry.
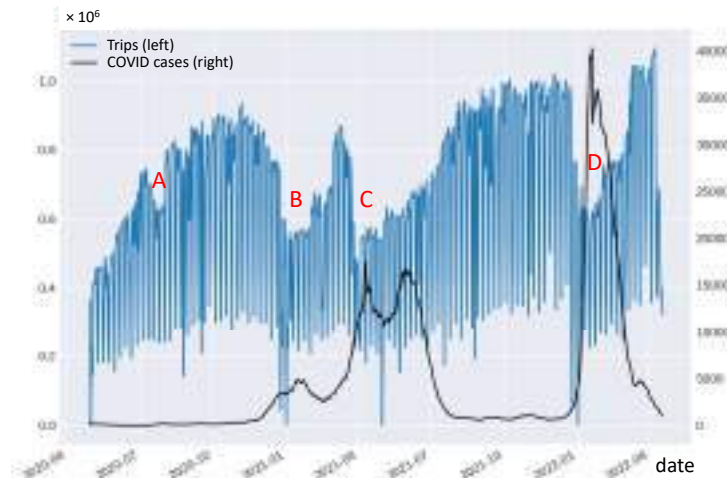

Fig. 3: Number of trips and COVID cases (April 2020 to May 2022)

Fig. 3 shows a clear relation between mobility in public transportation and the number of COVID cases. The number of trips reduced when a COVID outbreak happened, and the situation tended to normalize when COVID cases reduced. After the initial reduction of 70% in the first month after the sanitary emergency was declared, the number of trips recovered until the end of 2020. In Uruguay, the initial stage of the COVID pandemic was remarkable softer than in other countries. Only a minor increase of COVID cases was observed in August 2000, when the use of public transportation reduced about 10% (the small valley marked with 'A' in Fig. 3). Then, the first wave of COVID occurred in December 2020. The number of cases increased up to 5000, and the use of public transportation reduced more than 20% (the first large valley marked with 'B'). A new outbreak in May 2021 reduced more than 40% the number of trips (the second large valley marked with 'C'). The number of COVID cases dropped significantly between August and December 2021, and the use of public transportation returned to almost normal levels (almost a million trips daily). The second wave of COVID started in January 2022. The number of cases increased exponentially, up to almost 40 000 in January 2022. The use of public transportation decreased accordingly, almost 50%. When COVID cases reduced, citizens rapidly returned to their common mobility patterns using the public transportation system, with over one million tickets sold in May 2022.

The results clearly shows the correlation between the increase on COVID cases and the reduction on public transportation use in Montevideo, Uruguay. Fig. 4) reports the moving average (21 days) of the number of trips to remove peaks due to weekends and holidays, which results in a smoother curve for the characterization of the public transportation usage.
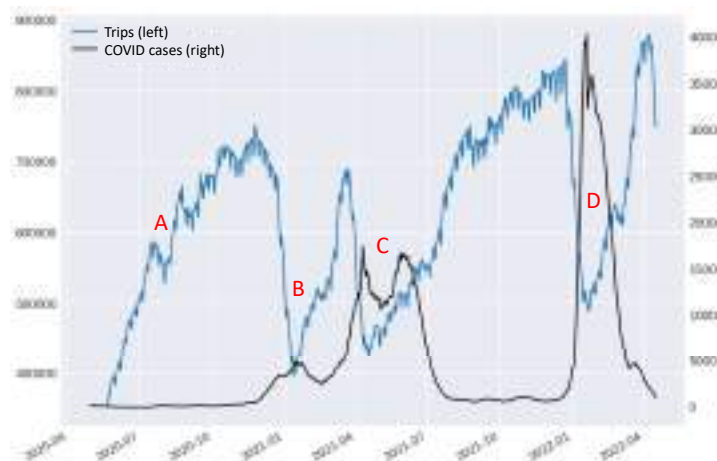

Fig. 4: Number of trips and COVID cases (smoothed average)

Characterization of daily trips. Neighborhoods in Montevideo have different socio-economic realities. To characterize the mobility patterns from/to different locations, the correlation between trips performed from each neighborhoods was studied. Since the dataset of trips does not contain information about neighborhoods, the shapefiles with the bus stops locations and with the polygons of each neighborhood in Montevideo were processed. The intersection between both shapefiles was computed to determine the neighborhood where each bus stop is located. The dataset of trips was grouped by neighborhood and the Pearson correlation between the number of trips from each neighborhood and the number of COVID cases reported in the city was computed. Fig. 5 shows the correlation between trips for the 65 neighborhoods in Montevideo and COVID cases.
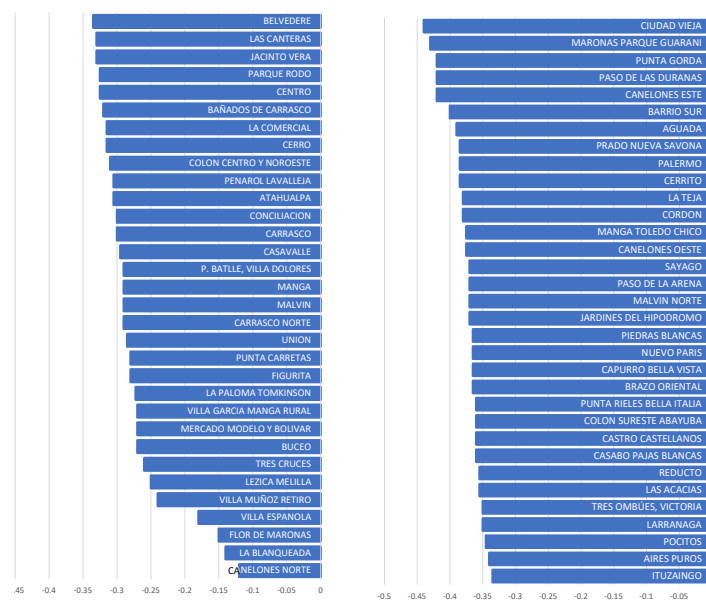

Fig. 5: Correlation between trips in the public transportation and COVID cases for neighborhoods in Montevideo

The correlation results in Fig. 5 shows three clear groups of neighborhoods: low negative correlation, medium negative correlation, and high negative correlation. Fig. 6 presents the results for the five neighborhoods with low negative correlation and for the five neighborhoods with high negative correlation.

An interesting fact emerges when considering the socio-economic reality of neighborhoods with low and high correlation between trips and COVID cases shown Fig. 6, according to the socioeconomic level index (INSE) [20]. Regarding neighborhoods with low correlation between trips and COVID cases, all of them have very low INSE values (2), except for La Blanqueada (6). In turn, all neighborhoods with high correlation between trips and COVID cases have high INSE values (7–9), except for Maroñas (3).

(a) low correlation (b) high correlation

Fig. 6: Neighborhoods of Montevideo with low and high correlation between trips and COVID cases

Results suggest that, on the one hand, citizens living in low income neighborhoods had no alternatives for commuting, but using public transportation. On the other hand, citizens with higher income and purchasing power significantly reduced using public transportation.

Figure 7 compares trips performed from Ciudad Vieja (centric neighborhood, high correlation) and La Blanqueada (centric neighborhood, low correlation).
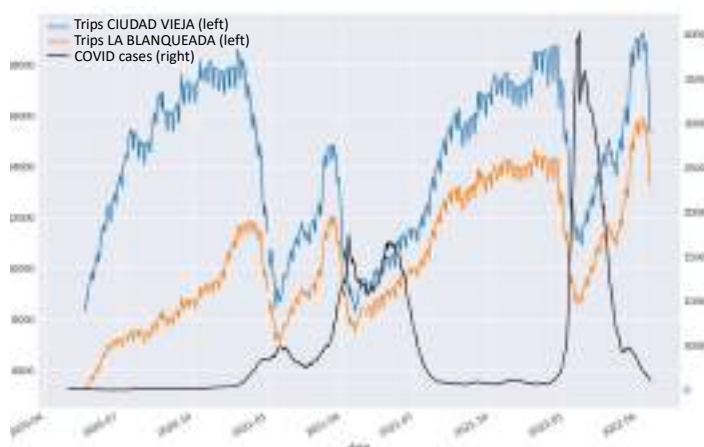
Fig. 7: Comparison of trips from Ciudad Vieja (high correlation) and from La Blanqueada (low correlation) and COVID cases

Figure 7 shows the difference between the reduction in the number of trips from Ciudad Vieja (54.5%) and from La Blanqueada (34.8%) in the first wave of COVID. In the second wave, the number of trips from Ciudad Vieja reduced 51,4% whereas trips from La Blanqueada reduced 35.7%.

Recovery of the use of the public transportation system. The recovery of the public transportation system was significantly faster in Montevideo, Uruguay than in other reported capital cities around the world. Table 1 reports the number of average trips per day for each month in the period in which the sanitary emergency was in force, and the percentage over the average pre-COVID trips.

2020								
pre-COVID	April	May	June	July	Aug.	Sept.	Oct.	Nov.
1024743	262008	357921	585612	860123	620732	805118	915852	925801
100.0%	25.6%	34.9%	57.1%	83.9%	60.6%	78.6%	89.4%	90.3%

2020	2021							
Dec.	Jan.	Feb.	March	April	May	June	July	Aug.
880519	650070	575294	720518	572381	590163	701371	738023	835182
85.9%	63.4%	56.1%	70.3%	55.9%	57.6%	68.4%	72.0%	81.5%

2021				2022				
Sept.	Oct.	Nov.	Dec.	Jan.	Feb.	March	April	
925830	996702	992601	990924	602185	712046	1050306	1082415	
90.3%	97.3%	96.9%	96.7%	58.8%	69.5%	102.5%	105.6%	

Table 1: Analysis of the recovery of trips in the public transportation system

Table 1 indicates that after a slow period of two months after the sanitary emergency was declared, the number of trips recovered fast, i.e., 84% of the reference value in just four months (July 2020). Despite a reduction in August 2020, by the end of the year the number of trips was almost the same than pre-COVID (90% in November). Then, the first massive cases of COVID generated a reduction of up to 56% in February 2021, and the same pattern occurred again, users steadily recovered the confidence in public transportation, until the first wave stroked hard in April-June 2021, causing a decrease in the number of trips up to 56% of pre-COVID numbers. The recovery of the number of trips was significantly faster after the first wave, reaching values over 90% in just three months (September 2021) and a full recovery in the last months of 2021. The second wave (Omicron strain) reduced the number of trips to 59% in January 2022, but the recovery was very fast: the number of trips exceeded the previous pre-COVID value in just two months, in March 2022.

The reported values demonstrate that despite the reduction on trips in public transportation as a consequence of the increase of COVID cases, citizens rapidly trusted again in the public transportation system. The periods for the recovery of the number of trips was shorter in each wave, and just a month and a half in 2022. This pace is significantly faster than the ones reported for other similar case studies in the world [3,13,28]. These facts allows concluding that the responsible freedom model was not only successful in mitigating the impact of the spread of COVID, but also in guaranteeing a rapid recovery of mobility patterns and the use of public transportation in Montevideo.

6　Conclusions and future work

This article presented a study and characterization of the use of public transportation in Montevideo, Uruguay, during the COVID-19 pandemic. Following a urban data-analysis approach, available open data about trips and statistics about the COVID-19 pandemic in Uruguay were analyzed.

The analysis confirmed a reduction of trips in public transportation of 71.4%, lower than values reported for similar cities. A negative correlation was detected between the use of public transportation and confirmed COVID-19. Neighborhoods with the higher correlation have lower sociodemographic levels, suggesting that low income citizens were forced to use public transportation. Trips in public transportation indicate recovered significantly faster than in other capital cities.

The main lines for future work include expanding the analysis considering other categories (e.g., age and tariff type) and performing a throughout analysis of the post-COVID situation, once more recent trip data are available.

References

1. Aloi, A., Alonso, B., Benavente, J., Cordera, R., Echániz, E., González, F., Ladisa, C., Lezama, R., López, Á., Mazzei, V., Perrucci, L., Prieto, D., Rodríguez, A., Sañudo, R.: Effects of the COVID-19 lockdown on urban mobility: Empirical evidence from the city of santander (spain). Sustainability **12**(9), 3870 (2020)
2. Andara, R., Ortego, J., Gómez, M., Ramírez, R., Navas, L., Vásquez, C., Gaitán, M.: Behavior of traffic congestion and public transport in eight large cities in Latin America during the COVID-19 pandemic. Applied Sciences **11**(10), 4703 (2021)
3. Awad, S., Julio, R., Gomez, J., Moya, B., Sastre, J.: Post-COVID-19 travel behavior patterns: impact on the willingness to pay of users of public transport and shared mobility services in Spain. European Transport Research Review **13**(1) (2021)
4. Beck, M., Hensher, D.: Insights into the impact of COVID-19 on household travel and activities in Australia. Transport Policy **99**, 95–119 (2020)
5. Bohte, W., Maat, K., van Wee, B.: Measuring attitudes in research on residential self-selection and travel behaviour: A review of theories and empirical research. Transport Reviews **29**(3), 325–357 (2009)
6. Bucsky, P.: Modal share changes due to COVID-19: The case of budapest. Transportation Research Interdisciplinary Perspectives **8**, 100141 (2020)
7. Cartenì, A., Di Francesco, L., Henke, I., Marino, T., Falanga, A.: The role of public transport during the second COVID-19 wave in Italy. Sustainability **13**(21), 11905 (2021)
8. Costabel, M.: Uruguay emerges as a rare pandemic winner in Latin America (2021), foregn Policy, July 21, 2020 [July 2022]
9. de Haas, M., Faber, R., Hamersma, M.: How COVID-19 and the Dutch 'intelligent lockdown' change activities, work and travel behaviour: Evidence from longitudinal data in the Netherlands. Transportation Research Interdisciplinary Perspectives **6**, 100150 (2020)
10. De Vos, J.: The effect of COVID-19 and subsequent social distancing on travel behavior. Transportation Research Interdisciplinary Perspectives **5**, 100121 (2020)
11. Denis, J., Massobrio, R., Nesmachnow, S., Cristóbal, A., Tchernykh, A., Meneses, E.: Parallel computing for processing data from Intelligent Transportation Systems. In: 10th International Supercomputing Conference in Mexico. pp. 1–15 (2019)
12. Fabbiani, E., Nesmachnow, S., Toutouh, J., Tchernykh, A., Avetisyan, A., Radchenko, G.I.: Analysis of mobility patterns for public transportation and bus stops relocation. Programming and Computer Software **44**(6), 508–525 (2018)
13. Gramsch, B., Guevara, C.A., Munizaga, M., Schwartz, D., Tirachini, A.: The effect of dynamic lockdowns on public transport demand in times of COVID-19: Evidence from smartcard data. Transport Policy **126**, 136–150 (2022)

14. Grupo Uruguayo Interdisciplinario de Análisis de Datos: Covid stats per department, https://github.com/GUIAD-COVID/datos-y-visualizaciones-GUIAD/blob/master/datos/estadisticasUYporDepto.csv [July 2022]

15. Hipogrosso, S., Nesmachnow, S.: Analysis of Sustainable Public Transportation and Mobility Recommendations for Montevideo and Parque Rodó Neighborhood. Smart Cities **3**(2), 479–510 (2020)

16. Hipogrosso, S., Nesmachnow, S.: A practical approach for sustainable transit oriented development in montevideo, uruguay. In: Smart Cities, pp. 256–270 (2022)

17. Jenelius, E., Cebecauer, M.: Impacts of COVID-19 on public transport ridership in sweden: Analysis of ticket validations, sales and passenger counts. Transportation Research Interdisciplinary Perspectives **8**, 100242 (2020)

18. Kłos, Z., Gutowski, P.: The outbreak of COVID-19 pandemic in relation to sense of safety and mobility changes in public transport using the example of Warsaw. Sustainability **14**(3), 1780 (2022)

19. Liu, L., Miller, H.J., Scheff, J.: The impacts of COVID-19 pandemic on public transit demand in the united states. PLOS ONE **15**(11) (2020)

20. Llambí, C., Piñeyro, L.: Índice de nivel socioeconómico (2012), cinve.org.uy/wp-content/uploads/2012/12/Indice-de-nivel-socioeconmico.pdf [August 2022]

21. Massobrio, R., Nesmachnow, S.: Urban Mobility Data Analysis for Public Transportation Systems: A Case Study in Montevideo, Uruguay. Applied Sciences **10**(16), 1–20 (2020)

22. Massobrio, R., Nesmachnow, S., Tchernykh, A., Avetisyan, A., Radchenko, G.: Towards a cloud computing paradigm for big data analysis in smart cities. Programming and Computer Software **44**(3), 181–189 (2018)

23. Massobrio, R., Nesmachnow, S.: Travel time estimation in public transportation using bus location data. In: Smart Cities, pp. 192–206. Springer (2022)

24. Massobrio, R., Pías, A., Vázquez, N., Nesmachnow, S.: Map-Reduce for Processing GPS Data from Public Transport in Montevideo, Uruguay. In: Simposio Argentino de Grandes Datos, 45 Jornadas Argentinas de Informática. pp. 41–54 (2016)

25. Nesmachnow, S., Iturriaga, S.: Cluster-UY: Collaborative Scientific High Performance Computing in Uruguay. In: Supercomputing, Communications in Computer and Information Science, vol. 1151, pp. 188–202. Springer (2019)

26. Odersky, M., Spoon, L., Venners, B.: Programming in scala: [a comprehensive step-by-step guide] (2008)

27. Palm, M., Allen, J., Liu, B., Zhang, Y., Widener, M., Farber, S.: Riders who avoided public transit during COVID-19. Journal of the American Planning Association **87**(4), 455–469 (2021)

28. Przybylowski, A., Stelmak, S., Suchanek, M.: Mobility behaviour in view of the impact of the COVID-19 pandemic—public transport users in gdansk case study. Sustainability **13**(1), 364 (2021)

29. Rodríguez, A., Wilby, M., Vinagre, J., Fernández, R.: Characterization of COVID-19's impact on mobility and short-term prediction of public transport demand in a mid-size city in Spain. Sensors **21**(19), 6574 (2021)

30. Taylor, L.: Uruguay is winning against COVID-19. this is how [corrected]. BMJ **370**, m3693 (2020)

31. Tirachini, A., Cats, O.: COVID-19 and public transportation: Current assessment, prospects, and research needs. Journal of Public Transportation **22**(1) (2020)

32. White, T.: Hadoop: The Definitive Guide. O'Reilly, Beijing, 4 edn. (2015)

33. Wielechowski, M., Czech, K., Grzeda, Ł.: Decline in mobility: Public transport in poland in the time of the COVID-19 pandemic. Economies **8**(4), 78 (2020)

Sistema de Análisis de la Movilidad Regular (Morebike): El Caso del Sistema ECOBICI de la Ciudad de México

Samuel Benitez[1] [0000-0001-9186-1591], Gilberto Martínez [2][0000-0002-8236-0469]
y Adolfo Guzmán[2][0000-0002-0105-1112]

[1] Instituto Politécnico Nacional (IPN), Av. Luis Enrique Erro S/N, 07738, Ciudad de México, México
sbenitezm1701@alumno.ipn.mx
[2] Centro de Investigación en Computación (CIC), Avenida Juan de Dios Bátiz S/N, 07738 Ciudad de México, México
{lluna,aguzman}@cic.ipn.mx

Resumen. Los sistemas de bicicletas compartidas son cada vez más una parte fundamental de la movilidad en las grandes ciudades del mundo como alternativa de transporte accesible y sostenible. Investigar los patrones de uso de las bicicletas en estos sistemas es clave para conocer la demanda y el comportamiento de los ciclistas y así optimizar sus procesos y mejorar su servicio.

A partir de los registros históricos de los viajes, en este artículo se presenta una herramienta de visualización de datos del sistema ECOBICI de la Ciudad de México para estudiar sus patrones y ofrecer su uso de forma pública. Se centra en el estudio de las colonias de la ciudad y los patrones que existen entre ellas, en días entre semana, fines de semana y en diferentes horarios del día.

Este caso de estudio pretende ofrecer una herramienta que ayude a resolver los problemas más comunes de estos sistemas que implican el análisis de la demanda de bicicletas, así como su rebalanceo en las diferentes zonas de la ciudad a través de la identificación de patrones de movilidad y la demanda de bicicletas y cicloestaciones. Se trata de un ejemplo de una aplicación de la Ciencia de Datos mediante herramientas de visualización de datos enfocadas en la movilidad urbana y en los sistemas de bicicletas compartidas.

Palabras clave: Sistema de bicicletas compartidas, Movilidad urbana, Ciencia de datos, Análisis exploratorio, Visualización de datos.

1   Introducción

Un sistema de bicicletas compartidas (SBC) es una solución de movilidad urbana que pone a disposición temporal un número limitado de bicicletas a los usuarios. Son parte de un enfoque de transporte sostenible de los gobiernos y agencias de planificación urbana para estimular la movilidad sostenible, reducir la congestión del tráfico,

el uso del automóvil, mejorar la calidad del aire, mejorar la conectividad y promover un estilo de vida saludable. [1]

Se basan comúnmente en el manejo de estaciones, lugares donde se pueden recoger las bicicletas para posteriormente poder dejarlas en la misma o en cualquier otra estación a lo largo de la ciudad en la que se encuentren, aunque también existen SBC sin estaciones.

ECOBICI es el SBC basado en estaciones de la Ciudad de México que integra a la bicicleta como parte esencial de la movilidad y transporte, dirigido a los habitantes de la capital, de sus alrededores y a los turistas. Permite a los usuarios registrados tomar una bicicleta de cualquier cicloestación y devolverla a la más cercana a su destino en trayectos ilimitados de 45 minutos brindando su servicio todos los días del año en un horario de 5 am a 12:30 am del día siguiente.

Comenzó su funcionamiento en el año 2010 y de acuerdo con su página oficial [2,3], en 2022 este sistema cuenta con más de 380,000 usuarios registrados, mientras que su servicio se encuentra activo en 55 colonias de la ciudad con 480 cicloestaciones disponibles y continua con planes de expansión en lo que resta del año.

Datos Públicos. ECOBICI pone a disposición pública todos sus datos históricos desde el año 2010 en su página oficial [4]. Los datos de los viajes son almacenados y publicados de forma mensual, es posible obtener los viajes de cada año y de cada mes hasta el año corriente, ya que al término de un mes se agrega un nuevo archivo CSV con los viajes registrados en dicho periodo.

2   Trabajos Relacionados

En esta sección se revisa la literatura relacionada a los sistemas de bicicletas compartidas, a sus problemas más comunes y las distintas soluciones propuestas para resolverlos, principalmente a través de la Ciencia de Datos y el uso o desarrollo de herramientas de visualización de datos.

Los procesos de planeación y desarrollo de estos sistemas comúnmente involucran actividades estratégicas, tácticas y operacionales, una continua toma de decisiones que depende de la investigación y evaluación de los datos, además de múltiples herramientas que faciliten los posibles ajustes y mejoras que estos requieran durante su gestión y desarrollo.

Tal como se describe en [5], existen diversos problemas a los que estos sistemas se enfrentan desde su diseño hasta su mantenimiento, en los que se incluye el diseño de las cicloestaciones, la administración del inventario, el rebalanceo estático y dinámico de bicicletas, la administración estática y dinámica de la demanda, entre otros.

Cada uno de estos representa un área de oportunidad y de mejora ya que requieren de un constante análisis de los patrones de movilidad y de las necesidades de los usuarios para cubrir con la demanda de forma óptima, es por ello que, es de suma importancia contar con herramientas que faciliten dicho proceso y permitan generar estadísticas y estrategias basadas en los datos para resolverlos.

Para el problema de la administración de la demanda existen propuestas como la mostrada en [6], la cual consiste en una herramienta para la predicción de la demanda de bicicletas y sus devoluciones en las estaciones a lo largo del día en un SBC en Grecia dirigida a los operadores del sistema. Para cumplir con este propósito se usaron modelos basados en algoritmos de regresión de aprendizaje máquina y se identificó una alta correlación entre el número de viajes y distintos factores de la estación: su ubicación y espacio, la temporada del año, el clima y la hora del día.

En el caso del rebalanceo de bicicletas, es decir, en la redistribución de las bicicletas para cubrir con la demanda de forma óptima, es posible encontrar soluciones como la propuesta en [7] que hace uso de técnicas de *Big Data* y datos geoespaciales de los viajes registrados en un SBC muy usado en China. Se realizó un análisis basado en el desarrollo de visualizaciones que ayuden a proporcionar una mayor comprensión sobre las zonas o ubicaciones geográficas con una alta demanda de forma gráfica y de esta manera concretar un rebalanceo más eficiente, además de la identificación de los viajes definidos como la *última milla,* viajes que usualmente tienen como origen y destino un lugar muy cercano en tiempo y distancia entre sí.

Por otro lado, existen diversas propuestas que resuelven estos problemas pero que dejan a un lado la creación y desarrollo de herramientas visuales y se limitan a realizar análisis numéricos o a la implementación de algoritmos o modelos de aprendizaje máquina. Tal es el caso de investigaciones como [8] y [9], trabajos en los que se hace uso de algoritmos con el objetivo de predecir la demanda de bicicletas y con ello realizar un mejor rebalanceo y manejo del inventario a lo largo del sistema y sus cicloestaciones en las ciudades en las que se encuentran.

La gran mayoría de estas soluciones se enfocan en la operatividad del SBC y están dirigidas a los tomadores de decisiones u operadores del sistema, sin embargo, dejan al usuario final sin la posibilidad de conocer las estadísticas de la movilidad y ayudarlo así a tomar mejores decisiones o simplemente informarlo sobre el estatus y progreso de los viajes registrados a través de los años, es por ello que, el presente trabajo busca cubrir con ambos objetivos.

2.1   Sistemas Existentes Similares a la Propuesta

Entre los sistemas de visualización de datos dirigidos a los usuarios de los SBC los más populares son *The Meddin Bike-sharing World Map* [10] y *Bike Share Map* [11], sin embargo, estos se enfocan en mostrar la información y estadísticas generales de los SBC de todo el mundo y no ahondan en los patrones o la movilidad de los usuarios, por lo que sólo permiten conocer datos básicos como el tipo de SBC, su operador, el número de cicloestaciones y bicicletas, su disponibilidad en tiempo real, noticias o eventos relevantes.

En el caso de ECOBICI, existen algunos sistemas de visualización y análisis de datos, entre ellos se encuentran SAHMI [12] y PLANBIKE [13], ambos desarrollados y mantenidos por el Laboratorio de Ciencia de Datos y Tecnología de Software (LCDyTS) del CIC. Dichos sistemas ponen a disposición pública diversas visualizaciones con el objetivo de difundir los patrones de movilidad en el sistema, un análisis histórico en el caso de SAHMI y un análisis de los viajes en el caso de PLANBIKE.

3   Sistema de Análisis de la Movilidad Regular en ECOBICI: Morebike

Morebike es un sistema y una página web (https://sites.google.com/view/morebike/) con el objetivo de analizar y brindar de forma totalmente pública visualizaciones para identificar patrones en la movilidad de los viajes realizados y registrados en el SBC ECOBICI de la Ciudad de México (ver Fig. 1) que surge como resultado del análisis de la movilidad regular presentado en [18].

Pretende ser una fuente de información confiable y dinámica para el análisis de la movilidad regular entre colonias de la ciudad y la identificación de patrones en distintos horarios del día, en días entre semana o en fines de semana.

Fig. 1. Morebike: Pantalla de Inicio

Dentro de sus principales características se encuentra un análisis bidireccional de los viajes en las colonias como origen y destino, 8 visualizaciones que describen distintos factores de la movilidad regular y un manual dirigido a los usuarios para explotar al máximo las capacidades y funciones de cada una de las visualizaciones, tales como: filtrado de datos, compartición de visualizaciones y descarga o uso de los datos de forma externa con distintos formatos que se ajusten a las necesidades del usuario.

Para lograr esto se hace uso del software de Tableau, una herramienta de análisis y visualización de datos especializada en la inteligencia de negocios [14]. Con esta herramienta, es posible desarrollar diversas visualizaciones y ofrecerlas de forma totalmente pública, además de permitirles a los usuarios interactuar, filtrar o incluso descargar la visualización o los datos completos para su uso particular.

Dichas visualizaciones son divididas de acuerdo con su objetivo y a la dirección de los viajes tomando como referencia a las colonias de la ciudad como origen (lugar del inicio de los viajes) o como destino (lugar del fin de los viajes).

De esta manera, en Morebike se hace uso de los datos abiertos de ECOBICI, sin embargo, sólo desde el año 2018, esto por simplicidad y para poder identificar patrones más cercanos a la realidad actual, especialmente durante la pandemia de COVID-19 y todos los efectos que esta tuvo en la movilidad y las costumbres de las personas en la ciudad.

3.1   Análisis de la Movilidad

Tal como se comentó, Morebike tiene el objetivo de analizar la movilidad de las colonias de la Ciudad de México, ya que se consideran zonas de la ciudad lo suficientemente grandes y representativas para identificar patrones en los viajes.

Dentro de las visualizaciones desarrolladas es posible conocer cuáles son las colonias con mayor movilidad en determinado mes o año, un comparativo entre los viajes entre semana y en fines de semana, la distribución de los viajes en los distintos horarios, meses y años, además de la movilidad entre colonias o la movilidad local en cada una de ellas, por mencionar algunos casos de uso.

Adicionalmente, cada uno de estos análisis se complementan al definir a las colonias como los orígenes o los destinos de los viajes, respectivamente y, de esta manera, estudiar ambos casos: de dónde vienen los ciclistas, cuándo y a qué hora lo hacen o hacia dónde se dirigen, cuándo y a qué hora lo hacen regularmente.

3.2   Visualizaciones

Las visualizaciones se dividen en dos secciones según la dirección de los viajes, sin embargo, son las mismas tanto para el análisis de las colonias como el origen o el destino de estos, en la Fig. 2 se muestra la estructura general de estas, además de la unidad de medida de cada gráfica y sus filtros activos. A continuación, se describe cada una de ellas.
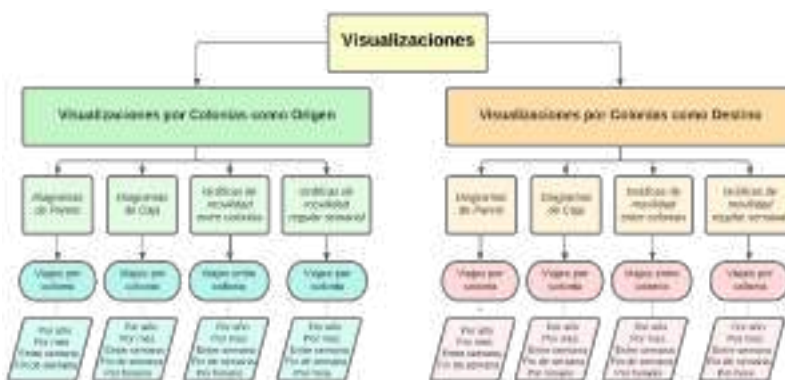

Fig. 2. Morebike: Estructura de las visualizaciones

Diagramas de Pareto. Se busca identificar si se cumple el principio de Pareto (también conocida como la regla del 80/20) el cual describe que el 80% de los efectos de un fenómeno estadístico resultan del 20% de todas sus causas [15]. Es de interés conocer cuáles son las colonias que aportan el mayor número de viajes mensuales y que conforman ese 80% del total de estos, ya sea en días entre semana como en fines de semana, en los distintos años y meses a partir del año 2018 (ver Fig. 3).

En el ejemplo de la figura 3 se observa que de las 55 colonias en las que el servicio de ECOBICI se encuentra activo son 17 aquellas que conforman el 80% de los viajes entre semana en el mes de marzo del año 2021, es decir, un aproximado del 30% de las colonias son las que aportan el mayor porcentaje de los viajes mensuales totales.
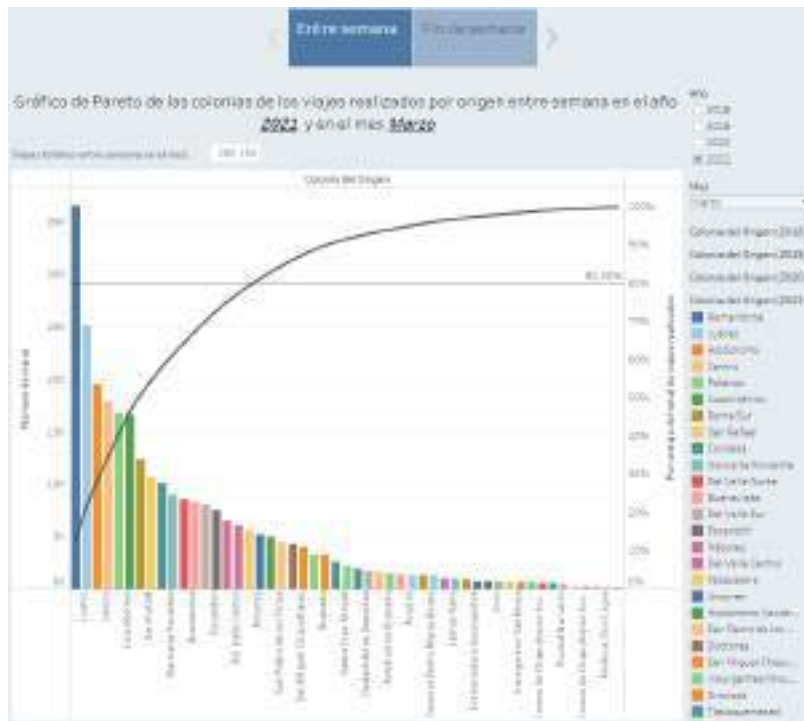

Fig. 3. Diagramas de Pareto: Distribución de los viajes entre semana y fin de semana por colonia y por mes

Diagramas de Caja. Es una herramienta fundamental para el análisis de datos puesto que nos permite conocer la distribución general de los viajes en las distintas colonias del sistema, así como también identificar a aquellas que se les cataloga como atípicas por tener una proporción de viajes significativamente mayor que el resto (ver Fig. 4). Estas colonias son representadas por los puntos que se encuentran por encima del bigote superior de cada diagrama u horario y están determinadas por la inecuación:

$$x > Q_3 + 1.5 \text{ IQR} \tag{1}$$

Siendo Q_3 el tercer cuartil e *IQR* el rango intercuartílico (el área de la caja).

Estas gráficas ofrecen una estadística descriptiva inicial mediante la mediana e información sobre la dispersión y asimetría de los datos, la colonia con el mínimo número de viajes, la colonia con el máximo y los cuartiles que los delimitan. De esta manera se puede realizar una comparación entre los distintos horarios e identificar la proporción de viajes realizados entre semana y en fin de semana en cada uno de estos.

Los horarios fueron definidos a partir de la identificación de las modas estadísticas en los viajes, siendo estos los distintos horarios en los que se presenta un aumento en la demanda y tomando en cuenta las horas en las que el servicio de ECOBICI se encuentra activo: 5 am – 12 pm, 12 pm – 4 pm, 4 pm – 12:30 am. Otra de las visualizaciones que ejemplifica mejor este comportamiento se observa en la figura 7.
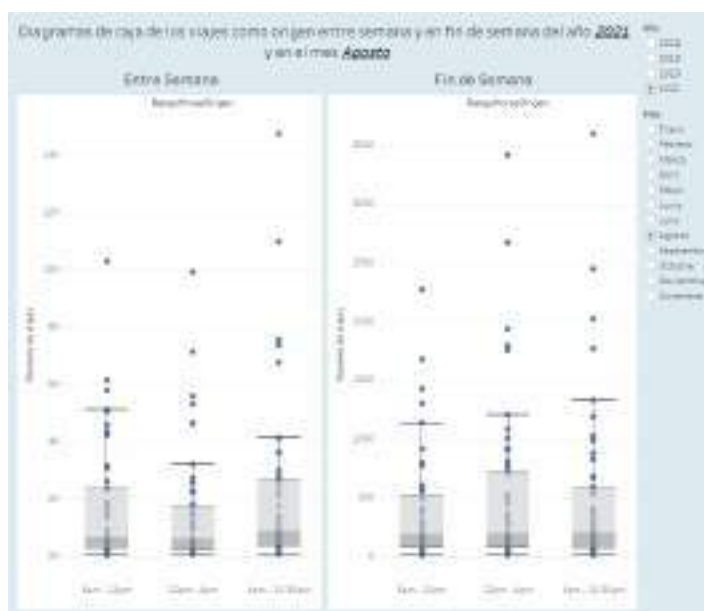
Fig. 4. Diagramas de Caja: Distribución de los viajes entre semana y en fin de semana por horario y por mes

Movilidad entre Colonias. En esta visualización es posible conocer la movilidad que existe entre las colonias con más viajes mensuales registrados en ECOBICI identificando los lugares a los que suelen ir los ciclistas o aquellos de los que suelen provenir, esto tanto en días entre semana como en fin de semana y en distintos horarios (ver Fig. 5). De esta manera, es posible conocer las relaciones entre distintas colonias y definir tres tipos de patrones recurrentes:

- *Movilidad local:* corresponde a las colonias con el mayor número de viajes realizados en sí mismas, es decir, el origen y destino de los viajes se ubica en la misma colonia. Estos viajes representan el problema de la última milla en la movilidad.

— Ej. La colonia Polanco cuenta con la mayor movilidad local del sistema (ver Fig. 5), registrando un gran porcentaje de viajes locales a lo largo del día y un porcentaje reducido de viajes hacia otras colonias.

- *Movilidad unidireccional:* colonias que realizan viajes hacia otras colonias pero que no necesariamente comparten la misma o similar cantidad de viajes entre sí.
  — Ej. De la colonia Juárez viajan constantemente a la colonia Centro, pero de la colonia Centro a Juárez no existe la misma proporción de viajes (ver Fig. 5).
- *Movilidad bidireccional:* colonias que presentan una fuerte relación por compartir viajes entre sí, tanto como origen como destino de los viajes.
  — Ej. La Colonia Hipódromo y Roma Norte comparten viajes recurrentemente a lo largo del día y con una proporción similar en cada horario (ver Fig. 5).

Fig. 5. Gráfica de Movilidad entre Colonias: Viajes compartidos entre las colonias con más viajes mensuales registrados

Podemos resumir estos patrones en dos: movilidad externa y movilidad local (ver Fig. 6). La mayoría de las colonias presentan una alta movilidad local dado el fenómeno de la última milla, sin embargo, los viajes externos suelen presentarse también en una gran proporción, dependiendo de la hora del día y las colonias referenciadas.

Fig. 6. Movilidad entre colonias: Externa (izquierda), Local (derecha)

Movilidad Regular Semanal. La última visualización corresponde a la movilidad semanal y describe la proporción de los viajes registrados a lo largo del día y en todos los días de la semana. Con estas gráficas es posible analizar la actividad de los viajes en cada una de las colonias en distintos meses y años, además de identificar los rangos de horas en los que usualmente aumentan los viajes (ver Fig. 7), esto lo definimos como las modas de los viajes.

Las colonias llegan a tener hasta 3 modas entre semana en la demanda a lo largo del día en los horarios que se definieron previamente: 5 am – 12 pm, 12 pm - 4 pm y de 4 pm - 12:30 am. La colonia Roma Norte, por ejemplo, cuenta con una demanda constante en estos tres horarios (ver Fig. 7), sin embargo, la mayoría de las colonias presentan dos modas a lo largo del día y sólo algunas una única moda.

Fig. 7. Gráfica de Movilidad Regular Semanal: Viajes a lo largo del día entre semana en la colonia Roma Norte

Este comportamiento cambia drásticamente cuando se habla de los viajes en fines de semana, ya que estos presentan una movilidad más errante y dinámica, sin un marcado aumento de la demanda en horarios. Siguiendo con el ejemplo de la colonia Roma Norte, podemos comparar estos dos comportamientos y observar la diferencia entre los días en fin de semana del mismo mes y año (ver Fig. 8).

Fig. 8. Gráfica de Movilidad Regular Semanal: Viajes a lo largo del día en fines de semana en la colonia Roma Norte

4   Resultados

Cada una de las gráficas nos permite extraer información histórica relevante y conocer patrones recurrentes en los distintos años y aquellos que han representado anomalías, como es el caso de la movilidad durante los años 2020 y 2021, afectados por la pandemia. Las aportaciones de este trabajo y el sistema Morebike radican en el análisis de estadísticas y patrones de ECOBICI de forma pública centrándose en el análisis de las colonias de la ciudad y los patrones recurrentes que existan entre ellas, brindando así una herramienta fiable de análisis de datos a sus usuarios y operadores, a su vez que promueve el uso y la mejora continua de estos sistemas.

A continuación, se describen patrones de la movilidad regular recabados de los análisis preliminares haciendo uso de Morebike y de sus visualizaciones.

4.1   Movilidad Regular y Patrones Recurrentes en Distintos Años

En el caso de los diagramas de Pareto, sin importar el año o si nos referimos a viajes entre semana o en fin de semana, son 17 o 18 colonias las que representan el 80% de los viajes mensuales, lo que equivale a poco más del 30% de todas las colonias, cercano al principio de Pareto, aunque este no se cumple en su totalidad. Además, las colonias que conforman este porcentaje suelen ser las mismas, con algunas excepciones en aquellas que delimitan a ese 80%.

De los diagramas de caja se resalta el hecho que, en la mayoría de los años y meses, el tercer horario que va de las 4 pm a las 12:30 am representa el de mayor cantidad y distribución de viajes en días entre semana, siendo este también el que tiene a las colonias con más viajes registrados históricamente, seguido del primer horario de 5 am a 12 pm y finalmente del segundo de 12 pm a 4 pm. Esto cambia drásticamente en los viajes en fin de semana, ya que en estos los 3 horarios presentan una movilidad similar entre sí, por lo que se realizan viajes de forma más dinámica a lo largo del día, a diferencia de los días entre semana que cuentan con horarios más definidos y una demanda que puede observarse más fácilmente.

Por otro lado, en las gráficas de la movilidad entre colonias es posible identificar patrones interesantes en algunas de ellas, sin embargo, es un proceso heurístico y de observación. De esta manera se puede conocer qué colonias presentan una mayor movilidad entre sí o aquellas que presentan altas cantidades de viajes en sí mismas, el hecho es que estas colonias suelen presentar los mismos patrones en los distintos años, aunque como es de esperarse, en los vividos en pandemia se observa una reducción significativa en el número de viajes registrados entre cada una de ellas.

Finalmente, es posible conocer en qué horarios la demanda de las bicicletas aumenta o disminuye en las distintas colonias gracias a las gráficas de la movilidad regular semanal. Se identifica el número de aumentos en la demanda a lo largo del día (de 1 a 3) y de esta manera se determina en qué horarios es posible que la mayoría de las bicicletas sean tomadas o, por el contrario, estén disponibles. Facilita el conocimiento de la demanda de bicicletas, pero también el de cicloestaciones, ya que para dejar una bicicleta debe existir un espacio disponible en la estación. De esta manera, un usuario puede determinar en qué lugares debe haber un mayor número de bicicletas disponibles en los horarios que comúnmente usa la bicicleta y en qué otros podrán encontrar lugares disponibles o simplemente definir otra estrategia para su transporte y hacer uso de otras cicloestaciones que se ajusten a sus necesidades.

4.2   Movilidad Regular en Años con COVID-19

Tal como sucedió con la mayoría de los transportes públicos, el uso de ECOBICI se vio extremadamente afectado por la pandemia de COVID-19, reduciendo el número de registros mensuales de un promedio de 700 mil en 2019 a 335 mil en 2020 y 350 mil en 2021 de acuerdo con el sistema SAHMI [16]. El año 2019 fue el último año con una movilidad y un crecimiento orgánicos con 8 millones 400 mil viajes registrados, sin embargo, estos fueron reducidos en un 50% con tan sólo 4 millones de registros en el año 2020 (ver Fig. 9). En 2021 y 2022 los registros se han recuperado pro-

gresivamente, sin embargo, sin la misma proporción que en años anteriores, aunque se estima que esto se modifique significativamente tras los planes de expansión a otras colonias de la ciudad y en especial, con la apertura de nuevas cicloestaciones, mismas que no se han visto en aumento desde el año 2018.
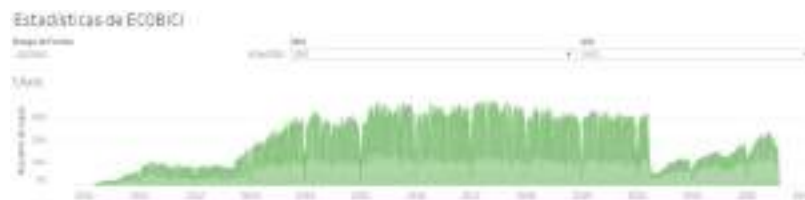

Fig. 9. Histórico de los viajes anuales registrados en ECOBICI

A pesar de la reducción considerable de los viajes, algunos patrones de movilidad se mantuvieron incluso en los años de pandemia. Tal es el caso del número de colonias que conforman el 80% de los viajes mensuales en los diagramas de Pareto, en los que, a pesar de no ser exactamente las mismas colonias en todos los años y meses, se mantuvo la proporción de aproximadamente el 30% de colonias que conforman ese 80% de los viajes en todos los meses.

Los horarios de los diagramas de caja también mantuvieron una proporción similar durante los años, siendo el horario de 4 pm a 12:30 am el que registró un mayor número de viajes, a excepción del año 2021 (ver Fig. 10). Sin embargo, en los meses de marzo, abril y mayo de 2021, los datos presentaron inconsistencias ya que cambiaron a un formato de 12 horas, omitiendo los tiempos am o pm lo que resultó en un incremento anormal en el horario de 5 am a 12 pm.
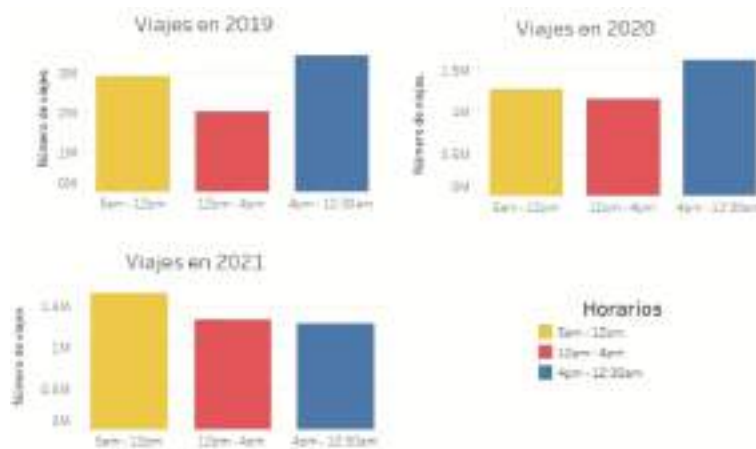

Fig. 10. Viajes registrados anualmente por horario

En la encuesta realizada en el año 2020 sobre el uso de las bicicletas [17], se reportó los horarios en que los usuarios regularmente realizan sus viajes (ver Fig. 11) en donde puede observarse que los horarios con mayor uso son de las 6 pm a 8 pm seguido del de las 6 am a 10 am, lo que reafirma también las observaciones.

Fig. 11. Horarios con mayor índice de uso de acuerdo con la encuesta del año 2020 de ECOBICI

5   Trabajo a Futuro

Morebike es una propuesta de una herramienta básica de visualización de datos que pretende seguir evolucionando según se identifiquen nuevas necesidades o se exploren los datos con diferentes aproximaciones. A continuación, se describen algunas propuestas como trabajo a futuro que representan mejoras significativas a la propuesta inicial del sistema.

Posicionamiento Geográfico. El desarrollo de visualizaciones con coordenadas geográficas sobre los viajes entre colonias que faciliten la observación de la distancia y la densidad de la movilidad en un mapa real de la ciudad.

Patrones en Tiempo Real. Hacer uso de los datos en tiempo real brindados por ECOBICI e implementar visualizaciones capaces de mostrar la movilidad al momento con el estándar GBFS (General Bikeshare Feed Specification).

Rutas Recurrentes. Identificación de los viajes más comunes entre colonias o viajes locales, es decir, aquellos viajes que se repiten constantemente a lo largo de los días, meses y años. Explorar también la posibilidad de identificar viajes recurrentes a nivel cicloestación bajo las mismas condiciones y filtros.

Modelos de Aprendizaje Máquina. Identificar la correlación con otras variables de los datos, como la edad de los usuarios, el clima o la temporada del año y con ello generar modelos de regresión que permitan predecir la demanda bajo ciertas condiciones. Con esto se podrá comenzar la exploración de los problemas de rebalanceo de bicicletas en ECOBICI y garantizar la satisfacción de sus usuarios.

6   Conclusiones

Morebike potencia la gestión y el uso del SBC de ECOBICI ya que permite tomar decisiones basadas en los datos para optimizar su funcionamiento y proporcionar información útil para el desarrollo de estrategias que incentiven a los usuarios a rentar o devolver bicicletas de acuerdo con la demanda esperada.

En la actualidad, los SBC representan cada vez más una alternativa ideal para muchas personas en su día a día, contribuyendo así a una vida mucho más saludable y un entorno sustentable, además de una reducción significativa de la contaminación y la saturación de otros medios de transporte convencionales. Es por ello por lo que, resulta tan importante generar más y mejores estrategias que permitan que estos sistemas evolucionen y atraigan a más personas.

El desarrollo de herramientas como Morebike son de gran ayuda para este propósito, además de que tienen el objetivo de informar y ayudar a los usuarios a conocer el sistema que usan para tomar más y mejores decisiones sobre sus métodos de transporte. Contar con más y diversas visualizaciones resulta en la identificación de distintos patrones de movilidad y se vuelve un proceso mucho más interactivo y enriquecedor para los usuarios finales y para los operadores de estos sistemas.

Referencias

1. Castellanos, S., De la Lanza, I., Lleras, N.: Guía para la Estructuración de Sistemas de Bicicletas Compartidas. Mecanismos y Redes de Transferencia de Tecnologías de Cambio Climático en Latinoamérica y el Caribe (LAC), pp. 17-20. Inter-American Development Bank (2019).
2. ECOBICI, What is ECOBICI? https://ecobici.cdmx.gob.mx/en/overview/, last accessed 2022/08/21.
3. ECOBICI, Statistics, https://ecobici.cdmx.gob.mx/en/statistics/, last accessed 2022/08/21.
4. ECOBICI, Open Data, https://ecobici.cdmx.gob.mx/en/open-data/, last accessed 2022/08/21.
5. Shui, C., Szeto, W.: A review of bicycle-sharing service planning problems. Transp. Res. Part C Emerg. Technol. 117, pp. 1–3 (2020).
6. Boufidis, N., Nikiforiadis, A., Chrysostomou, K., Aifadopoulou, G.: Development of a station-level demand prediction and visualization tool to support bike-sharing systems' operators. In: Codina, E., Soriguera, F. (eds.) EURO Working Group on Transportation Meeting, EWGT 2019, vol. 47. Elsevier (2020).
7. Gorgul, E., Chen, C.: A Visualization Based Analysis to Assist Rebalancing Issues Related to Last Mile Problem for Bike Sharing Programs in China: A Big-Data Case Study on Mobike. In: Yuan, P., Xie, Y., Yao, J., Yan, C. (eds) Proceedings of the 2019 DigitalFUTURES, pp. 145–153. CDRF 2019. Springer, Singapore (2019).
8. Gómez, H., López, R., Ramirez-Nafarrate, A.: A simulation-optimization study of the inventory of a bike-sharing system: the case of Mexico City Ecobici's system. Case Stud. Transp. Policy 9, pp. 1059–1072 (2021).
9. Zi, W., Xiong, W., Chen, H., Chen, L.: TAGCN: Station-level demand prediction for bike-sharing system via a temporal attention graph convolution network. Information Sciences 561, pp. 274-285 (2021).

10. The Meddin Bike-sharing World Map: Mexico City, https://bikesharingworldmap.com/#/mexicocity/, last accessed 2022/08/21.
11. Bike Share Map: Mexico City. https://bikesharemap.com/mexicocity/#/13.220450784310541/-99.204/19.4008/, last accessed 2022/08/21.
12. Sistema de Análisis Histórico de Movilidad Individual (SAHMI) Homepage, https://sites.google.com/view/sahmi/inicio, last accessed 2022/08/21.
13. PLANBIKE Homepage, http://148.204.66.79/neoecobiciweb, last accessed 2022/08/21.
14. Tableau, Why choose Tableau? https://www.tableau.com/why-tableau, last accessed 2022/06/14.
15. Tanabe, K.: Pareto's 80/20 rule and the Gaussian distribution. Phys. A: Stat. Mech. Appl. 510, pp. 635–640 (2018).
16. SAHMI, Histórico, https://sites.google.com/view/sahmi/inicio, last accessed 2022/08/22.
17. Encuesta ECOBICI 2020. https://ecobici.cdmx.gob.mx/wp-content/uploads/2022/07/encuesta_2020_rv4_2.pdf, last accessed 2022/08/23.
18. G. Martínez et al.: Visualization of the Regular Mobility of Trips Between Bike Stations in the ECOBICI System. In: M., Mata, R., Zagal, C., Barria (eds.) Telematics and Computing 11th International Congress, WITCOM 2022, Cancun, Mexico, November 7–11, 2022, Proceedings, CCIS, vol. 1659, pp. 1–24. Springer, Cham (2022).

Dispositivo IoT para monitorizar aerogeneradores Vortex

E. González-González [1][0000-0002-8025-2464], S. Lagüela[1][0000-0002-9427-3864], M. Sánchez-Aparicio[1][0000-0002-7931-9561], P. Andrés-Anaya[1][0000-0001-7708-3260], J. Martín-Jiménez[1][0000-0003-4383-9386] and S. Del Pozo[1][0000-0003-4869-3742]

[1] Universidad de Salamanca, Ávila 05003, Spain
egonzalezgonzalez@usal.es

Resumen. Un pilar esencial para el desarrollo de las ciudades inteligentes es la conectividad de dispositivos capaces de enviar y recibir datos que permitan tener la información necesaria en tiempo real. La tecnología que se emplea en dichos dispositivos depende del uso que se le dé a la red de comunicación, es decir, de la cantidad de datos que transfiera, del rango de cobertura que ofrezca, y del consumo de energía que tenga, entre otros. En el campo de las energías renovables, los sistemas que monitorizan el funcionamiento de las diferentes fuentes generadoras de energía están en pleno auge. En el presente trabajo se propone el desarrollo de un *data logger* autónomo con conectividad *LoRaWAN* para monitorizar y analizar el funcionamiento de aerogeneradores sin palas en tiempo real. Las pruebas realizadas demuestran el gran potencial de este tipo de redes en aplicaciones de registro de datos de ciudades, gracias a su largo alcance y bajo consumo.

Keywords: IoT-Devices, LoRaWAN, Smart-cities, Wind-Energy, Bladeless Wind Turbine, Vortex-Bladeless

1   Introducción

Con la aparición de nuevas tecnologías de comunicación se han desarrollado multitud de dispositivos conectados a internet (IoT, del inglés *internet of things*) capaces de enviar y transmitir información en tiempo real. Esto ha permitido el desarrollo de aplicaciones inteligentes y, con ello, la aparición del concepto de ciudades inteligentes [1].

El prototipo de IoT está definido por la conectividad entre diferentes dispositivos capaces de interactuar unos con otros y de realizar acciones autónomas [2] a través de una red global.

La existencia de gran variedad de sensores IoT permite que estos puedan ser empleados para monitorizar distintas actividades y lugares: supervisión de ciclistas, flujo de vehículos, aparcamientos públicos, o calidad del aire [3], entre otros. Dichos proyectos se basan en un control y análisis de datos recogidos por distintos sensores en tiempo real, por lo que es necesario contar con una red de conexión que permita transmitir dichos datos en todo momento. En función de la cantidad de datos, la frecuencia

de envío y la autonomía del dispositivo de medición (en caso de alimentación por baterías), será más o menos conveniente el empleo de un tipo de tecnología de comunicación u otra.

1.1 Aerogeneradores sin palas

En el contexto de la transición energética, la monitorización tanto de los elementos de generación como de los puntos de consumo se establecen como una aplicación de interés creciente para los sensores IoT. En el caso de la primera aplicación, los sensores IoT facilitan el control de la energía generada por diferentes tecnologías de explotación de recursos energéticos renovables, permitiendo por tanto su ajuste para optimizar la producción [4].

De entre las tecnologías emergentes para maximizar el aprovechamiento energético renovable, los nuevos diseños de aerogeneradores aparecen como un avance para la integrabilidad de la explotación del viento para generación de electricidad, favoreciendo el uso de dicho recurso energético para aplicaciones de autoconsumo, y por tanto democratizando su utilización de las grandes plantas generadoras a los usuarios finales. Considerando los puntos más desfavorables de los aerogeneradores convencionales, el diseño de aerogeneradores sin palas reduce la influencia en la fauna avícola, los efectos de interferencia en las bandas electromagnéticas de comunicación, mientras que el impacto visual y acústico es prácticamente nulo. Un ejemplo de este tipo de dispositivos es el modelo "Vortex Nano" de la empresa Vortex Bladeless [5]. Por su menor tamaño en comparación con los aerogeneradores convencionales, que permite su instalación en cubiertas de edificios o en jardines de viviendas, y por su mantenimiento (prácticamente nulo), estos modelos pueden equipararse a los paneles fotovoltaicos [6]. Además de ser tecnologías de aprovechamiento de recurso energético de características similares, la propuesta de hibridación de ambas (eólica sin palas y solar fotovoltaica) surge como una opción óptima para maximizar la disponibilidad de energía, compensando los aerogeneradores la falta de producción de los paneles fotovoltaicos durante periodos nocturnos o meses de menor radiación solar.

El funcionamiento de estos aerogeneradores se basa en el fenómeno conocido como vibración inducida por vórtices (VIV), recogiendo la energía producida en la parte superior de los mismos (que oscila) gracias a su diseño circular. Esta energía se transforma en electricidad gracias a un alternador alojado en su parte central.

Este trabajo presenta el desarrollo de un dispositivo para monitorizar aerogeneradores sin aspas de mayores dimensiones (modelo "Vortex Atlantis" de 7-10 m de altura), ubicados en zonas periféricas y próximas a entornos urbanos o puntos de consumo. Por lo tanto, la necesidad de comunicación de largo alcance (5-10 Km) hace necesario el empleo de una red *Low Power Wide Area Network* (LPWAN) con alimentación independiente y autónoma que permita minimizar los costes asociados al despliegue de infraestructuras de red o de energía. La Fig. 1 muestra diferentes tamaños y modelos de aerogeneradores sin palas.
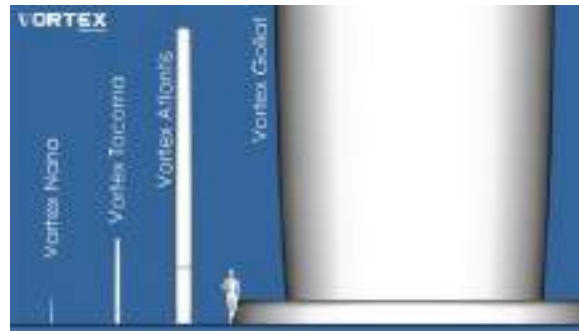
Fig. 1. Modelos de aerogeneradores desarrollados por la empresa Vortex Bladeless [7].

2   Necesidades y planteamiento

La monitorización del funcionamiento de aerogeneradores sin palas se planteó para un caso piloto con el modelo "Vortex Atlantis" de Vortex Bladeless. El sensor fue ubicado en el interior de la base del aerogenerador (Fig. 2), escogiendo una red LPWAN para la transmisión de datos. Este tipo de red se caracteriza por ser de bajo consumo y largo alcance. Concretamente, se seleccionó la tecnología *Long Range* (LoRa) y el protocolo de comunicación *Long Range Wide Area Network* (LoRaWAN) a través de la plataforma *The Things Network* (TTN) [8] configurada como servidor y aplicación de red. Los datos fueron enviados a una base de datos para su registro y posterior visualización y análisis telemáticos.

Fig. 2. Ubicación del dispositivo para la monitorización de datos de un aerogenerador sin palas.

2.1 Estado del arte

El avance de las tecnologías de comunicación y la aparición de nuevos sensores inter-conectados, han impulsado el desarrollo de las redes de sensores inalámbricas WSNs (del inglés *Wireless Sensor Networks*). El uso de WSNs tiene infinidad de aplicaciones en diferentes sectores como el industrial [9], el de las ciudades inteligentes [10], el transporte [11], el del ámbito sanitario [12], el de la agricultura [13] o el del control medioambiental [14].

El elevado coste que tienen los dispositivos convencionales condiciona la adopción de este tipo de soluciones por parte de los diferentes sectores productivos. Como resultado, han aparecido soluciones de bajo coste que permiten abaratar costes y elevar el grado de adaptación de este tipo de sensores a diferentes casos de uso [15].

La mejora tecnológica ofrecida por los sensores de bajo coste permite realizar una ins-trumentación más escalable y manejable, además de mejorar en aspectos como la adap-tación a entornos y aplicaciones específicas reduciendo costes de componentes innece-sarios [16].

Las redes LPWAN se caracterizan por alcanzar grandes distancias de comunicación con un bajo consumo de energía y una velocidad de trasferencia de datos baja. Por lo tanto, no es una tecnología pensada para transmitir señales de audio o vídeo, pero sí es ideal para dar conectividad a dispositivos en lugares remotos alimentados por baterías y con transmisiones de bajo volumen de datos [17].

LoRa es una tecnología de radio inalámbrica que permite la comunicación de un punto a otro alcanzando distancias kilométricas (en torno a 10-15 km en entornos rurales).

Las redes LoRaWAN son un tipo de redes LPWAN que utilizan la tecnología de co-municación LoRa. El protocolo de comunicación LoRaWAN especifica los parámetros requeridos en la arquitectura de red para gestionar el acceso y control de dispositivos dentro de la red, empleando para ello la tecnología de comunicación LoRa, que habilita la comunicación de largo alcance [18]. La Fig. 3 muestra la infraestructura de este tipo de redes.
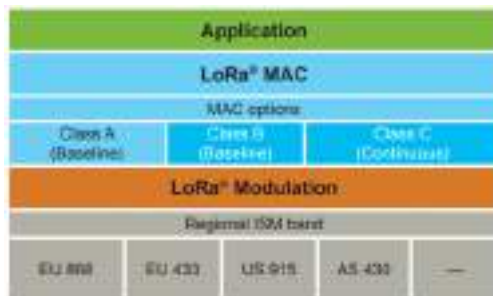

Fig. 3. Infraestructura de LoRaWAN [18].

Si bien es cierto que ya existen soluciones comerciales de dispositivos con conectividad LoRaWAN, estos dispositivos están diseñados para realizar registros con una cadencia

de tiempo grande para reducir el consumo y preservar la autonomía de las baterías. Por ello, se descartó hacer uso de este tipo de soluciones comerciales y desarrollar una propia que cumpliera con los requisitos que se precisan para monitorizar en tiempo real el funcionamiento de aerogeneradores sin palas. El dispositivo de medición diseñado, aparte de ofrecer la transferencia de datos en tiempo real, garantiza la alimentación al contar con un pequeño panel fotovoltaico como fuente de alimentación alternativa a la batería (finita). Además, cabe destacar que la apuesta por un diseño propio permite integrar los componentes periféricos y los sensores a medida de las necesidades o variables que se pretendan medir, reduciendo así los costes en componentes periféricos y otros requeridos en caso de haber hecho uso de una solución comercial.

2.2   Características del dispositivo

El dispositivo ha de cumplir dos principios básicos de diseño: autonomía energética y conectividad de largo alcance.

Para lograr autonomía energética, este dispositivo se alimenta de una batería que se recarga a través de paneles solares fotovoltaicos. Además, para prolongar la autonomía del dispositivo se redujo su consumo en la medida de lo posible reduciendo la cantidad de datos transmitidos. Esta solución fue adoptada para garantizar que la energía generada por los paneles fotovoltaicos fuera suficiente para recargar la batería, y que la capacidad de la batería fuera suficiente para alimentar el dispositivo ante periodos nocturnos, de días nublados o días lluviosos.

Las medidas realizadas con el dispositivo fueron: producción de energía, aceleraciones y geolocalización del dispositivo. Concretamente, el diseño supone la hibridación de los siguientes componentes:

- Microcontrolador Adafruit Feather M0 con señal RFM95 de LoRa [19].
- Módulo GPS Adafruit Ultimate GPS FeatherWing MTK3339 [20].
- Acelerómetro de 3 ejes ADXL343 [21].
- Batería LiPo 6000mAh / 3.7V [22].
- Cargador de batería solar para baterías LiPo de 3.7V [23].
- Placa solar de 5V y 500mAh [24].

2.3   Configuración de la red de comunicación

Red de largo alcance y bajo consumo - Low Power Wide Area Network (LPWAN)
Las redes LPWAN se caracterizan por alcanzar grandes distancias de comunicación con un bajo consumo de energía y una velocidad de trasferencia de datos baja. Por lo tanto, no es una tecnología pensada para transmitir señales de audio o vídeo, pero sí es ideal para dar conectividad a dispositivos en lugares remotos, alimentados por batería y con transmisiones de bajo volumen de datos. [25]

Este tipo de redes se configuran con una topología en estrella, donde un gateway recibe mensajes de los diferentes dispositivos o nodos. Las tasas de transferencia van de 10 Kbps hasta 100 Kbps, las tramas de datos transmitidas son de decenas de bytes y

el ciclo de envío está limitado para no saturar las bandas de frecuencia ISM (del inglés Industrial, Scientific and Medical) que usan este tipo de redes. Este rango de frecuencias ISM sin licencia se destinan a uso industrial, científico y médico y tienen una legislación dependiente de cada territorio. El uso de estas bandas de frecuencia y la potencia de transmisión dentro de ellas están reguladas por las legislaciones de radiofrecuencias correspondientes, y varían en función del territorio. [26]

Tecnología LoRa (Long Range).

LoRa es una tecnología de comunicación que utiliza una modulación de amplio espectro. Esto le permite tolerar ruido, múltiples caminos de señal y el efecto Doppler, manteniendo un muy bajo el consumo de energía. Como aspecto negativo, el ancho de banda es muy bajo comparado con otras tecnologías.
Las frecuencias de trabajo de LoRa emplean las bandas de radio ISM, que están por debajo de 1GHz y dependen de la legislación del territorio correspondiente [27], por ejemplo 433 MHz, 868 MHz, o 915 MHz.

The Thing Network - TTN.

Dentro de las redes LoRaWAN los nodos no están asociados con una puerta de enlace determinada, sino que los nodos emiten los datos y son las puertas de enlace las encargadas de transmitir los paquetes recibidos hasta el servidor de red.

La inteligencia y la administración de la red recaen en el servidor de red, que administra y filtra paquetes redundantes, comprueba la seguridad, y realiza ajustes en la transmisión de datos (ADR – del inglés Adaptative Data Rate) entre otros.

Por lo tanto, el servidor de red es uno de los pilares básicos dentro de la configuración de la comunicación del dispositivo de registro de mediciones o *data logger* a desarrollar.

Existen diferentes opciones a la hora de elegir un servidor de red, pudiendo ser de gestión propia o externa, y dentro de las gestiones externas, públicos o privados. La gestión propia del servidor de red supondría aumentar la complejidad del desarrollo del proyecto debido a la configuración del mismo, por lo que se optó por una gestión de terceros. Dentro de esta opción, se escogió el servidor público de redes de las cosas (TTN, del inglés *The Thing Networks*) debido a las ventajas que supone el empleo de su infraestructura de red ya existente de manera gratuita [8]. La Fig. 4 muestra el despliegue actual de la red TTN.

Fig. 4. Despliegue actual de la red TTN [28].

TTN es una iniciativa para establecer una red mundial de IoT-LPWAN, de código abierto, donde se permite construir e integrar una red de datos de IoT descentralizada, operada y mantenida por los propios usuarios. Las puertas de enlace TTN son de uso público, con lo cual se opta por aprovechar esta infraestructura ya existente y, dado el caso, colaborar en el despliegue de la red aumentando la cobertura de la misma e impulsando el uso de dispositivos IoT en una zona determinada [28].

Dentro de TTN también está la aplicación de red que gestiona los datos desde el nodo hasta la aplicación final del usuario y permite realizar integraciones con servicios. Dichos datos tienen una doble encriptación (AES-128), una de servidor y otra de aplicación, puesto que los datos son privados y sólo el usuario final tiene acceso a ellos [29]. La Fig. 5 se muestra los cifrados de la red a modo de esquema.
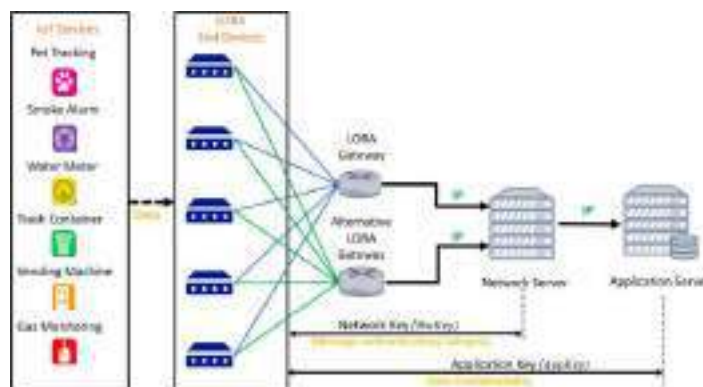
Fig. 5. Seguridad en las redes LoRaWAN [29].

3   Desarrollo y configuraciones

El *data logger*, tiene como objetivo principal analizar el comportamiento de los aerogeneradores que generan energía por la VIV. Por ello, además de monitorizar la energía producida, se analizaron las aceleraciones producidas en las oscilaciones del eje del aerogenerador.

La frecuencia de envío de datos se configuró respetando el uso de la red que establece TTN [30]. Las mediciones del estado del aerogenerador se establecieron cada 10 segundos, registrando el valor medio de producción energética durante este periodo y los valores de aceleración del mástil para analizar su actividad y los tiempos de reacción del aerogenerador. Adicionalmente, se envió la geolocalización del dispositivo, con la intención de evitar posibles robos de los equipos.

Otro pilar del diseño fue la autonomía del dispositivo. Por ello, se optó por una alimentación con baterías con capacidad para recargarse con la energía generada por paneles fotovoltaicos.

La autonomía del dispositivo se evaluó una vez desarrollado y con medidas de consumo reales ya que, en función de las potencias de transmisión (distancia al *gateway*), el consumo y el tiempo de envío varían significativamente.

3.1   Transmisión y registro de datos

Una vez que los datos se han transmitido a través de la red LoRaWAN, el servidor de red gestiona los paquetes de datos hasta las aplicaciones correspondientes, donde los datos son decodificados y recibidos por el usuario. Dentro de la consola de configuración de TTN se pueden configurar integraciones para transmitir los datos recibidos en otras aplicaciones, a modo de base de datos. En el caso que se plantea, se hizo uso de los siguientes softwares *open source*: NodeRed [31] para realizar una conexión a través del protocolo Mqtt [32] y transmitir los datos desde TTN a una base de datos Influxdb

[33]. Una vez registrados los datos en la base de datos, estos se visualizan a través de la plataforma Grafana [34].

La Fig. 6 muestra el flujo de datos seguido de forma general y la Fig. 7 la configuración del flujo de datos dentro del programa NodeRed.

Fig. 6. Esquema general de transmisión y registro de datos.

Fig. 7. Configuración de flujo en Node Red.

3.2   Pruebas de comunicación

Debido a que el propósito del uso de una red LoRaWAN es alcanzar grandes distancias de comunicación, se realizaron pruebas de cobertura a través de la plataforma TTN Maper [28], integrada dentro de TTN, para geolocalizar las señales recibidas por los diferentes *gateways* de la red y analizar la calidad de los paquetes de datos recibidos. Adicionalmente, dicha plataforma permite dejar registro de estos datos para que se puedan comprobar las zonas que ya cuentan con cobertura de la red TTN y la calidad de la misma. Tras comprobar dichas zonas, se estableció la zona de pruebas en la ciudad de Ávila (España) y más concretamente en la zona del Valle Amblés, por tratarse de un caso de uso de la red TTN favorable, pues su orografía permite la transmisión de datos en línea de visión directa (VLOS, del inglés Visual Line of Sight) prácticamente para toda su extensión (Fig. 8), condición necesaria para alcanzar grandes distancias de comunicación (10-15Km.)
.

Fig. 8. Perfil orográfico de la zona de pruebas ubicada en el Valle Amblés (Ávila, España) [33].

Además, esta zona contaba con una infraestructura de la red TTN (5 gateways) y bastó con emitir mensajes desde el dispositivo para comprobar la calidad de la señal recibida a través de los diferentes gateways. La Fig. 9 muestra las diferentes señales recibidas en la zona de pruebas.

Fig. 9. Cobertura de Red TTN en la ciudad de Ávila y el Valle Amblés [26].

3.3   Pruebas de autonomía

Con el objetivo de verificar el funcionamiento del dispositivo, la capacidad de recarga, y el consumo del mismo, se realizó una prueba de laboratorio disponiendo un panel solar [24] en posición horizontal en el poyete de una ventana orientada al este. Esta ubicación fue seleccionada de manera aleatoria, para testear la capacidad de generación del panel en cualquier condición posible, fuera de las condiciones más favorables (como sería la orientación sur, para el hemisferio norte) y así obtener resultados de autonomía más ajustados al uso del sistema por un usuario real. El panel fotovoltaico recibió radiación solar desde las 8:30h hasta las 13:00h durante dos días consecutivos en los que las condiciones meteorológicas fueron favorables (sin nubosidad). La Fig. 10 muestra la disposición del dispositivo próximo a la ventana donde se realizaron las pruebas.
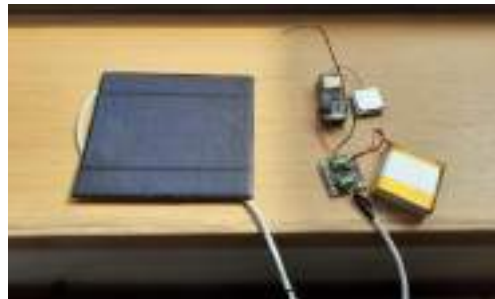

Fig. 10. Pruebas de laboratorio para analizar la autonomía del dispositivo de recogida y envío de datos.

4   Resultados

4.1   Resultados de comunicación

Se comprobó la recepción de datos en la zona de estudio establecida, cubriendo distancias de 17 Km en términos de máxima comprobada, considerándose suficiente. La Fig. 11 muestra el nivel de señal recibido por cada *gateway* durante las pruebas de cobertura.
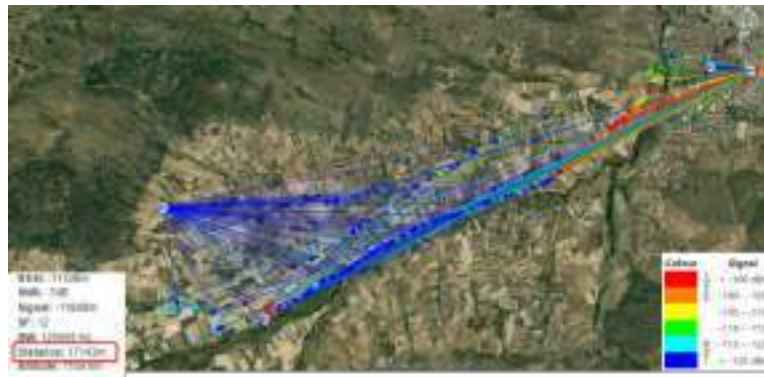
Fig. 11. Pruebas de cobertura del dispositivo desarrollado.

4.2   Resultados de consumo

Los datos de consumo energético y de autonomía se extrajeron de las pruebas efectuadas en el laboratorio durante dos días de funcionamiento continuo.

Como se ha mencionado, el dispositivo se ubicó en ventana con orientación este con incidencia solar directa sobre el panel fotovoltaico de 8:30h a 13:00h. Con esta energía solar disponible, el dispositivo fue capaz de recargar la batería para el resto del día, compensando la energía necesaria durante las horas sin radiación solar.

El gráfico de la Fig.12, creado a través de la aplicación de Grafana [32], muestra los niveles de tensión de la batería registrados en un intervalo de tiempo de dos días. Las pendientes ascendentes muestran la recarga de la batería cuando el sol incide de forma directa sobre el panel fotovoltaico, y las pendientes descendentes, relativas al consumo de la batería, al ser menos pronunciadas permiten compensar la energía generada y consumida y por tanto se consigue el balance energético neto.
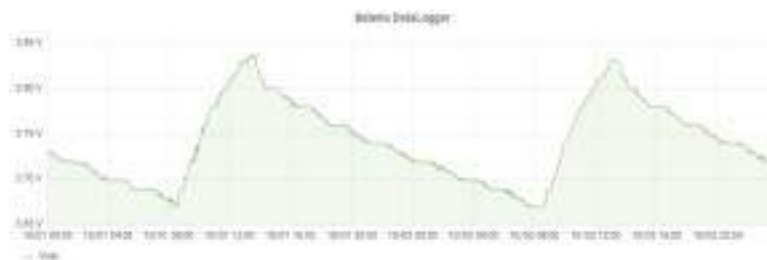

Fig. 12. Datos de recarga de la batería

5　　Conclusiones

Los resultados obtenidos tras las pruebas de cobertura y autonomía permiten pronosticar que las necesidades iniciales de diseño serán cubiertas de manera satisfactoria una vez que el dispositivo sea instalado de forma definitiva en el aerogenerador.

Los resultados de cobertura, cuya distancia de comunicación máxima a sido de 17 Km, demuestra la efectividad de las redes LoRaWAN para realizar comunicaciones a largas distancias. Aunque el alcance de cobertura de las redes depende de la orografía y de la ubicación de los *gateways* (zonas elevadas y con VLOS alcanzan mayores distancias), el uso de la red TTN permite la configuración y la integración de nuevos *gateways* para crear o reforzar la cobertura en una zona geográfica determinada.

Respecto de la autonomía del dispositivo, se ha verificado la capacidad de recarga de la batería con un panel fotovoltaico [24] a lo largo de un diferentes días soleados con inclinación horizontal y orientación este, por lo que la óptima colocación del panel (orientación sur) hará posible el aumento de horas de producción solar con respecto a las disponibles durante las pruebas de laboratorio. Así, la producción diaria de energía será mayor que el consumo, lo que permitirá dotar de mayor autonomía a la batería para compensar los días en los que la radiación solar sea menor (días nublados o con precipitaciones).

Cabe destacar que, aunque las pruebas iniciales han sido satisfactorias, hay capacidad de mejora en el consumo energético del dispositivo. Una de ellas, sería analizando las aceleraciones del aerogenerador y mediante detección de eventos (sacudidas), registrar datos de funcionamiento solo en los intervalos en los que el generador esté en movimiento, reduciendo el consumo de energía durante los periodos de inactividad.

Referencias

1. A. R. Al-Ali *et al.*, 'IoT-Based Shared Community Transportation System Using e-Bikes', in *2021 5th International Conference on Smart Grid and Smart Cities (ICSGSC)*, Jun. 2021, pp. 61–65. doi: 10.1109/ICSGSC52434.2021.9490509.
2. A. Botta, W. de Donato, V. Persico, and A. Pescapé, 'Integration of Cloud computing and Internet of Things: A survey', *Future Generation Computer Systems*, vol. 56, pp. 684–700, Mar. 2016, doi: 10.1016/j.future.2015.09.021.
3. H. Arasteh *et al.*, 'Iot-based smart cities: A survey', in *2016 IEEE 16th International Conference on Environment and Electrical Engineering (EEEIC)*, Jun. 2016, pp. 1–6. doi: 10.1109/EEEIC.2016.7555867.
4. O. Ordoñez and A. R. Duke, 'Wind Resource Assessment: Analysis of the Vortex Bladeless Characteristics in Puerto Cortés, Honduras', *IOP Conf. Ser.: Earth Environ. Sci.*, vol. 801, no. 1, p. 012019, Jun. 2021, doi: 10.1088/1755-1315/801/1/012019.
5. 'Vortex Bladeless - Energía eólica sin palas', *Vortex Bladeless Wind Power*. https://vortexbladeless.com/es/ (accessed Oct. 07, 2022).
6. 'Vortex Technical Paper - Bladeless Wind Turbines explained', *Vortex Bladeless Wind Power*, Jun. 07, 2018. https://vortexbladeless.com/download-green-paper/ (accessed Jun. 27, 2022).

7. 'Aerogeneradores sin palas, eólica 2.0. con Vortex Bladeless - Patentes y Marcas', Dec. 15, 2021. https://www.madrimasd.org/blogs/patentesymarcas/2021/aerogeneradores-sin-palas-eolica-2-0-con-vortex-bladeless/ (accessed Oct. 07, 2022).

8. T. T. Network, 'The Things Network', *The Things Network*. https://www.thethingsnetwork.org/ (accessed Sep. 27, 2022).

9. K. Tange, M. De Donno, X. Fafoutis, and N. Dragoni, 'Towards a systematic survey of industrial IoT security requirements: research method and quantitative analysis', in *Proceedings of the Workshop on Fog Computing and the IoT*, New York, NY, USA, Apr. 2019, pp. 56–63. doi: 10.1145/3313150.3313228.

10. B. Molina, C. E. Palau, G. Fortino, A. Guerrieri, and C. Savaglio, 'Empowering smart cities through interoperable Sensor Network Enablers', in *2014 IEEE International Conference on Systems, Man, and Cybernetics (SMC)*, Oct. 2014, pp. 7–12. doi: 10.1109/SMC.2014.6973876.

11. A. Hilmani, A. Maizate, and L. Hassouni, 'Automated Real-Time Intelligent Traffic Control System for Smart Cities Using Wireless Sensor Networks', *Wireless Communications and Mobile Computing*, vol. 2020, pp. 1–28, Sep. 2020, doi: 10.1155/2020/8841893.

12. M. Ilyas, 'Wireless Sensor Networks for Smart Healthcare', in *2018 1st International Conference on Computer Applications & Information Security (ICCAIS)*, Apr. 2018, pp. 1–5. doi: 10.1109/CAIS.2018.8442038.

13. Hu, X., Sun, L., Zhou, Y., & Ruan, J. (2020). Review of operational management in intelligent agriculture based on the Internet of Things. Frontiers of Engineering Management, 7(3), 309-322.

14. F. Mao, K. Khamis, S. Krause, J. Clark, and D. M. Hannah, 'Low-Cost Environmental Sensor Networks: Recent Advances and Future Directions', *Frontiers in Earth Science*, vol. 7, 2019, Accessed: Oct. 07, 2022. [Online]. Available: https://www.frontiersin.org/articles/10.3389/feart.2019.00221

15. F. Tauro *et al.*, 'Measurements and Observations in the XXI century (MOXXI): innovation and multi-disciplinarity to sense the hydrological cycle', *Hydrological Sciences Journal*, vol. 63, no. 2, pp. 169–196, Jan. 2018, doi: 10.1080/02626667.2017.1420191.

16. Chan, K., Schillereff, D. N., Baas, A. C., Chadwick, M. A., Main, B., Mulligan, M., ... & Thompson, J. (2021). Low-cost electronic sensors for environmental research: Pitfalls and opportunities. Progress in Physical Geography: Earth and Environment, 45(3), 305-338.

17. U. Raza, P. Kulkarni, and M. Sooriyabandara, 'Low Power Wide Area Networks: An Overview', *IEEE Communications Surveys & Tutorials*, vol. 19, no. 2, pp. 855–873, 2017, doi: 10.1109/COMST.2017.2652320.

18. 'Technical Overview of LoRa and LoRaWAN', p. 20, 2015.

19. A. Industries, 'Adafruit Feather M0 with RFM95 LoRa Radio - 900MHz'. https://www.adafruit.com/product/3178 (accessed Sep. 28, 2022).

20. 'Adafruit Ultimate GPS featherwing', *Adafruit Learning System*. https://learn.adafruit.com/adafruit-ultimate-gps-featherwing/overview (accessed Oct. 07, 2022).

21. 'adxl335.pdf'. Accessed: Oct. 07, 2022. [Online]. Available: https://www.sparkfun.com/datasheets/Components/SMD/adxl335.pdf

22. 'Datasheet-105050-2P-lipo-battery.pdf'. Accessed: Oct. 07, 2022. [Online]. Available: https://tienda.bricogeek.com/download/BAT-0012/Datasheet-105050-2P-lipo-battery.pdf

23. 'Solar_Charger_SKU_DFR0264-DFRobot'.   https://wiki.dfrobot.com/Solar_Charger_SKU_DFR0264 (accessed Oct. 07, 2022).

24. 'Solar Panel 2.5W 5V/500mAh Mini DIY Solar Panel Charger Kit (Solar Cell Only)', *ALLPOWERS*. https://iallpowers.com/products/diy-solar-panel-charger-kit (accessed Oct. 07, 2022).

25. U. Raza, P. Kulkarni, and M. Sooriyabandara, 'Low Power Wide Area Networks: An Overview', *IEEE Communications Surveys & Tutorials*, vol. 19, no. 2, pp. 855–873, 2017, doi: 10.1109/COMST.2017.2652320.

26. J. Sanchez-Gomez, J. Gallego-Madrid, R. Sanchez-Iborra, J. Santa, and A. Skarmeta, 'Impact of SCHC Compression and Fragmentation in LPWAN: A Case Study with LoRaWAN', *Sensors*, vol. 20, p. 280, Jan. 2020, doi: 10.3390/s20010280.

27. Yegin, A., Kramp, T., Dufour, P., Gupta, R., Soss, R., Hersent, O., ... & Sornin, N. (2020). LoRaWAN protocol: specifications, security, and capabilities. In LPWAN Technologies for iot and m2m applications (pp. 37-63). Academic Press.

28. 'TTN Coverage'. https://ttnmapper.org/heatmap/ (accessed Sep. 27, 2022).

29. H. Noura, T. Hatoum, O. Salman, J.-P. Yaacoub, and A. Chehab, 'LoRaWAN security survey: Issues, threats and possible mitigation techniques', *Internet of Things*, vol. 12, p. 100303, Dec. 2020, doi: 10.1016/j.iot.2020.100303.

30. 'Duty Cycle', *The Things Network*. https://www.thethingsnetwork.org/docs/lorawan/duty-cycle/ (accessed Oct. 04, 2022).

31. 'Node-RED'. https://nodered.org/ (accessed Oct. 04, 2022).

32. 'MQTT Version 3.1.1'. http://docs.oasis-open.org/mqtt/mqtt/v3.1.1/errata01/os/mqtt-v3.1.1-errata01-os-complete.html (accessed Oct. 04, 2022).

33. 'InfluxDB: Open Source Time Series Database', *InfluxData*. https://www.influxdata.com/ (accessed Oct. 04, 2022).

34. 'Grafana: The open observability platform | Grafana Labs'. https://grafana.com/ (accessed Oct. 04, 2022).

35. 'Google Earth'. https://earth.google.com (accessed Nov. 03, 2022).

Cyber-Physical System through Internet of the Things for the Monitoring of Meteorological Conditions

José-Isidro Hernández-Vega [1][0000-0002-2634-8828], Jonam-Leonel Sánchez-Cuevas[2][0000-0000-0000-0000] , Luis-Alejandro Reynoso-Guajardo[3][0000-0000-0000-0000] , Elda Reyes-Varela[4][0000-0000-0000-0000] , Lesly-Yamilett Treviño-Reyna[5][0000-0000-0000-0000] María-Ernestina Macías-Arias[6][0000-0000-0000-0000] ,

[1,3,4,5,6] Tecnológico Nacional de México/I.T. Nuevo León, Av. Eloy Cavazos No. 2001, Colonia Tolteca, Z.C. 67170, Cd. Guadalupe, Nuevo León, México
```
jose.hv@nuevoleon.tecnm.mx
luis.rg@nuevoleon.tecnm.mx
elda.rv@nuevoleon.tecnm.mx
lesly.tr@nuevoleon.tecnm.mx
ernestina.ma@nuevoleon.tecnm.mx
```

[2] Tecnológico Nacional de México/I.T. Saltillo, Av. Venustiano Carranza No. 2400, Colonia Tecnológico, Z.C. 25280, Saltillo, Coahuila, México
```
jonam.sc@saltillo.tecnm.mx
```

Abstract. The implementation of a cyber-physical system is presented through a network of sensors that monitor meteorological variables such as wind direction and speed, temperature, humidity, atmospheric pressure, rainfall, making use of the Internet of Things (IoT) through real-time measurements. The variation of the climatic conditions in the same region are changing due to the pollutants that are emitted to the environment, the climate can vary in metropolitan areas depending on the intensity of pollutants causing microclimates, that is, particular climatic conditions as a result of a modification of the climate due to ecological and environmental factors. The objective of the cyber-physical system is to monitor the meteorological variables in real time, flexible to be adapted in different areas and whose information is sent using the IoT, making a proposal on the subject of smart cities. The proposal is based on the steps of an iterative methodology for the design of a Cyber-Physical System (CPS). The results achieved so far is the development of the CPS in its experimental phase with the acquisition of environmental data using different kinds of sensors, sending the measurements to the IoT cloud, presenting results in a friendly graphical user interface and obtaining graphics of significant information on the behavior of the variables. The information represented in the graphs of the user interface shows the behavior of the meteorological variables in different zones, visualizing the variation of the climate due to environmental conditions.

Keywords: Internet of things, meteorological variables, cyber-physical systems, smart cities, microclimates, environmental pollution, sensors.

1   Introduction

Climate change is a global problem that is threatening the environment and humanity. One of the main causes of this climate change is global warming which we identify as the increase in the temperature of the planet caused by emissions into the atmosphere of greenhouse gases, gases derived from human activity cause variations in climate that would not occur naturally. The gases deteriorate the particles of the ozone layer of the plane-ta, this layer is responsible for protecting us from solar radiation.

The greenhouse effect is a natural process that allows the Earth to maintain the conditions necessary to harbor life. The atmosphere retains some of the heat of the Sun, without the greenhouse effect, the average temperature of the planet would be 18 ° C below zero, the current average is 15 ° C.

The greenhouse effect is produced by the action of several components of the planetary atmosphere: carbon dioxide, methane, water vapor, nitrogene oxide and ozone are some of them. The problem occurs when human activities increase the emission of greenhouse gases into the atmosphere and the atmosphere retains more heat than necessary, causing the average temperature of the plane-ta to increase and global warming to occur.

The global temperature increase has consequences that endanger the survival of the Earth's flora and fauna, including human beings. Among the impacts of climate change, the melting of the ice mass at the poles, which in turn causes the rise in sea level, which produces flooding and threatens the coastal coasts, even small island states are at risk of disappearing.

Climate change also increases the occurrence of more violent weather events, droughts, fires, the death of animal and plant species, the overflowing of rivers and lakes, the destruction of livelihoods and economic resources, especially in developing countries.

Another consequence is climate changes in regions, the so called microclimates are identified as a set of atmospheric patterns and processes that characterize a reduced environment and is influenced by ecological and environmental factors. A microclimate is not a specific size, but can vary from a few square meters to several hundred kilometers. Microclimates can be found in different parts of the world and there are two main parameters to define them within a given area: temperature and humidity.

There are microclimates in urban areas where the material of the buildings, such as concrete, absorbs heat, creating cold zones. On the other hand, the elevations of a region play a key role in the formation of microclimates.

Microclimates are also being affected by human activity due to the emission of pollutants, in urban areas there can be a temperature variation of 2-3 °C [1]. Strategies are sought for spaces in urban areas in order to improve the quality of current cities [2], research oriented to the effects of microclimates caused by environmental pollution is of great importance at present [3], finding solutions to solve these problems is the subject of this article.

The monitoring of meteorological variations in the same region is not currently being monitored in a timely manner, there are meteorological stations distributed by zones in large cities, but there are no portable monitoring stations that send information in real time to various sectors of society, monitoring of meteorological varia-

bles such as wind direction and speed, temperature, humidity, atmospheric pressure, rainfall in a specific area is a point of analysis of the effects of environmental pollution in specific areas.

The implementation of a cyber-physical system by means of a sensor network that monitors meteorological variables using the Internet of Things (IoT) by means of real time measurements, would establish the weather conditions of those areas. The system must be flexible as it can be adapted to different areas and the information would be sent to society using the IoT, making a proposal to the topic of intelligent cities in the approach of monitoring weather conditions and environmental pollution.

The article is organized as follows. First, in Section 2, we present the main concepts used in the project framework, in order to give a conceptual framework to the reader of the taxonomy used in the article. Secondly, in Section 3, we present the results of the main research works found in the context of portable weather stations. Thirdly, in Section 4, we present the approach to the problem and our model of solution of the cyber-physical system proposed by the authors using IOT technology. Fourthly, the integration model of the weather monitoring station is presented in Section 5. Fifth, the methodology used for the project is presented in Section 6. Sixth, Section 7 presents the main results achieved by the project to date, Section 8 presents the conclusions, and Section 9 presents future work to be developed.

2   Concepts

In order to know the taxonomy of the concepts used in this article, this section presents the main concepts involved. The industry 4.0 is impacting in the diverse activities of the human being. The IoT is part of these emerging technologies, the IoT combined with cyber-physical systems contribute to the development of techno-logical applications for Smart Cities.

2.1   Cyber-physical system.

A Cyber-Physical System, or CPS, is a system that integrates computing with the physical processes to form an Internet of Things, Data and Services, enabling agreater efficiency and intelligence in the system or environment where it is incorporated (transport, manufacturing, health, energy,city, home, etc.: Smart Everything Everywhere) [4].

The objective of the CPS is to improve the quality of life of citizens by monitoring and controlling the physical world in which they live using the capabilities of the cyber world. The CPS are systems that are used to monitor and control physical processes. They are perceived as the new generation of integrated control systems, so that CPSs are networked integrated systems [5]. The integration of the CPS are the result of the advances in information and communication technologies (ICT) in improving the interactions with physical processes, the aim is to integrate the cybernetic and physical worlds.

The components of a CPS are: communication, computation and control, monitoring and manipulation. The communication could be wireless or wired and could connect CPS with higher level systems, such as control centers, also the communication

could be with lower level components in the physical world. The computer and control part is where intelligence is integrated, control commands are received and detected measurements are received. The mo-monitoring and manipulation components connect CPS to the physical world through sensors to mo-monitor physical components and actuators to manipulate them [5]. The applications of CPS are varied, including: highly reliable medical devices, assisted systems, advanced traffic control systems, process control, energy conservation, environmental control, aeronautics, instrumentation, critical infrastructure control (electricity, water resources and communications systems), distributed robotics (telepresence, telemedicine), defense systems, manufacturing, intelligent structures [6].

Within the areas of research and challenges of CPS we can mention the following: the computer systems are procedural systems, sequential. However, the physical processes are concurrent and parallel, composed of multiple sub-processes with hardly sequential interrelationships. Designing robust and reliable cyber-physical systems, where there is a close interrelationship of the computational aspects of embedded systems with the physical processes that govern them requires a simultaneous mastery of both disciplines, development of embedded systems and development of general purpose applications. The integration of both aspects is a challenge: integration of procedural dynamics with concurrent dynamics, management of critical processes where response time is of utmost importance.

Among other challenges for CPS development, we mention: CPS engineering through new methods and tools to simplify its design, simulation, development, validation and verification. Data analysis for prediction and prescription based on mined data. Cybersecurity of PSCs in both internal and external environments. The robustness for the creation of dependencies in processes, multiplication of points of error, complexity. Training of professionals capable of addressing the solutions, integrated into collaborative and multidisciplinary teams, the legislation affecting the implementation of CPS and changes in societies (generational, behavioral, consumer).

2.2   Internet of Things (IoT)

The Internet of Things describes the network of physical objects (things) that carry integrated sensors, software and other technologies in order to connect and exchange data with other devices and systems through the Internet [7]. These devices range from everyday household objects to sophisticated industrial tools.

To be more specific, the term IoT refers to physical device systems that receive and transfer data through wireless networks without human intervention. What makes it possible is the integration of simple computer devices with sensors in all types of objects.

The technologies that make the Iot possible are: low-cost sensors, connectivity through a set of network protocols for the Internet has made it easy to connect sensors to the cloud and other things for efficient data transmission [8]. Cloud Computing Platforms, which allows both businesses and consumers to access the infrastructure they need to expand ca-pacity without having to manage it all. Machine Learning and Analytics, with access to huge amounts of data of a wide variety stored in the cloud, companies can gather information faster and more easily. Artificial Intelligence (AI) has brought natural language processing (NLP) to home IoT devices.

The future of the Internet will consist of heterogeneously connected devices that will further expand the boundaries of the world with physical entities and virtual components. The Internet of Things (IoT) will empower connected things with new capabilities [9].

2.3   Weather monitoring stations

A weather station is a device that takes data from different atmospheric variables of interest for meteorology, they are installed in any terrain and part of the world. An automatic weather station (AMS) is defined as a weather station where observations are made and transmitted automatically [10].

In an AMS, measurements made with instruments are read or received by a central data acquisition unit. Data obtained from the autonomous measuring devices can be processed locally at the AMS or elsewhere, for example, at the central processor of a network of weather stations. Automatic weather stations can be designed as an integrated concept of various measuring devices in combination with data acquisition and processing units. Such a combined system of instruments, interfaces and processing and transmission units is usually called an automated weather observation system or an automated surface observation system [10].

The main utility of a weather station is to collect and record meteorological data, with these data is created valuable information that can have the following features: Knowing exactly the weather conditions in that place, comparing that information with other weather stations in nearby locations, providing information for making weather forecasts from numerical models, creating climate information representative of the place where the data are taken, creating specific alerts for weather phenomena that could be of interest, correlating weather phenomena with risk situations, accidents, destruction of infrastructure, etc., in addition to providing information for agriculture in weather conditions.

The variables that a weather station could record are: air temperature, humidity, barometric pressure, wind speed, wind direction, precipitation, UV level, thickness of snow, soil temperature, soil humidity, solar radiation, visibility, pollution analysis, measurement of light hours, measurement of cloud height

There are different types of weather stations among which we can name: domestic weather stations, weather stations with PC connection, portable weather stations, professional weather stations, wireless or Wifi weather stations. The latter are stations capable of transmitting data to the Internet and broadcast them online, the proposal of this research work is oriented towards an automatic wireless weather station.

3   Related works

The advances in the management of meteorological stations with IoT and their relation with the problem of microclimates in urban areas are mentioned below:
In the literature review we found a prototype weather station applying IoT and Google tools, making use of a Spark Core card with IoT management capability. The variables to be measured in the prototype weather station were adjusted according to the

measurement variables that commercial stations have, such as ambient temperature, relative humidity, UV index, sunshine, rain sensor and solar energy capture. The variables are captured with analog and digital sensors connected to the card, which is in charge of processing the information of each one of them and publishing them in the cloud, to later capture them by means of a script that allows the reading of the variables and the publication in a spreadsheet and that will serve as data base of the collected information [11]. The disadvantage of this card is that it does not handle wind speed and direction.

Another work found is the design of the system with the use of Node MCU to make a low cost solution. This weather station is a product equipped with instruments and sensors to measure atmospheric conditions such as temperature, humidity, wind speed and direction, in order to make weather forecasts. By enabling IoT from the cloud, the user can access all atmospheric parameters measured by the weather station from anywhere in the world from any connected device [12]. This station is not available in an accessible way to users.

Another development is a model of a weather station to measure meteorological data: temperature, relative humidity, atmospheric pressure, direction of the wind, speed and rainfall. The measured data are transmitted wirelessly to the remote station for recording and displaying the information to different intelligent devices. This wireless connectivity has been planned through Wi-Fi connections that establish a mesh network for reliable data communication. The information from the station is used to help the inhabitants to take the necessary precautions in climatic changes [13]. Its application is oriented to urban use, in the related work was not found application in network mode of the stations.

A work is found through the solution of portable weather stations, proposes a wireless network of weather monitoring stations using GSM for an IoT middleware, responsible for retaining data and providing weather information to various applications focused on helping users in planning their daily routine [14]. The solution proposed by GSM limits the capacity of the graphical interface to present the information flexibly and graphically to the end user.

Another proposal is a system to monitor environmental parameters using multilevel IoT architecture. The proposed system will monitor changes in environmental parameters in the Hyderabad region. The proposed instrumentation operates on level II architecture on IoT. The proposed system consists of different sensors grouped in 5 sensor nodes that are invoked by switches in the gateway or from the web page. The sensors acquire the data and send it to a slave controller (PIC). In turn, the slave controller sends the acquired data to the master controller (Raspberry pi). The master acts as a gateway between the sensor nodes and the cloud. Master sends the data to the cloud and displays it as a web page via HTTP. Data is also received as SMS via GSM. Using the system, changes in the climatic conditions of the Hyderabad region were studied and information was provided to local farmers in terms of indicators that can be used to help them decide which crop (cotton, jowar, redgram) needs to be grown / harvested [15]. The disadvantage of this proposal is that it was not applied to weather parameters in urban areas caused by microclimates

4   Problem statement

The cost and benefits of global warming will vary greatly from area to area. For moderate climate change, the balance can be difficult to assess. But the larger the change in climate, the more negative the consequences will become. Global warming will probably make life harder, not easier, for most people.

The problems seem especially obvious in cases where current societal trends appear to be on a collision course with predictions of global warming's impacts: at the same time that sea levels are rising, human population continues to grow most rapidly in flood-vulnerable, low-lying coastal zones. Places where famine and food insecurity are greatest in today's world are not places where milder winters will boost crop or vegetation productivity, but instead, are places where rainfall will probably become less reliable, and crop productivity is expected to fall. The countries most vulnerable to global warming's most serious side effects are among the poorest and least able to pay for the medical and social services and technological solutions that will be needed to adapt to climate change[16].

5   Modeling

In this model we can observe the operation of the project, we have our Particle Boron (master) that is a powerful cellular enabled development kit and it is connected directly to the IoT Node that is a waterproof enclosure with a stackable adapter board for connecting the Particle Boron and the sensors. The temperature, humidity, pressure barometric and battery voltage ADC (Analog to Digital Converter) sensors are connected to the Particle Boron through the I2C communications bus. The meter kit sensors: rain gauge, anemometer and wind vane are connected through the analog and digital inputs. The Particle device needs an antenna to better capture of the network signal, also a lithium ion battery, and a solar panel to power the IoT Node; and all information of the sensors will be send to the Particle Cloud and at the same time the data is saved in Firebase DataBase in real time. Figure 1 shows a diagram of all sensors connected.

Fig. 1. Connection block diagram, Elaborated by the authors.

6   Methodology

6.1   Materials

For the development of the IoT Node for meteorological monitoring, the following components were necessary: IoT Particle Boron, IoT Node case integrated with Battery ADC Monitor and Barometric Pressure sensor, Anntena, Lithium Ion Battery, Temperature and Humidity sensor (AM2315), Solar Radiation Shield, Micro Sd Card, Solar Panel, Weather Meter Kit (containing rain gauge, anemometer and wind vane sensor). The Particle IDE software was used for programing the code and the Ubidots visualization plataform was used to graph all the information sensors. Sensor data is stored in a real-time database in Firebase.

6.2   Particle IDE and Particle Cloud

Every Particle device connects to the Particle Cloud – a secure, scalable, and reliable gateway between the devices and the web. Programming the device is over-the-air through the easy-to-use Web IDE, in which the programming code is written for the readings of the sensors, to activate relays and to send information to other platforms for viewing data as Ubidots. The programming language used in the Web IDE is C/C++ [21].

6.3   Ubidots

Ubidots is an Internet of Things (IoT) data analytics and visualization platform, it turns real-time sensor data into information that matters for business-decisions. Ubidots exists as an easy and affordable means to integrate the power of the IoT into your business or research [22].

6.4   Firebase Realtime Database

Firebase provides a real-time, back-end, tree-organized JSON database. The service provides application developers with an API that allows application information to be synchronized and stored in the Firebase cloud. The company enables integration with Android, iOS, JavaScript, Java, Objective-C, Swift and Node.js applications.

   Real-time synchronization of this database allows users to access their data information from any device in real time, sharing one Realtime Database instance, and every time a user makes a modification to this, this information is stored in the cloud and simultaneously notified to the rest of the devices [23].

6.5   System Integration

The device is programmed to obtain the information from the sensors, this information is sent via webhooks or "user's HTTP callbacks" to the display platform (Ubidots).

The sensors are polled every ten minutes and send the data to the cloud detecting any change in the weather. Data collection is at least ten minutes to avoid network congestion, and this time can be programmed. Figure 2 shows the webhook integration to the dashboard.

Fig. 2. WebHook.

6.6   Connections

I2C Bus is a synchronous protocol. I2C uses only 2 cables, one for the clock (SCL) and one for the data (SDA). This means that the master and the slave send data over the same cable, which is controlled by the master. I2C does not use slave selection, but addressing. Figure 3 shows an I2C diagram where all sensors are connected.
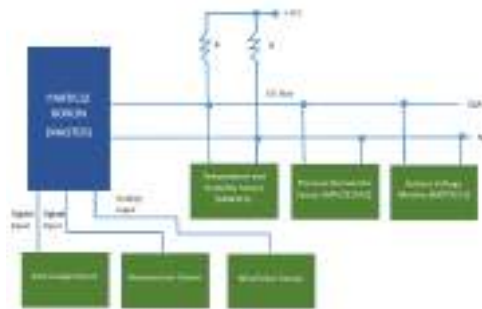
Fig. 3. Connections.

6.7   Algorithm

Algorithm is as follow:
- a) Start.
- b) Temperature and Humidity sensors sends data.
- c) The Rain Gauge, Anemometer and Wind Vane sensors sends data.
- d) The Pressure Barometric sensors sends data.
- e) The Battery Voltage ADC sends data.
- f) Data is collected.
- g) Data is sent to the Particle console and to Ubidots visualization platform.
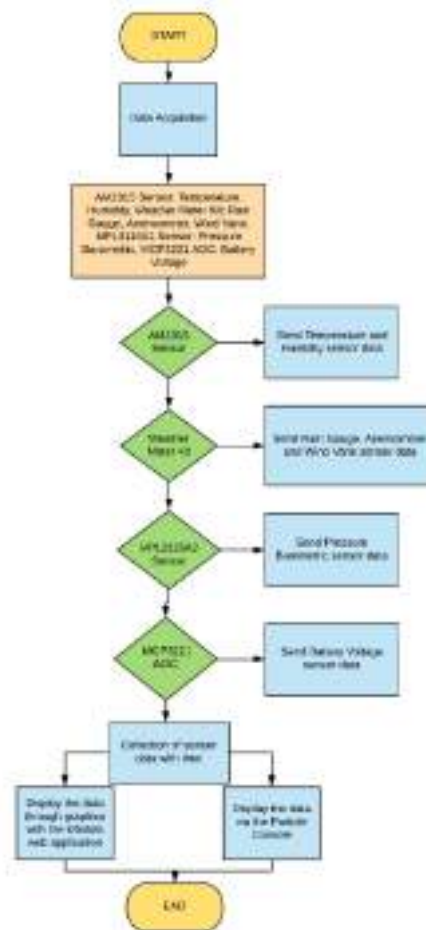- h) End

Figure 4 shows the flowchart.

Fig. 4. Flowchart

7   Results

This section describes the Solar Powered Cellular Weather Station, measuring wind speed, wind direction, rain, temperature, humidity, barometric pressure, and battery voltage in remote locations using Particle, Web IDE, Ubidots and Firebase.

   The cost of professional weather stations is high and they only measure a few variables. In this proposal, there is a semi-professional weather station with very precise values that involves the measurement of seven variables: wind speed, wind

direction, rain precipitation, humidity, temperature, battery voltage and barometric pressure. In addition, one of the advantages of this station allows us to connect up to 127 sensors that use I2C communication, and the assembly of this station is 1/3 of the value of a professional one.

7.1 Weather Station

The monitoring station is a CPS which allows real-time monitoring of the variables: wind speed, wind direction, rain precipitation, humidity, temperature, battery voltage and barometric pressure, and remote monitoring from anywhere in the world due to the CPS has an embedded system that connects to the Internet through cellular technology and, being on the Internet or in the cloud, requests can be made to this device programmatically from any IoT platform or from any web page programmed for this purpose.

The IoT Node board is designed to fit a hinged waterproof enclosure in which the temperature, humidity, atmospheric pressure and battery voltage monitor sensors are connected through the I2C communication protocol to the Particle Boron and the wind speed, rain precipitation sensors are connected through two digital inputs and the wind direction with an analog input on the same devices. Figure 5 shows inside of CPS.

Fig. 5. IoT Node

Figure 6 shows the weather station with each of its components to achieve the interaction of all measurements.

Fig. 6. Weather Station

7.2 Graphical Interface

Subsequently, a platform was integrated for the visualization of data in a graphic way, so the information can be represented as the final result of the project in the Ubidots Platform , the data are sent in real time every minute. Figure 7 shows the dashboard.

Fig. 7. Dashboard of the Sensors in Ubidots.

7.3　Wind Speed

Real-time wind speed monitoring is displayed at 1.39 km/h. The wind speed is the average of the measurements and polled every one minute, its unit of measurement is in kilometers per hour (km/h). Figure 8 shows the wind speed widget of the dashboard.

Fig. 8. Wind Speed Monitoring in Ubidots.

7.4　Wind Direction

Real-time wind direction monitoring is shown at 223.00 degrees and polled every one minute, the direction indicates where the wind is coming from, its unit of measurement is in degrees (clockwise rotation) where 0° is North, 90° is East, 180° is South, 270° is West, therefore, it is in Southwest(SW) direction. Figure 9 shows the wind direction widget of the dashboard.
.

Fig. 9. Monitoring of Wind Direction in Ubidots.

7.5　Rain Precipitation

Real time monitoring of rainfall level is shown which is at 14.81mm. It is the precipitation accumulated and polled every one minute, its unit of measurement is the millimeter (mm). Figure 10 shows the rain precipitation widget of the dashboard.

.

Fig. 10. Rain Precipitation Monitoring in Ubidots.

7.6 Humidity

Real time monitoring of humidity is shown which is at 38.00 %. The relative humidity is the average of the measurements and polled every one minute, its unit of measurement is in percentage (%). Figure 11 shows the humidity widget of the dashboard.
.

Fig. 11. Humidity Monitoring in Ubidots.

7.7 Temperature

Real-time monitoring of the temperature is displayed and is at 19.55 °C. It is the average outside temperature of the measurements and polled every one minute, its unit of measurement is in degrees Celsius (°C). Figure 12 shows the temperature widget of the dashboard.
.

Fig. 12. Temperature Monitoring in Ubidots.

7.8 Battery Voltage Monitoring

Real-time battery voltage monitoring is displayed with a value of 3,514.00 mV. The voltage is polled every one minute, its unit of measurement is in millivolts (mV). Figure 13 shows the battery widget of the dashboard.

Fig. 13. Battery Monitoring in Ubidots.

8 Conclusions

An autonomous monitoring station is developed since its power supply is through a battery connected to a 9 watt solar panel lightweight, waterproof, and designed for long term outdoor use in any environment. And this monitoring station is a CPS (Cyber Physical System) where the following variables are monitored in real time:

wind speed, wind direction, rain precipitation, humidity, temperature, battery voltage and barometric pressure. In addition, these variables can be monitored from anywhere in the world, since the CPS contains an embedded system connected to the Internet through cellular technology since it has a cell phone SIM. Once the embedded system is connected to the Internet or the cloud, from any IoT platform or any web page programmed for this purpose, data can be extracted from all the variables every certain programmed time, in this case, due to the number of sensors, it is recommended to take of readings at least every 10 minutes and avoid network congestion. This monitoring station is 1/3 of the total cost of a professional station, and one of the advantage of this station is precise values of environmental variables and with the ability to be autonomous and have the possibility of attaching up to 127 sensors through the I2C communication protocol.

Finally one of the advantages of this monitoring station, unlike LoRaWAN technology, is that this monitoring station does not need to be near a Gateway to connect to the Internet, since this station has an embedded system that connects to the Internet through a SIM cell phone, without the need for an intermediary such as a gateway to connect to the Internet.

9   Future Works

For future work we intend to add the measurements of environmental pollutants such as ozone, carbon monoxide, carbon dioxide, nitrogen dioxide, sulfur dioxide, particulate matter (PM10) and particulate matter (PM2.5), as well as generate our own web and mobile visualization platform with the data generated in the Firebase.

References

1. Schiller, S. D., Evans, J. M., & Katzschner, L. Isla de calor, microclima urbano y variables de diseño Estudios en Buenos Aires y Río Gallegos. Avances en Energías Renovables y Medio Ambiente, 5 (2001).
2. Tumini, I.. El microclima urbano en los espacios abiertos: estudio de casos en Madrid (Doctoral dissertation, Arquitectura) (2013).
3. Álvarez López, A. E. Cambio climático y microclimas urbanos en ciudades del centro de Cuba. Avances en Energías Renovables y Medio Ambiente, 8 (2004).
4. Fernández, M., Sáenz, D. Informe de Tendencias del ITI . Del Internet de las Cosas a los Sistemas Ciber- Físicos. Instituto Tecnológico de Informática, España.Instituto Nacional de Ecología y Cambio Climático (2015).
5. Humayed, A., Lin, J., Li, F., & Luo, B. Cyber-physical systems security—A survey. IEEE Internet of Things Journal, 4(6), 1802-1831 (2017).
6. Chandy, J. C.. Desafíos en el diseño de sistemas Ciber-Físicos. Ingenierías USBMed, 1(1), 6-14 (2010).
7. Mendez Mena, D., Papapanagiotou, I., & Yang, B. Internet of things: Survey on security. Information Security Journal: A Global Perspective, 27(3), 162-182 (2018).

8. Al-Fuqaha, A., Guizani, M., Mohammadi, M., Aledhari, M., & Ayyash, M. Internet of things: A survey on enabling technologies, protocols, and applications. IEEE communications surveys & tutorials, 17(4), 2347-2376 (2015).
9. Li, S., Da Xu, L., & Zhao, S. The internet of things: a survey. *Information Systems Frontiers*, *17*(2), 243-259 (2015).
10. Organización Meteorológica Mundial. Guía de instrumentos y métodos de observación meteorológicos (OMM N° 8). Secretaría de la organización meteorológica mundial, OMM, Ginebra Suiza. (2014).
11. Rodriguez, A., Figueredo, J. Selección e implementación de un prototipo de estación meteorológica aplicando IoT y herramientas Google. Serna, & Edgar, Desarrollo e innovación en ingeniería, 341-352. (2016).
12. D. K. Singh, H. Jerath and P. Raja, "Low Cost IoT Enabled Weather Station," *2020 International Conference on Computation, Automation and Knowledge Management (ICCAKM)*, Dubai, United Arab Emirates, pp. 31-37, doi: 10.1109/ICCAKM46823.2020.9051454 (2020).
13. Sarkar I., Pal B., Datta A., Roy S. Wi-Fi-Based Portable Weather Station for Monitoring Temperature, Relative Humidity, Pressure, Precipitation, Wind Speed, and Direction. In: Tuba M., Akashe S., Joshi A. (eds) Information and Communication Technology for Sustainable Development. Advances in Intelligent Systems and Computing, vol 933. Springer, Singapore. https://doi.org/10.1007/978-981-13-7166-0_39 (2020).
14. Monteiro, M. S., de Caldas Filho, F. L., Barbosa, L. A., Martins, L. M. E., de Menezes, J. T., & da Silva Filho, D. A. University Campus Microclimate Monitoring Using IoT. In 2019 Workshop on Communication Networks and Power Systems (WCNPS) (pp. 1-5). IEEE (2019).
15. Kishorebabu, V., & Sravanthi, R. Real Time Monitoring of Environmental Parameters Using IOT. Wireless Personal Communications, 1-24. (2020).
16. "Climate Q&A - Why is global warming a problem?", Earthobservatory.nasa.gov, 2020. [Online]. Available: https://earthobservatory.nasa.gov/blogs/climateqa/why-is-global-warming-a-problem/. [Accessed: 08- Nov- 2020].
17. "Boron LTE CAT-M1 (NorAm)", *Particle Retail*, 2020. [Online]. Available: https://store.particle.io/products/boron-lte. [Accessed: 08- Nov- 2020].
18. "Particle Cellular Flex Antenna 2G/3G/LTE 4.7dBi", *Particle Retail*, 2020. [Online]. Available: https://store.particle.io/products/cellular-flex-antenna-2g-3g-lte-4-7dbi?pr_prod_strat=copurchase&pr_rec_pid=4287708659781&pr_ref_pid=1654236086341&pr_seq=uniform. [Accessed: 08- Nov- 2020].
19. A. Industries, "Lithium Ion Battery Pack - 3.7V 6600mAh", Adafruit.com, 2020. [Online]. Available: https://www.adafruit.com/product/353#description. [Accessed: 08- Nov- 2020].
20. "AM2315 - Encased I2C Temperature/Humidity Sensor", Adafruit Learning System, 2020. [Online]. Available: https://learn.adafruit.com/am2315-encased-i2c-temperature-humidity-sensor. [Accessed: 08- Nov- 2020].
21. ["Particle Company News and Updates | Particle", Particle, 2020. [Online]. Available: https://www.particle.io/. [Accessed: 08- Nov- 2020].
22. "Ubidots: IoT Analytics and Visualization | PubNub", PubNub, 2020. [Online]. Available: https://www.pubnub.com/integrations/ubidots/. [Accessed: 08- Nov- 2020].
23. "Firebase", Es.wikipedia.org, 2020. [Online]. Available: https://es.wikipedia.org/wiki/Firebase#Realtime_Database[14]%E2%80%8B. [Accessed: 08- Nov- 2020]

A new approach to automate the connectivity of electronic devices with an IoT Platform

Juan José Flores-Sedano[1], Hugo Estrada-Esquivel[1,] Alicia Martínez Rebollar[1], Juan José Jassón Flores Prieto[1],

[1] TecNM/Centro Nacional de Investigación y Desarrollo Tecnológico CENIDET, Cuernavaca, Morelos, Mexico. C.P. 62470
{m20ce084, hugo.ee, alicia.mr, jose.fp}@cenidet.tecnm.mx

Abstract. At present, the Internet of Things is one of the most promising technologies considering a large number of applications domains. The IoT solutions imply the integration of electronic devices, communication protocols, the cloud as data storage and smart software systems to process the data. The complexity of current IoT solutions has given rise to the creation of IoT platforms to manage the implementation of the solutions, however, one of the most complicated tasks is the configuration of the electronic devices to send information to the cloud through a specific protocol and a specific IoT agent. Currently, this process is done manually and it represents a challenge for novel developers. In this paper a novel approach is presented to automate the connection of IoT devices with a specific Platform using IoT Agents. The evaluation of the proposed approach with users with different development knowledge levels is also presented in the paper.

Keywords: Internet of Things, IoT Platform, FIWARE.

1   Introduction

The Internet of Things (IoT) is a network of devices that are embedded with software, sensors, and network connectivity that collect and exchange data. The Internet of Things enables everyday objects to be "intelligent" by allowing data transmission and automates tasks, without requiring any manual intervention. IoT offers different opportunities and improvements in people's lives, being smart cities a concept that allows multiple technologies of this paradigm to be combined to generate solutions. Smart cities provide several digital services to sensorize and to automate different aspects of the city, such as the use of electricity, garbage management, city water management, pollution in different areas of the city, noise in the streets, etc. The proliferation of smart services based on IoT is largely due to the lower price of sensors and communication services. This cheapening of electronic devices has popularized the creation of applications that use sensor data to understand the context in which an object operates and the development of applications that capture and analyze this context data for decision making. The creation of IoT applications implies a great responsibility in software development, because the objects need to be in constant communication with the IoT platforms, which implies that the objects remain connected to the Internet all time. This situation causes the information produced by the sensors to be exposed to

computer threats, which must be addressed immediately in order to guarantee the integrity of the systems. As a consequence of this situation, intelligent agents were created as an intermediary between the information coming from the sensors and the software platforms and to also manage the security aspects produced.

This paper is organized as follows. Section 2 shows main concepts involved in the research. Section 3 presents the related work. Section 4 presents the proposed approach to automate the connection of electronic devices with an IoT Platform. Section 5 shows the experimentation, and finally, Section 6 details the conclusions and future work.

2   Background

This section presents the fundamental concepts involved in this research work.

2.1. Internet of things in the cloud

The constant growth in the number of "things" connected to the Internet and the large number of applications that require collecting and analyzing data from devices for decision-making was the origin of the Internet of Things (IoT). The Internet of Things considers the services and standards necessary to connect, manage and protect different IoT devices and applications. These devices can be sensors, actuators, mobile devices, etc. All the data collected by these devices is stored in the cloud, in order to have easy access to them, in addition to providing greater security in the event of a mishap [1].

2.2. Internet of things platform

The emergence of the Internet of Things gave rise to a set of solutions to manage all the interactions between hardware and application layers. These solutions, called IoT Platforms, must be able to manage the huge amount of data that smart devices collect. Today there are a large number of IoT platforms, some examples are Amazon Web Services, Google, Microsoft Azure, IBM and FIWARE [2].

2.3. FIWARE

FIWARE is one of the emerging IoT Platforms for the development and deployment of Future Internet applications. FIWARE provides a completely open architecture which allows developers, service providers, companies and other organizations to develop products that meet their needs. FIWARE comprises a set of technologies called generic enablers which provide open interfaces for APIs and support interoperability with other generic enablers, these enablers arise as a proposal to respond to the need for approaches for smart cities solutions [2].

2.4. **Orion Context Broker of the FIWARE Platform**

This component of the FIWARE Platform, which allows the publication of context information by entities, is a server that implements an application programming interface based on an NGSI information model. This component allows to execute the following operations [3]:

- Register context applications.
- Update context information.
- Be notified when changes to context information arise.
- Consult background information.

2.5. **Internet of things Agent**

The connection of objects to the internet implies overcoming a set of problems that arise in the different layers of the communication model. The lack of globally accepted standards for communication between objects has caused a heterogeneous environment to be required for devices using different protocols. For this reason, the IoT agents were created together with the FIWARE platform, so that the devices can send their data to the Context Broker using their own native protocols. Internet of Things Agents are intermediaries, a so-called bridge between IoT devices and platforms. In this context, the protocols used by the sensors are very relevant to select an appropriate IoT agent. Figure 1 shows the relationship between communication protocols, IoT agents and the Orion Context Broker [4].
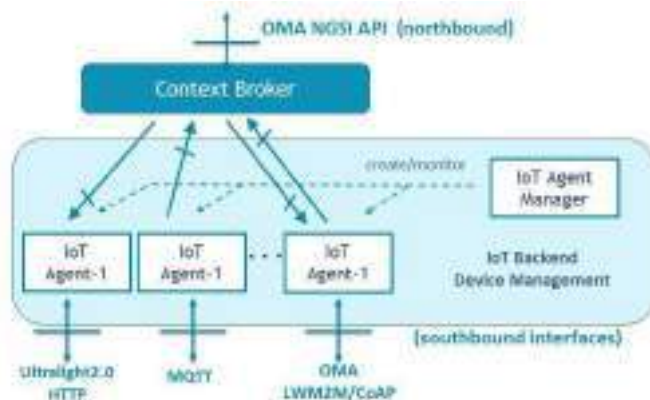

Fig. 1. Interaction between the Orion Context Broker, IoT agents and communication protocols.

The following are examples of IoT agents provided by the FIWARE Platform for communication between objects:

Table 1: IoT Agent list

IoTAgent-JSON.	IoTAgent loRanWAN
IoTAgent-LWM2M	IoTAgent OPC-UA
IoTAgent-Utralight	IoTAgent sigfox

3   Related work

This section presents the main research works related to the solution proposed in this paper.

In [5], the authors propose a model that allows the connection of services based on FIWARE OAuth 2.0 with the eID authentication provided by the eIDAS reference. With this model and its services that are already connected with an OAuth 2.0 identity provider can automatically connect with eIDAS nodes to provide eID authentication. To validate the proposed model, the authors have deployed an instance of the FIWARE identity manager connected to the eIDAS node. Later they registered 2 services; a private video conference system and a smart city deployment, in addition to expanding the functionalities to improve the user experience by taking advantage of. The authors conclude that the proposed solution facilitates the integration of FIWARE based generic OAuth 2.0 services for the eIDAS infrastructure, making the connection transparent for developers.

In [6], the authors demonstrate that the use of cloud services in the agronomic industry could be considered beneficial. In particular FIWARE, because it provides free and open-source development modules. The authors developed an application using the FIWARE components, and it has been validated in real crops located in a semi-arid area of southern Spain with the aim of reducing the amount of water needed for irrigation tasks.

In [7], the authors propose an authentication and identity management (IdM) method called YubiAuthIoT integrated with the FIWARE platform, as a way to provision and authenticate IoT devices. There are several benefits for IoT device authentication such as: device identity, scalability, offline crypto assets, revocation, and broadcast. YubiAuthIoT enables more decentralized device provisioning and management using subCAs, reducing the need for a discrete IdM service to manage devices. This approach provides more efficient and robust authentication and communication than the default on the FIWARE platform, which is based on HTTPS over HTTP/1.1 with JSON bodies, where authentication is provided by access tokens requested by each device/user and provided by the centralized IdM service.

In [8], the authors deal with the adoption of FIWARE for RPM development and, in general, for telehealth projects with the aim of supporting clinical centers interested in adopting cloud computing technology. Specifically, the authors presented a step-by-step approach to developing an RPM solution, investigating how the FIWARE platform and Generic Enablers (GE) could be adopted and integrated.

In [9], the authors present a customizable open source IoT platform setup using FIWARE. For the integration of existing building automation networks, this work extends an OpenMUC gateway with BACnet functionality and connects it to their platform via MQTT. The authors have successfully demonstrated the general setup with a website, by visualizing high resolution energy monitoring and control loop as basic requirements for the integration of more advanced control algorithms in future building energy management systems.

4   The proposed approach to automate the connection of electronic devices with an IoT Platform

One of the current challenges in the Internet of Things is the current connection between IoT devices and the FIWARE platform. This connection, which is currently done manually, involves configuring the physical devices to be able to link them with the appropriate IoT Agent. The selected IoT agent needs to be configured for each protocol, which implies in-depth knowledge of the operation of the protocol and the IoT agent. In case of request for a communication protocol that does not yet have a standard for the IoT agent, it is necessary to create a specific IoT agent. This involves encoding the necessary commands and attributes for the IoT agent to function properly. With the appropriate IoT agent, the connection between sensors and the Orion Context Broker can be made. This connection implies knowledge of the physical device, knowledge of the IoT agents and the Orion Context Broker. The difficulty of making this manual configuration has caused this connection to be made directly between the devices and the Orion Context Broker, completely omitting the use of IoT agents, which breaks with the ideal scheme and allows unauthorized access to the data read from the sensors [10].

The architecture of the solution proposed in this work aims to automate the device connection processes using a specific communication protocol towards an IoT agent and the automatic connection of the agents to the FIWARE Internet of Things platform. The proposed architecture uses the components of the FIWARE platform for the development of the application with the aim of generating a totally open-source system, which adapts to the standards provided by this IoT platform and also uses the concept of IoT agents that was developed by FIWARE to improve the security between the connection of devices and the cloud. The FIWARE components used in this work are: the Orion Context Broker, CrateDB and Grafana. The interaction between FIWARE and the created web system is done through a RESTful API. RESTful APIs are services with which we can exchange information through established protocols and standards such as HTTP. Figure 2 shows the proposed architecture, which is made up of the following layers: Application Layer, Services Layer and FIWARE services.

Fig.2. Architecture of the proposed solution.

The application layer contains the system developed in this research work, which is responsible for receiving, storing, processing and sending data from IoT devices. The services layer uses RESTful services to enable the interaction between the application layer and the FIWARE ecosystem, through requests to send data. The FIWARE service is responsible for receiving the data sent through the web system, in order to handle the data received by the Orion Context Broker. This layer makes a connection with the CrateDB module to create a database where all historical data sent to FIWARE is stored. This in order to connect to the Grafana module to display the data from the sensors graphically. The proposed system is made up of a series of modules that allow the automation of the connection process of IoT devices to the cloud of the FIWARE platform. These modules are presented in Figure 3.
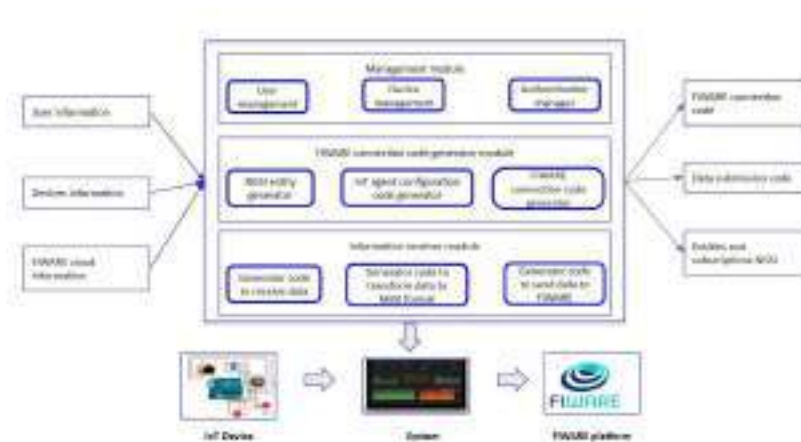
Fig. 3. Specific architecture of the proposed system

In following sections, the explanation of each module of the architecture is presented in detail:

4.1. **Manager module**

The manager module allows the system to manage user information (name, email and password), devices (name, readings, units, protocols) and FIWARE cloud details (Orion Context Broker address and IoT agent), as well as to take care of the authentication of the users who register in the system. This module connects to a database to store all the information it receives, this information is used to create the connection codes and data reception code of the device.

On the device registration screen (Figure 4) the user must fill in the form with the name of the device, units, maximum and minimum value of the device reading, the address of the Orion Context Broker server, the communication protocol and the Internet of Things agent that the device use and the readings of the device.
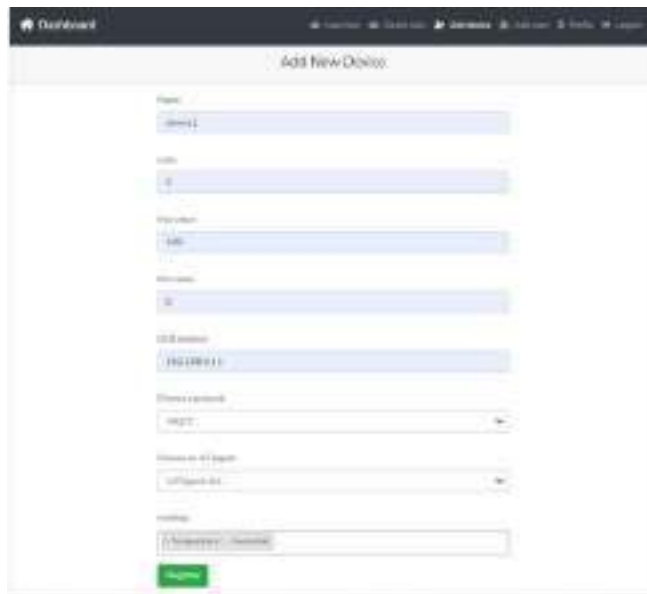
Fig. 4. device registration form

4.2.**FIWARE platform connection module**

The purpose of this module is to generate the necessary code to define the FIWARE entities corresponding to the devices that will provide data to the IoT system. The creation of NGSI entities and the generation of code in order to make the connection with FIWARE. The approach is based on the concept of entities that relate and entities with attributes and metadata. All communication between the different components of the OCB architecture is done through the NGSI v2 RESTful API. The context information in FIWARE is represented through generic data structures referred to as context elements, the context elements are composed of an identifier, a type associated with its entity, in addition to having attributes which contain a name, type and attribute value, these attributes in turn have metadata given which have a name, type and value, the metadata is optional when building the context elements. The values that are captured from the sensors must be represented using the concept of entities. Users must use the code generator to create the NGSI entities to define the map between the various sensors defined in the system and the various entities predefined by FIWARE, with the NGSI entities being JSON-type data formats that represent an object or thing in the system. real world with tangible attributes or characteristics. These entities help to send information to FIWARE, more specifically to the Orion Context Broker component, which uses a mongo database to store the current status of the entities, it does not store historical information of its changes. With the entities created, the users must select a

specific IoT agent using the submodule's code generator to configure an IoT agent according to the protocol defined in the sensor.

Figure 5 shows an example of the code generated to launch the FIWARE services. This code is composed of the following elements: the version of FIWARE cloud, the Orion Context Broker service, the dependencies such as mongodb, the ports it uses, in addition to including the configuration of the IoT agent. The information is obtained from the data that the user registers when adding a new device in the system, with the generated code the user can compile the code on the server where he wishes to host the FIWARE services.

Fig. 5. FIWARE connection code.

4.3. **Information receptor module**

This module aims to produce the necessary code so that the IoT system can obtain data from previously registered devices. In addition, it also aims to generate the code that allows the transformation of sensor data to the NGSI format (NGSI REST API) to be sent to the Orion Context Broker through a specific IoT agent. This code, which is

compiled later, allows the IoT system to take data from each sensor and pass it to the sub-module in charge of transforming it into the NGSI format for subsequent sending to the Orion Context Broker. To load the Arduino code to send data, in the Arduino code screen (Figure 6) the Arduino file is loaded so that the system inserts the code with the necessary data to send data, the code is made up of the id and the reading variables of the device, the address of the system, as well as the necessary libraries for the operation of the code which the user downloads and compiles to send data to the system .
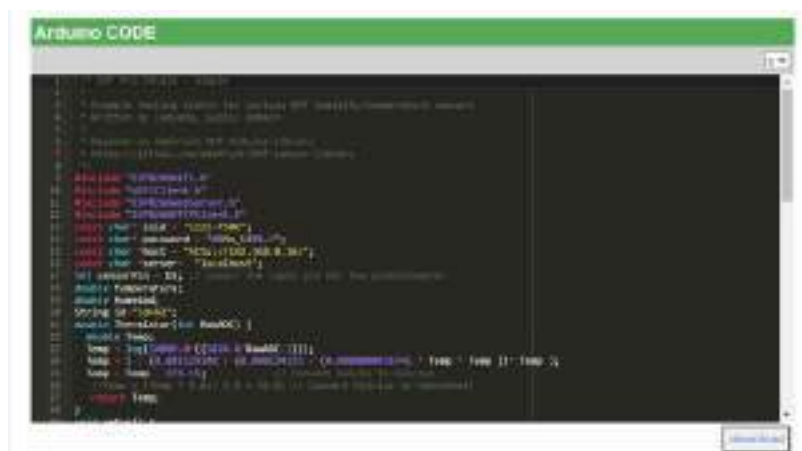
Fig. 6. Arduino code.

5   Experimentation

In order to validate the proposed approach, experimentation was carried out with developers with different levels of knowledge about sensors, cloud computing and the Internet of Things.

5.1. Phases of experimentation

The experimentation was carried out in three phases:

Phase 1. In this phase, participants were given an informed consent document explaining the objective of the experimentation, the procedures followed during the tests, and establishing that their personal information will not be disclosed. The participants read the consent document and signed it stating their agreement with the test plan.

Phase 2. In this phase, the functionality of the developed system is evaluated. The evaluation requires the development of 7 tasks. Each of the tasks must be evaluated with a questionnaire that allows knowing the functionality of the system and the times used for the participant to develop each of the tasks.

Phase 3. In this stage, the preliminary evaluation of the graphical interface of the system is carried out. The evaluation consists of a Likert-type questionnaire of 12 questions related to the interaction of the participants with the interfaces of the Web system in order to evaluate the usability of the system.

5.2. Experimentation participants

To carry out the experimentation of the new approach presented in this article, 8 male subjects (with ages ranging from 23 to 26 years) with different knowledge regarding the development in IoT environments and in the assembly and use of IoT devices were recruited. Regarding schooling, 4 participants are pursuing a master's degree and 4 of the participants are pursuing a computer science degree. The participants were summoned to a space where the computer with the developed system and the Arduino devices used to send data were located. In this environment, the 3 phases of experimentation were carried out continuously, ending with the preliminary evaluation of the graphical interface. The participants were divided into three groups (group 1: No IoT experience, group 2: Average experience in IoT, group 3: Advanced IoT expertise) according to their experience with devices, managing IoT agents and sending data to the cloud, whether from FIWARE or from another cloud service provider. The division was carried out through a brief questionnaire where the participants were asked about their experience using IoT devices, the management and configuration of Internet of Things agents, programming with Arduino and the configuration of the FIWARE cloud.

Table 2 presents the organization of the groups of participants according to their experience in the use of IoT or sending data to the cloud.

Table 2. Table of participants.

Participant	Age	Academic level	Experience
1	23	Master	Advance
2	23	Master	Average
3	26	Master	Advance
4	23	Master	Advance
5	24	Engineering	No experience
6	22	Engineering	Average
7	21	Engineering	No experience
8	24	Engineering	Average
9	21	Engineering	No experience
10	24	Engineering	Average
11	23	Engineering	Average
12	22	Engineering	Average
13	25	Engineering	No experience
14	23	Engineering	No experience
15	23	Engineering	No experience
16	24	Engineering	Advance

5.3.**Resources used in experimentation**

The resources used for the experimentation were the electronic devices, the informed consent document and the questionnaires to obtain feedback from the participants. Electronic devices: in order to reduce the problem in the availability of devices for the test, a set of devices that were used in the test sessions were made available to the participants. The devices that were made available to the participants during the test sessions are as follows:

- 3 generic Wemos D1 boards.
- 1 water sensor -SL067
- 1 Propane Gas Sensor – MQ-5
- 1 pulse sensor - MLM604362783
- 1 temperature and humidity sensor - Dht11A
- 1 accelerometer -MPU6050
- 1 Lenovo laptop with Windows 10, Arduino IDE in its latest version. The System was installed on this device.

Informed consent: the informed consent document has the purpose of informing the participants about the objectives of the testing phase, the procedure for the execution of the experimentation, and, above all, to make explicit the approval of the subjects to participate in the study. test plan and to record that the personal data of the participants will be anonymous. Evaluation questionnaires: the evaluation questionnaire was carried out after completing each of the tasks where the participant expressed the complexity of performing the task. The test plan considers that the participants of the experiment can perform a series of tasks with the system in order to send data generated by sensors to the FIWARE cloud, but using the concept of Internet of Things agents as intermediaries. The questionnaires developed for this test plan have the objective of evaluating the ease of use of the system's functionalities, the time used to perform each of the tasks and the usability of each of the modules.

5.4.**Experimentation procedure**

The main idea of carrying out the experimentation tasks is to make the connection between IoT devices and the FIWARE platform using the system. For this part, the system automatically performs the tasks of transforming the data read from the sensors into FIWARE entities in NGSI format and in accordance with a specific data model. In turn, the system automatically sends data to the FIWARE platform.

Phase 1 Start of experimentation

In this phase, participants were given an informed consent document explaining the objective of the experimentation, the procedures followed during the tests, and establishing that their personal information will not be disclosed. The participants read the consent document and signed it stating their agreement with the test plan.

Phase 2 Execution of tasks using the system

In this phase, the evaluation of the functionality of the developed system is carried out. The evaluation requires the development of 7 tasks which are:

- Task 1 User registration
- Task 2 Login
- Task 3 Device registration
- Task 4 Upload the Arduino code to the IoT device
- Task 5 Upload connection code with FIWARE
- Task 6 Reception of sensor data
- Task 7 Data visualization with Grafana

The objective of the tasks is to allow the participant to connect an IoT device to the system, and subsequently perform the configuration tasks that allow him to read the data from the device's sensors and send the standardized data to the FIWARE cloud. Each of the tasks must be evaluated with a questionnaire that allows knowing the usability of the system and the times used for the participant to develop each of the tasks.

Phase 3 Evaluation of the graphical interface

Once the 7 tasks were carried out using the Web system, the preliminary evaluation of the graphical interface of the web system was carried out in order to evaluate the usability of the system. The evaluation consists of a Likert-type questionnaire of 12 questions. Once the tasks and the questionnaires were completed, the evaluation was considered finished, which lasted an average of 15 minutes.

5.5. Functionality results

In order to have a first approximation to measure the ease of use of each functionality of the system, a functionality questionnaire was applied, which aimed to evaluate the complexity at the time of performing the tasks of the experimentation. The result of this evaluation made it possible to determine that all users were able to complete all the expected functionalities. The difficulty level of the average tasks is shown below:

- Task 1 User registration. Difficulty level (Easy 15 participants, Medium 1 participants and Difficult 0 participants).
- Task 2 Login. Difficulty level (Easy 16 participants, Medium 0 participants and Difficult 0 participants).
- Task 3 Device registration. Difficulty level (Easy 10 participants, Medium 5 participants and Difficult 1 participant).
- Task 4 Upload the Arduino code to the IoT device. Difficulty level (Easy 13 participants, Medium 2 participants and Difficult participants).
- Task 5 Upload connection code with FIWARE. Difficulty level (Easy 16 participants, Medium 0 participants and Difficult 0 participants).

- Task 6 Reception of sensor data. Difficulty level (Easy 12 participants, Medium 3 participants and Difficult 1 participants).
- Task 7 Data visualization with Grafana. Difficulty level (Easy 14 participants, Medium 2 participants and Difficult 0 participants).

The results of this evaluation allow us to establish that the system not only performs the tasks successfully, but also establishes that the functions are easy to follow and perform even for less experienced users in the Internet of Things area.

5.6. **Results of the evaluation of the time used for each of the tasks**

This section presents the results of the time that participants spent to perform each one of the tasks needed to operate the proposed system. Figure 7 shows the expected time (in minutes) that is expected to be used by the participant to perform the functionalities of the system. It is important to mention that expected time is based on the average time that an expert takes to use the functionalities of the system.
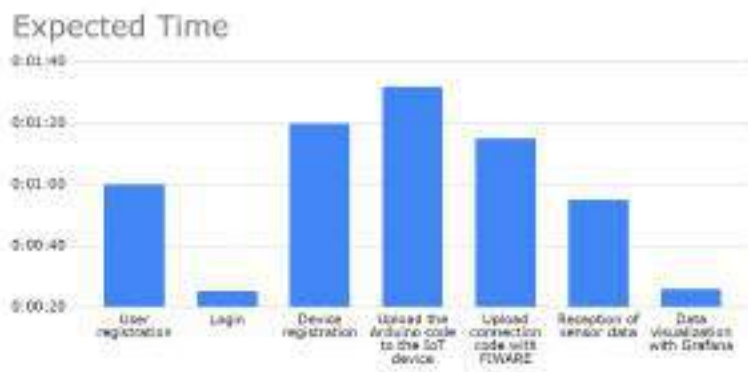
Fig. 7. Expected average time

The average time the user actually used to perform the evaluated activities is shown in Figure 8. The average time considers the time spent by the three groups of the evaluation: Advanced Participant, Average Experience Participant and Inexperienced Participant.
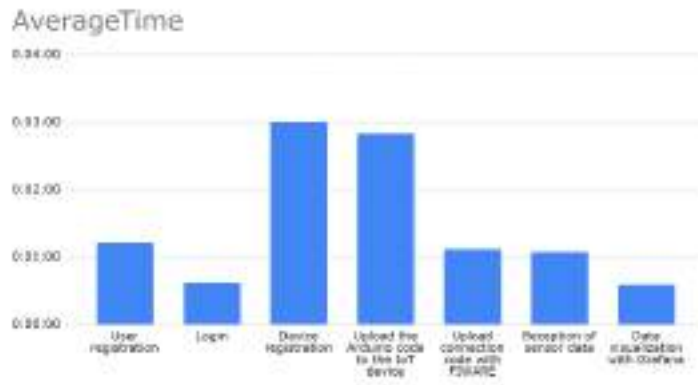
Fig. 8. Average time.

The analysis of the time used allowed us to detect that the times used in practice by the participants of the experiment were less than expected. In addition to the overall average time for all participants, the average time it took for each of the groups mentioned in the participants section of this document is also shown. The results for each of the participant groups are shown below.

5.7. **Group C results**

Figure 9 shows the average time it took group C (Advanced Participant) to perform the tasks. The tasks that required the longest time were task 3 "device registration" and task 4 "upload Arduino code". It is important to mention that the participants in the advanced group used more sensors than the other two groups, which led to the participants to take more time to register the devices that they were using and it also took more time to upload the Arduino code because it need it more processing resources because of the more sensor in the devices than the other group.
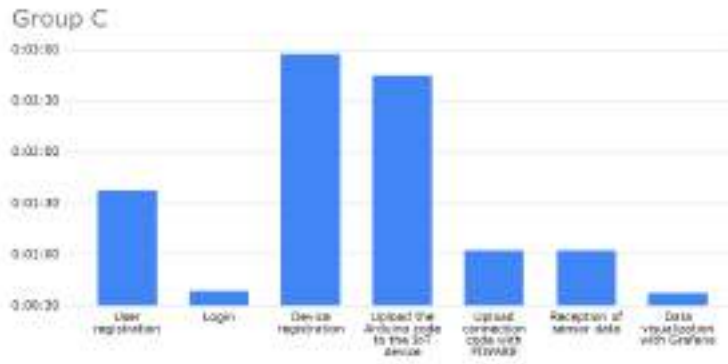
Fig. 9. Average time in group C.

5.8. Group B results

Figure 10 shows the average time it took group B (Average Experience Participant) to perform the tasks and, as well as the results of Group C. In this group, the tasks that also required the longest time were task 3 "device registration" and task 4 "upload Arduino code".
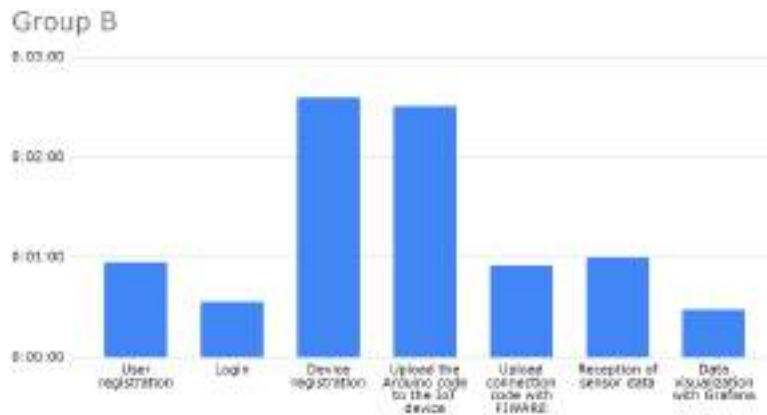

Fig. 10. Average time group B.

5.9. **Group A results**

Figure 11 shows the average time it took for group A (Inexperienced Participant) to perform the tasks and, as well as the results of groups C and B. Task 3 and 4 also required more time to be completed with times slightly higher than the other two groups.
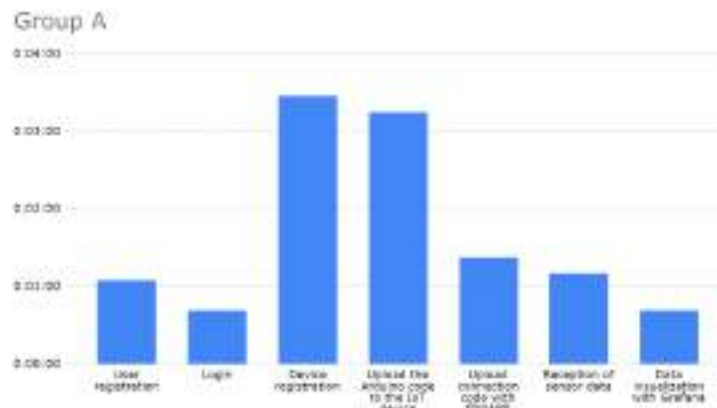

Fig. 11. Average time group A.

6   Conclusions

The research work presented in this paper has demonstrated that it is possible to automate the process to connect sensors to FIWARE Platform using the concept of IoT Agent. This paper presents the development of a software system that allows data to be sent automatically to the FIWARE platform using the CoAP and MQTT protocols in conjunction with Internet agents of Things. The proposed software system is responsible to obtain the needed information for registering the sensors of an IoT device and also to produce the code for a software module that obtains the data from sensors and establishes the connection with the FIWRE Cloud. The system was evaluated with a series of tests with young software developers, resulting in an effectiveness of 100% in all the functionalities of the proposed software system. The evaluation also considers the time that developers spent in developing each one of the tasks that compose the evaluation questionnaires. The results demonstrated that proposed solution fulfill the goal of automating the connection of IoT devices with the FIWARE Platform.

The developed system allows the user to save a significant amount of time when performing the connection and sending of data to the FIWARE platform. This type of system drives the transformation of traditional cities to smart cities, which have as obtained improve the quality of life of its inhabitants. The system presented in this work, being an intermediary between the devices and the platform FIWARE, allows

you to safely manage the data collected by the sensors of the devices, to later send them securely and automatically to the Orion Context Broker.

1.　　　References

1.　Bliznakoff del Valle, D. J. (2014). IoT: Tecnologías, usos, tendencias y desarrollo futuro. http://openaccess.uoc.edu/webapps/o2/bitstream/10609/40044/6/dbliznakoffTFM0 115memoria.pdf.

2.　FIWARE-ABOUT　　US,　　"ABOUT　　US»　　FIWARE,"　　2016. [Online]. https://www.fiware.org/about-us/.

3.　APRENDE FIWARE EN ESPAÑO, "Orion Context Broker" 2016. [Online]. https://fiwaretraining.readthedocs.io/es_MX/latest/ecosistemaFIWARE/ocb/.

4.　FIWARE,　　"Tuturial　　time　　series　　data"　　2018.　　[Online]. https://github.com/FIWARE/tutorials.IoT-Agent.

5.　Á. Alonso et al., "An Identity Framework for Providing Access to FIWARE OAuth 2.0Based Services According to the eIDAS European Regulation," in IEEE Access, vol. 7, pp. 88435-88449, 2019, doi: 10.1109/ACCESS.2019.2926556.

6.　López-Riquelme, J. A., Pavón-Pulido, N., Navarro-Hellín, H., Soto-Valles, F., & TorresSánchez, R. (2017). A software architecture based on FIWARE cloud for Precision Agriculture.　　Agricultural　　Water　　Management,　　183,　　123–135. doi:10.1016/j.agwat.2016.10.020.

7.　Sousa, P. R., Magalhães, L., Resende, J. S., Martins, R., & Antunes, L. (2021). Provisioning,

　Authentication and Secure Communications for IoT Devices on FIWARE. Sensors, 21(17), 5898.

8.　Celesti, A., Fazio, M., Galán Márquez, F., Glikson, A., Mauwa, H., Bagula, A., ... & Villari, M. (2019). How to develop IoT cloud e-health systems based on FIWARE: a lesson learnt. Journal of Sensor and Actuator Networks, 8(1), 7.

9.　Storek, T., Lohmöller, J., Kümpel, A., Baranski, M., & Müller, D. (2019, November). Application of the open-source cloud platform FIWARE for future building energy management systems. In Journal of Physics: Conference Series (Vol. 1343, No. 1, p. 012063). IOP Publishing.

10.　APRENDE FIWARE EN ESPAÑO, "Plataforma FIWARE," 2016. [Online]. https://fiware-training.readthedocs.io/es_MX/latest/ecosistemaFIWARE/plataformaFIWARE/.

An AC/DC hybrid microgrid: a case study at CE.D.E.R.-CIEMAT

Paula Peña-Carro[1], Oscar Izquierdo-Monge[1]

[1] CE.D.E.R.-CIEMAT, Autovía de Navarra A15 salida 56, 422290 Lubia (Soria), España, P.P.C.: paula.pena@ciemat.es; O.I.M.: oscar.izquierdo@ciemat.es

Abstract: This article presents the demonstrative development of the European project Towards Intelligent DC-based hybrid Grids Optimizing the Network performance (TIGON) at the facilities of the Centre for the Development of Renewable Energies - Centre for Energy, Environmental and Technological Research (CE.D.E.R.-CIEMAT). This project proposes the development of a microgrid with smart grid architecture based on direct current (DC) and integrated into the current energy system. It is proposed as a future solution to reduce energy losses caused by DC/alternative current (AC) conversions, increasing the performance and profitability of hybrid grids. To achieve the objectives set in TIGON, during the second year of the project, different power electronics equipment and exclusive protections are being developed. Their installation will allow the operation of a variety of generation systems (mini-wind and photovoltaic), storage (lithium batteries and lead acid batteries) and consumption (AC and DC) in both AC and DC at medium (MVDC) and low voltage (LVDC).

Keywords: AC/DC hybrid microgrid, DC microgrid, direct current (DC), AC/DC converters, DC/DC converters.

1   Introduction

Microgrids are energetic systems characterised by clearly defined limits and managed as one system. We can find them as; isolated microgrids in which they have no connection to the general energy distribution system and are 100% self-sufficient. Or, connected to the general distribution system via a point of common coupling (PCC) in which they have the possibility of consuming/pouring energy from/to the general system depending on the energy balance of the microgrid. Within any microgrid there are different sources of power generation systems, consumptions and, for the most part, storage systems, which help to manage the system´s energy. One of the benefits of microgrids is the possibility of using local resources such as wind, solar radiation, waterfalls or biomass to produce energy. All these resources should be near the generation and consumption points, reducing the distance and losses during transportation and, thus, improving the performance of generation-consumption ratio.

The sources for distributed generation are often renewable, being wind and photovoltaic systems the most used. These technologies generate energy in DC, be it directly or through a power converter. Storage systems are other elements operating in DC. They are an important part of the DC microgrid due to the intermediate energy production of renewable sources. Energy storage systems play an important role in the loads and power balance in the DC microgrid [1]. Taking into account what kind of current is used by the equipment conforming microgrids, we can see that DC prevails over AC.

In addition, modern electric equipment, computers, mobile phones, ventilation systems, electric vehicles, etc. also operate in DC [2]. On the contrary, most part of the infrastructure is centralized and the network works in AC. The reason behind this is that, comparing it to DC, AC at high voltages reduces the energy loss during transportation. Due to this difference in the type of current, and the generation and consumption modes, it is necessary to convert DC into AC using a DC/AC converter in order to use the devices connected to the grid. This conversion produces energy losses in the converter, with an approximate total energy loss of 10-25% [1], [3], [4], [2], and in transportation from the generation to the consumption points. At the same time, the efficiency of the electric systems is reduced.

All these disadvantages related to the consumption in AC, make DC grids attractive to the energetic sector [5], [6], due to the increasing DC loads such as LED lighting, charging stations for electric vehicles, energy storage, etc. and to recent expansion of distributed generation sources, thanks to which energy transportation is greatly reduced.

The main factors that fuel this change relate to the improvement of energy efficiency, flexibility, security and reliability that DC grids provide [2], [7], [8], increasing the sustainability of the energy distribution system.

The European Union's Horizon 2020 research and innovation program funds the TIGON (Towards Intelligent DC-based hybrid Grids Optimizing the Network performance) Project. Fifteen entities from eight European Union countries with different profiles of companies, associations and research organisations are participating in this project. All of them are involved in the design, management, production and demonstration needs of the project. The latter field includes Spain with CE.D.E.R.-CIEMAT and France with CEA, together with pilot use cases in a Finnish residential area and the Sofia metro system (Bulgaria) to analyse and solidify the replication beyond the development of the project.

TIGON aims to demonstrate the deployment and integration possibilities offered by DC architecture microgrids within current energy system. It proposes a four level approach to improve reliability, resilience, performance and cost efficiency through solution development in power electronics, monitoring systems and software tools and efficient DC grid control and management.

This document follows the next structure: section 2 will present CE.D.E.R., where the hybrid microgrid is located. Section 3 explains the monitoring systems installed at CE.D.E.R. to track the different equipment. Finally, section 4 describes the future work planned for this project.

2   Location: CE.D.E.R.-CIEMAT

The Centre for the Development of Renewable Energies (CE.D.E.R.) in Lubia (Soria, Spain) is one the demonstrator centres in the TIGON project. The centre is dependant of the Energy Department of the Centre for Energy, Environment and Technology Research (CIEMAT). CE.D.E.R. is specialized in applied research, development and promotion of renewable energies. It has large facilities for scientific and technological demonstrations, making it an ideal location for the installation and study of this project's hybrid microgrids.

The role adopted by the CE.D.E.R within the project is that of a demonstration centre. As will be explained below, a DC-based microgrid is being installed within the facilities, in which different generation systems, storage systems and consumption systems will be connected with all the necessary equipment for both DC and AC operation. Given that the use of DC microgrids is not a reality, all the equipment that enables operation in this mode is designed and manufactured exclusively for this project. One of the objectives we have as a demonstration centre is the operation of this microgrid and the creation of software for data collection and real-time action on the equipment. Subsequently, a study and analysis will be carried out at the equipment and global level, to extrapolate and replicate this case to the pilot cases and in the future implement it in more locations at an international level.

The centre can be considered as a microgrid itself. It has different generation systems like photovoltaic panels, wind turbines, biomass boilers, gasification systems and a small hydraulic turbine. In addition, there are different types of energy storage systems such as lead-acid, LFP and NMC batteries and diverse types of loads related to different consumption profiles (industrial, commercial and domestic). All of the above is operated and managed in real-time by a software. This software allows the remote switching on and off and the power variations of all the equipment instantaneously. Some of these controls are manual and other are automatic, as they have been programmed previously.

CE.D.E.R.'s general microgrid is connected to a 15 kV MVDC line. It is possible to identify 8 transformation centres that transforms this line to a 400 V three-phase low-voltage line. The demonstration of TIGON project will be done in an area inside the centre known as Pepa II (Fig. 1). Here, the microgrid with DC-based architecture will be located. This microgrid is going to be connected to the main AC grid through a Solid State Transformer (SST), making it possible to connect both the AC general grid and the DC microgrid. The Solid State Transformer is being developed exclusively for this project by one of its members. Thanks to this point of common coupling, whereby the connection between the LVAC and the MVDC is stablished, it is possible to operate either as an isolated microgrid or as a microgrid connected to the grid.

Fig. 1. Pepa II demonstration facilities.

At present, this is the second year of the project. All the equipment is being developed at the same time: the Solid State Transformer, the SiC medium-voltage DC/DC power converters and the WAMPAC and energy management system supported by a cybersecurity system.

Simultaneously, as a demonstrator centre, CE.D.E.R. is adapting its facilities to install to equipment.

In Figure 2, there is a diagram showing how the elements conforming the hybrid AC/DC microgrid are organized at Pepa II and its composition.

Excluding the equipment still in development, CE.D.E.R. has already installed the generation and storage systems at the AC side of the microgrid. They are working, enabling us to gather data for analysing in order to compare the production and consumption of an AC grid to those of a DC grid. Using the same equipment in different scenarios (meaning AC/DC) allows us to study production performance, costs, etc., while excluding factors such as the difference in the equipment or locations with different production levels, influenced by local resources. All the components of this project are detailed below.
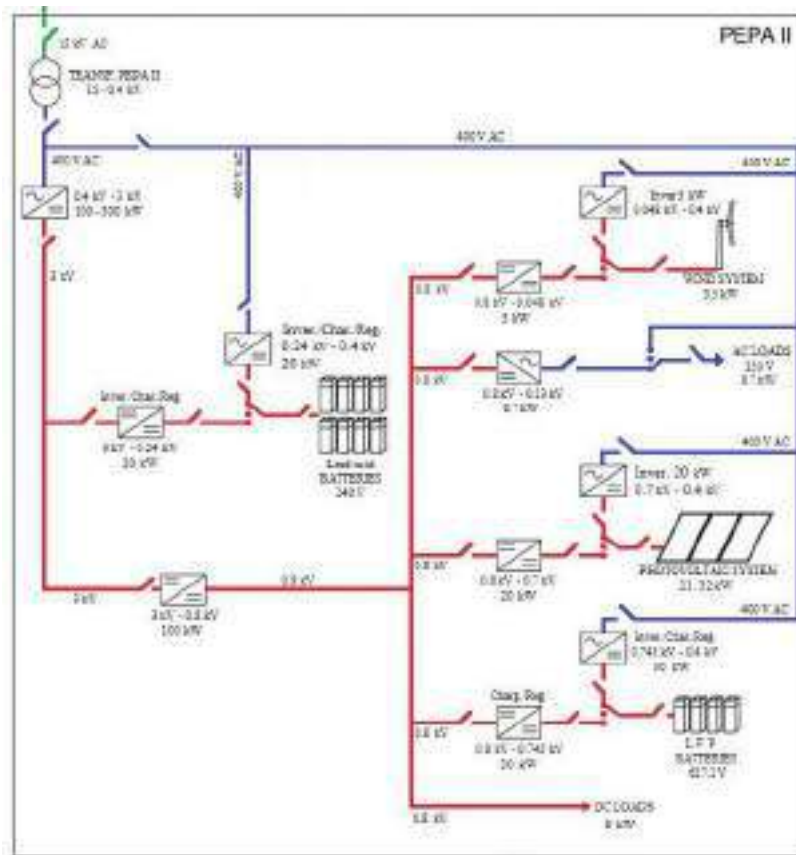
Fig. 2. *Hybrid AC/DC microgrid architecture scheme at Pepa II.*

Observing the DC part of the microgrid (red line), we can see a MVDC line where the lead-acid batteries are installed. In addition, in the photovoltaic system, wind turbine, LFP batteries and loads, there is a low-voltage line.

In the AC part (blue line), there are the AC loads from the centre such as offices, laboratories, computers, etc.

2.1   Generation systems

There are 2 generation technologies installed in the LVDC area for this project:
- The wind energy system is composed of a Ryse Energy E5 three-blade wind turbine with a nameplate power of 3.5 kW, horizontal axis while windward, and two power electronics equipment so it can operate in AC and another one

to operate in DC (see Fig. 3). All the components have been made by the company who manufactured the wind turbine. It is of interest to mention that the DC/DC equipment has been developed exclusively for this project due to the microgrid and technical requirements.

Fig. 1. Wind energy system composed of a Ryse Energy E5, a DC/AC inverter and a DC/DC converter.

- Photovoltaic system made of monocrystalline silicon. It is composed of 52 modules of 410 W connected in series-parallel. They are connected to an Ingecon Sun 3 Play inverter with a nameplate power of 20 kW to operate in AC (see Fig. 4).

Fig. 2. Photovoltaic system (photovoltaic modules and DC/AC inverter).

As seen before, this equipment must be able to work in DC in the low-voltage area. To achieve this, it is essential to install a device to adjust the operating photovoltaic system voltage to the low-voltage DC grid. This device is the DC/DC converter. The University of Valladolid is developing this device (Fig. 5), as they are not available for purchase.

Fig. 5. DC/DC photovoltaic converter in development.

2.2   Storage systems

The centre have two electrochemical storage systems available. One of them is a group of lead-acid batteries placed in the MVDC grid. The other is a group of LFP batteries in the LVDC grid.

- Lead-acid batteries: a group of batteries composed of 120 sets of 2 V each, a capacity of 1080 Ah (C120) and a total power of 2240 Vdc. This system is

able to work in AC, as it is doing now due to a connection to a 20 kW DC/AC inverter, or in MVDC (Fig. 6). This is the only device installed in the MVDC grid of the hybrid microgrid. To operate in the latter mode, some members of the project are developing a 20 kW medium-voltage DC/DC converter.

Fig. 3. Lead-acid batteries and DC/AC inverter.

- LFP batteries: composed of 2 racks, each of them have 14 modules with 14 cells of 3.2 V each module. The total voltage is 627.2 Vdc per rack and a nominal capacity of 50 Ah. All the system is controlled by a BMS, which is the one to internally manage the system loads and discharges to send the desired power to the Ingecom Sun 30 inverter (Fig. 7). The Ingecom Sun 30 inverter has been adapted to this system.

Fig. 4. LFP battery rack and inverter.

2.3 Loads

It is possible to differentiate three loads. The first one is CE.D.E.R.'s AC microgrid (computers, lighting, equipment, etc.). It is located upstream the transformation centre and is the one that contributes the most loads in terms of power.

The other two loading systems are already inside de microgrid itself, downstream from the SST. One of the systems is located in the AC grid and the other in the LVDC grid.

Regarding the AC loads, there are three AC2928 programmable loads (see Fig. 8). They have a power of 8.7 kW (2.9 kW each) and work as a master-slave scheme. There is one master and two slaves. Thanks to their daily and timely programmability, they allow us to set operational periods fitting the different desired consumption patterns.

In order to implement them into the hybrid microgrid, it is essential to install a device that let us transform the LVDC grid into AC, as it is how this system works. A Spanish company dedicated to manufacture power electronics devices is developing an 8.7 kW inverter.

Fig. 5. AC programmable loads.

Now, regarding DC loads, there are three resistive Enelec loads installed (see Fig. 9). They have different working modalities; three-phased, one-phased or direct, depending on the necessary requirements. Here, we decided on direct working mode, as it is possible to apply manually different percentages of the total power variation of the loads. This way, it is possible to achieve different consumptions and see how the microgrid reacts. As they are DC loads, there is no need to install equipment to adapt the voltage from the grid.

Fig. 6. DC loads.

2.4 Power converters and Solid State Transformer

It is possible to identify six converters in the proposed hybrid microgrid. Five of them are connected to the generation, storage and loads systems. The remaining transformer is the one in charge on transforming the MVDC line into a LVDC line.

The DC/DC converter enables us to convert 3 kV DC to 0.8 kV DC. Two members of the TIGON project are developing it under various premises. The material used for this is medium-voltage SiC with the objective of developing several power electronics building blocks (PEBB), which can be connected in series/parallel in order to achieve the desired final power and nominal voltage. All of this assures that settings are flexible and as easy to replicate as possible.

At present, the development is set to be finished by next year's summer, when the equipment will be installed at Pepa II. In addition, thanks to the delivery of the most important part of the microgrid, the solid state transformer, it will be possible to switch on the microgrid and to perform the planned tests.

Specifically, the solid state transformer is a device whose function is to transform the 400 V AC grid received directly from the transformation centre at Pepa II, into a 3 kV DC grid with 100 kW power. Given this function, the solid state transformer is a fundamental part of the project and the microgrid, as it is the device that creates the MVDC grid and to which all the other equipment is connected. The development of the SST is complex due to the functioning and protection requirements. Two members of the TIGON project are developing it.

3   Microgrid monitoring

In order for all the equipment that conforms the microgrid to work correctly, it is essential to manage said microgrid as efficiently as possible. This is the reason why it is necessary to know the actual value of certain parameters of the generation and consumption systems. Thus, developing a management system is indispensable. This

system should allow us to monitor in real-time the power consumed by loads, the power produced from renewable energy generation and the power consumed or delivered by the storage systems.

In most cases, the management systems communicates directly to each of the equipment's converters by using a ModBus communication protocol. If direct communication with a converter is not possible, it is necessary to install a smart metering system (grid analyser). This would allow us to measure the required parameters and for the converter to communicate with the management system by using a communication protocol.

Monitoring the grid let us see what happens in the microgrid in real-time and make immediate decisions to improve the performance, such as starting batteries, stopping loads, regulating power generation from the photovoltaic system by programming some protocols for the inverter, etc. This is the main objective of the WAMPAC system: to detect, prevent and mitigate all possible problems that may occur in the microgrid as fast as possible so big-impact effects like blackouts or the no supply of critical loads do not happen.

The monitoring and management system of CE.D.E.R.'s microgrid is based on three elements:

- Communications block: based on NodRed (see Fig. 10). It integrates the different communication protocols of the generation, storage and consumption systems at CE.D.E.R. (Modbus, MQTT, HTTP, etc.).
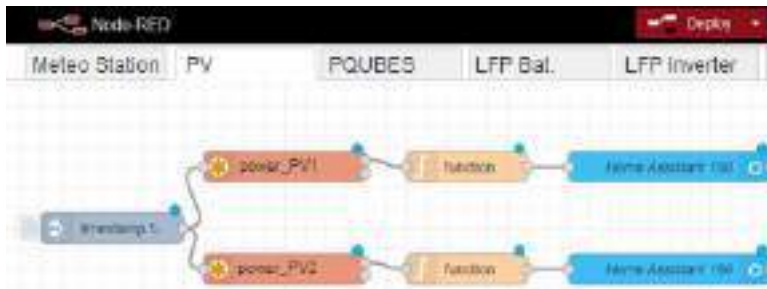

Fig. 10. Example from Nodered software

- Database: it is based on a database management system called MariaDB. The latter is a relational database that allows us to storage data per second in real-time thanks to programmed events and calculations (minute average or 15-minute average, as the ones used by the energy distribution company that supplies CE.D.E.R.) through the corresponding queries.

  This is important because, in addition to monitoring in real-time to make immediate decisions, it is of great interest to storage and analyse the data in order to stablish management strategies in the medium and long-term.

- Energy Management System (EMS) with a human-machine interface based on the Home Assistant software (see Fig. 11). This software allows monitoring all the necessary data from the equipment connected to the microgrid in real-time and giving instructions to each one. Furthermore, it is accessible from every point of the CE.D.E.R. communication network (meaning it is decentralized) and it can be accessed remotely with a smartphone application.

Fig. 7. Example from Home Asisstant Software

To achieve this, it is essential to connect all the elements of the microgrid as well as the management system to CE.D.E.R.'s data network (see Fig. 12). In this case, the equipment is connected to an Ethernet data network.
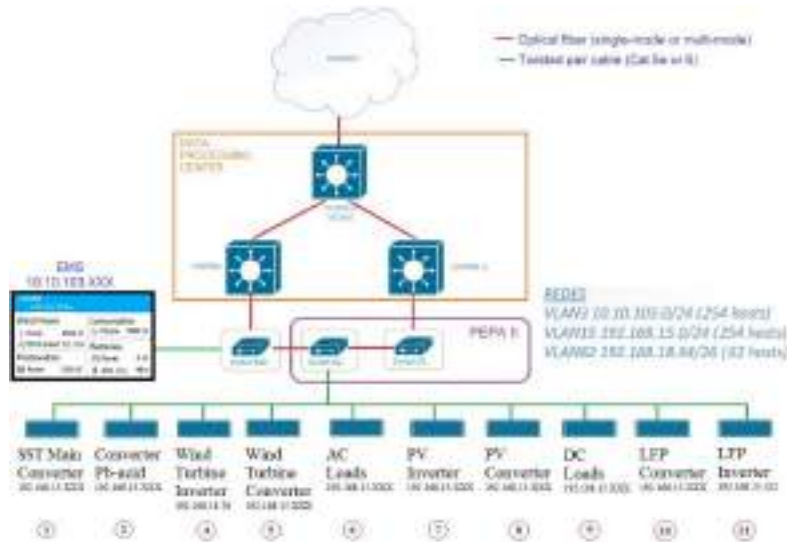
Fig. 8. Microgrid communication network

Cybersecurity is closely linked to the microgrid's management and control software. Due to the number of devices, entry points and protocols used, there is a bigger area susceptible to cyberattacks.

The modern cybersecurity market does not have the capacity to manage accurately such display for the entire power grid yet. Because of the latter, a member of the project is developing a security framework to provide a set of defensive measures in network attacking scenarios.

All of the above means that the operating mode and the cybersecurity system preparation is based on vulnerability evaluation and attack scenarios. The aim is to design a smart network architecture against malware. At the same time, the security performance will be analysed to reduce the impact of human errors and spear phishing campaigns.

4   Conclusions and Future work

As one of the demonstrator centres, CE.D.E.R. has, within its facilities, a hybrid AC/DC architecture microgrid. Here, we can find unique equipment designed specifically for this purpose and where different test will be held to answer the different viability and improvement questions raised by a hybrid microgrid when compared to an AC microgrid.

TIGON started in 2020, making this the second year of the project. Currently, we have all the generation, storage and consumption systems installed at Pepa II facilities,

as well as the necessary power electronics equipment; all of them ready to start working in AC. In addition, a DC/DC power electronics device for the small wind turbine and the rest of the equipment, that will make globally working in DC possible, are expected to be available at the end of 2023.

The microgrid working in DC supported by the developed management system, allows us to register all the data from the parameters that are being monitored, and to act instantly on the equipment. This enables us to do studies, comparisons and analysis about variation of performance, cost, benefits, and energy losses of the equipment or the grid. All of this, compared to the registers of a hybrid microgrid.

Doing these studies and analysis is part of the future work of this project. To reach this stage, as it has been described in this document, it is necessary to develop and research about SST, power converters and cybersecurity.

TIGON project conclusions have the objective of supporting in the decision-making process of electrical grid operators and directing interventions towards decentralized hybrid microgrids. Nowadays, the lack of DC microgrids prevents them from transforming from a promising solution for distribution networks to a commonly used technology.

All of the above is meant to achieve a positive impact thanks to the project's demonstration in our replicability facilities with the developed technology, and management and cybersecurity system, implemented by network operators and consumers. In addition, another goal is to become the foundation to stablish DC-based microgrids as an optimal solution and future perspectives to improve efficiency during energy generation and make the energy transition easier as stablished by the European Union's decarbonisation objectives.

Acknowledgments

References

1. Gunasekaran, M., Mohamed Ismail, H., Chokkalingam, B., Mihet-Popa, L., Padmanaban, S.: Energy Management Strategy for Rural Communities' DC Micro Grid Power System Structure with Maximum Penetration of Renewable Energy Sources. Appl. Sci. 8, (2018). https://doi.org/10.3390/app8040585
2. Fotopoulou, M., Rakopoulos, D., Trigkas, D., Stergiopoulos, F., Blanas, O., Voutetakis, S.: State of the Art of Low and Medium Voltage Direct Current (DC) Microgrids. Energies. 14, (2021). https://doi.org/10.3390/en14185595
3. Gao, L., Liu, Y., Ren, H., Guerrero, J.M.: A DC Microgrid Coordinated Control Strategy Based on Integrator Current-Sharing. Energies. 10, (2017). https://doi.org/10.3390/en10081116

4. Patterson, B.T.: DC, Come Home: DC Microgrids and the Birth of the "Enernet." IEEE Power Energy Mag. 10, 60–69 (2012). https://doi.org/10.1109/MPE.2012.2212610

5. Bosich, D., Vicenzutti, A., Grillo, S., Sulligoi, G.: A Stability Preserving Criterion for the Management of DC Microgrids Supplied by a Floating Bus. Appl. Sci. 8, (2018). https://doi.org/10.3390/app8112102

6. Saponara, S., Saletti, R., Mihet-Popa, L.: Recent Trends in DC and Hybrid Microgrids: Opportunities from Renewables Sources, Battery Energy Storages and Bi-Directional Converters. Appl. Sci. 10, (2020). https://doi.org/10.3390/app10124388

7. Mishra, S., Viral, R.K.: Chapter 6 - Introduction to hybrid AC/DC microgrids. In: Guerrero, J.M. and Kandari, R. (eds.) Microgrids. pp. 159–189. Academic Press (2022)

8. Aponte-Roa, D.A., Cabarcas, G.D.G., Weaver, W.W.: AC Vs DC Power Efficiency Comparison of a Hybrid Wind/Solar Microgrid. In: 2020 IEEE Conference on Technologies for Sustainability (SusTech). pp. 1–5 (2020)

SNS-Based Secret Sharing Scheme for Security of Smart City Communication Systems

Andrei Gladkov[1][0000-0002-9454-7618], Egor Shiriaev[1][0000-0002-2359-1291],
Andrei Tchernykh[2,3,*][0000-0001-5029-5212], Maxim Deryabin[4][0000-0002-6761-3667],
Ekaterina Bezuglova[5][0000-0002-7608-0452], Georgii Valuev[5][0000-0003-2049-7213],
Mikhail Babenko[1,3][0000-0001-7066-0061], and Sergio Nesmachnow[6][0000-0002-8146-4012]

[1] Faculty of Mathematics and Computer Science, North-Caucasus Federal University, 355017 Stavropol, Russia agladkov@ncfu.ru, eshiriaev@ncfu.ru, mgbabenko@ncfu.ru
[2] Computer Science Department, CICESE Research Center, 22860, Ensenada, Mexico chernykh@cicese.mx
[3] Control/Management and Applied Mathematics, Ivannikov Institute for System Programming, 109004 Moscow, Russia
[4] Computing Platform Lab, Samsung Advanced Institute of Technology, Suwon, 16678, South Korea max.deriabin@samsung.com
[5] North-Caucasus Center for Mathematical Research, North-Caucasus Federal University, 355017 Stavropol eksbezuglova@ncfu.ru, gvvaluev@ncfu.ru
[6] Faculty of Engineering, Universidad de la República, Montevideo 11300, Uruguay sergion@fing.edu.uy
*chernykh@cicese.mx

Abstract. A smart city has a complex hierarchical communication system with various components. It must meet the requirements of fast communication, reliability, and security without compromising data. In the paper, we discuss methods and techniques for increasing the speed and reliability of the mobile ad hoc networks with a sufficient level of security. We consider combining the secret sharing schemes and residual number systems (RNS) as an efficient security mechanism for a smart city dynamic heterogeneous network. We analyze the concept of data transmission based on RNS that divides data into smaller parts and transmits them in parallel, protecting them from attacks on routes by adadaptive multipath secured transmission. Proposed networks have the self-correcting properties that improve the reliability and fault tolerance of the entire system.

Keywords: Smart City, Residue Number System, Secret Sharing Schemes, Distributed Storage System, Reliability, mobile ad hoc network, Communication.

1   Introduction

A smart city is a set of interconnected solutions of Information and Communication Technologies (ICT) and the Internet of Things (IoT) integrated into the management environment of city property and services. As the main assets, various city systems and objects can act as distributed information systems, i.e., power plants, schools, transport,

law enforcement agencies, hospitals, and other public services. The main objective is to improve the living standard and urban service quality. ICT allows to analyze and manage the urban environment in real-time with a quick response. There are many scientific, commercial, and governmental solutions for implementing a smart city concept.

According to Deakin generalized definition [1], a smart city is a city that uses ICT to meet the needs of city residents. It is not only a set of technological solutions but the application of these technologies by local communities.

Let us consider the main hardware components of the smart city network. It consists of many elements, including video surveillance, emergency call systems, biometric systems, city and banking services, intelligent transport, and IoT solutions (Radio Frequency Identification [2], sensors for measuring temperature, illumination, pressure, etc.). The large-scale data sharing in a distributed environment is fraught with data security and privacy issues since data compromise can harm people and the entire system. Another important aspect is reliability. Failures can delay the response of emergency systems, medical, and rescue services. Thus, when building a smart city communication infrastructure, design methods that provide data security at the required level while having high reliability and speed are very important.

To solve this multi-objective problem, we consider the network as a distributed (DCS) rather than a centralized (CCS) computing system. It is well known that for large networks, centralized data processing imposes a large load on the central computing bottleneck slowing down the entire system. More detailed arguments about the positive and negative properties of a decentralized network can be seen in [3–5].

To ensure the security of such a network, we discuss a combination of the Secret Sharing Scheme (SSS) [6] and the Residue Number System (RNS). SSS is cryptographic technique that splits a secret into several shares and distributes them among participants, i.e., $S = \{s_1, s_2, \dots, s_n\}$. In the original SSS, to restore the secret, all n shares are required. In the most used threshold SSS, k shares from n are needed to restore the secret, where $k < n$. RNS is one of the most common non-positional number systems that represents the number in a positional system as a tuple of n numbers $(x_1, x_2, \dots, x_n)$, obtained by dividing numbers into residuals. Among many applications, we could mention the acceleration of operations due to the parallel implementation of basic arithmetic, information integrity control, digital signal processing, etc.

This paper is structured as follows: Section 2 considers data transmission in smart city networks. Section 3 discusses existing approaches to ensure security, as well as the advantages of SSS schemes based on RNS. Section 4 presents the RNS and SSS, as well as the proposed SSS-RNS. Section 5 discusses the SSS-RNS persistent. Section 6 is devoted to the presentation and analysis of the obtained experimental results. Section 7 presents the main conclusions and future work.

2   Data transmission in smart city networks

A wireless ad hoc network (WANET) and MANET are important concepts of smart city communication widely used for ensuring self-configuring and dynamic connectivity between sensors, humans, and devices that send and receive information.

Lobo et al. [7] study the Quality of Service (QoS) of MANET in smart city networks with an emphasis on healthcare. Several frameworks were considered that improve the quality of transmission in MANET, as well as individual elements, such as video signal transmission. Cardone et al. [8] discuss the MANET and Wireless Sensor Network (WSN) hybrid network for fast data collection in the smart city. The authors provide a transmission protocol based on modern data transmission standards considering IPv6. Pandey et al. [9] study methods to improve the reliability of MANET networks and propose a method of self-healing knots.

In this work, our goal is to increase the speed and reliability of the MANET communication with a sufficient level of security. To achieve this goal, we propose the use of RNS in MANET. In the original version, MANET solves the minimax optimization problem of finding the shortest path in the network. The smart city network can be represented as a directed graph, where the vertices are the communication nodes (devices in the network), and the arcs are the data transmission between the nodes. Let's establish that $G(V, E)$ – smart city network graph, with flow $v_0 \in V$. With path cost function $c: E \to R$. We assume that the set of vertices V split into two non-overlapping subsets V_A and V_B ($V_A \cup V_B = V, V_A \cap V_B = \emptyset$). Now we fix a pair of mappings:

$$s_A: v \to V_G(v) \ for \ v \in V_A \backslash \{v_0\}; \ s_B: v \to V_G(v) \ for \ v \in V_B \backslash \{v_0\};$$

where $V_G(v)$ – the set of ends of all arcs outgoing from a vertex v. We define the following subgraph $T_s = (V, E_s)$, generated by a set of arcs of the form $(v, s_A(v))$ and $(v, s_B(V))$. This subgraph has the property that for some given vertex $w \in V$, or there is a way $P_T, (w, v_0)$ from w to v_0 or there is no such path. In the latter case, moving from w along the outgoing arcs of the digraph T_s, uniquely get to some oriented cycle C_w. For an arbitrary vertex $w \in V$ define the value $\tilde{c}(s_A, s_B, w)$ as the sum of the costs of the arcs of the path $P_T, (w, v_0)$, if such a path exists T_s; if the path does not exist $P_T, (w, v_0)$ in T_s value $\tilde{c}(s_A, s_B, w)$ we will assume equal ∞ or $-\infty$ depending on the positivity and negativity of the sum of the costs of the arcs of the oriented cycle C_w; if the sum of the costs of the arcs of an oriented cycle C_w equals zero, then the value $\tilde{c}(s_A, s_B, w)$ equals the sum of the costs of the arcs of the path connecting the vertex w with cycle C_w. That is, a problem of the form $F(w) = \min_{s_A} \max_{s_B} \tilde{c}(s_A, s_B, w)$.

RNS allows us to approach the solution of this problem with less iteration. If, when solving the Minimak problem for one path, it is necessary to refine the optimal solutions up to one at each iteration, then in the case of RNS it is necessary and sufficient to refine such solutions to equal the number of modules in the RNS system. Thus, the use of RNS makes it possible to solve an optimization problem for a multiobjective problem. Consider the data transfer model (Fig. 1-2). It is known that MANET transmits using devices located on the infrastructure-less, distributed wireless networks without static located transmission stations.

It is an interesting and promising solution providing communication of a big variety of devices, from mobile devices to personal cars, from smart devices to public transport, etc. In addition, a smart city infrastructure also contains static nodes, such as data centers, storage, decision centers, etc. For such a dynamic heterogeneous network, we propose the concept of parallel data transmission based on RNS that divides data into
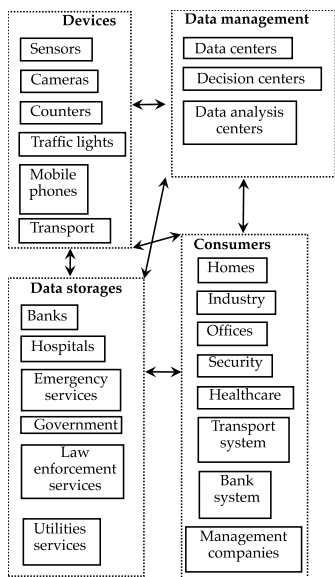
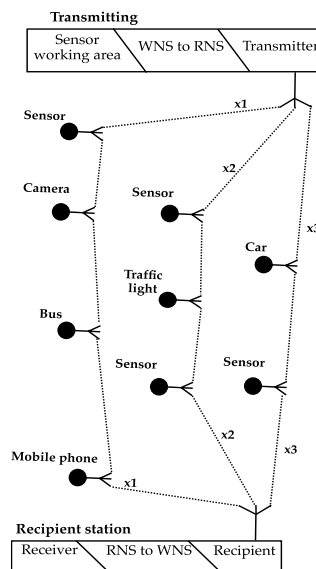**Fig. 1.** General model of data transmission

Fig. 2. Data transfer model

smaller parts and transmit them in parallel. The self-correcting properties of RNS can improve the reliability and fault tolerance of the entire system [10–13].

Let us consider a conceptual model described above (Fig. 1). Here, we group the elements of a smart city according to common features. They can be separated from each other by large distances and distributed like data management modules.

However, this model gives a general idea of the transmission network complexity. Each group of components is connected to other groups, and control personnel can communicate to any device on the network. In such a data transfer model, MANET provides a definite advantage. Any device, such as a sensor, can send data to a destination, transmitting it through other devices within the network. Let us take a closer look at how the smart sensor transmits data over the network to the intended destination.

Fig. 2 shows the data transfer model from the sensor to the recipient. The recipient can be a data warehouse, decision center, data processing center, cloud data analysis, etc. RNS allows you to transfer data in the MANET network in parallel breaking the message into several parts. It improves the system's speed since such parts are smaller than the message itself. The model of the data transmission packet is shown in Fig. 3.

Thus, the receiver collects pieces of information and combines them. The application knows how many parts have arrived and how many parts should arrive. If $k < n$ parts have arrived, the receiver recovers the entire message. Otherwise, it waits a certain time, and the packet is requested again or ignored. RNS is known to have self-correcting

properties. This allows to recover the message if one or several parts are lost or intentionally changed. As a result, we can get a network with increasing speed and reliability.
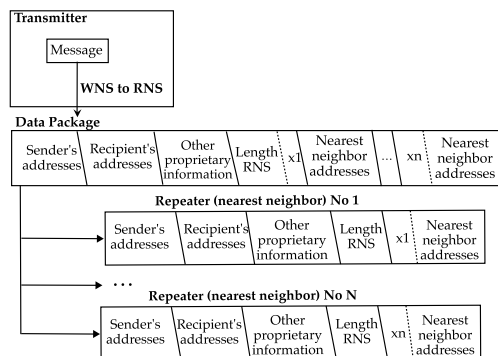

Fig. 3. Data packet model

3   DCS security: challenges and solutions

Our main approach is to use SSS to ensure the security of data transmission. Let us discuss and compare well-known solutions for providing reliability and security of distributed data storage and transmission. Four main methods are used to ensure reliability [14]: Replication, Erasure code, Erasure code modifications, and Error correction code.

Chang et al. [15] presented a modified data replication method, providing a high encoding and decoding speed. But it requires additional cryptographic primitives to ensure security and has a high redundancy compared to erasure codes.

Many different modifications of erasure codes have been proposed to create reliable methods for distributed data storage. The joint use of error correction and erasure codes maintains system performance and minimizes the load on the data transmission network when recovering lost fragments [16,17].

Erasure codes based on the Redundant Residue Number System (RRNS) [18] allow data to be processed in the encoded form [11]. So, it can be used both in the design of low-power wireless data transmission devices and distributed storage systems.

Secure distributed data storage and transmission systems are based on the use of cryptographic primitives - symmetric encryption algorithms (AES) and digital signatures based on RSA (Rivest, Shamir, Adleman) [19]. The advantages of these approaches are high speed of encryption and decryption and low data redundancy. The disadvantage is that an error in the encrypted data leads to its loss. To eliminate this shortcoming, the use of additional mechanisms for accessing data for a long time is required [20].

When building secure and reliable cloud storage, the following methods are used:

elliptic cryptography and erasure codes [21,22], access structures [23,24], error correction codes [25,26], graph-based algorithms and modified data replication algorithm [27], attribute-based encryption [28], etc.

An alternative approach is to use recovery codes [17], erasure codes and error correction codes based on RRNS [16]. However, recovery codes and erasure codes do not allow encoded data processing. Homomorphic calculations process encoded data without additional computational costs for decoding.

A significant breakthrough in the field of homomorphic computing came from the work of Gentry [29]. The authors proposed a fully homomorphic scheme to perform both addition and multiplication. The main disadvantages of this algorithm are significant data redundancy and lack of control over the results of arithmetic operations.

Particular attention should be paid to the distributed data storage model proposed in [30], guaranteeing security, privacy, homomorphism, reliability, and scalability. The authors propose two approaches to building systems based on homomorphic access structures in RRNS, with RRNS moduli being used as secret keys stored by users. Data processing leads to an exponential increase in the load on the network and memory, which makes this model inapplicable in practice in modern conditions.

Access structures [31, 32] ensure data security and confidentiality. RRNS implements the same functionality as the Mignotte scheme but allows you to control the results of data processing. Distributed cloud storage is also characterized by collusion risks [33]. Several approaches have been developed to prevent cloud collusion [23]. As mentioned above, the non-stationarity of the cloud environment reduces the efficiency, performance, reliability, and security of the system. The adaptive paradigm reduces uncertainty but is rarely used in cloud computing [33].

Let us consider the following scenario. The user has sensitive data and decides not to store it in single cloud storage. He divides them into several parts and stores them in different clouds. There are several types of security threats in this scenario.

Deliberate threats include unauthorized access to information, interception, falsification, hacker attacks, etc., in one or more clouds.

Random threats include errors, crashes, etc. They can lead to the loss of one or more pieces of data, inconsistencies between different copies of the same data, and/or the inability to restore the original data. Collusion threats are an illegal agreement between two or more adversaries (in the context of multi-cloud storage, the adversaries are cloud services) to gain full access to personal data. Cryptographic protocols can be used to mitigate the risks of deliberate threats, but this is not enough for random threats. To improve the security and reliability of storage systems, distributed storage mechanisms based on access structures and error correction codes are used, which distribute data across multiple CSPs and minimize the likelihood of theft or loss of information in the event of deliberate and accidental threats. Examples of such mechanisms are RACS [34], DepSky [35], and RRNS, using Approximate Rank RRNS (AR-RRNS) [25].

Let us consider four schemes for data sharing (Fig. 4). The first thresholding structure (Fig. 4.a) is a classic scheme where each store or channel has one share of data of the same size. An example of such a repository is DepSky [35]. The second threshold access structure (Fig. 4.b) is an extension of the previous scheme, see Miranda-Lopez et al. [33], where each store has the same number of short shares. In both schemes, data

can be recovered if the number of available shares exceeds a given threshold. Data splitting according to the traditional weighted access threshold structure means that the storages have one share of different sizes [6] (Fig. 4.c).

Babenko et al. [12] proposed a weighted threshold access structure WA-RRNS (Weighted Access – RRNS) based on a redundant residue number system, where each store has several short shares (Fig. 4.d). In the same work, a more efficient implementation WA-AR-RRNS was proposed, using an approximate value of the rank of the number represented in the RRNS to speed up the decoding procedure. With this approach, data can be recovered if and only if the sum of the share sizes is not less than a given threshold weight.
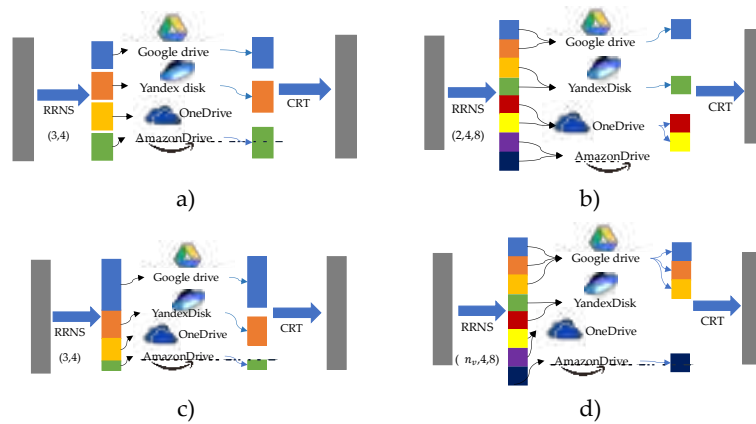

Fig. 4. Threshold access structure: a) One share per storage; b) Several short shares for each storage; c) Weighted threshold access structure (one share of different sizes per storage); d) Weighted threshold access structure (different number of shares of the same size per storage).

In the next sections, we show how the size and the total number of shares can change the reliability, security level, speed, etc. of data storage and transmission. These structures reduce the load on the transmission network compared to the classical replication mechanism and reduce the cost.

4   Residue Number System and Secret Sharing

RNS is one of the most common non-positional number systems [32]. Each specific RNS is determined by a system of coprime bases $\{p_1, p_2, \ldots, p_n\}$ and presentation range $P = \prod_{i=1}^{n} p_i$. Positional number X such that $0 \leq X < P$, in this system is represented as a tuple of n numbers $(x_1, x_2, \ldots, x_n)$, obtained by the formula:

$$x_i = X \bmod p_i , i = 1, 2, \ldots, n.$$

RNS has many applications, among which we can note the acceleration of operations due to the parallel implementation of basic arithmetic operations, information integrity control, and digital signal processing.

Modular calculus is based on the Chinese Remainder Theorem (CRT) [25], according to which the number X, $0 \leq X < P$, represented by remnants $(x_1, x_2, \ldots, x_n)$ in the system of moduli $\{p_1, p_2, \ldots, p_n\}$, then it can be uniquely calculated by the formula

$$X = \left| \sum_{i=1}^{n} \left| P_i^{-1} \right|_{p_i} P_i x_i \right|_P,$$

where $P_i = \frac{P}{p_i}$, $\left| P_i^{-1} \right|_{p_i}$ – multiplicative inversion P_i modulo p_i for $i = 1,2, \ldots, n$. This method is called the CRT method or the Garner method. However, it is computationally complex, since it requires division by a sufficiently large number P. It is worth noting that there are many well-developed methods for converting numbers back from RNS to a positional system, together with an efficient implementation of calculating the remainder of the division, make this system suitable for use as the basics of a secret sharing scheme [12, 23, 25].

Let us consider SSSs using Shamir's threshold scheme as an example [24]. As mentioned above, threshold schemes allow you to restore the secret k the parties, and $k < n$. The idea of this scheme is that the secret is represented as a polynomial $k - 1$ degrees. Then, to interpolate the resulting polynomial, it is necessary k points, and the polynomial can be divided into n shares. Then the secret sharing process is as follows. Let's say we need to share a secret M on n shares. To do this, take a simple number $p < M$, which specifies the final size field p. The following polynomial is constructed over this field:

$$F(x) = (a_{k-1} x^{k-1} + a_{k-2} x^{k-2} + \cdots + a_1 x + M) \bmod p$$

where $a_{k-1}, a_{k-2}, \ldots, a_1$ – random numbers that are only known when the secret is shared.

The secret recovery occurs due to the calculation of the Lagrange interpolation polynomial according to the following formula:

$$F(x) = \sum_i l_i(x) y_i \bmod p; l_i(x) = \prod_{i \neq j} \frac{x - x_j}{x_i - x_j} \bmod p,$$

where (x_i, y_i) – polynomial point coordinates. In addition, there is a limitation - all calculations are performed only in the final field p. In this scheme, an integer polynomial is used. Despite the low redundancy and high scalability, the field space p is not used efficiently.

Let us consider a scheme where a free coefficient represents information. This scheme was developed by Hugo Krawczyk in 1997 and, as in the case of the Shamir scheme, bears the name of its creator. Krawczyk scheme [36] appears to be a sharing scheme (k, n)- secret. It has a secret distribution protocol S among k participants randomly. In this case, the recovery of the secret is possible from k shares for a fixed value k, $1 \leq k \leq n$, while $k - 1$ shares do not allow you to recover the secret S. Thus, this scheme is a threshold.

Let us consider the information dissemination algorithm designated as IDA. This algorithm works for parameters n (total number of shares) and r (required number of shares for recovery). It includes a secure encryption function with a private key, which is designated as ENC. In addition, the algorithm implements a perfect (k, n)- secret sharing scheme, denoted as PSS. It is also worth noting that the space of both the secret and the message in this scheme is the same as for the encryption function ENC.

Share algorithm:

1. Choosing a random encryption key K; secret encryption S with ENC turnkey K, then $E = \text{ENC}_K(S)$.
2. IDA shares the encrypted E on n fragments, then $- E_1, E_2, \ldots, E_n$.
3. Further PSS, create n key shares $K_1, K_2, \ldots, K_n$.
4. Shares are sent $P_{i_j, j} = 1, 2, \ldots, n$ to each participant, as well as $S_{i_j} = (E_{i_j}, K_{i_j})$. Shares K_i sent P_i in encrypted form.

Recovery algorithm:

1. k participants combine their shares $P_{i_j, j} = 1, 2, \ldots, k$ together with $S_{i_j} = \left(E_{i_j}, K_{i_j}\right)$
2. Using IDA, restoration is underway E from assembled parts $E_{i_j} = 1, 2, \ldots, k$.
3. Further PSS restores the key K from $K_{i_j} = 1, 2, \ldots, k$.
4. Using K, decrypted E, after which it recovers S.

Thus, the scheme is a computationally secure, ENC is a secure encryption function, and PSS is the ideal secret sharing scheme. Every share S_i has a length $|S|_k + |K|$. Evidence of this, as well as confirmation of the secrecy of the circuit, is given in [36].

In this section, RNS has been considered, as well as two threshold SSSs. Despite the obvious advantages of these schemes (low redundancy, scalability, flexibility), they have several disadvantages, such as the inability to add new participants without restoring the secret and re-sharing it. As mentioned above, this circumstance is unsatisfactory for building a smart city. The advantages of SSS-RNS schemes, as well as these schemes themselves, will be discussed in more detail in the next section.

5   Secret Sharing System with Residue Number System

In this section, we introduce the basic concepts used in constructing SSS based on RNS. The most famous SSSs on RNS are considered - the Asmuth-Bloom and Mignotte. The main approaches used for SSS security analysis and their extension for SSS on RNS are presented.

Let us consider SSS using RNS and RRNS. Let each participant in the scheme have a unique number or identifier, the entire set of which we will call the universal set of numbers and denote U (in the simplest case $U = \{1, 2, \ldots, n\}$, where n – number of participants in the scheme). The set of allowed coalition numbers is called the allowed subset of the set U and is denoted by I. On the other hand, an unresolved subset is a subset $\tilde{I}$ numbers of members of any coalition that does not have the right to restore the secret. Scope of the secret S in this case, we will call the set that combines all possible values of the secret s.

In the Asmuth-Bloom scheme, p_0 is selected first. It defines the set of all possible secrets. Arbitrary secret s should be chosen so that $s \in Z_{p_0}$. Further base system $p_1 < p_2 < \cdots < p_k < p_{k+1} < \cdots < p_n$ is chosen, so that $\prod_{i=1}^{k} p_i > p_0 \prod_{i=0}^{k-2} p_{n-i}$. The last inequality is usually called the Asmuth-Bloom condition. At the stage of sharing the secret, a random number is generated r such that $s' = s + rp_0 < \prod_{i=1}^{k} p_i$. Secret s is divided so that $s_i = s' \bmod p_i$ is a share for member i, where $i = 1, 2, \ldots, n$. In this

method, any allowed set of participants with numbers from I can uniquely restore the secret; wherein $|I| = m \geq k$. First, using the Chinese remainder theorem, the position number is calculated x based on the modular representation $(s_{i_1}, s_{i_2}, \ldots, s_{i_m})$ in RNS with bases $p_{i_1}, p_{i_2}, \ldots, p_{i_m}$, where $i_j \in I$ for all $j = 1,2, \ldots, m$. The original secret is restored as the remainder of the division of the number x on p_0: $s = x \bmod p_0$.

To discuss the security of the Asmuth-Bloom scheme, consider the shares of some unresolved coalition of participants with numbers from $\breve{I}$. Then $|\breve{I}| \leq k - 1$, let $P = \prod_{i=1}^{k} p_i$ and $\tilde{P} = \prod_{i \in I} p_i$. All that will be known in this case is the number $\tilde{s} = s' \bmod \tilde{P}$. According to the Asmuth-Bloom condition $P/\tilde{P} > p_0$ and $(\tilde{P}, p_0) = 1$, then the set of numbers $\tilde{s}$, such that $\tilde{s} \equiv s' \bmod \tilde{P}$ and $\tilde{s} < P$, covers all residue classes modulo p_0. Thus, as shown in [31], a coalition uniting less than k shares of the secret, does not receive any useful information about the secret, which indicates the strength of the scheme. However, its serious drawback is the increase in the size of the shares of the secret relative to the size of the secret itself, which leads to a significant excess of output information. The following threshold secret sharing scheme is free from this disadvantage., (k, n)- Mignotte threshold circuit.

In Mignotte's scheme, the base system $p_1 < p_2 < \cdots < p_k < p_{k+1} < \cdots < p_n$ is chosen as a Mignotte sequence, the numbers which satisfy the inequality
$$\alpha = \prod_{i=0}^{k-2} p_{n-i} < \prod_{i=1}^{k} p_i = \beta.$$

To achieve stamina secret s is selected. At the same time, for an arbitrarily secret s from the gap (α, β) numbers $s_i = s \bmod p_i$, there are secret shares for each participant with a number i, where $i = 1,2, \ldots, n$. Any allowed set of participants with numbers can restore the secret. I, wherein $|I| = m \geq k$. Secret s is calculated using CRT number based $(s_{i_1}, s_{i_2}, \ldots, s_{i_m})$, presented in RNS with grounds $p_{i_1}, p_{i_2}, \ldots, p_{i_m}$, where $i_j \in I$ for all $j = 1,2, \ldots, m$. To ensure a security, Mignotte sequences with a large value $(\beta - \alpha)/\beta$ should be used [32]. This scheme is not stable, but it has practical applications due to reducing the amount of output data [37].

Below, we consider the concepts that play an important role in the theory of the absolute security of a circuit. Based on this approach, we can estimate the entropy of secret sharing schemes. In the absence of information about the shares of the secret, we denote the information entropy as $H(s \in S)$, where s there is a secret distributed in the secret definition area S. In this case, the entropy is maximum since only public information is considered. The entropy of the secret is denoted as $H(s \in S | s_i : i \in I)$, when the shares of the secret belong to a certain known set $I \subseteq U$. If I is the set of numbers of the allowed subset of participants, then $H(s \in S | s_i : i \in I) = 0$ since in this case, the secret must be correctly restored. For the opposite case, in which an unresolved set of participants is combined, it is important to achieve the maximum conditional entropy. This condition leads to the formulation of the scheme perfection condition based on the probabilistic approach. At the same time, the most important concept of the SSS theory is the decrease of the uncertainty, which is understood as the quantity
$$\Delta(s_i : i \in I) = H(s \in S) - H(s \in S | s_i : i \in I).$$

The decrease of uncertainty in the case where I is the set of numbers of the allowed subset of participants is equal to the unconditional entropy of the domain of the secret:

$\Delta(s_i : i \in I) = H(s \in S)$. Now let the set of participants be unresolved. A secret sharing scheme is perfect if for all unresolved subsets of numbered participants $\tilde{I}$ should
$$\Delta(s_i : i \in \tilde{I}) = 0.$$

However, as noted earlier, to analyze the security of SSS based on RNS, an additional concept to study the properties of SSS of this type by conventional methods [38] was introduced. Therefore, the concept of an asymptotically perfect SSS was introduced. The scheme is asymptotically perfect if, for all unresolved subsets of participants with numbers $\tilde{I}$ and for any $\varepsilon > 0$, there is such p, that, for $p_0 < p_1 < \cdots < p_n, p_i > p$ $(i = 0, 1, \ldots, n)$, and $\Delta(s_i : i \in \tilde{I}) < \varepsilon$.

The question of how exactly it is necessary to choose the parameters of the SSS on the RNS so that it has the asymptotic perfection property remains open. The work [38] shows the asymptotic perfection of the Asmuth-Bloom scheme when using "sufficiently close" coprime as the RNS base system. The work [37] considers so-called compact sequences of coprime numbers with an initial value p_0 when $p_n < p_0 + p_0^{\theta}$ for some real number $\theta \in (0,1)$.

Compact sequences of coprime numbers play an important role in studying the security of secret sharing schemes. The use of these sequences as a system of RNS bases makes it possible to build efficient and stable schemes, which is due to the proximity of numbers on the number line. The work [37] considers, it is shown that the Asmuth-Bloom scheme is asymptotically perfect when using compact sequences as the RNS base system. It should be noted that the Mignotte scheme is not asymptotically perfect. However, a robustness study would not be complete without an analysis of the computational robustness of the methods. In the future, we will assume that it is precisely the compact sequence of coprime numbers that are used as the bases.

Let us now turn to the concept of computational stability of a circuit. Let at some point in time some analysts managed to collect shares of an unresolved subset of participants with numbers $\tilde{I}$ for some SSS. The task of the analyst, in this case, is to recover the secret based on the available data. In a real situation, many S can be divided into two subsets. First subset S_1 will consist of all secret options that do not fit a secret role given the known data. Second subset S_2 will contain all remaining possible secret options. For example, if the Mignotte scheme knows the share of the secret s_j for module $p_j, 0 \le j \le n$, then the secret must satisfy the condition: $s \equiv s_j \bmod p_j$. Therefore, in this case $S_1 = \{s : s \in S \land s \not\equiv s_j \bmod p_j\}$ and $S_2 = \{s : s \in S \land s \equiv s_j \bmod p_j\}$. Note that if the SSS is perfect, then for it $S_1 = \emptyset$ and $S_2 = S$.

Thus, to find the original secret, it is necessary to go through all the options included in S_2 and the stability of the circuit depends on the cardinality of this set and on the computational complexity of exhaustive enumeration. It is necessary to generate the scheme parameters so that the analyst cannot, using modern computing resources, pick up the secret in a reasonable time. A circuit that meets these conditions will be called a computational rack. As a measure of computational security, we take the cardinality of the set S_2: $f(\tilde{I}) = |S_2|$.

For the Asmuth-Bloom scheme, considering its asymptotic perfection and the Asmuth-Bloom condition, $f(\tilde{I}) = |S| = |Z_{p_0}| = p_0$ for anyone $\tilde{I}$. It is easy to see that not all secure circuits are computationally secure. But, on the other hand, computationally

secure circuits are not always perfect. The most important in a practical sense is computational stability.

6　Modeling

In this section, an experimental study of the system considered above will be considered. The modeling was done by comparing two implementations of SSS-RNS, and is given: the Asmuth-Bloom implementation and the proposed implementation in section 5 (RNS implementation). The study was conducted as follows: the number of modules is selected from 4 to 6; the input is images of various sizes from 6 MB to 146 MB. The study will take into account the following characteristics: coding and decading time, redundancy in coding and decading. Let's consider the obtained results (Fig. 5).
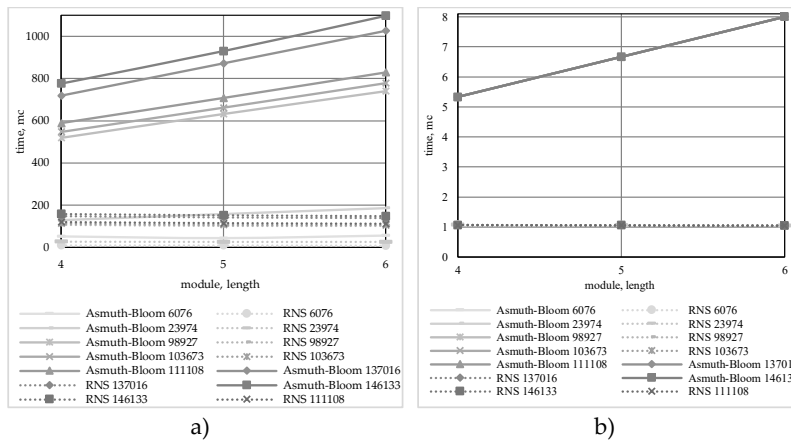

a)　　　　　　　　　　　　　　　　b)

Fig. 5. a) Encoding Performance. b) Coding Redundancy

Analyzing the obtained results, we can say that the proposed implementation has a high performance. The encoding time of all images is in the range from 1 to 180 ms. When as the Asmuth-Bloom implementation is between 40 and 1100 ms. This result is achieved due to the applied RNS methods in our implementation. It allows you to reduce computational complexity due to a larger number of precomputed constants. However, because of this, it is also necessary to conduct studies of the redundancy that appears when encoding information. Consider this study (Fig. 5b).

Analyzing this illustration, we can observe that the redundancy of the proposed implementation remains approximately at the same level, while the redundancy of the Asmuth-Bloom implementation is 5 times greater and increases with the number of modules used. Thus, in addition to efficiency in terms of performance, the proposed implementation also has better coding redundancy properties. When conducting decadence, similar results were obtained (Fig.6)

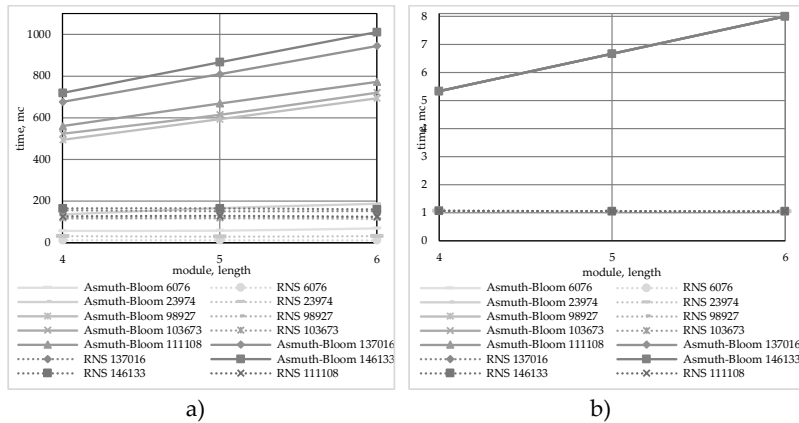a)   b)

Fig. 6. a) Decoding Performance. b) Decoding Redundancy

Considering the result obtained for decoding, we can say that similar results were obtained, as in coding. The proposed RNS implementation also has performance and redundancy advantages.

Thus, we can say that using the proposed implementation of SSS-RNS, it is possible to increase the speed of the system, as well as the redundancy of the processed data. However, this requires a larger number of precomputed constants, which is a manageable disadvantage when using a static set of RNS modules, but if you need to change the set of these modules, all precomputed values must be recalculated for the new set.

7   Conclusions

In this work, we study mechanisms for protecting and accelerating smart city communication systems. Security mechanisms based on different methods are considered. We show that the most suitable method for a smart city dynamic network is SSS. RNS can be used as an adaptive mechanism to increase security and reliability through effective correcting management. We propose MANET with RNS to improve the quality of service for each application used in the self-configuring and dynamic connectivity heterogeneous networks. The main advantage of RNS is the versatility of the data representation. On the one hand, RNS is a highly efficient tool for error-resistant coding of information based on the corrective abilities of redundant RNS. On the other hand, it is the basis for designing secret sharing schemes, including efficient computationally secure schemes. The proposed approach can increase the network's resistance to attacks of various kinds and the transmission confidentiality, along with high reliability using multipath routing. This approach does not have the disadvantages of traditional encryption transmission methods: the key management problem is solved by using SSS, and the problem of possible attacks on routes is solved by using an adaptive multipath transmission.

References

1. Deakin, M., Al Waer, H.: From intelligent to smart cities. Intell. Build. Int. 3, 3, 140–152 (2011). https://doi.org/10.1080/17508975.2011.586671.
2. Weinstein, R.: RFID: a technical overview and its application to the enterprise. IT Prof. 7, 3, 27–33 (2005). https://doi.org/10.1109/MITP.2005.69.
3. Weissman, J.B.: Gallop: The Benefits of Wide-Area Computing for Parallel Processing. J. Parallel Distrib. Comput. 54, 2, 183–205 (1998). https://doi.org/10.1006/jpdc.1998.1487.
4. Lange, D.B.: Mobile objects and mobile agents: The future of distributed computing? Presented at the (1998). https://doi.org/10.1007/BFb0054084.
5. Datla, D. et al.: Wireless distributed computing: a survey of research challenges. IEEE Commun. Mag. 50, 1, 144–152 (2012). https://doi.org/10.1109/MCOM.2012.6122545.
6. Attasena, V. et al.: Secret sharing for cloud data security: a survey. VLDB J. 26, 5, 657–681 (2017). https://doi.org/10.1007/s00778-017-0470-9.
7. Lobo, P. et al.: Quality of Service for MANET based smart cities. Int. J. Adv. Comput. Eng. Netw. 5, 2, (2017).
8. Cardone, G. et al.: Effective collaborative monitoring in smart cities: Converging MANET and WSN for fast data collection. In: Proceedings of ITU Kaleidoscope 2011: The Fully Networked Human? - Innovations for Future Networks and Services (K-2011). pp. 1–8 IEEE, Cape Town, South Africa (2011).
9. Pandey, J. et al.: Novel scheme to heal MANET in smart city network. In: 2016 3rd MEC International Conference on Big Data and Smart City (ICBDSC). pp. 1–6 IEEE (2016). https://doi.org/10.1109/ICBDSC.2016.7460339.
10. Shiryaev, E. et al.: Performance Impact of Error Correction Codes in RNS with Returning Methods and Base Extension. In: 2021 International Conference Engineering and Telecommunication (En&T). pp. 1–5 IEEE (2021). https://doi.org/10.1109/EnT50460.2021.9681756.
11. Babenko, M. et al.: Algorithm for Constructing Modular Projections for Correcting Multiple Errors Based on a Redundant Residue Number System Using Maximum Likelihood Decoding. Program. Comput. Softw. 47, 8, 839–848 (2021). https://doi.org/10.1134/S0361768821080089.
12. Babenko, M. et al.: RRNS Base Extension Error-Correcting Code for Performance Optimization of Scalable Reliable Distributed Cloud Data Storage. In: 2021 IEEE International Parallel and Distributed Processing Symposium Workshops (IPDPSW). pp. 548–553 IEEE (2021). https://doi.org/10.1109/IPDPSW52791.2021.00087.
13. Tay, T.F., Chang, C.-H.: A new algorithm for single residue digit error correction in Redundant Residue Number System. In: 2014 IEEE Int. Symposium on Circuits and Systems (ISCAS). pp. 1748–1751 IEEE (2014). https://doi.org/10.1109/ISCAS.2014.6865493.
14. Nachiappan, R. et al.: Cloud storage reliability for Big Data applications: A state of the art survey. J. Netw. Comput. Appl. 97, 35–47 (2017). https://doi.org/10.1016/j.jnca.2017.08.011.
15. Chang, F. et al.: Bigtable: A Distributed Storage System for Structured Data. ACM Trans. Comput. Syst. 26, 2, 1–26 (2008). https://doi.org/10.1145/1365815.1365816.
16. Dimakis, A.G. et al.: Network Coding for Distributed Storage Systems. IEEE Trans. Inf. Theory. 56, 9, 4539–4551 (2010). https://doi.org/10.1109/TIT.2010.2054295.
17. Lin, S.-J. et al.: Novel Polynomial Basis and Its Application to Reed-Solomon Erasure Codes. In: 2014 IEEE 55th Annual Symposium on Foundations of Computer Science. pp. 316–325 IEEE (2014). https://doi.org/10.1109/FOCS.2014.41.

18. Ye, R. et al.: RESIDENT: a reliable residue number system-based data transmission mechanism for wireless sensor networks. Wirel. Networks. 24, 2, 597–610 (2018). https://doi.org/10.1007/s11276-016-1357-1.
19. Stergiou, C. et al.: Secure integration of IoT and Cloud Computing. Futur. Gener. Comput. Syst. 78, 964–975 (2018). https://doi.org/10.1016/j.future.2016.11.031.
20. Lee, B.-H. et al.: Data security in cloud computing using AES under HEROKU cloud. In: 2018 27th Wireless and Optical Communication Conference (WOCC). pp. 1–5 IEEE (2018). https://doi.org/10.1109/WOCC.2018.8372705.
21. Zhou, S. et al.: ESDR: an efficient and secure data repairing paradigm in cloud storage. Secur. Commun. Networks. 9, 16, 3646–3657 (2016). https://doi.org/10.1002/sec.1571.
22. Hsiao-Ying Lin, Tzeng, W.-G.: A Secure Erasure Code-Based Cloud Storage System with Secure Data Forwarding. IEEE Trans. Parallel Distrib. Syst. 23, 6, 995–1003 (2012). https://doi.org/10.1109/TPDS.2011.252.
23. Tchernykh, A. et al.: AC-RRNS: Anti-collusion secured data sharing scheme for cloud storage. Int. J. Approx. Reason. 102, 60–73 (2018). https://doi.org/10.1016/j.ijar.2018.07.010.
24. Shamir, A.: How to share a secret. Commun. ACM. 22, 11, 612–613 (1979). https://doi.org/10.1145/359168.359176.
25. Chervyakov, N. et al.: AR-RRNS: Configurable reliable distributed data storage systems for Internet of Things to ensure security. Futur. Gener. Comput. Syst. 92, 1080–1092 (2019). https://doi.org/10.1016/j.future.2017.09.061.
26. Celesti, A. et al.: Adding long-term availability, obfuscation, and encryption to multi-cloud storage systems. J. Netw. Comput. Appl. 59, 208–218 (2016). https://doi.org/10.1016/j.jnca.2014.09.021.
27. Shen, P. et al.: SpyStorage: A Highly Reliable Multi-Cloud Storage with Secure and Anonymous Data Sharing. In: 2017 International Conference on Networking, Architecture, and Storage (NAS). pp. 1–6 IEEE (2017). https://doi.org/10.1109/NAS.2017.8026878.
28. Radha Devi, G., Kumar, A.: DROPS: Division and Replication of Data in Cloud for Optimal Performance and Security. Adv. Math. Sci. J. 9, 7, 5075–5083 (2020). https://doi.org/10.37418/amsj.9.7.73.
29. Gentry, C.: Computing arbitrary functions of encrypted data. Commun. ACM. 53, 3, 97–105 (2010). https://doi.org/10.1145/1666420.1666444.
30. Gomathisankaran, M. et al.: HORNS: A homomorphic encryption scheme for Cloud Computing using Residue Number System. In: 2011 45th Annual Conference on Information Sciences and Systems. pp. 1–5 IEEE (2011). https://doi.org/10.1109/CISS.2011.5766176.
31. Asmuth, C., Bloom, J.: A modular approach to key safeguarding. IEEE Trans. Inf. Theory. 29, 2, 208–210 (1983). https://doi.org/10.1109/TIT.1983.1056651.
32. Mignotte, M.: How to Share a Secret. In: Cryptography. pp. 371–375 Springer Berlin Heidelberg, https://doi.org/10.1007/3-540-39466-4_27.
33. Miranda-López, V. et al.: Experimental Analysis of Secret Sharing Schemes for Cloud Storage Based on RNS. CCIS, v. 796, 2018. https://doi.org/10.1007/978-3-319-73353-1_26
34. Abu-Libdeh, H. et al.: RACS. In: Proceedings of the 1st ACM symposium on Cloud computing - SoCC '10. p. 229 ACM Press, New York, New York, USA (2010). https://doi.org/10.1145/1807128.1807165.
35. Bessani, A. et al.: DepSky. ACM Trans. Storage. 9, 4, 1–33 (2013). https://doi.org/10.1145/2535929.
36. Krawczyk, H.: Secret Sharing Made Short. In: Advances in Cryptology — CRYPTO' 93. pp. 136–146 Springer Berlin, Heidelberg. https://doi.org/10.1007/3-540-48329-2_12.
37. Barzu, M. et al.: Compact sequences of co-primes and their applications to the security of CRT-based threshold schemes. Inf. Sci. (Ny). 240, 161–172 (2013). https://doi.org/10.1016/j.ins.2013.03.062.
38. Quisquater, M. et al.: On the Security of the Threshold Scheme Based on the Chinese Remainder Theorem. Presented at the (2002). https://doi.org/10.1007/3-540-45664-3_14.

IoT system for thermographic data acquisition of photovoltaic installations.*

Leonardo Cardinale-Villalobos[1][0000−0002−9649−6017], Luis Antonio Solís-García[2][0000−0003−0507−1425], and Luis Alonso Araya-Solano[3][0000−0002−7941−821X]

[1] Costa Rica Institute of Technology, San Carlos, Costa Rica
lcardinale@tec.ac.cr
[2] Costa Rica Institute of Technology, San Carlos, Costa Rica
antsolis04@estudiantec.cr
[3] Costa Rica Institute of Technology, Cartago, Costa Rica
luaraya@tec.ac.cr
https://www.tec.ac.cr/

Abstract. Infrared thermography (IRT) has been widely used to diagnose photovoltaic installations, however, its effectiveness needs to be improved to contribute to greater energy efficiency in Smart Cities. This research shows a solution that creates a database (DB) of IRT information, through an IoT solution that allows the process to be automated and accessed remotely. The functionality and accuracy of the system was validated in a real PV plant through an experiment inducing conditions that generate hot spots obtaining a temperature measurement error of less than 4 °C. During the investigation, 1.777 thermograms were generated and the ability to detect hot spots due to soiling, partial shading and short circuits in the module was verified. The DB generated by this solution will be used to establish better fault detection criteria for IRT, which is of high interest to thermographers and will benefit the users of distributed PV installations in Smart Cities around the world.

Keywords: IoT Applications · Photovoltaic· Infrared Thermography · Image Acquisition Systems

1   Introduction

For several years there has been a common trend that seeks the maximum possible use of renewable energy sources. Because of this, smart cities are characterized by the approach of strategies that incorporate distributed generation schemes that also consider an efficient use of energy and maximum exploitation over time. Solar photovoltaic (PV) energy is an option that adapts very well to the requirements of smart cities, making that in recent years it is being adopted in an accelerated way both at residential and industrial level, accompanied by

---

Internet of Things (IoT) solutions that automate and optimize their activities [1].

A PV installation will be exposed to a variety of factors that could slightly or significantly affect its performance during its lifetime. When a solar PV module experiences a suboptimal condition due to some external or internal factor, a reduction in delivered power occurs that manifests itself as a localized temperature gradient known as a *hot spot* [2]; this has been extensively verified, for example, several hot spots were analyzed in [3] causing a reduction in power greater than 11.9% in the cases analyzed. For the detection of hot spots in PV modules it is required to meet several conditions, in [4] a protocol is shown that is validated by a case study, however, a strict definition of the minimum delta temperature (DT) that exists in a hot spot is still pending, for example, in [5] it is defined in 10° C with an irradiance of 700 W/m^2, while in [6] it is defined in 20 °C for an irradiance of 600 W/m^2.

The transformation to smart cities that exploit PV technology is extending all over the world, even in cities with varying climatic conditions. Considering that a minimum irradiance of 700 W/m^2 is required for an infrared thermography (IRT) inspection and that the irradiance may vary abruptly, there is a risk that an IRT inspection may have to be suspended even after it has started, which implies an increase in costs for the users of this type of services. This research originates from the identification of the problem that the criterion of hot spot detection with IRT in PV modules requires environmental conditions that may be difficult to achieve for the users of distributed PV systems and that are a requirement for a correct application of the technique.

In order to create a new fault detection criterion, a large volume of thermographic information is required, including modules with hot spots and healthy modules, unfortunately there is no open database (DB) with this information. To contribute in the solution of this problem, the objective of this research was to create an IoT data acquisition system for the analysis of hot spots with IRT. The high volume of IRT information that will be generated with this system will allow future research to to the establishment of new criteria for the detection of hot spots in PV generation systems under irradiances less than 700 W/m2.

The research was developed in a distributed generation PV installation that has been in operation since 2018 at the Tecnológico de Costa Rica in Santa Clara of San Carlos. An IoT-based system was developed that periodically captures images and environmental variables that are useful in the analysis of IRT. The reading of temperatures in the thermal images is done automatically by means of digital image processing. To validate the performance of the system, 1,777 thermograms were taken and a fault-inducing experiment was developed by inducing hot spots through faults based on previous experience evaluated by [7].

This research has as its contribution: 1) The presentation of an IoT system for the acquisition of thermal information and 2) The under development generation of a large volume of thermographic information of modules under suboptimal and normal conditions. The mentioned DB its been used by a currently second stage of this research, that is processing the hot spot information for the definition of a

new criterion using artificial intelligence for irradiances greater than 300 W/m^2. This is an aspect of great interest for the managers of photovoltaic installations and thermographers, since it will facilitate the implementation of the technique and will contribute to improve its efficiency, as has been pointed out in [3] as an aspect to be solved. The DB creat by this system will later be accessible to all those who can contribute to this objective.

2   Related work

Works on IoT based solar module analysis using thermography are emerging, for example, [8] presents an analysis at normal and some faulty conditions using equipment like PV analyser, Solar Power Meter and thermal camera to compare PV performance for the monitoring of a generation plant. In regards to fault detection, hotspot detection using IRT has proven a effective technique to be used, see [9], where thermograms were analyzed by a hotspot detection algorithm called K-means clustering. Moreover, in a broader context, papers published on a special issue [10] have demonstrated that the autonomous monitoring and analysis approach is highly crucial in the performance monitoring, operation, and maintenance of PV systems. In [11] a summary of types and available fault detection techniques in photovoltaic installations is presented, visual inspection, IRT and analysis of electrical variables are among those techniques. In [12] several visual defects were detected in visual RGB and thermal orthomosaics, such as cracks, soiling, and *hotspots*. In addition, a procedure of semi-automatic *hotspots* extraction was also developed and is presented therein. Unmanned aerial vehicles were concluded as advantageous tools within the thematic of fault detection. The work on [13] identifies the main faults in PV arrays and correlates detection techniques that can detect them. In the study of [14] a metric to compare fault detection techniques is established. This metric takes into account detection capabilities like detection and classification, real-time detection, localization and fault isolation. The paper [15] compares fault detection techniques considering aspects such as: faults detected, level of diagnosis provided by the technique, on-line or off-line use, integration complexity and cost.

More pertinently, [7] establishes a comparison between multiple techniques to detect sub-optimal conditions in photovoltaic systems. The results showed that the visual inspection technique was the best at detecting soiling and partial shading with 100 % of effectiveness. IRT and electrical analysis had an effectiveness of 78 % and 73% , respectively, detecting the three types of conditions under study. Additionally, it's important to have a criterion over what is to be considered a fault. In regard to hotspots, [16] says hotspots temperature gradients larger than 20 °C, in any case, and even larger than 10 °C in certain conditions, are proposed as rejecting conditions for routine inspections under contractual frameworks. Also, hotspots can be considered failures if power variation goes over 4% [17].

3   Materials and Methods

The development of the solution started with the identification of the IRT requirements and the characteristics that the IoT system should have according to the conditions of the PV installation and the user.

The system was placed in a fixed location to maintain the conditions between thermograms following the requirements for this technique established in [4].

The photovoltaic installation used is located in the northern part of Costa Rica, 10°32' latitude and 84°31' longitude. According to the Köppen-Geiger system, the climate in this location is classified as tropical rainforest climate. The PV plant is located at the San Carlos Local Technological Campus in Santa Clara, Costa Rica. The PV panels model used is the Canadian Solar CS6k-280M tilted an angle of 15° and with an azimuth of 150 ° with respect to the North. Regarding the system instrumentation, a radiometric thermographic camera specialized for PV module inspection was used, and also sensors for irradiance, ambient temperature, relative humidity and cell temperature. The specifications are shown in Table 1 and Table 2. Due to the possibility of remote and on-site access to the system, the results obtained were validated from the beginning of the project.

Table 1. Characteristics of the FLIR VUE PRO R 336. Thermal camera used for the system.

Parameter	Value	Parameter	Value
HFOV x VFOV	25° x 19°	Weight	4 oz
Sensor (width x height)	5.764 mm x 4.351 mm	Accuracy	$\mp$ 5 ° C
Focal length	13.00 mm	Spectral band	7.5μ m -13.5 μ m
Image width x height	336 x 256	Thermal sensitivity	40 mK
Frequency	9 Hz	Power dissipation	2.1 W

Table 2. Characteristics of the components used for the sensing process

Component	Parameter	Value
DHT11 Sensor	Temperature range	$0°C$ to $50°C$
	Humidity Range	20% to 90%
	Accuracy	$\pm1°C$ and $\pm1\%$
DS18B20 Sensor	Temperature range	$-55°C$ to $+125°C$
	Accuracy	$\pm0.5°C$ for range $-10°C$ to $+85°C$
Spektron 210	Irradiation range	0 to 1500 W/m^2
	Accuracy	78.88 mV for each 1000 W/m^2

3.1   System validation

Temperature measurements were taken in a specific cell with IRT and with contact measurement at the back of the cell using the DS18B20 sensor, in order to compare them and evaluate the accuracy of the system measurements.

To evaluate its performance under hot spot conditions, an experiment were developed inducing failure conditions on the array. The test considerations are described below:

– Soiling, partial shadows and short-circuit conditions were induced in the cell.
– Each measurement was taken 10 minutes after inducing the fault condition and the next fault was induced by waiting at least 10 minutes after the previous measurement; this was done to eliminate residual effects between tests (to ensure inter-sample independence).
– All measurements were made applying only one fault condition at a time (no interaction).

The types of tests applied are described in table 3.

Table 3. Description of faults considered for the system evaluation.

Induced fault condition	Number of failures	Description
Shor circuit (SC)	11	Short-circuit through PV switch on module 8
Partial shading (PS)	6	Applied on modules 3, 6, 9 and 12 varying the shading area
Soiling (S)	9	Transparent plastic sheets with drawings of leaves and bird's dropping were randomly distributed in the array
Control module	26	In each test, module 2 was assigned as a non- faulty module to take its temperature as a reference

The experiment was carried out on March 2 and 9, 2022, starting at 07:30:00 and ending at 17:00:00. The system analyzes only the modules that are completely observed in the thermograms (see Fig. 1), therefore, modules 1, 4, 7 and 10 were not considered.

4   Automated fault detection in PV modules using IRT

This section describes in detail the data acquisition system developed for IRT analysis. It is subdivided into a) System requirements, b) General schematics,

Fig. 1. Segmentation of the solar array used by the system. Module 2 serves as a reference for the calculation of temperature gradients.

c) Position of the system with respect to the array, d) Thermographic image acquisition and processing, e) Data management.

4.1 System requirements

The following requirements were identified for the design of the system:

a) Automatic and synchronous acquisition of thermal images and environmental variables. In order to create a high volume of data, the system had to be able to activate a IRT camera automatically on a periodic interval. In addition, to improve the accuracy of a thermogram, it is necessary to know the relative humidity and ambient temperature of the site [18], therefore, the system had to measure both variables in real time. As the main future objective is to detect hot spots at irradiances below 700 W/m2, this variable had to be measured. Finally, all variables had to be acquired synchronously.

b) Automatic processing of IRT information. The technique allows indirectly measuring the temperature of the PV modules through a mathematical model that had to be applied automatically to each acquisition. Additionally, for each image the system had to be able to extract the specific IRT information for each module, discarding the information of the image that is not required (background).

c) Information management and remote access. The system had to be able to store the information in a cloud storage unit, with the possibility of accessing it from anywhere via the Internet. Additionally, all control of the system had to be able to be done remotely.

4.2 General schematics

Figure 2 shows a general schematic of the developed system. The main control unit (Raspberry Pi) combines wired and wireless links to access the measurement devices. All the IRT processing is done by the control unit and the information is stored in a DB. The measurement of irradiance and cell temperature is done

through wireless communication with another Raspberry Pi. Finally, like any IoT solution, the system can be accessed remotely by the user.
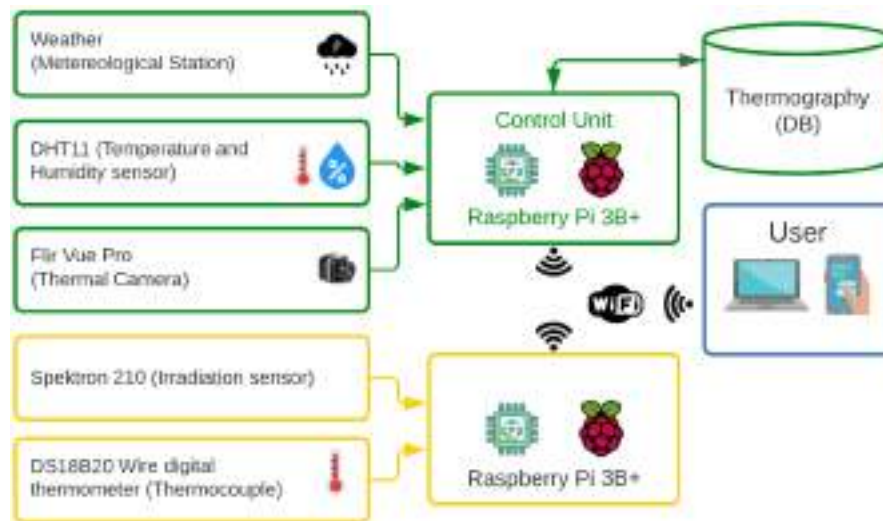

Fig. 2. General scheme of the IoT system developed for IRT analysis.

4.3 Positioning of the system with respect to the PV array

The final system was installed at a height of 7.05 m with respect to the ground, at an angle of 50° to the plane of the array at a distance of 9.2 m from the center of the array; in this way the thermograms meet the criteria established in [4] for correct temperature measurement at a resolution of PV cells. Since the system would be outdoors, the implementation considered that all electronic equipment be protected from rain. Figure 3 shows the solution installed on site in detail.

4.4 Thermographic image acquisition and processing

The algorithm of acquisition and processing of IRT information is represented in fig. 4. The system was configured to generate radiometric .rjpg images, so each thermogram generates 86.016 specific temperature measurements. To obtain temperature measurements of each particular PV module, the system segments the array and identifies each PV module with a specific identifier (see Fig. 1).

Each image taken is calibrated to obtain thermograms with an adequate level of accuracy. This is done automatically with the package *thermimage* [19], which
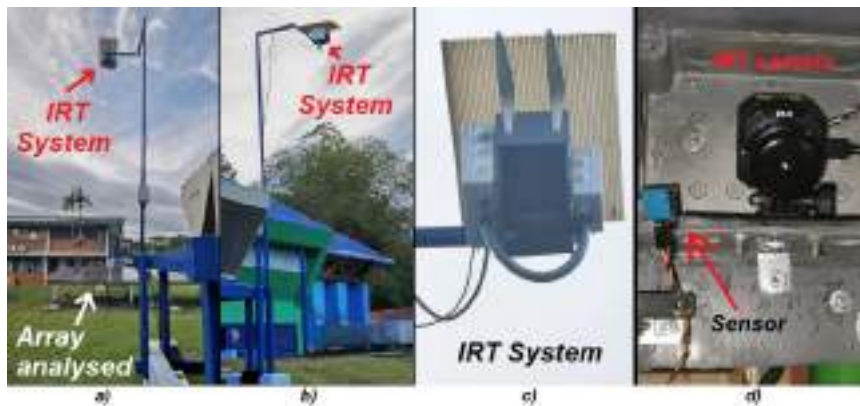
Fig. 3. a) Rear view of the system, b) side view of the system, c) front view of the system, d) IRT camera and temperature/humidity sensor.

applies the principles of Plank's law and the Stephan Boltzmann relationship. The table 4 shows the parameters used to obtain the temperature of each thermogram, in addition to the ambient temperature and relative humidity, which are updated in real time by the system's sensor, which in case of not obtaining such value, the value determined as default would be used.

Table 4. Parameters used to generate the thermogram of thermography.

Parameter	Value	Parameter	Value
Subject distance	10.41 m.	Emissivity	0.9
Atmospheric temp (default)	28°C	Humidity (default)	60%
Ir window transmission	1	Ir window temp	None

After acquiring the thermogram, a statistical analysis of the temperature values of each module is performed to obtain the maximum, minimum, average, mode and delta temperature (DT). DT is calculate with eq. (1); where, $T_{max,SM}$ corresponds to the maximum temperature of the module of interest and $T_{ave,REF}$ is the average temperature of the reference module (module 2). Finally, a color thermogram is generated to facilitate qualitative analysis (see Fig.5). All the information is stored in the DB automatically.
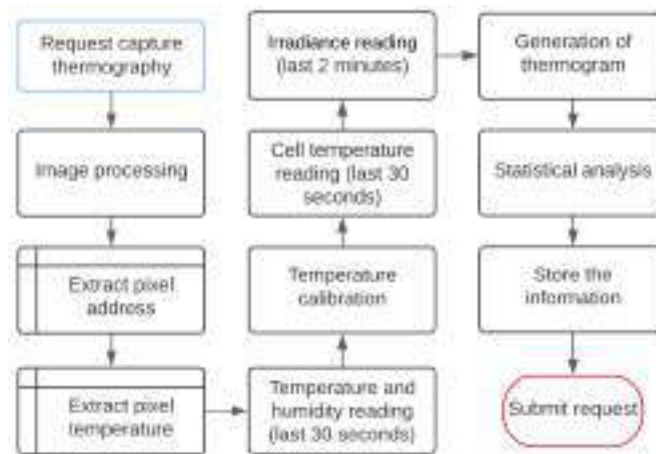
$$DT = T_{max,SM} - T_{ave,REF} \tag{1}$$

Fig. 4. Process implemented for the acquisition of thermal information, including external request sub-processes.
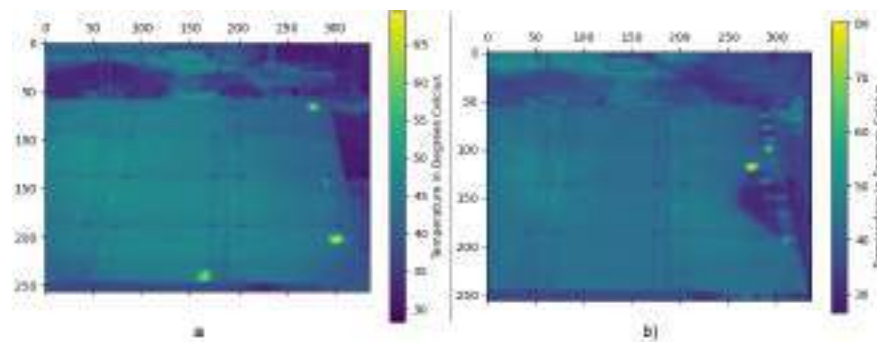

Fig. 5. a) color termogram of soiling test with hotspot of DT $= 23.7°$C with a irradiance of 224 W/m^2, b) Color termogram of partial shading test with hotspot of DT $= 37$ °C with a irradiance of 529 W/m^2.

4.5   Data management

The main control unit manages a DB with the processed IRT information. The table 5 shows in detail the main DB information that is stored for each PV module of each captured thermogram. The DB is backed up in the cloud and can be accessed remotely.

Table 5. Structure used for storing information in the experimentation DB. Temperature information is stored for each PV module.

Identifier			Electrical		Meteorological			Module temperature (°C)		
Date	Hour	ID	Power (W)	Irradiance (W/m^2)	State	HR (%)	Ta (°C)	T_{max}	T_{min}	DT

State: Clear, cloudy, rainy
HR: Relative humidity
Ta: Ambiente temperature

5   Results and discussion

This section describes, validates and analyzes the main results obtained by the developed system.

5.1   Temperature measurements

From 12 measurements between 08:09 am and 2:27 pm with values ranging between 36.7 °C and 55.25 °C, a variation of less than 4 °C was found between the measurements of the IRT camera and contact sensor. Considering that proportionality was found in the range of temperatures evaluated, and that the thermography is an indirect measurement on the front face and the contact measurement is on the back face, it is determined that the temperature measurements of the system are correctly taken with an accuracy of $\pm 4°C$.

5.2   System evaluation under induced faults

During the time the system was under test, 1,777 thermographs were captured, allowing to verify the continuous operation of the system.

With the experiment described in section 3.1, the relationship between the maximum DT value and irradiance was plotted (see fig. 6). We can observe that the DT of the hot spots increased with respect to the irradiance for SC and S type faults, which agrees with what was observed by [20]. On the other hand, for PS a decreasing trend was observed, which could be related to the activation or not of the by-pass diodes [21, 22], however, this requires a more detailed study by analyzing a larger amount of data. There were 26% and 8% of cases in areas C and D ($DT \geq 10°C$) of fig. 6, respectively, however, it is known that in all cases a fault condition was being induced to the array and that for other irradiance conditions a $DT \geq 10°C$ was reached for the same fault, therefore, new criteria should be generated to identify these faults for all possible range of irradiances. In area A, 42% of cases with a $DT < 10°C$ were identified, however, with the premise that at least 700 W/m^2 are required to perform the IRT analysis, these cases could not have been analyzed until the required irradiance conditions were reached, which represents a possible delay to be able to make the diagnosis in an agile way. Finally, it should be noted that for all types of induced faults there

were cases that did not meet the minimum value of DT for failure, therefore, this suggests that faults of different types could be identified with $DT < 10°C$; but for this new criteria need to be established.
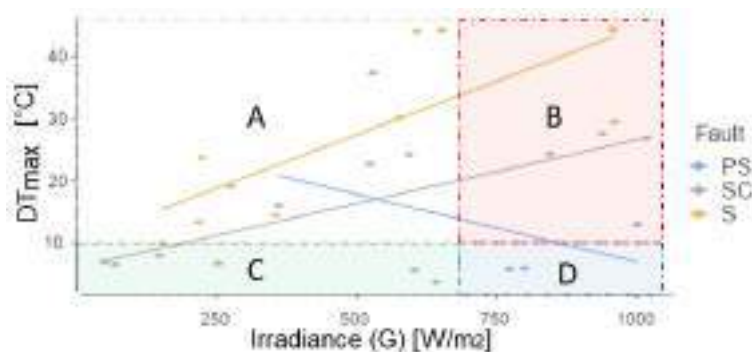

Fig. 6. Plot of the maximum DT(DT_{max}) found in each test with respect to the irradiance (G) present during each measurement. Shaded areas A and C correspond to $G < 700W/m^2$ and shaded areas C and D correspond to measurements with a $DT_{max} < 10°C$.

From a qualitative analysis of the figure 5, it is possible to observe that the thermograms are taken correctly, since it has a good focus of the PV array, it is possible to identify cases where a single cell is hotter than the neighboring cells and that by means of the color scales the user can easily identify the hot spots.

6   Conclusions

The developed system shows a viable alternative to automate the process of collecting IRT information continuously in photovoltaic installations for the creation of a high volume of IRT data of PV modules under suboptimal conditions. The temperature measurements obtained had an error of less than 4° C. The system validation process showed that under hotspot conditions, the developed system extracts information that is consistent with the theory, generating qualitative and quantitative information that is valuable for diagnosing faults in PV systems. The characteristics of the DB designed will allow to contribute to the improvement of the detection of hotspots through IRT analysis for a greater range of irradiance conditions than those currently established. The platform developed is an example of an innovative IoT solution for the optimization of energy sources usage in smart cities, which can be used by managers and inspectors of PV installations. It remains for future research to use the platform to perform an exhaustive analysis of the behavior of hot spot temperature with respect to irradiance for different types of faults, in order to establish better fault detection criteria.

Acknowledgement

References

1. Nasim Ghadami, Mohammad Gheibi, Zahra Kian, Mahdieh G. Faramarz, Reza Naghedi, Mohammad Eftekhari, Amir M. Fathollahi-Fard, Maxim A. Dulebenets, and Guangdong Tian. Implementation of solar energy in smart cities using an integration of artificial neural network, photovoltaic system and classical delphi methods. *Sustainable Cities and Society*, 74:103149, nov 2021.

2. John A. Tsanakas, Long Ha, and Claudia Buerhop. Faults and infrared thermographic diagnosis in operating c-Si photovoltaic modules: A review of research and future challenges, 2016.

3. Leonardo Cardinale-Villalobos, Carlos Meza, and Luis D. Murillo-Soto. Experimental comparison of visual inspection and infrared thermography for the detection of soling and partial shading in photovoltaic arrays. In Sergio Nesmachnow and Luis Hernández Callejo, editors, *Smart Cities, Third Ibero-American Congress, ICSC-Cities 2020, San José, Costa Rica, November 9-11, 2020, Revised Selected Papers*. Springer International Publishing, 1 edition, 2020.

4. Carlos; Cardinale-Villalobos, Leonardo; Rimolo-Donadio, Renato; Meza. Solar panel failure detection by infrared UAS digital photogrammetry: a case study. *International Journal of Renewable Energy Research (IJRER)*, 10(3):1154–1164, 2020.

5. International Energy Agency. Review on Infrared and Electroluminescence Imaging for PV Field Applications. Technical report, PHOTOVOLTAIC POWER SYSTEMS PROGRAMME.

6. International Energy Agency. Review of Failures of Photovoltaic Modules. Technical Report July, INTERNATIONAL ENERGY AGENCY.

7. Leonardo Cardinale-Villalobos, Carlos Meza, Abel Méndez-Porras, and Luis D. Murillo-Soto. Quantitative comparison of infrared thermography, visual inspection, and electrical analysis techniques on photovoltaic modules: A case study. *Energies*, 15(5), 2022.

8. Udit Kumar Phoolwani, Tanveer Sharma, Abhishek Singh, and Suresh Kumar Gawre. Iot based solar panel analysis using thermal imaging. In *2020 IEEE International Students' Conference on Electrical,Electronics and Computer Science (SCEECS)*, pages 1–5, 2020.

9. April Salazar and Erees Queen Macabebe. Hotspots detection in photovoltaic modules using infrared thermography. *MATEC Web of Conferences*, 70:10015, 01 2016.

10. Mohammadreza Aghaei. Autonomous monitoring and analysis of photovoltaic systems. *Energies*, 15(14):1–6, July 2022.

11. Siva Ramakrishna Madeti and S.N. Singh. A comprehensive study on different types of faults and detection techniques for solar photovoltaic system. *Solar Energy*, 158:161–185, 2017.

12. Yahya Zefri, Achraf ElKettani, Imane Sebari, and Sara Ait Lamallam. Thermal infrared and visual inspection of photovoltaic installations by uav photogrammetry—application case: Morocco. *Drones*, 2(4), 2018.

13. Mohammed Khorshed Alam, Faisal Khan, Jay Johnson, and Jack Flicker. A comprehensive review of catastrophic faults in pv arrays: Types, detection, and mitigation techniques. *IEEE Journal of Photovoltaics*, 5(3):982–997, 2015.

14. Albert Appiah, Xinghua Zhang, Ben Ayawli, and Frimpong Kyeremeh. Review and performance evaluation of photovoltaic array fault detection and diagnosis techniques. *International Journal of Photoenergy*, 2019:1–19, 02 2019.

15. A. Mellit, G.M. Tina, and S.A. Kalogirou. Fault detection and diagnosis methods for photovoltaic systems: A review. *Renewable and Sustainable Energy Reviews*, 91:1–17, 2018.

16. R. Moretón, E. Lorenzo, and L. Narvarte. Experimental observations on hot-spots and derived acceptance/rejection criteria. *Solar Energy*, 118:28–40, 2015.

17. Marc Köntges, Sarah Kurtz, Corinne Packard, Ulrike Jahn, Karl Berger, Kazuhilo Kato, Thomas Friesen, Haitao Liu, Mike Van Iseghem, john Wohlgemuth, David Miller, Michael Kempe, Peter Hacke, Florian Reil, Nicolas Bogdanski, W. Herrmann, C. Buerhop, Guillaume Razongles, and Gabi Friesen. Review of failures of photovoltaic modules. Technical report, 01 2014.

18. D. Roca S. Lagüela, L. Díaz-Vilariño. Infrared Thermography: Fundamentals and Applications. In Belén Riveiro and Mercedes Solla, editors, *Non-Destructive Techniques for the Evaluation of Structures and Infrastructure*, chapter 6, page 26. CRC Press, 1st editio edition, apr.

19. Tattersall, GJ. Thermimage: Thermal image analysis, 2021. R package version 4.1.3.

20. M Cubukcu and A Akanalci. Real-time inspection and determination methods of faults on photovoltaic power systems by thermal imaging in Turkey. *Renewable Energy*, 147:1231–1238, 2020.

21. Priya Ranjan Satpathy, Renu Sharma, Suraj Kumar Panigrahi, and Sobhit Panda. Bypass diodes configurations for mismatch and hotspot reduction in pv modules. In *2020 International Conference on Computational Intelligence for Smart Power System and Sustainable Energy (CISPSSE)*, pages 1–6. IEEE, jul 2020.

22. Pierluigi Guerriero and Santolo Daliento. Toward a Hot Spot Free PV Module. *IEEE Journal of Photovoltaics*, 9(3):796–802, may 2019.

Método para la transformación digital para espacios de salud (CLÍNICAS). Caso de estudio áreas de telemedicina

Fabian Leonardo Peñaloza Marín [1][0000-1111-2222-3333]

[1] Universidad, Cuenca, Ecuador
fabian.penalozam@ucuenca.edu.ec

Resumen

La investigación se enfocó en la propuesta de una metodología de transformación digital para espacios de salud del Sur de Ecuador con implementación de áreas de Telemedicina como caso de estudio. La metodología se basó en un estudio exploratorio con enfoque mixto con procedimientos cuantitativos y cualitativos para el manejo de la información. En el caso de los procedimientos cuantitativos, se contempla la aplicación de un instrumento de recolección de datos, en este caso, un cuestionario a los médicos del Centro Monte Sinaí, para conocer el grado de interés de este personal en la telemedicina, así como su nivel de cultura digital como aspecto relevante en la propuesta de una metodología de este tipo. En cuanto a los procedimientos cualitativos, se refiere a la revisión sistémica con publicaciones relevantes de ScienceDirect, IEEE, Scopus, y ACM de la literatura sobre las diferentes metodologías de transformación digital y sus casos de éxito en el campo de la salud. Los resultados evidenciaron que la metodología que más se ajusta a las necesidades de Ecuador para la implementación de transformación digital en el área de salud al sur de Ecuador, sería la de Cueva (2020), debido a que aborda los estados de madurez de los procesos de transformación digital, proporcionado herramientas al proceso de capacitación para el uso de la telemedicina para realizar servicios de Teleconsulta, servicios de Telemonitoreo, servicio de telecuidado para pacientes, garantiza requerimientos de pruebas de los pacientes remotos mediante TIC.

Palabras claves: Telemedicina, transformación digital, salud, teleconsulta y telemonitoreo

1   Introducción

La incursión vertiginosa de Internet y de las tecnologías de la información y la comunicación (TIC) ha provocado profundos cambios en la forma en que la sociedad se comunica, busca información, genera y comparte conocimientos. Esto significa que vivimos en una época de cambios constantes, en la que casi todos los ciudadanos tienen que adaptarse a ellos al mismo ritmo, tanto profesional como personalmente. Los avan-

ces tecnológicos han democratizado el acceso a Internet, incluidos los dispositivos móviles inteligentes, y han creado un entorno hiperconectado, impulsado por los datos y cada vez más digital (Cabrol y Pombo, 2021).

Por ello, casi todos los sectores productivos (incluido el sanitario) están en un proceso de transformación cuyo principal objetivo es adaptarse a la nueva era digital. En la sanidad, esta transformación digital ha sido más lenta que en otros sectores, quizá debido a la cautela en la integración de las innovaciones que es típica de las organizaciones, empresas o industrias en las que la vida de los usuarios puede estar en juego en la prestación de nuevos servicios, como la aviación o la energía nuclear (Bastias y Ulrich, 2019).

Pero en 2020, COVID ha cambiado la agenda global. Una pandemia que no conoce fronteras, naciones, clases sociales, edad o género ha frenado el impulso del siglo XXI. Todas las actividades humanas han sentido su impacto. En este nuevo escenario sanitario se ha dado empuje al concepto de salud digital, definido como el uso de las TIC para mejorar la salud humana, los servicios sanitarios y el bienestar de la población. Con una propuesta de valor que consiste en aportar soluciones digitales a los problemas actuales del sistema y de los pacientes, eliminando las barreras físicas, descentralizando los servicios hospitalarios, aumentando la autonomía y empoderando a los pacientes. Y todo ello con la ayuda de tecnologías como la telemedicina (Montero et al., 2020).

La tecnología se está convirtiendo cada vez más en una parte integral de todas las relaciones familiares, laborales y profesionales. Este tipo de interacción se ha generalizado en la asistencia sanitaria en todo el mundo y debido a la pandemia de la COVID-19 ha resultado en una digitalización acelerada e incluso forzosa, lo que convierte a la telemedicina en una herramienta eficaz y poderosa para facilitar la asistencia a distancia. En este contexto, la Organización Panamericana de la Salud (OPS), junto con el Banco Interamericano de Desarrollo (BID), ha apoyado el desarrollo de una herramienta para medir la madurez de los establecimientos públicos de salud en las Américas para que puedan adoptar servicios de telemedicina y apoyar el tratamiento de los pacientes a través de canales virtuales (Organización Panamericana de Salud, 2020).

A pesar de los beneficios potenciales de la salud digital, este nuevo paradigma también plantea nuevos retos para todas las partes interesadas en la salud, como la obtención de pruebas científicas y la creación de un marco jurídico que respalde las intervenciones de salud digital. Sabemos que cada vez más ciudadanos serán nativos digitales. Así, por su propia naturaleza, se enfrentarán al cambio y utilizarán cada vez más los servicios sanitarios a través de Internet y de dispositivos móviles (servicios sanitarios no presenciales). Por otra parte, el entorno cambiante hace necesario que los profesionales sanitarios adquieran y desarrollen determinados conocimientos, habilidades y actitudes relacionados con la salud digital y el uso de las TIC (Montero et al., 2020).

En este contexto de digitalización, se identificó una categoría en la que la mayoría de las barreras estaban relacionadas con la práctica clínica, en particular las diferencias en los registros clínicos y/o de diagnóstico y la incapacidad de acceder a toda la información sobre el historial clínico de un paciente. También se identificaron en este ámbito aspectos relacionados con las dudas sobre la calidad de los servicios prestados, la falta de protocolos o el desconocimiento de los consultores de algunas enfermedades locales (Saigí et al., 2021).

En cuanto a los profesionales implicados, hay que tener en cuenta la motivación y la voluntad de los profesionales de participar en este tipo de programas. En el caso de los profesionales locales, a través de la Fundación Ecuatoriana de Telemedicina y eSalud (FUNDETEL), se han impulsado proyectos de participación internacional para acordar directrices de implementación de Telesalud en cooperación con varios países, que de hecho obtuvo el primer lugar en América latina, se percibió además la motivación del personal médico en participar en estos proyectos con voluntad de fomentar el uso de la Telemedicina y e-Salud (Saigí et al. 2021).

En el caso de Ecuador, la penetración de internet en 2017 fue de solo el 57% de la población, lo cual es bajo e indica que el país aún tiene un largo camino por recorrer en cuanto al uso de la tecnología en la vida cotidiana. Por otra parte, la confianza en el uso de herramientas digitales, también dificulta su adopción. Ecuador ha realizado importantes avances en la mejora de su capacidad cibernética y en la lucha contra las amenazas, a lo que ha contribuido la creación de un grupo de trabajo para desarrollar una estrategia nacional de ciberseguridad (Cabrol y Pombo, 2021).

Aunque el sector privado ofrece algunos servicios de ciberseguridad, es necesario aumentar la concienciación sobre la ciberseguridad y la preparación ante las amenazas. Esto es importante porque la ciberseguridad es fundamental para nuestra prosperidad y seguridad. Las actividades cibernéticas maliciosas amenazan no sólo la economía, sino también el propio funcionamiento de nuestras democracias, libertades y valores. La seguridad futura depende de nuestra capacidad para transformar nuestras defensas contra las ciber amenazas tanto las infraestructuras civiles como las capacidades militares dependen de sistemas digitales seguros. Especialmente en el ámbito de la sanidad, donde se almacena tanta información sobre los pacientes en las historias clínicas que podría utilizarse de forma no deseada si cae en manos equivocadas (Cabrol y Pombo, 2021).

A esto se suma la falta de legislación clara sobre el uso de la Telemedicina en los diferentes países de América Latina. Incluso en Ecuador, no existe legislación específica sobre el uso de Telemedicina y han tenido que ser adaptados varios reglamentos, leyes y marcos legales que fueron creados para el uso de la tecnología en general, pero no específicamente. De ahí que se desprenden varios temas que no pueden ser adaptados adecuadamente por falta de un adecuado tratamiento. (Peralta et al., 2021).

En Ecuador también existe un vacío legal, hasta el punto de ser contradictorio en cuanto a la regulación de la telemedicina, ya que existen acuerdos ministeriales en materia de salud que, según el código de ética, prohíben ofrecer consejos o prescribir tratamientos médicos a través de cualquier medio de comunicación (Nº 14660 MINSAL, 1992); pero, a pesar de su antigüedad, no han sido abolidos (Vallejo, 2020).

Por el contrario, el Ministerio de Sanidad ha ido estableciendo el uso de la telemedicina, vigilando el cumplimiento de las normas necesarias, e incluso ha realizado algunas inversiones para desarrollarla, como en el caso del Hospital Vicente Corra (Vallejo, 2020).

En el caso de la telemedicina se presentan grandes barreras ya descritas, siendo las principales: las tecnológicas, las regulatorias y las de interoperabilidad, todas ellas im-

piden de alguna manera, ya sea física o regulatoria la prestación de servicios, sin embargo, no ha impedido que varios países tengan metodologías de transformación digital en el área de salud, incorporando algunos procedimientos en la telemedicina.

Por todo ello, es necesario evaluar la disponibilidad de todos estos factores en países como Ecuador, especialmente en el sur del país, a través de un análisis holístico que permita identificar requerimientos, condiciones, aspectos relacionados con la infraestructura de información, políticas de implementación, infraestructura física y legislación para proponer una metodología efectiva de transformación digital que sea parte de la solución sanitaria.

2   Método

2.1. Tipo de estudio

Para proponer una metodología de transformación digital para espacios de salud de Ecuador, se requiere conocer las diferentes metodologías existentes de este tipo que hayan sido aplicadas con éxito en diferentes países, en especial en América. Para ello se plantea un estudio exploratorio con enfoque mixto. De acuerdo a esto, Hernández et al. (2014), sugiere que este tipo de estudios permiten la familiarización con fenómenos poco estudiados o relativamente desconocidos para obtener una información más completa, en este caso la transformación digital en el área de la salud es un método novedoso que ha venido incorporándose paulatinamente en diferentes países y que ha tomado auge a raíz del Covid-19 por lo cual el presente estudio pretende ahondar en este tema.

De igual forma, se plantea el enfoque mixto, en cual comprende procedimientos cuantitativos y cualitativos para el manejo de la información. En el caso de los procedimientos cuantitativos, se contempla la aplicación de un instrumento de recolección de datos, en este caso, un cuestionario a los médicos del Centro Monte Sinaí, para conocer el grado de interés de este personal en la telemedicina, así como su nivel de cultura digital como aspecto relevante en la propuesta de una metodología de este tipo. En cuanto a los procedimientos cualitativos, se refiere a la revisión sistémica de la literatura sobre las diferentes metodologías de transformación digital y sus casos de éxito en el campo de la salud.

De acuerdo con Hernández et al. (2014), los procedimientos cuantitativos implican el uso de datos numéricos y procesos estadísticos de la información, mientras que las cualitativos buscan establecer una relación entre los participantes del proceso investigativo o entre los supuestos teóricos para extraer sus experiencias ideologías.

2.2. Métodos y técnicas de estudio

2.2.1. Métodos para el estudio

El método es un camino para investigar, conocer y distribuir (Baena, 2017). De acuerdo a ello, se considera para este estudio el método inductivo-deductivo, que consiste en la combinación de estos. Por una parte, el método deductivo que parte de leyes o enunciados generales para aplicar a casos particulares como de hecho sucede al analizar las diferentes metodologías existentes para la aplicabilidad de una de ellas. Por

otra el método inductivo en eventos particulares para llegar a una generalización, al tomar en consideración la percepción de los médicos para generalizar en el contexto.

2.2.2 Técnicas de Estudio

Es preciso considerar técnicas para recolectar los datos de estudio. Recolectar implica tener un plan detallado de procedimientos que conduzcan a obtener la información proveniente de las fuentes de estudio, para conseguir los objetivos (Hernández et al., 2014).

En este sentido, las técnicas a utilizar para el desarrollo del estudio son: la revisión bibliográfica-documental, la cual consiste en acoplar datos de fuentes escritas primarias o secundarias, a través de la exposición minuciosa de documentos que están relacionados con las variables examinadas (Hernández y Mendoza, 2018). En este caso se revisarán y analizarán las diferentes metodologías de transformación digital y su aplicabilidad en el sector de la salud por medio de la revisión sistemática de las mismas.

Además, se utilizó la encuesta, que es una estrategia oral o escrita para obtener información sobre un grupo o muestra en relación a su opinión sobre un tema específico (Arias, 2016). Esta encuesta se aplicará a los médicos del Centro de Salud Monte Sinaí.

2.2.2.1. Revisión sistemática

La revisión sistemática consiste en resúmenes estructurados contentivos de información hallada en artículos, fuentes informativas con un alto nivel de evidencia para dar respuesta a una interrogante contentivos (Moreno et al., 2018). En este caso se trata de   la revisión de artículos científicos, revistas, artículos académicos de fuentes confiables apoyados en buscadores especializados que dan garantía de confiabilidad de los datos suministrados. Para ello se consideraron los pasos de identificación de los temas relevantes, al respecto se tomaron como temas esenciales los relacionados con los objetivos los cuales conllevan a responder la interrogante de la investigación como lo son: mitologías de transformación digital, cultural digital, aplicabilidad de telemedicina, seguridad y tecnología en la transformación digital en el área de salud. Seguidamente se identificaron los artículos, documentos por medio de los *Abstract*, luego recopiló el material identificando sus autores, título, fuente, metodología, tipo de estudio, resultados y conclusiones, y finalmente, se revisó detalladamente el material con mayor relación.

El procedimiento para la revisión sistemática estuvo basado en la identificación de temas, identificación de artículos, recopilación de material, revisión detallada y análisis y discusión. Se estima la recopilación de al menos diez artículos por tópico de modo de dar rigor teórico al tema a desarrollar de acuerdo a los siguientes criterios de selección:

Criterios de inclusión

Para la selección de material, se cumplieron los siguientes criterios de inclusión: referencias actualizadas con no más de 6 años de vigencia, artículos o documentos con al menos uno de los tópicos siguientes: (Metodologías de transformación digital, & cultura digital) &, (aplicabilidad de telemedicina, o seguridad o tecnología en la transformación digital) & (en el área de salud.) y artículos con alta confiabilidad determinada por los buscadores especializados que ubiquen la revista o publicaciones en posición relevante: Scopus, ScienceDirect, IEEE y ACM

Criterios de exclusión

Para no seleccionar el material, se cumplieron al menos uno de los siguientes criterios de exclusión: referencias con data mayor de 6 años, artículos que no se relacionen con los temas indicados en los criterios de inclusión, artículos en idiomas distintos al inglés y español y artículos con procedencia dudosa.

Para seleccionar las dimensiones a considerar para el diseño del cuestionario se realizó la revisión de los artículos mencionados. Se revisó un total de 48 artículos en los diferentes buscadores mencionados con las variables: transformación digital, cultura digital, telemedicina.

En cuanto a la transformación digital, se seleccionaron 11 artículos de los 48 consultados, se excluyeron 37, de los cuales 12 estaban fuera del rango de fecha y 15 se relacionaban con la transformación digital en distintas áreas: pero contemplaban solo definiciones y no las dimensiones a considerar. En este sentido, los artículos tomados en cuenta se listan en la Tabla 1.

Tabla 1. Lista de artículos seleccionados

N°	Autor	Título	Dimensiones /aspectos	Fuente
1	Eberth, Cristof y Duarte Carlos	Digital Transformation	Cultura innovadora y colaborativa	Scopus
			Infraestructura de comunicación digital	
			Accesibilidad	
			Economía	
2	Vial, Gregory	Understanding digital transformation: A review and a research agenda	Competitividad	ScienceDirect
			Disponibilidad de datos	
			Estrategia digital	
			Cultura digital	
3	María José Sousa y Álvaro Rocha	Digital learning: Developing skills for digital transformation of organizations	Aprendizaje digital colaborativo	Elsevier
			Transformación digital	
			Habilidades organizacionales de negocios	
4	Peter C.Verhoefa, Thijs Broekhuizena, Yakov Bartb, Abhi Bhattacharyaa, John Qi Donga, Nicolai Fabiana Michael Haenleinc	Digital transformation: A multidisciplinary reflection and research agenda	Tecnología digital	Elsevier
			Competitividad digital	
			Comportamiento de clientes digitales	
5	Satish Nambisana, Mike	The digital transformation of innovation and entrepreneurship:	Apertura	Elsevier
			Posibilidades	

	Wrightb, Maryann Feldmanc	Progress, challenges and key themes	Generatividad	
6	Miguel Ángel Galindo, Martina María Soledad, Castaño Martínez, María, Teresa Méndez Picazo	Digital transformation, digital dividends and entrepreneurship: A quantitative analysis Digital transformation, digital dividends and entrepreneurship: A quantitative analysis	Estrategia digital	Elsevier
			Dividendos digitales	
			Emprendimiento	
7	Simon Chaniasa, Michael D., Myersb Thomas Hessa	Digital transformation strategy making in pre-digital organizations: The providercase of a financial service	Proceso-actividad	Elsevier
			Sistemas de información	
			Aprendizaje digital	
			Estrategia digital	
8	André Hanelt,René Bohnsack,David Marz,Cláudia Antunes Marante	A Systematic Review of the Literature on Digital Transformation: Insights and Implications for Strategy and Organizational Change	Condiciones contextuales (tecnologías y aplicaciones antecedentes)	ScienceDirect
			Mecanismos (de innovación y de integración)	
			Resultados (ambiental, económico, intraorganizacional)	
9	Jason Bloomberg	Digitization, Digitalization, And Digital Transformation: Confuse Them At Your Peril	Competencia	Open Source
			Iniciativas de digitalización	
			Estrategia de digitalización	
10	Francisco Vacas Aguilar	Transformación digital: del lifting a la reconversión	Estrategia de transformación (oportunidades)	ScienceDirect
			Estrategia funcional (competitividad)	
			Estrategia de negocios(recursos-competitividad)	
			Costos	
11	Kotarba, M	Digital transformation of business models	Clientes (relación/segmentación)	ScienceDirect
			Propuesta de valor/ventaja (competencia)	
			Recursos--canales-experiencia	
			Asociación de ecosistemas (compartir)	
			Finanza-economía	
			Cambio modelo de negocio	

2.2.2.2. Encuesta

Para la aplicación de la encuesta a la persona médica del Centro de Salud Monte Sinaí, se empleó como instrumento un cuestionario de diseño propio, con base en las

dimensiones de la variable de transformación digital: competitividad, estrategia digital y cambio cultural (innovación organizacional, cultura digital), la percepción y preparación sobre la aplicabilidad de la telemedicina en el área de la salud y las dimensiones de Telemedicina: servicios de asistencia remota, gestión administrativa de pacientes, Formación a distancia de profesionales de la salud, Evaluación e investigación colaborativa en red.

El cuestionario consta de 29 preguntas cerradas con opciones de respuesta tipo Likert, donde la escala es la siguiente: 1 = Nunca; 2= Casi nunca; 3= A veces; 4= casi siempre; 5= Siempre de acuerdo a la percepción o postura del encuestado sobre los aspectos mencionados.

Para la validez de su contenido, se someterá a juicio de los expertos en el tema y para la confiabilidad, se determinará a través del Alfa de Cronbach.

2.3. Población y muestra

2.3.1. Población

La población es a la totalidad de individuos, cosas hechos con características similares requeridas y medibles, que se tomen en cuenta para recoger la información y analizarla (Ñaupas et al., 2018). Por consiguiente, la población del presente estudio se encuentra conformada por 60 médicos pertenecientes al Centro Monte Sinaí.

2.3.2. Muestra

La muestra es la parte representativa de la población que se toma con el fin de investigar sus características y generalizar sobre el universo (Ñaupas et al., 2018).

En este orden, la muestra estará conformada por los 60 médicos del Centro Monte Sinaí, dada la característica de ser una población finita, conocida y pequeña.

3   Resultados

3.1. Presentación de resultados

Para la presentación de los resultados, se aplicó un "Cuestionario transformación digital", dirigido a personal médico del Centro Monte Sinaí, ubicado en la ciudad de Cuenca , conformada en 1990 por un conjunto de profesionales de la medicina con amplia experiencia en el sector y en el área administrativa, enfocados en ofrecer un servicio de salud a la región Austral y la Cuenca, dotado de implementación médica con tecnología de punta, para alcanzar la eficiencia y calidad en la atención de la salud de los pacientes, con una capacidad de 400 camas, y en el 2014 se realizó una habilitación del Centro Monte Sinaí, con una inversión $126 millones ($76 millones: construcción y $50 millones: equipamiento), con servicios disponibles de Unidad de Cuidados Intensivos, servicio de Emergencia y Sala de Primera Acogida, Hospitalización, Neonatología, área de Imagenología, Endoscopía, Colonoscopía, Broncoscopía y Colposcopía.

3.1.1 Diagnosticar la percepción y preparación del personal de salud del Centro Monte Sinaí de Ecuador en cuanto a la aplicabilidad de telemedicina.

En cuanto al diagnóstico de la percepción y preparación del personal de salud del Centro Monte Sinaí de Ecuador. Este diagnóstico se basó en un análisis estadístico en Statistical Package for the Social Sciences (SPSS) sobre la base de datos obtenida de la aplicación del instrumento. Finalmente, el resultado sobre los niveles de cumplimiento se observa en la Tabla 2.

Tabla 2 Diagnóstico de la percepción y preparación del personal de salud del Centro Monte Sinaí de Ecuador

Descripción	Escala de cumplimiento				
	0%	25%	50%	75%	100%
El Centro Monte Sinaí es competitivo en el ramo					X
Cambios dentro de la organización para promover la calidad total				X	
Los procedimientos responden a técnicas innovadoras que captan la atención de los usuarios					X
Considera que la estrategia competitiva contempla los procesos digitales				X	
La organización está actualizada frente a los distintos cambios tecnológicos			X		
Los planes estratégicos de la organización consideran el uso de recursos tecnológicos				X	
Han considerado organizativamente la implementación de procesos digitales de atención de la salud				X	
Se invierte en la organización en la adquisición de recursos con tecnologías de punta			X		
La organización plantea ideas de negocio adviertan un giro transformacional hacia lo digital					X
Las personas que trabajan en la organización están dispuestas a afrontar cambios hacia la digitalización de procesos					X
Usted está dispuesto(a) a afrontar cambios hacia la digitalización de procesos			X		
La organización invierte en capacitación y actualización tecnológica del personal					X
Se llevan a cabo cambios en productos y servicios dentro de este centro			X		
Se incorporan nuevos productos y servicios en este centro			X		
Se planifican procesos actualizados de atención					X
Está capacitado(a) para utilizar aparatos electrónicos de tecnología actual como parte de un proceso de cambio hacia la digitalización		X			
Sabe usar e interactuar medios sociales para el manejo de contenidos digitales de atención		X			
Considera que la telemedicina es una alternativa novedosa para la atención de procesos tradicionales de manera digitalizada		X			
Se siente capacitado para el uso de la telemedicina en los procesos que se cumplen en este centro		X			
Realiza servicios de Teleconsulta		X			
Realiza servicios de Telemonitoreo			X		
Se considera dentro del centro el servicio de telecuidado para pacientes			X		

Se atienden requerimientos de pruebas de los pacientes remotos haciendo uso de las TIC		X
Existe la posibilidad de facturar servicios al paciente de manera remota		X
Se propicia la educación continua para personal de salud para la promoción de la tecnología		X
El centro tiene espacios virtuales para la formación de los profesionales de salud		X
Comparte sus conocimientos a otros médicos por medios virtuales de acuerdo a su experiencia como profesional de la salud		X
Comparte sus experiencias de éxito sobre procedimientos o tratamientos con otros médicos a través de las Tecnologías de la información y comunicación		X
Se crean conocimientos de manera colaborativa a través de redes o entornos virtuales	X	

En relación a los resultados obtenidos de la encuesta, se dedujo que el 75% de los encuestados indicaron que casi siempre observan cambios en la organización para la promoción de la calidad total. Así mismo, el 100% de los encuestados indicó que casi siempre utilizan procedimientos que responden a técnicas innovadoras que captan la atención de los usuarios y los encuestados casi siempre consideran que la estrategia competitiva contempla los procesos digitales.

El 75% de los encuestados indicaron que casi siempre observan planes estratégicos de la organización que consideran el uso de recursos tecnológicos, mientras que el 75% restante indicaron que siempre han considerado organizativamente la implementación de procesos digitales de atención de la salud. Además el 50% indicó que casi siempre y el restante 25% consideró que se invierte en la organización en la adquisición de recursos con tecnologías de punta. De igual manera, cabe señalar que el 100% de los encuestados indicó que casi siempre consideran que la organización plantea ideas de negocio adviertan un giro transformacional hacia lo digital. El 100% de los encuestados casi siempre considera que las personas que trabajan en la organización están dispuestas a afrontar cambios hacia la digitalización de procesos. El 50% indicó que siempre personalmente se encuentran dispuestos afrontar los cambios hacia la digitalización de procesos.

El 100% indicó que a veces la organización invierte en capacitación y actualización tecnológica del personal. El 50% de los encuestados consideró que siempre se llevan a cabo cambios en productos y servicios dentro de este centro y además indicaron que siempre se incorporan nuevos productos y servicios en este centro de salud.   El 100% de los encuestados casi siempre consideran que se planifican los procesos actualizados de atención, y el 25% restante indicaron que siempre están capacitados para utilizar aparatos electrónicos de tecnología actual como parte de un proceso de cambio hacia la digitalización. Además el personal sabe usar e interactuar medios sociales para el manejo de contenidos digitales de atención.

El 25% restante opinaron que siempre consideran que la telemedicina es una alternativa novedosa para la atención de procesos tradicionales de manera digitalizada, así mismo, el 25% nunca se sienten capacitados para el uso de la telemedicina en los procesos que se cumplen en este centro.

Mientras que el 50% casi nunca y el 25% restante opinaron que a veces se realiza servicios de teleconsulta. El 50% casi nunca y el 25% restante opinaron que a veces se realiza servicios de telemonitoreo. El 50% opinaron que casi nunca se realiza servicios de telecuidado para pacientes y otros encuestados indicaron que nunca se atienden requerimientos de pruebas de los pacientes remotos haciendo uso de las TIC para pacientes.

El 50% de los encuestados indicó que nunca se facturan servicios al paciente de manera remota. Así mismo, nunca se ha propiciado la educación continua para personal de salud para la promoción de la tecnología, casi nunca el centro posee espacios virtuales para la formación de los profesionales de salud. De igual manera, se detectó que nunca comparte sus conocimientos a otros médicos por medios virtuales de acuerdo a su experiencia como profesional de la salud. En el mismo orden de ideas, se identificó que a veces comparten sus experiencias de éxito sobre procedimientos o tratamientos con otros médicos a través de las Tecnologías de la información y comunicación y nunca se ha creado conocimientos de manera colaborativa a través de redes o entornos virtuales.

Realizar análisis comparativo de metodologías de transformación digital cumplidas con éxito en otros países

En cuanto al análisis comparativo de metodologías de transformación digital cumplidas con éxito en otros países, se presentaron 6 autores de diversos países y su análisis se describe en la Tabla 3.

Tabla 3 Metodologías de transformación digital cumplidas con éxito en otros países

Autores	Título de la investigación	País	Metodología
Maliqueo, et al. (2021)	Gestión de personas y las barreras para innovar en la transformación digital	Chile	Se identificaron las principales barreras en la gestión de personas para la innovación en la transformación digital, las acciones de innovación más comunes, el tipo de tecnología utilizada en los procesos, el nivel de conocimiento que tienen los expertos en la materia y el nivel de posicionamiento estratégico de la unidad de las áreas, concluyendo que es necesario un nuevo enfoque estratégico en la visión de la dirección general sobre la gestión de personas y cambios en sus funciones, procesos y servicios.
Alayón (2021)	Tecnologías disruptivas en la transformación digital de las organizaciones en la industria 4.0	Venezuela	La investigación se basó en la descripción de las tecnologías claves que existen hoy y las metodologías exitosamente en las organizaciones para lograr la transformación; para alcanzar que la transformación digital como "educación digital", para mejor comprensión para avanzar hacia las siguientes tecnologías en la industria 4.0.
García, et al. (2022)	Tecnologías digitales para la formación en empresas y entidades de la economía social	España	Con el estudio se conocieron los datos empíricos y la realidad de la transformación digital de entidades de la economía social y el contexto de la formación en empresas, para lo cual se aplicó la técnica de encuesta, mediante dos cuestionarios creados *ad hoc*: uno para trabajadores y otro para cargos directivos de empresas y entidades de la economía

			social, lo cual arrojó que carecen de ciertas competencias necesarias para el mundo digital, empresas y entidades de la economía social priorizan la dotación tecnológica.
Vacas (2018)	Transformación digital: del lifting a la reconversión	España	Transformación digital: la estrategia de los siete pasos: identificar los objetivos prioritarios, inspeccionar los obstáculos internos y externos eficaces, determinar nivel de adopción tecnológica ayudaría a alcanzar los objetivos eficientemente, establecer plazo de una tecnología obsoleta, considerar las nuevas tecnologías introducidas, evaluar el coste de oportunidad de una tecnología concreta e imaginar las aplicaciones de las nuevas tecnologías, para adaptarlas al tipo de organización.
Cuencas, et al. (2020)	Transformación digital de los departamentos de relaciones públicas y comunicación de una muestra de empresas españolas	España	El estudio se basa en la madurez de la transformación digital de las empresas españolas a través de un cuestionario para comunicadores, del que se desprende que el 73,6% de los departamentos de comunicación de las empresas participantes han alcanzado un nivel de madurez alto en esta transformación, que requiere un cambio cultural en la gestión corporativa, la contratación de nuevos perfiles, la reorganización del trabajo y el enfoque en las áreas de mejora para maximizar el retorno de los recursos invertidos. El 85% de estos departamentos tienen una visión global de la comunicación digital, aunque son conscientes de que todavía es necesario automatizar una serie de procesos.
Cueva (2020)	Transformación digital en la universidad actual	Ecuador	La investigación se basó en valorar desde una perspectiva holística en la transformación en el ámbito universitario latinoamericano. La metodología contempla un proceso completo de transformación en los 5 estados de madurez: resistente digital, explorador digital, jugador digital, transformador digital y disruptor digital

3.1.2 Determinar los requerimientos de infraestructura tecnológica, física y de seguridad necesarios.

A continuación, se presentan los principales requerimientos de infraestructura tecnológica, física y de seguridad necesarios para implementar una transformación digital efectiva en el área de salud al sur de Ecuador, como se presenta en la Tabla 4 :

Tabla 4

Requerimiento de infraestructura tecnológica, física y seguridad para implementar una transformación digital efectiva en el área de salud al sur de Ecuador.

	Descripción	Aplicaciones
Requerimiento de infraestructura tecnológica	Mejoras en la base de datos	El *Scrum master* aprobará o desaprobará la puesta en marcha del suministro, por parte del *Product Owner*, de requerimientos técnicos de gerentes, empleados y/o clientes que usarán la aplicación hacia el equipo de desarrollo.
	Simplicidad de la base de datos	Facilitar el acceso fácil y rápido a las bases de datos a los usuarios con poca experiencia o poco conocimiento
	Desarrollo flexible.	Las herramientas para gestionar bases de datos deben tener la capacidad de evolucionar y actualizar su funcionamiento
	Digitalización	Incluye Big Data, internet de las cosas, blockchain, cripto monedas, entre otros.
	Base de datos para toma de decisiones	Gestionar *insights* y procesar variables de datos con una capacidad sobrehumana.
Requerimiento de infraestructura física	Redes corporativas	Redes corporativas está el Big Data, el Internet de las Cosas, el Mobile y Computación en la Nube.
	Infraestructura de TI	Soporte a todo ese proceso de cambios
	Creación del Product Backlog	Ordenar los requerimientos y analizar cada uno de ellos. Identificar usuarios autorizados del sistema
	Programación	Desarrollo de la aplicación con el lenguaje de programación PhP con base de datos en mySQL
	Plataformas	Para dispositivos móviles iOS/ Android, y para vista en la web.
Requerimiento de infraestructura de seguridad	Seguridad sin concesiones	Cloud Computing, Data Analytics y Ecommerce.
	Digital Security en la nueva era de transformación digital	Protección de datos, infraestructuras críticas o redes y sistemas de información, pero ninguna está enfocada específicamente a la transformación digital.
	Seguridad digital	Digital Risk Officer, DRO, Security Ombudsman, Data Security Scientist, DSS, Digital Ecosystem Manager, DEM, Chief of Staff for Security, CSS, servidores, redes de comunicaciones, nube, IA, IoT o IIoT, entre otros.
	Sistema de seguridad de la información bajo la norma ISO 27001	Requisitos necesarios para establecer, implantar, mantener y mejorar continuamente un sistema de gestión de la seguridad de la información en una organización.

3.1.3 Seleccionar la metodología que mejor se ajusta a las necesidades de Ecuador para la implementación de transformación digital en el área de salud al sur de Ecuador

En función de lo obtenido anteriormente de la investigación se dedujo que la metodología que más se ajusta a las necesidades de Ecuador para la implementación de transformación digital en el área de salud al sur de Ecuador, sería la de Cueva (2020), debido a que aborda los estados de madurez de los procesos de transformación digital. Ademas proporciona herramientas al proceso de capacitación para el uso de la telemedicina en los procesos que se cumplen en este centro, para realizar servicios de

Teleconsulta, servicios de Telemonitoreo, servicio de telecuidado para pacientes, garantiza requerimientos de pruebas de los pacientes remotos haciendo uso de las TIC, facturación de los servicios al paciente de manera remota, permite la educación continua para personal de salud para la promoción de la tecnología. Así mismo, proporciona espacios virtuales para la formación de los profesionales de salud, incrementa los conocimientos a otros médicos por medios virtuales de acuerdo a su experiencia como profesional de la salud. Tambien permite compartir conocimientos a otros médicos por medios virtuales de acuerdo a su experiencia como profesional de la salud y garantiza que se comparta las experiencias de éxito sobre procedimientos o tratamientos con otros médicos a través de las Tecnologías de la información y comunicación, mediante la resistencia digital, los exploradores digitales, los jugador digital, transformador digital: las capacidades de Transformación Digital y Disruptor digital, en complemento con los requerimientos de infraestructura tecnológica, física y de seguridad.

4. Discusion y Conclusion

4.1 Discusion

La metodología que resultó apta para desarrollar los estados de madurez de los procesos de transformación digital se basan en el uso de TIC en el proceso de capacitación para el uso de la telemedicina en los procesos que se cumplen en los centros de salud, la inversión en una infraestructura tecnológica y la educación continua para personal de salud para la promoción de la tecnología. En el mismo orden de ideas, cabe señalar que Baird (2021) considera necesario el estudio y planificación de la ejecución de productos opcionales de capacitación, consultoría y mantenimiento de los proyectos de desarrollo centrado en la información y resulta fundamental incorporar el reclutamiento internacional de profesionales que sean programadores y así poder optimizar sus funciones.
Mientras que Lema (2021) indicó que la transformación digital en el desenvolvimiento laboral se ve envuelto en un grupo de alteraciones tecnológicas que permiten que la institución adopte estrategias activas para conseguir soluciones inmediatas, así mismo, Lorenzo (2017) menciona que la transformación digital requiere un modelo interdisciplinario y multidimensional que permita a las empresas competir y satisfacer las necesidades de sus clientes y se encuentra en ascenso y emergen como mecanismo de evolución de capacidades de las empresas en esta era moderna.

4.2 Conclusion

Se evidenció que el centro de salud realiza esfuerzo para la promoción de la calidad total de los servicios, y además aplican procedimientos con técnicas innovadoras que captan la atención de los usuarios, adaptan a la estrategia competitiva en los procesos digitales, el personal se encuentra dispuesto afrontar cambios hacia la digitalización de procesos se plantean ideas de negocio adviertan un giro transformacional hacia lo digital. Sin embargo, existe una inversión insuficiente en la adquisición de recursos con tecnologías de punta, lo cual conlleva a que los servicios de teleconsulta. servicios de telemonitoreo y servicios de telecuidado para pacientes no cumplan con los estándares

de calidad exigidos en la telemedicina. Así mismo, nunca se ha propiciado la educación continua para personal de salud y la transferencia de conocimientos a otros médicos por medios virtuales de acuerdo a su experiencia como profesional de la salud.

Por lo cual, se concluyó que se requiere de una infraestructura tecnológica con simplicidad y mejora de base de datos, digitalización y desarrollo flexible; una infaestructura física en donde se maneje una infraestructura TI, programas de telemedicina, y una plataforma adaptada al centro de salud y los servicios de teleconsulta, telemonitoreo y telecuidado, y con una infraestructura de seguridad en donde considere la seguridad sin concesiones, digital Security, seguridad digital y sistema de seguridad de la información bajo la norma ISO 27001. Por otro lado, se concluyó que la transformación digital para que funcione en el centro de salud bajo la telemática debe orientarse en los 5 estados de madurez con una estructura organizada, iniciativas de transformación, objetivos corporativos, disrupciones en el mercado y un innovador modelo de negocio.

Referencias

1. Alayón, E. Tecnologías disruptivas en la transformación digital de las organizaciones en la industria 4.0. Revista Scientific, 6 (21) 1-8 (2021)
2. Baena, G. Metodología de la Investigación .3ra edn. Ciudad de México, México: Grupo Editorial Patria (2017)
3. Baird, J.. Plan de negocios para la creación de una empresa de desarrollo de soluciones web con metodología Scrum para la transformación digital de Pymes de la ciudad de Quito, [Tesis de maestría]. Universidad Internacional Sek, Quito, Ecuador (2021)
4. Bastias, E., y Ulrich, A.: Transformación digital del sector salud en América Latina y el Caribe: la historia clínica electrónica. LILACS, 1(40) 1-40 (2019)
5. Cabrol, M., y Pombo, C.: Posibles transformaciones en salud, educación y trabajo a través de la digitalización en la salida de la pandemia en América Latina y el Caribe: Publications BID 1(1), 1-16 (2021).
6. Cuencas, J., Matilla, K., & Compte, M. Transformación digital de los departamentos de relaciones públicas y comunicación de una muestra de empresas españolas. Scielo, 1-8 (2020).
7. Cueva, D. Transformación digital en la universidad actual. Scielo, 1-8 (2020)
8. García, P., Montiel, F., & Paz, M. Tecnologías digitales para la formación en empresas y entidades de la economía social. Revista científica de Educación y Comunicación, 1-19 24(1) (2022)
9. Hernández, R., Fernández, C., y Baptista, M. Metodología de la Investigación.6ta edn. McGRAW-HILL / INTERAMERICANA EDITORES, S.A. DE C.V. México DF (2014)
10. Hernández, R., y Mendoza, C. Metodología de la investigación. Mc Graw Hill Education México DF (2018)
11. Lema, K.. La transformación digital y el desempeño laboral en los empleados del departamento administrativo del Distrito de Salud 02D03 San Miguel, Provincia Bolívar, Zona 5 [Tesis de pregrado]. Universidad Técnica de Ambato, Ambato, Ecuador (2021)
12. Lorenzo, O. (2017). Modelos de Madurez Digital: ¿en qué consisten y qué podemos aprender de ellos? Boletín de estudios económicos, LXXI (2017)
13. Maliqueo, C., González, J., Mardones, R., & Ardiles, M. Gestión de personas y las barreras para innovar en la transformación digital. Revista Venezolana de Gerencia, 510-532 (2021)

14. Moreno, B., Muñoz, M., Cuellar, J., Domancic, S., y Villanueva, J. Revisiones Sistemáticas: definición y nociones básicas. Revista clínica de periodoncia, implantología y rehabilitación oral, 11(3), 184-186 (2018).
15. Montero, J., Merino, F., Monte, E., Ávila, J., y Cepeda, J.: Competencias digitales clave de los profesionales sanitarios. Educación Méd, 21(5) 338-344 (2020).
16. OPS Homepage, https://www3.paho.org/ish/index.php/es/telemedicine
17. Peralta, D., Cáceres, M., y Morocho, V.: Digital Identity Proposal for Unified Medical Record using Blockchain technology. Digital Indentify IEE 1(1) 1-6 (2021)
18. Saigí, F., Torren, J., Robles, N., Pérez, J., y Baena, M.: Estudio sobre Telemedicina in-ternacional en América Latina. Banco Interamericano de Desarrollo. 1(1) 1-285 (2021).
19. Vacas, F. Transformación digital: Del Lifting a la reconversión. CEF. Ciencia y educación, 10, 135-143. (2018)
20. Vallejo, J. La telemedicina y su regulación en Ecuador. Edición Médica, 22(17) 1-3 (2020).

Aplicación de tecnologías LPWAN basadas en LoRa en el monitoreo de fuentes hídricas de los páramos andinos

Luis González[1], Andrés Gonzales[1], Santiago González[1], and Alonso Cartuche[2]

[1] Department of Electric, Electronic and Telecommunication Engineering, Universidad de Cuenca, Av.12 de Abril, CP. 010203, Cuenca, Ecuador
luis.gonzaleza@ucuenca.edu.ec amauta.gonzales@ucuenca.edu.ec
santiago.gonzalezm@ucuenca.edu.ec
[2] Carrera de Ingeniería Ambiental y El Centro de Investigaciones Tropicales del Ambiente y Biodiversidad (CITIAB), Universidad Nacional de Loja, Ciudad Universitaria Guillermo Falconí, CP. 110150, Loja, Ecuador
victor.cartuche@unl.edu.ec

Abstract. This paper presents the design of a water source monitoring system based on LoRa technology for the Tres Lagunas Andean high-altitude wetlands ecosystem (Ecuador). The solution has been implemented using mainly an ATmega1284p microcontroller, an SX1278 transceiver and hydrological sensors. The data is transmitted from the study site to the TTN server and sent via the MQTT protocol to the Node-RED platform. On the other hand, a graphical interface has been developed that allows analyzing historical data of temperature, dissolved oxygen (DO), oxidation-reduction potential (ORP) and hydrogen potential (pH). Furthermore, energy consumption tests and LoRa physical layer experiments have been performed with the prototype. Results reveal the proper operation of the prototype. In particular, it has been observed that SF9 and SF10 present packet reception rates higher than 97 %. Regarding SF7 and SF8, they was discarded for this type of scenarios due to the packet loss rate higher than 10 %. The main contribution of this work is the proposal of a portable, low-cost and open source prototype, focused on the transmission of hydrological data obtained in Andean high-altitude lakes through IoT technologies for the administration, management and control of water resources that represent a fundamental component of a smart city.

Keywords: LoRa · Monitoring system · Wetlands ecosystem.

1. Introducción

Las aplicaciones basadas en tecnologías IoT (*Internet of Things*) constituyen una pieza fundamental en el ámbito de la innovación y el desarrollo sustentable [1]. En particular, las tecnologías de gestión de recursos hídricos son componentes vitales de las *Smart Cities* [2], promoviendo el uso de datos en tiempo real a

través de plataformas *online* con una eficiencia significativa frente a los métodos tradicionales [3]. Estos datos usualmente son potencial de hidrógeno, conductividad, oxígeno disuelto, entre otros. Los cuales son medidos a través de sensores y permiten determinar la calidad del agua [4]. Con respecto a las fuentes de agua, suelen estar ubicadas en zonas alejadas de la ciudad y carecen de servicios como acceso a Internet, energía eléctrica, entre otros, por tanto, soluciones basadas en IoT y redes de sensores (WSN) permitirían crear sistemas de monitorización que mejoren la gestión de los recursos hídricos.

Por otra parte, los recursos hídricos de los sistemas acuáticos son vulnerables ante el cambio climático debido a varios factores, por ejemplo, el aumento de temperatura puede contribuir a la evaporación de las lagunas, reducción del hábitat y alteraciones en la calidad del agua [5]. En tal contexto, en [6] se realiza una valoración económica del almacenamiento de agua y carbono en los bofedales de los páramos ecuatorianos. El área de estudio abarcó los páramos y humedales de los cantones de Nabón, Oña, Saraguro y Yacuambi, específicamente los sectores de Tres Lagunas y del río Shincata. Cabe indicar que a pesar de la existencia de 2 estaciones del INAMHI (Instituto Nacional de Meteorología e Hidrología), una en Oña (M421) y la otra en San Lucas (M32), debido a la ubicación de dichas estaciones no se puede determinar con exactitud las condiciones climáticas del área de estudio y por ende la comprensión de estos ecosistemas acuáticos es casi nula. En particular, las estaciones solo cubren las vertientes del sistema hídrico del Pacífico y Amazónico de la zona de estudio. Los datos recogidos de dichas estaciones, posiblemente presenten discrepancias con las condiciones reales del sitio, debido a los aportes de las lluvias, neblina y llovizna.

En relación a Tres Lagunas, este ecosistema contribuye a la subsistencia de las poblaciones cercanas debido a su gran valor ecológico, económico, social y cultural. La principal contribución es el suministro de agua para el consumo doméstico y el riego de cultivos. Además, es un lugar de suma importancia cultural para los 3 cantones porque se considera un lugar mágico, vinculado con las tradiciones religiosas ancestrales, la manifestación de poder y energía de la madre tierra [7]. Actualmente, este complejo de humedales se ve amenazado por varios factores, por ejemplo, la vía que conecta a Saraguro y Yacuambi cruza por esta zona y representa un gran riesgo para la conservación y protección de este sector. En este sentido, es indispensable conocer el estado de las lagunas con el objetivo de prevenir un déficit de los recursos hídricos, mejorar la calidad del agua y mitigar el efecto que pueda causar la contaminación antrópica como la circulación de vehículos, residuos de turistas, entre otros.

Tres lagunas no dispone de un sistema que permita monitorear el estado del clima y del agua, las estaciones más cercanas se encuentran a varios kilómetros. Factores como la distancia, condiciones climáticas adversas, limitaciones en el acceso a la red móvil e Internet han impedido la implementación de cualquier tipo de estación meteorológica en las lagunas de interés. Por consiguiente, el despliegue de estaciones de monitorización en el sector, representa una contribución para determinar el estado actual y las vulnerabilidades a las que se encuentran expuestas los ecosistemas acuáticos del sitio y brindar datos que permitan to-

mar decisiones a las instituciones correspondientes para la conservación y gestión estratégica de los recursos naturales.

En este contexto, el presente trabajo se enfoca en una solución tecnológica que permita monitorear el sitio Tres Lagunas, a través de un dispositivo de adquisición y transmisión de datos, desde el lugar de estudio hacia Internet. Este documento está dividido en 5 secciones, en la segunda sección se presenta el estado del arte, la tercera sección indica la arquitectura de monitorización, en la cuarta sección se presentan los resultados y se finaliza en la quinta sección con las conclusiones.

2.　　Trabajos Relacionados

La integración de soluciones IoT en *Smart Cities* permite mejorar los distintos servicios a través de nuevas tecnologías. Por ejemplo, la supervisión de los recursos hídricos permite una gestión sostenible de los servicios hídricos. La mejor opción cuando estos lugares se encuentran en zonas remotas, es utilizar redes de largo alcance como LPWAN (*Low Power Wide Area Network*). Por ejemplo, las redes basadas en LoRa (*Long Range*), poseen características para poder adaptarse a diversos escenarios. En este contexto, a continuación se discuten estudios relevantes relacionados con tales aplicaciones.

En relación con el registro de parámetros del agua, los dispositivos de recolección de datos requieren equipos especiales denominados sondas que suelen ser muy costosos [8]. Por consiguiente, es fundamental desarrollar prototipos que ofrezcan mayor accesibilidad para su uso. En cuanto a la implementación, el registro de estos datos ambientales se realiza mediante dispositivos tales como microcontroladores (MCU), donde la información medida por los sensores es preprocesada y almacenada internamente en la estación también conocida como nodo [9]. Cuando los nodos se usan en lugares remotos, el suministro de energía viene dado por baterías, en este contexto existen varios trabajos que han logrado incrementar el tiempo de duración de las baterías por periodos mayores a 1 año [10] [11].

En este sentido, en [12] se describe un prototipo, donde usan sensores de bajo costo para la adquisición de datos fisicoquímicos del agua. Durante un periodo de 45 días se probó el funcionamiento del dispositivo conjuntamente con un equipo profesional, obteniendo una alta correlación entre los datos de ambos equipos, verificando la calidad de la información del prototipo.

Por otra parte, el monitoreo de los ecosistemas hídricos es muy costoso en términos de recursos cuando se trata de sitios ubicados en lugares remotos y es necesario acceder de forma manual para recoger los datos [13]. Una solución es utilizar tecnologías de comunicación inalámbrica. En este contexto, una tecnología de transmisión adecuada sería LoRa/LoRaWAN. El protocolo de comunicación y la arquitectura de esta tecnología admiten comunicación bidireccional de bajo costo, móvil y segura, además está optimizada para un bajo consumo de energía y diseñado para escalar fácilmente [14]. Por ello, el uso de LoRa/LoRaWAN es cada vez más frecuente en diferentes aplicaciones y se adap-

ta a diversos escenarios. Por ejemplo, en [15] se destaca la importancia de las ventajas de LoRa en cuanto a la cobertura y rendimiento energético, lo cual facilita su funcionamiento en sitios poco caracterizados, como los de alta montaña y glaciares, permitiendo abrir nuevos campos de investigación de dichas zonas.

En lo que respecta a sitios remotos donde no hay acceso a la red eléctrica, el recurso energético de las baterías resulta crucial para su funcionamiento, como se discute en [16], estudio en el cual se realiza un monitoreo de aguas subterráneas, donde los nodos registran las variables y las transmiten a un *Gateway* LoRa, obteniendo 8 días de independencia energética. Otros métodos aumentan los recursos energéticos de los nodos mediante una combinación de fuentes energéticas, por ejemplo solar e hidroeléctrica, como se presenta en [17], que proporciona hasta 432 horas de autonomía a sus nodos.

En este sentido, uno de los factores de mayor consumo energético en los nodos LoRa se genera en la etapa de transmisión. En [18] se destaca la importancia de seleccionar los parámetros de transmisión adecuados, caso contrario la vida útil del nodo es más corta. Por ejemplo, el aumento de potencia para la transmisión de paquetes afecta drásticamente al consumo de energía como se reporta en [19], donde su estudio se centra únicamente en el resto de parámetros para mejorar la comunicación. En este contexto, el uso de valores de SF (*Spreading Factor*) bajos permitiría mejorar el rendimiento energético. Por ejemplo, en [20] los autores recomiendan usar SFs bajos (alta tasa de datos) y una potencia de transmisión alta solo para los nodos que se encuentren alejados del *Gateway*. Otro enfoque se describe en [21], donde se evalúan diferentes longitudes de *payload* y los parámetros de capa física para reducir el ToA (*Time on Air*), los autores recomiendan dejar el BW (*Bandwidth*) fijo y solo enfocarse en el SF y CR (*Coding Rate*), por otra parte indican que es necesario disminuir el *payload*.

En lo que respecta a escenarios de montaña, en [22] se presenta una evaluación de parámetros LoRa, los autores muestran que la potencia de transmisión de radio no es un parámetro dominante que afecte a la red, en cambio el BW, el SF y el CR juegan un papel más relevante. En estos escenarios de montaña, se han alcanzado coberturas de 3 km como se reporta en [23], donde evalúan la tecnología LoRa usando tres tasas de datos en la banda de 433 MHz, con una potencia de transmisión de 20 dBm, destacando que la línea de vista es un factor relevante para esta tecnología de transmisión.

En este contexto, se observa que el uso de LoRa para transmisión de datos ambientales es viable y permite una adaptación a diferentes entornos por su variedad de propiedades que pueden ser configuradas de acuerdo a los requerimientos. En el presente estudio se desarrolló un prototipo de adquisición de datos fisicoquímicos enfocado en lagunas de los páramos andinos al sur del Ecuador, empleando la tecnología de transmisión LoRa para el monitoreo de fuentes hídricas.

3.　Arquitectura de Monitorización

En esta sección se detalla el funcionamiento de la arquitectura de monitoreo, desde la implementación del prototipo hasta la presentación de los datos empleando servicios *cloud*.

3.1.　Implementación del Prototipo

La estación hídrica fue implementada mediante herramientas *hardware* y *software* que faciliten su reconfiguración. En la parte central de la estación, se usa un MCU ATmega 1284p de la familia *Pico Power* [24]. Por otra parte, la medición de variables fisicoquímicas del agua se realiza con sensores analógicos y digitales. En la Figura 1 se presenta la integración del prototipo.
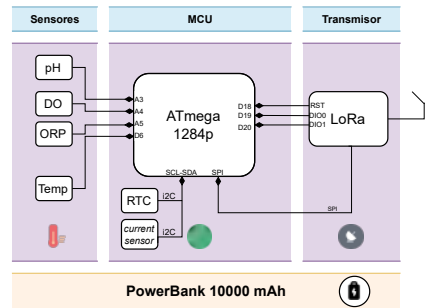
Figura 1: Diseño del prototipo.

Como se observa en la Figura 1 el prototipo consta de 4 sensores, tres son analógicos: Gravity pH [25], DO [26], ORP [27], y un sensor de temperatura digital DS18B20, las características técnicas más relevantes de estos equipos se presenta en la Tabla 1. Por otra parte, se agrega un sensor de corriente INA219 para medir los niveles de energía que consumen los periféricos y la estación de agua en general. Adicionalmente, se incorpora un módulo RTC (*Real Time Clock*) DS3231 que brinda las marcas de tiempo al sistema. Para el control de los sensores, se empleó librerías *open source* disponibles en [28]. En relación al protocolo de comunicación, los sensores digitales usan el protocolo i2C y los sensores analógicos son leídos con el ADC (*Analog-to-Digital Converter*) de 10 bits que incorpora el MCU.

En relación a la capa de red, está compuesta por el módulo LoRa RA-02 [29] y su configuración se realiza mediante las librerías MCCI-LoRaWAN-LMIC [30] para trabajar en una red LoRaWAN. De esta manera los datos se transmiten de forma inalámbrica hacia un *Gateway* que sube los datos al servidor *The Things Network* (TTN). Para el suministro de energía se incorporó un *PowerBank* de 10000 mAh. Finalmente, se diseñó una placa de circuito impreso (PCB) que

Tabla 1: Características técnicas de los sensores

Parámetros	pH	ORP	DO	DS18B20	Unidades
Rango de medición	0.1 a 14	-1500 a +1500	0 a 700	-55 a +125	pH,mV, %, ºC
Precisión	±0.2	±1	±2	±0.2	pH,mV, %, ºC
Tiempo de respuesta	0	0	0	750	ms
Consumo energético	3	3	3	1	mA

reúne todos los componentes para facilitar el manejo del prototipo, en la Figura 2 se observa como está implementada la PCB y sus componentes.
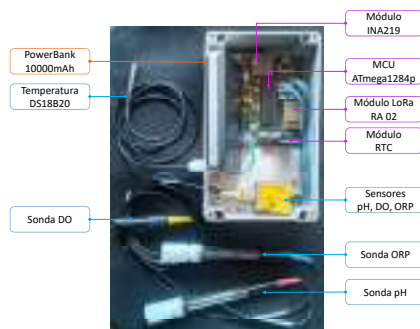
Figura 2: Componentes del prototipo.

3.2. Sistema de Monitoreo Hídrico

En la Figura 3 se presenta un diagrama funcional del sistema de monitorización. Para la programación del ATmega se utilizó la plataforma Arduino IDE [31], de esta manera la gestión de sensores y módulos es más flexible a partir de librerías disponibles para los equipos, promoviendo un desarrollo más eficiente.

En cuanto al servidor TTN, se requiere configurar los equipos de la red LoRaWAN. En particular, primero el nodo se configura en modo ABP (*Authentication By Personalisation*) y sus credenciales AppSKey y NwkSKey se registran en TNN así como en el *software* del nodo, con estas credenciales la información es encriptada y viaja desde el nodo hasta el servidor. Por su parte, el *Gateway* se configuró en TTN mediante la dirección MAC (*Media Access Control*) y se accede a Internet a través de la red móvil.

Los datos en TTN son descifrados y enviados a través de un servidor MQTT (*Message Queuing Telemetry Transport*) a la plataforma Node-RED, donde se implementa una API (*Application Programming Interface*) con los nodos de red (*network*): *http in* y *http response* que proporcionan *endpoints* con los datos almacenados, los cuales podrán ser visualizados de forma más amigable a través de
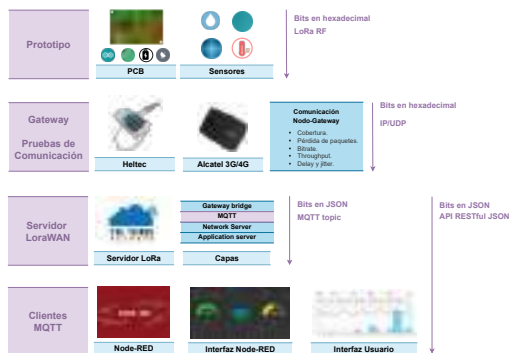
Figura 3: Diagrama funcional del sistema.

una interfaz desarrollada con JavaScript mediante la librería APEXCHARTS.JS. Actualmente, a efectos de la aplicación solo se ha desplegado un *endpoint* con el método *GET*, que permite recuperar la totalidad de datos de las variables disponibles. En esta interfaz el usuario puede observar los cambios de las variables respecto al tiempo, analizar resultados estadísticos de la información, acceder a datos históricos y descargarlos fácilmente. De esta manera el sistema es capaz de medir, transmitir y presentar al usuario variables fisicoquímicas obtenidas en lagunas alto andinas.

4.   Evaluación y Resultados

Esta sección presenta la caracterización del prototipo, tanto a nivel de red como en el proceso de adquisición de datos.

4.1.   Análisis del comportamiento del prototipo LoRa en diferentes escenarios

En la presente sección se examina el comportamiento del prototipo bajo distintas condiciones meteorológicas, distancias y configuraciones de los parámetros SF y CR tanto en una zona rural como en el alto páramo, examinando las métricas de PRR (*Packet Reception Rate*), *throughput/bit rate*, RSSI (*Received Signal Strength Indicator*), *delay* y *jitter*, mediante histogramas con intervalos de confianza.

Zona Rural. Se consideró evaluar primero la zona rural en lugar del páramo por la facilidad de ubicación del nodo-*Gateway* y de esta forma obtener datos de referencia como la tasa de bits, cobertura, la ubicación de la antena, que permitan apreciar las capacidades que posee el prototipo al enfrentarse a distintos entornos. La zona rural fue la parroquia de Urdaneta del cantón Saraguro.

(a) PRR.

(b) Bit Rate en Rx por SF.

(c) Bit Rate en Rx por CR.

(d) RSSI por SF.

(e) RSSI por CR.

(f) Delay por SF.

(g) Delay por CR.

(h) Jitter por SF.

(i) Delay vs jitter.
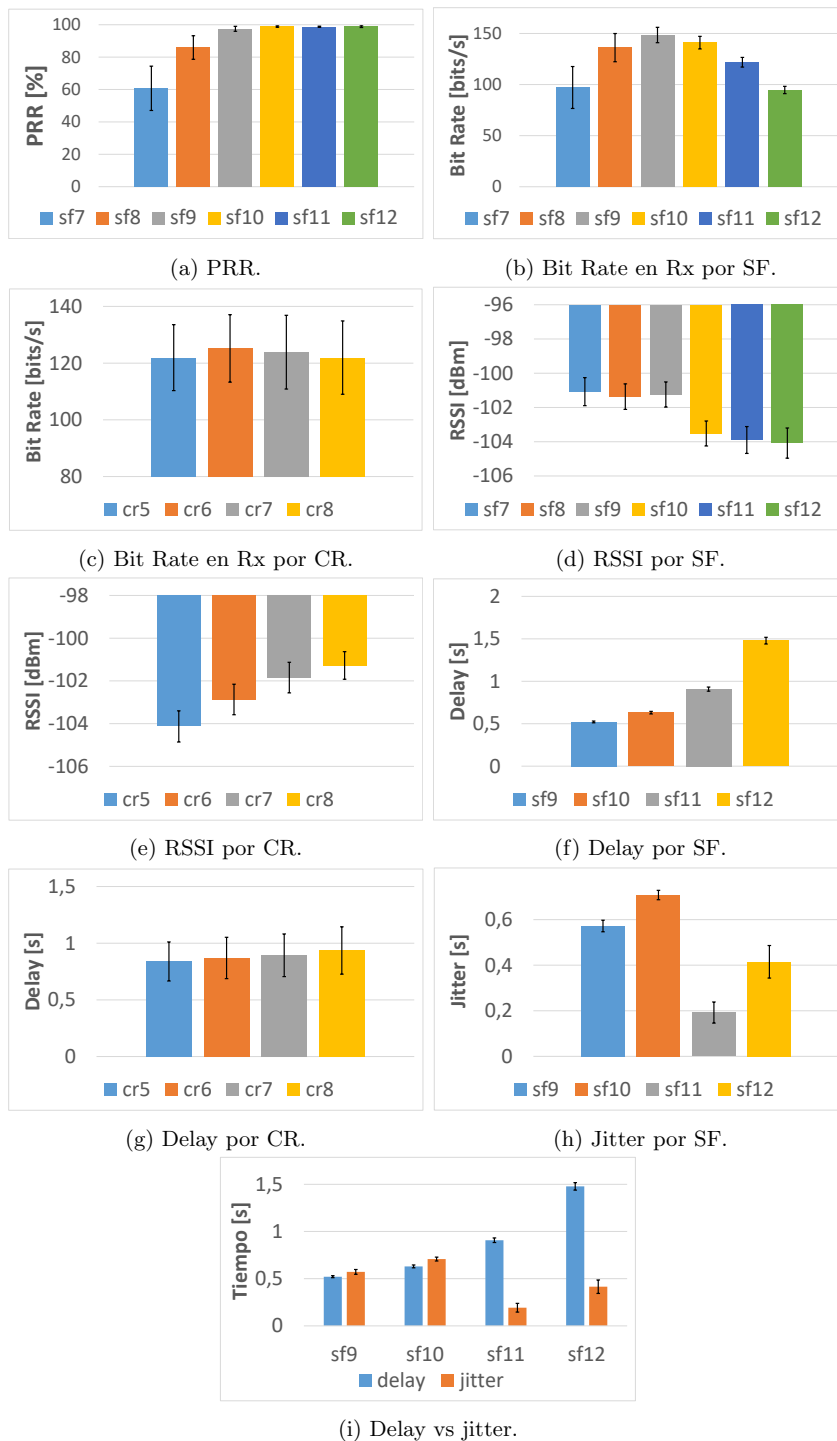
Figura 4: Resultados de las métricas obtenidas en la zona rural.

Urdaneta se encuentra aproximadamente a 30 km de distancia de Tres La-
gunas con una altitud de alrededor de 2490 m.s.n.m. Con respecto al entorno en
la zona rural, se observaron muchos arbustos y árboles altos entre el nodo y el
Gateway, sin embargo; no interfieren directamente en la línea de vista. Los expe-
rimentos se realizaron en 4 puntos a 500 m, 1 km, 1.7 km y 2.2 km de distancia
entre el nodo y el *Gateway*.

El histograma general de cada SF se presenta en la Figura 4a. Donde se
observa que tanto SF7 como SF8 tienen la tasa más baja, por lo tanto, son los
menos recomendables para este escenario. A partir de SF9 se obtiene un PRR
promedio mayor a 97 % con un intervalo de confianza muy bajo, lo que demuestra
estabilidad en la conexión.

En cuanto a los resultados generales del *bit rate* por cada SF, la Figura 4b
muestra una forma de campana, que se debe a la pérdida de paquetes obtenidas
para el caso de SF7 y SF8, por tanto el *bit rate* se ve directamente afectado. En
cambio, para SF10, SF11 y SF12, el PRR es del 99 %. Sin embargo, el *bit rate*
en el transmisor disminuye a medida que aumenta el SF, por lo tanto, la mejor
opción para este caso resultan los valores de SF9 o SF10, ya que están en un
punto intermedio y permiten obtener la tasa de bits más alta posible. Por otro
lado, el *bit rate* disminuye a medida que aumenta el denominador del CR (ver
Figura 4c), a excepción de CR5.

En los resultados del RSSI por cada SF de la Figura 4d, se observa que
los datos de potencia han variado muy poco entre sí, sin embargo; es clara la
tendencia de reducción de RSSI a medida que aumenta el valor del SF. Es decir;
que la señal es ligeramente más fuerte cuando el SF disminuye, mientras que
un mayor denominador en el CR mejora la potencia de la señal (ver Figura 4e),
generando cambios entre cada CR de aproximadamente 1 dBm de diferencia.

En la Figura 4f se presentan los valores de *delay* promedio para cada SF.
Existe una clara tendencia al aumento del *delay* a medida que se incrementa el
SF, lo que corresponde con la teoría, ya que un SF más grande representa mayor
ToA. Con respecto al CR, en la Figura 4g se puede observar que el retraso es
mayor cuando el denominador de la tasa de codificación es mayor, ya que existen
más bits para la transmisión. Sin embargo, la variación es muy pequeña, pasando
de 0.84 s al valor máximo de 0.94 s, por lo que la incidencia del CR en el *delay*
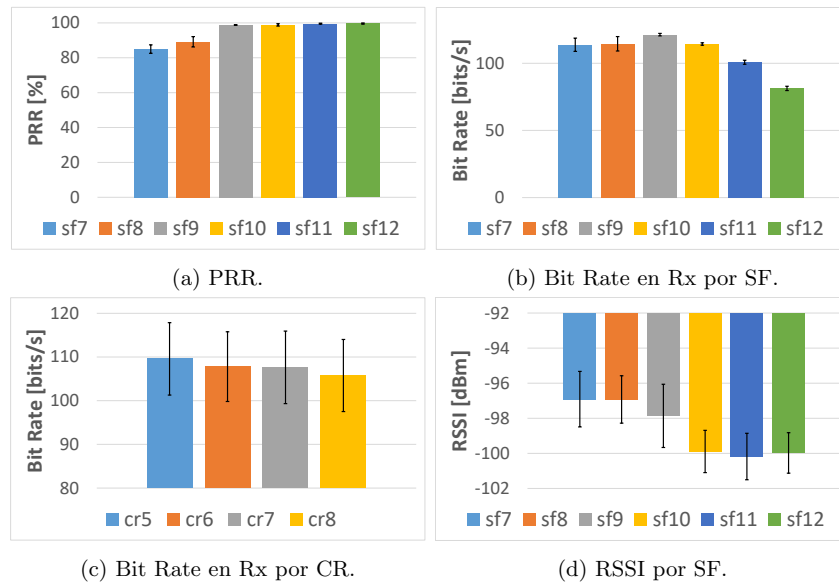no es considerable.

En cuanto a los resultados presentados en la Figura 4h respecto al *jitter*, di-
cho comportamiento está relacionado con la exactitud del RTC. En particular, el
dispositivo RTC (DS3231) posee una escala mínima dada en segundos, entonces
el *delay* mínimo es de 1 s, lo que produce que los retrasos de milisegundos o me-
nos, sean indetectables. Entonces, mientras más cercano sea el *delay* promedio a
valores enteros, existe menos probabilidad de varianza en el *delay*. Tal como se
observa en la Figura 4i, el *jitter* más bajo corresponde al SF con el *delay* prome-
dio más cercano a 1 s, en este caso SF11. Pero esto no quiere decir que al utilizar
SF11 tendrá menos *jitter* y una conexión más confiable, sino se trata de un error
en la precisión del RTC. Sin embargo, el *jiiter* afecta a las comunicaciones con

altas tasas de bits o aplicaciones que requieran datos en tiempo real, por lo que para este caso el comportamiento del *jitter* no afecta a la red.

Zona Alto Páramo. En el páramo, el entorno es el adecuado para LoRa, puesto que los resultados de la zona rural muestran un excelente rendimiento cuando la línea de vista está totalmente despejada y en Tres Lagunas no existen interferencias considerables. El lugar está en su mayoría cubierto de pasto, pequeños arbustos y plantas silvestres que no representan un obstáculo. Los dos puntos elegidos para la ubicación del nodo y el *Gateway* se encuentran a 1 km y 1.2 km de distancia entre sí.

En la Figura 5a se presenta el resultado general del PRR para todos los puntos y combinaciones de CR. El PRR tiende a aumentar a medida que el SF aumenta, llegando a tener un promedio de 100 % de paquetes recibidos en SF11 y SF12. Además, se observa que SF9 y SF10 tienen un excelente rendimiento, presentando un PRR promedio de 99 % con intervalos de confianza cercanos a cero. Por lo tanto, con respecto al PRR, es recomendable utilizar cualquier SF mayor a 9.

El *throughput* general para los valores de SF y CR se presentan en las Figuras 5b y 5c, respectivamente. La tasa de bits tiende a disminuir a medida que aumenta el SF, a excepción de SF7 y SF8, debido a la pérdida de paquetes. Por lo tanto, sigue siendo SF9 la mejor opción con respecto al *bit rate* para este escenario, ya que proporciona la tasa de bits más alta posible. En lo que respecta al CR, el *bit rate* disminuye mientras el denominador del CR incrementa, pero la variación entre cada CR es muy pequeña.

(a) PRR.

(b) Bit Rate en Rx por SF.

(c) Bit Rate en Rx por CR.

(d) RSSI por SF.

(e) RSSI por CR.

(f) Delay por SF.

(g) Delay por CR.
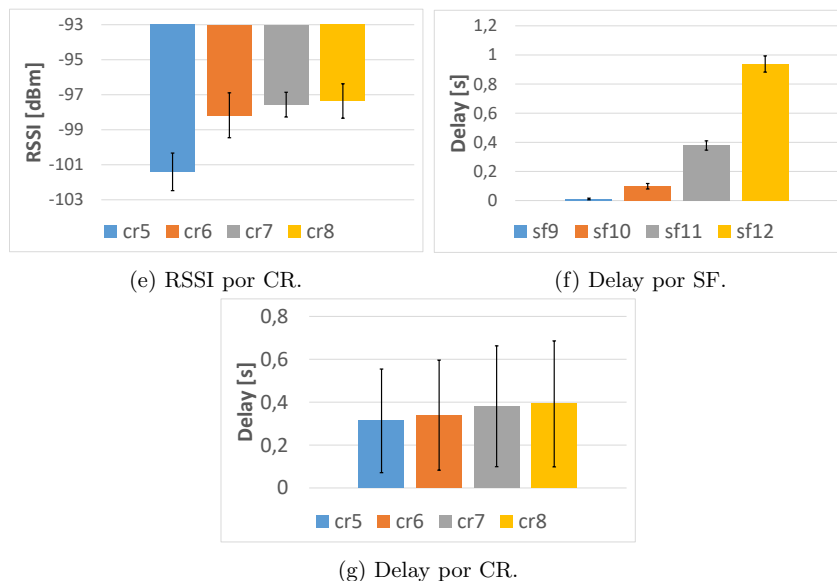
Figura 5: Resultados de las métricas obtenidas en la zona alto páramo.

Con respecto a los valores de RSSI por cada SF, la gráfica de la Figura 5d presenta una clara tendencia de disminución del RSSI a medida que aumenta el SF. Sin embargo, la degradación es bastante pequeña, por ejemplo, SF10, SF11 y SF12 tienen aproximadamente la misma media. Los valores de CR obtenidos en la Figura 5e muestran que el RSSI aumenta a medida que el denominador del CR es mayor, aunque la diferencia sea mínima. Al igual que en la zona rural, un denominador mayor de CR, mejora la potencia de la señal.

En la Figura 5f se presentan los resultados del *delay* para este escenario. Los datos corresponden con la teoría, porque a medida que el SF aumenta, también aumenta el ToA, lo que genera un *delay* mayor. El resultado más interesante se observa en SF9, donde existe un retardo de aproximadamente 10 ms y una variabilidad reducida, lo que se refleja en los intervalos de confianza. Observando SF9 y SF10, es evidente que los retardos también son muy pequeños en comparación con la zona rural, reiterando la importancia de la línea de vista para LoRa. Con respecto a SF12, el retardo es aproximadamente de 1 s. En cambio, en la Figura 5g se observa que a medida que el denominador del CR aumenta, también aumenta el retardo. Sin embargo, en este caso los intervalos de confianza son muy amplios como consecuencia de los valores de SF, puesto que el resultado corresponde a la media de todos los CR para cada SF y punto de prueba.

En la Figura 6, se presentan fotografías realizadas durante el desarrollo de los experimentos en los escenarios de estudio.

(a) Rural.   (b) Páramo.

Figura 6: Experimentos desarrollados en ambos escenarios.

4.2.   Consumo Energético

Considerando que el prototipo está alimentado por una batería, es muy importante tener una perspectiva general del consumo de energía durante su funcionamiento. En la Figura 7a se indica el consumo de corriente del prototipo durante un periodo de 30 min, las medidas se tomaron con un intervalo de 1 s y se graficaron los intervalos de confianza con un 95 % de fiabilidad. En cuanto a la interfaz LoRa, se usa SF9, BW 125 kHz, CR 4/5 y una potencia de 14 dBm en la frecuencia de 433.175 MHz.
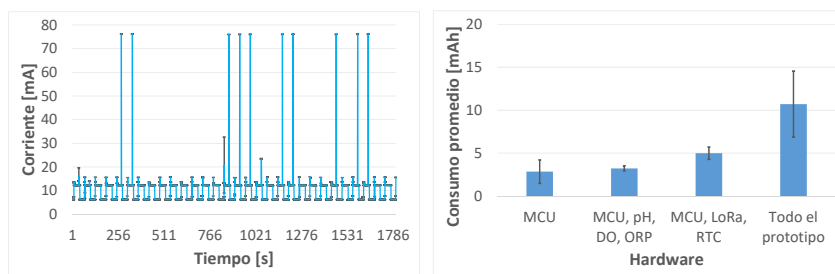
(a) Corriente requerida.   (b) Energía requerida.

Figura 7: Consumo energético del prototipo.

En la Figura 7a también se observa corrientes máximas de 76.26 mA y mínimos de 6.18 mA, el máximo se debe a los picos de corriente que causa la etapa de transmisión LoRa y el mínimo es durante las etapas de bajo consumo. En

cuanto a los módulos, sensores y periféricos del prototipo, para determinar la corriente que requieren se realizaron diversas mediciones, cuyos niveles de corriente promedio se indican en la Figura 7b. En relación al MCU, su consumo es de 2.84 mAh y al adicionar los sensores su incremento no fue significativo llegando a 3.22 mAh, en cambio al usar el módulo LoRa con el RTC alcanzó los 4.99 mAh y el consumo de todo el prototipo fue de 10.7 mAh.

Finalmente, se realizaron pruebas con una fuente energética de 10000 mAh para constatar el correcto funcionamiento del prototipo, donde se obtuvo aproximadamente sólo 8 días de autonomía. Debido a las pérdidas internas del *PowerBank* no se logró aprovechar toda su capacidad, sin embargo, el tiempo fue suficiente para realizar la instalación y evaluación del prototipo.

5.   Conclusiones

En este artículo se ha presentado una aplicación LPWAN basada en LoRa cuya función es monitorizar fuentes hídricas en los páramos andinos, donde los resultados muestran que es posible implementar el sistema en estos escenarios. Durante el análisis se observó que en general SF7 y SF8 tienen el peor rendimiento, además el PRR menor a 85 % es el aspecto más relevante que obliga a descartar estos factores. Entre las opciones restantes: SF 9, 10, 11 y 12, todas serían una buena opción, sin embargo, el *bit rate* disminuye a medida que el SF aumenta, por ejemplo SF12 en el páramo presenta un *bit rate* de 81 bits/s y para SF10 de 114 bits/s, lo que evidencia menos paquetes transmitidos y por lo tanto, menos recibidos a pesar que el PRR sea casi del 100 %. Con respecto al *delay*, también aumenta a medida que sube el SF y se observa claramente en el páramo, donde existe una diferencia de casi un segundo entre SF9 y SF12. Estos resultados reflejan que SFs mayores producen un mayor consumo de energía, porque requieren más tiempo para la transmisión. En el caso del RSSI, se observa que los SFs más bajos tienen una potencia de señal más fuerte, sin embargo, existe una mayor pérdida de paquetes. Es importante recordar que los SFs bajos son menos resistentes al ruido y tienen menos bits redundantes. Entonces, basados en las consideraciones anteriores, lo más adecuado es elegir el menor SF que presente un PRR alto, en el caso de la zona rural sería SF10 y en el páramo SF9. Con respecto al CR, la diferencia entre elegir uno u otro es mínima en todos los casos, a diferencia del SF, que sí afecta considerablemente a la red.

Comparar los resultados por cada punto facilita la elección del mejor escenario para LoRa, concluyendo que el mejor rendimiento corresponde con aquellos lugares que posean un área amplia libre de interferencias y con una línea de vista despejada entre el nodo y el *Gateway*. Esto se refleja claramente en la zona rural, donde el punto más alejado del nodo presenta mejores resultados que puntos más cercanos, esto es gracias a la línea de vista libre, ya que además el nodo y el *Gateway* se encontraban aproximadamente a la misma altura.

Mediante los análisis de consumo energético se observa que al usar un *PowerBank* el prototipo alcanzó una autonomía de 8 días, lo cual limitaría su

instalación por meses, para solventar esto se podrían evaluar otras baterías y agregar un sistema de carga, por ejemplo, usando paneles solares.

En este estudio no se desarrolló el diseño de un *Gateway* LoRa y se limitó a la operación de un sólo nodo. Como trabajo futuro se plantea evaluar la red empleando múltiples nodos y *Gateways*, permitiendo incrementar los puntos de monitoreo y una mejor cobertura de la red.

Referencias

1. Bellini, P., Nesi, P., Pantaleo, G.: Iot-enabled smart cities: A review of concepts, frameworks and key technologies. Applied Sciences 12(3), 1607 (2022)
2. Li, C., Su, Y., Yuan, R., Chu, D., Zhu, J.: Light-weight spliced convolution network-based automatic water meter reading in smart city. IEEE Access 7, 174359–174367 (2019)
3. Li, X.J., Chong, P.H.J.: Design and implementation of a self-powered smart water meter. Sensors 19(19), 4177 (2019)
4. Ramírez-Moreno, M.A., Keshtkar, S., Padilla-Reyes, D.A., Ramos-López, E., García-Martínez, M., Hernández-Luna, M.C., Mogro, A.E., Mahlknecht, J., Huertas, J.I., Peimbert-García, R.E., et al.: Sensors for sustainable smart cities: A review. Applied Sciences 11(17), 8198 (2021)
5. León Ortiz, P.: Influencia del calentamiento global en los ecosistemas terrestres del perú (2021)
6. Castro, M.: Proyecto "creación de capacidades para la valoración socioeconómica de los humedales altoandinos": Una valoración económica del almacenamiento de agua y carbono en los bofedales de los páramos ecuatorianos (2011)
7. Briceño Salas, J.P.: Percepción de los cambios ambientales en los humedales de Oña-Saraguro. Ph.D. thesis, UNIVERSIDAD TÉCNICA PARTICULAR DE LOJA (2014)
8. Ahmed, U., Mumtaz, R., Anwar, H., Shah, A.A., Irfan, R., García-Nieto, J.: Efficient water quality prediction using supervised machine learning. Water 11(11), 2210 (2019)
9. Mao, F., Khamis, K., Clark, J., Krause, S., Buytaert, W., Ochoa-Tocachi, B.F., Hannah, D.M.: Moving beyond the technology: a socio-technical roadmap for low-cost water sensor network applications. Environmental Science & Technology 54(15), 9145–9158 (2020)
10. Pieters, O., Deprost, E., Van Der Donckt, J., Brosens, L., Sanczuk, P., Vangansbeke, P., De Swaef, T., De Frenne, P., Wyffels, F.: Mirra: A modular and cost-effective microclimate monitoring system for real-time remote applications. Sensors 21(13), 4615 (2021)
11. Wild, J., Kopeckỳ, M., Macek, M., Šanda, M., Jankovec, J., Haase, T.: Climate at ecologically relevant scales: A new temperature and soil moisture logger for long-term microclimate measurement. Agricultural and Forest Meteorology 268, 40–47 (2019)
12. Méndez-Barroso, L., Rivas-Márquez, J., Sosa-Tinoco, I., Robles-Morúa, A.: Design and implementation of a low-cost multiparameter probe to evaluate the temporal variations of water quality conditions on an estuarine lagoon system. Environmental Monitoring and Assessment 192(11), 1–18 (2020)
13. Menon, G.S., Ramesh, M.V., Divya, P.: A low cost wireless sensor network for water quality monitoring in natural water bodies. In: 2017 IEEE Global Humanitarian Technology Conference (GHTC). pp. 1–8. IEEE (2017)

14. Moya Quimbita, M.A.: Evaluación de pasarela lora/lorawan en entornos urbanos (2018)

15. Kimothi, S., Singh, R., Gehlot, A., Akram, S.V., Malik, P.K., Gupta, A., Bilandi, N.: Intelligent energy and ecosystem for real-time monitoring of glaciers. Computers and Electrical Engineering 102, 108163 (2022)

16. Kombo, O.H., Kumaran, S., Bovim, A.: Design and application of a low-cost, low-power, lora-gsm, iot enabled system for monitoring of groundwater resources with energy harvesting integration. IEEE Access 9, 128417–128433 (2021)

17. Bathre, M., Das, P.K.: Water supply monitoring system with self-powered lora based wireless sensor system powered by solar and hydroelectric energy harvester. Computer Standards & Interfaces 82, 103630 (2022)

18. Bor, M., Roedig, U.: Lora transmission parameter selection. In: 2017 13th International Conference on Distributed Computing in Sensor Systems (DCOSS). pp. 27–34. IEEE (2017)

19. Ko, S., Song, H., Cho, Y., Chung, J., Kim, S., Yim, D., Jin, D., Smith, A.: Lora network performance comparison between open area and tree farm based on phy factors. In: 2018 IEEE Sensors Applications Symposium (SAS). pp. 1–6. IEEE (2018)

20. Cattani, M., Boano, C.A., Römer, K.: An experimental evaluation of the reliability of lora long-range low-power wireless communication. Journal of Sensor and Actuator Networks 6(2), 7 (2017)

21. Lopez Chalacan, V.H.: Performance evaluation of long range (lora) wireless rf technology for the internet of things (iot) using dragino lora at 915 mhz (2020)

22. Iova, O., Murphy, A.L., Picco, G.P., Ghiro, L., Molteni, D., Ossi, F., Cagnacci, F.: Lora from the city to the mountains: Exploration of hardware and environmental factors. In: Proceedings of the 2017 International conference on embedded wireless systems and networks (2017)

23. Zhang, Z., Zhang, B., Zhang, X.: Performance research of lora at high transmission rate. In: Journal of Physics: Conference Series. vol. 1544, p. 012177. IOP Publishing (2020)

24. Microchip: ATmega1284P, [Online]. Available: https://www.microchip.com/en-us/product/ATmega1284P. [Accessed: 18-Jun-2022]

25. Atlas-Scientific: Gravity™ Analog pH Kit, [Online]. Available: https://atlas-scientific.com/kits/gravity-analog-ph-kit/. [Accessed: 10-Sep-2022]

26. Atlas-Scientific: Gravity™ Analog DO Kit, [Online]. Available: https://atlas-scientific.com/kits/gravity-analog-do-kit/. [Accessed: 10-Sep-2022]

27. Atlas-Scientific: Gravity™ Analog ORP Kit, [Online]. Available: https://atlas-scientific.com/kits/gravity-analog-orp-kit/. [Accessed: 10-Sep-2022]

28. Atlas-Scientific: Gravity Analog Sensor/Meter Sample Code, [Online]. Available: https://files.atlas-scientific.com/atlas_gravity.zip. [Accessed: 10-Sep-2022]

29. Ai-Thinker: Módulo LoRa SX1278 433 Mhz, [Online]. Available: https://docs.ai-thinker.com/en/lora/man. [Accessed: 10-Sep-2022]

30. Github: User-friendly library for using arduino-lmic with The Things Network and other LoRaWAN® networks, [Online]. Available: https://github.com/mcci-catena/arduino-lorawan. [Accessed: 18-Sep-2022]

31. Arduino IDE, [Online]. Available: https://www.arduino.cc/en/software. [Accessed: 10-Sep-2022]

Assessment of a vertical Agrivoltaics installation in the area of Chanco, Maule Region in Chile

Roxane Bruhwyler[1], Hugo Sánchez[2],[3], Carlos Meza[2],[3], Frédéric Lebeau[1],
Pascal Brunet[4], Gabriel Dabadie[4], Sebastian Dittmann[2], Ralph Gottschalg[2],[5],
and Juan Jose Negroni[6]

[1] DEAL, BioDynE, Liège University, 5030 Gembloux, Belgium, f.lebeau@ulg.ac.be
[2] Anhalt University of Applied Sciences, 06366 Köthen, Germany
[3] Costa Rica Institute of Technology, 159-7050 Cartago, Costa Rica
[4] Naldeo Technologies Industries, 40220 Tarnos, France
[5] Fraunhofer-Center for Silicon Photovoltaics CSP, Halle, Germany
[6] Universidad Santo Tomás, 8370003 Santiago, Chile

Abstract. This paper presents a case study for a vertical agrivoltaic installation in Chile. Agrivoltaics has become a promising technique to improve land productivity, synergizing photovoltaics energy generation and crop production. However, most of the study cases have been developed for north latitudes and few for south latitudes, such as Chile.
The present research analyses a study case for a 100 kW$_p$ vertical agrivoltaic facility in the region of Chanco, Caunquenes Province, in Chile. The analysis explores the potential for the installation in two ways: first, the energy yield prediction for the photovoltaic component, and second, the water saved in evapotranspiration due to the reduced irradiation and the potential wind speed reduction that the vertical installation brings to the crop. A python library using mainly *PVLib* and *PVFactors* is used to evaluate the energy production while the evapotranspiration is predicted for a reference crop with the FAO 56 PM equation. Results for the year 2021 show that for the same capacity, a typical north tilted power plant would produced 15.7 % more energy than a bifacial vertical plant oriented East-West but the later improve the flexibility of grid operator with its two daily power peaks. As far as the water demand is concerned, in non-limited water condition, the reduction of irradiation caused by the vertical panels could save 550 m^3/ha of water while this effect combined with the potential wind speed reduction allows to save 2130 m^3/ha.

Keywords: agrivoltaics, vertical bifacial PV, evapotranspiration

1 Introduction

Food security and decarbonization require innovative schemes to fulfill the necessities of a growing world demand. And more important, growing sustainably. To address these challenges simultaneously, generating and studying new and innovative frameworks in the synergy of food and energy production systems is

necessary. In this sense, Agrivoltaics becomes a valuable opportunity to provide a holistic solution. It is defined as the synergy between solar photovoltaic energy and crop production [1]. Its potential is under study, however, one of the main benefits is the increase of the land equivalent ratio that refers to the combined productivity of the agrivoltaic system, compared with the productivity of traditional differentiated systems. [2, 3].

Agrivoltaic installations can be an alternative to conventional ground-mounted photovoltaic energy production. In this regard, traditional production of PV requires large areas that imply, in many cases, land competition. That could be an inflexion point for a stakeholder [4]. For this reason, new concepts will provide the capability to optimize the potential of the land [5, 6, 7]. Furthermore, it could generate several innovative production frameworks for food and energy generation.

One of the problems that solar production faces is the limited flexibility to allocate energy production on the grid as these technologies, if not associated to storage, are not dispatchable. One of the results of this problem is observed in the curtailment of solar installations [8]. It generates an interesting threshold effect, where it is necessary to use renewable energy sources, but power generation could be limited according to the time of day. The vertical solar plants can be an interesting complement for the electrical grid due to the capability to provide two peaks on generation in the mid-morning and afternoon, improving the flexibility of grid operators [9, 10].

In addition, vertical solar plants are compatible with crop operations at lower prices than elevated solar plants[11] and suit complex topographies. Agrivoltaics, depending on the PV plant configuration, are expected to mitigate climate change and protect the crop from radiation excess, water stress, night frosts and heavy rains or hails. In vertical Agrivoltaics, solar plants could act like windbreaks if perpendicular to the main wind direction. Windbreaks have numerous agronomic interests, including the reduction of water demand [12, 13].

Agrivoltaics installation has been studied in North America, and Europe with few study cases in the south hemisphere [14, 15]. In this regard, this paper wants to contribute to Agrivoltaics research in the Southern hemisphere, i.e., Chile. The rest of the paper is structured as follows, Section 2 presents the case of study and section 3 present the methodology followed. In section 4 the simulation results of the case study are presented and, finally, section 5 presents the conclusions and future work.

2   Case of study

This study analyzes the potential benefits of developing a vertical Agrivoltaics installation in Chanco in the Caunquenes Province, Maule Region in Chile. This region is rich in agricultural activities, more specifically for the production of horticultural berries, potatoes, cereals, fruit trees, forage plants, vineyards, and grapevines [16, 17, 18]. According to the Chilean Ministry of Agriculture, the Region of Maule, only 4% of the country region, represents the 17% of the agri-

cultural production in Chile [16]. Nevertheless, the region faces a water deficit as a result of climate change [19]. For that, the agriculture and production processes in the region will have to adapt to face the effects that climate change will have on them. For this reason, improving the region's water-use efficiency can help solve the problem. The present case study will analyze the implementation of a vertical agrivoltaics facility to contribute to the generation of innovative and resilient production schemes. The principal characteristics are shown in Table 1.

Table 1: Main Parameters for the site of analysis.

Location	Latitude [°]	Longitude [°]	Altitude [m.a.s.l.]	Total PV Capacity [kW$_p$]	Total Area [m^2]
Chanco	-35.735	-72.518	127.21	100	1000

We propose to evaluate a PV agrivoltaic vertical installation, which comprises four fences of 50 bifacial modules each (in two rows), with a midgap of 14 m. The gap will allow the utilization of farming machinery and provide enough space for the development of crops. For the simulation purpose, all the modules are connected to one central inverter. 1 shows a concept for the vertical installation PV for agrivoltaic.

Fig. 1: Vertical bifacial facility for agrivoltaics.

The area was chosen due to the special conditions of prevailing wind direction in the region in nearly West-East orientation [20]. The hourly data for 2021 was obtained from the National Aeronautics and Space Administration (NASA) Langley Research Center (LaRC) Prediction of Worldwide Energy Resource (POWER) Project funded through the NASA Earth Science/Applied Science Program [21]. As a confirmation, the wind direction at 10 meters height was analysed and presented in Figure 2. It is noticeable that the prevalent wind direction is between the southwest and the west.
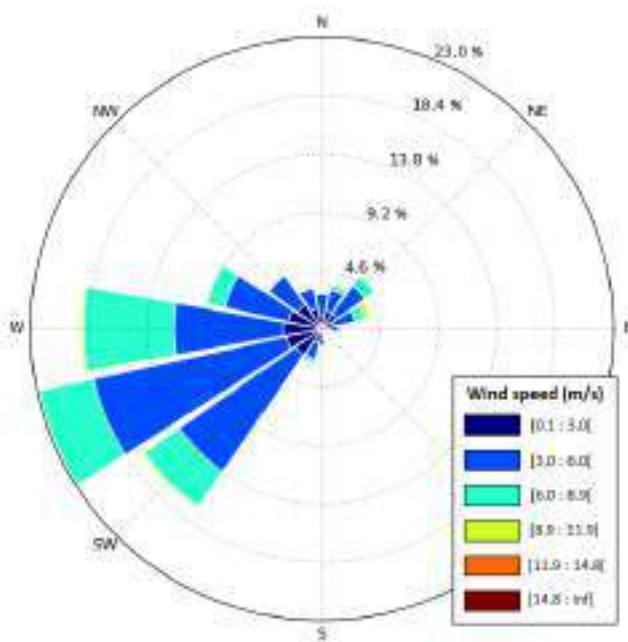
Fig. 2: Relative frequency of wind direction and speed for the area of Chanco in 2021.

The other meteorological data from the place is shown in Figure 3. The temperature (T), relative humidity (RH), and wind speed (WS) are represented as the overall hourly average meanwhile the global horizontal irradiance (GHI) is represented as the total monthly.
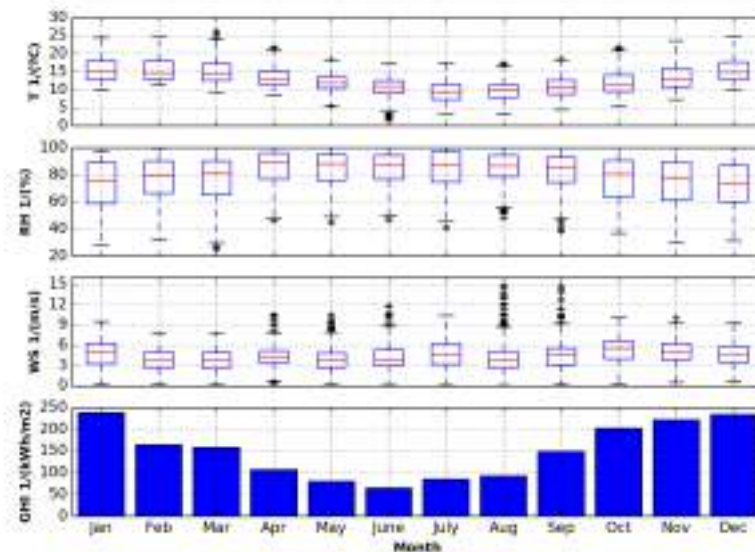
Fig. 3: Meteorological data for the area of Chanco in 2021. From top to bottom: Average Hourly Temperature, Average Hourly Relative Humidity, Average Hourly Wind Speed, and Monthly Global Horizontal Irradiance.

3   Methodology

Figure 4 represents a general overview of the methodology applied for the agrivoltaic facility assessment in the area of Chanco. The approach consists of two main components. The exploration of the energy production available and the evapotranspiration model. The block diagram represents the inputs required for the evaluation.

3.1   Energy yield calculation

For the energy yield calculation, a *Python* library is used for the energy prediction modeling using as the main framework the libraries *PVLib* [22] and *PVFactors* [23], using as the input data the Global Horizontal Irradiance, Average Temperature and Wind Speed. Then, the following steps are done for the simulation:

– **Modelling front side irradiance:** First the sun position is also estimated at the location using the NREL algorithm [24]. With that, the global horizontal irradiance is decomposed into the three main factors to the surface:
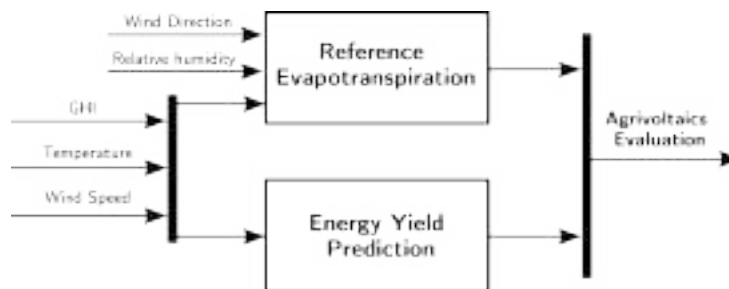
Fig. 4: Block Diagram Concept for the evaluation modeling for an Agrivoltaics Facility in Chile.

direct irradiance (*Ineichen Model*), diffuse irradiance (*Perez Model)*, and albedo.
- **Modelling rear side irradiance:** With the information from the decomposition model, the irradiance in the rear side of the module is estimated using the geometry and the decomposition of the light. The *ModelChain* method serves as a base for the segregation.
- **Electro-Thermal model:** with the decomposition in both sides of the solar module, the performance of the module is estimated. In this step the correction for the modules is selected using the *Desoto model*, the angular of incidence losses uses the *Martin-Ruiz* model, the spectral correction uses the SAPM and the temperature is corrected (*Faiman model)*
- **Final System Performance:** final corrections and losses are estimated using the SAPM method.

Some limitations and assumptions are considered for the simulation:

- There is no effect of self-shadowing between rows.
- The albedo is considered constant at the value of 0.2. However, the variance of albedo is clear in [25].
- The spectral mismatch in the different heights is neglected.
- Climping and thermal losses are not considered for the inverter.
- Bifaciality factor, the ratio of the nominal efficiency at the rear side, with respect to the nominal efficiency of the front side is set at 90%.
- Losses in the rear side contact are not considered.

3.2 Evapotranspiration calculation

The evapotranspiration model is based on the Penman-Monteith equation, known as the FAO 56 PM equation. It gives the daily potential evapotranspiration of a reference crop (ET0): a hypothetical green well-watered grass actively growing and completely shading the ground [26]. This model uses five input data (Figure

4), aggregating them into daily extremum of temperature and relative humidity, mean temperature, mean wind speed at 2 meters height and daily irradiation.

Two modifications of the agrivoltaic microclimate are considered to evaluate the difference in water demand between a crop growing in a control zone (open field) and a crop growing between the rows of vertical solar panels:

- **Residual daily irradiation:** Reduction in direct irradiance is evaluated with a geometrical model using $PVLib$ [22] for solar position and computing at a quarter-hour time step the shade projection of panels on the ground. Reduction in diffuse irradiance is computed considering a spatial mean view factor.
- **Residual wind speed:** The optic porosity of vertical panels is evaluated considering the 90 cm space between the ground and the first panel. A reduction factor of wind speed is then computed following [27].

Some limitations and assumptions are considered for the simulation:

- The albedo is considered constant at a value of 0.25.
- The reduction factor of wind speed, ratio between local wind speed and far field velocity, is evaluated at 0.85 for each days considering the prevalent wind direction and not considering the side-effects of a wind non perfectly east-west oriented.
- [27] presents wind reduction in windbreaks for homogeneous porosity while with vertical panels, all the porosity is located below the panels.
- Wind speed at 2 meters height is computed from 10 meters height data with the logarithmic profile of wind, considering a roughness lenght of 0.2 [7].
- Aerodynamic and surface resistances used in FAO 56 PM (70 s.m^{-1} and 208/U_2) are specific for the extensive grass surface with a height of 0.12 m. Displacement height is fixed to 2/3 of the crop height (0.8 m), roughness length governing momentum transfer is set to 0.123 the crop height (14,76 mm) and the roughness length governing transfer of heat and vapour is considered as 0.1 the roughness length governing momentum transfer (1,47 mm) [26].

4   Results

4.1   Energy yield calculation

Figure 5 shows a comparison, for the same capacity, between the PV production for the vertical agrivoltaics plant and the solar plant placed in a typically fixed tilt angle configuration (with the optimal angle of 35°). As expected, the vertical installation produces less energy compared to a north-facing tilt angle installation (0.2% during the summer solstice-December 21th-and 37% during the winter solstice- June 21th)

The overall production is presented in Figure 6, where the monthly energy for the vertical facility is compared with an equivalent power plant.

---

[7] https://wind-data.ch/tools/profile.php?lng=en

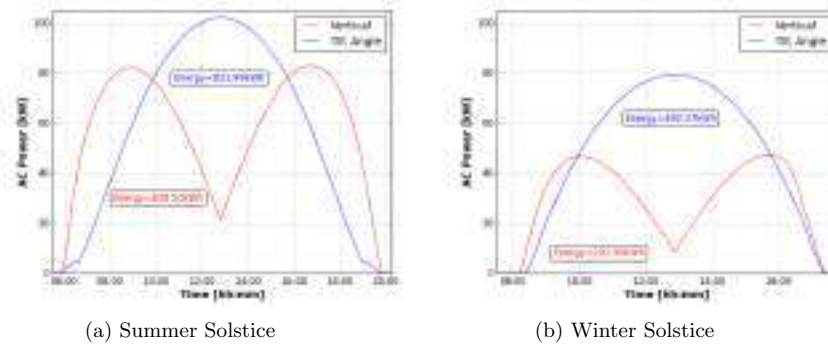(a) Summer Solstice   (b) Winter Solstice

Fig. 5: Comparison for the power generation profile for a vertical agrivoltaics solar plant and its equivalent for a classical tilt fixed in an optimal angle at the Summer and Winter Solstice in Chile.
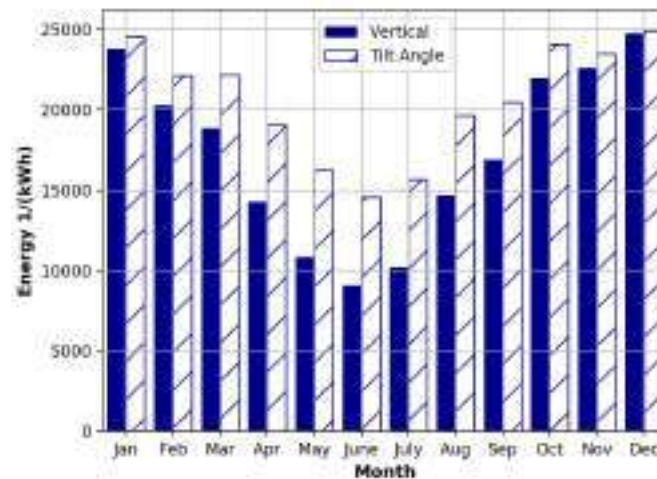

Fig. 6: Energy production for a vertical agrivoltaic plant and an equivalent with north tilt angle.

On average, the vertical PV installation will produce 208,14 MWh yearly compared to the tilt angle installation, which would generate 246,94 MWh yearly (an average difference of 15,71%). However, as described in the graph, the dif-

ference between the production in both installations can decrease up to 0,2%. However, the next section presents the benefits in terms of ET0 for this agri-voltaic facility.

4.2 Evapotranspiration calculation

Monthly potential evapotranspiration of a reference crop growing in the area of Chanco with non-limited water conditions, is presented in Figure 7, where a control scenario is compared with the agrivoltaic microclimate conditions created by the panels. The ET0 reduction caused by the decrease in irradiation is distinguished from the one caused by the wind speed reduction. The mean irradiation reduction for the year 2021 computed with the daily values is 30.2% going from 26.3% in December to 36% in July. Those irradiation reductions lead to a 5.6% decrease of ET0 on the whole year, corresponding to 55 mm of water saved (550 m^3/ha). As a reference point, the total amount of rain in 2021 was 806 mm. ET0 is reduced by 6.8% in November while only reduced by 0.2% in June. When the wind speed reduction is considered in addition to the shade conditions compared with the control scenario, yearly ET0 is reduced by 21.6%, saving 213 mm of water (2130 m^3/ha). Then, there are a 41.1% maximal reduction of ET0 in July and a minimal reduction of 16.9% in November.
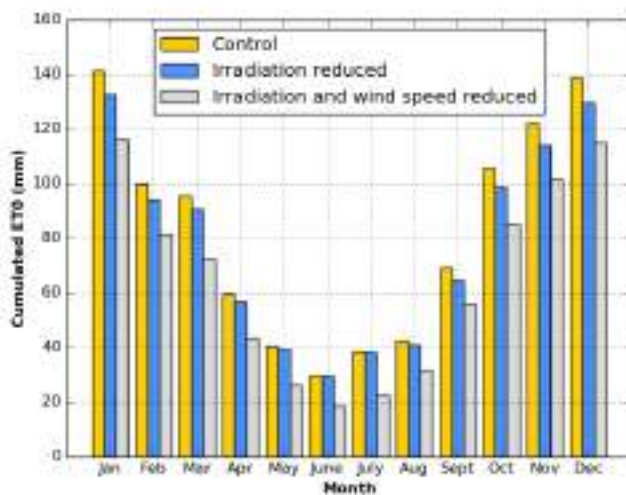
Fig. 7: Monthly reference evapotranspiration of a crop growing in the area of Chanco without any solar panel (control) and in the agrivoltaic microclimate.

Vertical solar plants could then play an essential role in water shortage in the area of Chanco due to this prevalent wind direction. However, this wind speed reduction rate of 0.85 employed to reduce the daily wind speed and the FAO 56 PM equation are simple assumptions that do not consider the complex effect of those special windbreaks on air flow conditions. Some evapotranspiration models allow to consider the real values of aerodynamic and surface resistances that can be evaluated through computational fluid dynamics (CFD) and measurement campaigns. It will be part of the future work to better assess heterogeneous air flow conditions and to integrate them into a more representative evapotranspiration model.

5 Conclusion and future work

This paper is a case study of a 100 kW_p vertical bifacial agrivoltaics facility in Chile. This theoretical vertical agrivoltaic installation represents synergy in the context of the energy oversupply sometimes occurring around the solar noon and the water shortage problem for agriculture. The water demand analysis is a preliminary study highlighting the importance of fluid dynamics in the microclimate created by vertical solar panels. Indeed, the basic assumptions made here evaluate that 2130 m^3/ha of water could be saved on one year thank's to a wind speed reduction factor of 0.85. Future work will focus on collaboration with industrial partners (TotalEnergies and Naldeo Technologies & Industries) to assess the actual effect of vertical panels on air flow conditions and thus on microclimate conditions and water demand.

Acknowledgment

Bibliography

[1] Goetzberger A, Zastrow A (1982) On the coexistence of solar-energy conversion and plant cultivation. International Journal of Solar Energy 1(1):55–69

[2] Trommsdorff M, Kang J, Reise C, Schindele S, Bopp G, Ehmann A, Weselek A, Högy P, Obergfell T (2021) Combining food and energy production: Design of an agrivoltaic system applied in arable and vegetable farming in germany. Renewable and Sustainable Energy Reviews 140:110,694

[3] Dupraz C, Marrou H, Talbot G, Dufour L, Nogier A, Ferard Y (2011) Combining solar photovoltaic panels and food crops for optimising land use: Towards new agrivoltaic schemes. Renewable energy 36(10):2725–2732

[4] Pascaris AS, Schelly C, Pearce JM (2020) A first investigation of agriculture sector perspectives on the opportunities and barriers for agrivoltaics. Agronomy 10(12):1885

[5] Sanchez H, Dittmann S, Tosello S, Meza C, Dullau S, Maren M, Scholz P, Tischew S, Gottschalg R (2022) Novel measurement concept for agripvplus systems-a triple use approach. In: 8th World Conference of Photovoltaic Energy Conversion. Milan, Italy

[6] Agostini A, Colauzzi M, Amaducci S (2021) Innovative agrivoltaic systems to produce sustainable energy: An economic and environmental assessment. Applied Energy 281:116,102

[7] Amaducci S, Yin X, Colauzzi M (2018) Agrivoltaic systems to optimise land use for electric energy production. Applied energy 220:545–561

[8] O'Shaughnessy E, Cruce JR, Xu K (2020) Too much of a good thing? global trends in the curtailment of solar pv. Solar Energy 208:1068–1077

[9] Chudinzow D, Nagel S, Güsewell J, Eltrop L (2020) Vertical bifacial photovoltaics–a complementary technology for the european electricity supply? Applied Energy 264:114,782

[10] Campana PE, Stridh B, Amaducci S, Colauzzi M (2021) Optimisation of vertically mounted agrivoltaic systems. Journal of Cleaner Production 325:129,091

[11] Bellini E (2021) URL https://www.pv-magazine.com/2021/03/26/cost-comparison-between-agrivoltaics-and-ground-mounted-pv/

[12] Béguin JM (1972) Observations sur le rôle des brise-vent. Fruits 27:745–764

[13] M Smith M, Bentrup G, Kellerman T, MacFarland K, Straight R, Ameyaw L (2021) Windbreaks in the united states: A systematic review of producer-reported benefits, challenges, management activities and drivers of adoption. Agricultural Systems 187, DOI 10.1016/j.agsy.2020.103032

[14] Jung D, Salmon A, Gese P (2021) Agrivoltaics for farmers with shadow and electricity demand: results of a pre-feasibility study under net billing in central chile. In: AIP conference proceedings, AIP Publishing LLC, vol 2361, p 030001

[15] Gese P, Martínez-Conde FM, Ramírez-Sagner G, Dinter F (2019) Agrivoltaic in chile—integrative solution to use efficiently land for food and

energy production and generating potential synergy effects shown by a pilot plant in metropolitan region. In: Proceedings of the International Conference on Solar Heating and Cooling for Buildings and Industry (SHC), Santiago de Chile, Chile, pp 3–7

[16] MINIAGRI (2022) Región del maule. URL `https://www.minagri.gob.cl/region/region-del-maule/`

[17] Sepúlveda Morales FA, Herrera Quinteros G, et al (2022) Acceso a la agricultura digital y tecnologías de información y comunicación para mejorar la comercialización de pequeños productores hortícolas y de berries de la región del maule. PhD thesis, Universidad de Talca (Chile). Escuela de Agronomía.

[18] Inostroza J, Méndez P, Espinoza N, Kramm V, et al (2017) Manual del cultivo de la papa en chile.

[19] Henriquez EMM, González PSN (2011) Análisis del déficit hídrico de la región del maule, chile. RIAT: Revista Interamericana de Medioambiente y Turismo 7(1):25–32

[20] Watts D, Jara D (2011) Statistical analysis of wind energy in chile. Renewable Energy 36(5):1603–1613

[21] NASA (2021) Nasa power. URL `https://power.larc.nasa.gov/docs/`

[22] Holmgren WF, Hansen CW, Mikofski MA (2018) pvlib python: A python package for modeling solar energy systems. Journal of Open Source Software 3(29):884

[23] Abou Anoma M, Jacob D, Bourne BC, Scholl JA, Riley DM, Hansen CW (2017) View factor model and validation for bifacial pv and diffuse shade on single-axis trackers. In: 2017 IEEE 44th Photovoltaic Specialist Conference (PVSC), IEEE, pp 1549–1554

[24] Reda I, Andreas A (2004) Solar position algorithm for solar radiation applications. Solar energy 76(5):577–589

[25] Dittmann S, Sanchez H, Burnham L, Gottschalg R, Oh S, Benlarabi A, Figgis B, Abdallah A, Rodriguez C, Rüther R, et al (2019) Comparative analysis of albedo measurements (plane-of-array, horizontal) at multiple sites worldwide. In: 36th European Photovoltaic Solar Energy Conference and Exhibition. Marseille, France, pp 1388–1393

[26] Allen RG, Pereira LS, Raes D, Smith M (1998) Crop evapotranspiration - guidelines for computing crop water requirements. FAO Irrigation and drainage 56

[27] Dewalle DR, Heisler GM (1988) Use of windbreaks for home energy conservation. Agriculture, Ecosystems and Environment 22-23:243–260, DOI 10.1016/0167-8809(88)90024-2, proceedings of an International Symposium on Windbreak Technology

Preparation of Zinc Oxide from Used Batteries as a Catalyst in the Transesterification of Recycled Oil to produce Biodiesel

Domenica Seminario[1,§][0000-0001-6208--9256] , Melisa Ortega[1,§][0000-0003-1162-3150] , Andrés Montero[1][0000-0001-5366-8029] , Paola Duque[2][0000-0003-4484-7273], Juan Cisneros[2][0000-0003-4484-7273], Paúl Álvarez[1][0000-0003-2146-5969] and Verónica Pinos[1,2*][0000-0001-8278-5873]

[1] IRCMA, Bioscience Department, Universidad de Cuenca, Cuenca 010107, Ecuador
[2] Departamento de Recursos Hídricos y Ciencias Ambientales, Universidad de Cuenca 010107, Ecuador
§ These authors contributed equally, thus equal first authors.
*veronica.pinos@ucuenca.edu.ec

Abstract

Nowadays, batteries and cooking oil consumption has been increasing in Ecuador. This is a big problem because the vast majority of used batteries are disposed of in landfills or in the trash; due to their composition, health and environmental problems are produced. Also, used cooking oil usually is disposed of in rivers and sewers, polluting water, and soil. For these reasons, the circular economy has been raised through the use of these environmental passives. Zinc oxide was obtained from spent batteries with a hydrometallurgical method to later be used as a catalyst. Zinc oxide showed a 98.49% purity, 56.20% of yield and a white coloration. Biodiesel was produced with treated recycled cooking oil, alcohol, and the obtained catalyst. Prepared biodiesel had a heating power of 37.553 kJ/g, a density of 0.8916 g/cm^3, a viscosity of 4.1887 mm^2/s, a water content of 0.001% and a 70.91% yield.

Keywords: zinc batteries, zinc oxide, catalyst, recycled cooking oil, biodiesel.

1. Introduction

Batteries such as alkaline and Zn-C are used as power sources of energy for various devices, most of which are disposable. It has been seen that in recent years the consumption of batteries in Ecuador has been increasing. Only 83.04% of Ecuadorian households, equivalent to 16.8 million people, used around 17 million batteries, of which 1.53 million were rechargeable (9.06%) [1]. However, after its use, most people tend to dispose of batteries in the common trash ending up in city landfills. This disposal practice causes pollution problems mainly to soil and water sources due to the formation of leachates with a high presence of heavy metals [2]–[4]. Currently, in Cuenca, around 35-40 kg of batteries are collected at the collection points each month. Etapa EP is the public company in charge of collecting them, and after conducting a stabilization process, they are confined indefinitely [5].

The ideal aim of a waste management program is to give the batteries a definitive treatment through innovative, economical, and environmentally sustainable processes. For example, alkaline batteries consist of a zinc anode and a high-density MgO_2 cathode, while Zn-C batteries are mostly made of zinc, followed by MnO manganese oxide. From this composition, for use as raw material in the industry, 33% of zinc and 29% of manganese oxide can be recovered [6]. Some authors have gone as far as obtaining zinc oxide from Zn-C batteries as Chen [7] used H_2SO_4 for reductive leaching and selective precipitation with NaOH at pH 10. Mahandra used an ionic liquid for battery leachate treatment [4], while Tanog used solvent extraction, electrodeposition, and precipitation methods [8].

On the other hand, cooking oil is a highly consumed product by the population in cities. But after its use, it usually tends to be disposed directly in the water sink ending up in rivers or in wastewater treatment facilities, affecting the ecosystem or the water treatment efficiency, respectively. This waste is considered hazardous due to its negative impact on the environment, mainly on water resources and aquatic fauna [9]. In Ecuador, 54 million liters of oil are discarded, 70% of which is vegetable oil. Etapa EP is the agency in charge of collecting and managing this waste. Currently, the collected oil is only stored. However, there are procedures, such as obtaining

biodiesel, that can be used to revalue this waste. Biodiesel is obtained from a transesterification reaction between oil and an alcohol in the presence of a catalyst [10]. Transesterification is a process where triglycerides from used cooking oil chemically react with alcohol and are converted into fatty acids methyl esters [11], see fig. 1.
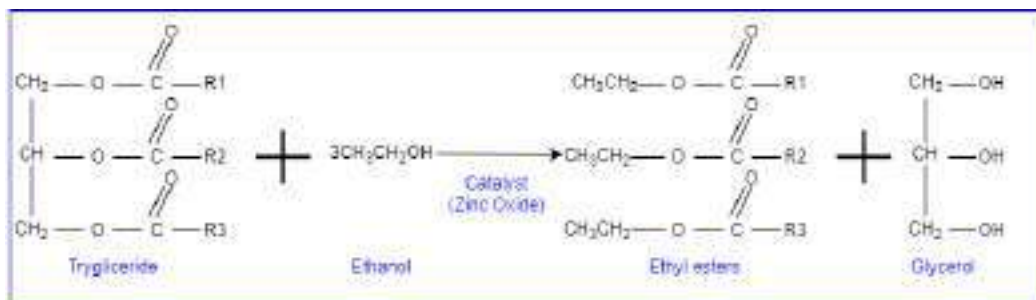

Fig. 1. Transesterification reaction

By using used cooking oil and zinc oxide from discarded batteries to produce biodiesel, it is possible to reduce the amount of hazardous waste that must be disposed of and therefore the costs of its management [12]. In Cuenca, collecting approximately 38 kg/month of batteries and 40 gallons/month of used cooking oil, 984 g of zinc oxide and 886 L of biodiesel can be obtained.

This research aims to find alternative processes that can revalue used cooking oil as battery components since these are currently not being adequately managed. Therefore, it is proposed to recover the zinc oxide from the Zn-C batteries through hydrometallurgical processes to obtain biodiesel by transesterified used cooking oil.

2. Materials and Methods

2.1 Cooking oil processing

Feedstock used for this research was used vegetable oil. This oil was obtained from a municipal company of Cuenca (ETAPA EP) that collects used oil mainly from restaurants and households and subsequently stores it in an open pool facility. The sample was first filtered in a chemical funnel using Whatman paper Nº40 to eliminate big-sized contaminants such as food residue. The oil was then washed, heating water and oil to 80 ºC, mixing and leaving the mixture in a decanter. Finally, water from the decanter was removed, and the oil was left in the stove at 115 ºC for 4 hours to eliminate the remaining water. For its characterization, the density was determined using a pycnometer, the kinematic viscosity was measured at 40 ºC by the Ostwald procedure, using water as the reference liquid. The water percentage in the sample was given by the Karl Fisher titration method. These parameters are shown in table 1.

### 2.2 Zinc oxide preparation and characterization

Used batteries were dismantled to obtain the zinc case and carbon rods. The carbon rods were then submerged in nitric acid at 30% and left for 24 h. Next, the carbon rods were washed until getting a neutral pH. Finally, the rods were dried in a stove at 110 ºC for 12 h, to remove residual water.

The zinc case was lixiviated to obtain zinc oxide with a pyrometallurgical method proposed by Chuquichanga [13]. Briefly, 115.6 g of the Zn case was lixiviated in 300 mL of hydrochloric acid at 37% in an Erlenmeyer at 100ºC during 60 minutes, obtaining 195.66 g of zinc chloride.

$$ZnO + 2HCl \rightarrow ZnCl_2 + H_2O$$
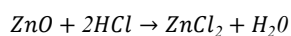
Subsequently, 250 mL of sulfuric acid at 50% was added. The solution was heated at 100 ºC for one hour. To the solution, 500 mL of distilled water was added to eliminate the impurities of the resulting zinc sulfate. The solution

was then heated to boiling and filtered through Whatman No. 40 paper. The filtered solution was allowed to cool down to room temperature for 24 h, getting 231.53 g of zinc sulfate crystals.

$$Zn^{+2}(ac) + H_2SO_4(ac) \rightarrow ZnSO_4(ac) + H_2 \uparrow$$
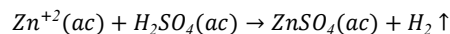
Sodium hydroxide (Fisher scientific., assay $\geq$ 98.9 %) at 30% was put on the crystals until a 6.5 pH was reached, obtaining zinc hydroxide and 341.46 g of sodium sulfate as a subproduct.

$$ZnSO_4(ac) + 2NaOH\ (ac) \rightarrow 2\ NaSO_4(ac) + Zn(OH)_2 \downarrow$$
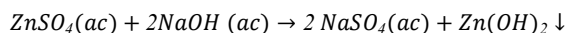
Although [14] mentions that sodium sulfate is harmful to the environment, [15] the concentration is low.
The solution was filtered through Whatman paper Nº 40. The paper with the solute was dried at 100 ºC for 1 hour. Finally, the dry paper was placed in a crucible and incinerated at 900 ºC for 6 hours in a muffle, obtaining zinc oxide.

$$Zn(OH)_2 \downarrow \rightarrow ZnO + H_2O(g) \uparrow$$
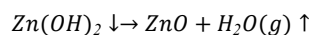
To prepare the supported catalyst, 0.96 mg of previously obtained zinc oxide was dispersed in water with a magnetic stirring hot plate at 300 rpm the dry carbon rod (4.8 g) was added to be impregnated with the oxide at 230 ºC until the solvent evaporated.

2.4 Biodiesel preparation and characterization

Transesterification was performed with the supported and unsupported catalyst with an ethanol/oil ratio of 6:1. The weights of non-supported and supported catalysts were 5% and 1% W/W (catalyst/solution). First, in a beaker, catalyst, and ethanol (98 %) were added. Later, the mixture was stirred in a magnetic hot plate at 300 rpm, 60 ºC per 20 minutes. Next, treated oil was added to the beaker. Conditions were held for one hour. This procedure was repeated in triplicate for each type of catalyst. The mixture was poured into the decanter. After three hours biodiesel was separated from biodiesel. The obtained diesel was washed and filtered with Whatman paper Nº42, to eliminate the remaining catalyst. Finally, it was dried at 80 ºC for 15 minutes.

Five parameters were considered for the biodiesel characterization: water percentage, specific heat capacity, density, viscosity, reaction yield. At first, water percentage was determined in a Karl Fischer titrator just by injecting the sample. Specific heat capacity was measured in a calorimetric pump [16]. Density was obtained using the pycnometer method. Viscosity was given by the Ostwald method using an Ubbelohde viscometer [17]. Finally, the reaction yield was calculated by measuring the FAME`s in the oil and in the biodiesel sample and applying the next formula.

$$\%Yield = \frac{FAME`S\ weight\ in\ biodiesel}{FAME`S\ weight\ in\ recycled\ oil} * 100 \qquad (1)$$

All these parameters were compared with three normatives for biodiesel; ASTM B 100, EN 590, INEN 2489 [16], [18], [19].

3.   Results and discussion

3.1 Zinc oxide preparation and characterization

Zn-C batteries provided by ETAPA EP were used. In the first place, batteries in good condition were selected (i.e., batteries without rust or spills). Subsequently, these materials were dismantled as shown in figure 2.

Fig.2. Battery dismantling procedure

Once the procedure mentioned in 2.2 was applied, zinc oxide was obtained as a white powder. The results of the catalyst characterization are shown in Table 1. Purity showed a percentage of 98.49%, which is greater than Chuquichanga who used the same principle (hydrometallurgical) [13]. Color was white as shown in the sample in figure 2. Yield is 56.20%, a percentage that is similar to that obtained by Chuquichanga of 54.7% [13] but it is lower when alcaline batteries are used, the percentage being 66.42% according Alvarado [20]. Finally, 20.92% of the sample is at the nanometric scale, which implies that the size reduction was not homogeneous.

Table 1. Zinc Oxide Characterization

Purity	98.49%
Color	White
Yield	56.20%
Particle size (1-10 nm)	20.92%

3.2 Cooking oil processing and characterization

Recycled cooking oil was given by ETAPA EP and was filtered, washed, and dried as mentioned in 2.1. We can observe this process in figure 3.

Fig .3. Cooking oil processing

Later, the treated cooking oil was characterized by the determination of density, viscosity, and water content. The results are shown in table 2. Density was 0.9646 g/cm^3, which is similar to the values registered by Lopez of 0.921 g/cm^3 [21] and Rodríguez of 0.9119 g/cm^3 [22]. Additionally, this parameter is close to the suggested by the normative ASTM D 1298 of 0.96 g/cm^3. Viscosity was 50.9117 mm^2/s, which is close to the viscosity reported from Rodríguez of 42.2 mm^2/s [22] and Tacias of 50 mm^2/s [23]. Water amount was 0.15% in the sample.

Table 2. Characteristics of recycled cooking oil

Oil characterization	
Density	0.965 g/cm^3
Viscosity	50.912 mm^2/s
Water amount	0.15%

Also, FAME (Fatty Acids Methyl Esters) were determined in a GC-FIT and the results are shown in table 3. The fatty acid in greater proportion is C 18:2 (linoleic acid) with 11.29%. For this reason, all the stoichiometric calculations took this fatty acid as a reference.

Table 3. Characteristics of recycled cooking oil

Fatty Acids	Percentage	Fatty acids´ weigh (g/mol)
C 16:0	4.15%	4.2591
C 18:0	1.43%	1.6311
C 18:1	7.91%	9.1216
C 18:2	11.29%	12.6597
C 24:0	5.75%	8.4828
Total	30.54%	36.15

3.3 Biodiesel

After the transesterification reaction of the recycled cooking oil and alcohol using the obtained zinc oxide as a catalyst, biodiesel was obtained and characterized. The results are shown in table 4. Heating power was 37.553 kJ/g, which is higher than what is registered from Rodríguez of 37.255 kJ/g [22] and Tondo of 35.912 kJ/g [24]. This may occur because zinc oxide is used in car engines to raise its heating power [25]. Density presented a value of 0.8916 g/cm3, which is in the ranges established by the normative INEN 1489 from 0.89 to 0.9 g/cm^3. However, the blank showed a value of 0.93, which is closer to the viscosity of the cooking oil. Viscosity was 4.1887 mm^2/s, which fits in the ranges of the normatives INEN 2482, ASTM B 100 and EN 590. The blank has a greater viscosity than the stipulated by the normatives, which shows that transesterification was not completed [26]. Water content showed a percentage of 0.001, which is in the ranges of the normatives INEN 2482, ASTM B 100 and EN 59. This also shows that the drying process of the cooking oil was efficient. Finally, the yield was 70.91% which is greater than the registered by of 49.78% [27], who used the same catalyst. On the other side, the obtained yield is

less when other catalysts are used. Fangfang, Sipayung and Sivarethinamohan obtained a yield of 98%, 91.8% and 95.57% using potassium hydroxide and calcium hydroxide respectively [28]–[30].

Although better results are obtained when catalysts other than zinc oxide are used, this is the most appropriate catalyst for obtaining biodiesel since it reduces the time and temperature necessary for the synthesis [31]. Furthermore, the performance can be improved by combining the zinc oxide with other compounds [32].

Table 4. Characteristics of biodiesel

Biodiesel Characterization	
Heating power	37.553 kJ/g
Density	0.8916 g/cm^3
Viscosity	4.1887 mm^2/s
Water amount	0.001%
Yield	70.91%

4. Conclusion

Zinc oxide was obtained from Zn-C batteries with a yield of 56% and purity of 98%. Supported catalyst was prepared with carbon bars from the batteries. Recycled oil was treated and characterized. This fatty acid in greater proportion was acid linoleic with 11.29%. The water percentage was 0.15%. Density was measured with a pycnometer obtaining 0.965 g/cm3. Viscosity was determined with the Ostwald method, having 50.912%. Both density and viscosity were the range given by ASTM normative. Biodiesel was obtained with pre-treated cooking oil and ethanol (6:1 P/P). In order to speed up the reaction catalyst was added. Water percentage, density and viscosity were 0.005%, 0.892 g/cm3 and 4.189 mm^2/s respectively. These parameters were in the ranges given by ASTM normative. Obtained catalysts helped to the generation of biodiesel due to the percentage of yield that was obtained being 70 % considered a high value of yield compared to the value obtained from the blank. Two residues considered as environmental passives were processed to products with added value. Leading to the implementation of a circular economy. Also, this investigation presents an alternative way of disposing batteries and cooking oil rather than storing them.

Bibliography

[1]   INEC, «Información ambiental en los hogares». 2020. [En línea]. Disponible en: https://www.ecuadorencifras.gob.ec/documentos/web-inec/Encuestas_Ambientales/Hogares/Hogares%202019/MOD_AMB_HOGAR_ESPND_2019_11.pdf

[2]   B. Ebin, M. Petranikova, B.-M. Steenari, y C. Ekberg, «Investigation of zinc recovery by hydrogen reduction assisted pyrolysis of alkaline and zinc-carbon battery waste», *Waste Management*, vol. 68, pp. 508-517, oct. 2017, doi: 10.1016/j.wasman.2017.06.015.

[3]   R. Farzana, R. Rajarao, P. R. Behera, K. Hassan, y V. Sahajwalla, «Zinc Oxide Nanoparticles from Waste Zn-C Battery via Thermal Route: Characterization and Properties», *Nanomaterials*, vol. 8, n.º 9, Art. n.º 9, sep. 2018, doi: 10.3390/nano8090717.

[4]   H. Mahandra, R. Singh, y B. Gupta, «Recycling of Zn-C and Ni-Cd spent batteries using Cyphos IL 104 via hydrometallurgical route», *Journal of Cleaner Production*, vol. 172, pp. 133-142, ene. 2018, doi: 10.1016/j.jclepro.2017.10.129.

[5]   O. Chicaiza, «Programa de gestión de pilas usadas», 4 de agosto de 2021.

[6]   B. Viswanathan, «Chapter 12 - Batteries», en *Energy Sources*, B. Viswanathan, Ed. Amsterdam: Elsevier, 2017, pp. 263-313. doi: 10.1016/B978-0-444-56353-8.00012-5.

[7]   W.-S. Chen, C.-T. Liao, y K.-Y. Lin, «Recovery Zinc and Manganese from Spent Battery Powder by Hydrometallurgical Route», *Energy Procedia*, vol. 107, pp. 167-174, feb. 2017, doi: 10.1016/j.egypro.2016.12.162.

[8]   K. Tanong, L.-H. Tran, G. Mercier, y J.-F. Blais, «Recovery of Zn (II), Mn (II), Cd (II) and Ni (II) from the unsorted spent batteries using solvent extraction, electrodeposition and precipitation methods», *Journal of Cleaner Production*, vol. 148, pp. 233-244, abr. 2017, doi: 10.1016/j.jclepro.2017.01.158.

[9]   Elgharbawy *et al.*, «A review on biodiesel feedstocks and production technologies», *Journal of the Chilean Chemical Society*, vol. 66, n.º 1, pp. 5098-5109, ene. 2021, doi: 10.4067/S0717-97072021000105098.

[10] L. Vásconez, «Convenios en cinco ciudades del Ecuador para reciclar aceites usados», *El Comercio*, septiembre de 2018. https://www.elcomercio.com/actualidad/ecuador/convenios-ciudades-ecuador-reciclar-aceites.html (accedido 1 de septiembre de 2021).

[11] P. Bardhan, A. Deka, S. S. Bhattacharya, M. Mandal, y R. Kataki, «Chapter 18 - Economical aspect in biomass to biofuel production», en *Value-Chain of Biofuels*, S. Yusup y N. A. Rashidi, Eds. Elsevier, 2022, pp. 395-427. doi: 10.1016/B978-0-12-824388-6.00003-8.

[12] D. Topi, «Transforming waste vegetable oils to biodiesel, establishing of a waste oil management system in Albania», *SN Appl. Sci.*, vol. 2, n.º 4, p. 513, mar. 2020, doi: 10.1007/s42452-020-2268-4.

[13] E. Chuquichanga y D. León, «Obtención de óxido de zinc a partir de pilas zinc carbono desechables», Perú, 2019.

[14] T. Samadhi, «Environmental impact of sodium sulfate decomposition in silicate glass manufacturing», jun. 2003.

[15] HERA, «Cover note of sodium sulfate». 6 de enero de 2006.

[16] INEN, «Biodiesel. Requisitos.» 2013. [En línea]. Disponible en: https://www.normalizacion.gob.ec/buzon/normas/2482.pdf

[17] ASTM, «Standard Test Method for Kinematic Viscosity of Transparent and Opaque Liquids (and Calculation of Dynamic Viscosity)», 20 de diciembre de 2021. https://www.astm.org/d0445-21.html (accedido 14 de marzo de 2022).

[18] ASTM, «Chapter 5 | Biodiesel», 2015. https://www.astm.org/mnl120170046.html (accedido 4 de enero de 2022).

[19] EN, «Combustibles para automoción. Combustibles par...», 2017. https://www.une.org/encuentra-tu-norma/busca-tu-norma/norma/?c=N0052852

(accedido 31 de agosto de 2022).

[20] E. Alvarado, E. González, y O. Mendoza, «Propuesta de un método para la recuperación de zinc de pilas alcalinas usadas bajo el enfoque de producción más limpia», Universidad del Salvador, El Salvador, 2010.

[21] J. Bocanegra, D. Malagón-Romero, y L. López, «Obtención de biodiesel a partir de aceite usado de cocina por trans-esterificación», *Ingenieria y Universidad*, vol. 19, p. 155, abr. 2015, doi: 10.11144/Javeriana.iyu19-1.odba.

[22] D. Rodriguez y J. Riesco, «Obtención de biodiesel a partir de mezclas de aceite de cocina usado y aceite de higuerilla por transesterificación», 2017. https://www.jovenesenlaciencia.ugto.mx/index.php/jovenesenlaciencia/article/view/1296 (accedido 5 de septiembre de 2022).

[23] V. G. Tacias Pascacio, A. Rosales Quintero, B. Torrestiana Sánchez, V. G. Tacias Pascacio, A. Rosales Quintero, y B. Torrestiana Sánchez, «Evaluación y caracterización de grasas y aceites residuales de cocina para la producción de biodiésel: un caso de estudio», *Revista internacional de contaminación ambiental*, vol. 32, n.º 3, pp. 303-313, ago. 2016, doi: 10.20937/RICA.2016.32.03.05.

[24] W. L. Tondo, F. Gurgacz, R. F. Santos, I. Werncke, F. F. Klajn, y A. M. Lenz, «Biodiesel as fuel for boilers», *Acta Scientiarum. Technology*, vol. 39, pp. 609-614, dic. 2017, doi: 10.4025/actascitechnol.v39i5.29501.

[25] R. Gavhane *et al.*, «Effect of Zinc Oxide Nano-Additives and Soybean Biodiesel at Varying Loads and Compression Ratios on VCR Diesel Engine Characteristics», *Symmetry*, vol. 12, n.º 6, Art. n.º 6, jun. 2020, doi: 10.3390/sym12061042.

[26] E. M. Sánchez Faba, «Obtención de biodiesel a partir de aceites vegetales empleando catalizadores sólidos nanoestructurados», 2021, Accedido: 5 de septiembre de 2022. [En línea]. Disponible en: http://ria.utn.edu.ar/xmlui/handle/20.500.12272/5187

[27] D. Diaz, G. Camargo, y M. Molano, «Evaluación de catalizadores de óxido de zinc y su actividad catalítica en la reacción de transesterificación para la producción de biodiésel», *AFINIDAD LXV*, pp. 299-305, 2008.

[28] F. Fangfang, A. Alagumalai, y O. Mahian, «Sustainable biodiesel production from waste cooking oil: ANN modeling and environmental factor assessment», *Sustainable Energy Technologies and Assessments*, vol. 46, p. 101265, ago. 2021, doi: 10.1016/j.seta.2021.101265.

[29] R. Sipayung y Budiyono, «Optimization of biodiesel production from used cooking oil using modified calcium oxide as catalyst and N-Hexane as solvent», *Materials Today: Proceedings*, ene. 2022, doi: 10.1016/j.matpr.2021.12.562.

[30] S. Sivarethinamohan, J. R. Hanumanthu, K. Gaddam, G. Ravindiran, y A. Alagumalai, «Towards sustainable biodiesel production by solar intensification of waste cooking oil and engine parameter assessment studies», *Science of The Total Environment*, vol. 804, p. 150236, ene. 2022, doi: 10.1016/j.scitotenv.2021.150236.

[31] P. Dasta, A. Pratap Singh, y A. Pratap Singh, «Zinc oxide nanoparticle as a heterogeneous catalyst in generation of biodiesel», *Materials Today: Proceedings*, vol. 52, pp. 751-757, ene. 2022, doi: 10.1016/j.matpr.2021.10.143.

[32] M. Guo, W. Jiang, J. Ding, y J. Lu, «Highly active and recyclable CuO/ZnO as photocatalyst for transesterification of waste cooking oil to biodiesel and the kinetics», *Fuel*, vol. 315, p. 123254, may 2022, doi: 10.1016/j.fuel.2022.123254.
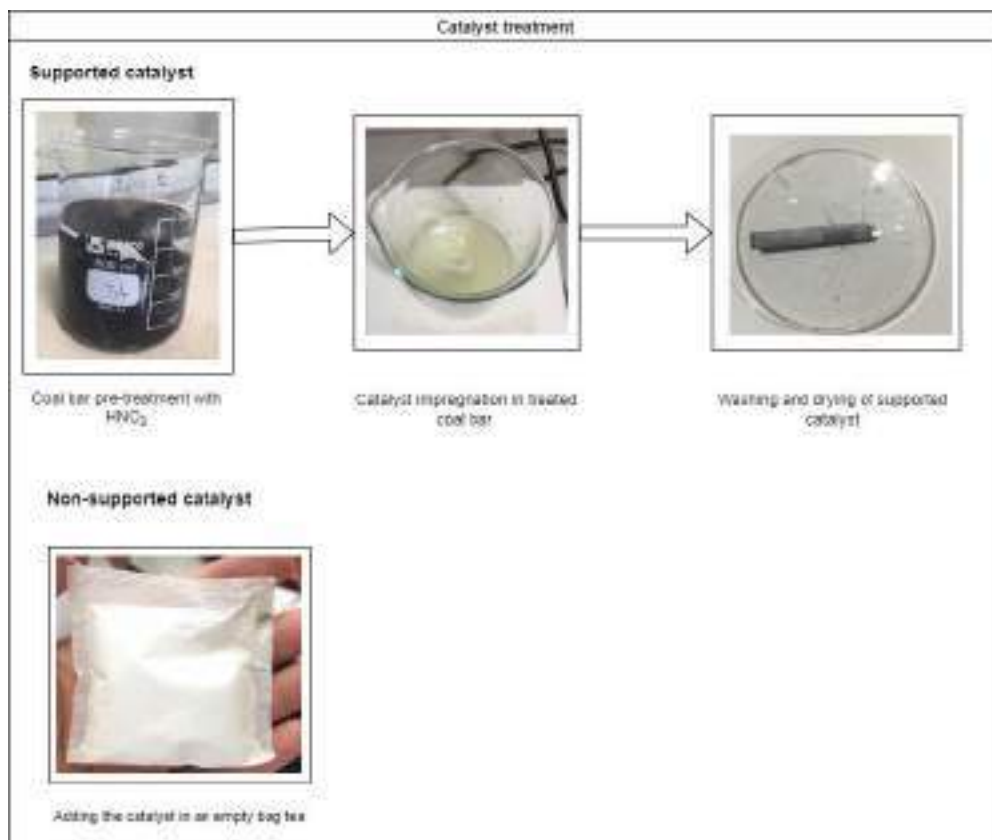
Annexes

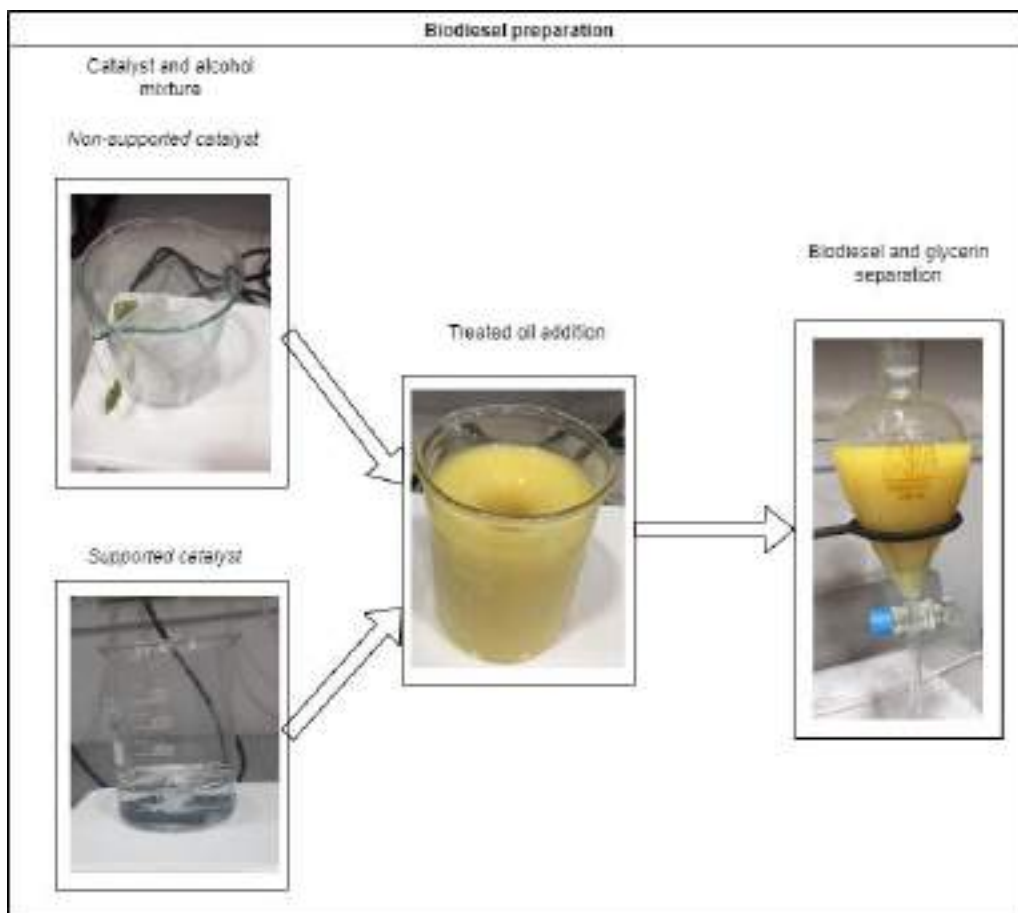**Annex 1. Obtainment of zinc oxide process**
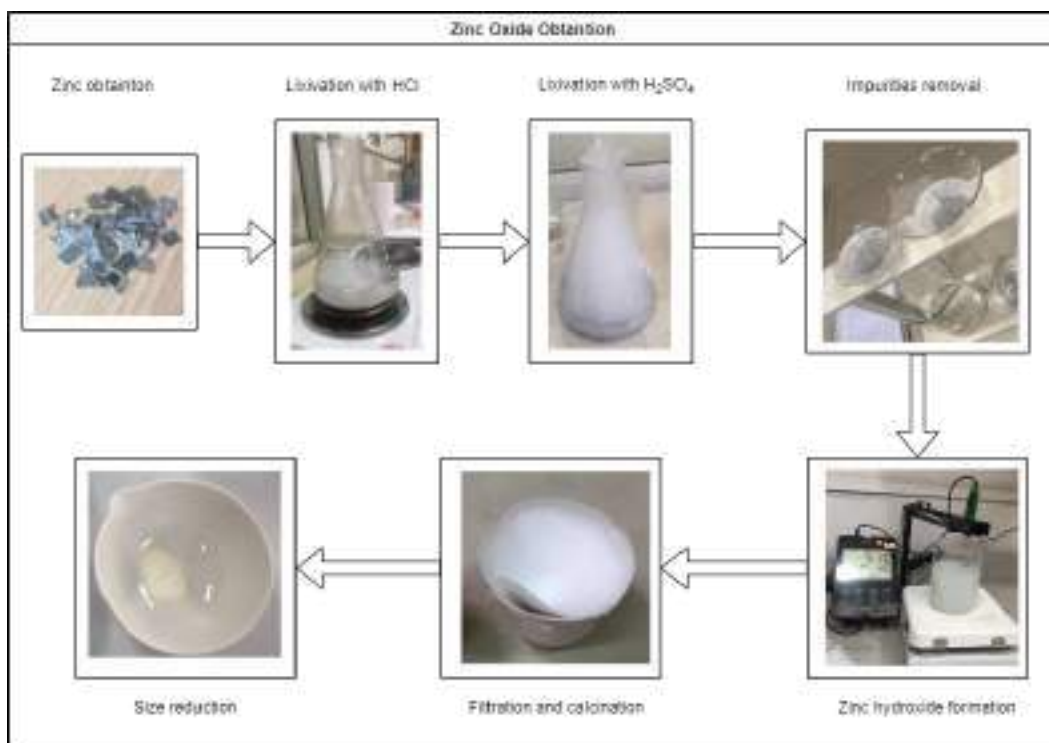
Annex 2. Recycled oil pre- treatment

Annex 3. Catalysts preparation

Annex 4. Biodiesel obtention

Annex 5. Biodiesel yield

Catalyst	Sample	Yield	Average (%)
Supported	SC1	74.5134	70.9088
	SC2	68.9701	
	SC3	69.2430	
B		0.5663	0.5663

Identificación automática de fases en redes de distribución en baja tensión mediante aprendizaje automático

Lluc Crespí-Castañer[1], Miquel Roca[1], Josep Lluís Rosselló[1], Lluís Juncosa[2] and Vicente Canals[1]

[1] Universidad de las Islas Baleares, Palma ES07122, España
[2] Vall de Sóller Energía, Sóller ES07100, España
lluc.crespi@uib.es

Resumen. Uno de los problemas recurrentes en la distribución eléctrica consiste en la determinación de las fases en que se encuentran conectados los diferentes consumido-res. La identificación de las fases es esencial para afrontar la problemática del desequilibrio en las redes de distribución de baja tensión puesto que, éste provoca pérdidas de energía significativas y reduce la vida útil de los componentes de la red, además de contribuir a una reducción de la calidad en el suministro.

Históricamente, no se ha venido registrando la distribución de las fases en el despliegue de los nuevos suministros. Adicionalmente, los métodos manuales de identificación tienen asociado un alto coste para las distribuidoras. A su vez, el reciente desarrollo de las redes inteligentes ha conducido a un despliegue masivo de equipos de medida telegestionables, con capacidad para monitorizar numerosas variables de los puntos de suministro. Lo que ha posibilitado el surgimiento de una serie de técnicas innovadoras basadas en el aprendizaje automático y Big data, que hacen posible resolver el problema de identificación de fases de forma automática y con un bajo coste asociado. Así, en el presente trabajo se aplica una metodología basada en aprendizaje automático para identificar las fases de los contadores inteligentes en redes de distribución ramificadas, a partir de los datos proporcionados por la empresa distribuidora Vall de Sóller Energía SLU, Islas Baleares (España). En concreto, el método implementado se basa en la clasificación de series temporales formadas por las tensiones medidas de los diferentes contadores de una red de distribución en baja tensión. Además, este método se fundamenta en una versión modificada del algoritmo Prim. Los resultados experimentales obtenidos sobre una red de distribución real, compuesta de 46 suministros son muy alentadores al haberse constatado como la correlación entre medidas de tensión se corresponde con la pertenencia a una determinada fase y viceversa. Posibilitando así la reducción de los desbalances en las redes de distribución y sus pérdidas asociadas.

Palabras clave: Constrained Multi-Tree, Identificación de fases, Redes inteligentes, Red eléctrica desequilibrada, Correlación de voltajes.

1　Introducción

Generalmente, la energía eléctrica se transfiere a los consumidores a través de redes de distribución trifásicas en baja tensión, debido a sus ventajas técnicas y económicas frente a las redes monofásicas. Los suministros de estas redes son mayoritariamente monofásicos, de modo que se conectan a una de las tres fases de la red. Muchas de estas redes se han ido desplegando a lo largo de los años con lo que no se ha mantenido el registro de las fases. Históricamente, la demanda energética era mucho menor a la actual, por lo que la identificación de las fases no era un factor relevante. De forma que, los suministros se conectaban sobre las distintas fases de la red de manera empírica. Actualmente, dado que la demanda es sustancialmente mayor, conocer a qué fase/s está conectado cada contador es fundamental para la disminución de las pérdidas de la red y la planificación de nuevos suministros.

Debe tenerse en cuenta, que la demanda de los usuarios depende de los hábitos de consumo de éstos, que son intrínsicamente variables. Por tanto, el reparto de los distintos contadores sobre las tres fases de la red es imprescindible para que ésta funcione eficientemente [1, 2]. Puesto que, el desequilibrio de cargas en una red trifásica tiene las diferentes implicaciones negativas. En primer lugar, el desequilibrio de fases produce pérdidas de energía adicionales durante la transmisión, debidas al efecto Joule. En segundo lugar, la capacidad de carga de los conductores y los transformadores de distribución disminuye, es decir, la máxima energía que puede ser transportada a través de la red se ve reducida. Por tanto, esto supone un factor limitante a la hora de realizar la conexión de nuevas cargas y el despliegue de la generación distribuida. En tercer lugar, puede producir daños y reducir la vida útil de los distintos elementos de la red. Como consecuencia del conjunto de estos factores, la calidad de la energía se ve afectada negativamente implicando, al final, un incremento de los precios de la electricidad.

Para resolver esta problemática de la identificación de fases existen diversas metodologías manuales que no suelen ser utilizadas en redes de distribución en baja tensión por su alto coste, en términos de mano de obra y recursos técnicos que requieren. No obstante, el incipiente desarrollo de las redes inteligentes pone al alcance de las empresas energéticas una enorme fuente de datos que permite la monitorización prácticamente completa de la red. La instalación de contadores inteligentes (Smart Meters) en casi todas las viviendas y demás puntos de consumo hace qué dicha monitorización no sea exclusiva de las redes de alta y media tensión, como era común, sino que también pase a abarcar las redes de baja tensión. Consecuentemente, este hecho ha permitido el surgimiento de diferentes metodologías innovadoras que, con la combinación de técnicas de aprendizaje automático y de análisis Big data, permiten mejorar y optimizar la gestión de las redes. En concreto, posibilitan la identificación de fases a partir de los datos de telemetría de los contadores inteligentes. La ventaja principal de estas técnicas se fundamenta en que no sea necesaria la implantación de costosos sistemas hardware adicionales ni que tampoco se requiera de un previo conocimiento de la topología de la red.

Los métodos actuales se distinguen principalmente por los datos de entrada que utilizan. Por un lado, los métodos que utilizan datos de consumo aplican el principio de conservación de energía, destacando el trabajo de V. Arya [3, 4]. Por otro lado, los

métodos que utilizan medidas de voltaje identifican las fases aplicando análisis de correlación, de regresión y métodos de clasificación basados en Machine Learning, destacando los trabajos de F. Olivier [5, 6] y de W. Wang [7].

V. Arya et al. [4] han propuesto una técnica para la identificación de las fases de contadores inteligentes basada en modelos de optimización matemáticos. El método propuesto determina las fases a partir de series temporales de medidas de consumo aplicando el principio de conservación de la energía. Se toman medidas de todos los contadores y del transformador de distribución que los alimenta de forma sincronizada. De esta manera, la carga total por fase del transformador deber ser igual a la suma de la energía consumida de todos los contadores sobre cada fase.

Por otro lado, el enfoque de F. Olivier et al., [5, 6] se basa en determinar la correlación entre series temporales de voltaje de las diferentes fases, del transformador y de los contadores. Como es natural, los voltajes de diferentes puntos de una misma línea de distribución diferirán entre si a causa de las caídas de tensión y otros efectos. Sin embargo, las medidas de voltaje tomadas sobre una misma fase deberían presentar correlaciones mayores entre sí que las tomadas sobre fases distintas. De esta forma, proponen resolver el problema mediante técnicas basadas en el aprendizaje automático de agrupamiento de características (Clústering). En concreto, han desarrollado un método basado en el algoritmo de Prim que toma como restricción que dos series temporales de voltaje, de dos fases diferentes de un mismo contador, deberán ser clasificadas en dos grupos distintos. Los resultados obtenidos se muestran muy satisfactorios, dado que el rendimiento del algoritmo para intervalos de tiempo de 15 minutos se aproxima al 100%.

Siguiendo en la misma línea de investigación, W. Wang et al. [7], proponen utilizar un algoritmo de clasificación K-Means con restricciones sobre los datos de voltaje. A diferencia del método anterior, no utilizan directamente las series temporales de voltaje, sino que extraen características de los datos teniendo en cuenta conocimientos específicos de la red de distribución. Por un lado, preprocesan los datos normalizándolos y aplicándoles un análisis PCA (Principal Component Analysis) para obtener sus características principales reduciendo, así, la dimensión de éstos. Por otro lado, aplican restricciones must-link y cannot-link. La restricción must-link implica que dos medidas deben estar en un mismo grupo. Mientras que, la restricción cannot-link implica que dos medidas deben ser clasificadas en diferentes grupos.

En el presente trabajo se propone la implementación del método Constrained Multi Tree, propuesto en [6], para la identificación de fases a partir de la clasificación de series temporales de voltaje, y la validación de dicho método con los datos de una red de distribución de baja tensión en la isla de Mallorca, España. Este documento se estructura de la siguiente forma: en la sección 2 se plantea la problemática de la identificación de fases enfocada como un problema de clasificación de aprendizaje automático y se expone el funcionamiento del método implementado. En la sección 3, se presenta el caso de estudio sobre el cual se ha validado el método, así como se presentan los resultados obtenidos para dicho caso de estudio. Finalmente, en la sección 4 se presentan las conclusiones.

2　　Metodología

La presente sección se desarrolla en dos partes. En la sección 2.1 se presenta el enfoque tomado para la identificación de fases del caso de estudio. Mientras que, en la sección 2.2 se describe el funcionamiento del método implementado.

2.1　La identificación de fases

Al analizar los voltajes de los contadores de una zona de distribución, es posible comprobar como los voltajes de los contadores conectados sobre la misma fase de la red están más correlacionados entre sí que los voltajes correspondientes a contadores que están conectados sobre diferentes fases. De esta forma, la identificación de fases se plantea como un problema de clasificación de aprendizaje automático. Así, el principio de funcionamiento del método implementado se basa en clasificar las fases de los distintos contadores, a partir de la correlación de sus series temporales de voltaje, en tres grupos o clústers distintos correspondientes a las tres fases de la red. Sin embargo, debe añadirse una restricción sobre la clasificación consistente en que dos fases de un mismo contador no puedan ser clasificadas en el mismo clúster.

Las series temporales de voltaje se componen de medidas de la tensión eficaz de la acometida de los diferentes contadores, tomadas a intervalos regulares. Para determinar debidamente la correlación entre dos series temporales de voltaje es necesario que la frecuencia de lectura sea alta y que las muestras se tomen en el mismo instante de tiempo para todos los contadores.

A fin de llevar a cabo dicha clasificación se ha implementado el método Constrained Multi Tree (CMT) [5]. La ventaja principal de este método reside en que la clasificación se efectúa teniendo en cuenta la estructura ramificada de la red.

2.2　Implementación del método CMT

La implementación del método CMT se basa en el algoritmo de Prim [6], que tiene como objetivo buscar el mínimo árbol de expansión de un grafo dado. Este algoritmo se ha adaptado para tomar en consideración las restricciones naturales y particulares del problema. Dado que, no puede aplicarse el algoritmo de Prim directamente, ya que se obtendría solamente un árbol. El objetivo consiste en obtener tres árboles, uno asociado a cada fase de la red trifásica. De esta forma, inicialmente se crearán tres árboles con sus respectivos nodos raíz correspondientes a las series temporales de voltaje de cada fase del transformador. La inicialización tiene que realizarse con tres medidas que realmente pertenezcan a fases diferentes. Por este motivo pueden utilizarse las medidas de un contador trifásico o las del transformador de distribución. Dado que la clasificación sigue una estructura de árbol como la de la red de distribución, asociando las medidas más correlacionadas entre sí en cada iteración, se tomarán las fases del transformador como nodos raíz. Olivier et al. [6] en un trabajo previo demuestra cómo se obtiene un mayor rendimiento utilizando las medidas del transformador en lugar de las medidas de un contador trifásico cualquiera. Seguidamente, el método realizará diferentes iteraciones para asociar las diferentes fases o nodos a los tres árboles. En cada iteración, en

primer lugar, se calculará la distancia entre las distintas fases sin clasificar y las fases previamente asociadas a un árbol. En segundo lugar, se asociará la fase más cercana al nodo del árbol correspondiente, en base a las distancias calculadas. De este modo, los árboles se van expandiendo iteración a iteración. Finalmente, los nodos pertenecientes a un mismo árbol son identificados como pertenecientes a la misma fase a nivel de la red. La distancia entre dos nodos o fases se corresponde con la medida de correlación entre sus series temporales de voltaje. Concretamente, la métrica de correlación utilizada es la de Pearson, descrita en la ecuación 1 para las series temporales de dos fases diferentes, en este caso las 1 y 2. El coeficiente de Pearson determina la dependencia lineal entre dos variables, valiendo 1 cuando ésta es perfecta y positiva y -1 cuando ésta es perfecta y negativa. De modo que, la distancia entre dos series temporales, definida en la ecuación 2, vale 0 cuando están perfectamente correlacionadas y 1 cuando no existe correlación. Cabe destacar que para prevenir el sobrecrecimiento de un árbol (o clúster) a expensas de los demás, primero se clasificarán las fases de los contadores trifásicos y, finalmente, las de los contadores monofásicos.

$$r_{F1,F2} = \frac{\sum_{i=1}^{n}(F1_i - \widehat{F1})(F2_i - \widehat{F2})}{\sqrt{\sum_{i=1}^{n}(F1_i - \widehat{F1})^2}\sqrt{\sum_{i=1}^{n}(F2_i - \widehat{F2})^2}} \tag{1}$$

$$d_{F1,F2} = 1 - |r_{F1,F2}| \tag{2}$$

A fin de detallar mejor el problema se utilizará un ejemplo ilustrando el grafo y los diferentes pasos del algoritmo. En este ejemplo, se tienen 5 contadores, 2 de los cuales son trifásicos (4 y 5), y un transformador. Por tanto, se tienen un total de 12 fases contando las de los transformadores.

La Fig. 1 muestra el grafo de partida para el cual el algoritmo deberá determinar los tres árboles de mínima expansión correspondientes a las tres fases de la red. En dicha figura se puede comprobar que no existen ramas que unan fases de un mismo contador, puesto que deben ser clasificadas como diferentes.
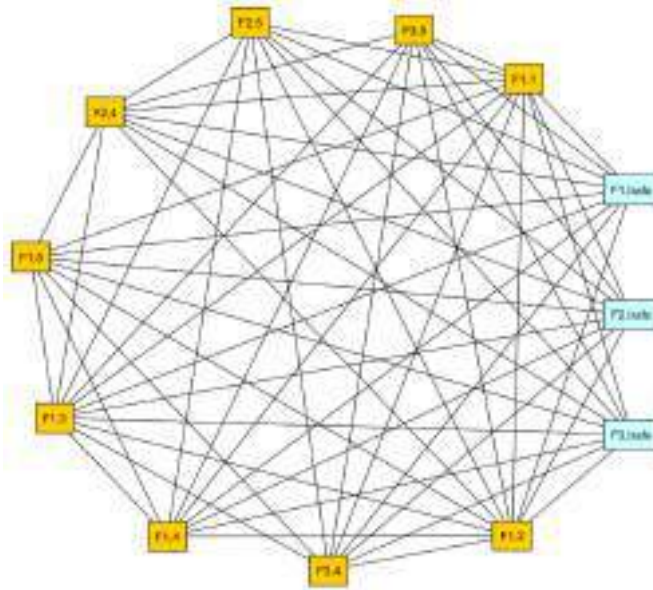
Fig. 1. Grafo de partida del método CMT

En el primer paso se asocian cada una de las fases del transformador de distribución a un clúster (Fig. 2).
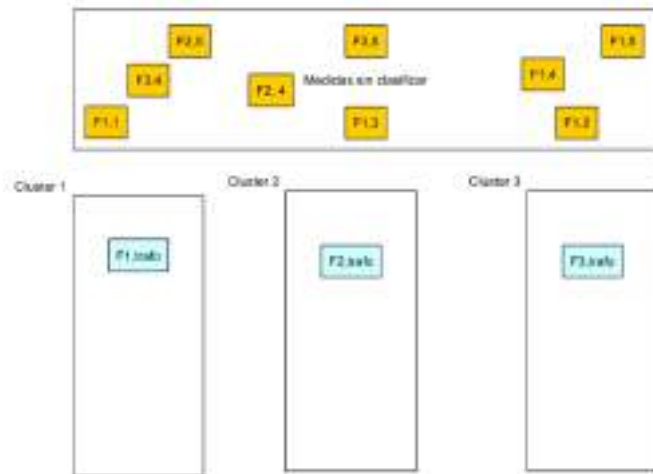

Fig. 2. Paso 1 del algoritmo CMT

El segundo paso (Fig. 3) consiste en calcular las distancias entre las diferentes fases de los contadores y las fases previamente asociadas a un clúster, en este caso las del transformador de distribución. Luego de haberse calculado las distancias, se ordenan las fases en base a las distancias calculadas de mayor a menor y se asocia la fase que presente la menor distancia al nodo correspondiente, expandiendo, así, uno de los tres árboles. Este procedimiento se repite hasta asociar todas las fases.
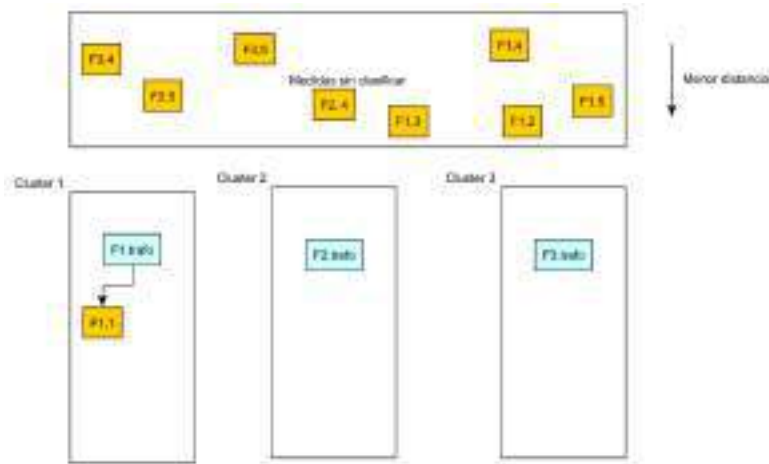

Fig. 3. Paso 2 del algoritmo CMT

Finalmente, se obtienen tres árboles de clasificación (Fig. 4), que se corresponden con cada una de las tres fases de la red de distribución en baja tensión.
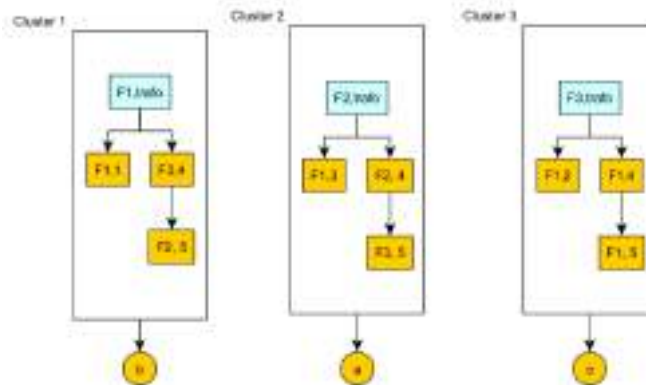

Fig. 4. Paso 3 del algoritmo CMT

En la Fig. 5 se presenta el diagrama de flujo de la metodología reseguida para la identificación de fases. Donde *D* representa la matriz de distancias o pesos del grafo entre las fases de los distintos contadores y los tres clústers.

En primer lugar, el algoritmo inicializa los tres clústers *C* asignando cada una de las tres fases del transformador de distribución ($F1_{trafo}$, $F2_{trafo}$ y $F3_{trafo}$) a un clúster diferente, según se detalla en la Fig. 2. Seguidamente, el algoritmo se ejecuta cíclicamente mientras existan fases de los *n* contadores sin clasificar. Realizando dos bucles diferentes, uno encargado del cálculo de las distancias y el otro encargado de la asignación de fases. El primer bucle se encarga del cálculo de las distancias entre las fases sin clasificar y las fases previamente asignadas en un clúster, según se muestra en la Fig. 3. En el diagrama de flujo de la Fig. 5, el término medida se refiere a la serie temporal de una fase perteneciente a un contador. Mientras que delta es el valor mínimo de las distancias entre una medida y las medidas asignadas a un determinado clúster. Se calcula delta para todas las medidas o fases aun no clasificadas, y su valor se almacena en la matriz de distancias *D*, que toma la dimensión de (*n* x *C* x *F*) como se muestra en la Tabla 1. Debe tenerse en cuenta que la clasificación de las fases de los contadores monofásicos no se lleva a cabo hasta concluir la clasificación de los contadores trifásicos.

Tabla 1. Matriz de distancias *D*

Contadores	F1 contador			F2 contador			F3 contador		
	C1	C2	C3	C1	C2	C3	C1	C2	C3
Contador 1	$d_{F1,C1}$	$d_{F1,C2}$	$d_{F1,C3}$	$d_{F2,C1}$	$d_{F2,C2}$	$d_{F2,C3}$	$d_{F3,C1}$	$d_{F3,C2}$	$d_{F3,C3}$
Contador 2	$d_{F1,C1}$	$d_{F1,C2}$	$d_{F1,C3}$	$d_{F2,C1}$	$d_{F2,C2}$	$d_{F2,C3}$	$d_{F3,C1}$	$d_{F3,C2}$	$d_{F3,C3}$
…	…	…	…	…	…	…	…	…	…
Contador n	$d_{F1,C1}$	$d_{F1,C2}$	$d_{F1,C3}$	$d_{F2,C1}$	$d_{F2,C2}$	$d_{F2,C3}$	$d_{F3,C1}$	$d_{F3,C2}$	$d_{F3,C3}$

Finalmente, una vez calculadas todas las distancias se procede a la asignación de fases a un clúster. Para ello, se calcula el valor mínimo de la matriz de distancias y se asigna la correspondiente medida o fase a un clúster.
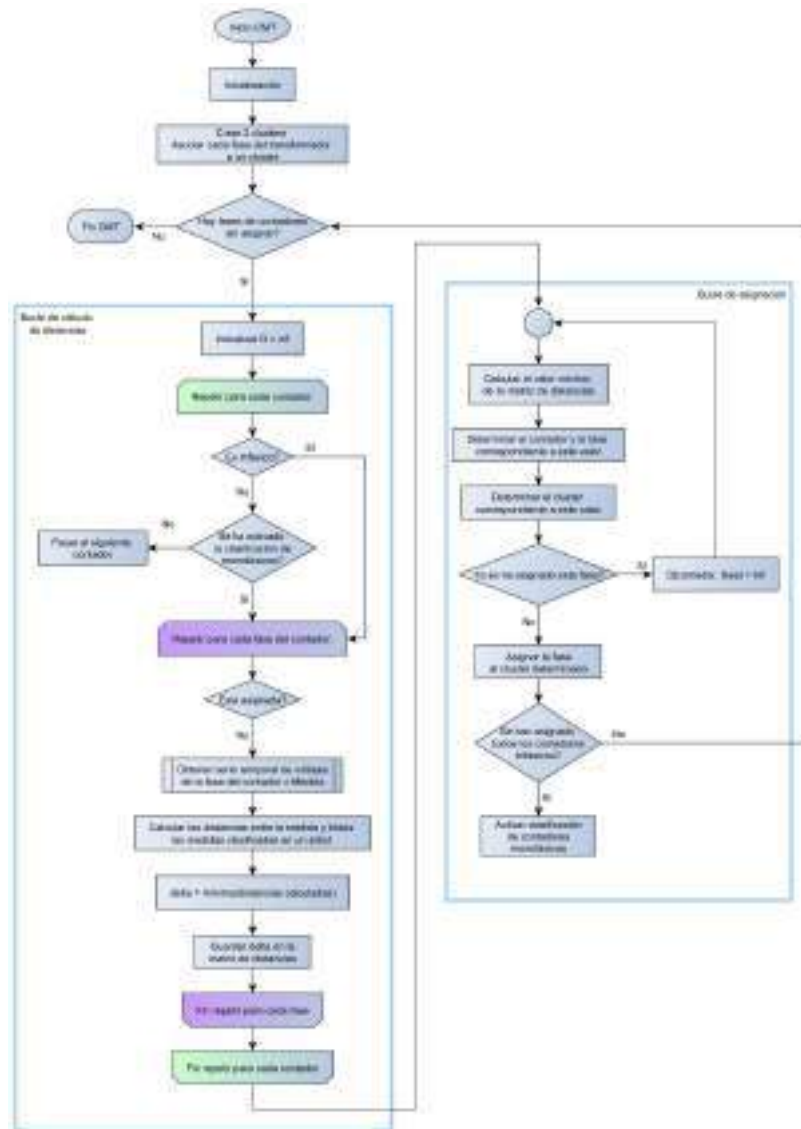
Fig. 5. Diagrama de flujo del algoritmo CMT

3   Caso de estudio y resultados

La presente sección se estructura en dos partes bien diferenciadas. En la sección 3.1 se presenta el caso de estudio mediante el cual se ha validado el método propuesto. Seguidamente, en la sección 3.2, se presentan los resultados de la identificación de fases para dicho caso de estudio.

3.1   Caso de estudio

El presente trabajo se ha podido desarrollar gracias a la colaboración con la empresa distribuidora Vall de Sóller Energía SLU, que ha proporcionado los datos de telegestión y la información técnica de la red de distribución, además de encargarse de realizar las medidas de campo para la comprobación de los resultados. Concretamente, ha facilitado los datos de tensiones y consumos de una zona de distribución de la ciudad de Sóller, Islas Baleares, llamada Binidorm. En esta zona existe un centro de transformación de Media Tensión a Baja Tensión (MT/BT), 10 contadores trifásicos y 36 contadores monofásicos. En cuanto a las medidas de voltaje, se han tomado desde el día 01/07/2022 hasta el día 07/07/2022, con una frecuencia de lectura teórica de 15 min. Así, con la frecuencia de recopilación de datos muestrales y previo filtrado de valores no válidos se ha dispuesto de 501 medidas de voltaje por fase y contador, con una frecuencia media real de 17 min. En cuanto a los datos de consumo, se ha dispuesto de la demanda energética horaria de cada contador para todo el año 2021.

3.2   Resultados

La empresa distribuidora Vall de Sóller Energía SLU disponía del registro de las fases de la red de distribución citada, dado que ésta se implantó recientemente. En consecuencia, esta información ha servido para comprobar los resultados del algoritmo con medidas tomadas a campo y, por tanto, verificar su funcionamiento. Concretamente, aportaron la identificación de 12 contadores monofásicos (Tabla 2). Al comparar la identificación obtenida del método CMT con el registro de las fases se comprobó que los resultados diferían para un contador determinado (resaltado en rojo en la Tabla 2). Teniendo en cuenta que el algoritmo había identificado correctamente el resto de las fases (11 de 12), se contactó nuevamente con Vall de Sóller Energía a fin de determinar si era posible realizar una nueva medición para el contador ZIV0034952257. La medida manual de este contador resultó ser la misma que la obtenida por el método automático. Por ende, el método propuesto ha logrado determinar correctamente la identificación de las fases de los 12 contadores de los que se disponía de registros.

Por otro lado, el resultado de la identificación de fases obtenido por el método CMT en conjunto con los datos de consumo de la red de distribución de Binidorm, citados en el apartado anterior, ha permitido evaluar el equilibrio de cargas de dicha red. En la Fig. 6 puede apreciarse como las distribuciones de demanda agregada por hora relativas a cada fase resiguen formas significativamente distintas. Por lo que, el consumo demandado por fase durante el periodo analizado ha sido muy dispar a lo largo del tiempo.

Además, se aprecia como la demanda de potencia sobre la fase 3, con una demanda media de 8,56 kW, es hasta un 41% inferior a la demanda media de las otras dos fases (12,7 kW para la fase 1 y 14,61 kW para la fase 2). Este hecho se explica principalmente mediante la identificación de fases realizada, que ha permitido verificar que el número de contadores monofásicos conectados sobre dicha fase era de tan solo 6, frente a los 12 instalados en la fase 1 y los 19 instalados en la fase 2.

Tabla 2. Resultados de la identificación de fases de la zona de distribución de Binidrom.

Contador	Fases de medidas experimentales[1]	Resultado de los métodos
ZIV0039450248	Trifásico	-
ZIV0034648582	2	2
ZIV0034648440	0	0
ZIV0034648577	0	0
ZIV0044545085	Trifásico	-
ZIV0034648272	1	1
ZIV0036240112	Trifásico	-
ZIV0034648438	1	1
ZIV0037417618	0	0
ZIV0034648274	2	2
ZIV0034701714	1	1
ZIV0034648252	1	1
ZIV0034952257	2	2
ZIV0034648439	1	1
ZIV0034648444	0	0

Adicionalmente, dado que la empresa cuenta con el listado de suministros de cada sublínea de la red, ha sido posible analizar el equilibrio de fases para cada una de estas sublíneas. Con lo que se ha podido determinar que ha existido un desequilibrio de cargas sustancial para las sublíneas 1 y 3, como puede apreciarse en la Fig. 7. En la sublínea 1 puede apreciarse que la demanda de la fase 3 es muy inferior a la de las otras dos fases. En concreto, se ha podido comprobar que no existe ningún contador monofásico sobre la fase 3 en dicha rama. Mientras que, para la sublínea 3, se aprecia como la demanda sobre la fase 2 es mucho mayor en relación con las otras fases. En este caso, se ha determinado que el número de contadores en dicha fase era de casi el doble respecto a las otras dos.

El análisis del equilibrio de cargas, tanto en el conjunto de la red como en cada una de las sublíneas de ésta, en base al reparto de las fases de los contadores sobre la red de distribución obtenido con la metodología presentada, posibilita analizar nuevas configuraciones de los contadores para minimizar el desequilibrio de la red, y por ende las pérdidas de distribución de ésta.

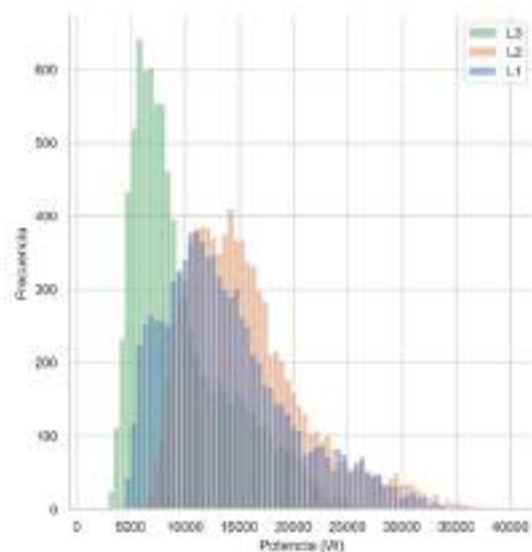[1] Aportadas por Vall de Sóller Energía SLU

Fig. 6. Histograma de demanda agregada por hora y por fase.
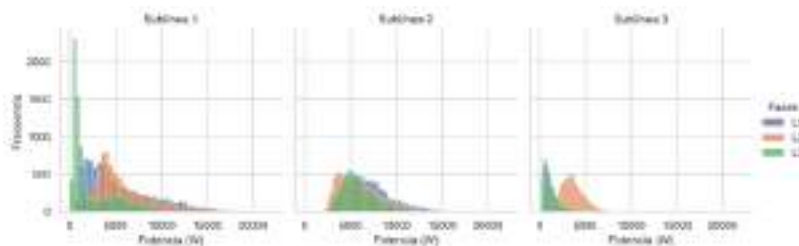

Fig. 7. Histogramas de demanda agregada por hora, fase y sublínea

4　　Conclusiones

Se ha aplicado una metodología basada en aprendizaje automático para la identificación de fases a partir de las series temporales de voltajes medidas en los diferentes contadores inteligentes de una red de distribución en baja tensión. Ésta se fundamenta en el uso de una técnica de aprendizaje automático no supervisado, denominada Constrianed Multi-Tree, que en base a la correlación entre las diferentes medidas permite extraer información acerca de la estructura física de la red de una red de distribución. Los resultados obtenidos sobre los datos de telegestión de una red de distribución real,

compuesta de 46 suministros (36 monofásicos y 10 trifásicos), son alentadores al haberse constatado como la correlación entre medidas se corresponde con la pertenencia a una determinada fase y viceversa. El análisis de la demanda agregada por hora relativa a cada fase ha mostrado como en la red de distribución analizada existe un desequilibrio de fases significativo, alcanzado el 41% de desequilibrio entre ellas. Por ello, la metodología presentada abre el camino a la reducción de los desbalances en las redes de distribución, tanto en cabecera como en los diferentes ramales de distribución.

Finalmente, diferentes aspectos prácticos relacionados con el rendimiento de la metodología han surgido a raíz de este trabajo. Siendo de gran interés continuar investigando la relación entre el rendimiento del algoritmo y la frecuencia de muestreo y el número de muestras.

5   Agradecimientos

6   Referencias

1.   Ni F, Liu JQ, Wei F, et al (2017) Phase identification in distribution systems by data mining methods. In: 2017 IEEE Conference on Energy Internet and Energy System Integration (EI2). IEEE, pp 1–6
2.   Modarresi MS, Huang T, Ming H, Xie L (2017) Robust phase detection in distribution systems. In: 2017 IEEE Texas Power and Energy Conference (TPEC). IEEE, pp 1–5
3.   Arya V, Jayram TS, Pal S, Kalyanaraman S (2013) Inferring connectivity model from meter measurements in distribution networks. In: e-Energy 2013 - Proceedings of the 4th ACM International Conference on Future Energy Systems. pp 173–181

4.   Arya V, Seetharam D, Kalyanaraman S, et al (2011) Phase identification in smart grids. In: 2011 IEEE International Conference on Smart Grid Communications (SmartGridComm). IEEE, pp 25–30

5.   Olivier F, Ernst D, Fonteneau R (2017) Automatic phase identification of smart meter measurement data. CIRED - Open Access Proceedings Journal 2017:1579–1583. https://doi.org/10.1049/oap-cired.2017.1143

6.   Olivier F, Sutera A, Geurts P, et al (2018) Phase Identification of Smart Meters by Clustering Voltage Measurements. In: 2018 Power Systems Computation Conference (PSCC). IEEE, pp 1–8

7.   Wang W, Yu N, Foggo B, et al (2017) Phase Identification in Electric Power Distribution Systems by Clustering of Smart Meter Data. 259–265. https://doi.org/10.1109/ICMLA.2016.0050

Análisis sobre la pérdida de las Lomas de Lima Este y su Impacto en la Reducción de los Servicios Ecosistémicos

Flor Karina Sueldo Nieto[1][0000-0003-3901] and Jorge Mírez[1][0000-0002-5614-5853]

1 Universidad Nacional de Ingeniería, Rímac, Lima, Perú
flor.sueldo.n@uni.pe
jmirez@uni.edu.pe

Resumen. En el presente artículo se analiza la reducción de los servicios ecosistémicos y se proponen propuestas de solución para su recuperación. Lima Este y los distritos que lo conforman, tienen varias brechas por cerrar respecto al cuidado de sus áreas naturales, existe una falta de compromiso por parte de los gobiernos locales, regionales e instituciones involucradas en la conservación y protección de las áreas naturales como las lomas. El alto déficit de áreas urbanas accesibles, la desprotección de las zonas de laderas y las zonas de lomas, han generado varios problemas como la ocupación ilegal, el tráfico de terrenos, la invasión informal, la perdida de áreas naturales y la degradación de las lomas. Al 2019 la loma de Amancaes se ha visto invadida en un 30%, la loma de Mangomarca en un 60% y la loma de Villa Maria del Triunfo en un 45%, como se observa la mayoría de las lomas que se encuentran del área urbano reciben una gran presión por parte de las invasiones informales Scudere et al (2019). Entre algunas líneas de acción se proponen la formalización de la conservación y protección de las lomas Payet y Mangomarca, a través del Gobierno regional, local y las instituciones involucradas la conservación de las áreas naturales. Creación de eco museos, circuitos eco-culturales, o la aplicación de propuestas como las de infraestructura ecológica de conservación, cuidado y un uso urbano - ambiental de los espacios, ayudaría conservar la infraestructura ecológica y a su vez brindar mas espacios abiertos a la comunidad. También es importante promover la participación de los colegios y la comunidad, para que la misma población proteja, cuide y pueda incluir un turismo sostenible como parte de sus actividades económicas, mejorando así su calidad de vida.

Keywords: Lomas, Servicios Eco-sistémicos, Ecología, Medio Ambiente.

1. INTRODUCCIÓN

En el presente trabajo se describen las lomas identificadas en Lima Este y los problemas de perdida de las lomas y sus servicios ecosistémicos, y sus diferentes causas entre las más principales la falta de protección legal por pararte de los gobierno regional, local y de las instituciones como el SERNAMP, quienes deben encargarse de proteger y conservar estas áreas naturales.

San Juan de Lurigancho es el distrito con mayor cantidad de habitantes y con mayor déficit de áreas verdes y/o espacios públicos, cuenta con 2 m2/Hab, por debajo de los 9m2/Hab recomendados por la OMS, PDU Lima Este (2022).

Los botaderos de basura que dejan la población que vive al costado de las lomas y el abandono de los sitios arqueológicos ha generado un ambiente ideal para los delincuentes y drogadictos, por lo que estos sitios son considerados inseguros, al encontrarse abandonados por las autoridades son vigilados por los traficantes de terreno, Scudere et al (2019)

Las lomas costeras son ecosistemas que han tenido una estrecha relación con las ciudades y/o asentamientos, a través de su historia, prueba de ello son las numerosas evidencias encontradas como cerámicos precolombinos, herramientas líticas, cercos y recintos que los antiguos peruanos utilizaban, como los encontrados en las lomas de Mangomarca, Nieuwland et al (2017).

Así mismo se detallan alguna propuesta para poder solucionar el problema como, la protección, la conservación no solo por parte de las autoridades sino también de la comunidad y el involucramiento de estos a través de talleres y capacitaciones.

La recuperación de las lomas, ayudara a incrementar los beneficios de los servicios ecosistémicos, también incrementaran las áreas verdes por habitante, áreas de esparcimiento donde la población pueda hacer caminatas, conocer y revalorar sus áreas naturales y así mejorar su calidad de vida.

2. AMBITO DE ESTUDIO

El ámbito de estudio se ubica al este de Lima metropolitana, limita por el norte con los distritos de Carabayllo, Comas e Independencia, por el Oeste con los distritos de Rímac, Cercado de Lima, San Luis, La Victoria, San Borja y Santiago de Surco, por el Sur con los distritos de San Juan de Miraflores, Villa María del Triunfo, Pachacamac y Cieneguilla, y por el Este con la Provincia de Huarochirí, se encuentra dentro de la provincia y el departamento de Lima, tiene un área total de 58606.94 Has de los cuales 30.47% (17856.63 has) de todo Lima Este corresponde al área urbana, Plan MET 2040 (2022).
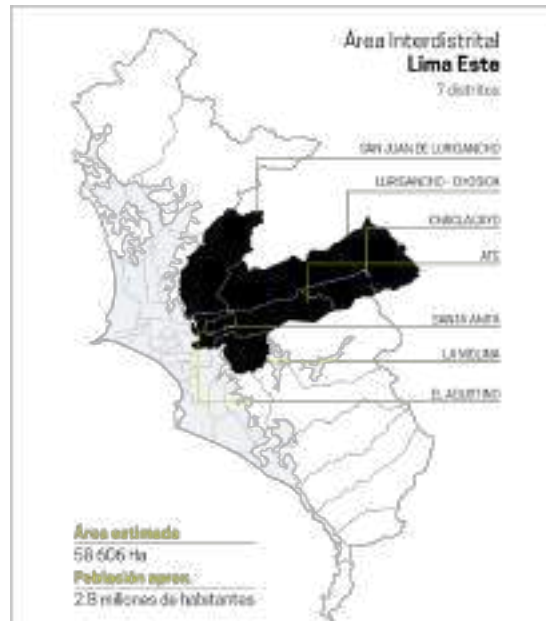
Fig 1. Mapa de la ubicación de Lima Este
Fuente: PDU Lima Este 2021-2031 (2022)

La costa peruana se caracteriza por ser una zona desértica, debido a sus características según su ubicación geográfica se ve influenciado por la Corriente del Humboldt, los vientos Alisios y la cadena de montañas, la humedad relativa está por encima del 80%, llegando al 100%, lo que produce la precipitación en forma de fina lluvia, conocida como garúa, SERNAMP (2019).

Las lomas son ecosistemas que se desarrollan en las zonas de neblinas invernales, usualmente estos se desarrollan en ambientes de colinas donde existe ingreso hídrico irregular producido por precipitaciones esporádicas y la presencia de neblinas estaciones cargadas de agua que se condensan al contacto con las superficies rocosas, presentándose como islas de vegetación que cubren las colinas y montañas.

Dentro de Lima Este se tienen 2 tipos de Lomas las estacionales que suman un total de 850.44 ha, y las extraordinarias con un área de 14926.09 has.

Fig 2. Las Lomas de Mangomarca diferentes vistas
Fuente: Scudere et al (2019)

Lomas Estacionales, Se denomina a aquellas lomas que se forman todos los años por las neblinas invernales entre los meses de mayo a octubre, dentro de Lima Este se identifican 4 zonas.

Lomas de Mangomarca con un área total de 516.10 ha, ubicada en el distrito de San Juan de Lurigancho (SJL).

Lomas Payet se ubica entre los distritos de Independencia y SJL, tiene un área total 402.89 ha. (RM.440-2018-MINAM), y el área ubicada en Lima Este en el distrito de San Juan de Lurigancho, tiene un área de 187.338 (ha).

Lomas de Amancaes se ubica entre los distritos del Rimac, Independencia y SJL, tienen un área total de 253.96 ha. (DS 011-2019-MINAM) y el área ubicada en Lima Este, en el distrito de San Juan de Lurigancho es de 66.551 ha.

Lomas de Villa María se ubica entre los distritos de la Molina y Villa María del Triunfo tiene un área total 627.94 (ha) (DS 011-2019-MINAM), el área ubicada en Lima Este, en el distrito de La Molina, es 80.446 ha.

Las Lomas registradas como Área de Conservación Regional del Sistema de Lomas de Lima son las Lomas de Amancaes y la de Villa María, mientras que las Lomas de Mangomarca y Payet, no están declaradas áreas de Conservación Regional, y actualmente reciben una fuerte presión por el crecimiento urbano, PDU Lima Este 2021-2031 (2022)

El 2018, la Dirección de Inventario y Valoración de los Servicios de Nacional Forestal y de Fauna Silvestre -SERFOR,   después de la identificación y caracterización de los estados de conservación incorporo una lista de 36 ecosistemas frágiles, dentro de esta lista se encuentran las Lomas Mangomarca, Payet y Villa María, se les considera frágiles por su baja resiliencia ante los eventos de tipo antropogénico que ha provocado una alteración en su estructura, de acuerdo con la RD 153-2018-MINAGRI-SERFOR.

Fig 3. Mapa de las Lomas Costeras de Lima
Fuente: Proyecto EbA Lomas,2017.

Lomas Extraordinarias, Se forman aquellos años cuando las condiciones climáticas son más húmedas o cuando ocurre fenómenos del Niño las superficies de estas lomas se amplían dando paso a las lomas extraordinarias con área aproximada de 14926.09 has dentro del ámbito de estudio, PDU Lima Este 2021-2031 (2022).

Déficit de áreas verdes

El déficit de áreas verdes, de Lima Este es alto 6 de los 7 distritos tienen entre 3 - 7 m2 por / habitante, solo el distrito de la Molina tiene un alto índice de áreas verdes por habitante de 20m2/hab aproximadamente, PDU Lima Este (2022).

Tabla 1. Índice de Áreas Verdes por población al 2021.

Tipo	Chaclacayo	Chosica	El Agustino	La Molina	Sjl	Santa Anita	Vitarte
Áreas Verdes(m2)	114920	473760	270751	2790705	1820930	439732	1297959
Espacios Públicos(m2)	135419	148298	372493	421887	784175	278722	742868
Total(m2)	250340	622058	643244	3212592	2605106	718454	2040826
Población al 2021	44201	283516	222197	160405	1178813	221999	671493
Índice actual(m2)	6	2	3	20	2	3	3
Déficit en base 9m2(Sugeridos OMS)	-3	-7	-6	11	-7	-6	-6

Fuente: PDU Lima Este 2021-2031 (2022)

Los Servicios Ecosistémicos

Son los beneficios que la gente obtiene de los ecosistemas; estos se dividen en servicios de base o soporte, que son los necesarios para la producción de los servicios de suministro, regulación y culturales (WRI, 2003).

Entre los principales servicios ecosistémicos que proveen las lomas de Lima Este son: El Soporte de conservación de recursos genéticos, mantiene ciclos de vida de aves migratorias, formación de suelos y la fotosíntesis.

La Provisión de agua y como este aporta en la recarga del acuífero subterráneo, de recursos genéticos endémicos, arbustos, flores y plantas silvestres que nos dan un paisaje hermoso. La Regulación de la calidad del aire y polinización.

Cultural nos brinda el ecoturismo, asimismo dentro de lomas Mangomarca se tienen 2 sitios arqueológicos los cuales se pueden articular a las visitas de las lomas y hacer circuitos eco culturales, o eco museos como lo propuesto por Scudere et al (2019), se pueden hacer investigaciones científicas, frente al déficit de áreas verdes las lomas

nos proveen de espacios abiertos Nieuwland et al (2017). a los cuales se pueden acceder pero aun de forma limitada, se requiere de una intervención para poder cuidar, conservar, brindar seguridad, frenar las invasiones ilegales, organizar la de manera que sean espacios con caminos, circuitos, áreas de descanso adecuados para que la población pueda   visitarlos sin perjudicar el ecosistema.

Fig 4. Servicios Ecosistémicos de las lomas costeras.
Fuente: SERNANP, 2017.

3.   PLANTEAMIENTO DEL PROBLEMA

La pérdida de áreas de lomas por degradación, ocupación indebida, tráfico de terrenos, crecimiento desordenado, déficit de nuevas áreas urbanas, entre otros aspectos generan la pérdida del servicio ecosistémico que esta ofrece a la ciudad.

Es importante proteger y conservar este ecosistema costero, por que ayuda a preservar una gran variedad de semillas que aguardan cada invierno para poder reverdecer. También ayudaría a reducir la gran brecha existente, en el déficit de área verdes que actualmente se tiene en casi todos los distritos de Lima Este, es una fuente de captura de carbono, la cual se va perdiendo según se pierden área de lomas.

4. METODOLOGÍA

Para la cuantificación del nivel de degradación de las lomas y saber la perdida aproximada de estas se realizó un mapeo en base a las imágenes libres del Google earth, el mapeo se realizó considerando el siguiente criterio:

Nivel de Degradación Media, aquella ocupación que tiene pocas viviendas dispersas y caminos, se consideran como las áreas con más probabilidades de recuperación y conservación debido a su poca intervención.

Fig 5. Vista de un área de degradación media, donde se observa que alrededor ya están lotizando las lomas.

Nivel de Degradación Alta, es aquella ocupación que tiene viviendas, galpones y algunas vías y caminos, se consideran como las áreas con algunas probabilidades de recuperación y conservación.

Fig 6. Vista de un área de degradación alta, también se observa la lotización que se está dando alrededor del área.

Nivel de Degradación Muy Alta, es aquella ocupación de viviendas y vías más concentradas y establecidas, se consideran como las áreas con menos probabilidades de recuperación y conservación debido a su alto nivel de intervención y asentamiento.

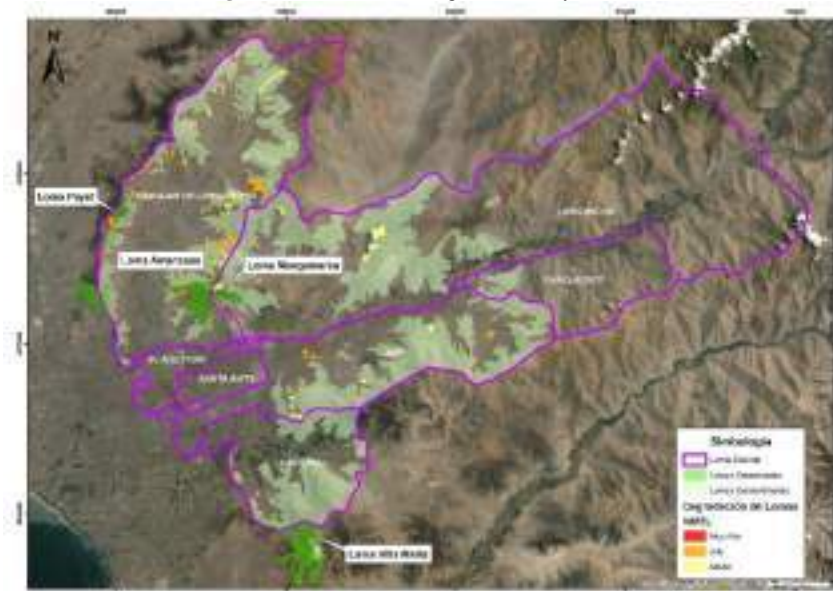**Fig 7.** Vista de un área de degradación muy alta

Fig 8. Mapa de la ubicación de las lomas y sus áreas de degradación en Lima Este
Fuente: Elaboración Propia

5.　RESULTADOS

Las áreas de lomas estacionales y extraordinarias que se encuentran sin afectación son 15212 has, es muy importante trabajar en estas áreas y buscar los medios para protegerlas y conservarlas de la ocupación ilegal, tráfico de tierras, ya que como se

observa en las fotos 1 y 2 están lotizando las áreas aledañas a lo mapeado, lo que significa que probablemente en un corto tiempo estas áreas podrían estar siendo ocupadas, lo que implicaría más perdidas de áreas de lomas.

Como se observa en el mapa de áreas degradadas, la loma estacionaria que tiene niveles más altos de degradación es la loma Payet, seguida de la loma Mangomarca.

En la siguiente tabla se muestran los porcentajes y áreas de degradación por niveles, el nivel muy alto de degradación es de 0.26% y los niveles alto y medio de degradación son del 1.68-1.64% del área total de las lomas. El 96.4% del total de las lomas aún se conservan, pero en un estado muy vulnerable sobre todo las de Mangomarca y Payet, por la falta de protección y conservación por parte del MINAM, SERNAMP y la falta de inclusión por parte de la Municipalidad Metropolitana de Lima como parte de las Áreas de Conservación Regional.

Tabla 2.Áreas y porcentajes del nivel de degradación y las lomas aun existentes.

Nivel de Degradación	Área (Has) Aprox.	Área (%) Aprox.
Muy Alto	41	0,26
Alto	265	1,68
Medio	259	1,64
Lomas	15212	96,42
Total	15777	100.0

Fuente: Elaboración propia.

Las lomas de Amancaes y Villa Maria, al formar parte de Áreas de Conservación Regional de Lima Metropolitana, se encuentran mejor protegidas y administradas.

Respecto a la loma de Villa Maria, existe una dicotomía ya que el área de la loma que se encuentra dentro del distrito de la Molina esta más conservada y protegida a diferencia del área de la loma que se encuentra en el distrito de Villa María, en esta última si existen problemas de degradación y ocupación informal, evidenciando que la participación del gobierno local es fundamental en el cuidado de estas áreas.

6. PROPUESTAS

Después del análisis de los diversos problemas que aquejan a estos ecosistemas frágiles, y cuantificando la degradación a través del mapeo, se observa que hay muchas brechas por cerrar pero también según la bibliografía revisada, se observa que hay estudios y iniciativas emprendidas antes de este articulo los cuales desde diferentes puntos de vista buscan proteger y revalorizar las lomas entre estos tenemos:

Entidades particulares como el Instituto de Cultura, Historia y Medio Ambiente(ICHMA), han trabajado activamente desde el 2002 en favor de la promoción, preservación y difusión eco-cultural de los sitios arqueológicos de la fortaleza Campoy, el Sitio Arqueológico Mangomarca y las lomas de Mangomarca, a través de actividades culturales, involucrando a los colegios del distrito para que los escolares puedan ser los defensores del patrimonio cultural y natural, promocionando visitas y rutas guiadas de circuitos turísticos, asimismo realizaron la propuesta de un parque arqueológico y ecológico de San Juan de Lurigancho.
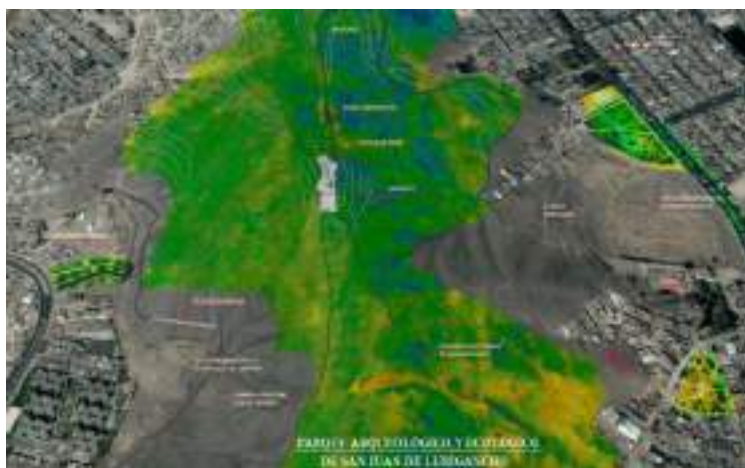

Fig 9. La Propuesta del Parque Arqueológico y Ecológico en SJL
Fuente: Una nueva Mirada de SJL desde su patrimonio cultural y natural. Instituto ICHMA, II Foro Ciudades como Vamos.

La concepción de las lomas como ecosistemas naturales y al mismo tiempo como espacios públicos es una propuesta denominada infraestructura ecológica, se basa en 3 principios: Principio de conservación de la biodiversidad el cual no solo busca el cuidado y protección de la flora y fauna amenazada sino también la protección del paisaje, principio de cuidado y mantenimiento de los servicios ecosistémicos su importancia radica en valorar funciones ecológicas de la naturaleza como la

purificación del aire, la captura del carbono y la captación de agua, y el principio multifuncional el cual tiene un enfoque de infraestructura ecológica que propone la posibilidad de uso urbano y ambiental de un mismo espacio, Nieuwland et al (2017).

Scudere et al (2019) después del análisis comparativo del porcentaje de invasión, problemas, potencialidades e iniciativas de conservación para las lomas de Carabayllo, Amancaes, Mangomarca y Villa María del Triunfo, concluye que las lomas de Mangomarca necesitan con más urgencia de un eco museo para poder frenar la desaparición de esta loma, en base a su análisis, realiza la propuesta para el eco museo, en el cual contempla se diseñen salas de exposición, la infraestructura tendría dos vista una a la urbanización Mangomarca y otra a las lomas, se plantea complementar el equipamiento para el circuito ecológico con programas comunales, se plantean 2 rutas una para el recorrido de las lomas y otra para los centros arqueológicos, así mismo plantea la creación de huertos urbanos cerca a los asentamientos humanos y la instalación de atrapanieblas las cuales puedan ayudar a regar las áreas de los huertos urbanos, la propuesta planteada es muy interesante y al hacer visible estas actividades se puede evitar la ocupación de los traficantes de terreno y degradación de las lomas.

Fig 10. Propuesta Urbana, Scudere et al (2019)

Algunas propuestas adicionales son proteger y conservar las Lomas Payet y de Mangomarca de una forma legal a través de una norma o resolución por parte de una

autoridad competente o a través del Gobierno Regional o local, para así frenar las invasiones informal.

- Realizar trabajos de conservación y recuperación sobre todo de las áreas de bajo nivel de degradación, ya que al ser las menos intervenidas, su recuperación puede ser más viable.
- Crear el parque ecológico en las lomas de Payet puede ayudar a realizar visitas de una forma más ordenada, segura, creando caminos y circuitos con señalización para que las personas que puedan visitar puedan ir informándose a lo largo del camino, como ya existe en las lomas de Lachay.

7. CONCLUSIONES Y RECOMENDACIONES

- Las lomas son áreas naturales sensibles y estacionales, las cuales albergan una gran variedad de semillas que esperan la humedad de los meses de invierno para poder florecer, pero al ser áreas naturales estacionales pueden verse afectadas, por la falta de conservación y protección, y quizá hasta desaparecer este importante servicio ecosistémico.
- Las lomas al tener una aparición estacional podrían verse afectado por el cambio climático.
- La pérdida de cobertura vegetal potencia el calentamiento global y reduce la captación de agua para la recarga de los acuíferos subterráneos y la captación de CO_2.
- Las lomas pueden ayudar a incrementar las áreas verdes por habitante, las áreas de esparcimiento, las áreas de treking y así ayudar a mejorar la calidad de vida de su población.
- Se recomienda proteger las lomas existentes, mediante normativas legales, las cuales puedan ser instrumentos que eviten la ocupación ilegal y tráfico de terreno de estas áreas naturales.
- Se recomienda promover en la comunidad, colegios, centros comunales el cuidado, protección y conservación de las lomas.

8. REFERENCIAS BIBLIOGRAFICAS

- Área de Conservación Regional Lomas de Lima, Perú. Disponible en: https://www.munlima.gob.pe/images/descargas/gerencias/GMA/AREA-DE-CONSERVACION-REGIONAL-LOMAS-DE-LIMA.pdf

- Decreto Supremo N° 011-2019-MINAM Decreto Supremo que establece el Área de Conservación Regional Sistema de Lomas de Lima https://sinia.minam.gob.pe/normas/decreto-supremo-que-establece-area-conservacion-regional-sistema-lomas

- Lleellish, M., Odar, J., & Trinidad, H. (2015). Guía de Flora de las Lomas de Lima. Disponible en: http://repositorio.serfor.gob.pe/handle/SERFOR/484

- Gestión Comunitaria de las Huacas y Lomas de San Juan de Lurigancho https://www.academia.edu/66944254/ICHMA_2021_Gestion_comunita ria_de_las_huacas_y_lomas_de_San_Juan_de_Lurigancho

- Plan de Desarrollo Urbano de Lima Este, 2022. Disponible en: https://www.imp.gob.pe/es/recursos/PDUS/Lima%20Este/Sintesi s%20y%20Propuesta/Documento/S%C3%8DNTESIS%20Y%20 PROPUESTA%20PDU%20LIMA%20ESTE.pdf

- Seoane Byrne, C., & Jeri Kukulis, J. J. Lomas de lima y el árbol de mito: amenazas y servicios ecosistémicos (Estudio de caso: Lomas de Pamplona alta).

- Gálvez Paredes, D. M. (2019). Impacto de la expansión urbana sobre las lomas costeras del Perú.

- Nieuwland, B., & Mamani, J. M. (2017). Las lomas de Lima: enfocando ecosistemas desérticos como espacios abiertos en Lima metropolitana. Espacio y desarrollo, (29), 109-133.

- Kato, A. (2018). Detrás de la neblina: lomas de Lima. Agenda Viva, (002), 9-15.

- Scudere Cardenas, A. B., & Zuñiga Alva, M. D. C. (2019). Ecomuseo en las lomas de Mangomarca: un camino hacia la conservación.

- Avendaño Cotrina, A. L.(2020) Valoración de los servicios ecosistémicos de lomas costeras en los criterios de diseño del espacio público en zonas de amortiguamiento. Lomas El Paraíso, Villa María del Triunfo.

- Servicios Ecosistémicos que brindan las Áreas Naturales Protegidas Documento de Trabajo No. 23, SERNANP 2016.

Posters

Smart cities and their relationship with ontological engineering

C. Espinoza-Aguirre[1]

[1]Universidad Carlos III de Madrid, Ciencia y Tecnología Informática, Madrid, España
100375266@alumnos.uc3m.es

Abstract. The article tries to relate smart cities and machine learning, so university dropout and its prevention through the implementation of machine learning have been analyzed. In this sense, the results of applying ontologies to understand the problem that revolves around university dropout and its application in smart cities are presented. Consequently, the use of ontologies has been implemented to contextualize a complex problem, as well as the relationship established between education and university dropout. This research will contribute to ontological engineering and education, enabling the construction of an information structure of the deserter's profile with semantic components that allow it to be an input for a more complex knowledge management model, such as artificial intelligence.

Planificación óptima de rutas de ambulancias eléctricas en situación de pandemia

Luis Santiago Martín[1], Mónica Alonso[1][0000-0001-9006-8196] and Hortensia Amarís[1][0000-0001-9487-0127]

[1] Universidad Carlos III de Madrid, Leganés, 28911, Madrid, Spain
monica.alonso@uc3m.es

Abstract. Las ambulancias juegan un papel crítico para el desempeño del co- rrecto funcionamiento de los sistemas médicos sanitarios, por lo que la planifica- ción óptima de las rutas a seguir para atender las llamadas de los pacientes es crucial. Atendiendo a los requerimientos de electrificación del transporte para reducir las emisiones de CO2, aparecen en el mercado ambulancias eléctricas, que incorporan nuevas acciones asociadas a la recarga de las baterías en el desa- rrollo de los planificadores de rutas. Además, la pandemia del COVID-19 impuso nuevas restricciones en la planificación de las rutas de las ambulancias al requerir un tiempo de desinfección del vehículo y de preparación de las medidas de pro- tección del personal sanitaria que viaje en ella. En este artículo se desarrolla un planificador de rutas para ambulancias eléctricas, con el objetivo de atender el máximo número de pacientes en el menor tiempo posible y optimizando el uso de las baterías de los vehículos eléctricos, considerando además los tiempos de desinfección del vehículo impuestos por una situación de pandemia.

Reciclado de Álabes de los Parques Eólicos implementados en Perú. Análisis y propuestas

A. León-Benavides[1], J. Mírez-Tarrillo[1]

[1]UNI, Universidad Nacional de Ingeniería, Rímac, Lima, Perú
walter.leon.b@uni.pe
jmirez@uni.edu.pe

Abstract. En el campo de las energías renovables, Los parques eólicos son considerados como energías limpias, pero tienen un componente que arrastran al final de su ciclo de vida como una mancha gris presente y esto es, la ausencia de un plan de cierre limpio y amigable con el medio ambiente. Los álabes no tienen una disposición final medioambientalmente apropiada. La fibra de vidrio y de carbono presentes en su estructura, son difíciles de ser tratados. El propósito del presente artículo, es dar un mirada a todo lo que se hace al respecto a nivel internacional y en el Perú. Las diferentes estrategias que están aplicando como extender la vida útil, reciclar, reutilizar, etc. Además, se revisa los aspectos legales y las oportunidades que surgen con la legislación actual en ese sentido.

Progressive regression model to project the behavior of photovoltaic generation in municipalities of Mexico City

López-Meraz R. A. [1][0000-0002-3236-3709], Reyes-Cárcamo Y.[2]
and Jamed-Boza L. O. [1][0000-0002-6378-758X]

[1] Universidad Veracruzana, Circuito Universitario Gonzalo Aguirre Beltrán s/n, 91000, México
[2] Instituto Tecnológico Superior de Huatusco, C. 25 Ote., Reserva Territorial, 94106, México
raullopez03@uv.mx: R.L-M.;yreyesc@huatusco.tecnm.mx: Y.R-M; lojb33@gmail.com: L.J-B.

Abstract. The work presents an analysis of the behavior of the daily energy production of two identical residential photovoltaic systems interconnected to the network, installed by the same company, located in neighboring municipalities of Mexico City. The measurement period is from December 11, 2020, to July 27, 2022. The product of this research offers a tool that more accurately estimates the nominal power of photovoltaic arrays (AFV) by identifying the site where the best conditions exist for achieve better efficiency. The characterization of the AFVs was carried out with the help of the statistical application software JMP and for the adjustment of the projection, the regression of three factors was used, reaching a totally significant approach.

A Review of Computational and Mathematical Techniques for Urban Mobility Data Analysis

Hugo Alatrista-Salas[1][0000−0001−5252−4728], Erick Cuenca[2][0000−0002−3996−2851], Rigoberto Fonseca-Delgado[2][0000−0002−8890−3911], Aracelis Hernandez[3][0000−0002−6094−4826], Saba Infante[2][0000−0001−8883−2730], Raúl Manzanilla[2][0000−0002−8456−0333], Diego Morales-Navarrete[2][0000−0002−6145−7608], Miguel Nunez-del-Prado[4][0000−0001−7997−1739], Israel Pineda[5][0000−0002−3950−2169], Pascal Poncelet[6][0000−0002−8277−3490] and Arnaud Sallaberry[6,7][0000−0001−7068−176X]

[1] Pontificia Universidad Católica del Perú, Lima, Peru
halatrista@pucp.pe
[2] Yachay Tech University, Urcuquí, Ecuador
{ecuenca, rfonseca, sinfante, rmanzanilla, dmorales}@yachaytech.edu.ec
[3] Universidad de Carabobo, Valencia, Venezuela
arhernan@uc.edu.ve
[4] Universidad Andina del Cusco, Cusco, Peru
miguel.nunezdelprado@vrin.uandina.edu.pe
[5] Universidad San Francisco de Quito, Quito, Ecuador
ipineda@usfq.edu.ec
[6] LIRMM, University of Montpellier, CNRS, Montpellier, France
{pascal.poncelet, arnaud.sallaberry}@lirmm.fr
[7] AMIS, Paul-Valéry University of Montpellier, Montpellier, France

Abstract. In recent years, the scientific community has increasingly studied urban mobility since around 55% of the world population lives in urban areas. Thus, individuals living in urban areas have to deal with phenomena like traffic jams, commute time, and pollution, which are difficult to understand and solve. Therefore, new innovative approaches such as mobility models, artificial intelligence, or visualization applied to urban mobility analysis problems shed new light on understanding the behavior of cities. In this work, we survey the current state of the mathematical and computational tools we have at our disposal to better understand the current situation of urban areas. Our work presents datasets, discusses relevant artificial intelligence and visualization techniques, and reviews mathematical tools to analyze urban data. We hope our work offers a valuable summary of these ideas and provides the base for future investigations.

Quantification of Resilience in the electric grid of CENTROSUR. A case study

Pablo Arias-Reyes[1], Antonio Barragán-Escandón[2], Javier González-Redrován[1] and Sergio Zambrano-Asanza[3,4]

[1] Centro de Posgrados, Universidad Católica de Cuenca, Camino a Patamarca y Cojimíes, Cuenca, Ecuador

[2] Grupo de Investigación en Energía, Universidad Politécnica Salesiana, Calle Vieja 12-30 y Ellia Liut, Cuenca, Ecuador

[3] Department of Electrical Engineering, Universidad Estadual Paulista "Júlio de Mesquita Filho"-UNESP, Ilha Solteira; SP, Brasil.

[4] Department of Planning, CENTROSUR Electric Distribution Utility, Cuenca, Ecuador
pariasr@ucacue.edu.ec

Abstract. The increase in the level of resilience in a distribution system is crucial due to the negative consequences and impacts on the electrical network that natural catastrophic events have due to the long times that are sometimes required for the restoration of the network and the services for end customers. Through an exploratory/descriptive and relational/explanatory study, resilience indicators and metrics was identified and developed for a part of the distribution utility network. The analysis was carried out in the CENTROSUR utility con- cession area that corresponds to the city of Cuenca and its associated primary feeder electrical networks. Zones vulnerable to high-impact, low-probability events (HILP) were identified by overlaying risk maps, georeferenced information, and data available from the electricity system in GIS format from the utility distributor. Vulnerable electrical zones and those with the highest reliability and resilience requirements were selected using qualitative and quantitative criteria. Reliability indices and resilience metrics existing in the literature was related and resilience metric models were determined for the proposed system under analysis. The information obtained was applied in the identification of resilient zones, infrastructure required to determine parameters for the electrical planning of the network, support of Microgrids, topological variants and priorities for reconfigurations and redundant investments of the network were exposed.

Energy Efficiency: characteristic that achieves the collaborative and sustainable perspective to incorporate IoT in a Smart City

Roberto Ferro-Escobar * Harold Vacca-González** Harvey Gómez-Castillo***

Universidad Distrital Francisco José de Caldas:
* rferro@udistrital.edu.co, https://orcid.org/0000-0002-8978-538X Universidad Distrital Francisco José de Caldas:
** hvacca@udistrital.edu.co, https://orcid.org/0000-0001-7017-0070 Universidad Distrital Francisco José de Caldas:
*** hagomezca@correo.udistrital.edu.co, https://orcid.org/0000-0003-4474-3642

Abstract. Una ciudad inteligente es un espacio urbano orientado a mejorar la calidad de vida de los ciudadanos que la habitan a través del uso intensivo de tecnología para afirmar desarrollos sociales y económicos, y en donde múltiples sectores cooperan sistemáticamente en lograr resultados sostenibles colectivos a todo nivel. En tal sentido, el uso de Internet ha llegado a un punto en el que se ha vuelto imprescindible en la vida cotidiana: la necesidad de tener la información a mano en el menor tiempo posible ha generado una revolución tecnológica centrada en la conexión constante con esta herramienta. Desde la vida personal y la relación con los objetos que se utilizan diariamente se ha creado la necesidad de monitorear e interpretar exhaustivamente lo que rodea al ser humano, de ahí el nacimiento del Internet de las Cosas (IoT); y la convergencia dada entre el medio ambiente junto con la interacción humana y la tecnología ha originado el concepto de ciudades inteligentes y sostenibles (SSC).

Sin embargo, dado el estado actual de estos conceptos, es necesario aplicar una revisión conceptual contextualizada introductoria sobre ciudades inteligentes y sostenibles, y luego caracterizarlas a partir del establecimiento de alguna amplia categoría con sus respectivas subcategorías: la Eficiencia energética (Energías Renovables, Gestión de Recursos Naturales y medición de parámetros ambientales –Emisiones-, Eficiencia del Consumo de Agua).

Teniendo en cuenta lo anterior, este trabajo aborda comparativamente conceptos sobre el presente de las SSC en colaboración con el IoT: destacando la Eficiencia Energética como aquella característica que confiere la perspectiva colaborativa y sostenible para incorporar IoT en una Ciudad Inteligente. Se da el caso de la ciudad- nación de Singapur a partir de su descripción cualitativa, realizando una evaluación cuantitativa en términos de Sostenibilidad, Capital Intelectual y Calidad de Vida, dentro de un modelo que se utiliza para clasificar las ciudades como inteligentes, es decir transitar desde una ciudad tradicional a una ciudad global moderna que oriente estos resultados para el mejoramiento de la calidad de vida de los ciudadanos.

Influencia del Desarrollo de Infraestructura Sostenible en el Sector Industria sobre la Vulnerabilidad Socioambiental

R. Villalobos-Núñez [1], J. Mírez-Tarrill [1]

[1] UNI, Universidad Nacional de Ingeniería, Rímac, Lima, Perú
rvillalobosn@uni.pe, jmirez@uni.edu.pe

Abstract. El artículo aborda puntos específicos de la historia de la humanidad dilucidando la influencia del desarrollo industrial sobre la vulnerabilidad socioambiental, plasmando cómo es que el ser humano ha ido transformando su entorno en miras a mejores condiciones de vida hasta llegar a un punto de inflexión donde continuar bajo los mismas paradigmas de desarrollo nos han conducido hacia la formación de una sociedad frágil y sin resiliencia. Se da a conocer, además, como lo expuesto está llegando a marcar un nuevo hito en la historia, sentando bases para el desarrollo de nuevos modelos industriales, como lo es la infraestructura industrial sostenible, esto gracias a la aplicación de nuevos conceptos como los de economía circular y simbiosis industrial, remarcándose mediante la exposición de casos de éxito, cómo es que en la actualidad ello ha calado en la formación de sociedades más resilientes.

EL PATRIMONIO DE LA HUMANIDAD COMO ELEMENTO COMPETITIVO Y DIFERENCIADOR PARA CIUDADES EN EL DESARROLLO ECONÓMICO DEL TURISMO DE NEGOCIOS

Hernández Andrés, Víctor[1] [0000-0002-5945-9567], De Frutos Madrazo, Pablo[2] [0000-0002-8206-984X], Martín Cervantes, Pedro Antonio[3] [0000-0002-8375-1613] y Frechoso Remiro, Juan Carlos[4] [0000-0001-7257-4749]

[1]Dpto. de Economía Aplicada, Universidad de Valladolid, 42004 Soria, España
victor.hernandez.andres@uva.es

[2]Dpto. de Economía Aplicada, Universidad de Valladolid, 42004 Soria, España
pablof@ea.uva.es

[3]Dpto. de Economía Financiera y Contabilidad, Universidad de Valladolid, 42004 Soria, España
pedroantonio.martin@uva.es

[4]Dpto. de Economía Aplicada, Universidad de Valladolid, 42004 Soria, España
juancfre@ea.uva.es

Abstract. Entre los principales desafíos de las ciudades inteligentes se encuentra el desarrollo económico sostenible. El turismo, constituye un motor para su desarrollo económico, pero frecuentemente está sujeto a una notable estacionalidad. No obstante, el denominado turismo de negocios rompe esta estacionalidad del turismo tradicional, desarrollándose a lo largo de todo el año en la ciudad destino. Contribuye al desarrollo económico a través de la atracción de viajeros cuya motivación son los negocios y cuya motivación está inicialmente diferenciada de las motivaciones de un turista vacacional. Su contribución puede ser directa derivada del desarrollo de negocios en dicha ciudad o bien por potenciales visitas posteriores (ya como turistas tradicionales) de los participantes de las reuniones y congresos. En este contexto, cabe preguntarse en qué medida las motivaciones que mueven a un turista vacacional, entre las que se encuentra el valor cultural o el patrimonio histórico de la región que visitan, pueden influir o determinar para que un turista de negocios tome la elección de un destino para la realización de un evento de negocios. En este estudio hemos contrastado si existe una relación entre el patrimonio cultural existente en una ciudad y el número de reuniones acaecidas a lo largo del año. Las conclusiones del contraste realizado son que, si bien el patrimonio cultural de una ciudad resulta significativo en relación al número de reuniones acaecidas, por sí sola esta variable no explica la elección de una ciudad como destino para la realización de un evento de negocios.

Herramienta de simulación de plantas de autoconsumo y su aplicación a un complejo turístico

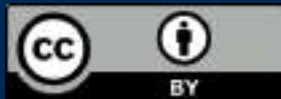Jacinto Vidal-Noguera, Victor Martínez-Moll, Ivan Alonso de Miguel, Andreu Moià- Pol y Vicente Canals

Universidad de las Isla Baleares, Departamento de Ingeniería Industrial y Construcción, Palma, Ctra. Valldemossa km 7.5, Campus UIB, Islas Baleares ES07122, España
jacinto.vidal@uib.cat

Abstract. El creciente aumento del precio del gas y la electricidad en la Unión Europea (UE) está afectando tanto a los pequeños consumidores como a los sectores industriales y de servicios. Esta situación ha conducido a un creciente interés en el despliegue de plantas de autoconsumo basadas en la combinación de fuentes renovables y fósiles. Ahora bien, determinar la planta de autoconsumo óptima para cubrir la demanda de un consumidor, no resulta simple dado el actual escenario de gran variabilidad en los costes energéticos y de la generación de las fuentes renovables. A su vez, para avanzar en la transición energética de la UE es clave poder generar energía de forma barata y eficiente.

Así, en este trabajo se ha desarrollado una herramienta numérica capaz de optimizar el predimensionamiento de las plantas de autoconsumo, así como la sistematización del análisis de su viabilidad técnico-económica. Para ello, la herramienta desarrollada analiza la demanda energética actual (eléctrica y térmica) de las instalaciones, como punto de partida para simular diferentes escenarios de autoproducción hasta hallar el que mejor se adapte a las características de estas. Finalmente, la herramienta numérica se ha aplicado sobre un complejo hotelero real de playa, que opera tan solo en la temporada de verano, y dispone de 477 habitaciones con una superficie construida de 25.000 m^2, ubicado en la isla de Menorca (España). Los resultados obtenidos muestran como las soluciones más rentables son la cogeneración y la trigeneración, siempre que los precios del gas natural canalizado no superen el umbral de los 0,10 €/kWh.

A Smart City is a framework composed mainly of Internet of Things systems and Information and Communication Technologies (ICT) integrated to develop, implement and promote sustainable development practices and face the challenges of urbanization. The Ibero-American Congress of Smart Cities (ICSC-CITIES) is a discussion forum that aims to create synergies among different research groups to promote the development of Smart Cities and contribute to their knowledge and integration in different scenarios.

This book constitutes the proceedings of the fifth Ibero-American Congress of Smart Cities (ICSC-CITIES 2022) held in a hybrid way (face-to-face and virtual) from November 28th to 30th, 2022, in Cuenca, Ecuador, hosted and sponsored by Universidad de Cuenca, Ecuador. Eighty-five technical presentations were given by researchers from 24 different countries during the ICSC-CITIES 2022. Papers were divided into four topics, i.e., Governance and Citizenship, Mobility and IoT, Infrastructures, Energy & Environment, and Energy Efficiency. All the papers accepted for publication in this book have been peer-reviewed.

UCUENCA

CITIES

CIUDADES INTELIGENTES TOTALMENTE INTEGRALES, EFICIENTES Y SOSTENIBLES

UVa

UNIVERSIDAD
DE LA REPÚBLICA
URUGUAY

UNIVERSIDAD AUTÓNOMA DEL
ESTADO DE MORELOS

UNIVERSIDAD NACIONAL DEL SUR
BAHIA BLANCA